



"Structural Integrity for the Next Millennium"

**The 1999 Meeting of the
International Committee
on**

Aeronautical Fatigue

12 - 16 July 1999

Conference: 12-13 July

Symposium: 14-16 July

**Meydenbauer Center
Bellevue, Washington - USA**

NATIONAL REVIEWS

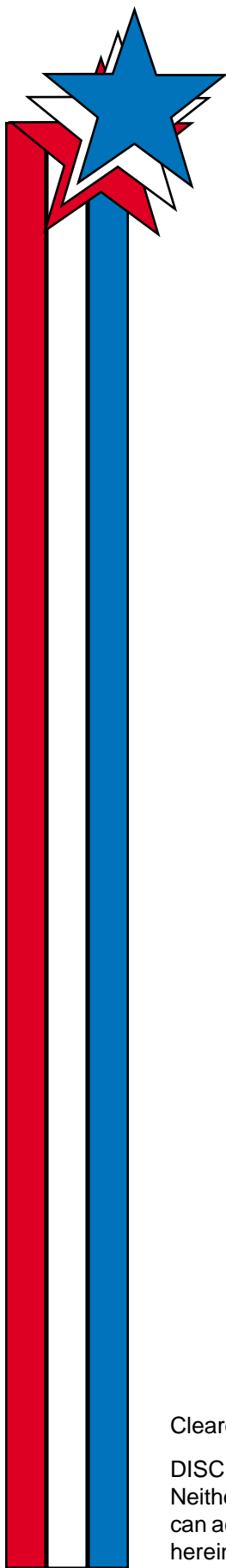
Minutes of the 26th ICAF Conference

Compiled by J.L. Rudd

Air Force Research Laboratory
Wright-Patterson Air Force Base, Ohio

Cleared for Public Release.

DISCLAIMER: These minutes contain summaries of work in progress. Neither ICAF as a body, nor the individual scientists or their organizations can accept any responsibility for the accuracy of data or other statements herein. This document should not be cited as a reference.



CONTENTS

Minutes of Previous ICAF Conferences

ICAF General Secretary's Review - 1997 to 1999

National Reviews for the Period 1997 - 1999

	PAGE
The Netherlands	1/1
United Kingdom	2/1
Sweden	3/1
Switzerland	4/1
Germany	5/1
France	6/1
Italy	7/1
Australia	8/1
United States	9/1
Canada	10/1
Israel	11/1
Japan	12/1
Conference/Symposium Agenda	13/1
National Delegates to the ICAF	14/1
Attendees to the 1999 ICAF Meetings	15/1
Photo Pages	16/1

MINUTES OF PREVIOUS ICAF CONFERENCES

Conf No.	Held at	Date	Establishment, Editor	ICAF Doc. No.
1	Amsterdam	1952	NLL, Plantema	14
2	Stockholm	1953	FAA, Noton	44
3	Cranfield	1955	RAE, Raithby	67
4	Zurich	1956	F+W, Keller	94
5	Brussels	1957	STAE(B), van Laer	115
6	Amsterdam	1959	NLL, Plantema and Schijve	126
7	Paris	1961	STAE(F), Barrois	220
8	Rome	1963	MDA, Villa	271
9	Munich	1965	LBF, Gassner	338
10	Melbourne	1967	ARL, Mann	412
11	Stockholm	1969	FFA, Wallgren	480
12	Miami	1971	NASA, Hardrath	561
13	London	1973	RAE, Pike	685
14	Lausanne	1975	F+W, Branger and Berger	800
15	Darmstadt	1977	LBF, Buxbaum and Franz	959
16	Brussels	1979	Admin. de l'Aeronautique, Maenhaut	1170
17	Noordwijkerhout	1981	NLR, de Jong and van der Linden	1215
18	Toulouse	1983	CEAT, Labourdette	1335
19	Pisa	1985	AIFE and U. of Pisa, Salvetti and Lazzeri	1489
20	Ottawa	1987	NAE, Simpson	1602
21	Jerusalem	1989	Technion, Berkovits	1681
22	Tokyo	1991	U. of Tokyo, Kobayashi	1816
23	Stockholm	1993	FFA, Blom	1950
24	Melbourne	1995	AMRL, Grandage and Jost	2054
25	Edinburgh	1997	DERA, Poole	2164
26	Seattle	1999	AFRL, Rudd	2265

REVIEW
on the activities of the
International Committee on Aeronautical Fatigue (ICAF)
during the period May 1997 to May 1999

25th ICAF meeting in Edinburgh in June 1997

The Meeting in Edinburgh was organized by Dr. Peter Poole, the U.K. National Delegate. It started with the 25th ICAF Conference on June 16-17, 1997 followed by the 19th ICAF Symposium on June 18-20.

At the Conference 12 National Reviews were presented. The Reviews were compiled in the Minutes of the Conference, published by the Defence Evaluation and Research Agency (DERA), Farnborough, England. Within half a year after the Conference these Minutes were available. More than 300 copies were distributed by the editor for dissemination in the ICAF countries.

The Symposium was opened by the 16th Plantema Memorial Lecture, named in honour of the late founder of ICAF, Dr. Frederick J. Plantema. It was presented by Dr. J. W. Lincoln. The title of his lecture was: "Aging Aircraft - USAF Experience and Actions." At the conclusion of his lecture, Dr. Lincoln received the Plantema Memorial Lecture Medal. In the Symposium 33 papers were presented by their authors, and a further 39 were presented in poster format. (This kind of presentation was initiated in 1993 in Stockholm, and has proven to be successful.) Both, papers and poster presentations were included into the Proceedings of the Symposium entitled "Fatigue in New and Ageing Aircraft." The book was edited by Messrs. R. Cooke and P. Poole, and was printed by EMAS in two volumes. It was also available about half a year after the Symposium, and it can certainly be recommended to everybody interested in aeronautical fatigue problems.

The Symposium was attended by 271 participants. It was generally appreciated that the host country had organized an efficient and interesting meeting. The participants enjoyed also gratefully an introduction into Scottish traditions and hospitality.

National Delegates of Germany and Switzerland

During the period of review two National Delegates retired, i.e. Dr. H. Huth from Germany and Mr. S. Michel from Switzerland.

Following suggestions coming from the respective countries the Committee Members had voted unanimously two new National Delegates, i.e. Dr. Claudio Dalle Donne, DLR Cologne in Germany and Dr. Michel Guillaume, SF Emmen in Switzerland.

ICAF Document Distribution

The number of documents distributed between the ICAF centres during the past two years is 66, which include 15 reports, 49 reprints (from journals and symposium books), and 2 books.

One ICAF Bulletin (No. 91, August 1998) and two Circular Letters (May 1998 and February 1999) were issued during the last period.

ICAF Status

Traditionally the Secretary's Review ends with a brief summary of ICAF Status.

ICAF is an international organization with informal rules written up in a one-page document, called the ICAF principles. ICAF has two objectives: (1) to stimulate contacts between people actively engaged in aircraft fatigue problems, and (2) to exchange information, experience, opinions, and ideas concerning aircraft fatigue.

The objectives are primarily realised by meetings like the present one, and by an exchange of ICAF documents between the member countries.

There is another document of two pages which refers to the tasks of the National Delegates. The Delegates are responsible for circulation of ICAF information and documents. Last and not least, each Delegate prepares and presents a review of the aeronautical fatigue investigations carried out in his home country. These reviews are most important reports, and all the work involved should be highly appreciated by all of us.

O. Buxbaum
General Secretary of ICAF

Review of aeronautical fatigue investigation in the Netherlands during the period March 1997 - March 1999

H.H. Ottens
National Aerospace Laboratory NLR
Anthony Fokkerweg 2
1006 BM Amsterdam
The Netherlands

1.1 INTRODUCTION

The present review gives a brief summary of the work performed in the Netherlands in the field of aeronautical fatigue, during the period from March 1997 until March 1999. The various contributions to this review come from the following sources:

- The National Aerospace Laboratory NLR
- The Faculty of Aerospace Engineering, Delft University of Technology (TU Delft)
- The Faculty of Mechanical Engineering, Eindhoven University (TU Eindhoven)
- Fokker Services
- Fokker Aerostructures
- Structural Laminates Industries (SLI)

The names of the principal investigator and their affiliation are presented between brackets at the end of each topic title.

1.2 LOADS

1.2.1 Determination of lateral gust loads (P.A. van Gelder, NLR)

Partly as a continuation of the "Fokker 100 Tail Loads Programme" that has been reported in previous ICAF meetings, NLR has carried out a research programme to test and validate newly in-house developed (unsteady) aerodynamic codes, especially with respect to the determination of lateral gust loads on aircraft. Calculations have been carried out with the Aero-elastic Simulation package (AESIM) for a Fokker 100 configuration and results will be compared with wind-tunnel data. The calculations were completed in 1998 and the final results will be reported in 1999.

1.2.2 Standard load sequences for aeronautical applications (P.A. van Gelder, NLR)

The National Aerospace Laboratory NLR has been actively involved, especially in the period between 1975 and 1992, with the creation and validation of standardised load sequences for fatigue analyses and testing.

In order to increase the accessibility, in terms of availability and application, and also to minimise the possibility of erroneous application of the data, all sequences (available at NLR) will be stored on one device (CD-ROM).

A database function will be added that will enable the generation of load/stress sequences for the appropriate stress levels from the basic data. Also an interface option for common crack-growth programs such as NASGRO (NASA) and CRAGRO (NLR) will be supplied.

The relevant describing reports will be added as well to this CD-ROM in a digital format (PDF).

The CD-ROM is expected to be completed in 1999.

1.2.3 FAA flight loads programme (P.A. van Gelder, NLR)

For the ageing aircraft programme FAA has installed Flight Data Recorders in a number of transport aircraft for load and usage monitoring. NLR was asked to advise FAA on this programme. One of the NLR tasks is to investigate whether the sampling rates that are currently used by onboard Flight Data Recorders is sufficient to supply statistically realistic and relevant loads data (cg-accelerations) and usage data (e.g. flap deflections). NLR carries out this investigation using NASA supplied flight data sampled at a high rate (20-100 Hz). This project is carried out as a co-operation between NLR the FAA and the Netherlands Airworthiness Authorities RLD.

1.2.4 Fatigue loads/usage monitoring of military aircraft

a. Structural fatigue load monitoring of RNLAf F-16 aircraft (D.J. Spiekhout, NLR)

The fatigue load monitoring programme of F-16 aircraft of the Royal Netherlands Air Force (RNLAf) has been continued. In the previous programme three aircraft per squadron were equipped with a four channel digital solid state recorder measuring wing root bending moment and three additional load quantities. This programme is gradually phased out and replaced by the FACE system.

The "Fatigue analysing and Air Combat Evaluation system (FACE)" was developed by RADA Electronics Industries Ltd. in Israel and will be installed in all RNLAf F-16 aircraft. To date in about 60% of the RNLAf fleet a FACE system has been installed. The FACE system allows a more extensive load monitoring on individual aircraft bases. Quantities measured to monitor structural fatigue loading include strains in five different structural locations: two indicative for wing root bending and outer wing bending, two at the rear fuselage dealing with horizontal and vertical tail loads and one in the fuselage center section indicative for fuselage bending. With these strain gages a number of flight parameters are measured simultaneously. The FACE system is also used to monitor engine loads and usage.

Apart from the continuous load and usage monitoring programme the FACE system is capable to do campaign measurements. The FACE system and its possibilities are described in Ref. 1.

b. Maritime Patrol Aircraft, P-3 Orion (A.A. ten Have, NLR)

NLR has developed software to perform fatigue life calculations of the P-3 Orion maritime patrol aircraft. These calculations provide the operator with a validated fatigue life indicator for the most critical wing location of the P-3 Orion airframe structure. This package is currently in use by the RNLN (as "PLEBOI"), the Spanish Airforce (as "SAFORI") and the Portuguese Airforce (as "POLICAL"). NLR performs structural data recording activities in RNLN and PoAF P-3 Orion to support theoretical fatigue life calculations.

c. Transport Aircraft, C-130 Hercules (R.P.G. Veul, NLR)

The Royal Netherlands Airforce operates two C-130H-30 Hercules aircraft that were delivered in 1994/1995. In order to optimize operational and maintenance aspects, NLR is setting up tailored C-130 structural life monitoring procedures. An in-flight data acquisition system will be installed in each of the C-130 Hercules airframes, generating operational usage and service loads data.

1.2.5 Helicopters (A.A. ten Have, NLR)

a. Lynx helicopter (A.A. ten Have, NLR)

To achieve Lynx life extension and to monitor and control maintenance of the main rotor and sponson (the Lynx undercarriage support structure) loads, the Royal Netherlands Navy RNLN has decided for a fleetwide installation of a multi-channel structural data recorder system, called the AIDA system. This AIDA system will also cover and replace engine cycle counter functionalities. NLR has provided extensive support to the RNLN by defining the AIDA functional specification, generating user-requirements and source selection input data, co-developing desired AIDA functionalities, performing airworthiness tests, and developing Host Station Software.

Current status as of April 1999, is that production AIDA systems are being delivered, Lynx airframes are being modified, and the AIDA certification process is being finalized. Developing the Host Station Software is still underway. Apart from the RNLN, German and Brazilian military operators also consider installation of this NLR developed AIDA system for their Lynx fleets. To support these operators in their decision-making process, NLR has provided input.

b. Bo-105, Chinook, Cougar helicopter (A.A. ten Have, NLR)

NLR has supported the Royal Netherlands Airforce RNLAf with structural integrity issues concerning the Bo-105, Chinook and Cougar. With respect to the Bo-105, these activities concern service life extension aspects of ageing airframes, with respect to the other helicopter types they concern optimization of new helicopters structural integrity issues. In particular, corrosion and crack logging and administrative usage monitoring procedures are under study.

1.3 ENGINES

1.3.1 Engine usage monitoring

a. Pratt & Whitney F100 engine (J.H. Heida, J.F. Slauerhoff, NLR)

Since 1991, NLR performs operational engine usage monitoring of the Pratt & Whitney F100 engines installed in F-16 aircraft. For this purpose, a number of multi-channel data-acquisition systems have been installed in the RNLA F-16 fleet registering parameters such as pressure altitude, calibrated airspeed, engine rotational speed and power lever angle. Engine damage accumulation is then calculated from the recorded engine cycles using specific algorithms. Furthermore, flight time and hot time envelopes (time spent in certain Mach number versus altitude regions) are determined to gain more insight in the RNLA F-16 mission profile. To date, more than 11000 RNLA F-16 sorties have been collected. On a routine basis, this operational RNLA engine data is transferred to the engine manufacturer for evaluation purposes and could be used as a basis for tailored engine maintenance procedures, e.g. affecting inspection intervals or retirement lives.

From 1997, the Fatigue Analysing and Air Combat Evaluation system (FACE) is being introduced in RNLA F-16 aircraft. FACE is a comprehensive maintenance management and flight debriefing system developed by RADA Electronic Industries Ltd in Israel. This system enables the recording of approximately 100 engine parameters of which a representative selection will be made in 1999. Ad-hoc campaign measurements will always allow other parameters to be temporarily monitored.

b. Rolls Royce Gem 42 engine (A.A. ten Have, NLR)

On a routine basis and employing four NLR developed engine cycle counters, NLR supports the Royal Netherlands Navy RNLN with Cyclic Life Control of their Lynx Gem engines. Currently, the RNLN is the only Lynx operator benefiting from tailored exchange rate in Gem engine maintenance procedures. In the near future the engine cycle counting is included in the AIDA system and the separate cycle counters will be phased out.

1.3.2 Life assessment of engine components (T. Tinga, NLR)

In order to do an accurate life assessment of a gasturbine component it is necessary to have detailed information on the gas turbine loads, thermal, aerodynamic and mechanical loads, and on the resulting stresses in the component.

The total loading of gas turbine components has two major contributions: thermal loading and mechanical loading. The loading of stationary (non-rotating) components like vanes is mainly thermal, caused by variations in temperature of the hot gas stream in which the components operate. Rotating components have additional mechanical loading, where the centrifugal loading due to the high rotational speed of the components is the most important contribution. At the NLR a method has been developed to determine both the thermal and centrifugal loading of any gas turbine component for any mission.

The basis of the analysis method is the Gas Turbine Simulation program (GSP), developed at the NLR. GSP performs a transient (gas path) analysis of a mission using power settings and flight conditions as input and giving, among others, gas temperatures, pressures and mass flows as output (see figure 1). The gas stream results of the GSP calculation are then used in a finite element (FE) analysis to calculate the temperature distribution in the component. The results of this thermal analysis are combined with the rotational speeds calculated by GSP to determine the stresses and strains in the component. Finally, the obtained stress spectrum is used to perform a life assessment of the component, which completes the analysis. The method has been applied to a real component, in this case a 3rd stage turbine blade of an F100-PW-200 turbofan engine.

1.3.3 Detailed analysis of engine components

a. Aerothermal loads analysis on engine components (R. Hagmeijer, NLR)

The theoretical aerodynamics department of NLR is responsible for providing thermal and aerodynamic loads on components due to the aerothermodynamics of the hot gas flow. The analysis is divided into two parts:

1) Computational Fluid Dynamics (CFD).

Based on solution of the 3D Reynolds-averaged Navier-Stokes equations, the thermal and mechanical loads are determined along the component boundaries. The set of five partial differential equations describes conservation of mass, momentum and energy respectively, for viscous compressible fluids. Accurate solution of a discretisation of this equation set is carried out by employing sufficiently dense grids to resolve all the relevant flow phenomena. Particularly, the heat transfer from the flow to the engine components is completely determined by the detailed shape of the temperature profile inside the boundary-layer. Extensive knowledge about the required grid resolution is available and employed. Until present CFD is carried out using commercially available codes on workstations. It is foreseen that one of these codes will be implemented on the NEC SX-5 supercomputer at NLR during 1999.

2) Asymptotic analysis.

To support design, verification and validation of other tools employed, e.g. CFD and physical experiments, an asymptotic analysis is carried out. Such analysis is based on asymptotic analysis of the 3D Navier-Stokes equations in boundary-layers where the flow field may locally satisfy similarity conditions. For example, the heat transfer from the flow to a stagnation point in the engine is predicted accurately by means of such asymptotic theory.

b. Thermal and thermo-mechanical analysis of engine components (A. de Boer, NLR)

In the framework of several projects on gasturbine components transient as well as steady state thermal analyses are carried out at NLR. The heat transmission coefficients that determine the heat flux from the gas flow to the gasturbine component are obtained from (in house) CFD analysis. The analysis may include internal component cooling.

Temperature dependent material properties such as the heat conduction coefficient and the specific heat are taken into account. At NLR thermal analyses are carried out with the finite difference program ESATAN and the finite element programs CFX, MARC and B2000. CFX allows a coupled CFD-thermal analysis. MARC is a commercial available structural finite element program. B2000 is a highly modular finite element program, which is used by NLR as a testbed for new developments and evaluation of (new) theories. PATRAN is used as geometry modeller and mesh generator for the structural finite element models. The heat transmission coefficients and corresponding surface co-ordinates obtained from CFD analyses can be read in PATRAN and interpolated to the structural node co-ordinates automatically. At NLR a mechanical-electrical 3D measuring device is available to measure geometries of gasturbine components with an accuracy of $1.5 \cdot 10^{-5}$ m.

Thermo-mechanical analyses using the aerothermal loads and the thermal analysis results as input. For the thermo-mechanical stress analyses it is not required to use the same mesh as for the thermal analyses. Within PATRAN there are features to map the thermal distribution field from the thermal finite element mesh on the finite element model for the stress analyses.

At NLR thermo-mechanical analyses are carried out with MARC or with B2000 for new developments. In the case of transient thermal analyses stress distributions are calculated for certain (interesting) time steps. In these analyses temperature dependency of the material properties (Youngs' modulus, expansion coefficient) can be taken into account. Creep is taken into account when appropriate. To this end a time and temperature dependent creep function must be defined in a MARC user subroutine. The parameters for this function can be measured in the NLR material laboratory.

The calculation of the heat transmission with CFD as was described, was validated with experiments carried out at the Von Karman Institute and published in Ref. 2. It concerns the heat transfer to a turbine blade, a 2D turbine cascade (see figure 2). The calculated and measured heat transfer (represented by the Stanton number) for different Reynolds numbers are presented in figure 3. It can be concluded that in the region where the flow is clearly laminar, the difference between the computed and experimental heat transfer is small for the two larger Reynolds numbers, but increases to about 20% for the smallest Reynolds number.

The procedure for thermal and thermo-mechanical analyses of a turbine blade with cooling channels and the with ENFLOW computed heat transfer as input is evaluated for the VKI blade. To this end the 2D geometry has been extended to a prismatic 3D model with 5 cooling channels. A typical steady state temperature distribution is depicted in figure 4. Due to the presence of cooling channels there exists a temperature gradient in the blade cross section at steady state. The resulting thermal stresses in the blade are presented in figure 5. Effects of centrifugal loads and creep behaviour on the stress and strain distribution are studied, too.

1.3.4 Behaviour of thermal barrier coatings under a thermal loading (M.F.J. Koolloos, TU Eindhoven, NLR)

The failure mechanism of thermal barrier coatings (TBCs) subjected to a thermal load is still not entirely understood. Thermal stresses and/or oxidation cause the coating to fail and hence must be minimized. During the present investigation TBCs with a thickness of 0.3, 0.68 and 1.0 mm were sprayed which withstood the high thermal stresses during thermal cycling. Owing to the substantial thickness the temperature at the top coat / bond coat interface was relatively low, resulting in a low oxidation rate. Furthermore, bond coats were pre-oxidized before applying a top coat. The performance of the TBCs during three different thermal loads was investigated. These loads were: thermal shock (short cycles, top coat surface is heated by flame), thermal cycling (long cycles, top coat surface is heated by flame), and furnace testing (long cycles, entire specimen is heated) The thick TBCs applied during this research exhibited excellent thermal shock resistance but performed very poor during furnace testing. A pre-oxidation treatment of the bond coat increased the lifetime during thermal loading where oxidation was the main cause of failure. Results are presented in figures 6 and 7 and in Ref. 3.

1.3.5 Modelling of thermal barrier coatings (M.F.J. Koolloos, TU Eindhoven, NLR)

Finite Element (FE) models that take into account the bond coat pre-oxidation and interface roughness were used to calculate the stresses occurring during thermal shock and furnace testing. The global-local approach was used. First the temperature and stress profile on a macroscopic scale were calculated. Next a small piece was excerpted from the global model. A new fine mesh was generated including a rough interface with very fine elements allocated for an oxide layer. The FEM analysis of the thermal shock process gives a first impression of the stress conditions on the interface undulations during thermal loading, but further development is required. The FEM analysis of the furnace testing elucidated that delamination occurred owing to stress concentrations at the free edge of the specimen. The experimental program is entirely performed at Eindhoven University of Technology, Department of Mechanical Engineering, Section Thermal Spraying (J.M. Houben)

1.4 FATIGUE AND DAMAGE TOLERANCE STUDIES

1.4.1 Fatigue of riveted lap joints (J.J.M. de Rijck, J. Homan, S.A. Fawaz, J. Schijve, A. Vlot, TU Delft)

Investigation on riveted lap joints as reported in the previous review were continued. The following topics have been studied.

a. Effect of the squeeze force on fatigue life

Experiments were carried out on GLARE specimens. The squeeze force has similar effect as previously shown for 2024-T3 lap joints, i.e. increasing of the squeeze force has a significantly favourable effect on the fatigue life. The fatigue lives for GLARE specimens, however, are much longer than for 2024-T3 specimens.

b. Correlation between the rivet squeeze force and the driven rivet head dimensions.

Manufacturing riveting machinery in the industry is equipped for displacement controlled riveting. The aim of the present investigation is to correlate the driven head dimensions (height and diameter) to the rivet squeeze force in order to check the rivet force as it was applied in production, and in this way to check the fatigue quality of riveted joints. Specimens have been made with the rivet diameter, rivet length, type of rivet and rivet materials as the variables. For each combination a range of squeeze forces was used. The correlation between squeeze force and driven rivet head dimensions is promising. Co-operation with Airbus industries should be mentioned.

c. Fatigue crack growth in riveted lap joint

The investigation reported in the previous Review has been continued. Previous work has been reported in the doctor thesis of Fawaz (Ref. 4) see also (Ref. 5). The present work is concentrating on stress intensity factors of fatigue cracks with oblique crack fronts and crack interactions of such cracks in adjacent holes in sheets under combined tension and bending. Experimental data were obtained on crack growth rates, crack shape development and crack interaction effects for fatigue cracks starting from different initial shapes in 2024-T3 sheet specimens with an array of holes. Although the fracture surfaces were quite tortuous, the crack growth history could be reconstructed by using marker loads introduced by reducing the maximum stress of the constant-amplitude baseline cycles. Crack growth histories were reconstructed

for cracks smaller than 1 mm (sheet thickness 2 mm). In the analytical part K-values were calculated for part-elliptical through cracks emanating from an array of holes subjected to remote tension and bending, and pin loading. The 3-dimensional virtual crack closure technique (3D VCCT) is used. Calculations for different crack shapes were made. Interactions between cracks of adjacent holes were studied by comparison to K-values for cracks from single holes. The comparison indicated that such interactions will become significant only late in the fatigue life. Application of the new K-values to prediction of the fatigue life showed a 10% underestimation of the life.

1.4.2 Fractography to study interaction effects during variable-amplitude loading (J. Schijve, TU Delft)

Fatigue crack growth tests were carried out on 2024-T3 and 7075-T6 central cracked specimens, described in Ref. 6. Variable-amplitude (VA) load spectra were used with periodic overload (OL) cycles added to constant-amplitude (CA) cycles. The fatigue fracture surfaces were examined in the SEM to obtain more detailed information on crack growth contributions of different load cycles. The striation patterns could be related to the load histories. An example is shown in the figure 8. SEM observations were associated with delayed retardation, the effect of 10 or a single OL on retardation, crack growth during the OL cycles, and crack growth arrest after a high peak load. Fractographs exhibited local scatter of crack growth rates and sometimes a rather tortuous 3d geometry of the crack front. Indications of structural sensitive crack growth under VA loading were obtained. Fractography appears to be indispensable for the evaluation of fatigue crack growth prediction models in view of similarities and dissimilarities between crack growth and VA and CA loading.

1.4.3 Comparison of the damage tolerance behaviour of two aluminium alloys (G. Jay, J. Schijve, TU Delft)

Various properties of 2024-T3 and 2024-T3A are compared. The second alloy was developed by Pechiney as a replacement of the first one. The test program includes static and fatigue tests (constant-amplitude and flight-simulation). Specimens to be used include blunt notch specimens, center cracked specimens and riveted joints (study of multiple-site damage). The first constant-amplitude fatigue crack growth results indicate that 2024-T3A is superior to 2024-T3.

1.5 FULL SCALE FATIGUE TESTS

1.5.1 Fokker 50 and 100 fatigue and damage tolerance tests (J.J. Veenstra, Fokker Services)

After completion of the fatigue and damage tolerance tests at 180,000 flight cycles, the residual strength tests and the tear down inspection programme, the structural inspection programmes of the Fokker 70/100 and Fokker 50/60 are now in the process of being completed by Fokker Services.

With the Fokker 50 and 100 fatigue test results also a verification programme is started on the fatigue inspection programmes of the F27 and F28 aircraft versions. Moreover these fatigue test results will be considered in the Ageing Aircraft programmes on Repair Assessment and on Widespread Fatigue Damage.

Continuous support and development of Non-Destructive Inspections techniques for fatigue and damage tolerance inspection tasks is provided for by ASNT level III specialists.

1.5.2 Fokker 60 fatigue and damage tolerance tests (N.J. Fraterman, Fokker Aerostructures)

The Fokker 60 is a derivative of the Fokker 50 propjet; the major changes consists of a stretched fuselage, higher design weights, increased cruise speed and a large cargo door (3*2 meter) in the forward fuselage. Due to these structural modifications the fatigue spectra has changed to such an extend that additional fatigue and damage tolerance tests were required for the certification of the Fokker 60 according to JAR 25. The airworthiness authorities required additional fatigue tests for areas, which were subjected to considerable higher fatigue loads than the Fokker 50, areas with newly designed structures and/or areas where the original Fokker 50 tests could not be extrapolated any further. The resulting test programme consisted of the wing-fuselage lugs, a stringer run-out in the lower wing skin and a section of the large cargo door plus surround have been tested successfully and have been reported in the ICAF review of 1997.

One of the component tests represents a fatigue critical panel joint in the lower skin of the outer wing. The fatigue spectrum consists of flight loads due to gust/ manoeuvre and ground loads due to taxi/ landing. This area is designed

and certified as a multiload-path structure and will therefore be tested for two and a half life times (=235000 FC) of which the last half life will be run with artificial cracks in order to verify the damage tolerance behaviour. The testpanel showed a crack in the cooling plate after approximately 40000 FC, which was repaired after monitoring the crack growth. The repaired panel has been tested for 92000 FC and a small crack has been found on another location. The slow propagation of this crack will be monitored, while the test on the panel is continued till a total of 235000 FC.

Another component test represents the mainframe, which is part of the wing-fuselage connection (see figure 9). The fatigue spectrum consists of flight loads due to gust/ manoeuvre plus cabin pressure and ground loads due to taxi, turning, landing impact and braking. The upper part of the mainframe has been designed and certified as a slow crack growth structure. Therefore it will be tested for two lifetimes (=180000 FC); thereafter artificial cracks of 0.05" will be inflicted at critical locations and the test will be continued for one and preferably for two lifetimes in order to demonstrate the slow crack growth behaviour. After 180000 FC a crack was discovered in a section of the machined mainframe. Investigations of the fracture showed that the crack was caused by an illegal hole that was drilled by accident and was surprisingly not discovered during the quality inspections. Microscopic analysis of the crack surface revealed that the crack has been initiated at ~90000 FC and propagated slowly until it was found at 180000 FC. The fact that the mainframe with the illegal hole sustained 180000 FC confirmed that the design was capable of handling extreme production defects. The cracked mainframe was replaced by a mainframe with artificial cracks of 0.05" at a number of critical locations in order to verify the damage tolerance behaviour. Up to April 1999 the mainframe with artificial cracks has been subjected to 60000 FC and none of the cracks did show any propagation. The mainframe will be tested till 180000 FC.

1.5.3 Thermoplast Main Undercarriage doors in the Fokker 50 (N.J. Fraterman, Fokker Aerostructures)

In order to gain experience in designing and building structural components in thermoplast CRFP-PPS the existing Aluminium Main Undercarriage (MUC) doors of the Fokker 50 were re-designed into CFRP-PPS version by Fokker Aircraft and Fokker Aerostructures. According to this design Fokker Special Products, using special developed forming and welding technology built one demonstrator. In order to be able to execute a service trial, a certification programme was agreed with the Dutch Airworthiness Authorities, which was based on a combination of tests and analysis. The test programme contained a full-scale static test on the door, static tests on samples and fatigue tests on a number of joints, including the welded joints. The fatigue tests on the welded joint showed a good behaviour in shear, but showed limited capability in tension. The fatigue properties were sufficient for the Fokker 50 MUC door design, but could be a limitation for other designs.

1.5.4 Testing the center section of a composite stabilizer (H.G.S.J. Thuis, NLR)

As part of a composite stabilizer technology programme a number of static and fatigue tests have been carried out on a "4-meterbox": a structurally complete composite center section of a stabilizer for the Fokker 100 aircraft (see figure 10). The purpose of the test program is to verify:

- a. the dynamic behaviour as determined by analysis
- b. the strain distribution as determined by analysis
- c. the "no damage growth concept" during fatigue loading
- d. ultimate load capability with Barely Visible Impact Damage (BVID)
- e. the damage tolerance behaviour

During the tests the "4-meterbox" was attached to a full size vertical stabilizer. The vertical stabilizer was connected to a rigid test frame. A number of hydraulic actuators (ten for the static tests and twelve for the fatigue tests) were used to introduce the appropriate loads. The overall test program contained a number of static tests at elevated temperature (80 °C) and increased humidity (85 % R.H). During these tests the "4-meterbox" was placed in an environmental chamber (7 x 3 x 2.5 m).

Two preliminary tests were carried out at ambient conditions and were reported in the previous ICAF review

Test no 1: Dynamic test

Test no 2: Static strain survey to Limit Load

After these tests the "4-meterbox" was saturated in the environmental chamber. During saturation the conditions in the chamber were 80 °C and 85 % RH. It required 10 months to reach a sufficient level of saturation.

Test no 3: Fatigue test

The fatigue test was performed at room temperature. An equivalent of 90000 flights (1 lifetime) was tested using a load enhancement factor of 1.18. The fatigue load sequence was reduced by omitting all small cycles, leading to an average of 2.5 cycles per flight. The fatigue test was completed successfully, no significant damage occurred.

After the fatigue test the “4-meterbox” was saturated again and two static tests were performed in the hot-wet condition

Test no 4: Static test to Ultimate Load with BVID’s

Test no 5: Static test to Limit Load with Visible Damages

Both tests were carried out without significant increase of the damages.

In the original test program static tests on the specimen with significant damages (failure of the front spar) were foreseen. It was decided, however, to keep the specimen intact to be able to use the specimen for tests in the future.

1.6 AGEING AIRCRAFT

1.6.1 Structural Maintenance of Ageing Aircraft (SMAAC) (W.J. van der Hoeven, NLR)

The NLR participates in the Brite Euram programme “Structural Maintenance of Ageing Aircraft (SMAAC)”. The programme started in 1996 and is sponsored by the Commission of the European Union. The activities of NLR were reported in the previous ICAF review. The work done in the last two years is:

a. Fractography of pressure cabin MSD (R.J.H. Wanhill, NLR)

Multiple Site Damage, MSD, fatigue initiation and early crack growth were fractographically investigated for fuselage longitudinal lap splices from three aircraft types, of which two from service (Fokker F 28, BAC 1-11) and one from a full-scale test (Fokker 100). The results were compared with those from a NASA investigation of a Boeing 747-400 full-scale test. The most MSD-critical rivet row was the upper one in the outer sheets of the lap splices. However, other rows were susceptible, especially the lower one in the inner sheets.

Fatigue initiation lives appeared to vary widely. However, there was no evidence from the series aircraft that corrosion was involved in crack initiation. Early crack growth rates were above 10^{-8} m/ cycle, which is significant for two reasons: (a) one should not expect differences between ‘short’ and ‘long’ crack behaviour, and (b) it makes questionable the usefulness of testing sub-scale specimens, which show much lower early crack growth rates.

More details are provided in the paper in the ICAF 1999 Conference Proceedings.

b. Effect of precorrosion on the fatigue life of riveted lap joint specimens (L. Schra, W. van der Hoeven, NLR)

The effect of precorrosion on the fatigue life of riveted lap joint specimens was studied. Riveted lap joints were made of 1.2 mm thick Alcad 2024 T3 sheets. The joints were representative for the longitudinal joint in medium sized jet aircraft. After drilling the rivet holes, but before riveting the sheets were precorroded. The precorrosion conditions were those described in ASTM G85, Annex 2, see for example figure 11 and resulted in some corrosion of the cladding layer close to the rivets and a moderate pitting attack inside the rivet holes.

After precorrosion, the specimens were riveted and fatigue tested to failure. During the fatigue test the specimens were loaded under constant amplitude loading since this type of loading simulates the cyclic stress variation in the fuselage skin due to cabin pressurisation. The fatigue lives were determined for three maximum stress levels: 80, 100 and 120 MPa. In addition, tests were done on uncorroded specimens. From the results, it was concluded that fatigue cracks initiate at the corrosion pits, but that the corrosion damage had no effect on the fatigue life of the joints (see figure 12).

c. Full-scale fuselage panel tests (R.W.A. Vercammen, NLR)

During the SMAAC project, residual strength tests were performed on three curved fuselage panels with artificial damage. The panels were supplied by the SMAAC partners Deutsche Aerospace and Alenia. The tests were carried out in the fuselage panel test rig of the NLR. In this test rig, the loads due to cabin pressurisation can be simulated. The hoop loads are introduced by pressurisation of the pressure chamber and the axial loads are introduced with an actuator. In the panels, saw cuts were made to simulate the presence of Multiple Site Damage. The damage consisted of a lead crack and many small cracks at the rivet holes in front of the lead crack. Before the static tests, the panels were loaded in fatigue to sharpen the tips of the lead crack.

During the residual strength test, only loads due to cabin pressure was increased until failure. The tests were successful in the sense that all panels sustained their ultimate design loads.

d. Crack initiation and crack growth models for MSD (F.P. Grooteman, NLR)

An MSD model for determination of the inspection intervals, threshold and follow-on inspections, for lap joints has been developed. It consists of a crack initiation and a crack growth model, both dealing with the MSD situation in which neighbouring cracks have influence on the crack initiation and growth.

The crack initiation model is based on P-S-N curves concept, where the S-N curves have a probability distribution, taking into account the variability in crack initiation lives. In order to account for the variability in the S-N curve data (P-S-N curves), at the start of an analysis a randomly generated probability value (chance) is added to every initiation site, determining from the P-S-N data the S-N curve for that site. Thus, every simulation results in a different crack initiation pattern

The stress intensity factors of the crack growth model for the MSD situation are calculated by the use of the compounding method, in which a stress intensity factor is determined by combining the known solution of the isolated cracked hole and its boundaries (edges, other holes or cracks) separately. Through cracks are assumed, because insufficient SIF-solutions exist for corner cracks. All the SIF solutions are based on a uniform stress distribution, which is not exactly the case here. Stress redistribution, is approximated by defining a finite width determined by the remaining net-section around a crack. Load transmission due to friction is only approximately modelled.

The model is currently based on flat sheets, leaving out the influence of the curvature, e.g. different stress-state in case of bulging

All the parameters from both, the crack initiation and crack growth model, can be treated as random variables and the stochastic problem is solved currently with the Monte-Carlo method. A more advanced stochastic method based on a Second-Order Reliability Method (SORM) has been developed recently.

A common problem with stochastic analysis is to obtain reliable data concerning the random variables. The probability density curves for the random variables are hard to obtain or even unknown. Therefore, data has to be obtained from literature and serve as estimation.

The program has been applied amongst others on a sheet with 14 holes of which the outer two holes were cold worked (low probability of failure). In figure 13 the calculated crack initiation period and crack growth period are plotted against each other for 1000 MC simulations. Also, contour ellipses have been drawn representing areas within γ percentile of the data points are included, under the assumption that both the crack initiation period and crack growth period are normally distributed. The major axis of the ellipses are not horizontally orientated representing the statistically dependency between the crack initiation period and the crack growth period, i.e. the longer the initiation period the shorter the crack growth period. The experimentally obtained results are represented by triangles.

In figure 14 the crack growth patterns at the various holes are shown for the longest (MSD situation) and shortest life (no MSD situation) obtained in the numerical analysis.

1.7 FIBER METAL LAMINATES

1.7.1 Dutch GLARE Technology research program

In the Netherlands a GLARE technology research program (GTO) is carried out. GLARE is a fiber metal laminate, which was initially developed for its excellent fatigue behaviour in terms of slow crack growth properties. The material appeared to have a lot more favourable properties, such as very high impact, corrosion and fire resistance capacity.

The GTO program is co-ordinated by Structural Laminates Industries (SLI). Other participants are Technical University Delft (TU Delft), the National Aerospace Laboratories (NLR) and Fokker Aerostructures (Fe). The program is sponsored by the Dutch government and is performed in close co-operation with DaimlerChrysler Aerospace Airbus (DA).

The research aims to achieve technology readiness for the application of GLARE laminates in very large transport aircraft. To do so, projects on the following working groups have been defined:

1. Materials & Processes
2. Methods
3. Design Concepts
4. Fabrication Technology
5. Maintenance
6. Durability

More than 90 subprojects were defined and are carried out in these working groups.

1. Materials & Processes

Main topics are material qualification and material properties and allowables. Another very important issue is the definition and the qualification of the splicing concept. With these splices it is possible to manufacture larger skin panels than with monolithic aluminium sheets. An example of how a splice in a GLARE panel looks like is given in the figure 15.

It is shown that with clever design and manufacturing a considerable cost reduction can be achieved which makes GLARE a very competitive material as compared with conventional sheet materials. The laminar built-up of GLARE allows a high degree of integration of structural details in one panel, such as splices and internal doublers.

2. Methods

This subject is focussed on the development of missing calculation methods (design tools) for GLARE structures. Research is aimed at prediction of basic material properties ("metal volume fraction" approach), stability of panels, residual strength and crack propagation.

3. Design Concepts

Design principles are under development to enable detailed design optimised for GLARE structures. Items such as panel arrangement, typical GLARE shell design, stringer design concepts, longitudinal and butt joints, door and window cut-outs are looked upon. Also certification aspects are under discussion.

4. Fabrication Technology

This subject is focussed on low cost and low risk manufacturing of GLARE fuselage skin panels. Although the actual material cost of GLARE is higher than for monolithic aluminium,

5. Maintenance

Maintenance concepts (with emphasis on cost aspects) and NDT inspection and repair methods for GLARE structures are under development. A lot of effort has been put into successful activities to acquire airline acceptance of GLARE.

6. Durability

Available test results show excellent properties related to durability of GLARE, but a large durability program is defined to take away some reservations, which still exist at aircraft manufacturers and operators.

A very interesting feature is the relation between reduction in mechanical properties due to environmental influences and the amount of downscaling to coupons and components. The more a test article resembles with the actual structure, the less the reduction of mechanical properties there will be.

1.7.2 Repair with bonded fibre metal laminate patches (A. Woerden, A. Vlot, TU Delft)

Because of ageing aircraft a need exists for safe, damage tolerant and cost-effective repairs. Different repair techniques are available, including mechanically fastened patch repairs and adhesive bonded patch repairs. Bonded repairs provide a more uniform and efficient load transfer into the patch and avoid high stress concentrations caused by additional holes necessary for riveted repairs. Adhesive bonded boron/epoxy repairs have the disadvantage of a large mismatch in coefficient of thermal expansion (CTE) between the repair and the aircraft structure. Moreover, the very high stiffness of boron/epoxy can lead to load attraction problems on the repair. Fiber Metal Laminate (FML) repair materials like GLARE® (GLASS REINFORCED) avoid these problems. Research into bonded repair FML repairs patches started in the early nineties between the Center for Aircraft Structural Life Extension (CASTLE) at the United States Air Force Academy (USFA) and the Structures and Materials Laboratory of the Faculty of Aerospace Engineering of Delft University of Technology in the Netherlands. Considerable research performed over the last years resulted in a better understanding of the physical background of bonded repairs, as well as significant improvements in bonded repair techniques. Current research focuses on the ability to accurately predict the crack driving stress intensity factor (K) at the crack tip of a crack under an adhesively bonded repair. This K is significantly lower than for an unrepaired crack, explaining the excellent fatigue behaviour of bonded repairs, as shown in the figure 16 with crack growth curves. This research is performed for both boron/epoxy and GLARE® patch repair materials. Models being used for the prediction of K include analytical models like the Rose model and finite element models. The Rose model gives an excellent analytical background, but secondaries bending for one-sided (i.e. asymmetrical) repairs and thermal stresses after curing are not accurately accounted for. Extensive experimental testing, see figure 17 with barrel test set up, and finite

element calculations are performed to investigate the influence of those two main variables, and to extend previous modelling.

Another part of current research focuses on in-service effects on patch performance and the experimental testing of realistic load sequences (variable-amplitude loading), including effects of overloads and underloads on crack growth of the repaired crack.

Research on in-service effects on patch performance, as yet hardly investigated, will concentrate on environmental influences on crack growth under a patch repair and on the growth of debonds between patch and adherent. Possible detrimental environments include cold, hot, humid and salty conditions, as well as combinations of those. In view of service experience, two bonded GLARE patches were installed on a C5-A Galaxy, which are inspected regularly.

A final goal of the "Repair Project" is the development of a repair tool for maintenance engineers, requiring little background knowledge of bonded repair. A first version of this tool, called CalcuRep® needs to be updated to accurately account for effects of secondary bending, influence of thermal stresses due to the curing cycle and effects of different environmental conditions.

1.7.3 Spliced Fibre Metal Laminates (T.J. de Vries and A. Vlot, TU Delft)

The maximum sheet width for 0.3 mm thick aluminium, and thus for GLARE laminates with this type of aluminium layers, is approximately 1.65 m. However, for the purpose of skin material in a fuselage, wider sheets are preferred to reduce the amount of necessary joints. This problem can be solved with the splicing concept; metal sheets are interrupted in the laminate and these splices are bridged by the fiber layers, see figure 18. With this concept the sheet width can be increased to 4 meters or more, depending on the autoclave size. Using these large sheet sizes can provide an additional weight and cost saving compared to monolithic aluminium structures due to a reduction of the number of riveted joints.

Fatigue and static strength tests on spliced laminates with varying fibre orientation were performed to determine design allowables. The disadvantages of local cross section reduction and the possible influence of moisture, which can penetrate in the uncovered splice, can be solved by covering the splice with a doubler. Bonding the doubler with prepreg over the splice appeared to be not favourable because of the low delamination resistance of the prepreg layer.

Possible solutions to maintain a smooth aerodynamic surface, even with bonded doublers, are now under development. Residual strength tests on spliced laminates with through cracks showed that the splices can effectively stop stable crack extension. In this case the crack has to reinitiate at the other side of the splice.

1.7.4 Service trial of a GLARE crownpanel in the A310 fuselage (N.J. Fraterman, Fokker Aerostructures)

An existing Airbus A310 will be installed with a large cargo door in the forward fuselage for a German customer. During the installation of this large door an Aluminium fuselage panel in the pressurised crown just aft of the door will be replaced by a GLARE panel. The installation of this GLARE panel is a service trial in order to gain more experience with GLARE in wide body aircraft under real loading and environmental conditions. The GLARE panel has the dimensions of 1600 x 4000 mm, is equipped with bonded Aluminium stringers and is attached to the existing frames with clips.

For the certification programme a number of static and fatigue tests on representative coupons of the panel will be performed. The fatigue tests include the circumferential and longitudinal lap joint of the GLARE panel to the existing surrounding structure and will be performed with a representative load spectrum. For some specimens also the environmental conditions (hot, wet) will be taken into account.

1.8 NON-DESTRUCTIVE INSPECTION

1.8.1 Inspection procedures (A. Oldersma, J.H. Heida, NLR)

For a number of RNLAf in-service inspection points of the F-16 airframe the detection of fatigue cracking led to a non-destructive and destructive evaluation of the parts concerned. The cause and extent of fatigue cracking was determined and, subsequently, changes in the inspection procedures of for example the Nose Landing Gear NLG shock strut piston radius and the flaperon root rib radius were proposed.

1.8.2 Reliability of inspection (J.H. Heida, F.P. Grooteman, NLR)

The possibilities within the Royal Netherlands Air Force (RNLAf) maintenance system to establish reliability data relevant for the in-service nondestructive inspection of F-16 airframe structure have been investigated. The principal inspection techniques herewith are manual and automatic eddy current inspection for the detection of fatigue cracking. Use was made of field inspection data registered in the Core Automated Maintenance System (CAMS) for specific airframe inspection points within the F-16 Aircraft Structural Integrity Program (ASIP). The available data include the registration of the number of cracks and the length of the largest crack found during the phased inspections. Further, use was made of crack growth data obtained from the aircraft manufacturer. An evaluation of the field inspection data and the crack growth data allows the estimation of the sensitivity and reliability of inspection for the structural details concerned, by constructing the Cumulative Distribution Function (CDF) of the detected crack sizes. An example of this approach is given in figure 19. The results of this evaluation can be used to revise the current values of the inspection intervals for the ASIP inspection points.

1.9 References

1. Spiekhout D.J., F-16 loads/ usage monitoring. RTO meeting 'Exploitation of structural loads/ health data for reduced life cycle costs' Brussels May 1998, RTO-MP-7.
2. Arts T., Lambert de Rouvroit M., Rutherford A.W., Aero-thermal investigation of a highly loaded transonic linear turbine guide vane cascade, Technical note 175, Von Karman Institute for Fluid Dynamics, 1990.
3. Koolloos, M.F.J. and J.M. Houben, Behavior of Plasma Sprayed TBCs During Thermal Cycling and the Effect of a Pre-Oxidised NiCrAlY Bond Coat, to be published in *Journal of Thermal Spray Technology*, 1999.
4. Fawaz, S.A., Fatigue crack growth in riveted joints. Doctor thesis, Delft University of Technology, 2 Sept 1997.
5. Fawaz, S.A. and Schijve, J., Fatigue crack growth predictions in riveted joints. Proceedings 2nd joint NASA/FAA/DoD Conference on Ageing Aircraft, Williamsburg, 31 Aug-3 Sept. 1998.
6. Schijve, J., The significance of fractography for investigations of fatigue crack growth under variable-amplitude loading. Delft University Press, Series 07: Aerospace Materials 09, 1998.

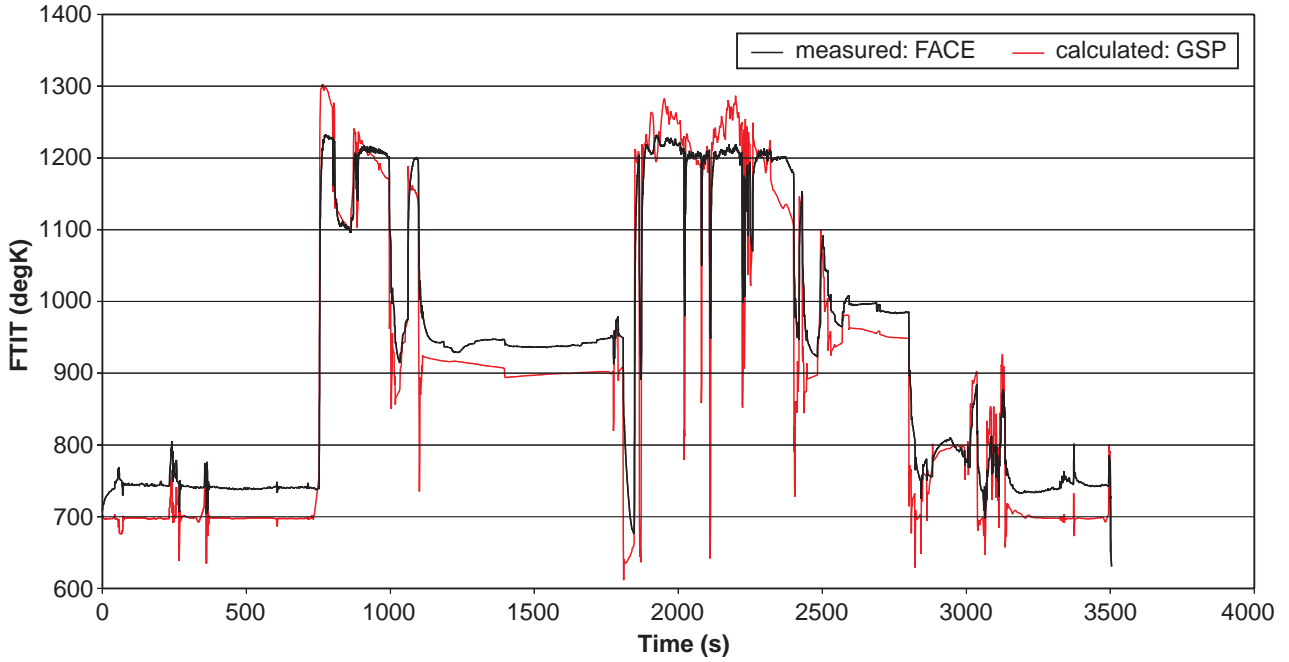


Figure 1 Comparison of fan turbine inlet temperature (FTIT) values during a mission as measured by FACE and calculated by GSP

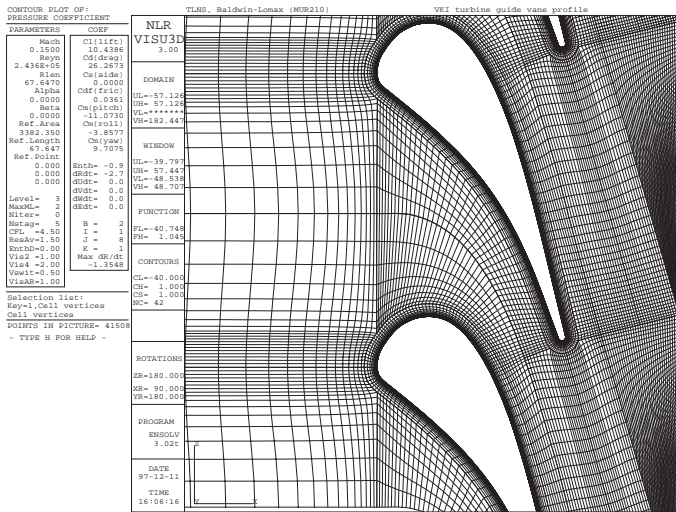


Figure 2 2D turbine blade cascade. Von Karmen Institute experiments are used for CFD validation

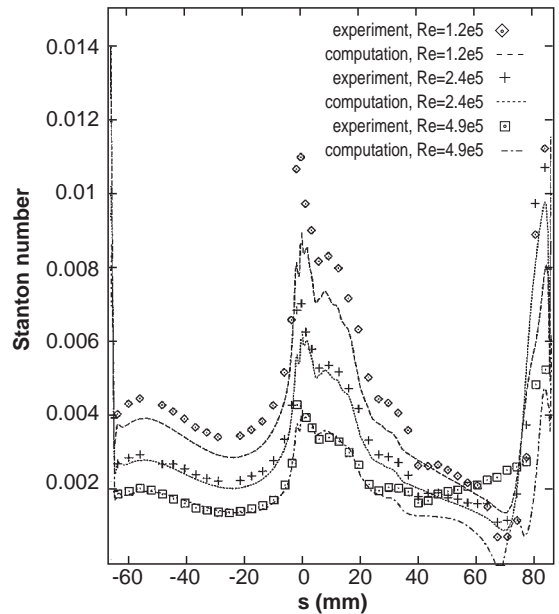


Figure 3 Calculated and measured heat transfer (represented by the Stanton number)

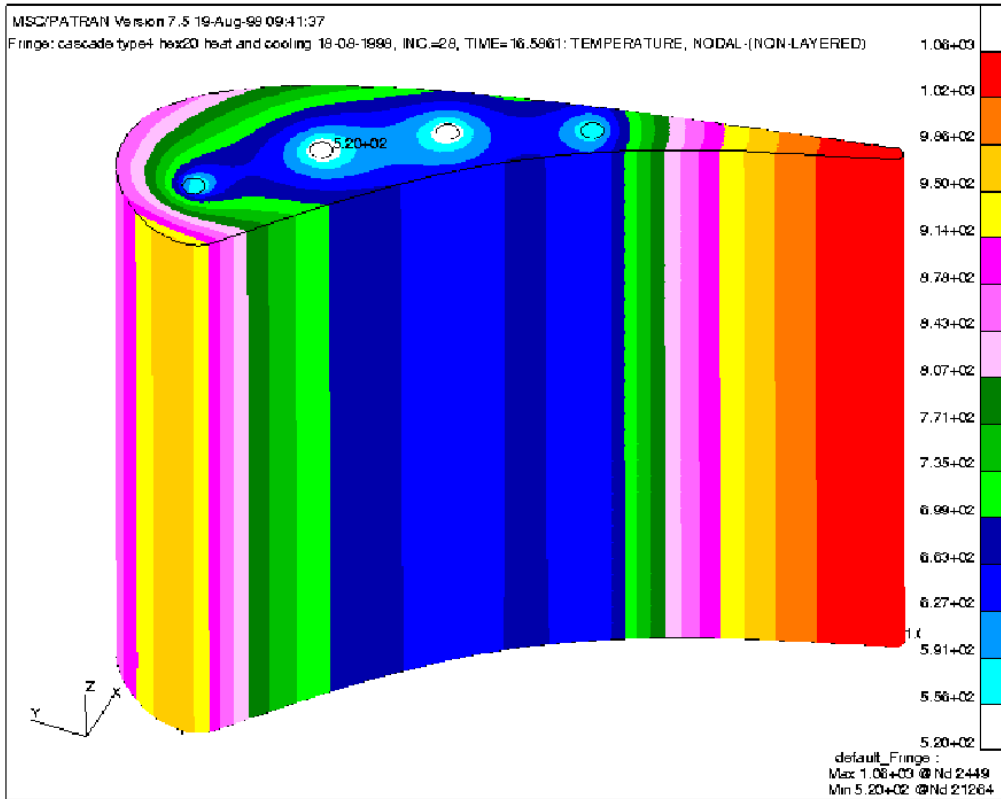


Figure 4 Steady state temperature distribution calculated for an internally cooled blade



Figure 5 Thermal stresses calculated for an internally cooled blade

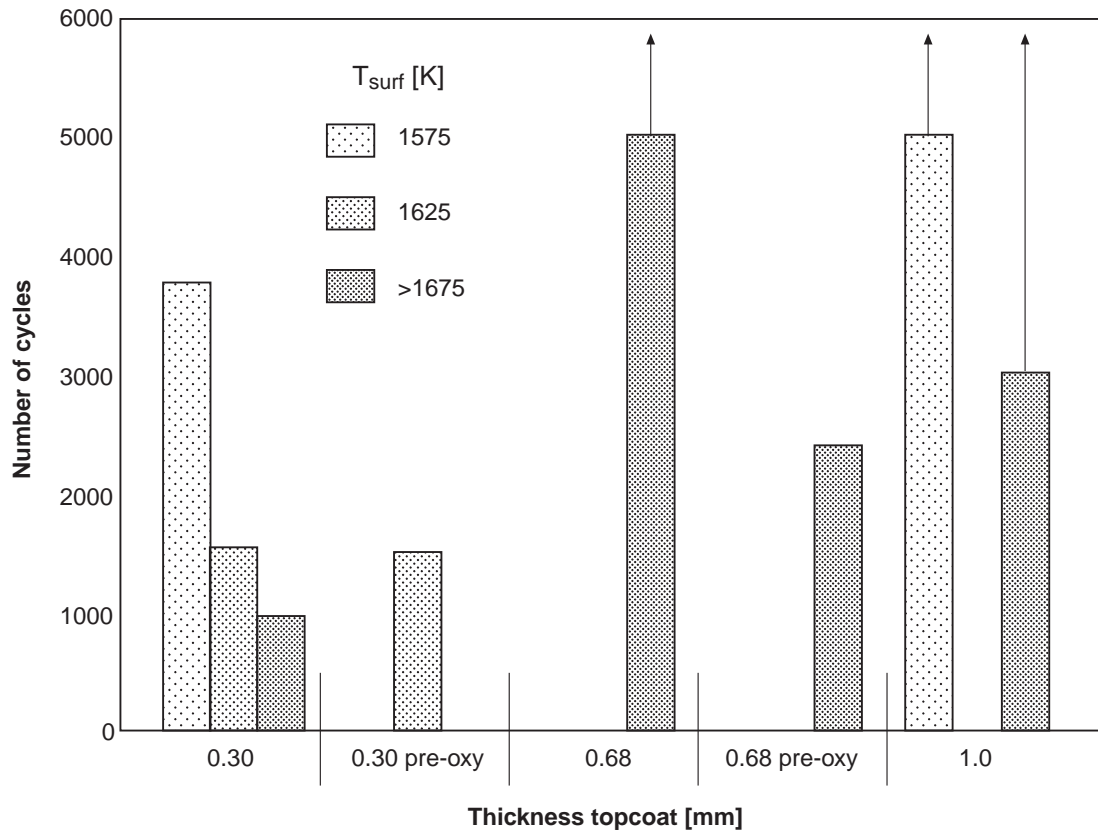


Figure 6 Number of thermal shock cycles to failure for several test temperatures, and for 0.3 and 0.68 mm (with and without pre-oxidized bond coat) and 1.0 mm specimens. Arrow on top of bar indicates that delamination did not occur within given number of cycles

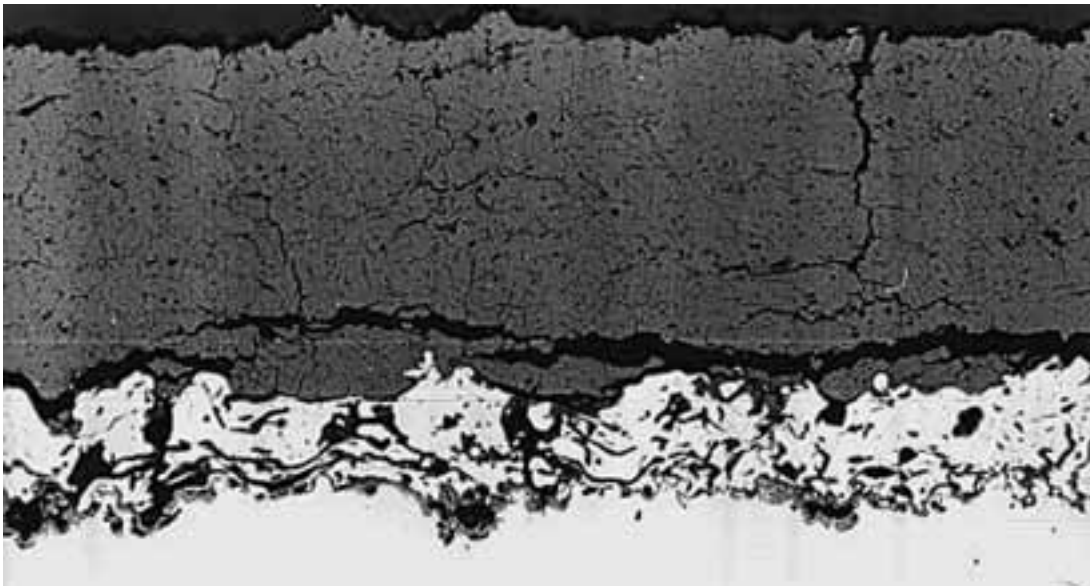


Figure 7 Failure mode of a TBC coating after thermal shock cycles

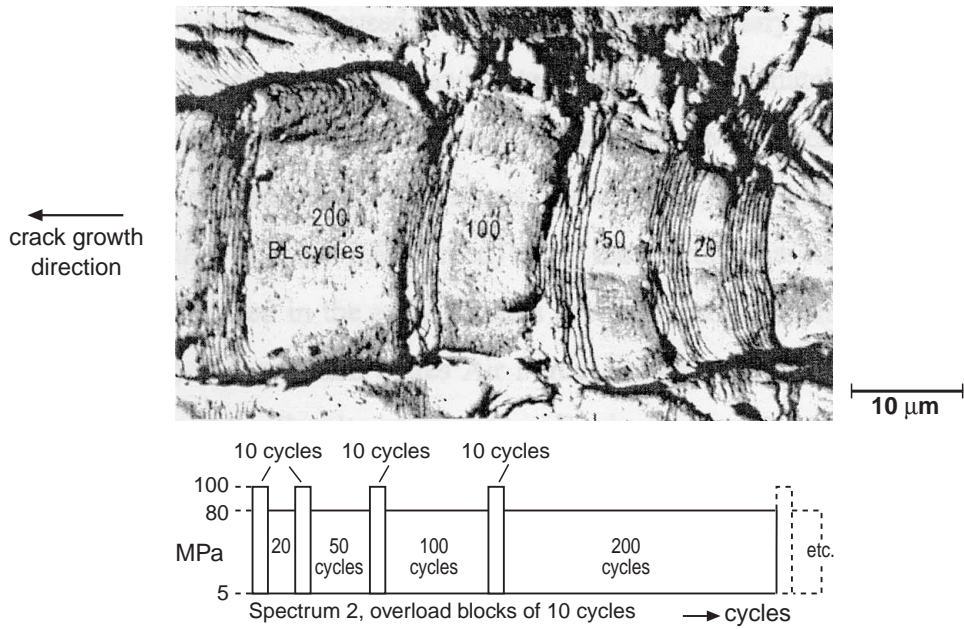


Figure 8 Overload cycle striations can easily be observed. The width of the intermediate bands of the baseline cycles is not proportional to the numbers of baseline cycles, which indicates a retardation effect

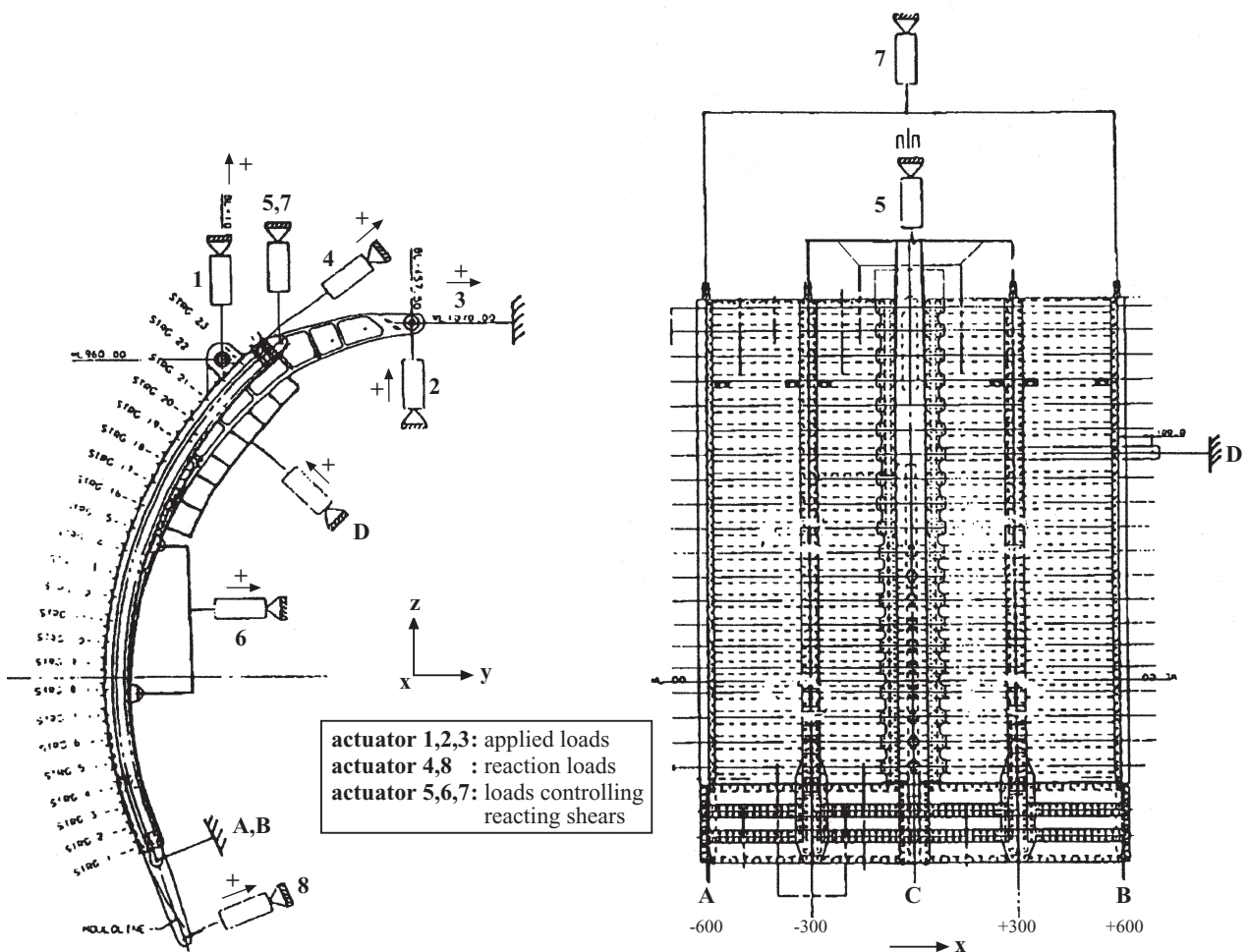


Figure 9 Fokker 60 wingfuselage connection; mainframe componenttest

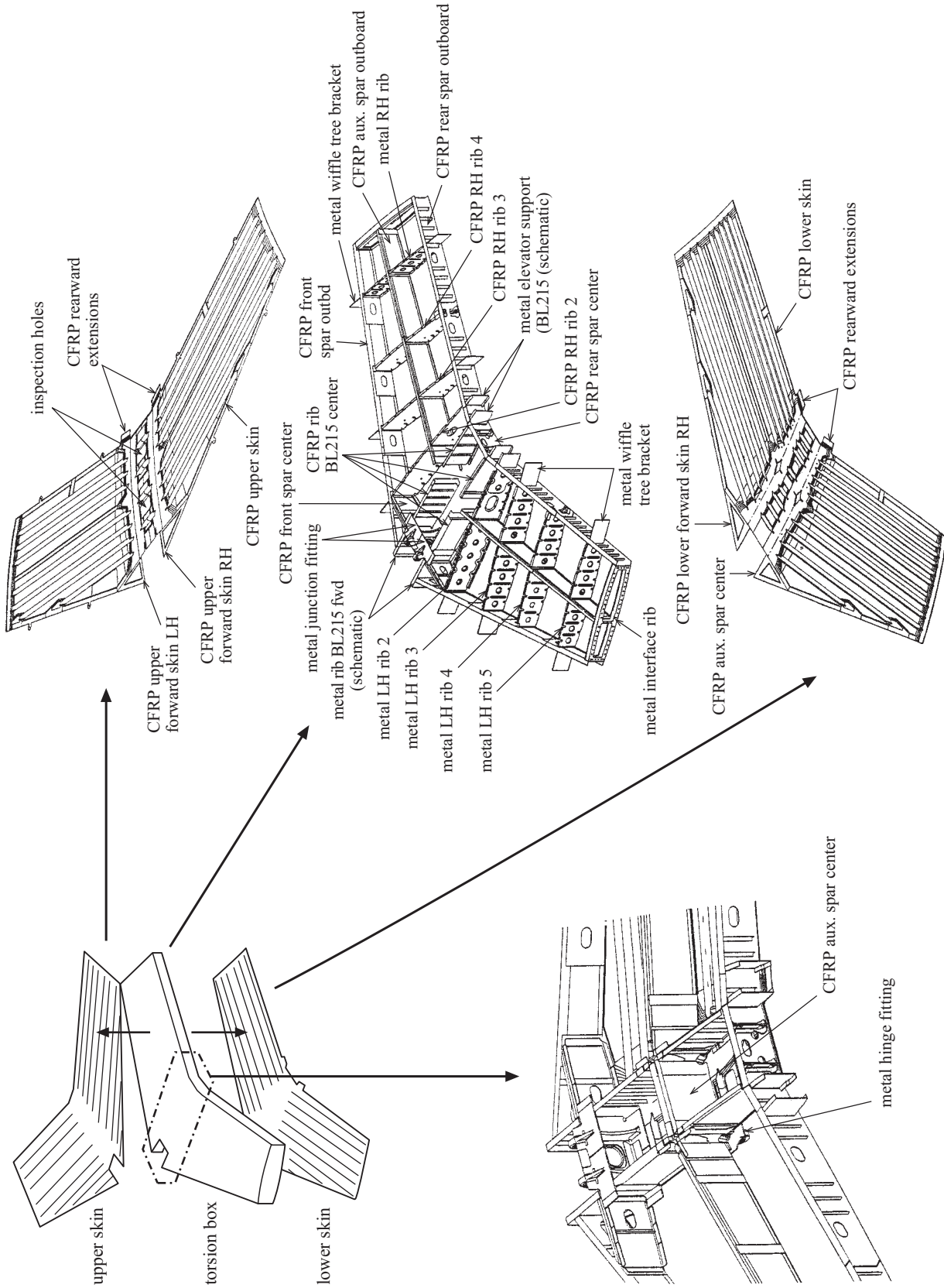


Figure 10 Structural lay-out of the "4-meterbox"

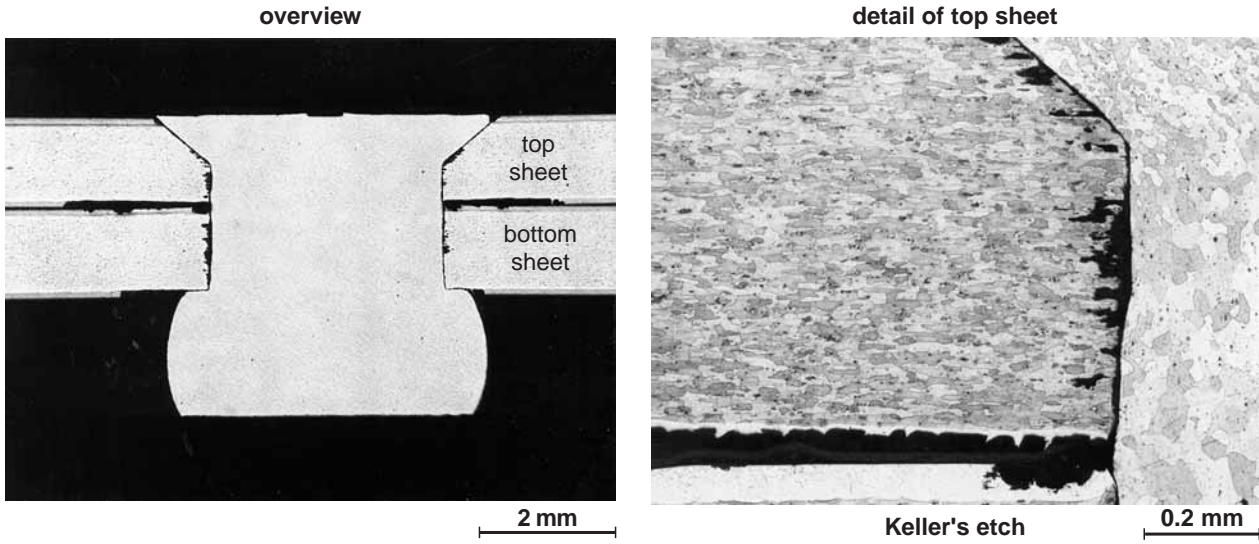


Figure 11 Cross section of a riveted top and bottom sheet

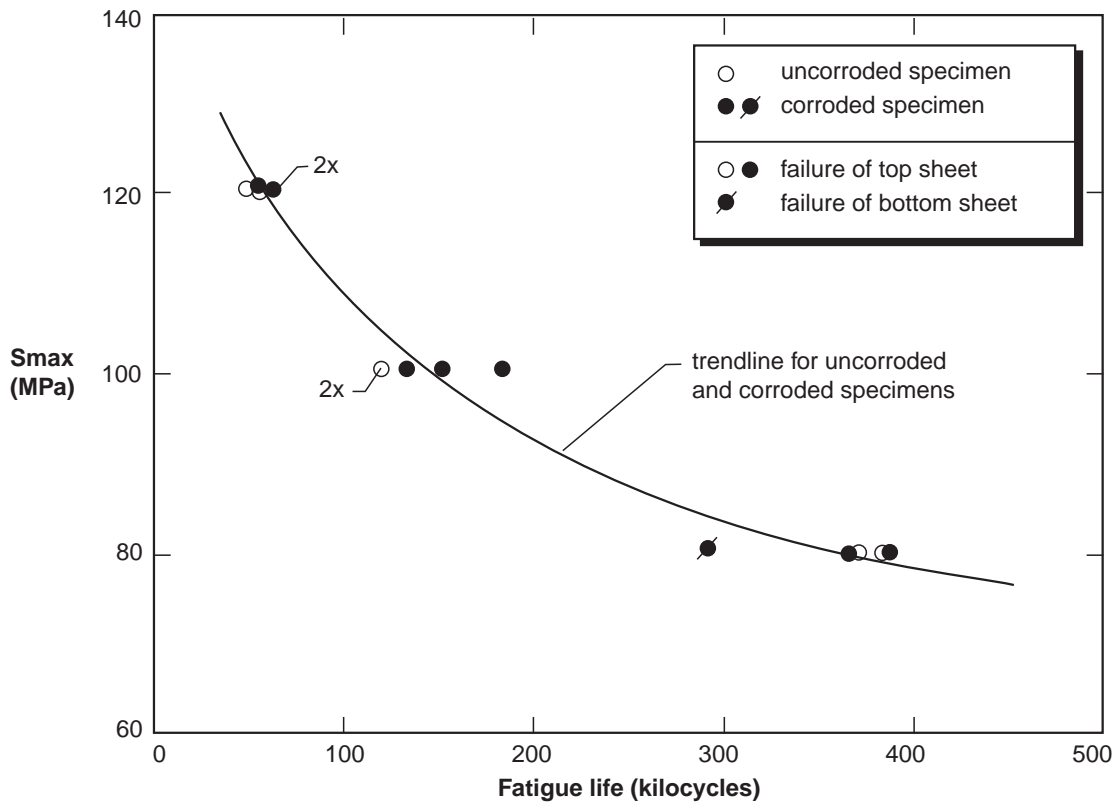


Figure 12 Fatigue lives as a function of maximum stress for uncorroded and corroded lap joint specimens, $R=0.1$

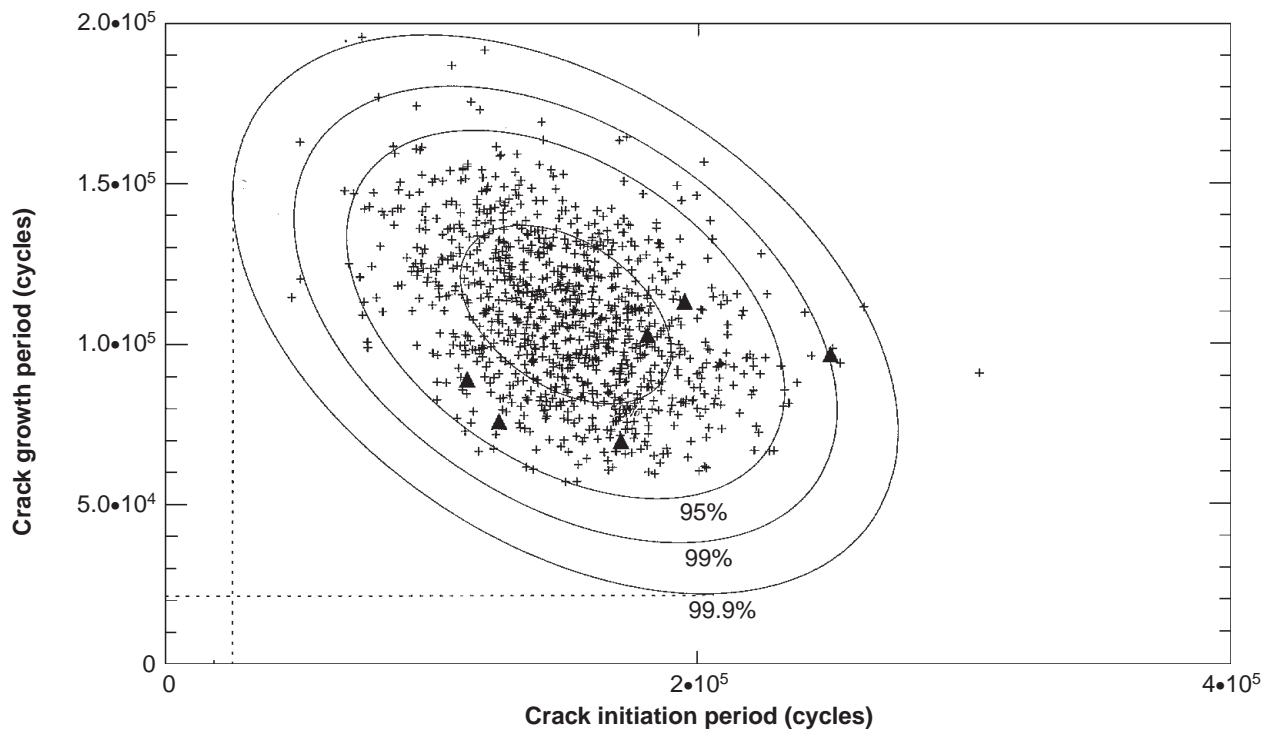


Figure 13 Crack initiation period versus crack growth period: numerical and experimental results

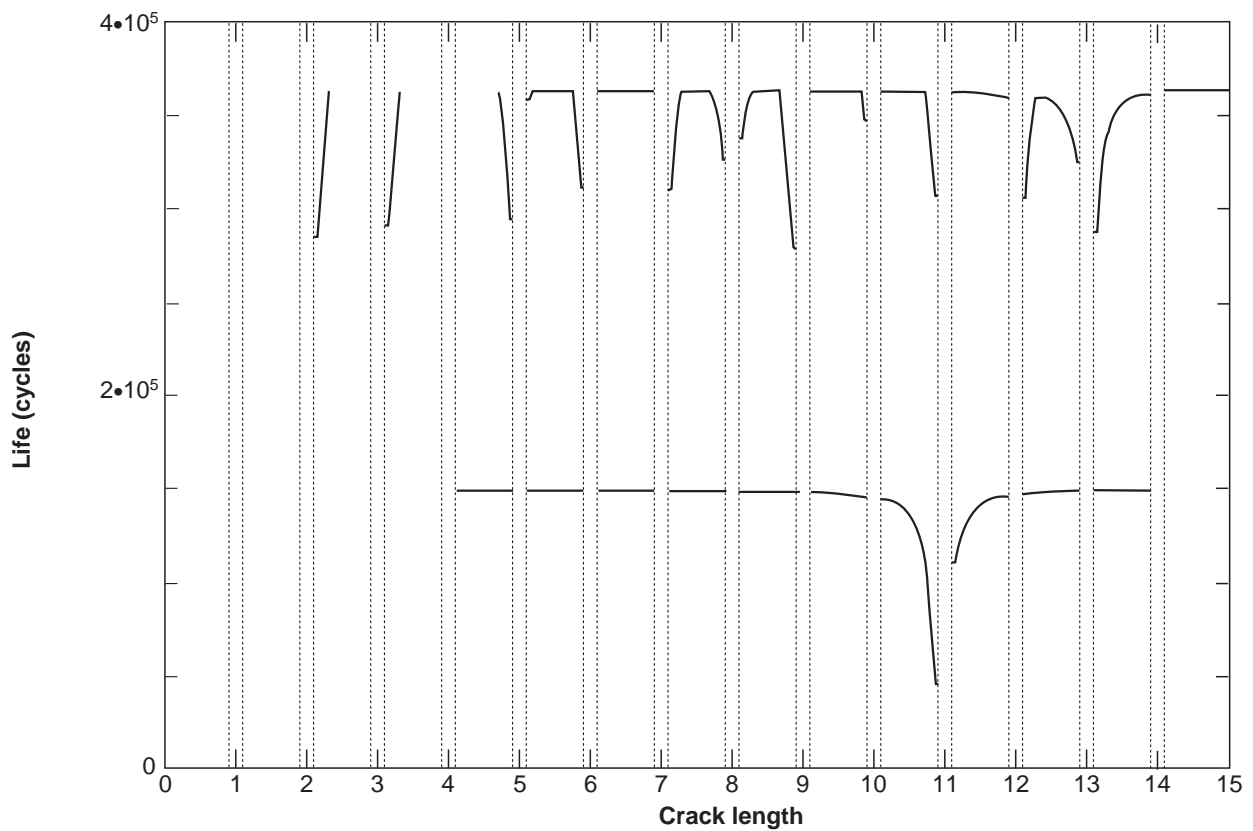


Figure 14 Crack growth pattern at the various rivets for the shortest and longest life obtained

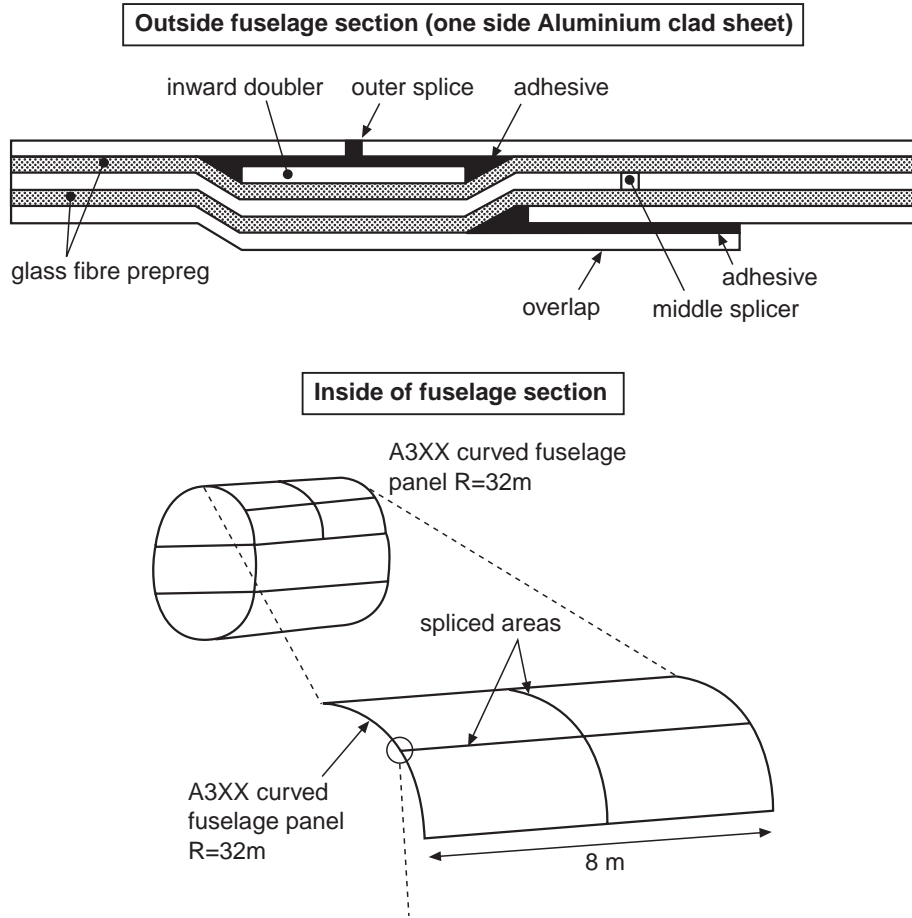


Figure 15 Splices in GLARE fuselage panels

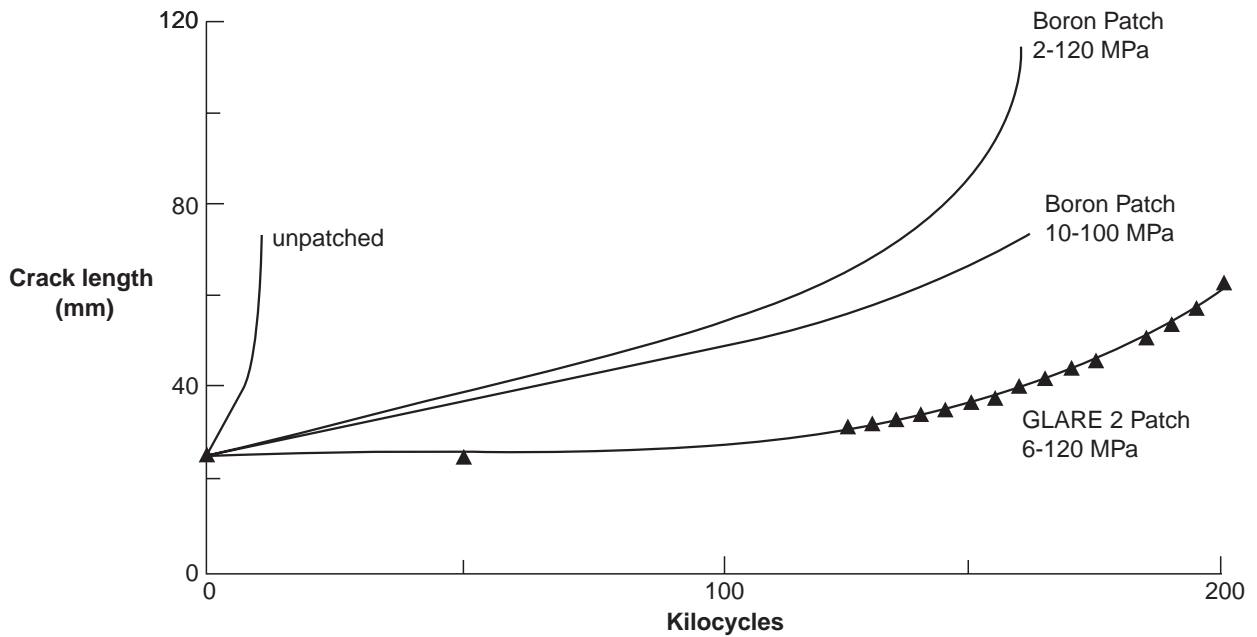


Figure 16 Crack growth curve for unrepaired and different adhesively bonded repairs

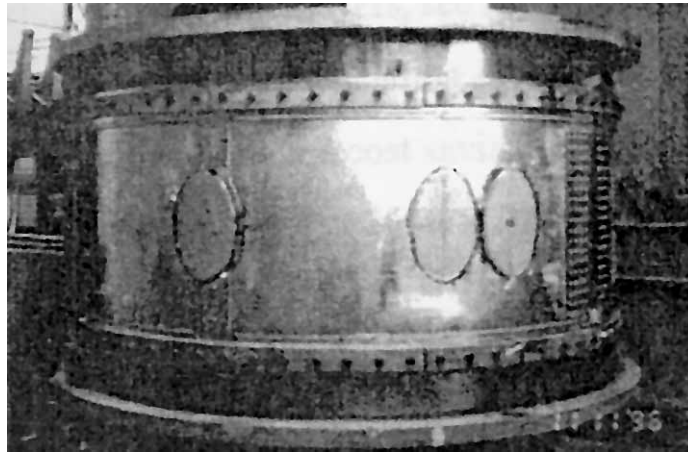


Figure 17 Example of experimental testing: barrel test setup

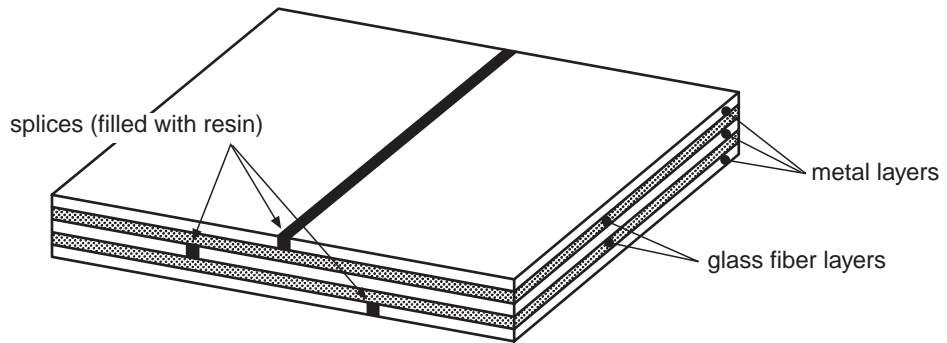


Figure 18 A spliced joint

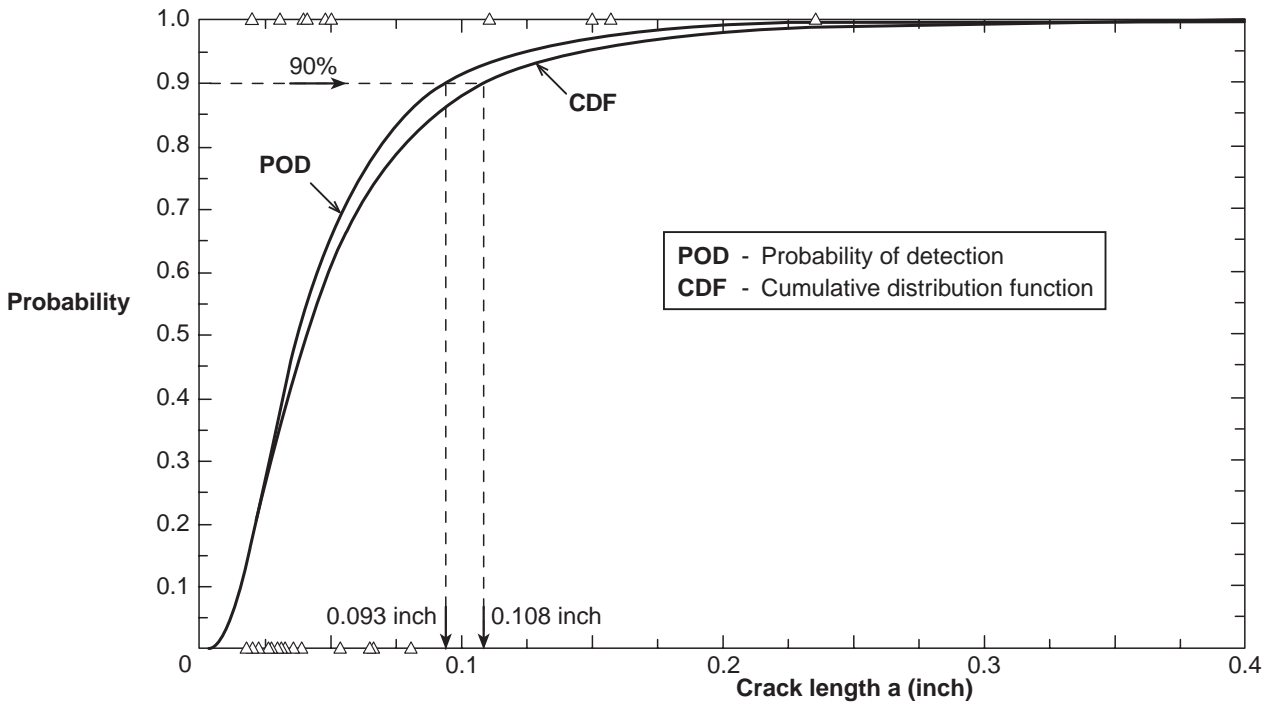


Figure 19 CDF of 28 “hit” data points and mean POD curve of 64 “hit/miss” data points for the manual eddy current inspection of a specific F-16 ASIP point

**REVIEW OF AERONAUTICAL FATIGUE
INVESTIGATIONS IN THE UNITED KINGDOM
DURING THE PERIOD MAY 1997 TO APRIL 1999**

compiled by

P Poole

Mechanical Sciences Sector
Defence Evaluation and Research Agency
Farnborough, Hampshire, UK

2.1 INTRODUCTION

2.2 LOADING ACTIONS

- 2.2.1 Structural Health Monitoring Programme for Eurofighter 2000 (I G Hebden and S R Hunt, British Aerospace MA&A, Warton)
- 2.2.2 VC10 Fin Load Measurement Exercise (VFLME) (C Hoyle, British Aerospace MA&A, Chadderton)
- 2.2.3 VC10 Undercarriage Load Measurement Exercise (VULME) (C Hoyle, British Aerospace MA&A, Chadderton)
- 2.2.4 The Hawk Fatigue Monitoring System (N Penistone, N McCusker and L Redmond, British Aerospace, MA&A, Brough)
- 2.2.5 Hawk – RAFAT Fatigue Monitoring (D J Jones and S C Reed, DERA Farnborough)
- 2.2.6 Operational Loads Measurement Programmes for Tornado, Jaguar and Harrier Aircraft (L Gill, British Aerospace MA&A, Warton)
- 2.2.7 Future Fatigue Monitoring Systems (D J Jones, DERA Farnborough)
- 2.2.8 Usage Monitoring in Helicopters – Estimation of Potential Fatigue Life Extension Benefits Provided by Usage Monitoring Systems (R A Hudson and P E Irving, Cranfield University)

2.3 FRACTURE MECHANICS AND DAMAGE TOLERANCE

- 2.3.1 An Alternative Crack Path Stability Parameter (L P Pook, University College London)
- 2.3.2 Advanced Boundary Element Methods for Prediction of Crack Behaviour in a Pressurised Aircraft Fuselage, P H Wen and M H Aliabadi, University of London; A Young, DERA Farnborough)
- 2.3.3 Dynamic Fracture Mechanics (P H Wen and M H Aliabadi; University of London; A Young and D P Rooke, DERA, Farnborough)
- 2.3.4 Applications of Experimental Mechanics (E A Patterson, University of Sheffield)
- 2.3.5 Damage Tolerance Design Principles in Metal Matrix Composites (E R de los Rios and J R Yates, Sheffield University)
- 2.3.6 Microstructural Fracture Mechanics (E R de los Rios, Sheffield University)
- 2.3.7 Fatigue Crack Growth from Cold Expanded Holes in Corroded Material (R Cook, DERA Farnborough; N Glinos, Kingston University)
- 2.3.8 Measurement and Prediction of Fatigue Crack Growth in the Presence of Residual Stresses in a Creep Resistant Aluminium Alloy (D J Smith, M J Pavier, A A Granada-Garcia and V Lacarac, University of Bristol)
- 2.3.9 Analysis of Crack Growth from Cold Expanded Fastener Holes (D Dai, British Aerospace Airbus, Filton, Bristol)
- 2.3.10 Damage Tolerance of Welded Aircraft Structures (G Bussu and P E Irving, Cranfield University)
- 2.3.11 Fatigue Crack Growth in Helicopters (P Wood, GKN-Westland Helicopters; P E Irving, Cranfield University; R Cook DERA Farnborough; I Austen, nCode International)

2.4 FATIGUE AND FRACTURE PROPERTIES OF ALUMINIUM ALLOYS

- 2.4.1 Reinforcement Distribution Effects on Fatigue and Fracture Behaviour in Al-SiCp Composites (J Boselli, I Sinclair and P J Gregson, University of Southampton; P Pitcher, DERA Farnborough)
- 2.4.2 Application of Soft Computing Modelling Methods to the Structural Performance of Aluminium Airframe Materials (O Feminella, I Sinclair, M Brown and P A S Reed, Southampton University)
- 2.4.3 Quantification and Modelling of Extrinsic and Intrinsic Contributions to Stage I Fatigue Crack Growth in Al-Li Alloys (Y Liu, I Sinclair and P J Gregson, Southampton University)
- 2.4.4 Numerical Modelling of Fatigue Crack Closure in Damage Tolerant Aerospace Materials (M Parry and I Sinclair, Southampton University)
- 2.4.5 Microstructural Assessment and Modelling of Overload Behaviour in Damage Tolerant Airframe Materials (Y Xu and I Sinclair, Southampton University; R Collins and J Haddock, BAe Airbus; J C Ehrstrom, Pechiney CRV)
- 2.4.6 In-situ SEM Studies of Small Crack Behaviour under Cyclic Load (P Bowen, M D Halliday and C Cooper, University of Birmingham; P Poole, DERA Farnborough)
- 2.4.7 Effect of Sequential Action of Corrosion and Fatigue on Fatigue Crack Initiation and Growth in 2024-T3 - Aluminium Alloy (I Rounge and P E Irving, Cranfield University)
- 2.4.8 Improving the Fatigue Crack Resistance of 2024-T351 Aluminium Alloy by Shot Peening (E R de los Rios, Sheffield University; A Levers, British Aerospace Airbus)

- 2.4.9 Fracture Toughness (G R Sutton, DERA Farnborough)
- 2.4.10 Fatigue, Fatigue Crack Propagation and Fracture Toughness of ALFSOTATS Sheet (S Scott, British Aerospace Airbus)
- 2.4.11 Development of Models for the Prediction of the In-Service Performance of Metal Matrix Composites (P M Powell and R Cook, DERA Farnborough)
- 2.4.12 Fracture Resistance, Fatigue and Corrosion Fatigue of Candidate Weldable Aluminium Alloys for Primary Aircraft Structure (P M Powell, M W Squibb and G R Sutton, DERA Farnborough)

2.5 FATIGUE AND FRACTURE PROPERTIES OF METALS OTHER THAN ALUMINIUM

- 2.5.1 A Fundamental Investigation of the Effect of Dwell Time, Grain Size and Environment on the High Temperature and Creep-Fatigue Resistance of Turbine Disc Alloys (N J Hide and P A S Reed, Southampton University; M B Henderson, DERA Farnborough)
- 2.5.2 Fatigue Life Studies of Sigma SiC Fibre Reinforced Titanium Metal Matrix Composites (Ti MMCs) (M P Thomas, P H Tranter, D Martin and S Sweby, DERA Farnborough)
- 2.5.3 Fatigue Studies of γ -TiAl-based Alloys (A Partridge, E F J Shelton and G F Harrison, DERA Farnborough)

2.6 FATIGUE OF METALLIC JOINTS AND STRUCTURES

- 2.6.1 Scatter Considerations in the Interpretation of Major Fatigue Tests (A Cardrick, DERA Farnborough)
- 2.6.2 Hawk – Structural Life Extension (R Shooter, British Aerospace MA&A, Brough)
- 2.6.3 Fatigue Analysis of Obliquely-Loaded Lugs (S K Walker, British Aerospace MA&A, Brough)
- 2.6.4 PC-9 Fatigue Testing “at a distance” (J Parish, British Aerospace MA&A, Brough)
- 2.6.5 Buffet Test Programme (R Randell and P C Cross, British Aerospace MA&A, Brough & Dunsfold respectively)
- 2.6.6 Hawk Tailplane (J A Anderson, British Aerospace MA&A, Brough)
- 2.6.7 Multiple Site Damage (R Cook and A Young, DERA Farnborough; S Chamberlain and I Taylor, RAF)
- 2.6.8 Assessment of Flaw Tolerance on the EH101 Airframe Structure (D Matthew, GKN Westland Helicopters Ltd., Yeovil)
- 2.6.9 Multi-Axial Fatigue Life Prediction of Ti-6246 Compressor Discs (P H Tranter, M B Henderson, G F Harrison, R Sahota, M J Lunt, M R Brown and D Painter, DERA Farnborough; R J Wilson, M Bache, J Evans and R Evans, IRC, University of Wales, Swansea)
- 2.6.10 Prediction of Fatigue Life for Bolted Joints (W Zhu, British Aerospace Airbus, Filton)
- 2.6.11 Full-Scale Panel Tests in Support of the A300 Life Extension Programme (S Kimmins and R Collins, British Aerospace Airbus, Filton)
- 2.6.12 Methodologies for the Assessment of Widespread Fatigue Damage in Aircraft Wing Structures (R Collins and S Kimmins, British Aerospace Airbus, Filton)
- 2.6.13 Structural Maintenance of Ageing Aircraft (SMAAC) (S Kimmins and R Collins, British Aerospace Airbus, Filton; R Cook and A Young, DERA Farnborough)

2.7 OTHER ASPECTS OF FATIGUE

- 2.7.1 Monitoring the Fatigue Exposure of Helicopter Components (A Cardrick, DERA, Farnborough)
- 2.7.2 Fatigue Regulations for British Military Aircraft (A Cardrick and A Mew, DERA Farnborough)
- 2.7.3 The Effect of Environment on Fretting Fatigue (D B Rayaprolu, DERA, Farnborough)
- 2.7.4 Boundary Element Analysis of Cracked Sheets Reinforced by Composite Patches (M H Aliabadi and D Widagdo, University of London)
- 2.7.5 Thermal-Acoustic Fatigue Programme (P D Green, British Aerospace MA&A, Warton)
- 2.7.6 Thermal-Acoustic Stress Prediction Programme (P D Green, British Aerospace MA&A, Warton)
- 2.7.7 Thermal-Acoustic Test Facility (R Randell, British Aerospace MA&A, Brough)
- 2.7.8 Strain-Life Data for Design (S H Spence, British Aerospace MA&A, Warton)
- 2.7.9 Effect of Service Temperature and Impact Damage on Bonded Composite Patch Repair of Aluminium Alloy Structures (P Poole, K Brown, D S Lock and A Young, DERA Farnborough)
- 2.7.10 Repair of Battle Damage (P Poole, K Man and A Young, DERA Farnborough)
- 2.7.11 Exposure Trials on CFRP Patch Repairs (G R Sutton and P Poole, DERA Farnborough)

- 2.7.12 Fatigue Crack Patching (A S Ball and C Edge, British Aerospace MA&A Farnborough; P Poole, DERA Farnborough)
- 2.7.13 Repair of Wing Leading Edge Skin Structure on In-Service Commercial Aircraft by Solid Phase Welding (G E Shepherd, British Aerospace Airbus, Filton)
- 2.7.14 Integrating P-S-N Curves Over Non-uniform Stress Fields (D Shepherd, G Harrison, M Lunt, A Boyd-Lee, M Brown and M Henderson, DERA Farnborough)
- 2.7.15 Fatigue Life Prediction (R S Sahota, DERA Farnborough)

2.8 FATIGUE PROPERTIES OF COMPOSITES

- 2.8.1 Fractographic Assessment of Fatigue Failures in Multi-Directional and Woven Polymer Composites (M J Hiley, DERA Farnborough)
- 2.8.2 Delamination Growth in Carbon-fibre Structural Elements under Fatigue Loading (S Singh and E Greenhalgh, DERA Farnborough)
- 2.8.3 Characterisation of Fatigue Crack Growth in Smart Hybrid Laminate Materials (M M Singh, J P Dakin, T S P Austin and P J Gregson, Southampton University; P M Powell, DERA Farnborough)
- 2.8.4 The Fracture Resistance of Fibre Reinforced Metal Laminates (G R Sutton, DERA Farnborough)
- 2.8.5 Ceramic Matrix Composite Lifting (P M Farries, M P Thomas and R Sahota, DERA Farnborough)

2.9 FATIGUE OF JOINTS AND COMPONENTS OF COMPOSITE MATERIALS

- 2.9.1 Fatigue of Adhesively Bonded Joints (I A Ashcroft, D J Hughes and S J Shaw, DERA Farnborough)
- 2.9.2 Lynx Composite Tailplane Fatigue Substantiation (J Nickolls, GKN Westland Helicopters Ltd., Yeovil)

2.10 NON-DESTRUCTIVE EVALUATION

- 2.10.1 A Systematic Approach to the Selection of Economic Inspection Methods and Intervals (S H Spence, British Aerospace MA&A, Warton)
- 2.10.2 Eddy Current (EC) Imaging and Inversion (D J Harrison, DERA Farnborough; J Bowler, Surrey University)
- 2.10.3 Detection and Characterisation of Corrosion (E A Birt, D A Bruce, D J Harrison, L D Jones and R A Smith, DERA Farnborough)
- 2.10.4 Adhesive Bond Inspection (D A Bruce, DERA Farnborough)
- 2.10.5 Ultrasonic Array Transducers (R A Smith and S J Willsher, DERA Farnborough)
- 2.10.6 NDE Reliability and Life Management (D A Bruce, DERA Farnborough)

2.11 DESIGN DATA (A C Quilter, ESDU International plc, London)

2.12 REFERENCES

2.1 INTRODUCTION

This review paper summarises aeronautical fatigue investigations which have been carried out in the United Kingdom during the period May 1997 to April 1999. The format of the paper is similar to that of recent UK ICAF reviews[1]; the topics covered include loading actions, fracture mechanics, repair and NDE, as well as fatigue of metallic and composite materials, joints and structures. A list of references related to the various items is given at the end of the paper.

The author gratefully acknowledges the contributions generously provided by colleagues in the aircraft industry and universities, and at the Defence Evaluation and Research Agency. The names of the principal investigators, and their affiliations, are shown in brackets after the title of each item.

2.2 LOADING ACTIONS

2.2.1 Structural Health Monitoring Programme for Eurofighter 2000 (I G Hebden and S R Hunt, British Aerospace MA&A, Warton)

The Structural Health Monitoring (SHM) system being developed for Eurofighter 2000 is resident on each aircraft and will enable the operators to monitor accurately fatigue consumption and significant structural events, thereby safeguarding the structural integrity of the aircraft. Different customer requirements for the SHM system has led to the development of a flexible system which can be configured, without recourse to software change, as either a parametric based or strain gauge based fatigue monitoring system.

System Development (Aircraft)

A full functionality version of the aircraft SHM system is installed and operating on the development aircraft. The in-service system is currently being worked on.

Flight data from both the SHM system and the flight test recording system is downloaded from the aircraft after each flight and analysed on-ground in the validation process for SHM. Validation of the G algorithms is progressing well. Validation of the damage algorithms is in progress; flight data from the development aircraft is being analysed in the validation process for both the strain gauge system and the parametric system. To date only the wing root locations have been analysed. Early indications show a very good correlation between the parametric solution and the strain gauge option for these locations.

System Development (Ground)

Current work is the pooling of 4 Nations requirements for inclusion into the design of the ground-based SHM. Each Nation has a different policy of Fleet Management and work is ongoing to agree how best to support the aircraft in service.

Production

Full production sensor locations for the strain gauge system, and testing requirements are currently being agreed within the EF consortium. Installation of strain gauges on production components has begun.

2.2.2 VC10 Fin Load Measurement Exercise (VFLME) (C Hoyle, British Aerospace MA&A, Chadderton)

Following completion of the VC10 Wing Load Measurement Exercise in July 1997, VC10 C Mk1 XR 810 was reconfigured for a limited fin OLM exercise in the lower fin area. A total of 21 strain gauges were affixed and ten flights were recorded in order to gain, in particular, a better understanding of the impact of hydrostatic pressure resulting from the fin fuel on the lower fin structure. As a result of this exercise significantly improved inspection periods have been obtained for the critical lower fin SSIs.

2.2.3 VC10 Undercarriage Load Measurement Exercise (VULME) (C Hoyle, British Aerospace MA&A, Chadderton)

Following completion of the VFLME in October 1997, the OLM aircraft XR 810 was reconfigured for a large scale undercarriage OLM exercise. The installation, calibration and commissioning was completed in October 1998 with 70 strain gauges affixed to the nose leg, 90 strain gauges affixed to the port main leg and 10 strain gauges on the starboard main leg for comparison purposes. This exercise, in the absence of either nose or main undercarriage fatigue tests, is required to produce representative fatigue spectra in order to calculate safe lives for the individual leg components. It will also provide a useful comparison, in terms of stress spectra, for the main undercarriage back-up structure. So far useable data from 30 flights have been obtained.

2.2.4 The Hawk Fatigue Monitoring System (N Penistone, N McCusker and L Redmond, British Aerospace, MA&A, Brough)

The latest variants of the Hawk are being marketed as aircraft with a 10000 or 12000 flying hours service life. In order to support this the aircraft incorporate airframe improvements and are fitted with a Fatigue Monitoring System (FMS). The FMS fitted to these latest variants of the Hawk aircraft provide the customer with the capability of monitoring fatigue consumption of all the major aircraft components. Monitoring is achieved by recording strain gauge and aircraft parameter data. Two main standards of strain gauge fit are used, a basic usage monitoring fit consisting of 7 or 8 gauges and an Operational Load Measurement (OLM) fit consisting of 21 gauges. OLM data are recorded as time histories whereas usage data are recorded in a peak valley format. When recording in OLM mode usage data are also recorded.

These are three main components to the system. A Data Acquisition Unit (DAU) which records the data on the aircraft. A Flight Line System (FLS) used to transfer data from the aircraft and a Desk Top System (DTS) used to analyse the usage data. Strain gauges are located on each of the major structural components; fuselage, wing, tailplane and fin. The gauge locations have been located to monitor the critical loading actions on each of these components. All gauges have at least one backup gauge with inaccessible ones having a second backup. The aircraft parameters measured on usage aircraft are normal acceleration, angle of attack, airspeed and pressure altitude. The acceleration provides significant data on the way the aircraft is being flown while the remaining three parameters allow a Dynamic Pressure-vs-Angle of Attack matrix to be created. This can be used to assess the amount of vibration the aircraft is subjected to. The availability of these data, from both strain gauge and aircraft parameters, allows the user to assess the impact of different sortie profiles on fatigue consumption and thus allow effective fatigue management of his fleet.

The FMS is configured to record data once the engine rpm is greater than 50% and Weight on Wheels (WoW) is False. This shall ensure that all flight data are recorded. It stops recording once the WoW has been true for 20 seconds. This means that ground loads from taxi and take off are not recorded and only limited landing loads. For the FMS the data are recorded in peak valley format with a programmable threshold gate set to remove non-damaging cycles and any unwanted perturbations and single noise.

The DTS is used to perform basic sanity checks on the downloaded data and to perform the fatigue analysis on that data. On board error checking covers max/min range exceedences, data spike detection, excessive chatter and low activity. It can be used to display the recorded data and to monitor and analyse fleet, squadron, aircraft and component usage data.

The fatigue analysis will be calculated using a range-mean-pair algorithm in conjunction with appropriate S-N curves and Miner's law.

All aircraft fitted with the FMS shall be subject to flight and ground calibrations. These are to ensure accurate fatigue monitoring in-service. The flight calibrations will initially be performed as part of the Production Flight Acceptance Trial (PFAT) where a predefined sequence of manoeuvres shall be flown. On the ground a dedicated calibration rig has been developed which will apply representative loads to all of the main aircraft components. To keep this rig to manageable proportions two of the gauges, subjected to fuel and cockpit pressurisations, are calibrated during the build sequence. The calibration exercise allows offset and positive and negative calibration factors to be generated. The aircraft will be re-calibrated periodically throughout its life or following changing of major components.

The OLM strain gauge fit provides an extension to the basic usage capabilities. This provides data as a continuous time history allowing assessment of aircraft loading actions and has duties above and beyond those of the basic FMS fit.

2.2.5 Hawk – RAFAT Fatigue Monitoring (D J Jones and S C Reed, DERA Farnborough)

The RAF Hawk fleet is in the process of undertaking its second Operational Loads Measurement (OLM) programme. The first [1985-88] did not include display flying with the RAF Aerobatic Team (RAFAT), or the Red Arrows as they are commonly termed, mainly because neither of the aircraft used were modified to RAFAT standards. The second OLM programme consists of a dedicated RAFAT aircraft and a second aircraft for the rest of the fleet use; DERA has been involved with BAe in the analysis of the data.

Results have shown that the buffet damage accrued can vary significantly between the display positions of the team aircraft and between individual sorties in the same display position. Consequently, the decision has been made to fit a strain-gauge based system to each aircraft in the RAFAT and other parametric data will also be collected (e.g. normal acceleration). Data will be collected as full time histories onto solid state memory and data processing will be undertaken on the ground.

It is intended to fit the system to the first 2 aircraft under a trial installation during the winter of 1999/2000 and the remainder the winter after.

2.2.6 Operational Loads Measurement Programmes for Tornado, Jaguar and Harrier Aircraft (L Gill, British Aerospace MA&A, Warton)

The Tornado Structural Usage Monitoring System (SUMS) continues to be operated within the RAF. It has now been running for approximately 15 years and more than 10000 flying hours of data have been analysed. Recently the ADV fatigue meter formula has been revised using this information. In addition SUMS data has been used to aid life extension studies for the IDS.

It is now 12 years since the first Jaguar airframe OLM was completed. Two separate, new, OLM programmes are now underway covering both the airframe and the undercarriage and associated back-up structure. Analysis of the first flights is now taking place. The results from the undercarriage OLM will be compared with the results from the on-going dedicated fatigue tests in support of life extension activities. A further OLM programme has been agreed for engine mounts.

The Fatigue Monitoring Computing System (FMCS) for Harrier is now in service. It is intended that the first 200 flights will be analysed by BAe.

2.2.7 Future Fatigue Monitoring Systems (D J Jones, DERA Farnborough)

Under a tasking placed by the RAF(ASI), DERA have produced an extensive report which considered the problems of existing systems and derived a policy for the future requirements of fatigue monitoring systems. Following this, a strategy was formulated which would use future OLM programmes to explore various aspects of the policy recommended.

Policy Recommendations:

- a. Future methods and improvements to fatigue monitoring should use a mixture of both direct and in-direct load monitors;
- b. Modern systems should be utilised to benefit from the increased scope and flexibility that is now available and proven in the following areas:
 - Number and type of monitoring channels available;
 - Type of sensors;
 - High sampling rates;
 - Memory capacity;
 - Ruggedness and improved reliability with use of solid state electronic modules;
 - Light weight/low cost.
- c. Avoid need for aircrew inputs;

- d. Ground analysis should be considered for final processing of data. For this work a global system of “Health and Usage Centres” should be developed;
- e. Consider benefits of advanced processing techniques, e.g. Artificial Neural Networks (ANNs);
- f. Event and Usage monitoring should be employed as part of the airborne system.

Way Ahead Strategy.

Future OLM programmes offer the opportunity to explore the potential of all the improvements that have been highlighted by the new policy. A programme of work has now been devised which will use these OLM programmes to consider initially the following aspects:

- a. Use of advanced systems;
- b. Artificial Neural Networks (initially in the area of data checking and validation)

This work programme is initially planned for 3 years, during which time it is hoped that the scope of the work can be expanded to include investigations into other elements of the policy, e.g. use of ANNs for the fatigue calculation exercise.

2.2.8 Usage Monitoring in Helicopters – Estimation of Potential Fatigue Life Extension Benefits Provided by Usage Monitoring Systems (R A Hudson and P E Irving, Cranfield University)

Service load data from 10 hours of instrumented helicopter flight of the Westland Lynx containing repeated examples of all 25 manoeuvres in the design spectrum were used for the investigation[2,3]. A rotor blade attachment component was selected for study. The damage content of each manoeuvre was calculated using Miners rule and component fatigue data supplied by the manufacturer, and the variability in damage assessed. There was great variability in the damage content of each manoeuvre type. Frequently the damage rate per second of a manoeuvre type, varied from zero to very high levels. An example of a cumulative distribution of damage rates is shown in figure 1. Forward flight manoeuvres comprising over 50% of the design spectrum were almost always undamaging. Taking the worst case damage for each manoeuvre and summing them to derive a total worst case design spectrum damage, showed that over 90% of the damage was contributed by just 5 manoeuvres. Similar results were obtained by summing all values of 50% probability of occurrence. These damage content data were used together with data on the variability of manoeuvre usage and assumed scatter of the component S-N fatigue curve in Monte Carlo simulations to calculate life distributions and probability of failure. It was found that damage variability in each manoeuvre has little effect, but changes in manoeuvre usage has very significant effects, as does the scatter in component S-N curves.

2.3 FRACTURE MECHANICS AND DAMAGE TOLERANCE

2.3.1 An Alternative Crack Path Stability Parameter (L P Pook, University College London)

It is well known that, under both static and fatigue loading, the directional stability of a Mode I crack in an isotropic material under essentially elastic conditions is governed by the T -stress, a stress parallel to the crack. If the T -stress is compressive, then a crack is directionally stable, and if the T -stress is tensile it is directionally unstable. In practice it is sometimes found that cracks are directionally stable even if the T -stress is tensile. Dimensional considerations mean that the T -stress does not provide a satisfactory measure of crack path stability. An alternative non-dimensional parameter, the T -stress ratio, T_R , has been proposed[4]. For a particular material there appears to be a critical value of T_R , T_{Rc} , below which a crack path is directionally stable. There is a size effect for geometrically similar configurations in that crack path stability increases with specimen size. Re-analysis of experimental data taken from the literature, for both static and fatigue loadings, gave T_{Rc} values from various materials ranging from 0.013 to 0.041. A general consideration showed that for many materials T_{Rc} is at least 0.021.

2.3.2 Advanced Boundary Element Methods for Prediction of Crack Behaviour in a Pressurised Aircraft Fuselage (P H Wen and M H Aliabadi, University of London; A Young, DERA Farnborough)

The aim of this project is to develop a more efficient and cost effective method for assessing the damage tolerance of pressurised fuselage structures. The proposed study includes investigation into linear, non-linear and time dependent problems, by combining new and advanced innovative computational methods with existing techniques. The recent

formulation by Dirgantara and Aliabadi[5] for modelling cylindrical shells has been extended to fuselage with frames and stringers[6]. Also developed are two techniques, direct integral method (DIM) and dual reciprocity method (DRM) for transformation of the domain integrals to the boundary[7]. Both concentric and eccentric stiffeners have been considered. Several test cases have been solved and compared to other published results[8].

2.3.3 Dynamic Fracture Mechanics (P H Wen and M H Aliabadi; University of London; A Young and D P Rooke, DERA, Farnborough)

The boundary element techniques previously developed for two-dimensional dynamic fracture analysis[9-11] have now been extended into three-dimensional dynamic analysis[12-16]. In this work, dynamic formulations of the dual boundary elements in the time domain method (TDM), in the Laplace transform method (LTM) and using the dual reciprocity method (DRM) are developed for analysis of crack problems subjected to dynamic loadings. Mode I and mixed-mode stress intensity factors were evaluated using crack opening discontinuity displacements directly by the time domain method and the dual reciprocity method and with the Durbin inversion technique by the Laplace transform method.

In figure 2, the mode I dynamic stress intensity factors $(\sqrt{\pi}K_I(t)/\sigma_0)$ are presented for an elliptical crack in a rectangular bar using the three boundary element methods. Also presented are the finite difference solutions due to Chen and finite element solutions due to Nishioka for comparison.

It was found that the computational time depends on the number of steps for TDM and LTM as in each step two new large matrices need to be calculated. As DRM is very fast way to obtain solution, it can be used to carry out approximate analysis for dynamic structure. LTM can be used to obtain more accurate solutions, but the time-stepping methods, DRM and TDM, were found to be more suitable than LTM for the analysis of crack growth.

2.3.4 Applications of Experimental Mechanics (E A Patterson, University of Sheffield)

Work has focused on the development and application of techniques in experimental mechanics to fracture mechanics. The principal techniques employed are transmission and reflection photoelasticity, thermoelasticity and caustics[17,18]. Most of the applications have been associated with the aerospace industry and those published during the period of the review include the effect of friction on crack propagation in compressor discs[19], and evaluation of SIF for cracks in a bolted joint[20,21].

Research is in progress on crack closure in collaboration with the University of Plymouth. Fatigue cracks have been grown in polycarbonate specimens which can be analysed using photoelasticity to determine the stress intensity factor during propagation and the contact stresses associated with closure. It is planned that the study will be extended by the use of reflection photoelasticity on metallic specimens. Funding has just been received which allow further development of work on the application of thermoelasticity[22] to fracture mechanics assessments. Experiments on the direct assessment of crack closure[23] will recommence shortly; further work on the evaluation of predominantly mode II stress intensity factors will also be undertaken.

2.3.5 Damage Tolerance Design Principles in Metal Matrix Composites (E R de los Rios and J R Yates, Sheffield University)

Based on microscopic observations of fatigue damage in MMCs, a micro-mechanical model of fatigue crack growth has been developed incorporating the basic material variables which control the fatigue properties of these composites: fibre constraints (strengthening) and fibre bridging. The fibres are assumed to constrain crack tip plasticity, so that crack plastic displacements are zero at the fully bonded fibres. The conditions for fibre debonding are then established and, when they are met, the fibre debonds, a process which depends on the interfacial shear strength of the fibre-matrix interface. The higher the interface strength, the higher the constraint and the lower the crack propagation rate. The other fatigue strengthening mechanism in these composites is the effect of fibre bridging developed by intact fibres within the crack wake.

This model was used to derive fundamental tools for damage tolerance design in fibre-reinforced MMCs. By deriving the limits of crack propagation (arrest) and composite crack instability, a damage map was constructed which determines the

bounds for crack arrest, stable fatigue crack growth and crack instability (figure 3). The application of the damage map in fatigue design with MMCs has been demonstrated[24-26].

2.3.6 Microstructural Fracture Mechanics (E R de los Rios, Sheffield University)

Microstructural Fracture Mechanics principles are used to study some engineering problems. i) Fatigue studies have been carried out on an aluminium 7010-T7451 alloy, under constant-amplitude and random loading conditions, using cylindrical plain hour-glass specimens. A crack growth model, which is capable of considering the mean stress effects on crack growth, was used to predict crack growth rates and fatigue life under random loading incorporating the root mean square (RMS) concept. This relatively simple approach predicted crack growth rates and lifetimes comparable to experimental results and implied that fatigue life under random loading can be predicted from constant amplitude experimental data, simply with the use of the RMS concept together with a pertinent crack growth law[27]. ii) A model based on Microstructural Fracture Mechanics principles has been used to study the short crack propagation in peened-notched components. The model reflects the typical features of the shot peening process, such as the relative fatigue resistance improvement, the existence of an optimum range of applicability and the detrimental effect of overpeening (figure 4)[28].

2.3.7 Fatigue Crack Growth from Cold Expanded Holes in Corroded Material (R Cook, DERA Farnborough; N Glinos, Kingston University)

Work on the effectiveness of hole cold expansion in the presence of corrosion has recently been completed at Kingston University[29,30]. It was reported in the last ICAF review that the effectiveness of hole cold expansion was reduced in corroded components because fatigue cracks initiated from corrosion pits in the tensile residual stress region remote from the hole, resulting in premature failures. The programme was conducted on open hole specimens manufactured from 7010-T76 alloy. Corrosion was introduced through exposure of the specimen to various corrosive environments for a range of exposure periods. Exposure to corrosive environments was conducted either before or after the cold expansion was performed. The results showed that specimens subjected to natural corrosion for several years prior to expansion failed prematurely from cracks initiating at corrosion pits, at most practical applied stresses. Premature failure was not observed at high applied stresses where failures initiated from cracks growing from the hole. The remainder of the test programme was conducted at a single applied stress level, close to the fatigue limit of cold expanded holes, which was of most interest for aircraft structures.

Exposure to a high corrosion severity environment (3.5% NaCl) prior to cold expansion resulted in premature failure even for very short exposure periods of a few minutes. However, when the severity of the corrosive environment was reduced to 0.35% NaCl, it was found that fatigue endurance were little affected at short exposure times but premature failures from cracks at corrosion pits occurred after longer exposure times. The change in failure mode was associated with a critical size and density of corrosion pits present. It was found that this critical size and density were exceeded in all tests exposed to 3.5% NaCl solution, which explains the behaviour described above.

Exposure to a high corrosion severity environment after cold expansion had little effect on fatigue endurance, accordingly testing was not performed with low corrosion severity. The sizes of pits formed in the vicinity of the hole were notably smaller than those found in specimens cold expanded after exposure to high corrosion severity atmosphere at equivalent exposure times. This could explain the lack of effect on fatigue endurance.

2.3.8 Measurement and Prediction of Fatigue Crack Growth in the Presence of Residual Stresses in a Creep Resistant Aluminium Alloy (D J Smith, M J Pavier, A A Granada-Garcia and V Lacarac, University of Bristol)

The aim of the current research is to gain an understanding of how residual stresses, generated as a result of cold working fastener holes, interact with fatigue loading. This is particularly at temperatures relevant to civil supersonic transport applications. There have been two main areas of work at Bristol; prediction and measurement of the 3D distribution of residual stresses around cold worked fastener holes, and fatigue crack growth studies for various fatigue loading and temperature conditions.

In predicting the development of residual stresses in a cold worked hole, and then examining the distribution of residual stresses after mechanical loading, it was realised that non-axisymmetric residual stresses occurred around the fastener hole.

Furthermore, using conventional through plate thickness measurement methods, such as the Sachs boring technique, gave erroneous results. Research at Bristol has developed a new experimental method called the Garcia-Sachs method that has provided accurate results[31]. For example, figure 5 shows the tangential residual stresses around a cold worked hole that has been subjected to creep stress relaxation. The tangential residual stresses have been normalised with respect to the yield stress of the material. A finite element (FE) prediction of the residual stresses is shown together with a simulation of the new measurement procedure. There is excellent agreement between the FE prediction and the results from the simulation of the method. Also shown are results obtained using the conventional Sachs method. These results are erroneous particularly near the hole edge.

The new measurement method has been applied to cold worked fastener holes that have been subjected to a wide range of external loading conditions. In general measurements, using the new technique, reveal that non-axisymmetric residual stresses occur around the fastener hole. As well as non-axisymmetric residual stresses there are also significant through thickness variations of the residual stresses. Figure 6 shows measured residual stresses at the entrance and exit faces of a cold worked hole. Also shown are the results from FE predictions using a complex hardening model for the material behaviour. The material model takes into account the unloading behaviour of the material after being subjected to prior plastic strain. Again there is excellent agreement between surface stress measurements and FE analysis.

Experiments have been carried out to measure the growth of corner cracks emanating from the edge of cold worked holes at the entrance face[32,33]. Crack closure and opening levels were measured optically using a digital camera, with the results used to interpret the influence of the residual stresses on crack growth. As might be expected there were improvements in fatigue lives of specimens containing cold worked holes compared to specimens containing non-cold worked holes. This is illustrated in figure 7, where fatigue crack growth rates are shown for non-cold worked and cold worked samples for different applied load ratios. The main reduction in cracking rates, in cold worked samples, is found for surface crack lengths around 2mm. Also shown are predicted crack growth rates. The predictions were made using an empirical relationship taking into account crack closure and the presence of residual stresses. The predictions clearly show the benefit of cold working fastener holes, and show that the benefit is a function of the load ratio.

Experimental studies have also explored how temperature and time influence residual stresses generated in cold working and hence fatigue life. Cold worked samples have been subjected to 150°C for different times, and then relaxation of the residual stresses measured. Although the residual stresses do relax, this relaxation is local to the cold worked hole. Fatigue crack growth studies reveal that some benefit from cold working is retained, with fatigue crack growth rates lower than non-cold worked specimens at the same temperature. Figure 8 shows an example of the results obtained.

2.3.9 Analysis of Crack Growth from Cold Expanded Fastener Holes (D Dai, British Aerospace Airbus, Filton, Bristol)

The cold expansion process leaves a complex residual stress distribution. An analytical method to predict the growth of a crack from a cold expanded fastener hole must therefore be able to model the steep stress gradient near the hole edge, with allowance for partial crack closure. In this project, the distributed dislocation method has been adopted; distributed dislocations are used to model the open parts of the cracks, whereas the boundaries of the structure are modelled by distributed dislocation dipoles. The method allows for partial crack closure, finite width effects, double cracks, and multiple site damage. The transverse stress ('T'-stress) can also be calculated for various crack configurations. The fastener is taken into account by appropriate dislocation influence functions; however, only interference fit is considered at the moment, where neither slip nor separation is allowed at the interface.

The method has been used to predict the growth of cracks under constant amplitude fatigue loading. The results shown in figure 9 are for specimens in 7075-T651 material, with an open hole of diameter 5.85 mm which was cold expanded by 4%. The specimens were subjected to cyclic loading at a stress ratio of 0.1, with two maximum stress levels (150MPa and 170MPa). The correlation between prediction and experimental results is very close.

Future work will include refinement of the 2D method to include interfacial conditions, non-slip and non-friction conditions at the fastener interface, separation and mixed boundary conditions. In addition, the model will be further validated against experiment measurements. A 3D model has also been developed, based on the distributed dislocation loop method. However, the method is computationally expensive to use, and significant improvements are required. A more robust 3D method for corner cracks will therefore also be developed.

2.3.10 Damage Tolerance of Welded Aircraft Structures (G Bussu and P E Irving, Cranfield University)

A number of major projects have been set up in the UK in the past two years to develop welding as an alternative to riveting in aircraft construction. Many of the projects have been concerned with development of high quality welding processes suitable for welding high strength aerospace aluminium, and titanium alloys. One project has investigated the damage tolerance behaviour of welds made in selected aluminium alloys using the friction stir welding and plasma welding processes. The project has considered both design and fatigue related issues in the substitution of welds for rivets.

As part of the design issues, the optimum location for welds in wing structures has been investigated, and finite element stress analysis used to identify the best location in terms of local stresses developed. Other considerations from a damage tolerance point of view are inspectability, and from a manufacturing aspect the weldability of particular joint configurations. The role of softened heat affected zones, and of residual stress fields caused by the weld, in promoting buckling behaviour during compressive loading of transverse welded joints has been studied using finite element analysis. It was found that transverse softened zones greatly reduced the compression strength of the structure. Fatigue properties (S-N curves) relevant to crack initiation behaviour of friction stir welds in 2024-T351 have been measured for both longitudinal and transverse weld orientations, in both as-welded and surface skimmed configurations[34]. Figure 10 and 11 show that the fatigue lives of as-welded joints were much less than those of the parent metal, and that surface skimming resulted in lives similar to those of the parent metal. Skimmed fatigue strength was superior to that of traditional riveted joints, but as-welded fatigue performance was inferior to that of riveted joints. Fatigue crack growth rates have been measured in the friction stir welds, both transverse and longitudinal to the weld direction. It has been found that the weld region exhibits anomalously fast crack growth rates relative to those measured in parent plate material. The work is continuing to develop a comprehensive picture of fatigue crack initiation and growth behaviour for welds in high strength aluminium alloys which can be used in damage tolerance analysis.

2.3.11 Fatigue Crack Growth in Helicopters (P Wood, GKN-Westland Helicopters; P E Irving, Cranfield University; R Cook DERA Farnborough; I Austen, nCode International)

A collaborative research programme was undertaken by the above organisations under the auspices of the UK Department of Trade and Industry LINK scheme. The five areas of investigation were described in the previous UK ICAF review, and included measurement of fatigue crack growth rates at high stress ratios, development of fatigue loading sequences for helicopter components, fatigue crack growth under spectrum loading, modelling of crack growth, and developing a robust damage tolerant design procedure for helicopter structures. Work has now been completed[35-37] and the main conclusions are presented below.

Two new loading sequences were defined, representing loads experienced by rotating components in the rotor head (Rotorix) and by a load frame (Asterix). Small amplitude cycles resulting from the main rotor motion contributed 90% of the crack growth in the spectra, for both Titanium (rotor head) and Aluminium-Lithium (lift frame) components, even at crack lengths as small as 1mm. Model predictions of crack growth under these load spectra were not predicted well by the models which were generally non-conservative. Linear summation methods (without load interaction effects) were also generally non-conservative, as illustrated in figure 12. The poor performance of the models was thought to arise for a number of possible reasons; failure to model accurately take-off and landing cycles, different fracture surface morphology between constant amplitude and spectrum loaded tests, poor definition of crack growth rates in the near threshold region and the dependence of threshold behaviour on crack length. These and other aspects will be investigated in a collaborative programme which commenced recently, sponsored by the UK Ministry of Defence and the UK Civil Aviation Authority.

2.4 FATIGUE AND FRACTURE PROPERTIES OF ALUMINIUM ALLOYS

2.4.1 Reinforcement Distribution Effects on Fatigue and Fracture Behaviour in Al-SiCp Composites (J Boselli, I Sinclair and P J Gregson, University of Southampton; P Pitcher, DERA Farnborough)

It is generally recognised that reinforcement distributions may have a marked effect on the failure behaviour of particulate reinforced Al-SiC_p MMCs. Whilst numerous methods have been presented to quantify particle distribution characteristics (such as Ripley's K-function, quadrat and nearest-neighbour tests), the identification of a tessellated region around a given secondary phase body such that every point within that region is closer to that particle than any other, has been recognised as

a uniquely powerful method to describe distribution characteristics on a particle by particle basis. In the present work[38-40], current concepts of Dirichlet tessellation have been extended to a 'finite body' tessellation, constructing cells from the actual interfaces of finite secondary phase particles, providing a more physically meaningful description of the high secondary phase volume fractions of most particle Al-SiC_p composites. Quantitative studies have shown Finite Body tessellation to be more sensitive to local microstructural character than the Dirichlet method when applied to real particulate composite systems. Statistical characteristics of tessellation measurements have been assessed, showing the coefficient of variation of mean interparticle separation to be a sensitive clustering parameter. This parameter has been applied to short fatigue crack growth behaviour in real composites and have shown to have a first order influence on growth rates. Initial microstructural finite element modelling has confirmed the influence of measured clustering effects on crack growth rates through a reinforced material.

2.4.2 Application of Soft Computing Modelling Methods to the Structural Performance of Aluminium Airframe Materials (O Feminella, I Sinclair, M Brown and P A S Reed, Southampton University)

Extensive scientific and technical know-how has been built up over the years on the processing and structural performance characteristics of aluminium aerospace materials. However, detailed quantitative modelling of materials performance in terms of actual commercial products remains largely untenable due to the underlying complexity of the materials and the associated commercial processing environment. Soft computing modelling methods, such a neural network analysis, represent a proven and efficient method of modelling such complex multi-variate physical systems, constituting a considerable improvement over simple regression analyses. The present project will particularly apply neurofuzzy network modelling methods to the fatigue performance of 2xxx and 7xxx series aluminium plate materials[41]. Neurofuzzy analysis represents an important progression of pure neural network techniques via reasonable straightforward inclusion of established physical knowledge (in terms of general physical dependencies) with the numerical heuristic model formation of pure neural networks. The models developed may be expected to provide direct contributions to production quality control (improving property minima and in-service reliability) and the identification of key process/alloy innovations.

2.4.3 Quantification and Modelling of Extrinsic and Intrinsic Contributions to Stage I Fatigue Crack Growth in Al-Li Alloys (Y Liu, I Sinclair and P J Gregson, Southampton University)

Investigations into the fatigue behaviour of commercial Al-Li alloys in damage tolerant plate and sheet forms have noted the occurrence of distinct macroscopic crack deviation at moderate to high ΔK levels in certain specimen orientations. Previous results have identified this behaviour with a combination of local crack-tip stress/strain conditions during crack growth, and the underlying crystallographic texture where sustained co-planar mixed mode fatigue crack growth may be produced at moderate mode II to mode I loading ratios parallel to preferred {111} plane orientations. Using an idealised combination of mixed mode crack growth testing geometry and specimen orientation, this behaviour is being used to quantify intrinsic Stage I fatigue crack growth behaviour as a function of mixed mode loading conditions and basic microstructural parameters. Results to date[42], have identified the limited efficacy of crack sliding contact closure under strongly mode II load conditions consistent with the unusually flat, crystallographic fracture surfaces that may be produced in these materials under mixed mode conditions. Furthermore, crack growth rates under mixed mode II/I and pure mode II conditions have been identified as consistently faster than nominal mode I results, with an energy based equivalent stress intensity parameter being identified as a useful descriptor of mixed mode crack growth behaviour. Further work is underway to clarify the role of intrinsic and extrinsic crack growth resistance to the apparent crack growth behaviour.

2.4.4 Numerical Modelling of Fatigue Crack Closure in Damage Tolerant Aerospace Materials (M Parry and I Sinclair, Southampton University)

The mechanics of crack closure arising from microscopic roughness of fatigue fracture surfaces, termed roughness-induced crack closure, are not fully understood. Many aerospace alloys exhibit deflected crack growth, and observed reductions in fatigue crack growth rates have been semi-quantitatively explained by this process. Models of this process within the literature are commonly restricted to two dimensions and relatively simple, unrealistic crack paths. The present programme is developing more representative finite element based models, particularly focusing on the three-dimensional surface features found in highly textured AA8090 plate material. Work to date has also addressed the issue of slip heterogeneity by introducing narrow low yield strength bands ahead of a propagating crack tip (simulating precipitate dissolution within cyclic slip bands), highlighting the important role this may play in producing mode II offset along a nominal mode I crack path, and consequent roughness induced closure behaviour.

2.4.5 Microstructural Assessment and Modelling of Overload Behaviour in Damage Tolerant Airframe Materials (Y Xu and I Sinclair, Southampton University; R Collins and J Haddock, BAe Airbus; J C Ehrstrom, Pechiney CRV)

Various micro-mechanical and microstructural influences on crack advance under variable amplitude conditions are established within the literature (e.g. associated with plasticity induced closure, crack tip blunting and/or branching, strain hardening, residual stress fields, etc.). However, variable amplitude lifing algorithms remain simplistic and to a significant extent empirical in nature. The present study seeks to quantify individual micromechanical contributions to overload events in a well controlled set of 2xxx-type materials, separating microstructural and mechanical effects. Work to date has concentrated on improved closure measurement methods, identifying a novel dual-curve fit compliance assessment method. Plain and deeply side grooved crack growth specimens are being used in conjunction with global and near-tip strain measurements to separate plane stress and plane strain contributions to load transients.

2.4.6 In-situ SEM Studies of Small Crack Behaviour under Cyclic Load (P Bowen, M D Halliday and C Cooper, University of Birmingham; P Poole, DERA Farnborough)

The small fatigue crack growth regime is being studied, particularly with regard to the aluminium alloys 2024-T351, 7010-T7651 and 8090-T8771. Cracks are self-initiated at plane, polished surfaces, usually from second-phase particles, under four point loading on a servo-hydraulic test machine and are grown on as 'thumb nail' cracks. Crack growth data are obtained from surface replicas. In-situ, high resolution observations and measurements of the micro-mechanics of crack growth are obtained at selected crack sizes using a 10kN cyclic loading stage mounted within an Hitachi S-4000 field emission gun SEM. Using these procedures it has proved possible to obtain crack closure data and near-tip crack opening displacement measurements for cracks of approximately 30 to 2000 microns total surface length. Testing has been conducted at positive and negative R ratios in laboratory air and at positive R ratios in distilled water and 3.5% aqueous sodium chloride environments. Comparative long crack growth data have been obtained in laboratory air using an automated threshold testing system based around a resonance-type testing machine[43].

The programme has provided information on the magnitudes and differences in small crack closure levels for various alloys, test conditions and environments. As an example, figure 13 shows measurements of closure over a range of crack sizes and environments for 7010-T7651 alloy. They show a tendency for the closure levels to reach higher values at smaller crack sizes and for an increase in crack closure with increasingly aggressive environment. However, despite increases in crack closure, a more aggressive environment can also produce enhanced crack growth rates, as shown in figure 14 for the same alloy. These experimental data have provided support for a closure model developed around the concepts of plastic deformation and surface roughness induced closure mechanisms[44], that is supported by finite element modelling[45]. Negative R ratios have also been shown to be detrimental to the small crack fatigue properties of the alloys. This appears to occur through the influence of mixed-mode fracture paths and the modification of crack closure by compressive loads. Measurements of near tip crack openings are being used as a parameter to examine the influence of environment and loading conditions on crack tip plastic deformation and the micro-mechanics of crack growth. Figure 15 shows an example of near crack tip opening displacement obtained from the 7010 alloy as a function of root distance behind the crack tip, a graphical presentation used previously[46]. The influence of environment at different crack lengths can be assessed by utilizing the gradient of these curves as in figure 16, where all the data are for a uniform surface stress of 0.8 x yield stress. The influence of simple load excursions on small crack growth has been examined in terms of crack tip opening displacements, crack closure and the finite element modelling of residual stresses ahead of the crack tip[46,47]. Fractographic observations have provided the basis for a suggested model of fatigue crack growth that extends from the growth of small cracks into stage II long crack growth[48].

The techniques outlined above are applicable to a wide range of metallic and composite materials, such as monolithic and fibre-reinforced titanium alloys, and are frequently employed in other in-house programmes of work. New, novel experimental procedures are being developed as part of the programme on small crack growth in the aluminium alloys. A facility for the continuous monitoring of small crack growth, rather than the intermittent measurements provided by replicas, that is consistent with previously developed systems for data acquisition, is currently under investigation.

2.4.7 Effect of Sequential Action of Corrosion and Fatigue on Fatigue Crack Initiation and Growth in 2024-T3 Aluminium Alloy (I Rounge and P E Irving, Cranfield University)

Samples of 2024-T3 containing a semi-circular notch 6mm in diameter were subjected to alternating periods of cyclic loading and corrosion, using the accelerating corrodant Exco[49]. Corrosion periods ranged from 15 minutes to 4 hours. The fatigue cycle numbers in the cyclic loading period ranged from 1250 to 10000. Corrosion periods of 15-30 minutes produced pit depths in the notch of 30-60 μm . Alternating this period with 10000 fatigue cycles produced a 65% reduction in fatigue life compared with the uncorroded state. Increasing the corrosion period up to 4 hours produced little further decrease in life. Reducing the cycles between corrosion periods to 1100 cycles, produced significant (95%) reductions in life compared with the original properties. Detailed observations of pit and fatigue development using replicas revealed a complicated picture. Pits produced multiple fatigue cracks and crack linking which decreased lives. Pit development also caused cracks to blunt and bifurcate, which increased lives.

2.4.8 Improving the Fatigue Crack Resistance of 2024-T351 Aluminium Alloy by Shot Peening (E R de los Rios, Sheffield University; A Levers, British Aerospace Airbus)

The effect of shot peening on the fatigue resistance of a 2024-T351 aluminium alloy was studied using an in-situ four point bending fatigue machine under an optical microscope. This system provided the possibility of continuously monitoring crack propagation during a fatigue test. Shot peening increases the fatigue life of aluminium alloy 2024-T351 over a wide range of stress levels. It was observed that the crack growth rate in peened specimens was at a minimum when the crack length was between 200-300 μm , which corresponds with the shot peening depth. Shot peening can be used for healing fatigue damage provided the crack length prior to peening is within the peening depth. For specimens with long initial cracks, shot peening has no healing effect and the endurance results coincided with those from unpeened specimens. For short cracks (between 200-300 μm) shot peening heals totally the prior fatigue damage which is manifested in the endurance results coinciding with the peened data for undamaged specimens, (figure 17) A fatigue crack model incorporating shot peening effects was used to derive the conditions for crack arrest and the results were presented in the form of a fatigue damage map (FDM). The FDM predicted accurately the fatigue damage healing ability of shot peening[50].

2.4.9 Fracture Toughness (G R Sutton, DERA Farnborough)

Further developments in plane stress K_R curve test methodology have been made. The use of a saw cut to simulate the initial fatigue crack has been verified for a wide range of aluminium alloys. Alternative methods of defining fracture resistance that would allow small test panels to be used have been reviewed. The most promising approaches were shown to be the crack-opening angle (CTOA) and energy dissipation rate (dD/da) methods. Although a lot of effort has been applied to developing the CTOA approach, further work is required to test the feasibility and repeatability of determining CTOA for a range of materials. Energy dissipation rate has been shown to offer a promising approach to deriving toughness values for real structures from small-scale tests, addressing the problems associated with determining the level of toughness needed to avoid catastrophic fracture in a particular structural application. Again, further work is required to clarify the geometry and crack length dependence of D and to understand the relationship of the method with the conventional R-curve approach. Also, a simple semi-empirical method of upward extrapolation of existing K_R curve data has been proposed which could allow valid critical stress intensity factors to be determined from comparatively small test panels.

2.4.10 Fatigue, Fatigue Crack Propagation and Fracture Toughness of ALFSOTATS Sheet (S Scott, British Aerospace Airbus)

A collaborative venture between British Aerospace Airbus, DERA Farnborough and British Aluminium has developed an aluminium lithium alloy defined as ALFSOTATS (Aluminium Lithium Fuselage Sheet Optimised for Toughness and Thermal Stability). Programme aims were to develop a damage tolerant fuselage skin material capable of achieving plane stress fracture toughness levels equivalent to that of alclad 2024-T3 sheet after a representative lifetime of thermal exposure due to the combined effects of high ambient temperatures and intense solar radiation. This work built on earlier experience with the 8090 RS-W alloy which has been reported previously.

Fatigue In general the fatigue endurance of ALFSOTATS tested in different environments and thermal exposure conditions was found to be superior to that of alclad 2024-T3 tested in air at room temperature. Fatigue properties of both plain ($k_t = 1$)

and notched ($k_t = 2.5$) specimens tested in the T-L orientation were characterised. Material was tested after different levels of thermal exposure, (no thermal exposure, 2000 hours at 90°C and 4000 hours at 90°C). The effects of different test environments (air at room temperature, air at -50°C and water) were also determined. For plain specimens the effects of chromic acid anodising were also determined.

The fatigue endurance of plain specimens was reduced by increasing levels of thermal exposure and by testing in water. Conversely, testing at -50°C improved fatigue endurance compared with that in air at room temperature. Anodising was found to provide an improvement in the endurance of thermally exposed material, but had no significant effect on unexposed material. The improvement associated with anodising was anticipated, and was similar to that observed in previous testing of 8090 RS-W material. The absence of improvement for unexposed material may be attributed to the testing being conducted at stress levels above the yield strength of the material, resulting in deformation of the substrate and cracking of the anodic layer.

The detrimental trends observed for plain specimens with respect to thermal exposure and testing in water were reversed for notched specimens. Testing at -50°C improved fatigue endurance compared to testing in air at room temperature.

Fatigue Crack Growth The fatigue crack growth performance of ALFSOTATS tested in either an unexposed or thermally exposed condition, in all orientations and environments of air or water, were substantially improved compared to alclad 2024 -T3 tested in air, with order of magnitude reductions in crack growth rates regularly apparent.

An extensive evaluation of the ALFSOTATS sheet has been made which involved an assessment of the effects of sheet gauge, test piece orientation, thermal exposure condition (material was tested in the unexposed condition and after both 2000 and 4000 hours thermal exposure at 90°C), and test environment (testing was conducted in air at room temperature, in air at -50°C, in water and in a 3.5% NaCl solution). 160 and 400mm wide CCT specimens were tested to establish fatigue crack growth rates over the range 7-50 MPa \sqrt{m} .

ALFSOTATS was found to be more isotropic in terms of fatigue crack growth than for 8090 RS-W with the difference between the (faster propagating) L-T orientation and all the other orientations being relatively small (figure 18). Testing at sub-zero temperatures was found to have little effect compared to testing in air at room temperature. In general thermal exposure had little effect on the fatigue crack growth performance of the material. Testing in water at 1 Hz was found to be similar to testing in air at 10 Hz (figure 19).

Tests were also undertaken to compare ALFSOTATS with alclad 2024-T3 tested using a simple block spectrum (1 cycle with $R = 0.1$ plus 10 cycles with $R = 0.7$, same peak stress). The tests were undertaken with 160mm wide CCT specimens tested in the L-T orientation. Results indicated that both materials tested using the block spectrum showed a reduction in crack growth performance compared to testing with $R = 0.1$. However, ALFSOTATS tested using the block spectrum was found to have a superior fatigue crack growth performance when compared with alclad 2024-T3 tested with $R = 0.1$.

Fracture Toughness Plain stress fracture toughness testing using 2m wide CCT test panels has been conducted. ALFSOTATS was shown to retain a high level of toughness even after prolonged exposure at elevated temperatures. ALFSOTATS thermally exposed for periods of up to 6000 hours at 90°C achieved greater or comparable levels of K_{IC} when compared with alclad 2024-T3 in an unexposed condition.

2.4.11 Development of Models for the Prediction of the In-Service Performance of Metal Matrix Composites (P M Powell and R Cook, DERA Farnborough)

DERA is participating in the Brite-Euram project 'Development of models for the prediction of the in-service performance of metal matrix composites (MISPOM)' along with Aerospatiale (France), Teksid (Italy), Erich-Schmid Institute (Austria), University Politecnica Catalonia (Spain), University of Ancona (Italy) and National University of Ireland Galway (Ireland). This three-year collaborative project commenced in April 1997 and will develop models to predict the static and fatigue behaviour of aluminium alloy based MMCs, reinforced with silicon carbide particulate. Two materials are being considered, namely wrought 2124-T4 + 17% SiC_p for aerospace applications and cast A359-T6 + 20% SiC_p for automotive applications.

A wide ranging programme of experimental characterisation is being carried out on the MMCs and on their unreinforced matrix alloys. This includes microstructural studies, residual stress measurement, tensile properties, S/N fatigue behaviour

and fatigue crack growth behaviour. DERA have studied the effect of stress ratio and stress concentration factor on the S/N fatigue behaviour of the MMCs and matrix alloys and have studied the fatigue crack growth behaviour of the 2124-T4 based MMC under constant amplitude loading and following overloads and underloads. Future tests will address the crack growth behaviour of the 2124-T4 based MMC under variable amplitude loading.

The experimental data is being used by partners to develop and validate micromechanical and fracture mechanics based models for predicting the fatigue performance of a helicopter rotor blade sleeve and an automotive brake drum under service loading. NUIG have modelled the static behaviour of the MMCs at the microscale using a finite element method (ABAQUS) and have obtained good correlation with the experimental data. They are developing the micromechanical models to predict the effect of microstructure (particles, porosity) on the fatigue behaviour. The R-curve threshold technique was used by Erich-Schmid Institute to predict the relationship between initial defect size and fatigue limit for the cast MMC and reasonable agreement was demonstrated with the experimental S/N data measured by DERA (see figure 20)[51]. DERA are also investigating the application of fracture mechanics based models (e.g. LOSEQ) to predict crack growth in the MMCs when subjected to overloads, underloads and variable amplitude loading. The final stage of the project will entail bench testing of the aerospace and automotive components under representative service loading, in order to assess and validate the models.

2.4.12 Fracture Resistance, Fatigue and Corrosion Fatigue of Candidate Weldable Aluminium Alloys for Primary Aircraft Structure (P M Powell, M W Squibb and G R Sutton, DERA Farnborough)

Welding offers airframe manufacturers the potential for labour saving assembly and increased cost efficient structures. At present however, welding of aluminium alloys is not generally approved or proven for airworthiness, mainly due to the historical inability to produce reliable defect-free welded joints. A collaborative research project, which has the aim of developing joining technology for the UK aerospace industry, has been carried out under the Innovative Manufacturing Initiative. The project is entitled “Cost Effective Manufacture: Welding Aerospace Materials (CEMWAM)” and includes sub-projects, which have addressed the structural welding of airframes using advanced welding process technology and the development of weldable airframe materials.

DERA has studied the damage tolerance of butt welded aluminium alloy sheet in a range of alloys, welded using the tungsten inert gas (TIG), plasma and metal inert gas (MIG) processes. The work demonstrated that the alloys could be welded successfully to produce good quality butt welds having consistent damage tolerance properties. In the damage tolerant alloys 2024-T3 and 6013-T4, R-curve fracture resistance was reduced by between 10 and 20% by TIG or plasma welding (see figure 21) and fatigue crack growth rates were up to five times faster in butt welds than in the parent sheet (see figure 22). In the higher strength 7475-T761 alloy, fracture resistance was reduced by up to 35% by TIG or plasma welding but little difference in fatigue crack growth rates were observed for butt welds and parent sheet. Welding of 8090-T34 aluminium-lithium alloy was shown to give rise to linear porosity along the fusion boundary and to prevent this, it was necessary to remove the surface of the sheet by milling prior to welding. It has been demonstrated however that the porosity had no significant effect on fracture resistance; the R-curves for welded 8090 panels were approximately 20 MPa√m lower than those for the parent alloy but the R-curves for the surface milled and welded sheet bracketed those for the unmilled sheet. The effect of the porosity on fatigue crack growth resistance is being assessed.

The corrosion fatigue behaviour of (TIG) and plasma butt welded joints of 6013-T4 and 2024-T3 alloys, in 3.5% sodium chloride solution, has been investigated and the results have been compared to those obtained in laboratory air. Radiographic and fractographic examinations of the welded joints have also been conducted. It was found that for 6013-T4 welded joints and parent sheet, fatigue crack growth rates were enhanced by a true corrosion fatigue mechanism at low values of stress intensity factor range (ΔK). For 2024-T3 parent sheet, evidence of stress corrosion fatigue was observed at a test frequency of 1 Hz, although this behaviour was not observed for the welded sheet. In addition, the fatigue performance of the welded 2024-T3 sheet was influenced by the position of the starter notch. Work is continuing and will evaluate two additional alloys, namely 7475-T761 and aluminium-lithium alloy 8090.

2.5 FATIGUE AND FRACTURE PROPERTIES OF METALS OTHER THAN ALUMINIUM

2.5.1 A Fundamental Investigation of the Effect of Dwell Time, Grain Size and Environment on the High Temperature and Creep-Fatigue Resistance of Turbine Disc Alloys (N J Hide and P A S Reed, Southampton University; M B Henderson, DERA Farnborough)

Sub-surface fatigue crack growth in turbine discs may lead to creep-fatigue in vacuum. High Cr content alloys are prone to σ phase formation (poor creep resistance) but are known to show better f.c.p. resistance. Small grain size is thought to promote grain boundary failure (through oxidation or creep) and promote irreversible slip (crack-tip plastic zone size containment) thus leading to more damage accumulation per cycle (poor f.c.p.). The γ' size effect is unclear as finer γ' increases slip heterogeneity affecting O_2 transport and possibly oxidation damage ahead of the crack tip. Finer precipitates may also be sheared more easily presenting a reduced resistance to crack advancement. This study considers f.c.p. behaviour of high Cr (U720) and low Cr (U720Li) alloys under cyclic and time dependent conditions in vacuum and air[52]. Variations in grain size and γ' size have also been studied.

In vacuum, cycle dependent behaviour is found at 650°C in both alloy variants, indicated by similar slopes (m values) of the crack growth curve and a predominantly transgranular cracking mode. Time-dependent behaviour is observed at 725°C in vacuum, with increasingly intergranular crack growth mechanisms observed at higher temperatures and longer dwell times. “True” creep-fatigue behaviour is apparently observed, with increased m-values under the most severe conditions indicating a contribution from static creep modes. In air, oxidation effects overwhelm any creep-fatigue behaviour and an intergranular oxidation mechanism of crack propagation predominates at all temperatures (similar m-values are observed at all temperatures). The lower Cr variant exhibits the best high temperature fatigue and creep-fatigue resistance. A larger grain sized variant of the low Cr U720Li alloy has been found to offer little advantage in the cycle dependent fatigue regime, but exhibits a significant improvement in creep-fatigue resistance.

Further work will evaluate the effects of γ' size variation on the high temperature fatigue and creep-fatigue mechanisms. By comparing the results from the grain size variant, then grain size and precipitate effects can be separated out. Interrupted tests will also identify the conditions ahead of the crack tip and FEG-SEM+EBSD techniques will allow subsequent elucidation of any element diffusion around the process zone as well as the degree of plastic damage ahead of the crack tip.

2.5.2 Fatigue Life Studies of Sigma SiC Fibre Reinforced Titanium Metal Matrix Composites (Ti MMCs) (M P Thomas, P H Tranter, D Martin and S Sweby, DERA Farnborough)

Low cycle fatigue behaviour of Ti-6-4 and Timetal 834 matrix MMCs, reinforced with two types of DERA Sigma fibre, is being studied. Tests are being performed over the temperature range room to 600°C, to simulate the gas turbine LP compressor environment. As well as fatigue-life curves, cyclic loads, strain and modulus are monitored throughout the tests. Data obtained from monolithic Ti specimens, fabricated using identical parameters as the MMCs, act as a baseline. Acoustic emission, emanating from fibre fracture and interfacial failure in the MMC specimens, is also collected and related to changes in cyclic strain. Figure 23 presents the S-N curves for one unidirectionally reinforced MMC, tested in the longitudinal orientation.

Additional studies are characterising the effect of the control mode (load or strain) on fatigue lives and damage accumulation in both monolithic and MMC material. The effect of the fibre orientation on fatigue lives of unidirectionally reinforced Ti MMCs is also being studied in both load and strain control.

Cyclic data obtained in these tests is being used to develop modelling techniques to predict the cyclic stress-strain response of Ti MMCs in gas-turbine component geometries.

2.5.3 Fatigue Studies of γ -TiAl-based Alloys (A Partridge, E F J Shelton and G F Harrison, DERA Farnborough)

γ -TiAl-based alloys have been identified as candidate materials for both high pressure compressor and low pressure turbine blades in future military and civil gas turbine aero-engines. TiAl alloys have a high modulus combined with a low density and excellent high temperature properties up to 700°C. However, they are inherently brittle and have very low fracture toughness compared to conventional alloys.

As part of an ongoing programme of work the tensile, creep and fatigue behaviour of two “XD alloys” (Ti-47Al-2Mn-2Nb-TiB₂/Ti-47Al-2Mn-2Nb-TiB₂) have been characterised. Constitutive equations and the relevant parameters needed to define the tensile, creep and LCF behaviour of these alloys have been developed which describe the material behaviour between room temperature and 750°C. The development of these equations have enabled lifing algorithms to be established and applied to conventional blade designs. This work has made a significant contribution to improving the understanding of the mechanical properties of TiAl alloys in the UK, and the ability to design and life TiAl components.

However, concerns do remain regarding the effect of Foreign Object Damage on TiAl components, due to their inherent brittleness and low fracture toughness. Therefore a further programme of work has been identified to assess the effects of damage and surface condition on the properties of TiAl components. Fatigue specimens with both cast and ground surfaces will be characterised, and the influence of introducing controlled damage (scratches) and uncontrolled (FOD) damage on the HCF/LCF behaviour will be assessed. The influence of complex loading on both specimens and components will also be evaluated and modelled. This work should lead to the formulation of a robust lifing strategy for TiAl components and increased confidence in our ability to predict safe lives for compressor and turbine components.

2.6 FATIGUE OF METALLIC JOINTS AND STRUCTURES

2.6.1 Scatter Considerations in the Interpretation of Major Fatigue Tests (A Cardrick, DERA Farnborough)

The author has considered how the philosophy used in deriving fatigue test factors for British military aircraft might be used to assist in the interpretation of the tests, to a minimum of twice the design service life, now required by FAR 25.571. The development of test factors has been traced from their introduction into AvP970 in 1959 to the present day. Reference has been made to the former use of a log₁₀ standard deviation of 0.176, the first measurements of the scatter of structures under variable amplitude loading (tests on Mustang wings) and the introduction of the ‘Safe S-N’ philosophy to enable account to be taken of the variation in scatter with endurance – the procedure has since been developed for adapting usage spectra for test purposes, identifying where supplementary evidence is needed to support these tests and positioning S-N curves for service loads monitoring. The application of this Safe S-N philosophy to the interpretation of the tests now required by the FAA, has been examined. Consideration has been given to the effectiveness of these tests, followed by tear-down inspections, in revealing those features which must be subject to a damage-tolerance evaluation and the extent to which the safe-life scatter factors might be reduced when failures originate from multiple-site damage (groups of nominally-identical features under the same loading). Finally, the author has considered how the Safe S-N philosophy might be used to derive the test factors needed to determine the inspection threshold (time to first inspection) corresponding to a prescribed probability of cracking, as might be required as part of a probabilistic analysis. This work will be described in a poster paper at the 20th ICAF Symposium.

2.6.2 Hawk – Structural Life Extension (R Shooter, British Aerospace MA&A, Brough)

The successful in-service operation of the Hawk aircraft in both flying training and weapons training roles as well as the Red Arrows aerobatics team led, in 1987, to the RAF requesting BAe to undertake a study to assess the possibility of extending the life of the airframe. A number of life extension targets were discussed, finally settling at 10200 Operational Hours, which equated to 15000 hours when viewed in terms of the normal acceleration design spectrum and 25000 Landings.

The main components of the life extension programme were:-

- a) The installation of a new wing standard to the Full Scale Fatigue Test, (FSFT), and its continuation as the Life Extension Fatigue Test, (LEFT).
- b) The assessment of items/components not fitted to the FSFT, such as the aileron which was tested separately and the flaps which had been cleared analytically.
- c) The assessment of build concessions (~5000), in-service modifications and repairs which were cleared against the original design requirements and again were not fitted to the FSFT.
- d) The development of modification, inspection and replacement strategies as required.

The volume of work generated from b) and c) in particular demanded that an efficient and systematic approach was developed, including the widespread use of Operational Loads Measurement (OLM) data and coupon testing where necessary. A poster paper describing the above programme will be presented at the 20th ICAF Symposium.

2.6.3 Fatigue Analysis of Obliquely-Loaded Lugs (S K Walker, British Aerospace MA&A, Brough)

Little information is currently available in published sources to allow estimation of fatigue life of obliquely-loaded lugs.

Stress concentration factors have been generated by finite element modelling of round-ended lugs with a range of width to diameter ratios. It was found by comparison with strain-gauge measurements that sinusoidally-distributed pin loading was inaccurate, particularly for low width to diameter ratio lugs. The use of non-linear elements to simulate contact between the pin and lug gave a much closer approximation of test results. Thirty-six load cases were run for each lug geometry representing varying pin loading angle.

The resulting database of stress concentration factors is being used as input to a computer program which will calculate fatigue life of lugs loaded at constant or varying pin load angle. The fatigue life will be either calculated internally via a nominal stress approach, or output of stress concentration factors will allow life to be calculated externally by other means, such as local strain analysis.

2.6.4 PC-9 Fatigue Testing “at a distance” (J Parish, British Aerospace MA&A, Brough)

The Pilatus PC-9 trainer has been developed from the PC-7 and certified under FAR part 23 regulations. There has been no full scale fatigue test (FSFT) of the airframe. British Aerospace (BAe) supplied the aircraft to the Royal Saudi Air Force (RSAF) from 1987. As co-ordinating Design Authority, BAe have underwritten the Fatigue Life of the airframe to satisfy RSAF requirements. However, the opportunity arose to participate in the Royal Australian Air Force (RAAF) FSFT program for their PC-9/A aircraft. This would give additional confidence in the airframe and assist in management of the structure over the full life of the aeroplane.

Two staff (an Aerodynamicist and a Structures/OLM specialist) were deployed for 18 months from mid-1993 to the Aeronautical and Maritime Research Laboratories (AMRL) in Melbourne to assist in the program, with a further Structures Engineer in support. Their main achievement has been the integration of the loads development activities with the rig design effort. The test formally started in December 1995 and had successfully completed the target life of 50,000 hours by February 1999. AMRL are now engaged on carrying out additional running to ensure full clearance for the structure, also clearance for some of the repairs that have been applied.

Once the BAe staff had finished their deployment, BAe continued to provide advice for the rig design and commissioning process and for the test-running phase, especially at the time of major reviews. In 1998 Pilatus also dedicated a Structures Engineer to AMRL to provide design information on repairs.

The main activity currently at BAe is to read the test data across to fatigue life clearance of the RSAF fleet, especially comparison of fatigue consumption and the possible application of inspection/repair techniques to the fleet. Pilatus are closely involved, covering the world-wide fleet of PC-9's as well as those for the RAAF and RSAF. One particular area that suffered damage was in the upper wing skin under mainly compression loading. AMRL, BAe and Pilatus all had a part to play in the design of the final repair at their respective offices, with BAe using their expertise in local strain fatigue analysis (Neuber) techniques.

2.6.5 Buffet Test Programme (R Randell and P C Cross, British Aerospace MA&A, Brough & Dunsfold respectively)

A number of test programmes are currently in progress to simulate buffet in combination with steady aerodynamic loads on large aircraft sections. This work is important for the clearance of aircraft extremes where dynamic contributions can be large and numerous when compared to steady manoeuvre loads.

A building block approach has been taken, from a proof-of-concept simple beam through to aircraft rear empennage testing. Using the vibration facilities, it is possible to control a number of response modes concurrently and work is continuing to develop an automated, combined buffet and manoeuvre load, flight spectrum.

One of these tests is being used to qualify, to United Kingdom requirements, the aft fuselage, fin and tailplane of Royal Air Force Harrier II Vertical/Short Take-Off and Landing aircraft. The structure in question is subjected to significant quasi-static manoeuvre loads, dynamic loads due to buffet at high Angles of Attack and jet turbulence on the ground. Previous Harrier II United States Marine Corps experience of fatigue cracking in the tailplane and UK fatigue predictions, which identified fatigue critical areas in the fuselage, have led to the need for a representative fatigue test. This would enable service aircraft to be flown safely without the need for extensive inspection requirements. The culmination of the development work was a test which could put the structure in multi-mode resonance under narrow band random excitation whilst under representative static manoeuvre loading. The fatigue test started running in June 1998 and reached 4,800 Equivalent Flying Hours in February 1999, producing useful results. It is due to restart in June 99; the test set-up is shown in figure 24.

A programme is about to commence on the development of test techniques to apply dynamic loads in combination with steady loads on major airframe fatigue test articles; initial work will be undertaken on the ex EF2000 development aircraft fatigue test article.

2.6.6 Hawk Tailplane (J A Anderson, British Aerospace MA&A, Brough)

Discovery of in service damage to the Hawk Tailplane has led to a detailed examination of the buffet environment experienced by tailplanes in service. The nature of the buffet was explored through Operational Loads Measurement (OLM) exercises which yielded the nature of the buffet in terms of magnitude, the frequencies at which the buffet was causing the tailplanes to resonate, the interaction of the buffet load with the mean load of the manoeuvre loading, the level of the buffet magnitude and the duration of buffet for any manoeuvre which induces the response. Analysis of the data produced fatigue allowables which were used for the design of the new tailplane. As fatigue testing formed part of the route to clearance for the newly designed tailplane, the data collected through the OLM exercise was used extensively to decide the testing spectrum which is formed by the excitement of 8 modal responses, 4 symmetric and 4 asymmetric and the level of manoeuvre loading. Known failures of pre-modification tailplanes were also used to correlate the theoretical spectra and the spectrum which has been applied to the test specimen.

The significant criteria for the test was to generate the correct modal response across the tailplane for each of the modes whilst simultaneously applying up to 4 modes, this was achieved with the use of a pair of electromagnetic shakers, one situated on the port side and one on the starboard side. Manoeuvre loading applied independently of the dynamic loading has been achieved by a more conventional wiffle tree and hydraulic actuator arrangement. Allowance for the mean manoeuvre load at which the buffet is applied to the aircraft is achieved through additional manoeuvre cycles, although the OLM data have shown that the level of the buffet mean load is much less than the peak tailplane load of a typical manoeuvre.

The test tailplane has been mounted on a rear fuselage (figure 25) and adjustments have been made through addition of ballast weights inside the fuselage such that the modal response of the tailplane was the same as that measured on the aircraft, confirmation of this was achieved by comparison of Ground Resonance Test results. Testing of the tailplane is currently underway with the program due to finish early 2002.

2.6.7 Multiple Site Damage (R Cook and A Young, DERA Farnborough; S Chamberlain and I Taylor, RAF)

Work to examine strategies for dealing with MSD in ageing aircraft structures is being performed at DERA in conjunction with the RAF, as described in the last UK ICAF review. Work on multiple column open hole coupons, 1.6 mm thick, has demonstrated that significant benefits in fatigue endurance can be obtained by cold expanding holes at which fatigue cracks have formed, and MSD is present. The programme showed that cold expansion was most beneficial where residual cracks were small, although crack growth was also slowed with cracks of up to 3mm present at 4.8mm diameter holes. Tests were also performed with lead cracks in addition to MSD type cracks. Lead cracks of 1, 2 or 4 fastener pitches were introduced prior to cold expansion. Benefits in fatigue endurance were found in all cases which accrued from crack retardation at successive holes as the lead crack propagated. Typical results are shown in figure 26 for 1 and 2 pitch lead cracks.

It was concluded that significant benefits could be gained from cold expanding holes in structures known to be susceptible to MSD. It was further recommended that this be carried out at an early stage of the life before any significant cracking was observed. The work is continuing and will examine the effectiveness of this procedure in lap and butt joints. Further work will also be undertaken to examine the effectiveness of over-pressurisation loads and composite patches to repair MSD where significant cracking has been found.

2.6.8 Assessment of Flaw Tolerance on the EH101 Airframe Structure (D Matthew, GKN Westland Helicopters Ltd., Yeovil)

In response to the 1989 changes to FAR/JAR 29, the certifying authorities (UK CAA and Italian RAI) required an assessment of the damage tolerance characteristics of the EH101 helicopter. A 'Fail Safe Design Considering Flaw Growth' approach was adopted and a major programme of testing and analysis undertaken to develop a viable method for application to helicopter structures. The test programme had four phases, each phase examined crack growth behaviour under progressively more complex load and geometry. In phase one, crack growth material data was generated for the aluminium lithium forging material (8090-T852) that forms the EH101 Main Load Path. The crack growth behaviour at R-Ratios of 0.1, 0.4, 0.7 and 0.9 was determined using compact-tension specimens. In phase two, structural elements representing the geometry of an 'I' section roof beam with a lightening hole were tested under constant amplitude load. Four tests were performed with artificially introduced flaws located at either the edge of the lightening hole or at the edge of the flange. In phase three, a full scale roof and side frame were tested under loads representative of three manoeuvre load levels. Cracks were successfully grown at three locations, though initiation of cracks from initial flaws proved difficult.

Each test from the first three phases was analysed using linear elastic fracture mechanics. The modelling procedure was refined based on the test results. The analysis demonstrated that flaw growth could be predicted to a reasonable level of accuracy. Flaw growth was then predicted at over thirty critical locations on the EH101 Main Load Path. The results showed that the high frequency vibratory flight loads cause rapid crack growth at short crack lengths, resulting in unacceptably short inspection intervals. Analyses of critical sites on the Lynx and Sea King airframe structures has led to similar conclusions to that on the EH101.

In the fourth phase, a full scale airframe (figure 27) was tested under low frequency manoeuvre and high frequency vibratory loads. An initial 5mm corner flaw was located on the top flange of a main roof beam. The crack was initiated using a factored load level and then grown under the representative flight loads. Fast fracture occurred when the crack was 10.5mm long after the equivalent of 28 flight hours. The fast fracture arrested at a lightening hole. After the equivalent of 0.6 flight hours, fast fracture occurred from the lightening hole and failed the rest of the frame (figure 28).

These results have led to the adoption of the 'Flaw Tolerant (Enhanced) Safe Life Approach' for the EH101 Main Load Path. An extensive programme of testing has begun using coupon specimens with either corrosion, impact or score damage. Reduced S-N curves derived from the test results will enable the generation of flaw tolerant safe lives.

2.6.9 Multi-Axial Fatigue Life Prediction of Ti-6246 Compressor Discs (P H Tranter, M B Henderson, G F Harrison, R Sahota, M J Lunt, M R Brown and D Painter, DERA Farnborough; R J Wilson, M Bache, J Evans and R Evans, IRC, University of Wales, Swansea)

Advances are being made in our ability to predict accurately the life of aeroengine Ti-6246 compressor discs. For such fracture-critical components it is necessary to declare lives so that the possibility of failure is extremely remote. Currently disc service lives are predicted using statistical analysis of results from full-sized disc spinning tests, where the low cycle fatigue life is given as the number of cycles required to nucleate an engineering crack of predefined dimensions. Nucleation and growth of such fatigue cracks is determined predominantly by the total equivalent stress range and maximum principal stress range respectively.

However, disc components with non-uniform sections are subjected to multi-axial cyclic loading owing to stress concentration features such as bolt holes and blade root fixings and thus the calculation of equivalent stress is not trivial. It is necessary therefore to use finite element (FE) methods to determine the equivalent stresses in the component. To this end, an extensive experimental programme is underway so that the constituents of constitutive FE models, such as an initial yield criterion and hardening rule, can be determined by correlation with results from specimens fabricated from actual Ti-6246

disc components. The construction of such constitutive models is further complicated because at high temperatures time-dependent (creep) deformation is active concurrently with low cycle fatigue deformation which can lead to over estimation of the relaxation of peak stresses. Therefore creep modelling is also included in the experimental programme as are non-proportional tension-torsion loading experiments and full-sized disc spinning tests.

Analysis of the results obtained to date, from plain Ti-6246 fatigued specimens, has shown that a rather complex modified hardening rule, combining components from other rules, predicts well the cyclic stress-strain behaviour of the material. The hardening rule is being used in the FE analysis of the multi-axial stress fields in notched specimens subjected to fatigue.

2.6.10 Prediction of Fatigue Life for Bolted Joints (W Zhu, British Aerospace Airbus, Filton)

In this project, a method has been developed to calculate the local stress in a bolted joint, which is used in combination with the material S-N curve and a multiaxial fatigue model to predict the fatigue endurance of the joint.

In order to determine the local stress, an analytical model has been developed to calculate the elastic stresses in a plate containing a fastener under any fastener load and remote applied stress. The results of this analysis have been validated against existing solutions and against finite element models. FE analysis has also been used to consider parameters which are currently not included in the analytical model (e.g. plasticity, friction between the fastener and hole and between the two plates, three-dimensional effects and clamping forces). As an example of this analysis, figure 29 shows the predicted stress around a titanium fastener in an aluminium plate. The multiaxial fatigue model is based on a combination of the maximum shear stress amplitude and the mean normal stress on the critical plane. The effect of the maximum shear stress on the fatigue life is also considered when the maximum stress reaches yield. However, more experimental data are required to determine the functional form of the relationship, and it may prove necessary to introduce other parameters, such as the equivalent shear stress amplitude.

The method has been used to predict the fatigue life of high load transfer joints with clearance fit fasteners, as shown in figure 30. In this case, the local stress was calculated through a 2D finite element analysis which included the effects of material plasticity, clamping force, friction between the fastener and the hole and friction between the plates. The friction between the two plates provides an alternative mechanism for load transfer, so reducing the stress at the edge of the fastener hole. A good agreement can be seen between the predicted endurance of the bolted joint specimens and the material S-N curve. However, it is apparent that there may be other influencing factors that were not included in this analysis.

In future work, the analytical model for calculating local stress will be extended to include plasticity, and load transfer due to friction between the two plates. The fatigue model will be improved to better represent the stress state of a bolted joint, and suitable parameters will be found to quantify fretting damage.

2.6.11 Full-Scale Panel Tests in Support of the A300 Life Extension Programme (S Kimmins and R Collins, British Aerospace Airbus, Filton)

Current operational statistics for the A300, the first generation Airbus, indicate that some early examples will reach their Design Service Goal (DSG) at the beginning of the next decade, at which point they would ordinarily be retired. However, as the aircraft continue to generate useful revenue, it has been suggested that the service life of the type be extended on economic grounds, provided that safety levels can be maintained. Airbus Industrie has therefore launched a general 'life extension' programme to justify these revised operational limits, and to allow the high-time A300 fleet to continue beyond 2003. This study will include an evaluation of the susceptibility of the design to Widespread Fatigue Damage (WFD), and the development of a programme for corrective action.

The prevention of WFD is central to the continued safe operation of ageing aircraft. In general, the primary source of test evidence in support of an assessment of Multiple Site Damage (MSD) or Multiple Element Damage (MED), the sources of WFD, follows from the full-scale aircraft structural fatigue test. It is generally recognised that full-scale fatigue test evidence is more accurate than the results of major component tests or coupon tests in predicting the fatigue endurance and the associated scatter in airframe structural components. Coupon or component test specimens are more likely than full-scale test specimens to have manufacturing processes, boundary conditions, and secondary load effects that are not fully representative of service aircraft. The experimental techniques adopted during coupon or components tests, such as the

environmental conditions and the cycle rate, may also be significantly different to that experienced by the aircraft during operational service.

Since the A300 full-scale wing fatigue test was limited to twice the DSG, the test does not provide evidence in support of continued operation beyond DSG. The A300 life extension programme will therefore include additional fatigue endurance and residual strength tests of the wing structure, with the specimens produced on a 'new-build' basis. The tests will be performed on full-scale (2m × 1m) panels representative of three areas of the wing structure identified as being susceptible to MSD/MED - the top and bottom chordwise skin joints at rib 9, and the stringer run-outs at rib 14. The test results will not be used directly to establish revisions to the inspection programme to prevent WFD; this will be done by analysis, using methods validated by the experimental evidence and calibrated against service experience

2.6.12 Methodologies for the Assessment of Widespread Fatigue Damage in Aircraft Wing Structures (R Collins and S Kimmins, British Aerospace Airbus, Filton)

In this study, the development of multiple site damage in typical wing structural assemblies was modelled. Simple analytical approximations were used to assess the fatigue aspects of the process, whilst an exact analytical approach formed the basis of the fracture mechanics calculations used to estimate the residual strength of a multiply cracked joint.

A probabilistic approach was used to model the crack initiation stage in a structure with multiple potential crack sites. The natural initiation of multiple fatigue cracks is linked to the fatigue endurance behaviour of simple laboratory test coupons, and a Monte Carlo procedure was used to generate a large number of different crack pattern scenarios. A deterministic approach was adopted to model the subsequent fatigue growth of cracks, with the assumption that a simple crack growth law, derived from single crack specimens, could be used. However, the fracture mechanics calculations requires that the interaction of adjacent cracks (or cracks with adjacent uncracked fastener holes) be allowed for, which was done in this study by using the approximate compounding approach to estimate the stress intensity factors. Although simplifying assumptions were made to facilitate the computational efficiency of the fatigue calculations, their accuracy was validated by supporting finite element studies.

These separate components were assembled into an overall methodology for the assessment of widespread fatigue damage in aircraft wing structures, which was used to investigate the behaviour of a number of representative test specimens. Current studies confirm other work in the field in that extensive secondary cracking can induce a significant reduction in the residual strength of a structure with a primary crack. The probability that such a scenario will develop can be determined using the procedures developed in this work, although the assumption of natural fatigue crack initiation makes such a scenario extremely rare. Scenarios of this type are more likely to develop if the scatter in the initiation process is reduced significantly, by corrosion for example.

2.6.13 Structural Maintenance of Ageing Aircraft (SMAAC) (S Kimmins and R Collins, British Aerospace Airbus, Filton; R Cook and A Young, DERA Farnborough)

The SMAAC (Structural Maintenance of Ageing Aircraft) project, which finished at the end of 1998, was a three-year collaborative research project partly funded by the European Union under the Fourth Framework Programme. The consortium of twelve partners included representatives from a range of European aircraft design, maintenance and overhaul organisations, as well as theoretical and experimental research centres.

As commercial aircraft approach the end of their original design service goal, there is an increased possibility of the development of Multiple Site Damage (MSD) or Multiple Element Damage (MED). These phenomena may eventually lead to Widespread Fatigue Damage (WFD), in which the residual strength of the structure is degraded below the required minimum level. The major objective of the SMAAC project was to develop methodologies and engineering tools for the assessment of MSD/MED, in order to determine the effect of extended service on the structural airworthiness of an ageing aircraft. This objective was addressed by:

- collecting in-service experience and data from teardown inspections, covering a wide range of the areas on the fuselage and wing identified as being susceptible to MSD/MED;
- conducting an experimental programme to enable detailed studies on different MSD/MED phenomena, including the influence of environmental effects such as corrosion on the development of MSD/MED, and

- developing and validating theoretical models, of different degrees of complexity, to assess the behaviour of structural components in the presence of MSD/MED.

As a result of these investigations, a common 'European' approach to the assessment of MSD/MED was established among the project partners. The conclusions of the SMAAC project have had, and will continue to have, a significant influence on discussions with regulatory authorities regarding continued airworthiness. The proposed methodology will be adopted in forthcoming ageing aircraft initiatives, and will enable revised inspection and maintenance programmes to be established in accordance with airworthiness requirements.

2.7 OTHER ASPECTS OF FATIGUE

2.7.1 Monitoring the Fatigue Exposure of Helicopter Components (A Cardrick, DERA, Farnborough)

Progress has been made in responding to the challenge of increasing the permissible fatigue lives of helicopter dynamic (rotating) components by providing a way of monitoring their fatigue exposure. Conventional loads-monitoring technology is difficult to apply because de-rotation problems inhibit the use of strain gauges for other than flight-test aircraft and the interpretation of parametric measurements is complicated by mechanical considerations. However, it has been recognised that for most components, the allowance for uncertainty in loading is sufficiently high and the stresses sufficiently low that there is scope to fit them with a miniature fatigue coupon that will indicate, by its fracture, when the component has received a prescribed amount of fatigue damage - the coupon always cracking well before the component, but having a substantially longer life than the permissible (safe) life of the component. There being no suitable miniature coupon available for this application, the feasibility of producing one has been examined. This has led to the definition of a prototype 'fatigue exposure indicator' (FEI) that seems likely to meet the challenging objectives that have been set. Exploratory tests have indicated that the coupons exhibit very low scatter and that, when they are fitted with miniature crack-growth gauges, it may be possible to monitor damage growth over the last 50% of the life. It is envisaged that, for service applications, the performance of the coupons, would be substantiated by fitting them to those components used for normal substantiation tests; the mean S-N curves for the coupons and the host components would then be located at the same time with no need for special component tests. The substantiation tests, which are done under mixed loading, would also reveal any significant differences between the cumulative damage characteristics of the coupons and the host components. For these substantiation tests and for production components, coupons, complete with crack gauges and a re-sealable connector, would be fitted under laboratory conditions. The whole would then be encapsulated to provide robustness and environmental protection; the encapsulated coupons would be termed 'Ladybirds' to reflect their small size and shape. At suitable maintenance intervals the [at-rest] crack-gauge readings would be taken in-situ. It is planned to develop Ladybirds with a range of cumulative damage characteristics so that component utilisation can be further increased by matching the Ladybird characteristics more closely to those of the component.

2.7.2 Fatigue Regulations for British Military Aircraft (A Cardrick and A Mew, DERA Farnborough)

There has been a second major review of the requirements since they were introduced in 1959. The new regulations, to be included in Issue 2 of Def Stan 00-970, overcome differences in interpretation that have arisen over the years, introduce improved compliance procedures and harmonise the aeroplane and helicopter requirements. Notable changes include the introduction of mandatory Operational Loads Measurement (Operational Data Recording for helicopters) and guidance on the use of the Safe S-N approach in adapting usage spectra for test purposes, identifying where supplementary evidence is needed to underpin tests and in positioning the S-N curves to be used in service loads monitoring.

2.7.3 The Effect of Environment on Fretting Fatigue (D B Rayaprolu, DERA, Farnborough)

The fretting fatigue behaviour of BS L65 aluminium alloy specimens in contact with steel or BS L65 pads has been investigated for various test environments, including air, water and water displacing penetrant WD40. Fretting pads were clamped onto two flat surfaces on each BS L65 specimen and fretting fatigue tests were carried out under constant amplitude loading at $R = -1$.

The fretting fatigue lives obtained in air with steel or BS L65 pads were much shorter than corresponding plain fatigue lives. At high axial stresses longer lives were obtained for BS L65 pads than for steel pads. These observations were consistent with corresponding variations in frictional coefficient.

When tests were carried out in the presence of WD40, rather than in air, significant improvements in fretting fatigue lives were obtained. Pad type had little effect, although slightly longer lives were obtained for BS L65 pads. When fretting fatigue tests were carried out in water, the lives obtained with steel pads were longer than in air but, in general, not quite as long as in WD40. For tests with BS L65 pads, the fretting fatigue lives in water were shorter than in WD40 and approached those in air. These observations were consistent with corresponding variations in measured frictional forces, i.e. the increased fatigue lives resulting from the presence of WD40 or water may be explained in terms of the observed reductions in frictional forces. For fretting fatigue tests where WD40 and water were sprayed alternately, average frictional coefficients and fatigue lives were similar to those observed for tests involving continuous spraying with WD40. Although relatively high frictional coefficients were observed initially in the presence of water, low values were rapidly obtained on application of WD40 and low average values were observed during subsequent alternate application of water and WD40.

Waveform analysis during fretting fatigue identified stick, micro-slip, macro-slip and slide regimes. In the presence of WD40, frictional force vs. axial force hysteresis loops were influenced by the rate of loading. In the case of similar metal contact, it was shown that fretting fatigue could lead to partial welding in the case of combined stick and macro-slip conditions. For $R = -1$ loading, with a peak stress of 140 MPa, it was shown that fusion occurred within the first 900 cycles of testing and that further fretting fatigue occurred mainly under stick conditions. Fast fourier transform analysis of frictional force data showed promise as a method for monitoring crack growth during fretting fatigue and will be investigated further. In addition, the effects of variable amplitude loading and surface treatments will be studied and an improved fracture mechanics model will be developed.

2.7.4 Boundary Element Analysis of Cracked Sheets Reinforced by Composite Patches (M H Aliabadi and D Widagdo, University of London)

In this project a new dual boundary element formulation is being developed for modelling cracked sheets reinforced by adhesively bonded composite patches. The formulation is the extension of the one developed by Salgado and Aliabadi[53] for isotropic patches. The discretization of the patches and corresponding region in the sheet into cells will be avoided through the use of fundamental and particular solutions used in the DBEM/DRM formulation, the crack boundaries can be excluded from the attachment regions boundary where the interaction between the sheet and patch takes place. Hence, after each increment of a crack propagation analysis, no changes are required to the existing attachment region even in cases where the sheet region overlaid by the patch contains a crack tip.

2.7.5 Thermal-Acoustic Fatigue Programme (P D Green, British Aerospace MA&A, Warton)

Endurance data for CFC/Nomex and SPF/DB Titanium sandwiches have been generated by random-amplitude vibration excitation of beams. This work[54] has shown that the integrity of “thin” sandwich panels under simulated acoustic loading are affected by design stress limits for Nomex core materials where particular ramp geometries are employed.

Three sheet corrugated core SPF/DB Titanium specimens have been tested and for the design tested, this has shown the landing to be more critical than the formed section. Depending on the magnitude of the RMS stress levels, failures were generated at the inner fastener line or at the bottom of the ramp diffusion bond line.

2.7.6 Thermal-Acoustic Stress Prediction Programme (P D Green, British Aerospace MA&A, Warton)

Structural response analysis tools are required by engineers who design and qualify structures subjected to severe environments such as acoustic, buffet and thermal sources. Structures exposed to these sources are also subjected to steady manoeuvre/steady in- or out-of-plane loads which modify the dynamic response making both stress magnitudes and accumulated cycles difficult to evaluate.

Analysis methods ranging from datasheets through to frequency- or time-domain finite element codes have been assessed and correlated against available test data. In most cases the level of stiffening caused by large deflection dynamic response, or by structures pre-stressed by tensile in-plane loads, is over predicted. A similar situation exists in panels with compressive

in-plane loads but here the complications caused by buckling make analysis difficult. Work is continuing to develop and fully evaluate suitable analysis methods and tools.

2.7.7 Thermal-Acoustic Test Facility (R Randell, British Aerospace MA&A, Brough)

The qualification of structures subjected to thermal-acoustic loads requires well proven and accurate tests to generate the required dynamic response. A new facility has been erected at the Warton site which will be capable of applying acoustic excitation at 175dB, with temperatures up to 300°C in combination with a range of in-plane loads up to 700KN on large structural elements.

Work to date has included facility running at 174dB with an acoustic progressive wave at grazing incidence to test articles in a duct. Efforts are continuing to provide the thermal loads within the duct and diffuse acoustic fields within or on the external wall of a reverberation chamber.

2.7.8 Strain-Life Data for Design (S H Spence, British Aerospace MA&A, Warton)

British Aerospace Military Aircraft has employed the local strain approach in the design process for fatigue durability for many years, particularly for the Goshawk T45A and some Harrier variants. A programme is currently underway extending the database to other materials and forms. This will allow the use of this fatigue lifing technique to be further extended across other aircraft structure where required.

Also within this programme of work is an evaluation of the effect of pre-strain on life. This involves testing at an applied strain amplitude which would give a life in the region of 10^7 cycles. However, the first cycle to be applied is of a significantly larger amplitude. The full database will be employed to investigate fatigue design curve rationalisation alongside a similar programme for stress-life data.

2.7.9 Effect of Service Temperature and Impact Damage on Bonded Composite Patch Repair of Aluminium Alloy Structures (P Poole, K Brown, D S Lock and A Young, DERA Farnborough)

Theoretical and experimental research has been carried out to investigate the effects of service temperature and impact damage on the efficiency of bonded composite patch repairs to aluminium alloy test pieces containing central, through-thickness fatigue cracks. CFRP and BFRP patches of similar stiffness were applied using a 120°C curing epoxy film adhesive. Some of the CFRP patches were manufactured with a layer of woven GRP on the surface to be bonded to the aluminium alloy specimen, and it was shown that the GRP layer had no significant effect on the retardation of fatigue crack growth due to patching. Thus, if it is necessary to use a layer of GRP to prevent galvanic corrosion, there will be no associated penalty of reduced patch effectiveness. An increase of the test temperature from ambient to 70°C resulted in very small reductions in crack growth rate for single sided BFRP or CFRP patched specimens. This observation was consistent with theoretical analysis which predicted that the opposing effects of reduced residual stresses and reduced adhesive modulus would result in a small reduction in crack growth rate. In contrast, for double sided repairs, a small increase in crack growth rate at 70°C was predicted. Theoretical analysis predicted that reducing the test temperature to -55°C would result in an increase in crack growth rate for patched specimens, owing to increased residual stresses having a greater effect than any accompanying increase in adhesive shear modulus. Fatigue testing at -55°C has not been carried out. However, when a single sided CFRP patched specimen was tested at -20°C, a significant decrease in crack growth rate was observed.

High energy impact [45 joules] resulted in severe damage of CFRP+GRP patches and acceleration of fatigue crack growth during subsequent testing of a double sided patched specimen. The increase in crack growth rate, and its variation with crack length, were consistent with theoretical predictions based on a conservative representation of the damage. Theoretical analysis of the effects of different forms of impact damage indicated that detailed information concerning the size and location of the damage was essential for accurate prediction of the effectiveness of damaged repair patches. Low energy impact [9 joules] resulted in localised patch damage and small increases in fatigue crack growth rate for double sided patched specimens. C-scans before and after fatigue testing did not detect significant growth of the damage introduced by either low or high energy impact. However, a narrow debond which developed at the patch/metal interface during fatigue testing was detected. In general, the effectiveness of the patch repairs predicted by numerical analysis was in very good agreement with that indicated by fatigue test results.

2.7.10 Repair of Battle Damage (P Poole, K Man and A Young, DERA Farnborough)

Theoretical and experimental research has been carried out to assess the use of adhesively bonded composite patches for the “permanent” repair of battle damage in aluminium alloy panels. The investigation involved the repair of simulated battle damage in the form of holes [up to 40mm diameter] with multiple cracks round the edges of the holes. Fatigue testing established that various damage configurations can be repaired effectively using precured carbon/epoxy patches bonded with a 120°C curing epoxy film adhesive. A 3-D BE/FE model was modified to allow the analysis of single and double-sided patch repairs to panels containing various hole/crack damage configurations, including multiple cracks at holes and kinked cracks. The model has been used to study the effects of damage configuration and crack front shape, as well as patch and adhesive variables. In general, good agreement has been obtained between theoretical predictions and experimental observations. Studies involving thick section repairs indicated that little improvement in patch repair efficiency was gained by reducing residual thermal stresses by the use of lower temperature curing materials. Work to investigate repair of surface battle damage in thick aluminium alloy sections commenced recently.

2.7.11 Exposure Trials on CFRP Patch Repairs (G R Sutton and P Poole, DERA Farnborough)

Earlier work has shown that fatigue damage in aluminium alloys can be successfully repaired using adhesively bonded CFRP patches. It was also shown that the durability of the patch bonds was good in hot/wet conditions. However, it was recognised that the exposure conditions used (2150 hours, 70°C, 84% RH, unstressed) were not particularly severe and that more searching trials were needed, using the materials that the RAF had adopted as standard. As a result two trials, comprising 6 years natural weathering under constant load at the hot/wet Pin Gin Hill cleared jungle and the Cowley Beach maritime sites in Australia, and 4 year exposure to cycling between 50°C/96% RH and –55°C, have been conducted. In the latter trial the patched panels were not under applied load, but the bond experienced considerable thermal stress during the –55°C phase of the cycle.

Pre-cracked 7075-T76 aluminium alloy test pieces were prepared for patching using a range of treatments which included grit blasting, silane swabbing and phosphoric acid anodising. Both pre-cured patches (bonded using epoxy adhesives) and wet lay-up patches were used. The panels for the natural weathering tests were primed and painted using a polyurethane topcoat.

For the panels exposed to the hot/wet/freeze cycle, it was clear that deterioration in patch performance occurred with exposure, particularly for wet lay-up patches. The wet lay-up panel treated by grit blasting only was completely disbonded with gross corrosion under the patch, whereas the panel with silane treatment was disbonded only at one corner only. Neither of the pre-cured, bonded patches showed any visual sign of disbonding at the edges.

The test panels for the natural weathering trials are currently being analysed. After exposure, the paint coatings were sound although slightly duller and faded. All except two panels withstood the exposure trial well, the exceptions being the wet lay-up panels from the beach site. These panels showed signs of lifting off after 5 years, and at the end of the 6 year trial these patches were completely disbonded with heavy corrosion over the patched area. At the end of the trial, all other panels were still fully bonded and showed no sign of degradation in fatigue performance when compared with the unexposed patched results. The wet lay-up patches from the jungle site showed an improvement in performance, probably due to an ongoing curing of the epoxy resin.

Panels containing central fatigue cracks have been repaired using pre-cured BFRP, CFRP or CFRP+GRP patches applied with a 120°C curing epoxy film adhesive. The CFRP+GRP patches had one ply of woven glass prepreg on the surface of the patch to be bonded. All panels have been exposed to 70°C/85%RH for 50 weeks. Fatigue testing in air at room temperature has commenced; additional tests will be carried out at 70°C/85%RH.

2.7.12 Fatigue Crack Patching (A S Ball and C Edge, British Aerospace MA&A Farnborough; P Poole, DERA Farnborough)

Work has been carried out to develop methods of repairing primary metallic aircraft structures using adhesively bonded composite patches. Following a review of known defects and potential applications of bonded composite patches, it was

decided that the early phase of the programme would investigate repair of a mechanically fastened splice joint and a wing spar.

A metallic splice specimen, representing a typical butt strap/splice configuration, was developed. The specimen was based on Harrier guidelines, using typical fastener pitches and assembly methods. The main objective was to demonstrate that bonded patches enhanced the fatigue performance of wet assembled splice joints when applied over counter-sunk fasteners. 20mm length fatigue cracks were grown from the central fastener holes in the two outer rows of holes. For selected specimens the two fatigue cracks were repaired using two precured CFRP patches bonded with a 125°C curing epoxy film adhesive. Constant amplitude fatigue testing established that patching reduced the rate of fatigue crack growth by a factor of 8; there was no evidence that significant debonding occurred during testing. However, it was shown that the fatigue performance of the unpatched wet assembled joints was influenced by the adhesive cure cycle, particularly if the cure temperature was increased from 125°C to 175°C.

Wing spar test specimens were cut from the rear spar of two scrap Hawk Mk1 wings supplied by the RAF. A 20mm long crack at a transfer hole in the spar web was introduced by spark erosion and fatigue loading. Constant amplitude fatigue testing under three-point bend loading established that patching was extremely effective in retarding crack growth. For example, patching was shown to arrest crack growth for 16.5 times the number of cycles it took the unpatched crack to grow 1mm. Furthermore, when the patch was removed from one specimen crack growth restarted within 750 cycles, which was 1% of the number of cycles the specimen achieved with the patch applied and no crack growth. There was no evidence of patch debonding due to fatigue loading. Compared to conventional metallic repairs, it was estimated that bonded composite patch repair of the spar web would result in manpower savings of 69% for repair application.

2.7.13 Repair of Wing Leading Edge Skin Structure on In-Service Commercial Aircraft by Solid Phase Welding (G E Shepherd, British Aerospace Airbus, Filton)

This project investigates the potential of using solid phase welding to repair skin cracks on in-service aircraft as a means of obtaining a better repair solution for the airline customer. The application of Friction Stir Welding in the In-service environment is being assessed and trials undertaken to explore the practical aspects associated with skin repair. The joining process requires a rotating tool to be plunged into the joint line of the material section. Frictional heat is generated by the tool, which contains the plasticised material under the tool head. The weld length is achieved by traversing the tool along the weld line and stirring the softened material together without it reaching melting point.

Coupon tests are being conducted to establish a life factor between the conventional skin structure and skin structure repaired by Friction Stir Welding. Fatigue analysis will be carried out to demonstrate the improved benefit that can be achieved by Friction Stir Welding to remove the notch created by the crack. For a conventional repair the crack may be stopped by a crack stop hole and reinforced by a skin plate for which the analysis considers a stress concentration for the notch and a stress reduction factor for the reinforcement. As the joining process will eliminate the notch, the local stress will be reduced, but the resulting fatigue life will need to be adjusted according to the life factor established.

Commercial and business implications, such as cost and benefit to the customer, are also being examined.

2.7.14 Integrating P-S-N Curves Over Non-uniform Stress Fields (D Shepherd, G Harrison, M Lunt, A Boyd-Lee, M Brown and M Henderson, DERA Farnborough)

The objective of the work is to provide the capability to integrate probabilistic S-N curves over arbitrary stress fields to give an estimate of the life distribution for components. This is achieved by deriving the equations giving the distribution of the life to failure as a function of both stress field and volume. However, this type of model differs from the conventional volumetric strength integrals common in the study of ceramics in that the random variable is cycles and not stress. Thus, the stress term only appears in the parameters of the model.

In this situation, the Weibull distribution suggests itself as a natural model, since it satisfies certain basic relationships with respect to volume. Initially, a simple 2-parameter based model was developed, which incorporates the assumption that the component has a non zero probability of failure for any life above zero cycles. However, this was subsequently extended by incorporating a more complex 3-parameter Weibull distribution which can account for features such as fatigue threshold and lower bounds for fatigue life. Also, a different approach has been developed which assumes that the life-to-first crack of a

component is distributed according to a lognormal density function. This has the advantage that it can be related to current aeroengine component lifing procedures much more easily, since the procedures which they use are based on Lognormal statistics.

2.7.15 Fatigue Life Prediction (R S Sahota, DERA Farnborough)

Mechanical loads of a cyclic nature are often experienced by aeroengine components such as blades and discs. Such conditions may induce failure in components with the choice of material and the component geometry being important factors in determining its occurrence. The ability to be able to forecast the transient mechanical behaviour is an important prelude to being able to predict failure. The fact that many elements of a gas turbine operate at high temperatures further accentuates the difficulty of this task

A study was carried out to compare and evaluate the material hardening rules available within the ABAQUS finite element package in order to discover whether or not they can be used to enhance fatigue life predictions. The relative merits of the isotropic, linear kinematic and nonlinear kinematic models were all investigated. Further work looked at the appropriateness of combining the isotropic and nonlinear kinematic rules.

The accuracy of each model was validated by comparing stress-strain hysteresis loops produced by a strain controlled uniaxial experiment with those of a finite element simulation. Peak stresses and total stress range were used to judge the suitability of particular models. The number of cycles to shakedown was also considered.

It was found that for the particular case under consideration (IMI 834 titanium alloy), the isotropic hardening rule gave a very poor portrayal of the characteristics associated with cyclic loading as seen in figure 31. No relaxation in the mean stress was evident and hence, with the exception of the first half cycle, the simulated hysteresis loops bore little resemblance to those produced by experiment. The prediction of total stress range was also poor.

The linear kinematic rule was also found to be unsuitable with again, extremely bad predictions of total stress range and the number of cycles to shakedown being a feature. The more advanced nonlinear kinematic rule was able to exhibit the phenomenon of stress-strain hysteresis loops dropping down along the stress axis. Cyclic softening was also in evidence but the simulation was still far from accurate. A number of attempts at improving the behaviour of the model failed and included modifying the input data used to describe hardening behaviour.

By contrast we can observe from figure 32 that the combined hardening model was found to produce an excellent prediction of the total stress range and cyclic softening was present throughout the simulation. Peak and mean stresses however were not described as well. Suggestions for further work centre on improving mean stress prediction by either modifying the isotropic component of the model or by altering the position of the yield surface in stress space by imposing a back stress.

FE models of notched specimens have been created for further testing and the analysis of LCF data supplied by a sub-contractor has been completed as a precursor to using the rules to help with the lifing of actual components.

2.8 FATIGUE PROPERTIES OF COMPOSITES

2.8.1 Fractographic Assessment of Fatigue Failures in Multi-directional and Woven Polymer Composites (M J Hiley, DERA Farnborough)

A fractographic study examining the micromechanisms of fatigue failure, under mode I (opening), mode II (shear) and mixed-mode (I+II) loading has been performed on unidirectional, multidirectional and woven carbon/epoxy laminates.

Initial 'in-house' fractographic studies examined the fatigue failure mechanisms in unidirectional laminates. Some work was also performed in conjunction with the European GARTEUR (AG20) Action Group on fractography. The aim of both studies was to characterise the fractographic features associated with fatigue failure in a range of unidirectional materials and to establish the use of these features for determining the rate and direction of crack propagation. A number of key fractographic features, including striations and matrix rollers were identified on many of the mode II dominated fracture surfaces. Striations were found in both the fibre imprints and occasionally within the matrix resin. The striations in the fibre imprints were oriented perpendicular to the crack growth direction and appeared either 'bright' or 'dark' depending on which side of the fracture surface was examined. A potential relationship between the crack growth direction and the

appearance of the striations, 'bright' or 'dark' was established. Several exceptions, which were attributed to fibre bridging, were however observed and further research is required to resolve these anomalies. The spacing of the striations, observed in the fibre imprints, was found to vary considerably across even a single fracture surface. The spacing appears to be influenced at very local level by stresses within the composite and the use of these features for determining crack growth rates appears limited. Fractographic studies performed on unidirectional materials, both 'in-house' and within GARTEUR (AG20) have now been concluded and reported[55].

Fractographic investigations have recently been extended to the examination of fatigue failures in laminates with plies of different orientations and those manufactured from woven fabrics. Mode I, mode II and mixed-mode delamination tests were performed, both statically and in fatigue, on multidirectional laminates containing 0/45 and 0/90 interfaces. Preliminary fatigue fracture surfaces were also generated in carbon/epoxy, containing a plain weave fabric. Significant differences were observed in the fracture morphologies of the two configurations of multi-directional laminate. Striations in the fibre imprints were observed on some of the mode II dominated fractures surfaces, but matrix rollers were not seen. Mode II dominated fractures generated in both the multidirectional and woven laminates were found to have one fracture surface that was resin rich and a mating surface that was fibre rich. The former tended to contain more striations within the fibre imprints. Initial studies of the fatigue fracture surfaces produced in the woven laminates, revealed the presence of striations in the matrix. At the point where the warp and weft fibres overlap, resin pockets were seen formed; this is where matrix striations tend to be observed. Preliminary experiments have also shown that R-ratio has a significant effect on the fracture processes occurring in polymer composites. Studies are currently evaluating the effect of R-ratio on fracture morphology.

2.8.2 Delamination Growth in Carbon-Fibre Structural Elements under Fatigue Loading (S Singh and E Greenhalgh, DERA Farnborough)

In this programme the fatigue behaviour of delaminations in tensile-loaded tapered structural elements was characterised experimentally, and analytical techniques for predicting such behaviour were assessed. The programme followed on from an earlier investigation into mixed-mode delamination growth in carbon-fibre coupons, results of which were reported at ICAF'97.

The structural elements, manufactured from carbon-fibre/epoxy matrix (Hexcel T800/924) pre-preg, were based on tapered ply drop-offs, as can be found at joints with stringers and at section changes. The specimens and their sub-laminates were balanced and quasi-isotropic (for short crack lengths the taper tips were unbalanced). Some of the specimens were curved. Delamination growth initiated from an artificial defect extending 10mm from the taper tip at 0°/0°, 0°/45° or 0°/90° strap/lap interfaces. Although the elastic load-displacement curves had the same gradient in all specimens, significant differences both in fatigue life and static strength were observed, depending on the interface and curvature. In 90°/0° specimens, crack-plane jumping[56] occurred immediately and the subsequent fatigue behaviour was very different from that of other specimens, which had stacking sequences chosen to generate single-plane delamination.

Strain energy release rates for the different specimens were evaluated using finite element analysis in conjunction with the virtual crack closure technique. The differences in the static strength were predicted using static mixed-mode (I/II) failure criteria; these were due to differences in the stiffness and in coupling terms of the unbalanced taper tip. When the finite element models were used to convert the load amplitudes to strain energy release rates, data obtained in this experimental programme fitted very well to the Paris curves previously measured for coupons. This indicates that these modelling techniques can be used in conjunction with coupon data to predict the behaviour in structural elements, when single-plane delamination is a valid assumption. It is becoming clear, however, that single-plane delaminations in real structures often do not remain single-plane[57,58].

The scatter in results, the steepness of the Paris plot and the narrowness of its domain result in the model being of far less value for composites than for metals (figure 33). Until better models are available, for components where delamination growth over short distances could prove critical, cyclic loads should be kept below the threshold levels for delamination growth[59], although limited smaller-scale degradation might be tolerated. The proportionately high fatigue threshold relative to static strength (when compared with metals) provides justification for accelerated testing by load truncation (though not by increased test frequency).

The next phase of work relating to delamination in structures will focus on developing realistic models for static failure, accounting for crack-plane jumping and statistical variation in properties; these will later be adapted for fatigue. A separate

new research programme will look at developing a general methodology for predicting fatigue life of composites under conditions not primarily governed by delamination growth. DERA and FFA (the Aeronautical Research Institute of Sweden) have been sharing information and comparing results relating to delamination fatigue and may collaborate in this area in the future.

2.8.3 Characterisation of Fatigue Crack Growth in Smart Hybrid Laminate Materials (M M Singh, J P Dakin, T S P Austin and P J Gregson, Southampton University; P M Powell, DERA Farnborough)

Hybrid laminates consist of alternate aluminium alloy and polymer composite laminae. The aim of the present work is to develop a unified model for crack growth and damage mechanisms encountered within the hybrid laminate, where fatigue cracks initiate at through-thickness fastener holes. Of particular interest is the interaction between regions of delamination associated with fatigue cracks and the fatigue crack growth rate. Incorporating fibre optic strain sensors into the fibre reinforced plastic laminae allows both experimental assessment of the fatigue damage process, and may provide an important in-situ monitoring tool in structural applications.

To minimise disruption, and hence deterioration, of the composite matrix, procedures for processing and embedding require that the optical fibres are carefully prepared. Fibres must be stripped of UV absorbent polymer buffer prior to the laser write process, after which a silane treatment is required to optimise the glass/epoxy interface. These techniques are already standard procedure in the telecomms and FRP industries respectively and, with a degree of care, facilitate reliable production of embedded sensors. Problems specific to the hybrid laminate that have been encountered include sensitivity to embedding losses and sensor reflectivity, but both have been addressed successfully. During the present investigation[60-63], hybrid laminate panels consisting of a single layer of unidirectional CFRP sandwiched between two layers of AA8090 have been manufactured. During the lay-up process a series of five fibre optic lines, each contained 8 in-fibre Bragg sensors distributed non-linearly over a 20mm length, have been embedded at 5mm intervals, the first located 20mm from the centre line of the panel. A multiplexing interrogation system has been implemented, continuously monitoring all 40 sensor locations during fatigue loading. In conjunction with an in-situ 'dry' C-scan technique for monitoring delamination development, load transfer in the fibre bridging region has been quantified. These results are being used to validate a three-dimensional finite element model of the crack growth/delamination process which incorporates crack growth behaviour in the skin alloy, the evolution of the delamination zone during crack growth and the load redistribution that occurs with ongoing crack growth.

2.8.4 The Fracture Resistance of Fibre Reinforced Metal Laminates (G R Sutton, DERA Farnborough)

Research on the damage tolerance of new and novel materials has included evaluation of the fracture toughness of glass fibre reinforced metal laminates (GLARE) in the presence of fatigue cracks. Plane stress fracture toughness tests have been conducted on three forms of typical aerospace structural GLARE laminates in the transverse orientation, i.e. at right angles to the design loading direction, on panels containing through-thickness cracks. Also, the effects of various amounts of fatigue damage on fracture toughness in panels loaded longitudinally, and the effects of limited buckling, have been evaluated.

The transverse fracture toughness properties of the GLARE materials were significantly affected by the type of aluminium alloy/glass fibre lay-up used. For laminates with balanced glass fibre lay-ups (i.e. equal number of fibres in the longitudinal and transverse directions), there was little effect of fibre orientation; the through-thickness-crack fracture toughness properties were dominated by the properties of the metallic unclad 2024-T3 layers. However, the transverse fracture toughness of a laminate with an unbalanced glass fibre lay-up was 17% less than in the longitudinal direction.

It was also shown that fatigue produced an area of delamination at the metal/prepreg interface which started to form at the fatigue initiation site. For a wide range of fatigue stress levels, and associated delamination areas, only a relatively small effect on the subsequent apparent fracture toughness occurred and the toughness integrity of the laminates was maintained.

Uncontrolled buckling in the region of a fatigue crack for a thin laminate, with one layer of cross ply glass prepreg between two aluminium alloy layers was shown to introduce a significant effect on toughness. Although the fatigue crack growth rate was unaffected by an increase in buckling, the toughness was reduced by 9%; however, the laminate material still outperformed the unclad 2024-T3.

2.8.5 Ceramic Matrix Composite Lifting (P M Farries, M P Thomas and R Sahota, DERA Farnborough)

The high temperature strength and stability of CMCs make them serious candidates for application in future gas turbine combustion and nozzle systems. A pacing technology, which is inhibiting application, is the lack of design data and appropriate lifting methodologies. Work has recently been started on the mechanical characterisation and modelling of ceramic matrix composite materials (CMCs) with the aim of formulating generic analysis and lifting methods for such materials. Testing will be carried out under conditions relevant to application of these materials in aeroengines. Low Cycle Fatigue testing at temperatures up to 1200°C will be included in the programme, as well as tensile and creep tests.

2.9 FATIGUE OF JOINTS AND COMPONENTS OF COMPOSITE MATERIALS

2.9.1 Fatigue of Adhesively Bonded Joints (I A Ashcroft, D J Hughes and S J Shaw, DERA Farnborough)

The aims of this work are twofold: firstly to investigate the failure mechanisms of adhesively bonded joints in fatigue, and secondly to develop the capability to predict the performance of adhesively bonded joints in service. Most of the experimental work has been concerned with CFRP materials bonded with epoxy adhesives, however, some work on the joining of PEEK and GFRP has also been undertaken. In service, environmental effects can significantly affect the performance of bonded joints and a major part of the current work has been an examination of the effects of temperature, humidity and pre-ageing on the fatigue performance of bonded joints. Other variables investigated include the effect of ply lay-up with CFRP adherends, the effect of joint geometry and the use of paste adhesives instead of film to investigate cost effective manufacture. A design methodology has been created based on a stress analysis and fracture mechanics approach. Lap-strap samples have been used to study fatigue crack initiation thresholds in unidirectional CFRP joints bonded with an epoxy film adhesive[64,65]. Temperature had little effect on the fatigue threshold for unaged joints tested at ambient humidity, however, there was a change in the dominant fracture path. Interlaminar failure of the composite was dominant at low temperatures whilst cohesive failure of the adhesive dominated at higher temperatures. Specimens that were aged in a humid environment and tested under high humidity at ambient temperatures showed little difference to those unaged. However, ageing in a humid environment and testing at high temperatures resulted in a large reduction in the fatigue threshold. A combination of temperature and high moisture content is therefore extremely detrimental to the fatigue resistance of these bonded joints. This was attributed to a lowering of the glass transition temperature of the adhesive by absorbed moisture, which meant that the test temperature was close to the reduced T_g of the adhesive. Results with a multidirectional CFRP substrate showed similar trends, with respect to environmental performance, to the unidirectional CFRP, but at significantly reduced threshold loads. This was consistent with both a stress analysis of the joints and calculations of strain energy release rates in the joints at failure.

Double lap joints with both unidirectional and multidirectional CFRP substrates bonded with an epoxy film adhesive were tested at -50, 22 and 90°C to produce S-N curves. The fatigue thresholds were significantly lower at 90°C for both substrate types. This difference to the behaviour of the lap-strap joints was attributed to the fact that creep of the joints was constrained in the lap-strap joint but not in the double lap joints. The existence of creep in the double lap joints at 90°C was confirmed by monitoring the increase in maximum displacement in fatigue at constant load amplitude. The multidirectional adherend joints were stronger than the unidirectional joints at -50 and 22°C, which was consistent with a stress analysis of the joints using maximum principal stress as a failure criterion. At 90°C, however, the unidirectional joints had the greater fatigue resistance. This could also be explained with the stress analysis, as the stresses in the middle of the joint were higher with the multidirectional adherend making it more susceptible to creep. Fracture paths in these samples were complex, but again showed a tendency to shift from the composite at -50°C to the adhesive at 90°C. Double lap joints were also used to construct S-N curves at room temperature, using two different MD lay-ups and a paste adhesive. One substrate type had 0° plies at the surface, the other had 45° plies. The failure mechanisms and fatigue threshold loads were similar for both substrate types.

Double cantilever beam specimens with unidirectional CFRP substrates bonded with an epoxy film adhesive were fatigue tested in displacement control at -50, 22 and 90°C. Again, there was a tendency for the locus of failure to shift from the composite at low temperatures to the adhesive at high temperatures. The static fracture energy, G_{Ic} , increased with increasing temperature, as did the fatigue threshold, G_{Ith} . This is illustrated in figure 34. DCB specimens with CFRP substrates and an epoxy paste adhesive were also tested[66]. Two ply lay-ups were used to encourage failure in the composite or the adhesive. The results showed that G_{Ith} and G_{Ic} were significantly greater for the adhesive than for the composite.

Single lap joints with CFRP adherends bonded with an epoxy paste adhesive were fatigue tested in load control to construct S-N curves. In this work, it was seen that removal of the adhesive fillet drastically reduced both the static strength and fatigue threshold, whereas reducing the bondline thickness improved both properties. Sandwich lap-shear joints were used to investigate the effect of test environment and pre-ageing on the fatigue performance of GFRP and CFRP adherends bonded to plasma-treated PEEK with epoxy film adhesive[67]. The results showed a deterioration in the fatigue resistance of the joints under both hot and cold conditions, and also under high humidity.

Work in progress is focusing on pure mode II and mixed-mode bend testing. In addition, fatigue threshold loads are being studied on lap-strap specimens manufactured by co-bonding, where the adhesive and composite and adhesive are cured in a single curing schedule.

2.9.2 Lynx Composite Tailplane Fatigue Substantiation (J Nickolls, GKN Westland Helicopters Ltd., Yeovil)

Due to the uncertain dynamic environment of helicopter tail structures, higher than anticipated loads were measured on the original Lynx metal tailplane. Various attempts have been made to address this, including reduction in span, addition of weights, and aerodynamic modifications. None of these have prevented limitations in the fatigue life, leading to frequent and difficult inspections. Therefore, a replacement composite unit has been designed which can be fitted without alteration of the surrounding aircraft structure (figure 35).

The new design consists of a tapering circular spar made from 44 plies of uni-directional carbon and glass pre-preg material. Spanwise glass and carbon plies provide the required strength and stiffness in bending, while +/-45 carbon plies satisfy the torsional requirements. The spar is bonded into the existing root end cuff with steel shear pins included in case of bond failure. An aluminium reinforcement is bonded inside the cuff to support the spar against local contact loads. The tailplane skins are two plies of woven glass pre-preg, bonded to a Rohacell foam core, which is in turn bonded around the spar. There are Stycast 2651 filled epoxy resin reinforcements top and bottom at the root end of the spar. Inboard and outboard closing ribs, and the trailing edge Gurney flap, are also made from woven glass.

Two fatigue tests were performed, a bare spar and a tailplane assembly. A bare spar was loaded to Ultimate Static Load prior to commencement of fatigue testing. Fatigue test loading was derived from high frequency flight loads measured on the existing metal standard tailplane. Loading was applied offset from the spar, at the centre of pressure, via a rig fitting clamped and pinned through a reinforced section of the spar. A single load level was applied, conservatively assuming that the maximum values of flap and lag bending, and torsional moment, occur together and in phase. A factor of 2.08 was included to account for strength and flight load variability. A total of 2.5×10^6 cycles were completed without failure or any sign of distress in the spar. After completion of the fatigue test, a residual static test demonstrated a strength of 1.73 times composite factored Limit Load.

A tailplane assembly fatigue test was performed to confirm the strength of the skins and foam core. Fatigue test loading was derived from flight test measurements using the new design. Loading was distributed over the tailplane lower skin via a whiffle tree, with the jack load at the centre of pressure, aft of the spar. A single load level was applied, which included the same 2.08 factor as the spar test and an additional 1.2 extrapolation factor. A total of 1.0×10^6 cycles were completed without failure. A residual static test demonstrated a strength of 1.34 times composite factored Limit Load.

The results of the fatigue tests were analysed against flight loads, demonstrating unlimited fatigue life. Fatigue Reserve Factors for the main components were 1.01 for the foam core, 1.11 for the spar, and 1.31 for the skins.

2.10 NON-DESTRUCTIVE EVALUATION

2.10.1 A Systematic Approach to the Selection of Economic Inspection Methods and Intervals (S H Spence, British Aerospace MA&A, Warton)

This study addressed the factors which must be considered when selecting inspection techniques and determining the associated inspection periods[68]. Fatigue related inspections are required when the safe life of a structure is less than the target service life (as a result of shortcomings in design, changes in usage, etc.) or where structural integrity support by inspection has been identified by a damage tolerance analysis. The increase in life extension programmes arising due to

contracting defence budgets is leading to an increasing dependence on inspections. Under these circumstances the structural integrity of a fleet or individual aircraft is safeguarded by inspection for fatigue cracks.

This study[68] specifically considered the inspection and repair of fastener holes, since the majority of fatigue cracks in airframe structures occur at such features. The inspectable crack size, inspection interval and cost are interdependent. The smaller the crack inspected for, the longer will be the period of growth to reach a maximum acceptable size. However, the associated preparation, inspection and down time costs will be greater. Further, for a given inspection technique, the probability of detection will be lower for a smaller crack and the chances of a false call are likely to be higher.

By optimising the inspection process, life-cycle cost benefits can be realised without compromising structural integrity. A schematic approach was developed in which a balance may be struck between inspection effectiveness, required inspection interval and the associated costs. This will enable the end users to determine the most economic maintenance programme provided that the effectiveness of potential inspection techniques can be sufficiently quantified.

2.10.2 Eddy Current (EC) Imaging and Inversion (D J Harrison, DERA Farnborough; J Bowler, Surrey University)

A. High frequency EC inversion methods for fastener hole inspection

A theory of eddy current interaction with surface cracks in the thin-skin limit was developed using a scalar Hertz transverse magnetic potential approach. The theory reduces the change in impedance of an EC coil due to the presence of a crack to three components each of which can be evaluated by a single integral along the crack mouth, greatly reducing computational time. This theory was initially used to calculate the EC response from long slots, showing good agreement with experimental data for both aluminium and mild steel.

A crucial feature required for the inspection of fastener holes is the ability to detect and measure cracks growing from corners at the edges of the layers or possibly around the fastener countersink. The theory was first extended to calculate the interaction with a rectangular slot, again showing very good agreement for both materials. The next step was to show that the EC interaction with slots of a much more realistic geometry than the rectangular slot could be calculated by first performing a conformal mapping to transform the slot geometry to an equivalent rectangular domain. The transformation could be carried out for semi-elliptical slots or for any smooth crack which can be represented sufficiently accurately by a series of elliptical cycloids. Using these solutions for realistic crack shapes the theory was used to predict the impedance changes for the four symmetric and asymmetric slots used in a TTCP collaborative programme, and again good agreement with experimental data was obtained.

Following the successful development of the forward models in the thin-skin theory, the model for curved slots was used as the basis for an inversion algorithm. The algorithm used the forward model to calculate the expected impedance changes as the coil is scanned along the crack axis, iteratively refining the assumed crack shape to minimise the error between the predicted impedance changes and the experimental. This was tested using data from the TTCP programme. The results showed that the algorithm could give a good representation of the slot profiles within about 10 iterations for the semi-elliptical slots and 35 iterations for the asymmetric ones. The accuracies obtained were within 10%, the algorithm showing a slight tendency to underestimate the maximum depth. The study concluded with an assessment of the application of the method to fastener hole inspection. The thin skin model has also been used to investigate the effects on EC inspection of current leakage across the face of a partially closed crack.

B. Inversion methods using transient eddy currents

A method of analysing the transient eddy currents was investigated using a Green's function formalism which would be suitable for incorporating in an inversion algorithm. The theoretical method used for describing the transient eddy current response to a planar crack followed the method which had been used successfully in the case of continuous excitation, by representing the crack as a sheet of current dipoles. An initial experiment to verify the theory compared predictions of the transient field to experimental measurements using a plate containing a rectangular slot cut into the blind side. Measurements and calculations were performed at several points along the length of the slot. These showed a reasonable agreement. It was noted that the calculation is very sensitive to the distance from the surface to the nearest point on the defect. In parallel studies the theoretical modelling of transients was investigated for a range of probe types and geometries, providing further verification of the capabilities of the forward models.

Following the successful calculation of the transients in the forward problem, the method was incorporated into an iterative inversion algorithm. This was tested using an aluminium specimen with an asymmetric slot cut in the blind side. The method was shown to give a good fit to the known slot profile, however it required almost 300 iterations to achieve this. It was noted that the algorithm was able to reproduce the slot profile most effectively where the slot approaches closest to the surface of the conductor, requiring only 120 iterations for this. The remainder of the time was required to give a good fit to the remainder of the slot profile.

Finally, the ability of the transient inversion scheme to represent volumetric defects such as corrosion was considered. A volume integral formulation was presented showing how the interaction between a transient eddy current and a defect in an unbounded medium could be calculated by a similar technique, again representing the defect by a cavity enclosed by a surface of current dipoles.

2.10.3 Detection and Characterisation of Corrosion (E A Birt, D A Bruce, D J Harrison, L D Jones and R A Smith, DERA Farnborough)

DERA has investigated the use of the following techniques for the detection and characterisation of corrosion:

- Conventional, single frequency eddy current methods
- Multi-frequency EC methods
- Transient EC methods
- Ultrasonic methods

DERA participated in an international comparative study of corrosion detection methods organised by TTCP. The study involved circulation to all of the participants of three specimens from the Canadian Institute of Aerospace Research specimen library. The specimens were sections of Boeing 737 lap joints, chosen to contain areas of suspected light, medium and heavy corrosion. Other participating laboratories used various eddy current, ultrasonic, thermal and optical methods for detection and quantification of the corrosion.

DERA participation included the use of each of the four above-mentioned techniques. EC and ultrasonic techniques were able to detect and map areas of suspected corrosion, although there were some notable differences between the findings of ultrasonic and EC methods. In particular it was found that measuring changes in the amplitude of reflected ultrasound provided the most sensitive technique. The areas of corrosion measured from amplitude changes were consistently greater than those observed in time of flight scans. The assignment will be concluded with a destructive examination of the panels to verify the results.

2.10.4 Adhesive Bond Inspection (D A Bruce, DERA Farnborough)

There is still an urgent need for an effective technique for bond inspection due to the adoption of bonded primary structure and repairs. The current state of the art is such that only gross faults such as disbonds can be detected with any confidence, although ultrasonic methods can detect suspect areas which may be partially bonded. A DERA-sponsored project at Imperial College investigating detection of environmental degradation of adhesively bonded aluminium joints suggested that environmentally driven failure mechanisms depend on moisture penetration through free volume along the interfaces rather than through the adhesive as had been thought. This suggested that there may be a secondary characteristic of the interfaces, such as inadequate penetration of the oxide layer, which might be detectable and which would give warning of poor environmental performance. A follow-on research project at Imperial College has investigated this effect. The results appear to show that it is not possible to detect any precursor of the environmental damage prior to the occurrence of a disbond. Loading of the specimens to cause failure has, however shown that cavitation occurs within the adhesive resulting in the formation of many microscopic voids around the disbond front. These can be detected by normal incidence ultrasound at a high frequency (50MHz).

2.10.5 Ultrasonic Array Transducers (R A Smith and S J Willsher, DERA Farnborough)

In order to speed up the fairly laborious hand scanning currently undertaken using single transducer systems like the DERA-developed Andscan[®] to characterise defects such as impact damage, the use of ultrasonic array transducers has been investigated. Novel array transducers have been developed in partnership with Diagnostic Sonar Ltd. and Buehler Krautkramer, specifically designed for use with scanning systems. The multiplexed active elements provide an array of overlapping square

transducers, incorporating the multiplexing electronics in the probe head. Trials of the array probes with the Andscan[®] system have shown that it is capable of inspecting a complete Harrier mainplane in only 6 hours.

2.10.6 NDE Reliability and Life Management (D A Bruce, DERA Farnborough)

The use of NDE to guarantee the integrity of a structure implies a knowledge of the reliability of the technique. Determining Probabilities Of Detection (PODs), or any other index of NDE performance, is a costly procedure and methods which can be used in the future to provide an inexpensive method of verifying inspection performance or a more efficient method of using the information would be valuable. In the past, efforts to gain NDE reliability data from service experience have not been successful possibly due to lack of data. The AGARD structures and materials panel identified this as a possible area for collaborative work. DERA have investigated the effects of using small samples and field inspection data to predict NDE performance and corresponding safety levels by the use of simulations. Existing methods for POD determination have been shown to suffer from systematic errors causing overestimation of the POD for large defects. Otherwise the use of a 95% confidence limit estimate for the POD is usually too conservative and results in excessively pessimistic estimates for the safety level. Alternative methods of interpretation, including a technique based on Bayesian inference which appears suitable for systematic incorporation of field data to refine safety level estimates, were shown to have considerable potential. This was presented at a NATO RTO workshop in 1998. The work will continue under a Canadian-led working group.

2.11 DESIGN DATA (A C Quilter, ESDU International plc, London)

During the period under review, ESDU International has extended and updated both the Fatigue – Endurance Data and the Fatigue – Fracture Mechanics Series with the issue of the following Data Items.

Data Item No. 97018 Standard fatigue loading sequences

The Item provides descriptions and analyses of three standard loading sequences for use in the fatigue assessment of aircraft structures. The three sequences presented are TWIST (and Mini-TWIST), FALSTAFF (and ENSTAFF) and Helix/Felix. A disk containing the loading sequences for each of the standards will be issued in due course.

Data Item No. 81031 Fatigue crack propagation rates and threshold stress intensity factor ranges for aluminium alloy plate, extruded bar and forgings

Data Item No. 81031 was updated in 1998. The updated Item included new data for two materials, 5083 and 6061 plate, and additional data for the 7010 alloy already featured in the Item. The opportunity was taken to revise the text in the Item to take account of recent developments in the field of fracture mechanics, particular attention being paid to the effect of stress ratio on fatigue threshold.

Data Items on CD ROM

Many of the past eighteen months have been spent converting all the Data Items in the ESDU Series to electronic format in order that they may be issued on CD ROM. The conversion process has involved re-typing the text and re-plotting the figures for all the Data Items; this work was completed in 1998 and both the Fatigue Series are now available on CD ROM. The electronic version of the Series includes comprehensive search facilities coupled with an index of all ESDU Data Items and software. Work on providing the facility of web delivery of Data Items and software is currently in progress.

Current Work

Data Item No. 97024 Derivation of endurance curves from fatigue test data including run-outs

Work on this Data Item is very nearly complete. The Data Item will be accompanied by two versions of a Fortran computer program; the two versions of the program are identical with the exception that one version provides graphical as well as numerical output. The method used by the program is applicable to data for both metallic and non-metallic materials as well as to data from tests on coupons or specimens representing structural features. The method deals with the low-cycle, high-cycle and endurance limit regimes. The program takes account of censored data such as run-outs in a mathematically

rigorous manner. The program also allows the user to make use of any knowledge of the expected shape of a particular curve by allowing certain parameters to be predefined, thus constraining the shape of the curve. The program output includes the equation of the derived curve, the coefficient of variation of the data, a measure of the goodness-of-fit of the curve to the data, and, depending on which version of the program is used, a plot of the curve and the data.

Data Item No. 99002 Computerised crack resistance curves

Work on this Data Item and the accompanying computer program is nearing completion. The Data Item presents a program based on the method described in Data Item No. 85031. The program uses either data from Item No. 85031 or data provided by the user to determine either the fatigue crack length that will cause fast fracture of a component under a given applied stress or vice versa. The program runs as a module within the Microsoft Excel spreadsheet program.

Data Items Nos. 82015 and 84003 Fatigue crack propagation rate data

Data Items Nos. 82015 and 84003 which give crack propagation rate data for titanium alloys and high alloy and stainless steels respectively are currently being updated. The updates will include the extension of the data for alloys already featured in the Items and the addition of new data for alloys not currently featured in the Items. The opportunity will also be taken to update the text of the Items to take account of recent developments in the field of fracture mechanics.

Cumulative damage program

Work on a Fortran program to perform cumulative damage calculations is in progress. The program will accompany Data Item No. 95006, "Fatigue life estimation under variable amplitude loading using cumulative damage calculations". That Data Item presents methods of estimating the fatigue life of a component subjected to variable amplitude loading and it is one of these methods, the rainflow method, on which the program is based.

Metallic Materials Data Handbook, ESDU 00932

Work on providing the Metallic Materials Data Handbook in the form of an electronic database is currently in progress. Two forms of database are envisaged, one based on the Microsoft Access database package and another that will form part of the MSC M-vision package. Both versions will include extensive search and information retrieval facilities and the latter will allow integration with various finite element analysis packages. The completion of both versions is planned for the summer of 1999.

2.12 REFERENCES

- [1] P Poole, Review of aeronautical fatigue investigations in the United Kingdom during the period May 1995 to April 1997, *DERA/SMC/SM2/TR970108*, (1997).
- [2] P E Irving and R A Hudson, The contribution of health and usage monitoring systems to calculations of damage state and future life of helicopter components under safe life and damage tolerant design, In: *Exploitation of structural loads/health data for reduced life cycle costs*, RTO-MP 7 Brussels, (1998).
- [3] P E Irving, J E Strutt, R A Hudson, K Allsop and M Strathern, The contribution of fatigue usage monitoring systems to life extension in safe life and damage tolerant designs, *Paper 19-1, CEAS forum on Life Extension – Aerospace Technology Opportunities*, Cambridge, Pub. RAeS, (1999).
- [4] L P Pook, An alternative crack path stability factor, ECF 12-Fracture from Defects, (Eds M W Brown, E R de los Rios and K J Miller), *EMAS*, pp 187-192, (1998).
- [5] T Dirgantara and M H Aliabadi, A new boundary element formulation for analysis of shear deformable shells, *International Journal of Numerical Methods for Engineering* (1999)
- [6] P H Wen, M H Aliabadi and A Young, Boundary element method analysis for shear deformable shallow shells, (to be published).

- [7] P H Wen, M H Aliabadi and A Young, Transformation of domain integrals to boundary integrals in BEM analysis of shear deformable plate bending problems, (*to appear in Journal of Computational Mechanics*).
- [8] P H Wen, M H Aliabadi and A Young, Boundary element method analysis for stiffened shear deformable plate, (to be published).
- [9] P Fedelinski, M H Aliabadi and D P Rooke, The Laplace transform DBEM method for mixed-mode dynamic crack analysis, *Computers and Structures*, **59**, pp 1021-1031, (1996).
- [10] P Fedelinski, M H Aliabadi and D P Rooke, A single region time domain BEM for dynamic crack problems, *Int. J. Solids and Structures*, **32**, pp 3555-3571, (1995)
- [11] P Fedelinski, M H Aliabadi and D P Rooke, Boundary element formulations for the dynamic analysis of cracked structures, *Engng Anal. Bound. Elem.*, **17**, pp 45-56, (1996).
- [12] P H Wen, M H Aliabadi and D P Rooke, Mixed-mode weight functions in three-dimensional fracture mechanics, *Dynamic, Eng. Fracture Mechanics*, **59**, pp 577-587, (1997).
- [13] P H Wen, M H Aliabadi and D P Rooke, Cracks in three dimensions: A dynamic dual boundary element analysis, *Comput. Methods Appl. Mech. Engrg.*, **167**, pp 139-151, (1988).
- [14] P H Wen, M H Aliabadi and A Young, A time-dependent formulation of dual boundary element method for 3D dynamic crack problems, *Int. J. Num. Methods for Engrg.*, (1999).
- [15] P H Wen, M H Aliabadi and D P Rooke, Three-dimensional dynamic fracture analysis with the dual reciprocity method in Laplace domain, *Engineering Analysis with Boundary Element Method*, pp 51-58, (1999).
- [16] P H Wen, M H Aliabadi and A Young, Dynamic analysis of crack problems by boundary element method, *Proc. ACME 99*, pp 203-208, (1999).
- [17] R A Tomlinson and E A Patterson, Measurement of residual stress associated with fatigue cracks, *Proc. SEM Conf. On Exptl. Mech.*, Belluvue, Washington, USA, pp 317-326, 1997.
- [18] J D Carazo-Alvarez and E A Patterson, The application to mixed mode cracks of a general methodology for automated analysis of caustics, In: *Experimental Mechanics*, I M Allison (ed.), Balkema, Rotterdam, pp 1217-1222, 1998.
- [19] R L Burguete and E A Patterson, The effect of friction on crack propagation in dovetail fixings of compressor disc, *Proc. I Mech. E., Part C*, **212**, pp 171-181, 1997.
- [20] S Gungor and E A Patterson, , A photoelastic determination of stress intensity factors for corner cracks in a bolted joint, *Trans. ASME JOMAE.*, 119(4), pp 276-280, 1997.
- [21] J W Jobbs, E A Patterson and R L Burguete, Photoelastic analysis of crescent shaped cracks in bolts, *Proc. Spring SEM Conf. On Exptl and Appl. Mech.*, Houston, Texas, pp 128-131, 1998.
- [22] R A Tomlinson, A D Nurse and E A Patterson, On determining stress intensity factors for mixed mode cracks from thermoelastic data, *Fat. Fract. Engrg. Struct. And Mater.*, 20(2), pp 217-226, 1997.
- [23] H Batchelor, E A Patterson and J R Yates, Detection of fatigue crack closure using thermoelastic stress analysis, *Proc. ASME 17th Int. OMAE Conf.*, 1998.
- [24] E R de los Rios, C A Rodopoulos and J R Yates, Fatigue damage design principles of fibre-reinforced titanium matrix composites, *Fatigue in New and Ageing Aircraft* (Eds. R. Cook and P. Poole) EMAS, Birmingham, pp 1051-1062, (1997).

- [25] E R de los Rios, C A Rodopoulos and J R Yates, Damage tolerant fatigue design in metal matrix composites, *Int. J. Fatigue*, **19**, 379-387, (1997).
- [26] E R de los Rios, C A Rodopoulos and J R Yates, The fatigue behaviour of metal-matrix composites under single overloads, *Fat. Fract. Engng. Mater. Struct.* **21**, 1503-1511, (1998).
- [27] Liwu Wei and E R de los Rios, Micro-fracture mechanics based modelling of fatigue crack growth in aluminium alloy Al 7010-T7451 under random loading, *Fracture from Defects* (Eds. M W Brown, E R de los Rios K J Miller) EMAS, Birmingham, 37-42, (1998).
- [28] C Vallellano, A Navarro and E R de los Rios, Application of microstructural fracture mechanics to shot peened components, *Fracture from Defects* (Eds. M W Brown, E R de los Rios K J Miller) EMAS, Birmingham, 145-150, 1998.
- [29] N Glinos, P G Wagstaff and R Cook, The influence of corrosion on the fatigue and fracture behaviour of 7050-T76 aluminium alloy specimens containing cold expanded holes, *Proceedings of the 21st ACS congress, Melbourne, Australia*, (1998).
- [30] R Cook, N Glinos and P Wagstaff, Role of surface pitting corrosion on effectiveness of hole cold expansion, In: *Fatigue in the presence of corrosion. NATO RTO Meeting Proceedings MP-18*, (1998).
- [31] A A Garcia-Granada, D J Smith and M J Pavier, A new procedure based on Sachs' boring for measuring non-axisymmetric residual stresses, Accepted for publication in *Int. J. of Mechanical Sciences*, (1999).
- [32] D J Smith, V Lacarac and M J Pavier, Growth of small fatigue cracks in the presence of residual stresses, Presented at *Engineering Foundation Conference*, Hawaii, USA, Dec, 1998, to be published.
- [33] A A Garcia-Granada, V Lacarac, D J Smith, M J Pavier, R Cook, and P Holdway, 3D residual stresses around cold expanded holes in a new creep resistant aluminium alloy, In: *4th Int. Conf. on Surface Treatment*, Assisi, Italy, (September 1999).
- [34] G Bussu and P E Irving, Fatigue performance of friction stir welded 2024-T351 aluminium joints, to be *Presented at 1st International Symposium on Friction Stir Welding*, California, (June 1999).
- [35] R G Buller, Investigation of helicopter loading spectra variations on fatigue crack growth in titanium and aluminium alloys, *PhD Thesis*, Cranfield University, (1999).
- [36] P E Irving and R G Buller, Prediction of fatigue life under helicopter loading spectra for safe life and damage tolerant design, In: *Fatigue and fracture mechanics, 29th volume*, Eds. T L Panotín and S H Sheppard, ASTM STP 1332, (1999).
- [37] R Cook, PC Wood, S Jenkins, D Matthew, P Irving, I Austen and R Buller, The development of a robust crack growth model for rotorcraft metallic structures, In: *Application of damage tolerance principles for improved airworthiness of rotorcraft*, NATO RTO Meeting Proceedings, (1999).
- [38] J Boselli, P Pitcher, P J Gregson and I Sinclair, Secondary phase distribution analysis via finite body tessellation. *J. Microscopy*, in press, (1999).
- [39] J Boselli, P Pitcher, P J Gregson and I Sinclair, Quantitative assessment of the effects of particle distribution and morphology on fatigue in Al-SiC_p composites. *Proc. ICAA6, Toyohashi*, **3**, pp 1927, (1998).
- [40] J Boselli, P Pitcher, P J Gregson and I Sinclair, Quantitative assessment of particle distribution effects on short crack growth in SiC_p reinforced Al-alloys, *Scripta. Mater.*, **38**, pp 839, (1998).

- [41] O Femminella, M J Starink, M Brown, I, Sinclair, C J Harris, and P A S Reed, Data preprocessing/model initialisation in neurofuzzy modelling of structure-property relationships in Al-Zn-Mg-Cu alloys, accepted for publication in *I.S.I.J.*, (1999).
- [42] Y Liu, I Sinclair, and P J Gregson, Extended slip band mixed mode fatigue crack growth in an AA8090 Al-Li alloy, In: *Engineering Against Fatigue*, Rotterdam: Balkema, 381, (1998).
- [43] M D Halliday and C J Beevers, Automation of fatigue crack growth data acquisition for contained and through-thickness cracks using eddy-current and potential difference methods, In: *Automation in Fatigue and Fracture: Testing and Analysis*, ASTM STP 1231 (Edited by C Amzallag), pp 164-185, (1994).
- [44] M D Halliday, P Poole and P Bowen, In-situ SEM measurements of crack closure for small cracks in aluminium 2024-T351, *Fat. Fract. Engng. Mater. Struct.*, **18**, pp 717-729, (1995).
- [45] J Z Zhang, M D Halliday, P Poole and P Bowen, Crack closure in small fatigue cracks – a comparison of finite element predictions with in-situ scanning electron microscope measurements, *Fat. Fract. Engng. Mater. Struct.*, **20**, pp 1279-1293, (1997).
- [46] M D Halliday, J Z Zhang, P Poole and P Bowen, In-situ SEM observations of the contrasting effects of an overload on small fatigue crack growth at two different load ratios in 2024-T351, *Int. J. Fatigue*, **19**, pp 273-282, (1997).
- [47] J Z Zhang, M D Halliday, P Bowen and P Poole, Three dimensional elastic-plastic finite element modelling of small fatigue crack growth under a single tensile overload, Accepted for publication in *Engineering Fracture Mechanics*, (1999).
- [48] M D Halliday, P Poole and P Bowen, New perspective on slip band decohesion as unifying fracture event during fatigue crack growth in both small and long cracks, *Mater. Sci. and Tech.*, **15**, pp 382-390, (1999).
- [49] I Roungos, The effect of sequential action of corrosion and fatigue on crack initiation and propagation in 2024-T3, Cranfield University MPhil, (1999).
- [50] E R de los Rios, M Trooll and A Levers, Improving the fatigue crack resistance of 2024-T351 aluminium alloy by shot peening, CEAS Forum: *Life Extension - Aerospace Technology Opportunities*, Cambridge, UK, pp 26.1-26.8, (23-25 March 1999).
- [51] B. Tabernig, P M Powell and R Pippan, Resistance curves for the threshold of fatigue crack propagation in particle reinforced aluminium alloys, In: *Fatigue Crack Growth Thresholds, Endurance Limits and Design*, ASTM STP 1372, Edited by J.C. Newman and R.S. Piascik, American Society for Testing and Materials, West Conshohocken, PA, (1999).
- [52] N J Hide, M B Henderson, A Tucker, and P A S Reed, to appear in *Proc. ICM8*, British Columbia, (May 16-21, 1999).
- [53] N Salgado and M H Aliabadi, The boundary element analysis of cracked stiffened sheet, reinforced by adhesively bonded patches, *International Journal of Numerical Methods in Engineering*, **42**, pp 195-217 (1998).
- [54] Study of thermal acoustic fatigue in ASTOVL aircraft structures - Phase 2, *BAe-WSS-RP-RES-SOR-000330*.
- [55] M J Hiley, AG-20 Fractographic aspects of fatigue failure in composite materials, GARTEUR Final Report TP112, May 1999.
- [56] S Singh and E S Greenhalgh, Micromechanisms of interlaminar fracture in carbon-epoxy composites at multidirectional ply interfaces, *Plastics, Rubber & Composites, Processing & Applications*, **27**, (1998).
- [57] E S Greenhalgh, and S Singh, Investigation of the failure mechanisms for delamination growth from embedded defects, *12th International Conf. on Composite Materials (ICCM-12)*, Paris, France, (5-9 July 1999).

- [58] E S Greenhalgh, S Singh, and K-F Nilsson, Mechanisms and modelling of delamination growth and failure of carbon-fibre reinforced skin-stringer panels, *Symposium on Composite Structures: Theory and Practice*, ASTM Committee D-30, Seattle, USA, (17-18 May 1999).
- [59] S Singh, and E S Greenhalgh, Interlaminar fatigue behaviour of epoxy-matrix composites: Implications for design and certification, *8th European Conf. on Composite Materials (ECCM-8)*, Naples, Italy, (3-6 June 1998).
- [60] J P Dakin, T S P Austin, P J Gregson, D K Guerrier, and K J Trundle, Miniature, multiplexed fibre-grating-array sensor for the interrogation of localised strain patterns during crack growth studies upon hybrid laminate panels, *SPIE Symposium Industrial and Environmental Monitors and Biosensors*, Boston, Proc. SPIE 3541B-38, (1998).
- [61] T S P Austin, M M Singh, P J Gregson, J P Dakin, and P M Powell, Damage assessment in hybrid laminates using an array of embedded fibre optic sensors, *SPIE Symposium Industrial and Environmental Monitors and Biosensors*, Boston, Proc. SPIE 3541B-28, (1998).
- [62] T S P Austin, P J Gregson, J P Dakin, P M Powell, and M M Singh, Fatigue damage in carbon fibre reinforced aluminium alloy laminates, *5th International Conference on Deformation and Fracture of Composites*, London, Conf. Proc. pp 191-200, (1999).
- [63] T S P Austin, M M Singh, P J Gregson, J P Dakin, and P M Powell, Numerical simulation of fatigue failure in carbon fibre reinforced aluminium laminates, *Proceedings of Computational Methods and Experimental Measurements IX*, Eds. G M Carlomagno and C A Brebbia, WIT Press, Sorrento, pp 47-56, (1999).
- [64] I A Ashcroft, D J Hughes and S J Shaw, Mixed mode fatigue testing of bonded composite joints, *Structural Adhesives in Engineering V*, Bristol, (1998).
- [65] I A Ashcroft, D J Hughes and S J Shaw, The effect of temperature on the fatigue of bonded composite joints, *Euradh 98, 4th European Conference on Adhesion, Germany*, (September 1998).
- [66] I A Ashcroft, D J Hughes, MT06.2 Bonded Joints: Progress Report FY 98-99, *AMCAPS-MC/TNM/H6/0000/13306*, (March 1999).
- [67] I A Ashcroft, R P Digby, S J Shaw, The effect of environment on the performance of bonded composite joints, *DERA/MSS1/TR980026/1.0*, Structural Materials Centre, DERA Farnborough, 1999.
- [68] S H Spence, A Systematic approach to the selection of economic inspection methods and intervals, *Proceedings of NATO R&T AVT panel Workshop, Airframe Inspection Reliability Under Field/Depot Conditions, Brussels*, (May 1998).

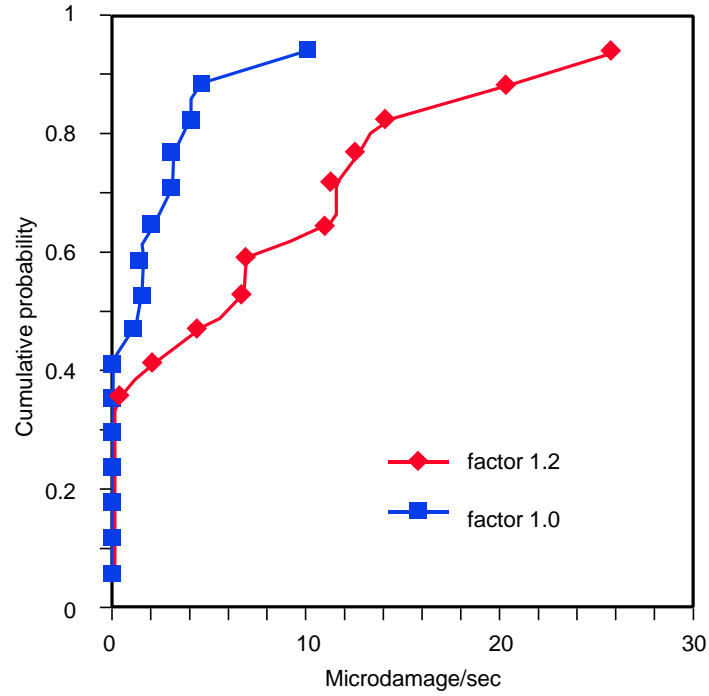


Figure 1 Cumulative distribution of damage rates for control reversal manoeuvres with loads factors of 1.0 and 1.2

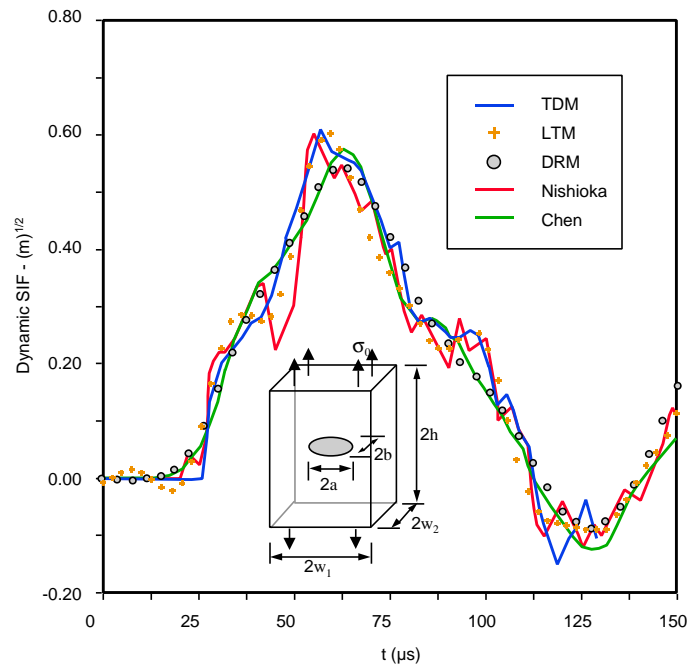


Figure 2 Dynamic stress intensity factors for an elliptical crack

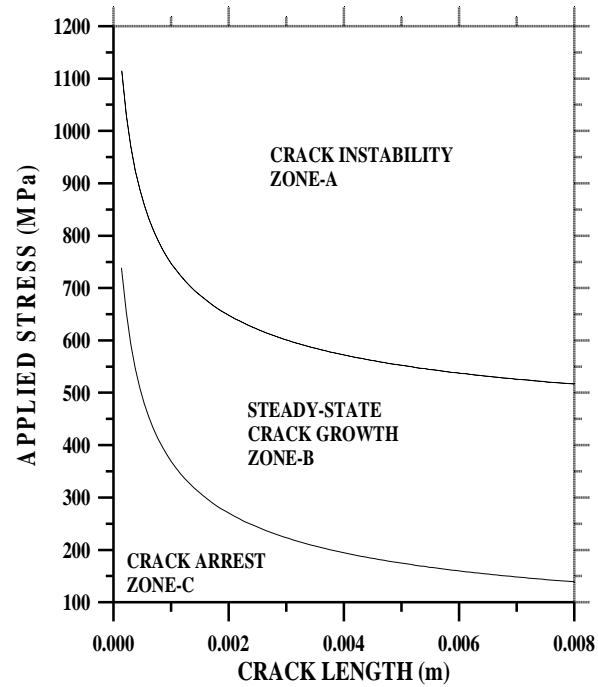


Figure 3 Fatigue damage map of MMC

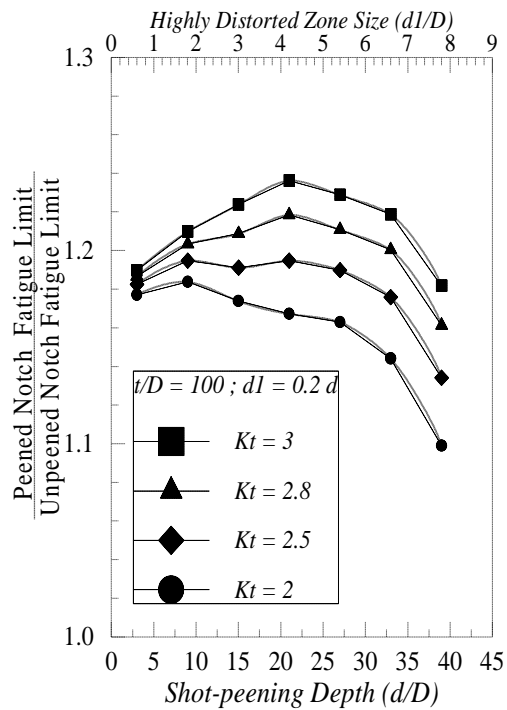


Figure 4 Effect of peening intensity and notch geometry on endurance limit

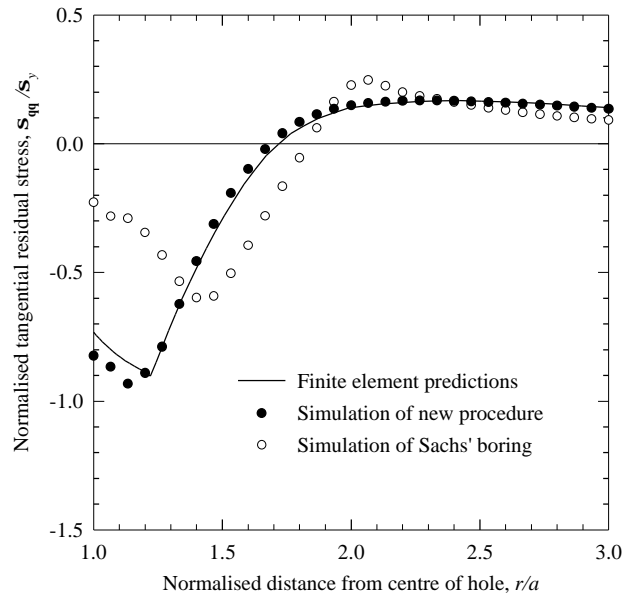


Figure 5 Comparison of tangential residual stress distributions in the vicinity of a cold worked hole.

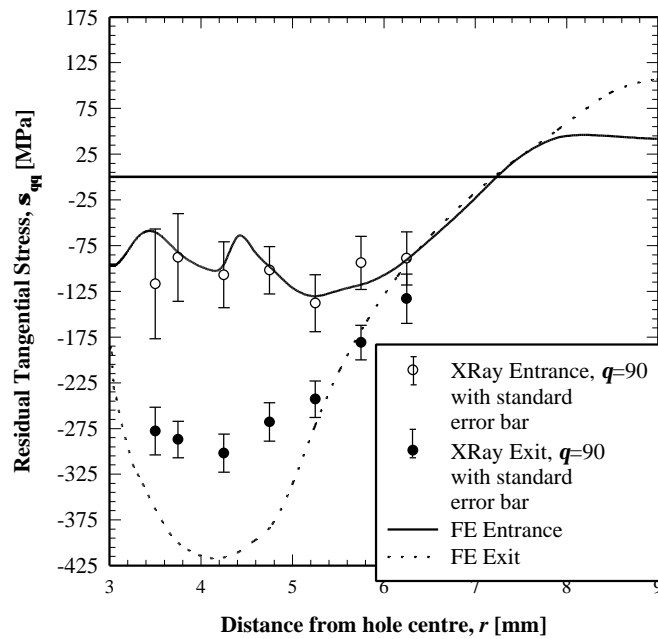


Figure 6 Comparison of surface tangential residual stresses obtained from finite element analysis and X-ray measurement

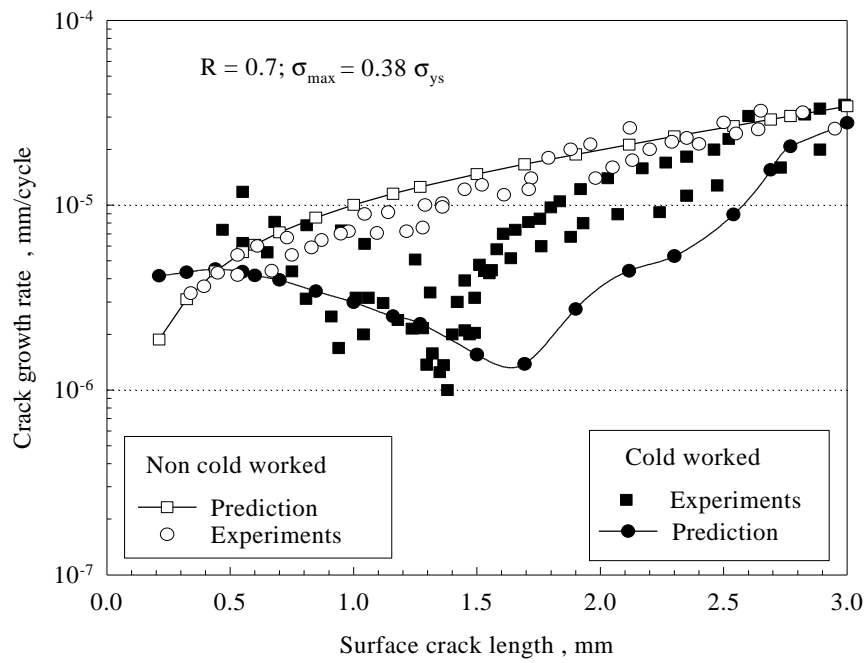
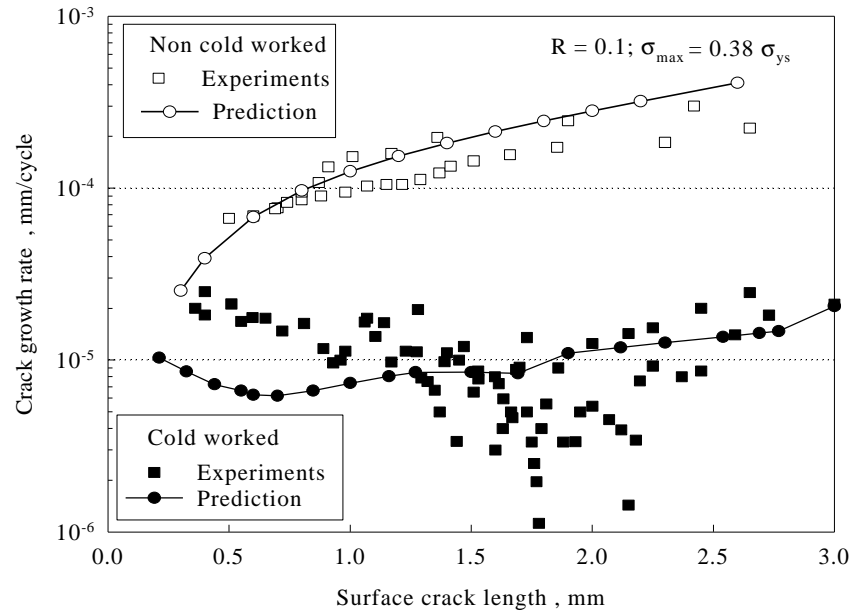


Figure 7 Fatigue crack growth rates from non-cold worked and cold worked fastener holes in aluminium alloy 2650

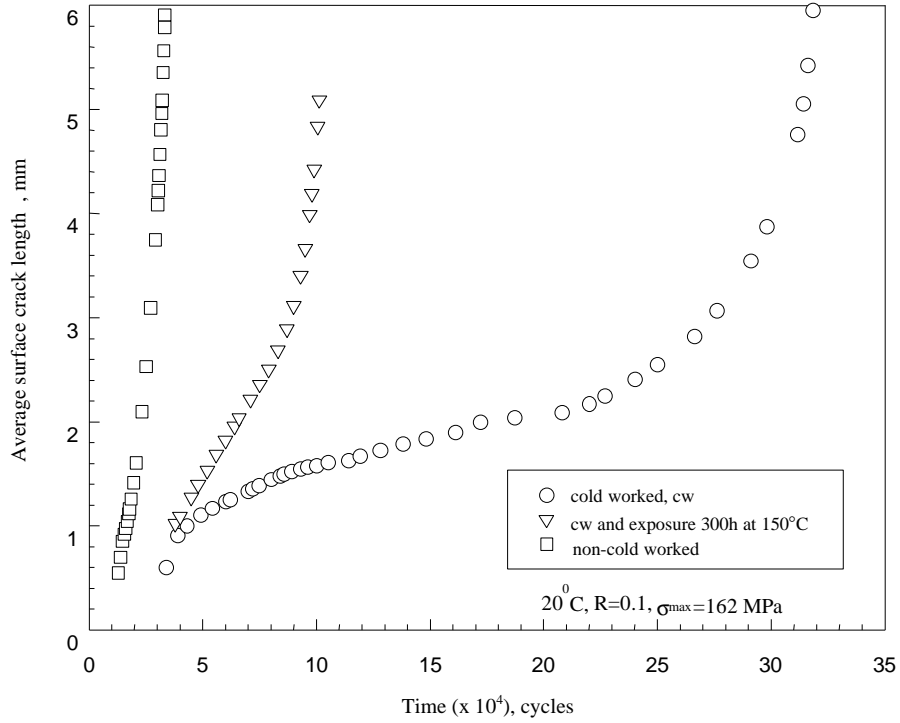


Figure 8 Fatigue crack growth from open holes in aluminium alloy 2650

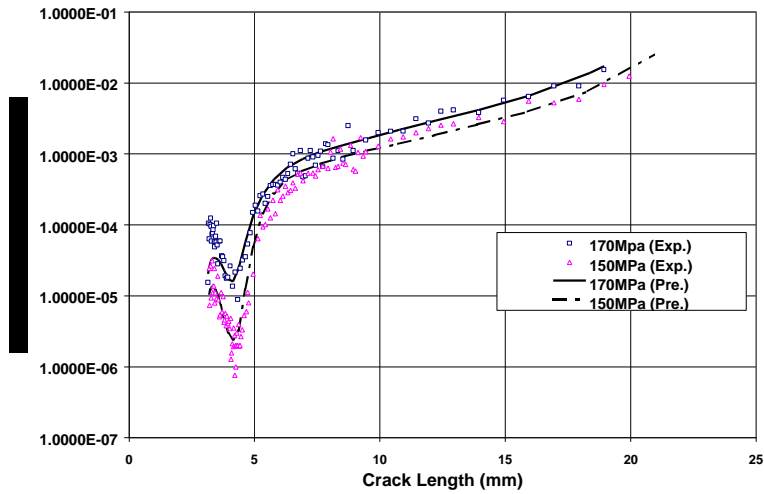


Figure 9 Comparison of predicted crack growth rate with test results

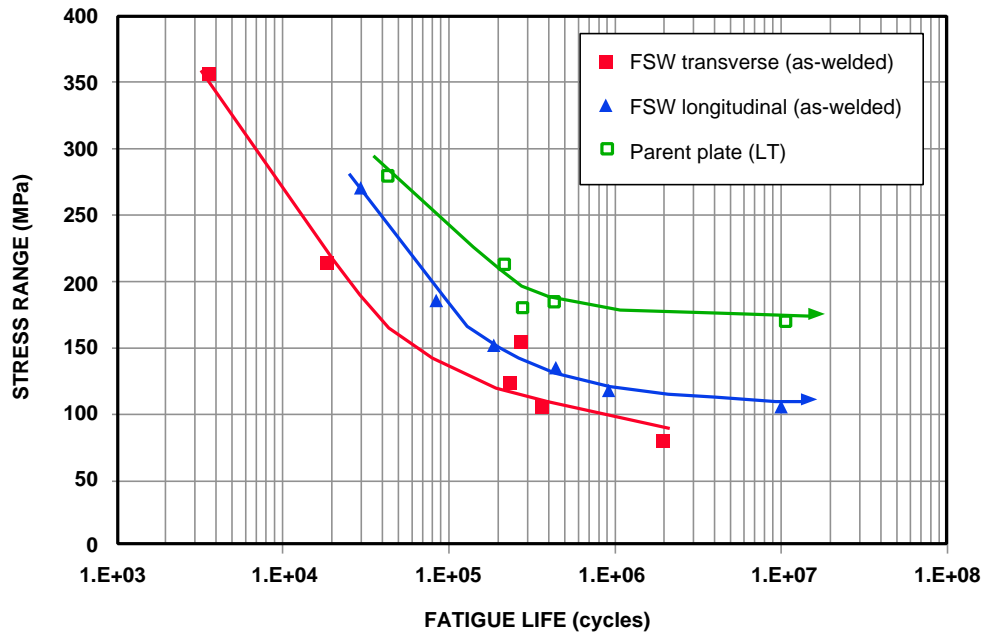


Figure 10 S-N curves ($R = 0.1$) of a parent plate and FSW

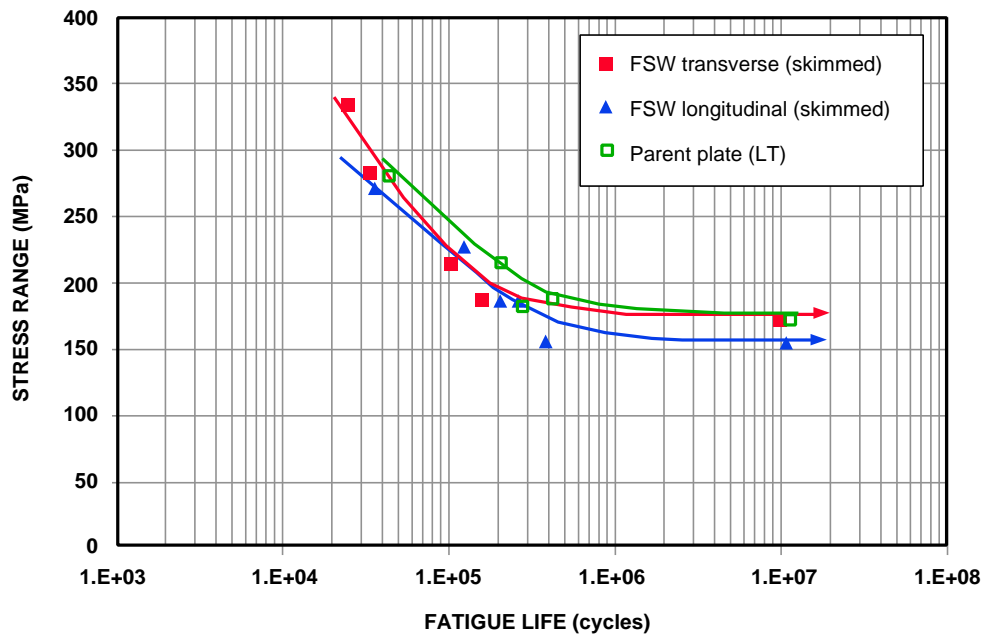


Figure 11 S-N curves ($R = 0.1$) of parent and FSW joints in surface skimmed conditions

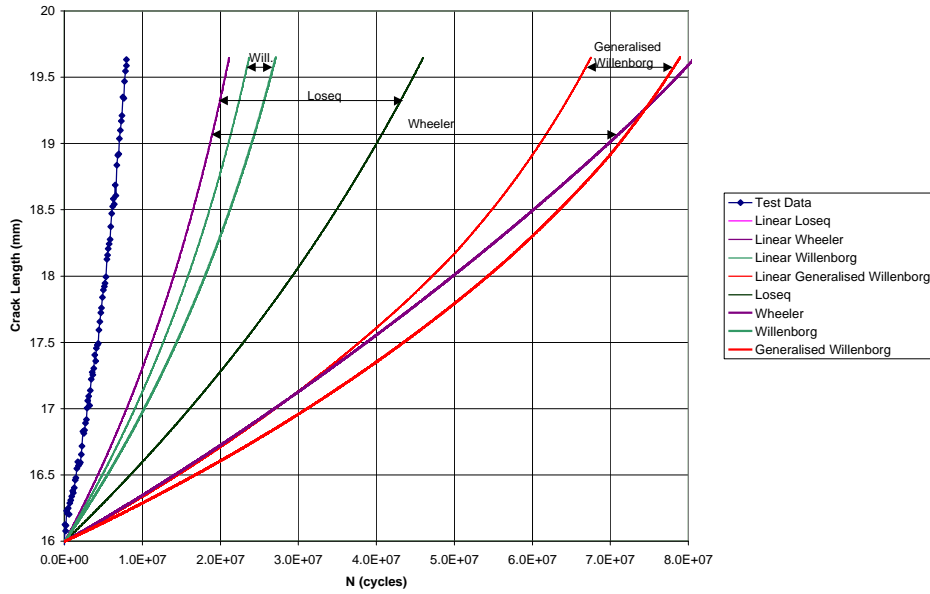


Figure 12 Effect of load interaction on crack growth predicted by various models

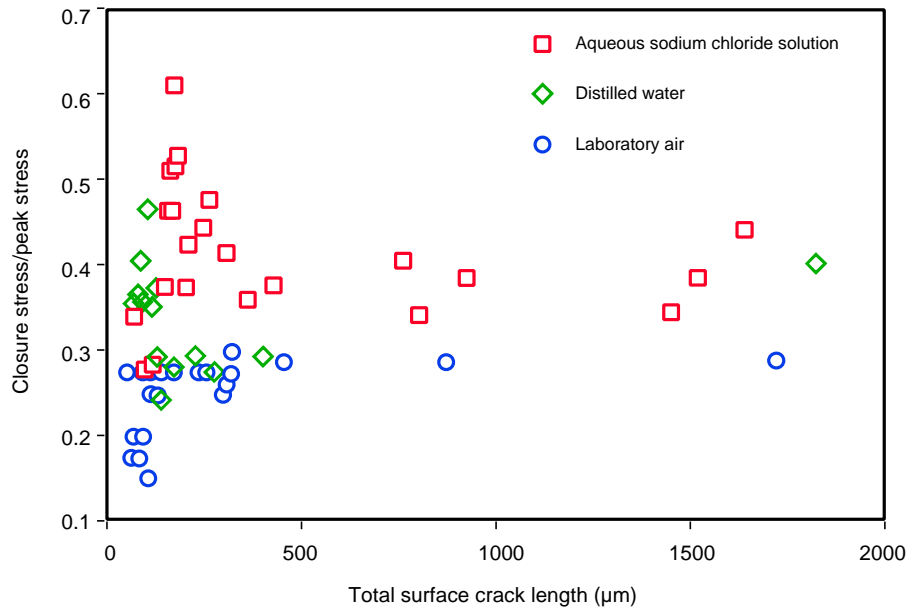


Figure 13 Alloy 7010-T7651 – graph of closure stress/peak stress versus total surface crack length for various environments

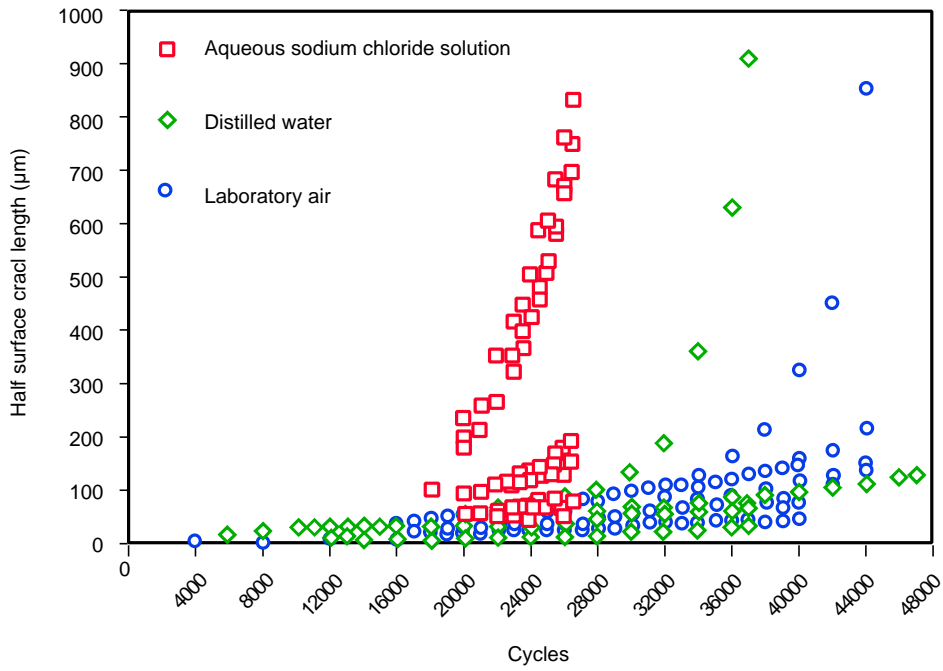


Figure 14 Alloy 7010-T7651 – graph of half surface crack length versus cycles for various environments

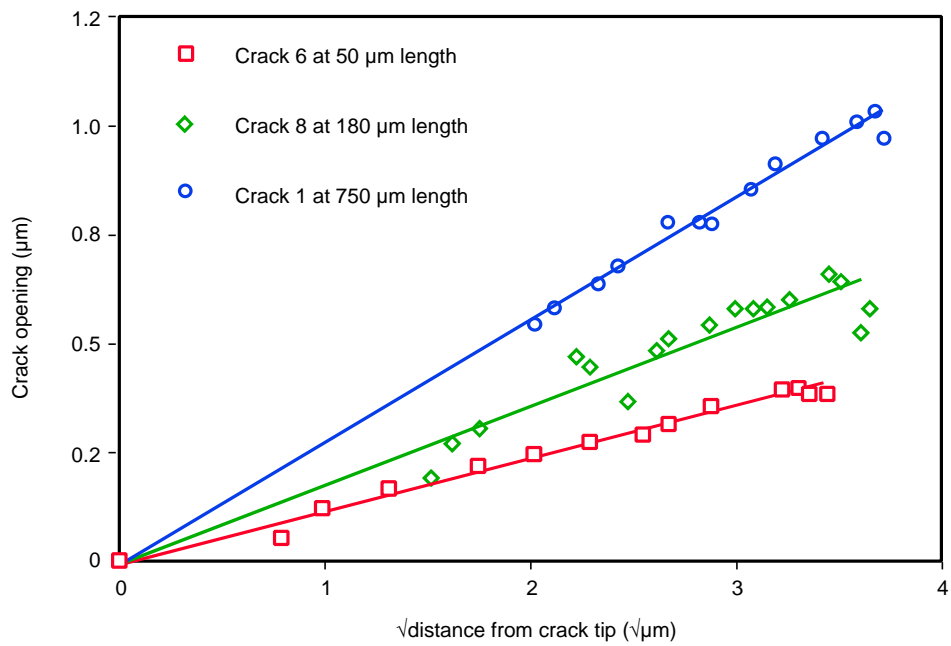


Figure 15 Alloy 7010-T7651 tested in aqueous sodium chloride solution - graph of crack opening versus square root distance behind crack tip

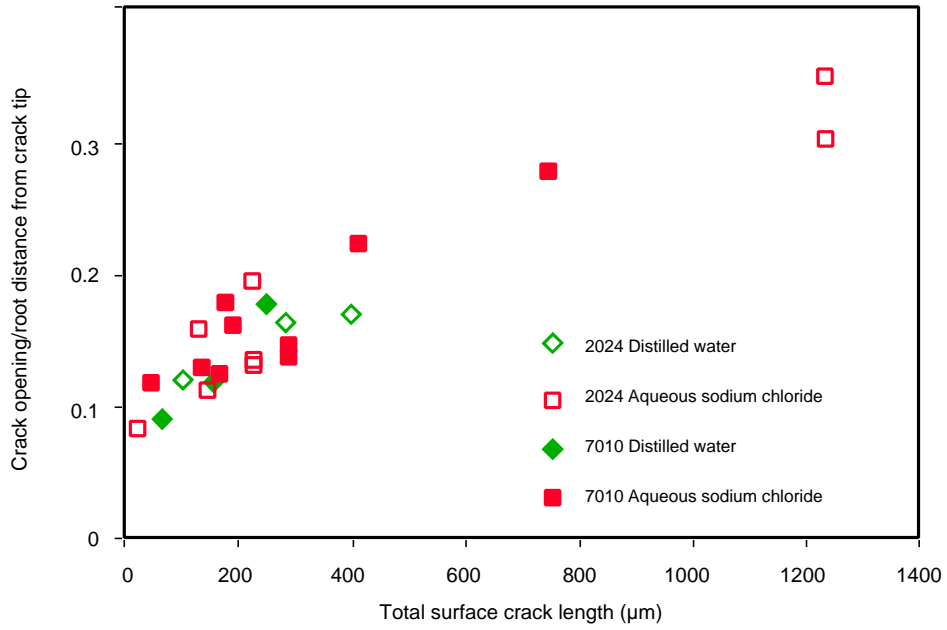


Figure 16 Graph of crack opening/ $\sqrt{}$ distance from crack tip versus surface crack length for alloys 2024-T351 and 7010-T7651 in distilled water and aqueous sodium chloride environments

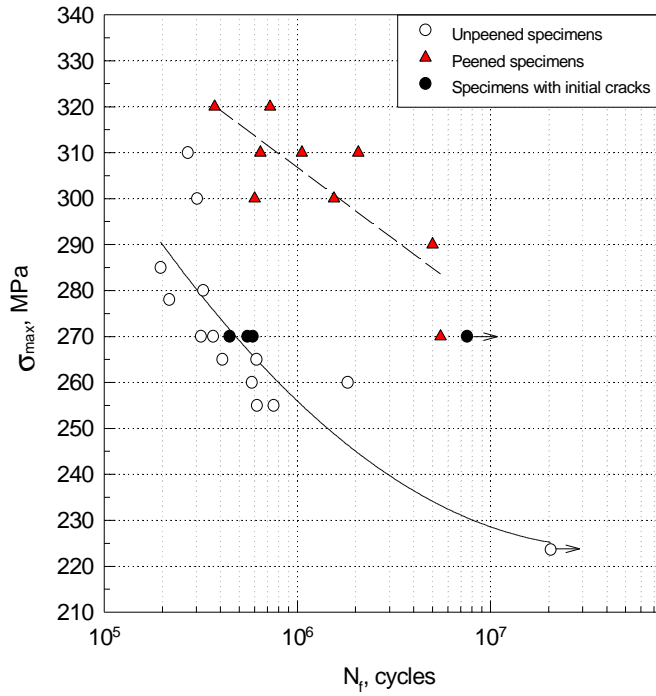


Figure 17 S-N curves for unpeened and peened specimens of 2024-T351, including results of specimens with initial cracks

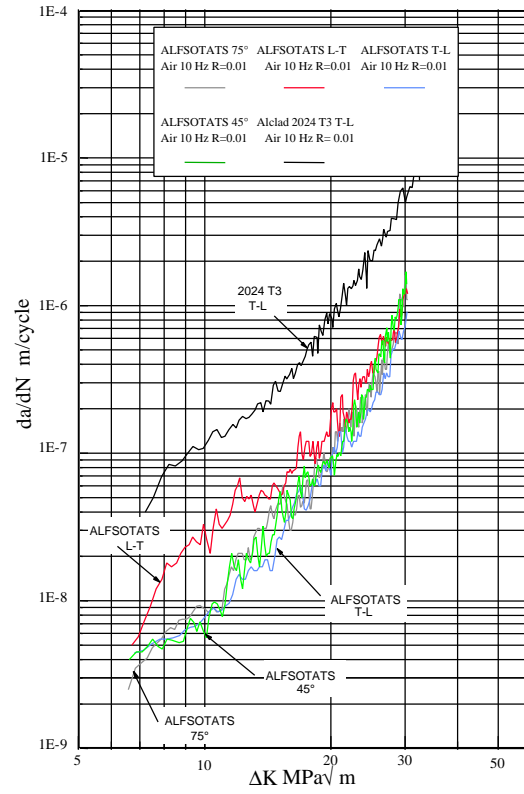


Figure 18 Effect of test orientation on fatigue crack growth rate for ALFSOTATS

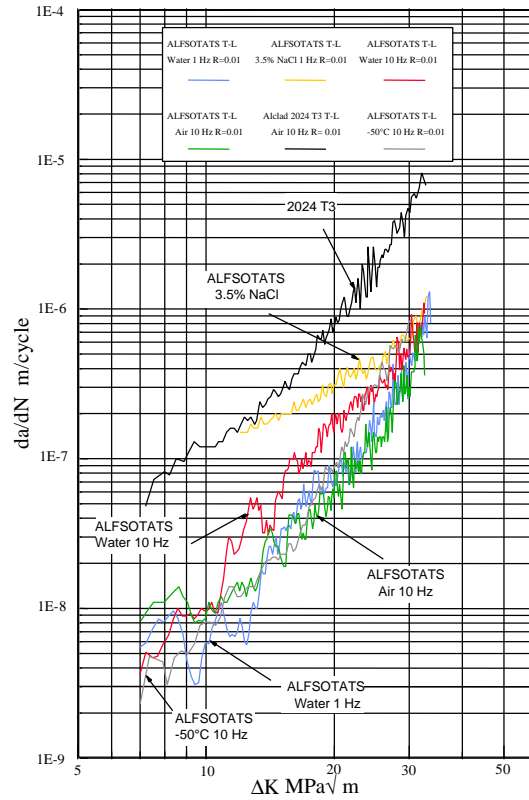


Figure 19 Effect of test environment on fatigue crack growth rate for ALFSOTATS

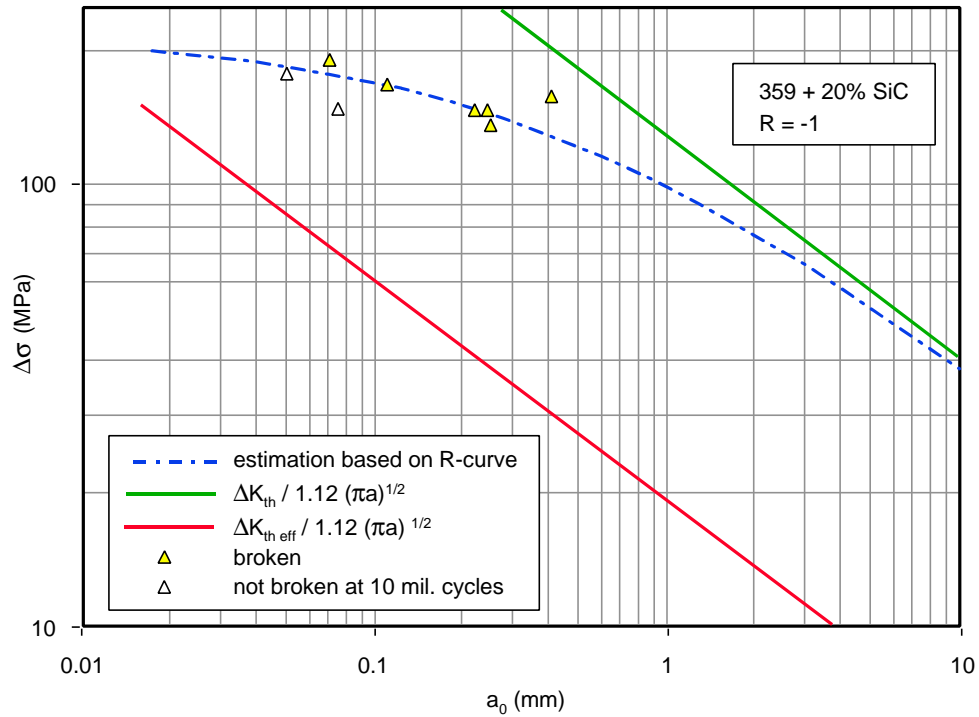


Figure 20 Kitagawa-diagram (fatigue limit vs defect size) for the A359 + 20% SiC_p aluminium alloy for load ratio R = -1

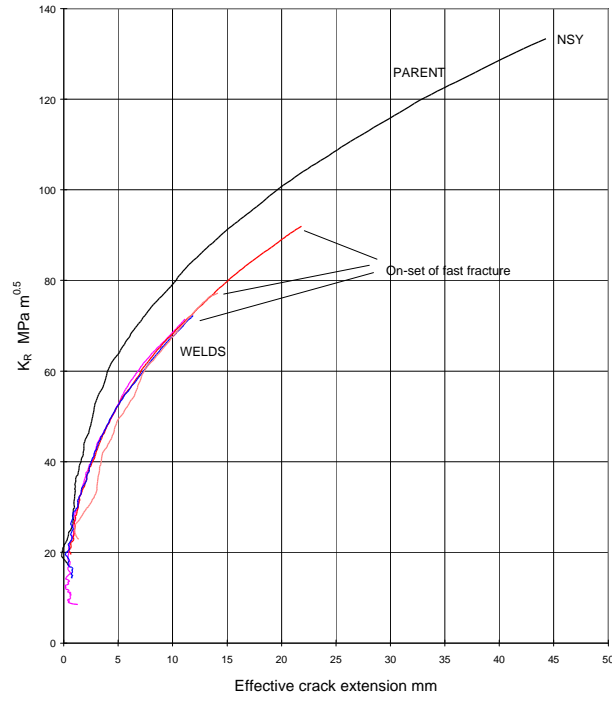


Figure 21 Summary graph showing the effect of welding 2024-T3 by the TIG and plasma techniques on R-curve behaviour

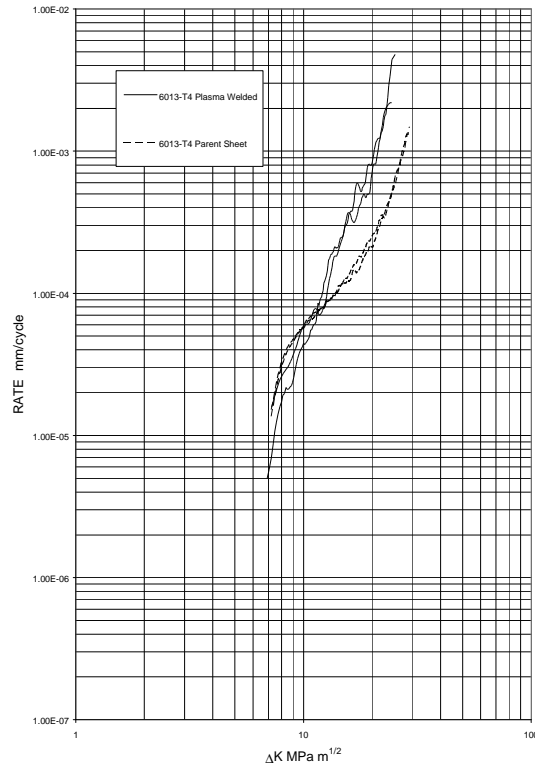


Figure 22 Comparison of fatigue crack growth rate curves for 6013-T4 TIG welded and 6013-T4 parent sheet (R=0.1 at 20Hz in air)

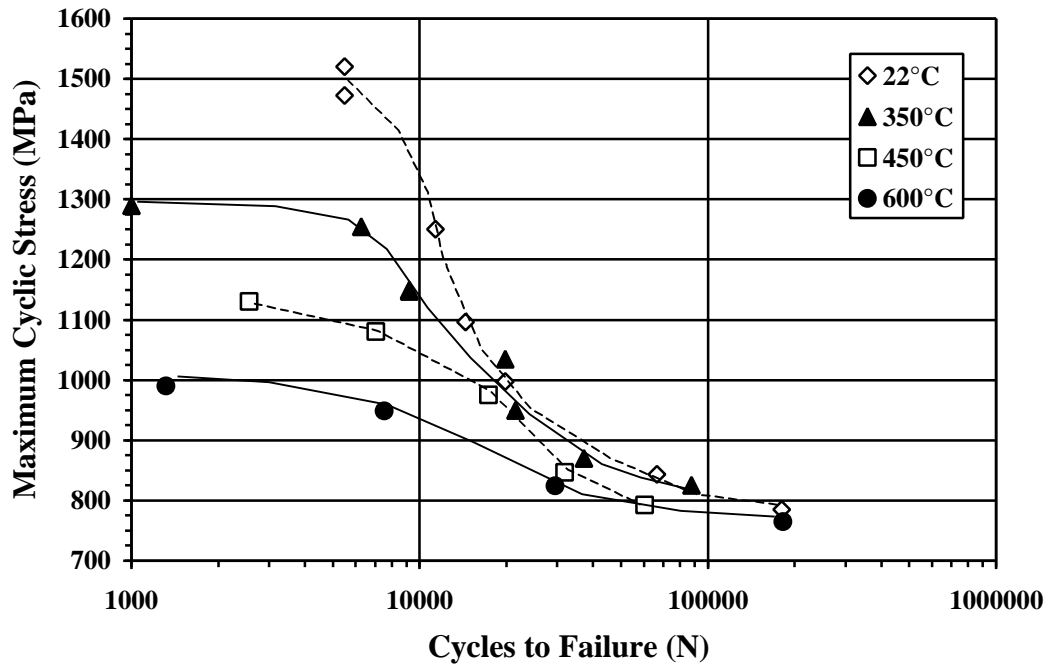


Figure 23 Effect of temperature on fatigue life in Ti-6-4 reinforced with Sigma SM1140+ fibres
Triangular Wave Form, $R=0.1$, Frequency = 0.1Hz, Load control



Figure 24 View showing Harrier empennage buffet test; tailplane in the foreground, steady load air actuator to left and electromagnetic shaker providing dynamic excitation to right of picture

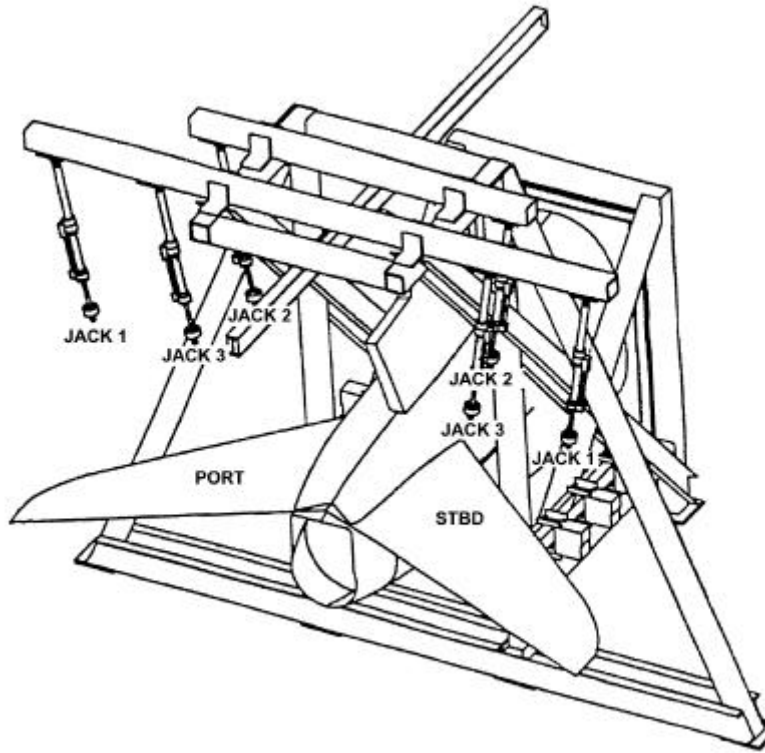


Figure 25 Export tailplane test rig – view showing manoeuvre actuators

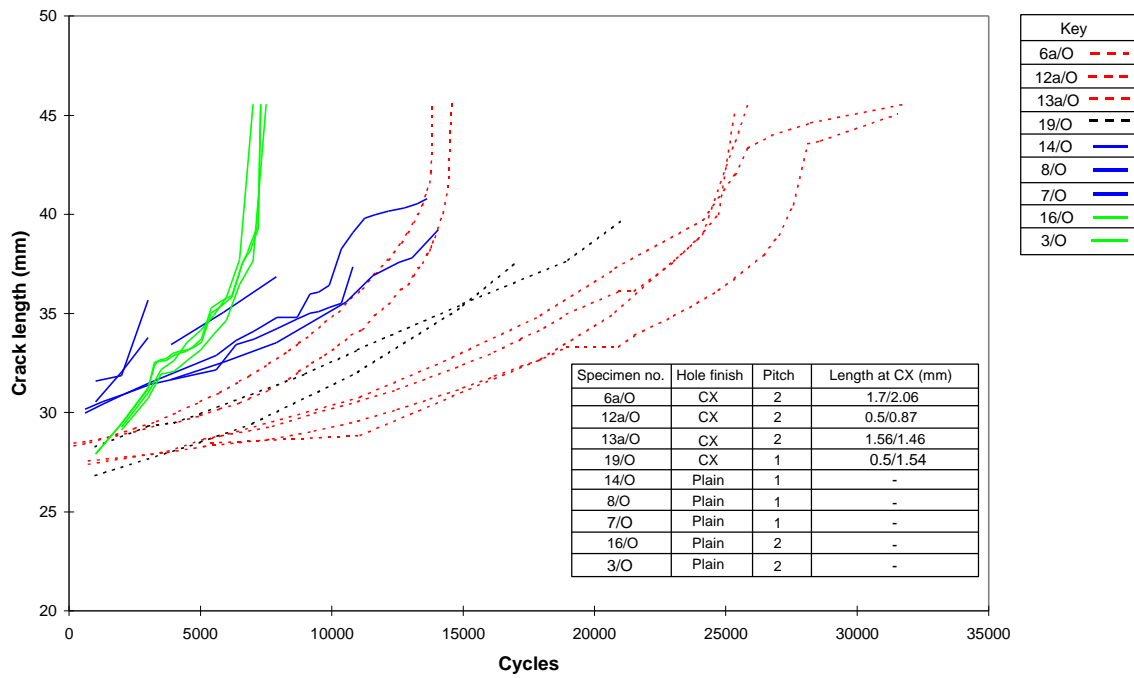


Figure 26 Effect of cold expansion on growth of 1 and 2 pitch lead cracks in the presence of MSD

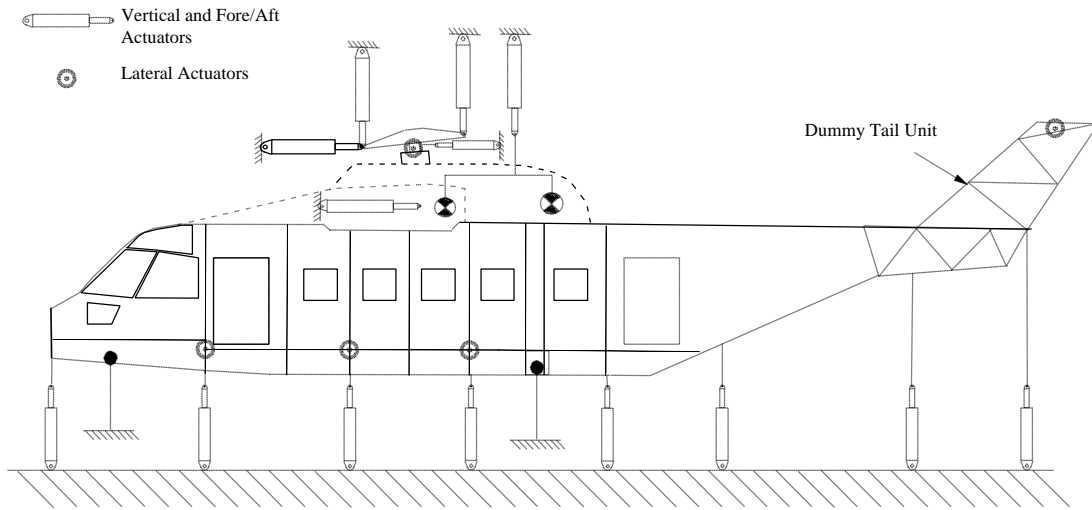


Figure 27 EH101 airframe full size fatigue/damage tolerance test geometry

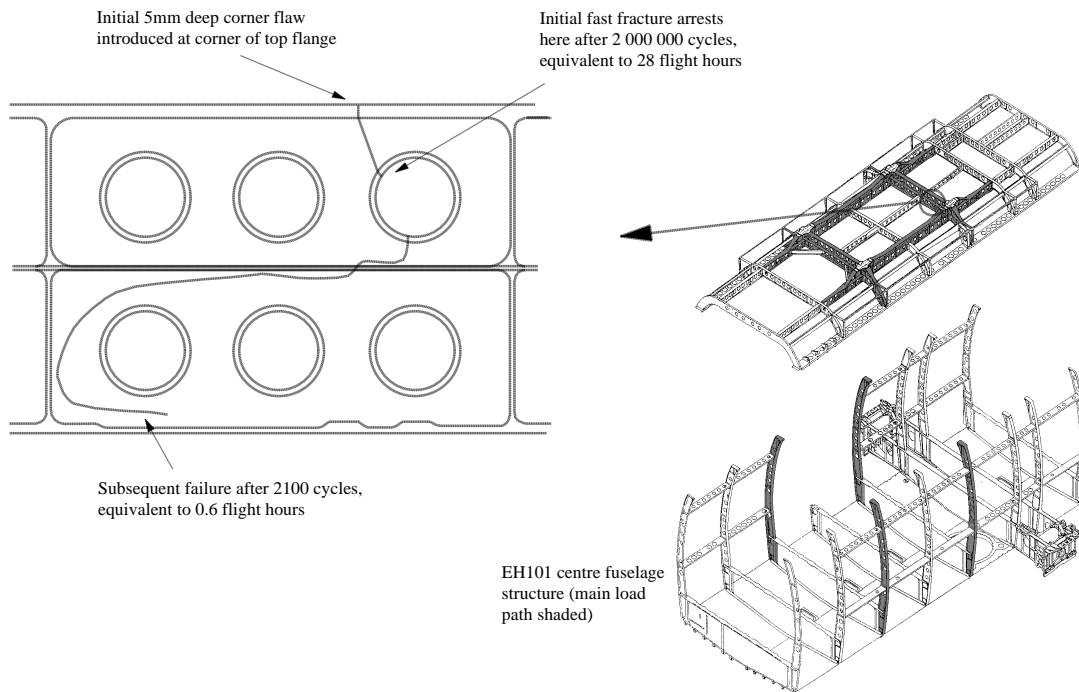


Figure 28 EH101 full size airframe flaw tolerance test

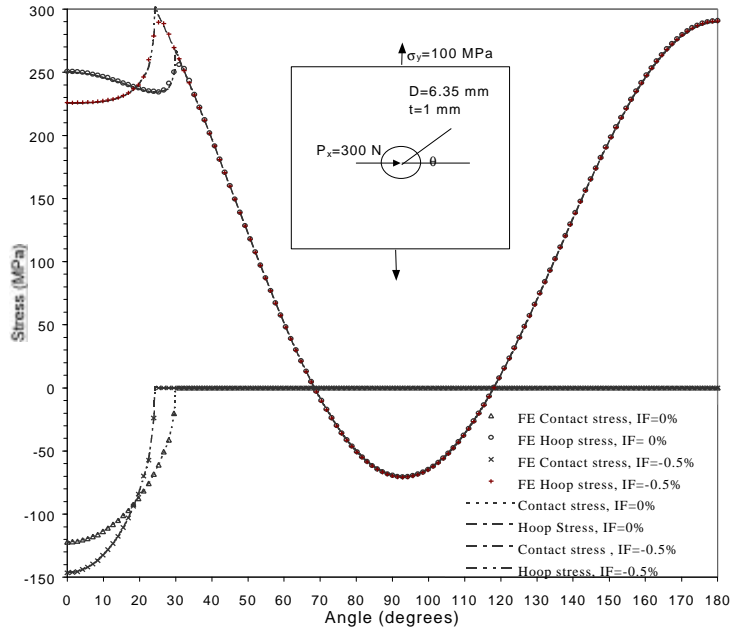


Figure 29 Comparison of analytical model with finite element results

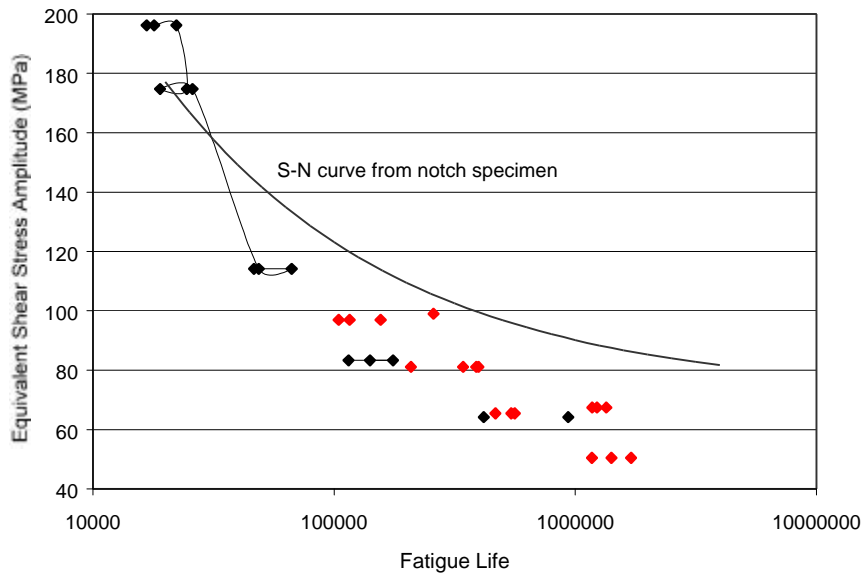


Figure 30 Prediction of fatigue lives of high load transfer joints with clearance fit bolts

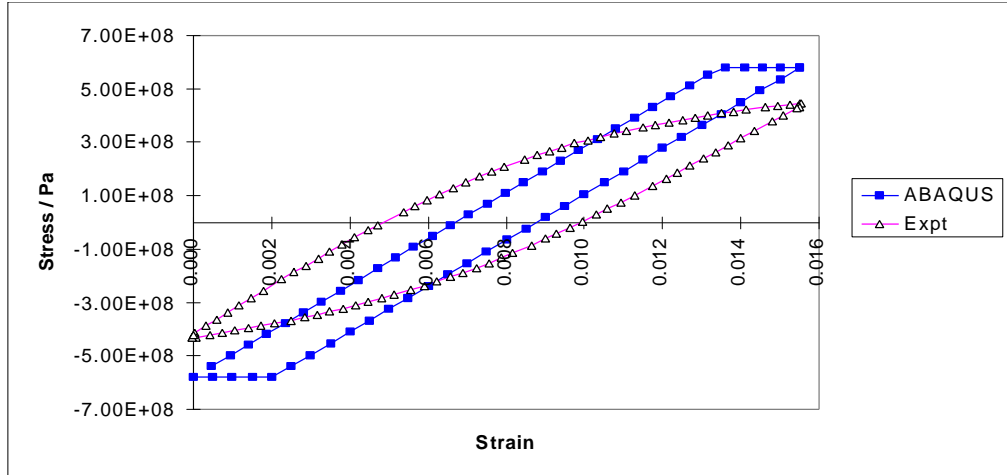


Figure 31 Hysteresis loops produced by both the ABAQUS isotropic hardening rule and by experiment at four hundred cycles (IMI 834 alloy)

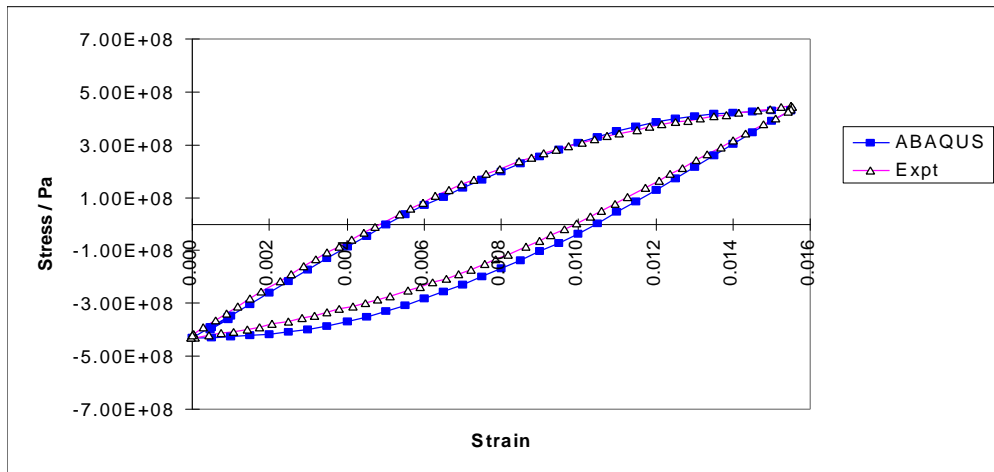


Figure 32 Hysteresis loops produced by both the ABAQUS combined hardening rule and by experiment at four hundred cycles (IMI 834 alloy)

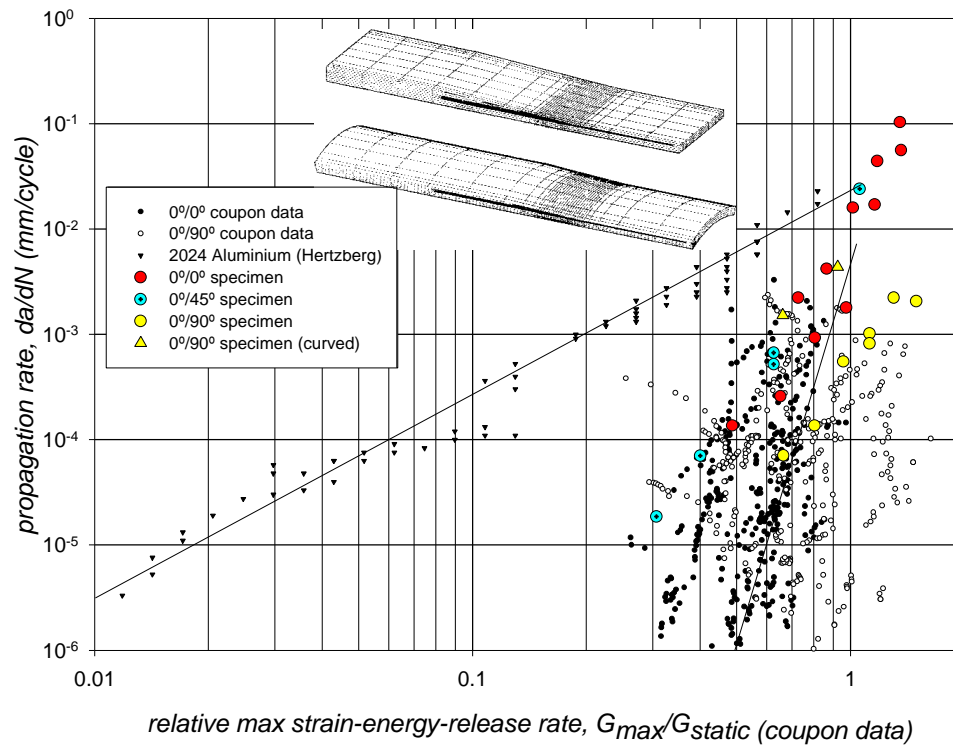


Figure 33 Paris plots for delamination fatigue in CFRP coupons and structural elements

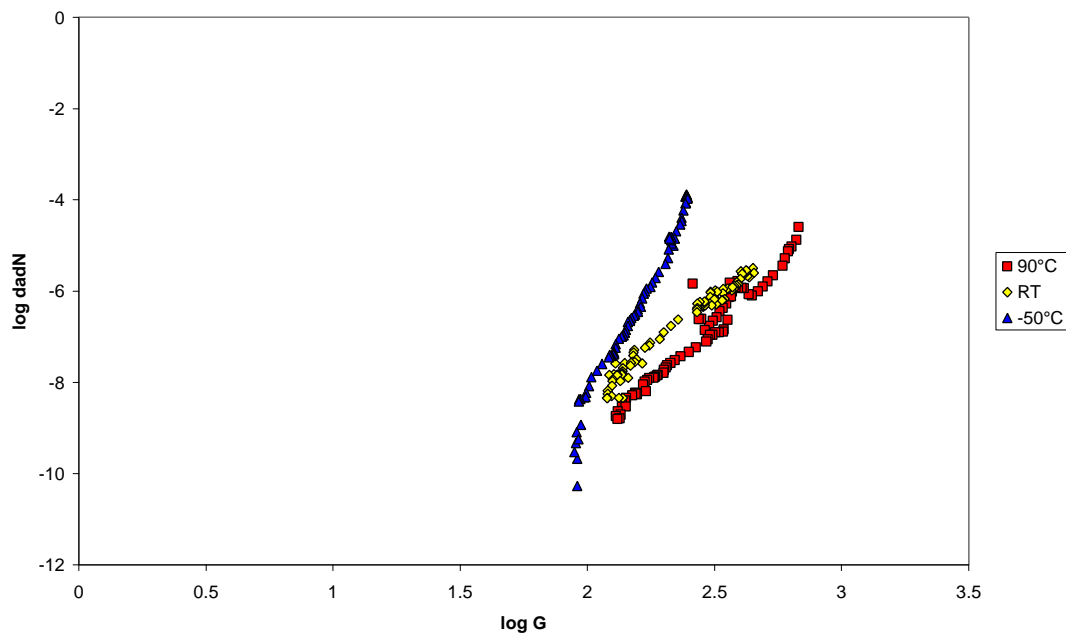


Figure 34 The effect of temperature on the fatigue resistance of CFRP-epoxy joints

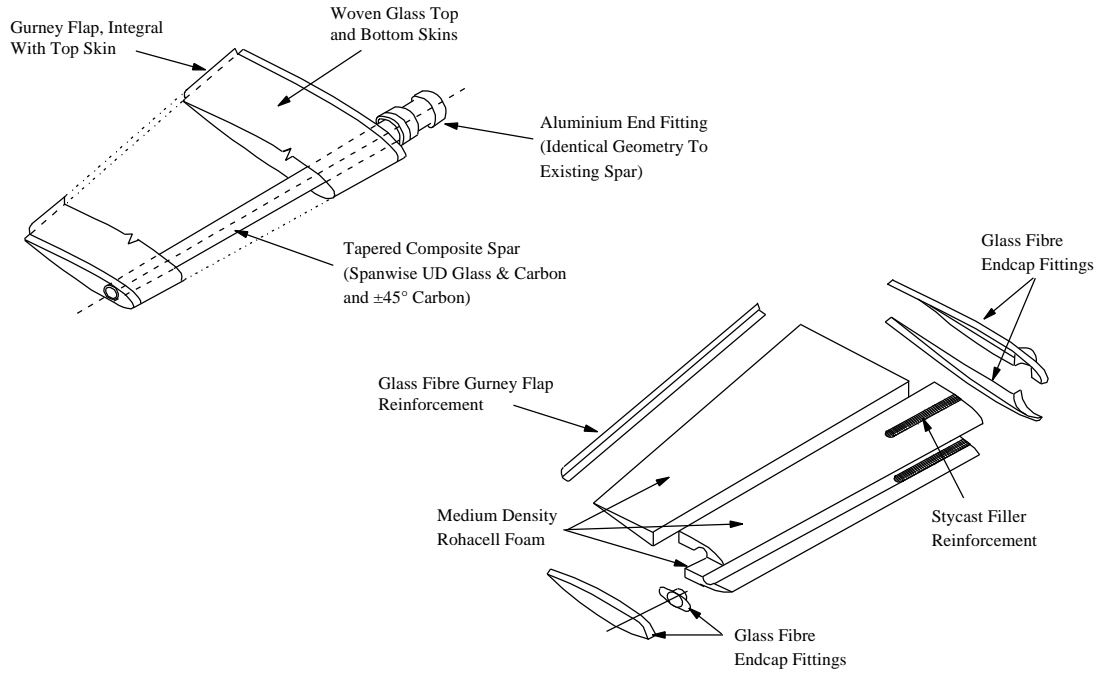


Figure 35 Lynx composite tailplane assembly

**A REVIEW OF AERONAUTICAL FATIGUE INVESTIGATIONS IN SWEDEN
DURING THE PERIOD MAY 1997 TO MAY 1999**

EDITED BY ANDERS F. BLOM

The Aeronautical Research Institute of Sweden

FFA

(FFA TN 1999-44)

CONTENTS

	<u>Page</u>
3.1 INTRODUCTION	3
3.2 FATIGUE LIFE TESTING AND PREDICTION	3
3.2.1 Temperature Exposure of Shot Peened AA7010 Parts	3
3.2.2 Qualification of Aerolock Rivets	3
3.3 JOINTS	3
3.3.1 Test Data on Fatigue Initiation of Butt Joints, MSD	3
3.3.2 Fatigue Behaviour of Mechanical Joints	5
3.3.3 Experimental Investigation of Fatigue Behaviour in Composite Bolted Joints	11
3.4 STRUCTURAL EVALUATION	13
3.4.1 SAAB 340 Full Scale Fatigue Test	13
3.4.2 The Saab 2000 Full Scale Fatigue Test	14
3.4.3 JAS39 Gripen Fatigue Testing	15
3.4.4 Research on High Speed Machined Aircraft Structures	15
3.5 STRESS ANALYSIS AND FRACTURE MECHANICS	16
3.5.1 Damage Zone Model with Multiple Cohesive Zones	16
3.5.2 Fast and Reliable 3D Fracture Mechanics Analysis in an Industrial Environment	17
3.5.3 Probabilistic 3D Multiple-Site Fatigue Crack Growth	17
3.6 FATIGUE CRACK PROPAGATION AND RESIDUAL STRENGTH	19
3.6.1 Strip Yield Analyses of Fatigue Crack Growth in Residual Stress Fields	19
3.6.2 Analyses of AGARD Small Crack Growth Test Results Based on the Post Yield Consideration	22
3.6.3 Stochastic Fatigue Crack Growth Analyses Based on Damage Accumulation Solution and Crack Closure Model	23
3.6.4 A Novel Probabilistic Fatigue Crack Growth Solution Based on the Crack Closure Model	25
3.6.5 Initial Fatigue Quality	27
3.7 COMPOSITE MATERIALS	28
3.7.1 Mode I Loaded Delamination Cracks Studied by High Magnification Moiré Interferometry	28
3.7.2 Rate Dependency of out-of-plane Properties of Composites	28
3.7.3 Evaluation of the Mixed Mode Bending Delamination Test	29
3.7.4 Methodology to Predict Strength of Impacted Sandwich Panels	29
3.7.5 Studies of Impact on Composite Structures	29
3.7.6 Damage Tolerance of Impacted CFRP Sandwich Panels	29
3.7.7 Methodology for Efficient Design of Composite Structures Exposed to Impact	30
3.7.8 Fatigue Delamination Growth Model for Composites	32
3.7.9 Load-Ratio Dependence on Fatigue Life of Composites	33
3.7.10 Coefficient of Friction of Composite Delamination Surfaces	33
3.7.11 A Numerical and Experimental Investigation of a Composite ENF-Specimen	33
3.7.12 Calculation of Mode-Separated Energy Release Rates during Delamination Growth	34
3.7.13 Interaction Between a Delamination Crack and a Matrix Crack	34
3.7.14 A Numerical and Experimental Investigation of Delamination Behaviour in the DCB-Specimen	35
3.7.15 Composite Fatigue	36
3.7.16 Fatigue after Impact and Bolted Joints in Fatigue	36
3.7.17 Certification Procedure	36
3.7.18 Equivalent Damage and Residual Strength for Impact Damaged Composite Structures	37
3.8 REFERENCES	37
3.9 SWEDISH ICAF-DOCUMENTS DURING MAY 1997-MAY 1999	42
ACKNOWLEDGEMENTS	42
FIGURES	43

3.1 INTRODUCTION

In this paper a review is given of the work carried out in Sweden in the area of aeronautical fatigue during the period May 1997 to April 1999. The review includes basic studies of fatigue development in metals and composites, stress analysis and fracture mechanics, studies of crack propagation and residual strength, testing of joints and full-scale structures, and fatigue life predictions. A reference list of relevant papers issued during the period covered by the review is included. Throughout this review references are made to the earlier Swedish ICAF review, Ref. [1].

Contributions to the present review are from the following sources:

- The Aeronautical Research Institute of Sweden (FFA)
Sections 3.2, 5.1, 5.2, 5.3, 6.1, 6.2, 6.3, 6.4, 6.5, 7.1, 7.2, 7.3, 7.4, 7.5, 7.6, 7.7, 7.8, 7.9, 7.10, 7.11, 7.12, 7.13 and 7.14
 - The SAAB Company
Sections 2.1, 2.2, 3.1, 4.1, 4.2, 4.3, 4.4, 7.15, 7.16, 7.17 and 7.18
- The Royal Institute of Technology (KTH)
Section 3.3

3.2 FATIGUE LIFE TESTING AND PREDICTION

3.2.1 Temperature Exposure of Shot Peened AA7010 Parts

Shot peening of aluminium plate 7010-T74 is used to guarantee the fatigue properties of many critical components. Temperature exposure of such shot peened surfaces will however impair the acquired strength due to material relaxation and loss of residual stress. Shot peened fatigue specimens with different notch factors have been tested after temperature exposure at certain times and temperatures. After 4 hours at temperature, specimens with $K_t=1.7$ had lost 15% and 35% respectively of stress at 10^6 cycles, compared to un-exposed specimens, see Figure 1. As-milled specimens had less reduction for the same temperature exposure.

3.2.2 Qualification of Aerolock Rivets

To qualify new rivets, for replacement of the rivet types AF139, MS20426 and MS20470 of material 2024 used today, fatigue tests of lap joints have been carried out. The rivets of material 2024 have to be stored refrigerated after solution heat treatment until short before installation. In order to simplify the rivet handling, a new rivet material, the 2017ID, is to be used without in house heat treatment and does not need ice box storing. In different fatigue test series, Aerolock rivets (designated AL90x) have shown to meet the fatigue properties achieved with the AF139DD and MS20470DD rivets (DD for the 2024-material). The AL907ID showed to be the best of the countersunk rivets, leading to the longest lap-joint fatigue life, both in constant amplitude and spectrum loading. The AL905ID, which was tested to less extent, showed to give similar fatigue strength of the joints as did the AF139DD. Of protruding head rivets, the AL906ID rivet showed to exceed the joint fatigue strength achieved with the MS20470DD rivet.

3.3 JOINTS

3.3.1 Test Data on Fatigue Initiation of Butt Joints, MSD

A test programme has been performed by SAAB in the Brite-Euram collaborative project BE95-1053, "*Structural Maintenance of Ageing Aircraft*". The programme has the following main objectives:

- To make a distinction between crack initiation and crack propagation in riveted joints of a given coupon configuration.
- To study the effect of pitting corrosion on fatigue in riveted joints of a given configuration and pre-corroded on selected areas before fatigue testing.
- To assess the damage pattern in a complex rivet configuration (several columns) by knowledge on a simple two columns configuration when loaded under the same conditions

Fatigue Initiation versus Crack Growth

Fatigue properties have been generated for an asymmetric two columns butt joint design, Figure 2. The testing was performed as constant amplitude tests with the stress ratio fixed, $R=0.1$. The stress level S and the stop criteria for interruption of a test setup are two commanded variables whereas the number of cycles recorded to reach the applied stop criterion is a random variable. The parameters *crack initiation period* and *crack propagation period* have been assessed. *Crack shapes* data, i.e. the data before the cracks are changed to through the thickness cracks, were assessed and *crack sizes* to be expected when the cracks can be detected by optical methods are discussed in SMAAC-TR-3.2-08-1.3/SAAB, Ref. [2].

The sheet material, used in all tests, is the same as used on the fuselage skin to SAAB 340 as well as SAAB 2000 i.e. aluminium 2024-T3 unclad. The surface treatment is of production standard, however, the sealants were excluded in order to make it possible to use the High Frequency Pulsator. The fasteners are countersunk aluminium rivets with 5/32" diameter and the rivet designation is AF138AD-5-5. The specimen design is illustrated by the Figure 2.

For the studied configuration, with respect to design and loading, the following conclusions have been extracted from [2]:

- ❑ The splice profile design, an extrusion loaded in the transverse direction, is too weak to control fatigue problem to the sheet material only and to prevent fatigue problem in the profile. Fatigue damages usually exist in the sheet material and in the splice profile material. Furthermore, the tests indicates that the failure mode is a function of the stress level.
- ❑ The test results at the maximum stress level 100 MPa have been described by fitting a distribution function to the data. The statistical variable adopted is the 10-logarithm of the fatigue life T . The normal distribution function, fully described by the two characteristic parameters μ and σ , was applied to the data. The mean value, μ , is strongly effected by the definition of fatigue life, in terms of acceptable damages in test specimens, whereas the standard deviation, σ , is more or less uninfluenced by the definition of fatigue life.
- ❑ When a fatigue crack become visual, i.e. can be detected by optical methods, it should be expected to read crack sizes which are 3 mm in length, recorded from the edge of the cylindrical hole or approximately 5 mm from the centre of the hole, Figures 3 and 4. The crack shapes are evidence for the existence of so called "*Secondary Bending*". Furthermore, the amount of fretting corrosion between the sheet and the splice profile, due to fatigue cycling, is classified as minor or not present.
- ❑ The mean damage growth period, from a visual crack to failure of the specimen, is $\leq 10\%$ of the mean total period to specimen fracture.
- ❑ The mean damage growth period, from small macro cracks to failure of the specimen, is at least 40% of the mean total period to specimen fracture.

Pitting Corrosion Effects on Fatigue

The effect of pitting corrosion on fatigue has been studied on small butt-joint specimens which were pre-corroded on selected areas before fatigue testing. The areas selected for exposure of corrosion media, two weeks to neutral salt spray in accordance to ASTM B117, are:

- ❑ The mating flat surfaces of sheets and splice profile.
- ❑ The rivet holes alone.

The depth of pitting was determined to be typically about 0.1 mm (100 μm). Corrosion on flat surfaces was developed on unprotected material surfaces by exposure to the neutral salt spray prior to drilling of rivet holes. Corrosion inside holes was developed by drilling the holes in bonding primed surfaces and exposure the material to the corrosive environment. Edges were masked prior to exposure. The riveting, in both cases, was the final operation. The specimen design is shown in the Fig. 5. Furthermore, the figure illustrates a typical 0.1 mm deep pitting.

The tested configurations are shown in Table 1.

Corrosion Prior to Fatigue Loading	Surface Treatment	Number of Specimen
About 0.1 mm deep pitting on mating surfaces	None	5
None	None	5 (reference)
About 0.1 mm deep pitting in rivet holes.	Phosphoric acid anodizing with bonding primer	5
None	Phosphoric acid anodizing with bonding primer	5 (reference)

Table 1. Test configurations

The fatigue testing was performed in a High Frequency Pulsator with a load cell of 100 kN. The specimens were mounted in mechanically fastened grips. When testing, the test frequency was about 70 Hz. Two stress levels were used for each specimen configuration, the pre-corroded ones as well as the references. The fatigue testing was performed at constant amplitude, $R \approx 0.1$, and the testing was continued to final rupture of the specimens. Stress-life distribution curves (SN-curves) has been established for each one of the tested configuration. For the studied configurations, with respect to design and loading, the following conclusions were made in SMAAC-TR-4.2-05-1.3/SAAB, [3]:

- ❑ A life reduction of 50 percent at pitting depth of typically 100 μm on mating flat surfaces of sheets and splice profile is likely. This life reduction can not be assigned to the loss in area due to pitting corrosion alone, Figure 6.
- ❑ The effect of typically 100 μm deep pitting in the rivet holes on fatigue life is negligible, when rivets were installed in precorroded holes which may have been affected by the subsequent riveting operation.
- ❑ The mean damage growth period, from a visual crack to failure of the specimen, is not affected by the studied pre-corrosion processes.

Structural Size Effects on Fatigue.

Fatigue properties have been generated for an twenty column joint, Figure 7. The testing was performed as constant amplitude tests with the stress ratio fixed, $R=0.1$. The stress level S was fixed at 100 MPa and the evolution of cracks as a function of number of cycles was monitored by optical inspection. Residual strength tests was performed on some panels when extensive cracking had developed. *Crack shapes* data, i.e. the data before the cracks are changed to through the thickness cracks, are assessed and crack sizes to be expected when the cracks can be detected by optical methods are discussed.

For the studied configuration, with respect to design and loading, the following conclusions are extracted from SMAAC-TR-3.2-12-1.3/SAAB, Ref. [4]:

- ❑ The splice profile design, an extrusion loaded in the transverse direction, is too weak to control fatigue problem to the sheet material only and to prevent fatigue problem in the profile.
- ❑ Strain measurements demonstrate a non-uniform distribution across the width of the specimen. Furthermore, it is obvious that the fatigue cycling affects the virgin stress distribution.
- ❑ When a crack can be detected by optical NDT it is likely to find cracks at both critical sites of the hole.
- ❑ When a fatigue crack become visual, i.e. can be detected by optical methods, it should be expected to read crack sizes which are approximately 4 mm in length, recorded from the centre of the hole, Figure 8.
- ❑ At or close to the fatigue life, i.e. failure of specimen, it is likely to have fatigue cracks in practically each hole of the fatigue critical holes.
- ❑ The residual strength in presence of cracks, sheet material, have been compared to a simple net section yield criterion for two sheets with extensive cracking, 1/3 and 1/6 of the crack free net section area. The used criterion overestimates the residual strength.

3.3.2 Fatigue Behaviour of Mechanical Joints

Aircraft structural joints are often the originating points of fatigue failures. Depending on the type of joint different mechanisms may initiate fatigue cracks. Additionally, cracks often initiate and grow subsurface, in the vicinity of a fastener installation. Hence, the fatigue behaviour of mechanically fastened joints is influenced not only by the type of joint, but by a vast number of parameters, i.e. both configuration and installation joint parameters.

Configuration parameters such as load transfer (LT) and secondary bending (SB) in low, medium and high load transfer joints have been identified for several joints and fatigue test results are interpreted based on these fundamental parameters. Additionally, installation parameters, as determined by traditional and high-performing

fastener systems, are investigated and their influence evaluated in terms of the same fundamental parameters, i.e. LT and SB.

EXPERIMENTAL DETAILS

Definition of Load Transfer and Secondary Bending

The load transfer is defined as the percentage of the applied load, which is transferred from one plate to the other by means of the fasteners and friction between the plates, see Fig. 9. Joints may be divided into four groups according to the amount of LT: no load transfer, low load transfer ($0 < LT < 10\%$), medium load transfer ($10\% < LT < 40\%$), and high load transfer ($40\% < LT < 100\%$).

Secondary bending is defined as the ratio of bending strain to axial strain in the section of interest. This leads to SB being a function also of the applied load level itself. The no-SB joints are of the double shear type, while the high-SB joints have a single shear configuration.

LT and SB measurements are performed on low- medium- and high-LT specimens instrumented with strain gauges on both sides of the “top”-plate. All in all ten different fastener systems have been investigated and evaluated.

Test Specimens

The experimental investigation, described in Refs. [5, 6], on fatigue behaviour of mechanical joints has been carried out on low, medium and high load transfer joints. The types of joints are described in the following.

The Double Reverse Dogbone (DRD) joint is a *low-LT, medium-SB joint*, representative of the lower wing skins attached to spars, see Fig. 10. The LT is dependent on the fastener type and fit, i.e. when a rigid fastener is used in combination with interference fit installation, LT has been measured to approximately 10%. If, however, a clearance fit fastener is used, the LT may disappear. Secondary bending measurements have been in the range of 0.1-0.25.

The 1 1/2 dogbone joint (D) is considered a standard design, originally developed by LBF (Laboratorium für Betriebsfestigkeit) in Germany with the aim of simulating the load conditions of runouts of stiffeners attached to the outer skin, see Fig. 10. The design goal for the LT was 40% and the SB was expected to be .5, making it a *medium-LT, high-SB joint*. This joint is sensitive to installation parameters and LT depends on fastener fit, clamping force and fastener flexibility. During the last 20 years, investigations indicated an LT of approximately 20-30%, Ref. [7], which is substantially lower than anticipated. However, recent measurements and corresponding detailed evaluation show values of LT well in agreement with the original design goal, Ref. [8].

Lap joints (L) are *high-LT joints* which, in their single shear configuration, are characterised also by *high SB* due to the asymmetric eccentricity of the load carrying members, see *Figure 2*. Load transfer in the two-row joint should be around 50% for each rivet row, but measured values give a range of $\pm 10\%$ possibly due to asymmetric effects of the formed and manufactured heads of countersunk (csk) fasteners, Ref. [8]. Secondary bending measurements were found to be in the range of 1.1-1.7. However, the SB in this joint is critically dependent on joint geometry, number of fastener rows and fastener characteristics as well as the use of anti-buckling devices.

Specimen Instrumentation

LT and SB are measured by use of specimens instrumented with strain gauges. This is a widely accepted practice that is considered standard procedure as exemplified in the AGARD collaborative programme on Fatigue Rated Fastener Systems, see Fig. 11.

For all medium- and high-LT specimens, all measurement positions are equipped with 120 Ω general-purpose strain gauges compensated in temperature for aluminium. The grid dimensions are 1.5 x 3 mm. The gauges have been glued to the specimens with Micro-Measurements M-200 room temperature curing single component cement and coated after installation with air drying polyurethane coating. All the gauges come from two batches with identical electromechanical characteristics. Each specimen has been instrumented with gauges coming from the same batch.

Regarding the low-LT specimen, see Fig. 12, a recently developed instrumentation technique was used which employs strip gauges, i.e. gauges consisting of a group of strain-sensitive grids mounted on the same carrier base, next to each other and with the sensible axis lying in the same direction for all of them, Ref. [9]. If the grids are soldered to each other in a series-type connection, a single, very wide strain gauge is obtained that has a total

resistance equal to the sum of the single grid resistance values and the same gauge factor. This new gauge will measure the overall strain value, or at least a value proportional to it. Hence, both data acquisition and evaluation procedures are simplified.

Artificial Defects

The low-LT specimens exhibited fatigue crack initiation sites far away from the fastener installations, often at the clamping area, Ref. [6]. This problem was pronounced for specimens assembled with high-performing fastener systems. Hence, it was decided that the fatigue investigation on low-LT joints was restricted to the fatigue crack growth process, thus omitting the initiation part.

Artificial defects were thus manufactured on both the faying surfaces of the specimen plates, see Fig. 13. The electrically discharge machined flaw is a corner defect with a radius of 1.5 mm on both sides of the fastener hole in the minimum net section perpendicular to the loading direction.

Fastener Systems

A fastener system includes all the fastener installation parameters that have to be determined when designing a joint. Thus, the type of fastener, hole geometry, amount of fastener fit, hole and faying surface quality, and clamping force all influence and characterise the joint.

Three different main configurations of fastener systems are used in this investigation, see Fig. 14, i.e. the Lockbolt and Hi-Lok screws, and the solid Aluminum rivet. Subgroups are formed based on fastener material, fastener fit and fastener pre-load after installation (i.e. the amount of clamping force (CF)). The fastener fit is dependent on the chosen fastener system. The Hi-Lok and Lockbolt systems are used with high (130 μm) and medium (50 μm) interference fit, and clearance fit (30 μm). All solid rivet systems are hole filling.

The manufacturers of Hi-Lok and Lockbolt fasteners guarantee a minimum fastener CF. The guaranteed magnitude depends on fastener diameter and is, for the chosen diameter, approximately 3 kN and 4 kN, respectively, which is, however, not a representative value of fastener CF. Experiments indicate substantially higher values. Thus, the tested Hi-Lok systems are characterized by a CF of approximately 5 kN and the Lockbolt system by a CF of approximately 7 kN, Ref. [8]. Further, the CF depends on the level of friction/lubrication between nut and plate as well as between fastener threads and nut. De Magistris et al [10] found a substantially higher clamping force in Hi-Lok systems when nut/plate and/or nut/threads were lubricated.

The solid rivet systems are characterized by almost zero CF, i.e. CF=0.0-0.5 kN. In design and fatigue life estimations the CF of rivet systems is usually neglected. All fasteners are countersunk (CSK) with a nominal diameter of approximately 5 mm. A compilation of joint configuration, fastener system, load spectrum and material is shown in Table2.

Joint Configuration	Fastener System	Material	Load Spectrum
Low, medium, high LT	Ti Lockbolt, interference	AA 7475-T76	FALSTAFF
Low, medium, high LT	Ti Lockbolt, high interference	AA 7475-T76	FALSTAFF
Low, medium, high LT	Ti Lockbolt, clearance	AA 7475-T76	FALSTAFF
Low, medium, high LT	Ti Hi-Lok, interference	AA 7475-T76	FALSTAFF
Low, medium, high LT	Ti Hi-Lok, high interference	AA 7475-T76	FALSTAFF
Low, medium, high LT	Ti Hi-Lok, clearance	AA 7475-T76	FALSTAFF
Low, medium, high LT	Steel Hi-Lok, interference	AA 7475-T76	FALSTAFF
Low, medium, high LT	Steel Hi-Lok, high interference	AA 7475-T76	FALSTAFF
Low, medium, high LT	Steel Hi-Lok, clearance	AA 7475-T76	FALSTAFF
Low, medium, high LT	Solid Aluminum rivet	AA 7475-T76	FALSTAFF

Table 2. Compilation of joint configuration, fastener system, material and load spectrum.

Flight Simulation Load History

The manoeuvre-spectrum FALSTAFF is representative for the wing root of a fighter aircraft. The sequence consists of 200 flights with a total number of approximately 36000 peaks and troughs, with an average of 90 cycles per

flight. Specimens tested with the FALSTAFF sequence were tested at two maximum gross stress levels equal to 150 MPa and 200 MPa.

Fatigue Testing Equipment

All fatigue tests were performed in an MTS 320 closed-loop servo hydraulic machine with a maximum capacity of 250 kN, controlled by an MTS Electronics TeStar II computer. The tests were carried out in load control with constant displacement rate giving a frequency variation between 4 Hz for high stress amplitudes to 16 Hz for low stress amplitudes. The average test frequency was about 10 Hz. The tests were performed in laboratory air environment at room temperature (18-21°C).

EXPERIMENTAL RESULTS

Detailed LT and SB measurements are presented in the following. Further, fatigue test results of low-, medium- and high-LT specimens are discussed.

LT and SB measurement results

An extensive experimental characterization of different fastener systems assembled in low- medium- and high-LT specimens was conducted by De Magistris et al [11] and Ricci Moretti et al [8] in terms of detailed LT and SB measurements. The investigation was aimed at characterizing high-performing fastener systems in terms of parameters as fastener fit, fastener pre-load after installation and fastener tilting stability and bending stiffness. A traditional rivet system was used as reference.

In order to take joint shakedown processes and, in some measure, fatigue wear into consideration, measurements on each joint configuration has been conducted at four consecutive runs with a particular load sequence inserted between each measurement repetition. The inserted sequences are 10, 100 and 1000 cycles long, respectively. Results from the third measurement sample (after 110 cycles) are presented in the following.

Fastener System	Low-LT		Medium-LT		High-LT	
	+30 μ m	-50 μ m	+30 μ m	-50 μ m	+30 μ m	-50 μ m
Fastener Fit						
Ti Hi-Lok (first run)	4.2	10.4	30.1	37.7	62.1	63.3
Steel Hi-Lok	5.2		35.0	40.6	62.1	64.2
Ti Lockbolt	5.4		36.0	42.0	59.6	59.4
Ti Hi-Lok (second run)	3.3					
Aluminum Rivet	5.4		35.5		60.4	

Table 3. LT measurements at maximum applied gross stress level (200 MPa) based on instrumented low-, medium- and high-LT joints.

When evaluating LT in low-LT joints the total LT through both fastener rows, including possible LT through friction, is reported. SB is reported based on the sections where LT is measured, thus a global measure of SB is obtained for the low-LT specimen which is, however, not common practice. For the medium-LT joint all measurements correlate to the total LT of the joint. For the high-LT joint all measurements correlate to the LT through the first fastener row in the joint. LT results are composed in Table 3. The SB is evaluated locally at the AGARD positions [3] for medium- and high-LT joints. SB results are composed in Table 4.

SB values are evaluated in the mid-position between the fasteners in the low-LT joint. For clearance fit this is the position with more pronounced SB, whereas for interference fit position C, see Figure 12, is characterised by the highest SB. The high-LT specimen is tested with anti-buckling guides affecting SB at stress levels above 70 MPa, Ref. [8].

Fastener System	Low-LT		Medium-LT		High-LT	
	+30 μ m	-50 μ m	+30 μ m	-50 μ m	+30 μ m	-50 μ m
Fastener Fit						
Ti Hi-Lok (first run)	0.05	0.04	-0.24	-0.41	-0.39	-0.51
Steel Hi-Lok	0.06	0.05	-0.26	-0.41	-0.46	-0.69
Ti Lockbolt	0.08		-0.28	-0.32	-0.50	-0.51
Ti Hi-Lok (second run)	0.06					
Aluminum Rivet	0.08				-0.40	

Table 4. SB measurements at maximum applied gross stress level (200 MPa) based on instrumented low-, medium- and high-LT joints.

In the low-LT joint, LT is heavily dependent on fastener fit. LT increases with approximately 100%, from 5% to 10%, when going from clearance to interference fit, and with almost 30% comparing interference fit (50 μ m) with high interference fit (130 μ m). SB, however, seem not to be particularly influenced by fastener bending stiffness, fastener tilting stability or fastener fit. SB is consistently below 10% at maximum applied load.

The medium-LT joint exhibit a fastener fit installation influence on LT of approximately 6% at maximum applied stress level (200MPa), irrespective of fastener type. In particular it may be noticed that although the bending stiffness of the steel Hi-Lok fastener is almost twice the bending stiffness of the Ti Lockbolt fastener, the higher clamping force in the latter seems to be more important for LT. Higher fastener tilting stability leads to higher SB and higher clamping force seems to lead to a higher SB. However, the most important installation parameter influencing SB in medium-LT joints is fastener fit.

In high-LT joints LT seem to be less influenced by the type of fastener system, including installation parameters as clamping force, fastener fit, fastener bending stiffness and tilting stability. However, SB is increased consistently when going from clearance fit to higher levels of interference fit.

Determination of Fastener pre-load after Installation.

High-performing fastener systems are characterised by a significant level of clamping force (CF). The CF is one of the main installation parameters influencing the fatigue performance of a joint. Often, the only values available for this parameter are those from the manufacturers' specifications. In order to obtain more information on the subject De Magistris et al [10] investigated the CF, with respect to lubrication influence, for three high-performing fasteners. The results are shown in Table 5.

The manufacturers' CF specification for the Steel and Ti Hi-Lok are close to 3 kN and for the Lockbolts approximately 4 kN. The manufacturers' guaranteed values are however minimum values and as shown, the actual CF exceed these values by 30% to almost 100% (Lockbolts). Previous research carried out by Ricci Moretti et al [8] indicated CF values for similar Hi-Lok and Lockbolt fasteners (from other batches though) in the region of 5 kN and 6 kN, respectively. Thus it is assumed that the actual value of CF may vary considerably between different batches of fasteners.

Fastener/Lubricant combinations	Average CF (kN)	Stand. Dev. CF (kN)
Ti Lockbolt	7.7	0.2
Ti Hi-Lok	4.2	0.6
Ti Hi-Lok, grease between collar/pin	4.5	0.3
Ti Hi-Lok, grease between collar/plate	4.5	0.4
Ti Hi-Lok, grease between collar/plate/pin	4.8	0.5
Steel Hi-Lok	4.0	0.4
Steel Hi-Lok, grease between collar/pin	4.6	0.5
Steel Hi-Lok, grease between collar/plate	5.1	0.3
Steel Hi-Lok, grease between collar/plate/pin	4.9	0.5

Table 5. CF measurement results.

Fatigue Testing of low-, medium- and high-LT specimens.

Studies of high-performing fastener systems (threaded fasteners) and a reference system with solid rivets assembled in low-LT joints of AA7475 material were conducted by De Magistris et al [12]. Results are shown in Figure 15. However, this investigation was restricted to the crack growth part of the fatigue life since all specimens were provided with initial defects. Also, Ricci Moretti et al [13] performed studies of the same high-performing fastener systems, but assembled in medium- and high-LT joints subjected to FALSTAFF flight-simulation loading. Results are shown in Figures 16 and 17, respectively.

Frequently the relation between log life and log stress for flight-simulations test results is assumed to be of a Basquin type:

$$\log N + m \log S = \text{constant}$$

The exponent m is called the slope factor, while it actually is the negative inverse slope of the relation:

$$m = - \frac{d(\log N)}{d(\log S)}$$

Hence, the slope factor indicates the life to be gained (or lost) if the stress level is reduced (or increased). Slope factors are presented in Table 6 and are in the same region as found in the literature for corresponding materials and flight-simulation loading. For single shear joints of AA7xxx material, the literature indicates for low-, medium- and high-LT joints slope factors of 4.3, 4.0 and 4.0 (weighted mean values), respectively. Note; the low-LT joint exponents in this investigation only comply with the fatigue crack growth process.

Fastener System	Low-LT <i>m (slopefactor)</i>	Medium-LT <i>m (slopefactor)</i>	High-LT <i>m (slopefactor)</i>
Ti Hi-Lok	2.8	2.9	2.6
Steel Hi-Lok	2.0	1.8	3.4
Ti Lockbolt	2.5	2.5	2.5
Aluminum Rivet	2.4	3.2	

Table 6. Slope factors for low-, medium- and high-LT joints subjected to FALSTAFF flight-simulation loading.

When comparing slope factors of Table 6, the fastener material seems to have significant influence on m depending on LT level. For low- and medium-LT joints an increased bending stiffness seem to decrease the slope factor whereas for high-LT joints the opposite holds true.

Fastener System Influence on Fatigue Life

Threaded fastener systems show significantly increased fatigue resistance compared to traditional solid rivet systems. This is generally true independent of type of test specimen, low- medium- or high-LT joints and type of testing procedure, fatigue life or fatigue crack growth part.

When evaluating medium-LT joints subjected to a fighter spectrum at a low gross stress level, 150 MPa, a lower fastener tilting implies a significantly higher fatigue resistance at high interference ($130\mu\text{m}$) and at clearance ($30\mu\text{m}$) fit. However, for interference ($50\mu\text{m}$) the opposite is valid since the fastener system with higher fastener tilting and CF is the best performing system which also is true for the same fit and spectrum loading at a high gross stress level, 200 Mpa, Refs [12, 13]. In fighter aircraft production, threaded fasteners are installed with interference fit ($50\mu\text{m}$).

Results of high-LT joints subjected to fighter aircraft spectrum loading at both a low gross stress level, 150 MPa, and at a high level, 200 MPa, show the same trend as for medium-LT joints. Low fastener tilting leads to significantly higher fatigue resistance at high interference and at clearance fit, but for interference fit ($50\mu\text{m}$) higher fastener tilting and CF promote fatigue resistance [13].

All high-performing fastener systems show extensive oxide debris at the fracture initiation sites, implying fatigue crack initiation due to fretting.

Fatigue Crack Initiation Characteristics

Depending on the fastener system there are several locations where fatigue cracks may initiate. For example, the crack initiation site may occur in the minimum net section at the edge of the fastener holes in the form of a part-elliptical corner crack, see Figure 18a. This type of crack initiation consistently corresponds to the fastener systems with no or minor clamping force, i.e. solid rivet systems. For a fastener system with a slightly higher clamping force and a stiffer fastener, the crack may also initiate at the intersection of the countersunk and the hole as shown in Figure 18b. For fastener systems with considerable clamping force, i.e. high-performing fastener systems, the fretting mechanism is dominant and cracks always initiate at some distance away from the fastener hole, see Figure 18c.

Summary

In low-LT joints, LT is significantly dependent on fastener fit. LT increases from 5% to 10% when going from clearance to interference fit. SB, however, seem not to be particularly influenced by fastener bending stiffness, fastener tilting stability or fastener fit. SB (global measure) is consistently below 10% at maximum applied load.

The medium-LT joint exhibits a fastener fit installation influence on LT of approximately 6% at maximum applied load irrespective of the type of fastener. Higher fastener tilting stability leads to higher SB and higher clamping force seems to lead to a higher SB. However, the most important installation parameter influencing SB in medium-LT joints is fastener fit.

In high-LT joints, however, LT seem to be less influenced by the type of fastener system, including installation parameters as clamping force, fastener fit, fastener bending stiffness and tilting stability. However, SB is increased consistently when going from clearance fit to higher levels of interference fit.

Thus, the most important installation parameter influencing configuration parameters such as LT and SB seems to be fastener fit.

Considering the fatigue performance of structural joints, CF seems to be the most important installation parameter. Significantly higher CF indicate an order of magnitude higher fatigue resistance compared to traditional solid rivets. CF measurements for several different high-performing fastener systems have been conducted. Results show that the actual value of CF exceed the guaranteed values by 30% to almost 100% (Lockbolts). However, it is assumed that the actual value of CF may vary considerably between different batches of fasteners.

Depending on fastener system there are several locations where fatigue cracks may initiate. Most often initiation occur in the minimum net section at the edge of the fastener holes in a form of a part-elliptical corner crack, which consistently corresponds to fastener systems with no or minor clamping force. For fastener systems with considerable clamping force, i.e. high-performing fastener systems, the fretting mechanism is dominant and cracks always initiate at some distance away from the fastener hole. Thus, in this particular case fretting cracks generally grow in the region which is less stressed and therefore this type of joint-fastener combination obtains higher fatigue resistance.

3.3.3 Experimental Investigation of Fatigue Behaviour in Composite Bolted Joints

Since aircraft structures are subjected to fatigue loading in service conditions fatigue behaviour of their sub components have to be clearly understood. Two extensive experimental programs on fatigue behaviour of composite bolted joints have been started and some obtained results are briefly summarised here, Refs [14,15].

Composite plates made of two lay-ups, quasi-isotropic (24/6-6-12) and 0° -dominated (24/16-4-4) ones, were fastened by two, four, or six Hexagon titanium bolts in either double-lap or single-lap joint configuration, Ref. [14]. The specimens were tested in fatigue loading, $R=-1$. In order to analyse joint behaviour during cyclic loading, various experimental measurements were carried out. Bolt-movement measurements were done to analyse fastener behaviour during fatigue loading. Strain gauges were applied to measure strain and to calculate the load transfer between different bolt rows. Relative displacement between the composite plates was measured by extensometers attached to the edge of the composite plates.

The fatigue results showed that the longest fatigue life was obtained for double- and single-lap joints fastened by six bolts. The dominating joint-failure mode was bolt failure. Analysis of the fatigue results has found that there is a linear dependence between the number of bolts and the fatigue life for those specimens which failed due to bolt failure, see Fig.19. If the applied load per bolt is calculated the fatigue results for the different joints collapses into a single fatigue curve.

The linear rule makes it possible to calculate the fatigue life for composite-structure joints with different configurations. First the load on each bolt should be estimated from the total load applied to the joint. Then, the joint's fatigue life can be found from the fatigue curve in Fig. 19. The linear method works for all lay-ups as long as the failure mode is bolt failure. However, the thickness of the composite plates needs to be the same as in the experiments.

Bolt-movement measurements showed that fatigue damage occurred at the bolts, such as wear particle formation, erosion of the hole surface, reductions in prestress in the bolts. This would significantly increase movement of the bolts, especially at the end of fatigue life, see Fig. 20. The initial decrease in bolt movement and grip displacement is believed to be due to an increase in the coefficient of friction between the plates.

Another way to analyse bolt behaviour during cyclic loading is to display measured bolt movement versus applied load loops. For instance, they indicate that the bolt movement consists of two mechanisms, bending and sliding as shown in Fig. 21. During loading when the friction force is overcome the bolt will slide in the bolt hole. This has been marked as st and sc in the figure. When the bolt gets in contact with the bolt hole it will begin to bend. This has been marked as bt, and bc in the figure.

Load transfer calculations show that the different bolt rows generally transferred the same amount of the total applied load. Generally, the experimental program found that the detailed measurements agreed well with each other and are consistent with the general behaviour of composite bolted joints during fatigue loading.

Another experimental program, Ref. [15], deals with fatigue of composite double-lap joints bolted by countersunk fasteners made of composite, titanium Torque-set, and Huck-comp. The specimens were tested at R=-1 fatigue loading and the dominant failure mode of the specimens were bolt failure. The obtained test results in terms of strain versus joint fatigue lives are presented in Fig. 22 together with the fatigue life results for double-lap specimens joined by six Hexagon bolts.

As seen the highest fatigue resistance was found for specimens joined with Huck-comp fasteners followed by those joined with Torque-set and composite (ACF) bolts. As can be noted both Huck-comp and Hexagon fasteners have a similar resistance to fatigue.

From bolt-movement versus applied load loops during one load cycle, it is possible to analyse different stages of bolt behaviour under cyclic loading. In the bolt movement loop for the first load cycle, see Fig. 23, there are some points of inflection. Initially, during loading most of the load is transferred by friction between the specimen plates. When friction is overcome, the bolt began to transfer load which resulted in its bending, point at.

It was also found that the strain distribution in the joint is affected by the bolt presence and, in particular, by its movement during cyclic loading. For example, if the measured strain for that strain gauge which was located between two bolts is plotted during one cycle as shown in Fig. 24, then it is possible to observe several inflection points in the loop.

The two points, at and ac, correspond to a moment when the friction force is overcome, and the bolts began to transfer the applied load. As a result, the bolt would bend in the bolt hole. However, the bolt bending would be restricted by the opposite hole edge, and that is why points bt and bc appear in the loop. If the results from the bolt-movement measurements and strain gauges are compared as shown in Fig. 25 for one quarter of a load cycle, it can be noted that the points of inflection in both curves appear almost at the same load levels.

It can be seen that while the bolt is bending (part m1-m2 in the EXT1 curve), the strain gauge shows a decrease in strain when the applied load increases (part at1-bt1 in the SG3 curve), thus reflecting how the bolt presence could affect the strain between the bolts.

Finally, some general conclusions can be drawn from the obtained experimental results. Despite the fact, that the bolted joints performed excellent fatigue resistance properties, especially those which were joined by Huck-comp fasteners, it seems that future work is needed in order to optimise the shape of countersunk fasteners. Fatigue tests of specimens with Hexagon and metal countersunk fasteners showed that joint's failure usually occurred after at least two bolts had broken. Thus, it gives time for the bolt failure to be discovered before the final failure will occur. Therefore, since a broken bolt can easily be detected by inspection and then replaced with a new one, it would seem that bolt failure mode has to be the most preferable mode of failure in bolted connections. The observed linear dependence between the number of fasteners and the fatigue life for specimens with different configurations has the potential to in the future reduce the required number of fatigue tests, and thus, the total experimental expenses associated with designing bolted joints.

3.4 STRUCTURAL EVALUATION

3.4.1 Saab 340 Full Scale Fatigue Test

General

The SAAB 340 Full Scale Fatigue test has presently been tested for 192000 simulated flights. The first 180000 flights of testing completed the fatigue phase of the test. This corresponds to two times of the current design life of 90000 flights. Artificial damages were embodied after the fatigue testing in order to verify the damage tolerance characteristics of the airframe structure. This damage tolerance phase testing is ongoing and presently 12000 flights have been simulated. The aim is to continue the damage tolerance testing up to 24000 which constitutes two times of the longest inspection interval outlined in the Maintenance Review Report.

An interim testing of the empennage structure of the SAAB 340 Full Scale Fatigue is also ongoing in order to verify the consequences of implementing some cold working of specific structural elements.

Damage Tolerance phase

The damage tolerance testing is conducted to verify and correlate the damage tolerance analysis of SAAB 340 in accordance with requirements presented in FAR/JAR 25.571

A total of 21 artificial damages were introduced before start of damage tolerance testing. The test specimen will be subjected to fatigue testing for at least 24,000 flights. The damages can be divided into two different types:

- Damages where the intention is to study the crack growth rate.
- Damages in fail safe structure, where the primary load path is removed. In this case the "residual fatigue life" of the remaining load paths, i.e. the time to initiation of secondary cracks, is of interest. The subsequent crack growth rate of possible secondary cracks will also be studied.

The following structural parts have been furnished with artificial damages:

- Wing: lower panels, lower spar caps, front and rear spar web, wing centre splice, wing to fuselage attachment.
- Fuselage: skin panels, skin splices, skin cut-outs
- Cockpit: pilot window posts
- Stabiliser: stabiliser spar/skin, stabiliser/fuselage attachment.
- Nacelle: upper longeron

The selected damages are considered to cover the relevant types of spectra, crack types and materials, in order to be a substantiation for the complete damage tolerance analysis of the SAAB 340.

The experiences from the damage tolerance testing will be taken into consideration in the damage tolerance analysis and the existing in service inspection program will be updated if necessary.

Cold working testing

A cold working technique is applied on the interface between the horizontal stabiliser spars and the fuselage of SAAB 340 Full Scale Fatigue test specimen. A limited number of fastener holes are cold worked and modification will be verified by additional fatigue testing of the horizontal stabiliser structure. The purpose of this modification is to improve economic life of some of the components and thereby avoid future time and cost consuming repairs. A

service bulletin is released for all SAAB 340 aircraft that calls out the implementation procedure of the cold working as retrofit modification.

3.4.2 The Saab 2000 Full Scale Fatigue Test

General

For the SAAB 2000, no complete airframe will be tested due to the commonality with the SAAB 340 .

Consequently, a number of full scale component tests are used. At the present, three fatigue and subsequent damage tolerance tests are ongoing.

Stabiliser fatigue test

This test includes the horizontal stabilisers and the attachment structure to the rear fuselage.

The fatigue phase of this test is completed comprising 150000 flights which corresponds to two times of the design life of 75000 flights. Subsequently testing is ongoing, the damage tolerance phase is performed in order to verify and correlate the damage tolerance analysis in accordance with the requirements in FAR/JAR 25.571.

A total number of four artificial damages have been embodied on the test specimen. The damages can be classified into two types as follows :

- Damages where the intention is to study the crack growth rate.
- Damages in fail safe structure, where the primary load path is removed. In this case the "residual fatigue life" of the remaining load paths, i.e. the time to initiation of secondary cracks, is of interest. The subsequent crack growth rate of possible secondary cracks will also be studied.

Following structural elements of the horizontal stabiliser have been subjected to artificial cracks. This was made by mechanical means in terms of sawing, grinding or cutting.

- Stabiliser/fuselage attachment
Study of crack growth rate for a crack in the stabiliser spar cap, from a fastener hole at the attachment to the fuselage frame.
- Rear spar web
Study of crack growth rate for a crack growing from an inspection hole.
- Upper skin panel
Study of crack growth rate for a crack growing from a fastener hole towards the honey comb core.
- Mid hinge
Study of crack growth rate for a crack growing from a fastener hole (LHS), study of residual fatigue life and crack growth of possible secondary cracks after complete failure of one of two parts in the mid hinge (RHS).

The rationale for selecting the aforementioned damages is that the damages shall cover relevant types of spectra , crack types and materials in order to constitute a justification of the damage tolerance analysis of the SAAB 2000 horizontal stabilisers.

At the moment, 9000 flights has been simulated with artificial cracks and the aim is to verify at least 24000 flights. In that case, the highest inspection interval (12000 flights) is verified.

Residual strength tests are to be carried out for those damages which are considered to require substantiation of the residual strength as a result of complex geometry and/or loading.

Detailed visual inspections are carried out each 500 flights where length of the cracks are recorded. NDT inspections in terms of X-ray and Eddy Current inspections are performed at each 3000 flights.

On the basis of the interim inspections up to 9000 flights, it can be concluded that the cracks in general have shown a small propagation.

The experiences from the from the damage tolerance testing will be taken into consideration in the damage tolerance analysis and the existing in service inspection program will be updated if necessary.

Wing/fuselage fatigue test

The test in question includes the centre and the rear part of the fuselage , the complete wing torque box and the rear part of the engine nacelles.

The wing detail design is changed compared to the SAAB 340 (machined spars with integral spar caps), and the wing/fuselage interface also. Furthermore the cabin pressurisation spectrum is more severe. The flight and landing loads on the fuselage is also more severe due to the slender fuselage of SAAB 2000.

The Wing/Fuselage Fatigue test will be tested to 150000 flights of fatigue loads with a subsequent damage tolerance testing. At the current date 110000 flights of fatigue testing have been completed.

Engine Mount structure fatigue test

The SAAB 2000 engine mounting structure is completely different in design compared to the SAAB 340. The structure is basically built up by eighth steel struts attaching to the forward engine mounts to the nacelle structure. Each of those eight struts is redundant in terms of continuing airworthiness if a strut is failed.

The fatigue phase of the testing is completed (verification of 150000 flights from fatigue point of view). A number of fail safe situations with respect to the fatigue behaviour are tested in order to check the fail safe characteristics of the trussgrid.

The damage tolerance phase with artificial cracks will be final phase of this test programme.

3.4.3 JAS39 Gripen Fatigue Testing

The strength verification programme with large components was completed during 1994. The only ongoing structural tests are two full-scale fatigue tests (single seater and twin seater).

Full scale fatigue test of the single seater

The configuration of the major fatigue test is almost identical to that of the major static test, both with regard to the structure and the test arrangement, see Fig. 26. The test set-up has about 90 control channels and is monitored by acoustic emission as well as by inspection by conventional methods. The test article has about 600 strain gauges installed and has been subjected to 16000 flh testing today (May -99). The test will continue to cover the export version of the Gripen. So far no significant cracking has occurred. The only cracks found are a few in parts belonging to the air brakes. These cracks were expected since they occurred also in the previous component test. The cracking is not a flight safety issue but the parts have been redesigned in order to avoid any cracking at all during the design life.

Full scale fatigue test of the twin seater

The configuration of the major fatigue test of the twin seater is designed to reflect the differences with the single seater, see Fig. 27. The test object is thus a fuselage consisting of the structure between the front of the engine bay and the radome. Attachment loads from the wings are applied via dummies. The whole test set-up has about 50 control channels and the structure is equipped with about 600 strain gauges. The test will be subjected to at least 4 x 4000 (4 x 5600 flights) of fatigue testing. Today (May -99) the test has reached 13000 flh and no cracking has yet occurred.

3.4.4 Research on High Speed Machined Aircraft Structures

A research project on high speed machined aircraft structures is ongoing. High speed machining (HSM) has become a powerful tool for cost efficient manufacturing of high performing metallic structures. Several advanced assemblies are scheduled to be manufactured by HSM in cost reduction campaigns for the Gripen fighter.

The purpose of the project is to:

- Establish knowledge, methods, data and procedures for design, sizing and qualification of complex metallic structures manufactured by high speed machining (HSM).
- Constitute a methodology for Process Window which treats the manufacturing process as an overall integrated process to secure the machined parts in aspects of gauges, tolerances and allowable material properties.

Work is going on to:

- Explain the mechanisms which affect the fatigue strength of aluminium alloys manufactured with HSM.
- Obtain fatigue strength properties specifically related to HSM and to correlate those to manufacturing process parameters.
- Develop methods for efficient part machining with predetermined process parameters.
- Implementation and evaluation of Process Window in a machine centre.
- Establish minimum gauges and tolerances of HSM manufactured articles.
- Develop methods and integrated procedures for fatigue and damage tolerance analysis of monolithic structures subjected to complex loading conditions.
- Extend the range of application of current methods for stability and buckling to cover design solutions feasible in HSM.
- Show by comparing analysis and tests that articles, utilizing HSM, are at least as durable, damage tolerant and compression stable as conventional assemblies are, but at a lower weight and produced to a lower cost.

The project consists of three major work packages:

1. Methods for Effective Part Production through Process Control
2. Machining Process Parameters Impact on Material Properties
3. Stress Methods Development & Detail Analysis Procedures

3.5 STRESS ANALYSIS AND FRACTURE MECHANICS

3.5.1 Damage Zone Model with Multiple Cohesive Zones

A method for analysis of structures with multiple cohesive zones has been developed, Ref. [16]. The main idea is to split a multiple-site crack problem into a global crack free problem and a number of local problems each containing a crack with surface loading, see Fig. 28. The different local solutions are superimposed in a way that the crack surfaces in the global problem becomes traction free, Ref. [17].

The tractions $q(x)$ on the crack surface is related to the crack opening $d(x)$ as,

$$q = F(d) \quad (1)$$

where the functional F depends on the material and the loading condition. The condition at the zone tip ($x = a$) in case of propagating damage is,

$$K_I = K_c \quad (2)$$

where K_I is the stress intensity factor in Mode I.

In order to solve the cohesive zone problem, the splitting method in Ref. [18] was modified so that the cohesive law (1) is satisfied, in a least square sense, on all cohesive zone crack surfaces. If the cohesive law is linear, this corresponds to solving a linear system of equations for the amplitudes of the loads applied in the local problems.

Consider, as an example a composite plate with six cylindrical holes, loaded in tension, see Fig. 29. The material in the plate is linearly isotropic and the cohesive law corresponds to linear softening, Equations (3). As the load is monotonically increased, the cohesive zones propagating from the hole boundaries, perpendicular to the loading direction. The lengths of cohesive zone are determined so that the conditions (1), (2) and (3) are fulfilled.

$$F(\mathbf{d}) = \begin{cases} q_c \cdot \left(1 - \frac{\mathbf{d}}{\mathbf{d}_c}\right) & \mathbf{d} < \mathbf{d}_c \\ 0 & \mathbf{d} > \mathbf{d}_c \end{cases}$$

$$K_c = 0$$

where

$$q_c = 581 \text{ N/mm}^2 \quad ; \quad \mathbf{d}_c = 0.12 \text{ mm}$$

(3)

The first cohesive zone forms at a global strain 0.300 %. At the strain 0.356 %, the maximum load carrying capacity of the plate is reached. The lengths of the cohesive zones at the strain 0.356 % are shown in Fig. 30. Error control and arbitrary accurate solutions are guaranteed by employing an *hp*-version of the finite element method.

3.5.2 Fast and Reliable 3D Fracture Mechanics Analysis in an Industrial Environment

A user-friendly interface and preprocessing facilities to the splitting method, described in Section 3.5.1 in Ref. [1] (see also Refs [18] - [22]), has been developed at SAAB and integrated in their automated design process, Ref. [23]. In the splitting method, the 3D fracture mechanics problem is splitted into a global problem where no cracks are modelled and a number of local problems where a single crack is modelled in detail (see Section 3.5.1).

By proper superposition of the solutions on the local domains and solutions on the global crack-free domain the solution sought is obtained. By employing the *hp*-version of the finite element, a set of solutions for K_I , K_{II} and K_{III} is obtained which converge exponentially fast to the exact mathematical solution of the problem.

The principles adopted in the SAAB development is that,

- parameterized mesh-generators automatically create the local FE-meshes using only global geometry information like radius, crack size a , crack ellipticity c/a etc.
- the global coarse mesh, without cracks, is created in the I-DEAS FE-preprocessor program
- 3D surfaces enclosing single cracks, needed when using the splitting scheme, are defined during the I-DEAS sejour in a simple way. A program module, linked to I-DEAS, was developed for this purpose.

In summary, the SAAB user interested in solving a 3D linear elastic fracture mechanics with multiple cracks of arbitrary number, sizes and locations, creates a coarse mesh of the global crack-free problem using I-DEAS and simultaneously identifies the locations where cracks are located. After defining crack-sizes, the splitting scheme implemented in the in-house FE-code STRIPE, provides a sequence of quickly converging 3D solutions for K_I , K_{II} and K_{III} .

The fatigue analysis tool developed is first to be applied to 3D crack growth studies in solid high speed machined parts.

3.5.3 Probabilistic 3D Multiple-Site Fatigue Crack Growth

Probabilistic multiple-site fatigue crack growth in riveted joints is treated in Ref. [18]. Multiple crack growth, where cracks are relatively large (i.e. 1-50 mm), is focused on. A 4-row rivet butt joint with 14 rivets/row is analysed in detail, see Fig. 31. In order to perform 3D probabilistic fatigue crack growth analysis of joints of the complexity shown in Fig. 31, a linear structural model that provides accurate approximations for the mode I stress intensity function $K_I(s)$ must be developed. From nonlinear analyses of the joint with damage, for a remote stress of 100 MPa, where plates and rivets are modelled as full 3D objects, it is concluded that, for a major crack of length less than about 50 mm, a) elastoplastic effects are small, b) nonlinear effects may be approximatively accounted for by introducing additional loads (i.e. bending moments), and c) the contact surfaces may be selected apriori, Fig. 32. The approximations seem to result only in minor errors in the calculated stress intensity function $K_I(s)$ for the case studied, see Fig. 33. The proposed linear structural model which is based on these assumptions is suitable for probabilistic fatigue analysis where $O(10^6)$ fully 3D fracture mechanics solutions are needed. A mathematical

splitting method is used to solve the fracture mechanics problems (Section 3.5.1 in Ref. [1], and Refs [18] - [21]. The splitting method gives, combined with the hp -version of the finite element method, 3D solutions which converge exponentially fast to the exact values of the stress intensity functions $K_I(s)$, $K_{II}(s)$ and $K_{III}(s)$ of interest, Refs [22, 24 and 25]. From the sequence of quickly converging solutions error control is obtained.

A benchmark problem. As a benchmark problem, consider a structural joint with 3D cracks of a characteristic shape. Fig. 34 shows calculated stress intensity functions $K_I(s)$ for different orders p in the splitting scheme. s is a coordinate along the crack front with $s=0$ at the vertex on the faying surface. Results from the splitting scheme can be compared with a nearly exact reference solution obtained by direct analysis of the complete domain with the cracks explicitly modelled. With increasing polynomial orders p of the splitting scheme, the stress intensity functions converge rapidly to the reference solution.

Comparison with experiments. In Fig. 35 experimentally observed, Ref. [26], crack lengths a_i as function of number of load cycles N are shown for one structural joint. In the figure, analytical results are compared with experimental ones for the five leading cracks (all twelve cracks were considered in the fatigue analysis). In all 600 full 3D fracture mechanics solutions were calculated, using the splitting method, in this single fatigue analysis. We see that the computational scheme described in Ref. [18] provides crack growth data, in case of multiple interacting cracks, that are in close agreement with experimental data.

Probabilistic analysis. A total of 15000 structural joints were analysed using three different scenarios for crack nucleation. The fatigue lifes of each of the 15000 plates were calculated explicitly. During the fatigue analyses, in all $3 \cdot 10^6$ full 3D fracture mechanics solutions were derived. Stress intensity factors needed in the cycle by cycle crack growth analysis were obtained by interpolating between the $3 \cdot 10^6$ 3D fracture mechanics solutions. One model for crack nucleation studied in Ref. [18] is based on the assumptions that two cracks, of lengths 1 mm, nucleate simultaneously at one hole at a certain load cycle. Such rivet holes are assumed completely randomly located. The probability of finding two cracks at a hole is assumed to be given by,

$$P(N) = k \cdot (N - 70000)$$

where $N > 70000$, and $k = 32 \cdot 10^{-7}$ (double cracks/hole/load cycle) was estimated from experiments in Ref. [26].

Fig. 36 shows the distribution functions $F_i(N)$ for the probability of finding the first crack of length a_i (mm) in a structural joint (Fig. 31) as function of the number of load cycles N . Results from the 5000 joints analysed are plotted in the figure (one filled circle/case analysed). If the first crack link-up event is considered, we see, in this type of graph, a significant msd-effect in 15 % of the structural joints.

Consider now the number of load cycles dN needed to propagate a crack in a joint from detectable size to critical size. Fig. 37 shows this distribution where the detectable crack size is assumed to be $a_i = 1$ mm and the critical crack size $a_i = 14$ mm (i.e first link-up). Two cases are plotted. In the first case, load cycles are measured from the cycle when the first crack in the structural joint becomes 1 mm. In the second case, cycles are measured from the cycle when the crack, that will link-up, is 1 mm. The distributions consist, roughly, of three straight line segments. The three parts correspond to the distinct cases of having a maximum three, two or "one" clustered crack pairs (in space).

Summary

The computational method derived in Ref. [18] makes it possible to perform 3D probabilistic multiple-site fatigue analysis of lap-splice joints of real-life complexity. For crack lengths of 1-20 mm, good agreement with experimental data was obtained. In an ongoing study, the splitting method is further developed to handle residual strength problems. Probabilistic analysis, including residual strength analysis of a complete fuselage section is in preparation.

3.6 FATIGUE CRACK PROPAGATION AND RESIDUAL STRENGTH

3.6.1 Strip Yield Analyses of Fatigue Crack Growth in Residual Stress Fields

In Ref. [27], a difficult analysis, the fatigue crack growth in residual stress fields, has been made and corresponding solutions have been achieved. An advanced procedure has been developed to analyse the fatigue crack growth in residual stress fields. The method is based on an extension of the strip-yield crack closure model for part-through crack problems. In this method, the residual stress relaxation due to both the fatigue loading and the crack growth is considered. It has been shown that the effect of the residual stress can be reasonably analysed using fracture mechanics methods as long as the residual stress field and its redistribution can be correctly evaluated and the elastic-plastic crack closure analyses are performed. Several examples are provided for the constant and variable amplitude loading conditions

The examples are based on a standard cruciform welded specimens with or without surface treatment on the weldment. The residual stress is first measured using the X-ray diffraction method on the surface along the loading direction away from the highest stress concentration. The residual stress measurements are shown in Fig. 38 for the residual stress in the virgin specimens as well as after various number of fatigue cycles under the spectrum loading. The experimental residual stress measurements indicate that the residual stress may be released after fatigue loading. However, there is no substantial change in the residual stresses for various fatigue load cycles. The time related release of residual stresses shows to be secondary. A comparison is made for the released residual stress field for only one maximum load. The release of the residual stress for one load has been analytically computed according to the initial residual stress field. The computed residual stress is shown in Fig. 38. A good agreement has been found between the residual stress field after various fatigue loading and the residual stress after only one maximum load. This result indicates that the release of residual stress under the fatigue loading may be well approximated using an analytical residual stress result for only one maximum load. Such a conclusion greatly reduces the analytical requirement to evaluate the residual stress release under the fatigue loading condition.

To verify the conclusion furthermore, neutron diffraction measurements have been made for the residual stress inside of the specimen for the initial residual stress as well as the residual stresses after various fatigue load cycles. The neutron diffraction measurement technique is demonstrated to be capable of detecting the whole residual stress field inside the critical location of the specimens with good resolution for a gauge volume up to 1 cubic millimetre. Since the neutron diffraction technique is a non-destructive method, it is therefore possible to measure the residual stress for the same specimen before the fatigue loading, and after various number of cycles. In the through-the-thickness direction, neutron detection results of the residual stresses for an as-welded specimen are shown in Fig. 39.

To consider a different initial residual stress field, a specimen with TIG dressing on the weldment is measured using the neutron diffraction method. The specimen has a very different initial residual stress field as shown in Fig. 41. The maximum residual stress is not located on the surface, but in about a quarter of the thickness. Fatigue cycles seem to have less effect on the residual stress inside of the specimen due to the stress concentration there is small. The main change of the residual stress occurs on the surface, the left side of the figure.

To complete the analyses of the residual stress field release, analytical residual stress fields are predicted according to the maximum stress level in the fatigue cycles. The predictions are shown in Fig. 40 and Fig. 41 as the solid curves. The analytical results are shown to be in reasonable agreement with the neutron diffraction measurements after various fatigue cycles for both the as-welded state and the TIG dressed state. Such a conclusion is furthermore verified using the neutron diffraction measurement for specimens loaded only once at the maximum stress level, shown for example in Fig. 41 as the “static” load case.

An important conclusion can therefore be made concerning the release of the residual stress field under the fatigue loading. The release of the residual stress field is mainly due to the extreme stress levels in the fatigue loading. This conclusion makes it possible to simplify the evaluation of the residual stress release under the fatigue loading. It is at least acceptable to estimate the release of the residual stress field based on only the elastic plastic stress analyses for the extreme load levels in a fatigue loading. According to this theory, the residual stress field may be stabilised after the specimen has experienced the extreme load level. This conclusion makes it possible to analyse the fatigue crack growth in the residual stress field according to the superposition principle.

It is theoretically possible to analyse the fatigue crack growth in the residual stress field only when the stress-strain response at the critical location can be identified. The stress-strain response can be divided into three different regimes as shown in Fig. 42. The first regime is shown as the dark shaded regime within which cycle yielding occurs. Typically this regime represents the large strain controlled deformation. In this regime, the whole material matrix will have plastic deformation under the fatigue loading. It is the physical property of the material matrix that determines the fatigue life. The failure occurs often with simultaneously numerous cracks in this case. No single, dominant crack can be defined as the main failure mechanism. Therefore, the fracture mechanics based methods are not applicable

The common case for the crack growth in the residual stress field is shown in Fig. 42 in the light shaded regime. In this regime, the plastic yield may occur even at a low load level due to the high possible stress resulting from the superposition of the stress caused by the load and the initial residual stress. As a result of the plastic yield, the residual stress field will be changed. If the load level is not extremely high, a stabilised residual stress field may be created due to the plastic yield. A new residual stress field will be created. Together with the stress due to the load, the stress-strain response may again behave linearly. The damage under the fatigue loading can be considered to consist of initiation and propagation of the fatigue cracks.

For even lower load level, there will be no plastic deformation under the fatigue loading. This is the case typically solved by the conventional fracture mechanics methods. In this case, no evaluation of the residual stress field redistribution is needed and the fracture mechanics solution can be used directly to analyse the fatigue crack growth problems with the implementation of the considerations for the effect of the residual stress field on the fatigue crack growth process.

A strip yield model, or the modified Dugdale model, is extended to analyse the fatigue crack growth in the residual stress field. The basic idea of the strip yield model is shown in Fig. 43. During the fatigue crack growth process, the plastic deformation due to the stress concentration at the crack tip is approximated as pure Mode I. Analytical solutions can be achieved according to this model for the plastic stretches ahead of the crack tip in the plastic zone. Under a fatigue loading history, the crack is simulated to grow into its own plastic zone, and the plastic stretches are left on the crack surface. Using numerical solutions for the boundary conditions for all the plastic stretches both in the plastic zone and on the crack surface, an important crack growth analysis parameter, the crack opening stress can be determined according to this model. The crack opening stress is then used according to Elber's crack growth law to evaluate the fatigue crack growth under general loading sequences.

The strip yield model has been extended for part-through crack problems based on the experimental observation of the similar fatigue striation patterns as shown schematically in Fig. 44. It is possible to establish a ring element arrangement similar to the fatigue striation to approximate the plastic stretches both in the plastic zone and on the crack surface. When a further assumption has been made that the crack front "a" may have approximately the same stress intensity factor as the crack front "c" for a naturally developed fatigue crack front, the weight function method can be used to solve approximately influence functions for the strip yield solution. According to this solution, the fatigue crack growth in the residual stress field can be analysed so long as a stabilised residual stress field can be determined under the general fatigue loading conditions.

The analytical procedure can be illustrated for the analyses of the fatigue crack growth under spectrum loading conditions for the cruciform specimens in both the as-welded state or the TIG dressed state. For example, linear finite element stress analyses may be made at first to identify the critical crack initiation locations as the stress results in Fig. 45 show for both the as-welded and TIG dressed specimen. Elastic plastic analyses may be made according to the initial residual stress field for the maximum stress level in the fatigue spectrum to determine the stabilised residual stress field if no experimental results are available. The crack growth can then be analysed according to the strip yield solution for a fatigue crack growing in a residual stress field.

To rationalise the fatigue crack growth when the residual stress field is considered, some interesting cases have been investigated. For example for the as-welded specimens under a tensile-tensile spectrum loading, the analytical crack growth results are compared to the test results as shown in Fig. 46. For this case, the spectrum consists of many small cycles around the mean stress level with spike overloads seldom occurring. Two comparison analyses have been made; one with the residual stress considered, the other with the residual stress ignored. The comparison is shown in Fig. 46a with the test results in an S-N curve. The fatigue crack growth analyses are performed using a physical initial flaw size of 0.1mm which is an average value from the weldment at the stress concentrations.

Reasonable agreement appears between the analytical results and the test results. An extraordinary result from the comparison shows that there is virtually no effect of the residual stress on the fatigue lives for the range of stress levels under consideration. It seems that the crack growth analysis can be adequately performed without considering the effect of residual stress. A close check into the analytical results revealed the mechanism behind the phenomenon. When the analytical crack opening stress is compared to the load spectrum as shown in Fig. 46b, it has been found that the crack opening stress is different when the residual stress is considered. When the residual stress is present, the crack opening stress is lower than that when the residual stress is ignored. The problem seems to be the load spectrum. As shown in the figure, the load spectrum has its majority of cycles concentrated around the mean value at the half of the maximum stress level. Most of the load cycles are above the crack opening stress level whether or not the residual stress is considered. It can be expected in this case that the crack closure analysis is not even needed at all. A simple cycle-by-cycle damage accumulation calculation may provide good analytical results.

The same situation exists also for the TIG dressed specimen as the comparison in Fig. 47 shows. The residual stress has no effect on the crack growth at all even though it significantly affects the crack opening stress. The reason is the same as for the as-welded specimens since the majority of the fatigue cycles in the spectrum are located higher than the crack opening stress whether or not the residual stress is considered. Again, this behaviour is mainly due to the spectrum, and the residual stress. Residual stresses induced by the welding are mainly of the tensile type at stress concentrations. Together with the tensile load, the local stress ratio is very high so that the change in the mean stress due to the residual stress will have negligible effect on the fatigue life.

The situation becomes quite different when a different load spectrum is considered. The second load spectrum is basically the same as the first load spectrum but with significantly reduced mean stress level. Instead of being a pure tensile-tensile spectrum, the second spectrum is a symmetrical load sequence with a gross stress ratio of $R=-1$. Again, the fatigue crack growth in the as-welded specimens is considered at first. The comparison between the test results and the analytical results is shown in Fig. 48. For this analysis, three considerations have been made. One for the residual stress free state, one for the initial residual stress field, and one for the stabilised residual stress-state. The predictions show that residual stress has significant effect on the fatigue life when the spectrum has changed. The fatigue life becomes more than an order of magnitude shorter for high stress levels. The fatigue life becomes about two orders of magnitude shorter for low stress levels. Apparently, ignoring the effect of residual stress will lead to a significant over estimation of fatigue lives. The comparison shows that when the stabilised residual stress is considered, the accuracy in the fatigue life analyses can be improved.

Concerning the crack opening stress, Fig. 48b shows that when the residual stress is not considered, the highest crack opening stress occurs. The high crack opening stress reduces significantly the crack growth driving force for majority of load cycles, resulting in a significant increase in the analytical fatigue lives. When the residual stress is considered, the crack opening stress is reduced due to the tensile type of residual stress. As a result, the crack growth driving force is increased for the fatigue cycles. Therefore, the fatigue lives are reduced.

There is a significant difference in the crack opening stress results between the considerations of the initial or the stabilised residual stress. The difference affects only a small part of fatigue cycles. Therefore, it doesn't affect significantly fatigue lives whether or not the residual stress relaxation is considered. This case may not be general since the load spectrum doesn't have many load cycles within the levels where the stress release shows difference. The effect of the residual stress release may become strong when the load level is increased since more release of the residual stress is expected.

The behaviour is similar for the TIG dressed specimens even though the initial residual stress is quite different. The comparison is shown in Fig. 49. In this case, the release of the residual stress doesn't have affect on the fatigue life since the release occurs mainly inside of the specimens which affect the fatigue life less. In the case of the TIG dressed specimens, the predicted fatigue lives may become more than two orders of magnitude longer if the residual stress is not considered.

In summary, the investigation demonstrates that the crack growth in the residual stress field can be satisfactorily solved according to the strip yield crack closure solution so long as the initial residual stress field, the stress analyses, and the residual stress relaxation under the fatigue loading have been correctly analysed. The residual stress may or may not have effect on the fatigue life depending on whether or not its effect on the crack opening

stress covers the fatigue cycles in the spectrum. Without the knowledge, the fatigue lives can not be reasonably analysed when a residual stress field is present in the path of the critical cracks.

3.6.2 Analyses of AGARD Small Crack Growth Test Results Based on the Post Yield Consideration

A procedure has been developed for post-yield fatigue crack growth analyses, Ref. [28]. The method is based on an extension of the strip-yield crack closure model. This procedure accounts for the post yield effect by considering residual stresses caused by the gross yield at the peak fatigue load. Three-dimensional weight function approach is used to solve influence functions as well as stress intensity factors needed to solve the crack closure. It has been shown that the method is very effective in dealing with part through fatigue crack growth problems under constant and variable amplitude fatigue loading conditions when gross yield occurs at the stress concentration.

The stress-strain response at a stress concentration can be divided into to three cases as shown in Fig. 50, depending on the load and the material. Under the fatigue loading, if the stress concentration under the extreme load level is less than the yield stress of the material, the stress-strain may have a linear relation as shown in Fig. 50a. The deformation will recover once the load is released. This is the case when most of modern fracture mechanics methods are valid when the fatigue life and crack growth is to be analysed. When the stress concentration exceeds the yield stress of the material, plastic yield may occur. None recoverable plastic deformation will change the linear stress-strain response under the fatigue loading. When the range of the fatigue loading is not significant, a linear stress-strain response may be re-established under the fatigue loading after the initial plastic deformation as shown in Fig. 50b. When the range of fatigue loading is severe and the load may be controlled by the deformation, cyclic plastic yield may occur as the case shown in Fig. 50c.

Most of the successful applications of fracture mechanics methods are valid only when the stress-strain response is linear at the stress concentration as shown as case (a) in Fig. 50. When plastic yield occurs, two cases should be separated whether or not cyclic yielding occurs. When cyclic yielding occurs at the stress concentration, the fatigue life is no longer determined only with the initiation and the propagation of the fatigue crack. The physical matrix property of the material may affect the fatigue life as well. Typical application is for the low cycle fatigue problems in high temperature application. In this area different method should be used to analyse the fatigue problems.

The common post-yield fatigue problems are represented by the case as shown in Fig. 50b. In this case, the extreme load level may create the plastic yield at the stress concentration. After the extreme load, the stress-strain response may return to a linear relation due to both the plastic deformation and the strain hardening. No plastic yield may occur for further fatigue cycles due to the increased yield stress from the strain hardening and the residual stress from the plastic deformation. The fracture mechanics method may be extended to analyse this post yield crack growth problem when the effect of the residual stress is considered, and the material parameters after the strain hardening are used in the analyses.

The strip yield crack closure model is extended to analyse the fatigue crack growth problems in the post yield regime. In this solution, the post yield effect is accounted for by using the residual stress caused by the gross yield as a modification in the analyses of the fatigue crack growth problems. The crack growth in the post yield condition is considered as the fatigue crack growth in a residual stress field caused by the yield. The solution is basically the same as for the analysis of the crack growth in a residual stress field.

According to the method, the AGARD small crack growth test results are analysed. The AGARD small crack tests are performed with the specimens shown schematically in Fig. 51. The specimen has a single notch on the side of the plate. The fatigue loading is the cyclic remote tension applied at clamping ends of the specimen. The notch has an average stress concentration factor of 3.17.

The fatigue test results are shown in Fig. 52 as symbols for various loading conditions. For many of the test load levels, plastic yield obviously occurred at the notch due to the high stress concentration for the alloy with a moderate yield stress. The yield is especially severe for the spectrum loading as well as the constant amplitude loading with rather high or rather low stress ratios.

The fatigue life has been analysed based on the strip yield model for the crack growth initiated at the metallurgical defects. Reasonable predictions have been made for the constant amplitude loading with the stress ratio of $R=0$, and for GAUSSIAN spectrum. Systematic shift can be observed between the test results and the predictions.

For the high, tensile dominated spectrum, the predicted fatigue lives are shorter than the test lives. For the compressive dominated loading, the predicted lives are longer than the test lives. A reasonable explanation is that the gross yield at the notch may affect the fatigue lives. Under large tensile load, plastic deformation may be created at the notch, resulting in a compressive residual stress field. This residual stress yield may reduce the crack growth rate and, in turn, the fatigue life. When a large compressive load is present, tensile residual stress may be created at the notch due to the plastic deformation. The tensile residual stress field may speed up the fatigue crack growth rate and reduce the fatigue life.

To verify the theory, finite element model has been created and the non-linear stress analyses have been performed for the load levels involved in the tests. Along the ligament away from the notch, the computed residual stresses are shown in Fig.53 for various load levels. The finite element analyses show significant yield in the specimen, with the plastic zone often larger than the radius of the notch. The residual stress is significant which can effectively affect the fatigue lives.

When the post yield effect has been taken into account, the fatigue lives can be re-analysed. The new prediction results are shown in Fig. 54, compared to the test results. There is a significant improvement in the prediction results when the post yield effect is considered. The predictions agree better with the test results as shown in Fig. 54, especially for the spectrum loading with high peak load or the loading with load stress ratio which may lead to the compressive yield and the tensile residual stress field.

The post yield effect may be better explained with an example for the crack opening stress compared to the loading sequence as shown in Fig. 55 for the FALSTAFF spectrum with a peak load of 205 MPa. The plastic yield at the peak load will lead to a gross yield at the notch and create a residual stress field. The residual stress will increase the crack opening stress since it is the compressive. In increased crack opening stress will exclude many load cycles from affecting the crack growth. The fatigue life is therefore prolonged.

To consider quantitatively the post yield effect, a better consideration for the distribution of the predictions and the test results for all the cases under consideration. Such a consideration is shown in Fig. 56 for all the results as shown in Fig. 54. To simplify the comparison, the mean fatigue lives are compared to the predictions in this figure. The comparison is made between the post yield mechanism ignored and for the post yield considered.

When the post yield is not considered, the prediction has in average 0.7 shorter fatigue life with a larger scatter (C.O.V of 0.6). If the “factor of two” criterion is considered between the predictions and the tests, there is only 75% probability that the predictions may be within the factor-of-two”. However, when the post yield is considered, the prediction becomes much closer to the test results in average, with slightly shorter life of 0.92. If the factor-of-two criterion is considered, the prediction gives about 90% probability compared to the test results. This is a significant improvement in the prediction results.

3.6.3 Stochastic Fatigue Crack Growth Analyses Based on Damage Accumulation Solution and Crack Closure Model

A total life probabilistic model, Ref. [29], has been developed based on both short and long crack growth data to analyse the fatigue crack growth under general loading conditions. The analysis is based on Elber’s crack closure model. An effective stress intensity factor is used as the major crack growth driving force in the crack growth analyses. Statistical fatigue crack baseline data from the constant amplitude loading tests are used as a basic governing function in the probabilistic crack growth analyses. A strip yield fatigue crack closure model is used together with a modified Miner-Palmgren’s damage accumulation model to account for uncertainties in the non stochastic crack growth process from the crack initiation to the final failure. In this model, effects of material inhomogeneity, initial flaws, and variations in geometry and applied load etc., have been considered for their individual effects. This model provides a probabilistic estimation of the fatigue crack growth for both small and large crack sizes. Several examples have been provided to illustrate a variety of problems that the model is capable of dealing with, and to clarify physical mechanisms behind some of the controversial experimental results.

Even for a wide range of crack growth rate data obtained from different laboratory under different stress ratios as shown in Fig. 57a, the crack growth rate can be expressed in an intrinsic form when the Elber’s stress intensity

factor is considered, see Fig. 57b. This simplifies both the deterministic and the stochastic crack growth analyses when the distribution of the crack growth rate can be reasonably defined, see Fig. 57b.

The problem with conventional stochastic crack growth analyses is that they are often developed based on the large crack growth data as shown in Fig. 58a which covers only a very limited range of the crack growth rate as shown in Fig. 58b. This leads to a great concern about the capability when these methods are intended to be used for the total crack growth analyses which covers the crack growth stage from the small crack to large crack.

Typical small crack growth test results are shown in Fig. 59. The crack growth shows larger scatter especially when the crack size is small. In the small crack growth stage, the crack growth is affected by the size of initial cracks as well as the small crack growth behaviour. Obviously, the stationary stochastic solutions based on the large crack growth test can not be applied for the small crack growth problems not only due the scatter, but also due to the crack growth rate range which is much lower than that for the large crack growth tests.

It seems necessary to characterise the whole range of probabilistic crack growth rate as shown Fig. 60 with large scatter assumed in the low crack growth rate regime. A simplification can be made when the intrinsic crack growth rate is considered as shown in Fig. 60 for the crack growth rate to be approximated piece-wise linearly according to the crack growth rate regime. A intrinsic presentation of the crack growth can be used as shown in Fig. 60b so that stochastic solutions may be considered for different regimes when the total fatigue life is considered. In this way, solutions for the long cracks can still be used when the crack growth rate is high.

When the intrinsic crack growth analyses are considered, the crack growth is due to the effective part of the load cycle, see the schematic as shown in Fig. 61. Under a spectrum loading condition, it is now possible to analyse the crack closure based on the strip yield model so that the range of effective load cycles can be translated into the range of effective stress intensity factor. By grouping the effective range of the stress intensity factor, numbers of cycles located in each intrinsic crack growth regime as shown in Fig. 60 can be determined. Therefore, stochastic solutions may be found based on the intrinsic consideration of the crack growth process.

A simplified model is established according to the schematic as shown in Fig. 62 according to the crack closure analyses and an extension of Miner-Palmgren's damage accumulation model. In this model, a deterministic crack closure analysis is performed for a deterministic load spectrum. Load cycles for each crack growth rate regime are computed as individual damage parameters. The cycles in each regime are used as a base to analyse the stochastic crack growth in each regime. If a spectrum has more effective cycles near the threshold, the fatigue life may have larger scatter. Otherwise, the crack growth may have similar feature as for the large crack case.

When the stochastic crack growth process has been solved, the effect of the initial flaws can be solved according to the model as shown in Fig. 63 by an integral. In this solution, the fatigue life may be determined with the small and large crack growth for the crack initiated at the physical initial flaws. In this solution, the crack nucleation stage is omitted since there is a very high probability that the initial flaw may be present in the engineering structure.

A comparison is shown in Fig. 64 between the analytical results and the test results in the scatter in the fatigue life for a wide range of load levels and spectrum for a crack initiated at a stress concentration. Two results are presented; one is with only the stochastic crack growth being considered, the other is with the effect of initial flaw distribution being considered. For the total life analyses, it has been shown that both the scatter in the initial flaws and in the crack growth process should be considered in order to achieve reasonable estimation of the scatter in the fatigue life. The simplified model seems to be capable of dealing with major feature in the stochastic crack growth process.

Together with a generalised solution for mechanical joints as shown in Fig. 65, scatter in the fatigue life may be analysed using an equivalent load, secondary bending, and the load transfer condition for the verification of the stochastic crack growth solution.

One case has been analysed for the fatigue live of the rivet hole specimens. Two cases have been considered; one with the rivet hole filled with a rivet, but there is no load transfer occurring through the rivet, the other with about 15% load transfer through the rivet. The stochastic crack growth model is used to analyse scatters in the fatigue lives for both cases. The comparison between predictions and the test results is shown in Fig. 66. There is a larger scatter in the crack growth for the specimens with load transfer for all the load cycle range. According to the analytical model, it has been found that the geometrical inconsistency has a significant effect on the scatter in the crack growth

process when load transfer occurs at the rivet hole. This solution seems to be reasonable since when load transfer occurs, the production inconsistency in the rivets affects more significantly stresses at the hole so that the fatigue life may be affected more significantly.

A significant outcome of the present solution is for the analysis of the scatter in the fatigue life when different loading conditions are involved. Fig. 67 shows an example for the test panel when two different fatigue sequences are used. In the tests, it has been found that the scatter in the fatigue lives becomes increasingly large when the fatigue life becomes longer (the low load level). The same trend is not observed when the same test items are subjected to variable amplitude loading conditions. The scatter in the fatigue lives seems to be “stabilised” under a variable amplitude loading condition. The behaviour is well accounted for using the present solution for the scatter in the fatigue lives as the comparison in Fig. 67 shows. The basic mechanism behind the test behaviour depends on the crack growth behaviour. For the constant amplitude loading, every load cycle will contribute to the crack growth process. When the fatigue life is long, the crack growth may be concentrated at the low end of the crack growth rate. According to the crack growth model, the low end of the crack growth rate will exhibit highest scatter in the crack growth rate and in turn, the greater scatter in the fatigue life. The scatter in the fatigue life may become infinite somewhere below the threshold.

The same mechanism applies to the crack growth under the variable amplitude loading. The difference is that under a variable amplitude loading condition, not every load cycle contributes to the crack growth process. Under a spectrum loading, some load cycles may be below the crack opening stress as shown in the schematics as shown in Fig. 61, they contribute to neither the crack growth or the scatter in the fatigue life. The longer the fatigue life becomes, the more the load cycles may be below the crack opening level. Even though the crack growth driving force for the remaining load cycles may be low and has larger scatter. The average effect may become constant so that the scatter in the fatigue life may not be dramatically changed. When such a mechanism is considered, even the simplified model yields a reasonable prediction for the scatter in the fatigue lives as the comparison in Fig. 67 shows.

3.6.4 A Novel Probabilistic Fatigue Crack Growth Solution based on the Crack Closure Model

The damage tolerance method requires assumption of cracks pre-existing at the highest stress concentrations in critical airframe structural details. The subsequent fatigue crack propagation should cover at least twice of the target life before failure occurs. If the crack propagation can not meet the requirement, an inspection of crack should be arranged at half of the fatigue life to prevent catastrophic failure. Fatigue tests from coupons up to the whole frame should be performed to complement the damage tolerance analyses. In spite of this, the damage tolerance method can still not guarantee an economical airframe life due to uncertainties in the initial fatigue quality, the materials, the usage, and the maintenance. Probabilistic analyses are needed to cover major sources of uncertainties. In Ref. [30], a procedure is presented based on a novel probabilistic fracture mechanics solution for analyses of the fatigue crack propagation. A practical example is used in the discussions to illustrate the procedure and to address important issues when uncertainties are involved. Compared to the deterministic damage tolerance method, it is shown that different consequences may appear in the analytical fatigue lives based on probabilistic considerations.

As an extension to the stochastic crack growth analysis model presented in Ref. [29], further development is made. The basic model is to create a stochastic solution for the crack growth process for spectrum loading involving the crack growth under both the small and large crack condition which is determined from the applied load as well as the spectrum as shown in Fig. 68a. The fatigue life is solved conditional to the initial flaw distribution in an integral as shown in Fig. 68b. This solution includes the non-stationary stochastic crack growth under the variable loading condition which is also affected by uncertainties in the geometry and the fatigue loading condition.

When the stochastic crack growth is determined, it is possible to investigate much more realistic scenarios in the management of fatigue problems, for example, when inspection and restoration are involved. For a structural detail in service, inspections may be performed. Repair may be made when crack damage has been detected. During the life span of a structure, more than one repair and inspection may be made for the critical details or the similar details in a large group of products, the fleet of a type of aircraft. Consideration should be made as shown in Fig. 69.

After a product has been put into use, inspection intervals should be determined for the critical details to prevent the failure. It is necessary to determine a inspection interval so that the safety of the structure is not compromised and in the same time, there is good probability that cracks may be discovered according to the inspection method. When

the inspections have been performed and the detected damage has been repaired, the safety of the structure should be re-analysed and the next inspection interval should be determined. These analyses are possible when acceptable crack growth analyses can be made.

One example is used to illustrate the solution. The example is for a forward fin attachment in a production aeroplane. The configuration is shown in Fig. 70. Fatigue test has been performed before to identify critical area and determine fatigue life for this item. A symmetrical fatigue load sequence is used in the fatigue test as shown in Fig. 71a. The most critical location found for this item is at the “leg” with a tested corner fatigue crack as shown in Fig. 70.

Fatigue crack growth has been analysed according to the stress results from the finite element analyses. The analytical results agree reasonably well with the test results as shown in Fig. 71b, indicating that the analytical method may be used for a reliable probabilistic analysis of the crack growth problem.

To simplify the fatigue life analysis, failure of the attachment is assumed when the crack begins to cross the thickness of the plate. This is used as criterion for the probability of failure (POF). According to this criterion, POF is computed based on the fatigue crack growth analyses. The analytical results are shown in Fig. 72a. Three results are presented in the POF results based on the order statistics consideration, representing POF for a fleet of 1, 10, and 100 aeroplanes. The computed POF is for the leading crack in the whole fleet. The results shows that POF is very high especially for the large fleet size, indicating at least reasonable inspection should be made before catastrophic failure. One inspection method is considered for a inspection threshold of $a(20/95)=20$ mm. This method is similar to the eddy current method.

A very high probability of detecting crack (PODC) can be found especially for the leading crack. It is meaningful to make inspection to detect the fatigue crack and implement repairs to keep the reliability acceptable. Solutions are developed to determine the inspection interval and re-evaluate the reliability when the effect of inspection and repair is considered.

Prediction examples are shown in Fig. 72. The first inspection procedure is based on the deterministic consideration based on the test results as shown in Fig. 71b. The fatigue test shows a fatigue life around twice of the design target. It may be assumed to be conservative to make inspection interval about one fourth of the test fatigue life, the half of the design life. This inspection procedure seems to provide a safety factor of four compared to the test results.

There is only one item being tested. The production uncertainty as well as the load uncertainty is not included. When these effects are considered, the POF can be analysed together with the consideration for the material inhomogeneity and the initial flaw distribution. The predicted results are shown in Fig. 73a as the symbol line. The prediction shows that there is a very high POF at the end of the first design life, more than 13% of POF. The first inspection has virtually no effect on POF. The prediction gives a different picture than what can be estimated from only the fatigue test.

If the inspection interval is further reduced to a quarter of the design life, POF can be reduced as the prediction in Fig. 73. The prediction shows that POF increases with the increase of the inspection before it is stabilised. The first inspection still has no effect on POF, perhaps due to the inspection threshold. The increased POF in the first several inspections is mainly due to the effect of missing the crack in the inspections. At the time of the inspection, the crack may have considerable size. If the crack has been missed in the inspection, it will lead to a higher POF at the next time of inspection. The sequence is stabilised only when significant inspection and repair have taken their effect.

The inspection procedure can be arranged according to another consideration, the variable inspection interval. According to the crack growth solution, it is possible to calculate inspection interval based on the given POF. The prediction results are shown in Fig. 73b for a given POF of 5%. This consideration shows that no inspection is required in the first 0.7 of design life. Very tight inspections are required after the first inspection. The inspection interval can be slightly increased when the repair has taken the effect. The inspection intervals seem to be periodic.

There is a very high POF no matter what inspection procedures have been used immediately after the inspection. The reliability of the component can not be restored to the original condition since there is a certain chance of missing the crack in the inspection. Therefore POF can not be recovered to the original condition. This may inspire another alternative to replace the component for a given POF to avoid the event of missing the crack in the

inspection. The consequence of this option is shown in Fig. 73b. For this option, the replacement will recover the component into the original condition. The replacement can take place for the next interval, the next 0.7 design life.

This option gives the best reliability and the minimum service. The concern for this option is mainly the cost. According to the probabilistic solution, the cost can be analysed in a term of the probability of repair. Assuming that a crack is immediately repaired after it has been detected. The probability of detecting crack is equal to the probability of repair (POR). For a given time duration, POR equals the sum of PODC in the time duration. For a short life duration, for example for 0.7 fatigue life, the cheapest option is to have no inspection or replacement at all. When one design fatigue life is considered, the variable inspection interval seems to be cheapest since it requires less inspections even though POR is nearly the same as that for the option of the fixed interval. The periodic replacement is the most expensive option.

The cost function changes dramatically when the fatigue life is considered, for example, for 1.4 times of the design life, the option of replacement becomes the cheapest since its POR is smaller and no inspections and repair are required with the corresponding costs. The cost for the variable interval is still less than that for the first interval. However, the difference is not dramatic, see Figure 74.

Based on the analytical model, the reliability of the component can be improved without changing the design parameter. For example, if the initial surface can be improved on the component to reduce the size of initial flaws. Better production method can be used for the component to reduce the difference between each component. These methods can increase the reliability so that POF can be reduced. An example is shown in Fig. 75 when both the initial flaw size and the product consistency have a 100% improvement. Under this improvement, POF can be dramatically change. For the requirement of POF of 5%, the first required inspection will be larger than the design life, which means that the design objective has been met. Again, if the component is required to operate beyond the objective, tight inspection and repair are required to guarantee the reliability.

A POF of 5% seems to be a very large number for a critical detail. The value in the analyses accounts however for all the uncertainties in the fatigue crack growth process including the uncertainty in the applied load as well as the uncertainty in the productions. These uncertainties are not included in a test item. In the fatigue test, the geometry is carefully measured. Stresses in the critical locations are often measured under the controlled load, and the loading is accurately controlled. Under this condition, POF for the test item is rather different from the actual component in service. An example is shown in Fig. 76 for two different considerations; one with actual uncertainties in both the load and the geometry, and the other with load and geometry controlled.

The computed POF is much lower when the production and load uncertainties are removed. In this case the POF is in an order of 10^{-3} for 0.7 design life where the first inspection is expected to occur in the same time when the computed POF is about 5% for the case when the uncertainties in both production and loading are considered. Understanding such a difference may be very helpful in translating the fatigue test results into a reliable fatigue life management program to minimise the failure probability and to improve cost efficiency.

3.6.5 Initial Fatigue Quality

The US Airforce model for initial fatigue quality, based upon the equivalent initial flaw size concept, has been implemented in a computer code at FFA. The implementation has been made such that two different approaches to obtain the parameters of the cumulative equivalent initial flaw size distribution, the time to crack initiation approach and the equivalent initial flaw size approach, are used and compared.

Fractographic data regarding crack growth are needed in order to apply the model. A rather extensive analysis of the experimental data may be performed to censor out data with anomalous behaviour and to calculate the parameters of the crack growth rate versus crack length relationship.

The FFA implementation of the model has been applied to the same set of fractographic data as was used by the US Airforce in order to verify the model. The results of these analyses show that the code is working as intended. Furthermore, it was found that the TICI and EIFS approaches in general results in different EIFS distribution parameters.

To test the model two different sets of fractographic data have been used. The first set refers to the data obtained in the AGARD co-operative investigation on "Short Crack Growth Behaviour". The second set refers to a data base of crack growth rate developed at FFA during recent years.

Using the first set of data it was found that the parameters of the EIFS distribution are sensitive to the procedures used to screen the fractographic data and to design variables. However, a single generic EIFS distribution was established for all 18 different groups of fractographic data which upon transformation to TTCI distributions for the individual data sets compared rather well to the cumulative TTCI distributions obtained by ranking TTCI-values for each data set and assigning probabilities according to their rank. Also, three different approaches to compute the EIFS-values were studied and it was found that the best fit of the TTCI distribution was obtained by using the deterministic approach.

Using the second set of data it was found that imposing the condition of a crack growth rate directly proportional to the crack length shifted the lower tail of the EIFS distribution considerably as compared to the result obtained using the true average value of the crack growth rate exponent.

Both data sets used effectively show the hypothetical nature of the EIFS distribution.

3.7 COMPOSITE MATERIALS

3.7.1 Mode I Loaded Delamination Cracks Studied by High Magnification Moiré Interferometry

An experimental/numerical study of the displacement fields around delamination cracks in carbon fibre/epoxy composites loaded in Mode I has been made, Ref. [31]. Four specimens with different stacking geometries were investigated. The delamination cracks were simulated using Teflon films. The measurements were made using moiré interferometry at high magnification. With moiré interferometry, the displacement field can be determined with an accuracy of 20 nm or better and by using microscope optics, a spatial resolution of about 10 μm can be achieved. The moiré interferometer used has the capability to switch between laser illumination for acquiring the displacement field and white light illumination to visualise the underlying microstructure. This made it easy to correlate the displacement fields to images of the fibre stackings.

The resulting displacement fields were compared to numerical solutions calculated using the finite element method. The comparisons indicate that the Teflon films for some of the specimens did not delaminate fully, a problem that raises doubt about the use of Teflon films to simulate delamination cracks. Otherwise the agreement was good, confirming that the displacement field around such cracks is satisfactorily described by linear fracture mechanics. The agreement was improved when a matrix rich region in front of the crack tip was included in the finite element model. Such matrix rich regions are often introduced in front of Teflon films during specimen manufacturing. Further, it was observed that a single cross-ply lamina has large effect on the displacement field at the surface due to different Poisson's ratios.

3.7.2 Rate Dependency of out-of-plane Properties of Composites

The ply out-of-plane tensile properties of carbon/epoxy composites were studied by use of static tests at FFA and dynamic tests in a tensile split Hopkinson bar apparatus at Luleå University of Technology, as reported by Melin & Asp [32, 33], Fig. 77. Miniature dog-bone unidirectional specimens were used since the directional structure of the specimens is unsuitable for conventional cylindrical specimens. The need for large strain rates at a sufficiently large load necessitated the use of specimens with a fairly small aspect ratio and associated large strain gradients. In the dynamic tests high speed Moiré photography was used to study the local strain field in the gauge section, which allowed for determination of the true stress-strain relation.

The dynamic tests were performed at strain rates between 100 /s and 800 /s. Several specimens were tested to fracture at strain rates between 300 /s and 800 /s . The corresponding crack speeds were up to 2300 m/s. The experiments did not reveal any increase in modulus with increasing strain rate but moderate increases in failure stress and strain, Fig. 78.

3.7.3 Evaluation of the Mixed Mode Bending Delamination Test

Based on previous static tests the Mixed Mode Bending (MMB) delamination test is now used in ongoing tests of delamination fatigue properties of composites. The static evaluation procedure for the MMB test is assessed in Ref. [34] which is focused on analytically equivalent evaluation models, expressed in load-displacement or load-only parameters. The analyses are compared with experimental results obtained with both evaluation methods. In particular, the assessment concerns the sensitivity of the interlaminar toughness to test rig forces as well as specimen material and geometrical properties. For a typical example, neglect of test rig forces causes a ten percent relative error in the calculated mixed mode ratio when using methods based on load only, Fig. 79. Neglect of test rig forces results in an overestimation of the mode dependent interlaminar toughness, since testing is done with a higher mode II fraction than anticipated. When all additional forces were considered both evaluation methods produced almost identical results, Fig. 80. Evaluation based on load only is convenient but is sensitive to variations in specimen flexural modulus and dimensions and had a larger scatter. The application of crack length corrections for calculating the mode I component is discussed in detail. The findings of the study are summarized in recommendations for the MMB test procedure and its subsequent evaluation.

3.7.4 Methodology to Predict Strength of Impacted Sandwich Panels

A systematic review of analytical models to predict failure of impacted sandwich panels, with focus on local compressive failure, is given in Ref. [35]. Thus, global buckling is not discussed. The study is limited to static failure modes, but may be of interest when developing models for fatigue failure of impacted sandwich panels. Impact damage in sandwich panels include a dent, delaminations, matrix cracks and fibre fracture in the face sheet and crushing of the core. The failure modes include wrinkling, inplane skin failure due to stress concentrations at the damage (Fig. 81a) and dent growth due to crushing of the core (Fig. 81c). Delamination growth caused by local outward buckling of a sublaminar (Fig. 81b) is considered unlikely due to the presence of an initial dent. A novel dent growth criterion based on energy balance considerations is suggested. All failure models were presented in a uniform notation and demonstrated on a number of published experimental studies. It is shown that dent growth and inplane failure due to stress concentrations are competing failure modes, which in many cases may occur at similar stresses. Several findings are also applicable to failure of monolithic laminates.

3.7.5 Studies of Impact on Composite Structures

Fatigue problems in composite structures are often associated with impact damage. The effects of impact on composite laminates and sandwich panels have been studied extensively at FFA by use of instrumented impact tests, fractography and static and fatigue tests of compression after impact. A comprehensive review of more than fifty studies in this area performed at FFA during 1986 to 1998 was given in Ref. [36]. However, the studies of fatigue properties after impact have been limited to two studies of impacted sandwich panels and one study on how impact induced matrix cracks affect the reliability of embedded fibre optic sensors.

3.7.6 Damage Tolerance of Impacted CFRP Sandwich Panels

An experimental investigation concerning static compressive strength, damage growth during fatigue and residual compressive strength of impacted CFRP sandwich panels was performed, Ref. [37]. The program includes determination of energy level for damage initiation (E_{IN}) and energy level to obtain a barely visible impact damage (E_{BVID}), i.e. a dent of 2 mm. Furthermore, specimens impacted at three different energy levels were tested with respect to static strength at room temperature and specimens with a barely visible impact damage were tested with respect to fatigue life both at room temperature (RT) and at hot-wet (HTW) conditions. After impact, and at intervals during fatigue loading, the damage was characterised by ultrasonic C-scan and by measuring the dent depth. Fatigue tests were performed with a symmetrical fin spectrum to a maximum of 6000 flight hours whereupon the residual strength was determined. Residual strength tests were performed at RT and at 100°C for specimens fatigue loaded at HTW conditions.

Low velocity impact damage were introduced in a drop tower using a falling weight with a 30 mm hemispherical tup guided by a tube, at room temperature and ambient environment. Both static and fatigue tests were performed in four point bending. The faces were made of 8 or 24 plies Fibredux 6376-HTA with a nominal thickness of 1 or 3 mm and the quasi-isotropic layups $(\pm 45/90/0)_S$ and $(\pm 45/90/0)_{3S}$. The core was made of aluminium honeycomb with

the densities 72 and 192 kg/m³. The test program was performed in a similar way as in a previous investigation performed on panels with skins of T300/914C. Dimensions of the specimens were 160x1000x50 mm (width by length by thickness). After trial impacts on specimens with the same lay-up and core material energy levels for impact was set to 1 (E_{IN}), 8 and 11 J (E_{BVID}) for the 8 ply specimens and to 8 (E_{IN}), 20 and 50 J (E_{BVID}) for the 24 ply specimens.

Results from static and residual strength tests are presented in Figs. 82 and 83 in terms of failure strain.

The sensitivity to impact of the failure strain of CFRP sandwich panels was clearly demonstrated since a reduction in strength with up to 80 % to the level of typical design values for composite structures was recorded. The reduction in failure strain combined with the rapid decrease of dent depth and thereby the visibility during fatigue loading is alarming since these results indicate the necessity to perform visual inspections after every mission. The cause for the decreased dent depth is relaxation of the top plies due to delaminations. It was also observed that the dent depth decreased with time when there was an interruption of several months between impact and fatigue testing.

Although the number of specimens in each group is too few to make a good statistical evaluation some tendencies can be recognised:

- The static failure strain of undamaged 24 ply specimens is higher than that of the 8 ply specimens.
- Reduction in static failure strain due to a BVID is more significant for the 24 ply specimens.
- Dent depth and consequently the visibility decreases rapidly after only a few flight hours of fatigue testing.
- Fatigue loads at RT cause damage growth and a reduction in residual strength. The effect seems to be more pronounced when the specimens were tested in HTW conditions.
- Strain concentrations in connection with the damage have been observed, and both for medium impact energy and a BVID the concentration has been recognised to extend more than 60 mm in the panels length direction.
- Nonlinearities in strain recordings on impacted panels indicates local buckling in the damaged area.

3.7.7 Methodology for Efficient Design of Composite Structures Exposed to Impact

Impact damage may cause severe reductions in the strength and stability of laminated composite structures. Most experimental studies have focused on *impact resistance*, which deals with the damage caused by an impact, and *impact damage tolerance*, which deals with the effect of the damage on strength and stability of the structure (Fig. 84). A more limited number of studies have focused on *impact response*, i.e. the structural response and formation of damage during impact, which provides deeper insight in the factors governing impact resistance. Analytical models of impact response and residual strength have gradually been developed at FFA to reduce the large costs of certification tests and to make design more efficient. A building block approach has been suggested which separately addresses major issues of importance for the effect of impact on composite structures. The ultimate goal of the work on impact is to efficiently combine impact resistance and impact damage tolerance in design to minimize undesired effects of a given impact. This may be termed a strive for *impact tolerance*. The work at FFA concerning impact damage has been summarized in Ref. [38]

The effects of impact on composite laminates and sandwich panels have been studied extensively at FFA by use of instrumented impact tests, fractography and static and fatigue tests of compression after impact. A comprehensive review of more than fifty studies in this area performed at FFA during 1986 to 1998 was given in [39]. However, the studies of fatigue properties after impact have been limited to two studies of impacted sandwich panels and one study on how impact induced matrix cracks affect the reliability of embedded fiber optic sensors.

FFA:s research on *impact damage tolerance* has been focused on compressive failure which involves strength and stability due to global buckling, local delamination buckling, delamination growth, in-plane failure and interacting failure modes. So far modeling work has focused on simulation of buckling induced delamination growth, and a program package has gradually been developed. A recent extension allows analysis of impacted skin-stiffener panels [40]. Previous experiments have demonstrated the need to also consider other failure mechanisms and the change of stiffness properties in the damaged region [41].

In general, an impact initiates elastic waves propagating from the impact point. For impact times in the order of the transition time for through-the-thickness waves, the response is dominated by three-dimensional wave propagation (Fig. 85a). For longer impact times, the response is initially governed by flexural waves and shear waves (Fig. 85b). For times much longer than the time needed by these waves to reach the plate boundaries the lowest vibration mode of the impactor-plate system predominates (Fig. 85c).

The impact response type is shown to depend on the impactor vs. plate mass ratio and appropriate models have been suggested for the various response types. Thus a distinction between *large mass impact* and *small mass impact* is more relevant than the common distinction between "high velocity" and "low velocity" impact. Figure 86 shows the difference in response and damage caused by 10 J impacts with a large and small mass, and illustrates that a small mass impact results in earlier damage initiation and larger damage at a given impact energy.

Evidently, response models for undamaged plates may predict damage initiation. For small deflections the delamination radius and plate boundary conditions have almost no influence on the critical load for delamination growth, which then is given by the following expression

$$F_{cr} = p\sqrt{32DG_{IIc}/(n+2)}$$

where D is the plate stiffness, G_{IIc} the mode II interlaminar toughness and n is the number of delaminations. The critical load for large deflections is obtained by accounting for membrane load contributions. For large mass impact the response may be predicted by a spring-mass system involving the impactor mass M , the effective plate mass M_p^* , the contact stiffness k_c , shear stiffness k_s , bending stiffness k_b , and membrane stiffness k_m of the plate under static load (Fig. 87). The corresponding initiation energy is obtained by summing contributions due to contact, bending, shear and membrane deformation. Further growth is highly dependent on the number of delaminations, but reasonable bounds for delamination size have been established.

At FFA several experimental studies have been carried out to characterize the impact damage for different geometries and boundary conditions. Laminate thicknesses have ranged from 2 to 6 mm and lay-ups have usually been quasi-isotropic, although a few studies have been done on orthotropic lay-ups. Our studies show that damage growth normally initiates by matrix cracking, followed by delamination growth and finally fiber fracture [44, 45]. Delaminations in thick laminates with span-to-thickness ratios of 10 to 20 typically initiate close to the impacted surface, while delaminations in thin laminates initiate close to the midplane [5] (Fig. 88).

Further delamination growth in thick laminates occurs in a "barrel shaped" region by growth of delaminations around the mid-plane, although a single large delamination may occur at the lowermost interface. Delamination growth in thin laminates occurs in a conical region by growth of delaminations towards the back face of the laminate [42]. The individual delaminations are more or less peanut shaped, extending along the fibers of the neighboring lower ply. In contrast, cracks with fiber failures generally follow the fibers of the neighboring upper ply and appear below delaminations as extensions of a matrix crack [42, 43]. The damage geometry and degree of fiber fracture depends on the span-to-thickness ratio and on how much the energy for damage initiation has been exceeded. Furthermore, the asymmetry of the damage has a strong influence on the global buckling load of the panel.

Recent work at FFA has concerned development of models with general non-linear kinematics to account for interaction of global and local buckling with contact for a panel with a single delamination of arbitrary shape located at the critical ply interface [40]. The finite element model developed is based on non-linear plate theory, using 4-noded mixed interpolation Mindlin/Reissner shell elements and a moving mesh technique. It is assumed that delamination growth is governed by linear elastic fracture mechanics parameters. The strain energy release rate, G , at local delamination growth is computed from the discontinuity in an energy momentum tensor component across the crack front [44].

Analysis of a plate or stiffened panel with a delamination is performed in the following steps: (1) Global buckling analysis. (2) Local buckling analysis of the delaminated member. (3) Postbuckling analysis from local buckling with contact iteration and automatic load increase until delamination growth criterion is attained. The growth criterion is currently based on the total critical strain energy release rate. (4) Delamination crack propagation by moving the FE mesh in the growth regions and continued postbuckling analysis.

By this approach, the evolution of delamination propagation is modeled performing a large number of incremental crack propagations. The developed model has been validated by experiments on artificially delaminated and impacted plates [41, 44] and stiffened panels [40].

Figure 89 shows the experimental and computed load vs. out-of-plane deflection results for two delamination depths. The numerical model is shown to capture the main observations regarding transverse deflections and buckling loads. Furthermore, critical loads, direction and shape of growth were also well predicted by the model. From a practical point of view the most important result of these studies seems to be that delamination growth for all cases occurred more or less at the global buckling load. Consequently, structures with delaminations should never be allowed to buckle globally. In reference [40] a preliminary analysis of stiffened composite panels is performed. In that study, a scheme for identification of the most critical ply interface is presented.

Test results for artificially delaminated, impacted and undamaged plates were compared [41]. A difference in maximum (global plate buckling) load is conspicuous in the load vs. out-of-plane deflections of the plates depicted in Fig. 90. The artificial delamination causes a 10 % reduction in global buckling load, while the reduction caused by impact damage is 20 %. These results imply that the reduced stiffness in the impacted zone has a fairly large effect on the panel buckling load. Thus, correct prediction of the buckling load of an impacted structure requires methods that consider influence/interaction of the stiffness reduction of the damaged zone.

In addition to delaminations which may promote buckling induced delamination growth, an impact damage may also be associated with local stiffness reductions which cause stress concentrations and in-plane "notch type" failure. Furthermore, such stiffness reductions will affect the delamination growth by reducing the buckling loads. In the literature it has also been suggested that a buckled sublaminar may act as a stress raiser causing in-plane failure.

Extensive fiber failure may also result in in-plane failure. For example, damage studies in [43] indicated more or less complete fiber failure in all plies in about one third of the total delamination width of 230 x 150 x 4 mm specimens impacted at 30 J. In the worst case such a damage may be comparable to the effect of a hole or slit, which may result in stress concentrations of three or more in a quasi-isotropic laminate. Available notch failure criteria will be incorporated as a competing failure mode in future development of the delamination growth FE-program.

3.7.8 Fatigue Delamination Growth Model for Composites

In order to calculate fatigue delamination growth in composite specimens a fatigue delamination growth rate law is needed. To experimentally measure the fatigue delamination growth rate for all possible combinations of energy release rate mode ratios and load ratios would be very expensive. The two constants in Paris law require that two points on the fatigue delamination growth curve are known. A model, Ref. [45] has been developed in which one such point is the fatigue delamination growth threshold which experimentally has been found to occur for a constant change in energy release rate, ΔG_{th} . In literature it has been reported that ΔG_{th} is independent of mixed mode ratio and Q -value. The Q -value is defined from

$$Q=R \quad \text{if } -1=R=1$$

$$Q = \frac{1}{R} \quad \text{if } R < -1 \text{ or } R > 1$$

where R is the load ratio, $R = \frac{S_{min}}{S_{max}}$. The threshold is here defined as the point where there is a "knee" in the delamination growth rate curve. The delamination growth rate, $\left(\frac{dg}{dN}\right)_{th}$, at which this "knee" occurs is usually about 10^{-6} mm/cycle. The second point occurs when static fracture takes place. The delamination growth rate, $\left(\frac{dg}{dN}\right)_C$, at which this takes place is usually between 10^{-1} - 10^{-2} mm/cycle. From these two points the constants in Paris law can be calculated for any energy release rate mode ratio and load ratio. The model is schematically shown in Fig. 91. The model predicts the exponent n in Paris law to decrease with decreasing load ratio Q and increasing amount of mode II fracture which agrees well with experimental observations.

3.7.9 Load-Ratio Dependence on Fatigue Life of Composites

Different composite structures in applications such as aircraft are often subjected to spectrum fatigue loading with different average load ratios, $R = \frac{S_{\min}}{S_{\max}}$. When characterizing the material for such structures constant amplitude fatigue data of coupons at the specific R -values are often used. This results in a large number of fatigue test having to be run which is expensive. Hence, there is a need to develop models for calculating the fatigue life of composites at different R -values. One such model has been developed, Ref. [46]. The basic assumption of the present model is that the fatigue life of a specimen is governed by delamination growth. When the delaminations have grown to a critical size the specimen will fail. This critical size is dependent on the peak load at failure. All other damage mechanisms, for example matrix cracking and fiber failure, are assumed to be of secondary importance and will only have a minor influence on the total life of the specimen. A consequence of this assumption is that the fatigue life of a specimen can be estimated by calculating the delamination growth rate in the specimen which is what the model does. Failure for specimens subjected to different R -values but the same peak load magnitude is assumed to occur when the critical delamination in the specimens has grown to the same length. This makes it possible to integrate Paris law to compare the number of cycles to failure for specimens at different R -values. The constants in Paris law are obtained from the model in Ref. [45]. The model works for all possible R -values as long as the basic assumptions are fulfilled. A comparison with experimental results, Ref. [46], for unnotched composites can be seen in Fig. 92.

3.7.10 Coefficient of Friction of Composite Delamination Surfaces

Composites are known to often fail due to delamination growth and it is important to have a good understanding of all the aspects involved in delamination growth. The crack surfaces in the ENF specimen will be in contact with each other where the support is located. During loading of the test specimen the surfaces will slide against each other and the resulting friction force will reduce the energy release rate of the delamination crack, Ref. [48]. In local delamination buckling the delamination surfaces are often in contact with each other at some points. At those points friction forces will be induced which affect the buckling problem and the energy release rate of the delamination front. In order to be able to include those friction forces in the modeling of local delamination buckling the coefficient of friction for delamination surfaces in contact is needed.

The coefficient of friction of delamination surfaces from graphite fiber/epoxy matrix (IM7/8552) composites has been measured in reciprocal sliding, Ref. [49]. The worn surfaces were examined with a scanning electron microscope and the friction and wear mechanisms were studied. The results show that the coefficient of friction is independent of normal load in the load range studied. The effective coefficient of friction depends on the amount of load carried by matrix/matrix, fiber/matrix and fiber/fiber contacts and their respective coefficient of friction as

$$m = \frac{1}{P} (m_{mm}P_{mm} + m_{ff}P_{ff} + m_{mf}P_{mf})$$

where P is the normal load, μ is the coefficient of friction and the subscripts mm , ff , and mf stands for matrix-matrix contact, fiber-fiber contact, and matrix-fiber contact, respectively. Of the three types of contact the matrix/matrix contact has the highest coefficient of friction, approximately 0.6. After an initial wear-in of the surfaces the coefficient of friction will decrease with increasing number of reciprocal cycles as more load is carried by fiber/fiber and fiber/matrix contacts. In Fig. 93 can the evolution of the coefficient of friction as a function of number of cycles be seen for $0^\circ/0^\circ$, $0^\circ/90^\circ$, and $90^\circ/90^\circ$ interfaces. The evolution of the coefficient of friction is related to whether the starting surfaces are covered with a matrix layer or if the fibers are visible. Any matrix layer will flow to the sides of the contact region, causing fibers to become visible. More of the load will be carried by fiber/fiber and fiber/matrix contacts and the coefficient of friction will decrease. Matrix debris forms at the boundary of the contact regions and no wear of the fibers was observed.

3.7.11 A Numerical and Experimental Investigation of a Composite ENF-Specimen

Delamination growth often plays an important role in composite failures. Thus, making it important to have a good understanding of the mechanisms and mechanics of delamination growth in order to use composites in advanced applications. The ENF specimen has been used to study static and cyclic mode II fracture, G_{II} for $0/0$, $45/45$, and $90/90$ interfaces and for carbon fiber reinforced epoxy materials IM7/8552, HTA7/6376, and T300/914, Ref. [48]. The ENF-specimen has also been studied with FEM. Results show that the material T300/914 has the lowest G_{IIc}

and that the 0/0 interface has the lowest G_{IIc} of the interfaces studied. The distribution of energy release rate for the different interfaces were calculated and the specimens with a 0/0 or 90/90 interface have fairly flat distributions with a small mode III component. The specimen with a 45/45 interface had an uneven distribution with a large mode III component. The FEM results were compared with beam models and it was found that for the specimen with a 0/0 interface were the beam models acceptable whereas for the specimens with a 90/90 and 45/45 interface did they show a large error. Instead a modified direct beam model was used for the specimens with a 90/90 and 45/45 interface which resulted in good agreement with the FE-solution, see Fig. 94. The influence from friction was studied with FEM and compared with a beam model. In Fig. 95 can the decrease in energy release rate for specimens with the different interfaces be seen together with results from a beam model. The results are for a coefficient of friction equal to 1.0. With a realistic coefficient of friction the decrease in energy release rate at a crack length of 25 mm is about 2%. The delamination crack changes interface for the specimens with a 45/45, and 90/90 interface and the direction it grows in is probably determined by the stresses at the crack tip. Two new stacking sequences are suggested with which delamination growth at 0/45 and 0/90 interfaces can be studied. By taking advantage of that the crack only wants to propagate in the positive z-direction, globally compressive side of specimen, a stacking sequence which results in a $0^\circ/45^\circ$ and $0^\circ/90^\circ$ interface can be designed, $[0^\circ_{12}/90^\circ/0^\circ_{11}]$ and $[0^\circ_{12}/45^\circ/0^\circ_{11}]$, where the off-axis ply is placed in the negative z-direction from the crack and // indicates the position of the delamination. The distribution of the normalized total energy release rate can be seen in Fig. 96 for a crack length of 25 mm. Both distributions are sufficiently flat for testing and can be analyzed with the modified direct beam model.

3.7.12 Calculation of Mode-Separated Energy Release Rates during Delamination Growth

In Refs [50, 51] delamination growth is analysed under the assumption that delaminations propagate in matrix rich layers close to ply interfaces. By only using results from the FE-solution inside the isotropic layer, when calculating stress intensity functions, several mathematical difficulties are avoided and standard fracture mechanics can be used. The energy release rates are then obtained from standard relations. As a benchmark example, a test specimen is analysed for a general load such that all three fracture modes are present. The results from the method, where the delamination propagates in a thin isotropic layer are compared with results for a perfect interface, see Fig. 97. The solution is for a $0^\circ/45^\circ$ interface with a 1 μm thick isotropic layer. A very good agreement between the two methods is found when the total energy release rates are compared. The comparison is also excellent for G_{III} and (G_I+G_{II}) , respectively. In Fig. 98 the influence of the thickness of the isotropic layer on energy release rate is shown from and the effect found to be small. By using the method with an isotropic layer the mode-separated energy release rate can be calculated for curved delamination fronts.

3.7.13 Interaction Between a Delamination Crack and a Matrix Crack

The interaction between a delamination crack and matrix cracks are studied in Refs [52, 53]. The point where a matrix crack intersects with a delamination front is often a vertex. A typical geometry can be seen in Fig. 99.

A notched specimen with a 6 mm hole was studied analytically. Typical matrix cracks and delamination shapes were taken from the experimental investigation, Ref. [54]. In the specimen one delamination grew parallel to the load direction and was bounded by matrix cracks, see Fig. 100. The type of vertex between a matrix crack and the delamination front shown in Fig. 99 occurred in this specimen.

Close to the vertex the stress intensity factors of the delamination crack front will be given by

$$K_I(\mathbf{z}) \approx \sum_{j=1}^J S^{(j)} \cdot \tilde{s}_I^{(j)} \cdot \mathbf{z}^{\text{Re}(\Lambda^{(j)})-1/2} + R_I$$

$$K_{II}(\mathbf{z}) \approx \sum_{j=1}^J S^{(j)} \cdot \tilde{s}_{II}^{(j)} \cdot \mathbf{z}^{\text{Re}(\Lambda^{(j)})-1/2} + R_{II}$$

$$K_{III}(\mathbf{z}) \approx \sum_{j=1}^J S^{(j)} \cdot \tilde{s}_{III}^{(j)} \cdot \mathbf{z}^{\text{Re}(\Lambda^{(j)})-1/2} + R_{III}$$

where $S^{(j)}$ are vertex intensity factors which are determined from the solution on the complete specimen, $\tilde{s}_I^{(j)}$ etc are vertex-edge stress intensity parameters which only depend on the local geometry close to the vertex, and $\Lambda^{(j)}$ are the vertex eigenvalues which also only depend on the local geometry close to the vertex. The $\tilde{s}_I^{(j)}$ and $\Lambda^{(j)}$ can be determined ones and for all from the local problem schematically shown in Fig. 99. The R_I , R_{II} , and R_{III} are smooth remainders. From the equations it can be seen that when the vertex is approached, i.e. $\mathbf{Z} \rightarrow \mathbf{0}$, the stress intensity factors will approach zero if $\text{Re}(\Lambda^{(1)}) > 1/2$ and infinity if $\text{Re}(\Lambda^{(1)}) < 1/2$. In Fig. 101, the five lowest vertex eigenvalues are shown for a $0^\circ/45^\circ$ interface.

Figure 101 shows that $\Lambda^{(1)}$ is less than 0.5 for all β studied. For a straight delamination crack, $\beta = 0$, $\Lambda^{(1)}$ is as low as 0.28. This means that the stress intensity factor will approach infinity when the vertex is approached. This might affect the fatigue delamination growth. It is reasonable to assume that the delamination crack will be curved towards larger β -values (as to have $\text{Re}(\Lambda^{(j)}) = 1/2$) which has also been observed in experiments. The stress intensity factors close to the vertex in the specimen in Fig. 100 were calculated with the vertex theory developed in Ref. [52] and with FEM. A comparison of the results can be seen in Fig. 102. The two solutions are in good agreement.

3.7.14 A Numerical and Experimental Investigation of Delamination Behaviour in the DCB-Specimen

One of the most common failure mechanisms in composites is delamination growth. Before delamination growth can be predicted in composite structures it is necessary to have a good understanding of delamination growth in generic test specimens, such as the DCB-specimen. The DCB-specimen has been studied in detail both numerically and experimentally, Ref. [55]. The critical mode I energy release rate, G_{IC} , was the same for the materials HTA7/6376 and IM7/8552 and $0^\circ/0^\circ$ interface, approximately 220 J/m^2 . The G_{IC} -value of T300/914 was about half that of HTA7/6376 and IM7/8552, about 110 J/m^2 . no toughening behavior was observed for the specimens with a $0^\circ/0^\circ$ interface. For the specimens with a $90^\circ/90^\circ$ and $45^\circ/45^\circ$ interface a R-curve behavior were observed. A fractographic study found that the crack propagates up and down in the off-axis plies bounded by the 0° plies in a repeating way. A detailed fractographic study found that several matrix cracks are nucleated before the delamination crack changes interface. After the crack has reached the $0^\circ/90^\circ$ interface the interest to change interface again increases as the cracks grow longer. The average energy release rate for DCB-specimens with different interfaces calculated with FEM was compared with results from beam models, see Fig. 103.

A model developed by Olsson showed the best prediction of the energy release rate. There is a large difference between G_{IC} and the approximate threshold value for fatigue loading. This leads to different load levels for delamination growth during static and fatigue loading. Given a delamination in a structure the ratio between delamination growth during static and fatigue loading is

$$\frac{G_{IC}}{G_{th}} = \left(\frac{K_{IC}}{K_{th}} \right)^2 = \left(\frac{\mathbf{s}_{static}}{\mathbf{s}_{fatigue}} \right)^2 \approx \frac{220}{80}$$

which gives

$$\left(\frac{\mathbf{s}_{static}}{\mathbf{s}_{fatigue}} \right) \approx 1.7$$

where σ_{static} and $\sigma_{fatigue}$ are the stress in the structure which causes the energy release rate of the delamination in the structure to reach G_{IC} and G_{th} , respectively. For mode II loading the situation is even worse with the ratio $\sigma_{static}/\sigma_{fatigue}$ being approximately 3. This should be compared with the ratio $\sigma_{DUL}/\sigma_{DLL}$ which often is 1.5 where σ_{DUL} and σ_{DLL} are the design ultimate load and design limit load. This means that a given delamination in a structure might not grow during static testing, but during fatigue testing it might grow.

3.7.15 Composite Fatigue

An experimental investigation has been carried out regarding load-sequence effects on the fatigue life of composite structures. Different elimination levels were considered for various load spectra and for constant amplitude block loading. The spectra considered were for an early design spectrum for the Gripen fighter aircraft, spectra associated with the aft fitting of the fin and to the upper fitting of the wing, and the compression dominated spectrum “Short Inverted Falstaff”. Both experimental and calculated results show, that the elimination level can be set to approximately 50% of the maximum range occurring in the load sequence. This means that considerable time and cost reductions in structural verification testing can be achieved. This will also have impact on a life prediction methodology since only a characteristic number of loading states needs to be considered. The resulting life for block testing, especially for a load ratio of $R=-1$, is highly influenced by truncation of high load ranges in the sequence. Spectrum fatigue test results accounting for ranges up to 90% of maximum range, the remaining load states eliminated, can be mapped on constant amplitude data. At chosen elimination levels approximately 80 to 90% of loading states were eliminated. Calculation results with the same technique, i.e accounting for a characteristic number of cycles, show promising results.

In Fig. 104 the influence of different elimination levels is depicted for the mixture of tension-tension and compression-compression loading (TT-CC) and for the full tension-compression loading (TC). It should be pointed out that only a limited number of tests has been performed (two specimens per level). For the TT-CC loading, elimination of cycles at 90% of ϵ_{\max} has a clear influence on fatigue life but for elimination of corresponding cycles at 50% of ϵ_{\max} the influence on fatigue life is almost within the scatterband for constant amplitude testing at the load ratio, $R=-1$. It can also be seen that for the calculated result, according to the theory outlined in Ref. [56]., the influence of elimination of cycles up to ~50% of ϵ_{\max} is negligible.

When the block-loading consists mainly of tension-tension and compression cycles, i.e TT-CC loading at $R=0.7$ and 1.43 , and those cycles are eliminated, the result still is close to constant amplitude testing at the load ratio $R=-1$. The reason is probably due to the fact that TT or CC dominated loading has very flat SN-curves and thus have a minor contribution to the life. It is also likely that if the TT-CC loading had been fully tension respectively compression loading, i.e $R=0$ and , the result would have been almost the same. In conclusion; accounting for only the $R=-1$ cycles gives reasonable prediction of life, though small contributions are due to the TT and CC cycles.

In Fig. 105 the test results for the different spectra are presented and compared to constant amplitude data. Figure 106 is an enlarged figure with embedded calculation results according to the theory outlined in Ref. [56]. The test results for the wing spectrum, OVKB, fall between $R=-0.5$ and -2 , and also match earlier spectrum testing with the short inverted Falstaff, labelled as SIF in the figure. The test results for the fin spectrum BFKB with two elimination levels, BFKB30 and BFKB50, i.e. loads less than 30 to 50% of maximum range were eliminated, do also match corresponding constant amplitude data very well if the effective number of cycles are accounted for in an appropriate way.

3.7.16 Fatigue after Impact and Bolted Joints in Fatigue

Currently an experimental program is running addressing fatigue after impact and bolted joints in fatigue loading. Both constant amplitude and spectrum testing are addressed with the purpose to find suitable elimination levels for use in verification testing and methodology development. For fatigue after impact preliminary results show that, see Figs 107 and 108 , loading in the compression regime is more critical than the combination of tension and compression loading that was the case for specimens with open holes. The failure in bolted joints is strongly dependent on the R -value with compression loading being the most beneficial. Elimination levels up to 50% of maximum range show promising result when compared to spectrum fatigue loading.

3.7.17 Certification Procedure

The current philosophy for for fatigue and damage tolerance substantiation of composite structures is based on a no-growth concept which is achieved by conservative strain limitations and extensive testing on a coupon level and on built-up structures. A major drawback in the certification work is the lack of relevant methodology, especially for life prediction, which makes it impossible to e.g investigate the consequences of a load change from design limit load (DLL). Of major concern within the substantiation work of composite structures is impact damage and the associated strength but also out-of-plane loading causing unexpected failure modes. There is an urgent need to come

to an agreement what a barely visible impact damage (BVID) is and the associated energy level. The situation today is that the substantiation work to a high degree, at least for certain aspects, is very project related. To have reasonable test times omission of low loads is necessary but the demands for metallic or composite structures differs and a clear methodology is lacking. The situation today is rules by the thumb.

The general requirements for the certification procedure could be found in Refs. [57] and [58] issued by FAA (Federal Aviation Administration) and JAA (Joint Airworthiness Requirements. In addition to those basic rules advisory circular Ref. [59] and the European version Ref. [60], with some editorial changes for consistency with JAR rules, covers specific composite aspects. The certification work is generally performed in what is called the building-block approach or Rouchon's test pyramid, Ref. [61], here shown in a schematic way in Fig. 109.

For military aircraft, and for naturally reasons, the requirements for certification are less coherent than for civil aircraft. To accomplish the general requirements stated, specific documents are written typical for the current project, see e.g Ref. [62]. Such a document typical covers stressing methods and how to verify static strength and how to meet the damage tolerance requirements. A comprehensive report covering certification methodologies was written within a national research program in Sweden, Ref. [63]. In Refs. [64] and [65] an extensive investigation was undertaken to develop a certification methodology. Various approaches were investigated, life scatter approach, load enhancement approach, ultimate strength approach and change in spectrum approach. Within a running national research program and within a european program EDACOS (Efficient Design and Verification of Composite Structures) two reports covering substantiation principles and the associated costs for the control surfaces of S2000 regional aircraft were written, Refs. [66] and [67]. The load enhancement and ultimate strength approach provides a convenient way to substantiation, see Figs. 110 and 111. The structural response variability, i.e one source to what is known as "Hot-Spot Failure", needs to be taken into account. It should be remembered though that damage tolerance due to in-service damage, like impact for instance, is not covered within those approaches. Repeated load tests with e.g impact damage are still needed on detailed sub-components in order to establish the appropriate shape parameter.

3.7.18 Equivalent Damage and Residual Strength for Impact Damaged Composite Structures

Determining structural durability and damage tolerance of aircraft-composite structures is an important task, not only in the design process but also when the aircraft is in operational use. There are many sources and types of damage e.g.: fatigue cracking, environmental degradation, or damage introduced by foreign objects. When occurring, all types of damage need immediate attention for determination of the effect on aircraft performance and functionality. There is a need in other words for simplified predictive methods for rapid assessment of occurring damage, where impact damage is the most important damage mode. Two residual strength models are presented, the so called soft inclusion and delamination buckling theory, and compared to experimental results on impact damaged composite structures in Ref. [68], see Fig. 112. Those experiments spans a variety of impact events, from 8J to 55J and different layups. The investigation has been supported by FE-technique for determination of the stress distribution in the buckled state and for characterisation of the damaged region. It can be concluded that for low-energy impact, though conservative assumptions on stiffness reduction, that the soft inclusion is un-conservative for residual strength prediction. In contrast the delamination buckling theory show good agreement for various impact energy levels, thicknesses and layups. The importance of repeated loading for composite structures with artificial delaminations is also demonstrated. If repeated loaded, the local buckling strain is strongly reduced as compared to a non- repeated loaded structure. It can also be shown that artificial delaminations, though deep-lying, can grow in a stable manner if pre-buckled.

3.8 REFERENCES

- [1] Blom, A.F. (Ed), "A Review of Aeronautical Fatigue Investigations in Sweden During the Period May 1995 to April 1997". FFA TN 1997-23, Stockholm 1997.
- [2] SMAAC-TR-3.2-08-1.3/SAAB, "Summary Of Laboratory Tests Performed By SAAB. Basic Specimen Design"
- [3] SMAAC-TR-4.2-05-1.3/SAAB, "Summary Of Laboratory Tests Performed By SAAB. Basic Specimen Design"
- [4] SMAAC-TR-3.2-12-1.3/SAAB, "Summary Of Laboratory Tests Performed By SAAB. Wide Specimen Design"

- [5] Ricci Moretti, L., Segerfröjd, G. and Palmberg, B., "Fatigue Behaviour of Mechanical Joints – A Programme Overview and an Introduction to Fretting and Fretting Fatigue with special Application to Joints", FFA TN 1998-03, The Aeronautical Research Institute of Sweden, Sweden, 1998.
- [6] De Magistris, F., Segerfröjd, G. and Palmberg, B., "Fatigue Programme on Mechanical Joints – Part II, Low Load Transfer Specimens", FFA TN 1998-62, The Aeronautical Research Institute of Sweden, Sweden, 1998.
- [7] Segerfröjd, G., "Fatigue in Mechanical Joints - A Literature Survey," FFA TN 1993-56, The Aeronautical Research Institute of Sweden, Stockholm, 1995.
- [8] Ricci Moretti, L., Palmberg, B. and Segerfröjd, G., "Experimental Characterisation of eight Fastener Systems – Detailed secondary Bending and Load Transfer Measurements in Joints", FFA TN 1998-29, The Aeronautical Research Institute of Sweden, Sweden, 1998.
- [9] Ricci Moretti, L., Palmberg, B. and Segerfröjd, G., "On a novel Instrumentation Design for Load Transfer Measurements in Joints", FFAP H-1373, The Aeronautical Research Institute of Sweden, Sweden, 1998.
- [10] De Magistris, F., Palmberg, B. and Segerfröjd, G., "Experimental Determination of Fastener pre-load after Installation – A Study of Lubrication Influence", FFA TN 1999-03, The Aeronautical Research Institute of Sweden, Sweden, 1999.
- [11] De Magistris, F., Segerfröjd, G. and Palmberg, B., "Experimental Characterization of different fastener systems assembled in low-LT Joints - Application of a new Instrumentation Concept", FFA TN 1999-draft, The Aeronautical Research Institute of Sweden, Sweden, 1999.
- [12] De Magistris, F., Segerfröjd, G. and Palmberg, B., "Fatigue Testing of Low Load Transfer Joints – A Study of High-Performing Fastener Systems", FFA TN 1999-12, The Aeronautical Research Institute of Sweden, Sweden, 1999.
- [13] Ricci Moretti, L., Palmberg, B. and Segerfröjd, G. "Fatigue Testing of Medium and high Load Transfer Joints – A Study of high-performing Fastener Systems", FFA TN 1998-30, The Aeronautical Research Institute of Sweden, 1998.
- [14] R. Starikov, "Experimental investigation of fatigue behaviour in composite bolted joints", Licentiate Thesis Report 99-24, Royal Institute of Technology, Department of Aeronautics, Stockholm, Sweden.
- [15] R. Starikov and J. Schön, "Experimental investigation of fatigue behaviour in composite bolted joints", To appear in the proceedings of 12th International Conference on Composite Materials, Paris, July 5-9, 1999. .
- [16] Alpman, J., "Cohesive zone modelling using the splitting method", Report FFAP H-1360, 1998-04-23, 13 pp.
- [17] Babuška I., Andersson, B. and Alpman, J., "A splitting method for 3D Multiple Damage Analysis". FFA Technical Note FFA TN 1998-69, Stockholm 1998
- [18] Andersson B., "Reliable analysis of 3D multiple-site fatigue crack growth", FFA Technical Note 1999-20, The Aeronautical Research Institute of Sweden, Stockholm 1999, 93 pp.
- [19] Babuška I. and Andersson B., "A Splitting Method for Multiple-Site Crack Problems", FFA Technical Note, FFA TN1996-23, Stockholm 1999, 74 pp.
- [20] Andersson B., Babuška I. and Stehlin P., "RELIABLE ANALYSIS OF 3D MULTIPLE-SITE FATIGUE CRACK GROWTH, PART I: The splitting method for fracture mechanics analysis", accepted for publication in *J Engnr Fract Mech*.

- [21] Andersson B., Babuška I. and Stehlin P., "RELIABLE ANALYSIS OF 3D MULTIPLE-SITE FATIGUE CRACK GROWTH, PART II: Statistical and worst scenario analysis", accepted for publication in *J Engnr Fract Mech*.
- [22] Andersson B. and Falk U., "Reliable stress and fracture mechanics analysis of complex aircraft components", Proceeding of the 17th International Committee on Aeronautical Fatigue, ICAF, Stockholm June, 1993, pp 389-412.
- [23] Ireman, P., "Fast and reliable 3D Fracture Mechanics Analysis Using a Splitting Method", Report FKH R-4134, Saab Military Aircraft, Linköping, Sweden, 35 pp.
- [24] Andersson B., Falk U., Babuška I. and Petersdorff T v, "Reliable stress and fracture mechanics analysis of complex components using a *h-p* version of FEM", *Int. J. Num. Meth. Eng.*, Vol 38, 1995, pp 2135-2163.
- [25] Andersson B, Babuška I. and Falk U., "Accurate and reliable determination of edge and vertex stress intensity factors in three-dimensional elastomechanics", Proceedings of 17th Congress of the International Council of the Aeronautical Sciences, Paper No: ICAS-90-4.9.2, 1990, pp 1730-1746.
- [26] Cattaneo G., Cavallini G. and Galatolo R., "Structural Maintenance of Aging Aircraft: Experiments on W.F.D., Testing of simple specimens", Document No SMAAC-TR-3.2-0.7-1.3/AEM, Department of Aerospace Engineering, University of Pisa, Italy, June 1998, 155 pp.
- [27] G. S. Wang, "Advanced Strip Yield Analyses of Fatigue Crack Growth in Various Residual Stress Fields", Technical Report FFA TN 1999-30 The Structures Division, The Aeronautical Research Institute of Sweden.
- [28] G. S. Wang, "Analyses of AGARD Small Crack Growth Test Results Based on the Post Yield Consideration", Technical Report, FFA TN 1999-29, The Aeronautical Research Institute of Sweden.
- [29] G.S.Wang, "Stochastic Fatigue Crack Growth Analyses Based on Damage Accumulation Solution and Crack Closure Model". Technical Report FFA TN 1999-28, The Aeronautical Research Institute of Sweden.
- [30] G. S. Wang and A. F. Blom, "A Novel Probabilistic Fatigue Crack Growth Solution Based on the Crack Closure Model". Technical Report, FFA TN 1999-xx, The Aeronautical Research Institute of Sweden.
- [31] L.G. Melin, H.T. Goldrein, J.M. Huntley, S. Nilsson and S.J.P. Palmer, "A Study of Mode-I Loaded Delamination Cracks by High-Magnification Moiré Interferometry", *Compos. Sci. Technol.* 58 (3-4), 515-525, (1998).
- [32] Melin, L.-G. and Asp, L. E., (1997), Effects of strain rate on transverse tension properties of a carbon epoxy composite: studied by Moiré photography, *Composites A.*, **30** (3) 305-316.
- [33] Melin, L.-G. and Asp, L. E., (1998), Dynamic transverse tensile behavior of a carbon/epoxy composite: monitoring crack initiation and propagation, Am. Soc. for Composites, 13th Technical Conf., Baltimore, 1998, *Proc. Am. Soc. Compos.*, Technomic, Lancaster, 354-370.
- [34] Juntti, M., Asp, L.E. and Olsson, R. (1999), "Assessment of evaluation methods for the mixed-mode bending test", *J. Compos. Technol. Res.*, **21** (1) 37-48.
- [35] Olsson, R., (1998), Methodology for predicting the residual strength of impacted sandwich panels, *FFA TN 1997-09*, The Aeron. Research Inst. of Sweden, Bromma.
- [36] Olsson, R., (1999), A review of impact experiments at FFA during 1986 to 1998, *FFA TN 1999-08*, The Aeron. Research Inst. of Sweden, Bromma.
- [37] Nilsson S. "Effect of Impact Damage in CFRP Sandwich Panels." FFAP H-1338, The Aeronautical Inst. of Sweden, 1997.

- [38] Olsson, R., Asp, L.E., Nilsson, S., Sjögren, A., "Methodology for Efficient Design of Composite Structures Exposed to Impact," To appear in ASTM STP 1383, also *FFA TN 1999-32*, The Aeronautical Research Institute of Sweden, Bromma, 1999.
- [39] Olsson, R., "A review of Impact Experiments at FFA during 1986 to 1998," *FFA TN 1999-08*, The Aeronautical Research Institute of Sweden, Bromma, 1999.
- [40] Singh, S., Asp, L. E., Nilsson, K.-F., and Alpman, J. E., "Development of a Model for Delamination Buckling and Growth in Stiffened Composite Structures," *FFA TN 1998-53*, The Aeronautical Research Institute of Sweden, Bromma, 1998.
- [41] Asp, L. E., Nilsson, S., and Singh, S., "An Experimental Investigation of the Influence of Delamination Growth on the Residual Strength of Impacted Laminates," *FFA TN 1998-52*, The Aeronautical Research Institute of Sweden, Bromma, 1998.
- [42] Giugno, D., "Effect of Geometry and Boundary Conditions on Impact Response and Damage in Composite Plates," *FFA TN 1998-17*, The Aeronautical Research Institute of Sweden, Bromma, 1998.
- [43] Menéndez Álvarez, E., "Characterization of Impact Damage in Composite Materials," *FFA TN 1998-24*, The Aeronautical Research Institute of Sweden, Bromma, 1998.
- [44] Nilsson, K.-F., Asp, L. E., Alpman, J. E., and Nystedt, L., "Influence of Delamination Depth on the Behavior of Globally Buckled Composite Laminates," *FFA TN 1999-04*, The Aeronautical Research Institute of Sweden, Bromma, 1999.
- [45] J. Schön, "Fatigue delamination growth model for composites", *FFA TN 1999-40*, Submitted for publication in *Comp. Sci. Tech.*
- [46] J. Schön and A. F. Blom, "Load-ratio dependence on fatigue life of composites", *FFA TN 1999-39*, Submitted for publication in the proceedings of 12th International Conference on Composite Materials, Paris, July 5th-9th 1999.
- [47] Gathercole, N., Reiter, H., Adam, T., and Harris, B., "Life prediction for fatigue of T800/5245 carbon-fibre composites: I. Constant-amplitude loading", *Fatigue*, 1994, Vol. 16, pp. 523-532.
- [48] J. Schön, T. Nyman, A. Blom, and H. Ansell, "A numerical and experimental investigation of a composite ENF-specimen", *FFA TN 1999-42*, To be submitted.
- [49] J. Schön, "Coefficient of friction of composite delamination surfaces", *FFA TN 1999-41*, To be submitted to *Wear*.
- [50] J. Schön and B. Andersson, "Calculation of mode-separated energy release rates during delamination growth", Proceedings of the American Society for Composites, 13th annual technical conference, Sept. 21-23, 1998, USA, pp. 654-675.
- [51] J. Schön and B. Andersson, "Calculation of mode-separated energy release rates during delamination growth", *FFA TN 1998-27*.
- [52] J. Schön and B. Andersson, "Interaction between a delamination crack and a matrix crack", *FFA TN 1998-34*.
- [53] J. Schön and B. Andersson, "Interaction between a delamination crack and a matrix crack", Proceedings of the American Society for Composites, 13th annual technical conference, Sept. 21-23, 1998, USA, pp. 676-710.
- [54] S. Nilsson, "Damage growth in notched carbon fibre/peek laminates under fatigue loading, *FFA TN 1994-24*, (1994), Sweden.

- [55] J. Schön, T. Nyman, A. Blom, and H. Ansell, "A numerical and experimental investigation of delamination behaviour in the DCB-specimen", FFA TN 1999-43, submitted for publication in *Comp. Sci. Tech.*
- [56] Nyman T., "Composite fatigue design methodology: a simplified approach", *Composite Structures* 35 (1996) 183-194.
- [57] Federal Aviation regulations Part 25.
- [58] Joint Airworthiness Requirements JAR25 large Aeroplanes (JAR25).
- [59] FAA, Composite Aircraft Structure, Advisory Circular AC20-107A, April 1984.
- [60] Composite Aircraft Structure ACJ25603.
- [61] Rouchon J., " Certification of LArge Airplane Composite Structures, Recent Progress and New Trends in Compliance Philosophy", ICAS-90-1.8.1.
- [62] Hellbom K. and Jangblad D., " Saab 2000. Stress Analysis and Structural Testing Requirements for Composite Components", TUKHK-89035, 1989.
- [63] Nyman T. and Blom A., "Aircraft Composite Primary Structures, Review of Certification Methodologies", TUDL R-4077/FFAP H-1308, 1997.
- [64] Whitehead R.S., Kan H.P. and Saether E.S., " Certification Testing Methodology for Composite Structure - Volume I-Data Analysis", NADC-87042-60, DOT/FAA/CT-86/39, October 1986.
- [65] Whitehead R.S., Kan H.P. and Saether E.S., " Certification Testing Methodology for Composite Structure - Volume II-Methodology Development", NADC-87042-60, DOT/FAA/CT-86/39, October 1986.
- [66] Nyman T., " Review of Certification Procedures at Saab", SAAB.T4.TR.1
- [67] Nyman T., " Review of S2000 Control Surface Substantiation", SAAB.T4.TR.2
- [68] T. Nyman, A. Bredberg and J. Schön, " Equivalent damage and residual strength for impact damaged composite structures". FFA TN 1999-38, Accepted for publication in *Journal of Reinforced Plastics and Composites*. Presented at the American Society Composite Materials Thirteenth International Conference, ASC 13th, in Baltimore, September 21-23, 1998.

3.9 SWEDISH ICAF-DOCUMENTS DURING MAY 1997 - MAY 1999

- 2214 Experimental Characterisation of Eight Fastener Systems – Detailed Secondary Bending and Load Transfer Measurements in Joints
Ricci Moretti, L., Palmberg, B. and Segerfröjd, G.
- 2215 Fatigue Testing of Medium and high Load Transfer Joints – A Study of high-performing Fastener Systems
Ricci Moretti, L., Palmberg, B. and Segerfröjd, G.
- 2216 Experimental Determination of Fastener pre-load after Installation – A Study of Lubrication Influence
De Magistris, F., Palmberg, B. and Segerfröjd, G.
- 2217 Fatigue Testing of Low Load Transfer Joints – A Study of High-Performing Fastener Systems
De Magistris, F., Segerfröjd, G. and Palmberg, B.
- 2218 Reliable Analysis of 3D Multiple-Site Fatigue Crack Growth
Andersson, B.
- 2219 Stochastic Fatigue Crack Growth Analyses Based on Damage Accumulation Solution and Crack Closure Model
Wang, G.S.
- 2220 Analyses of AGARD Small Crack Growth Test Results Based on the Post Yield Consideration
Wang, G.S.
- 2221 Advanced Strip Yield Analyses of Fatigue Crack Growth in Various Residual Stress Fields
Wang, G.S.

ACKNOWLEDGEMENTS

This work was supported by the Defence Material Administration. The assistance of Ms. Inez Engström in preparing the manuscript is gratefully acknowledged. The editor is also indebted to the following individuals who helped to write parts of this review:

Börje Andersson	FFA	(Sections 5.1, 5.2 and 5.3)
Hans Ansell SAAB		(Sections 4.3 and 4.4)
Anders Carlsson	SAAB	(Section 4.3)
Thomas Johansson	SAAB	(Section 3.1)
Lennart Magnusson	SAAB	(Sections 2.1 and 2.2)
Gunnar Melin FFA		(Section 7.1)
Sören Nilsson FFA		(Sections 7.6 and 7.7)
Tonny Nyman SAAB		(Sections 7.15, 7.16, 7.17 and 7.18)
Robin Olsson FFA		(Sections 7.2, 7.3, 7.4 and 7.5)
Björn Palmberg FFA		(Section 6.5)
Joakim Schön FFA		(Sections 7.8, 7.9, 7.10, 7.11, 7.12, 7.13 and 7.14)
Gabriel Segerfröjd	FFA	(Section 3.2)
Roman Starikov	KTH	(Section 3.3)
Stefan Thuresson	SAAB	(Sections 4.1 and 4.2)
Geng-Sheng Wang	FFA	(Sections 6.1, 6.2, 6.3 and 6.4)

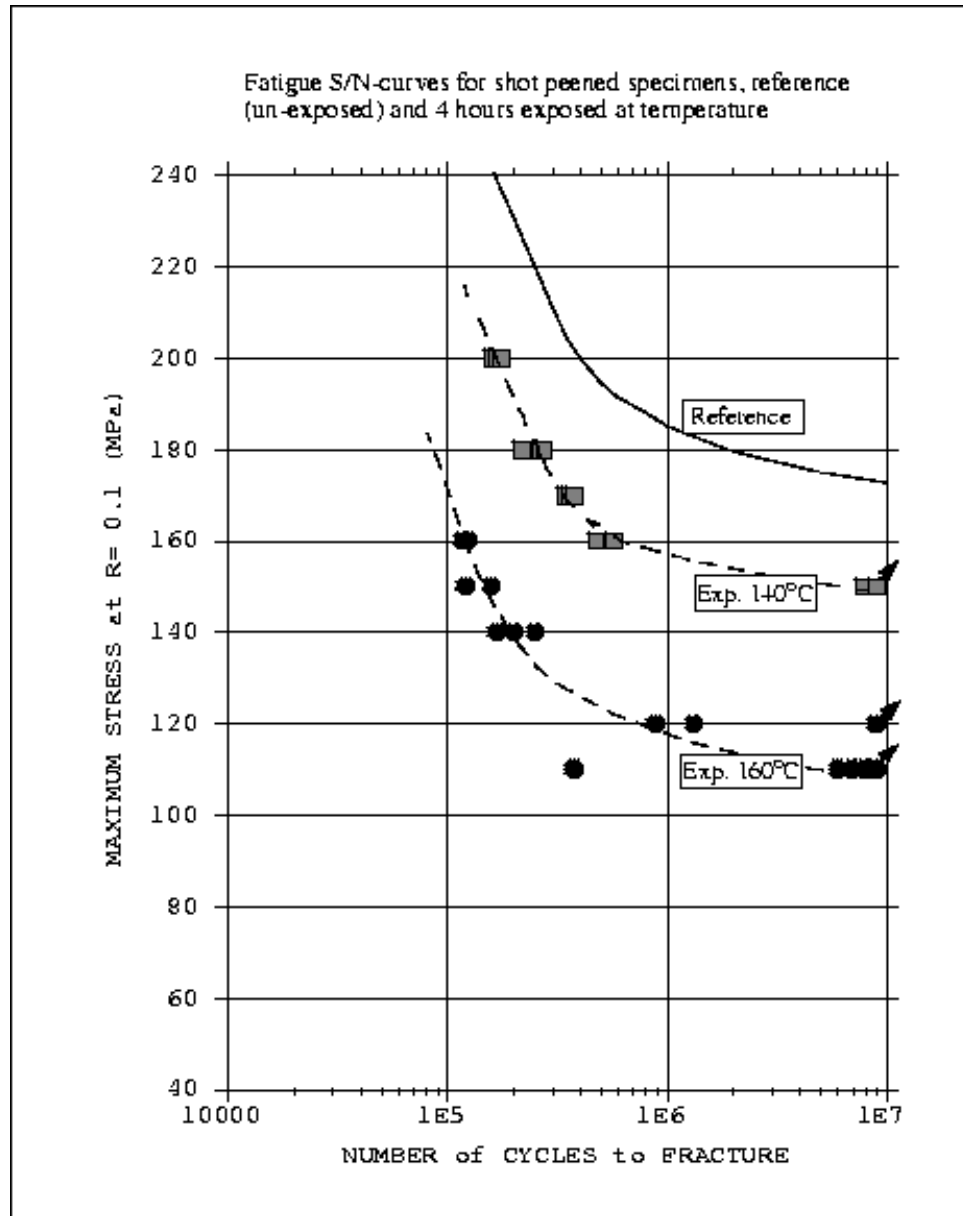


Figure 1 Fatigue test results for axially loaded test specimens, $K_t=1.7$, at $R=0.1$

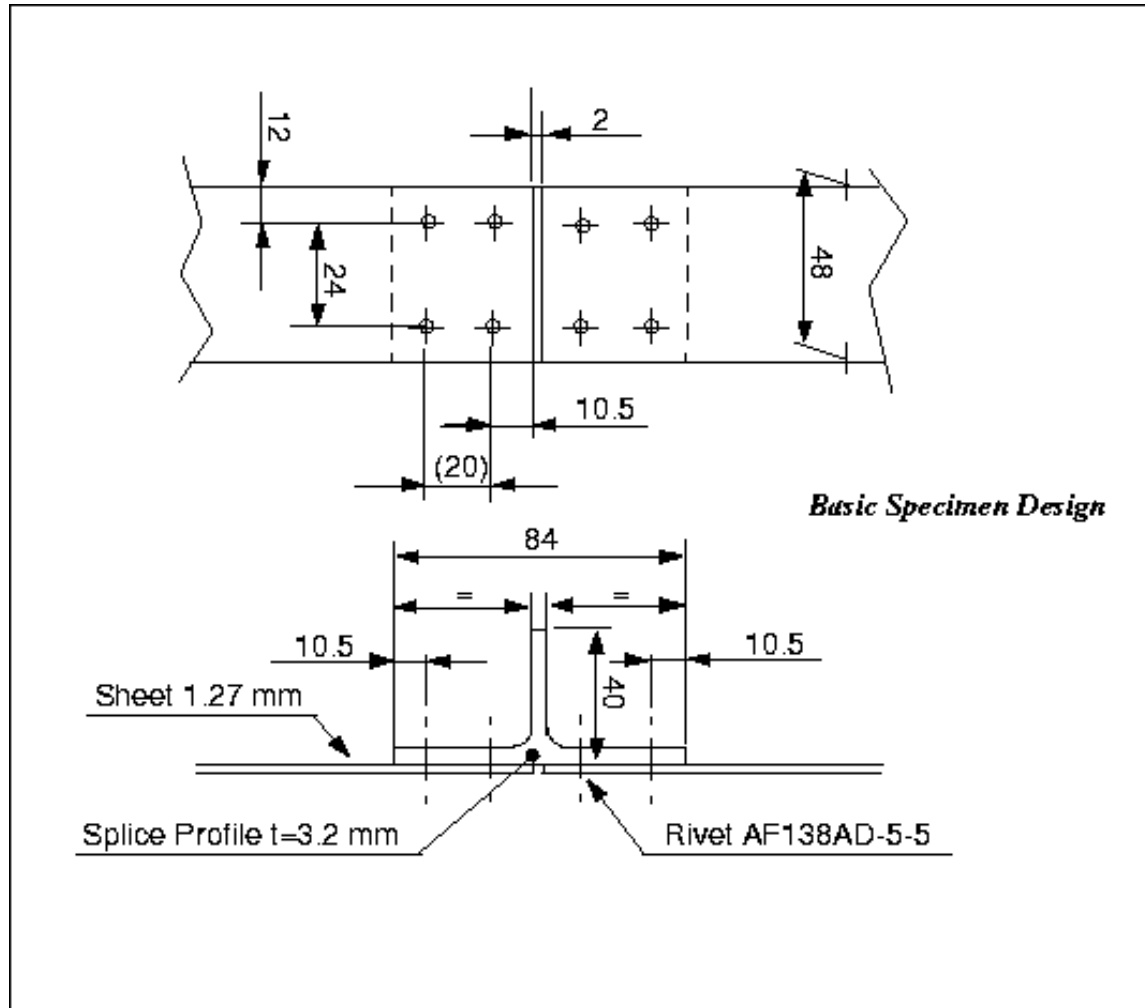


Figure 2 Basic Riveted Joint, Type 2C. To be loaded in the L-orientation of the sheet material.

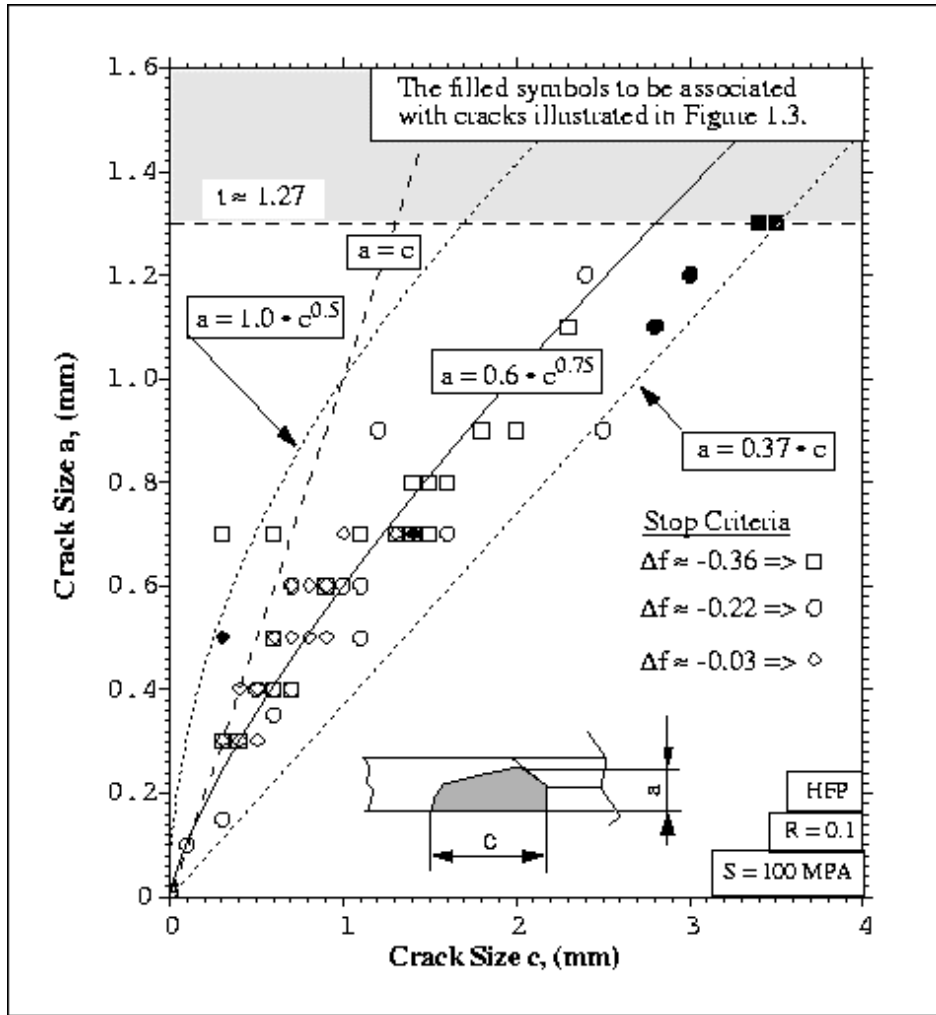


Figure 3 Crack shape data for the studied specimen design and the loading applied. The stop criteria for interruption of a test setup, Δf , is a pre-defined drop in frequency of the system.

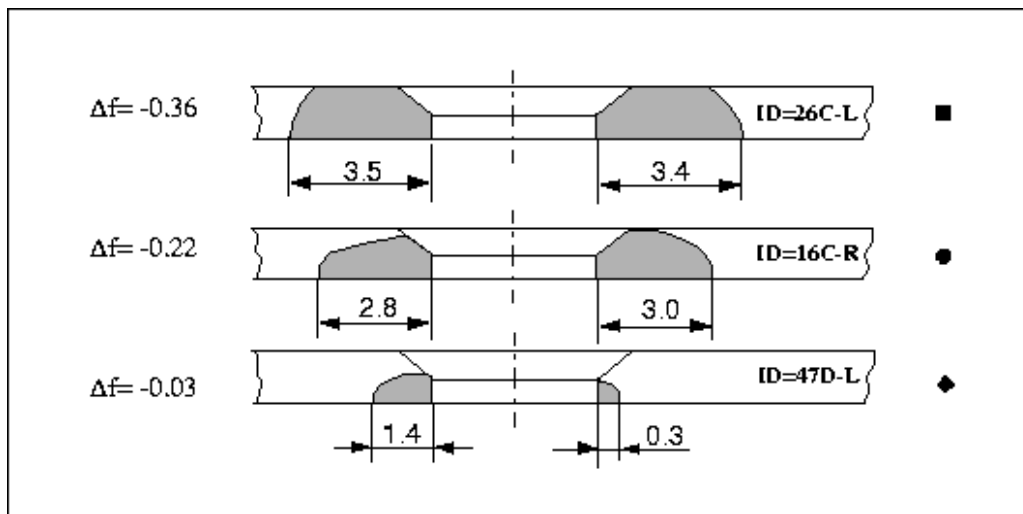


Figure 4 Fatigue crack sizes and shapes. Extreme values for crack sizes found in the studied populations as a function of commanded stop criteria.

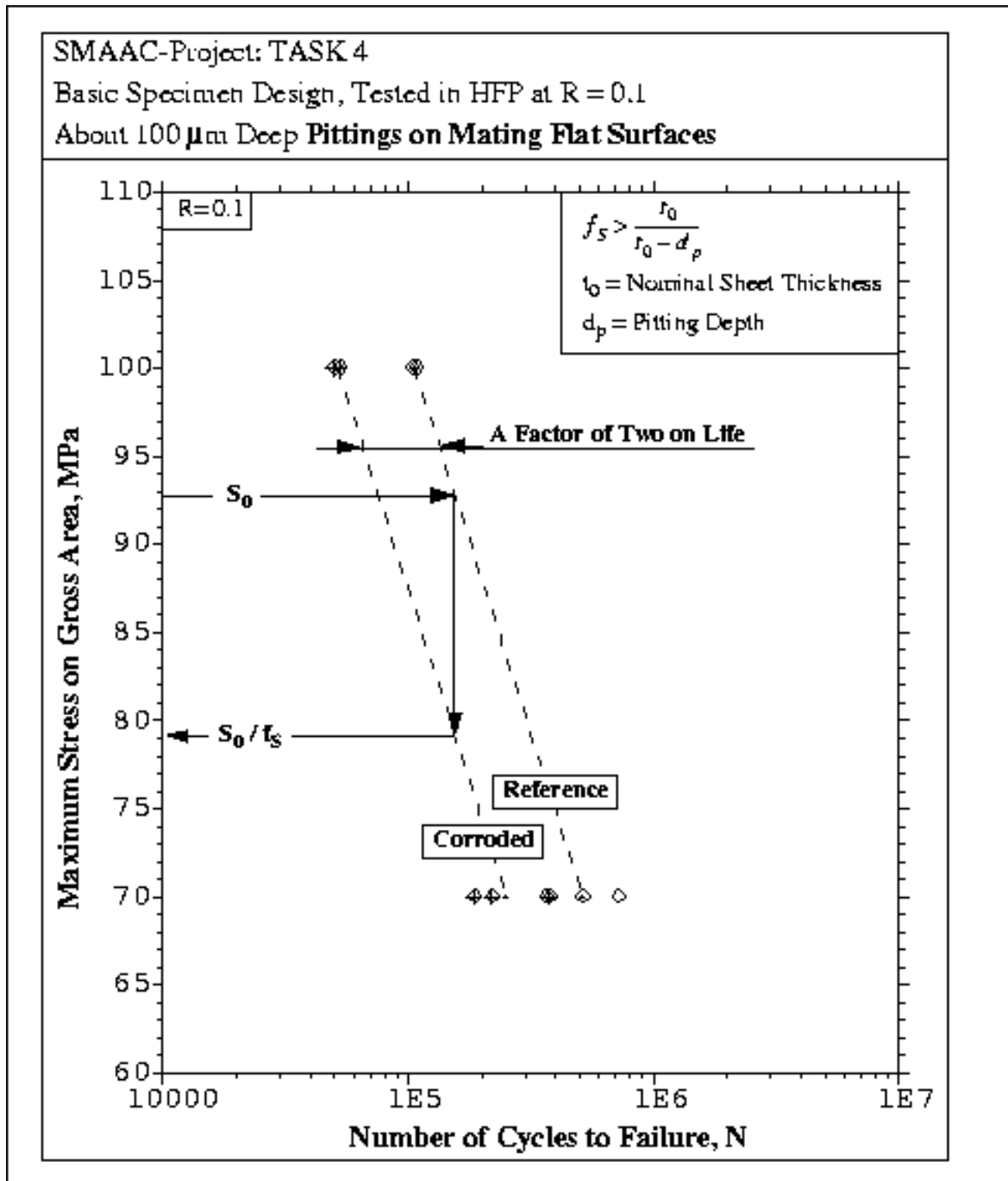


Figure 6 Comparison of fatigue data. The corroded specimen "100 mm Deep Pittings on Mating Flat Surfaces" versus the reference specimen "No Surface Treatment"

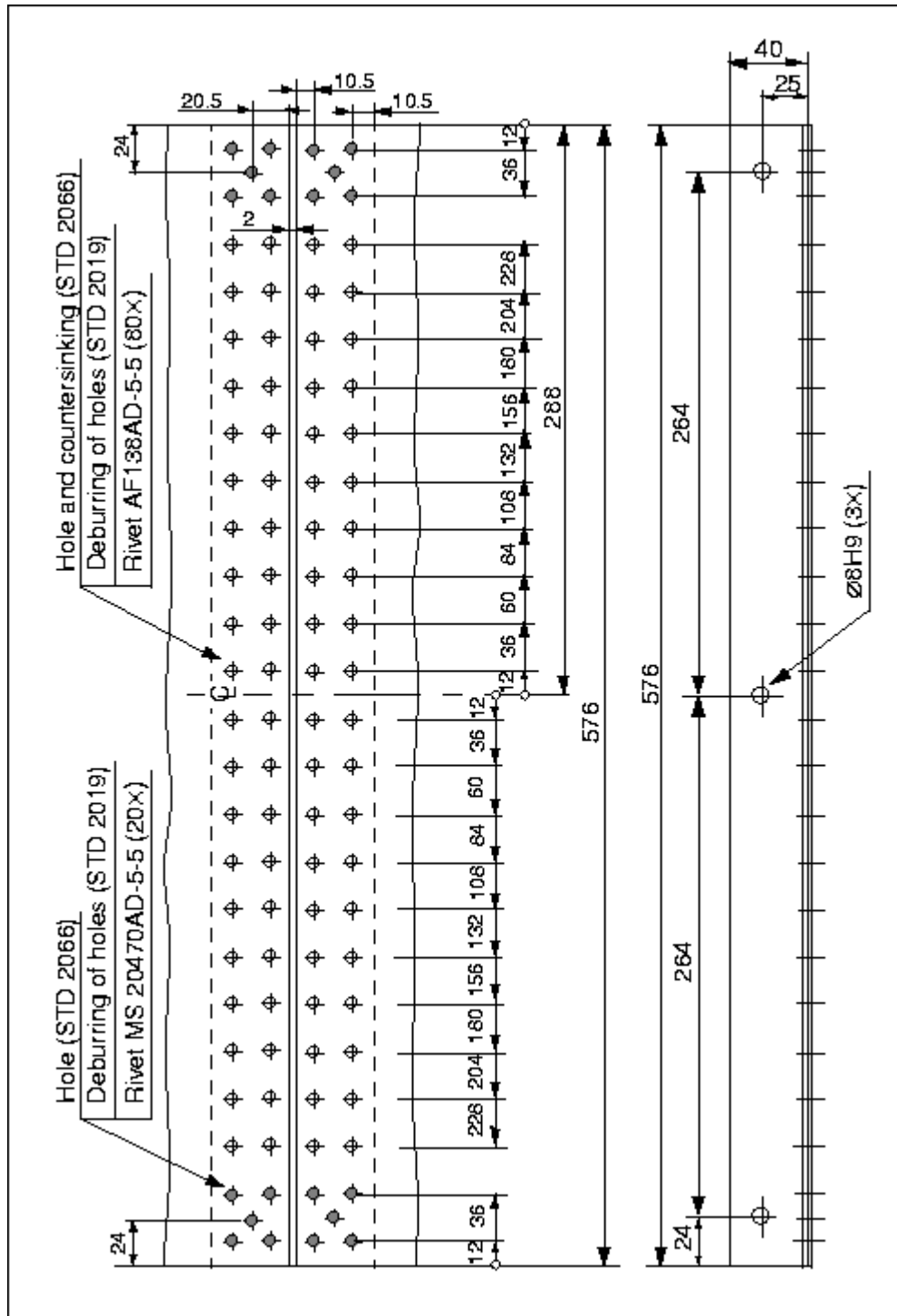


Figure 7 Wide Riveted Joint. Loaded in the L-orientation of the sheet material

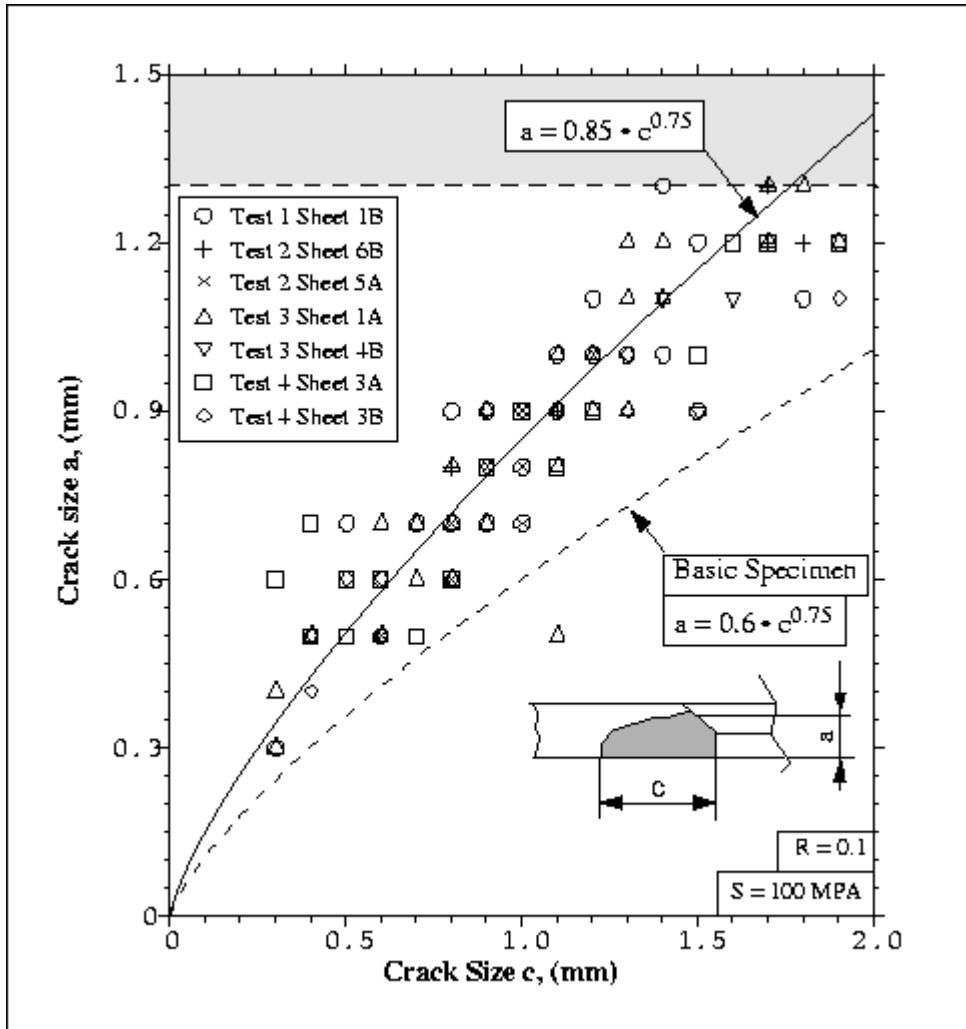


Figure 8 Crack shape data for the studied specimen design and the loading applied

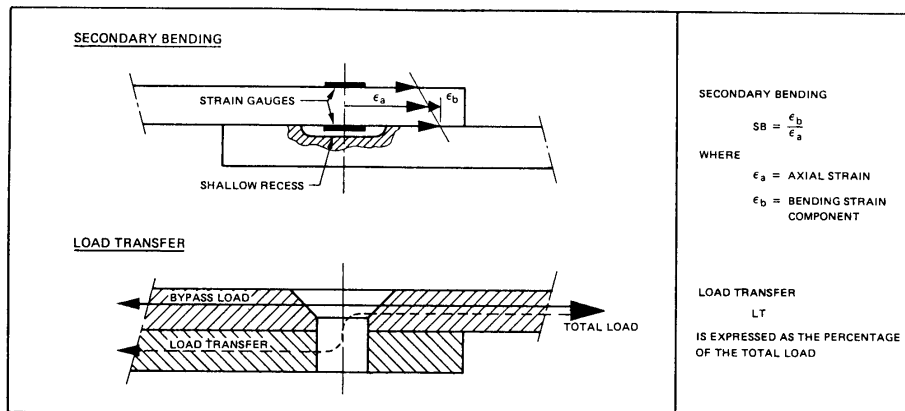


Figure 9 Load transfer and secondary bending definitions

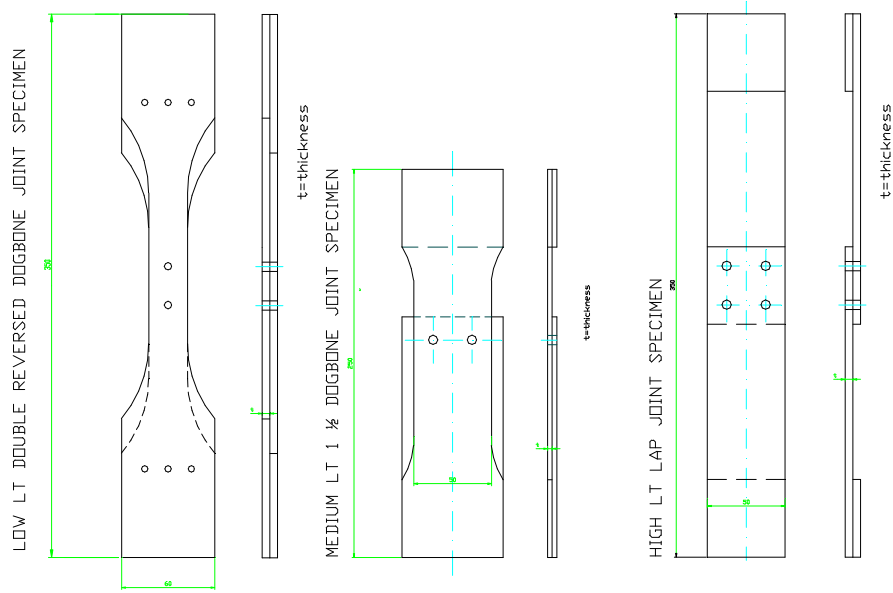


Figure 10 Low, medium and high load transfer joint specimens

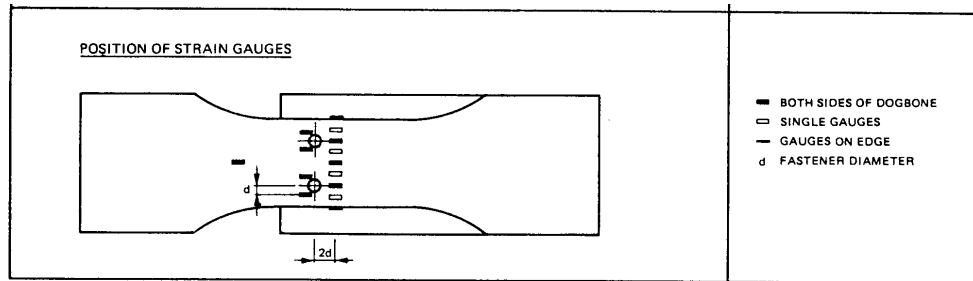


Figure 11 AGARD proposal to specimen instrumentation

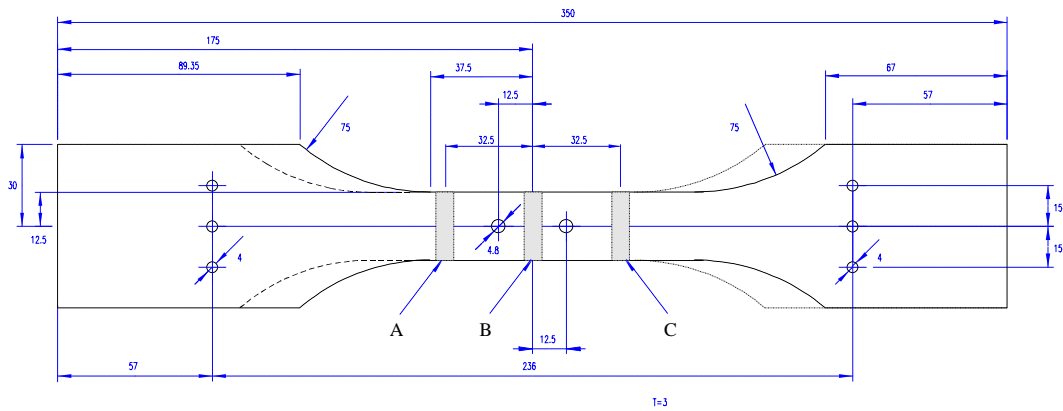


Figure 12 Instrumentation for low load transfer specimen

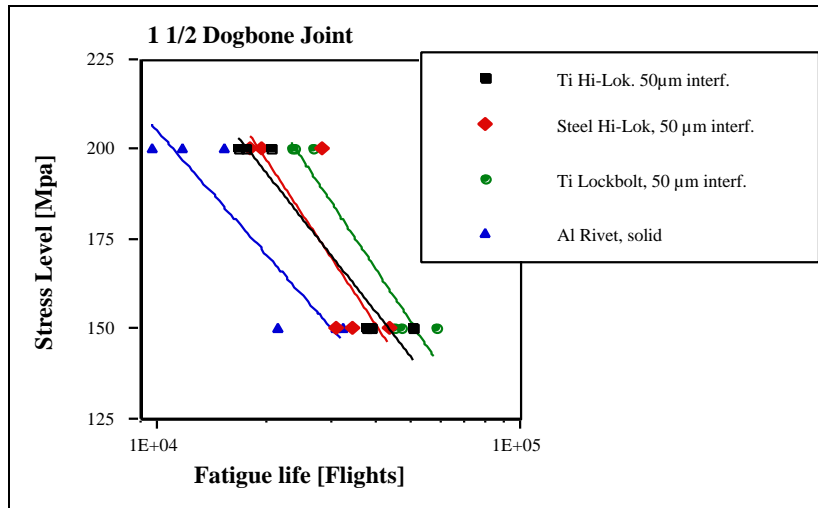


Figure 16 Fatigue test results of medium LT joints subjected to FALSTAFF flight-simulation loading.

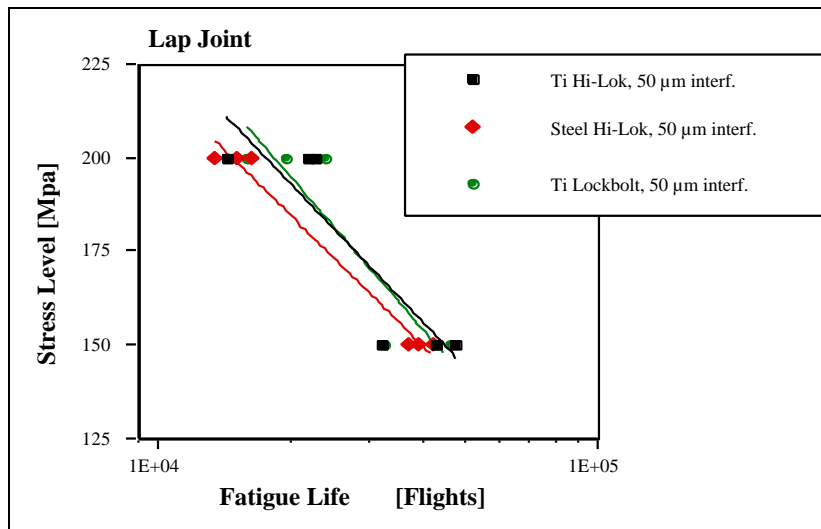


Figure 17 Fatigue test results of high LT joints subjected to FALSTAFF flight-simulation loading.

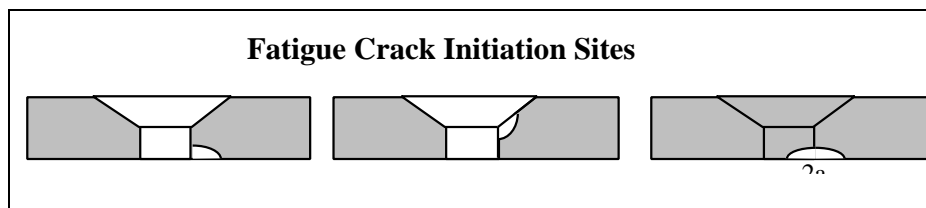


Figure 18 Fractographically observed fatigue crack initiation sites in medium-LT joint specimens.

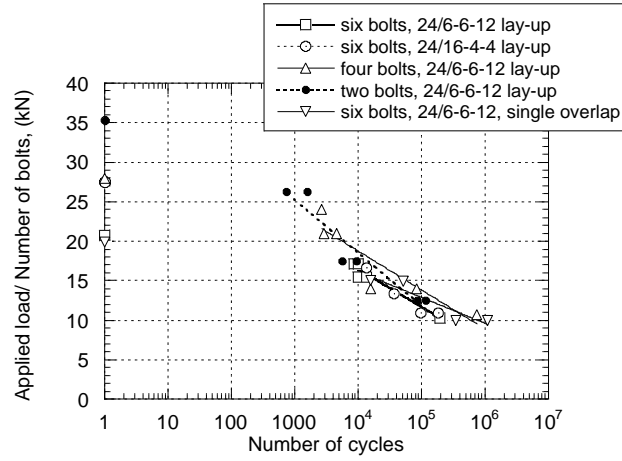


Figure 19 Fatigue test results of applied load per bolt versus number of cycles to failure

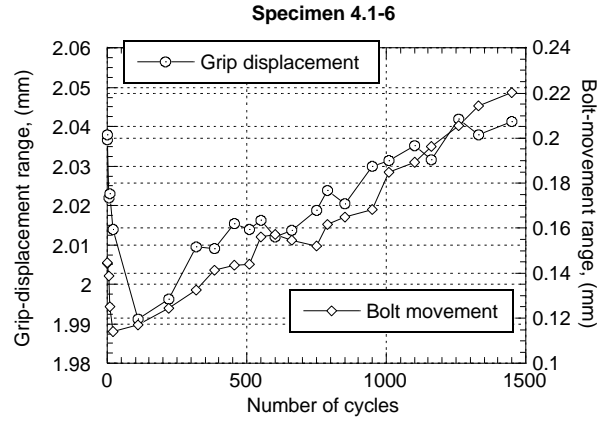


Figure 20 The results of bolt-movement measurements plotted together with grip-displacement data

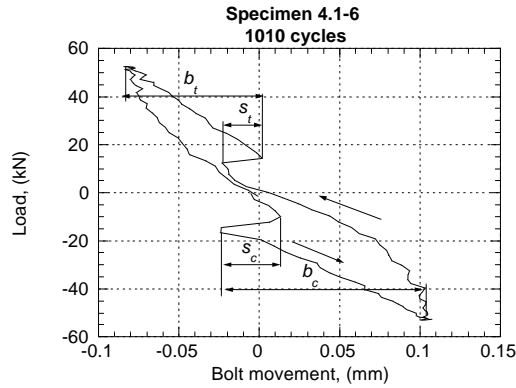


Figure 21 Bolt-movement loop plotted during one load cycle and containing sections of bolt sliding (s_t , s_c) and bending (b_t , b_c)

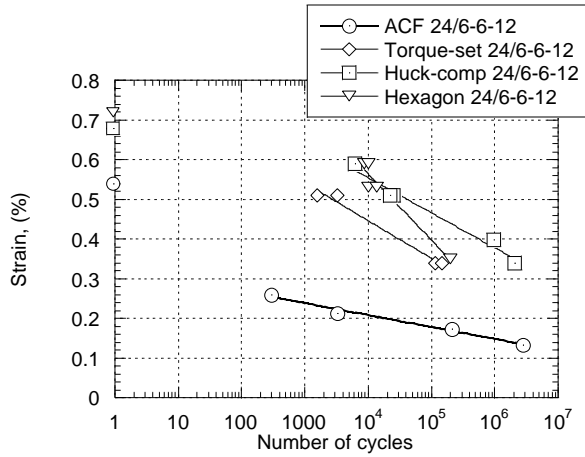


Figure 22 Fatigue life results for specimens with countersunk fasteners in comparison with those joined by Hexagon bolts

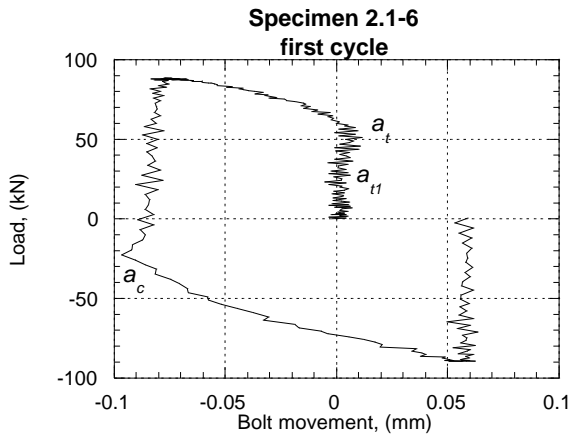


Figure 23 Bolt-movement loop containing points of inflection due to friction and bolt bending

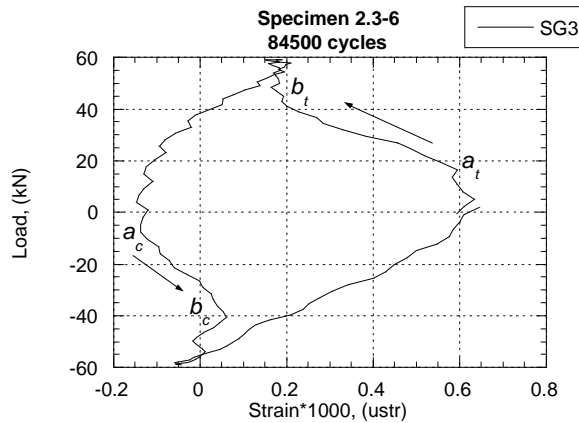


Figure 24 An example of strain versus applied load loop for a strain gauge located between two bolts

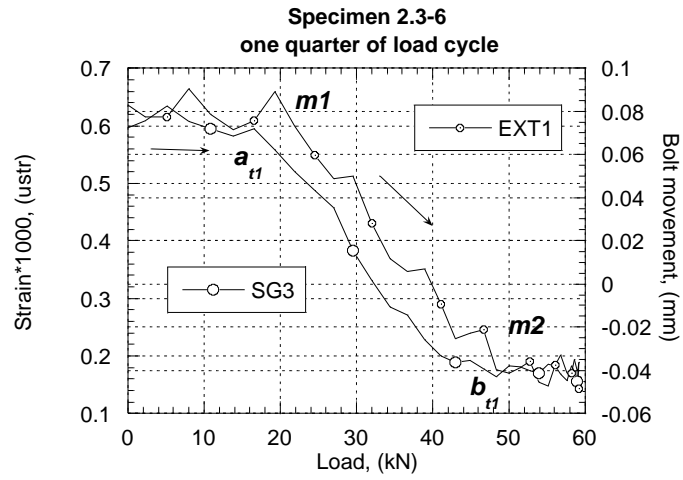


Figure 25 Comparison between bolt movement (EXT1) and strain (SG3) measurement



Figure 26 Photograph of the full-scale fatigue test of the Gripen single seater

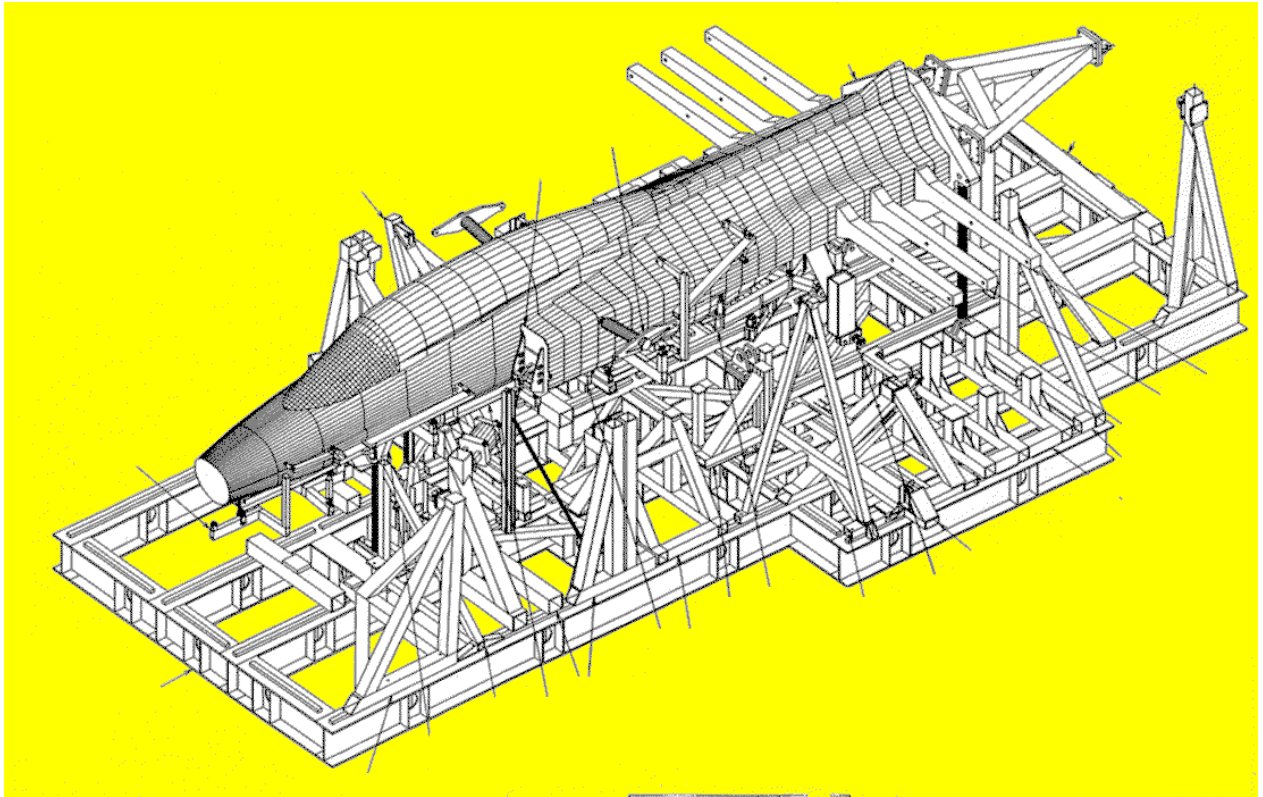


Figure 27 Schematic drawing of the full-scale test of Gripen twin seater

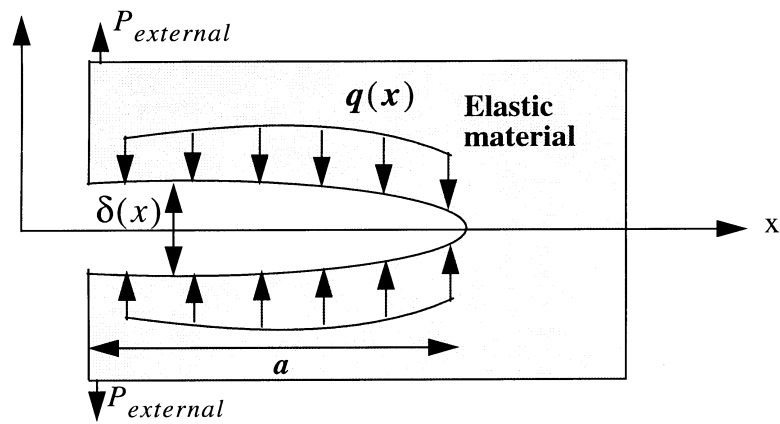
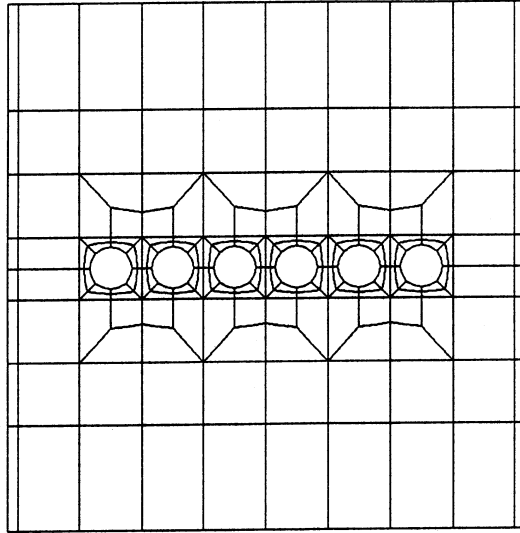


Figure 28 Definition of cohesive forces and crack opening displacements



FE mesh used in analysis of plate with 12 cohesive zones

Figure 29 Multiple cohesive zone problem

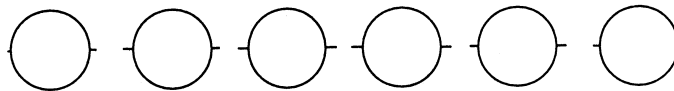


Figure 30 Lengths of cohesive zones at maximum loads
(solution is for polynomial order $p=7$)

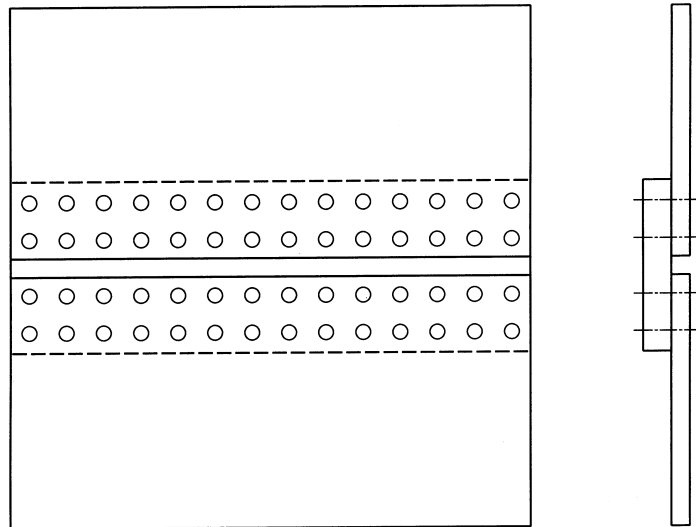


Figure 31 Butt joint with four rows with 14 rivets/row subject to a vertical y-displacements at $y=0$ and $y=c$ which corresponds to an average stress $S_y = 100$ MPa

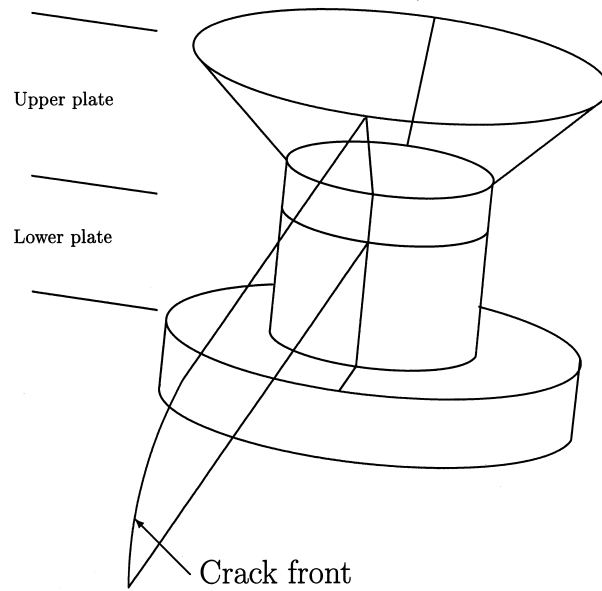


Figure 32 Rivet with apriori defined contact surfaces (sectioned) used in full 3D analysis of lap-splice joint

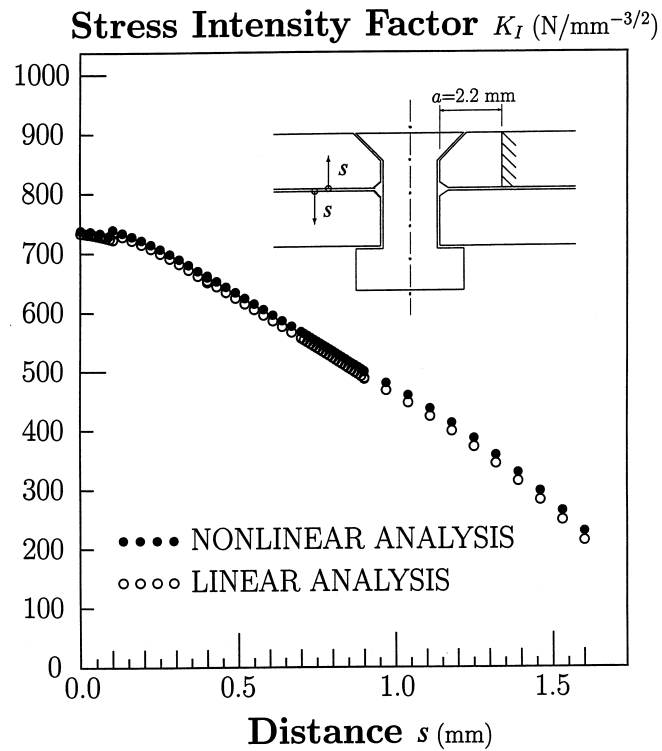


Figure 33 Comparison between calculated mode I stress intensity functions $K_I(s)$ for nonlinear solution scheme and linear solution scheme using apriori defined contact surfaces

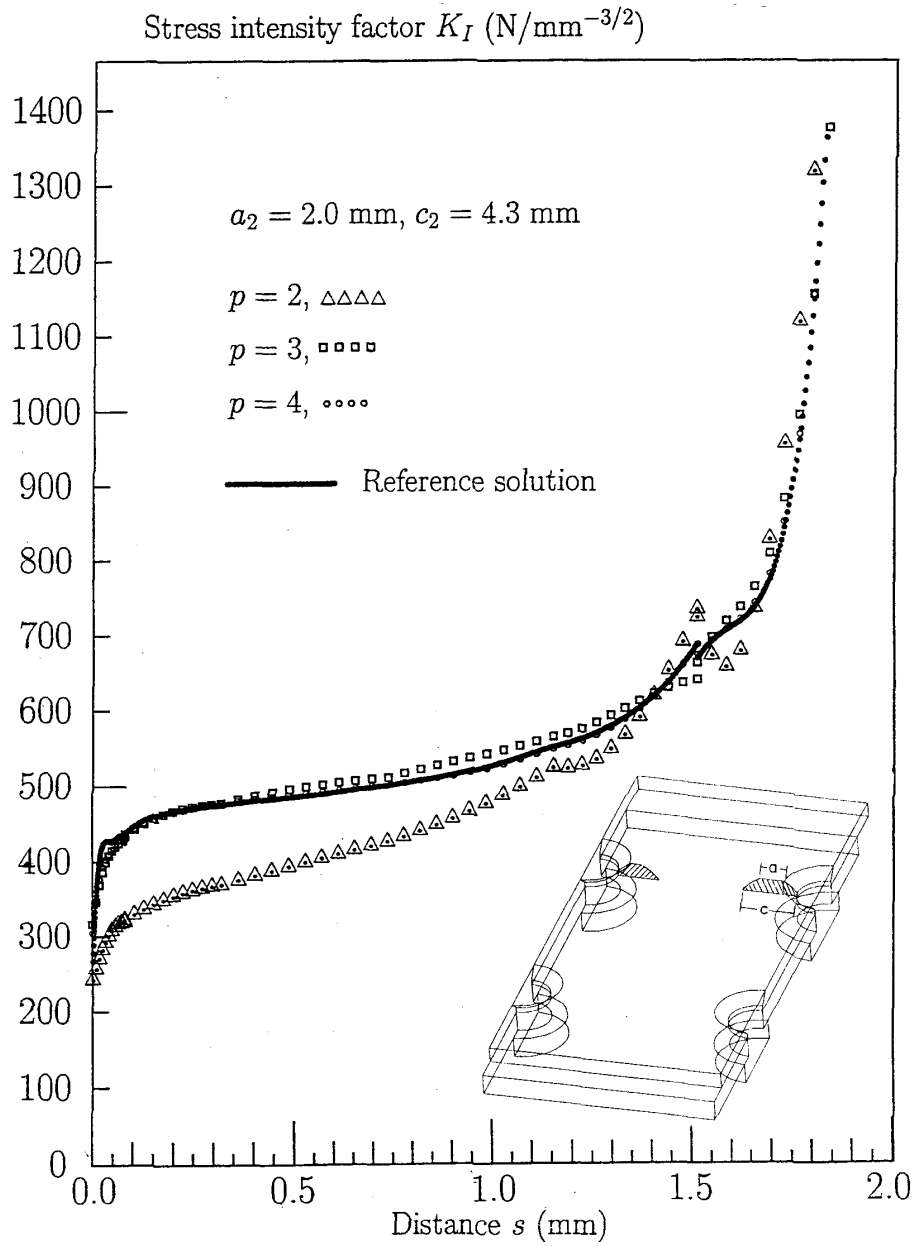


Figure 34 Calculated stress intensity function $K_I(s)$ for long crack with $a_i = 2.0 \text{ mm}, c_i = 4.3 \text{ mm}$ for different orders p in splitting scheme

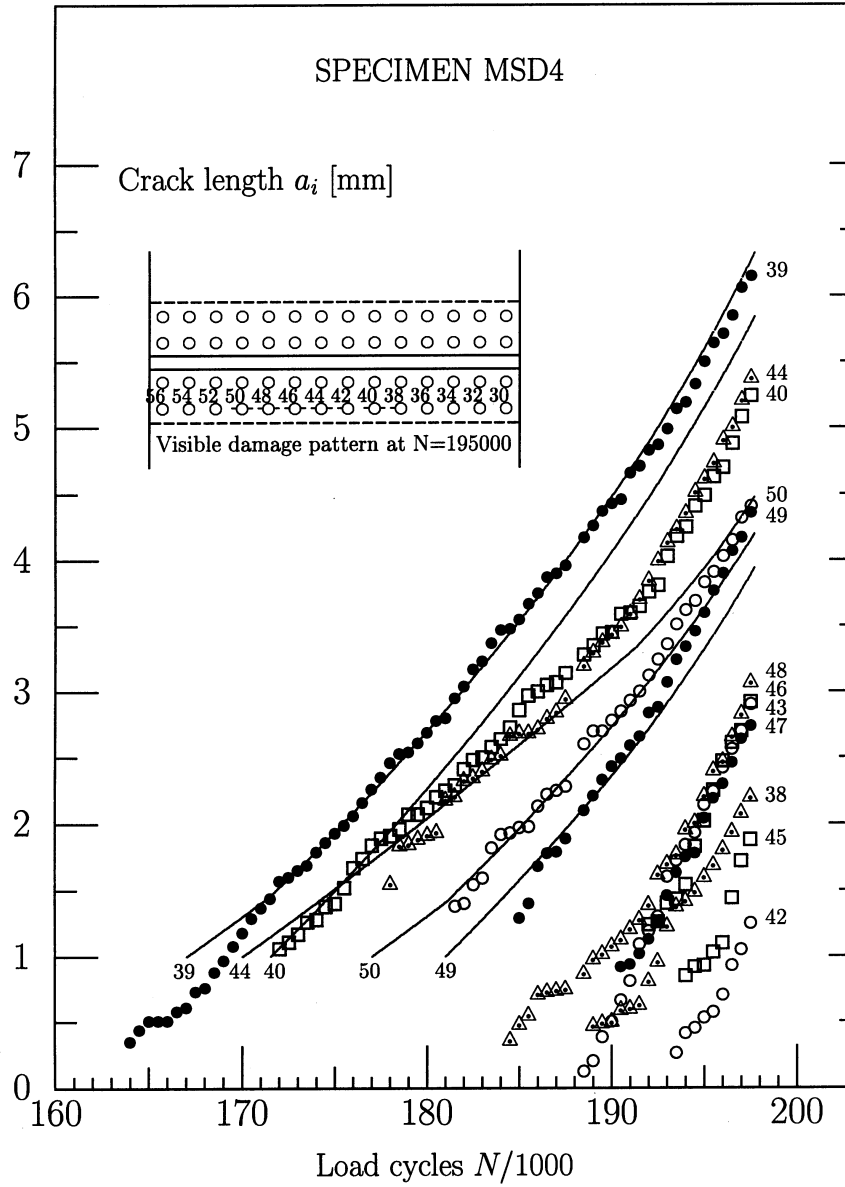


Figure 35 Calculated (solid lines) and experimentally determined [26] crack lengths a_i for specimen MSD4

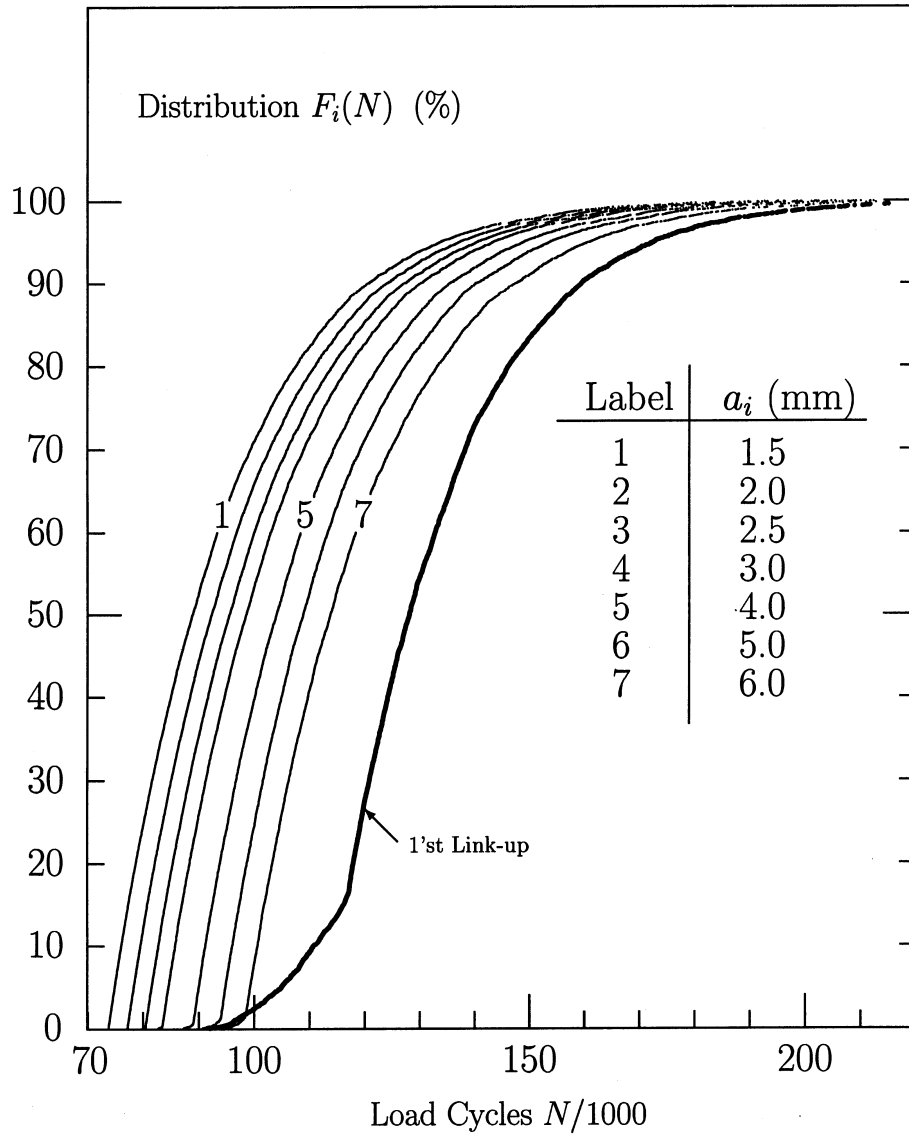


Figure 36 Distribution functions $F_i(N)$ showing the minimum number of load cycles N needed to form one crack of length a_i (mm). Data are from a Monte Carlo simulation using 5000 samples

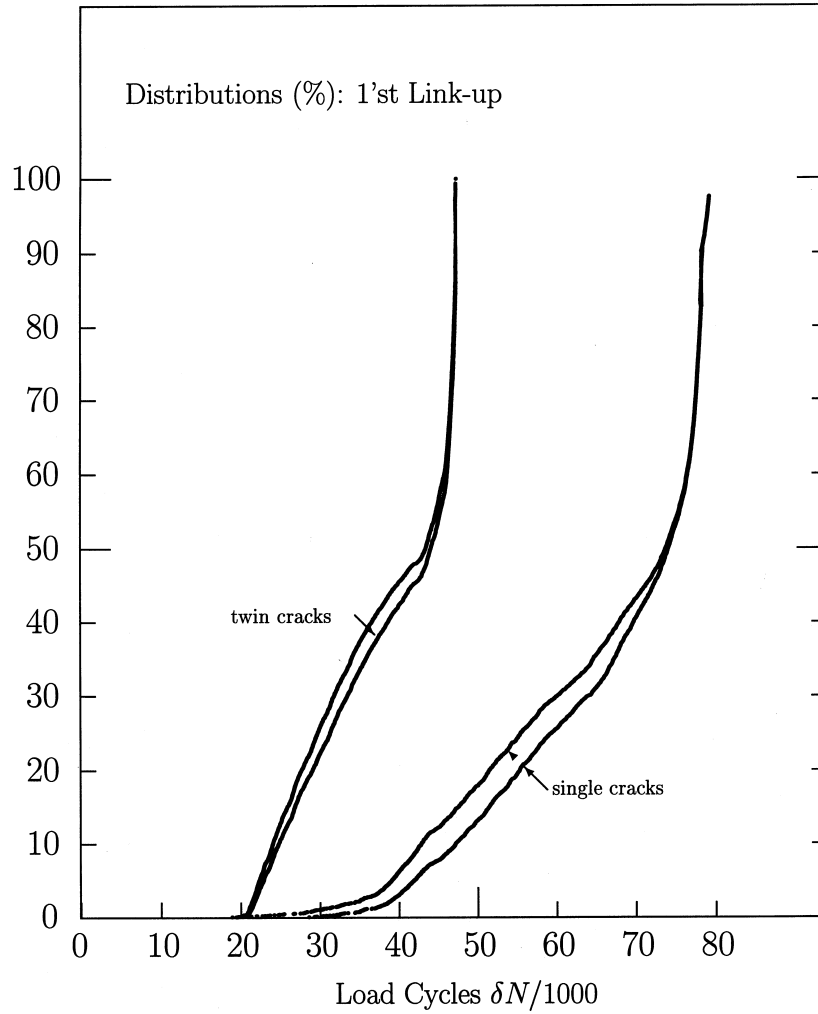


Figure 37 Distributions showing the minimum number of load cycles dN from detection of first 1 mm crack in the plate until 1'st link-up, respectively, time from first detection of 1mm crack, that will link-up, until 1'st link-up

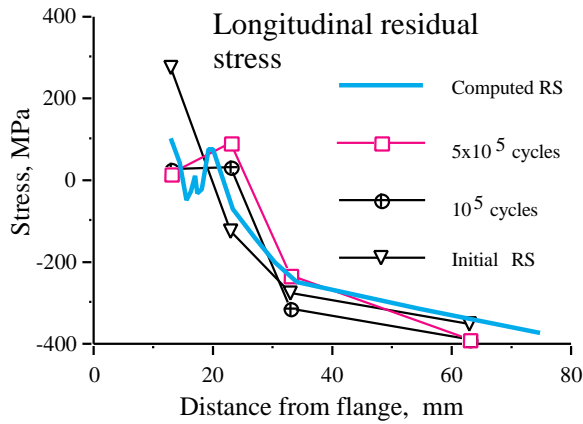


Figure 38 Residual stress and redistribution along the load axis on the surface of the as-welded specimen.

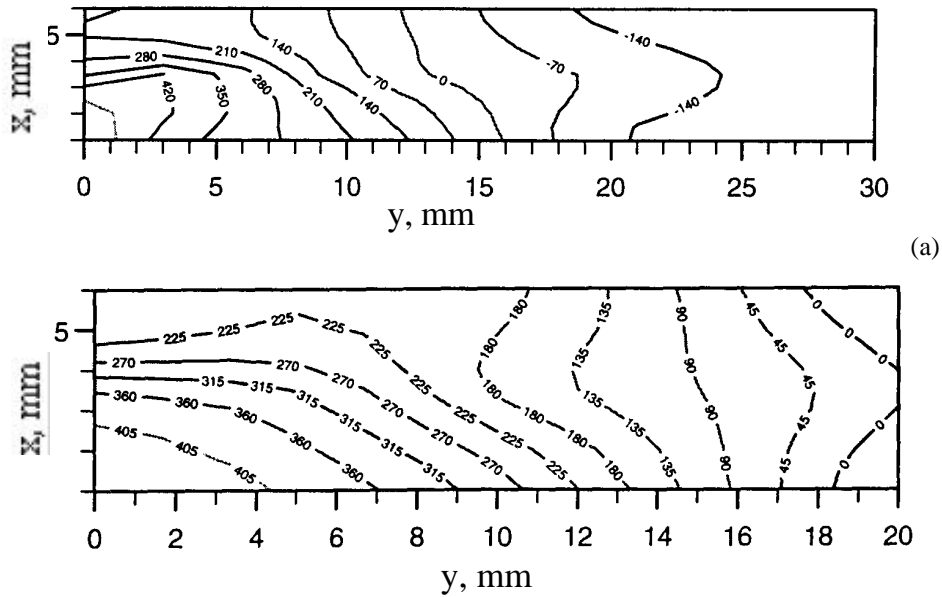


Figure 39 Examples of neutron diffraction residual stresses for the as-welded specimen. (a) initial residual stress, and (b) residual stress after 5×10^5 load cycles

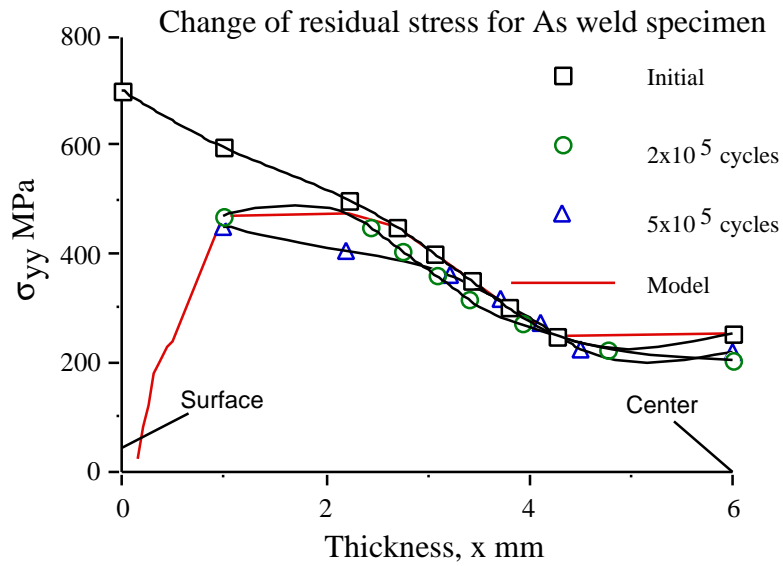


Figure 40 Comparison of the residual stresses before and after the fatigue loading for the as-welded specimen.

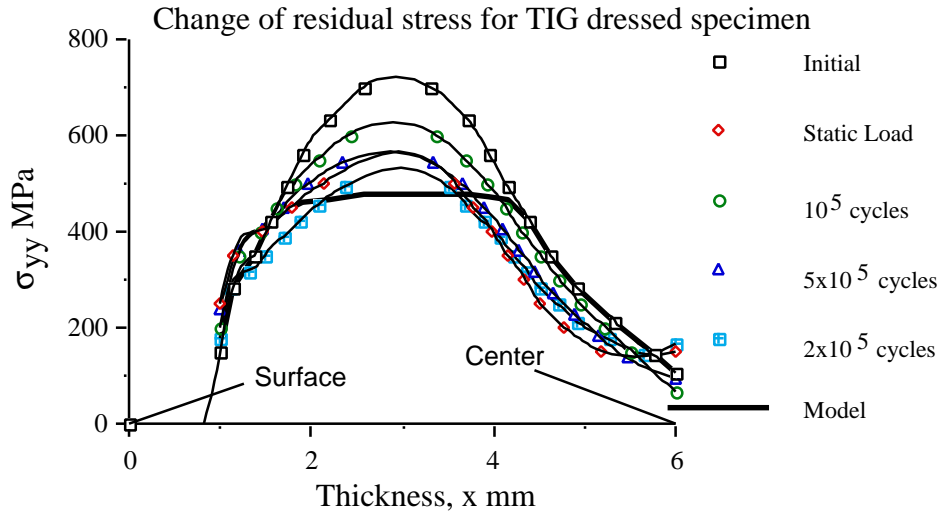


Figure 41 Comparison of the residual stresses before and after the fatigue loading for TIG-dressed specimens

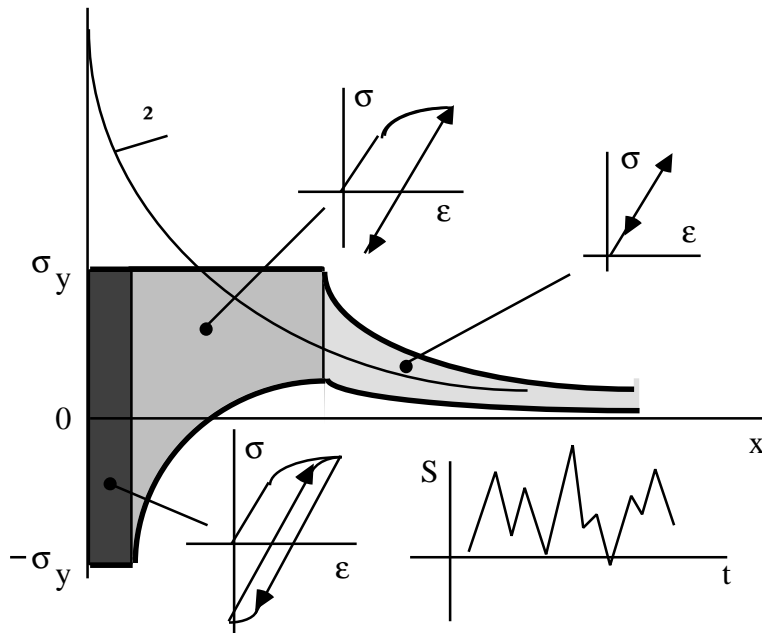


Figure 42 Schematic of the residual stress due to the plastic deformation under the fatigue loading

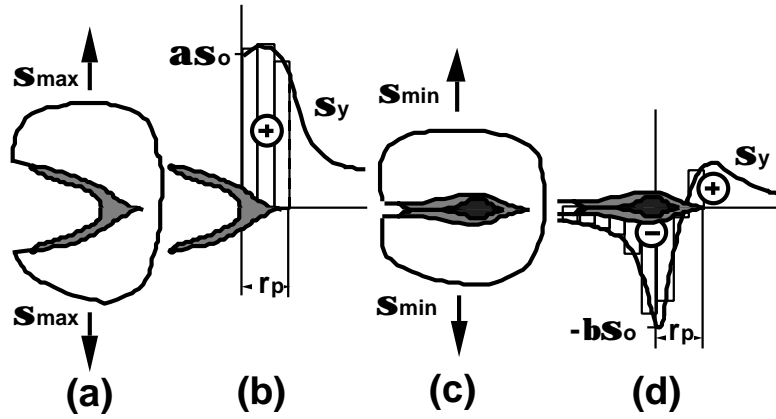


Figure 43 Schematic of the strip yield crack closure model

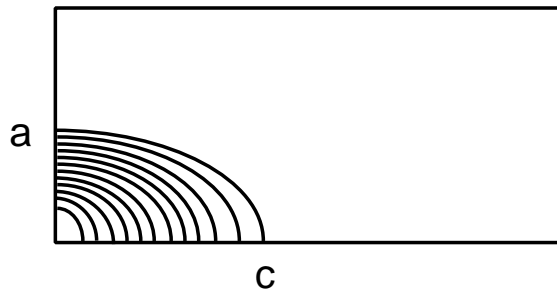


Figure 44 Schematic of the ring elements for the strip yield crack closure analysis

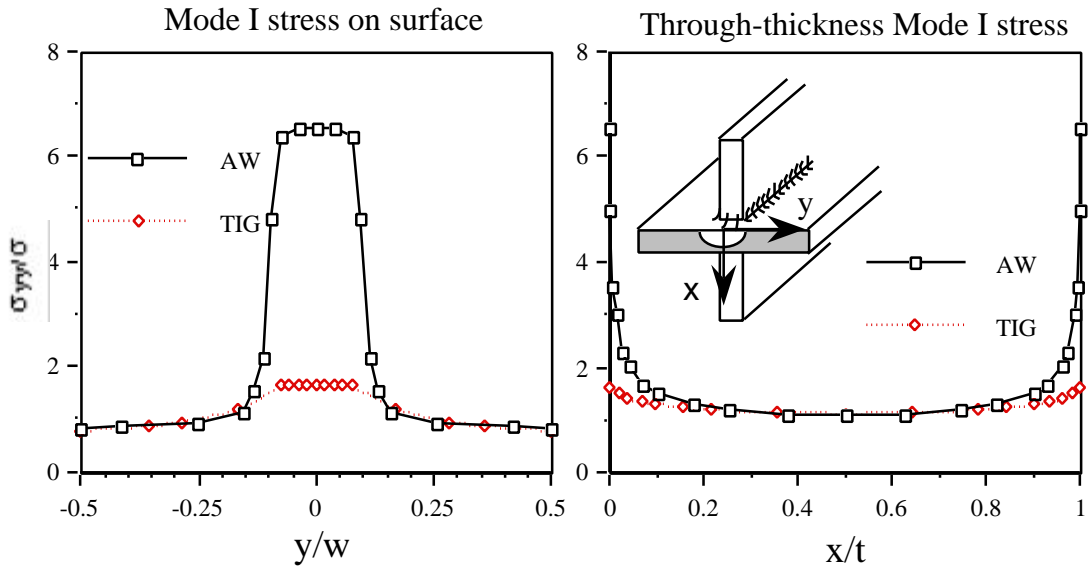
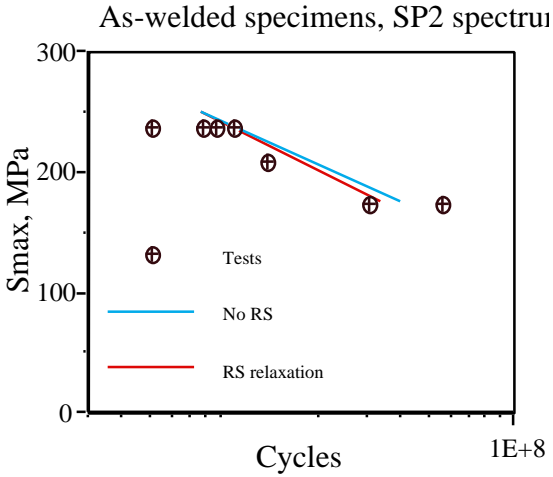
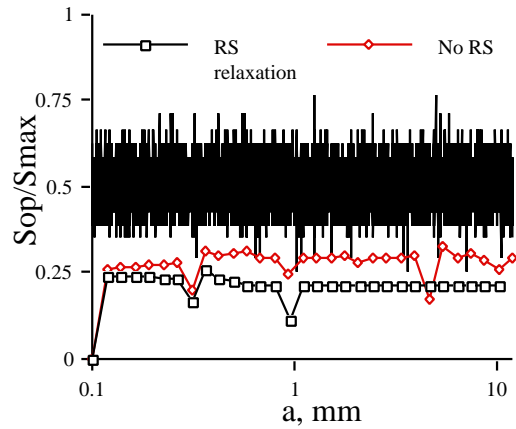


Figure 45 Elastic stress distributions on the specimen surface and in the depth at the stress concentration shown in the insert

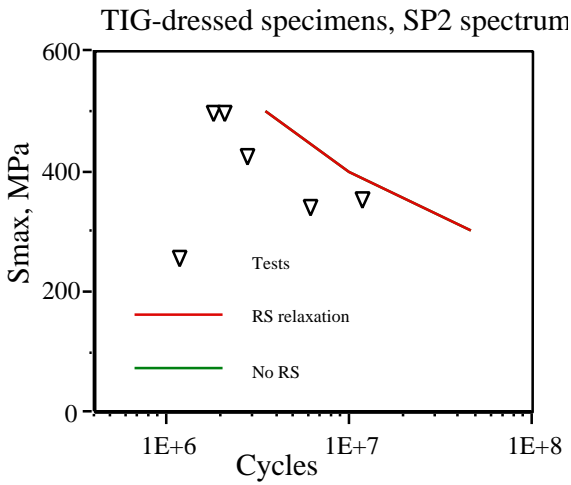


(a)

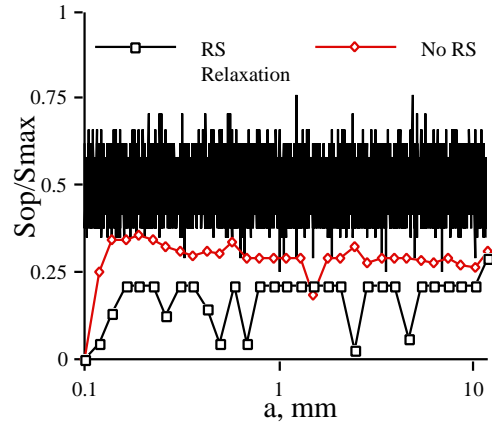


(b)

Figure 46 Comparison of experimental and analytical fatigue lives for the as-welded specimens under SP2 spectrum loading

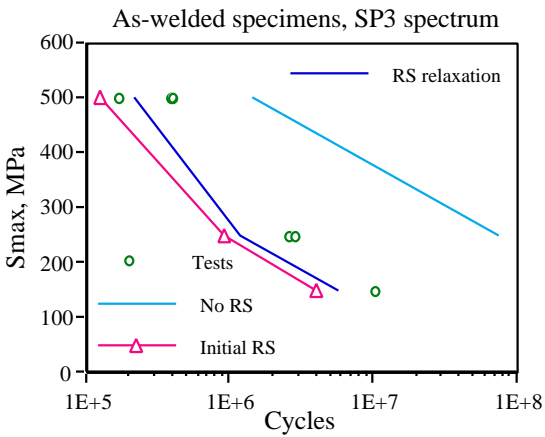


(a)

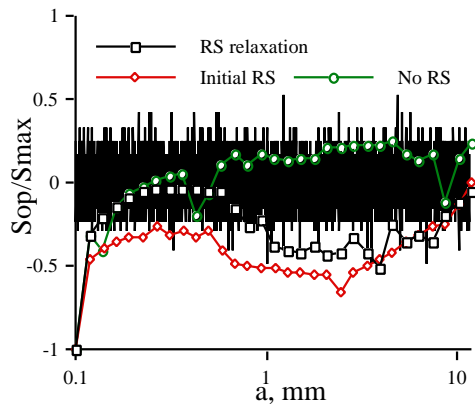


(b)

Figure 47 Comparison of experimental and analytical fatigue lives for TIG-dressed specimens under SP2 spectrum loading



(a)



(b)

Figure 48 Comparison of experimental and analytical fatigue lives for the as-welded specimens under SP3 spectrum loading

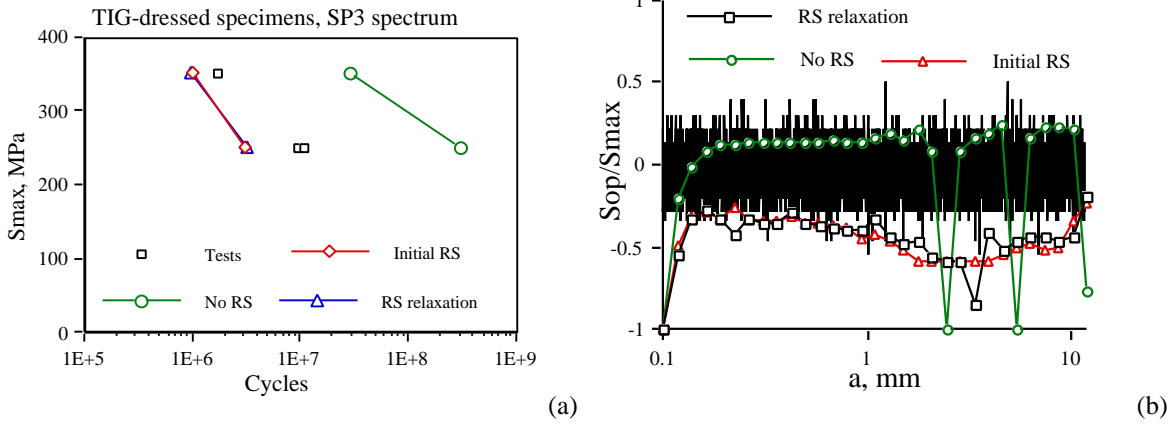


Figure 49 Comparison of experimental and analytical fatigue lives for TIG-dressed specimens under SP3 spectrum loading

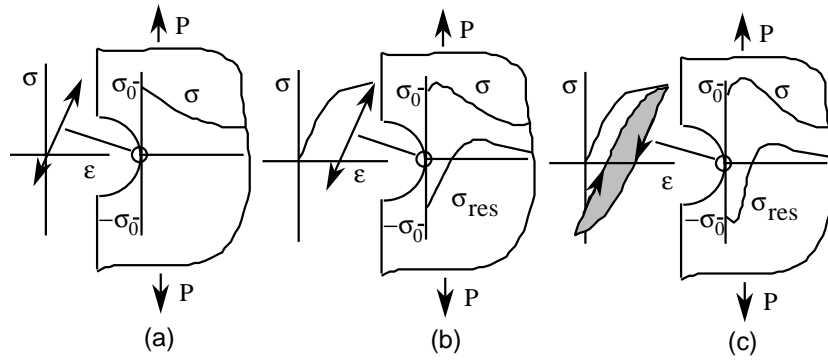


Figure 50 Various stress-strain responses at a stress concentration

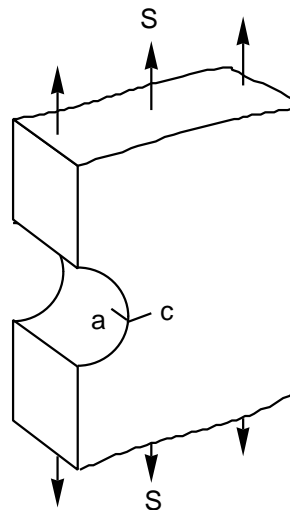


Figure 51 Schematic of AGARD small crack test specimen

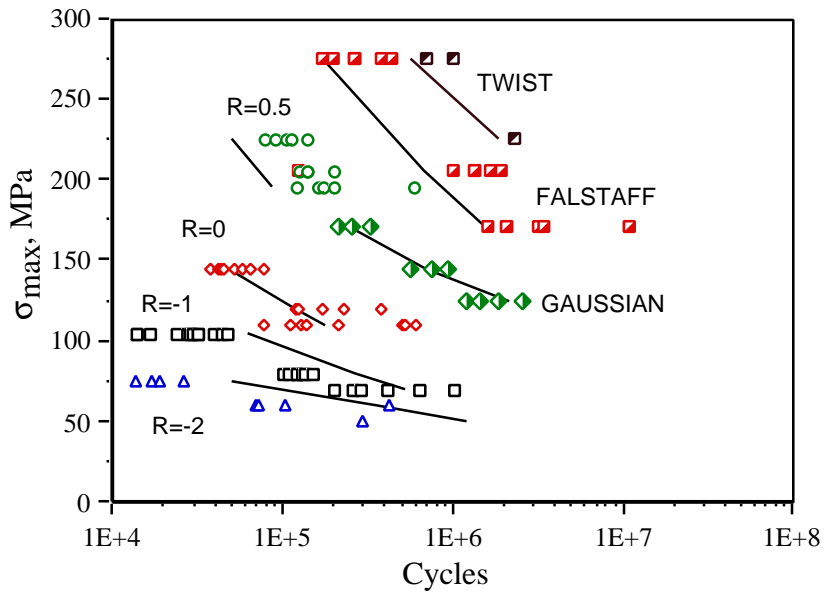


Figure 52 Comparison of test fatigue lives to predictions based on the fracture mechanics consideration

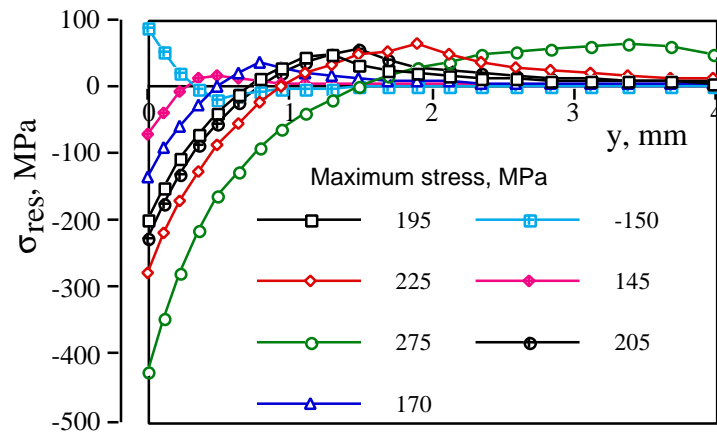


Figure 53 Finite element residual stress results for various load levels

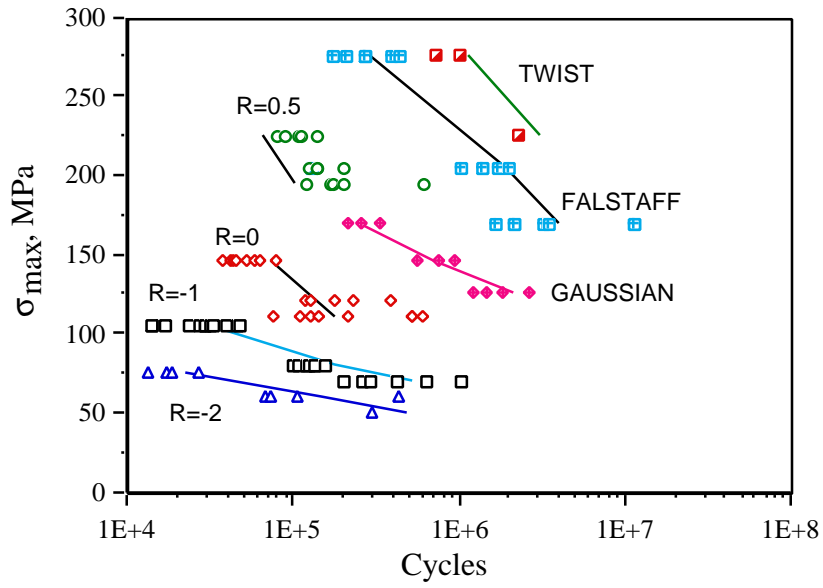


Figure 54 Comparison of the test results with the post-yield crack growth analyses

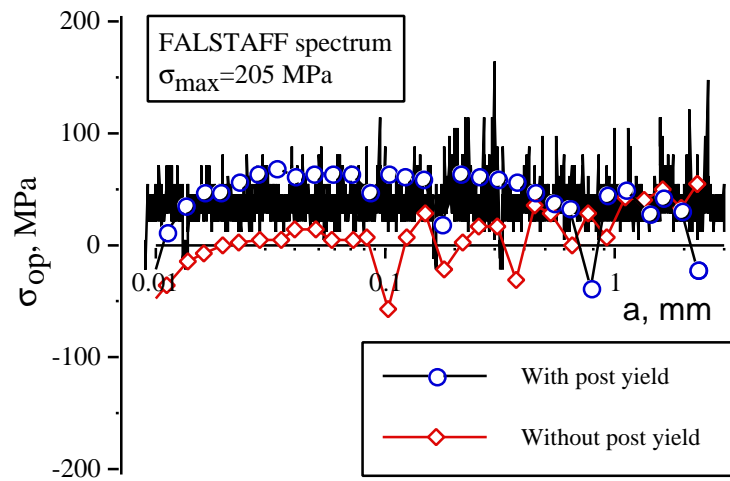


Figure 55 Comparison of crack opening stress with the load sequence

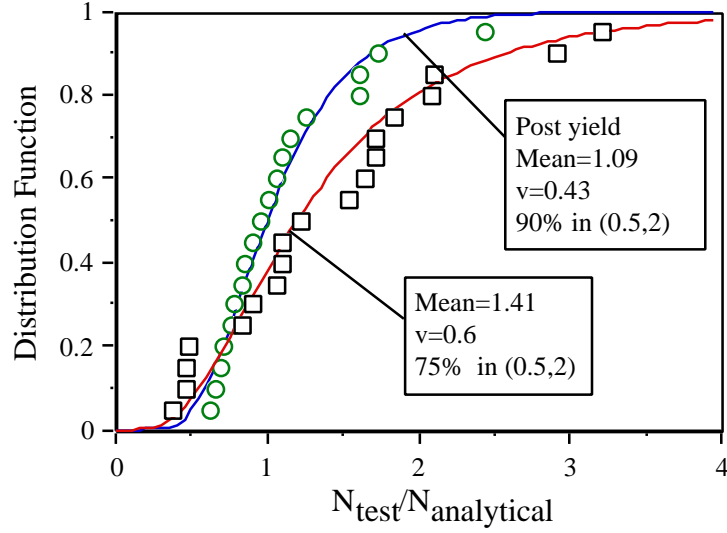


Figure 56 Comparison between predictions whether or not the post yield is considered

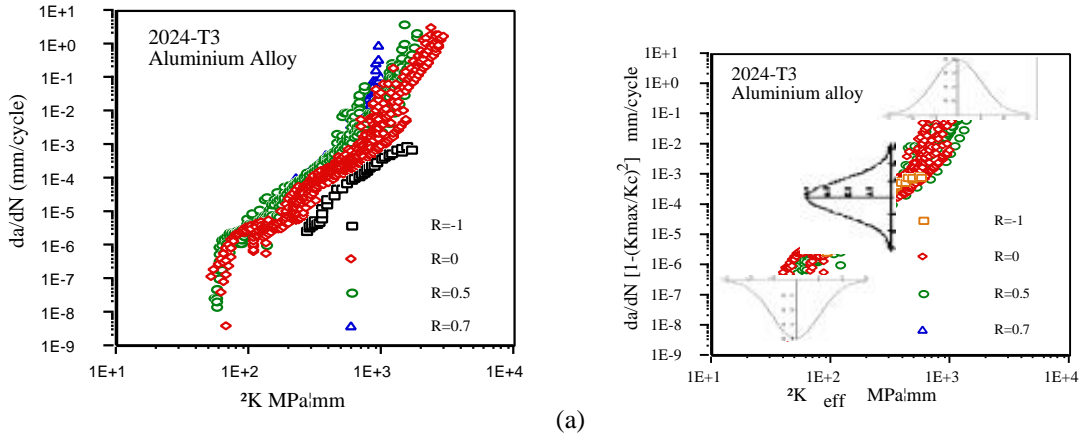


Figure 57 Crack growth rate as a function of the stress intensity factor range (a), and the effective stress intensity factor range (b)

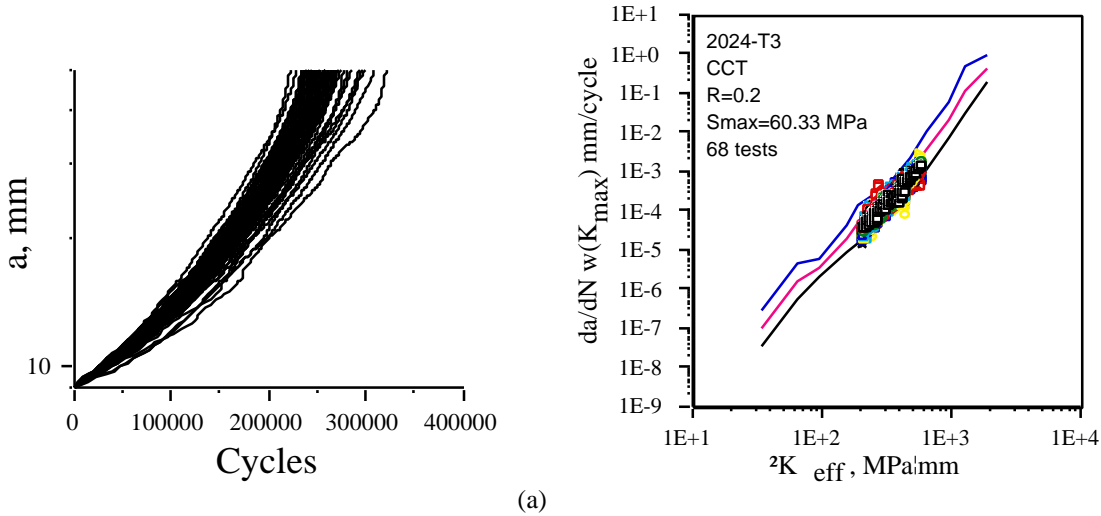


Figure 58 Probabilistic fatigue crack growth of long cracks

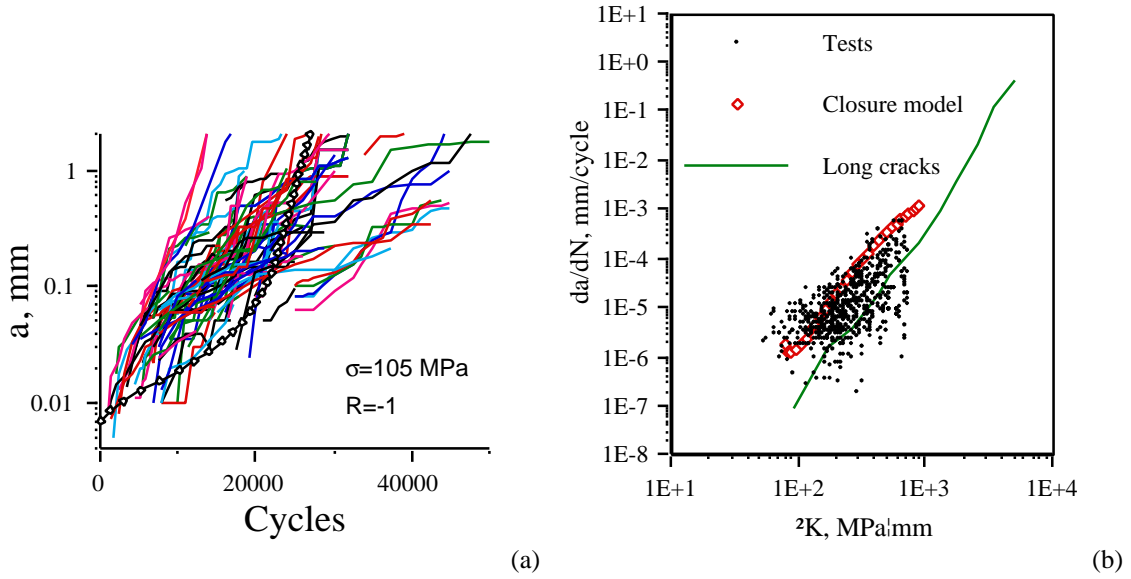


Figure 59 Probabilistic fatigue crack growth of small cracks

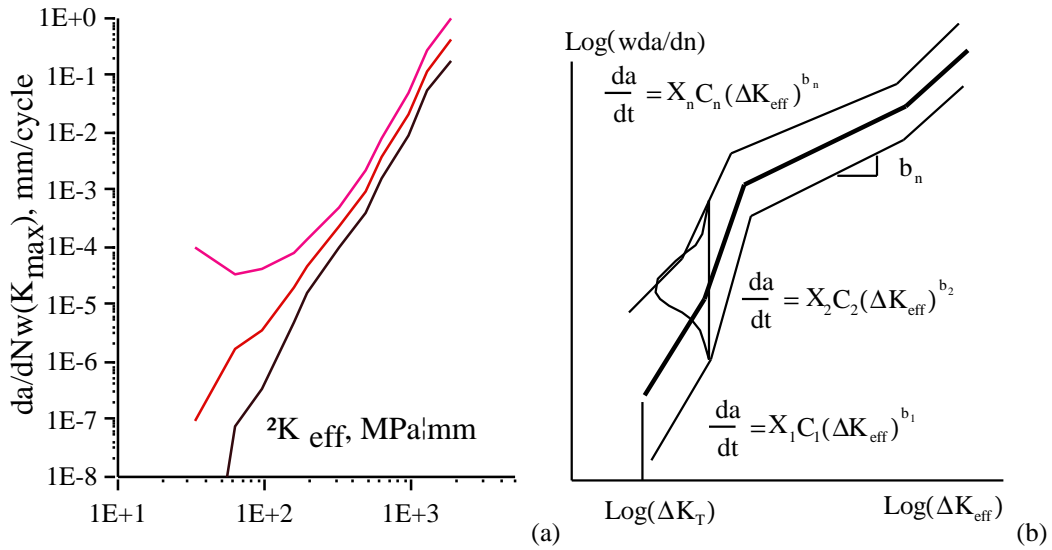


Figure 60 Comparison of crack growth rate for long and short cracks

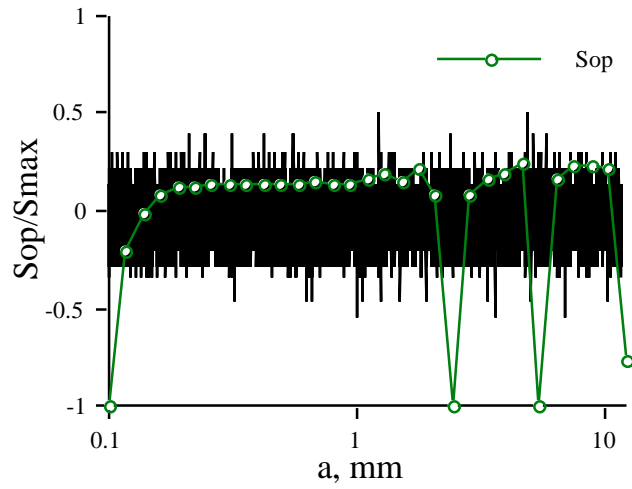


Figure 61 Crack closure compared to the spectrum loading

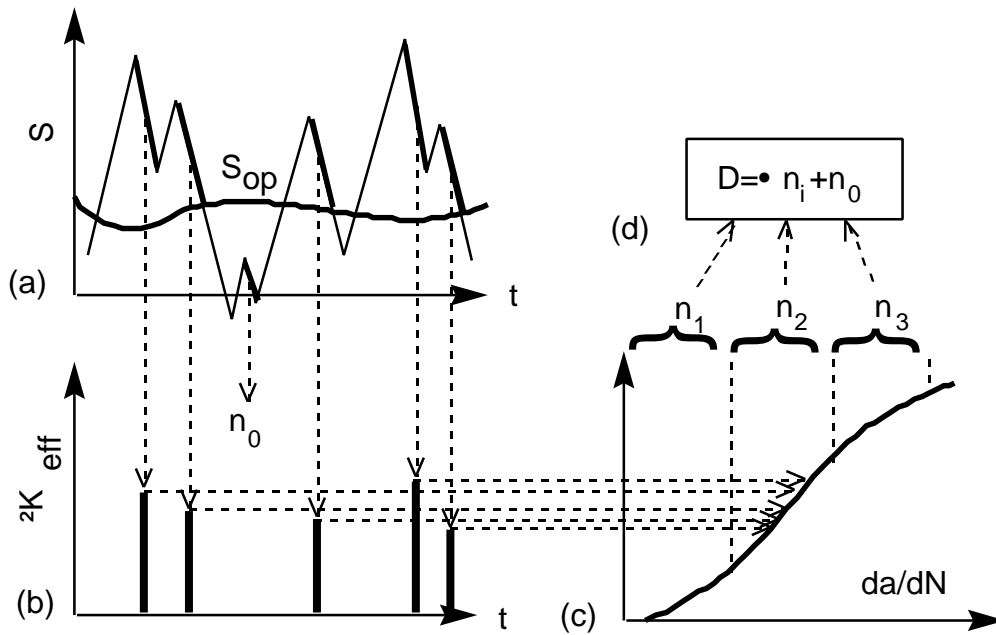


Figure 62 Schematic of the probabilistic damage accumulation solution for the fatigue crack growth analysis

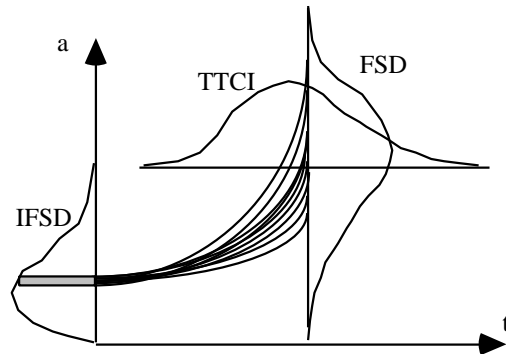


Figure 63 Effect of initial flaw distribution

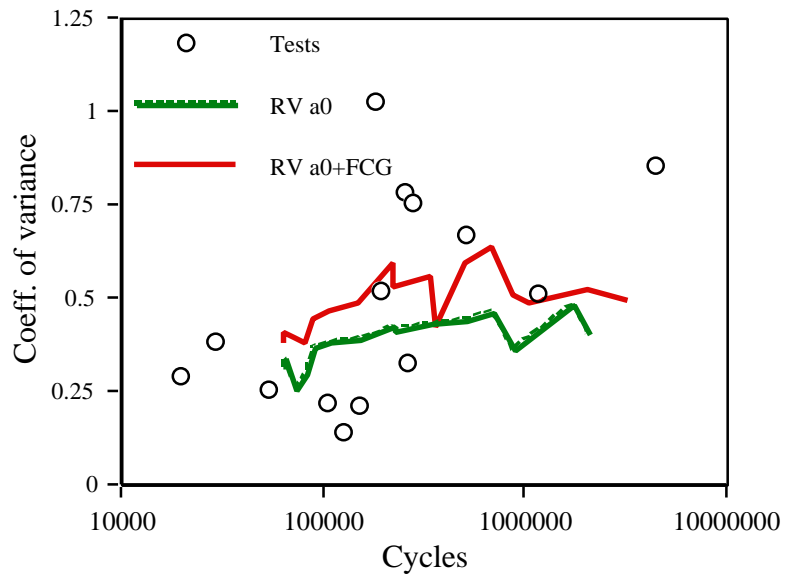


Figure 64 Comparison of COVs between the experimental small crack growth results and the different analytical results

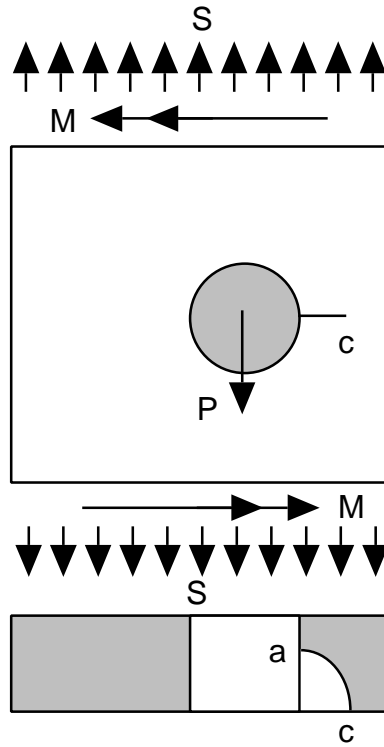


Figure 65 Basic geometry and load for the fastener specimens

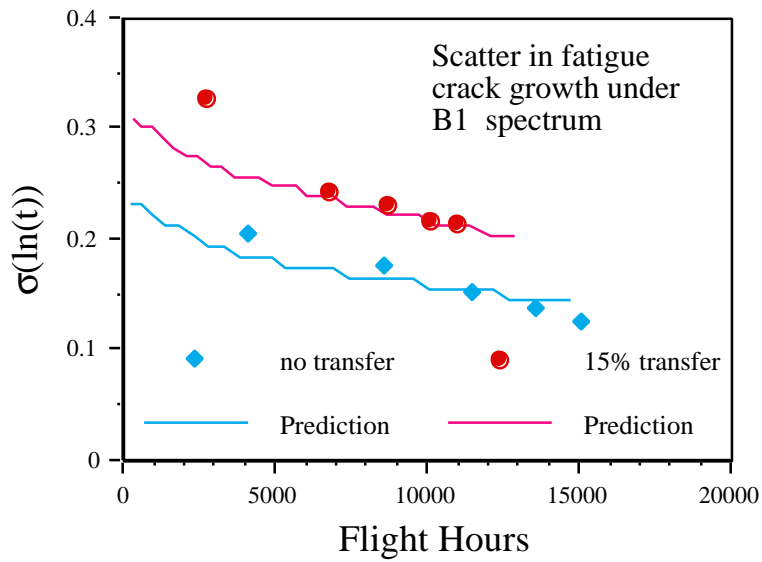


Figure 66 Comparison of log-normal scatter for two different fastener specimens

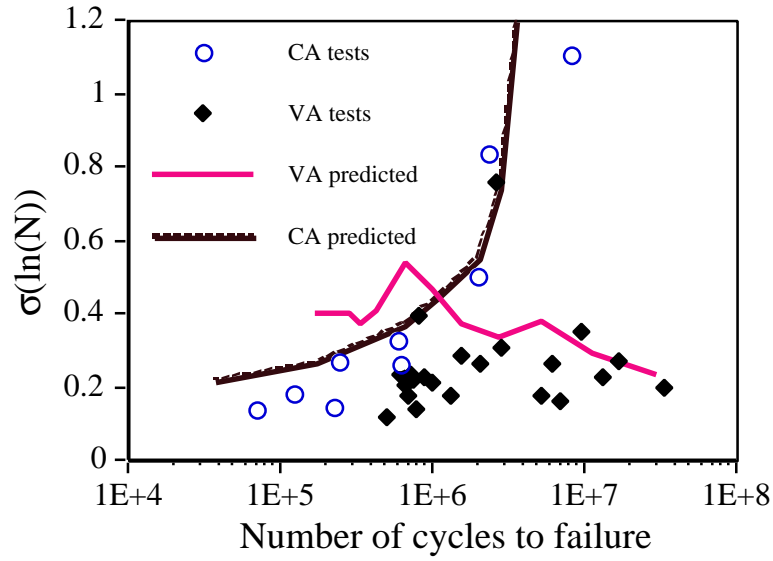


Figure 67 Comparison of log-normal scatter for the constant and variable amplitude loading

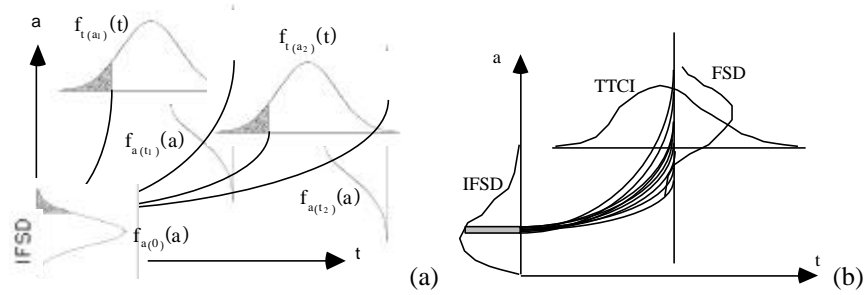


Figure 68 Schematic of the probabilistic crack growth analytical model

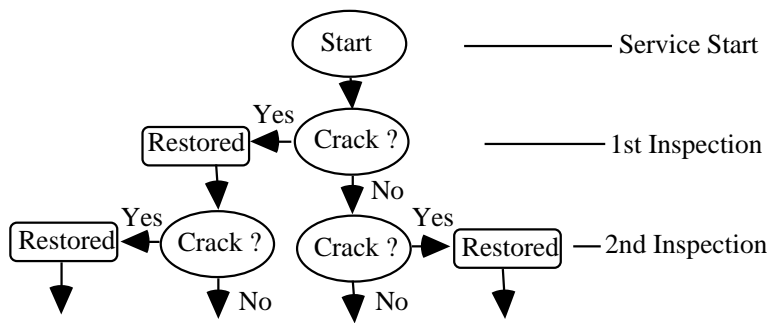


Figure 69 Schematic of the total probability solution

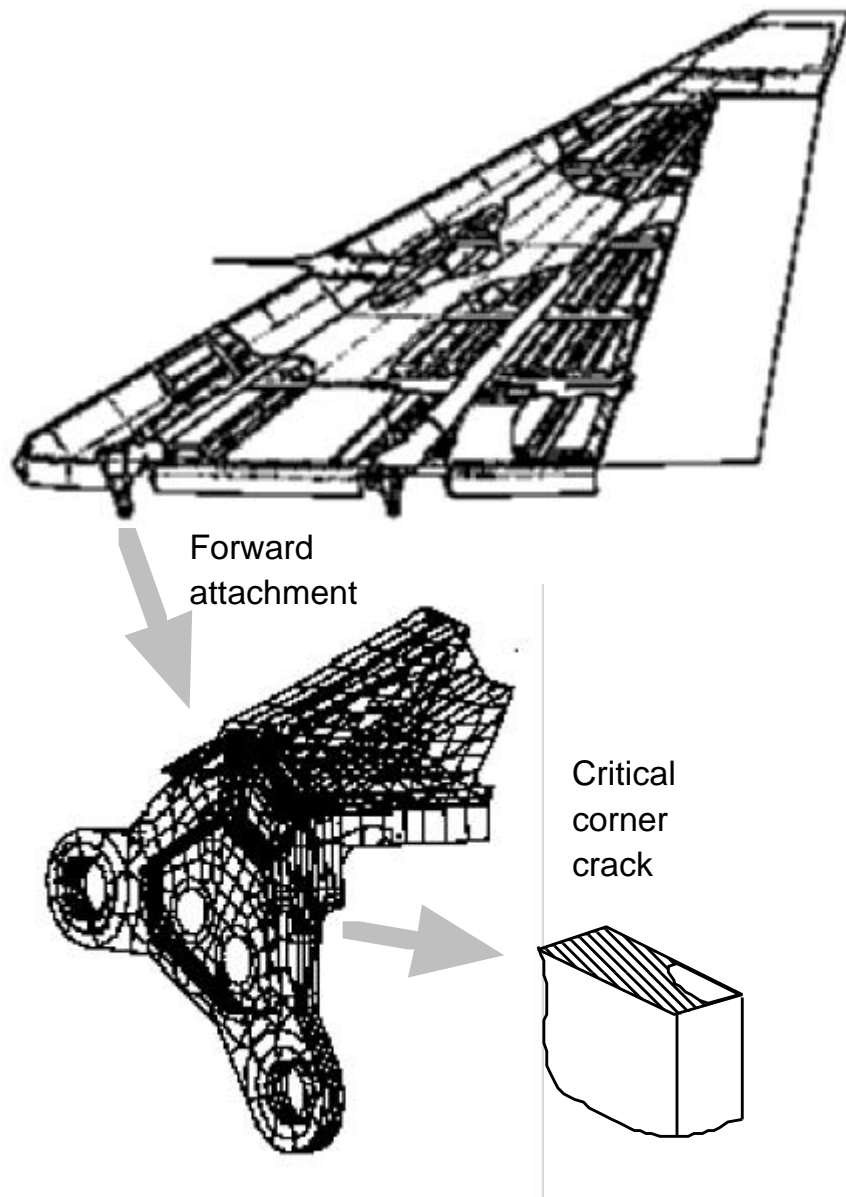


Figure 70 Finite element model of the forward fin attachment

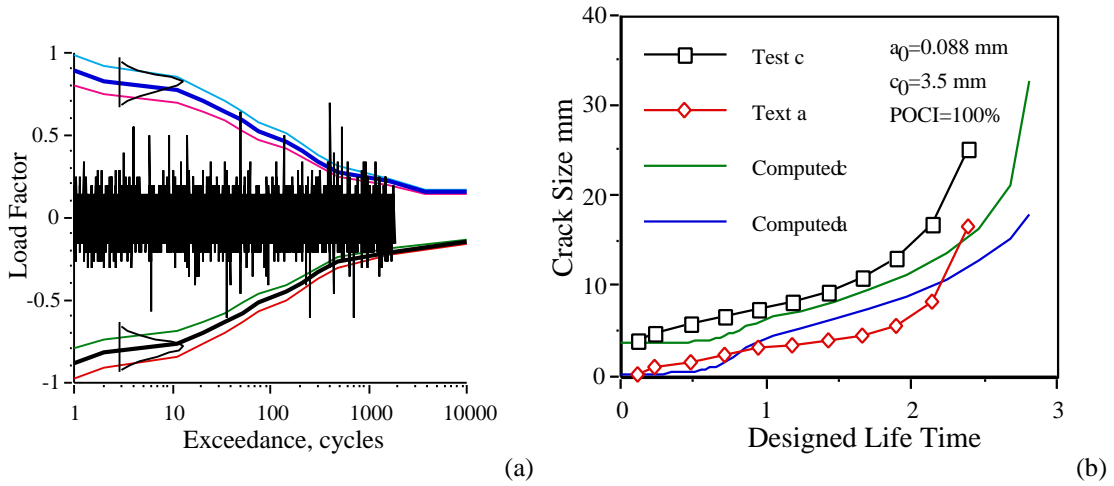


Figure 71 Load spectrum and comparison of analytical and test fatigue crack growth

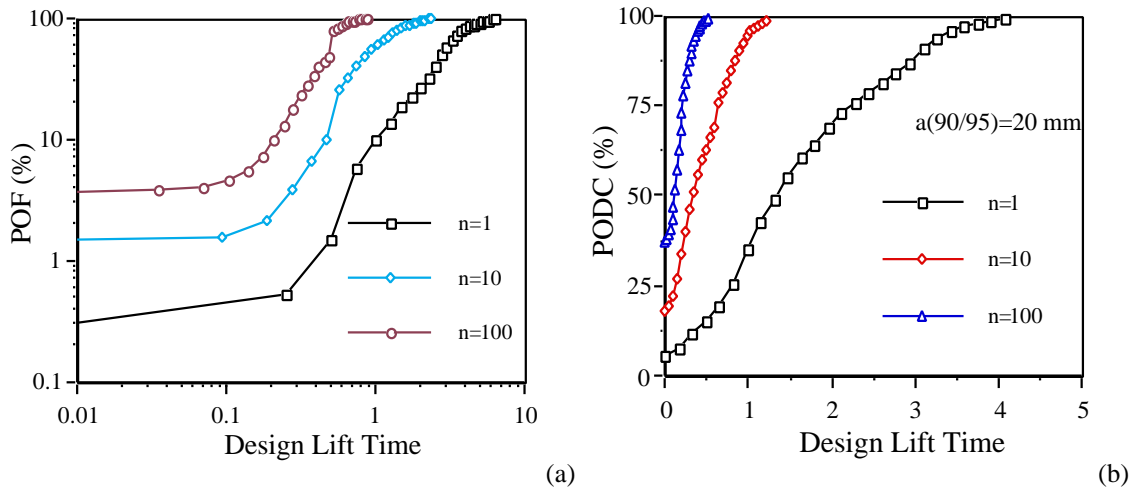


Figure 72 Probability of failure and probability of detecting crack

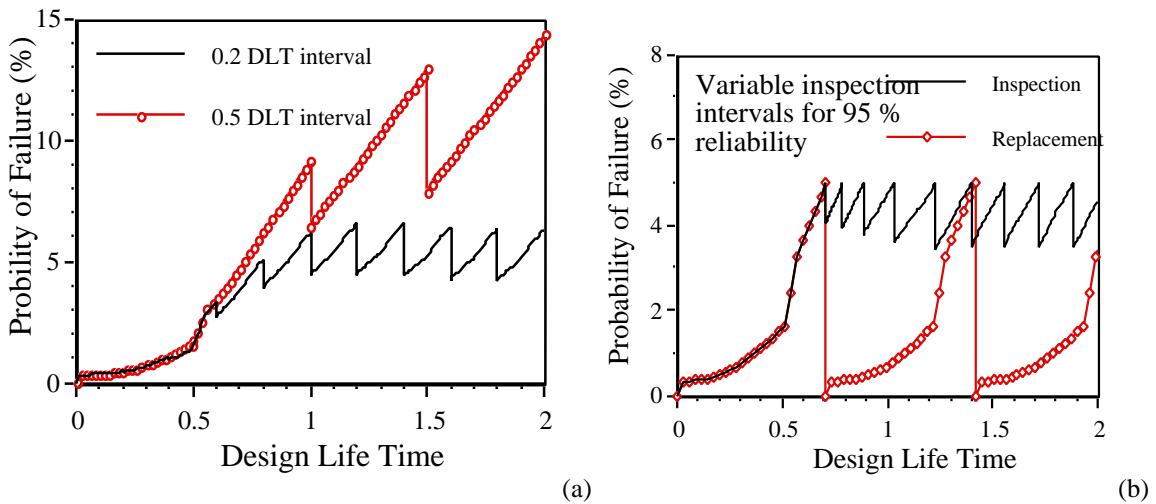


Figure 73 Comparison of constant and variable inspections

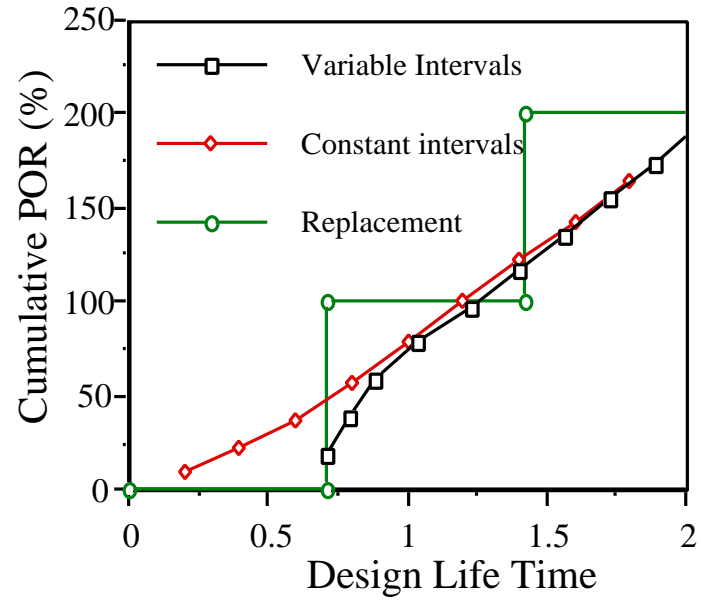


Figure 74 Comparison of the probability of repair for different options

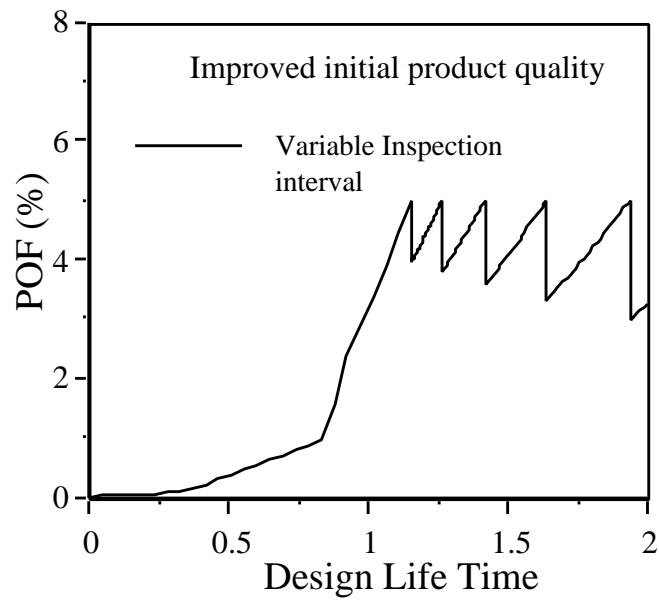


Figure 75 POF after the improvement in the initial flaw size and the consistency between components

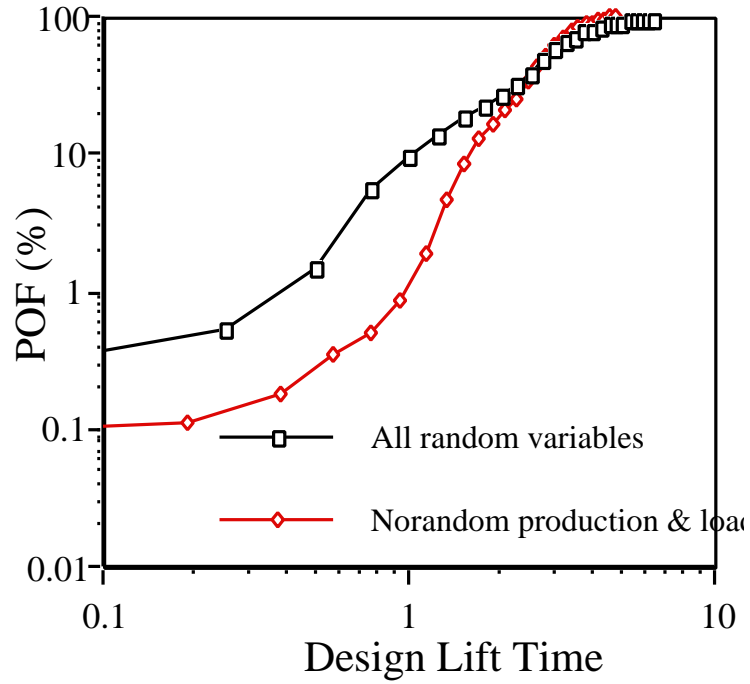


Figure 76 Comparison of various strategies

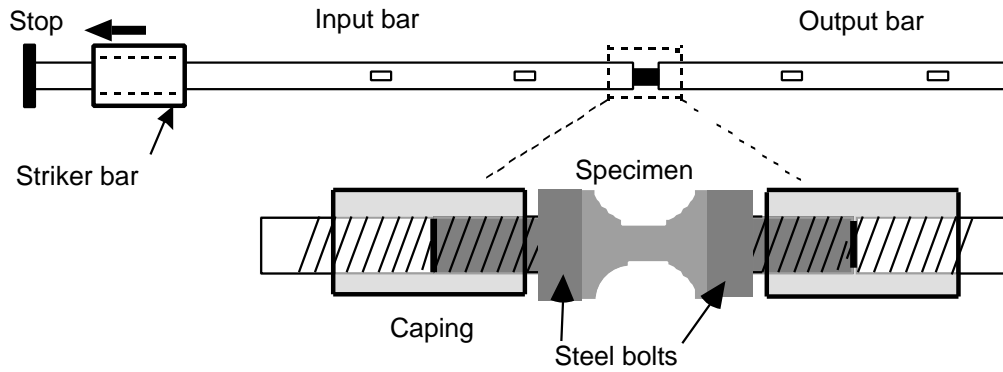


Figure 77 Split Hopkinson bar dynamic tensile test

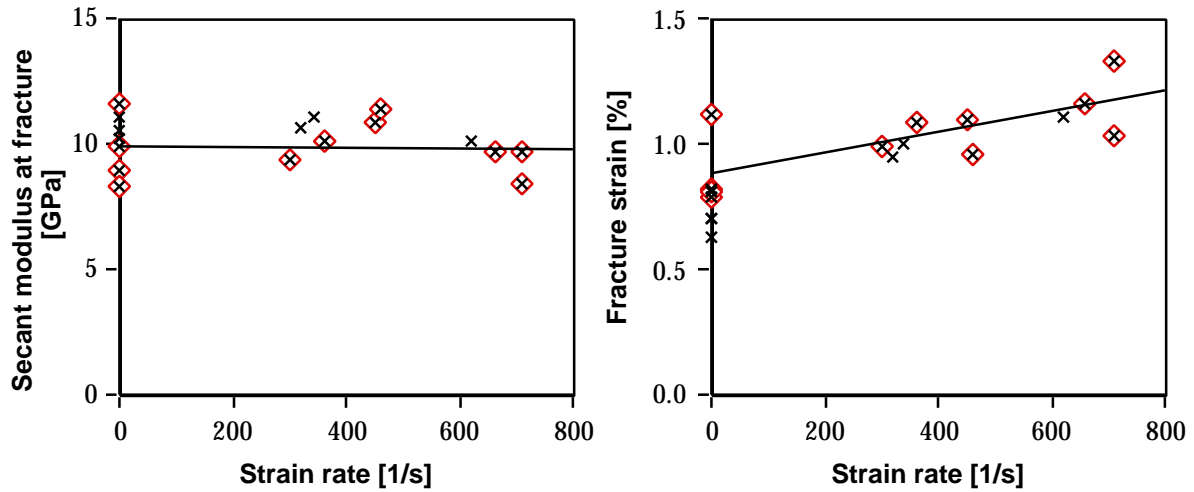


Figure 78 Dynamic out-of-plane tensile bulk properties

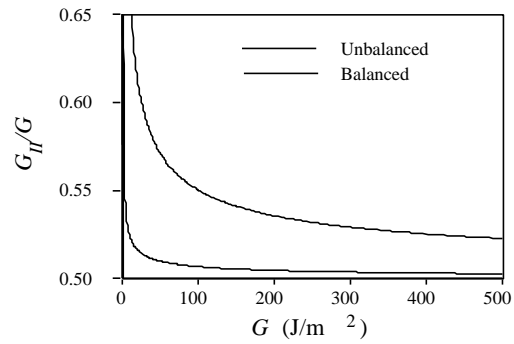


Figure 79 Mode-ratio at initiation of delamination growth for a balanced and an unbalanced test rig evaluated by load-only based methods.

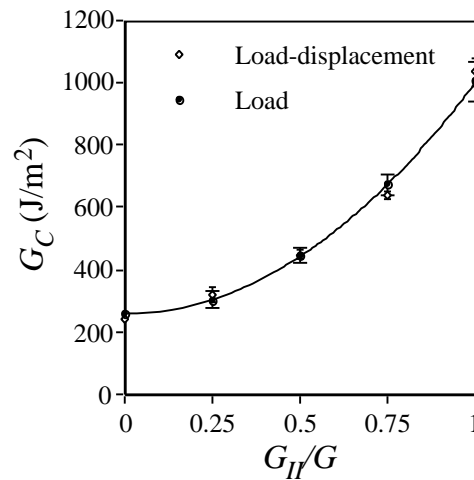


Figure 80 Delamination toughness vs mode mixity obtained by load-displacement evaluation and load only evaluation of an MMB-test with all rig forces eliminated.

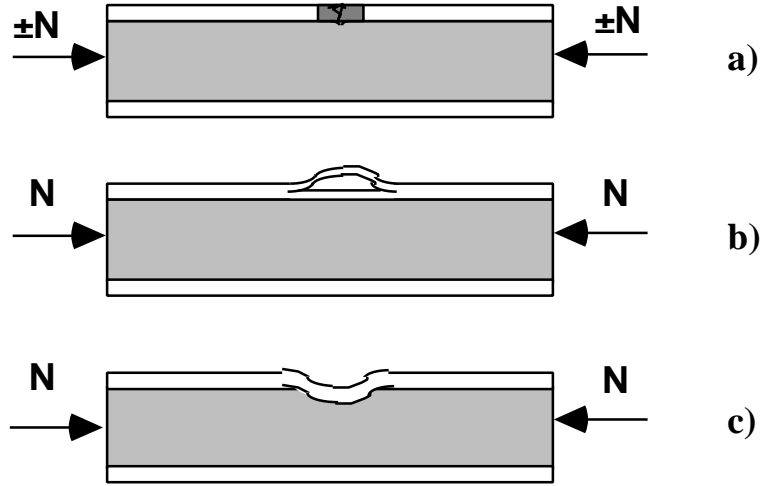
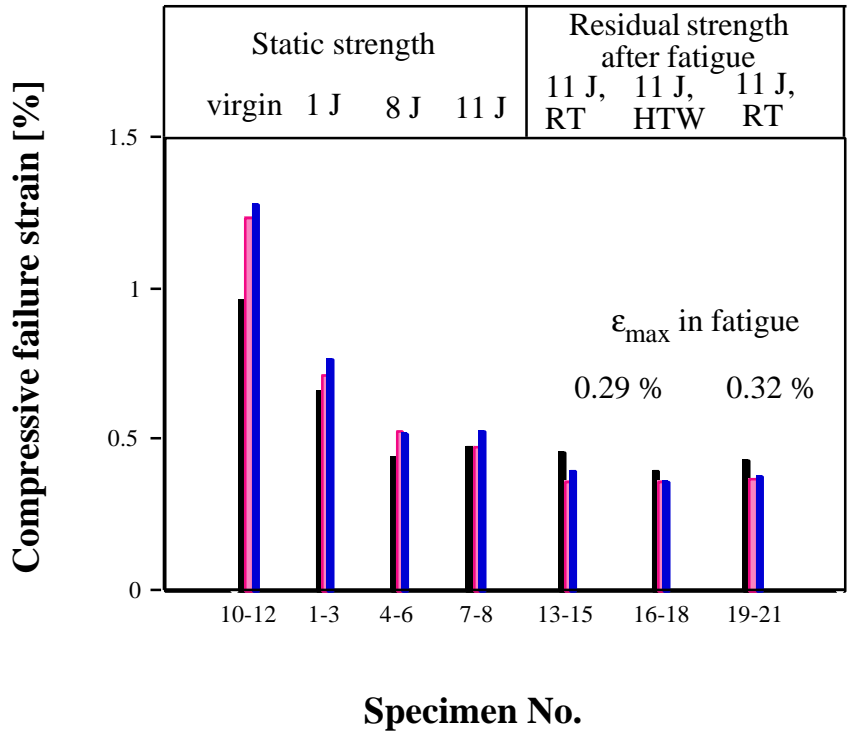
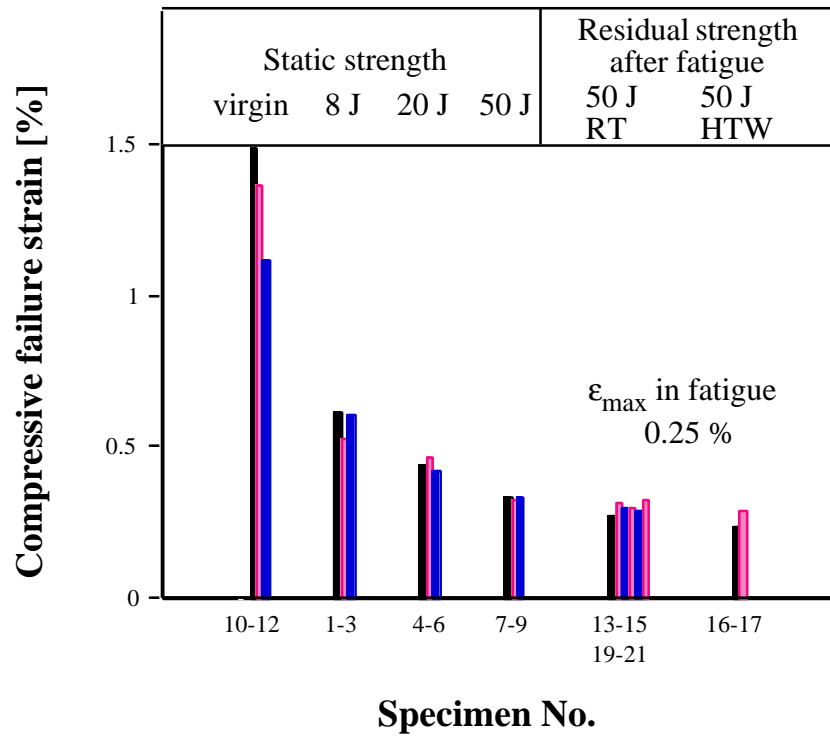


Figure 81 Local failure modes of impacted sandwich panels



Footnote. Specimen 10 failed by core shear.

Figure 82 Static and residual strength versus impact energy and fatigue loads, 8 ply specimens



Footnote. Specimen 12 failed outside the test region.

Figure 83 Static and residual strength versus impact energy and fatigue loads, 24 ply specimens

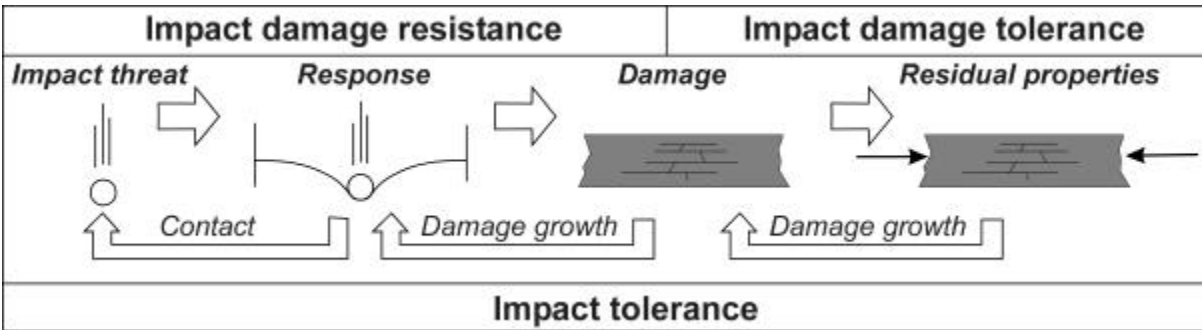
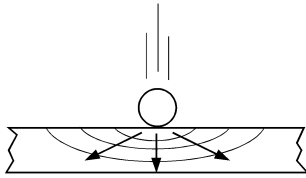


Figure 84 Major concepts of interest when considering effects of impact

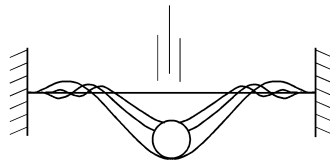
Response dominated
by dilatational waves



Very short impact times

a

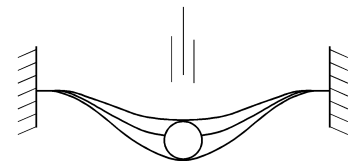
Response dominated
by flexural waves



Short impact times

b

Quasi-static
response



Long impact times

c

Figure 85 Response types during impact on plates

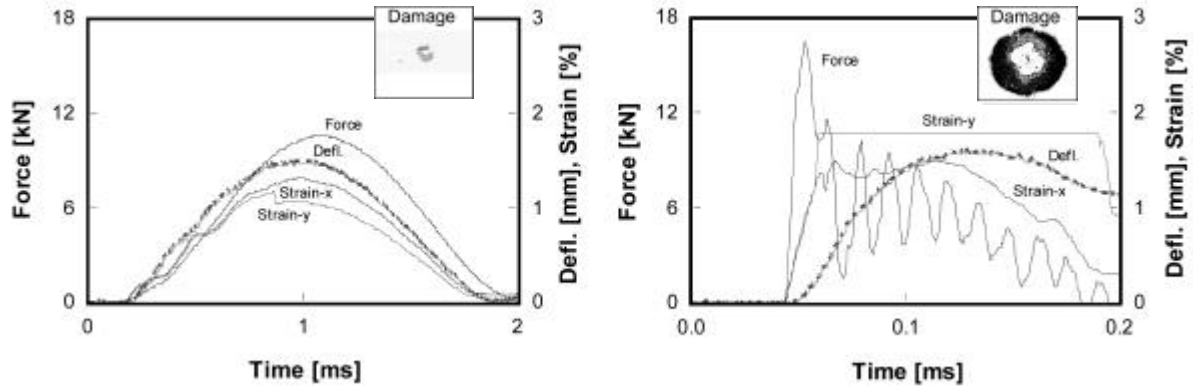


Figure 86 Response and damage due to 10 J impact by a large and small mass

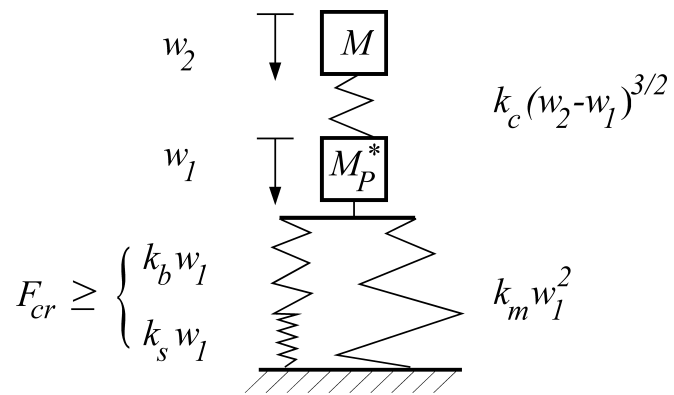


Figure 87 Structural model for quasi-static impact response

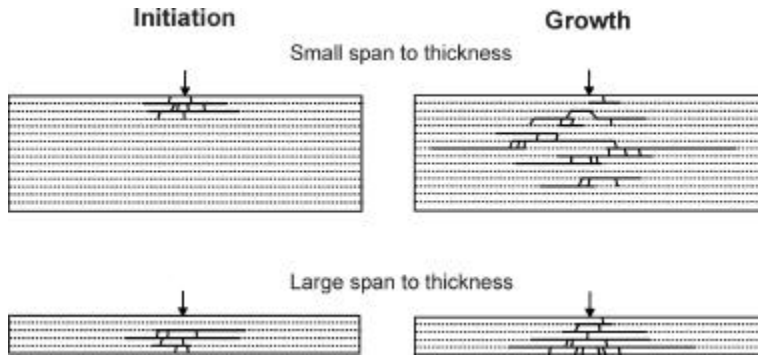


Figure 88 Delamination growth sequence in thick and thin laminates

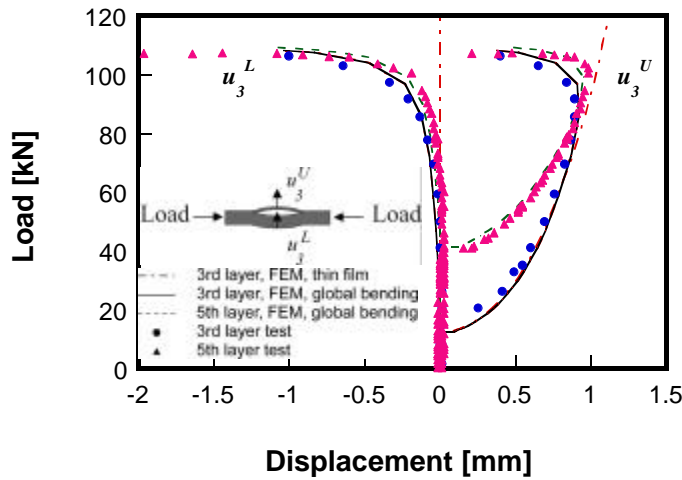


Figure 89 Computed and measured out-of-plane displacements for delaminations at two different depths

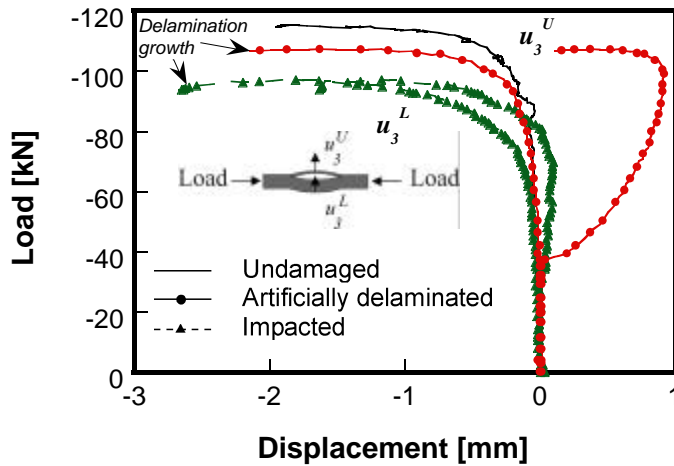


Figure 90 Load vs. out-of-plane displacements from experiments

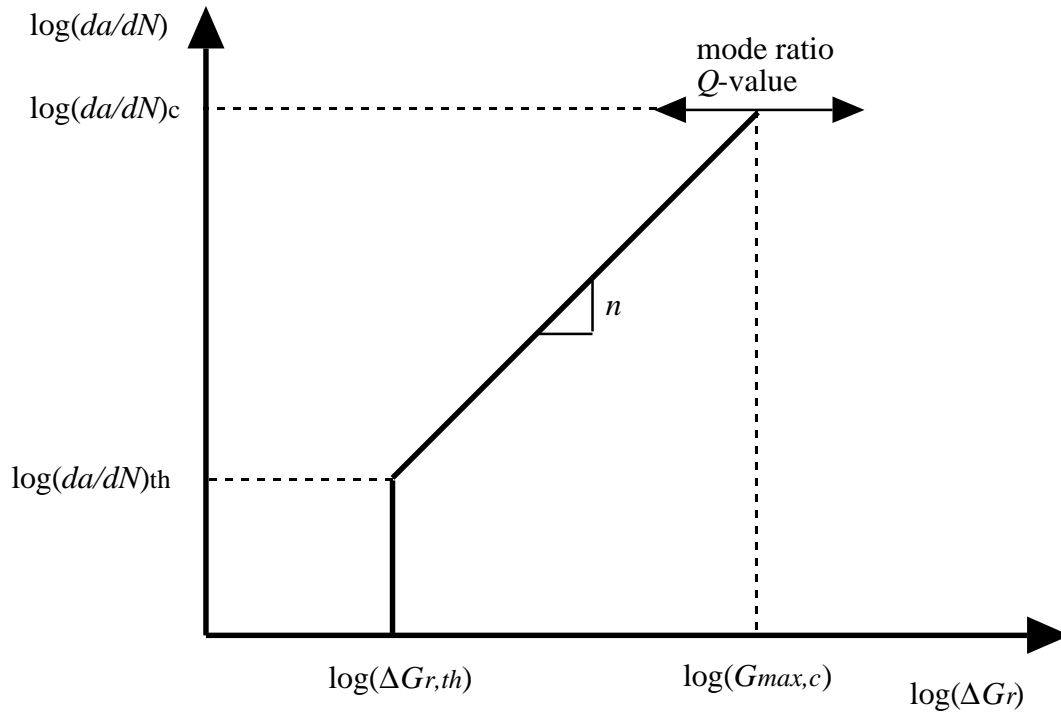


Figure 91 Schematic showing how the n -value changes with mode ratio and Q -value

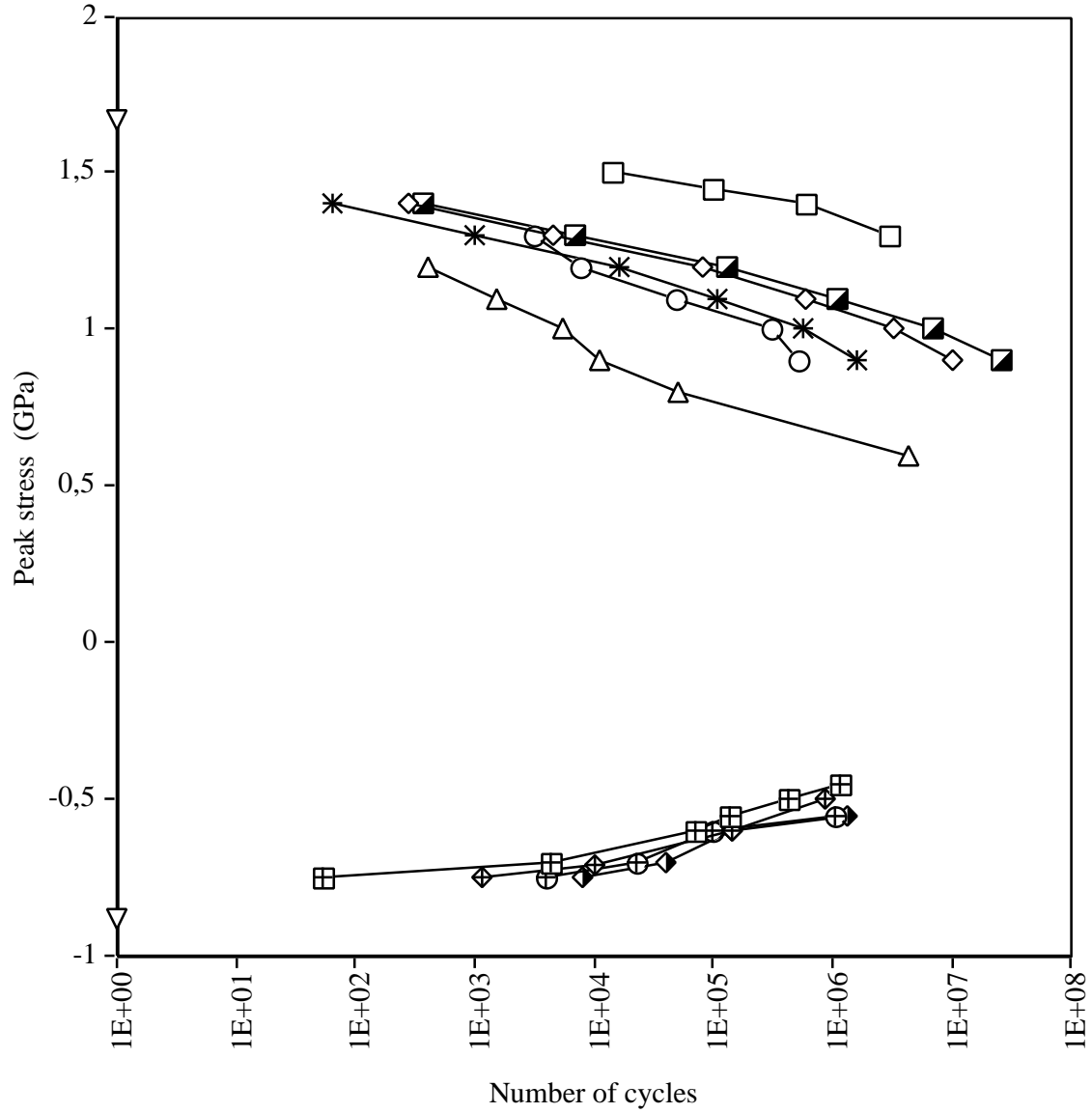
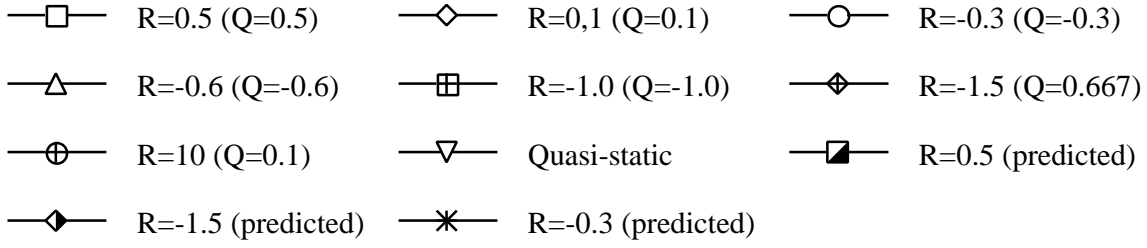


Fig. 92 Experimental [47] and predicted fatigue results.

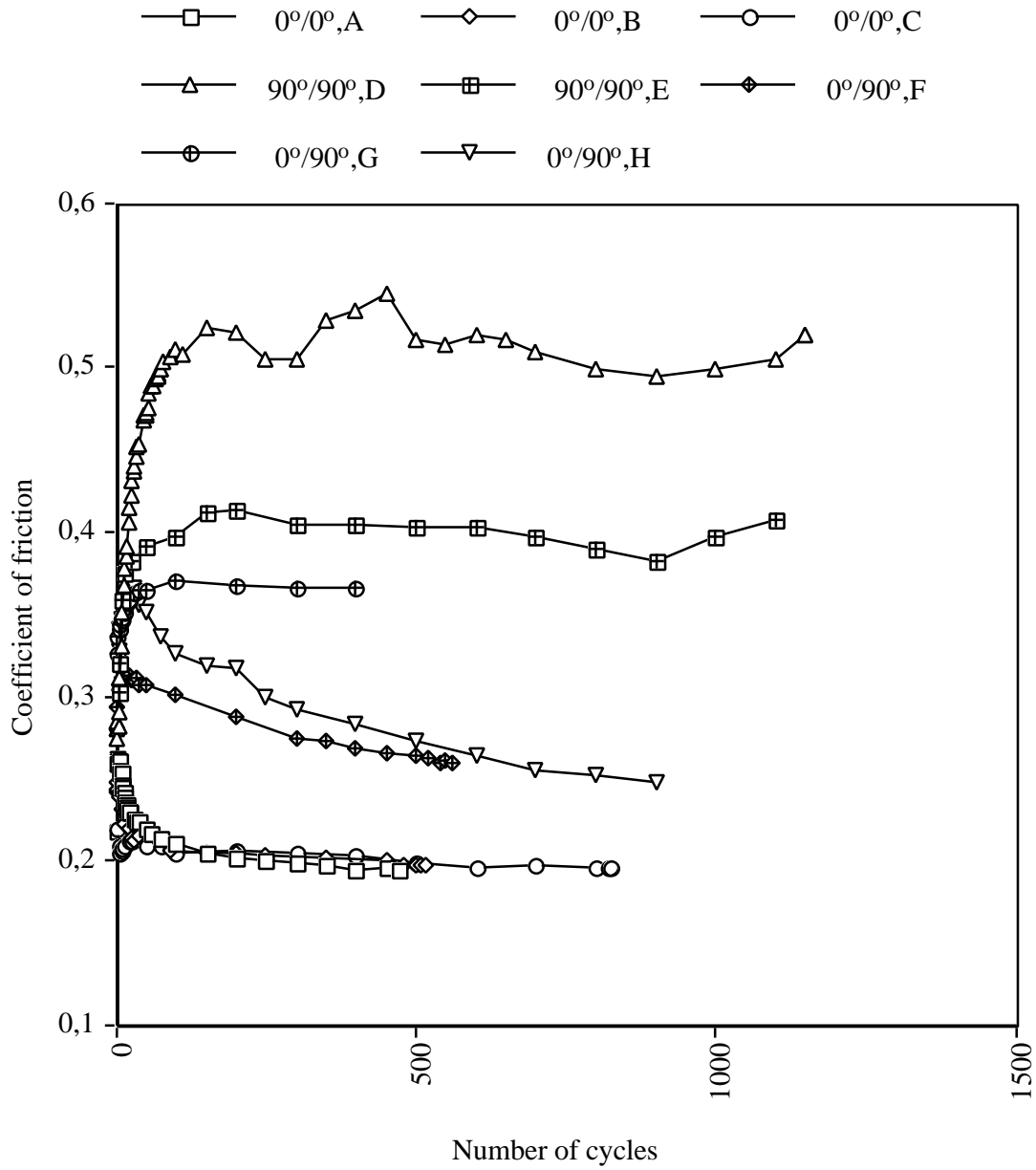


Figure 93 Coefficient of friction for different combinations of surfaces with fibers in 0° and 90° directions

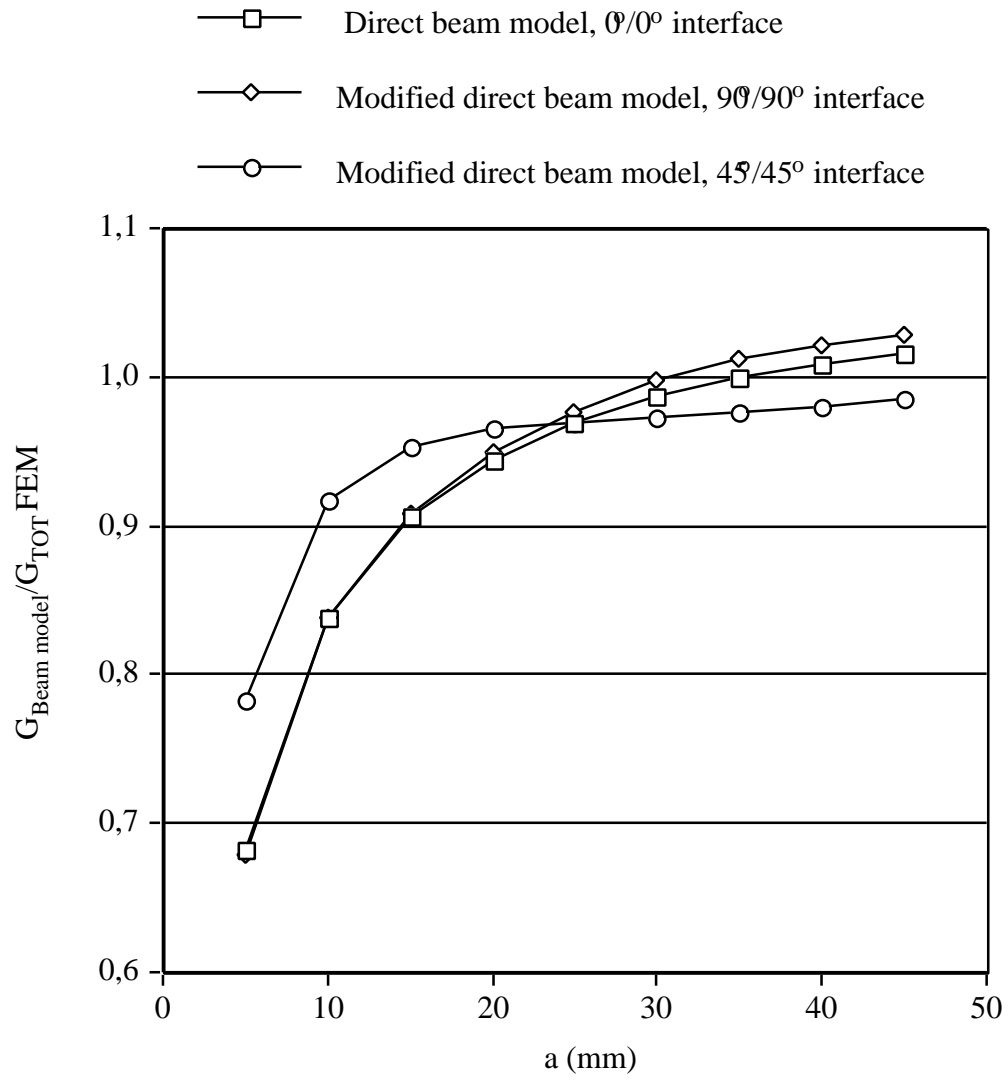


Figure 94 Comparison between results from beam models and FE-solution

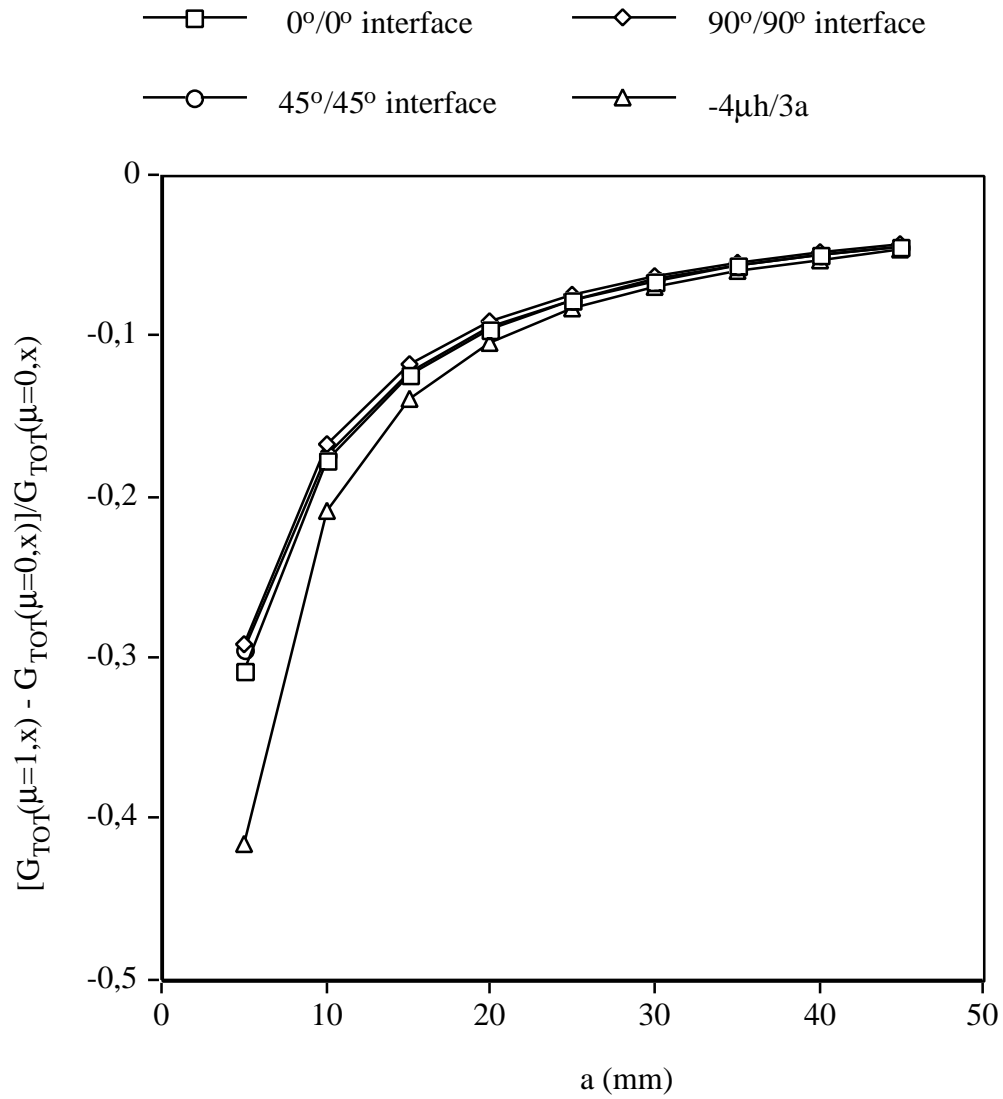


Figure 95 Change in total energy release rate as a function of crack length for different interfaces

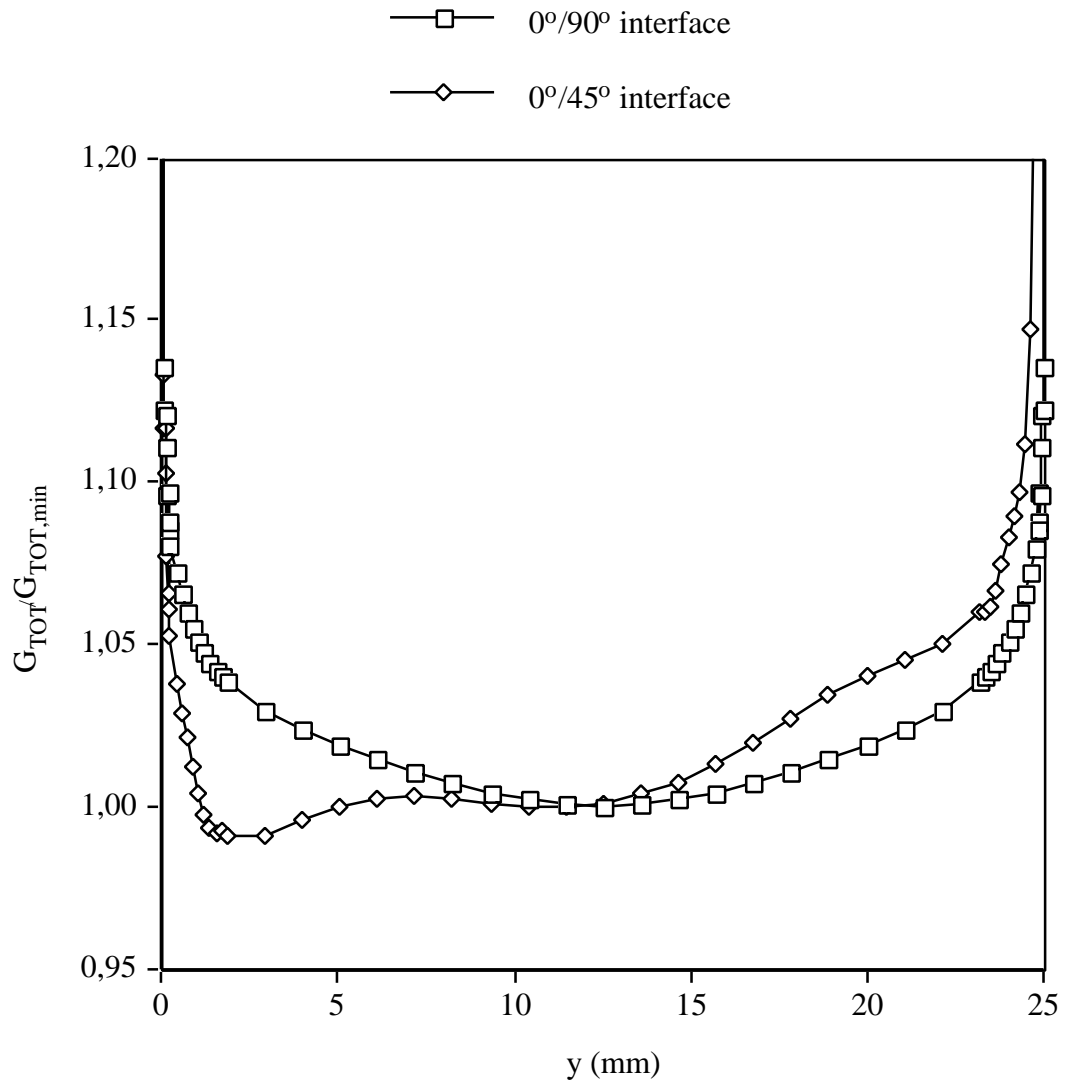


Figure 96 Distribution of total energy release rate for specimen with a 0°/90° and 0°/45° interface.

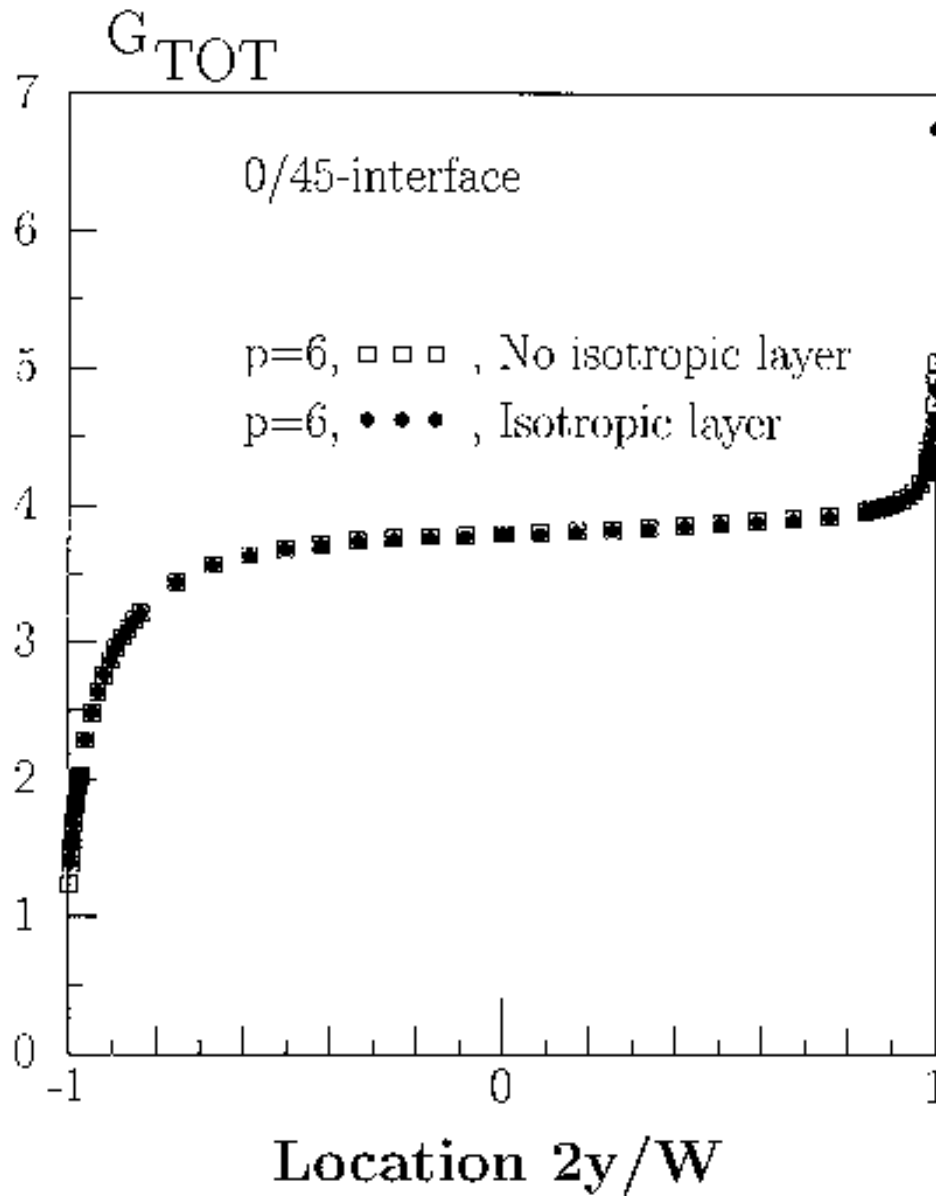


Figure 97 Total energy release rate for a $0/45^\circ$ interface with and without an isotropic material layer (1 mm thick)

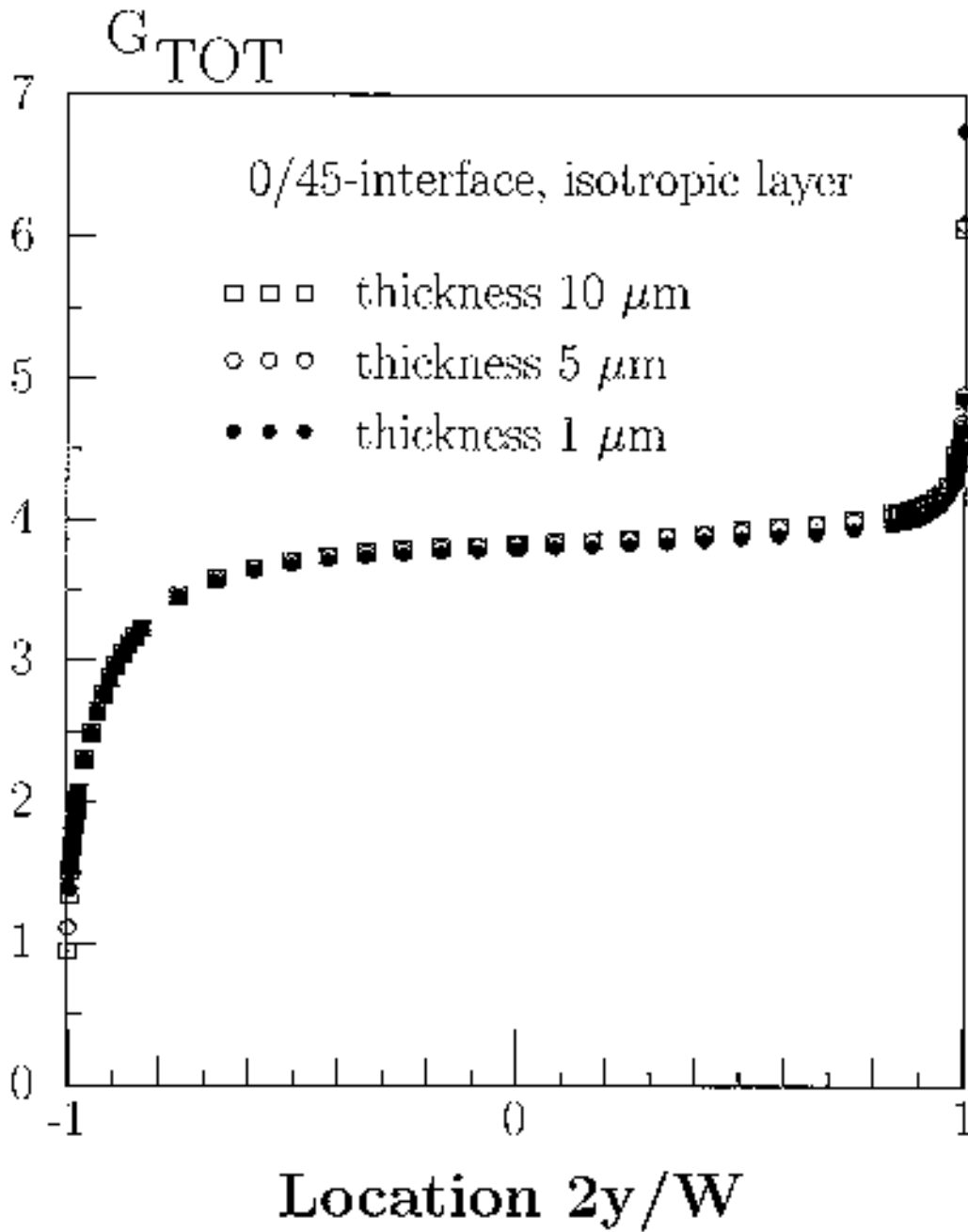


Figure 98 Total energy release rate for a 0°/45° interface with different thickness of the isotropic layer

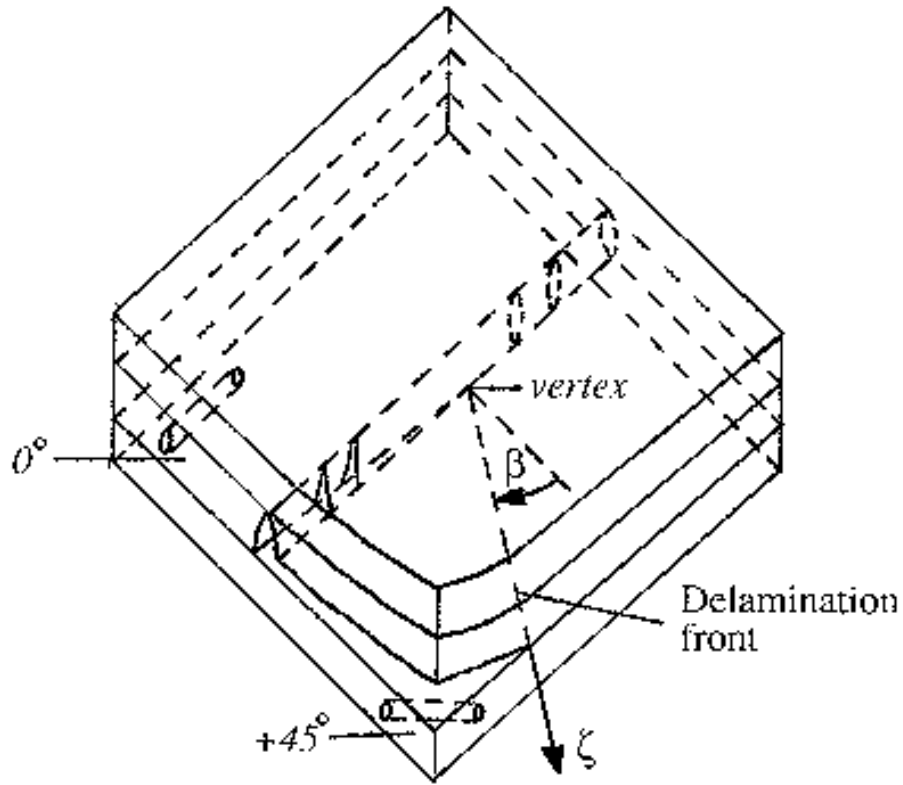


Figure 99 Geometry near intersection of delamination crack front and a matrix crack

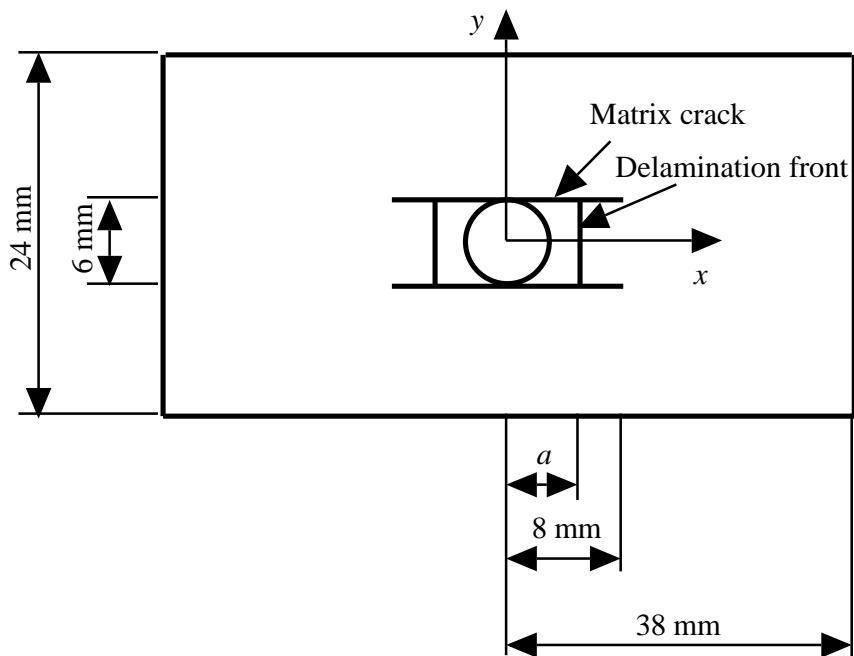


Figure 100 Specimen geometry

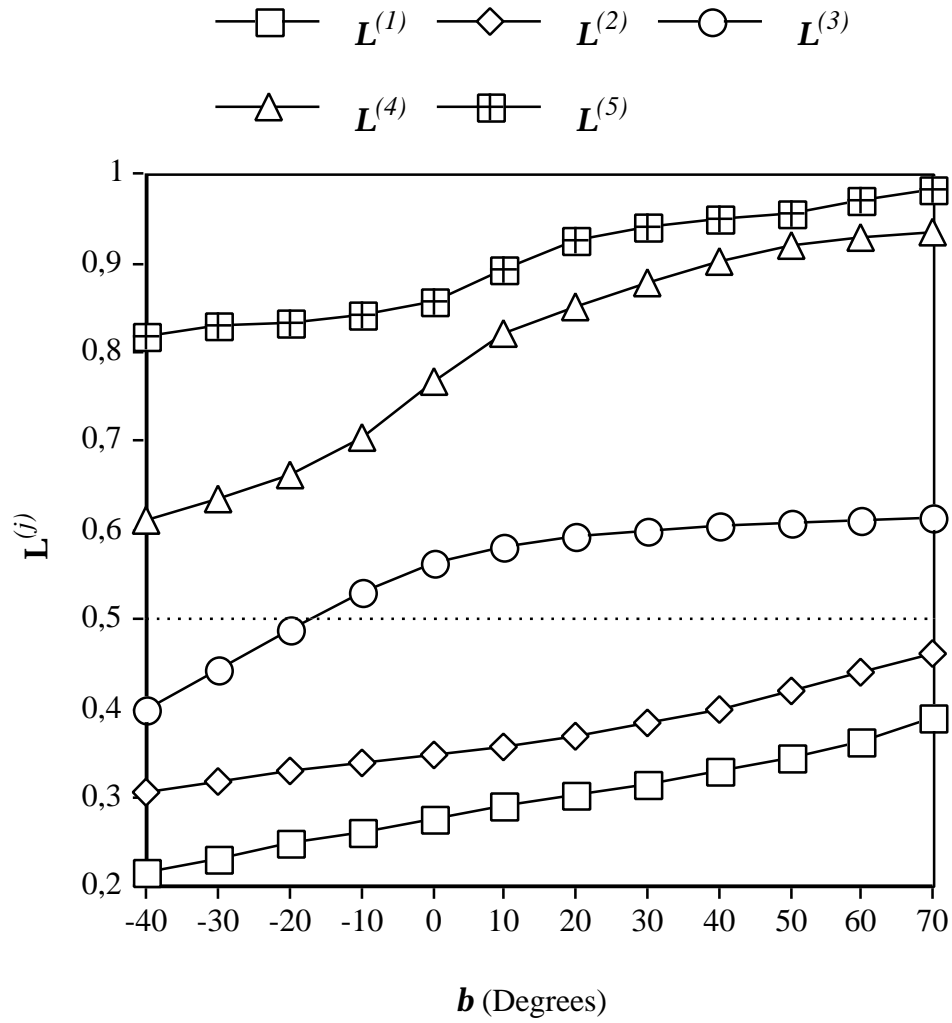


Figure 101 Vertex eigenvalues $\text{Re}(\Lambda^{(j)})$ as a function of b for a $0^\circ/45^\circ$ interface

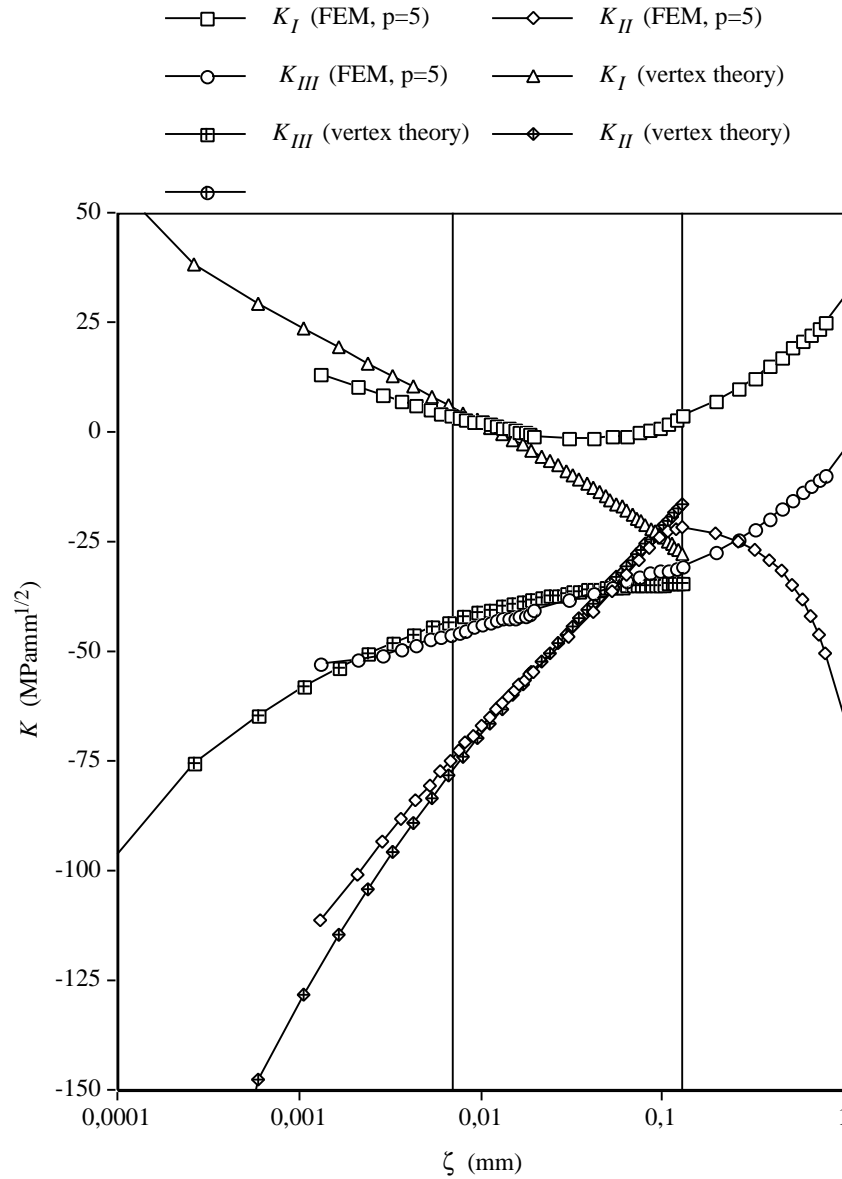


Figure 102 Values of edge stress intensity functions close to the vertex, computed using vertex data and edge data, respectively. In the figure the fiber diameter, 7 mm, and the ply thickness, 130 μm , are indicated.

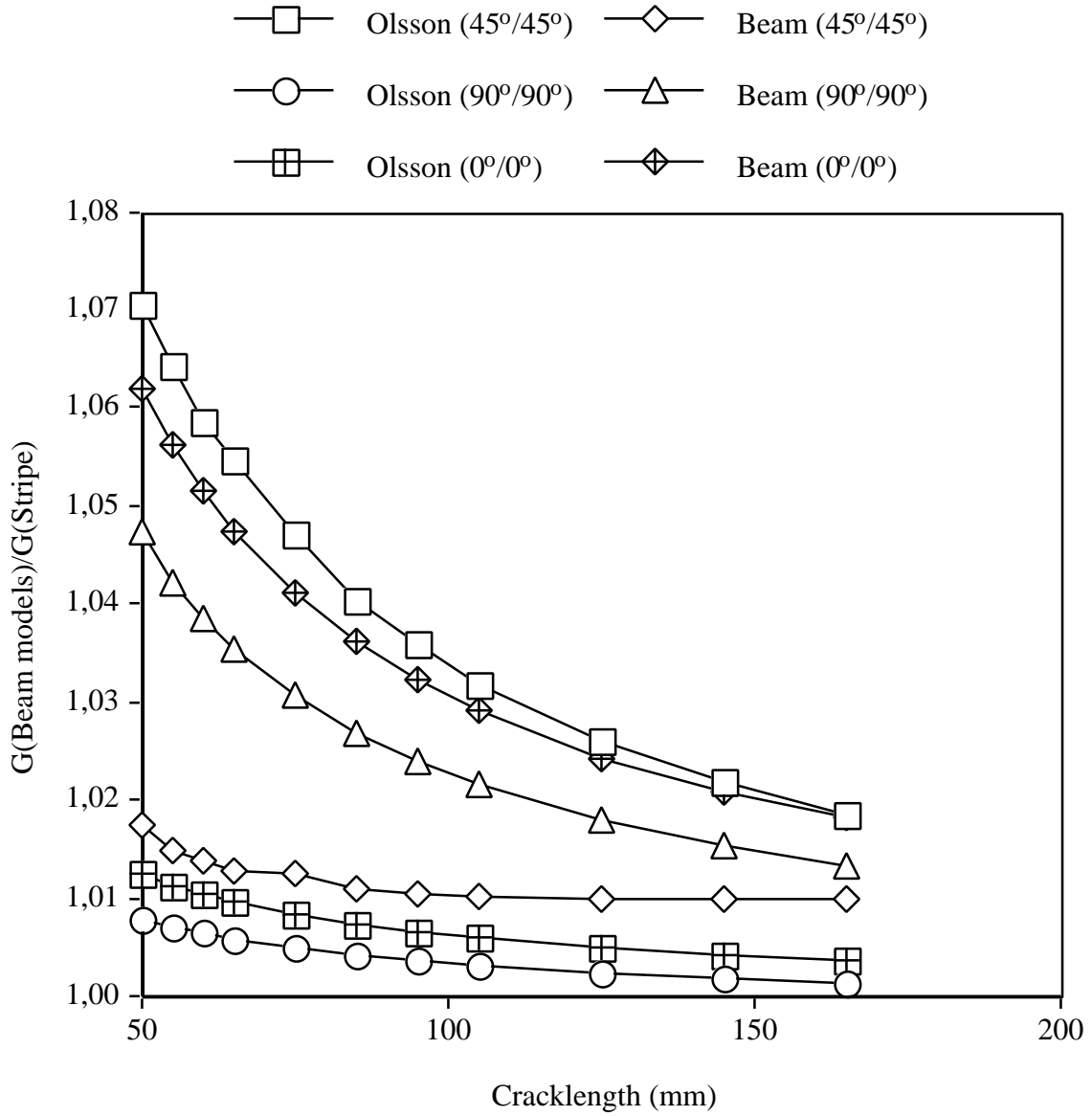


Figure 103 Comparison between FEM and different beam models

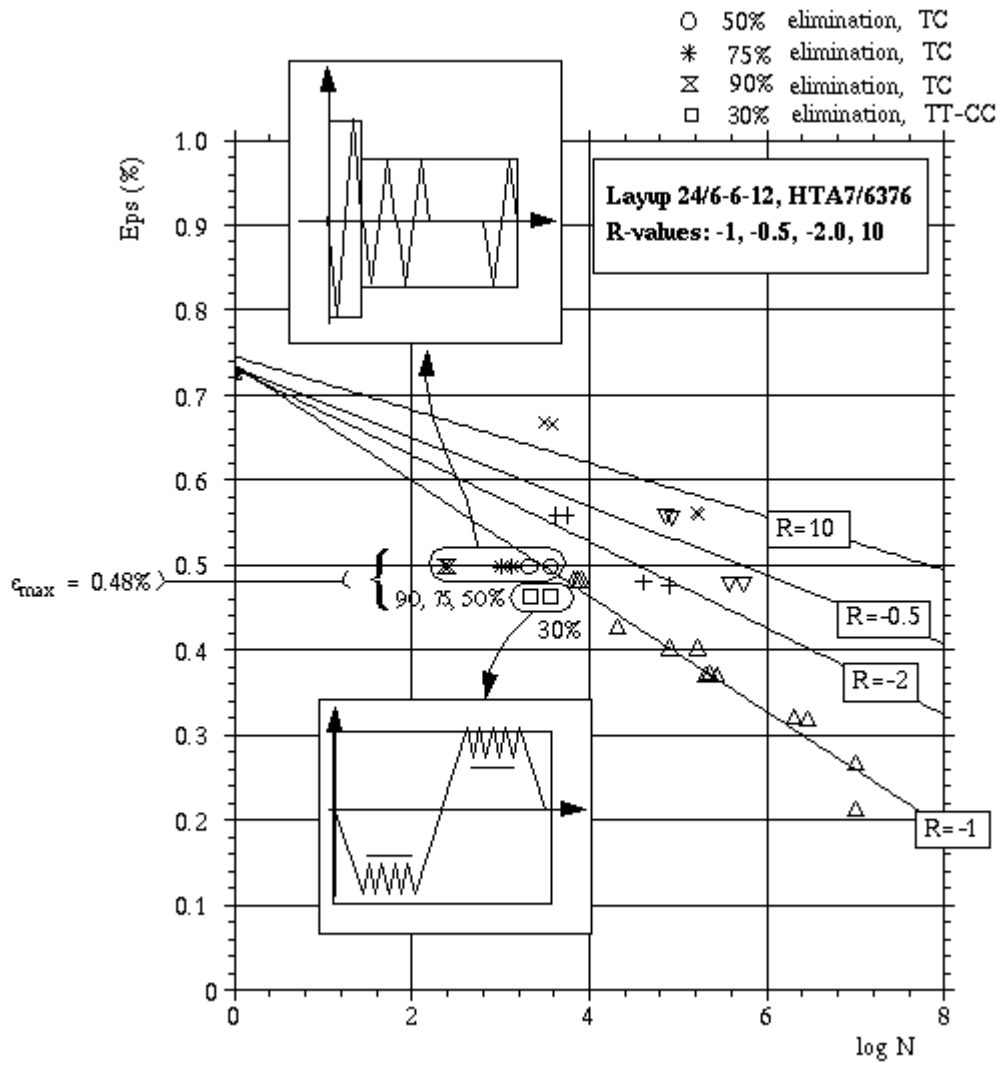


Figure 104 Comparison block testing with constant amplitude loading, where the block testing consists of a mixture of tension-tension and compression-compression loading (TT-CC) and full tension-compression loading (TC)

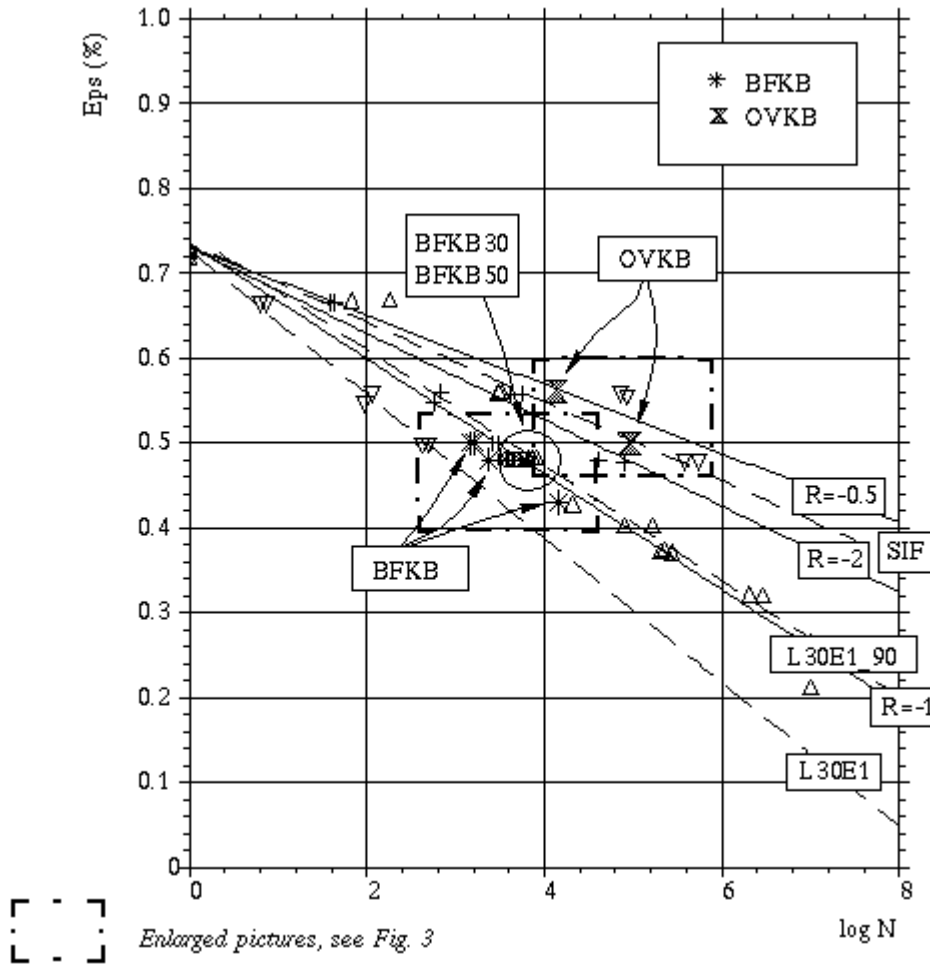


Figure 105 Spectrum test with L30E1, BFKB, OVKB and inverted short Falstaff (SIF) mapped on constant amplitude data accounting for a characteristic number of cycles. Depicted in the figure are also results from spectrum testing with different elimination levels, 30 and 50% of maximum range, indicated in the figure with BFKB30 respectively BFKB50.

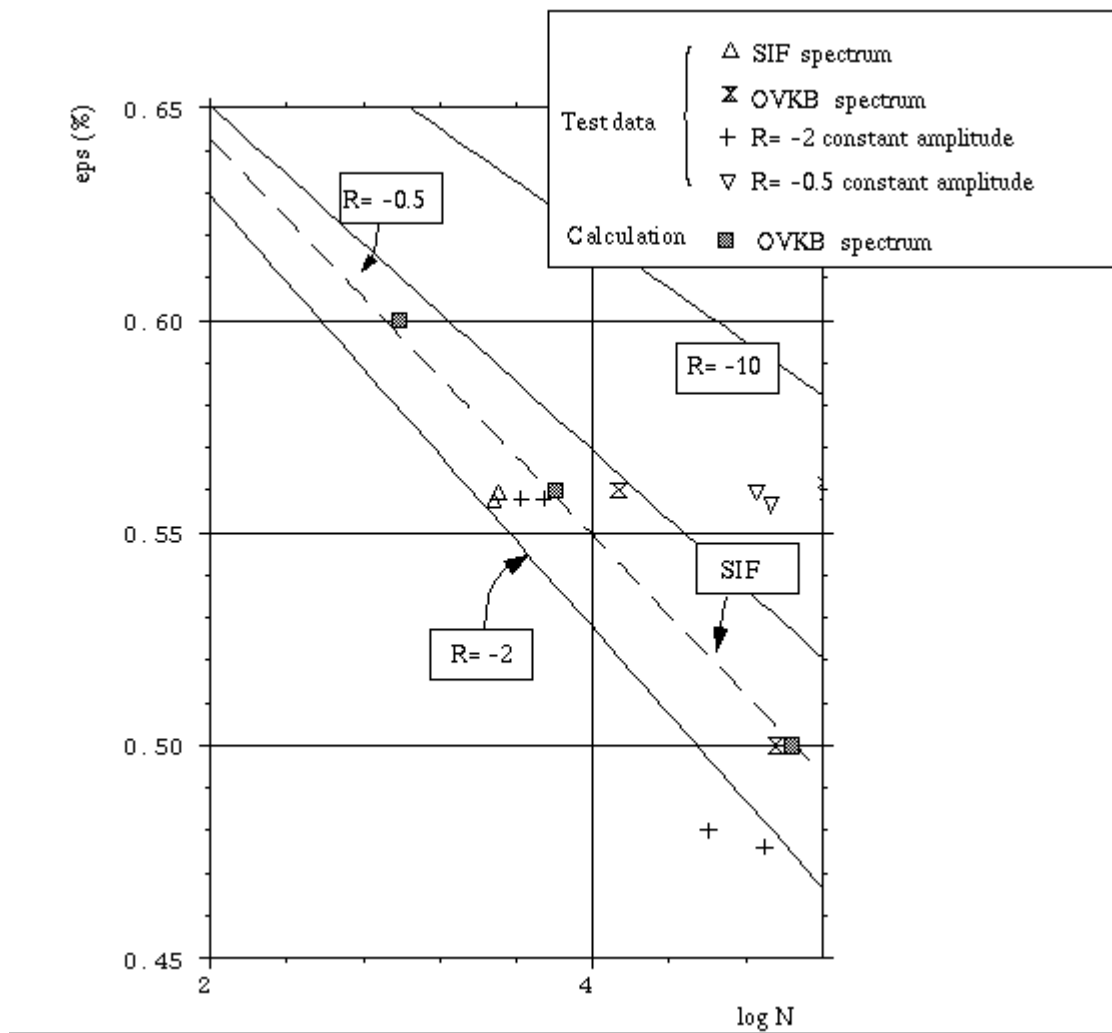


Figure 106 Spectrum test with OVKB and inverted short Falstaff (SIF) mapped on constant amplitude data, picture enlarged with embedded calculation results

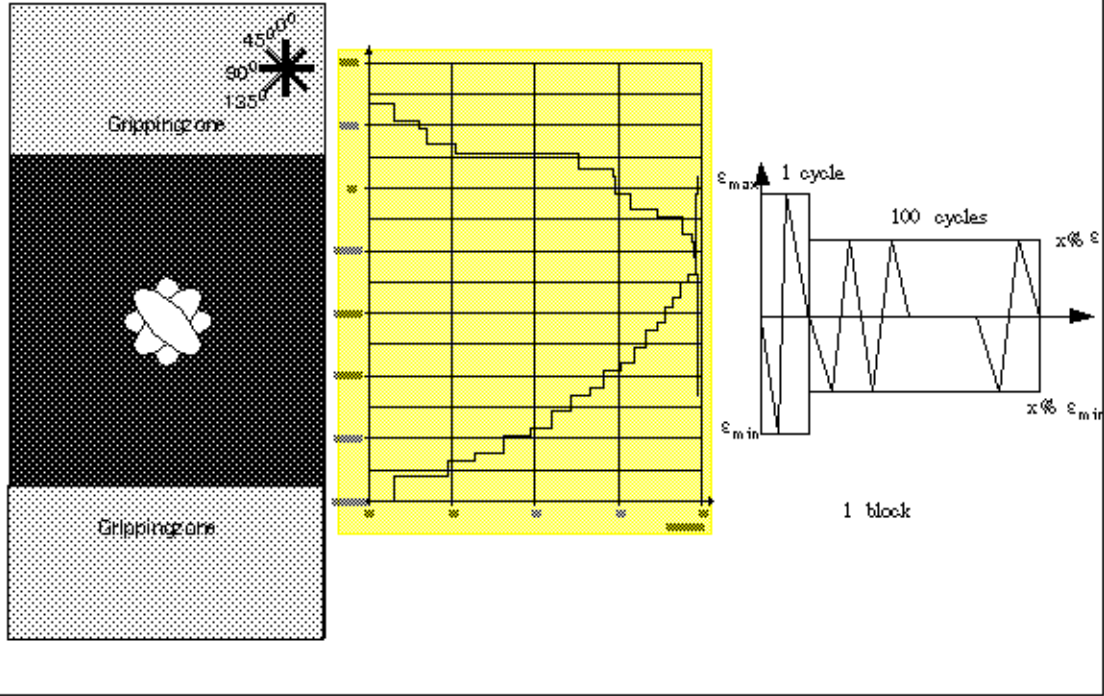


Figure 107 Schematic of fatigue after impact testing.

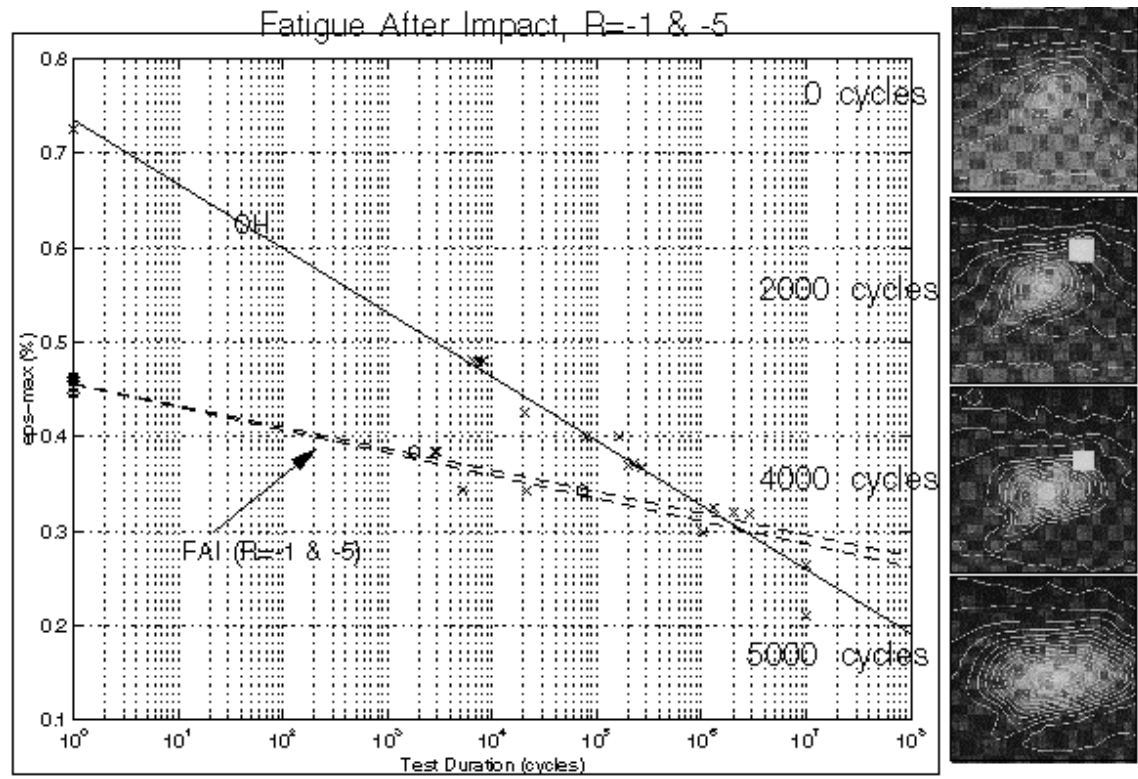


Figure 108 Fatigue after impact, constant amplitude loading.

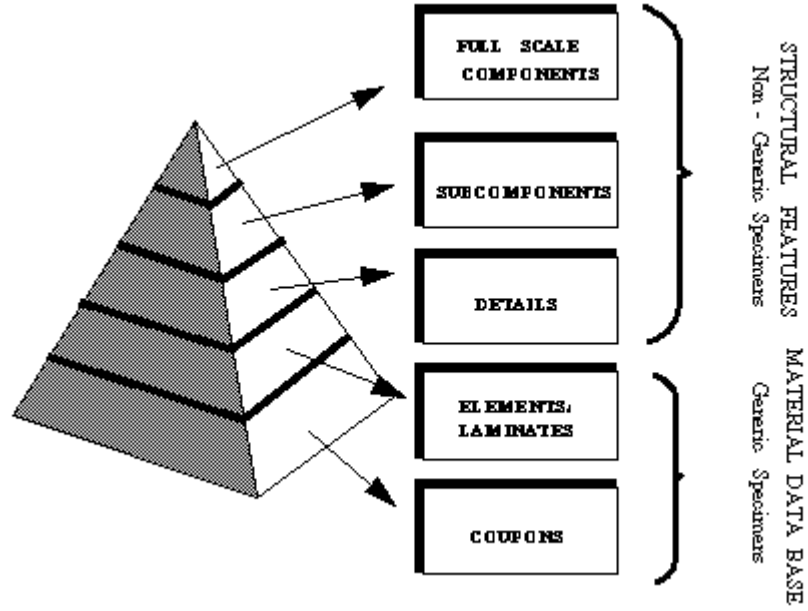


Figure 109 Schematic of testing requirements, Rouchon's test pyramid

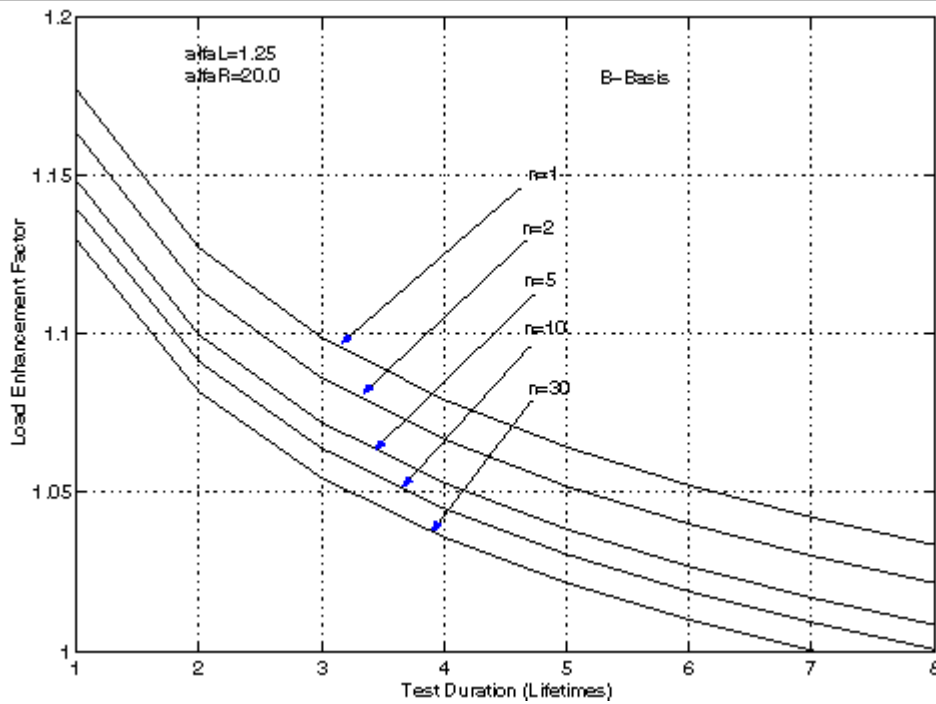


Figure 110 Load enhancement approach

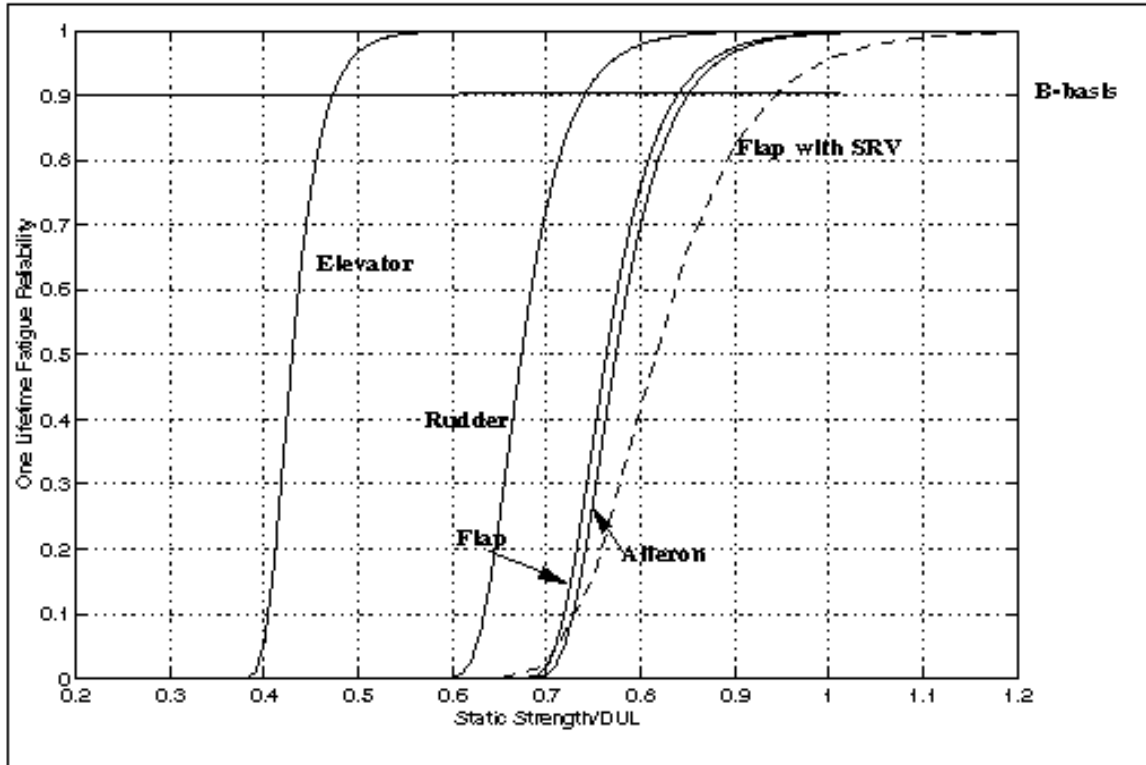


Figure 111 Ultimate strength approach, spectra comparison for control surfaces to S2000

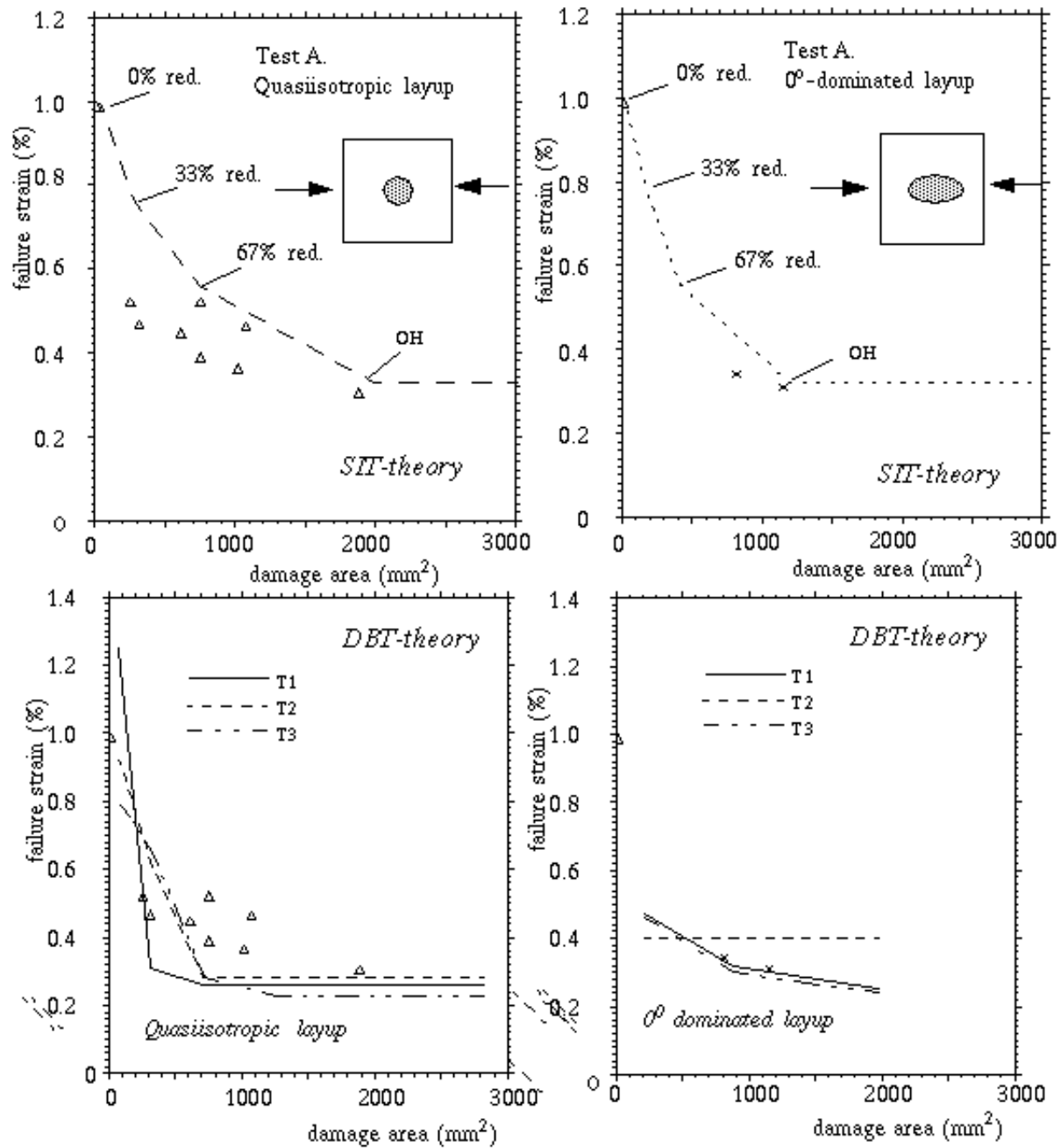


Figure 112 Predicted nominal failure strain with conservative assumed “soft inclusions” and with the delamination buckling theory v.s damage area.

**Review of Aeronautical Fatigue Investigations
in Switzerland**

April 1997 – June 1999

**M. Guillaume
Swiss Aircraft and Systems Enterprise Corp.
CH-6032 Emmen**

SUMMARY

The Swiss review summarizes fatigue work in Switzerland. It includes contributions from the Swiss Aircraft and Systems Enterprise Corporation (SF) which is responsible for the maintenance and engineering of the Swiss Air Force fleet and algroup Alusuisse (A-L) which was involved in investigations of fatigue properties of magnesium alloy. This document later forms a chapter of the ICAF conference minutes published by the conference host nation. The format of the review reflects ICAF requirements.

Prepared for the presentation at the 26th ICAF Conference
Seattle, 12 and 13 July 1999

TABLE OF CONTENTS

- 4.1 INTRODUCTION
- 4.2 MIRAGE III CANARD SERVICE EXPERIENCE
- 4.3 CRACKS IN MIRAGE III MAIN LANDING GEAR WHEELS
 - 4.3.1 Abstract
 - 4.3.2 Alloy composition and microstructure
 - 4.3.3 Fatigue Crack Propagation Rates and SN-Data
 - 4.3.4 REM-Fractography and Calibrated Initial Crack Length
 - 4.3.5 Summary and Conclusion
 - 4.3.6 Figures and Tables
- 4.4 ACTIVITIES FOR HAWK MK 66 FLEET
 - 4.4.1 Introduction
 - 4.4.2 Revision of the Hawk Mk 66 Fatigue Index Calculation
 - 4.4.3 Schedule of the Fic Revision
- 4.5 SERVICES EXPERIENCE OF TIGER F-5E/F
 - 4.5.1 15% Spar Wing to Fuselage Attachment Bolt Failure
 - 4.5.2 Horizontal Stabilizer Actuator Support Fitting
 - 4.5.3 15% Inboard Spar Cracks
- 4.6 F/A-18 SWISS STRUCTURAL INTEGRITY PROGRAM
 - 4.6.1 Swiss F/A-18 ASIP study
 - 4.6.2 Lif Test for close Tolerance Holes for each Spectrum
 - 4.6.3 Application of close tolerance Holes in Production
 - 4.6.4 Implementation of Swiss Modification in Production
 - 4.6.5 Swiss FSFT
 - 4.6.6 Development of Test Master Event Spectrum
 - 4.6.7 Coupon Test
- 4.7 F/A-18 FINITE MODEL INVESTIGATION FOR FULL SCALE FATIGUE TEST PROJECT
 - 4.7.1 FEA for the Swiss F/A-18 FSFT
 - 4.7.2 Fatigue Loads versus Test Loads, Fatigue Analysis
 - 4.7.3 Detail Stress Analysis for the F/A-18 FSFT
 - 4.7.4 The Baseline FE Model for the Swiss F/A-18 Full Scale Fatigue Test
- 4.8 REFERENCES

4.1 INTRODUCTION

This review paper summarizes fatigue investigations which have been carried out in Switzerland during the last two years from 1997 till 1999.

The contributions to this review come from the Swiss Aircraft and Systems Enterprise Corp (SF) and include the activities in the field of support for the Swiss Air Force to ensure the aircraft structural integrity of the fleet.

A part of the preparation of this review is sponsored by the Defence and Procurement Agency (DPA). This fond is gratefully acknowledged.

4.2 MIRAGE III CANARD SERVICE EXPERIENCE

(M. Guillaume; SF)

For the Swiss Mirage III upgrade program a Canard was developed between 1984 and 1987. The reason for this program was to increase the air combat performance of the Swiss Mirage III a/c.

The Swiss Canard is about 70% of the size of the Israeli Kfir version (Figure 4.2.1) and is a honeycomb structure with aluminum skin. The Canard (Figure 4.2.2) was tested in a component test using a block spectrum of 200 Flight Hours (FH). The spectrum was derived from flight data. The test was run up to 10'131 FH without any major incidences, and no damages such as cracks or failures in the honeycomb structure have been detected. In order to qualify the Canard also for its damage tolerance an additional test program with increased spectrum loads and artificially induced damages has been conducted afterwards. It resulted an inspection interval of 1200 FH.

The Swiss Mirage III fleet was upgraded by the Canard from 1988 till 1993. In 1998 the first Mirage III reached the limit of 1200 FH with a Canard installed. The Canard was dismantled from the aircraft and checked by an automatic ultrasonic scanner at SF Emmen. 12 locations with damage indications in the outer part of the front leading edge have been discovered. NDT specialists concluded that these damage indication must be disbanded areas between the honeycomb core and the aluminum skin. The Canard was then torn down and inspected in detail. The ultrasonic test results were confirmed.

The disbonding occurred in areas where structural vibration due to buffeting happen during specific flight maneuvers. This phenomenon was well known and reduced by a vortex generator in the early days of the Canard development. The effect of vibration was not simulated in the test. As of today 5 pairs of Canard were checked by ultrasonic and only one showed the same damage described above. The Swiss developed a repair procedure for the Canard using standard repair tools from F/A-18 structural repair manual.

The Mirage III S fighter version (29 aircraft) will be out of service by the end of this year. However the Mirage III RS fleet (16 reconnaissance aircraft) will remain in service.

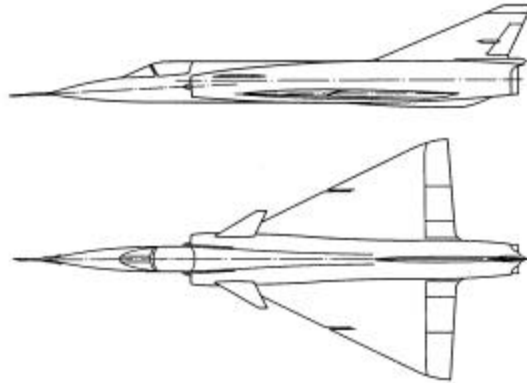


Fig. 4.2.1 Mirage III S with Canard CH 70

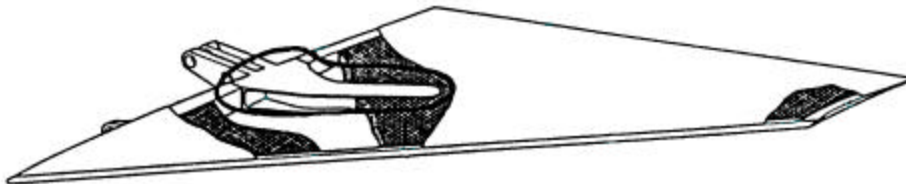


Fig 4.2.2 Canard CH 70 Structure

4.3 CRACKS IN MIRAGE III MAIN LANDING GEAR WHEEL

(R.Jaccard; A-L / M.Guillaume; SF / B. Wessicken; A-L / B. Meinck; A-L / S. Kysela; A-L)

Investigation of cracked Mirage III wheels results in a study for the fatigue properties of magnesium cast alloys MSR-TSM.

4.3.1 Abstract

After cracks were detected on some inner rims of the main landing gear wheel of Mirage III air planes as shown in Figure 4.3.1 it was decided to investigate the basic fatigue properties of magnesium cast alloys. Besides the standardized fatigue crack propagation rate measurements and SN-testing using one and two step loading conditions the microstructure and the fracture surfaces were studied.

Zinc and silver are grain size controlling elements of MSR-TSM magnesium sand cast alloys. The content of 6.6% zinc in the alloy of rim 1 lead to a 5 to 6 times larger grain than the silver content of 2.4% in rim 2. The roughness of the fatigue crack surface and the shrinkage porosity depend directly on the grain size. Although the Fatigue Crack Propagation Rate (FCPR) are much higher in the fine grain material of rim 2 the fatigue life is at least equal. The fatigue crack initiate at typical defects such as shrinkage porosity and inclusions. For constant amplitude loading the defect size can be defined by a calibrated initial crack length using a simple fracture mechanics model.

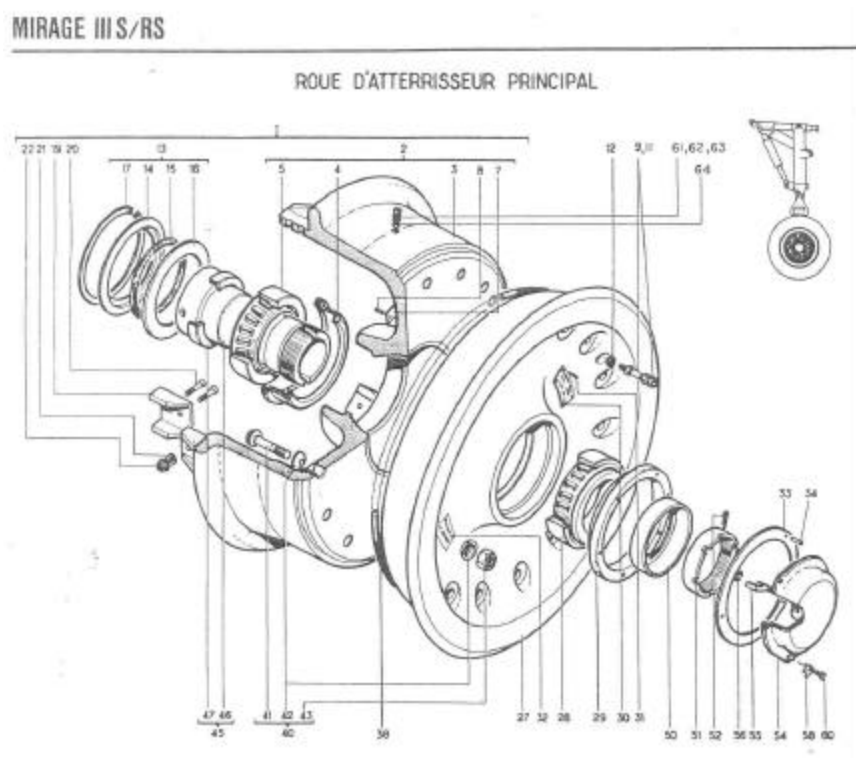


Fig. 4.3.1 Set Up of Mirage Landing-Gear Wheel

4.3.2 Alloy composition and microstructure

From four rims samples for metallographic analysis were taken. Since three rims showed more or less an identical chemical composition the results can be summarised into two groups as shown in Table 4.3.1.

	Rim No. 1	Rim No. 2
Silver	0.01	2.4
Aluminium	0.27	0.006
Copper	0.004	0.003
Iron	0.017	0.001
Manganese	0.023	0.016
Silicon	0.007	0.001
Zinc	6.6	0.023
Zirconium	0.005	0.50
Lanthanum	0.30	0.34
Cerium	0.12	0.20
Praseodymium	0.14	0.29
Neodymium	0.38	0.89
Dysprosium	0.001	0.014
Thorium	0.0001	0.0014

Table 4.3.1 Alloy Composition of Rim No. 1 and Rim No. 2 Chemical Element Content in %

The significant difference in the silver and zinc content of the two alloys affects some micro-structural features such as grain size, inclusions and shrinkage porosity.

Figure 4.3.2 shows the typical grain size and shape of the cast material of rim 1 with an average grain diameter of about 300 microns. In Figure 4.3.3 a representative area of characteristic defects such as micro voids and shrinkage porosity is visible. The elliptical voids of the shrinkage porosity are lined up to chains and the average size of a single void is about 20 by 60 microns. Figure 4.3.4 and 4.3.5 document the grain size and defects of the material of rim 2. The material containing 2.4 % silver has a 5 to 8 times finer grain and three to four times smaller voids, that are even dispersed over the sample area.

4.3.3 Fatigue Crack Propagation Rates and SN-Data

The fatigue crack propagation rates were determined according to ASTM E647 standard test method by using CT-Specimen of 60mm width and 10mm thickness. These investigations were completed by SN-tests to assist the defect-analysis and fatigue life prediction by using fracture mechanics. Different arrangements of the specimen for the two rims were selected for the SN-testing.

In Figure 4.3.6 quite a distinct polygonal shape of FCPR data is visible. The spacing between different R values are not regular as one would expect and what is known from other alloys such as aluminium alloys. We believe that magnesium alloys might exhibit higher scatter due to the hexagonal arrangement of the crystal lattice than aluminium alloys. The FCPR of two loading conditions for constant R conditions, i.e. $R = K_{\min} / K_{\max}$, and K_{\max} constant ΔK decreasing as defined in [1] are included in the diagram. The polygons represent the conservative envelope of the test data and were determined graphically.

W. A. Herman [2] published about ten years ago the " K_{max} constant" testing procedure to determine conservative FCPR to predict the cyclic life time of structural components and to describe the growth of short cracks. Since such FCPR [3,4,5] were generated for several aluminium, iron, and nickel-based alloys, it was decided to check the validity of the approach also for the magnesium alloys. In Figure 4.3.7. an appropriated set of K_{max} constant FCPR is conservatively combined with R constant data for the MSR-TSM Material of Rim 1 (6.6% Zn).

In the following two Figure 4.3.8 and 4.3.9 the FCPR of the two magnesium alloys of Rim 1 and Rim 2 are compared. In Figure 4.3.9. The FCPR of the aluminium cast alloy AlCu4Ti, EN AC-21100, is also included. Comparing the different FCPR it becomes obvious that grain size and crystal lattice have a significant effect on the rates. The aluminium cast alloy has the lowest and the fine grained magnesium alloy of 2% silver content the highest FCPR.

Considering the FCPR one could conclude that the silver containing magnesium alloy would have a shorter fatigue life compared to the magnesium alloy of rim 1. As it follows from the SN-data in Figure 4.3.10 and Table 2 this is not the case. In contrary the magnesium of rim 1 (6.6% Zn) has a much shorter fatigue life despite the lower FCPR due to the larger defect size related to the grain size, shrinkage and micro porosity (Figure 4.3.3 and 4.3.5). The fatigue fracture surface of this material is much coarser (Figure 4.3.12) than the one of rim 2 of 2.2% silver content (Figure 4.3.13).

4.3.4 REM-Fractography and Calibrated Initial Crack Length

In the last set of figures, Figure 4.3.13 to Figure 4.3.2, the result of REM fractography and the defect evaluation by using simple fracture mechanics models such as half-disk, half elliptical surface cracks and an embedded disk crack. As demonstrated in [6,7,8,9] for constant amplitude loading it is possible to use fracture mechanics to estimate the cyclic fatigue life of structural components by a fatigue life calibration, where a fictitious initial crack length is calculated based on a distinct SN-test under the assumption that the fatigue crack initiation consist mainly of a simultaneous growth of critical defects as individual short cracks leading to a technical crack length of one to two mm. Fatigue crack growth of short cracks can be estimated by K_{max} constant FCPR. If the defects are relative large and contain sharp notches such as e.g. the shrinkage porosity of cast alloys standard FCPR of long crack data can be used to determine the initial crack length.

Tensile specimen 1-09 sustained a stress range of 90 MPa at a stress ratio of 0.1 223000 times. Figure 4.3.13 contains the REM overview picture of the fatigue fracture surface and Figure 4.3.14 the detail of the initiation site. The fatigue life calibration using $R=0.1$ constant long crack FCPR suggests an initial half-disk crack of 0.414mm radius. This crack covers most of the area containing the fine dendrite arms. The bright area in the center is probably an inclusion particle and can be surrounded by an elliptical crack of 0.0834 mm width and a length of 0.36mm. This dimensions are found by a calibration using the K_{max} constant FCPR.

The next example on Figure 4.3.15 and 4.3.16 shows a typical initiation at a shrinkage porosity. The calibration based on K_{max} constant FCPR combined with the data of the applied R-ratio of 0.5 determined an initial half-disk crack of 0.288 mm radius.

In Figure 4.3.17 and 4.3.18 the defect is quite difficult to interpret. It consists of shrinkage porosity. Assuming a half-disk surface crack and K_{max} constant FCPR the fictitious initial crack length becomes 0.055 mm and 0.279 mm if the long crack constant R FCPR of the applied $R=0.1$ are considered. A better fit could be obtained by a half elliptical surface crack with a vertical main axes and if K_{max} constant FCPR would be used.

This was done in the last example of the series of rim 1 as shown in Figure 4.3.19 and 4.3.20 where the proposed initial crack length based on K_{max} constant FCPR and a vertically oriented half elliptical surface crack yields the best fit for the initial defect consisting out of a mixture of shrinkage porosity and inclusion particles. The half elliptical crack is 0.30 mm wide and 0.38 mm deep. The half-disk crack has a radius of 0.395mm.

The last two examples are fatigue fracture surfaces of the fine grain material of rim 2. Figure 4.3.21 and 4.3.22 show the REM pictures of the overview and the defect of tensile specimen 2-13 that was subjected to 333000 loading cycles at a R-ratio of 0.5 and a stress range of 50 MPa. The defect (Figure 4.3.22) is according to the results of the

microprobe a large zirconium inclusion 0.52 mm by 0.57mm. The half-disk surface crack models of the calibrations using both type of FCPR data do not fit the bright area of the inclusion site.

Figure 4.3.23 and 4.3.24 are the REM pictures of the fatigue fracture surface of specimen 2-20. The defect is a shrinkage porosity well embedded in sound material. This defect can be described by a disk crack. The best fit is obtained by considering the tensile part of the loading and FCPR of $R=0.1$. The radius is 0.285 mm. Assuming a $R=0.5$ long crack FCPR yields a radius of 0.09mm and the K_{max} constant FCPR predict such a radius of only 0.047 mm.

4.3.5 Summary and Conclusion

Zinc and silver are grain size controlling elements of MSR-TSM magnesium sand cast alloys. The content of 6.6% zinc in the alloy of rim 1 lead to a 5 to 6 times larger grain than the silver content of 2.4% in rim 2. The roughness of the fatigue crack surface and the shrinkage porosity depend directly on the grain size. Although the FCPR are much higher in the fine grain material of rim 2 the fatigue life is at least equal. The fatigue crack initiate at typical defects such as shrinkage porosity and inclusions. For constant amplitude loading the defect size can be defined by a calibrated initial crack length using a simple fracture mechanics model.

4.3.6 Figures and Tables

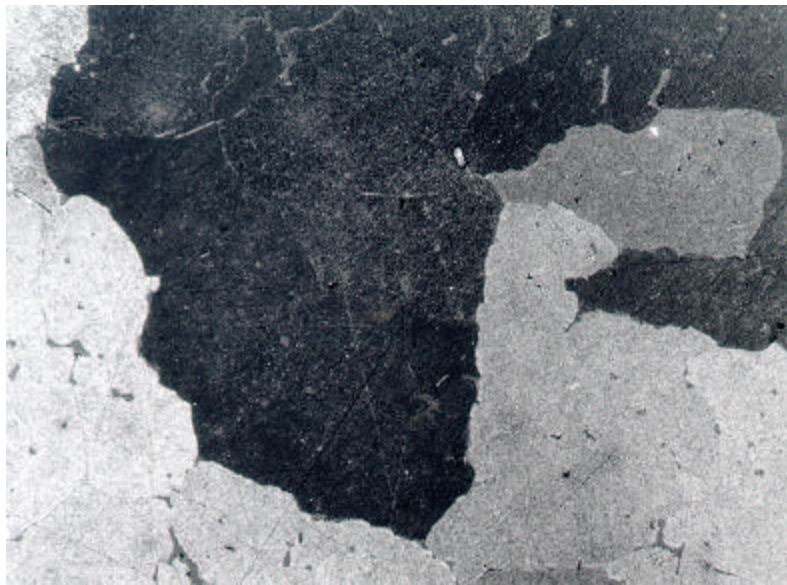


Fig. 4.3.2 Microstructure of cast material of Rim 1 Polished surface was etched 2 sec with 10% HF and illuminated by polarized light. Magnification 100x (Width of Picture 104mm)

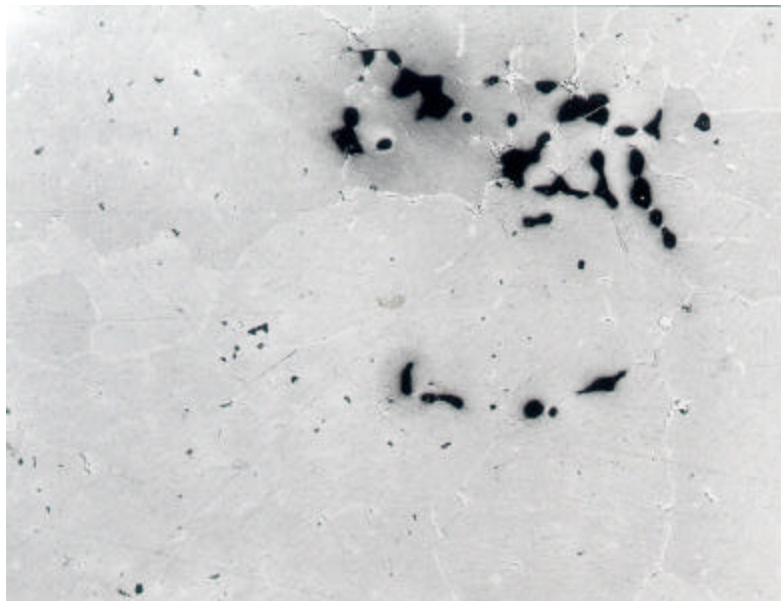


Fig. 4.3.3 Typical Defects of cast material of Rim 1 Polished surface was etched 2 sec with 10% HF and illuminated by polarized light. Magnification 100x (Width of Picture 104mm)

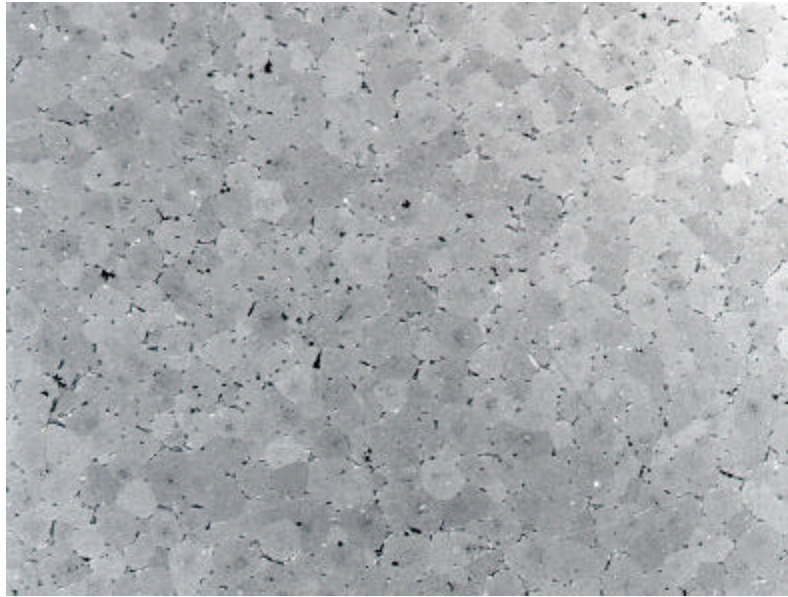


Fig. 4.3.4 Microstructure of cast material of Rim 2 Polished surface was etched 2 sec with 10% HF and illuminated by polarized light. Magnification 100x (Width of Picture 104mm)

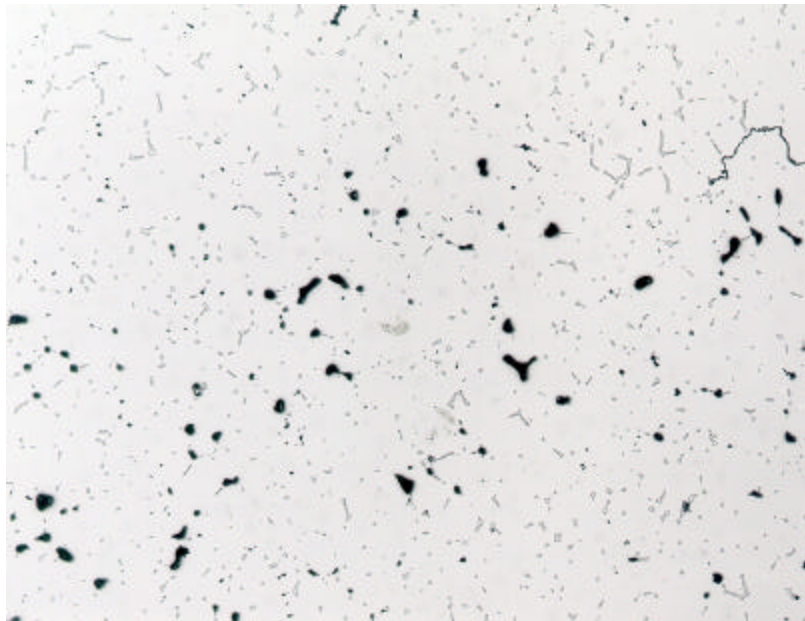


Fig. 4.3.5 Typical Defects of cast material of Rim 2 Polished surface was etched 2 sec with 10% HF and illuminated by polarized light. Magnification 100x (Width of Picture 104mm)

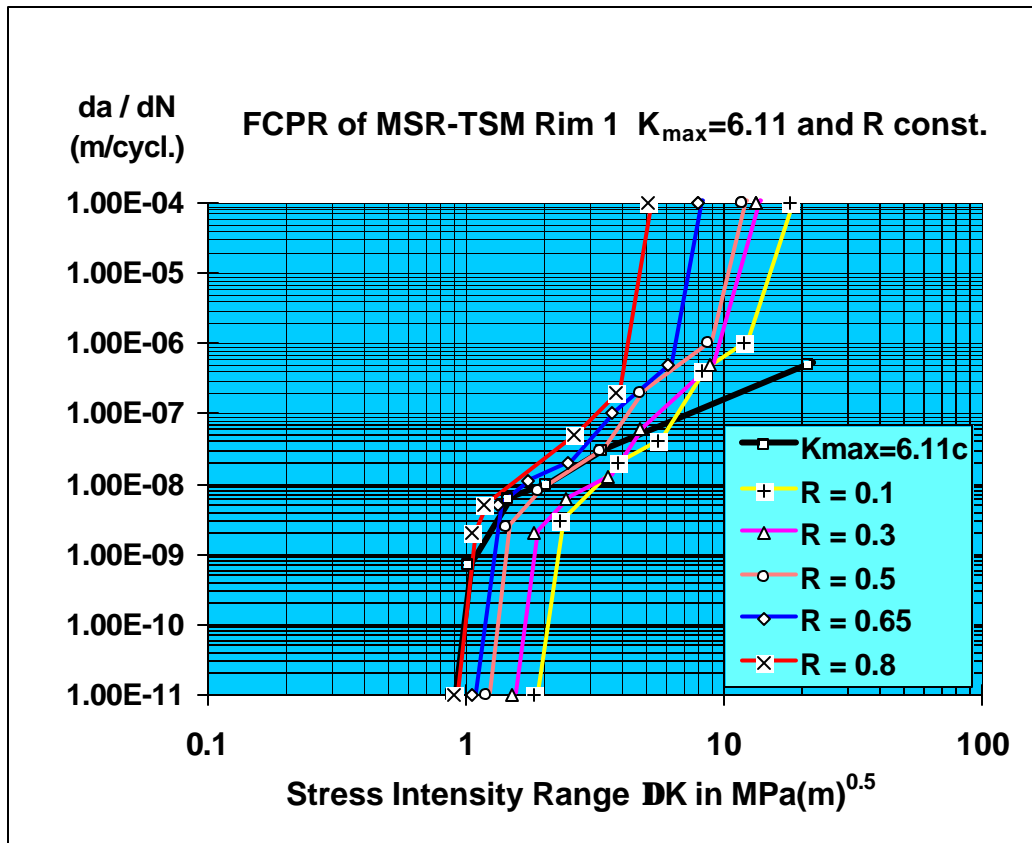


Fig. 4.3.6 Fatigue Crack Propagation Rates of MSR-TSM Rim 1 Material (6.6% Zinc content) Loading Conditions: (1) $R = K_{min}/K_{max} = \text{constant}$, (2) $K_{max} = 6.11 MPa(m)^{0.5}$ constant

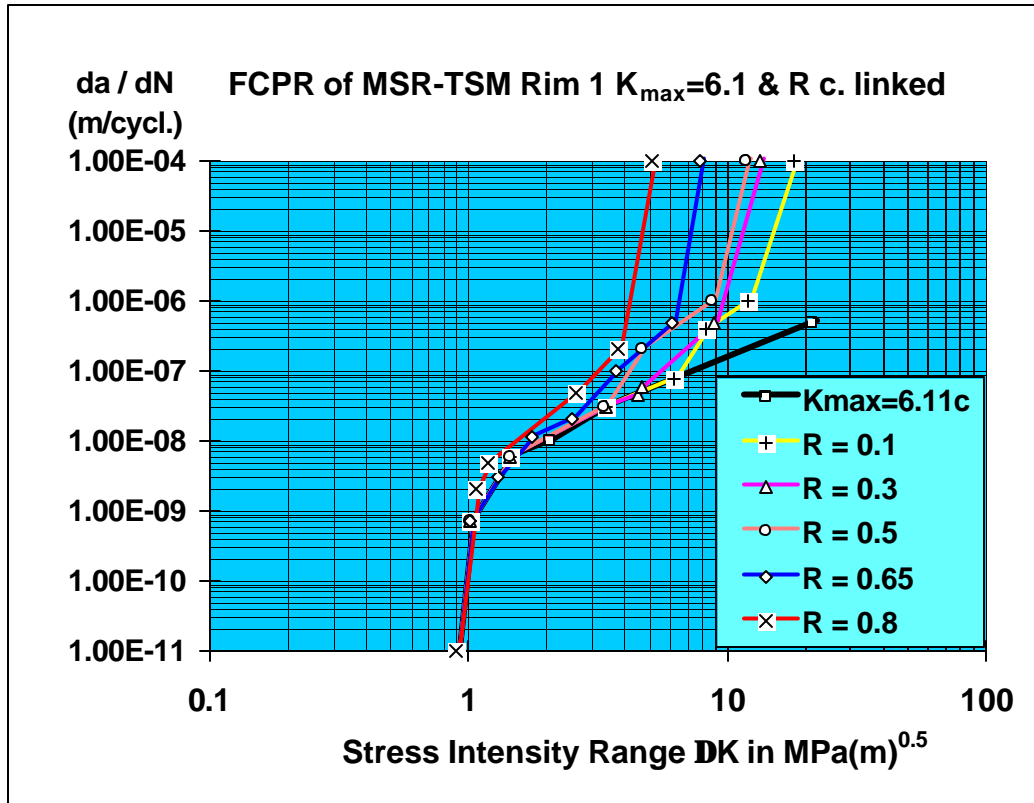


Fig. 4.3.7 Fatigue Crack Propagation Rates of MSR-TSM Rim 1 Material (6.6% Zinc content) $K_{max} = 6.11 MPa(m)^{0.5}$ const. combined conservatively with R constant

FCPR of MSR-TSM $K_{max}=6.1$ & $R=0.3$ Rim 1 vs 2

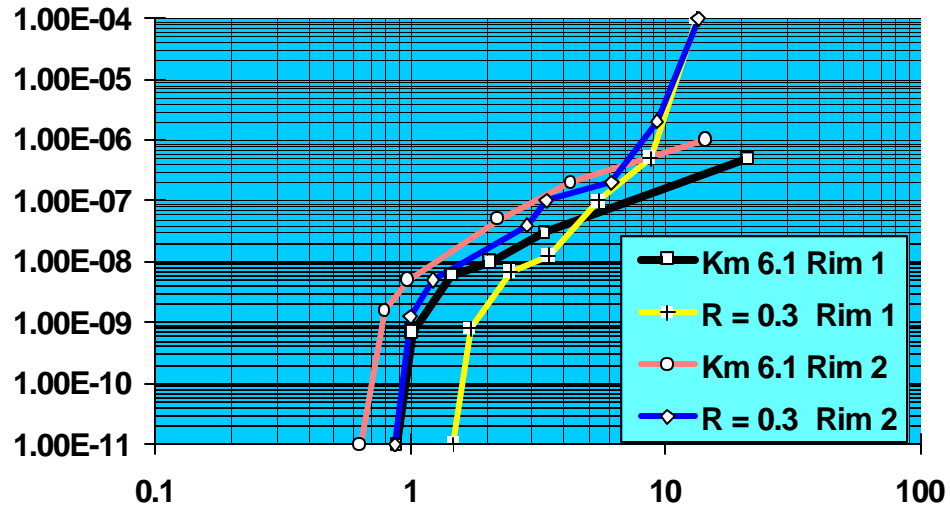


Fig. 4.3.8 Fatigue Crack Propagation Rates of MSR-TSM Rim 1 Material (6.6% Zinc content) compared to MSR-TSM Rim 2 Material (2.4% Silver content)

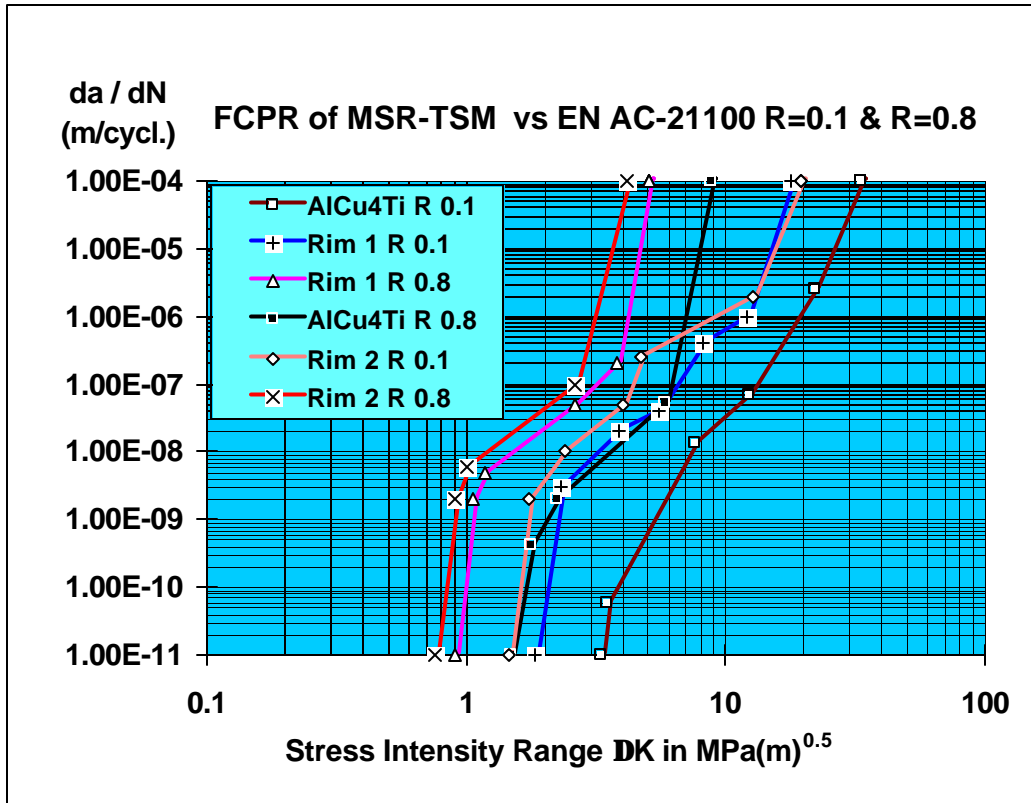


Fig. 4.3.9 FCPR of MSR-TSM Rim 1 (6.6% Zinc content) and Rim 2 (2.4% Silver content) compared to Aluminium Sand Castings AlCu4Ti EN AC-21100

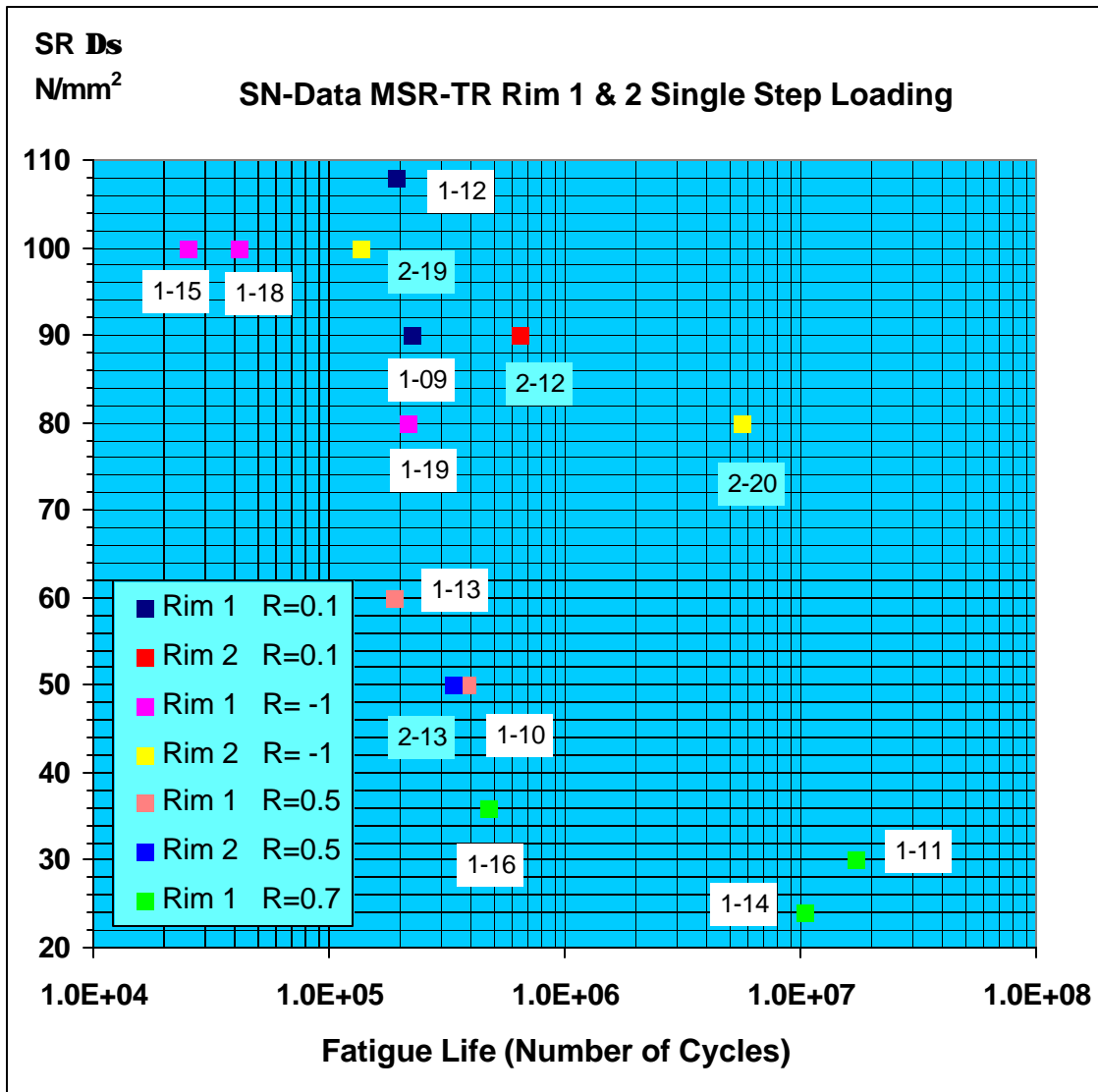


Fig. 4.3.10 SN-Data of MSR-TSM Rim 1 (6.6% Zn) compared to MSR-TSM Rim 2 (2.4% Ag)
(Stress range of R = -1 loading condition: SR = SR effective = ?_{max})

Specimen	Ds	R	Fat. Life Cycles	Specimen	Ds	R	Fat. Life Cycles
Rim 1:				1-15 E	200	-1	25100
1-12 E	108	0.1	192000	1-18 E	200	-1	41500
1-09 E	90	0.1	223000	1-19 E	160	-1	214700
1-13 E	60	0.5	190000	Rim 2:			
1-10 E	50	0.5	380000	2-12 E	90	0.1	640000
1-16 E	36	0.7	470000	2-13 E	50	0.5	333000
1-14 E	24	0.7	10300000	2-19 E	200	-1	135200
1-11 E	30	0.7	17000000	2-20 E	160	-1	5576400

Tab. 4.3.2 SN-Data of MSR-TSM Rim 1 (6.6% Zn) compared to MSR-TSM Rim 2 (2.4% Ag)
(Tabulated values of diagram in Fig. 4.3.10 above)

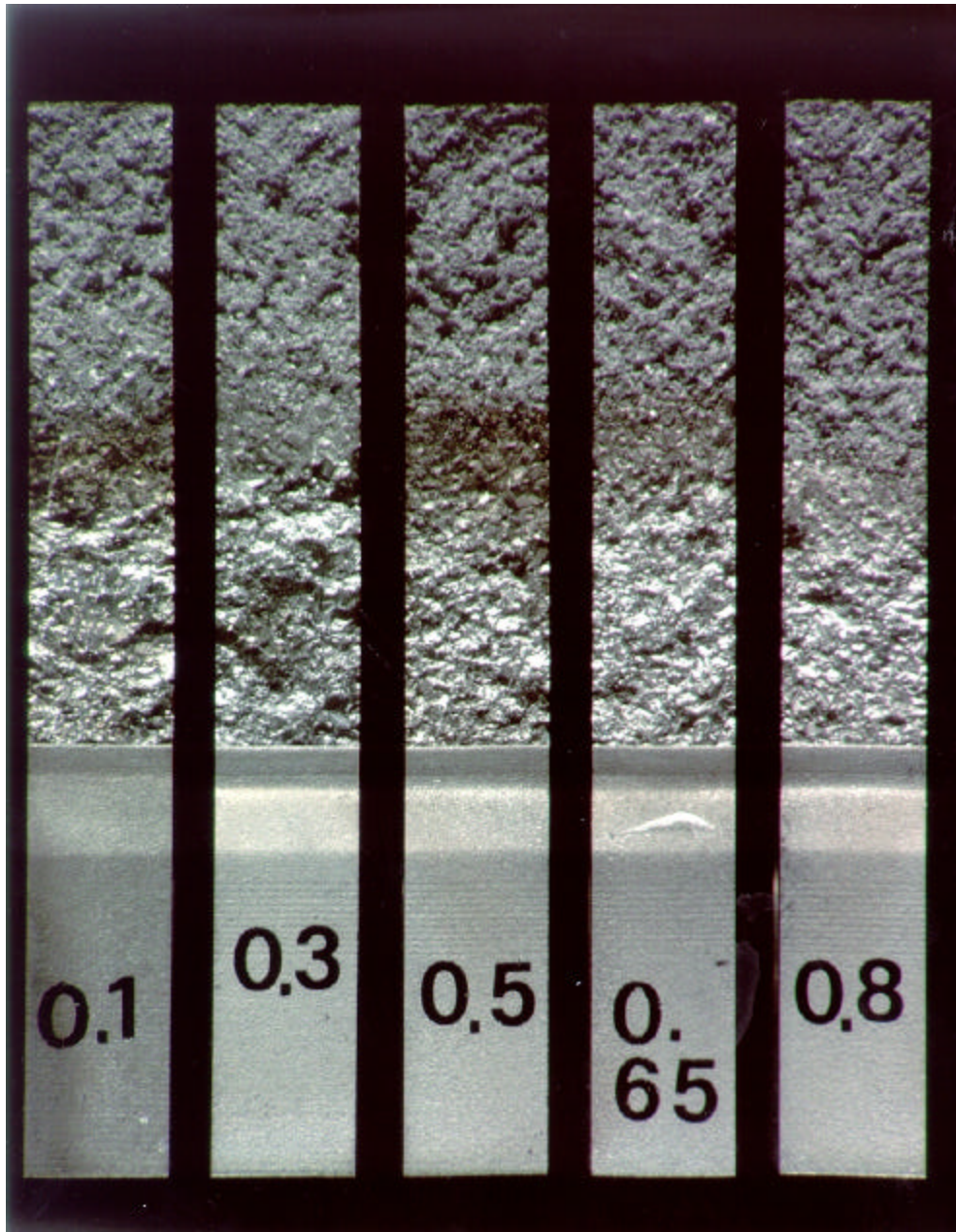


Fig. 4.3.11 Comparison of Fatigue Fracture Surfaces of CT-Specimen of FCPR Testing Sand Cast MSR_TSM Material of Rim 1 (6.6% Zn content)

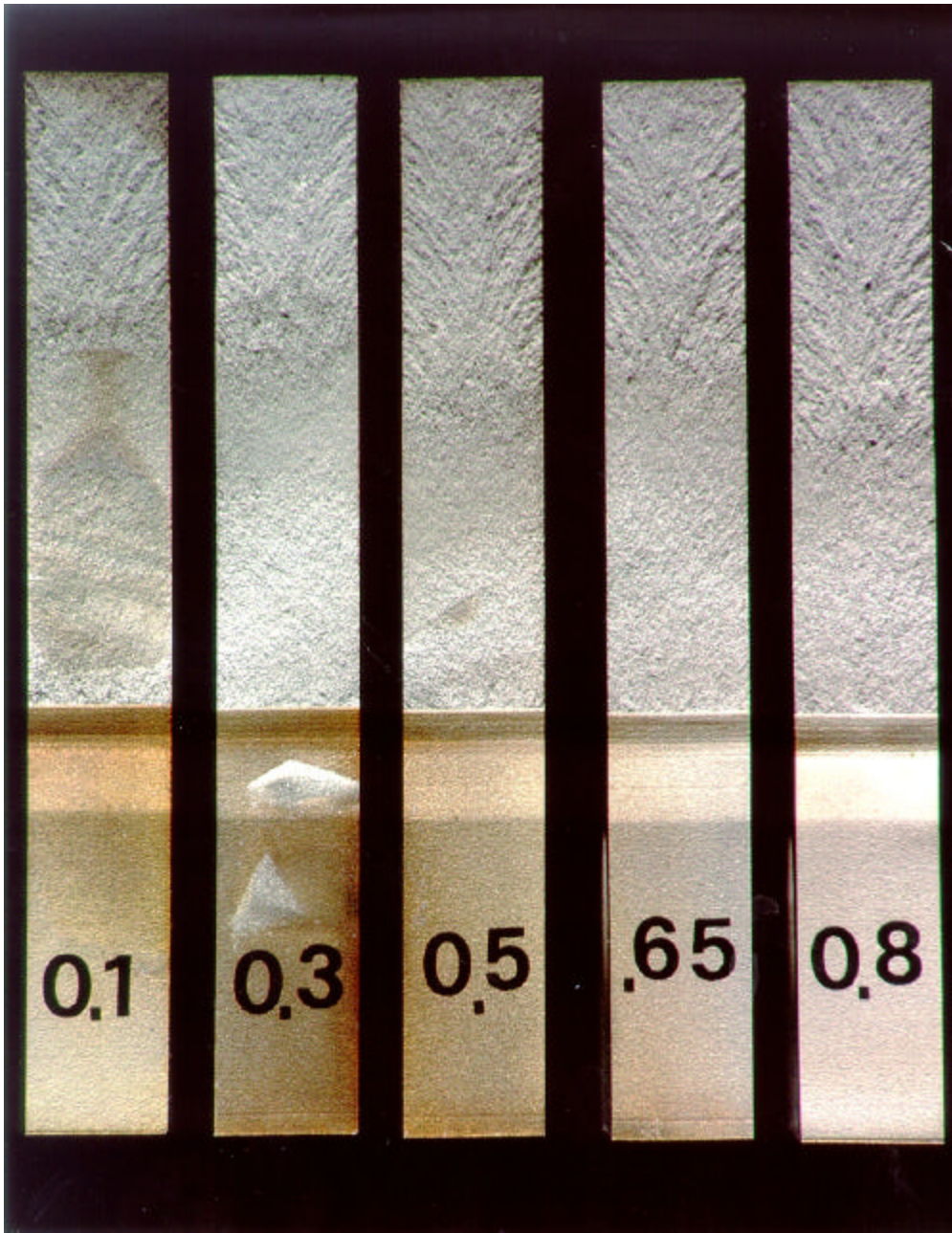


Fig. 4.3.12 Comparison of Fatigue Fracture Surfaces of CT-Specimen of FCPR Testing Sand Cast MSR_TSM Material of Rim 2 (2.4% Ag content)

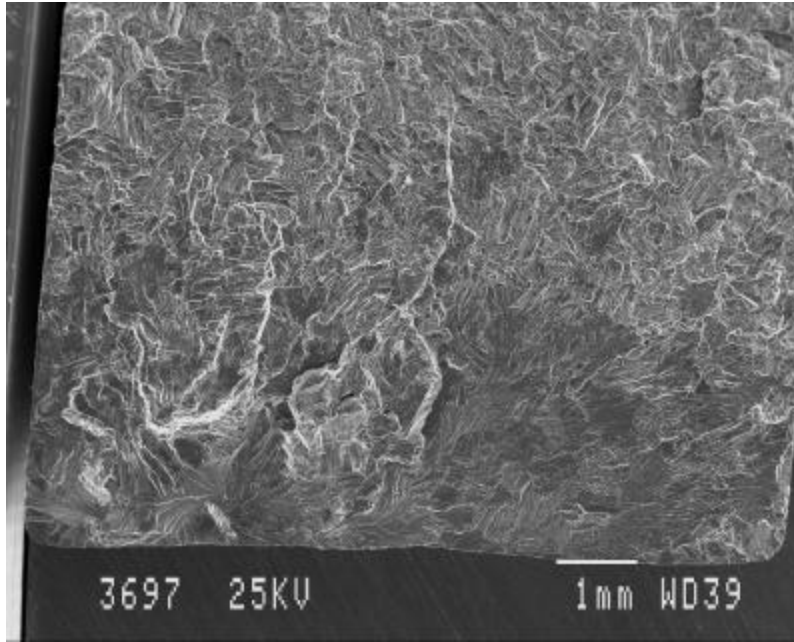


Fig. 4.3.13 REM picture of fatigue crack surface of specimen 1-09 of rim 1 loading condition: 1-step constant amplitude loading ($R=0.1$, $S_{max} = 100$ Mpa , Life $N = 223'000$ cycles)

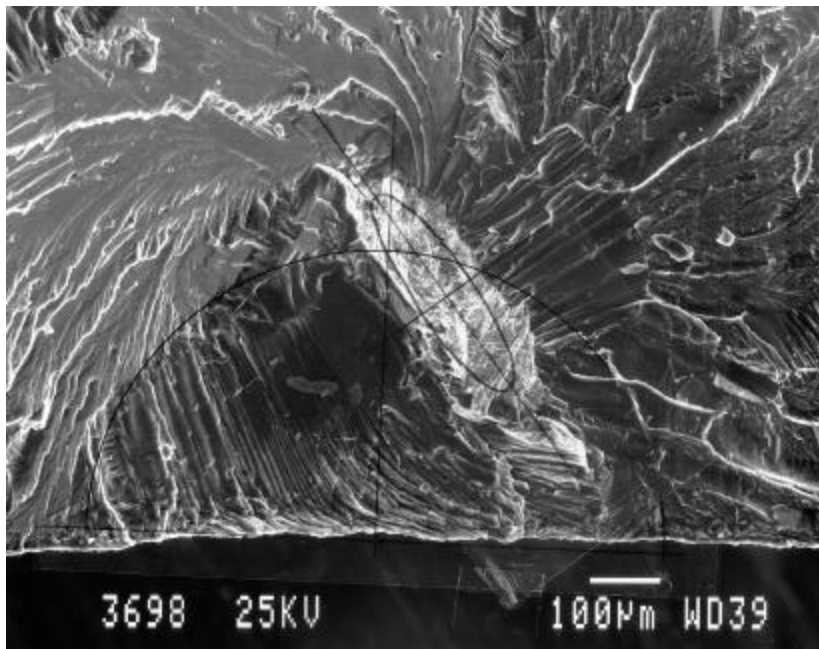


Fig. 4.3.14 Detail of Fig. 4.3.13 fatigue crack initiation of specimen 1-09 at inclusion particle (bright area surrounded by fine dendrites and shrinkage porosity)

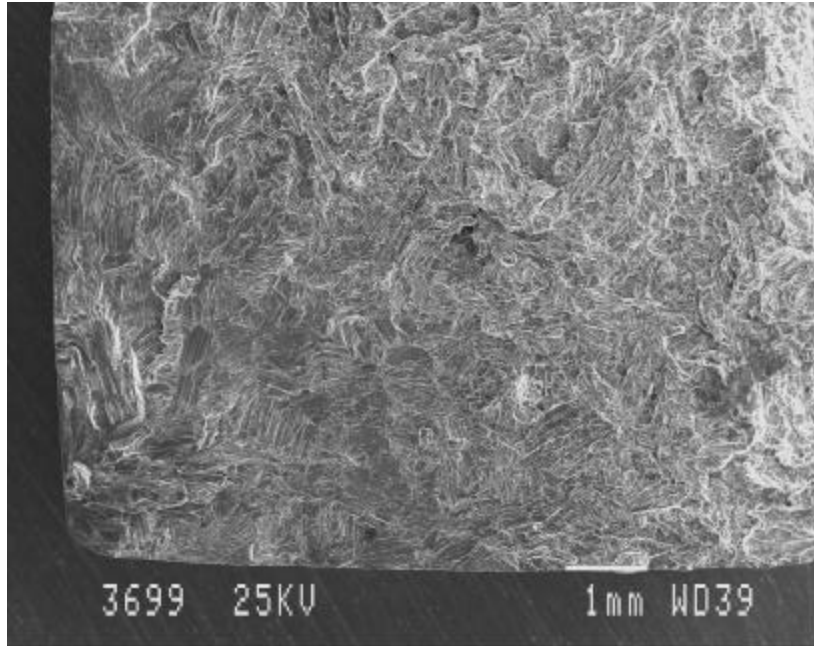


Fig. 4.3.15 REM picture of fatigue crack surface of specimen 1-10 of rim 1 loading condition: 1-step constant amplitude loading ($R=0.5$, $S_{max} = 100$ Mpa , Life $N = 380'000$ cycles)

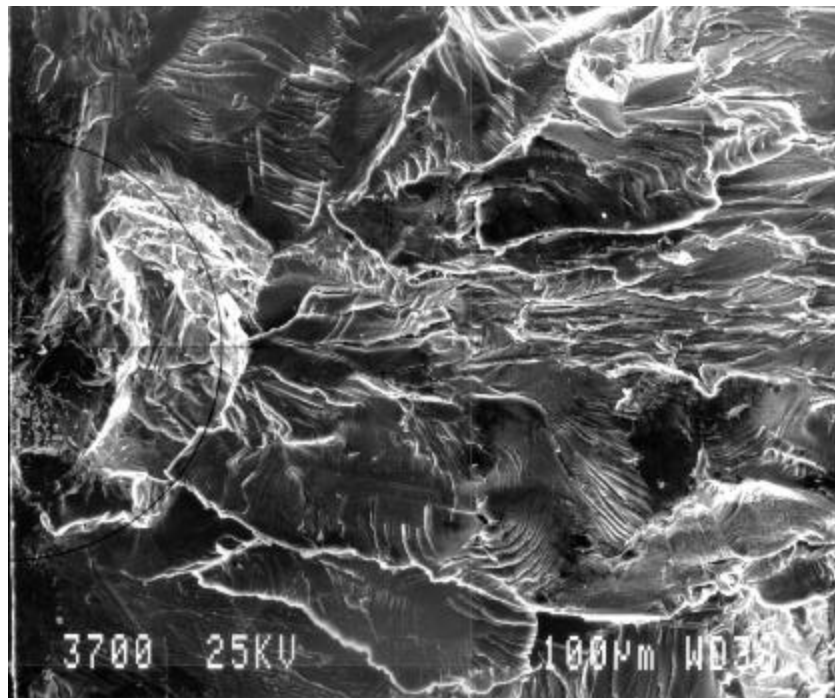


Fig. 4.3.16 Detail of Fig. 4.3.15 fatigue crack initiation of specimen 1-10 at a typical site of shrinkage porosity)

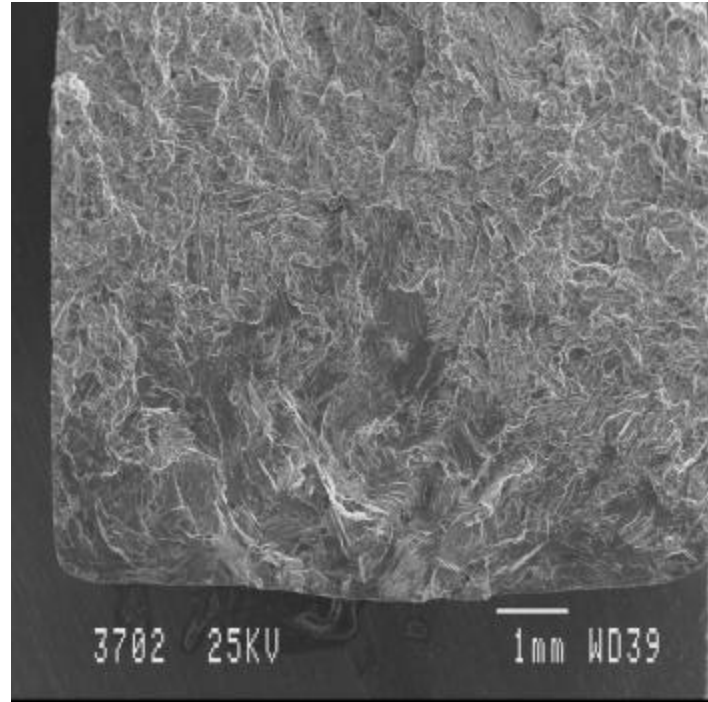


Fig. 4.3.17 REM picture of fatigue crack surface of specimen 1-12 of rim 1 loading condition: 1-step constant amplitude loading ($R=0.1$, $S_{max} = 120$ Mpa , Life $N = 192'000$ cycles)

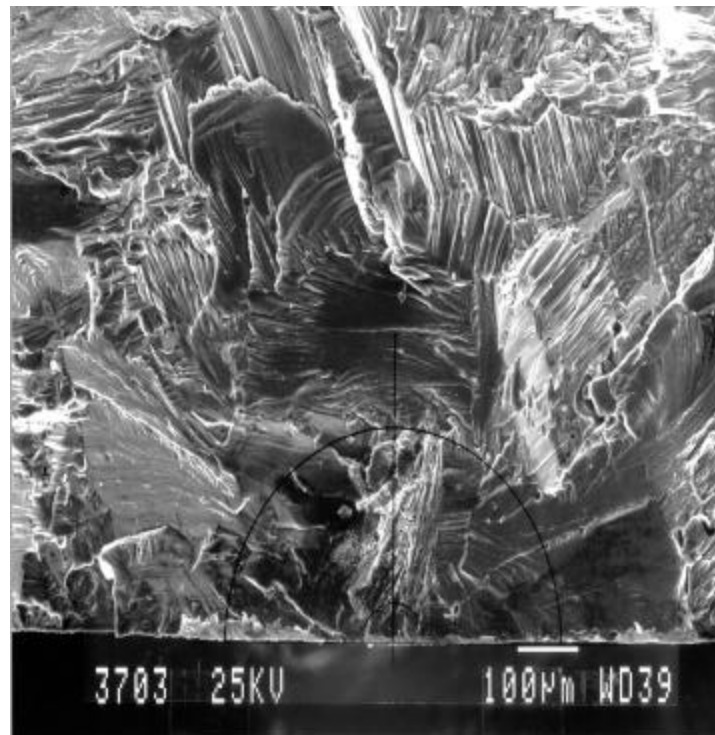


Fig. 4.3.18 Detail of Fig. 4.3.17 fatigue crack initiation of specimen 1-12 at a typical site of shrinkage porosity)

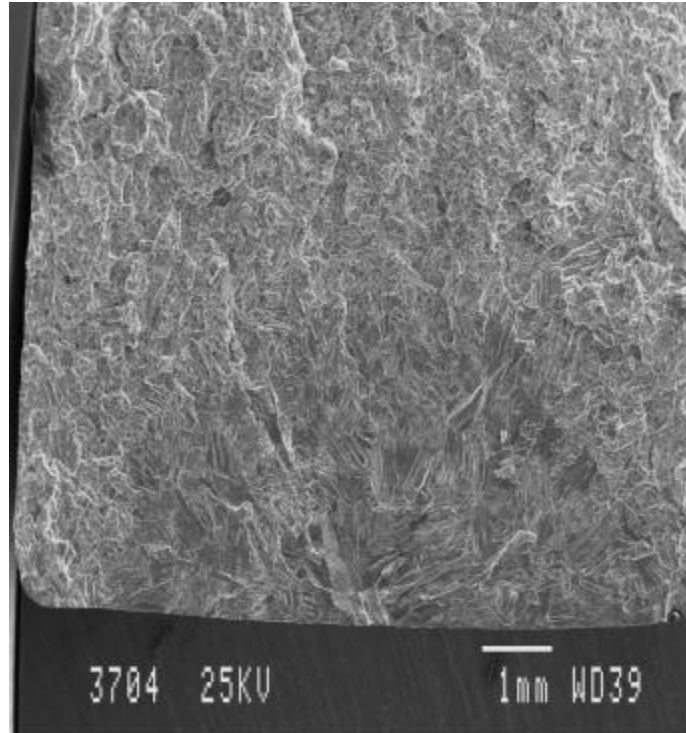


Fig.4.3.19 REM picture of fatigue crack surface of specimen 1-13 of rim 1 loading condition: 1-step constant amplitude loading ($R=0.5$, $S_{max} = 120$ Mpa , Life $N = 190'000$ cycles)

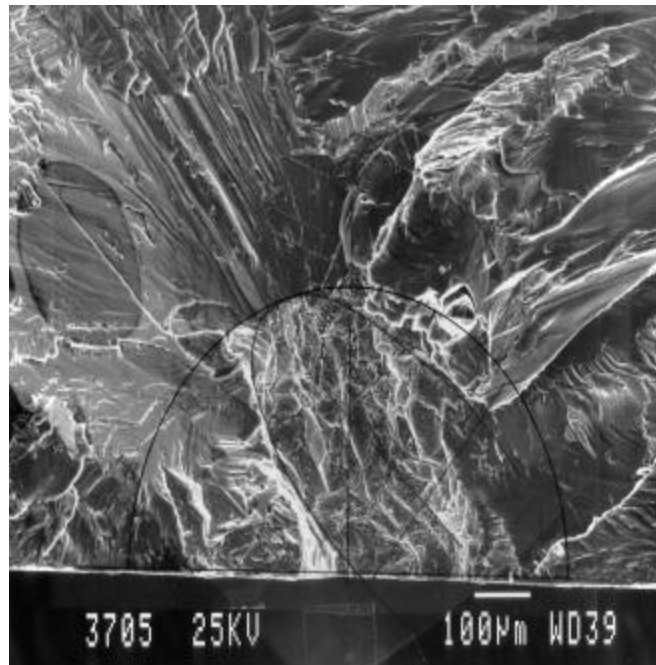


Fig. 4.3.20 Detail of Fig. 4.3.19 fatigue crack initiation of specimen 1-13 at a typical site of shrinkage porosity)

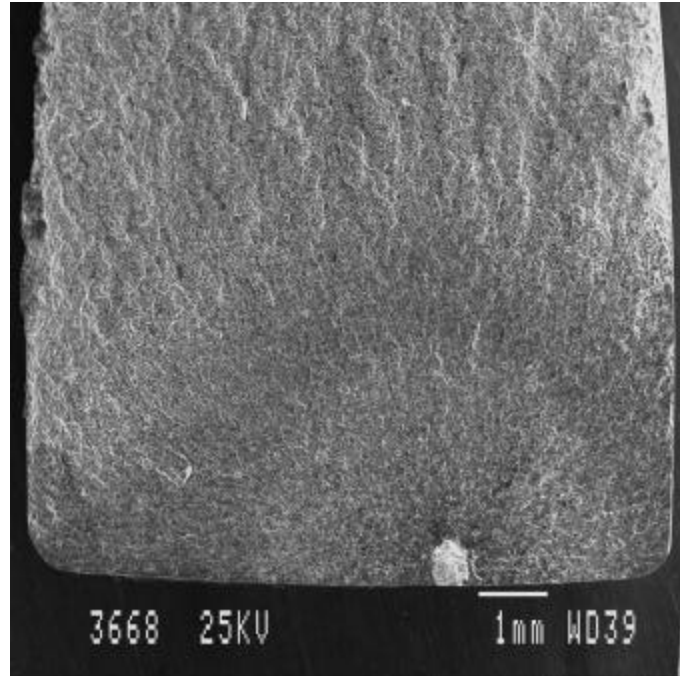


Fig.4.3.21 REM picture of fatigue crack surface of specimen 2-13 of rim 2 loading condition: 1-step constant amplitude loading ($R=0.5$, $S_{max} = 120$ Mpa , Life $N = 333'000$ cycles)

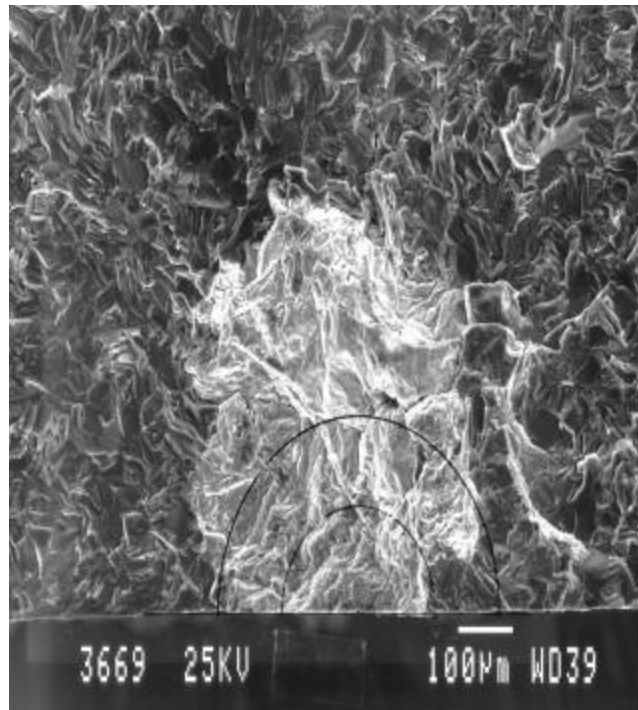


Fig. 4.3.22 Detail of Fig. 4.3.21 fatigue crack initiation of specimen 2-13 at a large zirconium inclusion (bright area) some oxides and shrinkage porosity are also apparent.

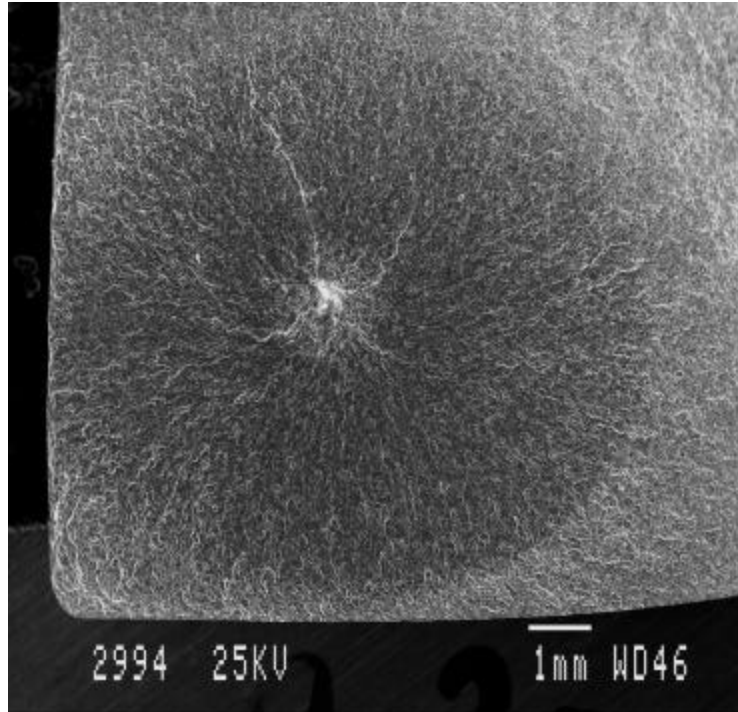


Fig. 4.3.23 REM picture of fatigue crack surface of specimen 2-20 of rim 2 loading condition: 1-step constant amplitude loading ($R=-1$, $S_{max} = 80$ Mpa , Life $N = 5'576'400$ cycles)

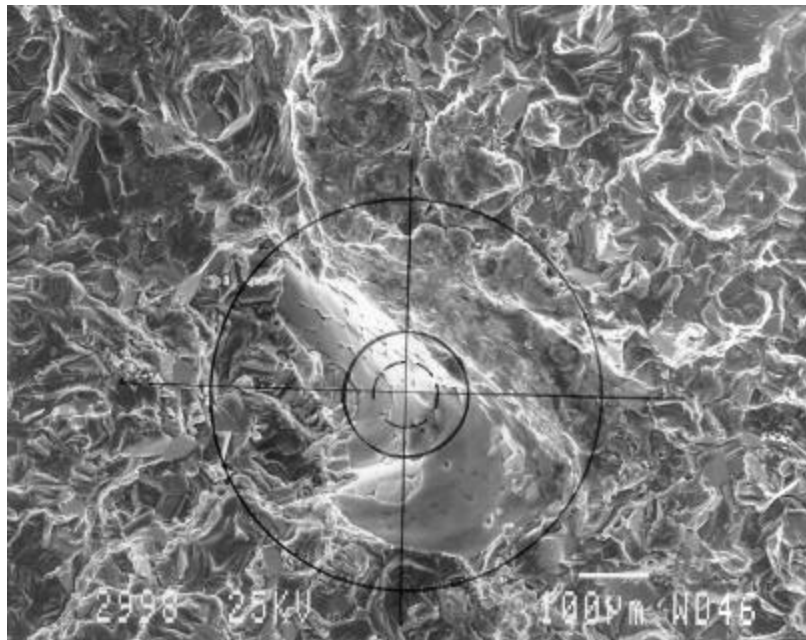


Fig. 4.3.24 Detail of Fig. 4.3.23 fatigue crack initiation of specimen 2-20 at a shrinkage porosity well imbedded in sound material lead to a long fatigue life

4.4 ACTIVITES FOR HAWK MK 66 FLEET

(I. Kongshaven; SF / P. Arebo; SF)

4.4.1 Introduction

The Swiss Hawk Mk 66 fleet consists of 19 aircraft, in-use as a jet-trainer since 1989. The Hawk was designed using a 'Safe Life' approach, and this philosophy has been fully adopted in its first 10 years of service. A Fatigue Index (FI) is calculated to compare Swiss usage to results from the Life Extension Fatigue Test (LEFT), currently on-going at British Aerospace (BAe) in England.

FI values for the wing, fin and tailplane are calculated on an annual basis to closely monitor Swiss usage. The FI is calculated from usage data measured by the Electronic Structural Data Acquisition (ESDA) System installed in every aircraft, see Figure 4.1.1. This system consists of an accelerometer to measure the vertical acceleration (N_z), as well as a strain gauge each at a critical location on the fin and on the tailplane. Such close monitoring of the fleet allows a reduction in the safety factor used in the FI calculation from 5 for an unmonitored fleet, to 3.33 for fleets which are monitored, thereby increasing the cleared service life. In order to optimize those parameters which are most representative for the FI calculation of each component, a sensitivity analysis and revision was carried out in 1998 and the FI re-evaluated for all years between 1989 to 1998.

4.4.2 Revision of the Hawk Mk 66 Fatigue Index Calculation

On the acquisition of the Hawk aircraft for the Swiss Air Force, a fatigue monitoring methodology was established to ensure the structural integrity of the Swiss Hawk Mk 66 fleet. This methodology outlines how to track the expended fatigue life of the aircraft through component tracking with the ESDA (Electronic Structural Data Acquisition System) and the calculation of an FI.

For the centre fuselage, wing, fin and tailplane, an FI each is calculated using the ESDA data. The first calculations were performed using parameters provided by BAe, primarily intended for the Hawk T. Mk 1. The initiative was therefore taken to revise and optimize the Hawk FI calculation based on Swiss Hawk Mk 66 specific parameters and recalculate the FI values for the years 1989-1997.

The improvements to the FI calculation (FIC) method have been performed according to the following schedule:

4.4.3 Schedule of the FIC Revision

Step 1:	Preparation of basic information	[Concluded end of March 1997]
Step 2:	Software revision	[Concluded end of August 1997]
Step 3:	Parameter revision	[Concluded end of October 1997]
Step 4:	Re-evaluation of flight data 1989-1997	[Concluded end of April 1999]
Step 5:	Final documentation	[Concluded end of June 1999]

The first step of the FIC revision aimed at reviewing the BAe FIC procedure, in order to integrate the experience from the OLM, Full Scale Fatigue Test (FSFT) and its sequel the Life Extension Fatigue Test (LEFT). The recorded strain sequences from these fatigue tests and the OLM serve as a reference loading to which the in-flight measured loading is compared. A correlation can be made between the design life and the monitored data, to indicate how much of the available safe life has been consumed.

A further important part of the first step of the FIC revision was a thorough calibration of the strains measured by the ESDA system for fin and tailplane including a verification of the strain gauge parameters and aircraft weight for different configurations and at different fuel states. Additionally, the strain to load factors for the components fin and tailplane were verified through load calibration tests. The parameters in the wing strain to load transfer function, which is based on the N_z sequence and weight of the Hawk aircraft, were also optimized. For this purpose, two aircraft were fitted with wing strain gauges and monitored for approximately 250 [FH].

For the calculation of an FI, not only knowledge of the structural response and the measurement system is required. It is also vital to be familiar with the loading of the different components. Therefore, studies into empennage

vibrations supported by flight measurements were launched. The result was to compensate for fin and tailplane vibrations outside the ESDA measuring range by an overall factor on the respective FI consumption.

As important as using the right input sequence from flights and tests in the FIC, is knowing the true material behaviour. Thus, SF carried out its own material testing of the aluminium alloy 2014-T651 used in the Hawk empennage. Based on these material tests, new empennage S/N matrices were developed for fin and tailplane. BAe also supplied new S/N matrices for the centre fuselage based on the LEFT.

One goal in the second step of the Hawk FIC revision was to introduce a new stress model specifically developed for the centre fuselage. Previously, the Fatigue Index for the centre fuselage was calculated indirectly by that of the wing and therefore omitted important fatigue loading induced from refuelling, inertia and changes in altitude. The centre fuselage stress model developed by SF is shown below and consists of three parts:

- s_0 , a constant from the pre-loading of the structure and centre fuselage fuel tank pressurisation
- $s_{fuel}(t)$, a variable accounting for the effect of the inertia forces of the fuel in the centre fuselage fuel tank. The loading of the tank floor depends on the fuel level and the current Nz.
- $s_{Nz}(t)$ is a function of Nz alone.

$$s(t) = s_0 + s_{fuel}(t) + s_{Nz}(t)$$

In the third step of the Hawk Mk 66 FIC revision, the following revised parameters were introduced into the FI calculation:

- Centre fuselage:
The model parameters for the centre fuselage stress program, for instance those in the function determining the pressure at the tank bottom, were validated in flight tests in 1997 and introduced together with the new S/N matrix for the centre fuselage.
- Wing:
The new parameters in the wing stress model, for instance those determining the Nz dependency, were introduced in the FIC software. These optimized parameters were found to reduce the calculated wing skin stresses by 15% to 30% depending on configuration.
- Fin:
 The correction factor on the FI consumption rate to account for the effect of fin vibrations was introduced. Also for the fin, a new S/N matrix from SF material tests was adopted for use in the FIC.
- Tailplane:
 As for the fin a correction factor on the FI consumption rate was introduced in the FIC to account for the effect of vibrational tailplane loads impossible to measure with the ESDA system. Additionally, a new S/N matrix developed for the tailplane based on SF material tests was included in the FIC.

In the fourth step of the FIC revision, a new evaluation of all collected flight data from 1989 to 1997 was performed with the optimized input data. During the re-evaluation, the LEFT component sequences were introduced as the new references for the FIC. The following results were obtained:

- The FI recalculation for the centre fuselage produced very high FI values which confirmed the information received from other fleet managers and BAe. This component is clearly heavily influenced from the fuselage fuel tank pressure and inertia loads.
- The wing FIC showed low consumption rates. Due to the similarity between the Nz spectrum for the Hawk Mk 66 with the reference spectrum from the LEFT, the calculated FI values represent well the Swiss Hawk usage.

- The fin FI values calculated for 1989 – 1997 are very low. The reason for the low FI consumption rates for this component is the too severe reference spectrum from the LEFT.
- For the tailplane, the FIC also produces very low consumption rates. Not only our experience however, indicate that the tailplane is fatigue critical. The reason for the low FI consumption rates are that the reference spectrum from the LEFT does not include vibration loading whereas the Swiss tailplane spectrum is vibration dominated.

A second phase in the monitoring of the Swiss Hawk Mk 66 has begun, in which the Safe Life approach is being better adopted to a Swiss specific fatigue life monitoring concept. Knowledge of in-service experience by other users is being used to introduce modifications that will extend the life of the centre fuselage, at locations affected by fuel system refuelling, inertia and changes in altitude loads.

In addition, we now know vibration loading in the empennage to significantly affect the fatigue life. The wing FI consumption rate is therefore not representative of the remaining life of the empennage. While the ESDA system captures the damaging 20Hz vibrations, damaging 70Hz and 90Hz vibrations are filtered out. A Swiss specific tailplane inspection concept is now being developed for critical locations, which will ensure Swiss Mk 66 fleet safety, coupled with Swiss specific modifications that will optimize the lifetime usage of the fleet.

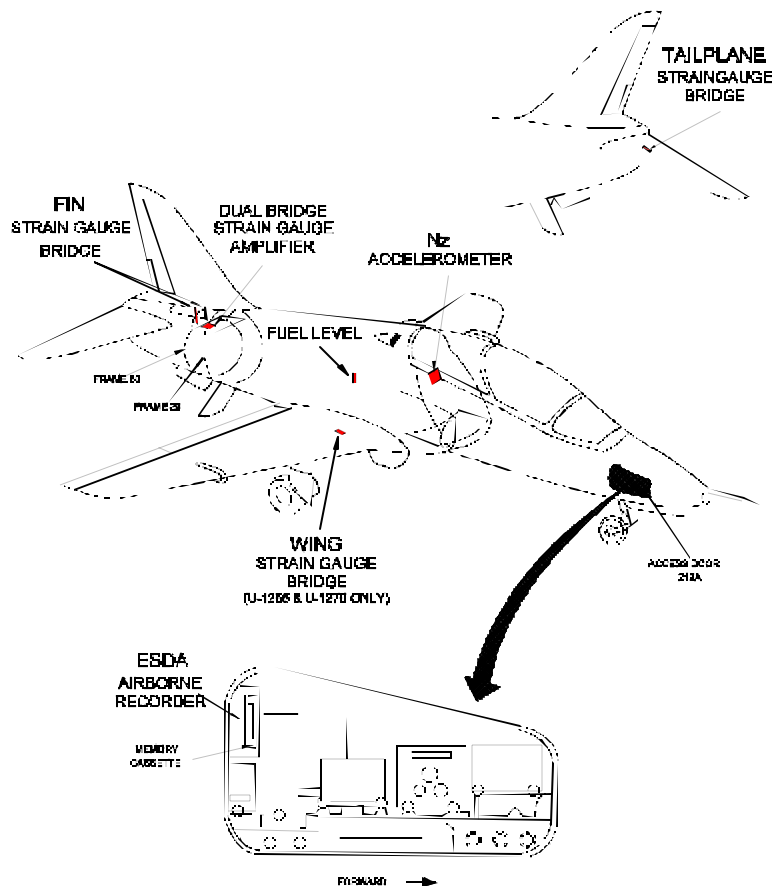


Fig. 4.4.1 The Electronic Structural Data Acquisition System (ESDA) used for loads history recording on Hawk Mk 66

4.5 SERVICE EXPERIENCE OF TIGER F-5E/F

(M. Nievergelt; SF / A. Uebersax; SF / A. Oswald; SF / A. Gasser; SF)

The 101 Tiger F-5E/F aircraft are the largest fleet of the Swiss Air Force. A comparison of fatigue damage taking into account the current amount of flight hours, as well as a spectra comparison with other users show that the Swiss F-5 usage is one of the most severe.

The following three subject describe major incidents in the period 1997-1999:

4.5.1 15% Spar Wing to Fuselage Attachment Bolt Failure

Incident

On March 13, 1997 the Fatigue Engineering Group was informed about the failure of a left hand side 15% bolt of an F-5F aircraft. The failure location was in the transition radius region of the threaded bolt extension. The failure of the bolt occurred at some unknown time during service. A thorough failure analysis was initiated by the Swiss Aircraft and Systems Company.

Since a failed 15% Spar Wing to Fuselage Attachment Bolt could result in the loss of the wing under certain flight conditions, subsequent loss of the aircraft and possible loss of the crew, the incident was considered to be highly safety critical.

An initial examination of the bolt fracture surface revealed evidence of a fatigue induced failure. Since there was no indication of the bolt failure being specifically due to in-service usage or inadequate maintenance of this particular aircraft, it had to be assumed that the whole fleet could possibly be affected by this type of failure. It was therefore decided to ground all aircraft until both 15% bolts had been replaced. At the same time, SF sent an information package about this safety critical incident to the F-5 Technical Coordination Group in order to inform all F-5 users worldwide.

During the replacement and subsequent Non Destructive Testing of all 15% bolts, a total of 5 damaged bolts were found. One of these bolts failed completely during the removal-process. A very low applied torque caused the total fracture of the bolt. Damage on the remaining 4 bolts was detected by Non Destructive Testing.

Bolt Function

The main wing loading including the wing torque is transferred through 4 bolts, see Figure 4.5.1.

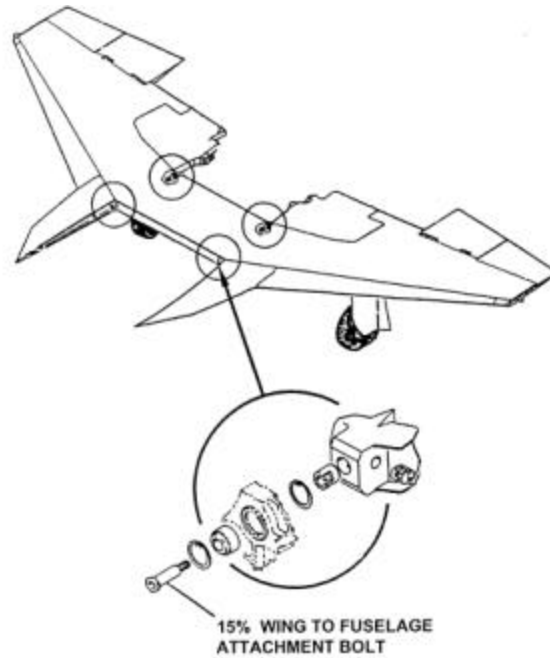


Fig. 4.5.1 Arrangement of 4 bolt on wing

The 15% spar bolt, Figure 4.5.2 is installed in a fixed position with regard to the wing. It is radially held by a wing integrated bushing. Axially it is held by a threaded bolt extension that is engaged within a barrel nut. On the fuselage side, a spherical bearing is axially held within the bulkhead bore by two snap rings. The bearing is free to slide axially on the bolt. The main loads for the 15% spar bolt are therefore vertical and lateral forces and the thereby resulting bending moments.

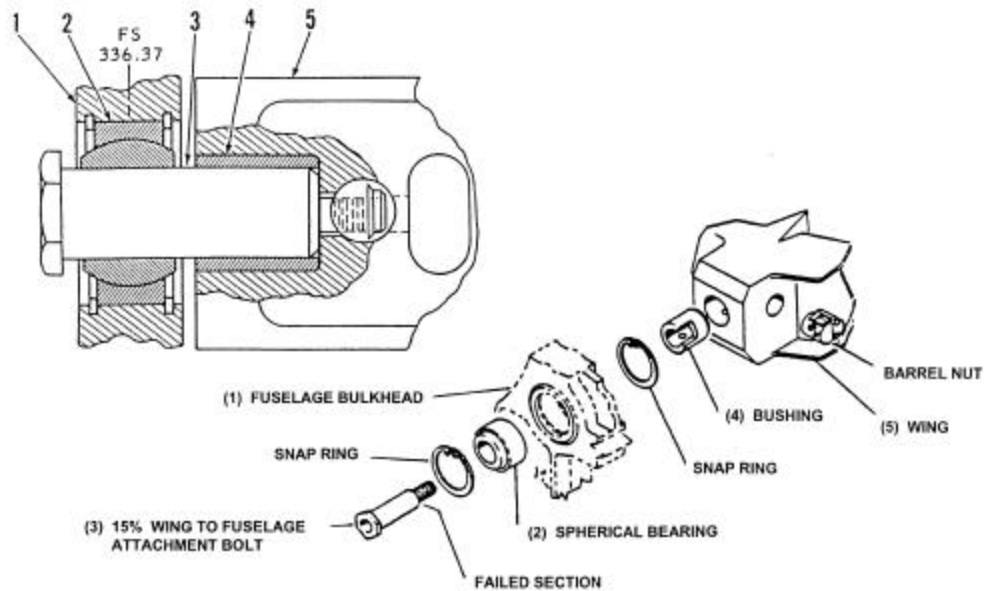


Fig. 4.5.2 Detail of bolt

Failure Investigation

The fatigue crack surface of the bolt Figure 4.5.3 is typical for parts with pre-cracked surfaces subject to a bending load. Therefore a crack must have initiated first around the whole circumference of the bolt before penetrating into the core. On the surface of the bolt, beach marks can be seen due to fatigue crack growth. The beach marks are horizontal lines, therefore indicating the presence of a bending moment caused by vertical loads.



Fig. 4.5.3 Fatigue crack surface of cracked bolt

The fatigue cracks initiated within the Nickel-plated surface in the transition radius region. The fatigue crack originated in machining grooves that had a sharp radius. Moreover, the brittle Nickel-layer shows multiple cracks penetrating into the steel matrix. Corrosion pits are also found. Further on, the Phosphorus content measured within the Nickel plating causes tensile internal stresses within the plating, see figure 4.5.4.

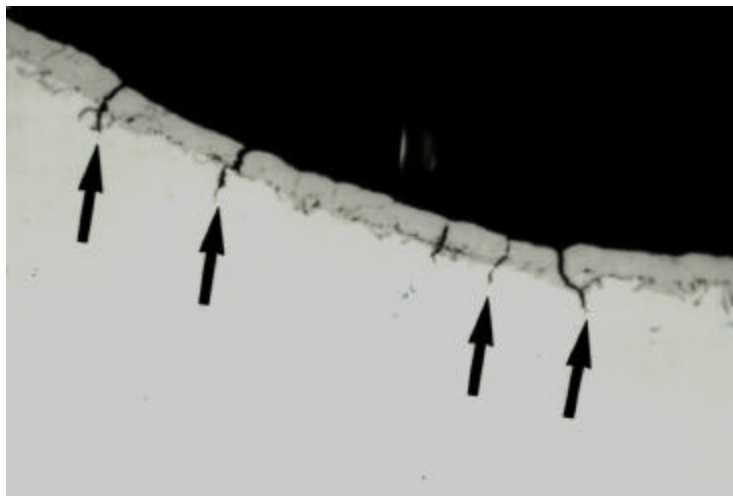


Fig. 4.5.4 Multiple cracks penetrating into steel matrix

Only one bolt shows a continuous grain flow at the thread indicating a rolling process according to requirements specified on the drawing. The other 4 bolts indicate a cutting process without rolling.

Conclusions and Actions

This incident shows clearly that the failure of the transition-radius section of the 15% bolt might have a severe impact on flight safety.

Because the failed section does not carry primary loads, neither a static analysis nor a Damage Tolerance Assessment had been performed by the aircraft manufacturer. However, the failure allowed axial slippage such that the bolt is completely out of position, causing the total loss of the bolts primary function.

All failures or damages of the 15% bolts are clearly due to fatigue. In all bolts, crack initiation took place within the brittle Nickel-plating, favored by sharp tool marks and corrosion pits at the critical transition radius.

Only 1 out of 5 bolts showed rolled threads according drawing specifications. The transition radius was far less than the 0.05 inches specified on the drawing. The electroless Nickel-plating process caused a brittle Nickel layer.

The Time Replacement Schedule according to aircraft manufacturer's technical orders requests replacement of the 15% bolts every 1200 flight hours. SF reduced the replacement interval to 600 FH for the Swiss F5 fleet and applied the same reduction for the technical orders.

Subsequently, the aircraft manufacturer developed an improved design of the bolt.

4.5.2 Horizontal Stabilizer Actuator Support Fitting

Incident

On August 27, 1998 the Fatigue Engineering Group was advised by the Technical Coordination Group (USAF) to perform a sample inspection on the Horizontal Stabilizer Actuator Support fitting (HSAS), see figure 4.5.5. After three cracks have been detected, SF decided to have all aircraft checked before the next flight. The inspection revealed about 25% of the aircraft with cracked fittings.

Fitting Function

The fitting is mounted on both sides in the aft fuselage and introduces the actuator loads into the surrounding fuselage structure.

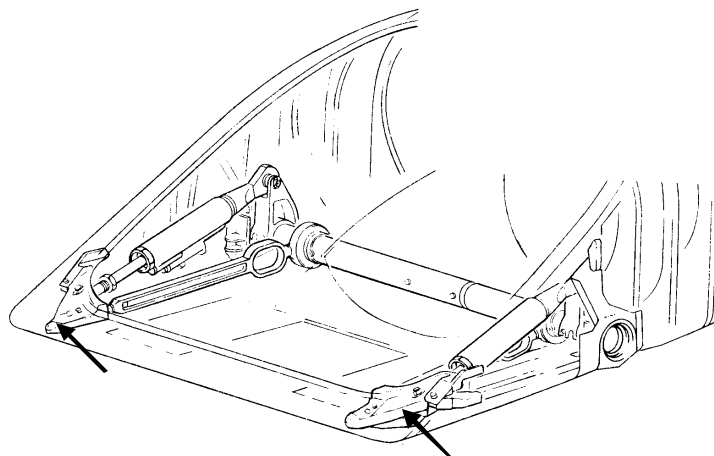


Fig. 4.5.5 Arrows show Horizontal Stabilizer Actuator Support fitting

Investigation

Three different crack types were found: Two on the lower fitting (LO1, LO2) and one on the upper fitting (UP1), Figure 4.5.6. Although cracks of 2.5 inches were found on the location LO1, see Figure 4.5.7, no failure of the fitting occurred. It seems that a significant amount of internal stress is introduced by an improper fit of the fitting's outboard flange with a titanium profile.

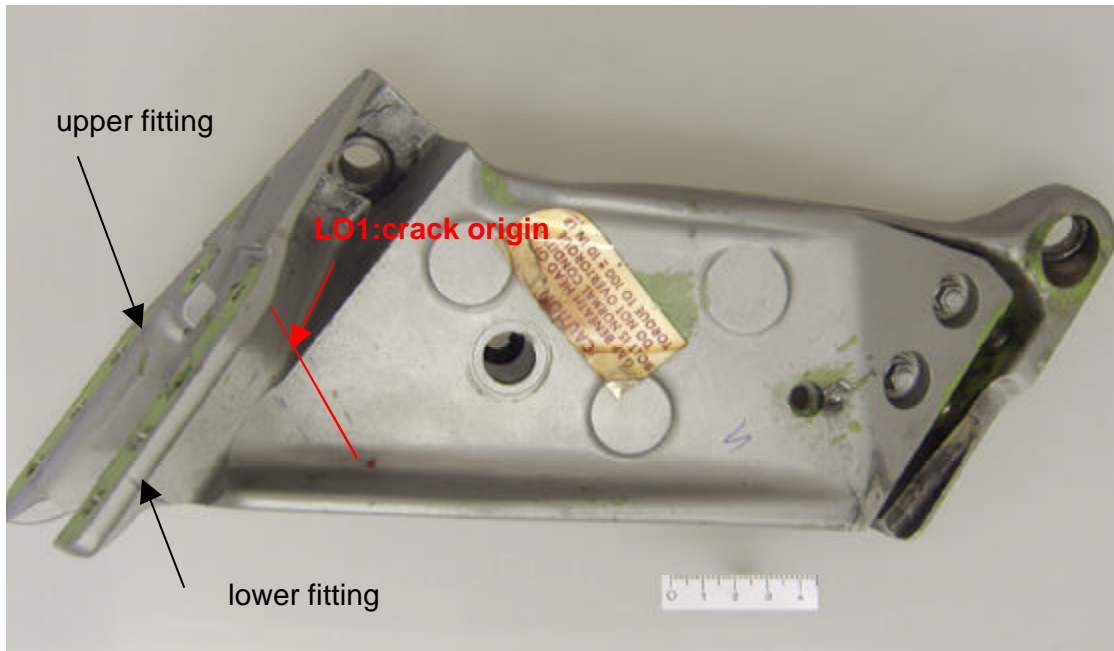


Fig. 4.5.6 Detail of Horizontal Stabilizer Actuator Support fitting

The performed fractographic analysis for the location LO1 (Figure 4.5.7) revealed pure fatigue cracking.

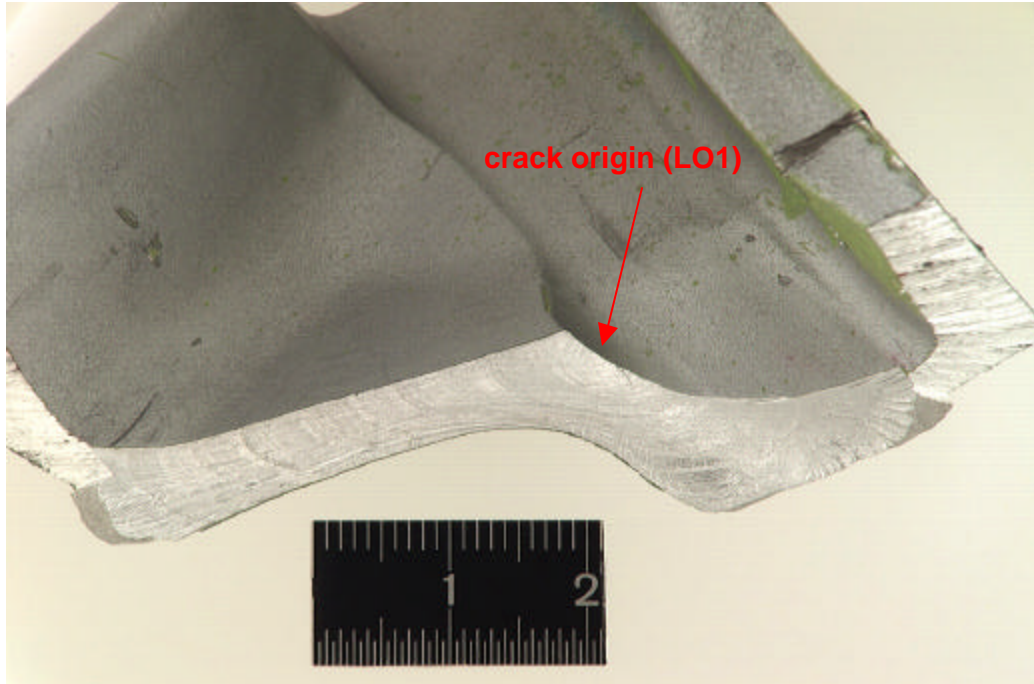


Fig 4.5.7 Location of cracks origin of LO1

Redesign

Without any spare parts available and an urgent need to get the aircraft airworthy again, SF was assigned to manufacture these fittings for the Swiss F-5E/F.

The FEM-model based on the 3D-solid-model for the original fitting showed stress concentrations in the same locations where the cracking originated. Therefore the decision was made to head for a geometrical redesign of the part.

Material Change

The material of the original fittings was a die forged 7075-T73 aluminum alloy. To reduce the lead times and keep the costs down, plate material was to be used as a replacement of the die forged material. After an analysis of fatigue strength data, the aluminum alloy 7075-T7351 was selected.

A fractographic analysis of the grain flow in some particular locations of the original fitting revealed the benefit of a forged part as minor or even not existent.

Geometrical Redesign

The geometrical redesign included beef ups of high stressed regions and a smoothed geometry in the regions of high stress concentrations (stiffness-gradients). Additional geometrical changes were introduced for a better fit in the structure.

The redesign was statically verified by FEM. The stress level in the critical section was decreased by 40%. The overall stiffness in the loading direction of the fitting was increased by only 12%.

Damage tolerance assessment (DTA)

There was no loading spectrum available. The performed DTA is therefore based on an artificial spectrum (matched with the design limit load conditions and with added vibration cycles). Calculations were made for the original as well as for the redesigned fitting, in order to get relative results.

The stress distributions in the uncracked fitting were taken from the FEM with the corresponding design load case. The improvement of the crack initiation life was evaluated by S-N curves.

Results:

Increase of crack initiation life at least by a factor 5

Increase of crack growth life at least by a factor 2.4

Due to the better overall fit of the fitting to the surrounding structure, less supplementary stresses are introduced

A coupon test program was performed to verify the analysis. A set of 3×3 specimen was tested to account for the effects of the material change and the stress reduction. The results showed that the performed crack growth calculation for the redesigned fitting is too conservative. With an adjusted analysis the CG life of the redesigned fitting will increase even more.

Fleet

The redesigned fittings are not installed preventively. The replacement is performed on aircraft with cracked fittings only.

Three aircraft are currently flying with the redesigned fitting. The production of 30 shipsets is in progress and installation is ongoing.

4.5.3 15% Inboard Spar Cracks

Incident

The critical location is covered (figure 4.5.8) in the fatigue relevant maintenance technical orders of the aircraft manufacturer. The Swiss F-5 are initially inspected at 1800 flight hours according to a damage tolerance analysis based on Swiss usage data. The majority of the Swiss F-5 already passed this inspection with no damage ever found. Only one single minor crack indication - that disappeared after a soft polishing - was observed on an aircraft in a subsequent inspection at 2400 flight hours.

On November 26. 1998 the Fatigue Engineering Group was informed about a crack exceeding 9 mm, found during the 2400 FH inspection.

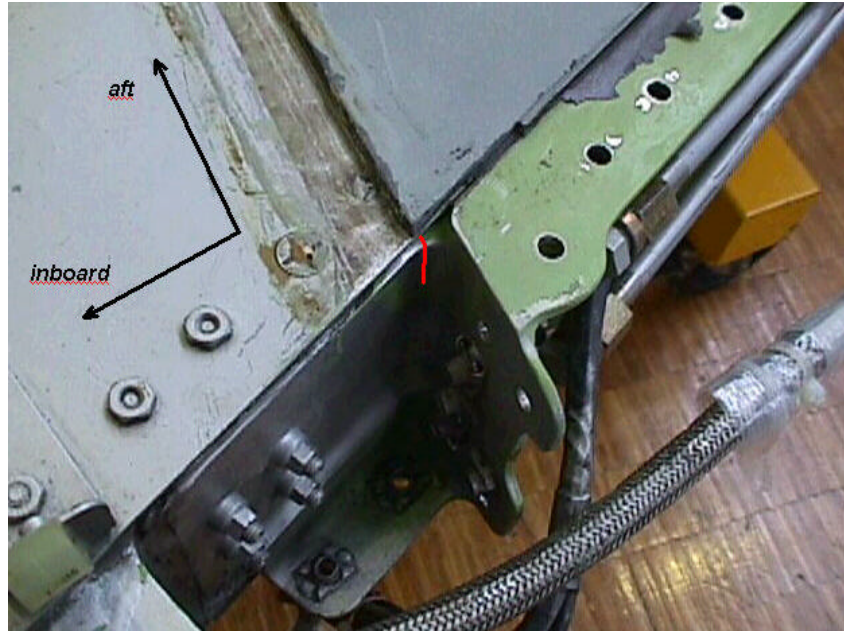


Fig 4.5.8 Critical locatin on 15% Inboard Spar

After the findings of 3 other aircraft with comparable cracks at the same location, SF decided to check all aircraft with more than 1800 FH within a week. During this inspection, 27% of the hole fleet was found with cracked spars. Wings with cracked spars are withdrawn from further flight service. Due to load transfer, the wing lower skin below the crack in the spar is subject to higher than normal stresses. Continued loading of this wing location could result in secondary damage in the wing lower skin being a highly safety and maintenance critical part of the F-5.

Spar Function

The wing torque box consists of the wing lower skin, the wing upper skin and 6 spars located between 15% and 44% of the aerodynamic chord. The 15% spar itself consists of 5 spliced parts, a center section, left and right inboard section and left and right outboard section.

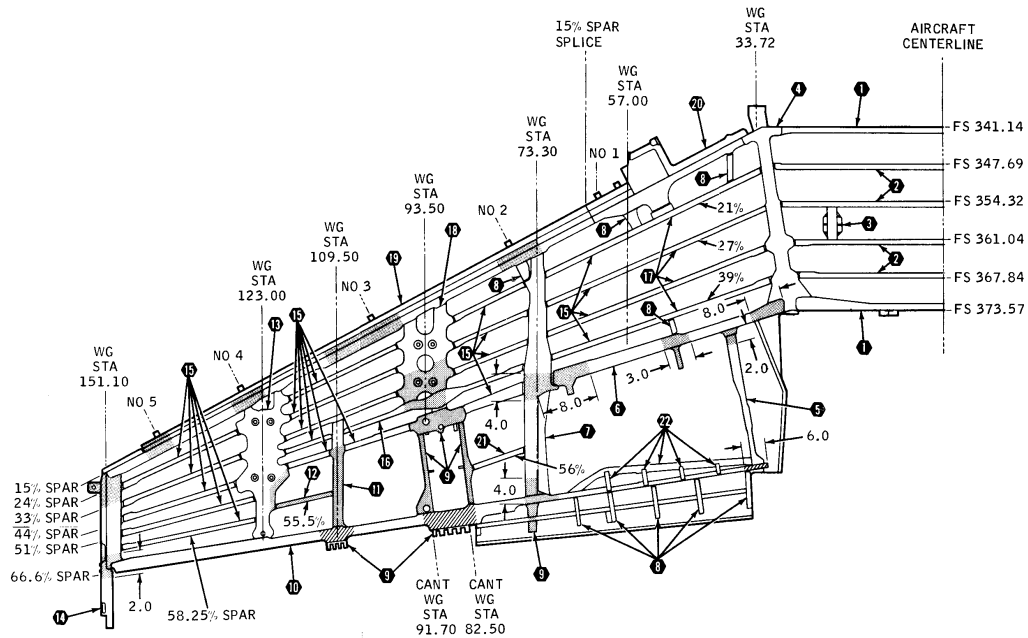


Fig. 4.5.9 Structure of F-5 wing inboard box

The main loading on the wing torque box, Figure 4.5.9 is the wing bending moment as well as the wing torque moment. The bending moment is taken by the skins acting as tension/compression components and by the spars mainly acting as shear transferring components. However, the spars are subject to the wing deformation and the flanges are tension / compression loaded comparable to the wing skins. In addition, 15% Inboard Spar extensions act as attachments for the Leading Edge Extension and as hard points for the trailing edge flap actuators.

The 15% Inboard Spar is machined from a forging oriented in such a manner that the longitudinal grain direction is optimized for the spar extensions parallel to the direction of flight. The grain flow is therefore orientated in the transverse direction with regard to the direction of tensile stresses. A flange step down and a spar extension act as a two dimensional stress raiser at the cracked cross section.

Conclusions and Actions

Because fast crack growth rates in excess of 20 mm per 150 FH, the recurring inspection intervals had to be reduced significantly.

The cracked 15% Inboard Spars reduced the Swiss F5 fleet availability and more findings are expected in the future. In addition, the replacement of the part requests a significant amount of effort and spare parts have drastic lead times. This combination would have resulted in a long term fleet shortage that would not have been acceptable. SF therefore decided to develop a temporary repair solution to overcome the period to a replacement of the part.

The primary goal of the repair was to compensate the strength and stiffness lost due to the crack within the spar so that the wing lower skin overload decreased to an acceptable value. In addition no structural degradation of the structure due to the application of the repair itself was permitted.

This goal was achieved by applying a tapered steel strap onto the wing lower skin. (Figure 4.5.10)

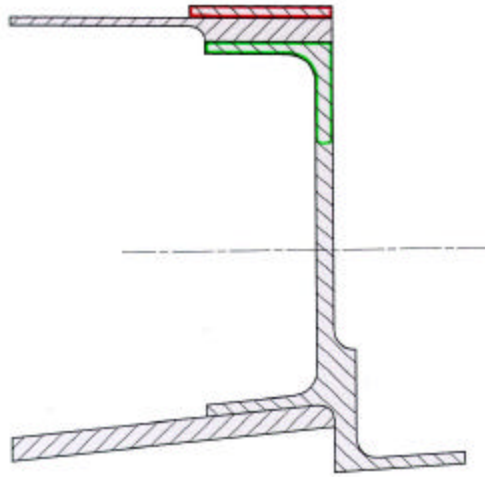


Fig. 4.5.10 Repair with tapered steel strap

Because the steel strap's length was limited by aerodynamic and geometrical requirements, the load introduction had to be designed and assessed very carefully. A damage tolerance analysis based on Swiss usage data was performed for the critical locations. The life of the temporary repair is limited by one of the fastener holes. Even under worst case assumptions, the fastener hole must be economically repairable after the repair's planned service life has expired.

The temporary repair for cracked 15% spars significantly increases the Swiss F-5 fleet availability during the next two years. Future findings of cracked 15% spars can easily be repaired in the same manner. The final replacement of the spars is planned and has to be finished before the expiration of the temporary repair's service life.

4.6 F/A-18 SWISS STRUCTURAL INTEGRITY PROGRAM **(M. Guillaume; SF / M. Gottier & A. Kuo; Engineering Consultants)**

4.6.1 Swiss F/A-18 ASIP Study

During the evaluation of a new fighter aircraft for the Swiss Air Force, the Swiss Defense Procurement Agency commissioned Boeing to perform an Aircraft Structural Integrity Program (ASIP) study to determine the F/A-18 structural parts which need to be modified to fulfill the Swiss service requirements. The static service requirement consists of a 9g symmetric limit load factor and a 6g asymmetric limit load factor applied to a higher average aircraft weight as the design weight of the United States Navy F/A-18. The Swiss service life criteria requires two life times of crack initiation (CI) life and two life time of crack growth (CG) life. One Swiss service life equals 5000 flight hours. The fatigue spectrum, which was the base for these requirements, consists of a design load factor exceedance curve and a point in the sky/configuration (PITS/ Config) usage criterion provided by the Swiss. The eight points in the sky defined by Mach number and altitude are combined with eight configurations. These points in the sky are determined for the average aircraft usage in contrast to the three points in the sky, representing the most severe aircraft usage. A more detailed description of the Swiss service life criteria is provided in reference [10].

The ASIP study performed at Boeing, revealed that the Swiss fatigue spectrum is at least two to three times more severe than the USN design spectrum, i.e. the Swiss CI-lives for the fatigue critical parts of the F/A-18 are two to three times shorter, than those of the USN. The reason is related to the proximity of the training area from the base, which eliminates almost the entire cruise time and therefore increases the percentage of the maneuver type of training per the total average sortie time.

Despite the more severe Swiss service requirements, it has been shown by the ASIP, study that the F/A-18 has structural growth potential: Only 5 structural parts required a major modification by changing the material from aluminum to titanium. However, the majority of the F/A-18 structure met the more severe Swiss service requirements with local structural modifications such as changing radii, increasing thicknesses of local areas, changing fastener types or improving holes by cold working or by installing interference fit fasteners. Table 4.6.1 shows the different types of structural changes for the major structural parts.

A total of 833 analyses have been performed during the ASIP study: 187 Static analyses, 528 CI analyses and 118 CG analyses. The majority of the structural changes were due to the Swiss fatigue requirements (see ref. [10]). The analytical fatigue method used to perform the ASIP study is based on fatigue test data from the USN FSFT. The method is described in detail in reference [11].

As mentioned before, the biggest number of structural changes were performed by improving fastener holes. Literature revealed that, a life improvement factor (LIF) of 3 can be taken into account by cold working a hole or installing an interference fit fastener. However, in some locations of the Swiss F/A-18, a LIF of 5 was needed to meet the Swiss fatigue requirement. This is the reason why a combination of cold working the hole prior to the installation of a interference fit fastener or a so called close tolerance interference fit fastener has been chosen. During the ASIP study, a coupon test program was conducted in order to verify the required LIF of 5. In chapter 4.6.2 an overview of the performed tests will be provided and a summary of the test results will be given.

4.6.2 LIF Test for Close Tolerance Holes for each spectrum

During the Swiss F/A-18 ASIP study a fatigue life improvement factor (LIF) of 5 was used to represent the beneficial effects of cold working fastener holes prior to the installation of interference fit fasteners. This is a factor of 1.67 over the LIF of 3 used for standard interference fit fasteners.

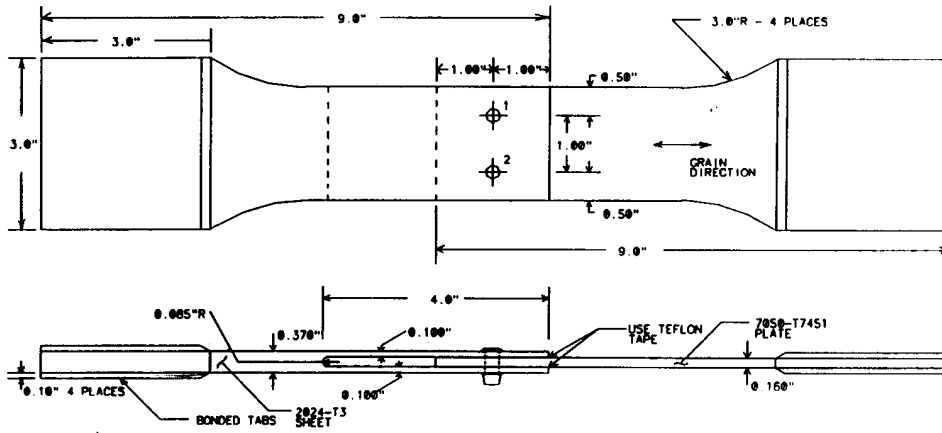
In order to verify this additional LIF of 1.67, a coupon testing program was conducted during the ASIP study using 3 different specimen configurations and two different spectra. The configuration of the specimens consists of double shear lap coupons with two (2), four (4) and six (6) fasteners and are shown in Figure 4.6.1. The reason for the three types of specimen was to determine which effect the ratio of bearing stress to through stress may have on the fatigue LIF (table 4.6.2). The coupons were tested with two randomized spectra of different severity. The test matrix is shown in table 4.6.3.

Early testing revealed very long fatigue lives for specimens with only interference fit fasteners. This was the reason why a control specimen of the same configuration without cold worked holes and interference fit fasteners was tested. The fatigue life of this coupon was 140 times shorter than the fatigue lives of the previously tested specimens with interference fit fasteners. It shows that this was due to high levels of fastener interference in the specimens.

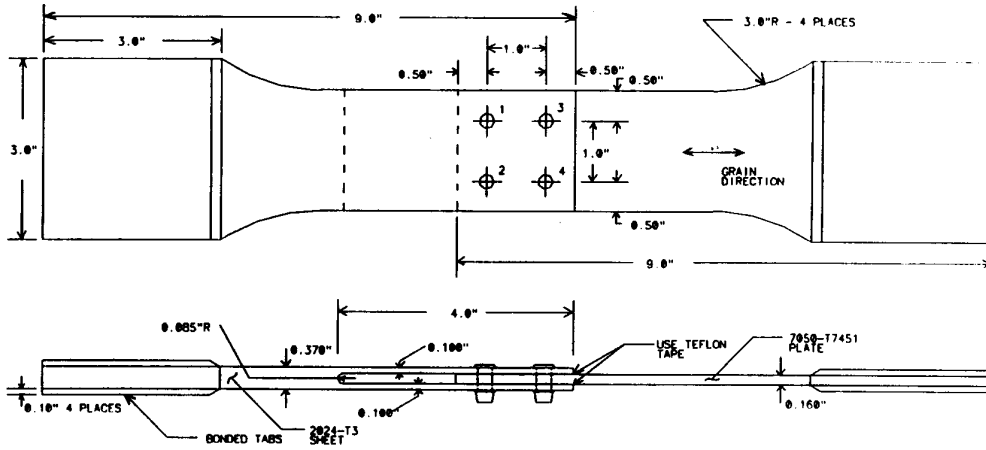
In order to induce earlier failure of the specimens, it was decided to increase the reference load for both spectra by approximately 20%. All testing was performed until either failure of the specimen occurred or 350'000 SFH was reached. The test results for each spectrum are summarized in Figure 4.6.2.

It can be concluded that the combination of a cold worked hole and an interference fit fastener resulted in fatigue LIFs which are between 4.75 and 9.55 (for details see table 4.6.4). These LIFs are all well above the desired LIF of 1.67 and therefore, the usage of a fatigue LIF of 5 in combination of a cold worked hole with an interference fit fastener versus a hole without any fatigue improvement has been validated by these tests.

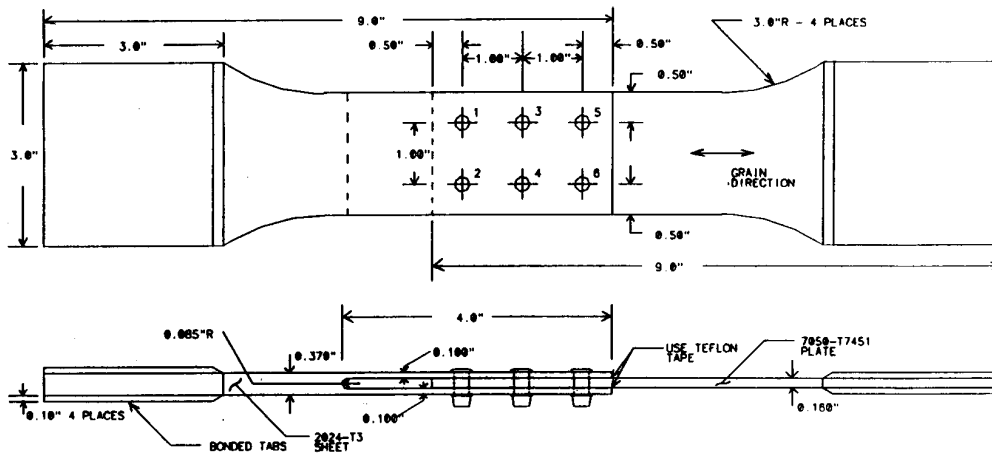
In addition, it reveals that most of the holes have a high interference due to the hole diameters, which were manufactured close to nominal dimensions resulting in a LIF, which is much bigger than 3 for a interference fit fastener hole versus an unimproved hole.



2 Fastener Specimen



4 Fastener Specimen



6 Fastener Specimen

Fig. 4.6.1 Test specimen for close tolerance holes

4.6.3 Application of Close Tolerance Holes in Production

The F/A-18 wing is composed of six major elements: the inner wing box, the outer wing box and four control surfaces (Figure 4.6.3). The inner and the outer wing boxes are highly loaded structural components consisting of several spars and ribs and one upper and one lower carbon-epoxy main box cover. Mechanical fasteners are used to attach the wing cover skins to the spars and ribs. The majority of the fasteners in the lower wing cover skin area are bolts with an interference fit whereas the upper wing cover skin fasteners are screws with a clearance fit.

In order to fulfill the Swiss fatigue requirements, most of the lower wing cover skin fastener holes have to be improved, i.e. in addition to the already existing LIF of 3, another factor of 1.67 was needed to achieve the LIF of 5. This improvement was accomplished by cold working the fastener holes prior to the installation of the interference fit fasteners. It revealed however, that this procedure was not practicable in the inner and outer wing box due to the inner metallic structure/carbon-epoxy wing cover skin combination: a fastener hole in a inner metallic part could not be cold worked through the composite skin due to the high risk of delamination of the composite structure. Cold working of all fastener holes with the wing cover skin removed was not possible either because of growth of the inner metallic structure. The reason for rejection of this procedure was based on a test performed on a spar. It revealed that after cold working the entire row consisting of approximately 120 fastener holes, the spar grew by at least one fastener diameter. As a consequence of this result, the fastener holes of the inner metallic structure would no longer align with the holes of the wing cover skin. This was the reason why a solution with close tolerance interference fit fasteners has been chosen for fastener holes where LIF of 5 was needed. Based on the results from the test program described in chapter 4.6.2, Boeing reduced the manufacturing tolerances of holes with interference fit fasteners by 0.001 inch.

The new tolerances of the interference fit fasteners are shown in table 4.6.5.

In order to be able to manufacture these tighter tolerances, Boeing had to improve the hole drilling process of their automatic drilling system. In addition, each hole had to be checked using a diatest digital ball measuring device (BMD). This device showed a much better precision than the mechanical ball gauge device and in addition, all measured data was stored and used for statistical process surveillance.

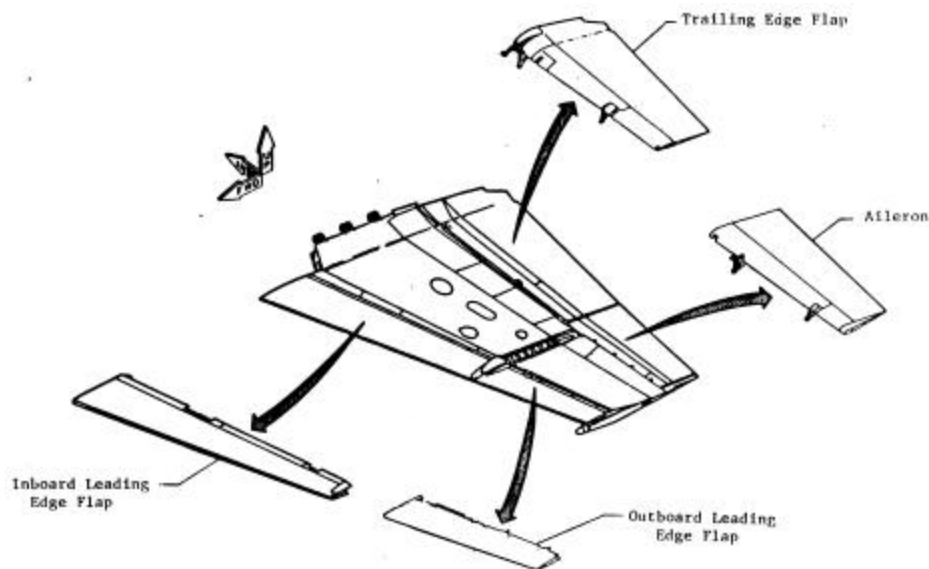


Fig . 4.6.3 Wing elements of F/A-18 including flops and inner/outer torsion box

4.6.4 Implementation of Swiss modifications in production

The implementation of the Swiss modifications into the production line was a major task for the manufacturers of the F/A-18 aircraft, i.e. The Boeing Company and Northrop Grumman. Many changes in their process specifications, work instructions and tooling were needed. Among all these changes, specifically one required a lot of effort until the required quality could be met; these are the interference fit fasteners with tight tolerances (see chapter 4.6.2 and 4.6.3). Each drill tooling needed to be modified in order to meet the requirement of the close tolerance holes. Especially the process of the automatic drilling machine had to be analyzed and additional tests were necessary to improve the system. In order to meet the more demanding requirements, it was also necessary to change the hole diameter measurement device due to the inaccuracy of the old device.

During production several problems also occurred: Mainly gaps between different structural parts of the wing, which could lead to a fatigue problem due to local fastener bending were an issue. This was the reason why an in depth analytical investigation was performed and new manufacturing standards had to be created. Based on these results the tolerance for liquid shimmed gaps was increased in some structural areas.

During manufacturing, other structural defects such as misoriented platenuts, short edge distances of end fastener holes in fatigue relevant parts and escaped fastener hole improvements were revealed. Most of these nonconformances occurred at the beginning of the Swiss production and corrective actions took place. However, a few of these nonconformances could not be corrected in early aircraft production and detail fatigue analyses were therefore needed for those aircraft. These analytical investigations revealed that most of these defects still meet the Swiss crack initiation requirements.

Despite of these positive results, it was decided to have some of these nonconformances built into the FSFT article. Based on this decision it will be possible to test the different configurations due to structural deficiencies of the Swiss F/A-18 fleet in the FSFT.

4.6.5 Swiss FSFT

In the summer of 1998, the Swiss Defence Procurement Agency (DPA) commissioned the Swiss Aircraft and Systems Company (SF) to perform a full scale fatigue test (FSFT) on the Swiss F/A-18 a/c. In order to perform this test in a most economical way with the most state of the art test set up and equipment, SF decided to team with IABG, a test and analysis center in Germany.

The goals to be achieved by the Swiss F/A-18 FSFT are as follows:

A basis of a safe operation of the Swiss F/A-18 fleet combined with a most economical maintenance program shall be established: the total fatigue life of critical components will be determined. In addition, inspection intervals established by analysis and inspection methods will be validated. Furthermore repair designs which occurred during the FSFT will be verified.

The redesigned Swiss F/A-18 structure based on the analytical approach used in the ASIP study shall be verified and validated: first the Swiss fatigue requirements of 10,000 service flight hours (SFH) of crack initiation, 10,000 SFH of crack growth and the residual strength load of $1.2 * P_{xx}$ have to be proven. Second the fatigue lives of those structural parts, which do not meet the Swiss redesign requirements, will be determined by test and validated. Third, the analytical approach used to redesign the Swiss F/A-18 structure will be verified, i.e. the pegging procedure described in ref. [11] will be verified by proving following relationship:

Analytical CI life / CI life determined by test = constant

In the ASIP study it was assumed that this relationship would be true for the USN and the Swiss design spectrum.

The Swiss FSFT program will be performed in the time frame between 1998 and 2004. These 6½ years are broken down in three major time periods with following mile stones:

- Summer 1998 - Start of pretest activities:
 To assemble the FSFT article,
 To define a detailed test concept, the test master event spectrum (MES) and fatigue relevant load cases,
 To carry out a coupon test program to verify the test MES,
 To convert FE data from CGSA/ CASD into NASTRAN/ PATRAN models and
 To build up a full FEM for the F/A-18 aircraft to support the FSFT.
- Fall 1999 - Start of test set up phase:
 To develop the test load spectrum and to set up the flight by flight test program,
 To determine the inspection concept and
 To build the mechanical test setup including equipment installation.
- Spring 2002 – Procurement and installation of test set up and performing of strain surveys.
- Fall 2002 - Start of test performance:
 To simulate the 10,400 test hours and to perform inspection based on the requirements of the inspection concept.
- End of 2004 - End of test phase I:
 The test should have been accomplished in a successful manner and at this time the data from the inspections during test should be processed.

The FSFT will be performed with the Swiss design spectrum, which was used for the ASIP study to define the structural modifications. However, in order to reduce the number of load cases for the FSFT, it was necessary to perform an extensive study to determine a test MES program. Chapter 4.6.6 describes the procedure to define this test master event sequence. The loading test set up is defined by means of a "push-pull" actuator system, which has already been applied successfully in FSFT of other fighter aircraft.

4.6.6 Development of Test Master Event Spectrum

The development of a master event spectrum (MES) for testing is one of the early activities specified in the Swiss F/A-18 FSFT program.

Each event in a MES is defined by a combination of an aircraft configuration and a point-in-the-sky (PITS). The loads on an aircraft are affected by these combinations. There are 25 combinations of PITS and configuration in the Swiss F/A-18 design criteria. During the Swiss F/A-18 ASIP study, the number of PITS/ Config combination was reduced from 25 to 11 equivalent combinations. The fatigue analysis of the ASIP study and the subsequent analysis to support manufacturing are based on these 11 PITS/ Config combinations. Therefore, the fatigue lives predicted by the 11 PITS/ Config will serve as the basis of developing a simplified MES suitable to the FSFT (see Figure 4.6.4). The reason to perform this task is related to the amount of fatigue loads relative to each PITS/ Config combination: the number of fatigue loads data increases with increasing the number of PITS/ Config combinations. For the ASIP analyses, fatigue loads were generated only for 17 selected locations in the F/A-18 airframe and for 11 PITS/ Config combinations. However, for the FSFT fatigue loads of the entire aircraft need to be generated. The effort to generate fatigue loads for the entire aircraft for the 11 PITS/ Config will be enormous. This is the reason why it is necessary to reduce the number of combinations of PITS/ Config in the MES to a manageable one for the FSFT while maintaining the fatigue damage within $\pm 10\%$ in terms of crack initiation (CI). It is to mention that CI is the primary fatigue design criterion for the F/A-18 aircraft.

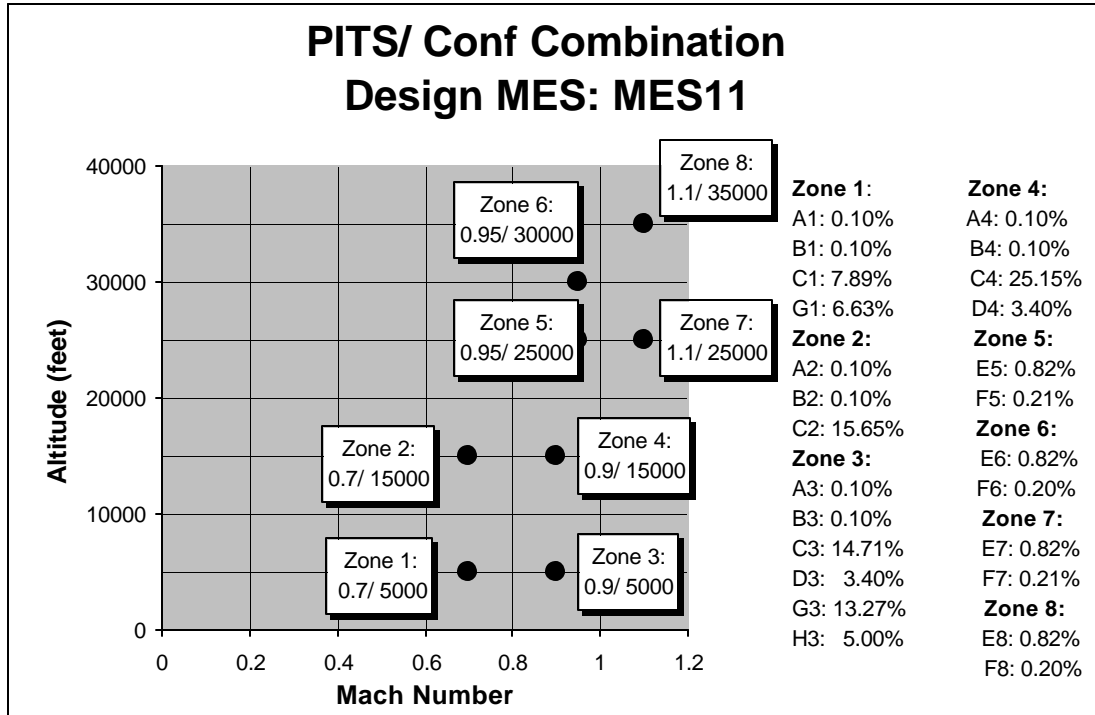


Fig. 4.6.4 PITS/Conf combinations for Design MES

The development of the test MES was carried out in two steps:

1. A reduction of PITS/ Config combinations was performed by comparing loads of the wing root location for those PITS/ Config combinations causing major fatigue damage. Using this approach, three MES were generated with a computer program for 11, 8 and 6 PITS/ Config as a starting point. Three Wing Root Bending Moment (WRBM) spectra were then created based on the MES of those PITS/ Config combinations. Based on these stress spectra the crack initiation (CI) lives were afterwards determined for the most extensively used material in the F/A-18 aircraft, i.e. titanium material, aluminum 7050 material and aluminum 7075 material.

The results are presented in Figure 4.6.5. The fatigue lives are normalized to the design spectrum consisting of 11 PITS/ Config combinations. It revealed that further adjustments of combining PITS/ Config was necessary leading into a second step with more detailed investigations in modifying the distribution of PITS/ Config combinations.

2. The procedure mentioned above was used to determine the CI lives at eight different locations of the F/A-18 aircraft for 6 PITS/ Configurations combinations with different distributions. The selected eight locations represent loads in the major components of the airframe. Several iterations were necessary in order to achieve the goal for the test MES spectrum with 6 PITS/ Config combinations

Based on this extensive analytical study the following conclusions can be drawn:

- A test MES for the FSFT was created with 6 PITS/ Config combinations (see Figure 4.6.6) meeting the $\pm 10\%$ CI life criterion at all eight fatigue relevant locations of the F/A-18 aircraft.
- A reduction of PITS/ Config combinations based on one material can result in an erroneous MES. All major materials used in the airframe should therefore be included in the investigation.
- The influence of each PITS/ Config on the load/ stress of the various major components in an airframe is significantly different. Thus, the PITS/ Config reduction study should include a number of locations whose load/ stress can be representative of the major components.
- Some PITS/ Config have a small percentage of usage, but have an major influence on the load/ stress of some locations. These PITS/ Config must be identified and included in the MES to meet the goal of the intended CI life criterion.
- The analytically determined test MES has to be verified by a coupon test program using specimens made of all major materials of the aircraft and different spectra with different stress levels.

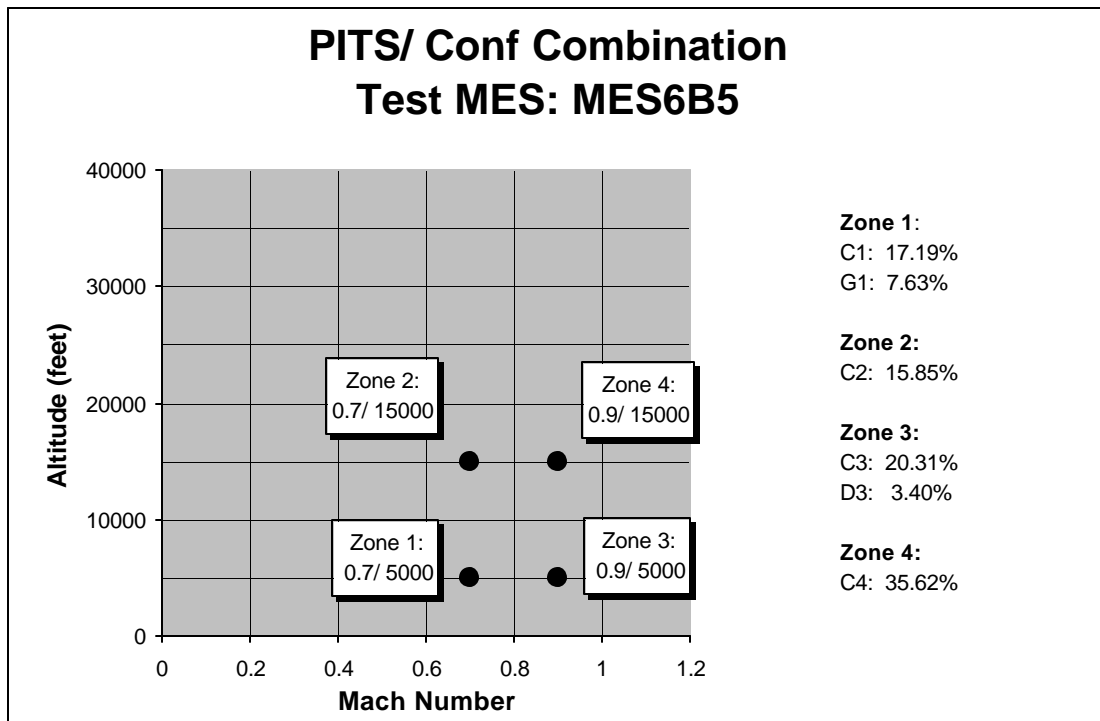


Fig. 4.6.6 PITS/Conf Combination for Test MES

4.6.7 Coupon Test

The Swiss Test MES was developed for the FSFT by reducing the number of PITS/ Config combinations without changing the number of events. Based on an analytical approach, the number of combinations were minimized while maintaining the crack initiation (CI) life within a tolerance range of $\pm 10\%$.

In order to qualify this Test MES program for the FSFT, a verification by a coupon test program was deemed to be necessary. The goal of the coupon tests is to compare the Swiss Design Spectrum with the Swiss Test Spectrum. This comparison will be accomplished based on the CI life. The CI life is defined as the fatigue life for the initiation of a 0.01 inch crack.

Because it is very difficult to detect such a small crack, the following procedure will be used in this test program: The test specimens will be cycled until a crack is automatically detected by an eddy current probe. Then the test will be continued up to failure while measuring the crack propagation with an optical device. The CI life is later determined by subtracting the crack growth (CG) life from the tested fatigue life. However, the CG life had first to be backtracked by analysis to an initial crack size of 0.01 inch.

The test specimens are finite width specimens with a $\frac{1}{4}$ inch centered open hole (see Figure 4.6.7).

In order to keep the number of specimens in a manageable size, a selection of parameter was required, resulting in the test matrix shown in table 4.6.6.

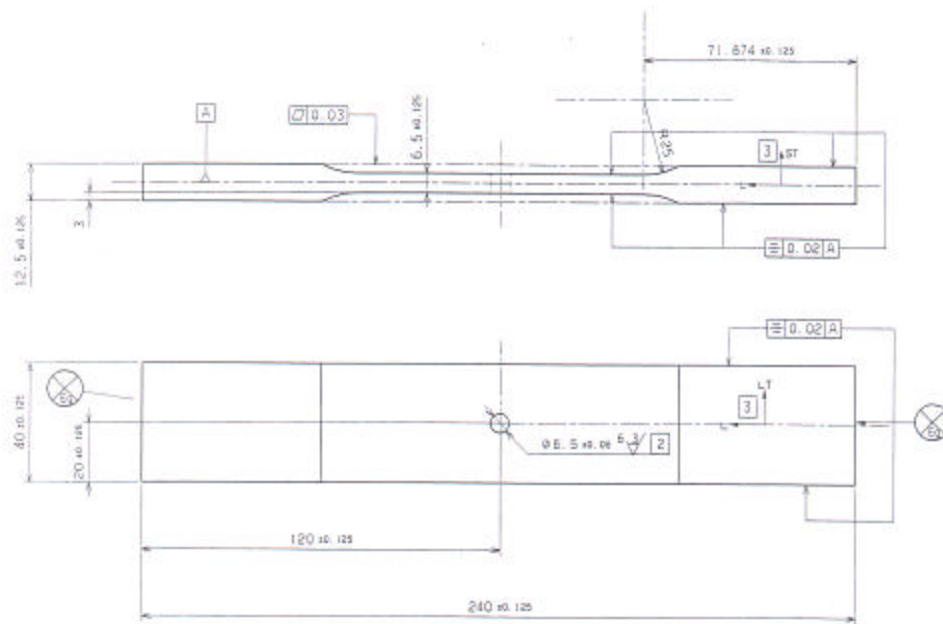


Fig. 4.6.7 Coupon Test Specimen for MES Testing

It is to mention, that each location represents a typical major structural assembly of the F/A-18; i.e. location A with the wing root bending moment spectrum (WRBM) represents the inner wing and location B with the center fuselage bending moment spectrum (CFBM) represents the center fuselage.

The coupon test program is in the progress of being accomplished. A first draft of processing data from the Al 7075 material coupons shows promising results. However, detailed data processing and analytical work is still ahead. An example of this task for the crack growth investigation is shown in Figure 4.6.8.

Table 4.6.1

Type of Modification	Structural	Major Structural Assembly	Structural Part
Change of Material (from Aluminum to Titanium)		Center Fuselage	Carry Through Bulkheads at FS 453, FS470.5, FS488 L/H and R/H Upper (Dorsal) Longeron between FS383 - FS557.5
Local Geometrical Modifications		Center Fuselage	Bulkhead at FS383 Former at FS508 Dorsal Deck between FS383 - FS557 L/H and R/H Upper Outboard Longeron between FS453 - FS557.5 L/H and R/H Lower Outboard Longeron between FS445 - FS557.5 Fuel Barrier Web between FS453 - FS557.5
		Inner Wing	L/H and R/H Lower and Upper Splice Fitting L/H and R/H Wing Spars L/H and R/H Win Closure Rib, Kick Rib, Fold Rib
		Outer Wing	L/H and R/H Front Spar L/H and R/H Fold Rib
Fatigue improvement method: - Change of Fastener, - Cold Working, - Interference Fit Fastener - Interference Fit Fastener and Cold Working - Close Tolerance Interference Fit Fastener		Forward Fuselage	
		Center Fuselage	
		Aft Fuselage	
		Inner Wing	
		Outer Wing	

Table 4.6.2

Load Ratio	Type of Specimen		
	2 Fasteners	4 Fasteners	6 Fasteners
$K_t \sigma_{brg} / K_t \sigma_{thru}$	Bearing only	2.03	1.06

Table 4.6.3

Type of Spectrum	Interference Fit			Cold Working & Interference Fit		
	2 Fastener	4 Fastener	6 Fastener	2 Fastener	4 Fastener	6 Fastener
Spectrum #1	10	10	10	10	10	10
Spectrum #2			10			10

Table 4.6.4

	Spectrum #1		Spectrum #2	
	2 Fastener	4 Fastener	6 Fastener	2 Fastener
Improvement Factor	4.75	8.11	6.03	9.55

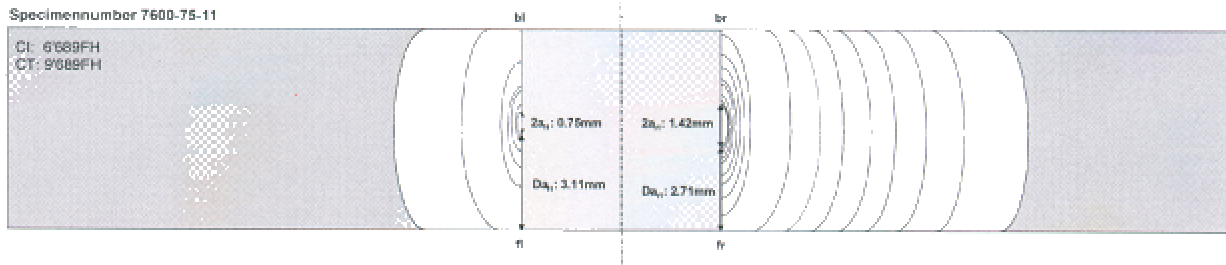
Table 4.6.5

Nominal Size [inch]	Fastener Diameter [inch]	Current F/A-18		Swiss F/A-18	
		Hole [inch]	Size Interference Fit	Hole [inch]	Size Interference Fit
1/4	.2490 - .2495	.2450 + .0030 - .0000	.0010 - .0045	.2445 + .0025 - .0000	.0020 - .0050
5/16	.3115 - .3120	.3075 + .0030 - .0000	.0010 - .0045	.3075 + .0020 - .0000	.0020 - .0045
3/8	.3740 - .3745	.3700 + .0030 - .0000	.0010 - .0045	.3700 + .0020 - .0000	.0020 - .0045

Table 4.6.6

Type of Spectrum	Al 7075 Material		Al 7050 Material		Ti Material	
	Stress Level 1	Stress Level 2	Stress Level 1	Stress Level 2	Stress Level 1	Stress Level 2
WRBM Design: Location A	3	3	3	3	3	3
WRBM Test : Location A	3	3	3	3	3	3
CFBM Design : Location B	3	3	3	3	3	3
CFBM Test : Location B	3	3	3	3	3	3

Fig. 4.6.8 Crack Growth Result of Coupon Testing



4.7 F/A-18 FINITE MODEL INVESTIGATION FOR FULL SCALE TEST PROJECT (M. Guillaume; SF / B. Bucher; SF / M. Godinat; SF / W. Stein; SF)

During the past three decades finite element analysis (FEA) has become an increasingly powerful tool for many technical or scientific applications. Computers, solvers and pre/post processing software have become more reliable, faster, and much more user friendly. FEA methods were employed in the development of the F/A-18 structure more than twenty years ago. Now SF is in the preliminary phase of an F/A-18 Full Scale Fatigue Test (FSFT) for the Swiss F/A-18 where FEA methods will again play a major role.

4.7.1 FEA for the Swiss F/A-18 FSFT

FEA is an important tool for the Swiss F/A-18 Full Scale Fatigue Test. Finite element (FE) models generate internal loads that can be used for subsequent stress and fatigue analysis. One of the many advantages of FEA methods over hand calculated methods of years past is the determination of primary load paths within the structure as a function of the relative stiffness of each of the structural components. All load carrying stringers, stiffeners, bulkheads, frames and skins will be reflected in the internal loads FE model. For a subsequent local stress analysis the stress analyst will have to decide, depending on the stress gradient, whether it would be necessary and beneficial to create a detail stress model with a finer mesh (more elements) or employ p-element formulation that would be more accurate for the location under consideration. SF's primary FEA tools for the Swiss F/A-18 FSFT are MSC/Patran/Nastran. This software package provides the full functionality of a state of the art FEA software package.

4.7.2 Fatigue Loads versus Test Rig Loads, Fatigue Analysis

For the Swiss F/A-18 FSFT, SF will select a set of fatigue load cases which represent the design usage of the aircraft (a/c). SF will take into consideration different PITS/CONFIG combinations as well as symmetric and asymmetric flight maneuvers at different normal and roll accelerations. Combined aerodynamic and inertia loads will be applied to the F/A-18 FE model as sets of balanced fatigue load vectors on select FEM node points. The fatigue loads are distributed over the whole a/c and represent net load pressure distributions. Test loads on the other hand will be coarsely distributed. This requires the SF stress analysts to investigate very carefully the local impact of whiffle tree load introduction into the test article. For each load introduction point proof of structural integrity must be performed. SF will implement this analysis first on static load and stress assessment utilizing MSC/Patran/Nastran and then on a fatigue analysis which is based on the CI89 crack initiation software procured from Boeing St. Louis. For fracture and maintenance critical parts selected crack growth analysis may be performed with the CG93 software procured from Boeing. MSC/Fatigue software was tested in 1998 at SF during the evaluation phase on a crack growth specimen.

4.7.3 Detail Stress Analysis for the F/A-18 FSFT

The internal loads FE model for the Swiss F/A-18 FSFT will be a baseline model for all subsequent stress and fatigue analysis. For more detailed stress and fatigue analysis local mesh refinement may be necessary. For local investigation a part of the structure may be isolated and interface loads or displacements may be applied as boundary constraints in order to perform a more detailed analysis. For load independent analysis SF employs reduced stiffness matrices which are extracted from and applied to a structure with Nastran ASET and GENEL cards, respectively.

The Boeing software Specgen can be used for local spectrum development for select locations in the structure with little stress gradient. During the Swiss Aircraft Structural Integrity Program (ASIP) study the sa0508 FEM baseline configuration was used to determine local stress spectra in the CTR/AFT portion of the F/A-18 fuselage. The reference stress for Specgen is retrieved from the most severe design load case for this particular location.

4.7.4 The Baseline FE Model for the Swiss F/A-18 Full Scale Fatigue Test

For the Swiss Full Scale Fatigue Test SF will base the stress analysis on a baseline FSFT FE model. This baseline FE model is derived from Boeing FE models which were used for internal loads analysis. Extensive conversion and verification procedures were performed on the forward fuselage, the LEX, the inner and outer wing box, the leading/trailing edge flaps, and the aileron. Former Boeing data had to be converted from CGSA/CASD (Boeing FEM Software) to MSC/Patran/Nastran. The CTR/AFT fuselage and the Vertical Tail FE models were created by Northrop Grumman as Nastran models and used for the Swiss ASIP Study, see Figure 4.7.1. Those FE models required little modification.

Considerable effort will be expended to generate balanced load sets by defining Nastran Force and Grid card files that can be applied directly to the baseline FE model. The loading distribution will be adjusted at specific locations where remeshing of component models was necessary. SF anticipates working with a full baseline FE model with coarse FE dummy structures included. The final decision whether SF will proceed with a full or half model will be influenced by the computer graphics adapter performance of our IBM WS 43P-150 computers.

With a full model, symmetric and anti-symmetric boundary conditions along the A/C plane of symmetry could be omitted, balance checks could be more efficiently performed, and the test set up would be simplified and easier to visualize. The test rig is anticipated as a coarse FE model. The test cylinder loads from the loading program will be applied to the whiffle tree FE model and redistributed to the a/c baseline FE model. The model will be statically constrained coincident with the test article constraint system.

The MSC/Patran/SuperModel software allows balance checks relative to any reference point. Also, graphical display of bending, shear and torque distribution can be plotted along any reference line. With this tool verification of applied fatigue load input is readily performed.

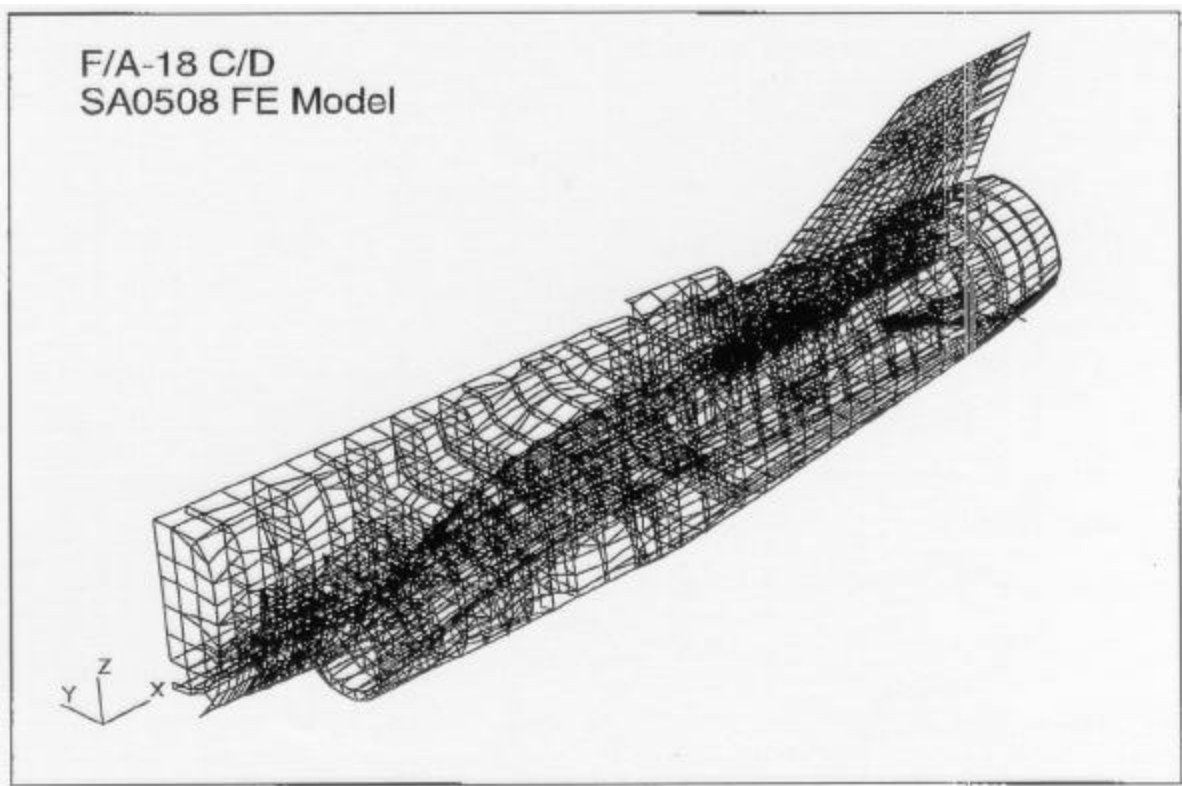


Figure 4.7.1 Swiss F/A-18 Nastran / Patran Center / After fuselage FE model

4.8 REFERENCES

- [1] W. A. Herman, R. W. Hertzberg, C. H. Newton and R. Jaccard, "A Reevaluation of Fatigue Threshold Test Methods". Fatigue 87, 3rd. Int. Conf. on Fatigue and Fatigue Thresholds, June 1987. Vol.. 2, pp. 819-828.
- [2] W. A. Herman, R. W. Hertzberg, and R. Jaccard, "A Simplified Laboratory Approach for the Prediction of Short Crack Behavior in Engineering Structures". Fatigue Fract. Engineering Materials and Structures Vol. 11 No. 4, pp. 303-320, 1988.
- [3] R. W. Hertzberg, W. A. Herman, T. Clark and R. Jaccard, "Simulation of Short Crack and Other Low Closure Loading Conditions Utilizing Constant $K_{max}DK$ -Decreasing Fatigue Crack Growth Procedures". Small -Crack Test Methods, ASTM STP 1149, J. M. Larsen and J.E. Allison, Eds., ASTM, 1992, pp.197-220.
- [4] Jaccard, R., "Fatigue Crack Propagation in Aluminium", IIW Doc. XIII-1377-90
- [5] R. Jaccard, "Fatigue Behavior of AlMgSi0.7 Aluminium Alloys - Evaluation of the Early Stage of Fatigue Crack Propagation Using SEM Microscopy and LEFM". RILEM Workshop, Naples, May 29th-31st, 1990.
- [6] R. Jaccard, "Fatigue Life Prediction of Aluminium Components Based on Local Stress Fields, Defect Conditions and Fatigue Crack Propagation Rates". 3rd Int. Conference on Aluminium Weldments, April 1985, pp. IV-5-40.
- [7] Graf, U., "Bruchmechanische Kennwerte und Verfahren für die Berechnung der Ermüdungsfestigkeit geschweisster Aluminiumbauteile", TU München, 3/92.
- [8] R. Jaccard, M. H. Ogle, "Aluminium Eurocode - Design for Fatigue", Int. Conf. on Performance of Dynamically Loaded Welded Structures." WRC Proceedings IIW, 1997
- [9] R. Jaccard, "Zum Bruchverhalten von Aluminiumbauteilen", Stahlbau 67 (1998) Sonderheft
- [10] ICAF 1997, Country review: Switzerland
- [11] M. Gottier, A. Kuo, S. Mc Cord, Application of Full Scale Test Result to Structural Modification, 17th Symposium of ICAF, June 9 – 11, 1993

**REVIEW OF AERONAUTICAL FATIGUE INVESTIGATIONS IN GERMANY
DURING THE PERIOD JUNE 1997 TO APRIL 1999**

Compiled by Claudio Dalle Donne

German Aerospace Center
Institute of Materials Research
D-51170 Cologne
Germany

Mailing Addresses of Contributing Companies and Institutes:

DA-BRE	DaimlerChrysler Aerospace Airbus GmbH, D-28183 Bremen
DA-HAM	DaimlerChrysler Aerospace Airbus GmbH, PO-Box 950109, D-21111 Hamburg
DA-LM	DaimlerChrysler Aerospace Airbus GmbH, LMT 21, PO-Box 801160, D-81663 Munich
DLR-WF	German Aerospace Center DLR, Institute of Materials Research, D-51170 Cologne
IABG	Industrieanlagen-Betriebsgesellschaft mbH, PO-Box 1212, D-85503 Ottobrunn
IMA	Materialforschung und Anwendungstechnik GmbH, PO-Box 800144, D-01101 Dresden
LBF	Fraunhofer Institute for Structural Durability, Bartningstraße 47, D-64289 Darmstadt
TUC-IMAB	Technical University of Clausthal, Institute for Plant Engineering and Fatigue Analysis, Leibnizstraße 32, D-38678 Clausthal-Zellerfeld
UniBw-M	University of the Federal Armed Forces Munich, Department of Materials Science, D-85577 Neubiberg
Uni-Si	University of Siegen, Department of Materials Science and Testing, D-57068 Siegen

The review has been prepared for presentation at 1999 Meeting of the International Committee on Aeronautical Fatigue.

1	METALS	5/4
1.1	FATIGUE BEHAVIOUR OF NOTCHED AND UNNOTCHED MATERIALS	5/4
1.1.1	Some Investigations on the Effect of Corrosion on the Fatigue Life of a High-Strength Al-Alloy	5/4
1.2	LOW CYCLE FATIGUE	5/5
1.2.1	Fatigue Testing of Thermal Barrier Coatings for Turbine-Blades under Realistic Testing Conditions	5/5
1.2.2	Influence of New Ti-Al Coatings on Fatigue Life of Ti-Alloys	5/6
1.2.3	The Effect of Environment on the Low-Cycle Fatigue Behaviour of a Near- γ Titaniumaluminide at High Temperatures	5/7
1.2.4	High-Temperature Deformation Behaviour and Damage Mechanisms of the Near- α Titanium Alloy IMI 834	5/9
1.2.5	The Influence of Hydrogen on the Mechanical Properties of β -Titanium Alloys	5/11
1.2.6	Effect of Pre-Deformation on the Cyclic Deformation Behaviour and the Microstructure of Particle-Strengthened Ni-Base Superalloys	5/12
1.3	CRACK PROPAGATION AND FRACTURE MECHANICS	5/14
1.3.1	A CTOD Approach to Assess Stable Tearing under Complex Loading Conditions	5/14
2	WELDED JOINTS	5/15
2.1.1	Fatigue Assessment of Aluminium Weldments	5/15
2.1.2	Fatigue Performance of Friction Stir Welded Butt Joints	5/16
3	FATIGUE LIFE ASSESSMENT	5/17
3.1.1	A New Stress Damage Parameter for the Fatigue Lifetime Prediction	5/17
3.1.2	Lifetime Prediction of Particulate Reinforced Aluminium Alloys under Cyclic Loading Considering the Statistical Size Effect	5/18
3.1.3	Dent Assessment Guideline: A Method to Assess Dents in Fuselage Skins Regarding Durability	5/19
4	FULL SCALE TESTING	5/20
4.1.1	Test to Determine the Effect of Multiple Site Damage on the Residual Strength Capability	5/20
4.1.2	Damage Tolerance Test of Curved Fuselage Panels	5/22
4.1.3	A340-600 EF2 Full Scale Fatigue Test for Center Fuselage and Wing	5/23
4.1.4	Eurofighter EF2000 Major Airframe Fatigue Test	5/25
4.1.5	Static Loading and Fatigue Life Test of Extra EA-400	5/26
4.1.6	Full Scale Fatigue Test with a CFRP Outer Wing Box	5/28
4.1.7	Fatigue Life Demonstration Tests on the CFRP Vertical Stabilizer of Airbus A 330-200	5/30
5	INVESTIGATIONS OF GENERAL INTEREST	5/32
5.1.1	Fatigue Strength of Smooth and Notched Specimens under High Mean Stresses	5/32
5.1.2	Experimental Investigation on the Cyclic Behaviour of Deformed Steel Sheets	5/33
6	REFERENCES	5/34

1 METALS

1.1 FATIGUE BEHAVIOUR OF NOTCHED AND UNNOTCHED MATERIALS

1.1.1 Some Investigations on the Effect of Corrosion on the Fatigue Life of a High-Strength Al-Alloy

R. Bochmann, DA-LM

All tests were carried out using flat specimens with $K_t=1.0$ cut from a 50 mm thick plate of 7075-T7351. The effect of corrosion on the fatigue life was investigated with pre-corroded specimens. These specimens were exposed for 168 h to a salt-fog of 3.5% salt solution at 35°C. Significant corrosion attack was observed after this exposure. FALSTAFF load spectrum was applied for the fatigue testing. The fatigue life degradation of the pre-corroded specimens compared to the base material is shown in Fig. 1.

A few samples were used to get information about a possibly more realistic corrosion scenario experienced in service. These specimens were first fatigue loaded for a pre-determined number of flights. Subsequently they were exposed to the corrosion environment as described above and finally fatigued until failure. The results in Fig. 2 indicate a not necessarily expected behaviour. The fatigue life to failure after exposure to corrosion seems to be independent of the initial fatigue loading.

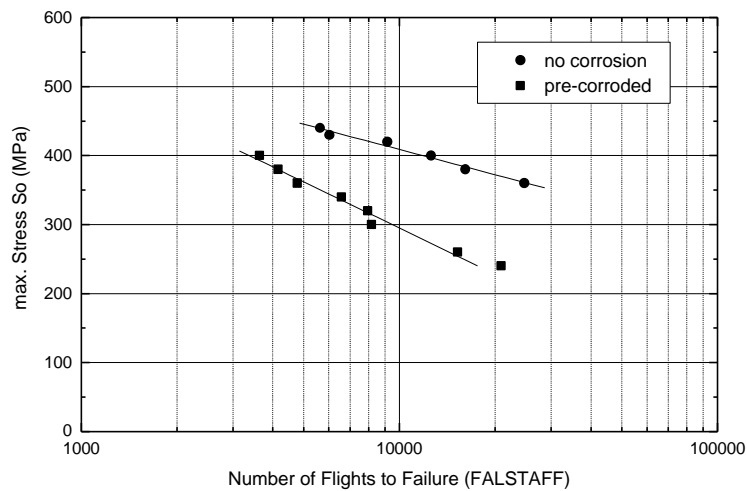


Fig. 1: Effect of corrosion on the fatigue life of 7075-T7351.

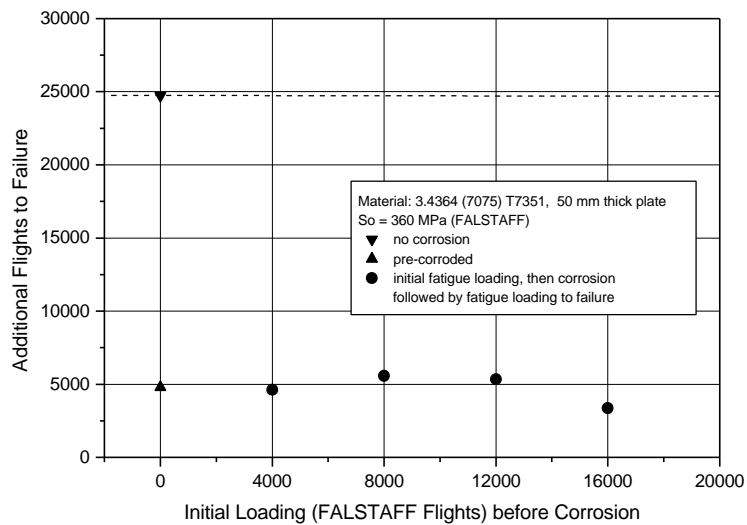


Fig. 2: Influence of the initial fatigue loading on the additional flights to failure after a corrosion exposure.

1.2 LOW CYCLE FATIGUE

1.2.1 Fatigue Testing of Thermal Barrier Coatings for Turbine-Blades under Realistic Testing Conditions

M. Bartsch, G. Marci, K. Mull and C. Sick, DLR-WF

Thermal barrier coatings (TBC) on components with inner cooling have a high potential with respect to higher turbine gas temperatures and hence reduced fuel consumption of turbine engines. To exploit this potential the coatings must however reliably withstand the extreme thermal and mechanical fatigue loading conditions in the turbines. Failure of the TBC at increased gas temperatures would lead to failure of the whole component.

Demonstration of TBC's reliability requires realistic testing, to make sure that lifetime determining mechanisms under testing conditions are the same as in real engines. Therefore a thermal gradient mechanical fatigue (TGMF) testing equipment was developed, which allows simultaneous mechanical and thermal loading, including thermo-shock [1, 2]. For heating, the radiation of four bulbs is focused on the specimen by elliptical mirrors. Sliders with integrated vents for cold air simulate the rapid cooling conditions of thermo-shocks, Fig. 3. Inner air-cooling of the hollow cylindrical specimens implies higher temperatures within the TBC than in the metallic substrate, Fig. 5. The strain in the TBC is imposed by the deformation of the metallic substrate.

The loading test-cycle was selected on the basis of a standard flight of an civil airliner with start, cruise and landing cycles, Fig. 4. The thermomechanical load is adjusted under the assumption that the metal blade or specimen substrate determines the thermomechanical loading conditions imposed on the TBC. Therefore thermomechanical load level is regulated by matching the life of a specimen without TBC to the life of a real turbine blade. The TBC-lifetime for different service conditions will be determined.

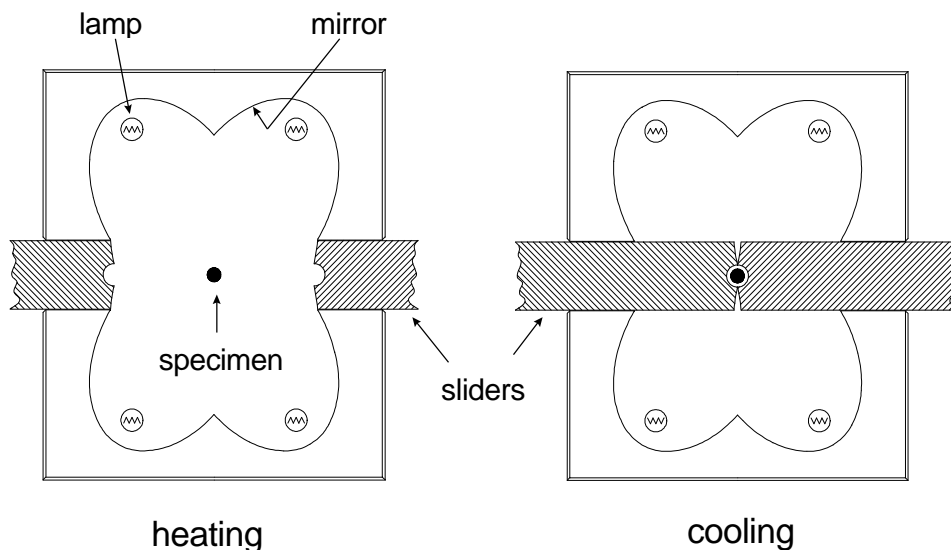


Fig. 3: Radiation heating system and sliders with integrated air-cooling to simulate thermo-shock conditions.

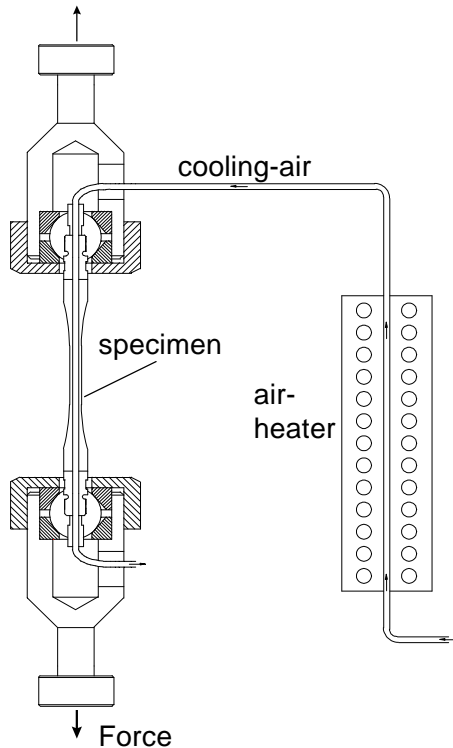


Fig. 5: Gripping arrangement for the cooled specimen.

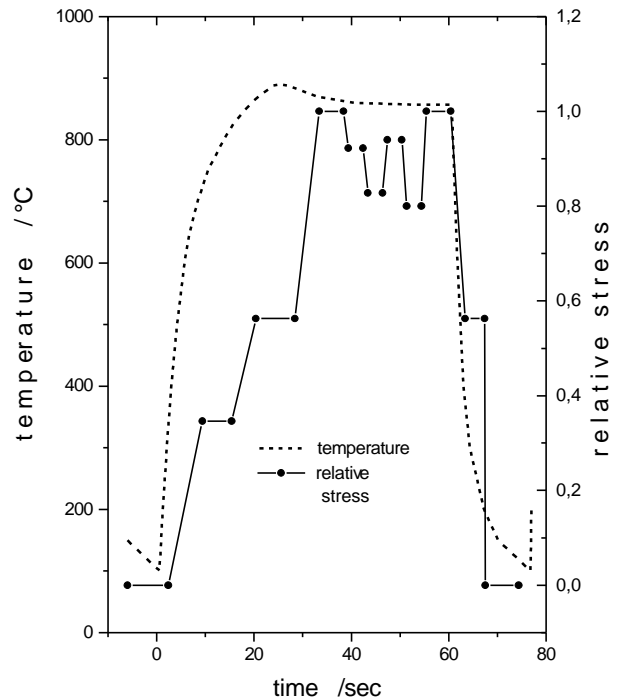


Fig. 4: Load and temperature spectrum during TGMF-tests simulating one flight cycle.

1.2.2 Influence of New Ti-Al Coatings on Fatigue Life of Ti-Alloys

C. Leyens, DLR-WF

Titanium alloys are prone to oxidising atmospheres due to the formation of non-protective, mixed oxide scales as well as the embrittlement of the subsurface zone. In order to expand the useful lifetime and even improve the high temperature capabilities of titanium alloys for aeroengine applications, researchers at the German Aerospace Center (DLR) have developed oxidation resistant coatings based on the binary Ti-Al system [3], which have proven to considerably decrease the mass gain after exposure as well as to prevent the embrittlement by penetration of oxygen and nitrogen. Furthermore, the coatings beneficially influenced the ductility of the base alloy after long-term exposure [4] and improved lifetime under creep conditions [5]. Probably most importantly, constant strain fatigue tests at $R_e=0$ of Ti-Al coated TIMETAL 1100 at 600°C revealed that the fatigue behavior was not significantly affected by the use of the coating systems, Fig. 6. In fact for 4µm thin magnetron sputtered multilayer and gradient Ti-Al coatings the fatigue data was identical with that obtained from the uncoated base material. Although an improvement of the fatigue resistance would be highly desirable from an engineering standpoint, it was probably the first time that coating systems on titanium alloys were shown *not* to *degrade* the fatigue properties of the substrate material [6]. Ongoing research is focussed on further improvement of the environmental resistance of the coating systems by the addition of ternary and quaternary elements and their impact on the fatigue behavior of the base alloy.

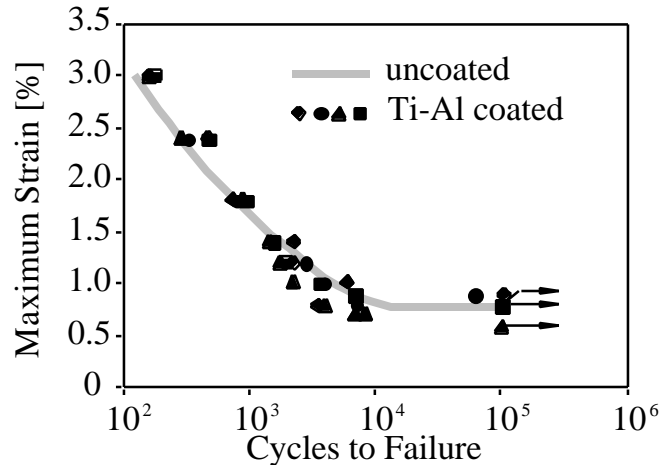


Fig. 6: Maximum strain vs. cycles to failure for uncoated and Ti-Al coated TIMETAL 1100 at 600°C in air.

1.2.3 The Effect of Environment on the Low-Cycle Fatigue Behaviour of a Near- γ Titaniumaluminide at High Temperatures

F.O.R. Fischer, H.J. Maier and H.-J. Christ, Uni-Si

Near- γ titaniumaluminides are promising candidate materials for various components in advanced gas turbine engines, as these alloys possess excellent weight-specific properties. In recent years much work has been directed towards improving the low ductility and poor fracture toughness of γ -TiAl at ambient temperature. As γ -TiAl alloys move closer to implementation, reliability under high-temperature service conditions is a key issue. Titanium aluminides, however, suffer from poor oxidation resistance. Environmental degradation might thus restrict the use of γ -TiAl for high-temperature components. Research addressing environmental effects on the high-temperature fatigue behaviour is still rather limited.

The material studied had a nominal composition of Ti-47Al-2Nb-2Mn (in wt-%). To improve low temperature ductility the material contained 0.8 vol.-% TiB₂. For fatigue testing smooth cylindrical specimens with a gauge length of 14 mm and a gauge diameter of 8 mm were machined from investment cast and hot isostatically pressed material. After heat treatment a duplex microstructure resulted. Prior to fatigue testing the gauge sections were electropolished to eliminate surface flaws. The fatigue experiments were performed under isothermal test conditions in fully reversed total strain control using a triangular wave-shape. The test temperature was varied in the range from 500 to 750°C, and the strain rate was kept constant at $3 \times 10^{-3} \text{ s}^{-1}$. Environment degradation was studied in fatigue tests run in air and high-vacuum ($p < 10^{-5} \text{ hPa}$), respectively. Fatigue testing was done both under symmetrical push-pull conditions, i.e. $R_e = -1$, and at $R_e = 0.1$. The latter tests allowed to assess the effect of mean stresses on fatigue life. Scanning electron microscopy (SEM) was employed to identify the relevant damage mechanisms. The evolution of the microstructure was characterized by transmission electron microscopy (TEM).

Fatigue behaviour was found to be drastically different below and above the brittle to ductile transition temperature, which is about 650°C for the alloy studied. At temperatures below 650°C, rapid initial cyclic hardening followed by a pronounced cyclic saturation state was observed. In tests run at 700 and 750°C cyclic softening dominated the cyclic stress-strain response. The cyclic stress amplitude for a given strain amplitude did not change much over the temperature range studied. However, fatigue life was found to increase by an order of magnitude if the temperature was increased from 500 to 700°C. Similarly, fatigue life was increased by at least an order of magnitude in high-vacuum as compared to tests run in air. The test results obtained in vacuum and air, revealed that the environmental effect on fatigue life was maximum at a test temperature of about 600°C.

At temperatures above the brittle to ductile transition temperature, large environmental effects are expected resulting from the poor oxidation resistance of the alloy. SEM indicated that at $T \geq 700^\circ\text{C}$ a thick titanium-rich oxide layer forms, Fig. 7. It

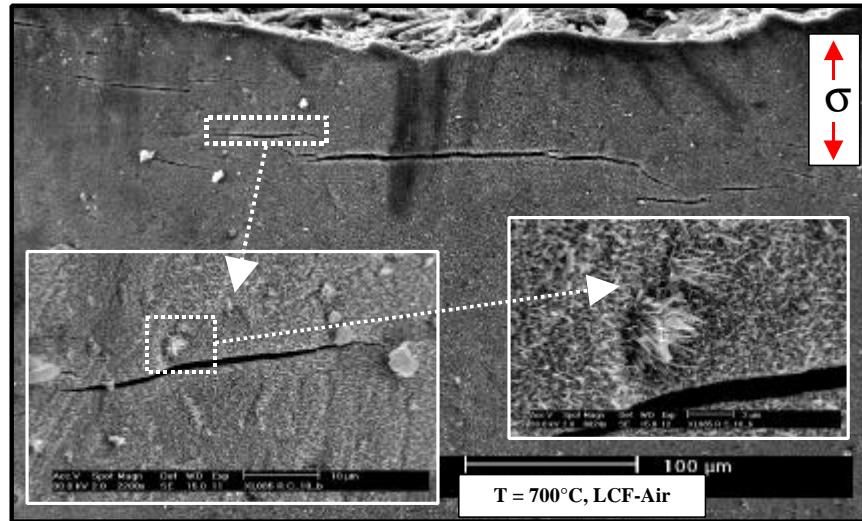


Fig. 7: Surface morphology of the low-cycle fatigue specimen tested in air at 700°C.

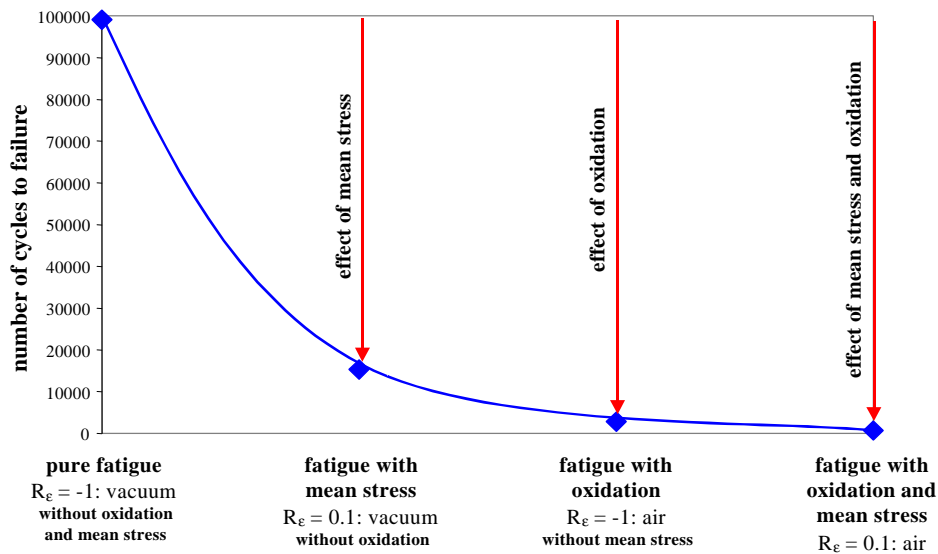


Fig. 8: Number of cycles to failure at 600°C for different test conditions.

is concluded that the fatigue properties are degraded as crack initiation and early crack growth are eased in the oxygen-rich embrittled subsurface layer that was formed underneath the non-protective outer oxide layer.

If the test temperature is lowered, oxidation kinetics is reduced and an increase in fatigue life should result. However, at a test temperature of 600°C, i.e. slightly below the ductile to brittle transition temperature, oxidation resistance was still rather poor. Initiation of small cracks was promoted by the oxide layer formed, and rapid crack propagation in the brittle material resulted in drastically reduced fatigue life as compared to tests run in high-vacuum. Consequently, environmental degradation is most pronounced at a temperature of about 600°C, where the material already behaves in a brittle manner and oxidation is still rapid. Fig. 8 quantifies the effect of environmental attack and mean stress on cyclic lifetime for this temperature.

1.2.4 High-Temperature Deformation Behaviour and Damage Mechanisms of the Near- α Titanium Alloy IMI 834

S. Hardt, P. Pototzky, H.J. Maier and H.-J. Christ, Uni-Si

The high-temperature fatigue and creep behaviour of the near- α titanium alloy IMI 834 was studied at temperatures up to 650°C. This titanium alloy was developed primarily for rotating components in the compressor part of jet engines. Initially, an upper service temperature of 600°C was envisaged for IMI 834. In some applications, however, the alloy is already used for high-temperature components where temperature excursions reach about 650°C. In order to identify the relevant damage mechanisms and their influence on fatigue life, fatigue tests were carried out under isothermal and thermomechanical conditions. The test program under isothermal conditions involved continuous cycling, dwell tests with hold periods in tension and compression, and asymmetrical strain-time cycles. All fatigue tests were carried out under true plastic strain control, with the exception of the tests containing hold periods.

If the maximum temperature does not exceed 600°C, planar dislocation slip prevails and similar microstructures are formed regardless of the test temperature and the testing mode in the fatigue test. Wavy dislocation slip was found to determine stress-strain behaviour when the maximum temperature was higher than 600°C. Independent of the test temperature, rapid initial cyclic softening was observed in all fatigue tests, Fig. 9. Initial cyclic softening was followed by moderate cyclic hardening at lower test temperatures up to 400°C. At intermediate temperatures cyclic saturation behaviour was found. At high test temperatures of 650°C the bimodal microstructure of the alloy, which is recommended by the manufacturer, was unstable throughout the fatigue tests. The coarsening of silicide precipitates and the disintegration of lamella boundaries resulted in continuous cyclic softening at 650°C.

Generally fatigue cracks initiate rapidly at planar slip bands that intersect the surface. As temperature is increased, oxygen diffusion into the matrix becomes important and a brittle subsurface layer is formed. Thus, environmental degradation becomes the dominant damage mechanism when the test temperature was 600°C or higher. Fatigue cracks initiated and propagated easily in the brittle oxygen-enriched layer. Thus, the fatigue cycles containing the highest tensile stresses led to the lowest fatigue life. This is shown in an exemplary fashion in Fig. 10, where fatigue cycles containing hold periods in the compressive part of the cycle yield the lowest number of cycles to failure. This was also found to be true for thermomechanical fatigue tests as shown in Fig. 11, where out-of-phase tests were much more detrimental than in-phase tests.

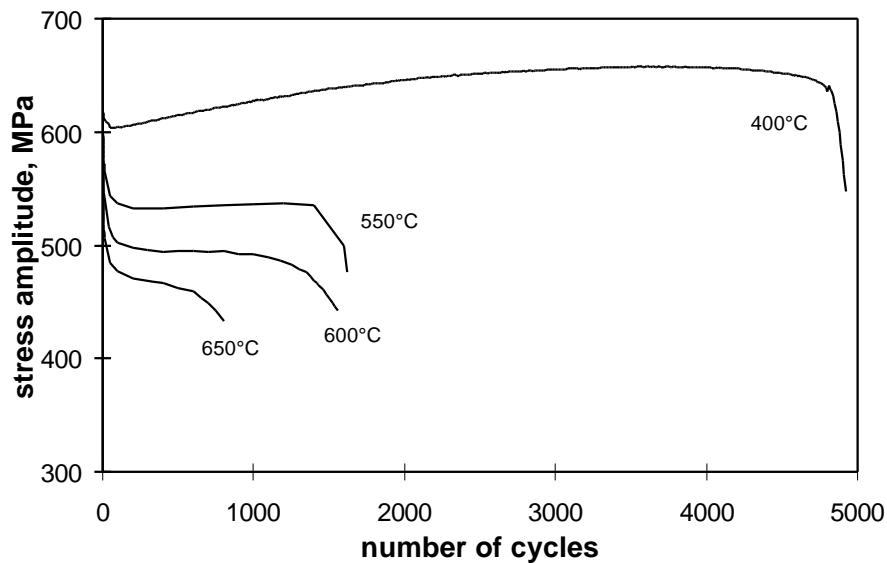


Fig. 9: Cyclic stress response of bimodal IMI 834 at different test temperatures and $\Delta\varepsilon_{pl}/2=0.2\%$. Plastic strain rate was $8 \cdot 10^{-4} \text{ s}^{-1}$ in each test.

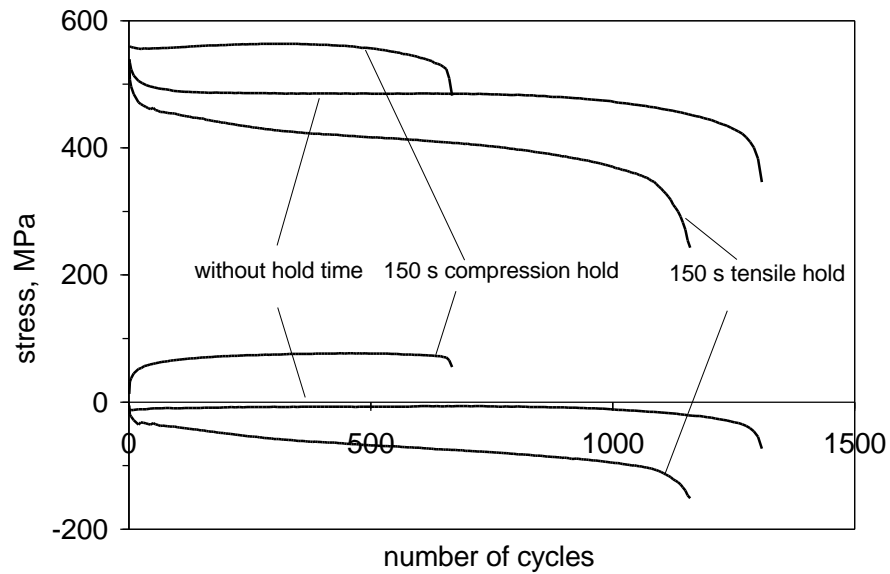


Fig. 10: Effect of hold time on cyclic stress response of bimodal IMI 834 in total strain controlled fatigue tests at $T = 600^{\circ}\text{C}$ and $\Delta\epsilon_{pl}/2 = 0.17\%$. Plastic strain rate was $8 \cdot 10^{-4} \text{ s}^{-1}$ in each test.

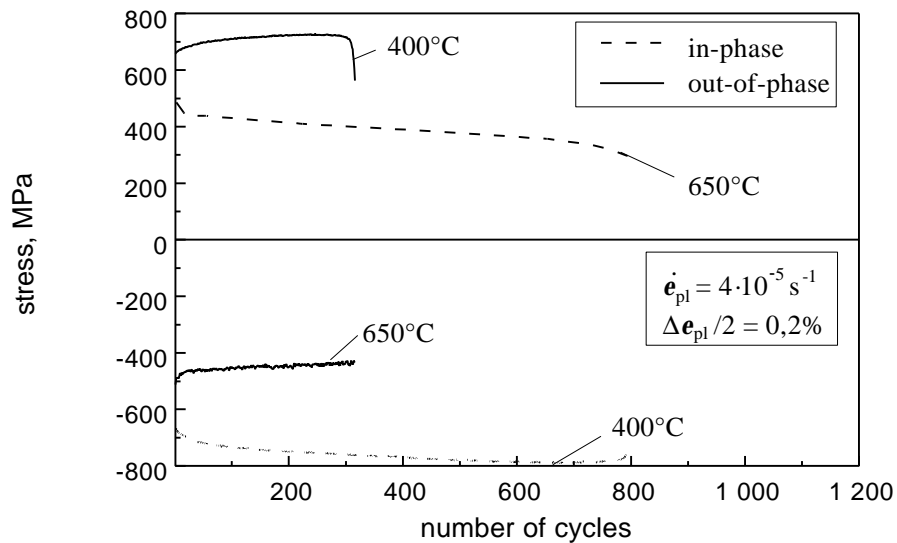


Fig. 11: Cyclic stress response of bimodal IMI 834 under thermomechanical conditions (upper part: maximum stress, lower part: minimum stress with respective temperature). In-phase and out-of-phase tests were carried out in the temperature range from 400 to 650°C.

1.2.5 The Influence of Hydrogen on the Mechanical Properties of β -Titanium Alloys

A. Senemmar and H.-J. Christ, Uni-Si

Titanium alloys are well-established for applications in the aerospace industry due to the combination of their high strength, their low density and their excellent corrosion resistance. However, the applicability of titanium alloys is strongly restricted because of their hydrogen susceptibility which can lead to serious embrittlement effects. On the other hand, β -titanium alloys as a special class of titanium alloys are considered to be quite insensitive against hydrogen embrittlement because of their high hydrogen solubility as compared to α and $\alpha+\beta$ titanium alloys. However, only little information exists on the influence of hydrogen on the mechanical properties of β -titanium alloys.

The objective of the present study is to investigate the effects of hydrogen on microstructure and to characterize the changes in mechanical properties of β -titanium alloys. For this purpose three different commercial β -titanium alloys were tested after being exposed to various hydrogen concentrations. The materials studied are the metastable alloys Ti 21S and Ti 10-2-3 as well as the stable β -alloy Alloy C (Ti-35Cr-15V). The mechanical properties were characterized by means of tensile tests, fatigue tests under total strain control, fatigue crack propagation tests and Charpy impact tests. It was found that hydrogen has an influence on the microstructure of Ti 21S and leads to a reduction of the mean size of the α -precipitates, in combination with a slight decrease on the volume fraction of the α -phase. The results of the fatigue tests on this alloy (Ti 21S) indicate that hydrogen reduces the strength and extends the cyclic lifetime of the alloy, whereas in the stable β -titanium Alloy C hydrogen leads to an increase of the strength and a decrease of the lifetime under cyclic loading conditions. Fig. 12 represents cyclic deformation curves of Ti 21S at a total strain amplitude of $\Delta\varepsilon/2=1.5\%$. The hydrogen was introduced into the material during the solution treatment (871°C, 2h) from the gas phase. Subsequently ageing at 538°C for 8h was carried out. Fig. 13 shows cyclic deformation curves of Alloy C at $\Delta\varepsilon/2=1.5\%$. There again, hydrogen was introduced into the material during solution treatment (815 °C, 2h) from the gas phase. The fundamental difference in the effect of hydrogen is mainly attributed to the hydrogen related microstructural changes.

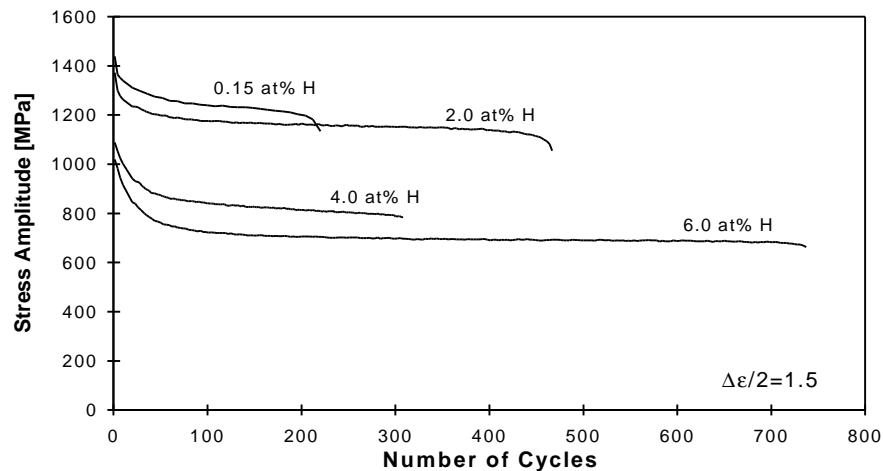


Fig. 12: Cyclic deformation curves of Ti 21S, hydrogen charged during solution annealing and subsequently aged.

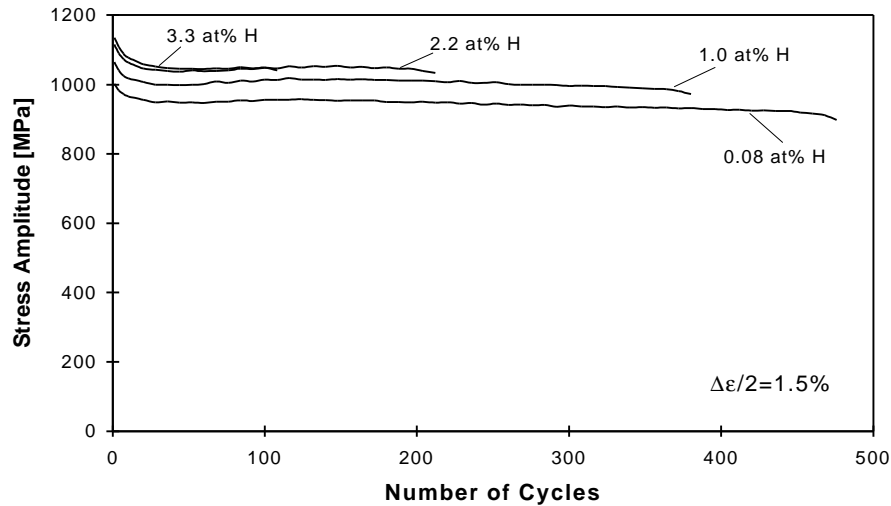


Fig. 13: Cyclic deformation curves of Alloy C in solution annealed condition with different hydrogen concentrations.

1.2.6 Effect of Pre-Deformation on the Cyclic Deformation Behaviour and the Microstructure of Particle-Strengthened Ni-Base Superalloys

K. Schöler and H.-J. Christ, Uni-Si

In most cases engineering materials undergo a (thermo-)mechanical pre-treatment in order to optimize their mechanical properties or just during the production process. Therefore, the influence of such a pre-history on the subsequent cyclic deformation behaviour is of particular interest. Unfortunately, the effects of a pre-deformation depend on several parameters and influence the macroscopic mechanical properties and the microstructure in a complex way. Especially for materials with planar-slip behaviour a monotonic pre-deformation leads to a reduction of the cyclic life and shifts the cyclic stress-strain curve to higher values.

The dependence of the cyclic deformation behaviour and cyclic life on the pre-history was studied on polycrystalline Ni-base superalloys (Nimonic 75 and Nimonic 105) in three characteristic precipitation conditions (precipitation-free, peak-aged and over-aged). Cyclic deformation tests were carried out in the temperature range from RT to 800°C under true plastic strain control with superimposed control of the plastic strain value at zero stress. This so-called bimodal control keeps the plastic strain amplitude (at zero stress) constant in spite of changes in Young's modulus. Monotonic pre-deformations were carried out at RT under total strain control up to given total tensile strains ranging from 1 % to 8 %.

Under most conditions a pre-deformation causes an increase of the resulting stresses, a pre-damage and leads to a reduction of cyclic life. However, in certain cases a small pre-deformation was found to act beneficial and increase cyclic life, Fig. 14. For the precipitation hardened Nimonic 105 this can be attributed to pre-deformation-induced changes of the microstructure. During subsequent cyclic loading at high temperatures with low plastic strain amplitudes slip bands once formed remain active and lower the resulting stresses and strains.

In order to describe the effects arising from a mechanical pre-history, a new pre-deformation parameter was developed and applied. This pre-deformation parameter was calculated from damage parameters resulting from tests with and without pre-deformation. Its value correlates with the dependence of the cyclic deformation behaviour on the pre-history. It was found that the dependence on pre-history increases with decreasing test temperature, increasing degree of pre-straining, decreasing plastic strain amplitude and increasing hardening effect of precipitates. Furthermore, it could be shown that for planar slip materials the value of the pre-deformation parameter correlates with the inverse normalized cyclic life in a wide field of deformation conditions, Fig. 15.

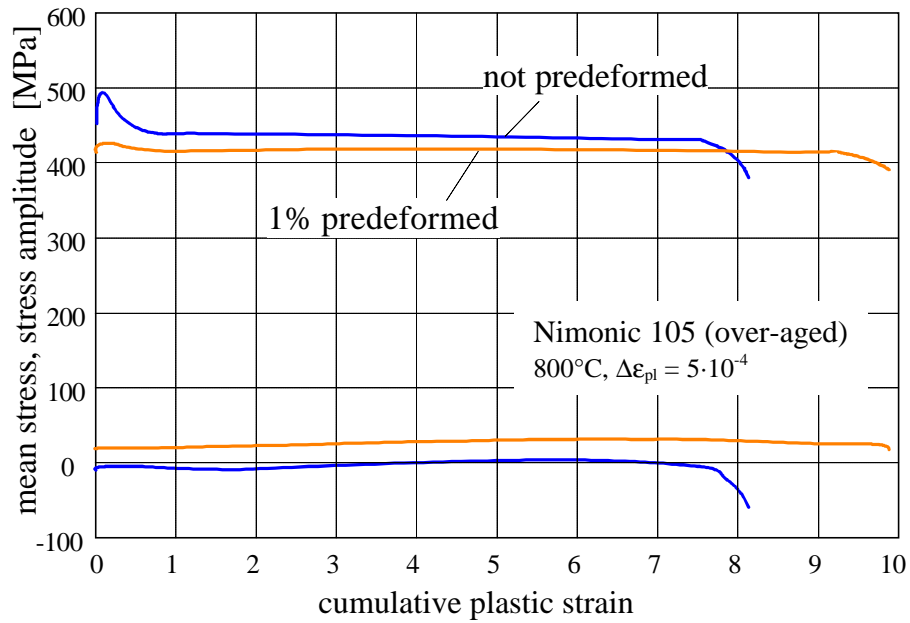


Fig. 14: Cyclic deformation curves of Nimonic 105 (over-aged) at 800°C and $\Delta\epsilon_{pl}=5\cdot 10^{-4}$ with and without pre-deformation.

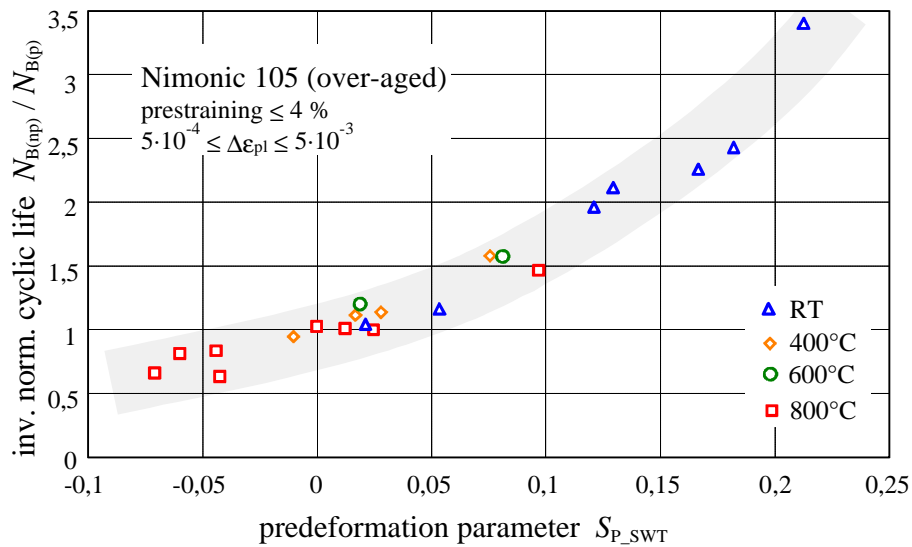


Fig. 15: Inverse normalized cyclic life versus the pre-deformation parameter of various fatigue tests under different conditions.

1.3 CRACK PROPAGATION AND FRACTURE MECHANICS

1.3.1 A CTOD Approach to Assess Stable Tearing under Complex Loading Conditions

C. Dalle Donne, DLR-WF

An engineering approach for assessing the ductile fracture of cracked thin structure based on the δ_5 crack tip opening displacement (ctod) is presented in [7, 8]. Standard laboratory tests and experiments with biaxially loaded cruciform specimens, Fig. 16, of 6 mm thick 2024-T3 sheets showed that the δ_5 -R-curves were reasonably independent of specimen geometry and applied loading conditions over almost the entire testing range. This was also found for inclined pre-cracks (mixed-mode I/II) and small cracks emanating from notches under biaxial loading. Only negative biaxial loading ratios, which lowered dramatically the constraint of plastic deformation ahead of the crack tip, led to an apparent increase of crack resistance. These constraint effects could however be quantified by a second parameter based on the linear elastic T-stress. The driving force was estimated with the Engineering Treatment Method (ETM), which required only the stress intensity factor and plastic limit load solutions of the considered structure as well as the material stress and strain power law as input parameters. Close agreement of ETM predictions to the experimental load versus δ_5 relationships or load-displacement curves can be achieved, if the proper plastic limit load solution of the cracked structure is available.

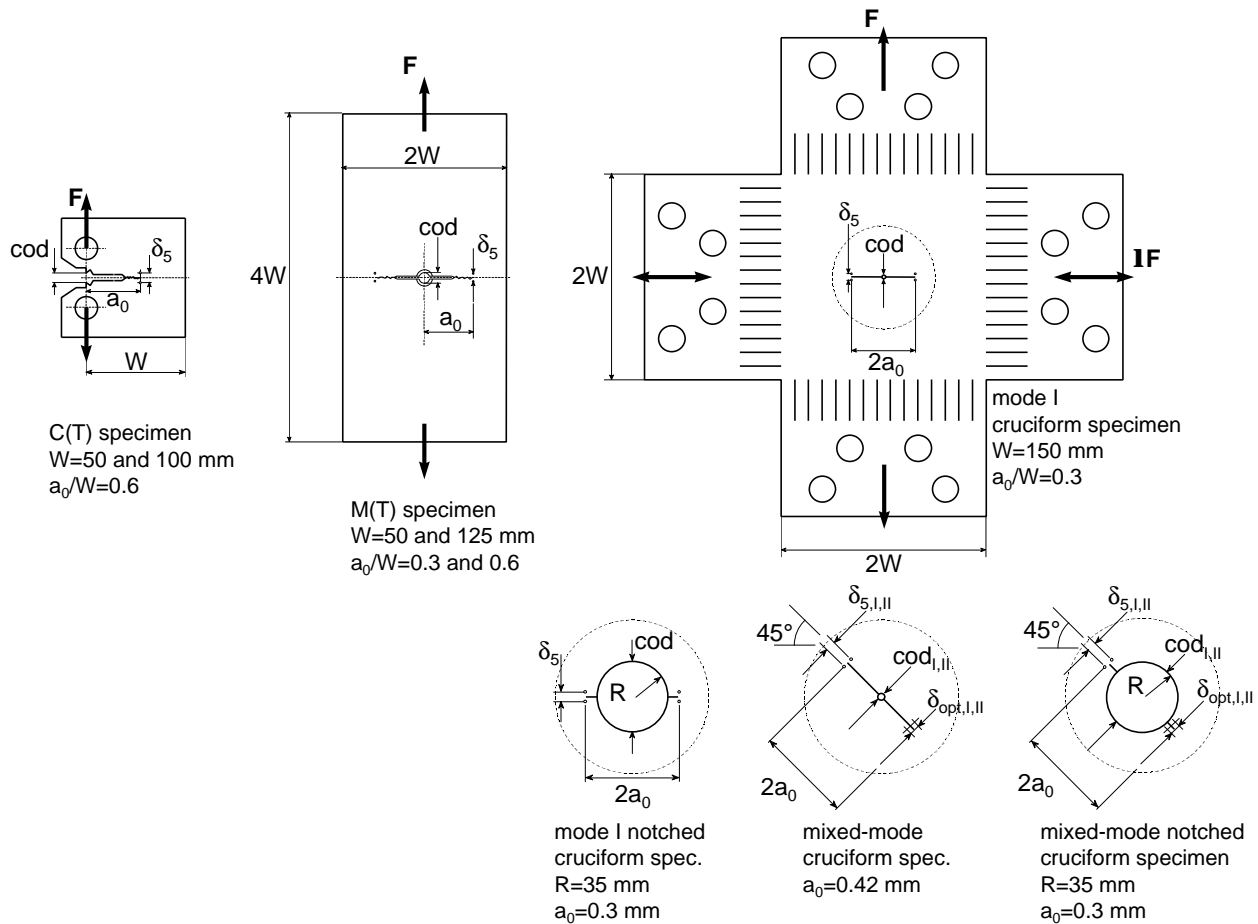


Fig. 16: Specimen configurations. The drawings in the lower right part of the figure show the cracked central part of the cruciform specimens.

2 WELDED JOINTS

2.1.1 Fatigue Assessment of Aluminium Weldments

U. Brandt, C. M. Sonsino, LBF

In this study, local approach and fracture mechanics concepts were used to predict the lifetime of aluminium weldments for a wide range of stress concentration factors. The fatigue behaviour of 5 and 25 mm aluminium-alloy butt weldments with full and incomplete penetration was investigated, Fig. 17. Such design details are found in different structures like truck frames, vessels, railway body-shells etc. Strain controlled fatigue tests of the 5083 aluminium-alloy base and 5183 weld metal were carried out to determine their cyclic material properties. Crack growth rate measurements were performed using center crack tension (CCT) specimens. Weldments with and without incomplete joint penetration (IJP) were fatigue tested under constant amplitude axial loading for stress ratios of $R=0$ and -1 . The fatigue life of the tested specimens was predicted using an analytical model which considers the lifetime to crack initiation and the crack propagation. As example, the comparison of the experimental and predicted lifetime of the 25 mm weldments is shown in Fig. 18 and Fig. 19.

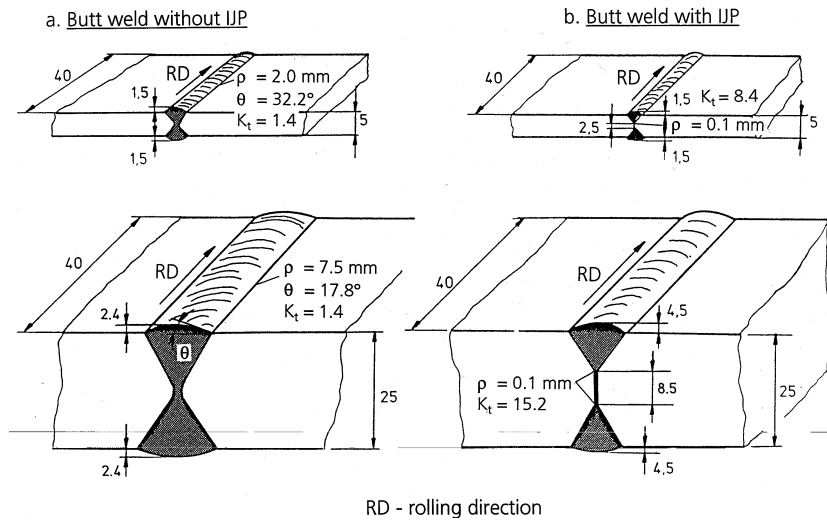


Fig. 17: Butt weldments with and without incomplete joint penetration (IJP).

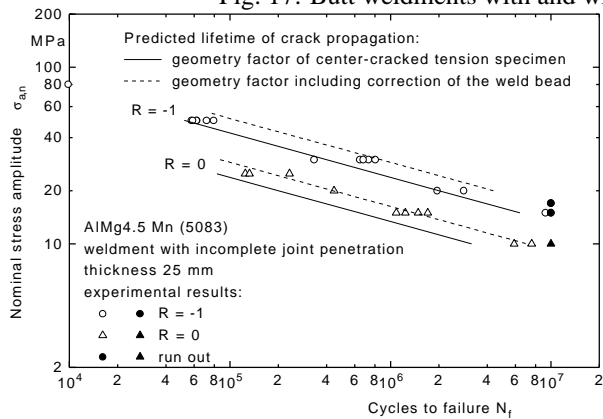


Fig. 18: Predicted crack propagation lifetime for 25 mm weldments with incomplete joint penetration.

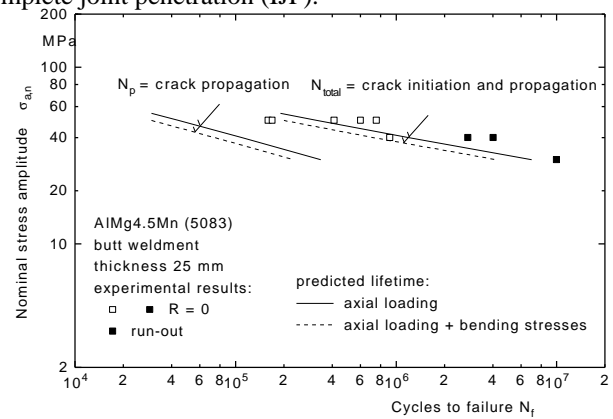


Fig. 19: Predicted lifetime for 25 mm full penetration butt weldments considering bending stresses.

2.1.2 Fatigue Performance of Friction Stir Welded Butt Joints

C. Dalle Donne and G. Biallas, DLR-WF

The friction stir welding (FSW) technique is a novel solid state joining process. It was developed by The Welding Institute (TWI) as an derivative of conventional friction welding processes. A friction stir butt weld is produced by plunging a rotating tool into the facing surfaces of the two plates, Fig. 20. The cylindrical tool consists of a shoulder and a pin emerging from it. As the rotating pin moves along the weld line, the material is heated up by the friction heat and stirred by the rotating pin in a process similar to extrusion. Since the temperatures are well below the melting point, problems associated with the liquid/solid phase transformation, such as porosity, solidification cracking, shrinkage and distortion are avoided. Therefore even high strength aluminium alloys like 2024 or 7075 which are generally considered as „difficult to weld“ with standard welding procedures can be joined with limited loss in joint strength.

Microstructural, mechanical and corrosive properties of FSW butt joints in 4 mm thick 2024-T3 were presented in [9, 10]. The sheets were joined on a milling machine using two types of proprietary tool designs (tool A and optimised tool B). Compared to the 2024-T3 base material following mechanical properties of the FSW joints were obtained:

- joint ultimate strengths of over 400 MPa or 80 % ultimate strength of the base material, with a maximum value of 432 MPa (87 %) for the optimised stirring tool
- better or comparable fatigue crack propagation behavior, Fig. 21
- fatigue strength amplitudes at 10^7 cycles ranging from 50 MPa to 100 MPa for the optimised tool in the as welded condition, Fig. 22
- higher or comparable crack resistance curves (R-curves) in terms of crack tip opening displacement

Currently FSW butt joints of 1.6 mm thick 2024-T3 are tested. The mechanical properties are even better than the ones of the 4 mm thick material. Ultimate joint strengths of over 90 % of the base material ultimate strength are obtained. The S-N data of the FSW-specimens tested in the „as welded“ condition fall in the base material scatterband [11].

Investigations on the corrosion properties revealed a certain sensitivity of the 2024-T3 joints to intergranular and exfoliation corrosion.

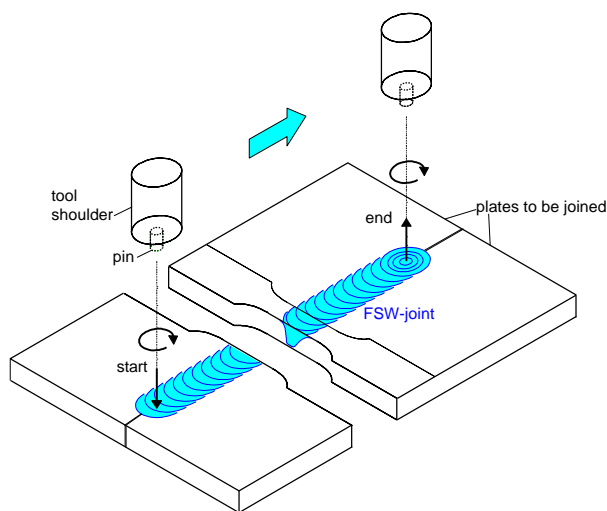


Fig. 20: Schematic of friction stir welding of butt joints.

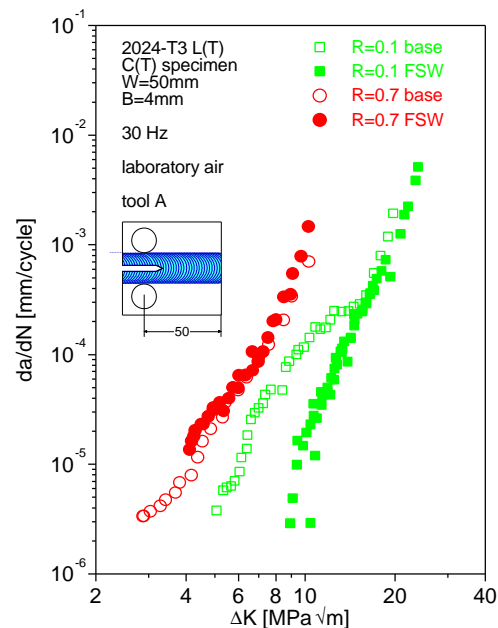


Fig. 21: Crack propagation rates in the friction stir welds produced with the tool A.

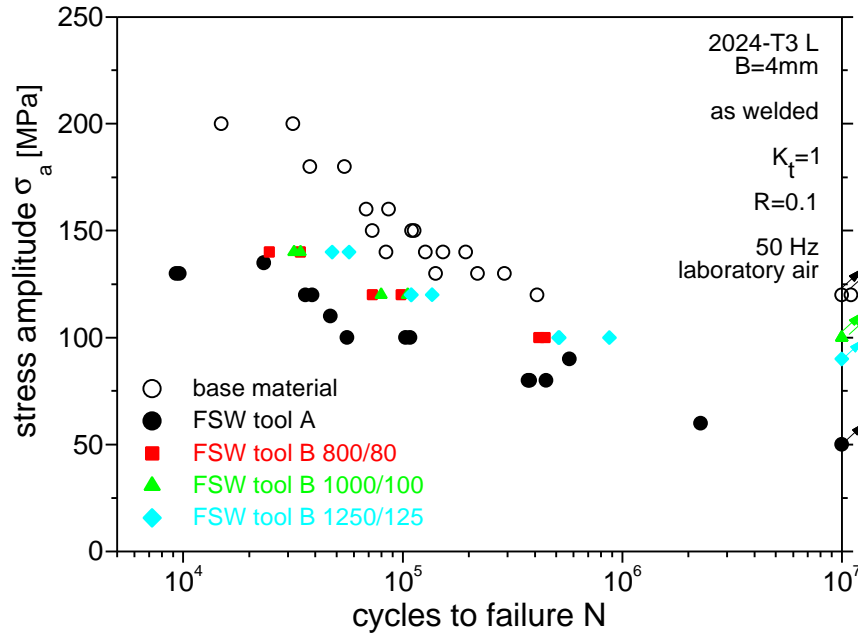


Fig. 22: Fatigue strength of base material and friction stir welded joints (the numbers in the legend indicate different welding parameters).

3 FATIGUE LIFE ASSESSMENT

3.1.1 A New Stress Damage Parameter for the Fatigue Lifetime Prediction

I. Bazios and H.-J. Gudladt, UniBw-M

Recently fatigue life predictions based on the accumulation of fatigue damage have received great attention. Especially for random fatigue loading various stress damage parameters have been developed to predict lifetime quantitatively by using an analytical concept. In general, there are two kinds of models: the first based on a global damage parameter and the second based on the formation of fatigue cracks propagating during the fatigue test. A stress damage parameter of the first type was proposed by Smith, Watson and Topper [12] and called P_{SWT} -parameter. The second type of parameter was proposed by Heitmann et al. [13] and labelled Z_d -parameter. In the first case, neither the notch geometry nor the size of the specimen has been taken into account. In order to estimate the influence of the specimen size on the fatigue life, a new stress damage parameter, P_{SI} , has been developed [14]. It is based on the P_{SWT} -parameter and includes the stress integral [15].

Fatigue tests have been undertaken with rolled AA6009-specimens with a central bore-hole ($K_t=3$) under constant amplitude loading. In Fig. 23 the stress amplitude is plotted against the crack initiation lifetime. A DC-potential drop method has been used for the determination of this lifetime. It was previously shown, that cracks with a length of at least $250 \mu\text{m}$ are detectable with this technique. It is clearly visible in Fig. 23 that the fatigue life prediction correlates very well with the experimental data, if the P_{SI} -parameter is used. Similar results have been found for random fatigue tests, as shown in Fig. 24. In this case, two different damage accumulation models (e.g. Miner as well as Manson) were taken into account. The stress-lifetime curve calculated with the new damage parameter P_{SI} correlates favourably with the 50% failure probability data, if the Miner damage accumulation model is used in the model.

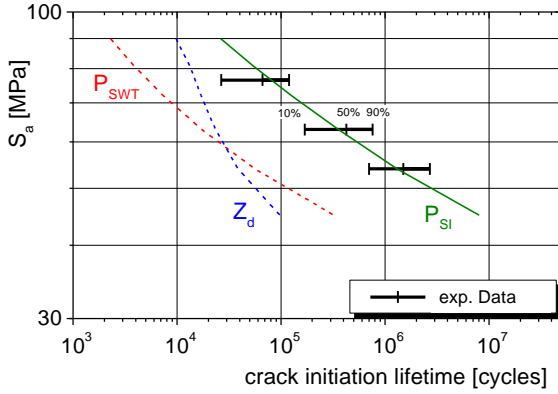


Fig. 23: Experimental constant amplitude stress versus life curves of AA6009-specimens with a central bore-hole ($K_t=3$) compared to the damage parameter predictions.

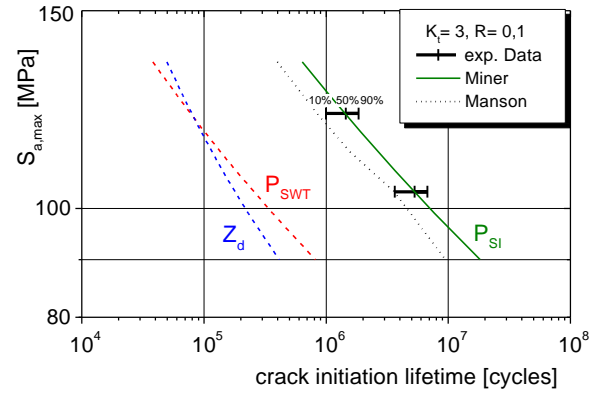


Fig. 24: Experimental random loading stress versus life curves of AA6009-specimens with a central bore-hole ($K_t=3$) compared to the damage parameter predictions.

3.1.2 Lifetime Prediction of Particulate Reinforced Aluminium Alloys under Cyclic Loading Considering the Statistical Size Effect

W. Berger, J.Bär and H.-J. Gudladt, UniBw-M

The statistical description of fatigue test data is necessary for a lifetime prediction of components. The standard specimen fatigue data is transferred to actual structure on the basis of the statistical size effect concept [15]. Further the stress conditions in the crack initiation region of the structure as well as the statistical distribution of the crack initiating defects in the material must be taken into account. Here the applicability of lifetime prediction models, which are based on a single crack initiating defect population, to metal matrix composites is investigated.

At the first glance, the assumption of a single crack initiating defect seems to be invalid for such a material [2], because of the heterogeneous structure and the variety of possible crack initiators, such as particle clusters, particle free areas and shots [16].

Metallographic examination of the extruded, aluminium oxide reinforced 6061-alloy showed a strong scatter in the particle volume content and an alignment of the particles in the extrusion direction. Further, cavities and non-metallic inclusions with diameter of up to 0.5 mm were found. The tests were carried out on a servohydraulic testing machine with smooth and notched specimens under uniaxial, stress-controlled cyclic loading until final failure of the specimens.

First, a statistical analysis is performed. On the basis of a Weibull distribution, the life lines for different probabilities of failure in double logarithmic S-N-diagram are described with the Basquin-equation $\sigma \cdot N^n = \text{const.}$. This equation enables the transformation of the unnotched specimen data to a constant cycle number $N = \text{const.}$. Now, the transformed stress values are presented as a cumulative frequency and analytically described with the general scatterband function:

$$P_{B,S}(\sigma_{\max}, N) = 1 - \exp \left[-Z \left(\frac{\sigma_{\max} \cdot N^n}{A_V} \right)^k \right] \quad (1)$$

The value $Z=S/S_0$ represents the ratio of the stress integrals of notched and unnotched specimens. The fit and the fit parameters are shown in Fig. 25.

For the life-prediction of the notched specimens the stress integrals of the respective specimen-geometry have to be calculated and have to be included in the scatterband function. This is done with the analytical solutions for stress integrals of cylindrical specimen according to Böhm [17]. The stress values predictions for the respective cycle number and for a given probability of failure P_B (10, 50 and 90%) are obtained by a transformation of the general scatterband function. The test data and the predicted life-lines for 10, 50 and 90% are presented in Fig. 26. The elastic-plastic notch stresses were calculated with the finite element method. The transformation of the maximum principal stress by the surface stress integral

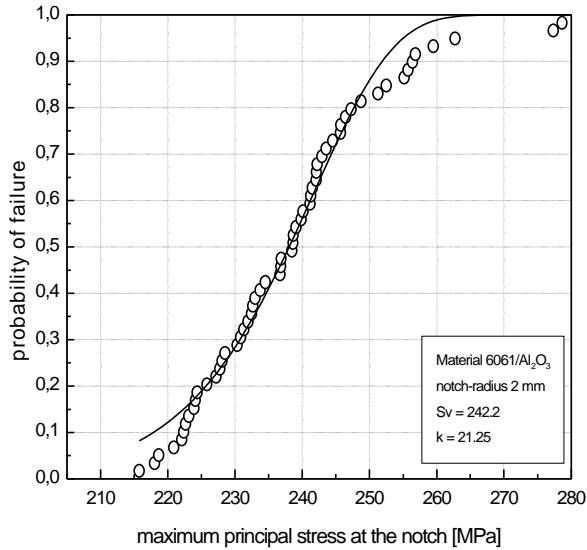


Fig. 25: Statistical data fit of notched specimen data (notch radius 2 mm).

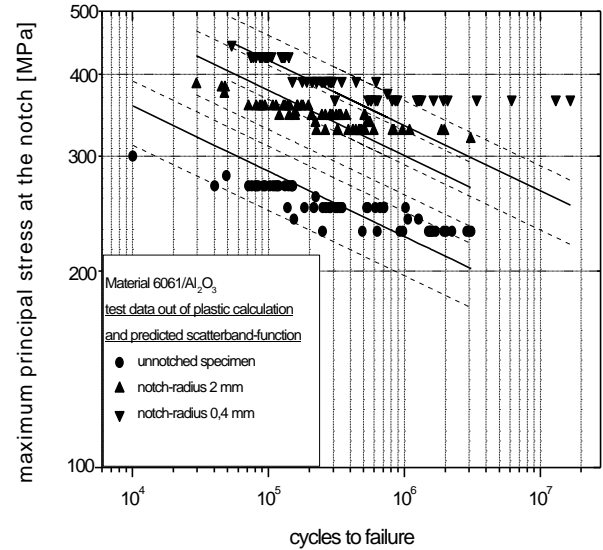


Fig. 26: Predicted stress versus life lines with scatterbands.

leads to good results and is always conservative. Consequently the fatigue life of simple components of metal-matrix-composites can be predicted with this approach.

3.1.3 Dent Assessment Guideline: A Method to Assess Dents in Fuselage Skins Regarding Durability

B. Schmidt-Brandecker, DA-HAM

In frame of the improvement program for the Structural Repair Manual (SRM) of all Airbus models DaimlerChrysler Aerospace Airbus (DA) developed a method which allows to assess dented fuselage skins by a simple approach. The aim of the method is to determine the fatigue life (durability) of the fuselage skin damaged by a dent. Based on the fatigue life factored by a sufficient scatter factor it can be decided whether a repair of the damaged area is necessary and when the repair has to be carried out.

The factored fatigue life is determined by a simple equation. A so-called basic factored fatigue life was defined for fuselage skin containing a dent with exactly defined details such as location, geometry, material, geometry of the dent, etc. The effect of deviating details can be easily assessed by determining factors considering the effect of the differences between the unique and the basic situation. The factored fatigue life THD for the unique dent is calculated by the following equation:

$$\text{THD} = \text{THD}_{\text{basic}} \times \text{STD} \times \text{DED} \times \text{MAD} \times \text{RID} \times \text{LOD} + \text{TID} \quad (2)$$

with:

THD _{basic} :	factored fatigue life of exactly defined geometry, loading and material
STD:	influence of the skin thickness
DED:	influence of the depth of the dent
MAD:	influence of the skin material
RID:	influence of location of adjacent riveting in relation to the dent
LOD:	influence of location of dented skin at the fuselage (considers the stress level)
TID:	time (number of flights) at incidence, to be added

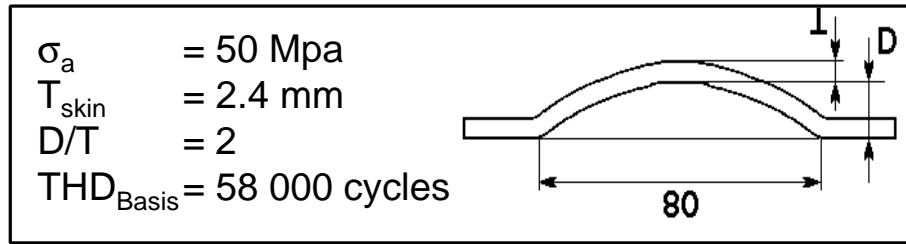


Fig. 27: Basic values for the Dent Assessment Guideline.

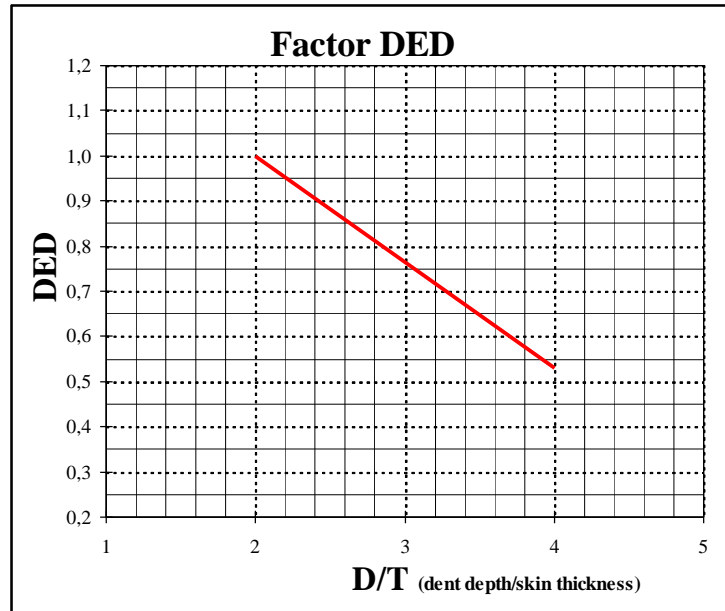


Fig. 28: Influence of depth of the dent.

The determination of all factors were supported by extensive coupon and component testing. The test program comprised: unstiffened coupons including dents, variations of the parameters described above and stiffened components containing dents at and between the stiffeners.

The basic fatigue life THD_{basic} is valid for the conditions shown in Fig. 27. As an example of the considered factors, the influence of the depth of the dent is shown in Fig. 28.

4 FULL SCALE TESTING

4.1.1 Test to Determine the Effect of Multiple Site Damage on the Residual Strength Capability

H. Trey, DA-BRE

Multiple Site Damage (MSD) in structural aircraft joints is defined as the simultaneous presence of cracks at multiple fastener holes that are of sufficient size and density whereby the residual strength of the joint is decreased by a certain value. Multiple Site Damage consequently leads to Widespread Fatigue Damage (WFD) where the structural joint will no longer meet the required residual strength. The examination of MSD phenomena therefore is a central item to the Ageing Aircraft Initiatives.

In frame of the European Ageing Aircraft SMAAC (Structural Maintenance of Ageing Aircraft) Project, which was partly funded by the European Commission under the BRITE EURAM programme, two large curved panels were tested at test facilities at NLR, Marknesse (NL).

The objective of these tests was to compare crack growth and residual strength of a complex pre-cracked structure without MSD (Panel 1) and in the presence of MSD (Panel 2). The two panels contained longitudinal lap joints, and were manufactured at DA. Both panels had the same overall geometry, but different crack scenarios were artificially created. The first panel (Panel 1) contained a lead crack only, whereas the second panel (Panel 2) contained an identical lead crack plus additional MSD cracks.

Fig. 29 illustrates the main features of both test panels. Both panels (3030 mm x 1128 mm) include longitudinal splice joints with a butt joint located over the central frame. An artificial crack (saw cut) of a length of $2a=530$ mm was cut symmetrically across the central butt joint in the upper rivet row (see Fig. 29). The central frame, clip and butt strap were also cut.

For the second panel an MSD-like situation was simulated by cutting small cracks at both sides of the artificial lead crack up to the end of the frame bay. These cracks extended 2.0 mm to both sides of each rivet (see lower left part of Fig. 29).

To initiate further fatigue crack growth at the tips of the lead crack up to a specified limit, both specimens were subjected to constant amplitude loading with the Airbus operational internal pressure at $R=0.1$.

The residual strength test was performed by a step-wise increase of the internal pressure up to a pre-specified limit or panel failure. The test results in Table 1 are related to the internal pressure at unstable crack extension of Panel 1, which was set to 100%. As indicated in Fig. 30, these results suggest a 15 % decrease of the residual strength of Panel 2 due to the presence of MSD cracks.

Table 1: Test results of large curved panels (the loads are related to the load at unstable crack extension of Panel 1)

Panel	Length of lead crack	MSD	Unstable crack extension at	Failure of specimen at
1	530 mm	no	100 %	> 150 %
2	530 mm	yes	85 %	> 150 %

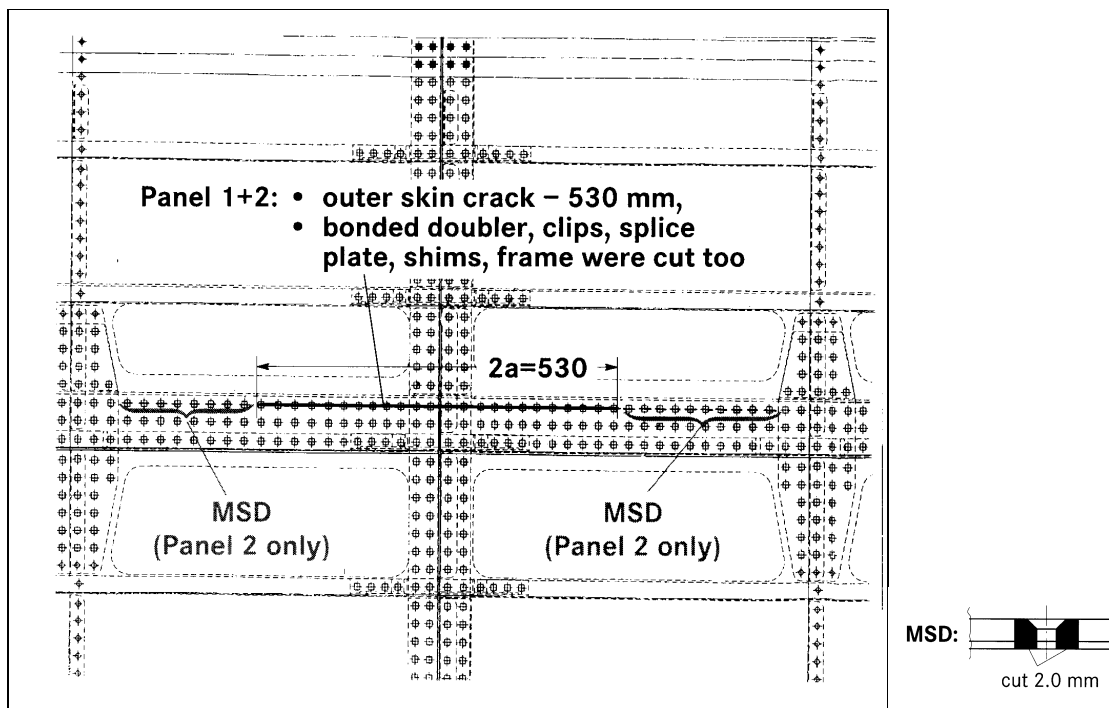


Fig. 29: Geometry of Test Panels 1 and 2. Panel 1 contains a lead crack (530 mm), while Panel 2 contains a lead crack (530 mm) plus additional MSD cracks. The MSD cracks were cut at both sides of each fastener hole, each crack having a length of 2.0 mm.

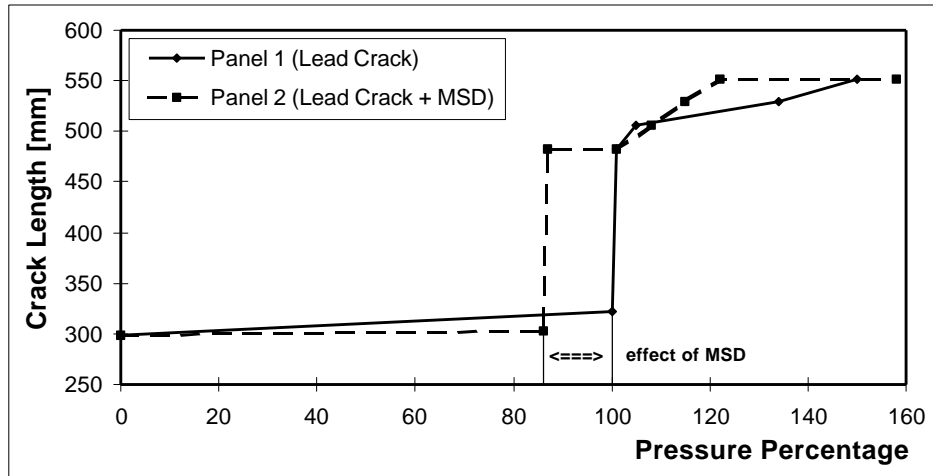


Fig. 30: Results of residual strength tests : MSD causes a 15 % load decrease in Panel 2

4.1.2 Damage Tolerance Test of Curved Fuselage Panels

Th. Fleischer, S. Goldbach, M. Semsch, IMA

In the years 1997 and 1998 several damage tolerance tests of fuselage sections were performed at IMA GmbH, Dresden. Curved fuselage panels with load introduction elements were mounted in a specifically developed testing machine, Fig. 31. This equipment simulates the loading conditions of real flights, such as cabin pressure and bending of the fuselage. The internal pressure p_i and the longitudinal ($F_{\text{längs}}$) and frame (F_{sp}) loads are applied by a pneumatic system and a servohydraulic loading equipment respectively, Fig. 32. The loading of the skin in circumferential direction is reacted by



Fig. 31: Test facility for curved fuselage panels.

Maximum loads of the test rig:

- Internal pressure: up to 1200 mbar
- Longitudinal force: up to 2 MN

Dimensions of the test specimen:

- Fuselage with 7 frames:
- Width: 2000 mm
- Length: 3500 mm
- Radius: 2820 mm

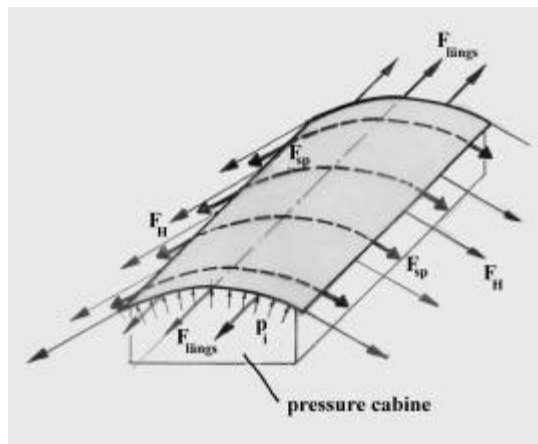


Fig. 32: Test principle.

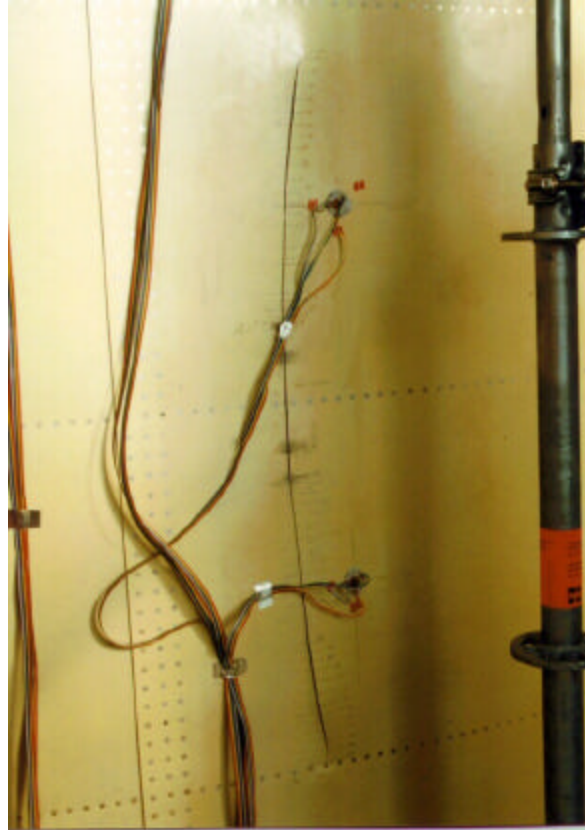


Fig. 33: Initial situation of residual strength test (two-bay-crack above broken frame).

forces F_H of the stiff connections between the fuselage panel and the test rig.

The damage tolerance tests of the fuselage panels consists of three parts, with following results:

- Crack propagation of circumferential skin cracks: the crack propagation rate of the crack between intact stringers is significantly lower than the crack propagation rate of a crack above a broken stringer. The crack above a broken stringer near the frame has a lower crack propagation rate than the crack in the middle of a skin field.
- Crack propagation of longitudinal cracks: the crack propagation of the crack between intact frames is faster than the crack propagation of the crack above a broken frame. The crack propagation in the middle of skin field is faster than the crack propagation of the crack which is situated near a stringer. The differences are due to reduced bulging near the stringer.
- Residual strength test of a two-bay-crack over a broken frame: the initial situation after a crack propagation test is shown in Fig. 33. The residual strength behaviour of the structure is influenced by the skin thickness of the fuselage, the fracture toughness of the skin material and of the frame material, the design of the frame and the riveting of skin and frames.

4.1.3 A340-600 EF2 Full Scale Fatigue Test for Center Fuselage and Wing

Th. Nielsen, DA-HAM

The A340-500/600 Commercial Transport Aircrafts are designed and will be certified as A340-200/300 derivatives according to FAR 25 Paragraph 25.571, including Amendment 45.

This review provides the principles of the EF2- test (EF2 = essai fatigue 2) for the center fuselage and wing boxes which will be performed at IMA Dresden. Since the A340-600 is designed for higher loads compared to the A340-500, it was decided to concentrate on -600 full scale testing. The -500 structure will be assessed on the basis of the -600 component

tests. In general, the test program is based on the A330/A340-EF2 test. It is divided into two phases: the fatigue tests are followed by damage tolerance investigations including damage propagation. Major topics of the test program are:

- Design Service Goal of 16600 flights,
- Verification of damage tolerance behaviour,
- 10000 simulated flights at the moment of A340-600 type certification,
- 44000 test flights (equivalent to more than 3 life times), blocked in a flight-by-flight program including 10 percent loads enhancement to reduce the test time
- 20000 flights with "detectable" artificial damages at typical locations for the A340-600

In order to provide the structural life justification and to identify possible fatigue sensitive areas of the new A340-600 passenger aircraft, a flight-by-flight fatigue test program is in progress. The test specimen, Fig. 34, is essentially a

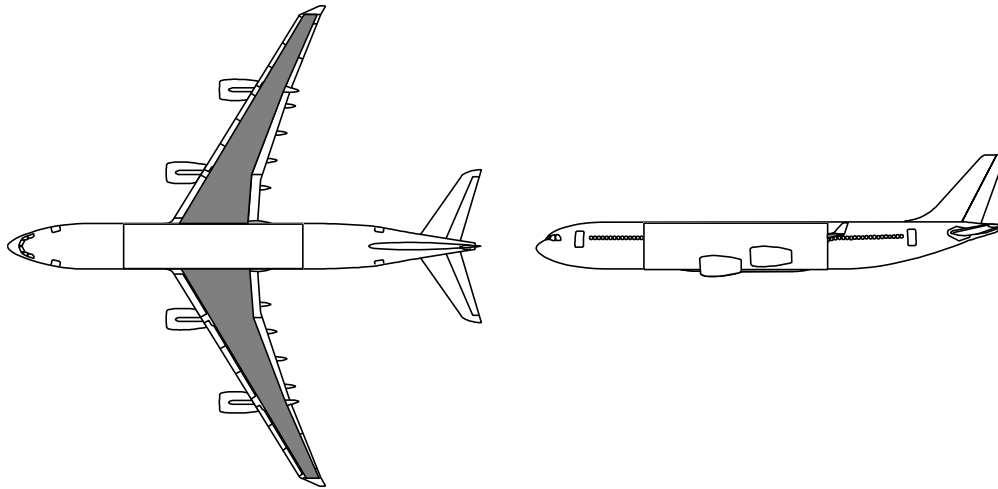


Fig. 34: Overview of the A340-600 test structure.

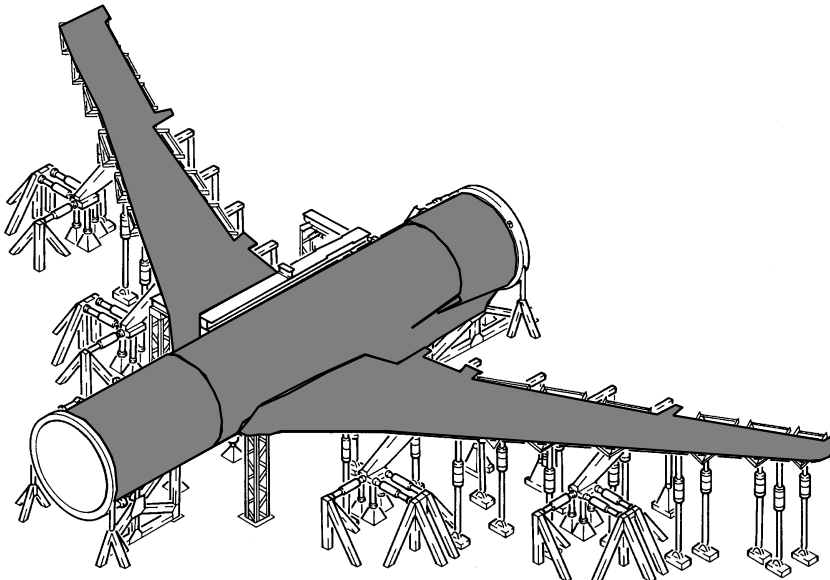


Fig. 35: Test set-up of the A340-600 EF2 full scale fatigue test.

production article. It consists of the center fuselage (length approximately 33m), the center wing, an outer wing box and of the attachments for the engine pylons, for the flaps, for the main and center landing gears with the respective dummy elements. The test specimen is controlled by 94 dual acting hydraulic jacks and is supported by 6 rods which are fixed at the dummy forward bulkhead of the center fuselage and at the main landing gears, Fig. 35. The load introduction is accomplished by bonded load pads on the wing lower surface to simulate the real load distribution. Additional loads are applied to the attachments of the flap track dummies, the engine pylon dummies, the main and center landing gear dummies as well as to the linkages at the passenger and cargo floor beams. Lateral flight loads are applied to the fuselage upper and lower shells by bonded pads.

The simulated test loads are increased by 10 percent and represent:

- Ground loads - 7 basic loads (1g) with superimposed incremental loads for taxiing, turning, take-off, rotation, landing impact, landing run and braking,
- Flight loads - 8 level flight loads (1g) with superimposed vertical and lateral incremental gust loads,
- Corresponding cabin pressure differential for each flight phase based on the typical flight profile.

Based on the previous test the test program following load cases are foreseen:

- 20 blocks of individual flight types of different severity,
- 2000 flights per block representing a randomized distribution,
- 21 flight types including 8 different airborne sub-flight types and 3 different ground sub-flight types,
- Random application of flight types and load cases.

To verify the damage tolerance behaviour of the A340-600 primary structure it is planned to install "detectable" damages based on scheduled in-service inspection methods. Also a number of standard repair solutions will be selected and installed on the test specimen to investigate the fatigue and damage tolerance behavior.

4.1.4 Eurofighter EF2000 Major Airframe Fatigue Test

C.Peters, IABG

The experimental fatigue life qualification of the Eurofighter EF2000 Major Airframe Fatigue Test (MAFT) was successfully performed at IABG's test laboratory in Ottobrunn from March 1993 till September 1998. The test specimen consisted of a complete airframe of the fourth Eurofighter prototype with front, centre and rear fuselage and fin and LH/RH wings without equipment. In the test rig a total of 66 hydraulic actuators, 4 retraction actuators for main/nose landing gear and airbrake, 6 struts and 4 pneumatic pressure systems were used to apply the required external and internal loads to the airframe structure. Fig. 36 shows a sketch of the entire test set-up.

The test loads were introduced into the test specimen by several fittings fastened to the specimen and a large number of rubber loading pads bonded to the surfaces of fuselage, fin and wings. A number of airframe components were replaced by dummy structures (landing gears, engines, radome, foreplane, pylons, slats, airbrake). These dummies simulated the real loadings at the respective attachment points. A fuel tank interconnection system was installed to enable fuselage and wing fuel pressurisation by a pneumatic system. The cabin with canopy seal and the intake ducts with diaphragm seals were also pressurised with air. The pressurisation volumes were reduced by polystyrene fillings. This increased the test rate and minimized the risk as well.

The main purposes of the test were:

- verification of a fatigue life of 6000 flight hours
- identification of fatigue sensitive areas
- determination of stress distributions with stress and deflection measurements and comparison of these data with the Major Airframe Static Test (MAST), Flying Aircraft (Structure Health Monitoring System) and FEM analyses

A randomised flight-by-flight test program of 18000 simulated flight hours (SFH) was necessary for the fatigue life verification of 6000 operational flight hours. The factor of 3 covered the scatter of the results. The program consisted of 3 missions with 17 different flights and about 800 different load cases.

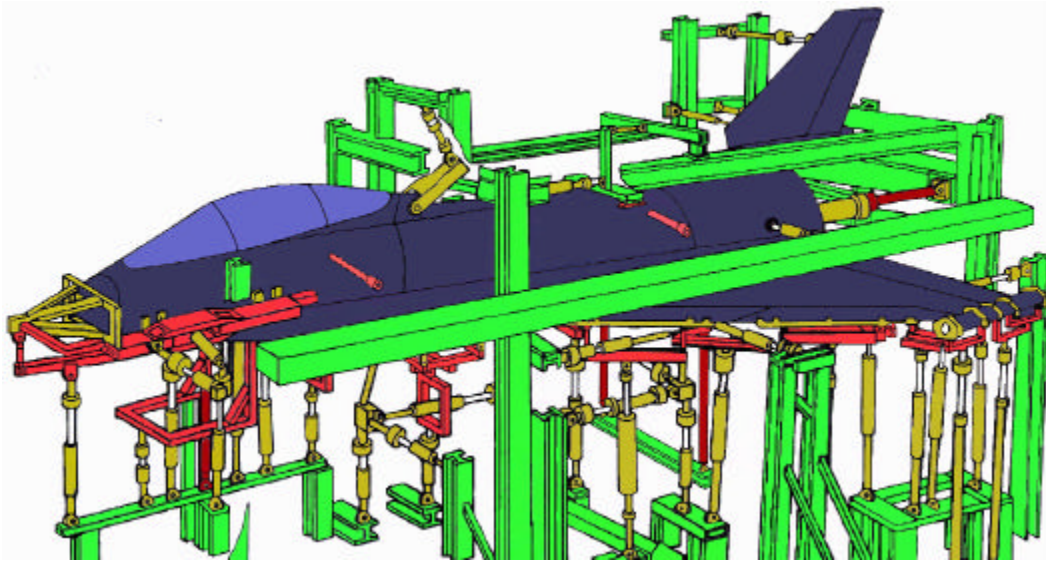


Fig. 36: Test set-up used for the EF2000 Major Airframe Fatigue Test.

Several static and spectra measurements were performed and extensive inspections were carried out during the performance of the test. The comprehensive inspection program included daily walk-around inspections, minor inspections every 1000 SFH and major inspections at 6000 / 12000 / 18000 SFH. The object of the inspections was to detect fatigue damages already at their initiation phase and to monitor propagation of cracks or delaminations.

Superficial inspections of easily accessible areas were carried out daily with no or only short test stoppage. These walk around inspections consisted of a normal visual check as well as close examinations of crack-suspect areas using adequate aids (magnifying glass). The complete aircraft was inspected within three days.

Every 1000 SFH a periodical inspection was carried out on selected critical areas. Every 6000 SFH a major inspection was performed on the complete aircraft. For the critical components, inspection locations and intervals were defined along with the desired inspection method. In general, visual inspections were specified. More sophisticated methods such as eddy current and ultrasonic were however required for specific areas. For a part of these inspections the polystyrene in the cabin, in the intake and in the tanks of the fuselage was removed. Further, some loading trees were dismantled and several panels, doors and covers at the fuselage were opened.

Pre-delivery and pre-test inspections of CFC components were performed by the Eurofighter Partner Companies. The locations of any delaminations, whether within the tolerances or outside the tolerances (defects) were recorded. Following the completion of rigging, which included attachment of loading trees and loading actuators, the ultrasonic inspections were repeated for the complete aircraft every 6000 SFH.

During fatigue testing, fuel tank leakage checks were performed every 3000 SFH. All panel joints, rivet rows and corners were scanned with a Helium Sniffer and inspected for leakage.

At the end of the MAFT test activities, a "Tear-Down" inspection was performed. To allow the full accessibility of the internal structure, the LH wing and the fin were disassembled and the upper skin of the wing and the LH skin of the fin were removed.

4.1.5 Static Loading and Fatigue Life Test of Extra EA-400

C. Peters, IABG

The EA-400 is a small business aircraft with six seats developed by the German company EXTRA Flugzeugbau GmbH. The aircraft with a pressurised cabin is completely manufactured in carbon fibre composite material. To obtain the certification for the EA-400 by the German authorities and the FAA, qualification tests were required. These tests included static loading and flight by flight fatigue tests. Additionally the behaviour of the connection engine mount/fuselage under engine burn

conditions had to be determined. A number of manufacturing failures and impact damages were introduced by the manufacturer at different locations in the main structures of the aircraft. This was done before the tests to check the damage tolerance behaviour of the composite structure.

This qualification test was performed at IABG's test laboratory in Ottobrunn. IABG designed and built the test set-up and installed the hydraulic loading system, the control and monitoring system and the measurement and data acquisition system. The entire test set-up consisted of frame which restrained the test article and of a number of load introduction systems (loading trees and hydraulic jacks). Fig. 37 shows a sketch of the entire test set-up.

The test article was mechanically loaded by 9 independent servo-hydraulic jacks. Pressurisation and depressurisation of the EA-400 cabin in relation to the test phases, was realised by a pneumatic system. For safety reasons and to reduce pressurisation and depressurisation time, the cabin was filled up with foam cubes. Sixty channels for the strain gauges and 12 displacement transducers were required to measure the behaviour of the structure during the static tests up to LL, UDL and during the residual strength test. For the fatigue life test 2 loops of the fatigue life program were required. Each loop consisted of 30 000 flights of a flight-by-flight loading program, giving a total of 60000 flights (which correspond to 2 x 20 000 flight hours). The fatigue test was carried out at room temperature and without moisture conditioning. Until March 1999 altogether 15000 flights were successfully simulated. A picture of the test set-up containing the EA-400 test article is given in Fig. 38.

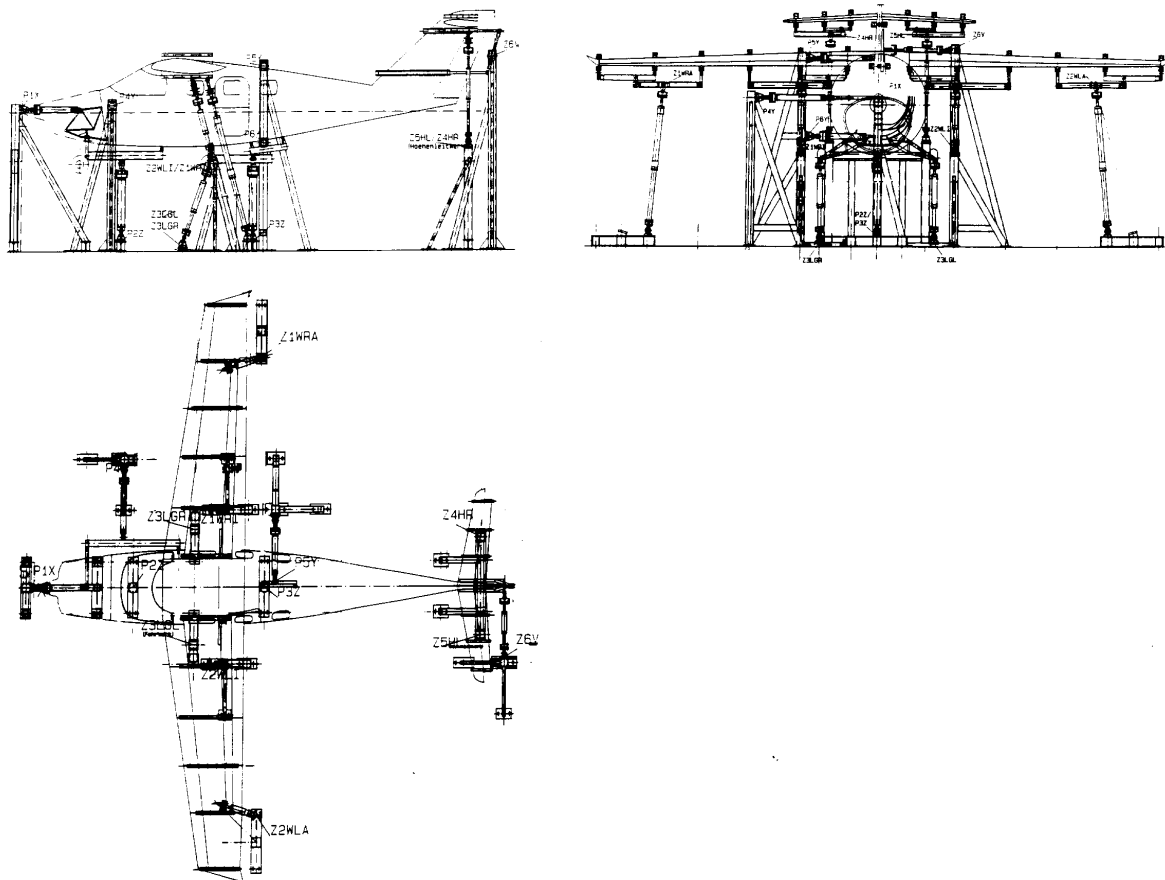


Fig. 37: Test set-up of the structural full scale Extra EA-400 tests.



Fig. 38 Completely assembled test set-up containing the EA-400 test article.

4.1.6 Full Scale Fatigue Test with a CFRP Outer Wing Box

H.-J. Mayer, DA-BRE, H.-C. Mühlmann and T. Müllert, DA-HAM

The technology project „CFRP Wing“ at DaimlerChrysler Aerospace Airbus (DA Airbus) is the first attempt in civil aeronautics to build and test a complete wing of CFRP (Carbon Fiber Reinforced Plastic). Development of this project started in 1994. The targets are:

- to minimize the technological risks by investigating design philosophies, feasibility and manufacturability,
- to tap economic potential in the manufacturing process
- to provide empirical verification of the design and the structural analysis and
- to be ready for development and production of a wing for a 100-seater, a A400M or the outer wing of a A3XX (Megaliner).

Testing on a complete wing, Fig. 39, has been in progress since July 1998. Based on a 100-seater definition a complete wing has been manufactured. This left hand (LH) wing consists mainly of CFRP; only load introduction elements are metallic. The design elements are: lower and upper skin stiffened by stringers in longitudinal direction, ribs in cross direction and front and rear spar. It is about 15 m long from root to tip and has a root width of 2.3 m. It has internal and external metal fittings for the attachments of the engine pylon (dummy), for the main landing gear (dummy), for moveable landing and take off aids (slats, flaps, aileron and spoiler) and for a fuselage connection. Its interior serves as a fuel tank.

The test rig simulates the special supporting and loading conditions of a wing. A center wing box is hinged between a trussed double steel frame as in an aircraft. On the left hand side, simulated wing loads are introduced in the root joint of the CFRP wing specimen. These loads are balanced by a RH wing dummy, which is attached to the center wing box. Further dummy structures are used for the load application to the engine pylon, to the main landing gear, to the slat and flap tracks and to the aileron. All loads are produced by hydraulic jacks supported by a basic rig connected with the double frame construction. Thus there is a closed loop for the forces.

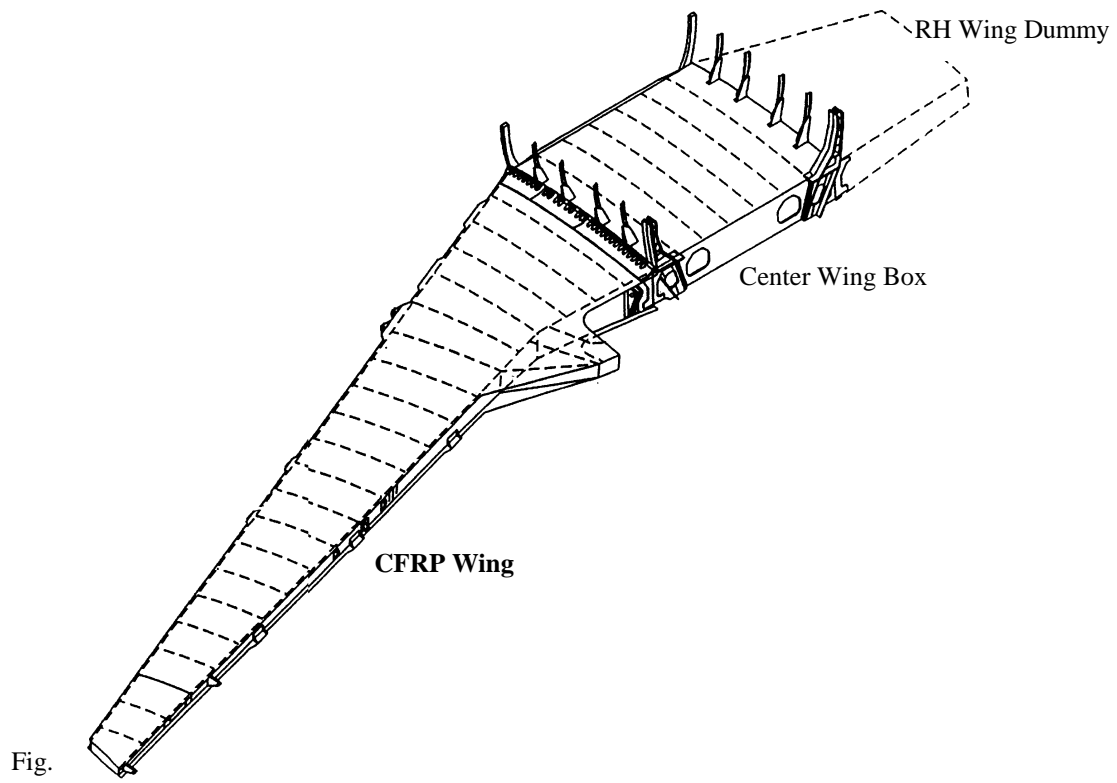


Fig.

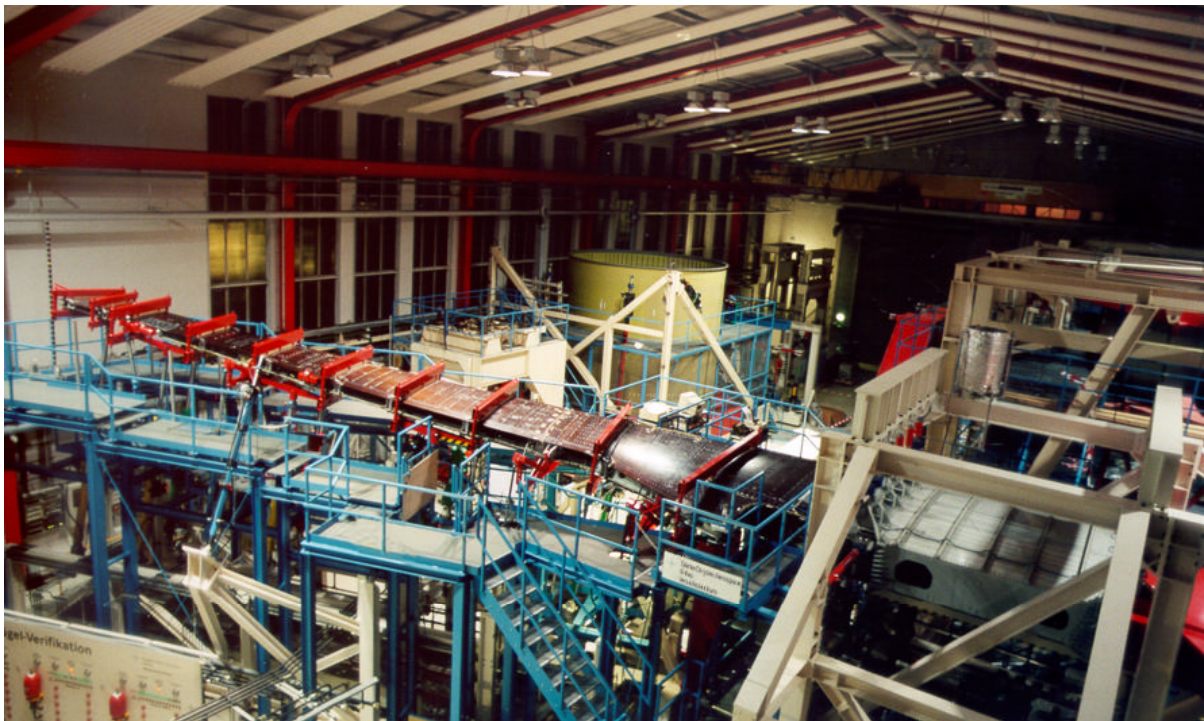


Fig. 40: CFRP wing during fatigue testing under positive gust, deflection at the wing tip of about 500 mm.

The test loads are applied by a total of 29 hydraulic jacks. The wing itself is attached to 12 jacks, which simulate the aerodynamic loads (bending, transverse forces and torsion). The loads are distributed via beams to the rib-spar nodes on the front and the rear spar. At the engine pylon dummy 5 jacks allow load application in 3 directions as well as rolling and yawing moments application. Loads in 3 directions are introduced with 3 jacks at the main landing gear dummy. The wing moveable surfaces have 3 jacks for the flaps, 2 jacks for the slats and 1 jack for the aileron loads. Correct internal loading is achieved through a jack which is located at the wing root attachment. The remaining 2 jacks at the RH wing provide the equilibrium loads. The loading system is digitally controlled and all hydraulic jacks are working simultaneously. A monitoring system serves for security. Another separate computer controls the overall flight-by-flight test procedure. The test is therefore running automatically night and day. To fulfil the requested environmental conditions of CFRP (moisture / temperature) the tank area is filled with heated water for the test time.

During the manufacturing process, the CFRP structure was damaged artificially to simulate manufacturing defects and handling stress (bonding failure, different impacts etc.), allowing their influence on strength and fatigue behavior to be studied.

The test program consists of a vibration test under three different specimen/load conditions, static tests for the main load cases, a fatigue test phase (one aircraft design life equals 60,000 simulated flights) and a damage tolerance test phase (another 30,000 flights). All fatigue loads are enhanced by a factor of 1.15. Sealing tests of the fuel tank area are performed in certain intervals as well as inspections using ultrasonic test methods. Finally, residual strength tests under special load conditions and a rupture test will be performed.

The wing fatigue test runs in a flight-by-flight manner, i. e. real life is simulated by repeated loads with variable amplitudes and load distributions. The flight load simulation comprises the 1 g airborne and on ground loads with superimposed environmental and maneuvering conditions. The 1 g loads are applied in the natural sequence from pre-flight taxi to post-flight taxi with 5 different airborne conditions in between. Superimposed incremental loads caused by taxi bumps, turning, engine run-up, thrust reversal, and braking on ground, vertical gusts in the air and spin up and spring back during the landing impact are applied. Special attention is given to the synchronization of the loads at the engine pylon, the landing gear and the wing. To cope with the dynamic gust load response of the engine pylon, 4 lateral pylon load cycles are applied simultaneously to one vertical wing load cycle.

The test is performed with a set of different flight types simulating different weather (gust), runway (bumps) and landing impact (sinking speed) conditions. Discrete loads were taken from the particular load spectra, distributed to the flight types and mixed to a random order. Five gust, 4 taxi bump and 4 landing impact flight types have been joined together to form complete flights. The joining effort was to combine e.g. large gust loads with low taxi loads and vice versa. So 19 joined flight types were obtained which are applied in a randomized sequence for a 4000 flights test block. Such a test block will be repeated 15 times to get one DSG (**D**esign **S**ervice **G**oal).

At present, the wing has completed its vibration test and the static tests up to limit load (under positive gust with about 900 mm deflection on the tip) successfully. Recorded data on the load behavior, strains, deflections and interior pressure (about 800 measuring points in all) indicates that the component properties correspond with calculated predictions very well. In the flight-by-flight fatigue test program, approximately 60,000 flights (1 life) have been performed at the end of April '99, Fig. 40. Inspections show no additional defects in the composite structure.

Till the end of 1999, it is anticipated that the completed test series will be finished including all necessary, additional coupon/component testing for higher component load flow e.g. for the Megaliner (A3xx) application. The total know how which comes out of this test program CFRP wing structure enable DA Airbus to design CFRP wing structure and thus to use all benefits of CFRP: weight saving from 15 % up to 25 %, no corrosion, vastly superior behaviour under fatigue loading and high fire resistance.

4.1.7 Fatigue Life Demonstration Tests on the CFRP Vertical Stabilizer of Airbus A 330-200

I. Malm and S. Jansen, DA-HAM

In connection with the new development of Airbus A 330-200 (Shrink), which has a length of 59 m and a wingspan of 60.3 m, a larger CFRP vertical stabilizer was also developed in a modified design. Higher stresses occur during operation of the new component, since the surface of the vertical stabilizer has been increased by 18% up to 52.9 m² compared with the basic component. Therefore extensive tests had to be performed to demonstrate sufficient fatigue life.



Fig. 41: Test setup for fatigue tests on the CFRP vertical stabilizer, A330-200.

The test specimen was composed of the fin box with the fuselage attach fittings, rudder actuator attach fittings, rudder bearing attach fittings and a rudder dummy with the original rudder spar. From the very beginning, the fin box had artificially applied manufacture, impact and repair defects.

A special test rig, simulating the representative loads resulting from gusts and manoeuvres, was developed. Three movable beams, used for rigging of the vertical stabilizer in its fuselage attach fittings, were integrated in a steel frame. With this movable beams, the reaction forces resulting from the air loads could be applied through a system of hinged supports and hydraulic jacks, which took the deformation behavior of the aircraft fuselage into account. In addition, the lateral loads were distributed over the surface of the vertical stabilizer via 19 hydraulic jacks with corresponding whiffle trees. Moreover, loads were introduced into the rudder axis area and rudder jack areas. Fig. 41 shows the test set-up.

During the fatigue test, all the loads as well as the deformation behavior of the structure were permanently monitored by a redundant system. The loading program included flight types of different duration (number of load conditions) and intensity (load level) in a cycle of 4.000 flights. This cycle was repeated fifteen times, so that a total of 60,000 flights = 1.5 times the fatigue life were simulated.

Climatic ageing was taken into consideration through a load factor. Periodical inspections involving different methods provided information on the structure's condition. In the course of the fatigue test, no change was noticed on the artificial damages of different kind and size. The final static test, in which the side shells were partially heated, demonstrated sufficient residual strength of the structure.

5 INVESTIGATIONS OF GENERAL INTEREST

5.1.1 Fatigue Strength of Smooth and Notched Specimens under High Mean Stresses

S. Narberhaus and H. Zenner, TUC-IMAB

Based on an extensive test series on notched and smooth specimens the influence of tensile mean stress on the fatigue strength and the cyclic deformation behaviour of the steel X22 CrMoV 12 1 and the ductile cast iron GGG 40 was investigated [18]. In 16 test series the fatigue strength was experimentally determined with the modified stair case method. The varied parameters were the notch factor K_t and the stress ratio R . In stress controlled tests the mean strain was measured. The main results of this research program can be summarized as follows:

- The determined dependence between mean strain and the number of load cycles is well fitted by an exponential function.
- In tests with combined HCF/LCF loading no influence of the LCF overloads on the fatigue strength or the cyclic deformation behaviour was found. The ratio of HCF load cycles to LCF was about 10^4 to 10^5 .

In the theoretical part of the research program, a creep model for the calculation of the cyclic deformation as a function of the load cycles was developed. Only static and cyclic material properties are needed to calculate the coefficients of the creep model. The proposed model is suitable for both materials investigated. It was successfully implemented in the ABAQUS finite element code. The calculated local strain versus number of load cycles plots showed good agreement to the experimental results.

On the basis of the experimental and theoretical results, a new approach for fatigue life prediction was developed. The concept combines the fatigue damage with the creep damage similar to Robinson [19]. Damage is divided in two parts: the fatigue damage is represented by the ratio of applied stress amplitude versus fatigue strength, whereas the creep damage is given by the ratio of total strain versus the strain at fracture. The calculated fatigue strength is in good correspondence with the experimental results. A comparison between the Combined Damage Rule (CDR) prediction and the test results is made in Fig. 42.

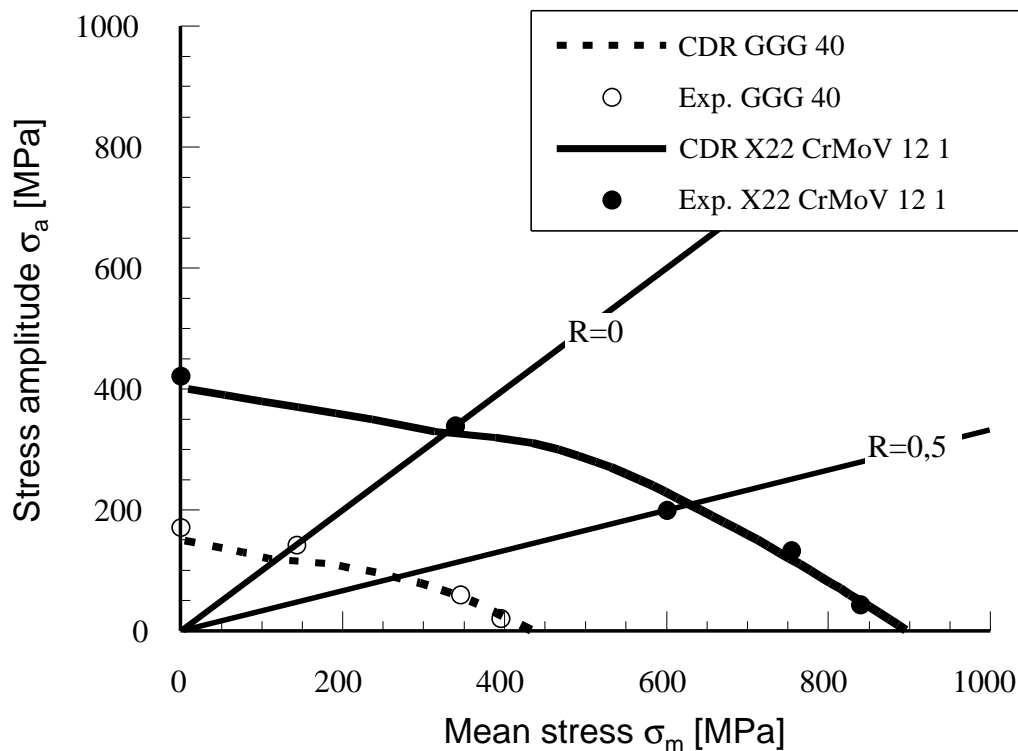


Fig. 42: Comparison between calculated and experimental fatigue strength.

5.1.2 Experimental Investigation on the Cyclic Behaviour of Deformed Steel Sheets

R. Masendorf and H. Zenner, TUC-IMAB

Sheet metal components are frequently subjected to severe deformation during the manufacture process. The service life of such components can be predicted on the basis of the local strain concept. The cyclic behaviour of the material, which depends on the degree of deformation and deformation ratio, must be known for the calculations. Since no approximate solutions for the cyclic characteristics of pre-strained sheet material are available so far, tests with St15 deep drawing steel sheet were carried out (ultimate strength $R_m = 314$ MPa, yield strength $R_{p0.2} = 190$ MPa, thickness 1 mm). The cyclic behaviour of the material was determined by constant amplitude, strain controlled tensile-compressive tests (zero mean strain). The test samples were cut out of pre-strained metal strips. Buckling of the specimen was prevented by friction-minimised supports.

The results of the strain-controlled tests are presented in Fig. 43 in terms of stress-strain curves and in Fig. 44 as ϵ -N curves. The ϵ -N relation is described by the Manson-Coffin equation

$$\epsilon_{a,t} = \epsilon_{a,el} + \epsilon_{a,pl} = \frac{\sigma'_f}{E} (N_A)^b + \epsilon'_f (N_A)^c \quad (3)$$

For strain amplitudes smaller than 2 mm/m, an increase in service life with increasing pre-straining is evident. In this range, the variation of the ϵ -N curve is governed essentially by the elastic strain components σ'_f and b . The variation of these characteristic values is plotted as a function of pre-straining in Fig. 45. Moreover, the parameters K' and n' , which describe the cyclic stress-strain curve are also indicated in Fig. 45.

In the future, the effect of pre-straining (degree of deformation and deformation ratio) on the cyclic behaviour of various steel and aluminium sheet materials will be investigated. The objective is to extend the uniform material law [20] by coefficients, which quantify the effect of pre-straining.

The work was supported by Deutsche Forschungsgemeinschaft (SFB 362 "Fertigen in Feinblech", TU Clausthal, Uni Hannover).

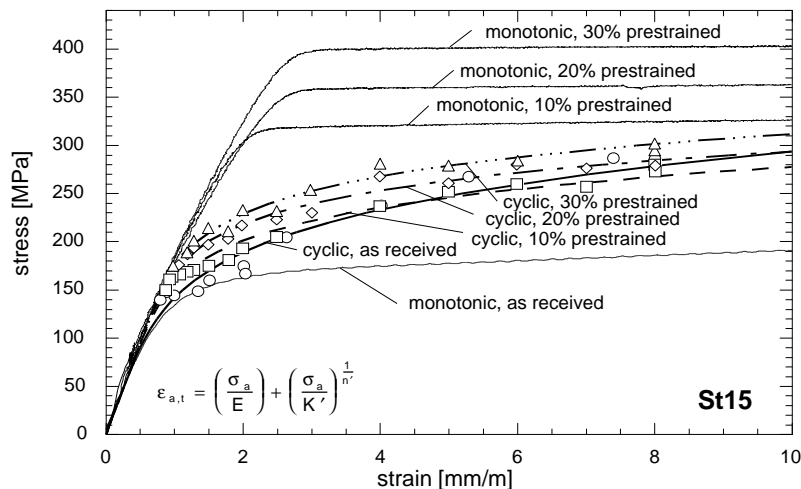


Fig. 43: Monotonic and cyclic stress-strain curves of pre-strained steel St 15.

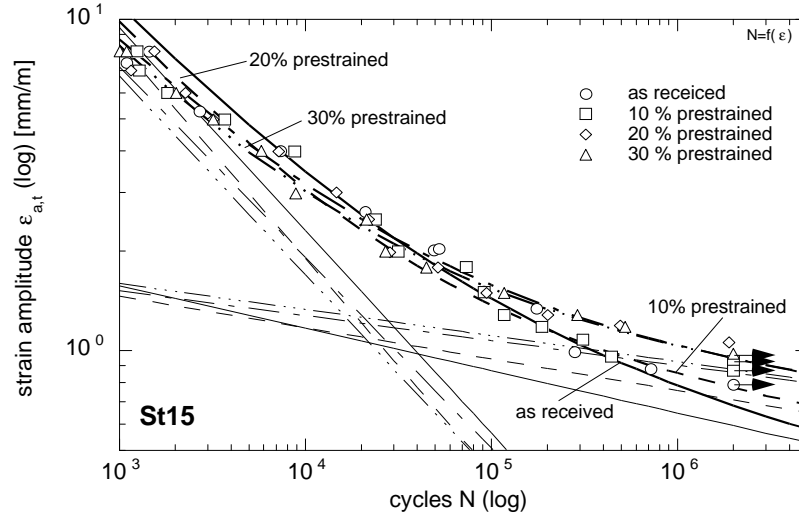


Fig. 44: Manson- Coffin curves of pre-stained steel St 15.

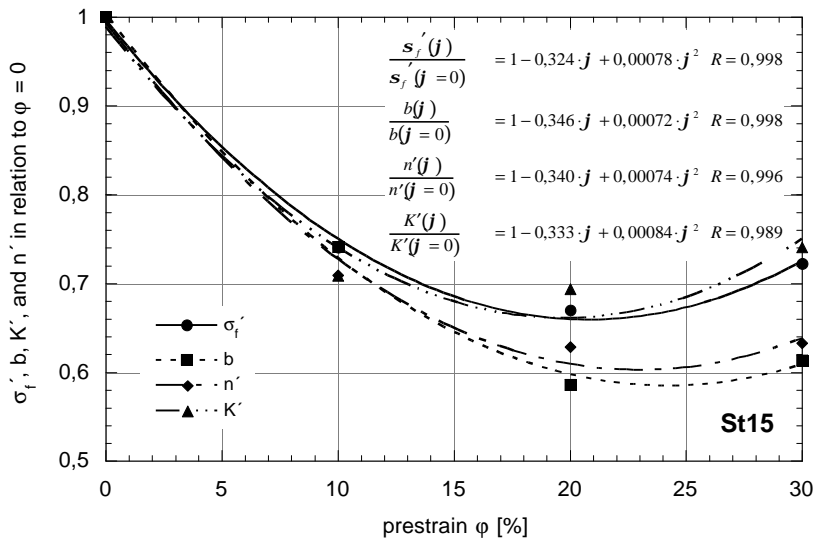


Fig. 45: Effect of pre-straining on the parameters σ'_f , b , n' , and K' related to the as-received condition.

6 REFERENCES

- [1] Marci, G., Mull, K., Sick, Ch., and Bartsch, M., New Testing Facility and Concept for Life Prediction of TBC Turbine Engine Components, 3th Symp. on Thermomechanical Fatigue Behaviour of Materials, Nov. 4-5, 1998, Norfolk, Virginia, ASTM STP 1371, in press.
- [2] Kaysser, W.A., Bartsch, M., Fatigue of Thermal Barrier Coatings, Proceedings of the 7th International Fatigue Congress - Fatigue'99, June 8-12 1999, Beijing, China, in press.

- [3] Leyens, C., Peters, M. and Kaysser, W.A., Oxidation Behaviour of Near- α Titanium Alloys and their Protection by Coatings, Proc. 8th World Conference on Titanium, Blenkinsop, P.A., Evans W.J. and Flower H.M. (Eds.), Birmingham, U.K.: The Institute of Materials, London, 1995, pp. 1935-1942.
- [4] Leyens, C., Peters, M. and Kaysser, W.A., Oxidation and Protection of Near-Alpha Titanium Alloys, Materials Science Forum, 251-254, 1997, pp. 769-776.
- [5] Leyens, C., Peters, M. and Kaysser, W.A., Influence of Intermetallic Ti-Al Coatings on the Creep Properties of TIMETAL 1100, Scripta Materialia, 35, 12, 1996, pp. 1423-1428.
- [6] Leyens C. et al., Influence of Intermetallic Ti-Al Coatings on the Fatigue Properties of TIMETAL 1100, Scripta Materialia, 36, 11, 1997, pp. 1309-1314.
- [7] Dalle Donne, C.: A CTOD Approach to Assess Stable Tearing under Complex Loading Conditions, The Second Joint NASA/FAA/DoD Conference on Aging Aircraft, NASA/CP-1999-208982/PART 2, Harris, C.E. (Ed.), 1999, pp. 555-564.
- [8] Dalle Donne, C.: The Crack Tip Displacement Vector Approach to Mixed-Mode Fracture, Mixed-Mode Crack Behavior, ASTM STP 1359, Miller, K.J. and McDowell, D.L. (Eds.), ASTM, Philadelphia, accepted 1999.
- [9] Dalle Donne, C., Braun, B., Staniek, G., Jung, A. and Kaysser, W.A., Microstructural, Mechanic and Corrosive Properties of Friction Stir Welded Aluminium Joints, Materialwissenschaft und Werkstofftechnik, 29, 10, 1998, S. 609-617.
- [10] Dalle Donne, C. and Biallas, G.: Fatigue and Fracture Performance of Friction Stir Welded 2024-T3 Joints, European Conference on Spacecraft Structures, Materials and Mechanical Testing, Stavrinidis, C., Rolfo, A. and Breitbach, E. (Eds.), ESA-SP 428, 1999, 309-314.
- [11] Biallas, G., Braun, R., Dalle Donne, C., Staniek, G. and Kaysser, W.A.: Mechanical Properties and Corrosion Behavior of Friction Stir Welded 2024-T3, to be presented at the 1st International Symposium on Friction Stir Welding, 14-16 June 1999, Thousand Oaks, Rockwell Science Center, California.
- [12] Smith K. N., Watson P., Topper T. H.: A stress-strain function for the fatigue of metals; Journal of Materials 5 (1970), pp. 767-778
- [13] Heitmann H., Vehoff H., Neumann P. Random Load Fatigue of Steels: Service Life Prediction Based on the Behaviour of Microcracks, Proc. Int. Conf. on Application of Fracture Mechanics to Materials and Structures, Freiburg, 1983.
- [14] Bazios I. Untersuchungen zum Ermüdungsverhalten einer AlMgSi-Legierung bei betriebsnaher Beanspruchung in korrosiven Medien, PhD-thesis, University of the Federal Armed Forces Munich, 1999.
- [15] Krä Chr.; Heckel K. Übertragung von Schwingfestigkeitswerten mit dem statistischen Größeneinfluß; Materialwissenschaft und Werkstofftechnik 20, 1989, pp. 255-261.
- [16] Gudladt, H.-J., Bär, J., Proc. of Euromat Topics, Vorsatz B. and Szöke E. (Eds.), 1994, pp. 319-337.
- [17] Böhm, J., PhD Thesis, Technical University of Munich, Germany, 1980.
- [18] Narberhaus, S., Zenner, H. and Kern, H., Hohe Mittelspannungen - Dauerschwingfestigkeit bei hohen Mittelspannungen, Forschungskuratorium Maschinenbau e. V., Frankfurt/Main, FKM-Forschungsheft, Aif-Nr. 10682, to be published in 1999.
- [19] Robinson, C. L., The Effect of Temperature Variation on the Long-Time Rupture Strength of Steels, Trans. ASME 74, 5, 1952, 777 -781.
- [20] Bäumel A. and Seeger, T., Materials Data for Cyclic Loading, Supplement 1, Elsevier Publ., Amsterdam, 1990.

ICAF'99 Conference - Bellevue, Washington, USA - 12-13 July 1999

**REVIEW OF AERONAUTICAL FATIGUE INVESTIGATIONS
IN FRANCE DURING THE PERIOD MAY 1997 - JUNE 1999**

Compiled by

Jean Rouchon

DIRECTION DES CENTRES D'EXPERTISE ET D'ESSAIS

Centre d'Essais Aeronautique de Toulouse

31056 TOULOUSE - FRANCE



CENTRE D'ESSAIS AERONAUTIQUE DE TOULOUSE

INTRODUCTION

The present review, prepared for the occasion of the 26th ICAF conference to be held in Bellevue (WA) USA, on 12 - 13 July 1997, summarises works performed in France in the field of aeronautical fatigue during the period May 1997 - June 1999.

Topics are arranged from basic investigations up to in-service reporting.

References, when available, are mentioned at the end of each topic.

Correspondents who helped to collect the information needed for this review in their own organisations are:

Mr Jean-Louis Chaboche for ONERA,

MM Louis Anquez and Daniel Gilletta de St Joseph for Dassault Aviation,

MM Cédric Meyer and Laurent Deféver for Aerospatiale-Matra, Aviation Branch,

Mr Bertrand Journet for Aerospatiale-Matra, Joint Research Center,

MM Pascal Hamel, Marc Langon, Yves Laporte and David Recorbet for CEAT.

They will be the right point of contact for any further information on the presented topics.

Many thanks to all of them for their contribution.

TABLE OF CONTENT

6.1 FATIGUE LIFE PREDICTION STUDIES AND FRACTURE MECHANICS	6/6
6.1.1 Fatigue crack initiation.....	6/6
6.1.1.1 Theoretical studies on aluminium alloys Wöhler curves (Dassault aviation).....	6/6
6.1.1.2 Follow-on activity concerning a new methodology to predict fatigue crack initiation (Dassault Aviation).....	6/6
6.1.1.3 Contact fatigue (Aerospatiale-Matra, Joint Research Center).....	6/6
6.1.1.4 Assessment of life prediction methods for turbine blades (O.N.E.R.A.).....	6/7
6.1.1.5 Engine material behaviour under thermo-mechanical fatigue (CEAT).....	6/8
6.1.2 Fracture mechanics.....	6/8
6.1.2.1 Fracture mechanics of Cold Expanded Holes (Aerospatiale-Matra, Joint Research Center).....	6/8
6.1.2.2 Stress corrosion (Dassault Aviation).....	6/8
6.2 COMPUTATIONAL TECHNIQUES	6/9
6.2.1 Finite element modelling of joints (Aerospatiale-Matra, Aviation Branch).....	6/9
6.2.2 Improvement of in-service performances (Aerospatiale-Matra, Aviation Branch).....	6/9
6.2.2.1 Allowables damages and repairs.....	6/9
6.2.2.2 Large cuts analysis in propagation and residual strength.....	6/10
6.3 EXPERIMENTAL TECHNIQUES	6/10
6.3.1 Assessing K-gauge capabilities for structure testing (CEAT).....	6/10
6.3.2 Development and running of a fatigue test facility for fuselage representative curved panels (CEAT).....	6/11
6.3.3 Biaxial fatigue testing facility for engine materials (CEAT).....	6/11
6.4 METALLIC MATERIALS AND TECHNOLOGY TESTING	6/12
6.4.1 Fatigue on landing gear representative specimens (Messier Dowty - CEAT).....	6/12
6.4.2 Validation of 2017 CP (Crack Proof) rivet use (Dassault Aviation).....	6/12
6.5 RULE MAKING SUPPORTING ACTIVITIES	6/13
6.5.1 Improvement of justification methods, prediction of widespread fatigue damage for ageing aircraft : A300 life extension (Aerospatiale-Matra, Aviation Branch).....	6/13
6.5.2 Improvement of justification methods, Initial flaw approach for design (Aerospatiale-Matra, Aviation Branch).....	6/13
6.5.3 Fuselage fatigue test on a retired Mercure 100 (Dassault Aviation & CEAT).....	6/13
6.6 - SONIC FATIGUE (Dassault Aviation)	6/14

6.7 FULL-SCALE FATIGUE TESTS NEWS	6/14
6.7.1 TBM 700 fatigue test (SOCATA and CEAT).....	6/14
6.7.2 Gazelle helicopter fatigue test (EUROCOPTER and CEAT).....	6/15
6.7.3 - Alphajet fatigue test (Dassault Aviation and CEAT).....	6/16
6.7.4 Transall structure life extension (Aerospatiale-Matra and CEAT).....	6/17
6.8 IN-SERVICE AIRCRAFT FATIGUE MONITORING	6/17
6.8.1 System general description and data collection (CEAT).....	6/17
6.8.2 Evolution of the system : MICROSPEES (Dassault Aviation and CEAT).....	6/18
6.8.3 Next generation of the system : HARPAGON (Dassault Aviation and CEAT).....	6/19

6.1 FATIGUE LIFE PREDICTION STUDIES AND FRACTURE MECHANICS

6.1.1 Fatigue crack initiation

6.1.1.1 Theoretical studies on aluminium alloys Wöhler curves (Dassault aviation)

C. Bleuzen (CEAT) analysed the scatter of high strength aluminium alloys (2024, 7010,...) using open holes specimens. A $\sigma/0.1\sigma$ fatigue loading was applied and three s levels were systematically investigated. The conclusion of this study was that there exists a range of σ where the probability of fatigue failure is no longer log-normal as it seems to be outside this critical range (figure 1).

Dassault then initiated a research programme on this subject since this experimental fact was considered as being important due to its possible consequences on damage cumulation in case of spectrum loading. This study, focused on the 2024 T3 alloy, pointed out that there exists one kind of inclusion of average size 10 μm (figure 2), very brittle, which fails when a given stress Σ is reached. Under constant amplitude loading, initiation arises from persistent slip bands in the bulk matrix when the maximum applied stress is lower than Σ and in the very surrounding of the broken inclusions when the maximum applied stress is higher than Σ . It appears that this last mechanism is definitely more damaging than the first. Then, the damage created by a low cycle (maximum stress lower than Σ) is not the same if the brittle inclusions are, or are not broken.

If we apply a spectrum loading on a structure leading locally to a maximum stress higher than Σ , some brittle inclusions will fail and, as a consequence, all the low cycles will produce higher damage than if they were applied alone. So, there is a need to determine a specific wöhler curve taking this fact into account.

Dassault propose to deduce this curve using the following methodology :

- experimental side : apply identical blocks consisting of one high load (such that s is higher than Σ) followed by a given number of low loads,
- theoretical side : use the hypothesis of linear damage cumulation in order to deduce the damage created by the low load when broken inclusions exist.

This has been done successfully on 2024 T3 aluminium alloy (figure 3).

Reference : M. XING Bin 'Confrontation of deterministic and statistical aspects in aluminium alloys fatigue initiation'. Thesis presented at the Ecole centrale de Paris (98-29).

6.1.1.2 Follow-on activity concerning a new methodology to predict fatigue crack initiation (Dassault Aviation)

The updated Neuber approach that has been developed by Dassault provides better previsions than the classical one (as already addressed in the ICAF'97 French National review).

Based on small scale yielding hypothesis, using the amplitude of the shear stress and the hydrostatic stress as active parameters (computed at a given, material dependant, critical distance from the free edge), the developed numerical tool takes local plasticity into account, but needs only elastic computation.

This specific development is now integrated into the fatigue analysis tool in ELFINI software.

Good previsions are obtained (figures 4 & 5), whatever the spectrum, for open holes and holes with loaded fasteners.

Dassault current effort aims at applying the same kind of procedure to the fatigue failure of the fasteners themselves.

6.1.1.3 Contact fatigue (Aerospatiale-Matra Joint Research Center)

Fatigue cracks often initiate in areas where contact takes place. Aerospatiale Joint Research Center has investigated several fatigue problems where contact is the main crack source. Pitting of gears and fretting fatigue are two examples of such problems and have been studied using the same analysis tools : a refined finite element analysis of

structural elements with contacting conditions and a fatigue analysis of the different stress histories through a multiaxial criteria.

In the case of gears, as shown in figure 6, the model uses a partial simulation of the wheel and the pinion. The finite elements are being used to analyse effects of real loadings and include friction between the two parts. Fatigue analysis is conducted on surface and subsurface elements, using Crossland or Dang Van multiaxial fatigue crack initiation criteria. Available fatigue data for the relevant materials (carburized steels, Duplex Hardening Steels) are used as input information to predict the component fatigue life. Depending on lubrication parameters, fatigue lives are minimum either on the extreme surface or in the subsurface elements. For example, if a high roughness is present on a pinion, a higher friction coefficient is expected between the two parts, thus generating low fatigue lives on the extreme surface. This numerical behaviour is typical of micropitting, experimentally obtained in the same conditions. On the contrary, if the components have a lower roughness, cracks tend to appear deeper in the material, as expected by the Hertzian theory. This model has shown a good efficiency in providing useful information on the gear properties needed for given running conditions.

In the case of fretting fatigue, as illustrated on figure 7, the same type of analysis can be conducted : the stress histories of different elements in a finite element model are analysed through a crack initiation multiaxial criteria. The effect of coatings are also analysed. Simulation are in good agreement with experiments currently underway on 30NCD16 steels. The beneficial impact of coatings on fatigue lives is particularly well reproduced. It should be noted that simulation results are usually conservatives in the conditions which have been explored. This is probably due to the fact that, in certain conditions of fretting-fatigue, cracks can be locally created in the vicinity of the contacting zone but do not propagate any more as soon as they have left this highly stressed area. This aspect of fretting-fatigue cannot be analysed using multiaxial criteria and will need further work with fracture mechanics tools.

6.1.1.4 Assessment of life prediction methods for turbine blades (O.N.E.R.A.)

Since a long time, Onera has developed constitutive and damage equations for the lifetime prediction of turbine components, especially turbine blades. In order to check the capabilities of these methods for thin walled turbine blades, a special experimental set up has been designed [1], [2]. Cyclic axisymmetric wall thermal gradients are applied on a tubular specimen (figure 8). The induction heating / air cooling system is able to reproduce thermal gradients of about 200°C over the 2mm wall thickness under permanent conditions (more during transient ones). A cyclic axial load is superimposed in order to represent centrifugal effects.

The life prediction method involves three main steps :

- a cyclic constitutive equation, involving several non linear kinematics hardening rules, is determined from standard cyclic tests over the whole temperature domain [3], [4],
- the cyclic inelastic analysis of the component is performed by finite elements. A sufficient number of successive cycles is calculated (typically 10 to 20) before the response stabilisation,
- a creep-fatigue-oxidation model is determined from a series of fatigue tests at various temperatures and frequencies and from creep tests. This model separates the macrocrack initiation into a microcrack initiation stage (incorporating the coating deterioration and oxidation effects) and a microcrack propagation (in the bulk material) during which creep-fatigue interaction does occur [5].

Applied on two turbine blade materials, the IN100 polycrystalline superalloy and the AM1 single crystal, the test results demonstrate clearly the life improvement obtained from the use of a single crystal (figure 9), The modelling method is able to predict correctly the observed lives on the two different materials. Let us note that the IN100 models were entirely determined 20 years before the present analysis [3].

References :

[1] Chaboche, J.L., Culé, J.P., Gallerneau, F., Nouailhas, D., Pacou, D., Poirier, D., Thin wall thermal gradient : experimental study, F.E. analysis and fatigue life prediction, 5th Int. Conf. On “ Biaxial/Multiaxial Fatigue & Fracture ”, Macha, E. and Mroz, Z., eds., Krakow, sept. 8-12, 1997, pp.237-250.

[2] Gallerneau, F., Chaboche, J.L., Fatigue life prediction of single crystals for turbine blade applications, to appear in Int. J. of Damage Mechanics , 1999.

[3] Chaboche, J.L., Policella, H., Kaczmarek, H., Applicability of the SRP method and creep-fatigue approach to the LCHTF life prediction of IN100 alloy, AGARD Conf “ Characterisation of Low Cycle High Temperature Fatigue by Strain Range Partitioning, Aalborg, 1978.

[4] Nouailhas, D., Development and application of a model for single crystal superalloy, Freed, A.D., and Walker, K.P., eds., “ High Temperature Constitutive Modelling – Theory and Applications ”, ASME, MD-26, AMD-121, New-York, 1991, p151.

[5] Gallerneau, F., Etude et modélisation de l’endommagement d’un superalliage monocristallin revêtu pour aube de turbine, Thèse de Doctorat, Ecole des Mines de Paris, 1995.

6.1.1.5 Engine material behaviour under thermo-mechanical fatigue (CEAT)

Aircraft engine hot-section components, such as turbine blades, are designed to operate in environments at elevated temperature, with high thermal gradients and mechanical loads. Repeated engine start-up and shut-down operations submit these components to cyclic strains which are generated both thermally and mechanically.

- In order to investigate the blade materials behaviour, CEAT developed a thermo-mechanical testing machine (figure 10), ten years ago. The test principle consists in measuring the stress-strain curves (elastic, plastic, thermal and total deformations) during a thermo-mechanical cycle. The test may be either stopped for performing metallurgical investigations when the stress-strain loop is stabilised, or carried out up to failure.

For the time being, an experimental programme is carried out to evaluate the damage of a single-crystal nickel base superalloy under thermo-mechanical cycling. Tests are performed on tubular specimens (figure 11), recovered or not, with a coating against corrosion and oxidation.

6.1.2 Fracture mechanics

6.1.2.1 Fracture Mechanics of Cold Expanded Holes (Aerospatiale-Matra, Joint Research Center)

In house fatigue crack growth tests on cold expanded holes, on aluminium alloys, have shown a tremendous crack retardation effect within the first few millimetres of crack advance (3 orders of magnitude). There is a need to take this gain into account for damage tolerance purpose. Together with Aerospatiale-Matra, Aviation branch, it was decided to run complementary tests and review the fracture mechanics of cracked cold expanded holes in order to calculate the stress intensity factor for the presence of residual stresses. The models given in the literature are too simplistic in their assumptions. The retardation effect has been modelled with a shape function. In order to have a more general purpose approach, the effort was placed on finite element analysis to calculate K. The steps are as follows :

- simulate cold expansion process using finite element analysis (joint work with BAe AIRBUS),
- introduce a crack in the mesh,
- apply the service fatigue stress,
- derive the stress field and calculate K,
- predict da/dN using an appropriate crack growth rate equation (short / long crack).

The predictions are satisfactory but the calculation will be refined (figure 12).

6.1.2.2 Stress corrosion (Dassault Aviation)

This investigation has been divided into two parts :

- derivation of the stress field installed by the interference of bushing and conic axis. This is achieved by F.E models (2D) - with constant conditions between :

- lug hole and bushing,
 - bushing and axis bushing,
 - axis bushing and axis.
- performance of an alternate immersion/emersion test on a service retired empennage fitting (Mystere 20). The observed propagation is then modelled by a damage tolerance approach.

Different parameter influences, as interferences and lug sizes, have been reviewed.

The results obtained are used to optimise the scheduled inspections in the maintenance manual.

This topic will be the subject of a presentation in the Session 5 of the symposium.

6.2 COMPUTATIONAL TECHNIQUES

6.2.1 Finite element modelling of joints (Aerospatiale-Matra, Aviation Branch)

In order to predict more accurately the circumferential butt joints fatigue life and to optimise their design, a fully representative non-linear model has been developed and validated by comparison with test results on coupons, flat stiffened panels and full-scale fatigue tests. Local stress fields and in-house fatigue procedures allow fatigue life to be determined at critical details (figure 13).

This model allows :

- to know the critical sites : strap, skin, splice, stringer,
- to estimate the load transferred by fasteners in these sites,
- to calculate the local stress concentration factor K_t ,
- to calculate fatigue life thanks to S-N curves extrapolations.

The geometrical non-linear behaviour of complex assemblies (skin, strap and frame) has to be taken into account. In fact, flexions bred stacking have unfavourable consequences on fatigue life.

Finally, this model makes possible to check the consistency and the reliability the results of tests performed by the CEAT on flat and curved panels (figure 14) in the frame of the project called 'Fuselage Nouvelle Génération Métallique' - FNGM - (i.e. New Generation Metallic Fuselage). Results are also compared with full-scale fatigue tests.

6.2.2 Improvement of in-service performances (Aerospatiale-Matra, Aviation Branch)

The aim of this axis is to better control allowable stresses in order to ease calculation limitations laid down to production (tolerances accepted, non conformity) and airlines (repairs, allowable damages, scratches, reworks, dents, customised inspection intervals,...).

The following items are studied :

6.2.2.1 Allowables damages and repairs :

Thanks to 3D geometrical and material non linear Finite Element models developed and validated by tests, it is expected :

- to calculate the stress concentration factor due to reworks in any kind of configuration : located in the middle of the pocket, in a fastening area,... Having this K_t factor, it is then possible to estimate fatigue lives,
- to simulate the dent created by an impact, and also the dent dress-out at a later stage,

- to calculate the stress concentration factor due to dents in some typical cases : in a uniform area of the fuselage, above a stringer, above the intersection between a stringer and a frame, in order to predict fatigue lives as a first priority.

6.2.2.2 Large cuts analysis in propagation and residual strength

The goal of this study is to increase the capability of damage tolerant structural items to resist to large cuts. That means, in particular :

- to reduce maintainability costs (replacing visual detailed or NDT inspection by general visual, reducing inspection intervals,...),
- to reduce weight thanks to the better damage tolerance capability offered by new alloys,
- to comply with high fatigue stress levels in the case of large aircraft,
- to comply with design and/or justification requirements (rotorburst, 2 bay crack criterion,...).

Thanks to 3D geometrical and material non-linear models developed in the frame of a project called 'Tol Dom 2000', it is now considered to reach :

- the calculation of circumferential crack growth due to mechanical loads, knowing the driving force curve (stress intensity factor versus crack length) and Forman law for the alloys used,
- the calculation of longitudinal crack growth due to internal pressure. The bulging effect remains as a field of investigations,
- the prediction of the residual strength in the presence of a circumferential or a longitudinal crack, including static failure of stiffeners, fastening system failure (shear) or instability of the skin (R-curve concept),
- the design of stiffeners which are able to sustain limit loads in the presence of a large cut (figure 15).

These models will be validated thanks to tests performed by the CEAT on the flat and curved (so pressurised) panels during the course of the FNGM programme (figure 16).

6.3 EXPERIMENTAL TECHNIQUES

6.3.1 Assessing K-gauge capabilities for structure testing (CEAT)

The K-gauge (figure 17) has been developed for the assessment of KI and KII through the strain field measurement at a crack tip.

First phase investigations, already mentioned in the ICAF'97 French National Review, had shown :

- a significant influence of an error in the axial positioning,
- an influence of the coefficient of biaxiality in complex loading conditions, mainly due to the distance between the strain state measurement points and the crack tip.

From the second phase that recently completed this study, a methodology able to correct K-gauge measurements of the influence of the stress field represented by the T-stress elastic term has been developed. This method, which requires a supplemental strain measurement, makes more universal and efficient the K-gauge usage and allows to measure the T-stress term. Sufficient previous testing and evaluation has now been done to be able to introduce this gauge in structure testing.

6.3.2 Development and running of a fatigue test facility for fuselage representative curved panels (CEAT)

A new test fixture has been set up at CEAT to subject full-scale fuselage curved panels to static and fatigue loads representative of those resulting from the fuselage pressurisation and bending. This fixture is capable of :

- fatigue tests under constant and variable-amplitude loads up to 1,200 kN and 700 mbar (10.15 psi) at frequencies up to 8 Hz and 0.25 Hz, for the axial and differential pressure loads respectively,
- residual strength tests, by applying axial and/or differential pressure loads up to 4,000 kN and 1,400 mbar (20.3 psi).

This fixture was designed to accommodate panels with a radius of 110 inches (2.8 m), typical of the AIRBUS A340 fuselage. The panel maximum dimensions are 4026 mm x 2268 mm (158.5 inches x 89.3 inches), with a varying frame pitch.

Special attention has been paid to the application of the tangential loads to the panel skin (use of non-impregnated glass fibres to reduce the shear effects resulting from the axial deformation) and the inspectability (reinforced-glass window over the central bays and motorised handling of the pressure chamber back door for quick access to the panel). The general drawing of this test facility is shown figure 18.

A typical test campaign on a single panel consists in propagating under combined fatigue loads an artificial crack along the circumferential direction. The panel is then repaired and a new crack is applied in another area of the panel along its axial direction. Then again, the propagation under combined fatigue loads is monitored by use of a remote control camera. The test is ended by residual strength assessment leading to the panel destruction.

Since August 1998, 3 panels have gone through such tests within the framework of an Aerospatiale-Matra research study aimed at defining the future AIRBUS A3XX fuselage. Results reported § 6.2.2.2 have been obtained with this test device.

6.3.3 Biaxial fatigue testing facility for engine materials (CEAT)

In the early nineties, CEAT has developed a biaxial fatigue machine capable to perform tests at elevated temperature (internal pressure + axial load on a thin walled tube, up to 1200°C).

This test facility is able to develop, in a FBA (Fatigue BiAxiale) specimen, tension-tension principal stresses which are representative of those existing in engine rotating discs. To start with, an experimental programme has been carried out at 650°C on the N18 alloy (a powder metallurgy nickel-base superalloy used for M88-2 discs, the Rafale's engine). The detrimental influence of biaxial loads on the lifetime has then been shown when compared to uniaxial test data.

- Since then, a study has been launched to have a better control of the test parameters (temperature and loadings). On one hand, thermal mappings, established during pressure cycling, have shown :

- a longitudinal thermal gradient smaller than 5°C on the external FBA specimen wall,
- an internal wall temperature cycle in phase with the pressure loading, but with a mean value lower than the external temperature (about 70°C with an induction heating system).

On the other hand, the finite element analysis , figure 19, (used to calculate the correct loading of the specimen) has been improved by using a material behaviour law (the elasto-plastic stress-strain curve) obtained from the first quarter cycle of a uniaxial fatigue test on a FBA specimen instead of a law extracted from a tensile test on a conventional plain specimen.

Now a widest study is aiming at :

- characterising the influence of test parameters (max loadings, loading ratios, phase difference between the axial and pressure loadings) by using experimental design,

- modelling and calculating the biaxiality effects with viscoplastic improvements on the material behaviour law and with a comparison between cumulative damage model combined with multiaxial criterion's.

6.4 METALLIC MATERIALS AND TECHNOLOGY TESTING

6.4.1 Fatigue on landing gear representative specimens (Messier Dowty - CEAT)

A fatigue test programme on specimens representative of landing gears components, in this particular case the landing gear trailing arm illustrated figure 20, which has already been mentioned in the last two National Reviews, is now completed. After having tested several materials as the aluminium alloys (7010 T74, 7175 T73 and 2618A T6) and the high strength steels (300M and 35NCD16), the last phase was dedicated to compare two shot peening processes : steel balls and glass balls. This experience has been carried out on 7010 aluminium alloy specimens treated by chromic anodisation. Results have shown :

- a comparable fatigue behaviour in the range of 10^5 cycles, regardless the ball material,
- for the two shot peening processes, a 25% decrease of the endurance limit in the 10^5 cycles domain, when compared to the untreated material.

Stress controlled fatigue tests carried out on uniaxial cut-up specimens - steel shot peening + chromic anodisation treated - have shown a fatigue strength reduction function of the number of cycles, with no significant improvement in the range of 10^5 cycles.

This general programme is now oriented towards the fatigue behaviour of main articulations (figure 21). The purpose is then to develop dimensioning rules allowing for the new requirements associated to future landing gears such as new endurance requirements, new maintenance conditions and new materials.

Fatigue tests undertaken on thirteen representative specimens are aimed at assessing the influence of various parameters such as the geometry, materials and lubrication conditions which govern the design of these articulations.

6.4.2 Validation of 2017 CP (Crack Proof) rivet use (Dassault Aviation).

Fatigue tests have been performed on specimens, with load transfer and without, representative of a Falcon stringer to skin attachment and a skin splice.

Various kinds of rivet installation have been tested :

- automatic (PRECA),
- manual,
- robot.

The effect of the countersink depth and de-burring at the skin faying surfaces turned out to be of major importance in fatigue performance. The fatigue life of 2017CP riveted assembly is demonstrated to be equivalent to the solution treated riveted assembly (figure 22).

6.5 RULE MAKING SUPPORTING ACTIVITIES

6.5.1 Improvement of justification methods, prediction of widespread fatigue damage for ageing aircraft : A300 life extension (Aerospatiale-Matra, Aviation Branch)

This subject leads Aerospatiale-Matra to work on multiple site damage modelling. In the framework of the European research program Brite-Euram SMAAC, a finite element based methodology has been developed and validated. This should allow to predict multiple crack initiation, propagation and residual strength in susceptible structures taking scatter and interaction effects into account (figure 23).

6.5.2 Improvement of justification methods, Initial flaw approach for design (Aerospatiale-Matra, Aviation Branch)

The concept of Initial Flaw Size has been used in US military aircraft for a long time (to assess the threshold and the inspection interval).

It is also currently used in Aerospatiale-Matra for damage tolerance analysis, especially to determine the inspection interval in simple and multiple load path structures.

Up to now, the threshold of first inspection has been calculated with a fatigue approach. Today, Aerospatiale-Matra is used to calculating with the following values : 1.25 mm for the manufacturing defects and 0.125 mm for the Equivalent Initial Flaw Size.

The objective of Aerospatiale-Matra research is to use efficiently the Initial Flaw approach for damage tolerance evaluations (Threshold and Interval assessment). This approach is now required by FAR/JAR 25.571.

The main tasks consist in :

- verifying the consistency of the values used so far (0.125 and 1.25 mm),
- determining Equivalent Initial Flaw Size and Manufacturing Defect distributions taking into account the various aeronautical configurations (material, geometry, technology...),
- defining new design criteria.

6.5.3 Fuselage fatigue test on a retired Mercure 100 (Dassault Aviation & CEAT)

After Mercure fleet retirement from operation in April 1995, the production line number 3 aircraft (registered under F.BTTC) was acquired by the airworthiness section of the French Official Agency SPAé. The fuselage has been taken to the Toulouse Aeronautical Test Centre facilities to perform a pressurisation fatigue test for 50,000 cycles in order to compare the results of this test, on an aged and corroded structure, with those obtained twenty years ago on the initial full scale test required for the Mercure 100 type certification. The purpose of this test is not at all to extend the life of this aircraft since the whole fleet is now retired from service, but to develop arguments that can be useful in rule making activities.

This fuselage was 18 years old and had accumulated 37,740 flights (or 31,970 flight hours). After installation in the test rig (see photography figure 24), a thorough inspection of the fuselage structure, performed by a joint control team of CEAT and Dassault Aviation specialists, identified the damaged state of the test article before the first pressure cycle. 141 damages, mainly from corrosion origin and a few short cracks, were then identified. These damages are monitored through the following inspection programme :

- basic inspections each 5000 cycles,
- deeper inspections each 20 000 cycles.

After this initial structure identification, the first test cycle took place in June 1996. This fatigue test has been recently completed and a static test up to 1.15 ΔP performed.

After 30,000 cycles, a major fatigue damage at the upper corner of the passenger door (figure 25) needed to be repaired (with an external steel doubler) for pursuing the test. As far as the other fatigue cracks discovered on the oblique rear pane frame fitting cap (see description in the ICAF'97 French National review) are concerned, decision was made to monitor their growth without any repair action. These damage did not show any significant evolution between 30,000 and 50,000 cycles, plus the residual (1.15 ΔP test). Nevertheless, during this period several fatigue ruptures have been experienced in the lock stops of the passenger and service doors.

A limited tear down to be launched soon will allow to comprehensively conclude this programme. As a first impression and as far as real ageing influence on fatigue behaviour was investigated, few lessons have been learnt due to the good corrosion resistance of this fuselage.

6.6 - SONIC FATIGUE (Dassault Aviation)

Extensive experimental works have been made by Dassault Aviation in the Sonic fatigue area. Since Falcon 10 inlet lifetime was considered as too short, it has been modified (with a lower stiffness) and the new structure design is now comparable to the MF 900 and F 2000 inlets.

The fatigue life of the modified inlet is deduced from strain gauges measurements on frames and skins.

As far as Mystere 20-5 and MF900B inlets are concerned, the two aircraft have the same engines and inlets, but the rate of crack detections (sonic fatigue) on Mystere 20-5 inlets is much higher than MF 900B rate.

An inlet equipped with strain gauges has been installed on a Mystere 20-5 and a MF900B. It has then been shown that the stresses around the de-icing holes increase very much above 92% N1 (engine regime). It is believed that the engine used on the Mystere 20-5 is more frequently used in a range between 90 and 98% N1, owing to the flight manual.

The frame 1 web should be reinforced. The effect of the nose buzz noise on stresses has also been evaluated.

6.7 FULL-SCALE FATIGUE TESTS NEWS

6.7.1 TBM 700 fatigue test (SOCATA and CEAT)

The TBM 700 is a monoturbo-prop aircraft with a 6/7 seat capacity, produced by SOCATA since 1991. Today, 130 aircraft have been delivered around the world with 19 ordered by French Air Forces for various liaison and training missions.

A full-scale static test on a complete structure, plus a pressure fatigue one (up to 10,000 flights) on the fuselage only, have been performed in the period 1989 - 90 for type certification. 3,300 flights were then released, by analysis only as far as other parts than the fuselage are concerned. In order to achieve the demonstration required for a 10,000 flight certification, a new complete fatigue test started in 1995 at CEAT (figure 26) with a specimen made of the previously tested fuselage plus brand new wings, empennage and landing gears.

Safety factors that were decided to be applied were 3 for the fuselage and 4 for the rest of the structure, leading to a 40,000 flight simulation. The fuselage having already supported 10,000 missions, there is one pressurisation cycle every two missions. Some complementary (severe) landing conditions have also been introduced in the load spectrum to meet Air Force specific requirements.

The 40,000 flight target was reached in August 1997, the main detected fatigue damages concerned the pressurised part, without requiring so far complex repair solutions :

- passenger door frame (between frames 10 and 12),
- junction bulkhead - windshield,
- exit door.

10,000 extra flights have then been added to fully substantiate the repair solutions introduced during the test. This last fatigue phase was completed by November 1998 and a residual static test has been performed in February 1999 before dismantling the test article.

Additional damage found during the last fatigue phase mainly concerned the already mentioned passenger door frame 12, that will require a slight drawing modification. This damage is illustrated figures 27 and 28.

The residual static test campaign which consisted in :

- a fuselage pressure test (1.1 ΔP),
- a positive wing bending (combined with fuselage pressure) up to Limit Loads,

did not reveal additional findings.

6.7.2 Gazelle helicopter fatigue test (EUROCOPTER & CEAT)

The gazelle SA341 is a combat light helicopter produced by Eurocopter for observation, liaison and anti-tank missions. This helicopter currently equips the French Army and, with machines built under license by Westland, the United Kingdom Forces.

The structure tests of this helicopter were performed in CEAT in the period 1974-78 with, in particular, a full-scale fatigue test that could release a 7,500 flight hours (FH) safe life time, extended by analysis to 10,000 FH later on. Taking into account the remaining potential of their own fleets, French and UK Forces wish to prolong the utilisation up to 15,000 FH. For this purpose, a second fatigue test, co-funded (25%) by the UK Forces, is in progress at CEAT (figure 29).

The test article, service aged and removed from the fleet, is made of a tail boom coming from the French Forces (5,440 FH accumulated) and a fuselage coming from the UK ones (7,500 FH accumulated).

The year 1996 was dedicated to design and build up the test facility while transforming the airframe in the test desired configuration.

The fatigue test started in December 1996.

Twenty seven load channels are used to simulate the three successive phases of the test programme :

- unarmed (clean) version : training and linking (28,125 FH),
- armed version without VIVIANE sight : day-time tactical flight (3,750 FH),
- armed version with VIVIANE sight : day and night-time tactical flight (5,625 FH).

Data from 16 strain gauges and 12 bridges are continuously acquired during the test by mean of a new CEAT device called MEFA. Considering the time needed from inspection and repairs, the total test duration should not exceed three years.

For a 37,500 flight hours test target $\{(3 \times 15,000) - 7,500\}$, 29,625 FH have already been simulated by June 1999. The first phase of the test (28,125 FH simulated in training and liaison version) was achieved in December 1998.

Around forty fatigue damages have been detected on the test article, most of them already found in service or during the first fatigue test. The most important are localised as follows :

- canopy welded frame,
- bulkhead (four damages) as there is an illustration figure 30,
- tailboom/fuselage junction bores,
- quarter hull skin.

Some so-identified damages have been repaired using permanent solutions already applied in service. New damages needed the design of specific repair solutions which are currently validated through this test.

The second phase of the test (day-time tactical flight without Viviane sight) started at the end of April 1999. 1,500 FH were simulated at the beginning of June, without significant damage on the test article.

6.7.3 - Alphajet fatigue test (Dassault Aviation and CEAT)

In-service in the French Air Force (FAF) since 1979, the Alphajet training and aerobatics aircraft has been the subject, since the end of 1994, of a life extension programme (reference 1) with the aim to define the actions to be taken so as to continue both economical and safe operations beyond the original service life. The resulting extended life should allow to fulfil the FAF's needs beyond 2001 and up to 2016 with 150 aircraft operating about 38,000 flight hours per year.

This programme mainly relies on a durability test currently (figure 31) performed on the airframe of the first aircraft having reached the original safe life limit of 180 Fatigue Index (FI) which was substantiated at the beginning of the serial production through an initial fatigue test carried out up to 540 FI (equivalent to 54,000 hours of the expected usage). Up to now, in addition to the 180 IF experienced in service, the test airframe has accumulated 290 FI corresponding 14,000 flight hours in the FAF's current average advanced training conditions.

In compliance with the scatter factors used for French military aircraft to promulgate service lives from full-scale fatigue tests, today, the test progress is not yet sufficient to release any life extension according to a, strictly speaking, safe life concept.

At the current stage of the fatigue test, the most significant damages detected on the test article are :

- failure of a retaining roof flap splice,
- cracks on wing skin,
- cracks in a wing/fuselage junction bore.

Some promising results have however already been derived from the durability test and from associated developments :

- most of the cracks revealed by the periodic inspection on the current test airframe had formerly been identified on the initial one. From these recurring damages, a fair correlation has been recorded between both FI values at the onset of cracking, and crack growth rates.
- with one exception for which a preventive repair has been developed, the disclosed cracking cases exhibit slow growths and appropriate NDI methods (with specific transducers in some instances) have been selected so that the modifications brought to the aircraft maintenance plan could be optimised.
- repair schemes ranging from interim repair to more definitive ones could be developed and the test airframe is used to assess the fatigue potential of the repaired airframes in anticipation of crack findings in the fleet that should therefore not unacceptably affect the aircraft availability.

Reference (1) : L. Deféver, T. Courbe, L. Le Tellier, 'Alphajet aircraft life extension programme', proceedings of the 19th symposium of the International Committee on Aeronautical Fatigue, Edinburgh, 1997.

6.7.4 Transall structure life extension (Aerospatiale-Matra and CEAT)

Developed in the 60's in a French-German cooperation, the TRANSALL C160 aircraft is a military transport aircraft. 67 of them are used by the French Air Force for tactical and humanitarian missions basically.

The service life extension for the Transall was decided in 1996 for the following major reasons :

- the advanced fleet age of aircraft in service,
- the estimated date of entry into service of the new generation military aircraft (around end of 2005).

The definition and substantiation of the life extension program will be based on the analysis of both :

- an extensive in-service damage collection with the establishment of a damage data bank,
- a full scale fatigue test on an aircraft retired from service.

The major participants in this process are : A.I.A (Atelier Industriel de l'Armement) from "Clermont-Ferrand", CEAT, SPAé (Service des Programmes Aéronautiques) and AEROSPATIALE.

A big concern was to define the load spectrum to be applied to the test airframe. A usage monitoring campaign was launched in 1996 to that end, based on :

- collection of general information about each flight of each TRANSALL aircraft (paper form containing the type of mission, flight duration, take-off and landing weights, door openings for droppings...),
- in-flight recording of flight parameters and stresses on 4 aircraft of the fleet, to derive the loads associated with each type of mission.

This campaign should come to an end in July 1999, after analysis of flight paper forms and in-flight records on more than 20,000 and 1,500 flights respectively.

At the same time, the assembly of the test fixture at CEAT will be completed (figure 32). It consists of 119 hydraulic jacks + fuselage pressurisation, and around 600 strain gauges.

After a few last adjustments, the test is expected to begin in September 1999, for a duration of approximately 4 years.

Tear-down inspections are expected at the end of the test to complement the fatigue test and in-service damage data, in order to establish the life extension conditions and updated maintenance program necessary to operate the fleet beyond 20,000 flights.

6.8 IN-SERVICE AIRCRAFT FATIGUE MONITORING

6.8.1 System general description and data collection (CEAT)

Most French military aircraft and a few ones of the same type operated by German and Italian Forces, are equipped with "fatiguemeters" g-counters. This device is able to count the number of times the vertical acceleration reaches or exceeds some predetermined levels during each flight. A debriefing form has to be filled in for each flight. The values of the counters, the mission code and the takeoff store configuration of the flight are written on the same form. Data collection, analysis and calculations on these individual aircraft recordings are performed by CEAT.

Simple calculation rules are used to provide, at any time during each aircraft lifetime, the cumulative fatigue damage at some points of the structure (pointed out as critical during the full-scale fatigue test for instance).

The cumulative fatigue damage is calculated on the basis of Miner's rule, assuming a representative K_t and an appropriate S-N curve . The relations between stresses and vertical acceleration are fitted to give a damage equal to one for one lifetime in the condition of the full-scale fatigue test.

First calculations were performed in 1974. Today, more than 800 aircraft are monitored by CEAT, representing the processing of more than 150,000 flight hours a year.

The load monitoring is not carried out on a sample of each fleet : each aircraft is equipped with a g-counter. Today the following fleets are monitored :

- Mirage 2000, Mirage F1 and Mirage IVP,
- Alphajet,
- Jaguar,
- Atlantique ATL1 (French, Italian, German),
- Falcon 10 Mer,
- Epsilon,
- Mystère 20.

For those fleets approaching their potential limitations, periodicity of processing and feed back to the Air Forces has been recently increased. This is the case for the Alphajet (every month) and the Mirage 2000 (every other month).

6.8.2 Evolution of the system : MICROSPEES (Dassault Aviation and CEAT)

Early production line Mirage 2000 for French Air Force (FAF) are equipped with the fatiguemeters (g counters) described § 6.6.1, the data of which are mostly representative of the loads supported by the wing root. With the development of new external load inventories, the M. 2000D aircraft, being now delivered to the FAF, are equipped with the "MICROSPEES" device.

This device - 5 analogic channels + 7 binary parameters data (no strain-gauge) - is able to record the history of different flight parameters such as : Mach, altitude, static and dynamic pressures, control deflections, fuel consumption. The analysis of the records sent to CEAT consists in deriving the stress history at different points of the structure and implementing these local stress spectra into models for fatigue crack initiation and propagation :

- fatigue crack initiation prediction is very similar to that performed on the other Mirage 2000 (on the basis of load exceedance records from g-counters) : a fatigue index (FI) is derived from the damage calculated on the basis of Miner's rule assuming an appropriate S-N curve. The only difference lies on the accuracy of the spectrum and the stress history which is taken into account by use of a RAINFLOW process,
- fatigue crack propagation prediction uses a model developed by ONERA : this model is based on the crack closure concept and accounts for stress history.

The first inspection is derived from the crack detection on the durability test airframe, by application of a reduction factor of 3 to the corresponding calculated Fatigue Index.

The crack growth investigation under various spectra and stress level outlines that the above mentioned "Fatigue Index" (FI), is penalising with regard to the definition of inspection intervals when considering more severe utilisation of aircraft. Thus, the subsequent inspection intervals are defined by a specific "Propagation Index" (PI) value corresponding to the application of a reduction factor of 2 to the calculated time necessary to reach the critical crack size.

The processing of the first MICROSPEES records raised some difficulties that have been overcome since then in new technical specifications. These are being implemented in a CEAT software to resume processing by the end of 1999.

6.8.3 Next generation of the system : HARPAGON (Dassault Aviation and CEAT)

HARPAGON is the name of the Health and Usage Monitoring System on the RAFALE aircraft. Part of it will be dedicated to fatigue damage calculation.

The approach is similar to that applied to the Mirage 2000-D fleet and described in §6.8.2. Fatigue and Propagation Indices (FI and PI) are derived from in-flight recorded parameters. The main improvements are the following :

- more parameters recorded (around 30),
- more structural points tracked (around 30),
- more advanced model for fatigue crack initiation (Dassault Aviation model),
- day to day assessment of the fatigue remaining potential and inspection interval performed by the Air Force and Navy themselves. These values are periodically updated by feed back and comparison to more extensive calculations performed at CEAT.

Today, the technical specifications for the calculations are being written, so that the computer programming may begin by the end of 1999. This should enable the system to be ready when the RAFALE enters into service.

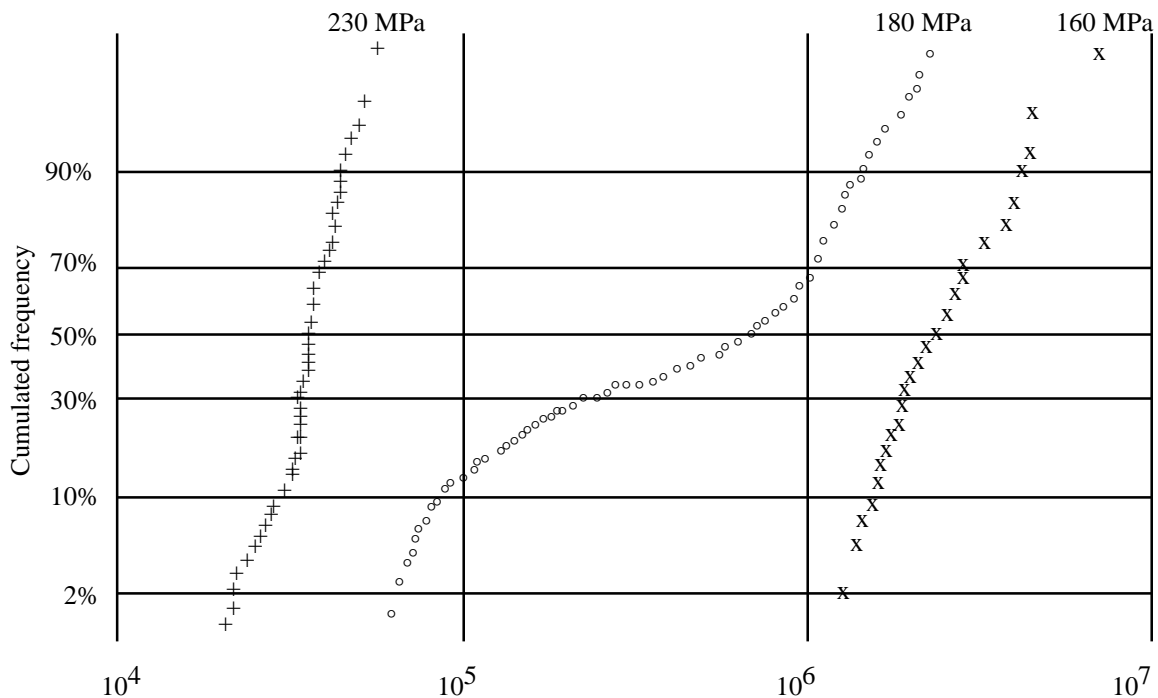


Figure 1 : 7010 T73651 aluminium alloy, fatigue results (two statistical populations co-exist in the intermediate stress level (180 MPa))

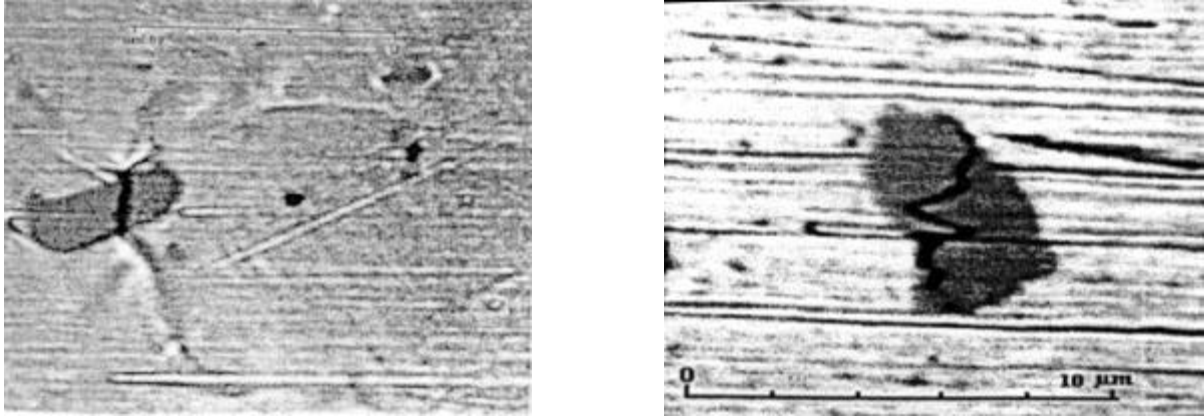


Figure 2 : inclusion failures leading to crack initiation sites

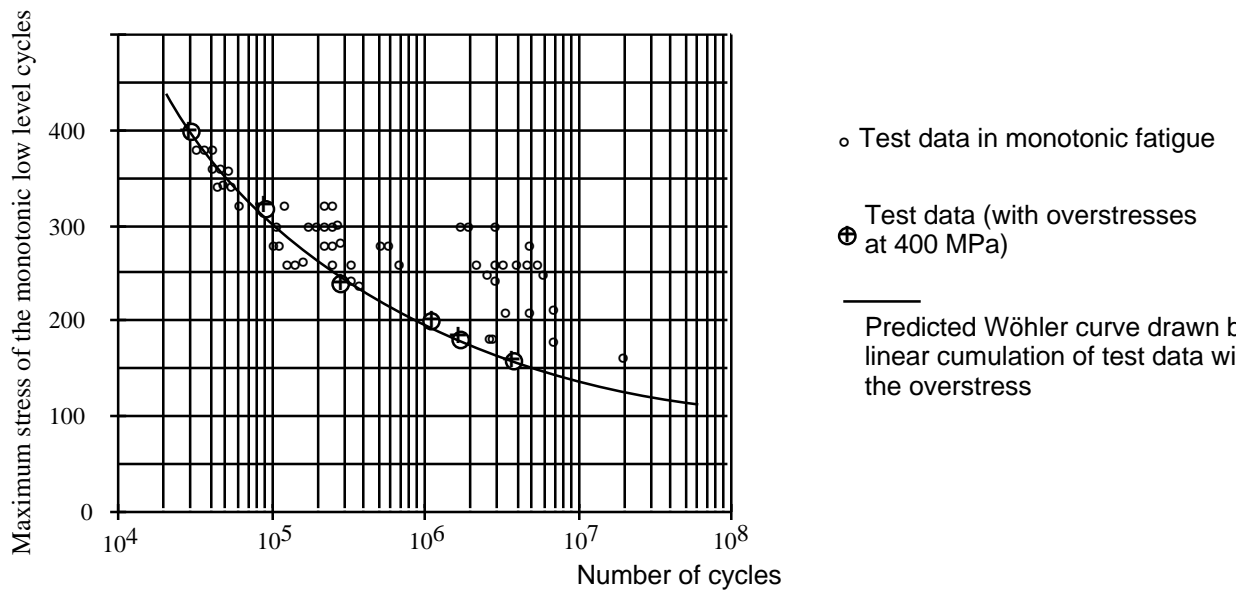


Figure 3 : correlation calculation/experience for the 2024 aluminium alloy

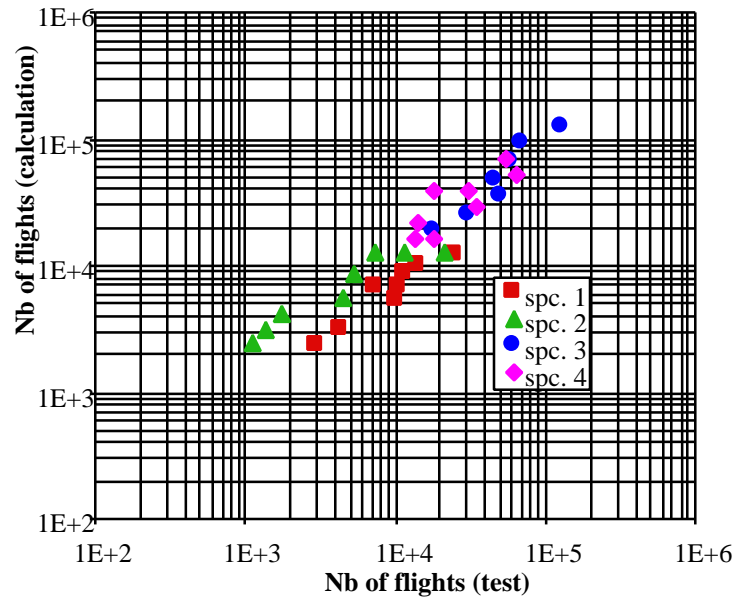


Figure 4 : correlation calculation/experience (open holes specimens)

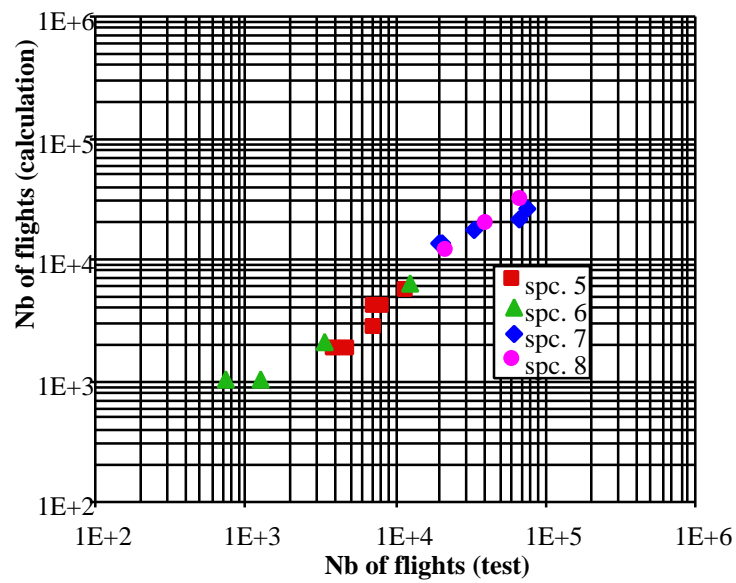


Figure 5 : correlation calculation/experience (open holes specimens with loaded fasteners)

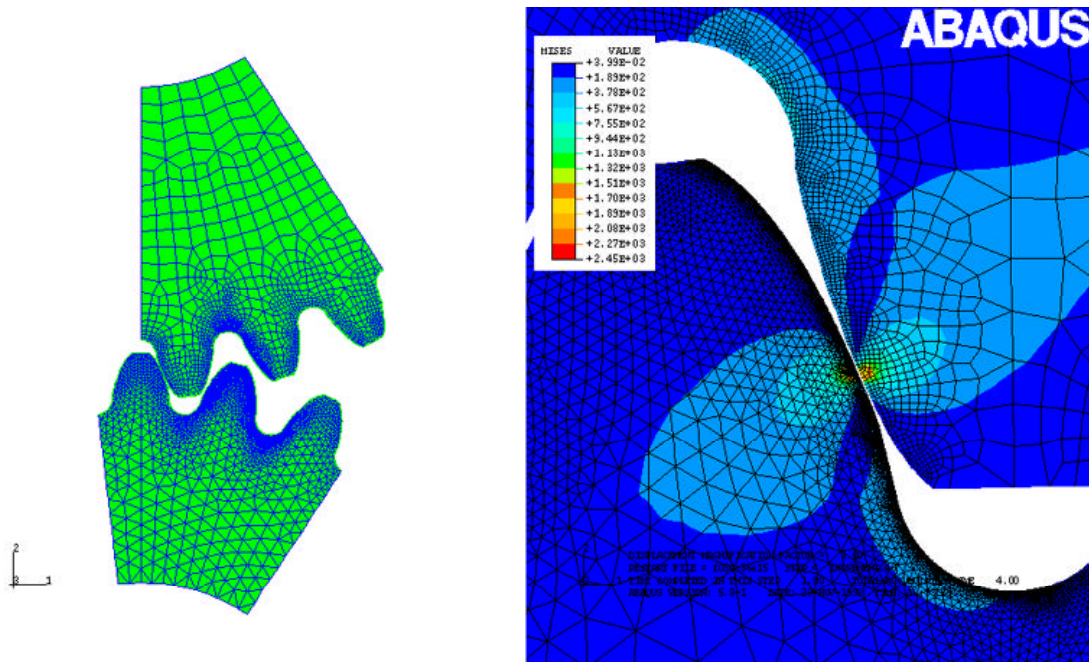


Figure 6 : Simulation of a gear, 3 pinion teeth and 3 wheel teeth (lefthand) and stress level for a given position (righthand) of the gear

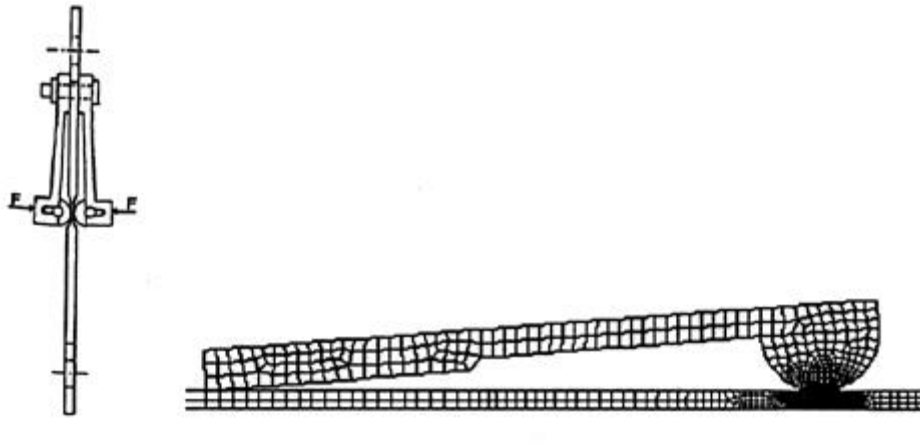


Figure 7 : Fretting fatigue behaviour, experimental equipment (lefthand) and associated finite element model (righthand)

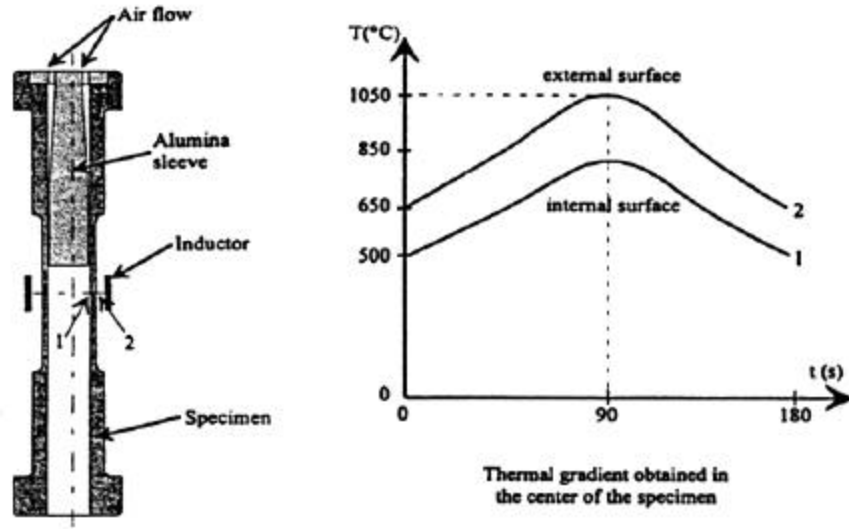


Figure 8 : Scheme of the heated/cooled specimen and temperature distribution

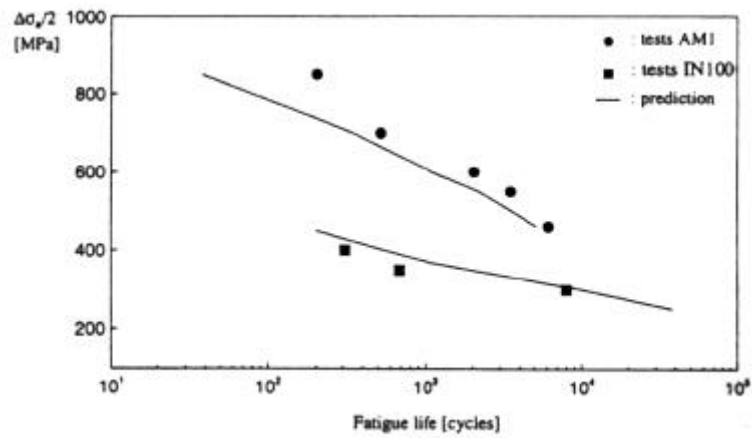


Figure 9 : Fatigue life (in cycles) comparison between experimental and calculated lifetimes

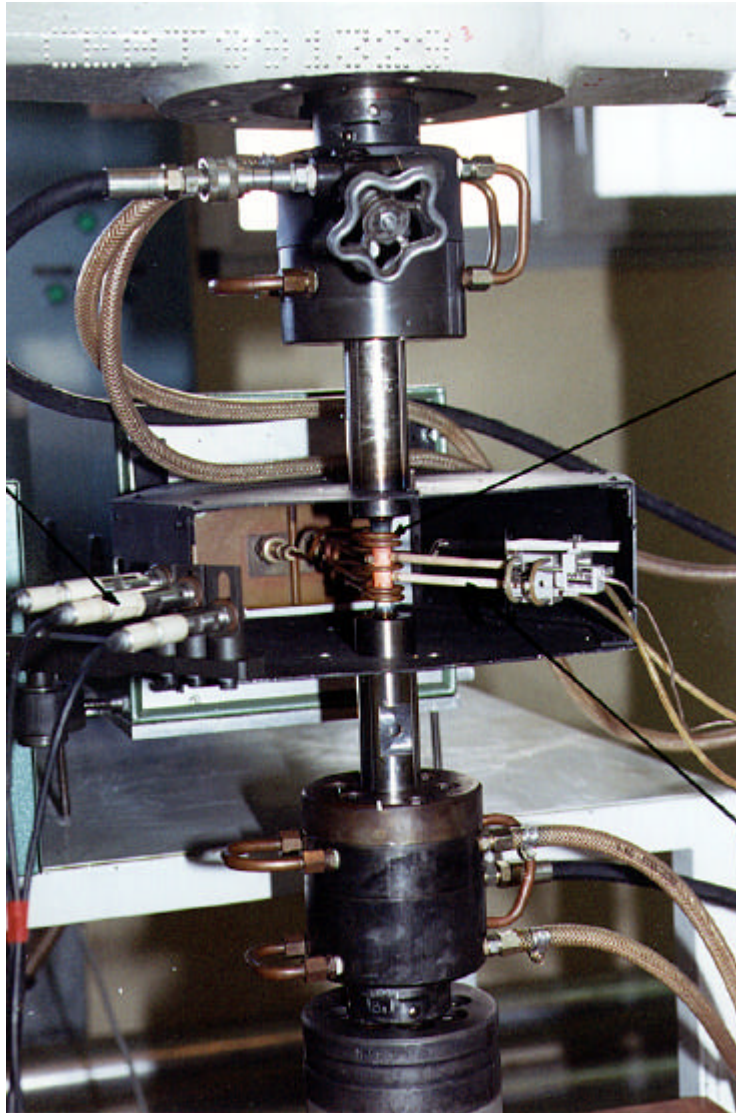


Figure 10 : CEAT's thermo-mechanical testing machine

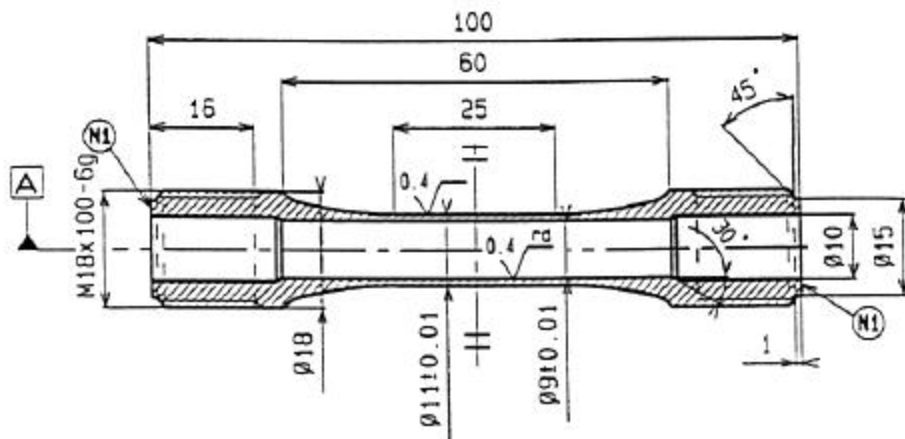
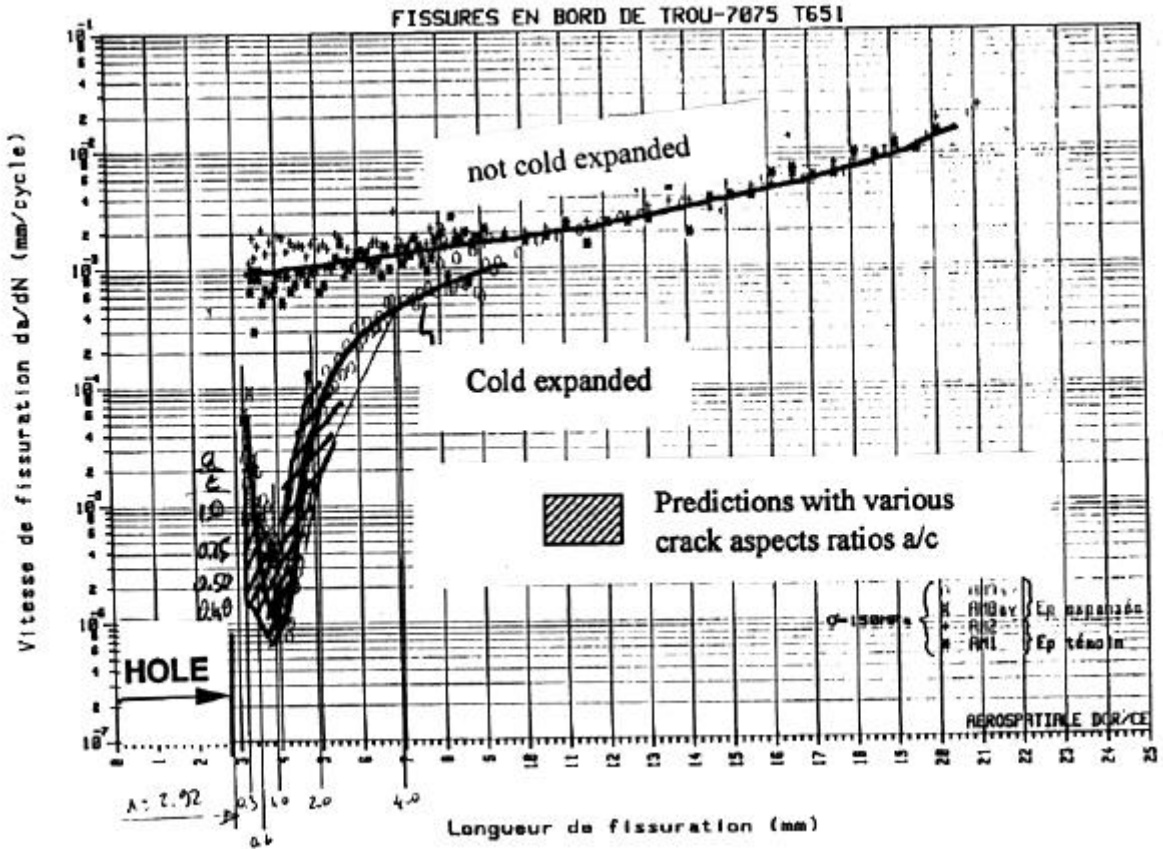


Figure 11 : Specimen developed for thermo-mechanical tests



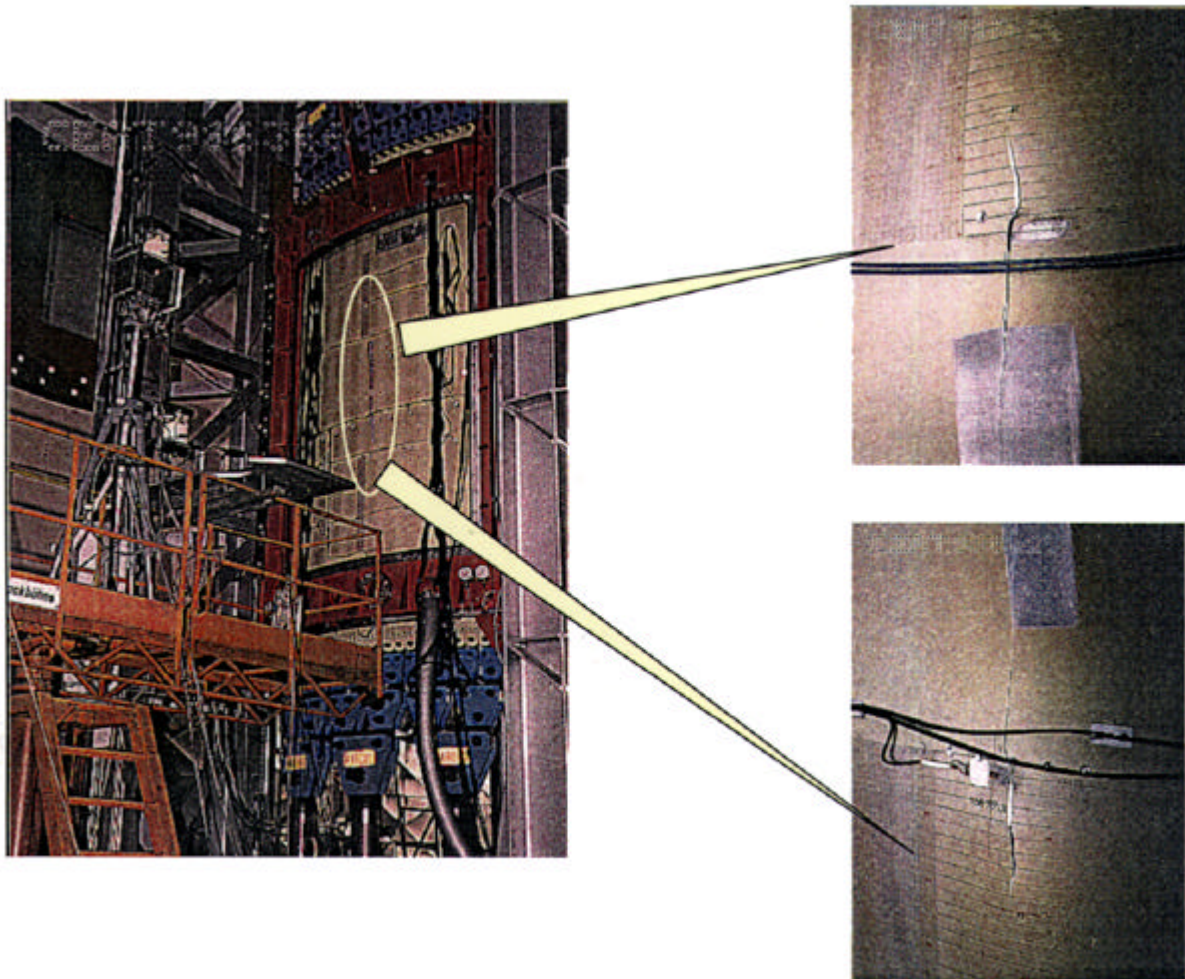


Figure 16 : Curved fuselage panel tested with a longitudinal large cut

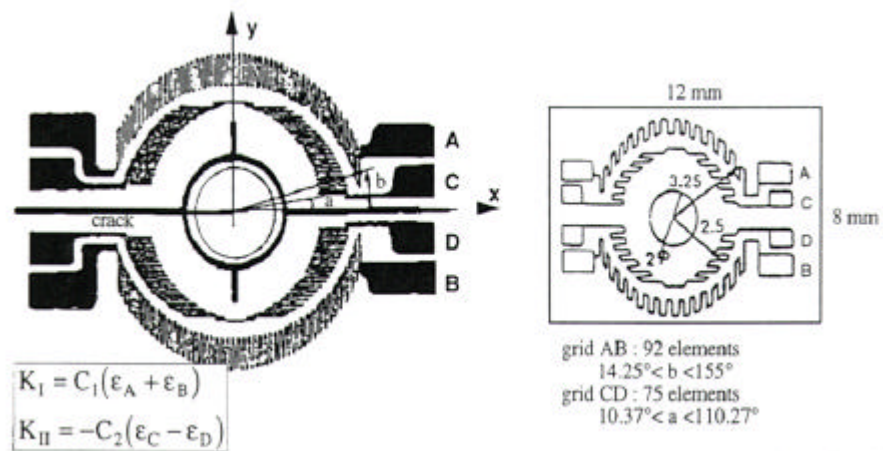


Figure 17 : K gauge principle

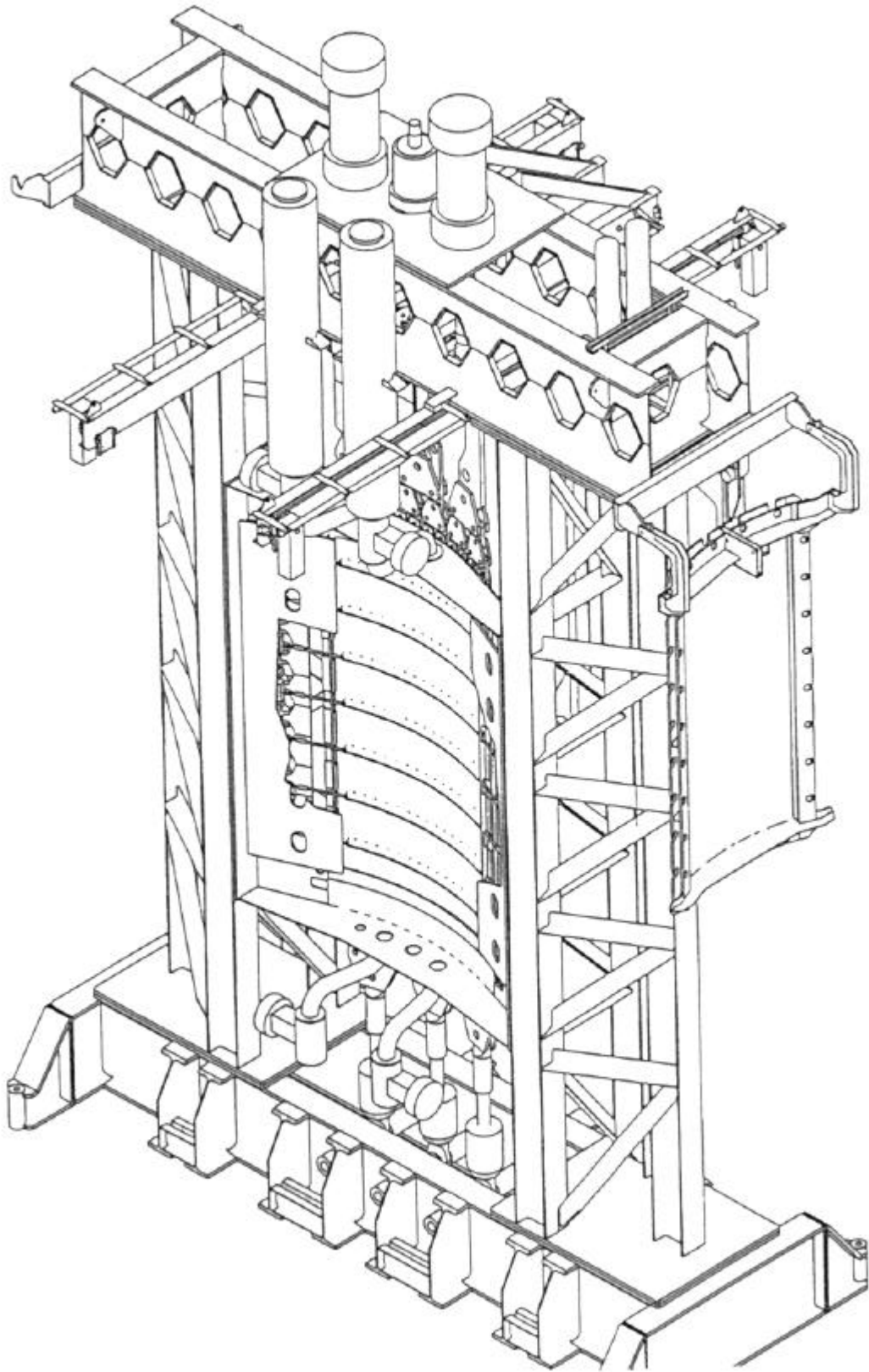


Figure 18 : CEAT's curved fuselage panel facility

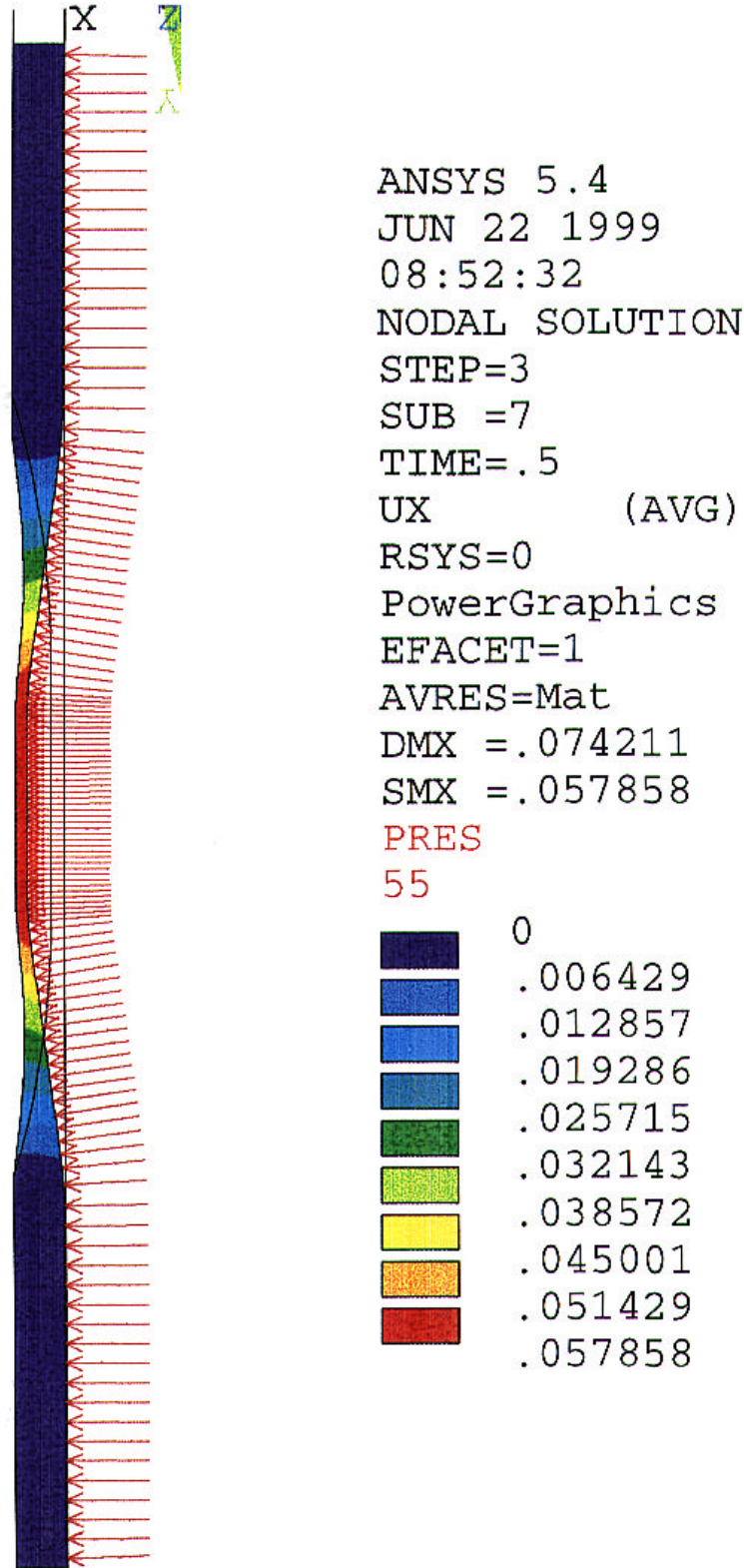


Figure 19 : Deformation of the biaxial fatigue specimen submitted to an internal pressure



Figure 20 : Landing gear trailing arm specimen

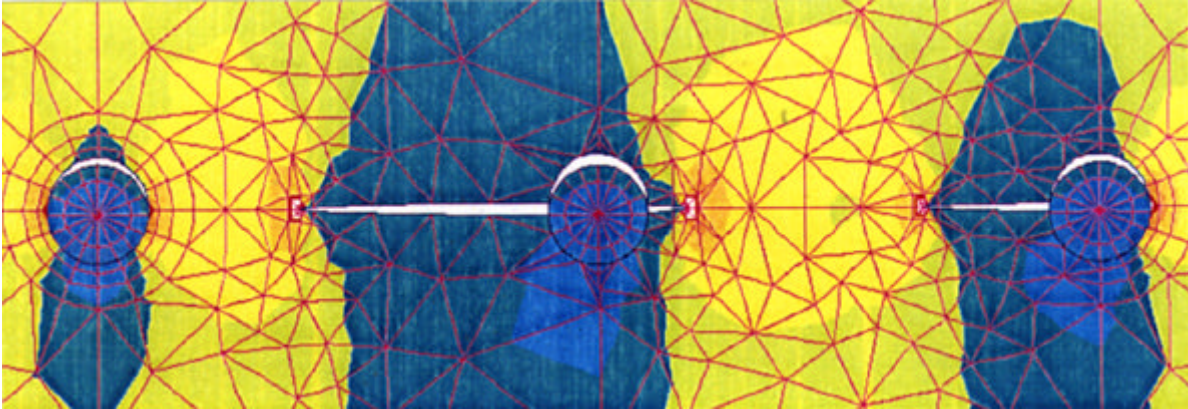


Figure 23 : Validated finite element model for MSD



Figure 24 : Mercure fuselage fatigue test

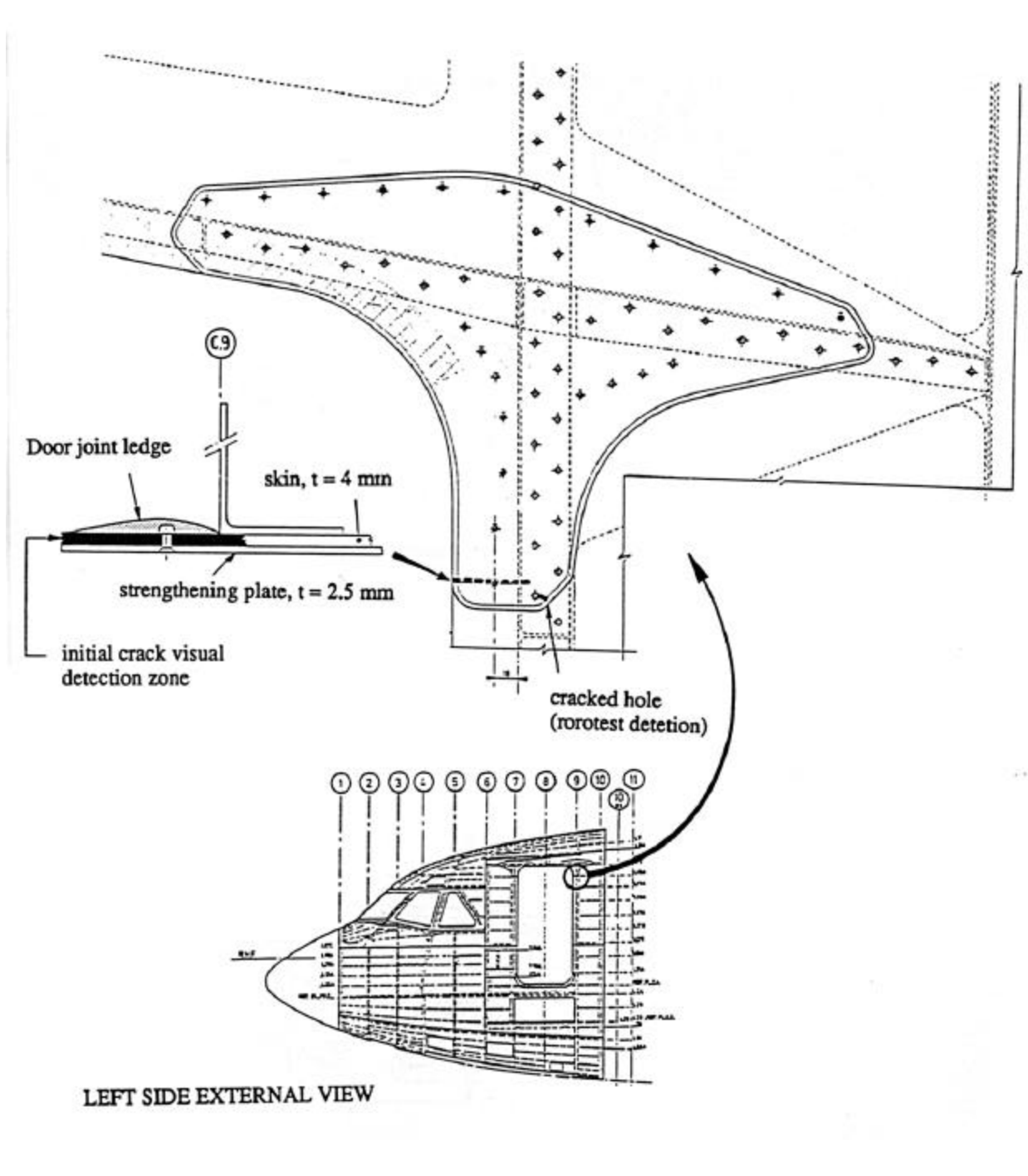


Figure 25 : Skin crack in the upper corner of passenger door at frame 9



Figure 26 : TBM 700 full-scale fatigue test

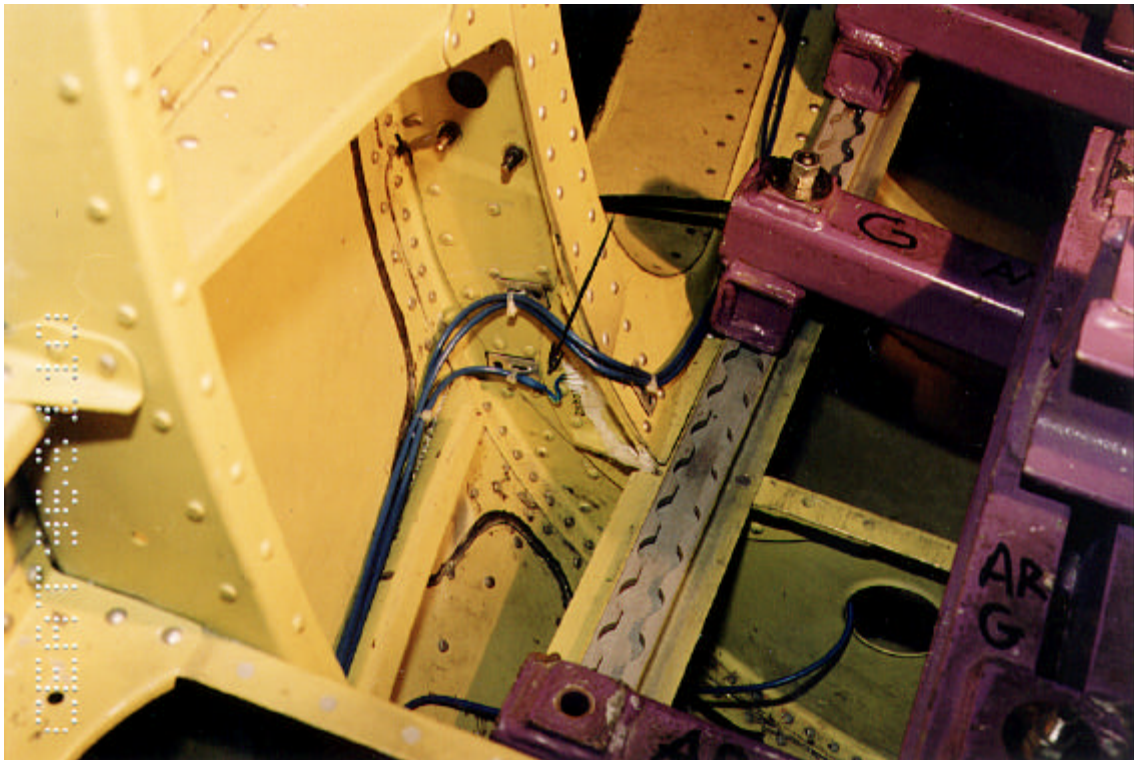


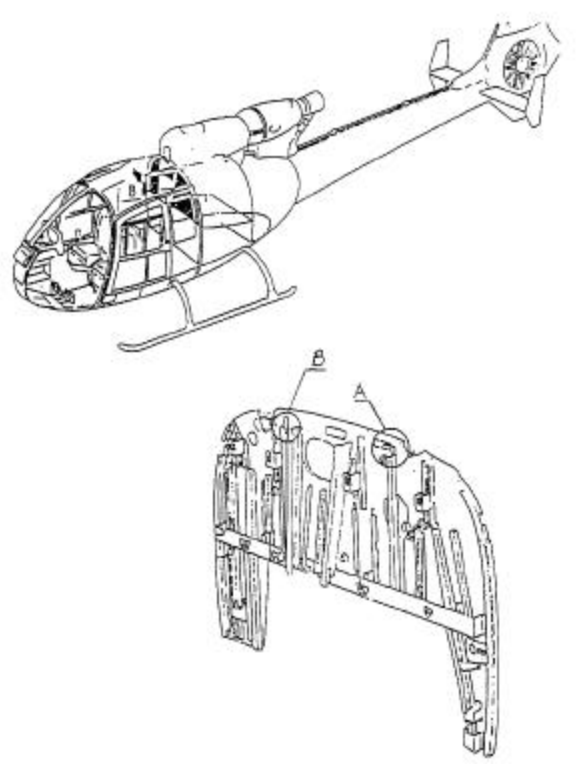
Figure 27 : TBM 700 location of the most significant fatigue damage



Figure 28 : TBM 700 fatigue failed component after taking-down



Figure 29 : Gazelle helicopter full-scale fatigue test



30 D
L = 12 mm



31 G
L = 14 mm



Figure 30 : Fatigue damage at the Gazelle bulkhead



Figure 31 : Alphajet full-scale fatigue test



Figure 32 : Transall full-scale fatigue test

Review of Aeronautical Fatigue Investigation in Italy during the period April 1997 to 1999

A. Slavetti
Universita di Pisa

1. INTRODUCTION

This paper summarises aeronautical fatigue investigations which have been carried out in Italy during the period April 1997 to April 1999. The different contributions have been arranged according to the topics, which are loading actions, fatigue and fracture mechanics of metallic materials, fatigue behaviour of composites, joints and full scale component testing. A list of references, related to the various items, is presented at the end of the document.

The review is based on the activities carried out within the various organisations belonging to A.I.F.A., the Italian Association for Fatigue in Aeronautics. The authors gratefully acknowledge the fundamental contribution, which has made this review possible, made by several A.I.F.A. members, who are the representatives of Universities and Industries in A.I.F.A.

2. MEASUREMENT AND ANALYSIS OF OPERATIONAL LOADS

2.1 - Design and installation of a structural monitoring system (Aermacchi)

On the basis of the requirements of a foreign customer, a structural Health, Usage and Monitoring System (HUMS) has been jointly developed by Aermacchi and Agusta; the system has been subsequently validated and installed on the S211 fleet in order to perform the Load/Environment Spectra Survey and Individual Aircraft Tracking functions.

The main guidelines followed in the development of such a system have been:

- Relative simplicity
- User friendly
- Ease of installation on aircraft already in service
- Limited use of dedicated sensors
- Reliable use of the S211 full scale fatigue test load histories

The recording and reduction of a limited number of in flight parameters time histories allow the analytical calculation of flight loads in the most significant items (see fig. 1). The loads analysis is performed with the aid of a computer on ground and is based on a sound and extensive flight load survey previously carried out during the certification phase of the S211 aircraft.

The relevant elements of the S211 HUMS system are:

1) IN FLIGHT

- Acquisition of flight parameters
- Data compression through the Peaks and Valley methodology
- Max N_z exceedences indication
- Automatic counting of spin turns

2) ON GROUND

- Data validation
- Loads/stresses calculation in the selected control points of the airframe
- Fatigue damage rate evaluation for each control point
- Consumed safe life and load severity indexes of the fleet

Fig. 2 shows the results obtained, with reference to the wing structure.

2.2 TORNADO life monitoring (Alenia Turin)

As already outlined in previous versions of the Italian National Review, the accounting for structural fatigue life of g-sensitive components applied to the entire Italian Tornado fleet continues to be managed by ALENIA using its own computer program that utilises g-meter readings and configuration/masses control. This activity is performed in parallel with the Maintenance Recorder System that is managed by Italian Air Force.

Updating of Maintenance Recorder System software (a monitoring system based on flight parameters recordings on board and fatigue life consumption calculation on ground) was performed. In addition, the software for filtering input data was improved, and a significant reduction of invalid recordings due to spikes was obtained.

A series of comparisons of Maintenance Recorder System results with outputs obtained by other computer programs, commonly used for calculations, took place. This activity was successfully concluded and resulted in the final validation of the system.

As far as the evaluation of the fatigue consumption of items not monitored by present monitoring systems is concerned, a complete review of qualification status and fatigue criticality of unmonitored items was performed.

The activity of measurements on statistical basis of actual service loads and spectra will continue in the next years; this will permit also to evaluate the possibility to extend the use of the aircraft.

An analysis dedicated to verify fatigue consumption of pylons carrying stores, that were not previously considered in the design of the aircraft, was carried out.

2.3 Fatigue monitoring of the AM-X (Alenia Turin/Aermacchi)

As already outlined in previous versions of the Italian National Review, the fatigue monitoring of AM-X is performed on each aircraft of the fleet by means of the computer program prepared by ALENIA; like for Tornado, the program is based on g-meter readings, configuration/masses and mission profiles.

Another structural fatigue monitoring system, developed and installed in collaboration with Aermacchi, based on 7 strain gauges and 1 accelerometer and called Airborne Strain Counter (ASC), is also used, but only on a limited number of aircraft, while all the others will be monitored via g-readings.

The reference stress spectrum is obtained by full scale fatigue tests and it is measured several times in order to minimise the scatter in the strain gauges readings.

A first comparison between the two systems was performed; such comparison activity will continue to find a reliable correlation between the two systems.

3. METALS

3.1 - Fatigue behaviour of notched and unnotched materials

3.1.1 Application of surface coatings for anti-wear purposes (Agusta)

Following the experiences of the previous years, a research activity has continued on the influence of anti-wear treatments on the fatigue behaviour.

Dynamic components of helicopters are quite often subjected to dynamic loads in presence of sliding contacts, which result in typical fretting fatigue conditions. For this reason, fatigue tests in fretting conditions have been carried out on Ti alloys, [1]. Test results obtained in fretting and non fretting conditions ($R=0.1$) are shown in fig. 3a, while the effect of two coatings (PVD: Physical Vapour Deposition; DG: Detonation Gun) is shown in fig. 3b.

By applying surface coatings necessary to reduce friction or surface damage, it is necessary to take into account the effect on the fatigue properties that the coating generates. Therefore, rotating bending fatigue tests are always carried out at any time that new surface treatments are evaluated. Fig. 4 shows how two new coatings under evaluation behave in comparison with the bulk material baseline and with previous test results.

3.1.2 Advanced surface treatments for transmission gears (Agusta)

New production routes for high performance gears and bearings, as well as possible process improvements, are continuously being developed; in the following, a description is given of some results about the fatigue evaluation of new surface treatments obtained during the last two years.

3.1.2.1 Development in nitriding and carburizing processes (Agusta)

The key processes commonly applied to improve the mechanical and fatigue properties of gear steels are the nitriding and carburizing processes.

The increased resistance and the residual compressive stresses introduced in the surface layer (case) usually play a fundamental role in fatigue performance.

Studies on both those processes are currently underway, together with fatigue testing to evaluate the influence on the performances at Politecnico di Milano - Dipartimento di Chimica Fisica Applicata and in Agusta company. The evidence of the effects of process improvements to fatigue will be available in the future months.

3.1.2.2 Duplex hardening (Agusta)

A Brite Euram program, funded by the EU, is aimed at the development of high performance surface materials, searching for the best compromise of core toughness, surface hardness, fatigue endurance and rolling contact fatigue resistance and elevated temperature resistance. Many parameters have conflicting consequences and the influence of any of them is evaluated.

One of the key areas is of course the surface hardness and the presence of a fairly thick hardened case showing compressive residual stresses. This can be achieved by duplex hardening (carburizing followed by nitriding), thus obtaining a hardened case over a tough core, see [2]. Fig. 5 shows the improvement in fatigue endurance which can be obtained with reference to a traditional carburized material.

3.1.3 Evaluation of high tempering temperature carburizing steel (Agusta)

Traditional carburizing steels for helicopter transmissions are usually limiting the performance of the gearbox by their temperature limits. In fact their carburized case cannot withstand temperatures higher than 150°C without softening. The choice of a material with higher tempering temperature is the most straightforward to allow higher temperature performance and to withstand longer loss of lubrication conditions, without introducing too many changes in the design. In fact for Pyrowear 53 (trade mark of Carpenter Technology), all the sophisticated processes applied to the gears remain almost unchanged. A comprehensive study was carried out to evaluate fatigue endurance properties of this new material compared to traditional AISI 9310.

The evaluation of the gear performance in fatigue is difficult because the carburized case must be tested possibly in the same stress concentration conditions of the actual gear. Tooth bending tests, though more similar to reality are subject to experimental pitfalls. A good solution seems the tensile tooth root fatigue specimen which is shown in fig. 6. By careful choice of the root radius, a good similarity with the situation of the actual gear tooth root can be achieved. For carburizing steel tests 1mm radius was chosen.

The tests on Pyrowear 53 showed very consistent results compared to AISI 9310, as shown in fig. 7. As these tests were run at ambient temperature, the advantage at elevated temperature in the transmission is expected to be noticeable.

3.2 - Crack propagation and fracture mechanics

3.2.1 Fatigue crack propagation and fracture analyses of some Al-Li alloys (Uni. Rome)

An experimental activity has been carried out to evaluate the crack growth resistance of three different commercial Al-Li alloys: 2091, 8090 and Weldalite 049 (2195). Fatigue tests were performed on compact tension (CT) specimens machined from the plates in the LT orientation with $B=9.5 \pm 12$ mm and $W=40$ mm. All tests were conducted with a sinusoidal constant amplitude loading, at $R=P_{min}/P_{max}=0.3$, with a maximum load P_{max} of 4 KN. The fatigue tests were carried out in two different environments (air and 3.5% NaCl aqueous solution) and at different frequencies (1, 2, 5

and 10 Hz). Fracture surfaces were examined using a scanning electron microscope (SEM). Some fracture surfaces were etched with a particular reagent in order to identify the crystallographic orientation of fatigue crack surface facets.

Figures 8 show the comparison between the fatigue crack propagation behaviour of the three studied alloys in air (a) and in NaCl aqueous solution (b). The scatter bands in the figures are the result of all the tests conducted on each alloy in the indicated environment.

The comparison between the three alloys in air does not show any appreciable difference in the crack growth behaviour. Only the 2091 alloy, near the threshold region, shows higher propagation rates. In aqueous chloride solution Weldalite 049 shows lower propagation rate at any ΔK . From all the results obtained, it is clear that there is not a direct correlation in the frequency range 1 - 10 Hz between the applied frequency and the fatigue crack growth rate both in air and in chloride solution

The good fatigue properties of this class of materials result from a series of phenomena that reduce the crack growth driving force. Usually Al-Li alloys show an intergranular fracture with evident signs of delamination. Delamination phenomena increase fracture toughness and fatigue crack growth resistance in the TL and LT orientations, because they divide the specimen into thin sheets and thus change the expected plane strain state (triaxial load) in a global plane stress state (biaxial load, lower stress level). However, the main phenomena that reduces the crack growth driving force are those related to the roughness induced closure mechanisms.

For a better and more complete analysis of the test data, a FE analysis has been carried out of the plastic wake and plastic zone utilizing the Dugdale strip yield model. The main objective of such an activity was a better interpretation of test results near the threshold, where significant contributions to crack closure come from the roughness. More details are reported in [3].

3.2.2 Application of aluminium lithium alloys (Agusta)

Application of Aluminium-Lithium alloys is quite extensive, where a strong weight reduction is required. The possibility to introduce 8090 material in condition T81 in lieu of the classical 2024-T3 is almost straightforward, as 8090 in this condition retains most of the mechanical properties of Clad 2024-T3, with also a slight improvement in fatigue endurance.

One concern was related to fatigue crack propagation, because new design of helicopter airframes is bound to damage tolerance certification criteria.

As it is well known, some of the properties of 8090 are dependent on the loading direction (typically yield strength). However the recrystallized condition, which is now employed for sheets of this grade, reduces the anisotropy effects. In particular, no influence of loading direction on the crack propagation rate was observed.

Crack propagation tests were performed on 1 mm thick sheets, milled tension specimens-ASTM E647, in three orientations (L, T, 45°), and three stress ratios (0.1, 0.3, 0.5) by the Department of Mechanics – Milan Polytechnic; a set of results is reported in fig. 9.

3.2.3 Evaluation of Fracture Mechanics characteristics of Al alloys for high temperature applications (Univ. Pisa)

Within the framework of a Brite-Euram project, aimed at the development of Al based alloys for applications in temperature up to 300 °C, the Department of Aerospace Engineering of Pisa has carried out some fracture mechanics tests on sheets, that were produced within the research by means of the Powder Metallurgy technique. Two materials were, at the end of the research, selected as candidates for the proposed applications: a quaternary alloy, Al-Fe-V-Si, and a Al-Mg-Li reinforced with 7.5% wt. Ultrafine Titanium dioxide. The two alloys showed rather different fracture toughness characteristics that were assessed by means of R-curve tests: good ductility for the quaternary alloy and a brittle behaviour for the MMC. Some of the crack-growth rate data are shown in figs. 10.

3.2.4 Residual strength evaluation of stiffened Glare panels (Univ. Pisa)

Within the framework of the ADPRIMAS Brite-Euram project, a collaboration has taken place between Alenia and the Department of Aerospace Engineering of Pisa, to study the residual strength of stiffened panels, with a Glare skin. The activity consisted of experimental tests carried out to evaluate the static properties of two types of fibre-metal laminate, named Glare X and Glare Y, produced by Alcoa for Alenia, that built three samples of each of the four

stiffened panel configurations that were object of evaluations. Two additional sheets were also provided to the Department of Aerospace Engineering, in order to evaluate the fracture resistance (R-curve) on Centre Cracked Tension (CCT) specimens.

The stable crack propagation, during the residual strength tests on the CCT specimens, as well as on the stiffened panels, was monitored by the Image Analysis technique. One sample for each stiffened panel configuration was extensively instrumented with strain gauges, to verify the stress distribution during the test. Some standard tensile tests were also carried out on small coupons cut from the skin of some stiffened panels after the residual strength test, to obtain the constitutive laws of the material, to be used in the numerical analyses (in progress).

The lay-up of the glass fibres was the same for both Glare types, i.e. Al/±45/Al/0₂/Al/±45/Al; the only difference was the aluminium alloy used: 2024-T3 for Glare X and 7475-T73 for Glare Y.

Two panel configurations had the skin in Glare X and two in Glare Y. However, other parameters were different in the various configurations, in addition to the skin material, such as the panel width, the type of the pad below the stiffeners and the type of joint between the skin and the stringers, as shown in Table I. All the panels had five stringers, made of 7075-T6 extrudate, with the central cut; different values of initial crack length were chosen, with a complete cut being introduced in the skin.

Both crack tips were monitored during the tests. The load increments were in steps of 50 MPa from 0 to 150 MPa, 5 MPa from 150 to 200 MPa and 2 MPa from 200 MPa to failure. Figs. 11 and 12 show the Load vs. Crack extension plot for the stiffened panels.

4. COMPOSITES

4.1 - Fatigue behaviour

4.1.1 Degradation of the fatigue endurance of composites due to impacting, notching and absorbing of water, oils, fuels and de-icing fluids (Pol. Milan)

An experimental research was carried out, with the purpose of studying the combined effects of moisture absorption and damages (due to low-energy impacting) or notches on the static and fatigue behaviour of composite laminates made of aramidic or graphite fabrics and epoxy resin; besides, the work evaluated the influence exerted by the absorption of typical aeronautical fluids, i.e. skydrol, jet-fuel and de-icing, as well as distilled water, on the tensile and compressive static and tensile-compressive fatigue behaviour of the same composite materials. The response of the different materials to low-energy impacts was investigated as well, and the shares of elastic re-bond and absorbed damaging energies were evaluated.

The mechanism of fluids diffusion into composites was deeply investigated, in order to set-up a methodology for the accelerated conditioning of these materials, able to experimentally reproduce the real phenomenon of water up-take.

Finally, static and fatigue testing were carried out on specimens previously dry- and wet-conditioned up to saturation; so doing, the effect of moisture absorption on plain, notched and impacted coupons was evaluated keeping, as a reference, the behaviour of dry-conditioned samples.

Furthermore, the influence exerted by notches and impact damages on the mechanical characteristics of the composites was analysed, at a parity of the environmental conditioning. By means of the opaque-enhanced dye penetrants stereo-radiography, the damage onset and growth was studied during the whole fatigue life, and the correlation between the decrease of the mechanical characteristics and the damage development was carried out.

In conclusion, the scanning electron microscopy (SEM) made feasible the investigation of the microscopic mechanisms of absorption and damage, and allowed the proposition of physical interpretative models.

4.1.2 Fatigue Evaluation of Composite Materials (Agusta)

One of the drawbacks of composite materials application is the extremely high cost of certification, due to the need of performing at different complexity levels tests in several damaged conditions, including the evaluation of the moisture effect. Fundamental studies are therefore quite useful, if they can be used to substantiate the reduction of certification tests.

To assess the effect of hot-wet ageing on the properties of a glass reinforced epoxy resin, static and dynamic tests were run in dry and moisture saturated condition. It has been found a reduction in the elastic properties and strength. On the other hand it seems that the hygro-thermal ageing has no marked effects on the fatigue curve at endurance loads,

whereas at low cycles a behaviour similar to the static case is observed.

More details and the main results and can be found in [4].

4.2 - Damage mechanisms and damage development

4.2.1 Damage tolerance evaluation of sandwich composite structures (Uni. Pisa/Agusta)

This program is focused in the improvement of structural evaluation of sandwich structures, to reduce the certification costs. Agusta is involved in the performance of tests and analyses, in collaboration with the Department of Aerospace Engineering of Pisa, to address the evaluation of delamination growth in the sandwich skin. The purpose is to improve comprehension of the driving parameters in delamination growth, deriving data to reduce the test plans on complex elements and subcomponents.

In the previous ICAF Symposium, a paper was presented, [5], describing the results of a test program carried out within “Damtos”, a Brite project. Sandwich panels, representative of real helicopter structures, were tested under the application of static and of fatigue loading, both in pristine and in damaged conditions; in this last case, impact damage was inflicted, or artificial delamination was introduced in a skin. One of the most interesting facts observed was that an artificial delamination may grow, under the application of a compressive fatigue load of constant amplitude, with a progressive decrease in the rate; in some cases, when the load range was low, the growth stopped and a sort of stable final shape was reached.

A FEM analysis was carried out of the above mentioned test results, with the purpose of assessing G , the Strain Energy Release Rate, the Fracture Mechanics parameter that is best suitable to describe fracture progress in composites. The total value of G is not particularly meaningful, but special attention must be paid to how G is divided into the contributions according to the fundamental Fracture Mechanics modes, i.e. mode I (opening), mode II (in-plane shear) and mode III (out-of-plane shear). The reason for this is that the fracture resistance has quite different values, when measured according to the various modes; in this respect, mode I is the most critical. As a consequence, the FEM mesh must be very detailed: the displacement field must be evaluated very accurately, keeping also geometrical non-linearity into account due to the occurrence of buckling of the sublaminates. For this purpose, a global-local approach was utilized; two FEM analyses are carried out, the first on a rather coarse mesh of the complete panel, and the second one on the central part, very finely described, where the displacements computed in the first analysis are applied. An example of the results obtained are shown in figs. 13, where the distribution of G contributions according to mode I and II are shown, for a generic delamination shape, observed in the experiments; it is interesting to note that, for an increase in delamination length, a strong decrease in mode I contribution occurs, while the mode II one increases. This explains why, in some cases, under the action of a small fatigue load, it was observed that the delamination evolved towards a stable shape: mode I is associated with a much lower interlaminar resistance than mode II.

The study of interaction between different mode partitions of G is therefore of particular interest and a material characterization will be carried out using the Mixed Mode Bending test procedure, developed by NASA, [6]. Other details about this activity can be found in [7].

5. JOINTS

5.1 - Riveted joints

5.1.1 Multi Site Damage in riveted joints (Uni. Pisa)

The main target of this research, carried out in collaboration with AerMacchi and within the Brite-Euram BE95-1053 (SMAAC), was the study of Multiple Site Damage (MSD) occurring in ageing aircraft, particularly at fuselage longitudinal joints. As a matter of fact, a number of small fatigue cracks, aligned with a long crack, can significantly reduce the residual static strength of the structure. To study this problem, an experimental activity has been carried out on specimens representative of a typical longitudinal riveted joint of a pressurised fuselage. The geometry of the selected single strap butt-joint specimen is shown in fig. 14; the material is 2024-T42 bare, $t=1.2$ mm. The research was carried out through the following phases:

1. fatigue crack nucleation on butt-joint MSD specimens;

2. fatigue crack nucleation on simple coupons, a strip specimen with a single row of rivets, obtained by cutting the MSD specimens longitudinally;
3. fatigue crack propagation in MSD specimens;
4. residual static strength of cracked MSD specimens;
5. analysis of fatigue crack nucleation and propagation;
6. prediction of residual static strength using different fracture criteria.

The Image Analysis technique was used in almost all the tests. This method has some advantages: a) it is possible to carry out fatigue crack nucleation and propagation tests automatically; b) it can be easily applied to complex geometries, even with multiple-site damage; c) there are no particular requirements for the specimen surface, and so in many cases surface preparation is limited to the paint removal by emery paper. The sketch of the test equipment is shown in fig. 15. It consists of commercial products: a Personal Computer, an Analog/Digital converter plug-in card, a Frame Grabber plug-in card, a black&white videocamera, an optic-fibre illuminator and a three-axes stage equipped with step motors. A computer code, named FATIMA (FATigue crack measurement by the IMage Analysis technique), was realized to control the equipment; it allows to perform fatigue crack nucleation and propagation tests, as well as residual strength tests.

The experimental activity has allowed the collection of a large amount of test data, that were quite useful for the activity described in par. 5.1.2. An additional activity, related with a few residual static strength tests on large MSD ($W=600$ mm) pre-damaged specimens (i.e. with a well-defined crack scenario), is planned to be carried out. The tests would show the stable link-up between cracks before the final failure.

A simple model has been used to predict the residual strength of damaged MSD butt-joints. The assumptions were the following: a) assigned load transfer ratio between the rivet rows; b) evaluation of K by means of the compounding method, considering also the interaction effect of neighbouring cracks; c) stable crack propagation evaluated by the R-curve of the material; d) link-up occurring when the plastic zones join; e) failure occurring at the average yielding of the net section or by reaching the K_c of the material. Preliminary results were very encouraging. A more complex model is under study, which is based on the use of the Crack Tip Opening Angle as a criterion for stable crack propagation.

More details about the results of this research activity can be found in a paper to be presented at the ICAF Symposium, [8].

5.1.2 Development of a fatigue design methodology based on the probabilistic approach (Uni. Pisa)

The PISA (Probabilistic Investigation for Safe Aircraft) code, written in Fortran, studies the modelling of the fatigue behaviour of typical aeronautical structures, such as riveted joints and stiffened panels or joints, in order to evaluate their number of cycles to failure. By means of the MonteCarlo method and utilizing the statistical distribution of the main parameters that influence the deterministic estimate of the component fatigue life, the code is capable to simulate the typical scatter in fatigue of metallic components.

Experimental activities have been carried out to provide the statistical distribution of some of the variables that influences the result. The variables considered are:

- a) nucleation of single cracks, through the Time to Crack Initiation model or the analogous Equivalent Initial Flaw Size;
- b) growth rate, through the coefficient C of the Paris law;
- c) failure of the structure, described by the fracture toughness K_c distribution;
- d) possible inspectionability of the structure, at prescribed intervals in terms of number of cycles, through the Probability of Detection curve.

The PISA code uses analytical models, available in the literature, to evaluate the corrective coefficients for K , keeping the various crack scenarios into account (interaction of a crack with a hole or with neighbour crack or with stiffeners). In the case of multi-rows riveted joints, the code considers also the Load Transfer for the different rows. The code, carrying out a high number of simulations, can provide an estimate of the probability of failure of the component examined.

The code has a modular structure and each module has been critically evaluated and, by means of comparison with results available in the literature, validated. In addition, a specific test activity has been carried out to provide data on real components, useful to evaluate the code in its globality, i.e. the accuracy/reliability of its results.

Future developments of the code will go in the direction to include a larger number of possible MSD critical components.

More details of this research activity will be described in a paper to be presented at the Symposium, [8].

5.1.3 Fatigue behaviour of riveted joints made in Glare (Univ. Pisa)

Within the framework of the Brite-Euram research project ADPRIMAS, a collaboration between the Department of Aerospace Engineering of Pisa and Alenia has taken place, focused on the study of the fatigue behaviour of riveted and bonded joints made of Glare. This is a part of a wider task, with the objective to develop a fuselage side panel, that shall be qualified in a full scale fatigue test.

Notwithstanding the experience gained in the design of metallic aircraft structures for so many years, joints are always critical elements; in the case of Glare, even greater attention must be paid to the study of the behaviour under the application of fatigue load cycles. The real problem is that fatigue damage develops in a quite different manner, with respect to metals, and therefore the design process must follow different rules. The fibres that are inside Glare have a very high resistance and fatigue cracking is limited to the metallic layers. The fibres act as crack stopper layers, that delay crack propagation in the thickness and reduce the crack growth rate within the Al layer; in addition to this positive action, it should be also considered that the fibres, even when all the metallic layers are completely cracked, after the application of many load cycles, make the joint still have a reasonable residual strength.

Alenia is in charge of the design of a fuselage side panel for a wide body aircraft, using Glare as the base material. For the skin, as a consequence of the large diameter, the pressurisation load condition requires a large thickness: therefore a Glare type 4/3 was selected, i.e. with four Al layers and three glass fibre layers. A very particular fibre lay-up with high shear stiffness and strength, namely Al/±45/Al/0₂/Al/±45/Al, has been chosen for that structural element, since it is subjected to large shear flows introduced by the floor beam. As a reference, the hoop direction has been assumed as 0-degree. This is a very “singular” lay-up, which has never been studied before; in the literature, only information about more “traditional” 0 or 90 degrees fibre orientations can be found.

As far as the aluminium alloy is concerned, the high static requirement has made it attractive to consider also the use of 7475 Al alloy, another “singular” choice for a fuselage skin, with respect to the much more common selection of 2024-T3.

The joints of this experimental investigation are representative of fuselage longitudinal joints. The test program comprised many different specimen configurations, that were designed by Alenia, in accordance with typical solutions utilized. The configurations evaluated are lap joints, with 2 or 3 rows of rivets, and butt joints, with single or double strap. In total, 16 different configurations (4 bonded and 12 riveted) were evaluated.

All the specimens were 140 mm wide, and each rivet row contained 7 rivets, spaced 20 mm apart (the external rivets were placed at a distance of 10 mm from the lateral edge); also the distance between rivet rows was 20 mm, while the edge margin (in the axial direction) was 12 mm. The specimens were manufactured by Alenia; the rivets were installed wet, using a PR 1773 B surface sealant, and their formed heads had a diameter equal to 1.3 times the shank diameter, a typical Alenia production standard.

For each configuration, the following test procedure was followed:

- a) one specimen was tested to evaluate the tensile strength;
- b) a few specimens, typically 5-6, were subjected to a fatigue loading up to complete failure, in order to obtain a traditional S-N curve; the aim of these tests was to define a realistic stress level to be used in the subsequent tests: a fatigue life of about 4-5 hundred thousand cycles was considered appropriate, because, divided by a typical scatter factor of 4, provides a realistic target fatigue life;
- c) the rest of the specimens was used to study the decay of the Residual Static Strength (RSS) with the fatigue damage accumulation: each specimen was subjected to a prescribed number of load cycles (C.A., R=0.06, S_{max} defined at the previous step), after which its residual strength was measured.

Some results are shown in figs. 16 and 17, where it can be seen that the joint is capable to retain a high percentage of the original strength after a considerable percentage of its fatigue life. This is very positive, from a Damage Tolerance point of view, but on the other hand fatigue cracks began to nucleate very early, on the mating surfaces, where bending stresses were high and a particular “knife edge” effect was present as a consequence of the reduced height of the cylindrical collar, where the rivet shank applies very high pressures. The end of the useful life for this type of joints seems therefore to be the evidence, on the outer metallic surface, of a fatigue crack; in these conditions, as already said, the joint has still reasonable strength capability, but safety reasons will never allow an aircraft to fly with externally visible cracks.

5.1.4 Fatigue behaviour of metallic lap joints (Univ. Pisa)

A research has been carried out at the Department of Aerospace Engineering of the University of Pisa about the role of the riveting technological parameters on the fatigue behaviour of metallic lap joints. For this purpose, the attention has been focused on lap joints in 2024-T42, thickness 1.2 mm, with two rows of rivets. A test program was defined and carried out to investigate the influence of the types of the head, the material, the heat treatment, the squeeze force on the fatigue behaviour. The material was anodised and protected by primer and topcoat; the rivets were wet installed. Contemporarily, a numerical analysis has been carried out; particular attention has been paid to study the influence of the specimen width, keeping also geometrical non-linearity into account, to compare the stress distributions in realistic joints with those obtained in typical laboratory coupons. Details of the results obtained are not given here as this item will be the object of a paper presented at the next ICAF Symposium, [9].

5.2 - Weldments

5.2.1 Mechanical properties of Variable Polarity Plasma Arc (VPPA) welded 2219-T851 joints (Uni. Pisa)

The Variable Polarity Plasma Arc (VPPA) welding technique used in the keyhole mode offers significant improvements compared to the traditional techniques, particularly in terms of higher bead quality associated with low production costs.

In view of these advantages, Alenia Aerospazio-Divisione Spazio has successfully developed and qualified a VPPA keyhole process to be applied on 7 mm thick joints of Aluminium Alloy 2219. The qualified process is applicable to the COLUMBUS module and to the Mini Pressurized Logistic Module structure manufacturing. The Department of Aerospace Engineering of Pisa has taken part to the qualification program, by performing fracture mechanics and susceptibility to stress corrosion tests on welded and un-welded plates. Residual stresses acting in welded plates were also measured. Some details about the results obtained were given in the previous review. The testing activity was concluded; a synthesis of the results obtained was given in [10].

The item of the residual stresses in welded joints was prosecuted numerically by using MARC, [11]. The solution is subdivided in two phases; in the first phase the welding process is simulated numerically. A mobile thermal source heats the plates; the intensity of the source is calibrated to have an area where the temperature exceeds the fusion temperature of the material as large as the weld bead. This analysis stops after the simulated cooling of the plates. Then the mechanical problem associated to the thermal history is solved. The interest in the prediction of the residual stresses acting in a welded component lies in the possible optimisation of the welding sequence to reduce the internal stresses or to reduce the deformations of the welded components. Also the effect of different constraints used to support the component during the welding process can be easily simulated by FEM. Fig. 18 shows an example of prediction of the residual stresses in an aluminium welded plate, compared with experimental results. Both the distribution than the numerical values of the residual stresses are quite accurately predicted.

5.2.2 Application of Titanium to fatigue critical parts (Agusta)

The work started in 1995 for the evaluation of a near β alloy Ti-10V-2Fe-3Al, and that was already mentioned in the last Italian National Review, has been concluded. This alloy has proven itself quite suitable for dynamic parts subject to severe fatigue load, especially for positive R ratios. Prototype parts were also produced and tested. On the other hand, the characteristics of fatigue propagation seem penalized with respect with annealed Ti-6Al-4V.

Some of the advantages of applying Titanium alloys, especially in the metallurgical conditions associated with enhanced fatigue and static properties, are counterbalanced by high material and machining costs. Studies are underway about the possibility of welding titanium parts by the Electron Beam process, starting from near final shape sub-components. A preliminary evaluation of fatigue performance of the welded joints was carried out and is shown in the fig. 19. All the failures took place in the Heat Affected Zone near the welding. As shown in the figure, the welded material fatigue limit can be considered approximately half of the bulk material.

5.2.3 Crack propagation in Ti-6Al-4V TIG welded plates under static and under fatigue load (Univ. Pisa)

Crack propagation tests were carried out on TIG welded Ti-6Al-4V plates, 200x600mm, thickness 2 mm, with the weld bead perpendicular to the load (crack in the weld bead or in the Heat Affected Zone) and with the weld bead parallel to the load (crack perpendicular to the weld bead). This material is typically used in space applications. The start notch was a surface crack. Some specimens were stress relieved to investigate the effect of the internal stress on the crack propagation rate. Comparative tests were carried out also on virgin material.

Welded plates were tested also for stress corrosion cracking; the corrosive environment was isopropilic alcohol. Preliminary fracture toughness tests were performed on two specimens; the crack was in the Heat Affected Zone; stable crack propagation was observed in the two tests at values of the stress intensity factor greater than 95 and 102 $\text{MPa} \cdot \sqrt{\text{m}}$. The maximum value before final failure was 116.5 $\text{MPa} \cdot \sqrt{\text{m}}$. Very long stress corrosion tests, up to five months, were performed. Crack propagation due to stress corrosion was observed under a stress intensity factor of about 100 $\text{MPa} \cdot \sqrt{\text{m}}$. The mean crack propagation rate observed was very low, about 4×10^{-3} mm/day. A comparative test, performed using 3.5% NaCl solution, gave the same result. The conclusion of this activity was the high resistance of welded panels to stress corrosion cracking. Some crack propagation tests under fatigue loading in corrosive environment were performed and the effect of the corrosive environment was evident in this case, fig. 20.

More details can be found in [12].

5.2.4 Susceptibility to Stress Corrosion of 7050-T7351 Electron Beam Welded Specimens (Univ. Pisa)

Susceptibility to stress corrosion tests were carried out on electron beam welded specimens made of 7050-T7451 aluminium alloy. As a comparison, specimens made of base material were tested too. The starting material was welded plates, 200x200 mm, thickness 27 mm, obtained by joining (EBW) two plates, cut in the longitudinal direction, along the transverse direction. The welded plates were machined to obtain small bars, which were milled to produce butt welded cylindrical specimens, diameter 4 mm, gauge length 26 mm.

The resistance of the welded material was high: the tensile properties were only slightly lower than those of the base material. After thirty days' exposure to a corrosive environment (alternate immersion in a 3.5% NaCl solution), the tensile properties of the welded material were considerably reduced, while the same properties were only slightly affected in the base material. The combined effect of stress and corrosion was only slightly detrimental for the base material and very detrimental for the welded material. At the lowest stress level tested, about 25% of the ultimate stress, the welded specimens failed after a mean life of 90 days.

Considerable residual stresses associated with the welding process were measured in a welded plate. A test was performed to verify the possibility of stress corrosion cracking promoted by the welding residual stresses. In actual fact, no cracks were observed, but the corrosion rate increased, particularly in the areas affected by the higher residual stresses. The results of the whole activity were given in [13]. Fig. 21 shows the Time-to-Failure results relevant to the welded specimens.

5.3 Bonded joints

5.3.1 Fatigue behaviour of bonded joints in Glare (Uni. Pisa)

As already described in par. 5.1.2, a large experimental activity was carried out, within the framework of the ADPRIMAS Brite-Euram project, to evaluate the fatigue behaviour of joints in Glare. The investigation about riveted joints was completed by the assessment of four bonded joints configurations; three differed overlap/thickness ratios were used (20, 30 and 40), plus a bonded and riveted configuration.

In the case of bonded joints, the failure mode was rather particular; the mating Al layer cracked at the overlap end, due to the stress concentration, and the crack propagated rapidly in the thickness and the width, cutting completely the metal layer. The fibre layer below acts efficiently as a crack stopper, so that the fatigue damage develops in the form of a delamination, between the cracked Al layer and the subsequent fibre layer, that offers minor resistance in comparison with the metal-to-metal bondline. The delamination grows in the overlap area, until the specimen separates in two parts.

6. COMPONENT AND FULL-SCALE TESTING

6.1 - Full-scale fatigue test of AM-X aircraft (Alenia Turin)

AM-X WAFT (Whole Aircraft Fatigue Test) ended after the application of 16000 simulated flight hours (SFH) and a major inspection was performed.

A second test, WAFT2, was programmed with two main objectives: 1) to qualify the main modifications of fuselage Main Frames in the area concerned by the wing-to-fuselage attachment; 2) to extend the AM-X fatigue life from 16,000 to 24,000 simulated flight hours. The test set-up is similar to that defined for WAFT Test and the loading sequence is the same. At present, 8,000 SFHs have been completed and the test article inspection program is in progress.

6.2 - Dassault Falcon 900 (Alenia Turin)

A damage tolerance test on the engine mount system was performed.

The theoretical crack propagation calculations were performed using a dedicated FEM model (fig. 22) to calculate ΔK and an ALENIA computer program calculating cycle by cycle the crack propagation rate. The analysis of results, including the comparison between calculations and test and the tuning of theoretical method, is now in progress.

6.3 - ATR 72 full-scale fatigue test – Tear down inspection (Alenia Naples)

The Full Scale Fatigue Test of ATR 72 Aircraft was defined keeping the specific load conditions expected in service into account. The ATR 72 A/C was designed to cover an operational life of 70000 flights. During the Full Scale Test the objectives were to demonstrate:

- Two Lifetimes for the structural parts designed as Damage Tolerant
- Five Lifetimes for the structural parts designed as Safe Life

As already reported in the last National Review, the Full Scale Fatigue Test was successfully concluded and the scheduled Tear Down Inspection (including non destructive and destructive checks) has been carried out.

Tear Down Inspection main objectives were:

- To find hidden cracks and to discover new critical areas, if any, not detected by inspections performed during the fatigue test;
- To verify the effectiveness of the inspection program for the ATR fleet;
- To assess the minimum detectable crack length provided by selected inspection methods, and to correlate it with the fractographic results;
- To determine the real crack dimension for damages detected during fatigue test;
- To analyze material and processes applied to the ATR, in order to verify the initial quality of the airframe structure.

The Tear Down Inspection results substantially confirmed the damage scenario detected during fatigue testing; some small differences were discovered after the disassembly of main components and can be attributed to the better accessibility conditions.

6.4 - Helicopter A119 Koala (Agusta)

A new single engine aircraft derived from A109, with 2720 kg of take off weight and a Pratt & Whitney engine of 1000 SHP. Civil certification is being carried out according to JAR 27.

Some significant dynamic parts are new design, the others were derived from A109. The fatigue test plan was completed on the main new assemblies, which are:

accessory gearbox, engine shaft, tail rotor drive line, 90° gearbox, landing skid, tail rotor mast, tail rotor controls, 'compact' main rotor head, with 'short' tension links and 'longer' blade root section (both composite items).

The usage spectrum and the flight conditions for the fatigue life calculations were derived and the preliminary fatigue lives were evaluated.

The final load survey and fatigue calculations are in progress at present for the Civil Type Certificate.

6.5 - ATR 42/72 Carbon Epoxy empennages (Alenia Naples)

As described in the last National Review, a new structural configuration of the empennages for the ATR aircraft has been defined in order to achieve a significant weight saving for the complete airframe. The new configuration resulted in a weight reduction of about 85 Kg in comparison with the metallic configuration. The main features were fully described in the last National Review; during the last two years, the Full Scale Fatigue test was successfully completed, reaching the target of 70,000 flights.

6.6 – EF Typhoon (Alenia Turin)

ALENIA prototypes (DA3 and DA7) are flying to perform the flight activity tests.

A simplified analysis for structural fatigue consumption of prototypes was performed, using flight test instrumentation, comparing design spectra with flown spectra of some significant flight parameters.

The Major Airframe Fatigue Test reached the target of 18000 simulated flight hours, covering the design safe life of 6000 hours (scatter factor of 3).

A very good behaviour of composite materials components was demonstrated; fatigue problems were limited to metallic parts.

An analysis of failures experienced on MAFT was performed getting indications for design improvements.

A fatigue test on wing tip DASS pod started in ALENIA Turin. The spectrum includes manoeuvres with associated buffet conditions and gust loads. The simulation of buffet was obtained by the statistical elaboration of buffet power density spectra. The PSD function of buffet response (fig. 23) has been elaborated into a probability density function (PDF) relevant to RMS of both Fz and My used as driving loads. The PDF was calculated for maxima assuming an identical, but opposite one, for minima. The negative part of the curve can be associated to maxima lower than 0 (or viceversa minima greater than 0). The range used for the construction of the spectrum was 0 to 4σ , and the analysis of this range has been performed by discretizing the curves of PDF into 13 intervals.

Studies for production aircraft and updating of spectra started, taking into account updating of aircraft characteristics and carriage of new stores.

6.7 - Fatigue test on the tail end fittings of the EH-101 helicopter (Aermacchi)

On behalf of Agusta a fatigue test is currently being performed at Aermacchi in order to qualify the end fittings of the EH-101 tail unit. The test rig assy and Test Article are shown in figure 24.

The design service life to be demonstrated is 10000 flight hours with a scatter factor of 4.

The test spectra include:

- Axial thrust loads of tail rotor
- Tail rotor reaction torque loads
- Tail surface down loads

Altogether, five types of load spectra have been adopted; the first 3 corresponding to 3 flights (one at high load factor, one at medium and the third at low G level). The last two correspond to high and medium vibration level. No cracks have been discovered insofar in the items under test

6.8 – Residual fatigue test on aged structural wing components (Aermacchi)

Within the frame of the Brite-Euram project SMAAC (Structural Maintenance of Ageing AirCraft), a residual fatigue test has been carried out on a pair of old MB-326 wing main spar. The spars were obtained from the Tear Down inspection of two very aged wings (35 years old) of an MB-326 trainer, whose expired safe life had been evaluated in about 90%, based on fatigue meter readings, for a total of 4902 flight hours.

The purpose of the test was to investigate the behaviour of aged thick items (steel and aluminium alloy) in presence of possible MSD and/or fretting corrosion phenomena.

The test rig is shown in figure 25. The adopted test spectrum was much more severe than that measured with fatigue meter (reference figure 26).

One end actuator was used to apply a flight by flight N_z – bending moment spectrum at the root of both test articles (RH and LH). The desired magnitude of the local stresses was controlled by means of strain gages throughout a calibration procedure. The RH lower steel wing attachment fitting (WAF) failed first after 5035 test hours; the failure section, shown in figure 277, indicated that multiple sites cracks initiations took place simultaneously from the corners of the first 3 bolts holes and subsequently by mutual interaction propagated up to the failure of the fitting. The test was then resumed by installing a dummy RH spar and introducing artificial saw cuts (1.5 mm deep) in the LH lower spar cap critical holes.

The second failure occurred after 5109 test hours in the lower spar cap (LH) at the first bolt hole for the connection of the MLG casting block (reference figure 28).

Both failures (WAF and spar cap) however were consistent with the results of the former MB-326 certification full scale fatigue tests.

6.9 – Wear/Fatigue test of YAK/AEM-130 canopy transparency (Aermacchi)

During the development phase of the YAK/AEM-130 canopy structure, a test has been carried out in order to investigate the wear resistance of the cast acrylic transparency at its connection with the forward frame of the canopy. A particular specimen with a teflon gasket at one end, representing a section of the upper zone of the transparency was inserted in a rig simulating the frame.

The test has been performed in two steps, corresponding to two specimen configurations:

- 1) Specimen horizontally fixed
- 2) Specimen inclined 35° and hit by UV lamp rays in presence of dust/powder to reproduce realistic environment conditions.

In both test steps the specimen was subjected to a cyclic displacement of ± 8 mm in order to simulate the relative movement of the transparency with respect to the frame.

Furthermore, a force $F = 25$ DaN normal to the specimen was constantly applied to reproduce the pressurization effect (reference fig. 29). The fatigue wear test has reached 94000 cycles in the first configuration and more than 50000 cycles in the second one without evidences of damages to the transparency.

6.10 - EFA wing centre/outboard pylons fatigue test (Aermacchi)

Certification fatigue tests on the center and outboard underwing pylons have been carried out in order to demonstrate a safe life of 6000 flight hours with a scatter factor of 3 according to the general design requirements. For both pylons the test spectra have been determined from the design N_z spectrum by analysing the aircraft maneuvers for each segment of the mission profiles and considering the external underwing stores which can be transported in the different missions. The Test Articles consisted for both pylons in the following items:

- Pylon body structure
- Dummy store
- Wing attachment fittings (spigot and yaw)

The test structures were connected to a rigid rig and the loads applied by means of 10 actuators (some on the store and other on the pylon) in order to better realize the theoretical spectra. In figs. 30 and 31, respectively for center and outboard pylon, are shown sketches of the Test Articles and of the actuators application points.

The pylons load spectra have been applied to the test structures in a flight by flight load sequence. A 1000 flight hours test block has been adopted, containing 74000 load cycles for the center pylon and 91867 load cycles for the outboard pylon.

The tests results for both components have cleared the desired fatigue safe life of 6000 flight hours, i.e., no cracks or failures have occurred after 18000 test hours.

7. FATIGUE SUBSTANTIATION OF NEW DESIGN AIRCRAFT

7.1 - Helicopter A109E and K2 (Agusta)

The Civil Certifications of the two variants were improved including:

- ❑ 20.000 ft altitude
- ❑ rescue hoist of 600 lb.
- ❑ Cargo hook of 1000 kg

Specific mission profiles were developed to derive the usage spectra for the fatigue life calculations of all the critical parts.

7.2 - Helicopter A129 International (Agusta)

This is a five blades variant of A129, with new and more powerful engines. The tail rotor RPM were increased to 107 % NR to improve performances.

The fatigue life evaluation was carried out based on a specific flight load survey including DEMO flight profiles.

7.3 - Helicopter NH90 (Agusta)

The NH90 is designed and manufactured by Eurocopter, Agusta and Fokker. Agusta designs and produces the drive system, the transmission support and the composite ramp door. The fatigue life calculation were carried out for the prototypes according to the preliminary load survey data related to the full operational envelope.

Although this is a military aircraft, civil FAR 29 requirements are taken into account, including damage tolerance for fatigue. This topic was deeply discussed providing a revised 'Fatigue Substantiation Criteria' document which addresses the constructor's proposal. The fatigue lives will be based on the well established safe life approach and the Flaw Tolerance / Damage Tolerance criteria is proposed only for setting inspections for accidental damage. The plan for flaw tolerance evaluation of Agusta parts was preliminary defined.

Agusta at present is approaching the D.T. evaluation of the Tail Rotor drive line showing fail safe capabilities of the couplings and 'no crack growth' by analysis carried out by the Dip. di Meccanica del Politecnico di Milano. The test proposal for the Main Case was defined considering degradation of multiple joints, by removal of the bolts, and flaws/scratches at the load concentration sections of the attachments.

7.4 - Helicopter EH-101 (Agusta)

Prototype monitoring was updated according to the present status of the fatigue evaluations, including the improved configurations for production.

The Civil variant -510 was certified in 1998 and is now in the final phase, the improved certification including 15000 ft altitude and the rescue hoist kit, which required specific usage spectra and comprehensive fatigue life calculations.

The evaluation of Damage Tolerance (DT) capabilities was almost completed as detailed in the paper [14], presented at RTO Meeting April 1999 in Corfu on D.T. for Rotorcraft.

Navy variant (Royal Navy and MMI). The most relevant fatigue testing activities for the Navy variant were focused on the evaluation of the MR Blade and Tail Unit folding conditions and the related structural components: the Tail Unit and the Rear Fuselage folding beams, the Inboard and the Outboard Tension Links. The ship trials data provided load recordings with wind gusts and ship induced loads.

Canada – SAR/Utility variant. The fatigue spectrum for the specific SAR missions addressed by Canada Air Force was developed and a preliminary fatigue life assessment was carried out for the critical parts.

7.5 – Helicopter AB139 (Agusta)

This is the new helicopter of 6000 kg gross weight, twin-turbine, multirole capability. The helicopter is in development phase. Civil Certification will be carried out according to JAR 29 Rules and therefore the fatigue assessment will require the Flaw Tolerance evaluation.

The fatigue substantiation criteria document was issued addressing the approach of compliance to the flaw tolerance requirements, detailing the proposed rationale to use either the Fracture Mechanics approaches or the enhanced safe life method, as far as applicable:

- ❑ the retirement life will never exceed the safe life evaluation
- ❑ in addition the flaw tolerance evaluations will prove tolerance to the ‘barely detectable flaw’ and inspections for the ‘clearly detectable flaw’.

The substantiation of composite parts (MR Blade, MR Tension Link, and TR Blade) will be carried out according to the AC 20-107A.

To minimize the inspections in metal parts, sizing for the ‘no growth’ of the rogue crack of 0.38 mm depth will be the preferred approach, including even slow growth if limited to loads with very low occurrence in the spectrum, like the start-stop or GAG cycles.

The substantiation criteria take advantage of the options currently addressed in the rule:

- ❑ fail safe capability, if double loading path can be applied in design;
- ❑ damage tolerance capabilities, if no crack growth is pursuing ;
- ❑ enhanced safe life, in the other cases, to prove tolerance to extreme but still realistic flaws.

The Department of Aerospace Engineering of Pisa and the Department of Mechanics of Milan Polytechnic will support Agusta in these evaluations, having identified specific areas of interest which are respectively: the complete metal fuselage for Pisa and the rotor parts for Milan.

7.6 – Tiltrotor AB609 (Agusta)

The relevant test activities on primary structures designed by Bell have already required the design of dedicated rigs by the Laboratorio Prove Strutturali. The most complex rigs are those for the testing of the Wing, the Prop Rotor Mast and the Swashplate Drivers.

For the wing tests, a common rig has been designed, capable of supporting a total of 48 actuators, to carry out the fatigue and the static tests.

8. INVESTIGATIONS OF GENERAL INTEREST

8.1 - Fatigue test on the window of a high speed train (Aermacchi)

A fatigue test on a window inserted in an aluminum frame of a high speed train is currently in progress. The design requirements are reported in the French rule “FICHE No. 566 OR”. This rule requires the window to be submitted to synusoidal pressurization cycles according to the following program:

- a) 10^5 cycles with $\Delta P = \pm 1500$ Pa at 6 Hz and with the load distributed on the total window surface
- b) 10^6 cycles with $\Delta P = \pm 2500$ Pa at 3 Hz and the load uniformly distributed on the window surface
- c) 10^5 cycles with $\Delta P = \pm 1500$ Pa at 6 Hz and the load uniformly distributed on the window surface.

The test rig and the window frame are shown in Figure 33.

8.2 Effect of Plasma Cutting on the Fatigue Resistance of Fe510 D1 Steel (Univ. Pisa)

A research programme has been carried out, concerning the effect of plasma cutting on the fatigue properties of Fe510 D1, thickness 8 mm, [9]. Plasma cutting is widely used in industry but in spite of the good quality obtained by

automatic processes, plasma cut edges in critical fatigue structures are often re-worked by grinding or mechanical profiling.

Comparative fatigue tests were carried out on dogbone specimens obtained from plate by milling or plasma cutting. The plasma cut surfaces did not look as regular as the milled surfaces; the edges were not straight and close tolerances are difficult to obtain. Besides, small scratches were present on the cut surfaces.

The optical microscope showed that the heat-affected zone of a plasma cut edge was composed of martensite, a harder structure than the basic ferrite; the hardness of this area was more than twice the hardness of the parent material.

A compressive residual stress of about 150 MPa was measured at the external surface of a plasma cut edge; this stress was superimposed on the thermal residual stress field, which involved the deeper layers of the specimen.

The results of fatigue tests carried out on milled and plasma cut specimens were fully comparable. So it can be concluded that plasma cutting in this material, is not detrimental from the fatigue resistance point of view. Additional fatigue tests confirmed the good fatigue resistance of plasma cut specimens after thermal relaxation even in the presence of small artificial defects in the hard layer produced by plasma cutting.

8. REFERENCES

- [1] L. Crippa, G. Merckling "Caratterizzazione meccanica a fatica in presenza di corrosione da contatto di leghe di titanio", Istituto Scientifico Breda, Milano (in Italian).
- [2] S Jenkins, D Davies, "Duplex hardening-an advanced surface engineering technique for future aerospace transmissions", 17th Conference on Aerospace Materials Engineering, 16.6.96 Paris.
- [3] S. Corradi, M. Marchetti, W. Stellino "Plastic envelope in propagating crack wake on Al-Li alloys subjected to fatigue cycles and to different heat treatments" RTA/AVT Workshop on New Metallic Materials for the Structure of Aging Aircraft, Corfu April 1999.
- [4] G Zaffaroni, C Cappelletti, U Mariani, M Rigamonti, "Hot Wet Ageing of Glass Reinforced Epoxy Resin", ECCM 8, Naples, 3-6 June 1998.
- [5] L. Candiani, U. Mariani, M. D'Alessandro Caprice, L. Lazzeri: "An evaluation of damage tolerance characteristics of sandwich composite structures", in "Fatigue in new and ageing aircraft", Proc. 19th ICAF Symposium, EMAS Publ., pp. 287-305.
- [6] Reeder, J.R. and Crews, J.H., Jr., "Redesign of the Mixed Mode Bending delamination test to reduce nonlinear effects" J. of Composite Tech. & Res., Vol. 14, No. 1, Spring 1992, pp. 12-19.
- [7] Lazzeri, L. and Mariani, U., "Damage tolerance characteristics of composite sandwich structures", paper presented at RTA/AVT Specialists' Meeting "Application of Damage Tolerance Principles for Improved Airworthiness of Rotorcraft", Corfu, April 1999.
- [8] G. Cavallini, R. Galatolo, G. Cattaneo "An experimental and numerical analysis of multi-site damaged butt-joints", Paper to be presented at the 20th Symposium of the International Committee on Aeronautical Fatigue, Seattle, 14-16 July, 1999.
- [9] M.Chiarelli, A.Lanciotti, L.Lazzeri " Fatigue behaviour of metallic lap joints: a study on the effect of riveting and of specimen geometry". Paper to be presented at the 20th Symposium of the International Committee on Aeronautical Fatigue, Seattle, 14-16 July, 1999.
- [10] A.Lanciotti, A.Belmondo "Mechanical Properties of Al 2219 VPPA Weldments" Paper presented at the 48th "International Astronautical Congress", Turin, 6-10 October 1997.
- [11] M.Chiarelli, A.Lanciotti, M.Manfredi "Measurements and Numerical Evaluation of the Residual Stresses in Welded Joints". Paper presented at the XIVth Conference of the Italian Association for Aeronautics and Astronautics, Naples, 20-24 October 1997 (In Italian).
- [12] A. Lanciotti, S. Ottaviano "Crack propagation in Ti-6Al-4V TIG welded plates under static and under fatigue load", Paper to be presented at the XVth Conference of the Italian Association for Aeronautics and Astronautics, Turin, 15-19 November 1999.
- [13] E.Ciampi, A.Lanciotti "Susceptibility to Stress Corrosion of 7050-T7351 Electron Beam Welded Specimens". Engineering Fracture Mechanics; n. 62, 1999; pp. 463-476.
- [14] U. Mariani, L. Candiani "Agusta experience on damage tolerance evaluation of helicopter components", RTA/AVT Specialists' Meeting on Application of Damage Tolerance Principles for Improved Airworthiness of Rotorcraft, Corfu April 1999.
- [15] M.Chiarelli, A.Lanciotti, M.Sacchi "Effect of Plasma Cutting on the Fatigue Resistance of FE510 D1 Steel". Paper accepted for the publication on the Journal of Engineering Materials and Technology (ASME).

Type	Stringer		Pad		Width W, (mm)	Skin material
	Bonded	Riveted	Bonded	Integral		
XR8A30		•	•		680	Glare X
WR1A30		•		•	680	Glare Y
XR7G60	•		No		740	Glare X
YR7G60	•		No		740	Glare Y

Tab. I – Configurations of the stiffened panels in Glare.

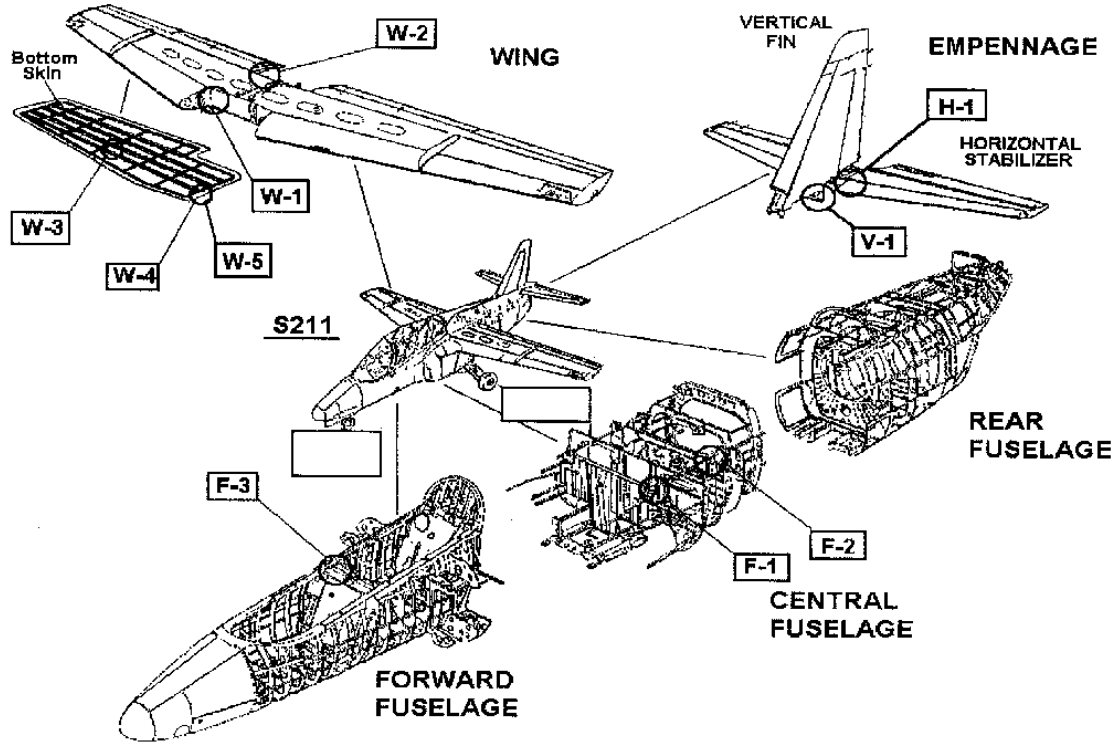


Fig. 1 Position of the most relevant items monitored by means of HUMS in S211 aircraft

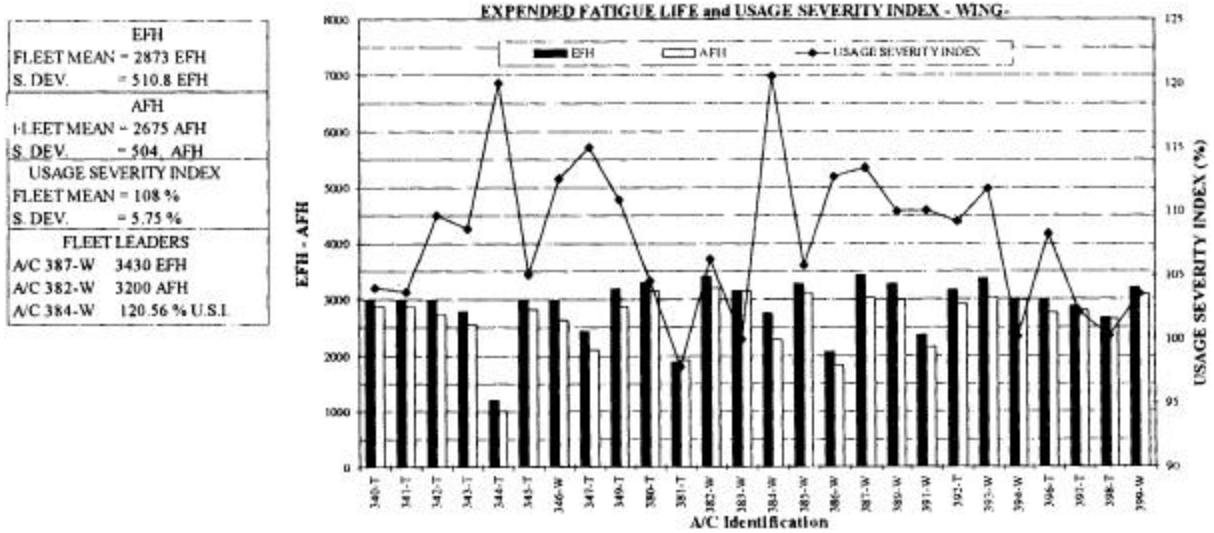


Fig. 2 Example of HUMS output chart

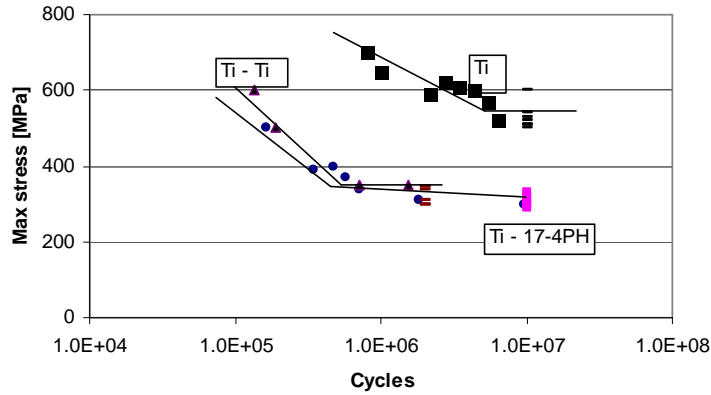


Fig. 3a Influence of fretting on Ti fatigue behaviour, for different contacting materials

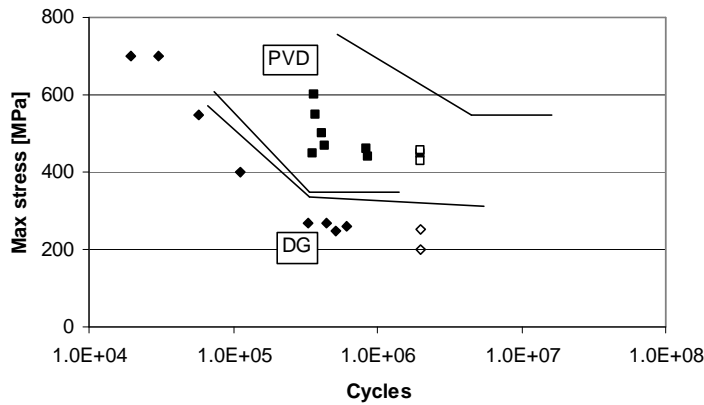


Fig. 3b Effects of surface coatings on Ti fatigue behaviour, contacting with 17-4 PH

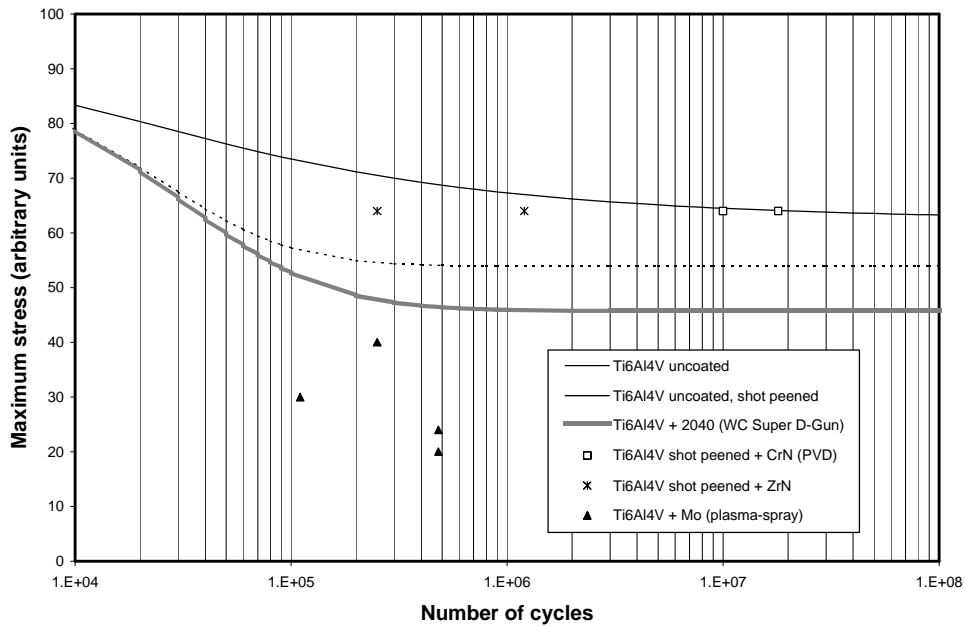


Fig. 4 Effects of different surface coatings on Ti fatigue behaviour (Rotating Bending)

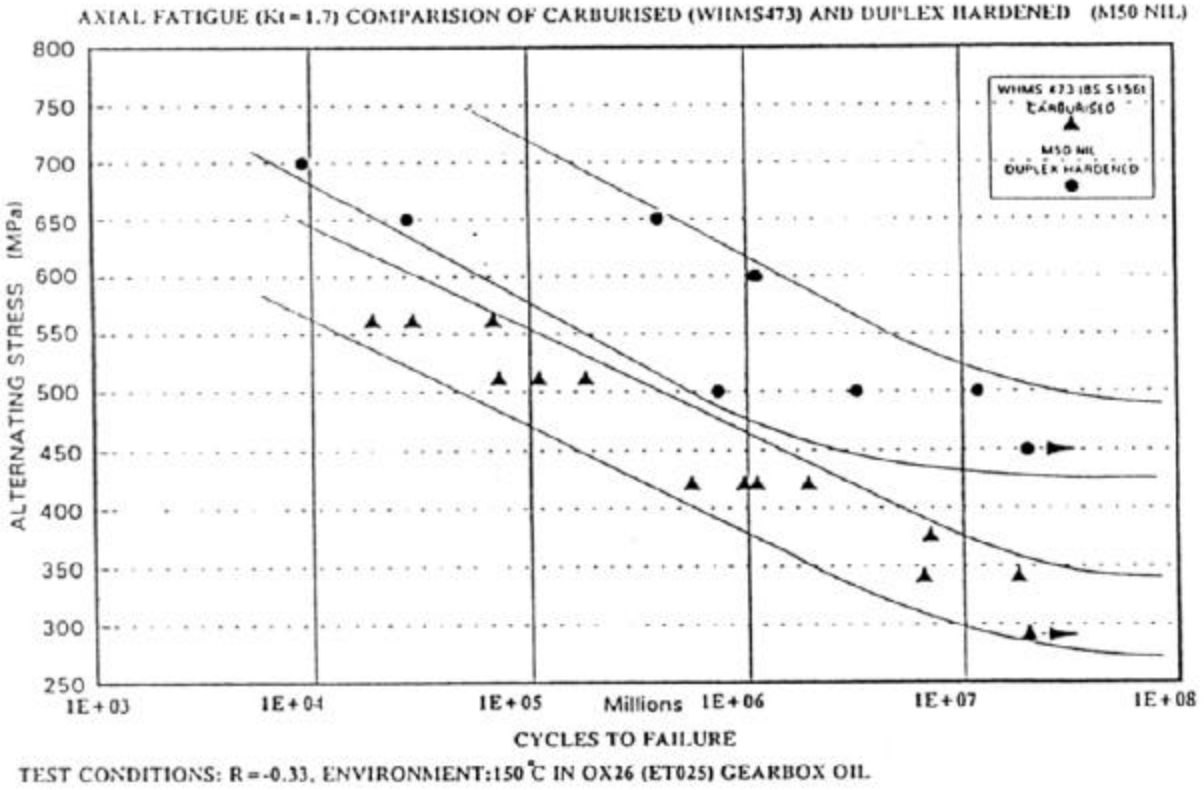


Fig. 5 Evaluation of fatigue behaviour of duplex hardened M50 NIL steel

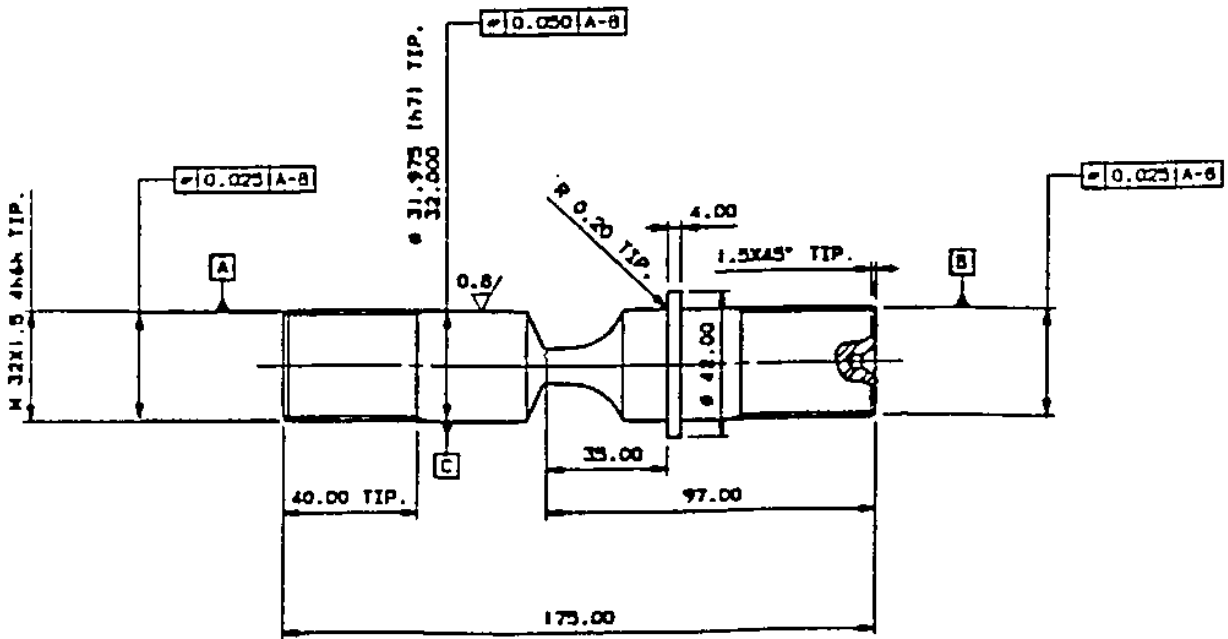


Fig. 6 Geometry of "tooth root" specimen

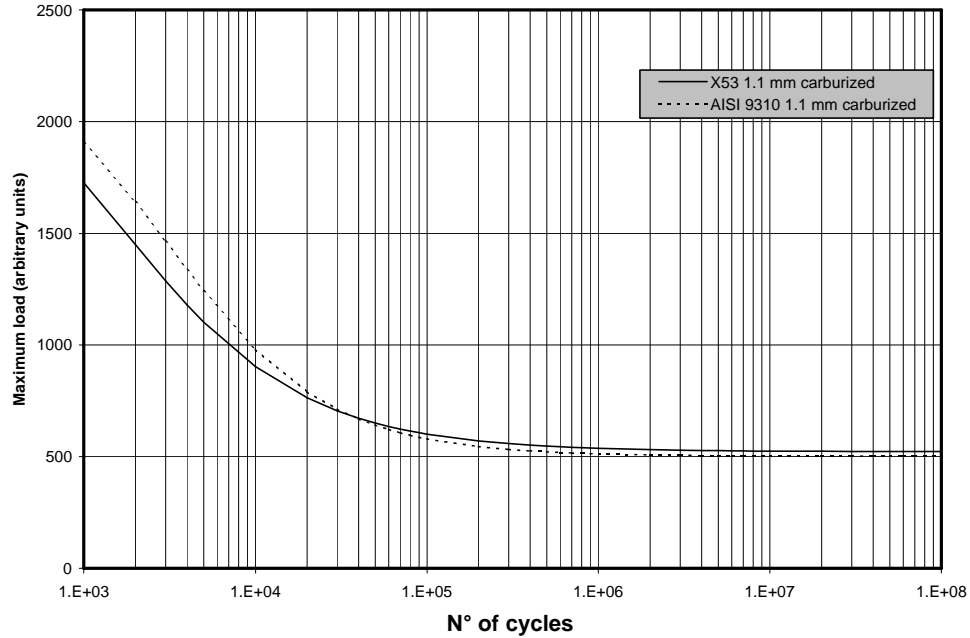


Fig. 7 Comparison of fatigue behaviour of Pyrowear 53 and AISI 9310, at room temperature

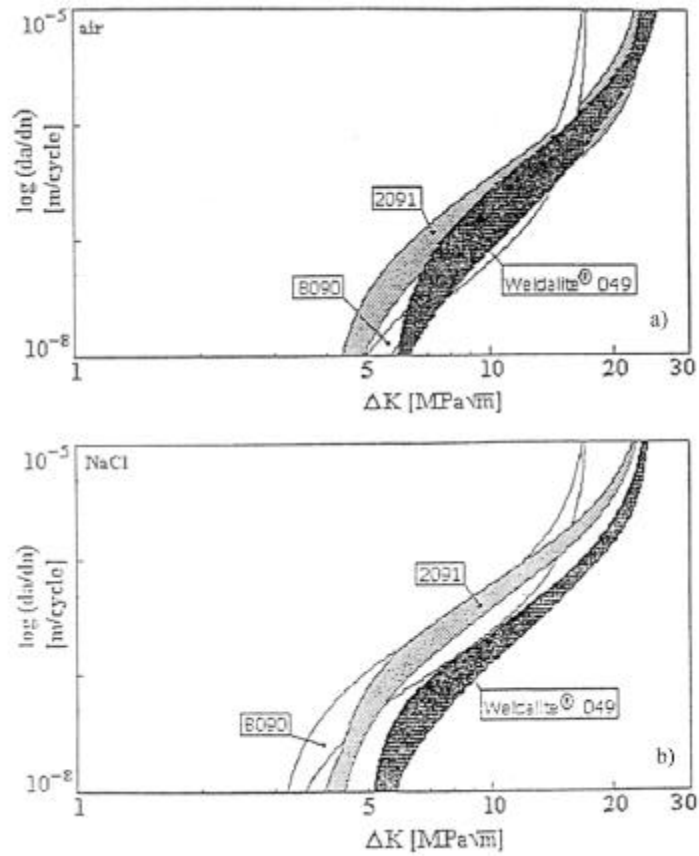


Fig. 8 Fatigue crack propagation rate of three Al-Li Alloys: a) in air; b) in NaCl aqueous solution

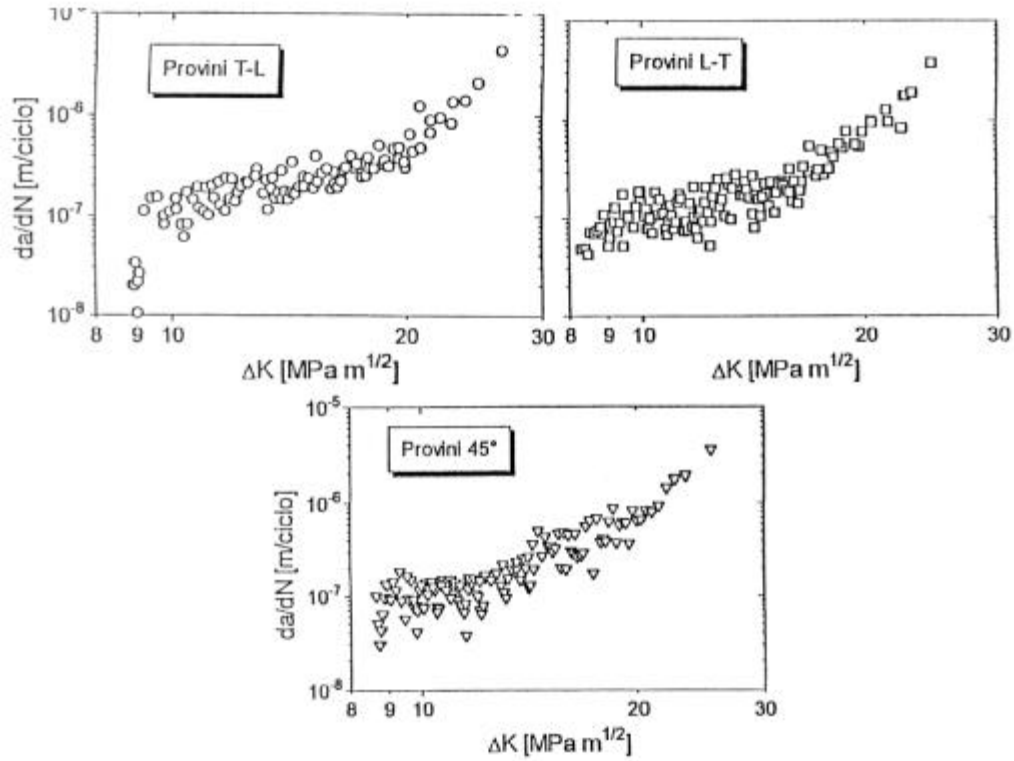


Fig. 9 Crack propagation in 8090-T81 sheets, 1mm thick, R=0.1, at different orientation

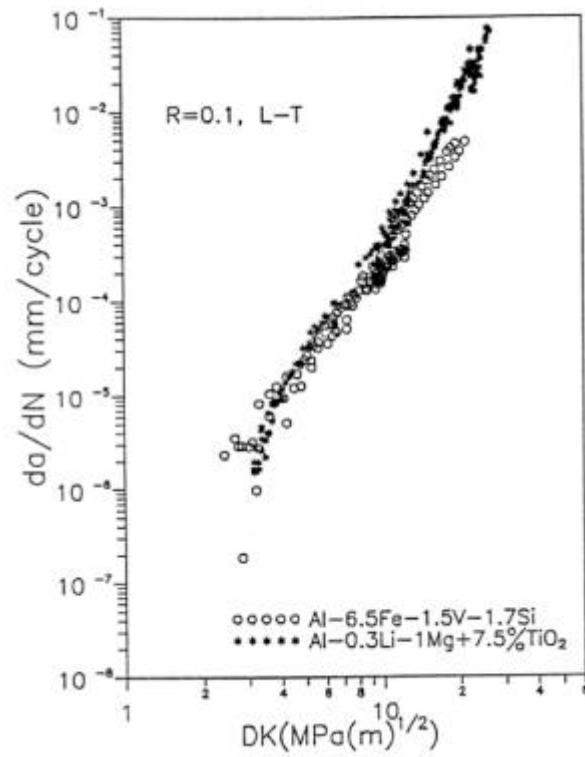


Fig. 10 Fatigue crack growth, R=0.1, L-T orientation: comparison between two Al Alloys for high temperature

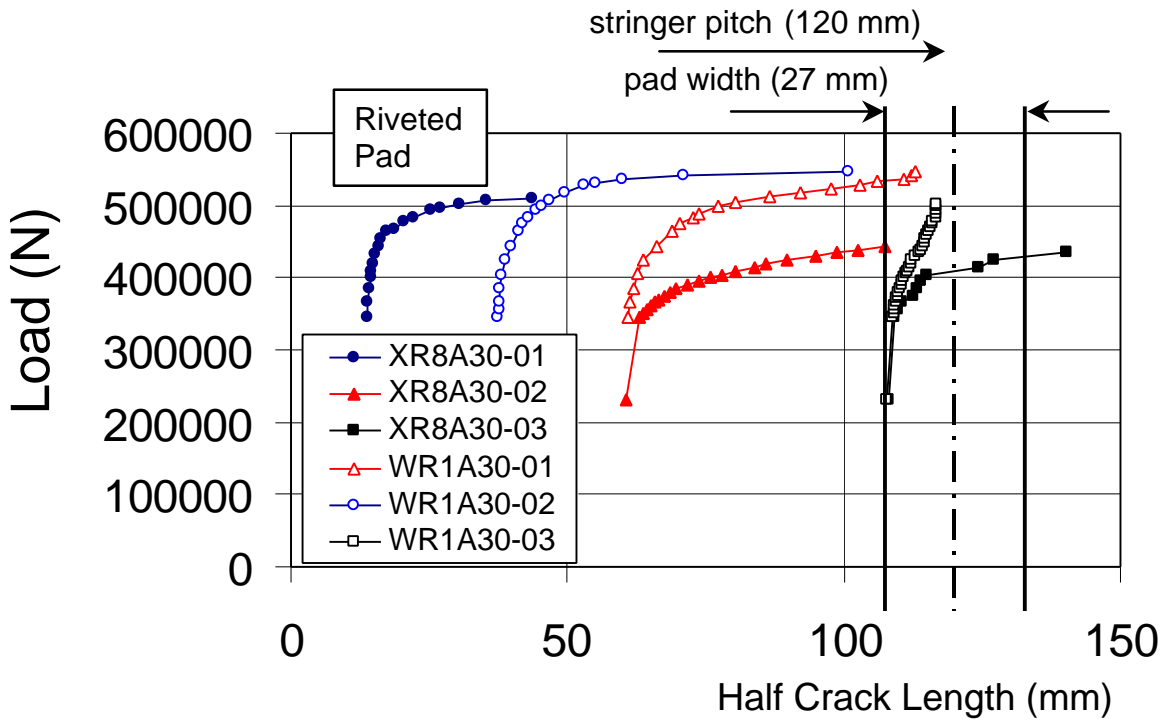


Fig. 11 Comparison of stable crack growth curves, riveted stringers

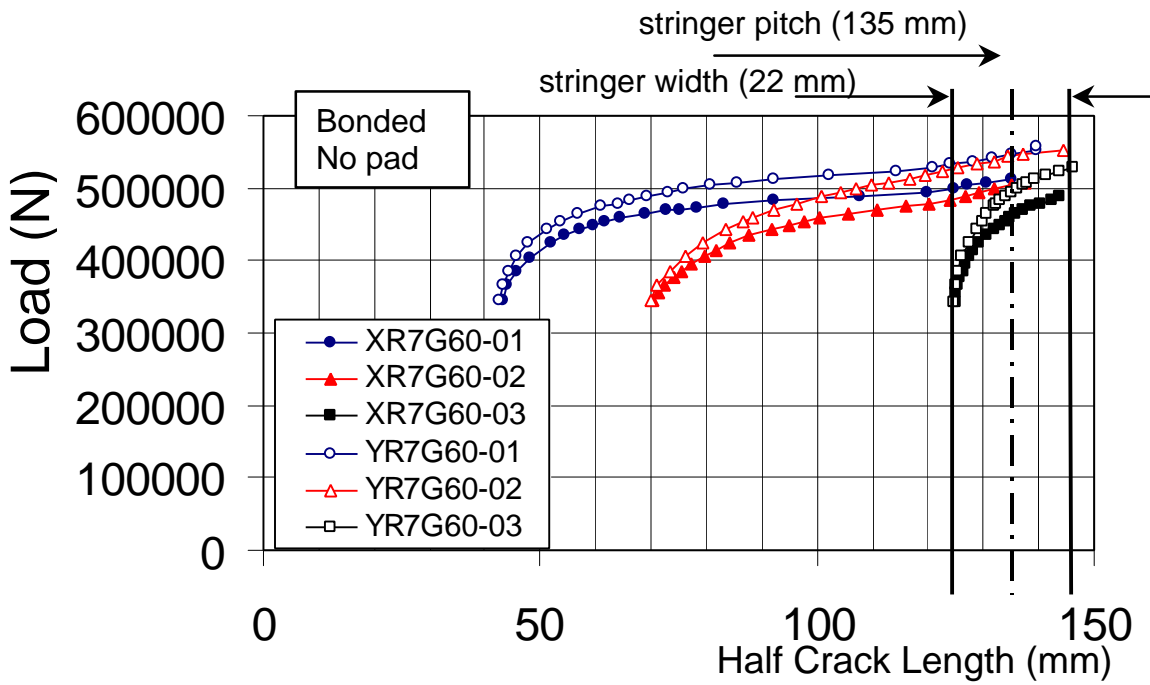


Fig. 12 Comparison of stable crack growth curves, bonded stringers

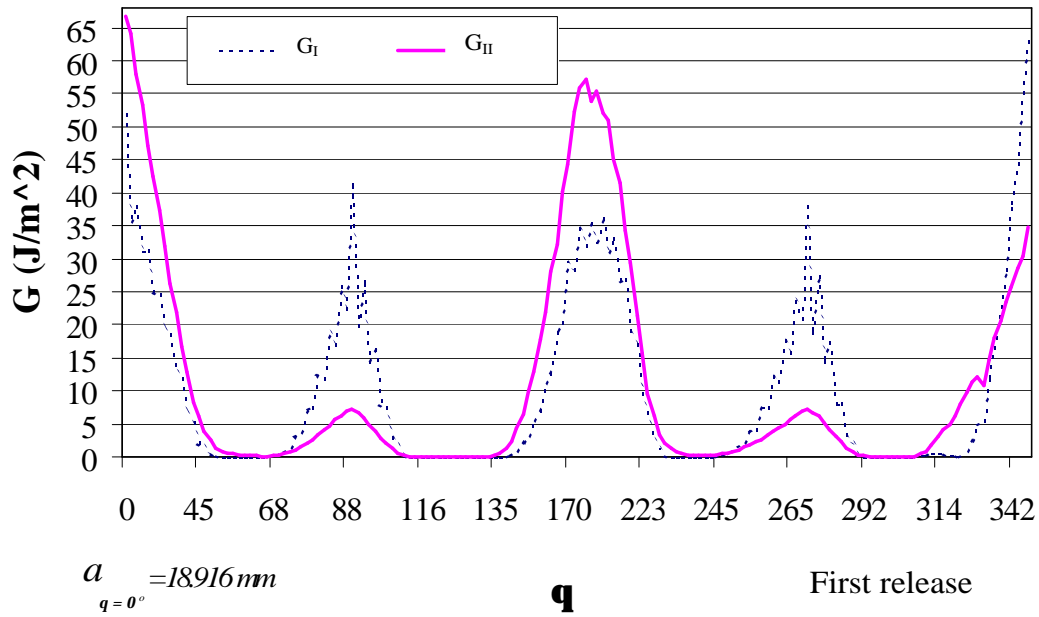


Fig. 13a Distribution of G_I and G_{II} contributions along the front of a generic shaped delamination (First delamination increment)

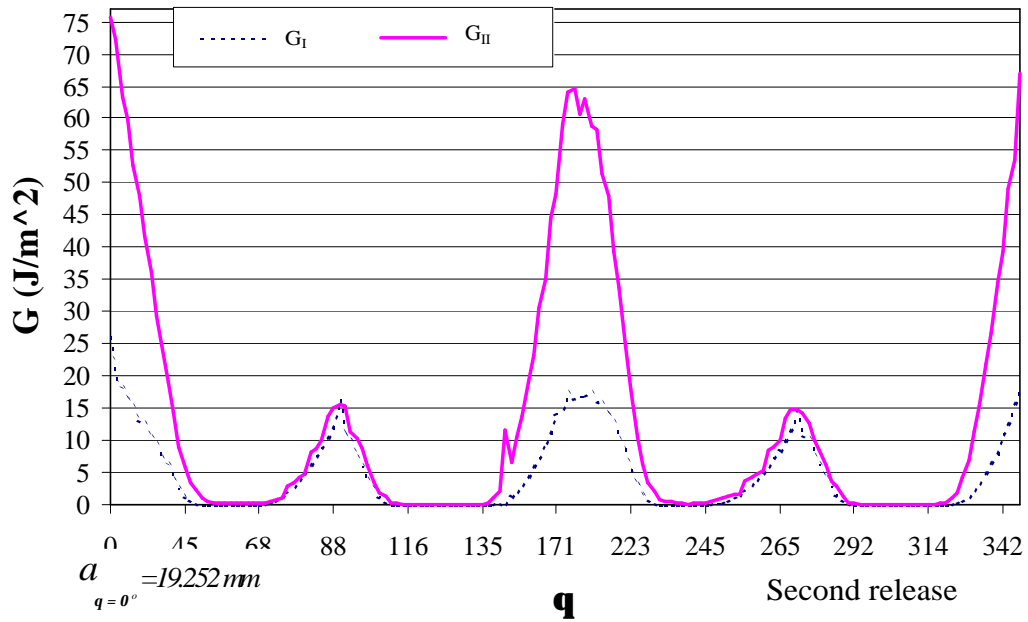
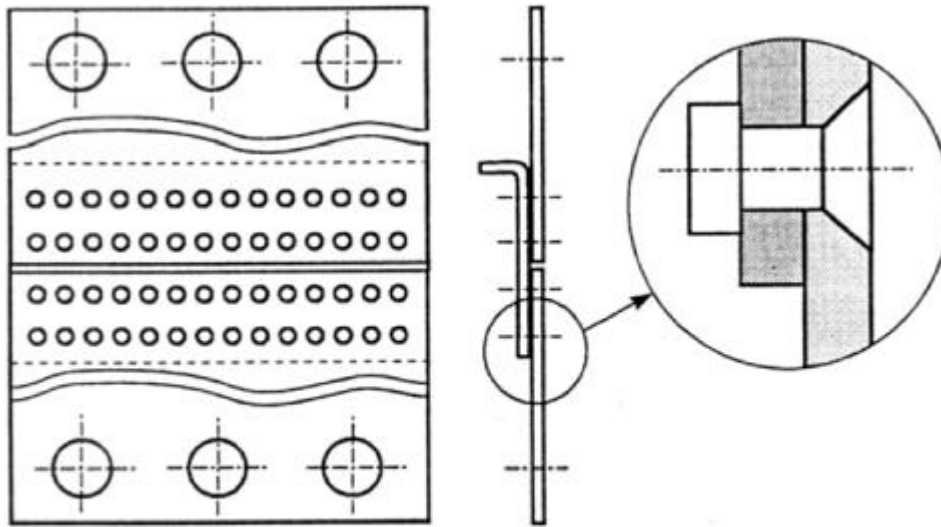


Fig. 13b Distribution of G_I and G_{II} contributions along the front of a generic shaped delamination (Second delamination increment)



W=280 mm ; 14 rivets per row
 W=600 mm ; 30 rivets per row

Fig. 14 Single-strap butt joint for MSD study

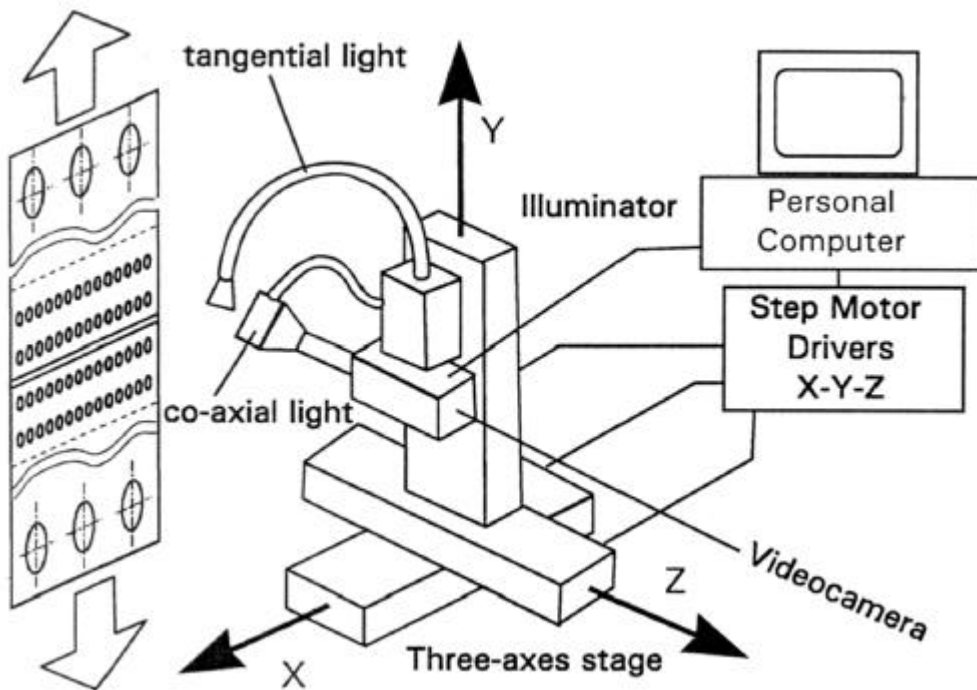


Fig. 15 Sketch of the test equipment

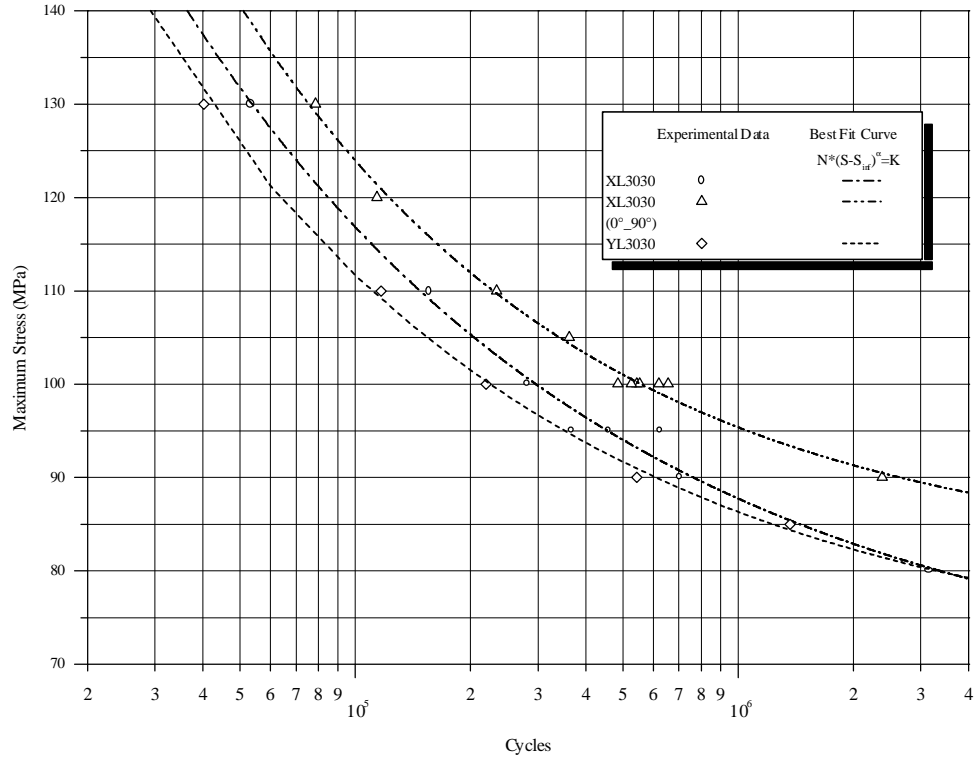


Fig. 16 Comparison of different S-N curves for 3 rivet rows joint configurations in Glare

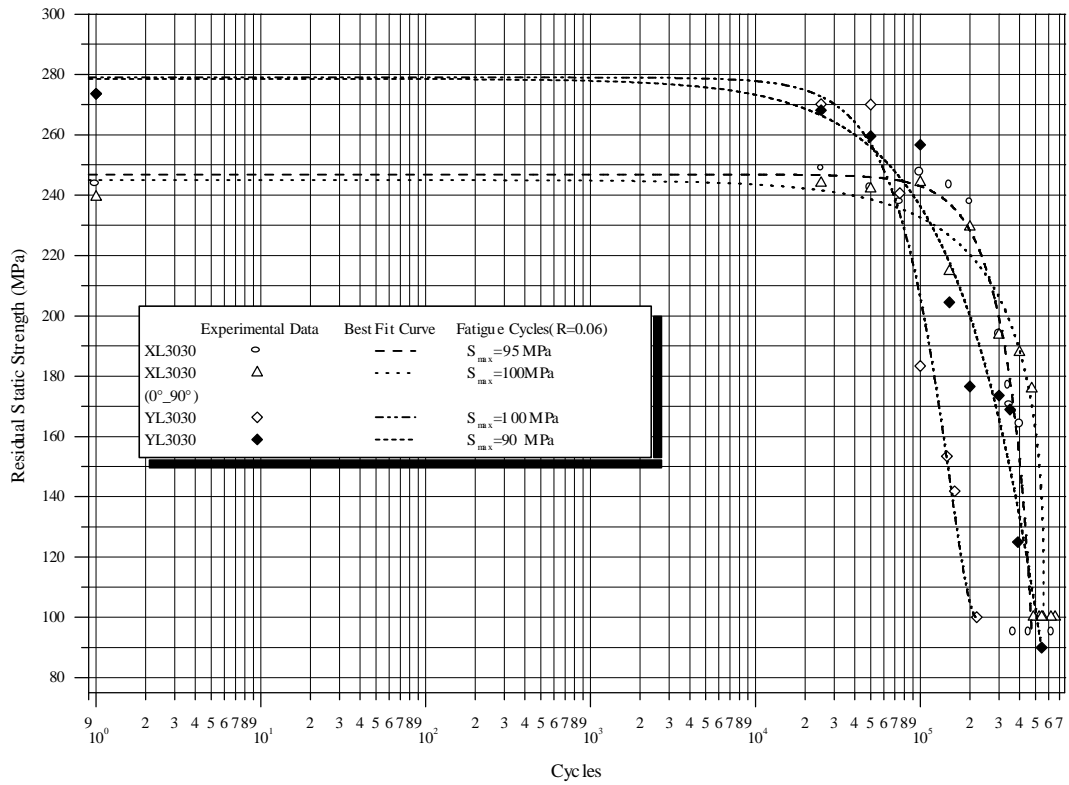


Fig. 17 Comparison of RSS curves for different Glare joints with 3 rivet rows

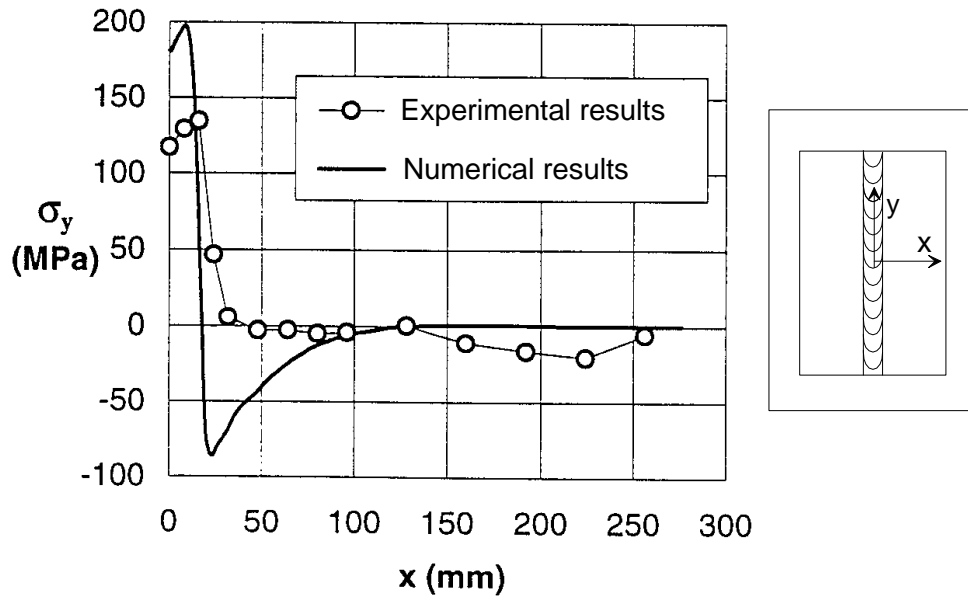


Fig. 18 Comparison between residual stress distributions evaluated experimentally and analytically

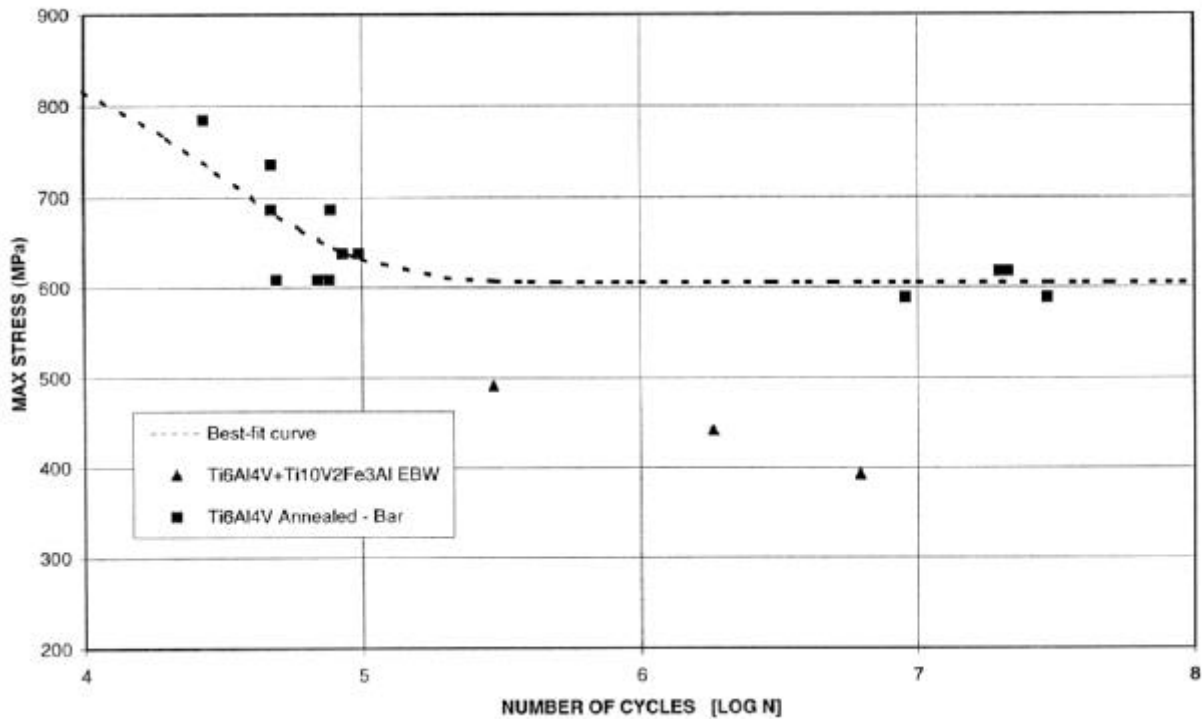


Fig. 19 Fatigue behaviour (rotating bending) of EBW Titanium alloys compared with Ti-6Al-4V annealed

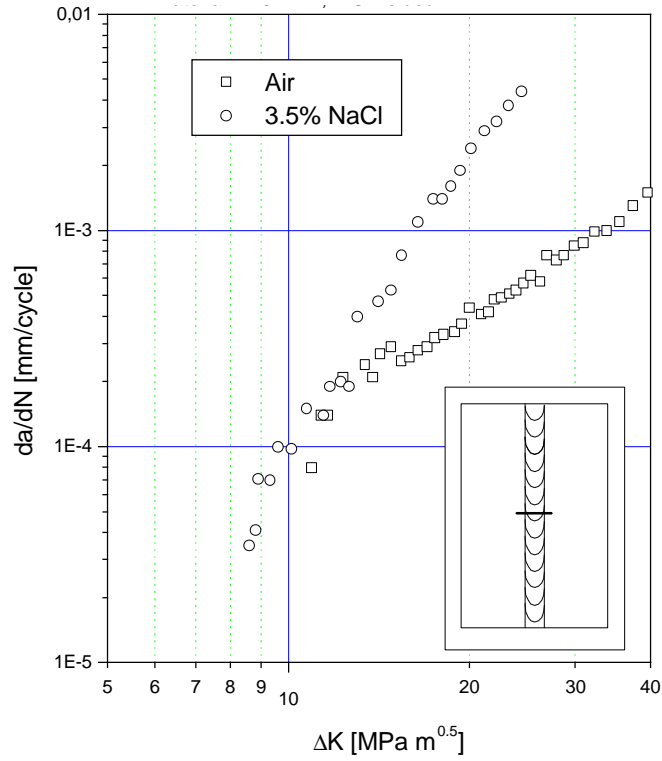


Fig. 20 Effects of the corrosive environment on fatigue crack growth in Ti-6Al-4V Welded

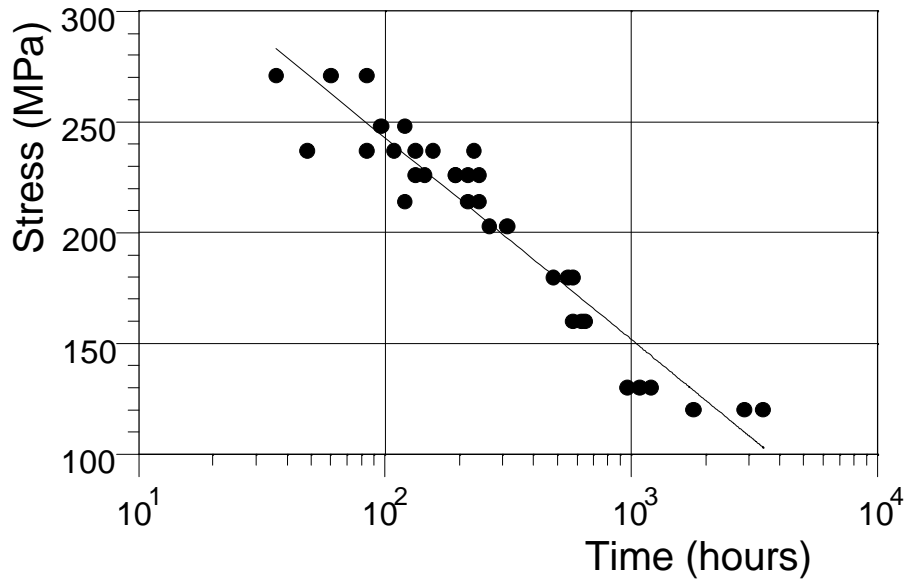


Fig. 21 Results of the Time to Failure Tests carried out on 7050-T7451 EBW specimens
Test condition: alternate immersion in a 3.5% NaCl solution

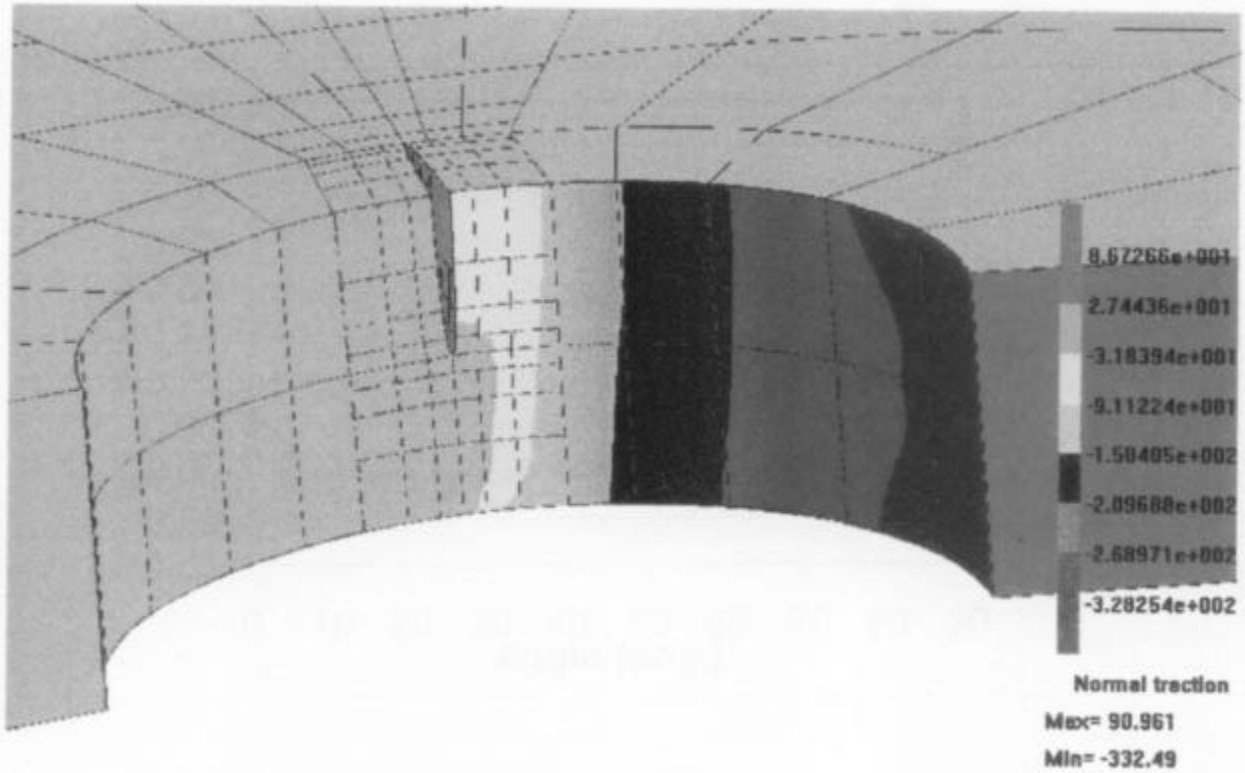


Fig. 22 FEM analysis for Stress Intensity Factor evaluation

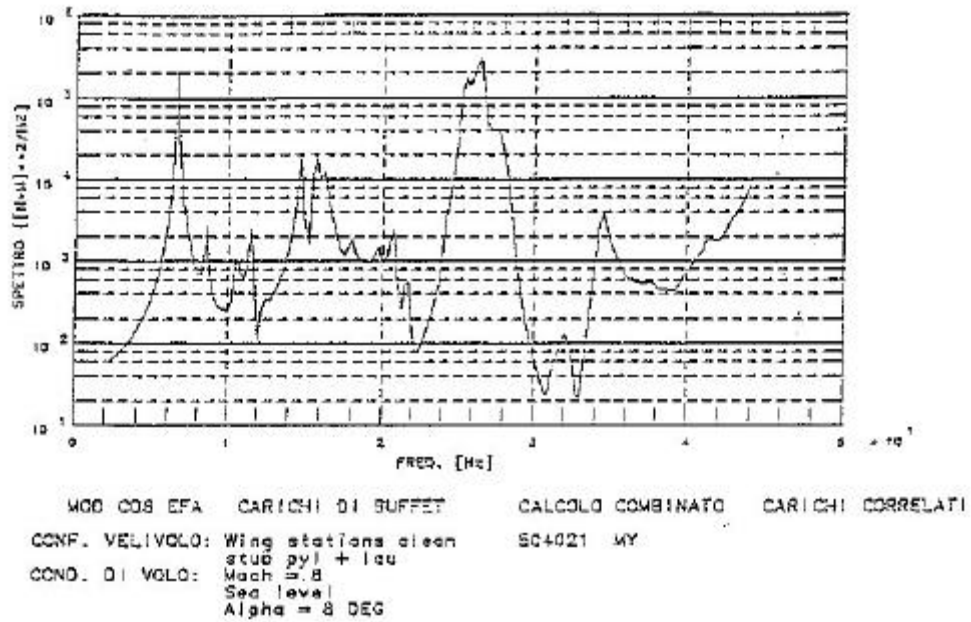


Fig. 23 PSD Function of Buffet response of the EF Typhoon aircraft



Fig. 24 Assembly for fatigue test of the EH-101 rear tail end fittings

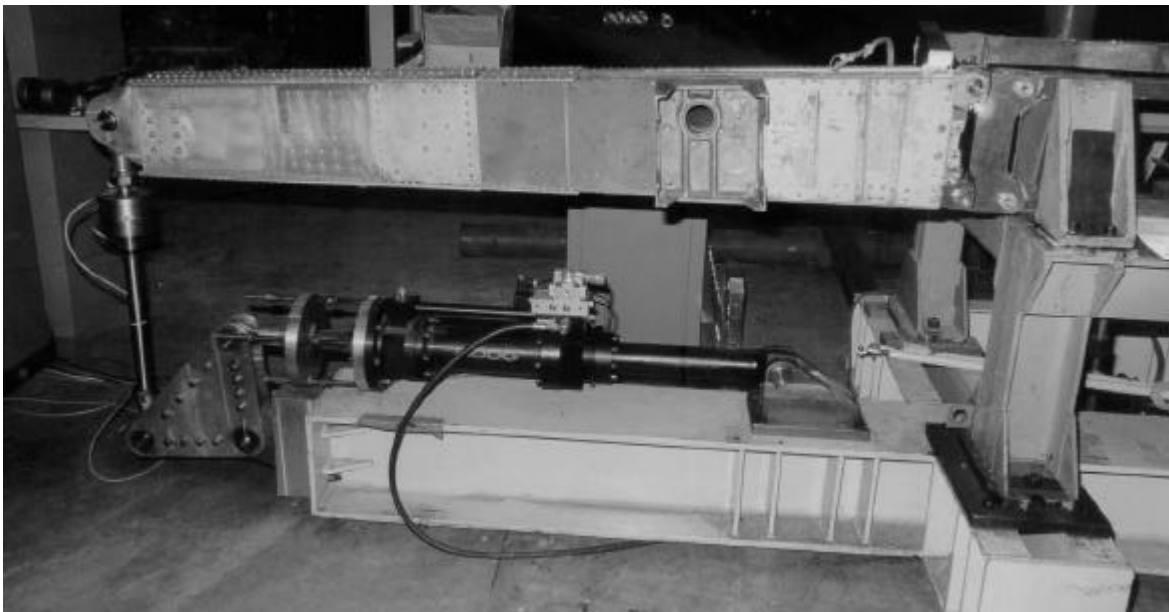


Fig. 25 Assembly for fatigue test of the MB-326 wing spar

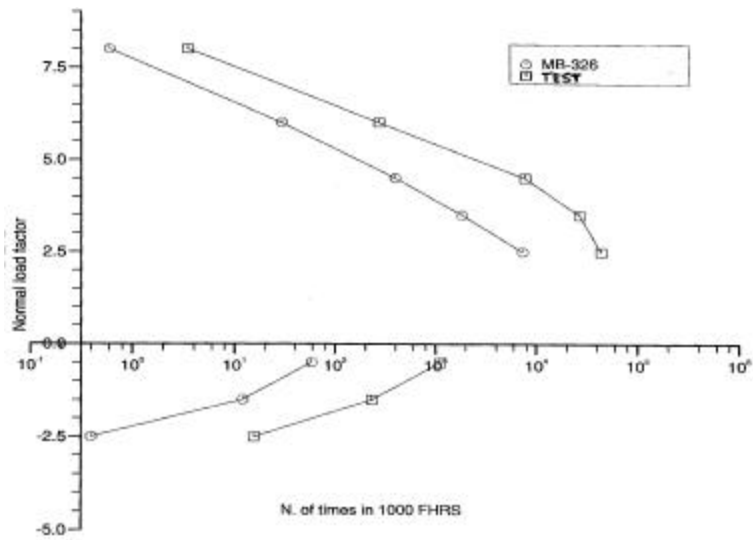


Fig. 26 Test load spectrum compared with measured MB-326 usage spectrum

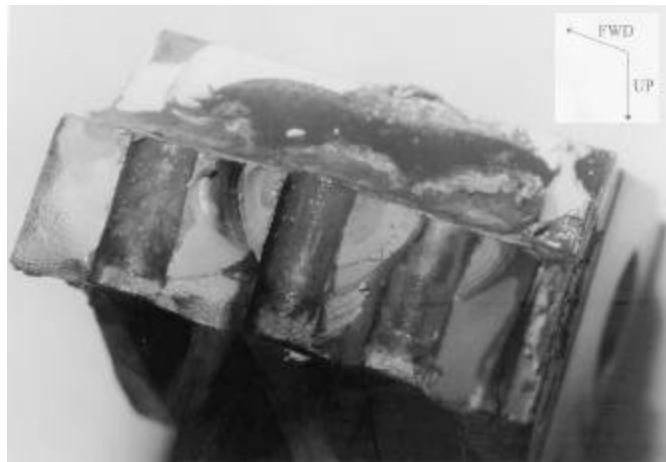


Fig. 27 Fracture surface of RH wing attachment fitting



Fig. 28 Fracture surface of LH spar cap

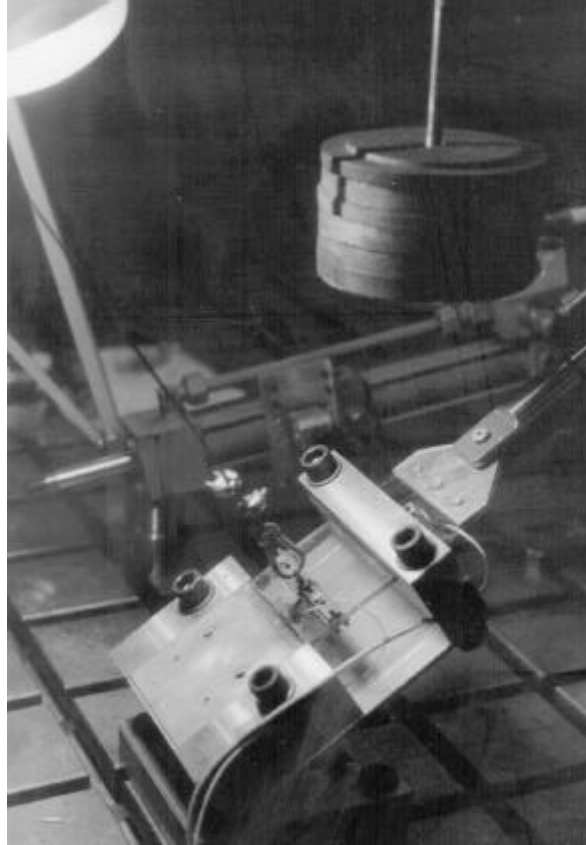


Fig. 29 Test rig for fatigue test of YAK/AEM-130 canopy transparency

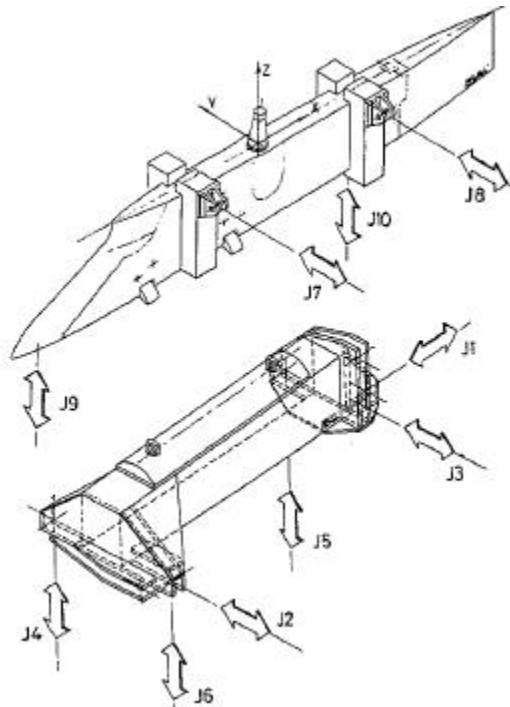


Fig. 30 EFA centre pylon test article and position of the actuators application points

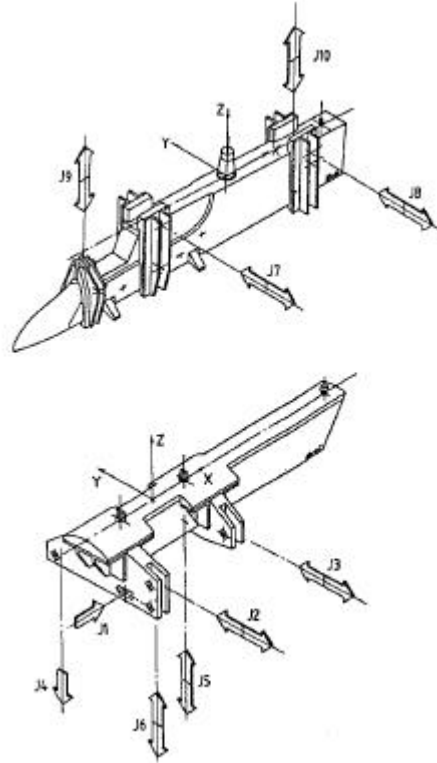


Fig. 31 EFA outboard pylon test article and position of the actuators application points

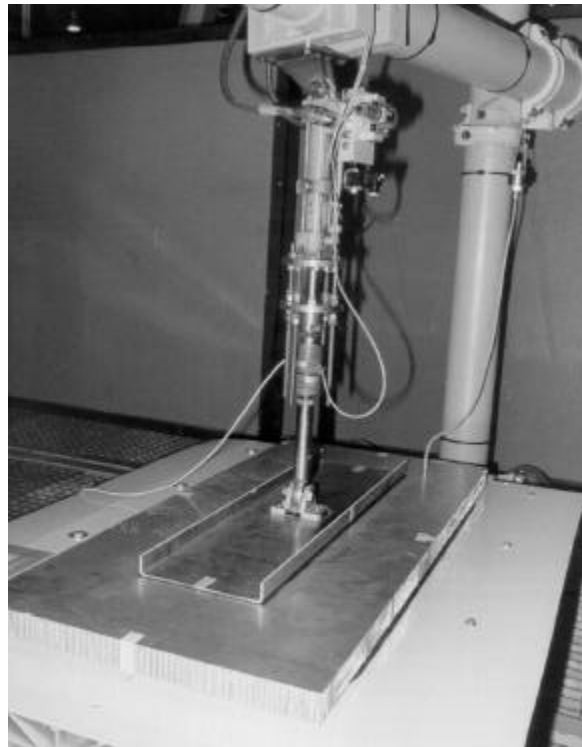


Fig. 32 Test rig of the window frame of a high speed train

**A REVIEW OF RESEARCH
ON
AERONAUTICAL FATIGUE IN THE UNITED STATES**

1997 – 1999

Compiled by
James L. Rudd
Air Force Research Laboratory
Wright-Patterson Air Force Base, Ohio, USA

FOR PRESENTATION AT THE MEETING
OF THE
INTERNATIONAL COMMITTEE ON AERONAUTICAL FATIGUE

12 – 16 July 1999

BELLEVUE, WASHINGTON, USA

Approved for Public Release: Distribution is Unlimited

TABLE OF CONTENTS

9.1.	Introduction	9/6
9.2.	Overviews	9/7
9.2.1	New Certification Procedures for Composites in Small Aircraft	9/7
9.2.2	Supplemental Inspection Documents for Commuters.....	9/7
9.2.3	Rotorcraft Fatigue and Damage Tolerance and the Use of a Health and Usage Monitoring System.....	9/8
9.2.4	Second International Symposium on Fretting Fatigue	9/9
9.3.	Loads.....	9/10
9.3.1	FAR23 Loads Program – Computer Aided Engineering for Airplane Loads to the Code of Federal Regulations.....	9/10
9.3.2	Variation in Load Factor Experience of Fokker F27 and F28 Operational Acceleration Exceedance Data.....	9/10
9.3.3	Flight Loads Data Collection Program, Large Transport Airplanes	9/11
9.3.4	Flight Loads Data Collection Program, Large Transport Airplanes	9/11
9.3.5	FAA Landing Parameter Survey Facility.....	9/12
9.3.6	Video Landing Parameter Survey at London City Airport, United Kingdom.....	9/12
9.3.7	Video Landing Parameter Survey, John F. Kennedy International Airport	9/13
9.3.8	Characterizing Aeroacoustic/Combustion Loads for Aging Aircraft Structures.....	9/13
9.4.	Fatigue and Fatigue Crack Growth.....	9/15
9.4.1	Determining the Initial Quality State for Materials.....	9/15
9.4.2	Equivalent Initial Flaw Size Test Program	9/15
9.4.3	Equivalent Initial Flaw Size Using Small Crack Data	9/16
9.4.4	Boundary Correction Factors for Elliptical Surface Cracks at Countersunk Rivet Holes	9/17
9.4.5	Comparison of Boundary Correction Factor Solutions for Two Symmetric Cracks In a Straight-Shank Hole.....	9/17
9.4.6	Fatigue Crack Growth Under Variable-Amplitude Loading in a Titanium Alloy	9/18
9.4.7	Part Through Crack Behavior in Aluminum Alloys Under Spectrum Loading	9/19
9.4.8	Experimental Verification of T* Theory.....	9/19
9.4.9	Fracture Analyses of Surface Cracks in Brittle Materials	9/20
9.4.10	Modeling K_{max} Effects on Fatigue Crack-Growth Rates.....	9/21
9.4.11	The Manson-Coffin Relation for Determining Cycles Until Failure	9/22
9.4.12	Fatigue Crack Growth Lives Under Repeated Spike Overloads and Underloads	9/22
9.4.13	Assessment of Low Cycle Fatigue of Powder Metallurgy Disk Superalloy U720	9/23
9.4.14	Residual Strength Analysis Methodology.....	9/23
9.4.15	Analyses of Buckling and Stable Tearing in Thin-Sheet Materials	9/24
9.4.16	Fracture Simulations of Wide Panels Need the Plane-Strain Core	9/25
9.4.17	Fatigue Crack Growth at Machined Pockets.....	9/26
9.4.18	T-38 Lower Wing Skin Machined Pockets Analysis and Test.....	9/26
9.4.19	Fatigue Analysis of Padded Single-Shear Lap Splices.....	9/27
9.4.20	Application of Small-Crack Theory to a Rotorcraft Material	9/28
9.4.21	Fretting Damage in Advanced Propulsion Systems	9/28
9.4.22	Fretting Fatigue in Riveted Aircraft Structures.....	9/29
9.4.23	Advanced Crack Growth Modeling (using AFGROW) and Testing	9/30
9.5.	Widespread Fatigue Damage.....	9/31
9.5.1	Analytical and Test Evaluation on the Linkup of Multiple Cracking in Stiffened Fuselage Panels	9/31
9.5.2	Fracture Analyses of FAA/NASA Stiffened Panels with Multiple-Site Damage	9/31
9.5.3	FAA-NASA Stiffened-Panel Fracture Tests	9/32
9.5.4	Widespread Fatigue Damage Evaluation	9/33
9.5.5	Bulging Factors for Predicting Residual Strength of Fuselage Panels with WFD	9/33
9.5.6	Engineering Approach to Predict Residual Strength of Fuselage Panels with WFD	9/34
9.5.7	Engineering Model for Residual Strength with Multiple Site Damage.....	9/34
9.5.8	Transport Risk Assessment Containing Widespread Fatigue Damage: TRACWFD.....	9/35

9.6.	Corrosion and Corrosion/Fatigue	9/36
9.6.1	Modeling Corrosion Growth on Aircraft Structure	9/36
9.6.2	Experimental Study	9/36
9.6.3	Importance of Chemically Short-Crack-Growth on Fatigue Life	9/37
9.6.4	Prediction of Fatigue Life of Pre-Corroded Specimens	9/37
9.6.5	An Engineering Crevice Corrosion Model in KC-135 Lap Joints	9/38
9.6.6	Corrosion Fatigue Predictive Modeling with Pit Depth as a Controlling Factor	9/39
9.6.7	A Life Prediction Methodology for Evaluating Corrosion-Fatigue Interactions.....	9/40
9.6.8	Joint FAA-Air Force Corrosion Fatigue Interaction Research Program	9/41
9.6.9	Corrosion Monitoring of Field Sites	9/42
9.6.10	An Environmental Corrosion Severity Index for USAF Airbases	9/42
9.6.11	Evaluation and Quantification of Fretting Fatigue Induced Damage	9/43
9.6.12	Effect of Prior-Corrosion Damage on Cold-Expansion Hole.....	9/43
9.6.13	Corrosion Fatigue Structural Demonstration	9/43
9.6.14	Computerized Model for Lap Joint Corrosion Prediction.....	9/44
9.6.15	Corrosion Fatigue Structure Demonstration Program.....	9/45
9.7.	Probabilistics and Risk Assessment	9/46
9.7.1	Probabilities of Occurrence and Detection of Damage in Airframe Materials	9/46
9.7.2	Fatigue Variability and Life Prediction: A Probabilistic Approach.....	9/47
9.7.3	Probabilities of Occurrence – Model Estimation Versus Field Measurement	9/48
9.7.4	Probabilistic Residual Strength Model for Uni-Axial Fatigue of Composites	9/49
9.7.5	Risk Analysis as a Force Management Tool -- Updates	9/49
9.7.6	Reliability Management for Structural Certification and Life Extension	9/50
9.8.	Joints	9/51
9.8.1	3-D Finite Element Modeling of Cracked Mechanically Fastened Joints	9/51
9.8.2	Analysis Tools for Durability and Damage Tolerance Analysis on Riveted Lap Joints	9/51
9.8.3	Crack Growth in High-Strength Bolts.....	9/52
9.8.4	Qualification of Hand Held Low Voltage Electromagnetic Riveting	9/53
9.8.5	Damage Tolerance Testing and Analysis of an Integral Skin Stringer Fuselage Panel	9/54
9.8.6	Fatigue Testing of a High Load Transfer Joint	9/55
9.9.	Testing.....	9/56
9.9.1	Longitudinal Test of a B737 Fuselage Section	9/56
9.9.2	Dynamic Vertical Drop Test of a Shorts 330 Airplane	9/56
9.9.3	Full-Scale Fuselage Panel Test System.....	9/57
9.9.4	777 Main Landing Gear Fatigue Test	9/58
9.9.5	Beechcraft 1900 Airliner Dynamic Drop Test Report	9/58
9.9.6	737-800 Full Scale Fuselage Fatigue Test	9/59
9.9.7	Advanced Actuators for Active Control of Sonic Fatigue Dynamic Environments.....	9/60
9.10.	Composites.....	9/61
9.10.1	Thermomechanical Fatigue Durability of T650-35/PMR-15 Sheet Molding Compound.....	9/61
9.10.2	Analysis of Thermally Induced Strains in Continuous Fiber Reinforced Composites.....	9/62
9.10.3	Methodology for Delamination Growth Assessment in Composite Material Aircraft Structures	9/62
9.10.4	Prediction Methodology for Impact-Damage Composite Structure.....	9/63
9.10.5	Compression Testing of Composite Materials	9/64
9.10.6	Handbooks for Advanced Composites	9/65
9.10.7	Strength Prediction of Notched Thin-Skin Honeycomb Sandwich Structures.....	9/66
9.10.8	Effect of Long-Term Isothermal Aging in Air on IM7/K3B and IM7/5260 Composites Laminates	9/67
9.10.9	Crack Growth and Residual Strength of Hybrid Laminate Open-Hole Tension Specimens.....	9/67

9.11. Repair.....	9/69
9.11.1 Installation of Composite Doubler on L-1011 Aircraft in Delta Airlines Fleet	9/69
9.11.2 Shot Peening Effects on Fatigue-Crack Growth	9/70
9.11.3 Bonded Composite Doubler Repairs at Warner Robins Air Logistics Center	9/70
9.11.4 C-130 Center Wing Lower Surface Corrosion Bonded Composite Doubler Repair.....	9/71
9.11.5 The Panther Skin Project – A Joint FAA/FIU Investigation.....	9/73
9.11.6 Composite Repair of Aircraft Structure Program.....	9/74
9.11.7 Effects of Artificial Disbonds on Patching Efficiency over Thicker Structures.....	9/74
9.11.8 Assessing the Effect of Repairs on Damage Tolerance of Airplane Fuselage Structure.....	9/75
9.11.9 Damage Dosimeter and Durability Patch.....	9/76
9.11.10 Repair Assessment Procedure and Integrated Design (RAPID) User Evaluation.....	9/76
9.12. Nondestructive Inspection/Evaluation.....	9/78
9.12.1 Investigation of Fatigue Cracks in Riveted Specimens Using the Light, Electron and Acoustic Microscopes	9/78
9.12.2 Effects of Maximum Nominal Applied Stress on Fatigue Crack Orientation and Growth in Riveted Specimens.....	9/78
9.12.3 Eddy-Current Methods for Crack Detection	9/79
9.12.4 Superconducting Quantum Interference Devices for Detection of Hidden Cracks.....	9/80
9.12.5 Eddy-Current Detection of Small Cracks.....	9/80
9.12.6 Self-Compensating Ultrasonic Technique	9/81
9.12.7 Development of a Novel NDE Probe to Detect and Measure Corrosion of Aging Aircraft	9/82
9.12.8 Thermal Wave Imaging of Disbonding and Corrosion in Aircraft Structures	9/83
9.12.9 Economical Eddy-Current for Engine Components.....	9/83
9.12.10 Early Fatigue Detection and Characterization using the Meandering Winding Magnetometers.....	9/84
9.12.11 Visual Inspection Reliability.....	9/85
9.12.12 NDE Capabilities Data Book	9/85
9.13. Engines.....	9/87
9.13.1 Uncontained Turbine Engine Debris Characterization and Vulnerability Analysis.....	9/87
9.13.2 Containment of Turbine Engine Failures	9/87
9.13.3 Resistance of Titanium Aluminide to Domestic Object Damage Assessed	9/88
9.13.4 Enhanced Turbine Rotor Material Design and Life Methodology.....	9/88
9.13.5 Fleet Octane Requirements for Unleaded Fuels.....	9/89
9.13.6 Simulation of Crack Propagation in Engine Rotating Components Under Variable Amplitude Loading	9/90

9.1. INTRODUCTION

1. Leading government laboratories, universities and aerospace manufacturers were invited to contribute summaries of recent aeronautical fatigue research activities. Their voluntary contributions are compiled here. Inquiries should be addressed to the person whose name accompanies each item. On behalf of the International Committee of Aeronautical Fatigue, the generous contribution of each organization is hereby gratefully acknowledged.

- + **The Boeing Company**
- + **NASA - Langley Research Center**
- + **NASA - Glenn Research Center**
- + **Federal Aviation Administration- William J. Hughes Technical Center**
- + **University of Utah**
- + **Lehigh University**
- + **USAF Warner Robins Air Logistics Center**
- + **US Navy – Naval Air Systems Command**
- + **Rensselaer Polytechnic Institute**
- + **Purdue University**
- + **Analytical Processes/Engineering Solutions, Inc**
- + **NCI Information Systems, Inc.**
- + **R - Tech**
- + **Lockheed Martin Aeronautical Systems**
- + **Northwestern University**
- + **Florida International University**
- + **Lynntech, Inc**
- + **Air Force Research Laboratory**

2. References, if any, are listed at the end of each article. Figures are compiled at the end of the review.
3. The assistance of Ms. Charlotte Burns, Universal Technology Corporation, in the preparation of this review is gratefully appreciated.

9.2. OVERVIEWS

9.2.1 New Certification Procedures for Composites in Small Aircraft

Donald Oplinger

FAA William J. Hughes Technical Center

NASA Langley Research Center together with various elements of the FAA has been working with the Advanced General Aviation Transport Experiments (AGATE) consortium of small aircraft manufacturers since 1994 to revitalize the U.S. small airplane manufacturing industry. One of the major thrusts under AGATE, the Integrated Design and Manufacturing (ID&M) effort, is to enhance competitiveness of U.S. small airplane airframe manufacturers through development of low-cost production methods based on the use of composite components. The William J. Hughes Technical Center, through its research program on Advanced Materials (along with other units of the FAA including the Small Airplane Directorate and the Aircraft Certification Service), has been providing financial and technical support to AGATE/ID&M since its inception in 1994.

A major barrier to lowering the cost of aircraft using composite structural materials has been the cost of certification. To a large extent the high certification cost has been due to the need for individual manufacturers to develop large and costly data on structural and chemical properties of the materials selected for use in aircraft construction. The conventional and AGATE/ID&M certification procedures are compared in Figure 1.

In the conventional approach shown at the left, individual companies are required to develop the total database; several companies desiring to apply the same material to a number of components are each required to develop the same database. Thus, the considerable effort involved in generating the database may have to be duplicated several times. In the AGATE/ID&M process shown on the right, the group of small aircraft companies making up the consortium agree to use a common material for each of their applications and only one database development is needed. The cost of generating the database is then shared by the whole group of companies making up the consortium, resulting in a sizeable savings to each of the partners. It is estimated that after development of the common data base, the certification cost of each company is reduced from \$350,000 to \$50,000, with a concurrent reduction in time to complete the development of the property base from as much as 24 months to as little as 6 months.

Essential to the success of this effort was the participation of various organizations within the FAA. The Small Airplane Directorate (ACE) agreed to accept the group certification approach; individuals within ACE also worked as associate members of the consortium to give guidance to the small airplane manufacturers as to details of the test plan that had to be followed in generating the database. William J. Hughes Technical Center participation included co-funding of the data gathering effort — conducted by Wichita State University — and consultation support where coordination with the MIL-HDBK-17 Composite Materials Handbook was required.

POC: Donald Oplinger, AAR-431, FAA William J. Hughes Technical Center, Atlantic City International Airport, NJ 08405, (609) 485-4914.

9.2.2 Supplemental Inspection Documents for Commuters

Dr. Xiagong Lee

FAA William J. Hughes Technical Center

Increased utilization, longer operational lives, and the high safety demands imposed on currently operating air carrier airplanes have indicated that there is a need for a program to provide for a high level of structural integrity for all airplanes in the commuter transport fleet. Supplemental Inspection Programs (SIP) have been used successfully to provide this level of safety in the large transport segment of the industry.

To extend this concept to commuter category airplanes, the FAA proposes changes to require all airplanes operated under FAR Part 121, all U.S.-registered multiengine airplanes operated under Part 129, and all multiengine airplanes used in scheduled operations conducted under Part 135 to undergo inspections after their 14th year in service to ensure their structural integrity. The proposed rule would also require that damage tolerance (DT)-based SIP be developed for these airplanes before specific deadlines. (See Figure 2.) This proposal represents a critical step toward compliance with the Aging Aircraft Safety Act of 1991. It ensures the continuing airworthiness of aging

airplanes by applying modern DT analysis and inspection techniques to older airplane structures that were certificated before such techniques were available.

Many commuter airplane manufacturers and operators do not have the large engineering staffs, budgets, or fleet sizes to support a program as extensive as the large transport program. To ease this burden, the FAA is assisting U.S. manufacturers of selected airplane models to develop Supplemental Inspection Documents (SIDs) which could then be used by operators to develop SIPs. In addition, other manufacturers can also use SID guidance material as they develop the documents for their aircraft models. SIDs are under development for two models of aircraft representing a cross section of the commuter fleet: Cessna 402 and Fairchild Metro 227.

Cessna has developed a SID for the Model 402 through the use of DT-based analyses. (See Figure 3.) Fairchild established inspection thresholds and intervals for each of the principal structural elements (PSEs) in the Metro 227 through the use of DT-based analyses. The inspection thresholds and intervals and recommendations and descriptions of inspection techniques will form the basis for the SID, which is to be completed early next year.

POC: Dr. Xiagong Lee, AAR-431, FAA William J. Hughes Technical Center, Atlantic City International Airport, NJ 08405, (609) 485-6967.

9.2.3 Rotorcraft Fatigue and Damage Tolerance and the Use of a Health and Usage Monitoring System Mr. Dy Le FAA William J. Hughes Technical Center

Rotorcraft flight envelopes are extremely complicated due to high oscillatory loads. Therefore, in the design of rotorcraft structural components, fatigue is critical and is a prime area that significantly effects the safety of rotorcraft.

Damage tolerance (DT) design practice is based on the premise that should serious fatigue, corrosion, or accidental damage occur within the operation life of the rotorcraft, the remaining structure can withstand the limited load without catastrophic failure or excessive structural deformation until the damage is detected through scheduled inspection intervals. The approach is based upon fracture mechanics and nondestructive inspection (NDI) techniques. It has been concluded that the damage tolerance approach and reliability of improved and advanced NDI techniques would minimize the catastrophic failure in aging rotorcraft, and at the same time, reduce the life-cycle costs by extending their useful structural component life.

The FAA is currently supporting the development of a comprehensive understanding of the damage tolerance methodology for rotorcraft through several efforts. (See Figure 4.) The results of these efforts will be used for developing or revising applicable Advisory Circulars and FARs that the FAA engineers could use in certifying new components or making safety-related decisions in order to reduce the accident rate due to structural failures in rotorcraft.

Operational Evaluation of a Health and Usage Monitoring (HUMS) program, conducted by Bell Helicopter Textron Inc., is designed to evaluate structural usage monitoring and damage tolerance methodology using data collected concurrently during a helicopter flight program. The previous effort involved a Bell Helicopter Model 412 equipped with a Health and Usage Monitoring System and data recorder and operated by Petroleum Helicopters Inc. (PHI) during the 1996 Summer Olympic Games in Atlanta, Georgia. The Atlanta Short Haul Mission (ASHM) included many short flights but with a large number of maneuvers to provide pickup and delivery services. The collected usage data was used to compare with certification data and to data collected from a previous study for the Gulf Coast Mission (GCM). The usage data was also used to perform fatigue life calculations and determine relative crack growth rate on the rephrase and collective lever, the main rotor spindle, and the main rotor yoke.

The results indicate that the calculated lives for the GCM and ASHM are much higher than that certified for the rephrase and collective level and the main rotor spindle with a pressure altitude split at 3000 feet. For the main rotor yoke, with the altitude split, the GCM calculated lives are higher, and the ASHM calculated lives are about the same as that of those certified.

The calculated crack growth life, using three different spectra, indicated relative short inspection intervals for components that were designed using a safe-life philosophy.

A final report of this effort was published in April 1998 documenting the fatigue life analysis and damage tolerance analysis, Operational Evaluation of a Health and Usage Monitoring System (HUMS), AR-97/64.

The expansion of the usage database will continue with Bell and PHI using a HUMS-equipped Bell Helicopter Model 412 to examine a variety of different missions. The evaluation of the damage tolerance analysis and its comparison to the traditional safe-life methodology is also continuing.

POC: Mr. Dy Le, AAR-431, FAA William J. Hughes Technical Center, Atlantic City International Airport, NJ 08405, (609) 485-4636.

**9.2.4 Second International Symposium on Fretting Fatigue, Salt Lake City, Utah,
August 31 - September 2, 1998
D.W. Hoepfner, and V. Chandrasekaran
University of Utah**

The Second International Symposium on Fretting Fatigue was held at the University Park Hotel in Salt Lake City, Utah on Aug. 31-Sept. 2, 1998. The Quality and Integrity Design Engineering Center (QIDEC) at the University of Utah, in conjunction with Fatigue and Structural Design Engineering Incorporated (FASIDE), sponsored the event along with MTS Systems Corporation, and United Technologies Corporation. This symposium is a follow-up to the First International Symposium on Fretting Fatigue held at the University of Sheffield in April, 1993.

The symposium featured keynote lectures by researchers from numerous countries. In addition, sessions featured invited papers as well. A total of 40 papers were presented by researchers around the world that represent a broad spectrum of research and development activities. Figure 5 shows the distribution of papers by country. Figure 6 shows the distribution of fretting fatigue papers by topic.

Papers that were presented at the symposium will be published by the American Society for Testing and Materials (ASTM) as a Special Technical Publication (STP) entitled *Fretting Fatigue: Current Technology and Practices*. Drs. D.W. Hoepfner, V. Chandrasekaran and C.B. Elliott of QIDEC are functioning as the editors for the STP 1367.

9.3. LOADS

9.3.1 FAR23 Loads Program - Computer Aided Engineering for Airplane Loads to the Code of Federal Regulations

Mr. Thomas DeFiore

FAA William J. Hughes Technical Center

The FAR23 Loads Program was developed to approximate loads on small airplanes from preliminary airplane geometry using methods acceptable to the FAA. The program includes 20 modules that are each self-contained sub-programs designed for specific application.

Most of the detailed flight loads are developed from the flight envelopes specified in 23 CFR Parts 333 and 345. At every point specified in the flight envelope, the airplane is balanced by a tail load reacting to the specific linear normal acceleration and the aerodynamic lift, drag, and moment about the center of gravity. The data needed to make these balancing calculations consists of (1) the weight at the center of gravity, (2) aerodynamic surface geometry, (3) structural speeds, and (4) aerodynamic coefficients. After the balanced loads are developed, the critical structural loads are determined for each component. For the critical conditions, the air, inertial, and net loads are calculated. Aileron, flap, tab, engine mount, landing, and one engine out loads are also calculated. Landing loads are calculated from the landing geometry, landing load factor, weight, and center of gravity data.

The FAR23 Loads Program provides a procedure for calculating the loads on an airplane according to the Code of Federal Regulations, Title 14 - Aeronautics and Space, Chapter I - Federal Aviation Administration, Subchapter C - Aircraft, Part 23 - Airworthiness Standards: Normal, Utility, Aerobatics, and Commuter Category Airplanes, Subpart C - Structures.

The FAR23 Loads Computer Program is documented in an FAA Technical Report, DOT/FAA/AR-96/46, User's Guide for FAR23 Loads Program. Computer Aided Engineering for Airplane Loads to Federal Air Regulations.

POC: Mr. Thomas DeFiore, AAR-431, FAA William J. Hughes Technical Center, Atlantic City International Airport, NJ 08405, (609) 485-5009 and Mr. Richard Micklos, AAR-432, FAA William J. Hughes Technical Center, Atlantic City International Airport, NJ 08405, (609) 485-6531.

9.3.2 Variation in Load Factor Experience of Fokker F27 and F28 Operational Acceleration Exceedance Data

Mr. Thomas DeFiore

FAA William J. Hughes Technical Center

Fatigue meter data obtained during operational flights of Fokker F27 and F28 aircraft were reprocessed and analyzed to study the variation in load experience between different aircraft of the same model type.

The data covered about 470,000 flights which were made by 101 aircraft belonging to 51 different operators. A simple algorithm was developed to quantify the load factor experience in terms of fatigue damage per flight. The data were subjected to a statistical analysis where considerable variations in load experience were obtained. See accompanying Figure 7 for the F27 and F28. The results give an indication of the potential benefits which can be gained from individual aircraft load monitoring. Similar studies are planned on data for US carriers when sufficient flight data are obtained.

This research was performed under a memorandum of cooperation between the Federal Aviation Administration and the Netherlands Aviation Department. As part of this effort, the National Aerospace Laboratory was contracted to participate in this research effort.

A final technical report was published, DOT/FAA/AR-96/114, Variation in Load Factor Experience of Fokker F27 and F28 Operational Acceleration Exceedance Data, December 1996.

POC: Mr. Thomas DeFiore, AAR-431, FAA William J. Hughes Technical Center, Atlantic City International Airport, NJ 08405, (609) 485-5009.

9.3.3 Flight Loads Data Collection Program, Large Transport Airplanes
Mr. Thomas DeFiore
FAA William J. Hughes Technical Center

The FAA has reestablished a flight loads data collection program for large transport airplanes. The FAA system is operational and the analysis procedures have been established and verified by industry. Presently, data from 21 B-737 airplanes, 6 MD-82 airplanes, and 12 B-767 airplanes are being received. The actions have been put in motion to collect data from 40 A-320s, 5 B-757s and an additional 24 B-737s from another airline. FAA funding has purchased the majority of the necessary equipment; however, in two cases the airlines themselves supplied the necessary funding.

The initial results from a year ago have been confirmed with the additional collected data. Specifically, at high altitude the gust exceedance experience is considerably lower than that from the old National Aeronautics Civil Agency (NACA) reports; yet, conversely, at low altitudes, the gust experience is considerably greater than that which was reported in the previous NACA data.

An FAA technical report on the B-737 data was published, DOT/FAA/AR-98/28, "Statistical Loads Data for Boeing 737-400 Aircraft in Commercial Operations." This report contained a summary of 11,721 flights, 19,105 flight hours of typical service for 17 B-737/400 airplanes. New and improved methods and criteria for processing and presenting large transport airplane flight and ground loads data were developed and reported. These included (1) The definition of service related factors which affect the operational life of commercial aircraft, (2) design of an efficient software system to reduce, store, and process large quantities of optical quick access recorder data, and (3) provide processed data in formats that will enable the FAA and the airplane manufacturers to reassess existing certification criteria. The data included statistical information on accelerations, speeds, altitudes, flight duration and distance, gross weight, speed brake/spoiler cycles, thrust reverser usage, and gust velocities encountered. A similar report containing 4000 flights, 7100 hours of MD-82 usage, has been drafted and is scheduled to be published in early FY99.

When completed, the research program will have provided large quantities of typical usage data for the major categories of large transports including twin engine on wing, twin engine on aft fuselage, wide-body fuselages, and fly-by-wire airplanes. At the program's conclusion, one lifetime of data is expected to be collected for each model type instrumented.

POC: Mr. Thomas DeFiore, AAR-433, FAA William J. Hughes Technical Center, Atlantic City International Airport, NJ 08405, (609) 485-5009.

9.3.4 Flight Loads Data Collection Program, Large Transport Airplanes
Mr. Thomas DeFiore
FAA William J. Hughes Technical Center

The Federal Aviation Administration has re-established a flight loads data collection program for large transport airplanes.

The FAA system is operational, and the data collection and analysis procedures have been established and verified by collecting and reporting on approximately 900 hours of operational data on a B-737 (DOT/FAA/AR-95/21, Flight Loads Data for a Boeing 737-400 in Commercial Operation, 1996). An additional 18,000 hours of B-737 data and 8000 hours of MD-82 data have been collected and are currently being reduced and analyzed. Another technical report summarizing the new data is expected later this year.

A number of initial results are already available. As an example, see Figure 8. At high altitude the gust exceedance is considerably less than that from the National Administration of Civil Aeronautics (NACA) reports, yet, conversely, at low altitudes the gust experience is considerably greater than previous NACA data.

Equally important is the merging of three FAA programs for on-board data monitoring sources. Researchers from the subject program and the Flight Operational Quality Assurance and Automated Performance Measuring System have been sharing data from their respective systems. See Figure 9. For the Flight Loads Program, we purchased

only 12 Optical Quick Access Recorders, yet are receiving data from 27 recorders with expectations of data from an additional 16 during the next fiscal year. Host airlines are gaining an interest in on-board data monitoring and are purchasing their own recorders and making these data available to the FAA for research.

Airframe manufactures strongly support this research effort and played a major role in defining the data reduction formats presented in the referenced FAA report. A second and yet more extensive set of statistical requirements has been jointly researched by the FAA and aircraft manufacturers.

As the program matures even further, additional recorders will be installed by the airlines in different type airplanes to develop a balanced database. The next installations are expected to be on B-767 airplanes.

POC: Mr. Thomas DeFiore, AAR-431, FAA William J. Hughes Technical Center, Atlantic City International Airport, NJ 08405, (609) 485-5009.

9.3.5 FAA Landing Parameter Survey Facility

Mr. Thomas DeFiore

FAA William J. Hughes Technical Center

The FAA William J. Hughes Technical Center established a permanent video landing parameter data collection facility at Atlantic City International Airport, New Jersey, to collect operational landing impact parameters year round under a wide variety of weather conditions. In addition to the regular commercial airplane arrivals, frequent U.S. Air Force KC-10s and cargo jets conduct touch-and-go training operations at the airport. Inclement weather data collected at this facility will supplement regular survey data from high activity airports which has been collected during the four prior 10- to 12-day surveys.

Using this facility, the FAA hosted a Boeing Flight Test Team consisting of an MD-90 airplane and 28 crew members, engineers, and flight test personnel for a research effort to compare FAA and Boeing sink speed measurements. This effort will correlate landing ground contact parameters obtained from the FAA-Navy Aircraft Approach and Landing Data Acquisition System (NAALDAS) with those from the Boeing, Douglas Products Division on-board flight test Internal Navigation System (INS). (See Figure 10.) Approximately 75 complete-stop landings were performed between April 13-17 of this year for measurement and analysis by the respective FAA and Boeing data acquisition systems. Ground contact information such as sink speed, approach velocity, pitch, roll, and yaw, obtained from prior and future NAALDAS surveys at high-activity commercial airports, are planned to be used to assess the validity of existing FAA certification criteria.

POC: Mr. Thomas DeFiore, AAR-433, FAA William J. Hughes Technical Center, Atlantic City International Airport, NJ 08405, (609) 485-5009.

9.3.6 Video Landing Parameter Survey at London City Airport, United Kingdom

Mr. Thomas DeFiore

FAA William J. Hughes Technical Center

Personnel from the Propulsion and Systems Section AAR-432 lead a joint research team, from the FAA William J. Hughes Technical Center and the Naval Air Warfare Center, Patuxent River, MD, to conduct a extensive video landing parameter survey at London City Airport (LCY), United Kingdom. Landings at both Runways 10 and 28 were video taped. This was the fourth of a series of surveys conducted by the FAA to more fully characterize the landing contact conditions of transport aircraft in routine operations. Prior surveys were conducted at JFK International, Runway 13L, Washington National, Runway 36, and Honolulu International, Runway 8L.

LCY is a relatively new, commuter only, airport in East London, UK, near the dock lands. LCY has a single east-west runway, 3800 feet long which requires aircraft to descend with a minimum 5.5 degree glide slope (3.0 degrees is typical). The data acquisition system was expanded to monitor both ends of the LCY runway, and six cameras were used to collect the landing video images. Approximately 80% of the total daily operations at LCY were recorded. A total of 430 landings, mostly BA-146's and FK-50's, were digitally video taped at LCY during the two week period from June 23 to July 4.

UK Civil Aviation Authority (CAA) and British Aerospace (BAe) researchers have indicated that the foremost missing element in their usage performance data is a precise characterization from the time the airplane is over the runway threshold to landing impact. Another important missing element is a description of the dispersion of the actual touchdown locations. The landing parameter data acquisition survey conducted on this 5.5 degree glide slope airport is expected to provide the CAA and BAE researchers with much of the landing ground contact data needed for new future regulations regarding steep approaches.

POC: Mr. Thomas DeFiore, AAR-431, FAA William J. Hughes Technical Center, Atlantic City International Airport, NJ 08405, (609) 485-5009.

9.3.7 Video Landing Parameter Survey, John F. Kennedy International Airport

Mr. Thomas DeFiore

FAA William J. Hughes Technical Center

The Federal Aviation Administration William J. Hughes Technical Center is conducting a series of video landing parameter surveys at high-capacity commercial airports to acquire a better understanding of typical contact conditions for a wide variety of aircraft and airports as they relate to current aircraft design criteria and practices.

The initial survey was conducted at John F. Kennedy (JFK) International Airport in June 1994. Four video cameras were temporarily installed along the north apron of Runway 13L. Video images of 614 transport (242 wide-body, 264 narrow body, and 108 commuter) aircraft were captured, analyzed, and the results presented in FAA Technical Report DOT/FAA/AR-96/125 Video Landing Parameter Survey - John F. Kennedy International Airport, published this year. Landing parameters presented include sink rate; approach speed; touchdown pitch, roll, and yaw angles and rates; off-center distance; and the landing distance from the runway threshold. Wind and weather conditions were also recorded and the landing weights were available for most operations. Since this research is concerned with overall statistical usage information only, all data were processed and presented without reference to the airline or flight number.

The video landing data acquisition system has proved to be a practical, cost-effective technique for collecting large quantities of typical landing parameter data at major commercial airports.

While the initial indications are that the heavy wide-body aircraft (B-747, MD-11, DC-10, L-1011) land with a higher sink rate than other jet transports, the rather limited number of these large jets suggest that additional data on these aircraft need to be collected before any conclusions concerning their landing performance can be made. See Figure 11.

The commuter data collected during this survey may not reflect typical operations for this category aircraft since these aircraft landed on a 10,000-foot runway with heavy jets in the landing pattern.

POC: Mr. Thomas DeFiore, AAR-431, FAA William J. Hughes Technical Center, Atlantic City International Airport, NJ 08405, (609) 485-5009.

9.3.8 Characterizing Aeroacoustic/Combustion Loads for Aging Aircraft Sustainment

Mr. Clare Paul

Air Force Research Laboratory

The Air Force needs to be able to predict the dynamic loads associated with aging aircraft problems. Currently these loads cannot be predicted for all the various dynamic loads associated with aging aircraft. The goal of this work is to characterize these loads and format them on a CD-ROM for easy access. When completed the aging aircraft community will be able to readily and reliably predict the loads contributing to fatigue cracking of aircraft structure.

The objectives of this effort are to formalize and compile an extensive aircraft acoustic loads data-base, develop an OASPL acoustic loads prediction methodology, develop modal characteristics for frequency and amplitude, and conduct a sensitivity analysis of structural response to acoustic spectra.

The approach will consist of developing a database of all available loads data for attached and separated flows, cavities, engine inlet/combustion /nozzle, and exhaust plume(screech). The data base will be then be enhanced by

utilizing a novel prediction technique, which was developed by the principal investigator and is based on first principles. Sensitivity analysis of structural response to different acoustic spectra will be conducted. The results will then be formatted into a CD-ROM for application to aging aircraft loads prediction.

9.4. FATIGUE AND FATIGUE CRACK GROWTH

9.4.1 Determining the Initial Quality State for Materials

Craig L. Brooks, Scott Prost-Domasky, and Kyle Honeycutt
Analytical Processes / Engineered Solutions

This project developed a key element in a holistic approach to fatigue life computations for metallic structures. A holistic life assessment model provides the range of probable fatigue lives of the structure that accounts for all phases of cracking due to operation and environment from the as-manufactured condition to final unstable fracture. The effort was conducted for the USAF Corrosion Program Office to support the development of analytical techniques to predict the impact of corrosion interacting with fatigue on service life capability. The methods developed provide major improvements in Durability and Damage Tolerance predictions and thus provide opportunity to improve the economics of maintaining and continuing service of aircraft.

The key element of the process is the method of computing the Initial Quality condition or state of the bulk material. The computed distribution of initial crack sizes, similar to equivalent initial flaw computations but under disciplined criteria and requirements, in fracture mechanics scenarios accurately represents the statistical variation of life observed in coupon test from time zero for a wide range of variables. This technique thus captures the inherent scatter observed in fatigue testing while providing a physical characteristic that can be measured and understood. This approach provides a technique to establish the initial analysis conditions and guidelines that will enable predictions and assessments of:

- the on-set of widespread fatigue damage, and multiple-site damage
- comparison of life capability of aircraft designed by either USAF or USN criteria
- design features to optimize for Joint Service Life Design capabilities
- effects of corrosion interaction with fatigue
- damage tolerance assessments with age degradation influences
- quantitative measure for material discriminator and selection

Figure 12 schematically shows this initial quality state concept, the results for 2024-T3 and 7075-T6, and the benefits to life assessment methods. Figure 13 illustrates how closely the results compare to those found by expensive full scale fatigue test, scanning electron microscope, complex spectrum element test, and measured defects. This concept utilizes the benefits and strengths from two distinctly different life prediction techniques “initiation”(aka ‘nucleation’) and “growth” to understand the shortcomings of each and result in an improved holistic prediction process. The improved process provides improved estimates for maintenance and service life decisions, and insights to solving many of the Aging Aircraft problems requiring prediction methods.

Reference:

1. C. L. Brooks, S. Prost-Domasky, and K. Honeycutt, “Determining the Initial Quality State of Materials”, Proceedings of the 1998 USAF Aircraft Structural Integrity Program Conference, San Antonio, Texas, December 1998 (also available from www.APESolutions.com under "Links")

9.4.2 Equivalent Initial Flaw Size Test Program

Dr. Paul Tan

FAA William J. Hughes Technical Center

As a partner in a FAA contract with the Boeing Commercial Airplane Group, the United States Air Force (USAF) at Wright Patterson Air Force Base has conducted tests of 16 spliced panels to determine the equivalent initial flaw size distribution of cracks emanating from rivet holes. These experimental data will be used to verify small crack growth methodology developed by the FAA and NASA as part of an integrated methodology to predict the point of widespread fatigue damage (WFD).

Four different common types of splice joints were considered. A total of 16 specimens were fabricated, 4 of each splice type. The specimens were 22 inches wide and 56 inches long. The splices represent three types of fuselage longitudinal splices and one type of fuselage circumferential splice, as shown in Figure 14.

The three longitudinal splice types were (a) a lap joint with two finger doublers and a longeron, (b) a longitudinal lap joint without doublers but with a longeron, and (c) a longitudinal butt joint with a splice plate, a doubler, and a longeron. The circumferential splice type was a circumferential butt joint (d) with a butt splice plate and a finger doubler. The skins were made of 2024-T3 aluminum alloy, the longerons were made of 7075-T6 aluminum alloy, the doublers and splice plates were made of either 2024 or 7075 aluminum alloy.

The edges of the splices were bonded by FM-73 material together with the edge blocks to prevent premature edge crack during the tests due to Poisson's ratio effects. All specimens had eight strain gages, located back to back in pairs, to determine if uniform load was induced in the splice joints. One specimen of each splice type had an additional 16 strain gages located in the tangential line of the critical rivet row to measure the secondary bending due to the unsymmetrical geometry.

Pretest analyses were conducted to determine the internal loads, the stress concentration (K_t) of the critical rivets, the fatigue lives, and the crack growth live estimations in the various types of splice joints. The internal loads were determined by finite element analysis using NASTRAN and FRANC2D/L codes, including the fastener flexibility. The K_t and fatigue lives were determined using S-N curves and accumulative damage approach. The crack growth lives were determined by FASTRAN-II predictions with small crack growth rate data.

During the fatigue tests, periodic inspections were conducted by a rotating self-nulling eddy-current probe developed at the NASA Langley Research Center. These nondestructive inspection (NDI) findings were documented.

The tests and analyses were correlated using the NDI data and SEM data. The closure-based crack growth prediction model, FASTRAN-II, was used for the analyses. The parameters considered include the test specimen geometry, the test load history, magnitude of applied far-field stress, bending stress factor, bypass stress factor, neat-fit pin factor, and the effects of adjacent holes with cracks. The effects of the countersunk hole and the interference between the rivets and the sheet are also being investigated. A correlation factor, as a function of crack length normalized to hole radius, was calculated for one specimen to obtain good agreement between analytical prediction and the experimental results for that specimen. This factor was subsequently used as the correlation for all other specimens. This factor provided good correlation for larger crack sizes, but poor correlation for small crack sizes. Further analysis and experimental correlation will be performed upon crack growth data as it becomes available.

POC: Dr. Paul Tan, AAR-431, FAA William J. Hughes Technical Center, Atlantic City International Airport, NJ 08405, (609) 485-6665.

9.4.3 Equivalent Initial Flaw Size Using Small Crack Data

R. P. Bell, S. Shah, And R. E. Alford

WR-ALC, Robins AFB, Georgia

Aircraft fleets are approaching their design service life goals and are expected to be operated past those goals. This requires that maintenance actions be developed that will allow the fleet to operate safely.

The development of maintenance actions and evaluation of Fail Safety requires an equivalent initial flaw size distribution and MSD (Multi Site Damage) consideration. Both of these require that small crack growth rate (da/dN) be known. However, most of the available crack growth rate data are based on large cracks.

The results of the research performed by Dr. J. C. Newman, Jr. and his associates at NASA Langley Research Center (LaRC) to investigate the Small-Crack effects in High-Strength Aluminum Alloys were reviewed. (Ref. 1). The results of this research allowed Lockheed Martin Aeronautical Systems (LMAS) to extend the large crack growth rate data in to small crack region. This in turn was used to derive an equivalent initial flaw size distribution for cracks occurring on C-141 wing panel weep holes. The detail of C-141 wing weep holes is shown in Figure 15. The equivalent initial flaw size distribution for weep holes based on cracks detected during full-scale fatigue test,

tear down inspection and field inspections is shown in Figure 16. This distribution compares well with the microstructure and fractographic examinations performed on the weep holes.

Reference:

1. Newman, J. C. Jr., Wu, X. R., Venneri, S. L and Li, C. G., (1994), Small-Crack Effects In High-Strength Aluminum Alloys, NASA Reference Publication 1309, NASA Langley Research Center, Hampton, Virginia, USA.

9.4.4 Boundary Correction Factors for Elliptical Surface Cracks at Countersunk Rivet Holes

Dr. John Bakuckas

FAA William J. Hughes Technical Center

To predict crack growth and residual strengths of riveted joints, accurate stress and fracture analyses of corner and surface cracks at a rivet hole are needed. Stress-intensity factor (SIF) solutions of cracks emanating from countersunk rivet holes under tension, bending, and wedge load conditions were calculated. The crack size, shape, and location were selected to represent typical experimental observations. The crack shape was defined as the ratio of the elliptical crack length in the thickness direction (a) to that in the width direction (c) and was varied from $a/c = 0.5, 0.75, \text{ and } 1$. The ratio of the length of the straight-shank portion of the hole to the plate thickness (h/t) was varied from 0.05, 0.25, and 0.50. Cracks at five locations were analyzed: (1) corner cracks passing through the middle of straight shank portion of the rivet hole, (2) corner cracks passing through inner knee of the rivet hole, (3) breakthrough cracks passing through the middle of the inclined surface of the rivet hole, (4) breakthrough cracks passing through the upper knee of the rivet hole, and (5) through-the-thickness cracks passing through the inner and outer surfaces of the plate.

A global-intermediate-local modeling technique was used to generate the stress-intensity factor solutions. The effect of the shape of the crack, the location of the crack, the height of the straight-shank portion of the countersunk rivet hole, and applied loading were determined. The boundary correction factor was determined along the crack front in terms of the physical angle measured from the inner surface of the plate to a given point on the crack front. In general, as shown in Figure 17, the values of boundary correction factors increased moving along the crack front from the inner surface of the plate towards the hole boundary (i.e., as the value of θ increased). For points on the crack front near the inner surface of the plate ($\theta=0$), the value of the boundary correction factor increased as a/c increased. When moving along the crack front from the inner surface to the hole boundary, boundary correction factor solutions for the three values of a/c merged.

For the five crack locations considered (See Figure 18), the inner surface of the plate has less of an influence on the boundary correction factor than the hole and outer surface boundaries. The values of the boundary correction factor were highest for the crack fronts closest to the hole boundary.

POC: Dr. John Bakuckas, AAR-431, FAA William J. Hughes Technical Center, Atlantic City International Airport, NJ 08405, (609) 485-4784.

9.4.5 Comparison of Boundary Correction Factor Solutions for Two Symmetric Cracks in a Straight-Shank Hole

Dr. John Bakuckas

FAA William J. Hughes Technical Center

Accurate stress-intensity factor (SIF) solutions are required to conduct thorough damage tolerance analyses of structures containing cracks. Exact closed form SIF solutions for cracks in three-dimensional solids are often lacking for complex configurations; therefore, approximate solutions must be used. In this study, a three-level global-intermediate-local (GIL) hierarchical approach was developed using finite element method (FEM) for fracture mechanics analysis of cracks in three-dimensional solids. Verification studies of the GIL approach were conducted using a problem consisting of two symmetric cracks emanating from a straight-shank hole under remote tension. First, convergence studies were done to determine the level of mesh refinement needed for the global, intermediate, and local models. Next, the use of conventional and singularity elements in the local model was assessed. The use of conventional elements was found to be sufficient to obtain accurate solutions. The solution obtained from the GIL approach was verified and compared to the solutions obtained by several investigators using

a variety of methods including the equivalent domain integral method (DIM), semi-empirical SIF equations, the finite element alternating method (FEAM), the boundary element method (BEM) in conjunction with the crack opening displacement approach (FRANC3D) and a direct approach using special crack-tip elements (FADD3D), and the Weight Function Method (WFM).

The results of the various methods are shown in Figure 19 as the boundary correction factors along the crack front in terms of the parametric angle, ϕ . Excellent agreement was obtained among the methods. All solutions fell within a band of $\pm 3\%$ about the average solution. (See Figure 20.)

POC: Dr. John Bakuckas, AAR-431, FAA William J. Hughes Technical Center, Atlantic City International Airport, NJ 08405, (609) 485-4784.

9.4.6 Fatigue Crack Growth Under Variable-Amplitude Loading In A Titanium Alloy

E. P. Phillips and J. C. Newman, Jr.

NASA Langley Research Center

The objective of this work was to compare the fatigue crack growth lives measured under repeated spike overload and underload sequences for thin-sheet Ti-6Al-2Sn-2Zr-2Mo-2Cr (Ti-62222) titanium alloy with those calculated from the crack-closure model, FASTRAN. Phillips [1] conducted repeated spike overload and underload tests on middle-crack tension specimens made of 1.65-mm-thick titanium alloy. All specimens were fatigue precracked under constant-amplitude loading ($S_{CA} = 138$ MPa at $R = 0.1$) until a 3.8 mm crack was produced. Then a repeated spike overload/underload sequence was applied every 2500 cycles until failure. Overload ratios (S_{OL}/S_{CA}) ranged from 1.5 to 3.5. Some tests with an overload ratio of 2.5 also had an underload applied immediately following each overload. The ratio of the minimum load of the underload cycle to the precrack maximum fatigue load (S_{UL}/S_{CA}) ranged from -1 to -3. The number of cycles required to grow the crack from the initial size to failure N_f was recorded. Some specimens were fatigue precracked at a low stress and then fractured to determine the fracture toughness.

The repeated spike overload tests indicated that the cyclic load history influenced the fracture behavior of the specimens. Figure 21 shows the tests that were fatigue pre-cracked at low loads and then pulled to failure (open symbols). The solid symbols show results from the repeated spike overload tests using the final crack length and the overload stress to compute the elastic (apparent) fracture toughness, K_{Ie} . These results show that the toughness is elevated with higher cyclic loads. The curves are from the Two-Parameter Fracture Criterion (TPFC) [2] fitted to the open symbol data. The two-parameters for the room temperature results (solid curve) are $K_F = 238$ MPa \sqrt{m} and $m = 0.8$; and the elevated temperature results (dashed curve) are $K_F = 330$ MPa \sqrt{m} and $m = 0.8$. The TPFC is used in the FASTRAN code to terminate the fatigue crack growth analysis. The FASTRAN code does not account for the influence of cyclic load history on toughness.

Using constant-amplitude crack-growth rate data on the titanium alloy and an estimate for the constraint-loss regime, the baseline ΔK_{eff} - rate relation was established. (In the closure model, the constraint factor is denoted as α , where plane stress is $\alpha = 1$ and plane strain is $\alpha = 3$.) The fatigue crack-growth lives, N_f , for various repeated spike overload magnitudes are shown in Figure 22 as symbols. The longest fatigue life occurred at an S_{OL}/S_{CA} ratio of 2.5. The curves show the predicted lives for room and elevated temperature using the respective baseline relations with the constraint-loss option (low rates are plane strain and high rates are plane stress). The predicted lives were generally within a factor of two of the test data.

References:

1. Phillips, E. P., "Periodic Overload and Transport Spectrum Fatigue Crack Growth Tests of Ti62222STA and Al2024T3 Sheet," NASA/TM-1999-208995, 1999.
2. Newman, J. C., Jr., "Fracture Analysis of Various Cracked Configurations in Sheet and Plate Materials," ASTM STP 605, 1976, pp. 104-123.

9.4.7 Part Through Crack Behavior in Aluminum Alloys under Spectrum Loading

Suzanne A. Masterson

Boeing

Inspection intervals for aircraft depend on the calculated growth rate of part through cracks under spectrum loading, so accuracy in predicting growth for these cracks is essential. Boeing conducted a test program in collaboration with Southwest Research Institute of San Antonio, Texas, to verify an analytical model for predicting crack growth of short cracks (less than through-thickness). The model uses the crack closure method to simulate the load history effect observed for short cracks growing under spectrum loading.

Two specimen geometries were used, flat plate with a crack at a hole and flat plate with a crack at one edge. Some crack-at-a-hole specimens were tested with open holes and some with holes filled with close tolerance bolts. Specimens were notched using electro-discharge machining, as shown in Figure 23. The specimens were then fatigue cycled using one of six flight spectra. The spectra tested represented wing upper and lower surfaces and fuselage crown loading. Southwest Research Institute, Mechanical and Materials Engineering Division, used specimens fabricated from three 2xxx-series and three 7xxx-series aluminum alloys, including plate and extrusion forms, and the Boeing Structural Materials Laboratory repeated tests on one material from each series. An example of the test results from the two laboratories and the corresponding prediction is shown in Figure 24.

Constant amplitude and K gradient tests using compact tension specimens were also conducted to characterize crack growth properties for each lot of material used in the spectrum tests.

Analytical predictions showed good correlation with test results for tension-dominated spectra for all materials tested. The model gave unconservative results for spectra that are highly compression dominated. Cracks growing under these spectra tended to develop multiple initiation sites through the thickness, accelerating the crack growth.

9.4.8 Experimental Verification of T^* Theory

Dr. Paul Tan

FAA William J. Hughes Technical Center

The FAA Center of Excellence for Computational Modeling of Aircraft Structures, Georgia Institute of Technology (GIT), has developed an elastic-plastic crack growth criteria which is based on strain energy at the crack tip, T^* . This criteria has been successfully used to predict crack growth in stiffened and unstiffened flat panels. It has been proposed that T^* is a material property and thus the objective of this work was to experimentally measure this quantity.

The specimens used consisted of fatigue precracked, thin, single-edged notched (SEN) and center notched (CN), 2024-T3 aluminum alloy specimens. The orthogonal displacement components surrounding the crack tip was measured by Moiré interferometry using a cross-diffraction grating of 40 lines/mm prior to and during stable crack growth. T^* software, developed by the FAA Center of Excellence for Computational Modeling of Aircraft Structures was modified to evaluate T^*_ϵ integral using Moiré fringe data along a given part rectangular contour which moved with the moving crack tip. The T^*_ϵ integral and the crack opening angle (CTOA) were determined during successive increments of stable crack growth. Simultaneously, the SEN specimens were analyzed by GIT and the CN specimens were analyzed at the University of Washington (UW) using the ABAQUS finite element (FE) code. These results were then compared with the experimentally determined T^*_ϵ .

Figure 25 shows the results of the experimentally and numerically determined T^*_ϵ in the region closest to the crack tip where distinct Moiré fringes are observed.

Concurrent with these experimental and numerical efforts were efforts to extend the T^*_ϵ theory to mixed modes I and II loading as well as to the growth of a curved crack.

POC: Dr. Paul Tan, AAR-431, FAA William J. Hughes Technical Center, Atlantic City International Airport, NJ 08405, (609) 485-6665.

9.4.9 Fracture Analyses Of Surface Cracks In Brittle Materials

J.C. Newman, Jr.

NASA Langley Research Center and

W.G. Reuter.

Idaho National Engineering Laboratory

Prediction of failure loads for surface-cracked specimens under tension and bending loads have eluded the technical community for many years. The present work [1] concentrated on elastic-plastic finite-element stress analyses of the surface crack in a plate subjected to tension and bending loads. The variations of a hyper-local constraint factor (α_h), based on the average normal stress in the plastic zone along the surface-crack front, was studied to identify the critical fracture location. Linear-elastic fracture mechanics was applied to fracture of surface-crack specimens made of a high-strength D6AC steel. Two methods to characterize fracture: the K^2 -integral around the crack front and K at a critical fracture location (ϕ_c). These two methods were used to evaluate the fracture toughness at both crack-initiation and maximum failure loads. Only the results for crack initiation will be considered here.

An International Cooperative Test Program on Surface-Crack Specimens [2] was conducted in the mid-1990's to investigate a wide range of surface-crack configurations made of a brittle material, D6AC steel, tested under remote tension and bending. The nominal range of crack-configuration parameters tested were: $a/t = 0.25, 0.45, 0.65$ and 0.85 , and $a/c = 0.2, 0.4$ and 1.0 with $W = 50.8$ or 101.6 mm and a thickness (t) of 6.35 mm.

A combination of the hyper-local constraint factor, $\alpha_h(\phi)$, and the stress-intensity factor, $K(\phi)$, as functions of the parametric angle, ϕ , were used to determine the critical fracture location. The objective was to develop a rational to predict the critical fracture location ϕ_c . The stress-intensity boundary-correction factor, F_b , and the constraint factor, α_h , variation as a function of ϕ for a surface crack under remote bending is shown in Figure 26. The maximum F_b (or K) occurs at the free surface but here the constraint factor is low (nearly plane stress). In contrast, at the maximum depth location where the constraint factor is high (nearly plane strain), the F_b (or K) value is very low. Thus, fracture should initiate in the interior but not at the maximum depth location and, probably, not at the free surface. From the fracture test, the crack-initiation region was measured from 6 to 17 degrees [2], as denoted by "test range". Using a simple product of $F_b\alpha_h$ (or $K\alpha_h$), as shown by the dash-dot curve, the peak value occurred at 14.4 degrees. This value fell within the experimental test range. The rational is that the region where the "stress-intensity factor and constraint" maximizes would be the most likely location for fracture to initiate.

The stress-intensity and constraint-factor variations were then used to determine the critical fracture location ϕ_c and the critical stress-intensity factor at that location. This approach was applied to the fracture tests conducted by the NASA Ames Research Center (ARC) and Idaho National Engineering Laboratory (INEL). The results of fracture tests at the crack-initiation loads using K_ϕ at the critical location (ϕ_c) produced the correlation shown in Figure 27. Here the average of the bending specimens was extremely close to the average of the tension tests. The average value from all tests was $(K_\phi)_{Ic} = 61.5 \text{ MPa}\cdot\text{m}^{1/2}$ with 93% of the data falling with $\pm 20\%$. The toughness from the surface-crack specimens was somewhat higher than the K_{Ic} value ($53 \text{ MPa}\cdot\text{m}^{1/2}$) from through-crack bend specimens.

References:

1. Newman, J. C., Jr., W. G. Reuter, and C. R. Aveline, Jr., "Stress and Fracture Analyses of Semi-Elliptical Surface Cracks," Presented at the 30th National Symposium on Fatigue and Fracture Mechanics, St. Louis, MO, June 1998.
2. Reuter, W. G., Elfer, N., Hull, D., Newman, J. C., Jr., Munz, D., and Panontin, T. L., "Fracture Toughness Results and Preliminary Analysis for International Cooperative Test Program on Specimens Containing Surface Cracks," ASTM STP 1321, J. H. Underwood, B. D. Macdonald and M. R. Mitchell, Eds., 1997, pp. 146-166.

9.4.10 Modeling K_{max} Effects On Fatigue Crack-Growth Rates

R. S. Piascik and J. C. Newman, Jr.
NASA Langley Research Center

The use of constant- K_{max} test procedures have greatly increased. This test procedure produces, closure-free, low crack-growth rate data much more rapidly than the constant-stress-ratio (R) load-reduction procedure without the questionable load-interaction, closure-affected results at low R. But recently, using K_{max} testing, researchers have generated data at high R that produce K_{max} -affected data. Testing at high R, in the absence of crack closure, are producing different crack-growth rates at the same applied ΔK (or ΔK_{eff}) values. For 2024-T3 aluminum alloy, these test results show an increase in micro-void growth as the crack grows at higher K_{max} values [1]. Research work at NASA Langley [1,2] has been initiated to explain and to develop equations to correlate data at constant-R and constant- K_{max} testing. Fatigue crack-growth rate data plotted against ΔK or ΔK_{eff} , commonly show a “sigmoidal” shape as a crack grows to fracture. To account for this shape, the Elber-Paris power relation was modified by

$$dc/dN = C (\Delta K_{eff})^n / H \quad (1)$$

where $H = 1 - (K_{max}/K_c)^q$. The function H accounts for the rapid crack-growth rates approaching fracture [2]. The parameter K_c is the cyclic fracture toughness. The cyclic fracture toughness is generally higher than the static toughness for cracks grown at a low load and then pulled to failure. This is caused by the shielding effect of the plastic wake. The cyclic fracture toughness, like the elastic fracture toughness, is a function of crack length, specimen width, and specimen type.

Riddell and Piascik [1] tested small extended compact tension (ECT) specimens ($B = 2.3$ mm and $W = 76$ mm) under constant- ΔK values for a very wide range in stress ratios. Some typical results at 5.5 MPa \sqrt{m} are shown in Figure 28 as symbols. The upper axis shows the ratio of K_{max}/K_c for these test data ($K_c = 50$ MPa \sqrt{m}). The solid curve is the predict results from equation (1) with a power $q = 2$. The power of $q = 2$ had been previously selected for aluminum alloys. The dotted lines show a ± 40 percent scatter-band about the solid curve. The dashed curve shows the calculated results using only ΔK_{eff} without the K_{max} term.

Dubensky [3] tested middle-crack tension specimens ($W = 305$ mm) over a wide range in stress ratios ($R = 0$ to 0.7) at extremely high applied stress levels ($0.6 \sigma_{ys}$ to σ_{ys}). Only some of the data are shown in Figure 29 as ΔK plotted against rate (symbols). Open and solid symbols are high and low R data, respectively. The dotted curve is the ΔK_{eff} baseline curve. The solid and dashed curves are the predicted ΔK against rate results from FASTRAN [2] for specimens tested at low and high R. These results show that K_{max} or stress-level effects are present even at low stress ratios, if the tests are conducted at high stress levels. Note that these tests were cycled to failure and that the cyclic fracture toughness K_c (chosen to fit the asymptotes) was 100 MPa \sqrt{m} .

These results show that equation (1) can account for some K_{max} effects at low and high ΔK levels. But how cyclic crack growth and static fracture modes interact needs further study.

References:

1. Riddell, W. and Piascik, R. S., “Stress Ratio Effects on Crack Opening Loads and Crack Growth Rates in Aluminum Alloy 2024,” *Fatigue and Fracture Mechanics: 29 Vol.*, ASTM STP 1331, T. L. Panontin and S. D. Sheppard, Eds., 1999, pp. 407-425.
2. Newman, J. C., Jr., “An Evaluation of the Plasticity-Induced Crack-Closure Concept and Measurement Methods,” NASA TM-208430, August 1998.
3. Dubensky, R. G., “Fatigue Crack Propagation in 2024-T3 and 7075-T6 Aluminum Alloys at High Stress,” NASA CR-1732, 1971.

9.4.11 The Manson-Coffin Relation for Determining Cycles Until Failure
Dr. Milton J. Torres and Dr. Kuang-His Wu
Florida International University

$$\frac{\Delta \varepsilon}{2} = \frac{\sigma_f'}{E} (2N_f)^b + \varepsilon_f' (2N_f)^c$$

$\Delta \varepsilon$	input	Strain Range
$\frac{\sigma_f'}{E}$	=0.008632	One Reversal Intercept of Elastic Strain vs Life Line
ε_f'	=0.18	One Reversal Intercept of Plastic Strain vs Life Line
b	=-0.071	Slope of Elastic Strain Amplitude vs Fatigue Life
c	=-0.645	Slope of Plastic Strain Amplitude vs fatigue Life
N_f	output	Cycles Until Failure

Fatigue Life Extension

Foam Thickness (inches)	0	1.25	2	2.75	3.50
Microstrain @ 6.5 psi Cabin Pressure	916.6	883.4	847.4	819.5	799.1
% Reduction Strain		3.6%	7.6%	10.6%	12.8%
Cycles until Failure	4.53E+17	7.62E+17	1.37E+18	2.19E+18	3.13E+18
Increase Fatigue Life N Fold	1.0	1.7	3.0	4.8	6.9
Microstrain @ 7.5 psi Cabin Pressure	1041.8	1008.0	971.0	941.4	919.3
% Reduction Strain		3.2%	6.8%	9.6%	11.8%
Cycles until Failure	7.47E+16	1.19E+17	2.01E+17	3.11E+17	4.35E+17
Increase Fatigue Life N Fold	1.0	1.6	2.7	4.2	5.8
Microstrain @ 8.5 psi Cabin Pressure	1165.9	1131.6	1093.7	1062.7	1039.1
% Reduction Strain		2.9%	6.2%	8.9%	10.9%
Cycles until Failure	1.53E+16	2.33E+16	3.76E+16	5.64E+16	7.74E+16
Increase Fatigue Life N Fold	1.0	1.5	2.5	3.7	5.1

9.4.12 Fatigue Crack Growth Lives Under Repeated Spike Overloads And Underloads
D. S. Dawicke and J. C. Newman, Jr.
NASA Langley Research Center

The objective of this work was to compare the fatigue crack growth lives measured under repeated spike overload and underload sequences for thin-sheet 2024-T3 aluminum alloy with those calculated from the crack-closure model, FASTRAN. Dawicke [1] conducted repeated spike overload and underload tests on middle-crack tension specimens made of the 2.3 mm-thick aluminum alloy. All specimens were fatigue precracked under constant-amplitude loading ($S_{CA} = 70$ MPa at $R = 0.02$) until a 12.7 mm crack was produced. Then a repeated spike overload/underload sequence was applied every 2500 cycles until failure. Overload ratios (S_{OL}/S_{CA}) ranged from 1.125 to 4, and underload ratios (S_{UL}/S_{CA}) ranged from 0 to -3. The number of cycles required to grow the crack from the initial size to failure N_f was recorded. Using constant-amplitude crack-growth rate data on the aluminum alloy and an estimate for the constraint-loss regime, the baseline ΔK_{eff} -rate relation was established. (In the closure model, the constraint factor is denoted as α , where plane stress is $\alpha = 1$ and plane strain is $\alpha = 3$.) Predictions of fatigue crack growth lives for all of the repeated overload and overload/underload tests were made, see Figure 31.

The fatigue crack-growth lives, N_f , for various repeated spike overload magnitudes are shown in Figure 30 as symbols. The longest fatigue life occurred at an S_{OL}/S_{CA} ratio of 2. When the overload ratio reached 3.75, the specimen failed on the first application of the overload. The solid curve shows the predicted lives using the baseline relation with the constraint-loss option (low rates are plane strain and high rates are plane stress). The predicted lives were generally within a factor of two of the test data. Comparing the fatigue surfaces for the constant-amplitude case and the small overload ($S_{OL}/S_{CA} = 1.125$) case, it became obvious that the small overload caused enough crack surface roughness to produce fretting-product-debris on the surface. The increased closure due to the debris was not accounted for in the analysis. Thus, the model under predicted the fatigue lives for the small to moderate overloads. To illustrate why the constraint-loss regime is needed, predicted fatigue lives under a constant constraint factor of 2 (nearly plane strain) are shown by the dashed curve. Here the predicted results can be as much as an order of magnitude in error.

The crack-closure model matched the experimental test data quite well and demonstrated why it is importance to include the influence of the constraint-loss regime on crack growth behavior for thin-sheet alloys.

References:

1. Dawicke, D. S., "Overload and Underload Effects on Fatigue Crack Growth Behavior of 2024-T3 Aluminum Alloy," NASA CR-201668, 1997.
2. Newman, J. C., Jr., "Prediction of Crack Growth under Variable-Amplitude Loading in Thin-Sheet 2024-T3 Aluminum Alloys," Engineering Against Fatigue, University of Sheffield, March 17-21, 1997.

9.4.13 Assessments of Low Cycle Fatigue of Powder Metallurgy Disk Superalloy U720

Tim Gabb, Jack Telesman, Pete Bonacuse, Pete Kantzos, Joe Sweeney
NASA Glenn Research Center

The fatigue lives of modern powder metallurgy disk alloys can be influenced by variabilities in alloy microstructure and mechanical properties. These properties can be dependent on parameters within any of the various steps of materials/component processing: during powder atomization, consolidation, extrusion, forging, heat treatment, and machining. It is important to understand the relationships between the statistical variations in life and these factors, as well as life variations due to the fatigue loading conditions. The objective of this study was to evaluate the fatigue life response of a nickel-base disk superalloy U720 produced using powder metallurgy processing. Strain-controlled fatigue tests were performed at 538°C (1000°F) using multiple tests at limited, carefully selected sets of test conditions. Analyses were performed to assess variations of microstructure, mechanical properties, and LCF failure initiation sites as functions of disk processing variables and different test conditions. Statistical evaluations were applied to compare fatigue life frequency distributions and minimum life estimates using data from multiple tests at unique test conditions and pooled data from different test conditions.

Significant variations in life were observed as functions of the disk processing variables evaluated. Furthermore, the failure initiation sites for tests performed at a strain ratio $R_\epsilon = \epsilon_{\max}/\epsilon_{\min}$ of 0 were different from those in tests at a strain ratio of -1 (Figure 123). However, the lives of all specimens could still be combined and statistically evaluated together. Evaluations indicated the natural logarithm of life could be modeled as normally distributed. Mean and minimum life estimates from a curve generated with the combined data of various strain ranges and strain ratios compared well to estimates generated with multiple tests at fixed strain conditions.

9.4.14 Residual Strength Analysis Methodology

D. S. Dawicke and J. C. Newman, Jr
NASA Langley Research Center

The NASA Aging Aircraft Programs have developed a residual strength prediction methodology for aircraft fuselage structures. This methodology has been verified for structures ranging from laboratory coupons up to full-scale structural components [1-4]. This methodology uses the critical crack-tip-opening-angle (CTOA) fracture criterion to characterize the fracture process and a geometrically and material nonlinear finite-element shell code to perform the structural analyses.

The CTOA fracture criterion assumes that stable crack growth will occur when the angle made by the upper crack surface, crack tip, and the lower crack surface reaches a critical value. Evaluation of the CTOA fracture criterion requires an elastic-plastic finite-element analysis. The critical CTOA value is determined by simulating the behavior of a small laboratory coupon specimen to obtain the angle that best describes the observed experimental behavior. This critical CTOA value is then used to predict the behavior of other, more complex and larger structures.

The critical CTOA value appears to be independent of specimen width and crack length. However, it is a function of material thickness and local three-dimensional constraint. Similar to the fracture toughness (K_{IC}) of a material, the critical CTOA value changes with material thickness, and generally decreases in value with increasing thickness. The influence of local three-dimensional constraint is a result of the fracture process that causes the local stresses to be neither plane stress nor plane strain condition, but something in between. This local constraint requires either a full three-dimensional finite-element analysis or a two-dimensional analysis with an approximation of the three-dimensional constraint. One such approximation, the "plane strain core" which uses plane-stress conditions everywhere except for a strip along the crack path where plane strain is assumed. The height of the strip (dimension perpendicular to the crack path) determines whether the approximation is closer to plane stress or plane strain behavior and generally increases with increasing thickness. Current research has evaluated the fracture behavior of 2024-T3 aluminum alloys with thickness of 0.04 to 0.09 inches. The critical CTOA and plane-strain-core height, as shown in Figure 32, were determined from small laboratory specimens. Using these parameters, the CTOA fracture criterion was used to predict the behavior of middle crack tension specimens up to 40 inches wide, flat panels with riveted stiffeners, and multiple-site damage cracking, 18-inch-diameter pressurized cylinders, and full scale curved stiffened panels subjected to internal pressure and combined loads.

References:

1. Dawicke, D. S. and Newman, J. C., Jr., "Residual Strength Predictions for Multiple Site Damage Cracking Using a Three-Dimensional Finite Element Analysis and a CTOA Criterion," *Fatigue and Fracture Mechanics: 29th Volume*, ASTM STP 1332, T. L. Panontin and S. D. Sheppard, Eds., 1998.
 2. Dawicke, D. S., Gullerud, A. S., Dodds, R. H., Jr., and Hampton, R. W., "Residual Strength Predictions with Crack Buckling," *Second Joint NASA/FAA/DoD Conference on Aging Aircraft*, Williamsburg, VA, 1998.
 3. Starnes, J. H., Jr. and Rose, C. A., "Stable Tearing and Buckling Responses of Unstiffened Aluminum Shells with Long Cracks," *Second Joint NASA/FAA/DoD Conference on Aging Aircraft*, Williamsburg, VA, 1998.
- Young, R. D., Rouse, M., Ambur, D. R., and Starnes, J. H., Jr., "Residual Strength Pressure Tests and Nonlinear Analyses of Stringer and Frame Stiffened Aluminum Fuselage Panels with Longitudinal Cracks", *Second Joint NASA/FAA/DoD Conference on Aging Aircraft*, Williamsburg, VA, 1998.

9.4.15 Analyses of Buckling and Stable Tearing in Thin-Sheet Materials

B. R. Seshadri and J.C. Newman, Jr.

NASA Langley Research Center

This study was conducted to analyze flat panels with cracks that fail with severe out-of-plane displacements (buckling) using STAGS (STRUCTURAL Analysis of General Shells) code [1] and the critical crack-tip-opening angle (CTOA) fracture criterion. The critical CTOA was determined from small laboratory coupons that were restrained against buckling. STAGS and the critical CTOA were then used to predict load-crack-extension and residual strength of restrained and unrestrained panels. (Note that these results were generated before the plane-strain core option was incorporated into the STAGS shell code.)

Comparisons between STAGS analyses and experimental measurements of applied stress against crack extension on middle-crack tension M(T) specimens (restrained and unrestrained from buckling) are shown in Figure 33. The analyses predicted the influence of buckling on the tearing behavior quite well. Parameters like crack-length-to-width ratio, sheet thickness (B), crack configuration, and material fracture toughness (CTOA) had a strong influence on buckling response [2]. A plot showing the ratio of the buckling-failure load to the failure load for a restrained cracked panel are shown in Figure 34 for aluminum alloys and steels [2,3]. The STAGS analyses predicted the load ratio as a function of the initial crack-length-to-sheet-thickness (c_i/B) ratio reasonably well. The oscillations were due to buckling mode changes for larger values of c_i/B ratios. The STAGS analyses and the critical CTOA fracture criterion were able to predict the influence of buckling and out-of-plane displacements on the tearing behavior of

thin-sheet materials. These capabilities are needed to predict the residual strength of cracked fuselage structures that exhibit out-of-plane deformations.

References:

1. Brogan, F. A., Rankin, C. C., Cabiness, H. D. and Loden, W. A., "STAGS User Manual Version 2.3, Lockheed Martin Missiles and Space Co., Inc., Palo Alto, CA, 1994.
2. Seshadri, B. R. and Newman, J. C., Jr., "Analyses of Buckling and Stable Tearing in Thin Sheet Materials," ASTM STP 1332, T. L. Panontin and S. D. Sheppard, Eds., 1999, pp. 114-134.
3. Forman, R. G., "Experimental Program to Determine Effect of Crack Buckling and Specimen Dimensions on Fracture Toughness of Thin Materials," AFFDL-TR-65-146, 1966.

9.4.16 Fracture Simulations Of Wide Panels Need The Plane-Strain Core

J. C. Newman, Jr.

NASA Langley Research Center

Cracks in thin-sheet materials, such as fuselage materials, develop high constraint conditions, like plane strain, around the crack front, but away from the crack front plane-stress conditions prevail. To account for this effect in two-dimensional finite-element fracture simulation codes, a plane-strain core concept was developed [1] for use with the critical crack tip opening angle (CTOA) fracture criterion. This study was conducted to verify the CTOA fracture criterion and the plane-strain core concept for wide panels made of a thin-aluminum alloy material.

Eichenberger [2] conducted fracture tests on middle-crack tension M(T) specimens made of 2.5-mm thick 2219-T87 aluminum alloy. Specimen widths (W) ranged from 90 to 1200 mm with a wide range of crack lengths conducted for some of the widths. The failure loads from all specimens were used to determine the critical CTOA value and the plane-strain core height by a trial-and-error procedure using the finite-element computer code, ZIP2D [1]. The critical CTOA value was then used to calculate the failure loads on all specimens using either plane-stress, plane-strain, and the plane-strain core concept. The critical CTOA was determined to be 4.7 degrees with a plane-strain core half-height (h_c) of 1.9 mm. The CTOA fracture simulation with the plane-strain core predicted the failure loads on all specimens within about 5 percent. To demonstrate the need for the plane-strain core, the critical angle of 4.7 degrees was then used to calculate failure loads under both plane-stress and plane-strain conditions. Figure 35 shows a normalized failure stress (S_f / σ^*) plotted against the specimen width for specimens with a crack length to width ratio of 1/6 (symbols). The solid curve is the CTOA analysis with the plane-strain core, whereas the dotted and dashed curves are the calculations for plane stress and plane strain, respectively. These results clearly show why the plane-strain core is needed for analyzing fracture of thin-sheet alloys. Figure 36 shows failure stress plotted against $2c/W$ for $W = 305, 610$ and 1200 mm. The CTOA analysis with the plane-strain core predicted the failure stresses very well over a wide range of panel widths and crack lengths.

Fracture of thin-sheet alloys is neither plane stress nor plane strain, but is a mixed combination of the high (plane-strain) constraint around the crack front and plane-stress behavior elsewhere. In lieu of conducting three-dimensional fracture analyses, the plane-strain core is a simple approach to approximate fracture of thin-sheet alloys.

References:

1. Newman, J. C., Jr., Booth, B. C. and Shivakumar, K. N., "An Elastic-Plastic Finite-Element Analysis of the J-Resistance Curve using a CTOD Criterion," ASTM STP 945, 1985, pp. 665-685.
2. Eichenberger, T. W., "Fracture Resistance Data Summary," Report DA-20947, The Boeing Company, June 1962.

9.4.17 Fatigue Crack Growth At Machined Pockets

Mohan M. Ratwani

R-Tec

James Helbling and Maro Heimerdinger

Northrop Grumman Corporation, El Segundo

Machined pockets in lower wing skins of an aircraft have shown propensity for crack initiation and propagation during service. It is necessary to perform damage tolerance analysis and design repairs for these locations. A test program (Reference 1) was carried out to obtain crack growth at machined pockets representative of a lower wing skin pocket. The specimen configuration shown in Figure 37 was used. A semi-circular part through flaw was used as an initial flaw. The fatigue testing was done under T-38 lead-in-fighter spectrum loading. During the testing it was observed that the crack tips in both the test specimens were growing at almost the same rate for the initial 1500 flight hours of spectrum testing. However, when the crack tip adjacent to the end of the machined pocket was closer to the pocket edge, it grew much slower compared to the other tip which was away from the edge of the pocket. The crack growth rate was found to be significantly different at the crack tips as shown in Figure 38.

To make crack growth predictions, analytical stress intensity factors were modified to account for the presence of the machined pocket radius along the crack plane. The modified stress intensity factors were used in Forman equation for crack growth predictions under spectrum loading. The unequal crack growth at the crack tips was accounted for by modifying crack growth constant c in the Forman equation. As the test data indicated crack growth rate at one crack tip to be one half of that at other crack tip, average value of c equal to 0.75 times the normal value was taken in Forman equation for crack growth predictions. A comparison of predicted crack growth and observed crack growth is shown in Figure 38. The figure shows a good correlation between predicted and observed average crack length.

Reference:

1. Helbling J, Heimerdinger M, and Ratwani M M, "Composite Patch Repair Applications to T-38 Lower Wing Skin," Presented at The Second NASA/FAA/DoD Conference on Aging Aircraft, Williamsburg, Virginia, 1998.

9.4.18 T-38 Lower Wing Skin Machined Pockets Analysis And Test

Mohan M. Ratwani

R-Tec

James Helbling and Maro Heimerdinger

Northrop Grumman Corporation, El Segundo

As a part of a program to extend the life of T-38 lower wing skin (Reference 1) a test and analysis program was carried out to obtain stresses in the machined pocket area of the lower wing. A test specimen was designed to simulate the local details and laboratory testing conducted (Reference 2) to obtain strains in the region. Two different detailed finite element analyses using a fine mesh and a coarse mesh were carried out to obtain strain distribution in the pocket area.

Structural testing of the T-38 wing at Wright Patterson Air Force Base is being carried out under T-38 Lead-in-Fighter spectrum loading as a part of "Advanced Technology redesign of Highly Loaded Structures Program". Prior to the fatigue testing of the wing, strain gages were applied to the lower wing skin pocket area. The location of the strain gages on the wing is shown in Figure 39. Two different strain surveys were performed on the wing. In the first strain survey, an inadequate amount of torsional load was applied. Subsequently, additional cylinders were added to provide the required amount of torsion. The strain survey was carried out for the two most critical load conditions (namely S0985 and 10556) to 50% of limit load. The results of the two strain surveys for the pocket between the 39% and 44% spar are shown in Figure 40 for the two conditions. The figure shows about 8% higher strains for the second strain survey compared to the first survey. The figure also shows the strains from the coupon test strain survey of reference 2. Correlation between strains from the wing test and coupon test is very good for both conditions. This indicates that the coupon specimen provides an accurate simulation of the wing pocket area.

The comparison of test and analytically predicted strains, obtained from coarse mesh and fine mesh finite element models, for the pocket between 39% and 44% spars is shown in Figure 41. The figure shows that for condition

S0985, both finite element models show a good correlation with the test results. However, for condition 10556, only the fine mesh results correlate well. The coarse mesh results are shown to be slightly higher.

References:

1. Helbling J, Grover R L, and Ratwani M M, "Analysis and Structural Test of Composite Reinforcement to Extend the Life of T-38 Lowe Wing Skin", Proceeding of Aircraft Structural Integrity Conference, San Antonio, Texas, December 1998.
2. Helbling J, Heimerdinger M, and Ratwani M M, "Composite Patch Repair Applications to T-38 Lower Wing Skin," Presented at The Second NASA/FAA/DoD Conference on Aging Aircraft, Williamsburg, Virginia, 1998.

9.4.19 Fatigue Analysis of Padded Single-Shear Lap Splices

Tom E. Sovar
Boeing

Longitudinal single-shear lap joints are used to join aircraft fuselage skins in a very straightforward and inexpensive manner. However, these joints may be problematic in terms of fatigue performance. To increase the fatigue life of aircraft structure at lap splices, the skin thickness may be increased locally at the joint. This is typically done by either bonding a doubler in this area or milling the skins down to their final thickness, thus leaving thicker pads in the joint region (see Figure 42). This procedure is commonly referred to as padding the skins.

Boeing has developed a method to predict the fatigue performance of padded lap splices using one-dimensional, flat-shell models of the joint. The flat shell models have closed-form solutions, which can be solved on a computer to provide quick estimates of the bending moments at the end fastener rows. These bending moments are used, along with the tension load and percentage of load transferred, to predict the peak stress at the edge of the fastener hole via stress concentration (K_t) factors. By combining this information with an existing method for predicting the fatigue life of an unpadded single-shear lap splice, it is possible to make the life predictions for padded lap splices.

The analysis procedure for the padded lap splice has several steps. First, the peak stress in the actual padded lap joint is estimated by superposing the predicted peak stress due to each of three load components at the end fastener rows -- skin bending moment, load transfer, and the bypassing stress. The flat shell model gives the skin bending moment at the end fastener rows. The percentage load transferred at these rows is estimated using existing stiffness-based methods, and the bypass stress is determined from the applied load once the percentage of load transfer is known.

The filled hole K_t associated with each load component is used to determine the peak stress value for that component. To account for hole filling effects, the K_t due to bending and the K_t for the bypass stress are assumed to be 60% of the open hole solutions.

Next, a model of an unpadded lap joint is made with a skin thickness equal to the pad thickness of the padded joint. By varying the load that is applied to this unpadded lap splice, the peak stress can be matched to that in the actual padded lap joint. Then a life prediction is made for the unpadded lap splice for this applied load. Since the peak stresses are the same at the same end fastener detail in both the padded and unpadded lap joint models, the assumption is made that the fatigue lives of the two joints are the same.

Several analytically predicted trends have been verified by fatigue tests. These include pad thickness as the primary parameter affecting fatigue life, and pad orientation as also very important. A pad that has the added material on the side toward the faying surface is much more effective at increasing the fatigue life at the end fastener row (in that same pad) than a pad that has the added material away from the faying surface. Conversely, a pad oriented toward the faying surface has a lower fatigue life at the fillet where the pad-up starts than a pad oriented away from the faying surface. This behavior is displayed in Figure 43 for aluminum joints with one particular configuration. Another effect which is predicted is that a joint with increased overlap width will have a longer fatigue life than an otherwise identical joint that is simply narrower (less overlap). This is because the wider joint undergoes less rotation, resulting in lower bending stresses at the first fastener rows. This behavior is displayed by Figure 44 for a simple unpadded lap joint with two .040" thick aluminum skins.

9.4.20 Application Of Small-Crack Theory To A Rotorcraft Material

J. C. Newman, Jr.

NASA Langley Research Center and

R. A. Everett, Jr.

U.S. Army Research Laboratory

Studies on the growth of small cracks have led to the observation that fatigue life of many engineering materials is primarily “crack growth” from micro-structural features, such as inclusion particles or from manufacturing defects. This work applied a plasticity-induced crack-closure model [1] to predict fatigue lives of metallic materials using “small-crack theory” under various loading histories. Constraint factors, to account for three-dimensional effects at the crack front, were selected to correlate large-crack growth rate data as a function of the effective stress-intensity factor range (ΔK_{eff}) under constant-amplitude loading. Modifications to the ΔK_{eff} -rate relations in the near-threshold regime were needed to fit measured small-crack growth rate behavior. The model was then used to predict total fatigue lives, for notched and un-notched specimens under constant-amplitude and spectrum loading using micro-structural flaws.

Swain et.al [2] conducted large-crack tests on middle-crack tension specimens made of 4340 steel. These test data were used to obtain the ΔK_{eff} -rate relation. Fatigue tests were also conducted on single-edge-notched tensile (SENT) specimens with a stress concentration $K_T = 3.3$. Examination of the initiation sites for 35 specimens gave information on the distribution of crack-initiation site dimensions. Two types of particles were observed: a spherical particle and a stringer particle, see Figure 45 (a) and 45 (b). The spherical (calcium-aluminate) particle was by far the most dominate crack-initiation site particle. The cumulative distribution function for these defects is plotted against an equivalent semi-circular defect radius based on the actual area of the defect in Figure 45 (c). The mean defect is about 13- μm in radius but selecting 8- to 30- μm defect radii would cover over 80% of the all defects.

Results of fatigue tests conducted on circular hole specimens under the Felix-28 load sequence [3] are shown in Figure 46 as symbols. The maximum stress in the spectrum is plotted against the cycles to failure. Predictions of total fatigue life under the Felix-28 load spectrum were made using the FASTRAN code [1] by calculating the number of cycles necessary to grow a crack from the assumed initial defect size, located at the center of the open hole, to failure. The predicted results for the two initial defect sizes bounded the test data quite well.

References:

1. Newman, J. C., Jr., “Application of Small-Crack Theory to Aircraft Materials,” Small Fatigue Cracks: Mechanics and Mechanisms, Oahu, Hawaii, December 1998.
2. Swain, M. H., Everett, R. A., Newman, J. C., Jr. and Phillips, E. P., “The Growth of Short Cracks in 4340 Steel and Aluminum-Lithium 2090,” AGARD R-767, 1990.

9.4.21 Fretting Damage in Advanced Propulsion Systems

Mr. G. Harish, Ms. P.A. McVeigh and Prof T.N. Farris

Purdue University and

Prof M.P. Szolwinski

Rensselaer Polytechnic Institute

The area of contact between the blade root and disk in high-performance turbomachinery (Figure 45 (d)) has been identified as a critical area for the nucleation of fatigue damage leading to premature and often catastrophic component failures. The interaction of small-scale, oscillatory relative displacements or slip at the contact surfaces and the sharp gradients of near-surface contact stresses induced by fretting contact is responsible for the nucleation of fatigue damage in these components. An ongoing program strives toward the development and validation of analysis tools for assessing quantitatively the threat of fretting fatigue to the integrity and subsequent performance of jet engine components.

Two computational approaches—one relying on a quasi-analytical formulation and another employing the finite element method—for characterizing the interfacial conditions arising in experimental setups used to simulate conditions of fretting in the blade/disk contacts [1]. The nominally flat nature of these contacts leads to sharp gradients in near-surface conditions. The quasi-analytical formulation provides a computationally efficient approach

for analyzing arbitrary contacting profiles. It is also shown that predictions from the analyses compare favorably to interfacial damage observed in an ongoing series of fretting fatigue tests of a titanium alloy used commonly in turbomachinery components, Ti-6Al-4V. Other modeling efforts have targeted the effects of LCF/HCF interaction on the near-surface stress field [2].

These near-surface stress fields have also been combined with a multiaxial fatigue life parameter and uniaxial strain-life data from smooth-bar Ti-6Al-4V specimens to provide predictions of fretting fatigue failures in dovetail-like contacts [3]. As shown in Figure 45 (e), correlation between initial test data and these predictions is encouraging, lending support to the use of this mechanics-based approach in ensuring the integrity of current and next-generation engine designs.

References

1. McVeigh, P.A., Harish, G., Farris, T.N. and Szolwinski, M.P., "Modeling Interfacial Conditions in Nominally Flat Contacts for Application to Fretting Fatigue of Turbine Engine Components," *International Journal of Fatigue*, 1999, accepted for publication.
2. Szolwinski, M.P., Matlik, J.F. and Farris, T.N. "Effects of HCF Loading on Fretting Fatigue Crack Nucleation," *International Journal of Fretting*, 1999, accepted for publication.
3. Szolwinski, M.P., Harish, G., McVeigh, P.A. and Farris, T.N., "The Tribological and Fatigue Performance of Ti-6Al-4V Fretting Contacts, in 4th National Turbine Engine High Cycle Fatigue (HCF) Conference, Monterey, CA, Universal Technology Corp., 1999, CD-ROM proceedings.

9.4.22 Fretting Fatigue in Riveted Aircraft Structures

Prof M.P. Szolwinski

Rensselaer Polytechnic Institute and

Mr. G. Harish and Prof T.N. Farris

Purdue University

Fretting, a synergistic damage mechanism experienced at clamped, contacting surfaces in a wide variety of mechanical systems subjected to oscillatory loading, plays a particularly critical role in the nucleation of fatigue cracks in aging aircraft systems. The localized near-surface stresses, strains and surface microslip associated with fretting contact lead to a detrimental tripartite combination of corrosion, wear and fatigue damage in riveted lap joints. Understanding fretting fatigue in these joints is crucial to those interested in not only airframe structural design but also technologies for life prediction and maintenance of aging aircraft systems, both civilian and military.

The goal of this research was to formulate a mechanics-based approach that linked the localized stress and strain fields at and around the rivet/hole interface to the nucleation of fretting fatigue damage in riveted lap joint structures. As summarized in Figure 45 (f), this effort integrated results from well-characterized experiments and modeling efforts to produce a validated methodology for predicting the fatigue performance of lap joint structures from knowledge of applied load histories, manufacturing parameters and basic fatigue properties.

Figure 45 (g) presents an overview of the components of this predictive framework. Initial steps were taken to formulate a three-dimensional shell-element model of a riveted lap joint [1]. This model resolved both the load transfer among rivet rows and contact at and around the rivet/hole interfaces. The interfacial conditions at the rivet/hole contact were found to be similar to those generated in a well-characterized fretting fatigue test system with a reduced contact geometry [2, 3]. Furthermore, the results also identified a strong link between the mechanics of load transfer in the joint and the through-thickness restraint offered by the installed fastener.

In light of these results and the obvious influence the residual stress field induced during fastener installation has on fatigue performance, a finite element model of force-controlled rivet installation was developed [4]. This model revealed a through-thickness gradients in the residual stress field and a change in the distribution of residual hoop stress near the rivet/hole interface with changes in the installation force. The data from this simulation were then used as input into a two-dimensional finite element model of a single lap joint structure that was validated by a thermal imaging technique [5]. This model was exercised in conjunction with a multiaxial fatigue life parameter to identify both the critical location and number of cycles for fatigue crack nucleation. Comparison between these predictions and observed failures in single lap joint test articles has been favorable [6].

References:

1. Harish, G. and Farris, T. N., "Modeling of Skin/Rivet Contact: Application to Fretting Fatigue," in *A Collection of Technical Papers, Proceedings of 38th AIAA/ASME/ASCE Structures, Structural Dynamics and Materials Conference, Volume 4*, Kissimmee, FL, 1997, pp. 2761-2771.
2. Szolwinski, M. P. and Farris, T. N., "Observation, Analysis and Prediction of Fretting Fatigue in 2024-T351 Aluminum Alloy," *Wear*, Vol. 221, No. 1, 1998, pp. 24-36.
3. Szolwinski, M. P., Harish, G., Farris, T. N., and Sakagami, T., "In-Situ Measurement of Near-Surface Fretting Contact Temperatures in an Aluminum Alloy," *ASME Journal of Tribology*, Vol. 121, No. 1, 1998, pp. 11-19.
4. Szolwinski, M. P. and Farris, T. N., "Linking Riveting Process Parameters to the Fatigue Performance of Riveted Aircraft Structures," in *A Collection of Technical Papers, Proceedings of the 40th AIAA/ASME/ASCE/AHS/ASC SDM Conference*, St. Louis, MO, AIAA, 1999, in press.
5. Sakagami, T., Harish, G., Farris, T. N., and Szolwinski, M. P., "Observing and Modeling the Onset of Widespread Fatigue Damage in Riveted Aircraft Structures," in *1999 Society of Experimental Mechanics Spring Conference & Exposition*, Cincinnati, OH, Society of Experimental Mechanics, 1999, in press.
6. Szolwinski, M. P., Harish, G., McVeigh, P. A., and Farris, T. N., "Experimental Study of Fretting Crack Nucleation in Aerospace Alloys with Emphasis on Life Prediction," *Fretting Fatigue: Current Technology and Practices*, ASTM STP 1367, D. W. Hoepfner, V. Chandrasekaran, and C. B. Elliott, Eds., American Society for Testing and Materials, West Conshohocken, PA, 1999, accepted for publication.

9.4.23 Advanced Crack Growth Modeling (using AFGROW) and Testing**Mr. Clare Paul****Air Force Research Laboratory**

The goal of this research program is to expand the capabilities of predicting growth of cracks in aircraft structure. New technology and material data will be developed and implemented into *AFGROW*. Specifically, the multiple crack growth modeling project currently underway (Multiple Crack Growth Verification Testing,) will be expanded to include additional in-service cracking scenarios of cracks nucleating and growing from several locations in one structural element; for example, a row of fasteners in a single bay of a fuselage lap-splice joint or a row of fasteners in a span- or chord-wise splice of a wing skin. The current effort does not cover the wide variety of cracking scenarios seen in-service; thus new stress intensity and interaction factors must be developed and experimentally verified. Additional stress intensity factor solutions will be developed for cracks growing in stiffened panels if said solutions are not available in the open literature. In addition, the ability to model cracks growing from highly stressed joints (lugs with interference fit bushings installed for example) is needed by ALC engineers.

9.5. WIDESPREAD FATIGUE DAMAGE

9.5.1 Analytical and Test Evaluations on the Linkup of Multiple Cracking in Stiffened Fuselage Panels

Dr. John Bakuckas

FAA William J. Hughes Technical Center

Widespread fatigue damage (WFD) in the form of small cracks rivet holes in a fuselage lap joint can degrade the load carrying capacity of an aircraft. The reduction in emanating from multiple residual strength of flat panels due to multiple cracking has been demonstrated experimentally. Research is currently ongoing to develop and validate analytical and computational models to predict the reduction in residual strength of stiffened, curved structures with multiple cracks.

As part of model validation, testing on full-scale, stiffened, curved panels was conducted. The test articles for this fixture contain structural details resembling those found in a commercial transport aircraft. Residual strength tests were performed on a panel with two different multiple cracking configurations. The first configuration consisted of a two-bay skin lead crack with multiple smaller collinear cracks spanning an intact central strap. The second configuration consisted of a two-bay lead crack in the upper row of an unbonded longitudinal lap splice with multiple smaller collinear cracks spanning a broken central strap. The data obtained from these tests can be used to validate the analytical and computational models now under development to predict the residual strength of aircraft panels.

In addition to testing, engineering analyses were performed to predict the remote stress at linkup. In these analyses, linkup (See Figure 47) was assumed to occur when the ligament between adjacent crack tips becomes completely plastic. Curvature was taken into account by applying a bulging factor. Mathematical expressions for the bulging factor as a function of applied stress, crack length, and other parameters were developed. These expressions contained unknown constants that were determined from curve fitting of geometric nonlinear finite element results. The derived expressions for the bulging factor were used in conjunction with a displacement compatibility analysis which was applied to include the effect loads carried by rivets that attach the frames and the tear straps to the skins.

The calculated linkup stresses were conservative in comparison with test data in most cases. In general, the predicted linkup stresses were within 25% of the experimental values. Stable tearing had a relatively weak effect on the calculation of linkup stresses. The bulging factor had a significant effect on predicting linkup stresses, as shown in Figure 48.

POC: Dr. John Bakuckas, AAR-431, FAA William J. Hughes Technical Center, Atlantic City International Airport, NJ 08405, (609) 485-4784.

9.5.2 Fracture Analyses Of Faa/Nasa Stiffened Panels With Multiple-Site Damage

J.C. Newman, Jr., B. R. Seshadri and D. S. Dawicke

NASA Langley Research Center

The objective of this study [1] was to analyze a series of fracture tests conducted jointly by the FAA and NASA on stiffened and unstiffened panels with multiple-site-damage (MSD) cracking. The panels were made of 2024-T3 sheet (B = 1.6 mm) with five 7075-T6 flat stiffeners (with the central stiffener severed). Severe out-of-plane displacements, due to local buckling along the crack plane, were observed in all tests. The analyses were conducted using the STAGS (STRUCTURAL Analysis of General Shells) code to describe the structural non-linearity and the critical crack-tip-opening angle (CTOA) fracture criterion to predict stable crack growth. The STAGS code with the "plane-strain" core option was used in these analyses to account for the effects of through-thickness constraint on the fracture process.

A critical CTOA value was determined from a wide (unstiffened) panel with anti-buckling guides. The plane-strain core size was estimated from previous fracture analyses and was about equal to the sheet thickness. Rivet flexibility and stiffener failure was based on methods and criteria, like that currently used in the aerospace industry. STAGS and the CTOA criterion were used to predict load-against-crack extension for the wide panels with a single crack and multiple-site damage cracking at many adjacent rivet holes.

Test results and the STAGS/CTOA analyses made on a wide stiffened panel with a single crack is shown in Figure 49. The load-crack-extension measurements are shown as symbols and the analysis by the solid curve. The insert shows the relative location of the stiffener. Crack extension was measured until the crack went underneath the stiffener. Once the crack grew outside of the stiffener, the panel failed (solid symbol). Whether failure of the panel was due to sheet failure or stiffener failure could not be determined. Failure of either would immediately result in panel failure because the stiffeners were carrying about one-half of the applied load. A comparison of the measured and predicted load-against-crack extension for the wide stiffened panel with a lead crack and the 1.3-mm MSD is shown in Figure 50. Again, the insert shows the relative location of the lead crack, open holes, MSD, and the intact stiffener. The measured load-crack extension values for the data underneath the stiffener were inferred from the load-time trace recorded on this specimen. As the crack linked up with the open hole at about 125 mm, the sheet failed with all 24 MSD cracks linking. Panel failure then occurred at about a 10% higher load to break the stiffeners. The predicted load-crack extension behavior matched the test results very well. These results indicated that the STAGS code and the CTOA failure criterion could predict stable tearing in the presence of MSD in a stiffened structure with severe out-of-plane deformations, typical of what may occur in an aircraft fuselage under pressure.

Reference:

1. Seshadri, B.R., Newman, J. C., Jr., Dawicke, D. S. and Young, R. D., "Fracture Analysis of the FAA/NASA Wide Stiffened Panels," Second Joint NASA/FAA/DoD Aging Aircraft Conference, Williamsburg, VA, 1998.

9.5.3 FAA-NASA Stiffened-Panel Fracture Tests

Dr. Paul Tan

FAA William J. Hughes Technical Center

NASA Langley Research Center and the FAA William J. Hughes Technical Center have jointly conducted fracture tests on 40-inch-wide sheets of 0.063-inch-thick 2024-T3 aluminum alloy. Five different crack configurations were tested: a single center crack, a single center crack with a line of 24 holes collinear with the crack, and three configurations with a single center crack with equal multiple site damage (MSD) cracking at each hole. The MSD cracks were introduced by fatigue precracking at a low stress range. For each crack configuration (three MSD sizes), identical specimens were tested with and without riveted tear straps. During the tests, measurements were made of load, crack extension, applied end displacement, strain, and displacement fields.

The significant feature of these tests are that they are the first wide panels with MSD fatigue cracks rather than saw cut cracks. The MSD cracks were introduced through a unique four-step process: (1) undersized holes were drilled into the specimen and small notches were machined into both sides of each hole; (2) the specimen was fatigued and the resulting crack growth at each hole was measured optically; (3) whenever the crack at any hole reached the desired value, a nut-washer-bolt system was used to transfer load around the crack, stopping the crack growth and letting the other holes catch up; and (4) after all the crack at all the holes reached the desired length, a long center notch was machined and fatigue precracked to a length of 8 inches. This method resulted in MSD cracks within 0.002 inch of the desired lengths.

The photograph in Figure 51 shows one of the 40-inch-wide specimens in the servo-hydraulic loading frame. In the foreground are the two cameras used to measure the out-of-plane displacements using a digital image correlation technique. The measurements of out-of-plane displacement and crack extension as a function of applied load are being used to verify a three-dimensional, geometrically nonlinear, elastic-plastic residual strength prediction model for aircraft fuselage structures.

POC: Dr. Paul Tan, AAR-431, FAA William J. Hughes Technical Center, Atlantic City International Airport, NJ 08405, (609) 485-6665.

9.5.4 Widespread Fatigue Damage Evaluation

Jin-Chyuan Yu

Boeing

Under sponsorship of the FAA and NASA and, later, the USAF, Boeing has undertaken the task of evaluating the effects of multisite damage (MSD) on the integrity of aircraft structures since 1996. MSD, a subset of WFD, usually refers to collinear cracks along a row of fastener holes. The project is expected to be completed in the Year 2000. The emphasis is on the prediction of MSD initiation and critical damage configuration that causes the residual strength to drop below the design level.

Fatigue tests were conducted on 16 22-in-wide splice panels, of four splice types, to generate data for use in an equivalent flaw initiation size (EIFS) study. Crack growth as predicted by FASTRAN, a closure-based crack growth model, was compared with the measured curves to determine the EIFS. For aluminum 2024-T3 sheet, 0.063-in thick, the EIFS obtained, based on limited test data, are in the neighborhood of 0.008 in.

The residual strength study on MSD in splice joints involves prediction of linkup between two cracks and final unstable fracture. Two fracture criteria are primarily used for this purpose: the FAA-developed T^* [1] and the crack tip opening angle (CTOA) [2]. T^* is incorporated in the code EPFEAM, and CTOA is implemented in the NASA code STAGS. Both criteria account for the large yielding in the ligament between cracks.

The investigations are focused on four splice configurations with MSD along the joints. For simple lap joints in 2024-T3 sheet, 0.063-in thick, the initial results show that 20% of residual strength will be lost with an MSD crack size of 0.05 in at each hole with a pitch of 1.14 in, and 30% if the MSD crack size is 0.1 in. A series of tests will be performed to generate data for correlation with analysis. Sixteen flat splice panels, consisting of four splice configurations, and six spliced curved panels, with splice either in axial or circumference direction, will be tested, with testing scheduled to start in the second quarter of 1999.

References:

1. Wang, L. et al., "The Elastic-Plastic Finite Element Alternating Method (EPFEAM) and the Prediction of Fracture Under WFD Conditions in Aircraft Structures." Computational Mechanics, V 19, pp 370--379.
2. Newman, J. C. Jr., "A Fracture Criterion for Widespread Cracking in Thin-Sheet Aluminum Alloys," 17th International Committee on Aeronautical Fatigue.

9.5.5 Bulging Factors for Predicting Residual Strength of Fuselage Panels With WFD

Dr. John Bakuckas

FAA William J. Hughes Technical Center

An engineering approach for evaluating the residual strength of fuselage panels with widespread fatigue damage (WFD) is being developed by the FAA. The approach, developed by Broek and Swift, uses the residual strength diagram modified to include multiple-site damage (MSD) cracks. It is assumed that the MSD crack will be absorbed by the main lead crack through plastic collapse of the net section ligament. Referred to as the plastic zone linkup criterion, this occurs when the plastic zones from the lead crack and MSD crack meet. The geometry of the plastic zones is determined from appropriate values of the stress-intensity factors (SIF).

A two-part investigation was conducted to generate bulging factors for pressurized unstiffened and stiffened fuselage structures. In the first part, bulging factors and crack profiles were calculated for a variety of configurations using a global-local hierarchical (GLH) approach using nonlinear finite element analyses. Comparisons with bulging factors β from the literature (Riks and Chen and Schijve) were used to validate the GLH approach. Once validated, results showed that, for the unstiffened cases, the bulging factor increases as the crack length increases and decreases as the applied pressure increases. (See Figure 52) For the stiffened cases, the effect of an intact and broken central strap on the bulging factor and strap stresses was studied. An intact central strap significantly reduces both the bulging effect and the stresses in the adjacent strap compared to a broken central strap.

In the second part, results from the GLH approach were used to derive a generalized expression for the bulging factor for unstiffened fuselage panels using a dimensional analysis. The shape of the bulging profile was accurately

modeled and used in an energy balance approach to derive an expression for the bulging factor. (See Figure 53) For all cases, the derived expression was within a few percent of the results generated using the GLH approach.

The reported solutions for the bulging factors will be used in future work to predict the residual strength of fuselage panels containing widespread fatigue damage.

POC: Dr. John Bakuckas, AAR-431, FAA William J. Hughes Technical Center, Atlantic City International Airport, NJ 08405, (609) 486-4784.

9.5.6 Engineering Approach to Predict Residual Strength of Fuselage Panels With WFD

Dr. John Bakuckas

FAA William J. Hughes Technical Center

Widespread fatigue damage (WFD) in the form of small cracks emanating from multiple rivet holes in the fuselage lap splice joint can degrade the load carrying capability of an aircraft below the original certification requirements. Tools and methodologies to evaluate the effect of WFD on the structural integrity of aircraft are under development. One of these tools, an engineering approach for evaluating the residual strength of fuselage panels with WFD, is being developed by the FAA. The approach, developed by Broek and Swift, assumes that the smaller crack will be absorbed by the main lead crack through plastic collapse of the net section ligament. Referred to as the plastic zone linkup criterion, this occurs when the plastic zones from the lead crack and smaller crack meet. The geometry of the plastic zones is determined from appropriate values of the stress-intensity factors (SIF).

The engineering approach has been successfully applied to predict the residual strength in flat panels containing various multiple crack configurations. (See Figure 54) The flat panels were tested by the FAA at the National Institute of Standards and Technology (NIST). On average, the difference between the experiments and the predictions of the fracture strength was 13%. The engineering approach is appealing since it can be used in numerous parametric studies to screen a large number of cases to identify critical configurations, which may then be analyzed in more detail.

To further develop the engineering approach to predict the residual strength of curved fuselage panels with WFD, the effect of bulging has been incorporated into analysis. Finite element results generated in a parametric study were used to derive an expression for the bulging factor for unstiffened shells using dimensional analysis. The shape of the bulging profile was modeled and used in an energy balance approach to derive an expression for the bulging factor, which was incorporated into the engineering approach. The resulting methodology was used to predict the residual strength of an unstiffened fuselage panel with multiple-site damage (MSD). (See Figure 55) The difference between the experimental and the prediction of the fracture strength was 7%.

POC: Dr. John Bakuckas, AAR-431, FAA William J. Hughes Technical Center, Atlantic City International Airport, NJ 08405, (609) 485-4784.

9.5.7 Engineering Model For Residual Strength With Multiple Site Damage

J. E. Ingram and Y. S. Kwon

Lockheed-Martin

Nonlinear finite element analyses were conducted to develop an engineering model for predicting residual strength of skin panels with multiple site damage (MSD). The STAGS finite element code was used to conduct parametric analyses of numerous configurations of lead and MSD cracks. The analyses were directed at developing a method to predict the link-up behavior in ductile alloys such as 2024-T3 aluminum. Recent enhancements to STAGS by the Langley Research Center (LaRC) and Lockheed Martin Missiles and Space Co. (LMMSC) have enabled the code to accurately predict stable tearing and link-up of cracks with the elastic plastic behavior and local plane strain effects accounted for. These enhancements include the automatic node release (crack extension) feature and the plane strain formulated shell elements. The nodes are released when the STAGS-calculated crack tip opening angle (CTOA) reaches the critical value for the material.

Before starting the parametric analyses, the accuracy of the STAGS code and the CTOA criteria were investigated by comparing the STAGS calculations to existing test results. First, a middle crack tension specimen was analyzed

with STAGS, and the critical value of CTOA was obtained which gave the best agreement with the K_R curve for the 2024-T3 material. Figure 56 shows a comparison of the measured and STAGS-calculated K_R curves. Next, the geometry of the MSD test panels used in the Foster-Miller tests were simulated in STAGS. The comparison of the STAGS calculations and the test results are shown in Figure 57. The average error for the 15 link-up predictions was 2.3%.

Based on the good agreement between STAGS and the MSD tests, a series of elastic plastic analyses were conducted to obtain a parametric set of link-up stresses for varying sizes of lead and MSD cracks, and ligament lengths (distances between the adjacent crack tips). A scheme for curve fitting and interpolating on these results was incorporated into a subroutine, used in the residual strength computer program. The interpolation routine allows numerous configurations of MSD crack geometries to be investigated in a fraction of the time that separate elastic-plastic finite element solutions would require.

9.5.8 Transport Risk Assessment Containing Widespread Fatigue Damage: TRACWFD

Dr. Catherine Bigelow

FAA William J. Hughes Technical Center

As aircraft age, damage accumulates throughout the structure. The onset of widespread fatigue damage (WFD), as well as the structure's residual strength, are not deterministic quantities, rather there is some probability that either the onset of WFD has occurred or the residual strength has fallen to unacceptable levels. Not only are these calculations a function of the underlying physical processes but they are also a function of the maintenance and inspection procedures performed on the aircraft.

A probabilistic analysis tool has been developed to assess the damage progression in aging aircraft and such damage's impact on the onset of widespread fatigue damage, the residual strength, and maintenance and inspections. The analysis tool combines the results of previous FAA, U.S. Air Force, and National Aeronautics and Space Administration developments into a fast, efficient mechanics model for the aging aircraft fleet. This computer model has been named **TRACWFD** – Transport Aircraft Risk Assessment Containing Widespread Fatigue Damage.

TRACWFD can be used to assess the effect of a variety of factors on the overall risk of commercial and military aircraft operation under the conditions of aging. The program analysis has been divided into two phases. The first phase of the analysis for a particular aircraft structure is deterministic where the nominal behavior is calculated in terms of local damage conditions, stress concentrations, and crack driving forces. Figures 58 and 59 show typical results of the deterministic analysis. The second phase of the analysis involves the probabilistic modeling of the mechanics models, loads, and inspection procedures. Some of the damage mechanisms that can be addressed with TRACWFD are crack initiation, linear and nonlinear curved-panel stress analyses, fatigue crack growth, corrosion, corrosion fatigue, nondestructive inspections (NDI), and residual strength analyses.

Studies have been conducted examining the longitudinal lap splice, the wing, and circumferential lap and butt splices in a narrow-body jet. Predictions of the time dependent probability of the onset of widespread fatigue damage and the loss of residual strength have been made. In addition, the minimum crack sizes that must be able to be detected to maintain a risk level have been predicted.

POC: Dr. Catherine Bigelow, AAR-431, FAA William J. Hughes Technical Center, Atlantic City International Airport, NJ 08405, (609) 485-6662.

9.6. CORROSION AND CORROSION/FATIGUE

9.6.1 Modeling Corrosion Growth On Aircraft Structure

D.W. Hoepfner, V. Chandrasekaran, Young In Yoon and A.M.H. Taylor
University of Utah

State of the Art Review

A state of the art review was prepared on *corrosion and corrosion fatigue predictive modeling* for NCI Information systems, Fairborn, OH. The major sections of the report discussed the following three major areas:

- Corrosion in Aircraft Structural Aluminum Alloys,
- Pitting Corrosion,
- Microstructure and environment effects on “short” crack behavior of materials.

The review of the literature clearly showed that much progress has been made on modeling the effects of corrosion on material behavior and structural integrity. It is clear that to date the models have centered around characterizing the corrosion and modeling the effects of the corrosion as one or more of the following:

- section change that affects the area/volume that modifies the stress.
- nucleation of localized debris that may modify the stress (part of pillowing) that modifies the stress or stress intensity.
- nucleation of intergranular corrosion that is involved in pillowing that modifies the stress or stress intensity.
- nucleation of localized corrosion (pitting, fretting, etc.) that modifies the local stress and may ultimately nucleate cracks.
- production of products of corrosion that produce localized embrittlement effects that may alter the material behavior and produce accelerated crack propagation.

As a part of this program, an experimental study was conducted to characterize corrosion damage quantitatively in relation to fatigue life of 2024-T3 aluminum alloy specimens as briefly discussed below.

9.6.2 Experimental Study

D.W. Hoepfner, V. Chandrasekaran, Young In Yoon and A.M.H. Taylor
University of Utah

The primary focus of this study was to correlate corrosion "damage" using pit depth as a controlling factor with the fatigue life of prior corroded 2024-T3 aluminum alloy specimens. The analysis of fracture surfaces clearly showed that fatigue cracks nucleated from corrosion pits propagated deeper into the specimen subsurface when compared to cracks nucleated from uncorroded areas. For example, refer to Figure 60. In general, the greater the range of pit depth, the lower the fatigue life of the specimens. Also, as shown in Table 1, the greater the range of pit depth, the less the distance the crack propagated into the specimen subsurface before fracture as observed from fractography. In addition, in another study, the quantified pit depth was correlated to "short" fatigue crack nucleation and growth on prior corroded 2024-T3 aluminum alloy specimens.

Table 1: Results from Fatigue Experiments

Material: 2024-T3; σ_{\max} (Net Stress) = 20 ksi; R = 0.1, f = 10 Hz.

Specimen ID	Range of Pit Depth (μm)	Average Pit Depth (μm) (a_0)	Crack Depth (Fractographic study) (mm) (a_c)	Fatigue Cycles at Fracture
Specimen #1	35-66	50.5	1.4	10,208,000
Specimen #2	60-110	85	0.5	1,084,200
Specimen #3	50-230	140	0.26	316,000
Specimen #4	55-90	72.5	1.4	2,919,500

9.6.3 Importance of Chemically Short-Crack-Growth on Fatigue Life

R.P. Wei

Lehigh University

Commercial and military aircraft are exposed to deleterious environments (such as atmospheric moisture and salt spray) that enhance the fatigue crack-growth (FCG) rates in aircraft structural alloys. This phenomenon, generically termed corrosion fatigue (CF), is explicitly taken into account in the development of life prediction and management methodology. It is increasingly recognized that CFCG behavior may be separated into two regimes: a chemically long and a chemically short regime of growth. For aluminum alloys used in aircraft construction, experimental data show that the CFCG rates are up to 10X those in an inert environment in the long-crack regime. In the chemically short regime, the growth rates are further enhanced by up to 3X, with the effect extending out to crack lengths of up to 6 mm. For accurate damage tolerant life management and design, the accelerated CFCG rates in the chemically short-crack regime must be considered. For example, this regime of crack growth can span over nearly one-quarter of the inter-rivet distance in typical fuselage lap-splice joints. Characterization of the chemically short crack-growth response of 2024-T3 and 7075-T6 aluminum alloys were determined at Lehigh University. Estimates of the impact of this regime showed reductions in fatigue lives that are commensurate with the increased crack growth rates.

Typical crack growth response under constant crack driving forces ΔK , showing the chemically short-crack effect in a 7075-T6 aluminum alloys in a 0.5M NaCl solution, is shown in Figure 61. The effect is reflected by a faster FCG rate for a 0.5 mm-long crack relative to that of one 6 mm long; the extent of increase depended upon the ΔK level. Overall the 7075-T6 alloy is more susceptible to corrosion fatigue crack growth than the 2024-T3 alloy. The sensitivity to chemically short crack-growth for 7075-T6 alloy is also greater, exhibiting a factor of three increase in FCG rate at 0.5 mm over that of a long-crack at a ΔK of $5 \text{ MPa m}^{1/2}$ versus a factor of two for the 2024-T3 alloy. Comparisons of simple estimates of number of cycles required to extend a fatigue crack from 0.03 to 1 mm (fatigue crack growth lives) for the two alloys, based on short-crack and long-crack data, are shown in Figures 62 and 63. These estimates recognize that for the model used in for these estimations, over 95% of the crack growth life would be spent in the early growth from 0.03 to 1 mm, and the disappearance of the effect at higher ΔK levels. The reduction in fatigue lives is greater for the 7075-T6 alloy relative to the 2024-T3 alloy. The reduction is commensurate with a doubling of chemically short FCG rates relative to the chemically long FCG rates, and is significant in relation to long-term service.

References:

1. Evan J. Dolley and Robert P. Wei (1999). "Importance of Chemically Short-Crack-Growth on Fatigue Life". *2nd Joint NASA/FAA/DoD Conference on Aging Aircraft*, Williamsburg, VA, 31 August-3 Sept. 1998, Charles E. Harris, ed., NASA/CP-1999-208982/PART 2, 679-687.
2. Evan J. Dolley, Jr. (1999). "Chemically Short-Crack Behavior of the 7075-T6 Aluminum Alloy", Ph.D. Dissertation, Lehigh University.

9.6.4 Prediction of Fatigue Life of Pre-Corroded Specimens

R.P. Wei

Lehigh University

The fatigue life of an engineering structure fabricated of aluminum alloys may be reduced as a result of exposure to corrosive environments. One form of corrosion is pitting which can act as nuclei for fatigue cracking. Research at Lehigh University showed that the fatigue life of a pre-pitted aluminum alloy could be estimated accurately from the initial pit size and the corrosion fatigue crack growth properties of the material.

Notched specimens of 2024-T3 aluminum alloy were pre-corroded in a 0.5 M NaCl solution from 48 to 384 hours (or 2 to 16 days) and tested in fatigue in air at room temperature. The results showed that pre-corrosion significantly reduced fatigue lives (Figure 64); for example, the lives of specimens after 384 hours of pre-corrosion (corresponding to the deepest pits) were more than one order of magnitude lower than those of uncorroded specimens. The crack nucleating pit sizes were determined from post-fracture examinations by scanning electron microscopy, and ranged from 20 to 70 μm . The reduction in fatigue life showed better correlation to the nucleating pit size than the duration of pre-corrosion. This finding is consistent with that of Harmsworth on a 2024-T4 aluminum alloy tested in rotating bending.

Based on the measured crack nucleating pit sizes and by assuming that the pits may be represented by equivalent semi-circular surface cracks (aspect ratio of unity), fatigue lives for the 2024-T3 and 2024-T4 alloys were estimated by considering crack growth alone, using fatigue crack growth data obtained at Lehigh University on the 2024-T3 alloy. The estimated lives are shown to be in good agreement with the actual fatigue lives (Figures 65 and 66); the scatter in the results reflected inaccuracy in the pit size measurements and variations in the actual aspect ratio. The agreement suggests that (i) the number of cycles required to nucleate a crack from a corrosion pit was relatively short and may be neglected, and (ii) pitting corrosion had effectively eliminated the early crack growth portion (or commonly viewed as the initiation portion) of fatigue life. Based on the measured distribution in pit sizes from specimens that had been pre-corroded for 384 hours, estimates of the distribution in fatigue lives were made by Monte Carlo simulation for aspect ratios of 0.6 and 1.0, which covered the range of observed aspect ratios. The estimated distributions are shown in Figure 67 and are in good agreement with the experimental observations.

The results show that fatigue lives are determined principally by crack growth (*vis-à-vis*, initiation), and can be accurately estimated on the basis of crack growth properties and the sizes of crack nuclei (*e.g.*, corrosion pits). The distribution in fatigue lives is directly related to the distribution in the size of crack nuclei, but is also expected to reflect variations in crack growth properties. This finding provides a direct connection between the conventional and fracture mechanics based approaches to corrosion fatigue in that it suggests that S-N response might be directly predicted from linear fracture mechanics considerations of crack growth.

References:

1. Evan Dolley, Baekho Lee and R. P. Wei (1999) "The Effect of Pitting Corrosion on Fatigue Life", submitted to *Fatigue & Fracture of Engineering Materials & Structures*.
2. C.L. Harmsworth (1961) "Effect of Corrosion on the Fatigue Behavior of 2024-T4 Aluminum Alloy". *ASD TR-61-121*, Aeronautical Systems Division, Wright Patterson Air Force Base, Ohio, 1-29.
3. D. G. Harlow and R. P. Wei (1994) "Probability Approach for Prediction of Corrosion and Corrosion Fatigue Life". *American Institute of Aeronautics and Astronautics* **32**, 2072-2079.
4. R.P. Wei (1997) "Corrosion Fatigue-Science and Engineering". *Proc. of Recent Advances in Corrosion Fatigue*, 16-17 April (to appear).
5. AFGROW Life Prediction Software, (1998); (available from the following web site: <http://fibec.flight.wpafb.af.mil/fibec/afgrow.html>).

9.6.5 An Engineering Crevice Corrosion Model In KC-135 Lap Joints

Marina Altynova

NCI Information Systems, Inc.

At the present time there is no fundamental scientific model of the crevice corrosion within a lap joint. Moreover, the conditions inside these joints are too poorly understood to allow quantitative determination of the evolution of the corrosion rate and type given input conditions such as the environment to which aircraft is exposed.

An engineering model for the corrosion growth predictions inside the aircraft lap joints is proposed. It uses the probabilistic approach, where initial corrosion damage and corrosion rates for certain environmental conditions are used in the form of Weibull Probability Density functions.

The engineering approach uses as input:

1. Information of initial corrosion condition of the aircraft from Non-Destructive Inspection (eddy current technique), Figure 68.
2. The corrosion rates distribution obtained from SQUID (Superconducting Quantum Interference Device) that measures the magnetic fields induced by the corrosion currents within the lap joint exposed to the certain environment (chloride concentrations, humidity, temperature, etc.), Figure 69.

The model allows predicting corrosion damage of the aircraft after a period of time Δt since NDI spent in specific environmental condition, for which the corrosion rate information is known.

Mathematical model implementing this engineering approach has been developed by NCI. It uses as input:

1. NDI results in the form of distribution function $NSD(h)$ (Number of Sites of given Depth), Figure 70.
2. Corrosion Rate information for given environmental condition in the form of distribution function $FOR(p)$ (Frequency of Occurrence Rate), Figure 71.

The output of the mathematical model is information about corrosion condition after time period Δt in given corrosion conditions in the form of distribution function $PNSD(h)$ (Predicted Number of Sites of given Depth), Figure 72.

This function $PNSD(h)$ is a result of convolution of two input functions:

$$PNSD(h_f) = \int_{p=0}^{p=\frac{h_f}{\Delta t}} NSD(h_f - p * \Delta t) * FOR(p) dp \quad (1)$$

Probability distribution function $PNSD(h_f)$ carries all the information about predicted corrosion condition in the lap joint after time Δt . An example of calculated $PNSD$ of final pits distribution of the KC-135 lap joint after 10,000 hours in 2.0 M Cl⁻ solution is shown in Figure 72.

User-friendly VB applications program has been developed that uses both functions as input and produces solutions for different specific problems about future corrosion damage of the lap joint, see Figure 73.

References:

1. "SQUID Measurements of the Rate of Hidden Corrosion", presented at the Corrosion Fatigue and Corrosion Predictive Modeling Technical Interchange Meeting, NCI/USAF, Dayton, (May 1998)
2. FINAL REPORT FOR CORROSION/FATIGUE EFFECTS ON STRUCTURAL INTEGRITY (CONTRACT NO. F09603-97-C-0349, TASK ORDER 9128 CDRL No. A001) submitted by NCI Information Systems, Inc.

9.6.6 Corrosion Fatigue Predictive Modeling With Pit Depth As A Controlling Factor

D.W. Hoepfner and V. Chandrasekaran

University of Utah

Since October 1997, FASIDE International Incorporated, Salt Lake City, Utah has been performing research related to modeling corrosion growth on aircraft structure for the NCI Information systems, Fairborn, OH. As a part of this program, an experimental study was conducted to characterize corrosion damage quantitatively in relation to fatigue life of 2024-T3 aluminum alloy specimens. The primary focus of this study was to correlate corrosion "damage" using pit depth as a controlling factor with the fatigue life of prior corroded 2024-T3 aluminum alloy specimens. It is believed that pit size in terms of pit depth has an important role in crack nucleation. Under fatigue loading conditions, "small" cracks nucleate from pits reducing the residual strength and fatigue life of the materials.

Corrosion pits were artificially produced on 2024-T3 aluminum alloy specimens. The depth of pits was varied by changing the exposure time of the specimens in solution. Prior to testing, the confocal microscope was used to quantify the depth of pits that were artificially produced on 2024-T3 aluminum alloy specimens. A pit depth in the range from 35 to 230 μm was obtained on the corroded area of the specimens. Then, the range of pit depth was correlated to the fatigue life of prior corroded aluminum alloy specimens. The summary of the results from fatigue experiments that were conducted on prior pitted 2024-T3 aluminum alloy specimens is presented below.

In general, the greater the range of pit depth, the lower the fatigue life of the specimens. An analysis of the photographs of fracture surfaces was conducted and it revealed that fatigue cracks always nucleated from the corrosion pits and propagated to fracture. In addition, an extensive fractographic study was conducted and the analysis of the fracture surfaces revealed that cracks propagated deeper from the pitted area when compared to the uncorroded area of the specimens. During fatigue testing numerous "small" surface cracks from corrosion pits as well as from uncorroded area of the specimens were observed. However, the analysis of fracture surfaces clearly showed that fatigue cracks nucleated from corrosion pits propagated deeper into the specimen subsurface when compared to cracks nucleated from uncorroded areas. Also, the fractography results indicated that fatigue cracks that nucleated from the corroded area resulted in the final fracture of the specimens. This observation was supported by

the appearance of fatigue striations and secondary cracks on the fracture surface corresponding to the prior corroded area of the specimen.

Moreover, the SEM analysis of fracture surfaces clearly showed that fatigue cracks that formed from an uncorroded area of the specimens had a negligible effect on the fatigue life of the prior corroded 2024-T3 aluminum alloy specimens. In other words, cracks that nucleated from an uncorroded area of the specimens remained as surface cracks and did not propagate further into the specimen thickness. This observation was supported by the fractographic analysis as the characteristic features of fatigue fracture were not seen on the fracture surfaces corresponding to the uncorroded area of the specimens.

Finally, a fatigue life estimation model for prior-pitted 2024-T3 aluminum alloy specimen was presented incorporating the quantified pit depth. The estimated fatigue life of prior-pitted 2024-T3 specimens was found to correlate fairly well with the experimental results.

9.6.7 A Life Prediction Methodology for Evaluating Corrosion-Fatigue Interactions **Craig L. Brooks, Scott Prost-Domasky, and Kyle Honeycutt** **Analytical Processes / Engineered Solutions**

A versatile engineering approach has been formulated to include real time age degradation environments in structural service life analyses. The initial application predicted the influence of corrosion on the fatigue life capability of a typical fuselage lap joint. The analyses used fracture mechanics methods and fundamental engineering principles. The primary steps in the lap splice assessment were:

- Determine the initial “as-built” quality condition of the structure and basic material for the initial starting condition;
- Formulate multi-site damage (MSD) models and scenarios;
- Model the effects of micro/macro surface topography changes in time due to corrosion growth;
- Include the time dependence of any mechanically induced deflections due to corrosion by-products (corrosion pillowing) and effects of material loss;
- Juxtapose and superimpose corrosion effects with cyclic fatigue crack growth using the appropriate environments; and
- Select the appropriate residual strength method and failure criteria

Crack growth life analyses were performed to isolate each of the variables to show the relative life impact of each of the corrosion metrics. The effects of initial quality states (Reference 1), corroded surface topographies, corrosion-induced pillowing (Reference 2), and multi-site damage in lap joints are included, as illustrated by Figures 74-78. For example, typical surface topographies created by real time in-service corrosion in a lap joint were evaluated. The local stress amplification due to the corrosion roughness reduced the localized crack growth capability of a surface crack by 70%. The impact of sustained stresses caused by corrosion by-product build-up (pillowing) in a lap joint degraded structural life 25 to 35% for a crack adjacent to a fastener hole. These results represent the level of potential life degradation that could be realized in corroded regions. Analysis results emphasize the need to include corrosion parameters in a component service life assessment, as shown by Figure 79.

A simulation of a pressurized fuselage skin splice was used to illustrate the analytically derived impact to the life and safety of the joint in the presence of corrosion, thus demonstrating the synergistic effects of cyclic fatigue and the corrosion effects described above. The analysis included time-dependent effects of corrosion into the structural life prediction for a multi-site damage (MSD) scenario. Twenty and fifty year corrosion assumptions were used based upon conditions found in existing aircraft. Figure 80 shows the results of this “whole shebang” scenario relative to the traditional damage tolerance analyses that would be used to maintain the structure. Although this scenario uses conservative assumptions, it does represent a lower bound. These results indicate that this location should be identified as a potential safety issue. Corrosion effects are both interdependent with and independent of the cyclic domain and the synergistic effects of the two are problem specific. More detailed results of this approach can be found in Reference 3. This effort was performed for the USAF Corrosion Program Office to support their efforts for quantifying the effects of corrosion on the integrity of the aging aircraft fleet.

References:

1. C. L. Brooks, S. Prost-Domasky, and K. Honeycutt, "Determining the Initial Quality State of Materials", Proceedings of the 1998 USAF Aircraft Structural Integrity Program Conference, San Antonio, Texas, December 1998.
2. Komorowski, J.P., N.C. Bellinger and R.W. Gould. "The Role of Corrosion Pitting in NDI and in the Structural Integrity of Fuselage Joints", Proceedings of the 19th Symposium of the International Committee on Aeronautical Fatigue, 16-20 June 1997, Edinburgh.
3. C. L. Brooks, S. Prost-Domasky, and K. Honeycutt, "Corrosion is a Structural and Economic Problem: Transforming Metrics to a Life Prediction Method", Proceedings of the NATO RTO's Workshop 2 on Fatigue in the Presence of Corrosion, October 1998, Corfu, Greece. (Access to these papers are available through www.APEsolutions.com under "Links")

9.6.8 Joint FAA-Air Force Corrosion Fatigue Interaction Research Program

Dr. Thomas Flournoy

FAA William J. Hughes Technical Center

The problems of corrosion and fatigue associated with aging aircraft are common to both civilian and military aircraft. The interaction of pre-existing corrosion with fatigue is being examined by testing fuselage panels supplied by the US Air Force obtained from disassembly of retired Boeing 707 and C/KC-135 airplanes.

Both fatigue and static strength tests are being done on the FAA Aging Aircraft Test fixture located at and operated by Foster-Miller, Inc., under contract with the Volpe National Transportation Systems Center. The test fixture accommodates panels that are approximately 10 feet in length by 6 feet along the circumference with a 74-inch radius of curvature. Prior to the current test program, only laboratory panels had been tested in the fixture. The work in progress demonstrated that panels from actual aircraft can be tested in the fixture.

Various nondestructive inspection (NDI) techniques are being applied to the panels before testing to detect any hidden corrosion or fatigue cracking from in-service usage. These methods include thermal wave imaging, magneto-optic imaging, D-sight, pulsed eddy current, and ultrasonics. These NDI methods will be validated by panel teardowns after the test program is completed.

To date fatigue testing has been completed on two Boeing 707 panels taken from the same airplane. The airplane had been in service for 23 years and accumulated 22,071 flight cycles and 77,742 flight hours. One panel was taken from a location forward of the wing and had a nominal skin thickness of 0.040 inch. The other panel was taken at a location aft of the wing and had a skin thickness of 0.062 inch. Both panels were tested in fatigue with pressures varying from 1 to 9.5 psi.

The first panel tested, the panel with the thinner skin, was characterized as having light corrosion by the NDI techniques. The first fatigue crack was found after 36,000 fatigue cycles. Linkup of two adjacent cracks occurred after 47,500 cycles. Linkup of several adjacent cracks occurred after 48,616 cycles resulting in a single crack length of over 14 inches in length. At this point, fatigue cycling was stopped and a static residual strength test was performed. The internal pressure was increased at a rate of 0.2 psi per second from 0.5 psi until panel failure occurred at 13 psi. The residual strength test revealed that the tear straps provided sufficient crack arrest capability to create a safe decompression during failure as shown in Figure 81.

The remaining panels will be inspected using the NDI techniques to detect any corrosion or cracks prior to testing and then tested in a similar manner to the first panel. The fatigue and residual strength tests on all the panels will be completed by the end of 1998.

POC: Dr. Thomas Flournoy, AAR-430, FAA William J. Hughes Technical Center, Atlantic City International Airport, NJ 08405, (609) 485-5327.

9.6.9 Corrosion Monitoring of Field Sites

W.H. Abbott

Battelle-Columbus

Work has been in progress for several years to directly measure the corrosive severity of a variety of military bases worldwide. This work is being done for several reasons. One is to provide a test for current mathematical models which attempt to predict corrosion rates based on available environmental data. A second is to provide “hard” data on a number of relevant materials and in the process gain additional knowledge about the base environments. The latter refers, in particular, to data relating to total reactive chlorides and/or humidity levels which are recognized to be major “drivers” of corrosion processes. A third reason, has been to develop and validate simple, inexpensive, and reliable methods for obtaining such data.

To date about 50 bases have been monitored over a 1 year period with results obtained on a quarterly schedule. This work has proceeded smoothly and with no apparent problems to affect data quality. As a result, corrosion rate data have been obtained on copper, two grades of aluminum, and steel. One additional material, silver, has been used as a unique chloride monitor.

The results have shown that the absolute severity levels of military bases monitored to date differ by a factor of about 150:1 for aluminum and even more for steel. Initial attempts have been made to relate these values to actual effects reported on aircraft such as corrosion related maintenance actions. Such a correlation appears to exist and with a relationship showing a very rapid increase in such actions with increasing severity.

The work has shown a good and somewhat surprising correlation among the corrosion rates of this diverse matrix of materials. This is significant, since this knowledge has been developed into an additional check on data quality and has provided a basis in the future for further simplification of monitoring procedures.

New and important data have been developed on chloride levels in the base environments. It has been learned that chlorides (possibly in various forms) are ubiquitous and have been found at virtually every base studied to date. This includes both coastal and inland locations. These data have shown a good correlation between average chloride levels and corrosion rates with two important conclusions. One is the very low levels of chloride coupled with humidity necessary to produce severe corrosion even at some inland locations. The second is that the “prediction” of chloride levels is not a simple matter and one which may not be simply related to distance from ocean sources. From current data, average chloride levels appear to vary by a factor in excess of 300:1 at military bases worldwide.

Finally, tests have been made between these actual corrosion rate data and currently available models/algorithms. The agreement between these results has been poor. In particular current models appear to underestimate severity for those bases in the more severe environments. The reasons for this are being examined. One possible reason is inadequate environmental data necessary for such calculations.

9.6.10 An Environmental Corrosion Severity Index For USAF Airbases

DR. Robert Summitt & Dr. C. T. Lynch

RSC&L, Inc.

Environmental data are used to compute a numerical Environmental Severity Index (ESI), normalized to the most severe environment. Published equations derived from exposure tests were utilized to develop the algorithms for computation. Accuracy and validity of the underlying equations were demonstrated using experimental data from the open literature. Algorithms are of a general nature, and may be applied to any location for which data are available. The environmental corrosivity may be described in terms of a few of the factors that effect corrosion, including water, oxygen, and temperature, which are necessary for corrosion; and chloride ion, sulfur dioxide, and nitrogen oxides, which accelerate corrosion. The computed ESI values are for four alloy base metals, zinc, aluminum, steel, and copper. Extension to another alloy is accomplished by comparing its corrodibility to that of these metals. Environmental data have been compiled for the more than 150 worldwide USAF, AFRES, and ANG bases, and ESI values were computed for each of them. Documentation is provided so that the basic algorithms can be modified to meet future requirements. The resulting indexes are compared with corrosion damage from testing programs and with aircraft maintenance experience. The results show that the location specific Environmental Severity Index can be used as part of the assessment program in establishing maintenance requirements.

9.6.11 Evaluation and Quantification of Fretting Fatigue Induced Damage

D.W. Hoepfner, V. Chandrasekaran, Young In Yoon and A.M.H. Taylor
University of Utah

Fretting fatigue experiments were conducted on 7075-T6 and 2024-T3 Aluminum alloy specimens. The primary objective of this study was to quantitatively characterize fretting damages that resulted on the fatigue specimens. Fretting fatigue experiments were performed in laboratory air at various maximum fatigue stress levels at a constant normal pressure. From the confocal microscopy analysis of fretting damages, it was observed that fretting-generated *multiple cracks* on the faying surface could be responsible for the fracture of 7075-T6 aluminum alloy specimens (see Figure 82) where as the fracture of 2024-T3 aluminum alloy specimen could be attributed to fretting-generated *multiple pits* on the faying surface (see Figure 83). From the results, it is proposed that fretting nucleates damages of different nature depending on the material microstructure as well as its composition and the methods to alleviate fretting should consider issues pertaining to a specific material.

In addition, fretting damages were quantified in terms of material removal by characterizing the depth as well as the geometry of fretting-generated pits on the faying surface of the specimen. Pit size in terms of pit depth (P_d), pit area (P_A), and pit dimension perpendicular (P_{Dy}) as well as parallel (P_{Dx}) to the applied load also were quantified. The quantified fretting-nucleated pits revealed a fair correlation between the pit depth and the area of the pits (see Figure 84).

Our recent research to characterize the effect of prior-corrosion damage on cold-expansion hole is briefly stated below.

9.6.12 Effect of Prior-Corrosion Damage on Cold-Expansion Hole

D.W. Hoepfner, V. Chandrasekaran, Young In Yoon and A.M.H. Taylor
University of Utah

The process of cold expansion of rivet holes has proved to improve the fatigue performance of airframe structural joints. However, as aircraft age, the process of corrosion and corrosion fatigue are expected to affect the integrity of the cold-expanded rivet holes. Therefore, a research program is being performed in conjunction with the Fatigue Technology Incorporated (FTI) to quantitatively characterize the effect of corrosion damage on the nucleation and propagation of "short" cracks from prior-corroded 2024-T3 and 7075-T6 aluminum alloy specimens with cold-expanded holes.

Concluding Remarks

At the ICAF'99 symposium three papers will be presented in detail with the results generated from the above mentioned research programs.

9.6.13 Corrosion Fatigue Structural Demonstration

D.W. Hoepfner and A.M.H. Taylor
University of Utah

QIDEC, along with other subcontractors, is working with Lockheed-Martin Aerospace Systems on a program to model the interaction of corrosion and fatigue on aircraft as part of the Aircraft Structural Integrity Program. This work will lead in the end to a software to be used to corrosion fatigue behavior of aircraft structure.

QIDEC and the other team members have just begun this effort. Further progress is envisioned throughout 1999.

9.6.14 Computerized Model for Lap Joint Corrosion Prediction
Dr. Xuejin Zheng
NCI Information Systems, Inc.

In a project to assess corrosion/fatigue effect on aging aircraft for the USAF, a computerized model was developed to calculate corrosion growth inside lap joints of KC-135 aircraft. The computerized model is a probabilistic/engineering model developed by NCI Information Systems, Inc. A corrosion damage distribution ($NDS(h_{t_0})$) is obtained from the most recently non-destructive inspection (NDI), and a distribution of corrosion growth rates ($FOR(r)$) for a given environment is obtained by Superconducting QUantum Interference Device (SQUID) measurements. This given environment is related to USAF base(s) through environmental severity indexes (ESIs) which were developed by NCI. The model assumes that for any spot inside lap joints exposed to a given environment, the probability of the corrosion growth rate at the spot is determined by the distribution of corrosion growth rates in the environment, i.e., a predicted corrosion damage distribution ($PNDS(h_t)$) at time t given by:

$$PNDS(h_t) = \int_{r=0}^{\frac{h_t}{t-t_0}} FOR(r) \bullet NDS(h_t - r(t-t_0)) dr$$

where t_0 is the time when the most recently NDI was conducted, r is the corrosion rate and h_t is the corrosion thickness loss at time t . Two-parameter Weibull functions have been used for representing the distributions of corrosion damage and corrosion growth rates. Because of mathematical complexity of the integration above, the integration has to be solved numerically. A Microsoft Visual Basic program has been developed not only carrying out the numerical integration, but also incorporating a corrosion database of the ESI for virtually all the USAF bases and corrosion growth rate distributions. The main content and functionality of the program include the following:

- (1) data input: entering aircraft tail number, MDS number, lap joint materials, corrosion damage distribution parameters from NDI, etc. into the specimen database (or directly entering them on the deployment plan screen, and entering deployment plan on the deployment plan screen,
- (2) accessing the databases: accessing the specimen database and selecting related data and transferring them onto the deployment screen, and accessing the corrosion database to select ESIs for USAF bases according to the deployment plan, and then select the corrosion growth rate parameters according to the lap joint materials and ESIs; all the corrosion related data are listed on the corrosion parameters screen,
- (3) PNDS calculation: carrying out the numerical integration to obtain $PNDS(h_t)$,
- (4) reliability calculation: calculating a critical thickness loss based on the maximum probability of corrosion failure which the user can withstand,
- (5) results output: PNDS and cumulative distribution of PNDS, as well NDS and cumulative NDS, are tabulated and graphically shown on screen, and the data can be save as a binary file,
- (6) cost assessment of corrosion:¹ calculating costs of corrosion based on the user's choice of maintenance policy and the best maintenance policy (i.e., with the lowest cost) based on Markov's model.

To enhance the program, a specimen database for lap joint specimens was recently integrated into the program. The specimen database can store aircraft information, including tail number, MDS number, deployment history, TCTO, PDM, and visual and NDI results for specimens. These data can be transferred to data input for corrosion growth prediction.

Figure 85 shows the flowchart of the computerized model design, and Figures 86-90 are some screens of the model.

¹ Corrosion Cost Model

9.6.15 Corrosion Fatigue Structural Demonstration Program
Mr. Clare Paul
Air Force Research Laboratory

The objective of the Corrosion Fatigue Structural Demonstration program is to develop, verify, apply, and demonstrate analytical techniques that include the effects of corrosion and cyclical fatigue on aircraft structural integrity. Once developed, these techniques will be applied to primary and secondary structural components of aging aircraft to aid in determining inspection intervals, remaining structural life, and residual strength.

In this effort, a short term concentrated evaluation and planning study will be conducted early in the program to assess the availability and maturity level of existing analytical techniques, and to select the baseline structural component(s) for demonstration of the techniques. Thereafter, a series of structural element and sub-component tests will be conducted that are representative of in-service aircraft subject to a corrosion/fatigue environment. These tests will then be used to develop analytical models and to correlate predictions with in-service results. Once analytical techniques are verified on a sub-component basis, the capability of the developed model will be validated through a final demonstration test(s) of structural component(s).

The intent of this effort is to enhance engineering support of aging aircraft structures by developing tools to predict the effects of corrosion on structural integrity. For example, instead of immediately fixing corrosion damage if it is found, the maintenance engineer may determine that maintenance actions may be deferred until the next programmed depot maintenance cycle. These tools will influence the timing and extent of the inspections and repairs/modifications required by the force structural maintenance plan. Thus, lower sustainment costs, less downtime and improved readiness will result from the development and use of these tools.

9.7. PROBABILISTICS AND RISK ASSESSMENT

9.7.1 Probabilities of Occurrence and Detection of Damage in Airframe Materials

R.P. Wei

Lehigh University

Airworthiness, in a structural context, requires the assurance of continued structural integrity and safety of an aircraft throughout its planned period of operation from its current state to the next scheduled inspection and maintenance (Figure 91). Its accurate assessment depends critically on the development of a quantitative methodology that integrates information from state-of-the-art nondestructive evaluation (NDE) with validated methods for prediction of damage accumulation and structural integrity assessments. The mechanistic aspects of damage accumulation and the probabilistic aspects of its evolution and distribution are not adequately addressed in current methodologies. The criticality, or structural significance, of damage in relation to its probability of detection (PoD) by NDE techniques is not well established.

As a part of the research at Lehigh University, the issue of probability of occurrence (PoO) of damage versus PoD was addressed, and an approach and methodology for predicting the PoO of damage was developed. A simplified mechanistically based probability model for localized (pitting) corrosion and corrosion fatigue crack growth was used to illustrate the critical functions of modeling and detecting structural damage. The model facilitates the prediction of the evolution and distribution, and the PoO of damage in terms of their size, geometry and location. Experimental data on pitting corrosion and fatigue crack growth for a 2024-T3 aluminum alloy were used for estimating the PoO of damage in an open-hole specimen subjected to typical fuselage pressurization-depressurization stresses.

Typical results on damage evolution, with and without corrosion, are shown in Figure 92, and the PoO of damage are compared with a typical PoD curve for eddy-current inspection in Figure 93. These results show that the service lives are significantly reduced by early corrosion damage. They serve to highlight the dichotomy between the probability for damage accumulation and its detection, in that the PoD is too low for structurally significant corrosion and early fatigue damage. In its current usage, the PoD simply represents the probability for detecting the existence of damage above a given size. PoD in the fullest sense, however, is much more complex, and must include information on size, geometry and location of damage, and it must account for the dependence on inspectors and techniques. In other words, the fatigue life is compromised by the presence of corrosion at a scale level that is 10 to 50 times smaller than current NDE capabilities. To take advantage of that fatigue life reserve, an aggressive stance in terms of corrosion prevention and protection must be taken. Otherwise, early detection and intervention of very small damage must be facilitated. In the latter instance, the PoD needs to exceed 90% for damage sizes that are 10 to 50 times smaller than the current level of 1 to 2 mm; *i.e.* at about 0.1 mm. In either case, the ability to provide accurate NDE measurements of damage sizes is essential for making reliable airworthiness assessments.

The study showed that the proposed methodology facilitates the prediction of the evolution and distribution, and the PoO of damage in terms of their size, geometry and location. It can serve as a basis for quantitative estimations of the distribution of damage for use in WFD analyses to replace the more *ad hoc* approaches used heretofore. It is clear that current state-of-the-art NDE methods are not adequate for detecting damage at the sizes that can significantly affect life prediction and reliable assessment of airworthiness. It is recognized that both modeling and detection of damage need to be substantially improved in the development of effective tools for airworthiness assessment and fleet management. Because of the importance of corrosion in aging aircraft and because corrosion damage is not clean, accurate NDE measurements are a challenge, especially in detecting corrosion damage underneath a rivet head or in the second and third layers of a typical joint.

References:

1. R.P. Wei, C. Li, D.G. Harlow and T.H. Flournoy (1998). Probability Modeling of Corrosion Fatigue Crack Growth and Pitting Corrosion. *ICAF97: Fatigue in New and Aging Aircraft*, vol. 1. R. Cook and P. Poole, eds. London: Engineering Material Advisory Services Ltd., 197-214.
2. A.P. Berens (1989). NDE Reliability Data Analysis. *Nondestructive Evaluation and Quality Control, Metals Handbook 9th Ed.*, Vol. 17. ASM International, Metals Park, OH, 689-701.

3. F.W. Spencer and D. Schurman (1995). Reliability Assessment at Airline Inspection Facilities Volume III: Results of an Eddy Current Inspection Reliability Experiment. DOT/FAA/CT-92/12, III.
4. R.W. Hyatt, G.E. Kechter, and R.G. Menton (1991). Probability of Detection Estimation for Data Sets with Rogue Points. *Mater. Eval.* 49, 1402-1408.
5. C.-M. Liao (1997). Particle Induced Pitting Corrosion of Aluminum Alloys. Ph.D. Dissertation, Lehigh University.
6. D.G. Harlow and R.P. Wei (1994). Probability Approach for Prediction of Corrosion and Corrosion Fatigue Life. *AIAA J.* 32, 2073-2079.
7. G.S. Chen, K.-C. Wan, M. Gao, R.P. Wei and T.H. Flournoy (1996). Transition from Pitting to Fatigue Crack Growth - Modeling of Corrosion Fatigue Crack Nucleation in a 2024-T3 Aluminum Alloy. *Mater. Sci. & Engng A* 219, 126-132.
8. D.G. Harlow and R.P. Wei (1998). A Probability Model for the Growth of Corrosion Pits in Aluminum Alloys Induced by Constituent Particles. *Engng Fract. Mater.* 59, 305-325.
9. A.P. Berens, P.W. Hovey and D.A. Skinn (1991). Risk Analysis for Aging Aircraft Fleets: Volume 1 - Analysis. USAF WL-TR-91-3066.

9.7.2 Fatigue Variability and Life Prediction: A Probabilistic Approach

B.M. Hillberry

Purdue University

In aging aircraft structures, the remaining life and its corresponding variability are of particular interest for risk analyses and remaining life computations. The equivalent initial flaw size (EIFS) approach has been used to determine an equivalent distribution of initiating flaw sizes, however, determining the distribution is very time consuming. Newman, et al. (1) in the AGARD studies observed that in aircraft structural materials, cracks formed at constituent particles very early in life. In our work we have also found that the cracks form at these particles and in addition the size of the particle can be considered to be the size of the initiating flaw (semicircular for surface crack). By measuring the particle sizes on the crack growth plane (3800 plus particles measured with a scanning electron microscope using IMIX software) and assuming that the initiating flaw is a semi-circular crack with an area equal to that of the particle, a distribution of initiating equivalent flaw sizes inherent to the material is obtained. This distribution closely fits a log-normal distribution function. Using this initiating distribution, a crack growth model that accounts for short and long crack growth behavior (FASTRAN II, Newman (2)), and a Monty Carlo simulation, the fatigue life and its variability is predicted. The prediction is illustrated as a cumulative distribution function (CDF) that characterizes the fatigue lives and associated variability. To verify the model, single edge notched specimens, similar to those used in the AGARD study, were tested (3). Fatigue cracks formed in the notch at the inclusion particles and the lives were measured as the cycles to grow the crack to a through-the-thickness length. The predicted lives and associated life variability showed excellent agreement with the experimental results. The model has been validated with our test results and AGARD test results at three different stress levels with 2024-T3 aluminum alloy, and our test results of 7075-T6 (3,4). Further verification included measuring the size of the actual particles that initiated fatigue cracks. As expected, the initiating particles were from the tail of the log normal distribution.

The probabilistic model has also been used to predict the remaining fatigue life of corroded 2024-T3 aluminum alloy (5). The distribution of pit sizes, that was assumed to be the initiating flaws, fit the Gumbel extreme value distribution. The model closely predicted experimental results and the cracks were observed to form at the pits, demonstrating that the pits were the initiating sites.

The model provides a probabilistic approach for predicting the fatigue lives by means of comparing the CDF. It can be readily incorporated into risk analyses. The model can be used with either a Monty Carlo simulation or conditional probability. The model has been incorporated into an open hole multi-site-damage model for predicting failure probability.

References:

1. Newman, J.C., Jr., and Edwards, P.R., "Short Crack Growth Behavior in an Aluminum Alloy - An AGARD Cooperative Test Programme," AGARD Report No. 732, 1988.
2. Newman, J.C., Jr., FASTRAN II Manual, NASA TM No. 104159, 1992.

3. Laz, P.J., and Hillberry, B.M., "Fatigue Life Prediction from Inclusion Initiated Cracks, International Journal of Fatigue, Vol. 20, pp. 263-270, 1998.
4. Gruenberg, K.M., Craig, B.A., and Hillberry, B.M., "A Probabilistic Method for Predicting the Variability in Fatigue Behavior of 7075-T6 Aluminum," AIAA-98-2055, Proceedings, 39th AIAA/ASME/ASCE/AHS/ASC Structures, Structural Dynamics and Materials Conference, pp. 2965-2975, Long Beach, CA, April 1998.
5. Zamber, J.E., and Hillberry, B.M., "A Probabilistic Approach to Predicting Fatigue Lives of Corroded 2024-T3," AIAA-982054, Proceedings 39th AIAA/ASME/ASCE/ASH/ASC Structures, Structural Dynamics and Materials Conference, pp. 2976-2984, Long Beach, CA, April 1998.

9.7.3 Probabilities of Occurrence – Model Estimation versus Field Measurement

R.P. Wei

Lehigh University

The reliability of airworthiness assessment and management of fleets of aircraft depend critically on the quality of tools for predicting damage nucleation and accumulation and its detection (*i.e.*, on the probabilities of occurrence and detection), and the accuracy of the information on damage size provided by nondestructive inspection. The probability of occurrence (PoO) provides estimates of the size and distribution of damage at future times and is used in assessing an aircraft's airworthiness in the projected future states. The probability of detection, along with information on damage size, provides information for assessing its current airworthiness and serves as a "validated" starting point for estimating its future airworthiness. As a part of the program of research on corrosion and corrosion fatigue of airframe aluminum alloys at Lehigh University, a mechanistically based probability approach has been developed for estimating the PoO of damage. A model has been formulated for one plausible scenario involving localized pitting corrosion and subsequent fatigue crack nucleation and growth. In this study, estimations of the PoO of damage in the lower wing skin of transport aircraft were made and compared to the measurements made from the tear-down of two B707 aircraft that had been in commercial service by the United States Air Force (USAF).

The USAF has elected to convert retired B707 aircraft into E-8C Joint Surveillance Target and Attack Radar System (JSTARS) aircraft. As a part of its structural integrity assessment program, teardown inspections were conducted on two B707 (one 100 series and one 300 series) aircraft that had been in commercial service with a number of carriers worldwide. The left wing of each aircraft was disassembled, and sections of the lower wing skins and stiffeners were inspected. Damage (crack) sizes were measured visually at 20X with the aid of dye-penetrants at fastener holes in the lower wing panels (aluminum alloy 2024-T3) and the companion fastener holes in the stiffeners (aluminum alloy 7075-T6). For this study, focus is placed on the multiple hole-wall crack (MHWC) data collected from the inspection of numerous fastener holes in the wing panels. The measured data, consisting of over 500 individual measurements per aircraft, were analyzed and are shown on Weibull probability plots in Figures 94 and 95.

The evolution of corrosion and fatigue damage in the lower wing skins and stiffeners was estimated from the model by considering the primary loading to be ground-air-ground cycles only, which are adjusted for "average" gust loading, and an estimated average utilization. Reasonable values (including their variance) for the localized corrosion and fatigue crack growth rates, statistically estimated from the data obtained at Lehigh University, were used. The estimated PoO of corrosion and corrosion fatigue damage for each aircraft (solid line) is compared against the measurements in each figure. The PoO from the simple mechanistically based model and the teardown data are in remarkable agreement. Similar comparisons for the stiffeners are being made and will be reported later.

Thus, the efficacy of the approach and its relevancy to airworthiness assessment and fleet life management are demonstrated. It is hoped that these results will encourage further model developments and validation against laboratory and field data.

References:

1. D.G. Harlow and R.P. Wei (1994). Probability Approach for Prediction of Corrosion and Corrosion Fatigue Life. *AIAA J.* **32**, 2073-2079.
2. D.G. Harlow and R.P. Wei (1998). A Probability Model for the Growth of Corrosion Pits in Aluminum Alloys Induced by Constituent Particles. *Engng Fract. Mater.* **59**, 305-325.
3. A. J. Hug (1996). Laboratory Inspection of Wing Lower Surface Structure from 707 Aircraft for the J-STARS Program. Boeing Report D500-12947-1.

9.7.4 Probabilistic Residual Strength Model for Uni-Axial Fatigue of Composites

David J. Thomas and Wieslaw K. Binienda

University of Akron

Composite materials have been moving into applications demanding more precise and reliable fatigue modeling capabilities. This is especially true for ceramic matrix composites that are being envisioned for use in the next generation of high-speed propulsion systems. Recent work has focused on a phenomenologically based fatigue model for uni-axially-loaded composites. The research effort addressed the probabilistic nature of composite life by treating material strength (initial as well as residual) and number of cycles to failure as random variables. The framework established is adaptable to new material and modeling advancements.

The current work was based on a fatigue model originally proposed by Yang and Liu [1]. A Kachanov type rate equation was assumed to govern the strength degradation. The cyclic rate of strength reduction is taken to be inversely proportional to the residual strength raised to the power of some empirical constant. The proportionality factor was posed as two unknown functions (f and g) dependent on the variables of loading. A three-parameter Weibull representation for the initial ultimate strength and for the number of cycles to failure was introduced. Inherent problems of original work have been corrected. Namely, the strength degradation model no longer predicts negative threshold behavior, and the magnitudes of the fatigue parameters are all comfortably within the range of computational accuracy.

As part of the search for the functional forms of f and g the linear representation of $S-N$ data on a log-log plot was examined. In the case of a stochastic material, for each applied load, S , there will be a distribution in the observed fatigue life, N . Adopting a Weibull representation for this data (analogous to the Weibull representation for ultimate strength), a linear relationship can be established between the applied load and the characteristic life. As such, the characteristic life was expressed in terms of the applied load and the two empirical linear curve-fit parameters. Mathematical manipulation of the event statement for the probability that the number of cycles to failure is less than or equal to some value, n , allows for f and g to be evaluated.

With f and g known, the strength degradation law can be finalized, along with the distribution functions for cycles to failure and residual strength. Both of these distribution functions appear in the format of a three-parameter Weibull expression. Additionally, the threshold values predicted by both functions are mathematically always greater than or equal to zero, thus providing physically meaningful answers.

Example results are presented in Figures 96 and 97 for fatigue scatter and residual strength, respectively. Experimental data for a [90/45/-45/0]_s graphite/epoxy material system was taken from the literature [2]. Predicted distribution functions based on the new model, as well as Yang's original model, are presented and compared to ranked experimental data. In the case of the fatigue scatter, the new model appears to have done a better job in matching the ranked data. In addition, the threshold prediction (11,487 cycles) by the new model was both greater than zero, and less than the minimum observed cycles to failure. For the residual strength results, both models return similar results, generally picking up the trend of the data but slightly over-predicting the measured data.

References:

1. Yang, J.N. and Liu, M.D., J Comp Matls, Vol 11, 1977.
2. Yang, J.N., Miller, M.D. and Sun, C.T., J Comp Matls, Vol 14, 1980.
3. Thomas, D.J. and Binienda, W.K., NASA-CR to be published, 1999.

9.7.5 Risk Analysis As A Force Management Tool - Updates

R. P. Bell

Lockheed-Martin

The latest use of our risk analysis methodology is to study whether aging transport aircraft are still failsafe. Most aging civil aircraft were shown to be failsafe by test and analysis during their original design phase. These requirements, both civil and military typically specified an initial damage state that the structure had to sustain;

either at limit load or some percent thereof. The question now becomes whether these aircraft can still meet these failsafe criteria after being in service for up to 40 years.

The FAA Aging Aircraft Program has continued to look at the effects of multi-site damage along longitudinal splices caused by fatigue. Our approach is to assume that this initial damage state can come into being at any time during the life of the aircraft. This damage can be caused by engine debris from an unconfined engine explosion, ground incidents that are unreported, battle damage, fatigue or other unanticipated events. In any case, this initial damage state is not just due to fatigue cracking, and it may be unconservative to assume this to be the case.

The risk analysis method used for this calculation uses standard inputs. These inputs are a master crack growth curve; a probability of detection curve for the Non Destructive inspections used on the aircraft; a loads/probability curve per flight hour; and an initial flaw size distribution. Using these inputs, the probability that the loads exceed the strength at a given point in time can be calculated. For standard distributions, this calculation can be done using simple equations such as Normal, Lognormal or Weibull distributions. Data for these inputs is fairly well defined except for the initial flaw distributions. Work continues on defining and estimating these parameters so that meaningful calculations can be performed.

In summary, our method is as follows:

- 1) Given that an initial damage state exists in the aircraft structure.
- 2) Calculate the probability that the adjacent structure will not fail at any point in time though out the life of the aircraft and remove aircraft from service when this value is unacceptable.

9.7.6 Reliability Management for Structural Certification and Life Extension.

Margery Hoffman and Paul Hoffman
Naval Air Systems Command

Structural reliability assessment methods are being developed to aid program managers in making decisions for life extension and fleet management. A systematic approach is needed by the US Navy to make consistent optimal decisions with respect to structural life goals, especially in light of reduced and stretched out acquisition programs. The need to quantify the risk of decision alternatives in engineering programs is critical. This program is a preliminary study in the development of prototypical methodologies to define, calculate and quantify reliability. The promising methodologies will then be expanded to functional tools for future fleet tracking and management.

As the initial step, a basic model was assembled to calculate the probability of crack initiation and fast fracture at fatigue critical locations on naval aircraft. Probabilistic crack initiation and probabilistic crack growth were combined into a probabilistic total life model. (Figure 98) The approach was demonstrated on a single location in a single component. Results were compared to fleet findings of cracks. Results can be used to schedule component replacement and order additional parts for inventory.

The F-5E aircraft was selected for demonstrating the model because it is a relatively controlled population and many of their upper cockpit longerons have cracked. The part replacement requires a long lead-time (over one year), so a projection of how many may crack in upcoming years is beneficial to the program manager. A generic fastener hole in the longeron was selected as the representative case. The repair options were enumerated as component replacement after a selected number of flight hours, inspect and replace, or delay and replace. The probabilities of failure for the uncracked and unrepaired longerons were computed with existing algorithms. The research demonstration was the formulation of the prototypical example for exhibiting the applicability of the algorithms. The product was the enumeration of the probability of the failure in various practical forms for the repair decision.

9.8. JOINTS

9.8.1 3-D Finite Element Modeling Of Cracked Mechanically Fastened Joints

Y. S. Kwon and J. E. Ingram
Lockheed-Martin

Existing stress intensity (K) solutions for cracks in multiple fastener joints, such as fuselage skin splices and wing chordwise joints do not account for fastener force redistribution as a lead crack extends from one fastener hole to the next. Using engineering judgment, crack growth analysts have typically considered the load transfer effect on K only for the loaded hole at the crack origin, and assumed that the load transfer was zero after the crack extended to the adjacent hole(s), or to a free edge. This assumption followed the reasoning that the local stiffness of the attachment dropped so severely, due to the cracked hole, that no appreciable load transfer could occur. An additional shortcoming in existing solutions for multiple fastener joints, is the absence of information regarding the contribution to K from the fastener force ahead of the crack. Further, an increased load develops at this “next” fastener as a result of load shedding in the “wake” of the crack that has never been quantified or accounted for. Without this load redistribution information, the normal procedure has been to treat the next fasteners as open holes. Recently, there has been an additional need to account for these effects because of the possibility that multiple site damage (MSD) may exist in the skin splices. Accurate K solutions are needed for MSD-cracked skin splices to improve the accuracy of predicting the time to onset of widespread fatigue damage and the effect on residual strength.

Detailed three-dimensional solid element models are being used to analyze skin splices with multiple site damage. The models are developed in a parametric language using the Lockheed Martin DIAL code to facilitate analyses of numerous crack shapes and sizes. The parametric models will be created for various configurations of skin splices (2-row, 3-row, single and double shear, etc.). Accurate fastener force redistribution and the effect on the K solutions at each crack is accomplished by using interface (contact-type) elements at all bearing surfaces. The lead and MSD cracks in the models are quarter-elliptical corner cracks (as shown in Figure 99) as well as through-the-thickness cracks. The 3D Virtual Crack Closure Technique (3DVCCT) [1] is used to calculate K along the crack front.

Reference:

1. Shivakumar, K. N., Tan, P. W., and Newman, J. C., Jr., “A Virtual Crack-Closure Technique for Calculating Stress Intensity Factors for Cracked Three Dimensional Bodies,” International Journal of Fracture 36, 1988.

9.8.2 Analysis Tools for Durability and Damage Tolerance Analysis on Riveted Lap Joints

Dale A. Cope, Pat S. Johnson, Joe J. Luzar, Angela Trego and Jerry D. West
Boeing

Two specific concerns that could affect safety limits for aging aircraft are the effects of corrosion damage and widespread fatigue damage (WFD) on structural integrity. A common joint in fuselage structure is the riveted lap joint, which overlaps two fuselage skin panels. This design creates complex loading conditions that require various analysis methods for accomplishing a durability and damage tolerance (DaDT) analysis. Under an Air Force research project, Boeing evaluated the capabilities of several advanced analysis tools for assessing these effects on the structural integrity of riveted lap joints (see references 1 through 4). Boeing evaluated existing structural analysis tools (Figure 100) capable of performing stress analysis, fatigue crack growth analysis, residual strength analysis, and risk assessment. The advanced structural analysis tools that were evaluated included

- Finite-element code, FRANC2D/L, for determining stress distributions and stress intensity factors of cracks
- Crack growth analysis code, AFGROW, for estimating fatigue crack growth life
- Finite element codes, FRANC2D/L and FRANC3D/STAGS, for predicting residual strength
- Risk analysis code, PROF, for determining the probability of cracking.

These existing structural analysis tools were evaluated for their capabilities to address crevice corrosion and multiple site damage (MSD) associated with WFD in fuselage lap joints. The evaluations investigated the capabilities of the tools to account for two primary effects of crevice corrosion -- material thinning and corrosion pillowing, and for two primary effects of WFD -- MSD cracks and small cracks (cracks less than 0.05 in). The tools demonstrated the

capabilities to perform stress analysis, crack growth analysis, risk analysis, and residual strength analysis on (1) structural components with multiple cracks, (2) thin structural components with multiple layers of material, and (3) large structural shell components such as fuselage panels.

Three case studies were performed in the evaluation on structural items having features common to a typical lap joint. To validate the tools, two case studies were conducted to compare analysis results with experimental test data on corroded coupon specimens from two previous research efforts. The first case study investigated flat, unstiffened panels with open holes containing MSD, and the second case study investigated lap joint coupon specimens. The third case study was a demonstration of an analytical method for assessing corrosion damage and MSD on a full-scale fuselage panel with a lap joint. For case studies 1 and 2, analysis results showed good agreement between predicted and experimental fatigue life and residual strength data for both the baseline and corroded configurations. The case 3 study illustrated how estimates could be made to evaluate the effects of corrosion damage and MSD cracks on the fatigue crack growth life and residual strength of a fuselage panel with a lap joint.

Evaluations showed that analysis tools could account for material thinning and MSD cracks, but limitations in some of the tools prevented a complete evaluation that accounted for corrosion pitting or small cracks. With further improvements in analysis tools and techniques, the analytical framework would be useful in assessing the impact of corrosion damage and MSD on the integrity of an aircraft structural component.

References:

1. Cope, D. A. and J. J. Luzar, "Analysis Tools for DADTA on Riveted Lap Joints," 1999 SAE General, Corporate & Regional Aviation Meeting & Exposition, April 20--22, 1999.
2. Cope, D. A. and P. S. Johnson, "Fracture Mechanics Tools for Analysis of Corrosion and Fatigue in Fuselage Lap Joint," 1998 USAF Aircraft Structural Integrity Program Conference, December 1--3, 1998.
3. Cope, D. A., P. S. Johnson, A. Trego, and J. D. West, "Analytical Framework for Assessment of Corrosion and Fatigue in Fuselage Lap Joint," The Second Joint NASA/FAA/DoD Conference on Aging Aircraft, August 31--September 3, 1998.
4. Cope, D. A., P. S. Johnson, A. Trego, and J. D. West, "Analytical Methodology for Assessing Corrosion and Fatigue in Fuselage Lap Joints," 1998 Air Force Corrosion Program Conference, April 8--9, 1998.

9.8.3 Crack Growth in High-Strength Bolts

Mark L. Thomsen,
Boeing

A great deal of research has been conducted in determining the nucleation of cracks in threaded fasteners due to the combination of loads and stresses at the critical tooth of the connector. The behavior of cracks nucleating at the thread roots of bolts is a relatively well understood phenomenon; however, very little research has been conducted on fatigue crack nucleation in the grip length of threaded fasteners. This is mainly because the load distribution is not well understood. The main concern for fatigue cracking in the grip length of bolts and threaded fasteners is due, for example, to scratches, gouges, nicks, and dings associated with the installation, use, or removal of these components. Therefore, the main purpose of this research was to apply and verify a stress intensity solution for circumferential surface cracks in bolts and threaded fasteners through numerical and experimental techniques.

The experimental verification of the stress intensity solution was accomplished by testing 28.575 mm (1.125 in) and 31.750 mm (1.250 in) diameter bolts manufactured from two strength levels of Inconel 718, a nickel-based steel alloy and MP159, a cobalt based multiphase steel alloy. To simulate surface imperfections encountered in service, an artificial defect of 2.032 mm (0.080 in) in depth and approximately 16.256 mm (0.640 in) in circumferential length was utilized to locate the sites of cracking. This artificial defect was induced in the material by means of an electro-discharge machine (EDM). Cracks nucleating from the EDM flaw will be allowed to propagate from the initial notch length to fracture under constant amplitude loading conditions.

To measure the growth of fatigue cracks in the threaded fastener specimens, the technique of direct current electrical potential difference for continuous in situ monitoring of fatigue crack propagation was used. The test setup is shown in Figure 101. For this experiment, the depth of the crack is defined as being along the short axis of the specimen, and techniques are employed to determine the crack aspect ratio (a/b where a = crack depth and b = half-

circumferential crack length) as the crack propagates through the specimen. A schematic of the cracking pattern is shown in Figure 102. The results were analyzed using linear elastic fracture mechanics to produce average crack growth rates; nondimensional stress intensity geometric corrections, β ; critical crack depths, a_{cr} ; and stress intensity factors, K_I . The verification of an accurate stress intensity factor for bolts and the experimental techniques will be useful in predicting crack growth rates and fracture strengths. This data will assist in designing safe structural components and establishing standards for inspection intervals for connectors used in critical attachment capacities. Typical bolt crack growth data are presented in Figure 103.

9.8.4 Qualification of Hand Held Low Voltage Electromagnetic Riveting

Mark A. Ofsthun

Boeing

Designing and producing a durable commercial airplane requires balancing good detail design and good manufacturing processes. Wings are one of the most severely fatigue loaded components of an airplane. Boeing Commercial Airplanes Group has used fatigue-rated machine riveting of wing skin to stringer joints for almost 35 years. Automated drilling and hydraulic squeezing of rivets provides fluid tightness, excellent fatigue performance, and good fabrication flow time.

In order to hydraulically rivet the wing skin to the stringer, temporary fasteners are used every 15 to 20 fastener locations to hold the parts together. On completion of the hydraulic riveting, these temporary fasteners are removed. The holes are reamed for coldworking, then cold worked and reamed to final size, then rivets are installed by hand. Cold working is a time-consuming process, but is necessary with hand installed rivets in order to achieve sufficient fatigue quality. This study evaluated the feasibility of using a new riveting process called hand held low voltage electromagnetic riveting (for brevity called EMR in this summary), developed by ElectroImpact™, to replace hand installation at the temporary fastener locations. The driving gun (head side) and the gun that forms the rivet button (tail side) are shown in Figure 104. The lift systems that support the guns are not shown.

EMR installs rivets using electromagnetic impulses that send two masses toward the rivet and form it in approximately two milliseconds. By comparison, the hydraulic system takes about one second to form the rivet. One of the features of the EMR system is normality sensors that ensure alignment to minimize the possibility of shanking the fasteners. This provides uniform hole fill and optimizes the chance of obtaining fatigue-rated hole filling.

During the development of the EMR process, strain lines were discovered in higher strength 7XXX-series rivet material. An example of strain lines can be seen in Figure 105. Strain lines are caused when the deformation of the rivet is so rapid that the material cannot flow around corners and edges. Because strain lines can lead to cracks in rivets by stress corrosion cracking (SCC), the decision was made to change the rivet material to a 2XXX alloy, which has less stress corrosion susceptibility.

The specimen selected for fatigue testing was a 15 fastener specimen with very low load transfer (less than 2%), which is representative of typical wing skin-stringer structure. The specimen uses the same plate and extrusion materials as those of wing lower surfaces. Multiple rivet diameter and material stack-up combinations were included in the evaluation.

Specimens were assembled on the automated hydraulic production machines, leaving holes 6, 8, and 10 open for EMR-installed rivets. These specimens were compared to specimens with all 15 fasteners installed using the automated hydraulic machine process. Additional specimens were assembled with all EMR-installed rivets. This specimen data could be used for future wing repairs.

All fatigue testing was done in MTS™ fatigue-test machines under uniaxial, constant amplitude loading with a stress ratio (f_{min} / f_{max}) of -0.2. To ensure that a proper “head-to-head” comparison was being made, all the materials for the specimens came from the same heat lot, the hydraulic riveting was done at the same time on the same machine, and the tests were conducted with the same test machines.

Figure 106 compares the results for specimens simulating temporary fastener replacement relative to the baseline hydraulic riveted specimens. The EMR process resulted in a 5% to 30% reduction in fatigue life at the tack fastener locations. Regular hand riveting without cold working results in a 50% to 75% reduction in fatigue life compared to

hydraulic riveting. Failure analysis indicated that the cracks originated in the extrusion material on the fastener button (tail) side at the EMR-installed rivet locations.

Figure 107 shows that when all the holes in the specimens were filled with EMR rivets rather than only three of the holes (6, 8, and 10), some recovery in terms of fatigue life was observed. This may be because the EMR-installed rivets had a different hole-fill pattern than the hydraulically installed rivets. This different level of hole fill could attract more load (i.e., increased load transfer), which tends to have a negative influence on fatigue. The best fatigue performance is with uniform fastening.

The impact of fatigue life reduction using EMR at temporary fastener locations was assessed and found to be contained within the design margins, so the EMR was qualified for use in production. The use of the EMR system resulted in reduced fabrication flow time and reduced potential for employees developing repetitive motion injuries with only a small decrease in fatigue quality. The EMR process reduces the flow time for temporary fastener replacement on each set of wing panels from 24 hr (three shifts) to 8 hr (one shift). The elimination of cold working accounted for half of the time saved.

9.8.5 Damage Tolerance Testing and Analysis of an Integral Skin Stringer Fuselage Panel

Keith E. Wilkins and Mike L. Gruber

Boeing

An integrally machined, full-scale widebody pressure panel was tested under fuselage pressure loading to measure its crack growth and residual strength performance. This testing was part of a larger test program performed in support of the NASA Integral Airframe Structures (IAS) program [1].

The curved test panel, which was 10 ft. wide by 10 ft. long, with a 127 inch radius, was similar in general configuration to typical widebody fuselage structure consisting of shear-tied frames riveted to a local skin pad. The integral aspect of the panel was that the skin and stringers were monolithic, machined from 1.5 inch thick 7475-T7351 aluminum plate. In addition, the frames were machined from a 1.5 inch thick 7050-T7451 plate. A photograph of the panel, with an illustration of the configuration, is shown in Figure 108.

The fixture used in testing the panel was a 20 ft long barrel section that had a rectangular cutout designed to accept test panels of varying configurations. Compressed air was used as the pressurizing medium. The skin, stringers, and frames were instrumented with 121 strain gages to determine how the stress distribution varied as the crack grew, and video cameras were used to capture panel behavior both inside and outside the fixture.

The first test, which consisted of a five inch skin crack centered on an intact frame, was introduced in the lower portion of the panel. The skin crack grew by cyclic loading at 8.6 psi to approximately 38 in (frame pad to frame pad) in approximately 10,300 cycles. The central frame was then cut and a residual strength test conducted. The crack dynamically extended at 9.8 psi then arrested at approximately 40 in when both crack tips entered the shear-tie fastener holes. A photograph of the panel in this condition is shown in Figure 109. The test was terminated at this point, and the site was repaired to prepare for a second test run on the upper portion of the panel.

In the second test, a 38-in crack centered on a broken frame was created in the upper portion of the panel. A residual strength test was conducted after small 0.05-in sawcuts were made at the edges of the shear tie fastener holes to represent multiple site damage. These flaws were introduced to make sure the fastener holes did not stop the crack extension, as in the first test. At a pressure of 9.9 psi, the 38-in crack ran dynamically and catastrophically failed the panel.

Predictions of panel stresses, crack growth rates, and residual strength were made prior to testing, using results from nonlinear finite element analyses. In the finite element model, the major panel elements (skin, frames, and stringers) were modeled using shell elements, while beam elements were used to model fasteners connecting the skin to the frame. A frame-centered crack, with lengths ranging from 5 to 45 in, was introduced in the skin, and stress intensity factors were determined and used to make crack growth and residual strength predictions. Predicted stresses correlated well with test strain gage results, as shown in Figure 110; however, crack growth predictions were very conservative. Finally, the panel residual strength was predicted using an R-curve approach to be 9.4 psi, which compared very well with the test results.

Reference:

1. Munroe, J. D., Gruber, M. L., Metschan, S. L., Wilkins, K. E., "Integral Airframe Structure (IAS): Validated Feasibility Study of Integrally Stiffened Metallic Fuselage Panels for Reducing Manufacturing Costs," NAS1-20014, November 1998.

9.8.6 Fatigue Testing of a High Load Transfer Joint

Ian C. Burford

Boeing

The Boeing 767-400ER is a new version of the existing 767. The wingspan has increased from 156 feet on the current 767 to approximately 171 feet for the 767-400ER. In addition, the gross weight of the 767-400ER has increased by approximately 10%. These changes resulted in higher loads, which necessitated a redesign of the wing-to-body joint. The 767-400ER wing is made of three major sections -- right and left outboard sections, and a center section that passes through the fuselage. The outboard wing sections meet the center section at the fuselage sidewall. Structural joints at the upper and lower wing surfaces and front and rear spars provide continuity between the outboard and center portions of the wing. The joint at the lower surface is critical for fatigue loading because each fastener in the joint must transfer a significant load (high load transfer). A test panel representing the 767-400ER lower wing surface joint between the outboard wing and center section wing was fatigue tested to verify joint durability. The joint was designed and sized using analytical methods, and the primary purpose of the test was to validate the assumptions used in the analysis.

The panel was tested in the Boeing Materials Test Laboratory 500,000-pound MTS test frame. It was cycled for 300,000 (ground-air-ground) constant amplitude cycles. Cycling was conducted between maximum panel stress levels of approximately 21 ksi in tension and slight compression. The panel was inspected at regular intervals by eddy current, pulse echo, and visual inspection techniques during cycling. Strain data was taken at intervals during testing. Three fatigue cracks were found and repaired during cycling. Testing was concluded at 300,000 cycles, when the design quality was verified. Figure 111 a close-up view of the panel in the fixture.

The panel was instrumented with 109 axial strain gages, 16 rosette strain gages, and various crack wires. The gages were used to validate the finite element model used in the design of the joint, as well as to ensure that the panel was behaving as expected during the test. Crack wires were installed on the panel outside the joint in areas that were not being inspected with NDI methods in order to detect unanticipated damage to the test specimen that would jeopardize the testing of the joint portion of the panel. Some of the gages and crack wires are evident Figure 111.

During the test, several cracks initiated prior to the conclusion of cycling. One of these, not in the joint area, was repaired, and cycling continued. The remaining joint cracks occurred late in the test, when the desired fatigue performance was already demonstrated. After the cause of the cracking was determined, appropriate corrections were made to the analysis and the production design.

9.9 Testing

9.9.1 Longitudinal Test of a B737 Fuselage Section

Gary Frings

FAA William J. Hughes Technical Center

A 10-foot transport airframe section was longitudinally impact tested at the Transportation Research Center (TRC) Inc. in East Liberty, Ohio, in November 1997. The test measured the structural responses of and the interaction between the overhead stowage bins, auxiliary fuel tank, and the fuselage under simulated severe, but potentially survivable, impact conditions. The TRC facility features a test area 88 feet wide and 95 feet long, with a deceleration area of 35 feet wide, 142 feet long, and a 24-inch-diameter Hyge Shock Tester. The Hyge principle, as applied to safety testing, simulates the deceleration conditions of an impact but in reverse. The Hyge system was programmed to test the various test specimens that were mounted onboard the aircraft, such as overhead bins and an auxiliary fuel tank system, at three different deceleration levels: 6, 9, and 16 g's.

The airframe test section, supplied by the FAA William J. Hughes Technical Center, was configured with a 120-inch overhead stowage bin on the left (or pilot) side, with a 60-inch overhead stowage bin on the right (or co-pilot) side, and with a 500-gallon auxiliary fuel tank located in the cargo area. The photograph in Figure 112 shows the airframe test section as the specimen was being prepared.

The first dynamic test, the 6 g test, unseated the auxiliary fuel tank from its tracks and attachments but did not damage the tank itself and did no damage to the overhead stowage bins or the fuselage structure. The second test at 9 g's used only the overhead bin compartments. Results showed that none of the furnishings onboard the aircraft were affected by the dynamic forces. In the final test, the aircraft section was exposed to a harsh 16 g deceleration; this last test was 7 g's more than the required FAA certification tests for aircraft furnishings. This acceleration level resulted in a dramatic failure of one of the overhead stowage bin compartments as it detached from the aircraft. The response data collected in these series of tests will be used to determine dynamic response characteristics of the airframe installation and will be combined with data from similar tests previously conducted to help determine the standard for future Federal Aviation Regulations pertaining to cabin interior items of mass.

POC: Gary Frings, AAR-431, FAA William J. Hughes Technical Center, Atlantic City International Airport, NJ 08405, (609) 485-5781.

9.9.2 Dynamic Vertical Drop Test of a Shorts 330 Airplane

Mr. Gary Frings

FAA William J. Hughes Technical Center

On August 20, 1998, the FAA William J. Hughes Technical Center conducted a vertical drop test of a 30-passenger Shorts 330 airplane at its Dynamic Vertical Drop Test Facility. The airplane, with a wingspan of 75 feet, a length of 58 feet, and weighing 21,210 pounds, was the largest ever dropped at the Technical Center. This test is part of a series of drop tests conducted at the Technical Center to define impact behavior across all airplane classes in order to develop dynamic g-level seat requirements.

The objective of the test was to determine the loads and forces acting upon this class of airplane, particularly a high-wing airplane, in a severe but survivable impact. The airplane was equipped with 28 dummies, of which 7 were anthropomorphic test dummies instrumented to measure the forces that would be felt on the human body due to the impact forces. The airplane also carried 3885 pounds of simulated fuel, two simulated engines, and 28 seats. The airplane was dropped from a height of 14 feet, which generated a final vertical velocity of 30 feet per second. One hundred eighteen channels of data were recorded for the test.

Since this was a severe impact, the airplane was heavily damaged. Both wings broke at impact. (See Figure 113.) One of the engines separated from the airplane. The fuselage cracked aft of the main spar. Both overhead fuselage fuel tanks lost their integrity causing the simulated fuel to spill inside and outside the airplane.

Preliminary data analysis indicates that over 100 g's were experienced by the fuselage. The passenger cabin, although severely damaged, maintained a habitable environment for the occupants.

Further data analysis will determine the relative survivability of the occupants. Six to nine months of data analysis will be required before the final technical report of this test can be published. The analyzed data will provide direction for regulatory action, if any, to improve survivability characteristics of future aircraft.

POC: Mr. Gary Frings, AAR-431, FAA William J. Hughes Technical Center, Atlantic City International Airport, NJ 08405, (609) 485-5781.

9.9.3 Full-Scale Fuselage Panel Test System

Dr. John Bakuckas

FAA William J. Hughes Technical Center

The Full-Scale Fuselage Panel Test System is capable of testing full-scale, curved-panel specimens under conditions representative of those seen by an aircraft in actual operation. The data obtained from the tests will be used to validate analytical models being developed by the FAA. All testing will be monitored using state-of-the-art video equipment for continuous observation. The test system was developed under contract with the Boeing Company, Long Beach, CA, and features a unique adaptation of mechanical, fluid, and electronic components, which will be capable of applying pressurization, longitudinal, hoop, and shear loads to a curved-panel test specimen.

The internal pressure will be applied using water as the media, eliminating the possibility of a catastrophic accident. The system is capable of dynamically cycling the internal pressure as well as performing a static pressurization to levels above flight gradients.

The hoop and longitudinal stresses are simulated by the controlled application of distributed loads around the perimeter of the test panel. Hoop forces will be distributed by individual loading linkages using a two-tier coaxial whiffle tree assembly, which generates four equal forces from each controlled load point. A total of seven load points are used on each side of the specimen, creating a total of 28 attachment points. Longitudinal forces are created using similar loading devices on each end of the panel, consisting of 4 load control points and 16 attachment points. Similar devices are available to apply bending and tension loads at each end of a frame.

An innovative shear loading system was developed that uses two load distribution points in the longitudinal direction at the edges of the specimen. The force is applied as a couple and is reacted by a couple in the hoop direction. A unique feature of the shear loading system is the elastomeric coupling between the loading mechanisms and the test specimen. The elastomer, which has a soft shear modulus, creates a close approximation to uniform shear distribution in both the applied and reacted couples. (See Figure 114)

All forces are generated using water as the fluid medium. The external loads are generated by applying water pressure to bladder-type actuators, which are controlled by pressure activated dome valves. The dome valves are automatically controlled by the use of electro/pneumatic control valves. The valves are driven by a computer-controlled system in a closed-loop configuration. A graphical interface allows the operator to control the loads, speed, and type of test desired. Data acquisition from strain transducers, load transducers, pressure transducers, etc., will be displayed on color monitors in real time as well as stored for off-line analysis. A unique video data acquisition capability is also a part of the system. A remote video system will be integrated with the test rig to track and record crack propagation and measure crack opening during the testing of the curved panels. The video system will automatically track and record the crack growth and has a very high zoom range to be able to either cover the entire test panel or to zoom into a narrow field of view to observe the crack tip behavior. (See Figure 115)

The design and construction of the Full-Scale Fuselage Panel Test System has been completed and preliminary testing has been conducted at the Boeing facility in Long Beach, CA. The fixture has been delivered and acceptance testing will be completed early next year. The video data acquisition system will then be installed.

The finite element method (a typical mesh is shown in Figure 116 (on the right)) was used to conduct an analytical strain gage survey of the fuselage panel under simulated test loading conditions in preparation for the acceptance testing. This data (typical results are shown in Figure 116 (on the left)) will be used during the acceptance testing to ensure that the test fixture performs in accordance with the desired design specifications.

POC: Dr. John Bakuckas, AAR-431, FAA William J. Hughes Technical Center, Atlantic City International Airport, NJ 08405, (609) 485-4784.

9.9.4 777 Main Landing Gear Fatigue Test

Gregory G. Eggers

Boeing

The fatigue (safe life) requirements identified in FAR and JAR 25.571 (c) require that “the structure be able to withstand the repeated loads of variable magnitude expected during its service life without detectable cracks.” To demonstrate compliance, the Boeing 777 main landing gear and its support structure have been tested in fatigue by subjecting it to a minimum of five lifetimes of complete takeoff-landing flight cycles.

A left-hand production 777 main landing gear, minus the hydraulic and electrical systems, and its supporting structure were installed in an inverted position in a test fixture at the Boeing Structural Component Test Laboratory. The test fixture, shown in Figure 117, includes a dummy rear spar to simulate rear spar stiffness, and welded steel structure that supports the landing gear and provides reaction points for the load systems. The dummy spar provided the interface for rear spar fittings, which included the forward trunnion support, the outboard gear beam support, and the drag strut support fitting. At the inboard end of the gear beam, the hanger link attaches to the test fixture.

The tires, wheels, and brake assemblies for the landing gear were simulated with wheel block and brake block test fixtures. Vertical, side, and drag loads were applied to each wheel block, shown in Figure 118, to simulate ground handling, take off, and landing load conditions. The gear retraction loads were applied to the structure using the production retract actuator and two test hydraulic actuators. The test hydraulic actuator loads were vectored to emulate the full range of retract actuator motion. Inboard flap loads were applied to the inboard end of the gear beam at the flap support extension using a single actuator in a fixed geometry. All load systems used servo-controlled hydraulic actuators with electronic load cells to provide the system feedback.

The applied fatigue test spectrum was developed using a basic spectrum of operating loads derived from available landing and ground operations data. The test spectrum contained loading that simulated towing, taxiing, turning, braking, take off and landing, and retraction-extension conditions. The load conditions were similar to those applied during the Model 757 and 767 main landing gear fatigue tests. The main difference is that the 777 fatigue loads were applied in a flight-by-flight sequence, which allowed damage accumulation representative of actual service. The flight-by-flight load sequence required the shock strut to be repositioned during cycling to simulate landing and taxi conditions. This was accomplished using the main landing gear internal hydraulic pressure.

Prior to the beginning of fatigue cycling, portions of the landing gear and its supporting structure were coated with a birefringent photoelastic coating for a photostress survey. Critical load conditions were applied to the landing gear to determine approximate magnitudes (locations and directions) of principal stress differences. Strain gages were installed at select locations to establish reference component stresses and to determine maximum and minimum principal stresses. Additionally, a static deflection survey using approximately 40 electronic deflection indicators was conducted in conjunction with the strain gage survey. Data gathered from the strain gage survey has been used in the establishment of 777 derivative aircraft safe-life limits.

In December 1998, the 777 landing gear fatigue test reached its goal of five lifetimes of complete takeoff-landing flight cycles applied to all main landing gear components. Final teardown inspections are currently being performed. The inspection results will be included in the documentation submitted to the regulatory agencies to substantiate the final safe-life limits for the main landing gear components. Results from the fatigue test are being used to improve the design for future 777 aircraft.

9.9.5 Beechcraft 1900 Airliner Dynamic Drop Test Report

Mr. Gary Frings

FAA William J. Hughes Technical Center

A vertical impact drop test of a commuter category Beechcraft 1900C airliner was conducted in the Vertical Dynamic Drop Tower at the FAA William J. Hughes Technical Center. (See Figure 119) The test measured the impact response of the fuselage, cabin floor, cabin furnishings (including standard and modified seats), and

anthropomorphic test dummies. This test was conducted to simulate the vertical velocity component of a severe but survivable crash impact. This test entailed dropping the low-wing, 19-passenger fuselage from a height of 11.2 feet that resulted in a vertical impact velocity of 26.8 feet per second. The airframe was configured to simulate a typical flight condition, including seats, simulated occupants, and cargo. Results of this test indicate that

- the fuselage experienced an impact in the range of 140-160 g's with an impact pulse duration of 9-10 milliseconds
- the occupants experienced g levels in the range of 32-45 g's with a pulse duration of 44-61 milliseconds
- this test was considered to be a severe but a definitely survivable impact
- the fuselage structure maintained a habitable environment during and after the impact
- the seat tracks remained attached to the fuselage along its entire length
- all standard seats remained in their tracks after the impact
- all exits remained operable
- all the test dummies experienced lumbar loads in excess of the current requirements found in FAR 23.562(c)(2)

The data collected in this test will supplement the existing basis for improved seat and restraint systems for commuter category Federal Aviation Regulation (FAR Part 23) airplanes.

POC: Gary Frings, AAR-431, FAA William J. Hughes Technical Center, Atlantic City International Airport, NJ 08405, (609) 485-5781.

9.9.6 737-800 Full Scale Fuselage Fatigue Test

Christopher M. Conley

Boeing

The 737-800 fuselage fatigue test exposes a production-quality fuselage to a typical set of operating loads experienced by the Next-Generation 737 fleet. A 5x5 flight spectrum (five load levels and five flight types) is applied to the fuselage in a cyclic manner to simulate 60 years of service. The 20 year design service objective is 75,000 flight cycles. The test is considered a Boeing structural validation test and is not required for type certification.

The primary purpose of the 737-800 fuselage fatigue test is to identify fuselage fatigue design and production issues to be considered for corrective action in advance of the fleet. Information obtained from the test will be utilized for verification of analysis methods. In general, the test will not be used to validate repair procedures.

Development of the 737-800 fuselage fatigue test loads spectrum is based on the concept of applying loads as realistically as possible while remaining within cost and time constraints and test equipment limitations. Test loads are derived from the 737-800 short-flight fatigue mission, defined as 0.6 hr and 170 nmi, as depicted in Figure 120. Discrete hydraulic actuator loads are calculated to produce shears, moments, and point loads equivalent to the design values. These loads are applied to the fuselage through a series of load fittings and simulated airplane structure. The major load introduction points for the 737-800 fuselage fatigue test are through side-of-body straps, passenger and cargo floor systems, a simulated vertical stabilizer, a simulated horizontal stabilizer, main landing gear beam lugs, nose landing gear, and the wing box front spar. In concert with hydraulic load application, the fuselage is pressurized to 7.5 psig during the flight profile as required for the short-flight fatigue mission.

Fatigue test loads are applied in blocks of 7,500 flights using five different flight types. These five flight types (A, B, C, D, and E) are combinations of five alternating load levels (I, II, III, IV, and V) for load conditions simulating various severity of gust and maneuver-type loading. The procedures for developing this 5 x 5 variable amplitude fatigue test spectrum were standardized for the full-scale testing of the 757, 767, and 777.

The test began on September 21, 1998, and is scheduled for completion the first quarter of the year 2000. Figure 121 is an image of the test setup.

9.9.7 Advanced Actuators for Active Control of Sonic Fatigue Dynamic Environments

Mr. Clare Paul

Air Force Research Laboratory

Dynamic/acoustic environments, which cause sonic fatigue on aircraft structures, need to be controlled. If they are not the structure must be designed to withstand the higher loads resulting in a significant weight penalty. If the structure is not properly designed secondary structural failures will occur. Passive flow control techniques have not been able to provide sufficient control authority to effectively suppress the dynamic/acoustic environments. The objective of this effort is to develop advanced active flow control actuators and validate the effectiveness of active control of acoustic and dynamic flow environments.

The approach will consist of conducting an extensive survey to determine all of the current flow actuators, which are applicable to the dynamic environments causing sonic. Laboratory and flow tests will be conducted to evaluate the effectiveness of the various actuators. The most promising ones will be selected for further testing, optimization, and application to active control. New and unique actuators shall be considered and evaluated. A final recommendation will be given for the best actuator for the various flow environments and active control methodology. Data from flow tests will be provided to substantiate the recommendations.

9.10. COMPOSITES

9.10.1 Thermomechanical Fatigue Durability Of T650-35/PMR-15 Sheet Molding Compound

Michael G. Castelli

Ohio Aerospace Institute

James K. Sutter

NASA Glenn Research Center

High performance polymer matrix composites (PMCs) continue to be the focus of a number of research efforts aimed at developing cost effective, light weight material alternatives for advanced aerospace and aer propulsion applications. These materials not only offer significant advantages in specific stiffness and strength over their current metal counterparts, but present a further advantage in that structures can be designed and manufactured to eliminate joints and fasteners by combining individual components into integral subassemblies. This makes these materials extremely attractive for commercial applications. With the current emphasis on low cost manufacturing of advanced composite structures, there is heightened interest on high performance sheet molding compounds (SMCs). SMCs effectively serve to reduce the costs associated with component production using prepregs where variable costs are generally associated with labor, secondary processes and scrap. Using compression molding, SMCs can be molded into complicated shapes facilitating the use of simple charge patterns, part consolidation and molded-in inserts that can reduce labor, equipment, and operation costs for preparatory and secondary processes.

Researchers at the NASA Glenn Research Center, in cooperation with Allison Advanced Development Company, have completed an investigation examining the use of T650-35/PMR-15 SMC for a mid-stage inner vane endwall application within a gas turbine engine compressor. The inner vane endwall is in the engine flow path and is subjected to high airflow rates, elevated temperatures and high pressures. This application is unique in that it represents a very aggressive use of high performance SMCs, raising obvious concerns about durability and property retention in the presence of microstructural damage. Therefore, it is necessary to evaluate the fatigue behavior and damage tolerance of this material subjected to a representative thermomechanical fatigue (TMF) mission cycle, as shown in Figure 122. Damage progression was tracked through changes in the macroscopic deformation and elastic stiffness in the loading direction. Additional properties, such as the glass transition temperature (T_g) and dynamic mechanical response were also examined. The fiber distribution orientation was also characterized through a detailed quantitative image analysis. Material damage tolerance was quantified based on residual static tensile properties after a prescribed number of TMF missions. Detailed microstructural examinations were conducted using optical and scanning electron microscopy to characterize the local damage.

Results indicate that the imposed TMF missions had only a modest impact on material durability as measured by the mechanical properties. Some microstructural damage was observed after 100 h of TMF cycling which consisted primarily of fiber debonding and transverse cracking local to predominantly transverse fiber bundles. No statistically significant degradation occurred in the residual tensile properties. Some of the more aggressive TMF scenarios examined, however, did promote notable creep damage and excessive strain accumulation leading to rupture. In some cases, this creep behavior occurred at temperatures in excess of 150 °C, below the commonly cited values for T_g . Consequently, thermomechanical exploratory creep tests were conducted and revealed that the SMC was subject to time dependent deformation at stress/temperature thresholds of 150 MPa/230 °C and 170 MPa/180 °C.

Reference:

1. Castelli, M.G., Sutter, J.K. and Benson, D., "Durability and Damage Tolerance of a Polyimide/Chopped Fiber Composite Subjected to Thermomechanical Fatigue Missions and Creep Loadings," *Time Dependent and Nonlinear Effects in Polymers and Composites*, ASTM STP 1357, R.A. Schapery and C.T. Sun, Eds., American Society for Testing and Materials, 1999.

9.10.2 Analysis of Thermally Induced Strains in Continuous Fiber Reinforced Composites

Gary R. Halford and Vinod K. Arya
NASA Glenn Research Center

Recent analytic research /1/ examined the linear-elastically calculated stresses and mechanical strains induced by thermal gradients in unit cubes of a 33 volume percent continuous-fiber (silicon carbide, SCS6) reinforced titanium Metal Matrix (Ti-15-3) Composite (MMC). Stand-alone matrix material was also analyzed as a baseline of comparison. Each cube was exposed to a fixed heat flux on one face with the opposite face held at a fixed low temperature. Other faces were insulated and all faces were forced to remain parallel. Each cube was a sub-element of a much larger non-warping structural element. A comprehensive range of 11 different composite ply lay-up and heat flux orientations were analyzed. The cubes are shown schematically in Figure 122 (a). The large X drawn on the hottest surface (or portions of the surface) indicates that surface to be the one containing the highest induced thermal strains. Thermally induced stress and strain results were calculated for the global composite cube assuming it to be a continuum/1/. However, these results are not presented herein. The most significant results were those from the local micro-mechanics linear elastic analyses. For every one of the 11 composite architectures studied, the micro-mechanical strains in the matrix in every direction exceeded the maximum strains in the stand-alone matrix by approximately a factor two. To emphasize the significance of these findings, only those strains operating perpendicular to a fiber are considered. Because this is by far the weakest direction in a composite, it is particularly alarming that the thermally induced strains in this direction are nearly always a factor of two greater than the largest strain computed in the stand alone matrix cube. The results are presented in Figure 122 (b) wherein the computed strains are normalized by the value of the maximum thermal strain induced in the stand-alone matrix cube; all for exactly the same applied heat flux. The normalized mechanical strain ranges varied between 1.75 and 2.18 depending upon the specific architecture. The combination of large thermal strains acting in the weakest possible directions within MMCs is expected to reduce their thermal fatigue resistance far below that of monolithic materials. This finding is expected to severely limit the application of MMCs in structural applications involving appreciable thermal cycling. Thermal fatigue resistance is not one of the structural advantages of metal matrix composites.

Reference:

1. HALFORD, G. R. and Arya, V. K.: Thermal Stresses -- The Achilles' Heal of Continuous Fiber Reinforced Metal Matrix Composites. *Thermal Stresses '97, Proceedings of the Second International Symposium on Thermal Stresses and Related Topics*, Rochester Institute of Technology, NY, June 8-11, 1997, pp.41-44.

9.10.3 Methodology for Delamination Growth Assessment in Composite Material Aircraft Structures

Mr. Peter Shyprykevick
FAA William J. Hughes Technical Center

Delamination growth is a common failure mode in laminated composite aircraft structures. Delaminations occur in critical areas of the structure, as shown in Figure 124, and need to be addressed to satisfy damage tolerance requirements during certification and in-service to guide inspection and repair activities. Presently, the criticality of the delaminations, by size and location, is determined by tests. An efficient analytical methodology to reduce testing will also reduce the costs of certification and aircraft maintenance.

Such a methodology has been developed for the prediction of delamination growth in laminated composites at Syracuse University under FAA grant sponsorship. To predict delamination growth, the available energy to create a new surface area through delamination, defined as strain-energy-release rate, G , is compared to a critical value of that energy or toughness. If G at a particular delamination tip exceeds the material toughness, the delamination will grow. The developed methodology addresses both the computational difficulties and complexities of determining G and the experimental determination of material toughness for practical structural details (as shown above) found in composite aircraft structures.

The developed methodology uses a crack-tip element (CTE) analysis based on classical plate theory. The CTE analysis provides closed-form expressions for G and for its components, G_I (crack opening mode) and G_{II} (sliding mode), respectively, in terms of force and moment resultants in the vicinity of delamination tip. Such quantities are usually available from a global finite element analysis (FEA) of the structural component. As this procedure is computationally efficient it can be used at a large number of interfaces where delamination growth is likely. Once G

is calculated it is compared to material toughness at the appropriate mode mix ratio (G_I/G_{II}) to determine delamination growth initiation. In addition, the CTE approach allows non-classical definitions of the individual G components. This is useful for many laminated composites when classical linear elastic fracture mechanics (LEFM) is inapplicable. For those cases where the near-tip damage zone is small and the classical definitions of G apply, solutions by the CTE approach have been compared to FEA showing excellent correlation and computing efficiency. See comparisons on the next page for a laminate with a delamination under compressive loading. The predictions match not only the total G but also the mode mix as shown by the G_{II}/G plot.

The experimental part of the methodology has established testing requirements to characterize fracture properties or toughness for various mode mix ratios of the composite material. Standard ASTM tests and newer methods were used to determine number of tests required and the specimen configurations. Data reduction of these tests was studied extensively and it was found that the CTE method provides a robust procedure to obtain a single value of toughness for the full range of mixed mode ratios.

Although the developed methodology has been demonstrated to work for unidirectional laminates of one material system, for the method to be accepted by the aircraft industry it must be shown to work for other material systems and other lay-ups and must be compared to test results of more complex structural details. This work and the extension to repeated load environments are underway.

The developed methodology has the potential of profoundly affecting design, analysis, and certification procedures for composite aircraft structures. First, it will allow a relatively rapid assessment at a large number of possible locations, under a wide range of loadings, as to whether delamination growth is likely. This will provide an early identification of possible failure sites that may not be found by the current selective testing approach resulting in improved flight safety. Second, knowledge of the critical size and location of delaminations will reduce maintenance activity as it will serve as a guide for repair actions. Finally, this methodology may allow the implementation of a more economic certification procedure based on a mix of analysis and testing to assure a damage tolerant structure, similar to that presently in-use for metallic structure. (See Figure 125)

POC: Mr. Peter Shyprykevich, AAR-430, FAA William J. Hughes Technical Center, Atlantic City International Airport, NJ 08405, (609) 485-4967.

9.10.4 Prediction Methodology for Impact-Damaged Composite Structure

Mr. Donald Oplinger

FAA William J. Hughes Technical Center

Composite aircraft structures exposed to low-velocity impact can sustain extensive internal damage without visual signs of damage on the impacted surface. This internal damage can cause significant reduction in the compression strength of the structure. Concerned about the strength degradation caused by the nonvisible damage, the FAA requires that composite structures containing barely visible impact damage be able to sustain the design ultimate load. Compliance of this damage tolerance requirement is usually demonstrated by tests. Research was undertaken to provide an analytical tool to estimate the residual strength of the composite structure after an impact event. The developed analytical tool provides better understanding of the behavior of the structure and reduces some of the expensive testing in the certification process.

The semiempirical method developed by Northrop Grumman Military Systems Division, which can run on a PC, combines all internal damage resulting from a low-velocity impact into an equivalent region of reduced stiffness. The model captures the effects of all significant impact and structural configuration parameters. The parameters considered are laminate lay-up, laminate thickness, material toughness, support condition, impactor mass and diameter, and structural arrangement. In this model, the degree of stiffness reduction for a given material system and impact condition is assumed to depend on the impact energy. The resulting stress or strain distribution in the structure due to the effects of the damage region is determined using an elasticity formulation. The influences of the other parameters that affect the postimpact compression strength of a laminate are empirically incorporated. To accommodate practical usage, a cutoff energy level and a threshold energy level (to accommodate observed behavior) can be used to predict residual strength.

The computer program of the stiffness reduction model can also be used together with the damaged structure reliability analysis model developed previously by the FAA. The reliability model integrates the residual strength prediction technique, the strength data scatter, and the impact threat distribution into a single reliability computation. The residual compression strength and the impact threat are combined to form a compounded probabilistic distribution to determine the damage structural reliability at a given applied stress (or strain). This is shown schematically in Figure 126. Also shown in Figure 126 (a) is the postimpact strength data scatter at different energy levels. The stiffness reduction model discussed above is employed to establish the relation between the postimpact strength and the impact energy. A two-parameter Weibull distribution is used to describe the scatter of the strength. The impact threat distribution that is obtained empirically for a given location in the structure is also required for analysis. It is shown as a Weibull distribution in Figure 126 (b) for this example. The postimpact strength and the impact threat are combined to form a compounded distribution to determine the impact damage tolerance strength reliability at a given applied stress (or strain), as shown in Figure 126 (c).

Although a structural damage tolerance evaluation was conducted using the enhanced methodology and the results were compared to those obtained previously, validation with test data is needed for this analytical tool to be used for design and certification. This does not negate the usefulness of the developed model for sensitivity studies, such as might be performed by the FAA to judge safety risk, and for preliminary design.

POC: Mr. Donald Oplinger, AAR-431, FAA William J. Hughes Technical Center, Atlantic City International Airport, NJ 08405, (609) 485-4914.

9.10.5 Compression Testing of Composite Materials

Mr. Donald Oplinger
FAA William J. Hughes Technical Center

A major accomplishment in 1997 was the development of the Combined Loading Compression (CLC) test for in-plane compression strength of organic-matrix fiber reinforced laminates. The difficulty of measuring the in-plane compression properties of composite laminates has been a major barrier to rapid development of composite structural applications in aircraft and other applications. The achievement of a new, lower cost, and more reliable test method to supplement accepted test methods, such as the Illinois Institute of Technology Research Institute (IITRI) compression test incorporated as ASTM standard D3410 some years ago, has long been a goal of the composites community. The CLC test developed at the University of Wyoming under FAA support appears to achieve this objective.

The IITRI D3410 and CLC test fixtures are compared in Figures 127 and 128. The principle of the CLC specimen shown in Figure 128 is to introduce compression load in the test specimen by a combination of friction-induced shear load and direct column loading. In comparison, in the IITRI fixture shown in Figure 127, the specimen loading is introduced entirely by shear stresses produced by contact with the wedge grips which are squeezed against the specimen by the geometry of the arrangement. Although the IITRI fixture is capable of providing high quality test results, great care and understanding of requirements of the test are required to do so. Moreover the fixture is extremely cumbersome to install and its considerable weight adds to the difficulty of a correct installation. The CLC fixture has been evaluated by several industrial organizations and has been found considerably lower in cost than the IITRI fixture as well as easier to use, while providing results at least as consistent as those of the IITRI fixture.

In preparation for adaptation of the CLC compression test as an authorized method by the MIL-HDBK-17 Composite Materials Handbook and as a new ASTM standard, an extensive program for evaluating the details of the CLC specimen has been undertaken within the past year by Peter Wegner, a graduate student in the University of Wyoming's Composite Materials Research Group (CMRG). Issues of interest which were investigated in the Wyoming effort were identified by the members of the MIL-HDBK-17 Test Methods Group as the key to confirming the acceptability of the CLC method. Typical of the results obtained in the Wyoming study of the CLC test were those related to dimensional tolerance requirements on fixture components for achieving consistent results. Several popular test methods were compared with the IITRI and CLC tests. For the most part, both the IITRI and CLC methods are found to give higher average values with less scatter than most of the competing methods. As an example of industry interest in the CLC test method, Mr. John Adelman of Sikorsky, cochairman of the MIL-HDBK-17 Test Methods Group, has developed an internal company specification for use of the CLC method for compression characterization of laminates.

POC: Mr. Donald Oplinger, AAR-431, FAA William J. Hughes Technical Center, Atlantic City International Airport, NJ 08405, (609) 485-4914.

9.10.6 Handbooks for Advanced Composites

Mr. Donald Oplinger

FAA William J. Hughes Technical Center

With the increased use of advanced composite materials in fabrication of commercial aircraft parts, there is a need to have readily available pertinent information on composites for use by the regional FAA offices. The information would be used to aid engineers and manufacturing inspectors in their certification and continued airworthiness activities.

Two handbooks "Fiber Composite Analysis and Design: Composite Materials and Laminates, Volume I" DOT/FAA/AR-95/29,I and "Handbook: Manufacturing Advanced Composite Components for Airframes" DOT/FAA/AR-96/75 have been published to provide this needed information. Both were complete revisions of texts that were first published in the nineteen-eighties.

The "Fiber Composite Analysis and Design: Composite Materials and Laminates, Volume I" provides an extensive background on the characteristics and mechanics of fiber reinforced composites which permits engineers experienced in the evaluation of structures involving conventional materials, especially metals, to extend their competence to the assessment of fibrous composite structures. The emphasis is on the definition of the nature and magnitude of the differences associated with the use of composites compared to conventional metallic materials and particularly on explaining the reasons for the differences and their implications for design evaluation. Accordingly, a broad spectrum of technologies is involved, ranging from detailed methods of analysis to more qualitative discussions on methods of analysis and design. The material is divided into two major categories: (1) composite materials and laminates, treated in Volume I; and (2) structures covered in a separate FAA technical report (DOT/FAA/CT-88/18, Volume II), which is currently undergoing similar revisions and should be available in early 1998. Volume I has been revised to include significant advancements in the design of composite structures as well as in the analysis mechanics of composites.

The design process for composites is essentially the same as for conventional metals. With composites, however, there is an additional requirement that the material be designed along with the structure. There are more steps required in the design cycle than heretofore with metallic structures, as illustrated in Figure 129.

Thus, with composites, the possibilities of improvement in the design by reiteration of the design cycle are increased by the added steps in the design cycle. In other words, the structural efficiency of a design may be improved by changes in constituent properties and laminate configurations.

The "Handbook: Manufacturing Advanced Composite Components for Airframes" is a compendium of information on methods of manufacture of advanced composite components for airframes. It is aimed at familiarizing the reader with the common industry standards and aspects of using composites in aircraft applications. The contents are drawn from various sources and are condensed into an easy-to-read, comprehensive format.

The contents of the handbook include introductory background on composite materials describing fiber reinforcements, matrix systems, core types and styles, handling, related practices found in the manufacturing and fabrication as well as the use of these materials, the concepts of producing parts using tooling, various manufacturing methodologies, processing, machining, quality assurance, assembly, repair, and related safety and environmental issues.

The organization and flow of the handbook are arranged to mirror that of the conventional processing of a composite part.

First, as with any material, an understanding of the basic materials with details on their unique properties are covered. Next, the steps required in the fabrication of a composite, beginning with the lay-up and orientation of the material in the mold, are described. From there, bagging, processing (cure), trimming, and installation of the

composite parts are covered. Other topics include inspection, damage identification, repair, and safe handling requirements.

The handbooks will provide FAA personnel with a better understanding of composites. The topics addressed in these handbooks are considered essential for proper assessment of the engineering, design, and manufacturing qualities of composite parts used in civil aviation today and in the future. The handbooks are also distributed to the aerospace community who have found them to be useful.

POC: Mr. Donald Oplinger, AAR-431, FAA William J. Hughes Technical Center, Atlantic City International Airport, NJ 08405, (609) 485-4914, and Mr. Peter Shyprykevich, AAR-431, FAA William J. Hughes Technical Center, Atlantic City International Airport, NJ 08405, (609) 485-4967.

9.10.7 Strength Prediction of Notched Thin-Skin Honeycomb Sandwich Structures

Mr. Hamid Razi

Boeing

Thin-skin honeycomb composite sandwich structures are being used in several aircraft control surface and fairing components. These structures are susceptible to impact damage from ground hail and from ground handling equipment. One method of reducing the frequency of repair is to increase allowable damage limits. Accurate residual strength prediction of damaged composite honeycomb structures is a key to increasing allowable damage limits. This review describes a generalized analysis method based on a bilinear material strain-softening law combined with a damage zone model to predict residual strength of thin skin honeycomb sandwich structures with damage such as holes and slots. This method was developed as an engineering tool for evaluating the strength of damaged composite aircraft structures. The method can be extended to determine the strength of impact damaged composite structures.

Numerous models with varying capability, accuracy, and required computational effort have been developed for failure analysis of damaged composites. The models are non-progressive and do not include damage formation and progression, such as the point-stress criterion and average-stress criterion. The limitation of such approaches is that the characteristic distance is dependent on the laminate geometry, material, and layup, and has to be determined through fitting experimental residual strength data. In a composite material, a zone of damage is developed in front of a notch prior to failure. Recent research indicates that the damage zone manifests itself in the form of strain-softening material behavior.

The method presented here for predicting the notched strength of composite materials is based on the damage zone model (DZM). During increasing external load on a composite structure with a notch, a damage zone (DZ) will form and grow in the stress intense region at the notch. To simplify calculations, the DZ is projected onto a straight line and modeled as a crack, with cohesive stresses assumed to be acting on the "crack" surfaces. An increase in the damage zone within the material is postulated to correspond to an increase in "crack" opening and reduced cohesive stress. A bilinear relationship between cohesive stress (σ) and crack opening displacement (v) was assumed in this analysis. The area under the σ - v curve represents the apparent total fracture energy per unit area of free crack surface and is denoted by G_c^* .

Four laminate properties must be determined prior to evaluating residual strength. These properties are the unnotched laminate strength (σ_0), bilinear relationship between cohesive stress (σ) versus crack opening displacement and bilinear material properties a and b , and the characteristic damage zone size (L_{ch}). The relationship between L_{ch} and material apparent strain energy release rate, G_c , is given by the following equation, where E_x , E_y , G_{xy} are elastic moduli:

$$L_{ch} = \frac{G_c E_x}{\sigma_0^2} \left[\frac{2E_y/E_x}{\sqrt{E_y/E_x - \nu_{yx}} + E_y/2G_{xy}} \right]^{0.5}$$

The analysis method was correlated to 365 test data points from several carbon fiber- and glass fiber- reinforced epoxy laminates and sandwich panels. The predictions correlated well to the data, with errors within 5%. Figures 130 and 131 show the comparison between test data and analysis predictions for two material systems. Figure 131 shows that a linear strain softening law resulted in a large error in the prediction of residual strength, thus prompting the need to use a bilinear material law.

9.10.8 Effect of Long-Term Isothermal Aging in Air on IM7/K3B and IM7/5260 Composite Laminates

Mr. Roger D. Bradshaw

Boeing

Carbon fiber/bismaleimide (IM7/5260) laminates were isothermally aged in air for up to 60,000 hr (6.8 years) at temperatures ranging from 149° to 204°C. After aging, mechanical testing was performed that evaluated lamina shear modulus/strength, quasi-isotropic modulus/open-hole compression strength, and mode II fracture toughness. In each case, the IM7/5260 laminates showed significant property degradation. As an example, the normalized lamina shear modulus is shown in figure 132 for three different aging temperatures (the other tests had similar findings). After 60,000 hr at 149°C, the shear modulus falls by more than 70% from its unaged value, while at 204°C only 6,000 hr is required for a similar reduction. If the aging temperature only affects the rate of the underlying degradation process, results at various temperatures should collapse onto a single curve if the time scales are adjusted appropriately. Figure 132 shows that the 177°C and 204°C data does indeed shift nicely to the 149°C data set with experimentally determined values of a_T . Thus, aging at elevated temperatures can accelerate the aging process so long-term data can be gathered more quickly.

One contribution to degradation of IM7/5260 is the sensitivity of the matrix to oxygen attack. This is shown visually in figure 133, in which a thin slice (microsection) of an aged quasi-isotropic IM7/5260 laminate is illuminated using through-transmission light. Scans of the original image permit a line to be drawn along the border between the damaged and undamaged material. The area between the line and the free surfaces has suffered oxygen damage. Such oxygen attack occurs at all exposed surfaces and leads to a loss of matrix material which, in turn, leads to the reduced mechanical properties shown in figure 132.

In addition, carbon fiber/polyimide (IM7/K3B) laminates were isothermally aged in air for up to 55,000 hr (6.3 years) at temperatures of 149° and 177°C. After aging, mechanical testing was performed that evaluated quasi-isotropic modulus/open-hole compression strength, compression after impact strength, and microcrack density after thermocycling. Little difference was observed between the aged and unaged specimens (the exception was that an increase in microcrack density did occur with aging). These results indicate that IM7/K3B is much less sensitive to oxygen attack than IM7/5260 at the tested temperatures.

9.10.9 Crack Growth and Residual Strength of Hybrid Laminate Open-Hole Tension Specimens

Ms. Elaine Worden

Boeing

This study examined crack growth and residual strength in hybrid titanium/graphite (TiGr) laminate open-hole tension specimens. A more complete discussion of this study can be found in reference 2. TiGr laminates are composed of titanium foil and polymer matrix composite (PMC) plies. TiGr has been considered for various uses on a High Speed Civil Transport (HSCT) for its potential advantages over titanium or composite materials. The strength and stiffness of a TiGr laminate can be tailored, as with traditional composite materials. Because of the crack-bridging effect of the PMC plies, fatigue life and crack growth resistance of the titanium plies is improved. Because titanium is used in the outer plies, the PMC plies are protected from an oxidative environment (i.e., ambient air) and UV radiation. As well, better conductivity improves the lightning strike potential, and impact damage is more readily detected than in composite materials.

This study used the following materials and processes to manufacture TiGr: The titanium alloy was 0.005-in thick Ti 15V-3Al-3Cr-3Sn (Ti 15-3) foil. An aliphatic sol-gel was used to prepare the surface of the Ti 15-3 foil for bonding with the PMC; the surface was then primed with BR[®]x5. The PMC used was PIXA/IM7; the PMC plies were about 0.0054-in thick in the finished laminate. Three layouts of TiGr laminates were investigated: TiGr 4-2-2 ([Ti/90/Ti/0]s), TiGr 2-6-2 ([Ti/0/90/0₂]s), and TiGr 7-12-4 ([Ti/90/0₂/Ti/0₂/Ti/0/90/0/Ti/0/90/0/Ti/0₂/Ti/0₂/90/Ti]).

Twenty-seven specimens were manufactured of each TiGr layup. The specimens were 3 by 12 in, with a 0.25-in diameter center hole. Three specimens of each layup were used to obtain baseline open-hole tension (OHT) strengths. The remainder of the specimens were fatigue cycled at a load ratio of 0.1 to preselected crack lengths. Following OHT testing, the lengths of the fatigue cracks in the separate titanium plies were measured in the broken specimens. The results are shown in figure XX.17-1; the net stress shown in this figure is the maximum load divided by the specimen thickness and the specimen width less the hole diameter.

Despite extensive cracking in the titanium plies, there was a negligible or small loss of residual strength in the laminates. In many instances, the residual strength increased over that of the uncracked specimens. Researchers at MIT have studied the damage modes in TiGr after fatigue cycling [1]. They showed that concurrent to cracking in the titanium plies, there is cracking in the 90° PMC plies and splitting in the 0° PMC plies. Most likely, splitting in the 0° PMC plies reduced the stress concentration at the hole, negating the effect of cracking in the titanium plies.

References

1. Burianek, D. A., and S. M. Spearing, "Fatigue Damage in Titanium-Graphite Hybrid Laminates," The 39th AIAA/ASME/ASCE/AHS/ASC Structures, Structural Dynamics, and Materials Conference, AIAA-98-1959, 1998.
2. Li, E., "Residual Strength Study of Fatigued Open-Hole Titanium-Graphite Hybrid Composite Laminates," The 39th AIAA/ASME/ASCE/AHS/ASC Structures, Structural Dynamics, and Materials Conference, AIAA-98-1960, 1998.

9.11. REPAIR

9.11.1 Installation of Composite Doubler on L-1011 Aircraft in Delta Airlines Fleet

Mr. James Newcomb

FAA William J. Hughes Technical Center

A boron epoxy doubler was applied as a door corner reinforcement on an operational Delta Airline, L-1011 on February 18 and 19, 1997. The installation occurred while the airplane was undergoing a heavy maintenance visit (D-check). The installed doubler passed all the planned inspections and was in service as of February 28. The FAA Airworthiness Assurance Nondestructive Inspection Validation Center (AANC) performed additional inspections of the doubler in order to accumulate history regarding the long-term doubler endurance under actual flight conditions. This activity represents the completion of the FAA-sponsored project which involved the services of the following organizational participants:

- 1) FAA provided oversight and regulatory format approval.
- 2) AANC provided project management, NDI development, validation, and structural testing.
- 3) Lockheed provided doubler design analysis and OEM approval documents.
- 4) Delta installed the doubler, issued process specifications, and provided engineering oversight.
- 5) Textron provided doubler materials and installation training.

The bonded composite doubler has numerous advantages over the mechanical fastened repair. They are:

- 1) adhesive bonding eliminates the stress concentrations caused by additional fastener holes,
- 2) the composite laminate was easily formed to fit the contour of the fuselage section,
- 3) corrosion resistance,
- 4) a high strength-to-weight ratio, and
- 5) economic advantages.

Delta's maintenance program indicates that the installation of the conventional metallic repair requires approximately 600 man-hours. The composite doubler installation and inspection required approximately 250 man-hours.

From an engineering view, the door corner application, shown in Figure 135, provided a good showcase for composite doubler capabilities. The design, fabrication, and installation challenges included large heat sinks, severe bending loads (shear stresses), a cutout in the center of the doubler, a complex complex geometry, multiple taper directions and an extremely thick (72 ply/0.040 inch) doubler.

The data resulting from this study serves as a comprehensive evaluation of a bonded composite doubler for general use. The associated documentation package provides guidance regarding the design, analysis, installation, damage tolerance, and nondestructive inspection of the doubler. The documentation package for this validation effort resides in the public domain. The FAA Atlanta ACO maintains the documents under the FAA project number SP1798T-Q. The engineering data and process specifications will also be published in a series of FAA DOT reports.

Currently, a composite doubler project with Boeing (Long Beach) and Federal Express is underway. Activities include the selection of candidate composite doubler repairs on Federal Express aircraft and identifying the specific tasks necessary to produce a composite repair installation on a DC-10 aircraft.

The main goals of the current composite repair program is to move the technology and associated validation into the repair regime, expand composite doubler sponsorship to another original equipment manufacturer, and complete the technology transfer to another carrier. A major emphasis is to streamline the design-to-installation process in order to make composite doubler technology more attractive for wide-scale use.

POC: Mr. James Newcomb, AAR-433, FAA William J. Hughes Technical Center, Atlantic City International Airport, NJ 08405, 609-485-5720.

9.11.2 Shot Peening Effects On Fatigue-Crack Growth

R. A. Everett, Jr.

U.S. Army Research Laboratory

J. C. Newman, Jr.

NASA Langley Research Center

Crack growth tests are being conducted on 2024-T3 aluminum alloy specimens to assess the effects of shot peening on fatigue-crack growth. This work is of current interest to the U.S. Air Force as well as the rotorcraft community. The results of these tests are important to the Air Force because the F-22 fighter is one of the first fighters to not use shot peening in much of its manufacturing process. The Sikorsky S-92 commercial helicopter will also be one of the first helicopters not to use shot peening. The reason for not shot peening these current aircraft comes from arguments which are based on the premise that the shot peening compressive residual stress depth is much less than the 0.05-inch initial damage tolerance crack size. Therefore, shot peening should have no beneficial effects toward retarding crack growth.

To evaluate the effects of shot peening on fatigue-crack growth, crack growth lives for non-shot peened tests were compared against tests on specimens with a nominally level of shot peening. The specimen configuration used was a double-edge notch to keep bending to a minimum. Initial starter cracks of about 0.05 inches were grown from small machined corner flaws in the notches to simulate the damage tolerance rogue-flaw size of 0.05 inches. Constant amplitude tests were conducted at a stress ratio of 0.1 at maximum stress levels of 15 and 20 ksi in order to keep the local stresses below the yield stress so that the residual stresses resulting from the shot peening would not be negated.

Figures 136 (a) and (b) show crack length against cycles for the normal (non-shot peened) and shot peened test specimens at 15 and 20 ksi, respectively. The average life of the non-shot peened specimens was 65,000 cycles at the lower stress level and 25,000 cycles at the highest stress level. For the shot peened specimens, the average life at the lower stress level was 210,000 cycles and 47,000 at the highest stress level. This trend towards a higher life for shot peened specimens is as expected. The large scatter in the shot peened data is disturbing since a designer would have to design to the lowest crack growth life. From these results, very little benefit from shot peening would be indicated. However, a closer evaluation of the test data showed that the longer crack growth lives were tending to come from the tests where the starter cracks were the shortest. More tests are needed to correlate crack growth lives with the initial crack lengths. But these results tend to show a potential benefit in crack growth lives from shot peening (factors of two to four increase in the average crack growth lives).

9.11.3 Bonded Composite Doubler Repairs at Warner Robins Air Logistics Center

W. Schweinberg

Warner Robins Air Logistics Center

Bonded Composite Repair Technology

- Relatively new technology which provides a repair option in situations where normal bolted/fastened sheet metal repairs are technically unsuitable or not cost effective.
- Especially helpful for aging aircraft problems such as fatigue cracks and corrosion.
- Industrialized and proven at Robins, used more here than all other DOD facilities combined.
- Developed and patented a highly effective NDI method to inspect the repairs.
- Very adaptable method, but not a panacea.
- Requires highly trained repair and engineering personnel.
- Requires specialized and modified equipment.

Applications (See Figure 137)

- C-141 Weep Hole
 - Bonded composite repairs were the only real repair option; alternative was total panel replacement – which was accomplished in some severe cases.
 - Initial installations in 1993
 - Over 400 repairs accomplished on over 130 aircraft.
 - Over 1200 bonded doublers, two inside the fuel tanks and one outside.

- No failures to date of the repairs.
- Net savings over panel replacement approximately \$39,000,000.
- Other C-141 Repairs.
 - Over 35 repairs on 25 aircraft.
 - Sizes up to 24" x 44".
 - Repairs include Vertical Stabs, panel cracks, corrosion, battle damage and fuselage.
 - All repairs have been on primary structure.
- C-130 Applications
 - Four Egyptian Air Force C-130 aircraft repaired in Egypt.
 - Over 40 repairs on 25 Air Force aircraft.
 - Sizes up to 28" x 15".
 - All repairs have been to primary Inner Wing structure.

Repair Mobility (See Figure 138)

- Deployable (air or ground) tractor/trailer capability developed to better serve the users.
- Avoids the cost, time and safety concerns of a one time flight to a depot for repair.
- Allows us to go to the aircraft; by road or air.
 - Capability is unique to Robins, designed and built at Robins.
 - Totally self-sustained, needs only work stands and fuel systems support from the field units.
 - Generator, Compressor, Filtered Air, Freezer, Heaters, Bond Controllers, Grit Blaster, NDI, Lab Sink, Numerous specialized tools and equipment.
 - Quick response, hours if by road, about 1½ days if by air.
 - Specifics are:
 - 8 feet wide, 8 feet 1½ inches high, 36 feet 2 inches long.
 - Weight 24,500 lbs.
 - Can be airlifted by C-130 and larger aircraft, drive on, drive off.
 - Overall mobile capability since Jan 1995.
 - One smaller older backup unit being phased out, new full capability unit in development.
 - 46 aircraft repaired to date by mobile trailer including 4 in Egypt.
 - 3 Overseas locations.
 - 8 Stateside locations.
 - Considerable savings in time and money.
 - Approximately \$100,000 saved per aircraft compared to bringing the aircraft to a depot (if possible) or contractor facility for repair.
 - Total Net savings of over \$4,200,000 (not including the Egyptian aircraft).
 - Time savings to the customer is very large, a cost for this is not factored in.

Further Efforts and Technology Transfer

- Engineering research efforts (organic and contractual) to expand understanding and range of applications.

Bottom Line

- Bonded composite repairs have proven to be a technically sound, durable, adaptable, cost effective, quick response and mobile repair method that is currently unique to Robins at this level of effort.

9.11.4 C-130 Center Wing Lower Surface Corrosion Bonded Composite Doubler Repair

W. Schweinberg

Warner Robins Air Logistics Center

Problem:

The Inboard Aft Nacelle Fairings, immediately aft of the #2 and #3 engine nacelles, were experiencing cracking problems due to acoustic fatigue. The fairings are approximately 35 inches by 38 inches, and while the fairings are not structural in nature, they are critical to assure the laminar flow of the engine exhaust and prevent stagnation of the hot exhaust which could (and has) lead to overheating and buckling of the lower wing skin panels. Lockheed

addressed the problem on later model C-130's, and all others by TCTO, by installing a semi-rigid and porous foam inside the fairings to dampen the vibration. (See Figure 139)

In the free state the foam is significantly higher than the space under the fairing and is firmly compressed during installation. (See Figure 140) As such the foam is in intimate contact with the lower wing skin panels. Due to the moisture, grit retention and abrasive properties of the foam, a less than optimum primer and paint system on the wing panels, no inspection intervals on aircraft with less than 2000 flight hours and the fact that the area is hidden under the fairing, a subsequent and severe corrosion problem has developed on the wing panels and fasteners. The wing panels in the area of concern are approximately 0.120 thick. Analysis has shown that isolated corrosion damage up to 0.020 deep can be simply removed and no repair is required. However the corrosion has been found to be much deeper and wide spread and long-term durability, and in the worst cases structural integrity, dictate a repair. (See Figure 141)

The extent of the corrosion problem was first noted in 1997 on three Egyptian Air Force aircraft during a Warner Robins depot field team effort to repair a heat damaged Nacelle fairing. The heat damaged aircraft and three corrosion damaged aircraft were repaired by the Warner Robins field team using bonded composite repairs. The first serious cases on Air Force aircraft were noted in the summer of 1998 by the Delaware ANG and shortly thereafter on the Combat Talon II fleet.

The standard Technical Order (T.O.) repair for general structural damage to the lower wing panels is to install a fastened metal doubler. However the size and severity of the T.O. repaired damage is very restricted due to the loading, type of construction, the need to install a large number of additional interference fit fasteners which causes additional structural, damage tolerance and durability problem.

Solution:

Since the large majority of the damages are well beyond normal T.O. limits and cost and logistics considerations make a panel, wing replacement or expanded metal repair unfeasible, an alternate repair methodology had to be developed. The solution was to use damage specific (size and thickness tailored for the damage) bonded composite doublers. The repair is multi-stepped and requires: (See Figure 142)

- Removal of all button head fasteners in the damaged area.
- Eddy current inspection of all fasteners holes for flaws.
- Very careful buffing to remove the corrosion damage.
- Reinstallation of all fasteners with new interference fit flush fasteners.
- Design and fabrication of a composite doubler tailored to the extent and depth of the damage.
- Special preparation of the wing panel surface for a long term durable bonded repair.
- Adhesive bonding of the composite doubler to the wing surface with a heat curing structural adhesive.
- Inspection of the completed repair with thermography.

The ISO Inspection workbook was also changed to require the field units to remove the Aft Nacelle Fairing during every ISO inspection and to inspect for corrosion. As a result, other aircraft of the same time group have been identified with the same problem. To date 27 aircraft with corrosion problems have been repaired, all but one were from manufacture year groups 1983 thru 1990.

Bonded composite doubler repairs have been used quite successfully on the C-141 since 1993 to repair fatigue cracks in the weep holes, other areas of the lower wing panels and other primary structure. Over 450 repairs on over 170 C-141 aircraft have been accomplished by WR-ALC/TI to date. This relatively new repair technology offers many structural and durability advantages. However, the technology is very process sensitive and requires specialized equipment and specially trained engineers and mechanics which currently limit the repair methodology to a depot level approach which to date is limited within the DOD almost exclusively to WR-ALC/TI. In order to better support the user, WR-ALC/TI has developed a self contained bonded composite repair tractor/trailer combination that can be taken, via road or air lift, to a field site to accomplish the repair. This approach has proven quite successful and saves the users approximately \$100,000 per aircraft over a depot "drop-in" for repair. WR-ALC/TI currently has a primary repair trailer and a reduced capability backup trailer (the original prototype) which is being taken out of service and a second, full capability, unit is being developed.

In addition to the corrosion problems, similar bonded composite repairs have been accomplished on six other C-130 aircraft where a metal repair was not feasible. (See Figure 143)

Key Points:

- Composite repairs for corrosion problems accomplished on 27 aircraft to date either at depot or by deployable repair trailer at field location.
- 6 aircraft at WR-ALC, either depot status or speed line drop in. 10 aircraft at Billy Mitchell Field, Milwaukee WI (AFRC)
 - 9 aircraft were Milwaukee assigned aircraft
 - 1 aircraft from Niagara Falls
 - 3 Egyptian Air Force aircraft
 - 3 aircraft at Kadena Air Base, Okinawa, Japan
 - 3 aircraft at Mildenhall RAF Air Base, UK
 - 1 aircraft at New Castle Airport, Wilmington DL (ANG) 1 aircraft at Ogden ALC, depot status
- 26 of the 27 aircraft have been 1983 thru 1992 year aircraft.
- 40 repairs total
 - Repair sizes from 11" by 11" up to 25" by 16"
 - Damage depths from .032 to full panel depth (.120)
- Three known aircraft needing repairs, suspect additional aircraft as ISO inspections are completed.
- Cost savings of bonded composite repair vs. replacement or expanded metal repairs has not been evaluated.
- Depot deployable repair trailer repair vs. depot repair savings is 18 aircraft x \$100,000. per aircraft = \$1.8 million. (See Figure 144)

**9.11.5 The Panther Skin Project - A Joint FAA/FIU Investigation
Dr. Milton J. Torres and Dr. Kuang-Hsi Wu
Florida International University**

The Panther Skin Project has been underway at Florida International University since 1989 in an attempt to alleviate the aging aircraft problems that exist today. Thus far the objectives accomplished are listed as follows:

- EXTENDED AIRCRAFT LIFE - An FAA Finite Element Study has indicated that with 2 inch thickness of Panther Skin a 2.5 lifetime extension can be expected for aircraft and for 3.5 inches a 5.1 lifetime for the aircraft can be expected.
- REDUCED STRAIN - Stops metal fatigue on aircraft fuselage structures. Adds strength to structural integrity.
- CRACK PROPAGATION REDUCED - On the EF3 of an Airbus A340 it reduced the crack propagation for an inch and a half thickness a factor of 1.5.
- LANDING/TAKE OFF BURN SAFETY - With 1.5 inches of thickness and an outside temperature of 3000 F it only reaches on the inside surface 100 F after 25 minutes.
- CHEMICAL RESISTANCE - Panther Skin resists all petroleum based solvents and most corrosive reagents.
- LOW MOISTURE ABSORBANCE - In ambient air absorbs less than .025% water.
- CORROSION RESISTANCE- The Naval Warfare Surface Center exposed Carbon Steel Lascor Panels to ASTM B-117 and to two years at sea with no corrosion evident.
- INSULATION - Lowest K factors of all known insulation materials.
- LIGHT WEIGHT - Densities between 2 - 3 pcf will provide buoyancy from 58 - 60 pcf.
- LOW COST - Relatively inexpensive to apply to aircraft.

REFERENCES:

1. Kolcum, E. H. 1990, "Process Would Use Foam to Alleviate Fatigue, Corrosion in Aging Aircraft", *Aviation Week & Space Technology*, 133(9):93
2. 1991, "Foam Process Makes Planes Stronger, More Fire Resistant," *Design News, Engineering News*, 47(7):26
3. December 1995, "Big Money On Campus" *Florida Trend*, 18(8):66
4. August 1996, Periscope, Technology, Bombproof? *Newsweek*, CXXVIII(9):6

9.11.6 Composite Repair of Aircraft Structure Program

Mr. Clare Paul

Air Force Research Laboratory

OBJECTIVE

- The objective of the Composite Repair of Aircraft Structures effort is to develop, verify, and transition techniques to design, install and predict the effectiveness of bonded composite repairs to metal aircraft in order to increase aircraft structural safety/durability and reduce cost.
- Work closely with the ALCs to insure work meets their needs and capabilities

APPROACH

- Survey Air Logistics Commands (ALCs) and other potential users on their exact needs and capability to support composite repair technology.
- Survey the existing state-of-the-art in composite repair and establish where improvements may be made to support users needs.
- Improvements in design techniques will be made and demonstrated on sub-component and full-scale test articles to certify their effectiveness and usefulness for the ALCs.
- The ALCs will be directly involved throughout the program to insure transition of this technology.

PAYOFF

- This program will reduce supportability costs by providing simplified methods to design and implement repairs to aging aircraft.
- Repairs to stop or decrease crack growth in fatigue damaged aircraft
- Repairs to decrease stress concentrations which could cause fatigue cracks
- Repairs to replace material removed due to corrosion
- These repair techniques will increase the effective life of existing aircraft structural components before replacement is required.

TECHNOLOGY DELIVERABLES

- All program results, software, and records will be documented in a manner that yields a technology sufficiently mature for transition to the aircraft support community. The major deliverable items include;
 - Lessons Learned Document – Includes information on previous and on-going work with recommended repair “best practices” and materials resulting from down-selects, novel repair designs, extensions of composite repair technology, and remaining issues requiring future programs
 - Supportability Plan – This will provide the basis of a plan for the practical implementation of composite repairs among the ALCs standard practices and accompanying logistics considerations.
 - Integrated Analysis Codes – An integrated software package which covers strength/durability analysis and repair design including required databases will be provided.
 - Program Report – This document will contain technical documentation on analysis modules, test results for coupon, panel and large demonstration tests, test analysis/correlation results, and a general record of the program.

9.11.7 Effects of Artificial Disbonds on Patching Efficiency over Thicker Structure

Mr. Clare Paul

Air Force Research Laboratory

This paper describes ongoing work aimed at developing the ability to predict and quantify the effects of disbonds on the fatigue response of cracked aluminum structure with bonded composite reinforcement. Studies by a number of authors have demonstrated reduced patching efficiency caused by disbonds at and around the crack tips for relatively thin structure (0.040 inch <1 mm> and 0.063 inch <1.6 mm>) representative of fuselage skins and control surfaces. However, little has been done to extend such work to thicker structure, such as 0.125 inch <3.2 mm>, more representative of primary structure such as wing planks. The patching system under study consisted of center-cracked, 0.125 inch thick, 7075-T6 aluminum sheets repaired with boron-fiber reinforced composite patches bonded with both film and paste adhesives. Constant amplitude fatigue crack growth studies were run at 5Hz and a peak stress of 17.4ksi (120MPa) and crack growth data was recorded as crack length versus number of cycles. Variables

under examination included disbond size (ranging from 0% to 20% of the total bonding area) and location, with special emphasis placed on the documentation of any disbond growth beyond those artificially induced. Different adhesives were also used and illustrated the effects of thermal stresses from the curing process.

Results showed a slight general trend of decreasing life as the percentage of the disbanded area directly over the crack tip increased. For the cases using paste adhesive, life improvement factors over an unpatched panel varied from 9.6 for the completely bonded case to 7.1 for the case with a full width disbond. When a higher-temperature curing film adhesive (AF 163-2M) was used, significant residual thermal stresses were evident and a large amount of out-of-plane bending was associated with the tests. Nevertheless, these patched panels offered life improvement factors over the unpatched case ranging from 6.7 for the completely bonded patch to 3.8 for the cases with a full width disbond.

After fatigue cracks had been grown to the edges of the patch, many of the panels were tested for residual strength. Even with a crack length nearly twice the critical length of the unpatched panels, these specimens all exhibited residual strength in excess of 30ksi (210MPa), or roughly half the yield strength of the aluminum

No disbond growth was seen from any pre-existing disbonds (either manufactured or naturally occurring) as a result of cyclic loading. Cyclic disbonding was observed only in the wake of the crack tip. These results point to the ability of bonded composite patches to perform their intended purpose under room temperature/dry conditions despite the presence of large disbonds. Further work is necessary to extend these results to the issue of long-term bond durability in the presence of aggressive environments.

9.11.8 Assessing the Effect of Repairs on Damage Tolerance of Airplane Fuselage Structure **Mr. Randall I. Elliott** **Boeing**

A pending FAA operational rule will require the assessment of repairs to fuselage pressure boundary structure. This review describes the process Boeing used to develop a repair assessment approach, and the way operators will implement that approach to comply with the regulatory requirements.

The Boeing approach is based on damage tolerance principles. The steps taken to develop the approach included the following:

1. Develop a process to evaluate the existing repairs on the airplane. This will allow operators to determine if existing repairs should remain on their airplanes.
2. Determine the loads for the different structural details that will be evaluated.
3. Develop or set up a basic inspection program. This is used to determine if an operator's basic maintenance program includes adequate inspection of some of the repairs.
4. Analyze each structural detail to determine the crack growth rate.
5. Determine how each repair will affect the inspection of the original structure.
6. Develop inspection requirements for each repair type.

On the basis of these steps, the document was set up as a three-stage process. The three stages include determining which repairs need to be assessed, evaluating those repairs, and determining the required inspections.

The first stage, determining where to look, allows operators to reduce the potential impact of this program. The areas or repairs determined to be damage tolerant when inspected with a basic inspection are eliminated from assessment. Repairs not covered by the basic inspection program move on to the second stage for assessment.

During the second stage, operators will assess these repairs and place them into one of three repair categories, designated as Category A, B, or C. They are defined as

Category A: A permanent repair where normal maintenance inspections are adequate to ensure continued airworthiness (inspectability is equivalent to unrepaired original structure).

Category B: A permanent repair that requires supplemental inspection beyond a specified supplemental inspection threshold to ensure continued airworthiness.

Category C: A temporary (time-limited) repair that will need to be reworked or replaced prior to an established time limit. Supplemental inspection may be necessary to ensure continued airworthiness prior to this limit.

The third stage allows the operators to determine the inspection requirements for the Category B and C repairs. The inspection requirements are presented in graphical or tabular form. With the inspection requirements determined, the operators must then incorporate them into their maintenance programs.

9.11.9 Damage Dosimeter and Durability Patch

Mr. Eric D. Haugse

Boeing

The damage dosimeter has been designed to fill a void in commercially available data recorders. The U.S. Air Force often has the need to measure structural strains and temperatures on in-service aircraft in order to diagnose difficult-to-analyze structural conditions, including high-cycle fatigue. To perform these functions, a rugged, small, and lightweight data acquisition unit, called the damage dosimeter, has been constructed (see figure 145). Powered by a small battery, the damage dosimeter measures three channels of strain at sample rates as high as 15 kilo-samples per sec and a single channel of temperature. The dosimeter is programmable in C code and can be configured to autonomously collect, analyze, and store data as required. It merges the functionality of both analog signal conditioning and a digital single-board computer on one 3.5- by 5-in card. The entire unit (excluding battery) weighs less than 1.5 lb. Although currently designed to monitor analog strain and temperature data for flight vehicle applications, the damage dosimeter can be easily modified to monitor other inputs, such as acceleration. The dosimeter can be used for both ground and flight applications.

The durability patch design process uses the damage dosimeter to develop repairs for secondary structure damaged by high-cycle fatigue [1]. The approach is to restore structural integrity and increase the structure's damping in the repair region. Increased damping leads to a reduction in resonant response and a repair that will survive the life of the aircraft. In order to design a repair with effective damping properties, the in-service structural strains and temperatures must be known, since damping material properties are a function of both frequency and temperature. The damage dosimeter allows an engineer to easily instrument an in-service aircraft to obtain the structural characteristics necessary to properly select damping materials. This information, in conjunction with analysis and design procedures, will result in design of a repair with optimum effectiveness. An overview of the durability patch design process is shown in figure 146.

Reference

1. Rogers, L. C. and Searle I. R., "Durability Patch: Repair and Life Extension of High Cycle Fatigue Damage on Secondary Structure of Aging Aircraft," DOD/FAA/NASA Conference on Aging Aircraft, July 8--10 1997, Ogden UT.

9.11.10 Repair Assessment Procedure and Integrated Design (RAPID) User Evaluation

Mr. Chen Chen

Boeing

Structural repairs and modifications to airframe structures have caused some concerns about structural integrity of aircraft in recent years. To ensure continuing airworthiness and operational safety, all scheduled-operation airplanes must meet static strength requirements and have implemented, or plan to implement, the damage tolerance based inspection programs for repairs and modifications to aircraft. The incorporation of static strength and damage tolerance analysis methodologies in repair practices and the maintenance of aircraft requires profound understanding of complex structural details and computational techniques. The required resources can be lacking, particularly for small operators, independent repair facilities, and military repair depots. In an effort to address this need, an automated repair analysis/design tool, RAPID, has been developed under the cosponsorship of the Federal Aviation Administration and the U.S. Air Force.

RAPID is a PC Windows[®]-based software repair tool capable of static strength and damage tolerance analyses of fuselage skin repairs. The current version of the software, RAPID 2.11, deals with common circular and rectangular

repairs, complex lap and butt joint repairs, and repairs over stiffeners for large transport aircraft. The proximity effect between two rectangular repairs can also be accounted for in the analysis.

In RAPID, generic load spectra have been developed and built into the program for narrowbody and widebody aircraft. A conservative engineering approach is used to convert the load spectrum into the stress spectrum for damage tolerance analysis of the repair. An option is available for a user-provided stress spectrum. Load transfer at critical fastener locations and skin stresses have been obtained using a two-dimensional finite element method, and are built into a database. An engineering approach is used to estimate stress intensity factors of pertinent crack configurations. Fracture toughness and crack growth rate data for common skin materials are included in the database. An option is also available for user-supplied tabular material data. The fracture toughness approach with Feddersen's correction method for small cracks is used to evaluate the residual strength of the repair. The crack growth analysis is carried out using either the simplified method or the cycle-by-cycle method, with an option to use the generalized Willenborg retardation model.

RAPID is an automated repair analysis/design tool. It was developed with an open modularized system architecture, providing easy implementation of tool upgrades and new features. Developmental effort is continuing, with applications for general aviation and the Air Force, including skin modifications for antenna installation and repairs near openings.

9.12. NONDESTRUCTIVE INSPECTION/EVALUATION

9.12.1 Investigation of Fatigue Cracks in Riveted Specimens Using the Light, Electron and Acoustic Microscopes

Z.M. Connor, M.E. Fine and J.D. Achenbach
Northwestern University

This project was undertaken to study the growth of fatigue cracks that initiate in the subsurface of riveted panel joints. Subsurface fatigue cracks in riveted lap-joint specimens were viewed using the scanning acoustic microscope. Fatigue testing was interrupted at intervals to obtain crack length measurements of these subsurface cracks. Testing was discontinued and specimens were disassembled after various stages of subsurface fatigue cracking as revealed with the scanning acoustic microscope. After disassembly, the panel containing the fatigue crack was pulled in tension until fracture, and the fracture surfaces were examined microscopically.

Crack growth measurements of subsurface cracks in riveted lap-joint specimens were obtained at intervals of 10,000 cycles using the scanning acoustic microscope. The results of these measurements were plotted as crack length vs. number of cycles and compared with the results of crack growth measurements obtained with the use of the light microscope after the crack broke through to the surface. Comparison of the crack lengths subsurface and on the surface after they break the surface show that the cracks are longer below the surface than on the surface. In one specimen, the number of cycles between the first observance of a crack on the acoustic scans and the observance of surface rumpling, which is an indicator that there is a subsurface crack, was 55,000 cycles. The C-scan image shows a longer crack than what appears on the surface even when the crack is quite long. This is true for both eyebrow and center line crack types. Increasing the maximum load from 4kN to 8 kN and keeping the same R ratio, 0.1, the crack configuration changed from the eyebrow type to the centerline type.

Fractographic examination has revealed that fatigue cracks initiate and grow from the hidden side of the countersunk panel as semi-elliptical cracks. Analysis of the fracture surface of a specimen with a crack barely visible under the acousting microscope revealed several crack initiation sites on each side of the rivet hole. The acoustic micrograph and the electron micrographs of this specimen are shown in Figures 147 and 148 respectively.

References:

1. Z.M. Conner, M.E. Fine and J.D. Achenbach, "Fatigue Crack Initiation and Propagation on Hidden Surfaces: Riveted Joints of Alclad 2024", *Proceedings of The First Joint DoD/FAA/NASA Conference on Aging Aircraft*, Vol I, July 8-10, 1997, Ogden, Utah, pp. 665-685.
2. Z.M. Conner, M.E. Fine and J.D. Achenbach, "Acoustic Electron and Optical Microscopy Visualization of Surface and Sub-surface Cracks", *Review in Progress in Quantitative Nondestructive Evaluation*, Vol 17B, 1997, pp. 1581-1588.

9.12.2 Effects of Maximum Nominal Applied Stress on Fatigue Crack Orientation and Growth in Riveted Specimens

Z.M. Connor, M.E. Fine and J.D. Achenbach
Northwestern University

The objective of this research was to investigate microscopically the effects of load variation on fatigue crack orientation and growth in riveted specimens of Alclad 2024T3 and to compare observations of sub-surface fatigue crack growth rate and growth path using the scanning acoustic microscope (SAM) with surface observations using the optical microscope. [1,2]

Sub-surface fatigue cracks were examined with the SAM and optically after selected numbers of cycles and then returned to the fatigue apparatus for further cycling. In some experiments testing was discontinued after subsurface fatigue cracking was revealed in C-scans produced with the SAM and the specimens were disassembled. After disassembly, the panels containing the fatigue cracks were pulled in tension until fracture to reveal the fatigue fracture surfaces which were then examined microscopically using the scanning electron microscope (SEM). Some tests were continued until the cracks broke through to the surface. Comparisons were then made between the crack lengths of such cracks below the surface and on the surface.

Specimens were tested at maximum nominal stresses of 206 MPa, 180 MPa, 154 MPa, 129 MPa and 103 MPa. The R ratio was 0.1 for all tests. At 206 MPa, 180 MPa and 154 MPa, the fatigue cracks which formed were located radially at 3 and 9 o'clock around the rivet with respect to the stress direction, but at 129 MPa and at 103 MPa, the fatigue crack was an eyebrow type crack. (A similar behavior was noted on stress increase with seven rivet specimens). At the high stress of 206 MPa, the rivet began to pull out, and there was competition between fracture due to the crack or from the rivet pulling out. The initiation sites of the cracks in specimens fatigued at 103 MPa were some distance from the rivet hole and on the inner surface of the countersunk panel, while the fatigue cracks for the specimens fatigued at 154 MPa started at the corner where the knife edge intersects the hidden surface. (See Figures 149 and 150) These cracks began to grow in shear and then quickly turned propagating normal to the direction of the applied stress. Both kinds of cracks are seen in aircraft skins.

Measurements, using the scanning acoustic microscope, of crack lengths in specimens fatigued at maximum nominal stresses of 103 MPa and 154 MPa were made at cycle intervals. The results of these measurements were plotted as crack length vs. number of cycles and compared with the measurements obtained with the use of the optical microscope after the same cracks broke through to the surface. For both stress levels, the length of the same crack on the back surface of the countersunk panel remains longer than the length of the same crack on the front surface of the specimen. Reasonable agreement was obtained between crack length vs. number of cycles curves for a maximum nominal stress of 103 MPa acquired with the use of the SAM and the curve predicted with FASTRAN-II* analysis assuming an initial flaw size of between 15 and 30 μm .

*FASTRAN-II is a fatigue crack growth structural analysis program developed by Dr. James C. Newman, Jr. at NASA Langley Research Center.

References:

1. Zayna M. Connor, Morris E. Fine, Jan D Achenbach and Mark E. Seniw, "A Study of Sub-surface Defects and Crack Propagation in Materials Using the Scanning Acoustic Microscope", *JOM*, 50(11) (November, 1998), *JOM-e*
2. Z.M. Connor, M.E. Fine and J.D. Achenbach, "Quantitative Investigation of Surface and Subsurface Cracks Near Rivets in Riveted Joints Using Acoustic, Electron and Optical Microscopy", presented at The Second Joint NASA/FAA/DoD Conference on Aging Aircraft, August 31 – September 3, 1998, Williamsburg, Virginia, in press.

9.12.3 Eddy-Current Methods for Crack Detection

Dr. Christopher Smith

FAA William J. Hughes Technical Center

A novel pulsed eddy-current instrument (originally developed for use in detection of hidden corrosion in lap splices) has been adapted to detect small fatigue cracks in layered aircraft structures by researchers at the FAA Center for Aviation Systems Reliability–Iowa State University. (See Figure 151) The advantages of pulsed eddy-current techniques include the wide bandwidth attainable, which permits a single probe and a single measurement to provide information over a broad frequency range. Pulsed eddy-current signals can be used to characterize cracks and locate them in the depth of the material. Time gating of the pulsed eddy-current signals provides a means to discriminate against interfering signals from lift off, air gaps, and fasteners.

The principal advantage of the instrument developed in this program, as compared to the commercially available pulsed eddy-current instrument, is that this instrument can be adapted for use with any commercial probe and used in any type of geometry normally inspected with eddy currents. The commercial instrument employs a rotating Hall-effect sensor and is designed specifically for fastener inspection. The ability to scan and image areas up to 8 x 20 inches in size is a considerable advantage. The time-gating feature included in this instrument is a unique capability that has no parallel in commercial instrumentation.

Samples of laboratory-produced fatigue cracks are being obtained from Prof. Morris Fine and Ms. Zayna Connor of Northwestern University for further development of the technique. Work is continuing on optimizing probe design for flaw detection and increasing the scanner resolution to improve the detection of very small cracks. A constant current probe drive has been constructed and will be tested in the coming year. Demonstrations of the instrument at the FAA Airworthiness Assurance Nondestructive Inspection Validation Center (AANC), Northwest Airlines, and Foster-Miller, Inc. are anticipated next year.

The instrument has been licensed to Sierra-Matrix, a California-based company, for commercialization. (See Figure 152)

POC: Dr. Christopher Smith, AAR-433, FAA William J. Hughes Technical Center, Atlantic City International Airport, NJ 08405, (609) 485-5221.

9.12.4 Superconducting Quantum Interference Devices for Detection of Hidden Cracks

Dr. Christopher Smith

FAA William J. Hughes Technical Center

Pulse-excited superconductive quantum interference devices (SQUIDs) are a new technology for eddy current evaluation of aircraft structures. Their high sensitivity at extremely low frequencies enables penetration of 15 mm of aluminum (0.6 inch) through multiple layers to identify submillimeter fatigue cracks and material loss of less than 5 percent. In combination with emerging eddy-current scanning techniques, this technology is capable of a three-dimensional view of defects in sublayers and tomographic imaging of multilayer structures. (See Figure 153)

In recent years the price and capability of superconducting technology have arrived at a point where near-term (2-3 year) implementation in airframe manufacturing environments, and subsequently in airframe maintenance facilities, is possible. This and the FAA's increasing interest in thicker structure motivated the FAA to fund a Phase I Small Business Innovative Research proposal submitted by SQM Technology in late 1995.

Results of the Phase I work include:

- Detection of a 1 mm change in thickness through 5, 10, and 15 mm of aluminum plate to demonstrate deep penetration of pulsed eddy currents with SQUIDs.
- Resolution of the lengths of millimeter size cracks through 10 mm of aluminum plate with SQUID pick-up loops of 1 mm diameter.
- Time discrimination of pulsed eddy currents that separates surface effects, like lift-off and tilt, from signatures of deep cracks.
- Submillimeter sampling at scan rates of 1mm/sec or more over a 25 mm swath.
- Demonstration of the feasibility of a small hand-held unit suitable for a field environment.

(See Figure 154)

POC: Dr. Christopher Smith, AAR-433, FAA William J. Hughes Technical Center, Atlantic City International Airport, NJ 08405, (609) 485-5221.

9.12.5 Eddy-Current Detection of Small Cracks

Dr. Christopher Smith

FAA William J. Hughes Technical Center

Over the past few years the FAA Airworthiness Assurance Nondestructive Inspection Validation Center (AANC) has conducted numerous experiments using a variety of eddy-current inspection equipment to inspect for small cracks from beneath rivets. All of the experiments were performed as blind experiments. That is, the person or persons performing the inspections did not know whether any specific inspection site contained cracks or not. In this way the inspections mimicked conditions of actual inspections that would take place in normal use conditions.

Equipment included in the study were the following off-the-shelf equipment: Nortec 30 Eddyscan, Krautkramer Branson Crackfinder, Hocking FastScan, Nortec 19e with sliding probe procedure, and MIZ22 with pencil probe and template procedure. Also included were instruments or probes recently developed that are not readily available to the public. These include the Northrop-developed low-frequency eddy-current array (LFECA), the NASA-developed rotating self-nulling probe, and a McDonnell Douglas Aerospace/GK Engineering surface scanning probe used with an Elotest B1 minirotor.

Eddy-current procedures commonly employed in aircraft inspection are capable of reliably detecting cracks as small as 0.050 inch while maintaining false calls below 1 percent. However to achieve such detection rates requires careful settings of threshold levels and appropriate standards for setup.

There are newly developed techniques and instruments that are capable of doing better. The NASA self-nulling rotating probe demonstrated that it could reliably be used to find cracks as small as 0.032 inch and the Northrop LFECA demonstrated a capability of reliably detecting cracks as small as 0.040 inch. These rates were achieved without an increase in false calls. (Illustrative probability of detection curves for the NASA probe are shown in Figure 155.)

Other experimenters have reported that the Hocking FastScan, Nortec-30 Eddyscan, Northrop LFECA, and GK Engineering/Elotest are capable of detecting surface cracks 1.0 mm (0.040 inch) in length under flush-head aluminum rivets. The AANC study extends these results and indicates that although capable of detecting this size crack, the probability associated with routinely detecting them (at false call rates < 0.01) are approximately 0.23 (FastScan), 0.74 (Eddyscan), 0.88 (LFECA), and 0.67 (GK).

The effect of inspecting through paint (0.003 to 0.005 inch) is often a decrease in the probability of detection. However, this effect seems to be due primarily to the difficulty in properly centering the probe over the rivets rather than because of the paint layer. Techniques that give the operator signal feedback that can be used to assure proper centering were shown to be effective in removing this level of paint as a major reliability factor.

The AANC also addressed methodology issues for estimating probability of detection curves from signal data. Specifically, they have shown that the traditional “ \hat{a} versus a ” analysis that looks at NDI signal strength versus flaw size can be generalized by considering an analysis performed on crack flaw predictions based on the signal strength.

The predicted values are treated as the dependent variable with the flaw characteristics as the independent variables in the traditional “ \hat{a} versus a ” analysis to estimate the probability of detection curve. This proposed methodology was shown to be equivalent to the “ \hat{a} versus a ” analysis when there is a single dimensional signal, but offers the capability of extending the analysis to multiple dimensions of a signal.

POC: Dr. Christopher Smith, AAR-433, FAA William J. Hughes Technical Center, Atlantic City International Airport, NJ 08405, (609) 485-5221.

9.12.6 Self-Compensating Ultrasonic Technique

Dr. Christopher Smith

FAA William J. Hughes Technical Center

Encouraged by their success on the DC-9 T-cap application, Igor Komsky and Jan Achenbach of Northwestern University are further developing the self-compensating ultrasonic technology to detect and characterize defects in other aircraft structures.

The self-compensating approach ensures sensitivity and reliability by eliminating the need for a manual calibration for each test. The measuring device as a unit is placed on the structure. An appropriate combination of the measurements yields data that is uncoupled from the measurement device. Work is in progress on the detection and characterization of radial cracks emanating from fastener holes. Applications for crack detection in a second layer are specifically directed to the detection and characterization of fatigue cracks in the second layer of a bolted spar-cap/strap connection of the DC-10 and to multilayered wing structures of Boeing and commuter airplanes.

The second generation prototype of a rotational scanning system was tested in June 1998 at the Northwest Airlines Maintenance Facility (shown on the right). The prototype scanning system has been integrated with a commercially available ultrasonic flaw detector to image cracks around the fasteners. A three-step inspection procedure was developed to, first, determine the quality of the sealant in between the layers, then, to inspect the joint for second-layer cracks, and finally, to image the detected cracks.

A new calibration specimen for the DC-10 spar-cap/strap connection has been manufactured to model the complete line of 12 fasteners with nonuniform spacing around fasteners and various sizes of the fastener heads. The specimen was used to calibrate the scanning system for quantitative characterization of the cracks and the quality of the sealant.

The feasibility of crack detection in the T-chord of a B777 body splice has been demonstrated. Using the airplane skin as the inspection surface, a triangular EDM notch (0.2"x0.2") was detected at the T-chord-paddle fitting interface. Also, an inspection procedure was developed to determine the presence of the sealant at the skin/T-chord interface.

The self-compensating ultrasonic technique makes it possible to detect and size fatigue cracks, stress corrosion cracks, and material corrosion loss in internal layers of airplane structures. The inspection can be done from the outside of the structure. Considerable cost-savings have been achieved by users of the technique in the DC-9 T-cap application.

(See Figure 156)

POC: Dr. Christopher Smith, AAR-433, FAA William J. Hughes Technical Center, Atlantic City International Airport, NJ 08405, (609) 485-5221.

**9.12.7 Development Of A Novel NDE Probe To Detect And Measure Corrosion Of Aging Aircraft
Jinseong Kim, Anuncia Gonzalez-Martin, and Dalibor Hodko
Lynntech, Inc.**

Lynntech has developed a lab-scale prototype of a novel non-destructive evaluation (NDE) probe for the detection of hidden corrosion in aircraft metallic structures. The NDE system is based on electrochemical impedance (EI) measurements. Impedance signals at the selected frequencies are highly sensitive to the degree of corrosion of the sample under study.[1] Thus, real time, on-line evaluation of the corrosion process by the EI-NDE probe has been easily achieved using characteristic frequencies.[2,3] The probe is simple in design, portable, low in cost, and will not require trained personnel to operate. Another advantage of the probe design is that the use of liquid electrolytes is eliminated.

Figure 157 shows the performance of Lynntech's NDE prototype probe on a painted Al7075-T6 coupon. The coupon had several intentionally damaged sites. Three probes of different sizes were used. A single frequency was used for the inspection. The first step was to inspect the entire surface with the largest probe. When the impedance value was less than the value of the impedance magnitude corresponding to a damaged-free surface, that area was identified as "damaged". Next, the "damaged" area was inspected with the medium size probe to further localize the flaw. The damaged sites identified by the smallest probe are shown as the darkest shadows. This successive inspection with probes of different sizes reduces the time-labor to inspect a large area of a substrate. Also, this procedure will save time and cost during the repair process, because repair will be limited to those sites where flaws are localized with the smallest probe.

The probe has also been used to successfully determine a relative value of corrosion rates around rivets and lap joints present in part of a fuselage from an aged Boeing 727. Both, the impedance magnitude at one frequency and the relative corrosion rates were calculated for each one of the rivets. Figure 158 shows two gray-scaled maps indicating the degree of corrosion. The first map was obtained from the values of relative corrosion rates and the second one from the inverse of the value of the impedance magnitude at a single frequency. An excellent correlation exists between both maps, indicating that the impedance at the selected frequency is a direct reflection of the degree of corrosion damage experienced by the inspected area. Determination of corrosion rates is extremely valuable because it contains quantitative information on the severity of the problem and on the need for immediate repair and/or future inspection schedules.

References:

1. A. Gonzalez-Martin, J. Kim and D. Hodko, "New NDE/I Probe for the Detection of Early Stages of Corrosion in Aircraft", Proceeding of "The First Joint DoD/FAA/NASA Conference of Aging Aircraft", 8-10 July 1997, Ogden, Utah.
2. J. Kim, A. Gonzalez-Martin and D. Hodko, "Novel NDE/I Probe for the Detection of Corrosion in Aircraft Metallic Structures Based on Electrochemical Impedance", Proceeding of "The Second Joint DoD/FAA/NASA Conference of Aging Aircraft", 31 August-3 Sept. 1998, Williamsburg, Virginia.

3. A. Gonzalez-Martin, J. Kim and D. Hodko, "Novel NDE Probe for the Detection of Corrosion in Aircraft Based on Impedance Spectroscopy", The 1998 USAF Aircraft Structural Integrity Program Conference, 1-3 December 1998, San Antonio, Texas.

9.12.8 Thermal Wave Imaging of Disbonding and Corrosion in Aircraft Structures

Dr. Christopher Smith

FAA William J. Hughes Technical Center

Infrared (IR) thermal wave imaging, developed by R. L Thomas and his team at the Center for Aviation Systems Reliability-Wayne State University, is a new technology with applications to aging aircraft. The technique uses pulsed surface heating (with flashlamps) and fast, synchronous IR video imaging of the surface temperature to form rapid (two or three second), wide-area (more than a square foot) images of subsurface structure, such as skin corrosion and disbonded doublers or tear straps. Images of doublers resemble x-ray images, with the disbonds showing as bright contrast on a dark background. On typical aircraft skins, thermal wave imaging is capable of measuring corrosion thinning with a sensitivity of better than 2 percent material loss. (See Figure 159)

During two 1997 visits to Northwest Airlines (NWA) and one to Boeing-Wichita the Thermal Wave Imaging (TWI) System demonstrated the capability to inspect painted aircraft without applying water soluble paint. In earlier versions of the TWI system, it was necessary to temporarily apply a water soluble paint to the area of the fuselage to be inspected. The inspection results were as good or better than results from the same area when paint was applied and were in agreement with independent inspections by NWA and Boeing personnel. This new capability significantly reduces the inspection preparation and cleanup time and should relieve recurring industry concerns regarding the application of paint to inspection areas.

Based on these demonstrations, Northwest Airlines has asked Boeing to authorize the use of thermal wave imaging for both the repetitive inspections and the terminating actions called for in service bulletins. United Airlines has also asked Boeing to authorize the use of thermal wave imaging for similar authorization for a separate inspection application. Boeing intends to pursue activities required to add thermal wave imaging to their nondestructive testing (NDT) manual. (See Figures 160 and 161)

POC: Dr. Christopher Smith, AAR-433, FAA William J. Hughes Technical Center, Atlantic City International Airport, NJ 08405, (609) 485-5221.

9.12.9 Economical Eddy-Current for Engine Components

Dr. Christopher Smith

FAA William J. Hughes Technical Center

In an effort to eliminate potential service inspection problems before they result in serious consequences, the FAA Engine Titanium Consortium (ETC) is working with the airlines to identify common servicing needs of the most popular engine models. As a result of their efforts, there now exists a suite of eddy-current tools which allows controlled scanning and digital data acquisition for a variety of applications.

A portable scanner and data acquisition system have been developed for use in airline overhaul and maintenance shops. (Figure 162) The portable scanner consists of a generic mechanical scanning system with application specific tooling for probe positioning and manipulation. Adapter plates are used to mate the mechanical scanning system to a variety of engine disks by using the bolt hole patterns to align the system to specific disks. A lunch box computer has been used for data acquisition and analysis. The system has been interfaced with a variety of commercially available instruments as well as conventional and wide field probes, including the ETC-developed probe.

A series of onsite meetings at airline maintenance and overhaul facilities and a survey of over 50 national and international engines were used to determine the features of the final product. The ETC scanning tools have been demonstrated at the ATA NDT Forums annually since 1994. This continues to provide valuable input to the application of the tools. In addition to the commercial aviation community, the portable scanner concept has been discussed with potential military users including demonstrations at several Air Force sponsored meetings. Key inspection personnel from the Tinker AFB Air Logistics Command, Oklahoma City, and the Wright Patterson R&D staff will participate in the upcoming demonstration at American Airlines.

To date, bore scans (axial motion), web scans (radial motion), and slot scans have been demonstrated on engine hardware from all three engine manufacturers involved in ETC: Pratt & Whitney, General Electric Aircraft Engines, and AlliedSignal. Validation testing has been completed at United Airlines and Northwest Airlines where efforts focused on inspection of the 14th and 15th stages of the JT9D compressor disks. Additional validation testing is under way with AlliedSignal and is planned with American Airlines. Signal processing tools are being developed at Iowa State University for use in the AlliedSignal applications. (See Figure 165)

The Northwest Airlines Atlanta facility has expressed interest in conducting validation testing in late 1997 or early 1998. To date the scanner and data acquisition system have been successfully adapted for use with six instruments at various airline facilities. In addition to the intended jet engine applications, minimal adaptation has enabled the system to be applied to inspection of propeller blades, reportedly saving the industry over \$10 million.

Commercialization discussions began with applicable vendors in 1996 and led to the recent partnership with Uniwest. The first commercial version of the scanner is expected to be on the market in early 1998. Several airlines and OEMs have expressed interest in purchasing the scanner for future inspection initiatives.

POC: Dr. Christopher Smith, AAR-433, FAA William J. Hughes Technical Center, Atlantic City International Airport, NJ 08405, (609) 485-5221.

**9.12.10 Early Fatigue Detection and Characterization Using the Meandering Winding Magnetometers
Dr. Christopher Smith
FAA William J. Hughes Technical Center**

A thin, conformable eddy-current sensor and associated grid measurement algorithms invented at the MIT Laboratory for Electromagnetic and Electronic Systems was further developed under FAA and DoD sponsorship by JENTEK Sensors, Inc. The Meandering Winding Magnetometer (MWM™) measures electrical conductivity profiles as a function of depth from the outer skin surface. The sensor has the capability to:

- provide manufacturing quality control and fatigue and thermal degradation monitoring for coated and uncoated engine components (e.g., thermal degradation of thermal barrier coatings, overtemperature for 718 alloy blades, and degradation of diffused aluminide coatings for turbine blades)
- detect signs of unusual material distress in aircraft skins and structural members prior to the formation of detectable cracks, which may provide evidence of the onset (or absence) of widespread fatigue damage

The patented MWM sensor shown in Figure 163 has demonstrated the capability to measure the thickness variation of thermally grown oxide layers under thermal barrier coatings with a precision of better than 1 micron. The MWM sensor is essentially a transformer confined to a single plane. The impedance (secondary voltage/primary current) magnitude and phase is converted to electrical properties at each applied frequency using a patented measurement approach. The measurement grids (look-up tables) are generated off-line (in advance) using a model of the MWM interactions with multiple-layered media, such as an aircraft skin lapjoint. These grids are then stored in a grid library. The grids and GridStation™ software provide real-time electrical property profile measurement as a function of depth from the exposed surface. The MWM is thin and flexible permitting inspection of complex geometries such as the leading edge of an airfoil/root transition region for a turbine blade.

Figure 164 shows the results of single frequency MWM measurements on aluminum and stainless steel bending fatigue specimens. Photomicrographs of sectioned aluminum specimens show microcrack clusters approximately 1-3 mills deep near the surface for specimens at 70% of the estimated fatigue life. These microcracks could not be detected with focused liquid penetrant testing. The stainless steel specimens showed no microcracking at 75% of the estimated fatigue life. JENTEK is working on similar curves for titanium and nickel alloys used in engine components.

JENTEK Sensors, Inc. has continued this technology development under an FAA Phase I Small Business Innovative Research (SBIR) for commercial aircraft applications, and under a Navy Phase II SBIR for military aircraft. JENTEK plans to continue the testing and validation of this technology on the Boeing 737 test bed and engine test specimens at the FAA AANC. The MWM and portable GridStation™ system are now commercially available from JENTEK Sensors, Inc. For more information contact Dr. Neil Goldfine at (617) 926-8422.

POC: Dr. Christopher Smith, AAR-433, FAA William J. Hughes Technical Center, Atlantic City International Airport, NJ 08405, (609) 485-5221.

9.12.11 Visual Inspection Reliability

Dr. Christopher Smith

FAA William J. Hughes Technical Center

The FAA Airworthiness Assurance Nondestructive Inspection Validation Center (AANC) has completed benchmark experiments on the reliability of visual inspection. The experiments are part of a coordinated effort to examine a broad range of visual inspection tasks. The experiments used professional aircraft inspectors, inspecting real aircraft, and were designed to be broadly applicable to a large class of visual inspection tasks.

The primary test beds consisted of a Boeing 737 and a Fairchild Metro II commuter aircraft. Both aircraft are part of the AANC's collection of test specimens. Simulated lap splice specimens with well-characterized cracks were also used in the experiments.

The experimental program consisted of two different phases. The first phase used the Boeing 737 as a test bed and included 12 inspectors from four different major airlines who have the Boeing 737 in their fleets. The second phase used the Fairchild Metro II and included 11 inspectors from North American commuter and cargo operators with the Fairchild Metro in their fleets. Each of the inspectors spent two days at AANC performing different inspection tasks specific to their background. Both groups also inspected the simulated lap splice specimens.

Following are some significant observations coming from these experiments.

1. Substantial inspector-to-inspector variation in performance existed. Figures 165 and 166 (Transport and Commuter PoDs) show probability of detection curves fit to results of the simulated lap splice inspection for cracks from beneath rivets. Comparable inspector-to-inspector variation, as well as an overall level of detection, is exhibited in each of the population of inspectors. The commuter inspectors spent more time on the task and produced more false calls. This is as expected since the specific task was more familiar to the transport inspectors.
2. Performance levels were task specific. An inspector's good performance (relative to other inspectors) on one task did not necessarily indicate a relatively good performance on other tasks.
3. The AANC investigators were able to distinguish inspector failures of detection specific to the searching for cracks from a decision failure in calling an indication a crack. The search component of the process was the larger factor in determining performance levels, although the decision process accounted for much of the worst performance. The implications here are that most, if not all, inspectors can benefit from training interventions that address search procedures.
4. Both test-beds contain several cracks that were found by only one or two of the inspectors, and not the same inspectors. The lengths of these test-bed cracks did not significantly contribute in predicting the number of inspectors that would detect them. The implication of these results is that probability of detection curves as a function of crack length are meaningful only within specific inspection tasks and conditions of inspection.

POC: Dr. Christopher Smith AAR-433, FAA William J. Hughes Technical Center, Atlantic City International Airport, NJ 08405, (609) 485-5221.

9.12.12 NDE Capabilities Data Book

Dr. Christopher Smith

FAA William J. Hughes Technical Center

An FAA program, conducted by the Nondestructive Testing Information Analysis Center (NTIAC), is in progress to collect, analyze, and organize documented probability of detection (PoD) data and information for a variety of nondestructive evaluation (NDE) methods, procedures, materials, and applications related to aircraft inspection. PoD has been used as a quantitative measure of NDE reliability and capability for a number of years. Originally developed as a data presentation approach to meet functional engineering analysis needs, the concept has grown into a recognized approach for comparison of the performance capabilities of various NDE procedures, for quantification of improvements in NDE procedures, for validation and management of NDE system performance, and for

personnel skill development and qualification. Compilation of this information into an *NDE Capabilities Data Book* provides an engineering reference for use in NDE engineering analyses and for development and validation of new NDE procedures. PoD reference data in the Data Book can be used in selecting an NDE procedure for a specific application and for assessing the potential equivalency of an alternate NDE procedure.

The current edition of the *NDE Capabilities Data Book*, available in both hard copy and on compact disk, contains 284 PoD curves presented and organized by NDE method. A documentation page precedes each PoD data set and provides a condensed description of the test object, test artifacts, NDE procedures, and results summary. The PoD curves for varying test object, test artifact, and data collection conditions are presented as a function of crack length and as a function of crack depth and crack depth-to-thickness ratio for selected datasets. Original reference source information is provided for each data set. Work is continuing on upgrading the Data Book with additional PoD information, such as the visual inspection reliability data developed by the FAA Airworthiness Assurance Nondestructive Inspection Validation Center (AANC).

(See Figure 167)

POC: Dr. Christopher Smith, AAR-433, FAA William J. Hughes Technical Center, Atlantic City International Airport, NJ 08405, (609) 485-5221.

9.13. ENGINES

9.13.1 Uncontained Turbine Engine Debris Characterization and Vulnerability Analysis

Mr. Robert Pursel

FAA William J. Hughes Technical Center

Uncontained turbine engine events have led to catastrophic aircraft failures. The FAA saw a need to update advisory material addressing uncontained turbine engine failures. An Aviation Rulemaking Advisory Committee (ARAC) was tasked to update Advisory Circular (AC) 20-128, "Design Considerations for Minimizing Hazards Caused By Uncontained Turbine Engine and Auxiliary Power Unit Rotor and Fan Failure." The group determined that there was a need to better characterize the types of failures, number of fragments, velocity of fragments, and damage caused by these fragments. Engine and airframe manufacturers, who considered this data to be proprietary, had collected much of the data needed to do this. Therefore, in 1995, the FAA William J. Hughes Technical Center entered into an interagency agreement with the Naval Air Warfare Center, Weapons Division (NAWCWD), China Lake, CA, to gather this data and conduct an analysis of the data which could then be used to update AC 20-128. Data was given freely to NAWCWD because this organization had pre-existing nondisclosure agreements with most engine and airframe manufacturers and could therefore protect the proprietary nature of the data.

The data has now been analyzed and the results have been made available to members of the ARAC to use for the update of AC 20-128. The results of this characterization of uncontained debris are being published in an FAA report prepared by NAWCWD. Additionally, the data characterization will also be used to prepare stochastic models of uncontainment events of various types to be used in conjunction with the development of vulnerability assessment tools for civilian aircraft.

Existing vulnerability assessment tools (FASTGEN3 and COVART 4.0) have been used by the military to assess the vulnerability of their aircraft to hostile threats. Vulnerability analyses of commercial airframes to the threat from uncontained engine debris will be conducted by modifying the military codes for use by civilian airframe manufacturers.

The final result of this effort will be a validated tool kit to improve the certification process and provide a means of compliance with the proposed revision to AC 20-128 that will include design for multiple fragment threat.

(See Figure 168)

POC: Mr. Robert Pursel, AAR-430, FAA William J. Hughes Technical Center, Atlantic City International Airport, NJ 08405, (609) 485-6343.

9.13.2 Containment of Turbine Engine Failures

Mr. Robert Pursel

FAA William J. Hughes Technical Center

A Kevlar ring, using a patented design, was developed by Pepin Associates, Inc. and tested in a full scale test at China Lake, CA. The ring was fabricated with a 0.014-inch titanium inner and outer sleeve. One-inch-thick Kevlar 29 ballistic fabric made up the primary structure of the containment ring. The ring was reinforced with titanium rods inserted through the fabric and laser welded to the inner and outer sleeves. The ring was tested on a T53-L-13L engine installed in an UH-1 Huey helicopter. The second stage power turbine disk was notched so that the disk would rupture at approximately 20,400 rpm. The engine was started and immediately accelerated to minimize the chance of a premature rupture. The test was recorded on high-speed film at 4000 pictures per second. The disk ruptured as the engine accelerated through 19,629 rpm. The disk ruptured into three equal sections (approximately 3.6 lbs. each). The photograph in Figure 169 shows the containment ring after the test.

All three fragments penetrated through the combustor case and were embedded inside the containment ring. Minimum interactions between the immediate engine components and fragments were observed. The result was a contained tri-hub burst with minor bulging of the containment ring and little sign of distress to the airframe.

The test demonstrated the capability to contain a tri-hub burst on a medium-sized turboshaft helicopter engine. The full-scale test demonstrated that the fiber material, Kevlar 29 reinforced with titanium rods at 45° angles, is a good baseline ballistic fabric for containment structures. This is based on the specific containment fragment energy of the containment ring. Practical issues related to clearance for maintenance on a day to day basis as well as design for ring expansion during the failure are difficult challenges that must be considered for production of this type of a system. An FAA technical report (Turbine Fragment containment Test, AR-98/22, June 1998) on this work has been published.

POC: Mr. Robert Pursel, AAR-430, FAA William J. Hughes Technical Center, Atlantic City International Airport, NJ 08405, (609) 485-6343.

9.13.3 Resistance of Titanium Aluminide to Domestic Object Damage Assessed

Brad Lerch
NASA-GRC

A team consisting of General Electric Aircraft Engines, Precision Cast Parts, Oremet, and Chromalloy were recently awarded a NASA sponsored *Aerospace Industry Technology Program (AITP)*. This ATIP will develop a design and manufacturing capability leading to engine test demonstration and eventual implementation of a γ -Ti-47Al-2Nb-2Cr (at. %) titanium aluminide (TiAl) low pressure turbine blade for commercial service. One of the main technical risks of implementing TiAl LPT blades is the poor impact resistance of TiAl in comparison to the currently used nickel-based superalloy. The impact resistance of TiAl is being investigated at the NASA Glenn Research Center as part of the AITP and HITEMP program.

The overall objective of this work is to determine the influence of impact damage on the high cycle fatigue life of simulated TiAl low-pressure turbine blades. To this end, impact specimens were cast to size in a dog-bone configuration and given a typical processing sequence followed by an exposure at 650°C for 20 hours to simulate embrittlement at service conditions. The specimens were impacted at 260°C under a 69 MPa load. Steel projectiles with diameters 1.6 and 3.2 mm were used to impact the specimens at 90° to the leading edge. Two different impact energies (0.74 and 1.5 J) were used to simulate moderately severe domestic object damage on a low-pressure turbine blade.

Fatigue tests were performed at 650° C and at a frequency of 100 Hz. In addition, three different loading ratios, R, were used to assess the effect of mean stresses. As expected, the specimens impacted at the higher energy levels failed at lower fatigue stresses due to the larger “defect” associated with the impact. Both energy levels resulted in fatigue strengths that were significantly lower, yet predictable, than for the smooth bars (i.e., non-impacted specimens). In addition, a Goodman mean stress approach could be used accurately to model the fatigue data for all impacted specimens (Figure 170).

The industry-NASA team is using the results of this study minimize the technical risks associated with impact issues. The actual damage tolerable for low-pressure blade application will be determined by a combination of fatigue testing and consideration of actual engine conditions. The current evaluations indicate that Ti-47Al-2Nb-2Cr possesses the level of damage tolerance required for implementation into service.

Reference:

1. Susan L. Draper, J. Michael Pereira, and Michael V. Nathal: Impact Resistance of γ -Ti-48Al-2Nb-2Cr, NASA CP 10192, Vol. II, pp. (25-1) - (25-13), 1997.

9.13.4 Enhanced Turbine Rotor Material Design and Life Methodology

Mr. Joseph Wilson
FAA William J. Hughes Technical Center

Commercial airline service experience by turbine-powered aircraft has shown that despite the current rigorous safe-life design approach toward failure critical components, material and manufacturing anomalies can reduce structural integrity and increase failure risk. The photograph in Figure 171 shows a cutaway of one such anomaly, a hard-

alpha defect in titanium engine material. The FAA, working closely with the engine industry through the Rotor Integrity Subcommittee of the Aerospace Industries Association, has developed supplemental design and lifing methods that formed the basis for this research program.

A major, ongoing, multiyear program has been established through an FAA cooperative grant to Southwest Research Institute with engine company partners General Electric, Pratt & Whitney, AlliedSignal, and Allison. The program is developing a standardized, damage tolerance-based, probabilistic code to address the structural integrity issues of failure critical turbine engine rotors. A methodology and a computer program have been developed to assess rotor disk design considering the uncertainties of alloy melt-related hard-alpha defects (size, location, and occurrence rate), stresses, crack growth, inspection effectiveness (PoD), and shop visit time. Version 1 of the DARWIN (Design Assessment of Rotors With Inspection) code was delivered in April 1997 and reviewed by participating engine companies. DARWIN 2.0 was delivered in June 1998. DARWIN integrates finite element stress analysis, defect growth analysis, and nondestructive inspection simulation with probabilistic analysis to assess the risk of rotor disk fracture with in-service inspection. The code has the ability to model random inspection schedules and probability of detection and compute the probability-of-fracture as a function of flight cycles with and without inspection. In addition to the Monte Carlo simulation method, advanced tailored probabilistic methods have been developed to efficiently compute failure probability. A graphical user-interface has been developed to assist the user in preparing DARWIN inputs with a unique capability to divide the structure into stress or inspection-based zones and define zone-based parameters for fracture mechanics modeling. It is anticipated that DARWIN will be used as a tool to reveal critical information for optimal design and inspection planning. The methodology can be applied to other structures that are characterized by rare defects. The framework of DARWIN has been designed to anticipate future expansion to cover other materials and multiple failure modes.

When completed, the code will be the basis for an acceptable design and lifing method referenced through an FAA Advisory Circular that engine companies may incorporate into their design systems. The anticipated outcome when implemented will have the potential to reduce the uncontained rotor disk failure rate while providing more realistic inspection schedules.

POC: Mr. Joseph Wilson, AAR-432, FAA William J. Hughes Technical Center, Atlantic City International Airport, NJ 08405, (609) 485-5579.

9.13.5 Fleet Octane Requirement for Unleaded Fuels

Mr. Stewart Byrnes

FAA William J. Hughes Technical Center

The 1990 Clean Air Act Amendments passed by Congress called for the elimination of the use of tetraethyl lead in all fuels. Since that time the FAA has been encouraging a partnership between government and industry to oversee the development of a fuel to replace the primary fuel used by the general aviation industry known as 100 low lead (100LL). The lead in this fuel provides the octane rating necessary for the safe operation of high performance general aviation piston engines.

In February of 1995, a Coordinating Research Council (CRC) Committee was formed with members from the FAA and private industry to oversee the development of a replacement fuel for 100LL. This forum has served as a mechanism to allow the competitive interests of individual segments of the general aviation industry to share information and help foster the development of a new unleaded aviation gasoline.

Soon after its formation the CRC agreed that determining the octane requirement of the general aviation fleet was the most important parameter that demanded immediate attention. Data generated by the William J. Hughes Technical Center on test engines, shown in Figure 172, has yielded a draft report documenting the validation of a ground based procedure for determining an engine's octane requirement. That procedure was balloted for consideration at the June 1998 American Society of Testing and Materials (ASTM) semiannual meeting to become an approved ASTM procedure. Comments on the procedure were addressed and it will be balloted again for approval at the December 1998 ASTM meeting. Work has also begun on the octane rating procedure for the more complex turbocharged engines.

Octane rating tests determined that to date no engines have performed with 100% satisfaction on primary reference fuels. This has forced the generation of new formulations by the participating oil companies of unleaded primary reference fuels that will have octane ratings higher than 100 without lead. Prior to this development, primary reference fuels required lead to get a rating higher than 100. The first of these samples arrived in September of 1998 and will be tested in early FY99.

A fuel matrix, comprised of several different components, was agreed to by the CRC. This matrix will spur the submission of industry-supplied candidate fuels. Candidate formulations specified in the matrix will be submitted to various laboratories to determine the octane rating of each formulation. The results will be used to determine which candidates are the most promising and worthy of actual engine octane rating testing. These developments should lead to significant advances in the coming year in the search for safe and effective replacement for 100LL.

POC: Mr. Stewart Byrnes, AAR-432, FAA William J. Hughes Technical Center, Atlantic City International Airport, NJ 08405, (609) 485-4499.

9.13.6 Simulation of Crack Propagation in Engine Rotating Components Under Variable Amplitude Loading **P.J. Bonacuse**

U. S. Army Research Laboratory

L. J. Ghosn

Case-Western Reserve University

J. Telesman and A. M. Calomino

NASA Glenn Research Center

P. Kantzos

Ohio Aerospace Institute

The crack propagation life of tested specimens has been repeatedly shown to strongly depend on the loading history. Overloads and extended stress holds at temperature can either retard or accelerate the crack growth rate. Therefore, to accurately predict the crack propagation life of an actual component, it is essential to approximate the true loading history. In military rotorcraft engine applications, the loading profile (stress amplitudes, temperature, and number of excursions) can vary significantly depending on the type of mission flown. To accurately assess the durability of a fleet of engines, the crack propagation life distribution of a specific component should account for the variability in the missions performed (proportion of missions flown and sequence). In this report, analytical and experimental studies are described that calibrate/validate the crack propagation prediction capability for a disk alloy under variable amplitude loading. A crack closure based model was adopted to analytically predict the load interaction effects. Furthermore, a methodology has been developed to realistically simulate the actual mission mix loading on a fleet of engines over their lifetime. A sequence of missions is randomly selected and the number of repeats of each mission in the sequence is determined assuming a Poisson distributed random variable with a given mean occurrence rate [Figure 173]. This assumes that an aircraft will perform the same mission repeatedly while stationed with a specific unit and an overhauled engine will go to a randomly selected unit. Multiple realizations of random mission histories are generated in this manner and are used to produce stress, temperature, and time points for fracture mechanics calculations. The result is a cumulative distribution of crack propagation lives for a given, life limiting, component location. This information can be used to determine a safe retirement life or inspection interval for the given location. While the mean of the simulated crack propagation lives is relatively insensitive to the value chosen for the Poisson distribution the spread in the increases dramatically.

As can be seen in Figure 174, there is a strong dependence of the crack propagation life on the mission sequence and particularly on the mean block length (expected number of mission repeats between engine removal for overhaul). The expected crack propagation life variance caused by the mission mix loading will necessitate a reduction in the estimated lower bound crack propagation life.

Reference:

1. Bonacuse, P. J., Ghosn, L. J., Telesman, J., Calomino, A. M., and Kantzos, P., "Simulation of Crack Propagation in Engine Rotating Components Under Variable Amplitude Loading," in NATO Research and Technology Organization, Applied Vehicle Technology Panel (formerly AGARD Propulsion and Energetics Panel (PEP)) meeting proceedings: RTO-MP-8, Feb. 1999.

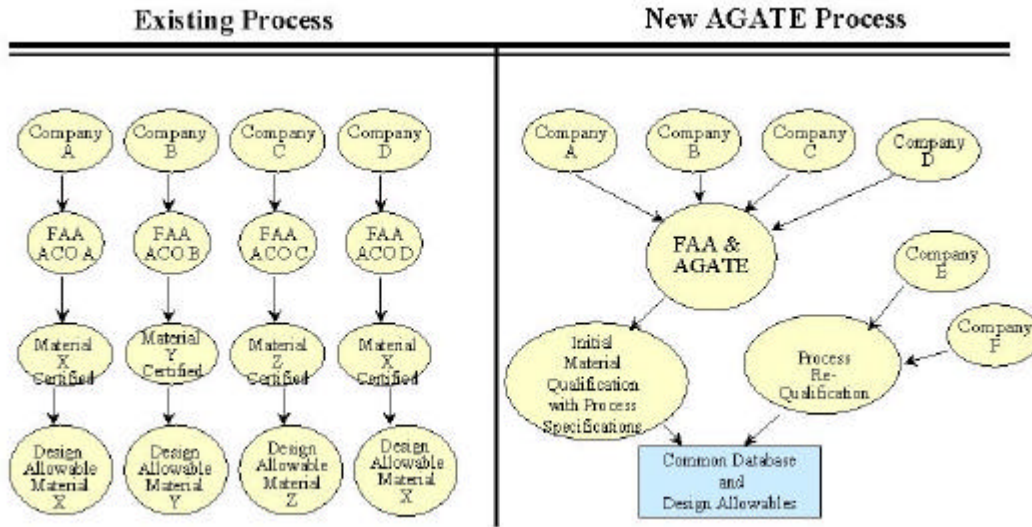


Figure 1.



Figure 2.



Figure 3.



Figure 4.

Second International Symposium of Fretting Fatigue
August 31 – September 1, 1998
The University Park Hotel, Salt Lake City, Utah

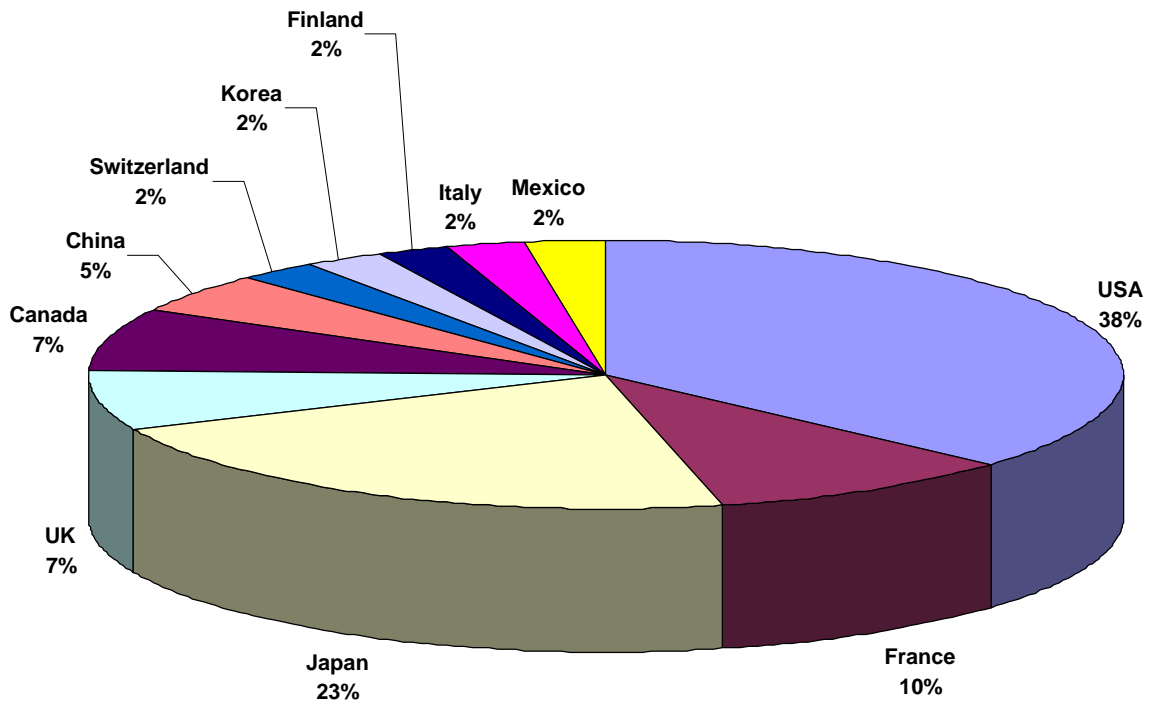


Figure 5. Distribution of Papers – By Country

Second International Symposium on Fretting Fatigue
 August 31 – September 2, 1998
 The University Park Hotel, Salt Lake City, Utah

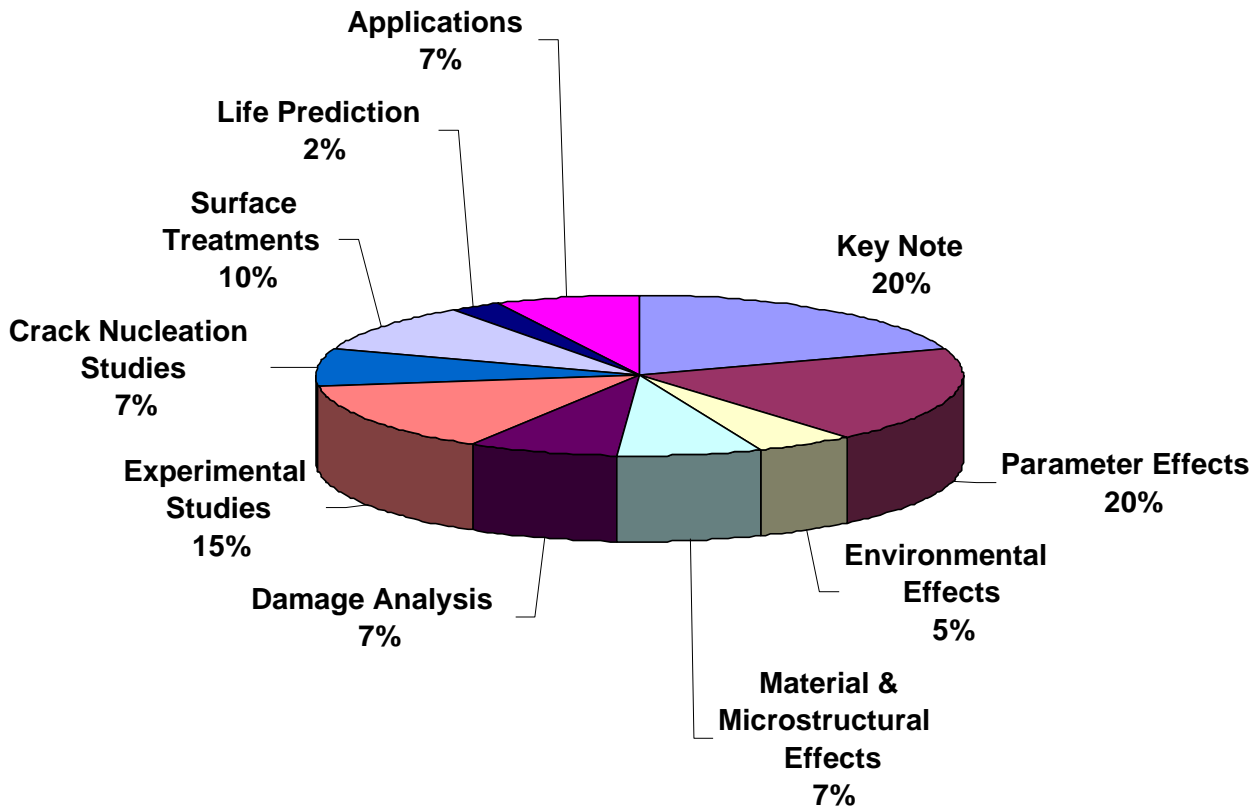


Figure 6. Distribution of Papers – By Topic

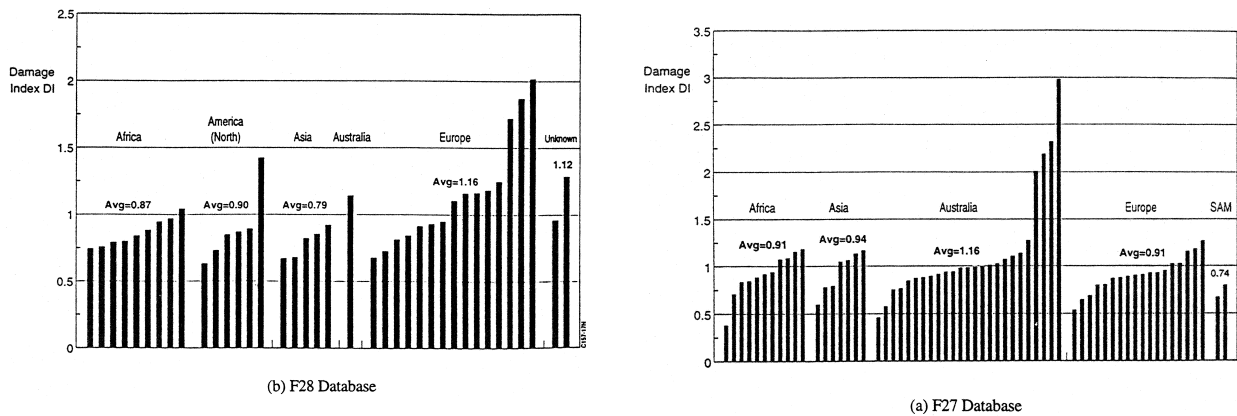


Figure 7.

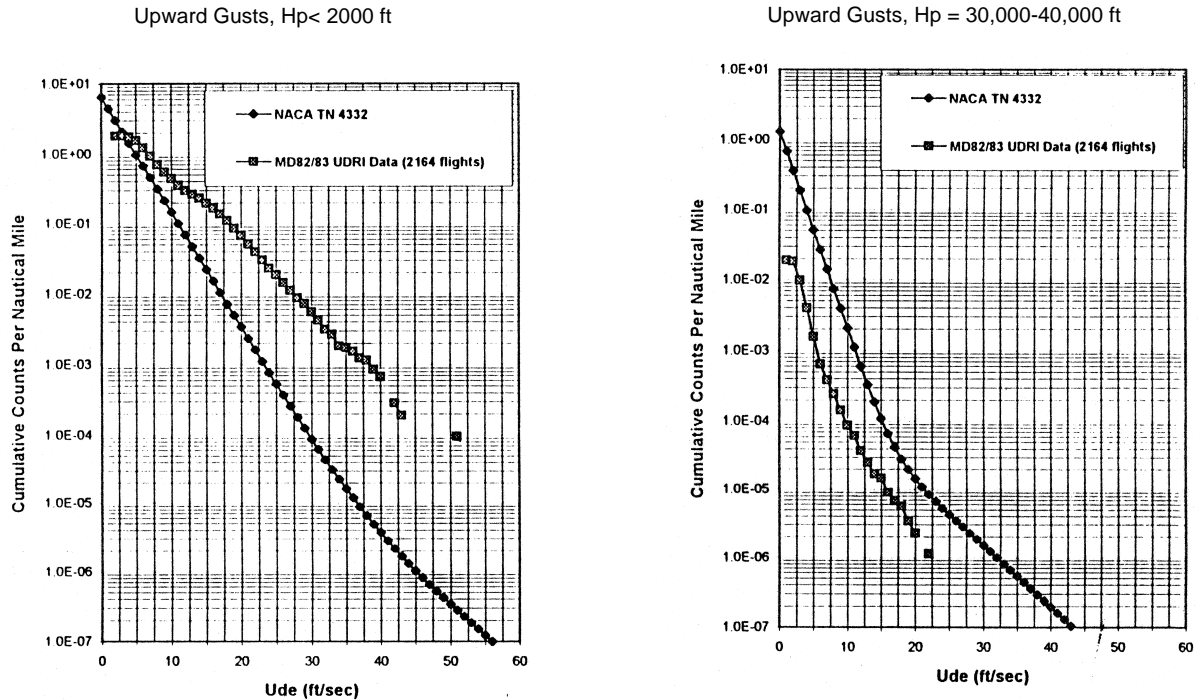


Figure 8. Derived Gust Velocity Cumulative Peak Counts

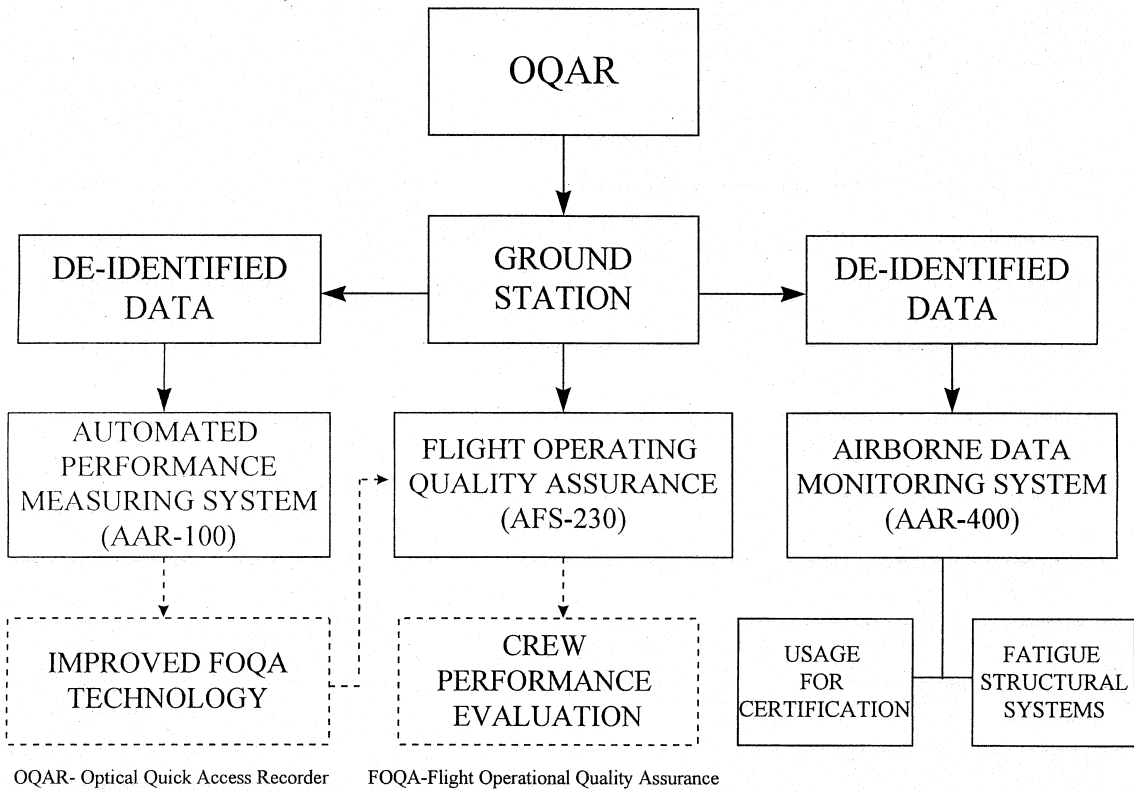


Figure 9.



Figure 10.

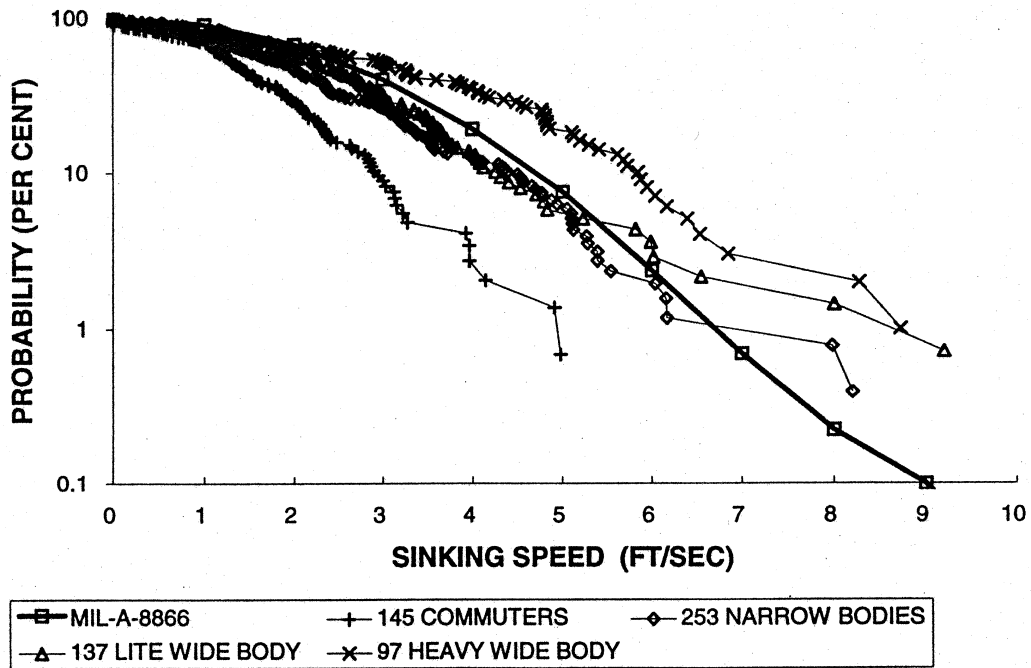
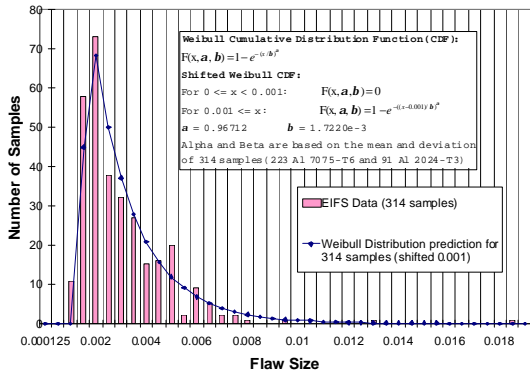
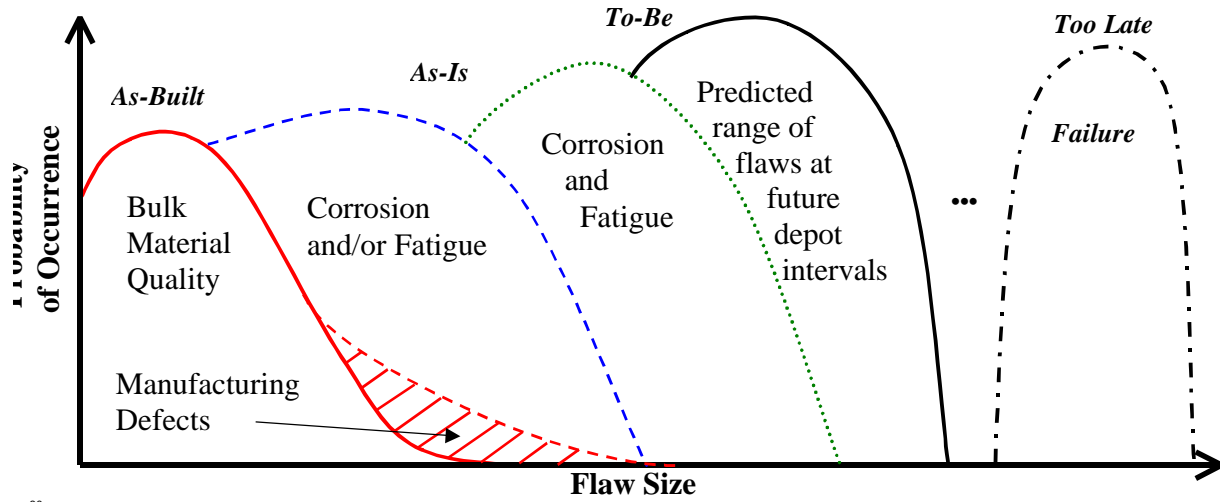


Figure 11. Probability of Distribution of JFK Survey Sinking Speeds



Inputs, Improvements & Benefits

- WSD, MSD
- Applicable to USAF/USN criteria
- Joint Service Life design features
- Corrosion-fatigue interaction
- DTA with environmental effects

Figure 12.

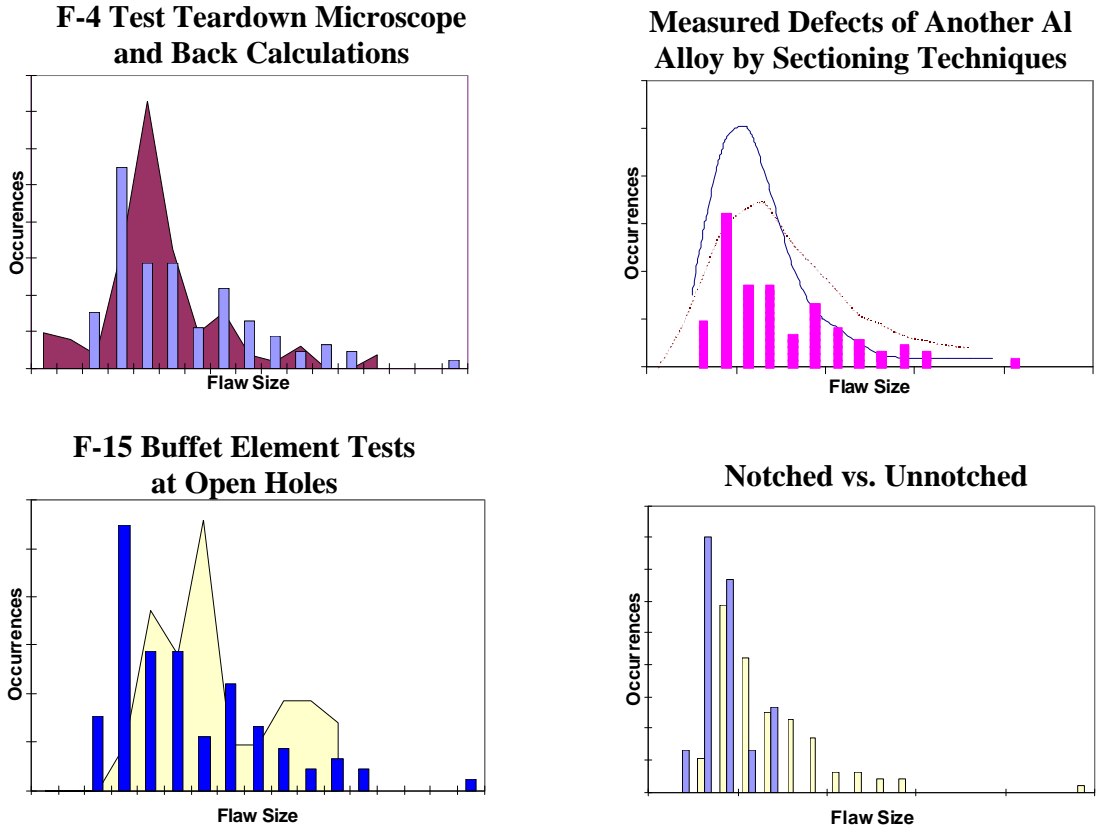


Figure 13. Methods & Concept Substantiated by Several Techniques

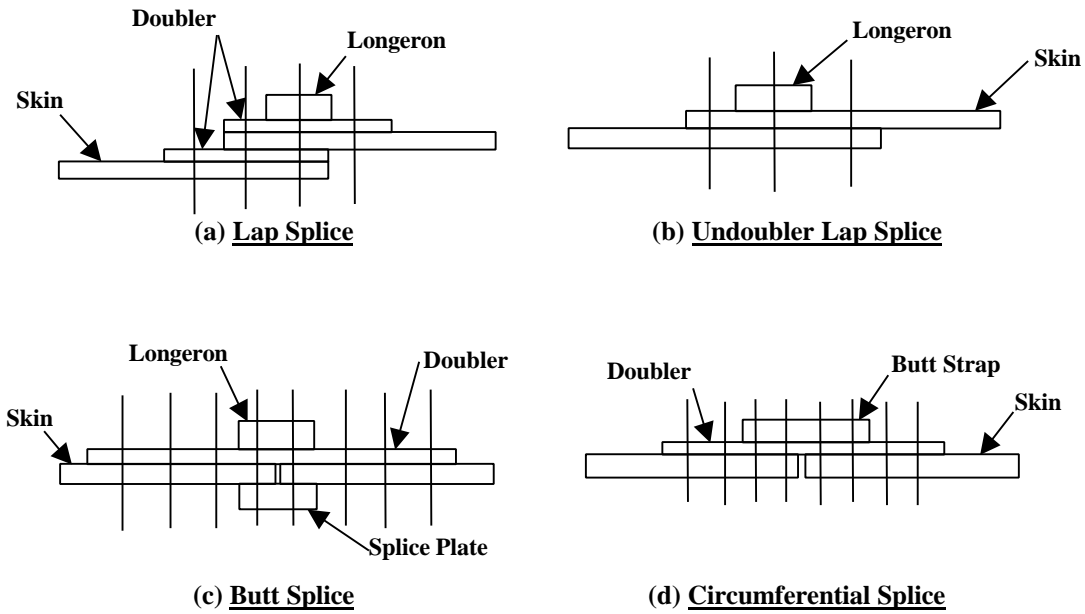


Figure 14.

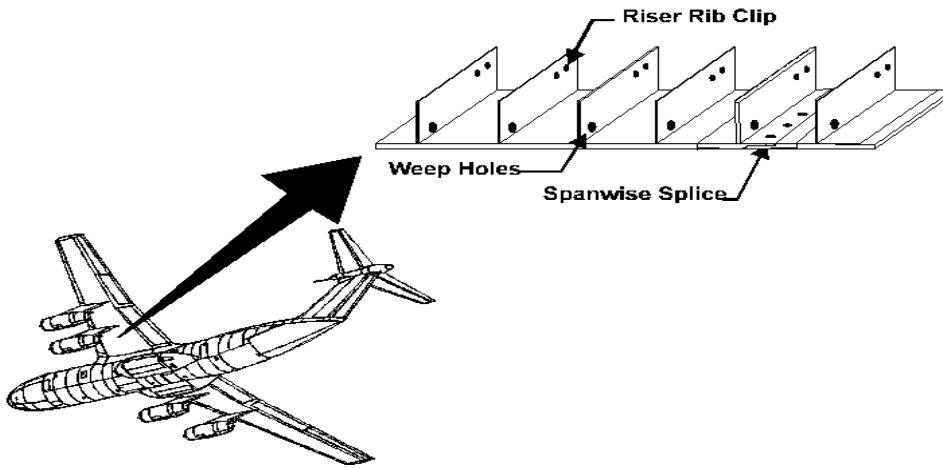


Figure 15. C-141 Wing Lower Surface

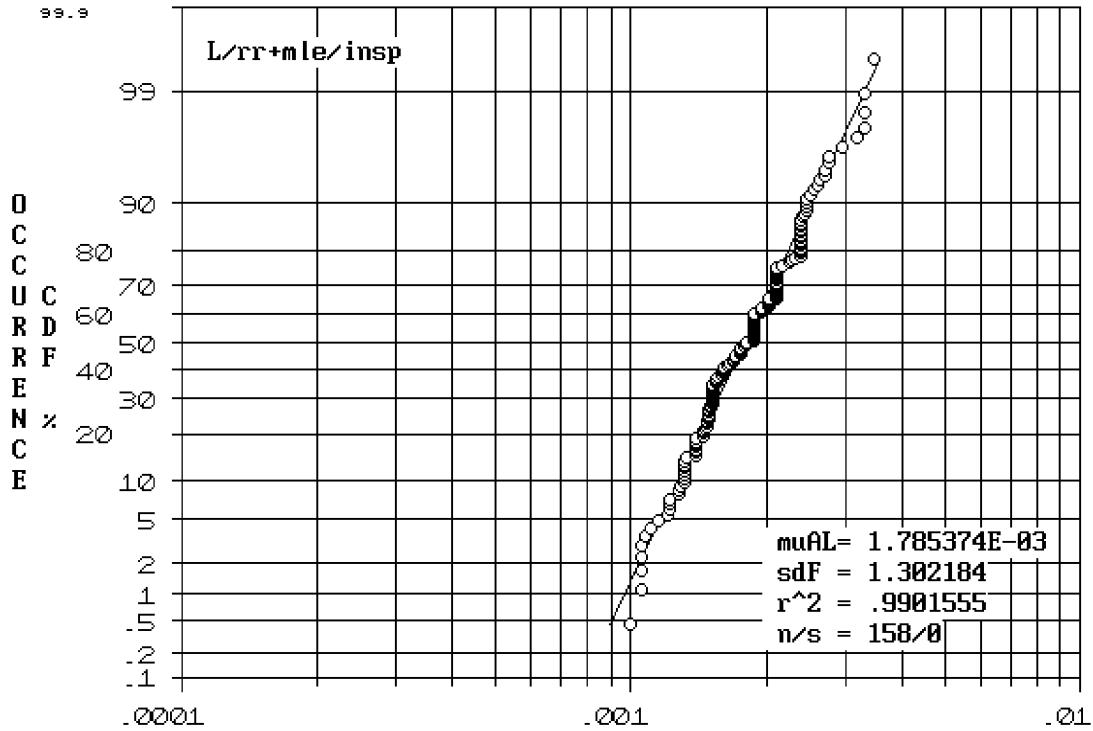


Figure 16. Cumulative Number of Weep Hole Cracks vs. Crack Length-Fatigue Test, Tear Down Inspection and Field Inspections

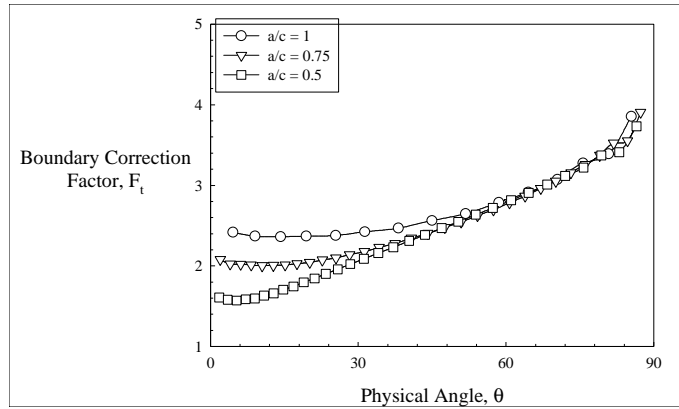


Figure 17.

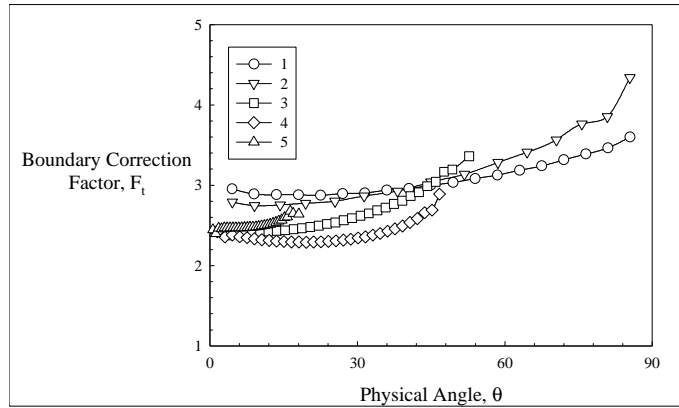


Figure 18.

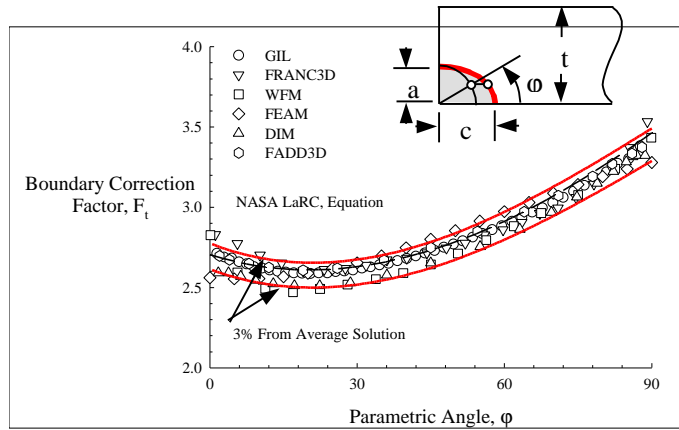


Figure 19.

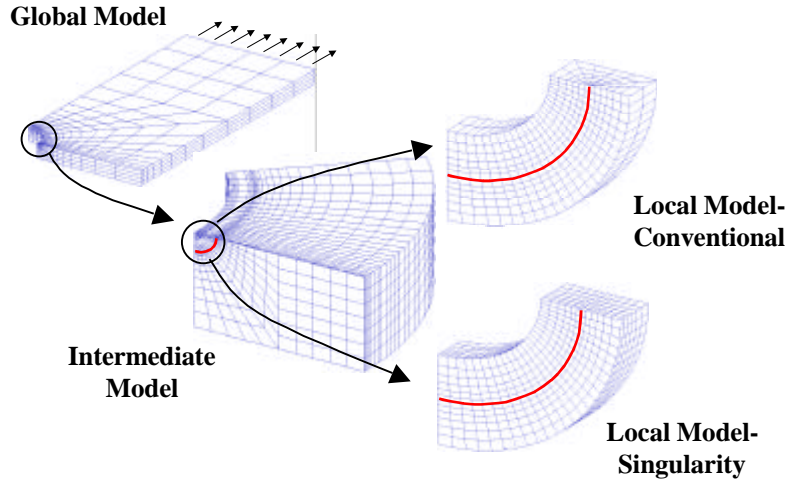


Figure 20.

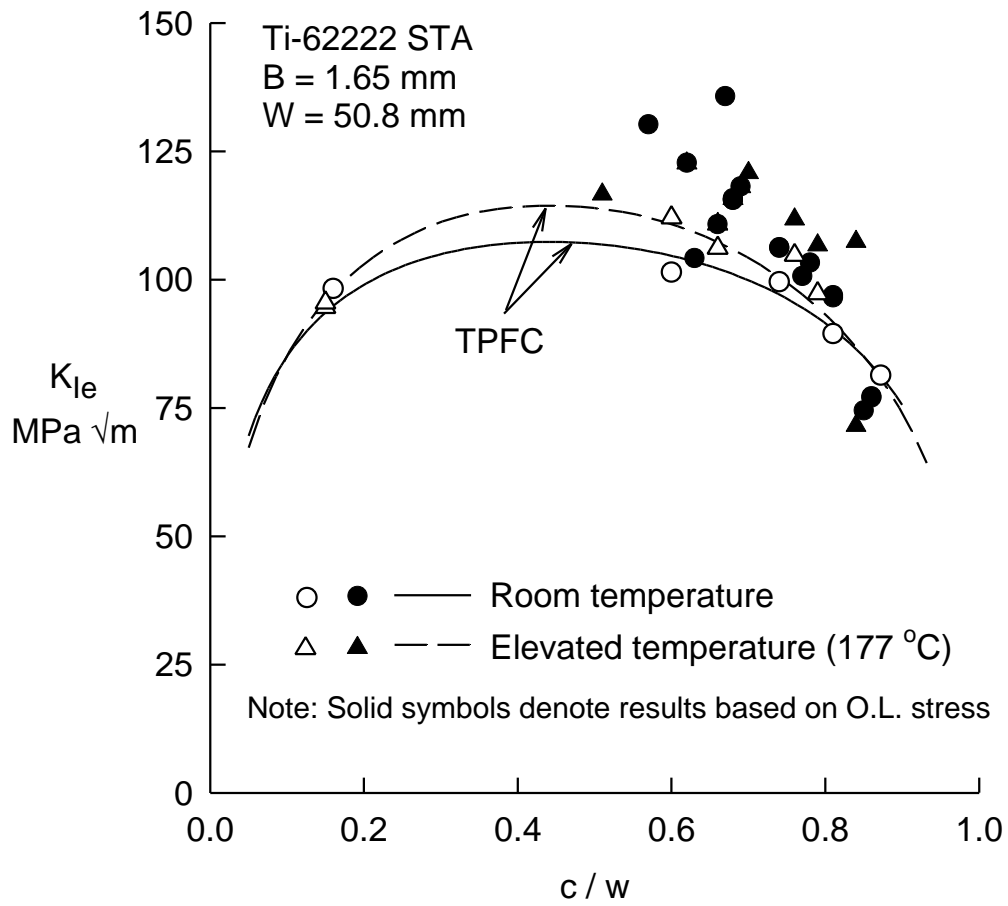


Figure 21. Fracture Data for Ti-62222 Titanium Alloy at Room and Elevated Temperature

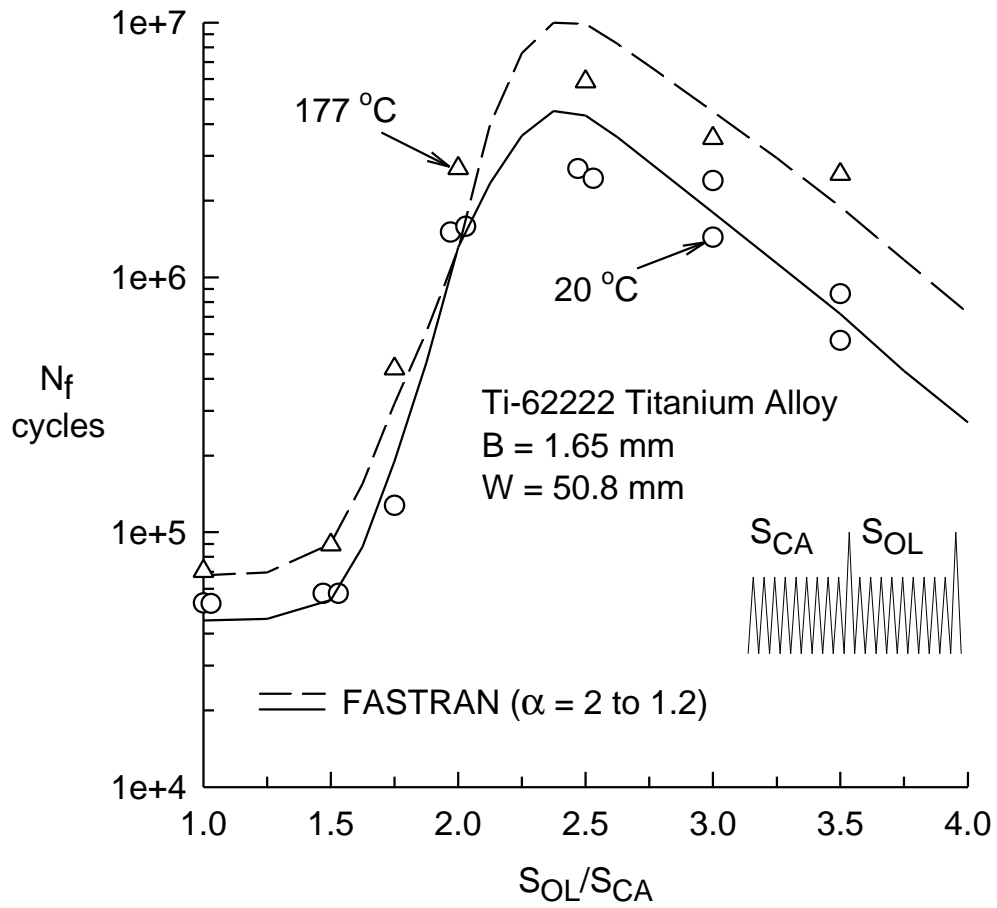


Figure 22. Comparison of Measured and Predicted Crack Growth Lives for Repeated Spike Overloads for Room and Elevated Temperature for TI-62222 Titanium Alloy

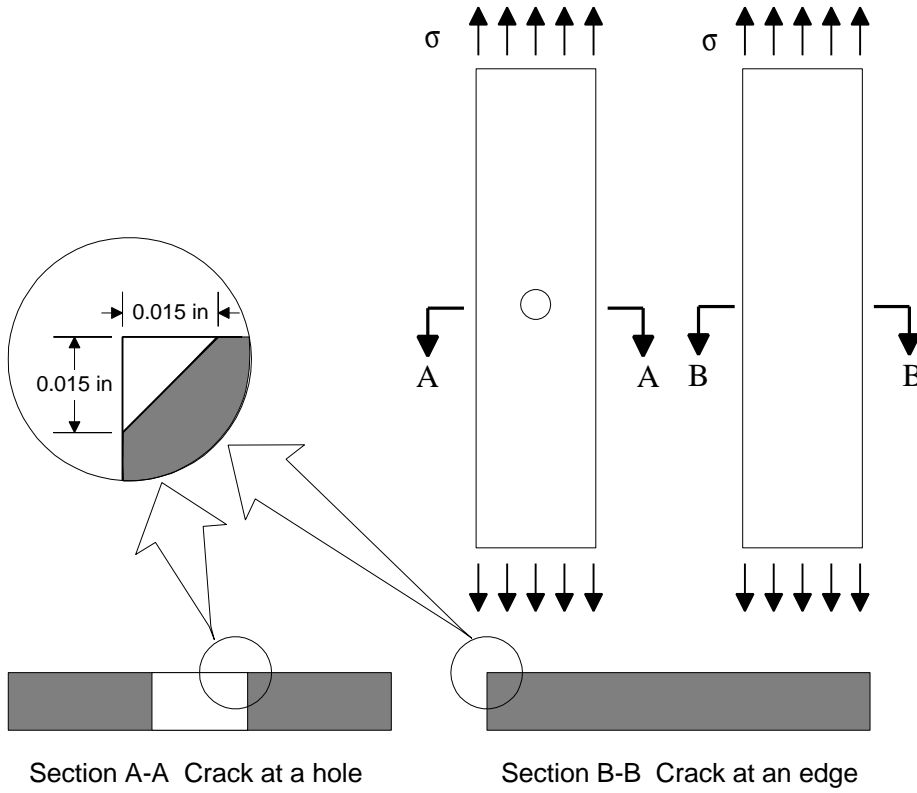


Figure 23. Crack Starter Notch Location on Spectrum Test Specimens

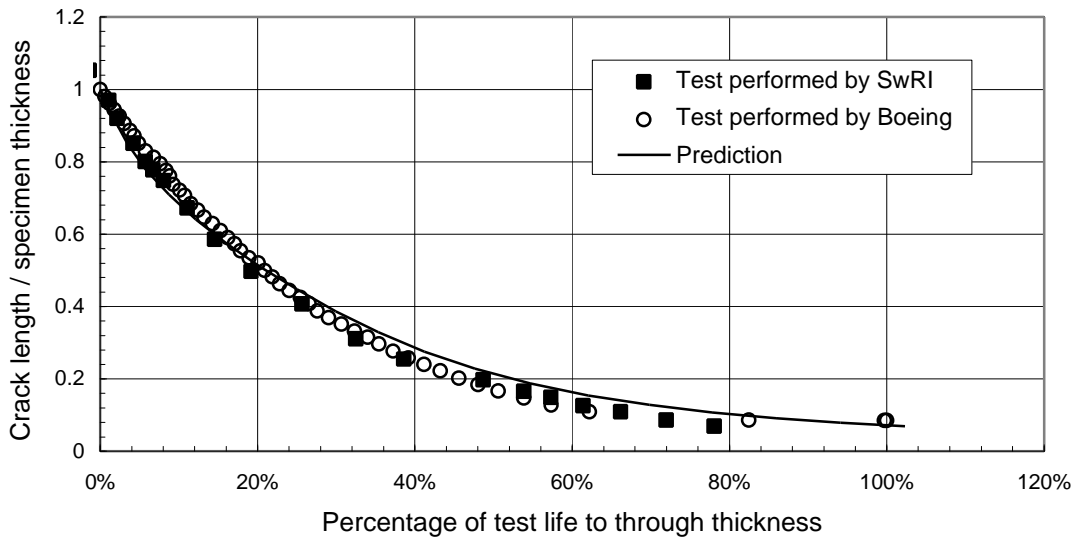


Figure 24. Predicted Crack Length Compared to Test Crack Length for Wing Lower Surface Spectrum Loading Applied to a 2324-T9 "Crack-at-a-Hole" Specimen

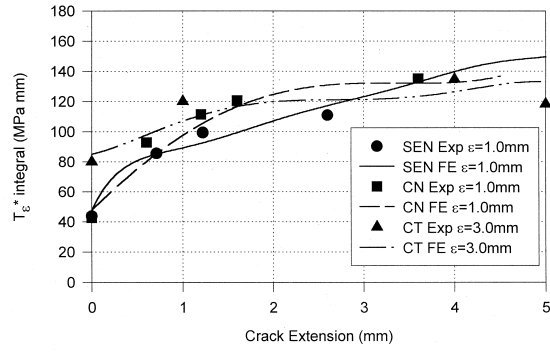


Figure 25.

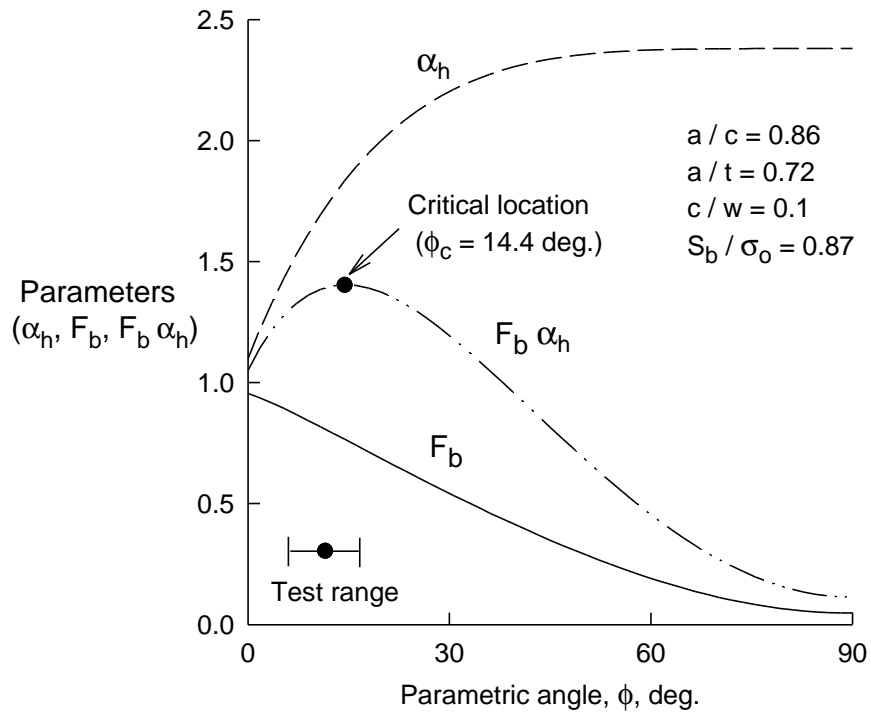


Figure 26. Determination of the Critical Fracture Location for Surface Crack Under Bending Loads

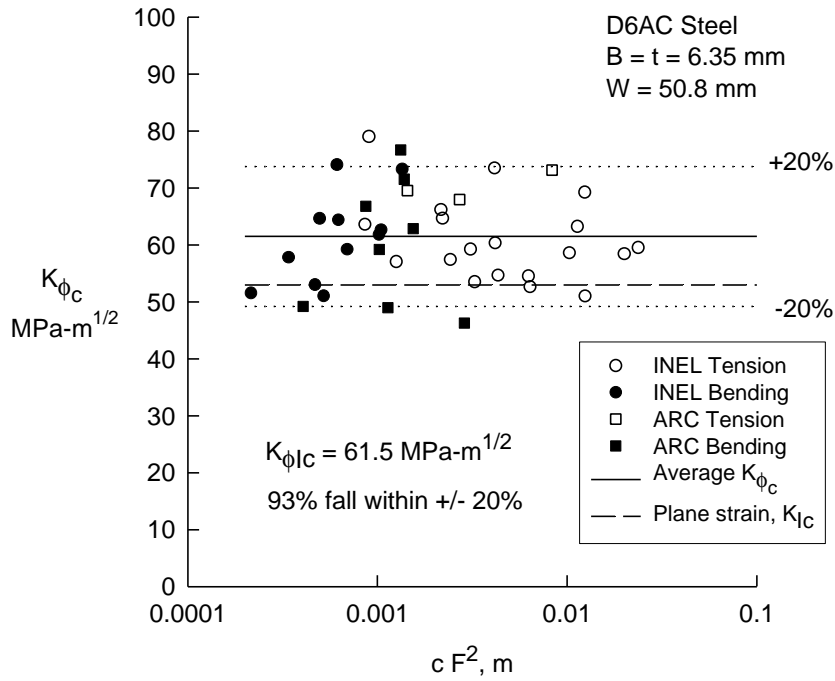


Figure 27. Critical Stress-Intensity Factor at Critical Location for D6AC Steel at Crack Initiation Under Either Tension or Bending Loads

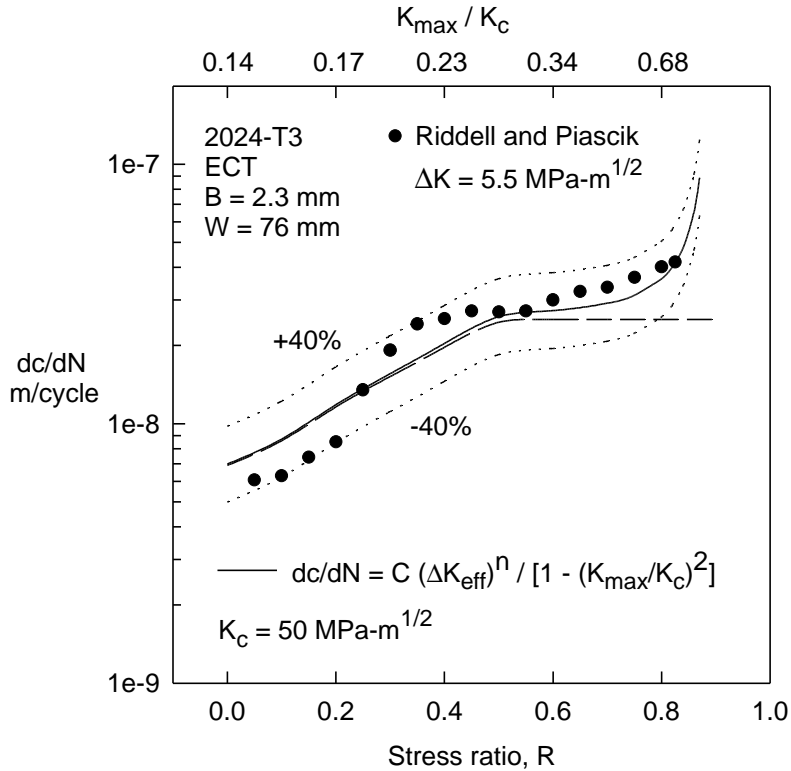


Figure 28. Measured and Calculated Crack-Growth Rates at Constant ΔK Value

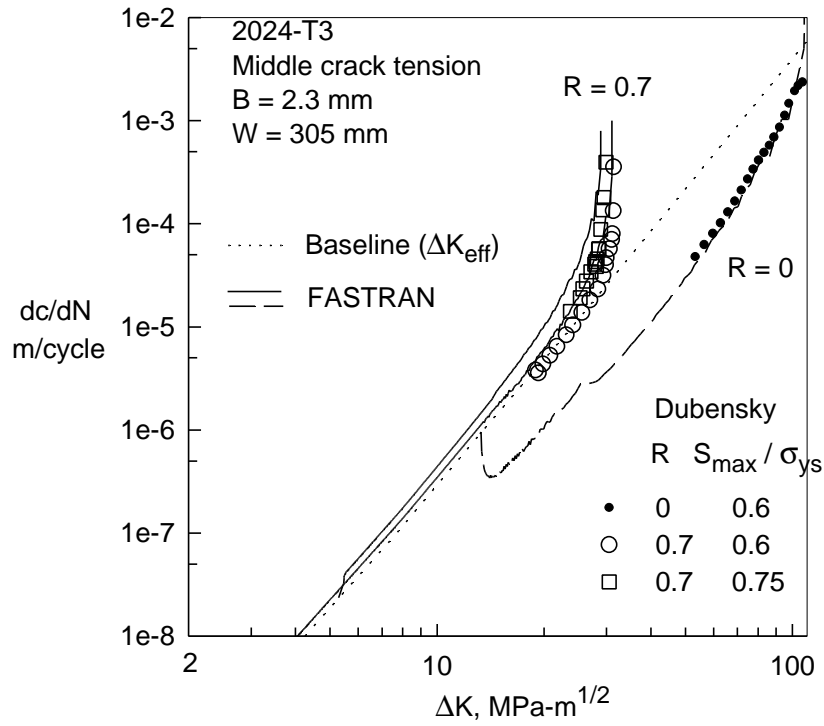


Figure 29. Measured and Calculated Crack-Growth Rates for High Stress Levels at Low and High Stress Ratios

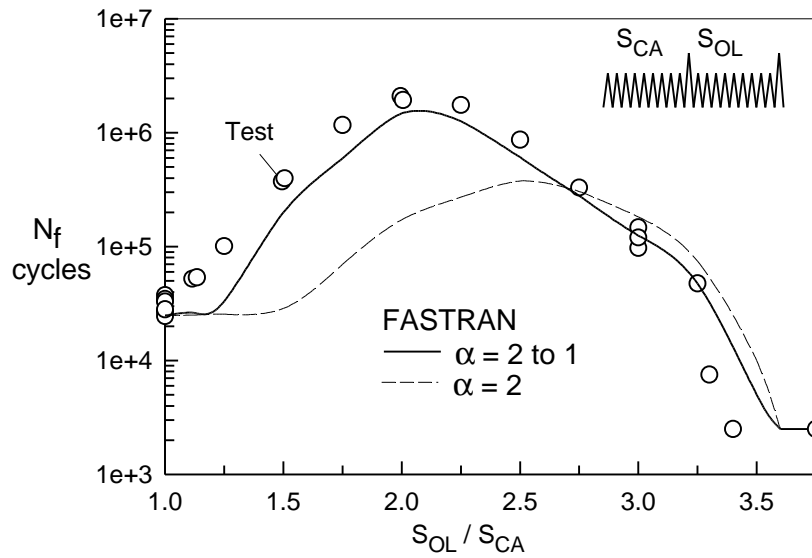


Figure 30. Measured and Predicted Cycles to Failure During a Repeated Spike Overload Sequence

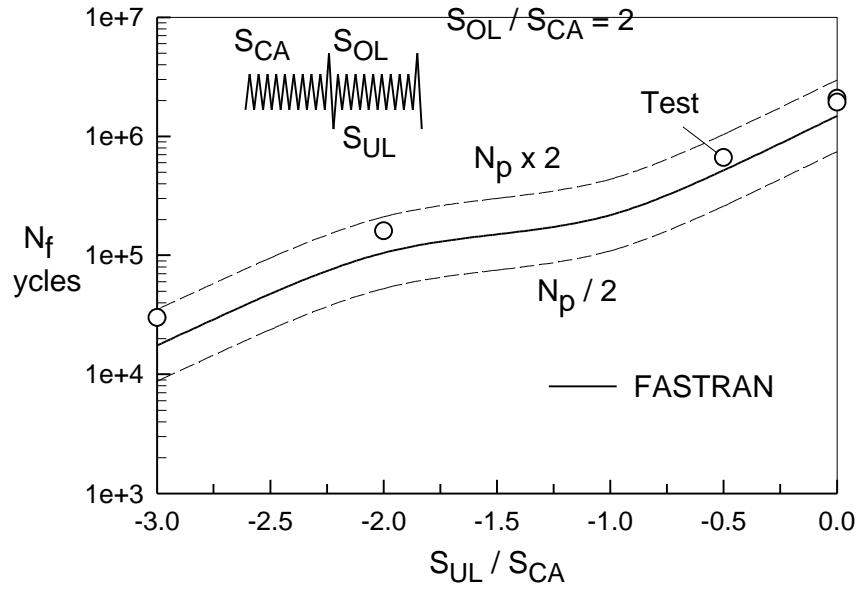


Figure 31. Measured and Predicted Cycles to Failure During a Repeated Spike Overload and Underload Sequence

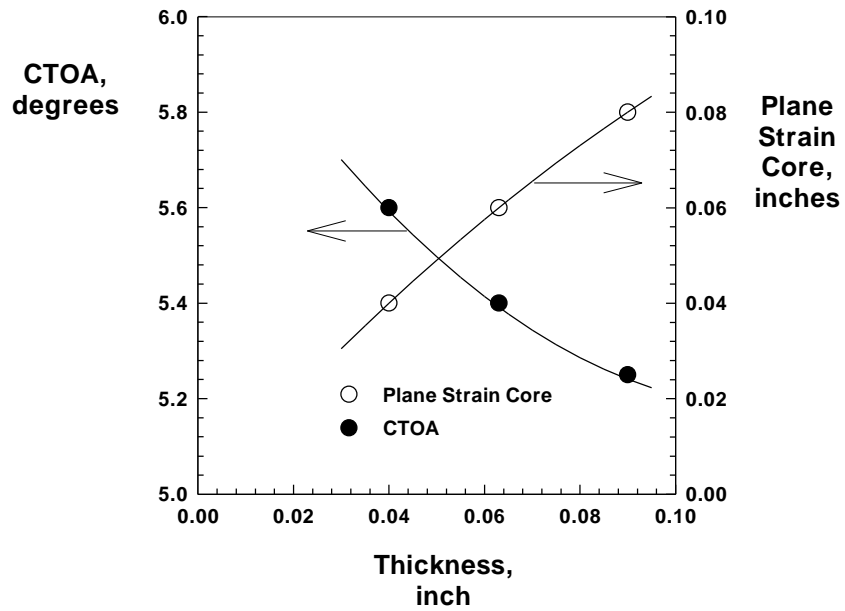


Figure 32. Variation in Critical CTOA and Plane-Strain Core Height as a Function of Thickness for 2024-T3 Aluminum Alloy

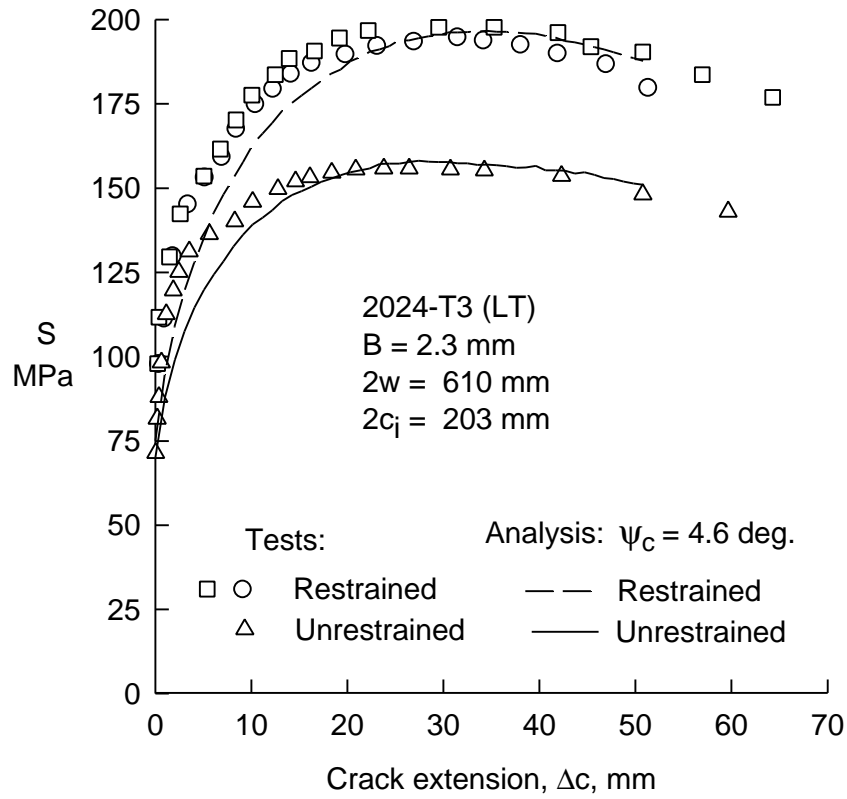


Figure 33. Measured and Predicted Stable Crack Growth for Restrained and Un-Restrained (Buckling) Panels

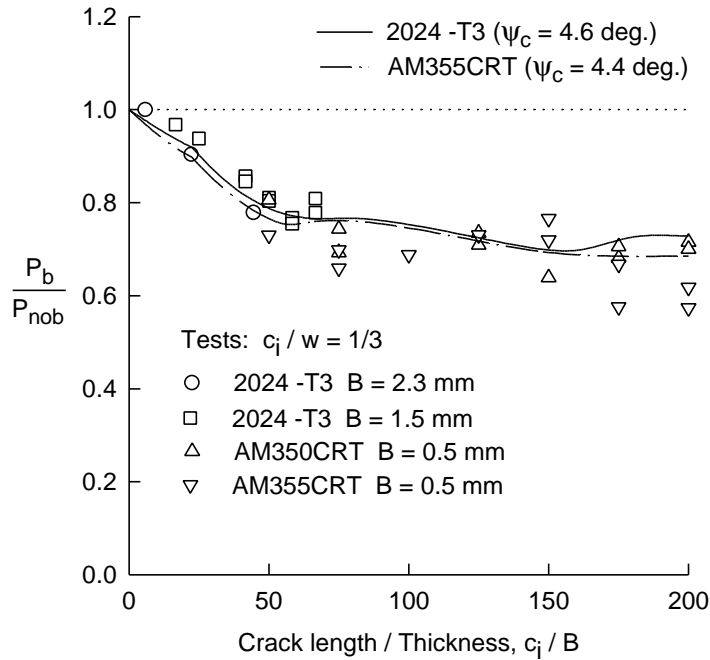


Figure 34. Measured and Predicted Effects of Buckling on Failure Loads for Thin Aluminum Alloys and Steels

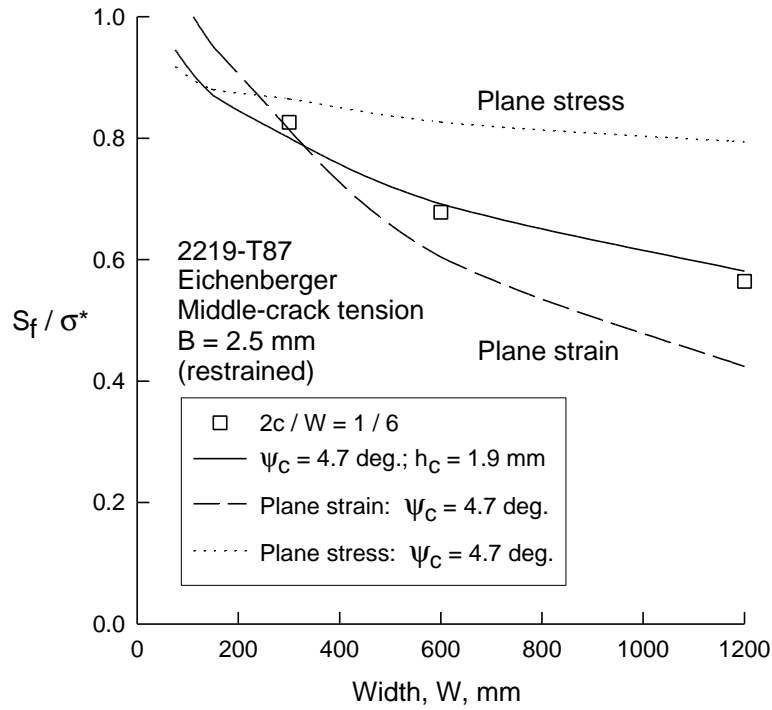


Figure 35. Measured and Predicted Failure Stresses as a Function of Specimen Width Using Plane-Stress, Plane-Strain, and the Plane-Strain Core Concept

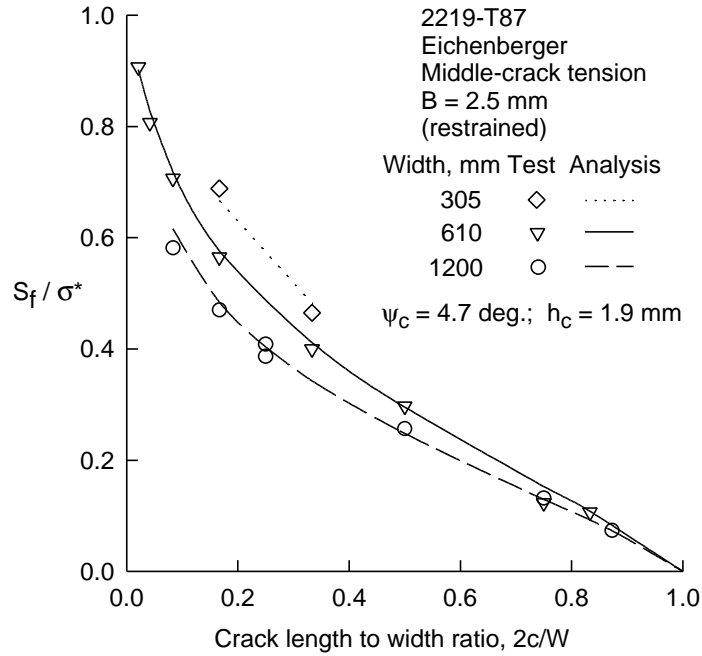


Figure 36. Measured and Calculated Failure Stresses as a Function of Crack Length for Various Width Specimens

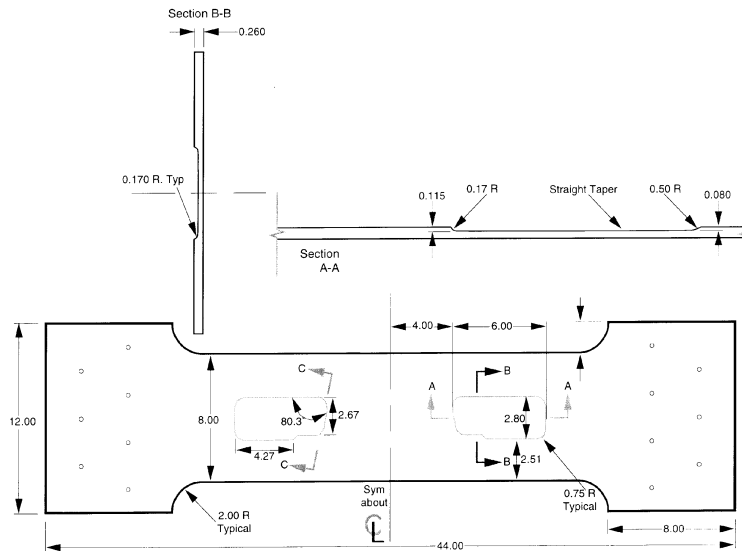


Figure 37. Test Specimen Geometry Simulating Machined Pockets

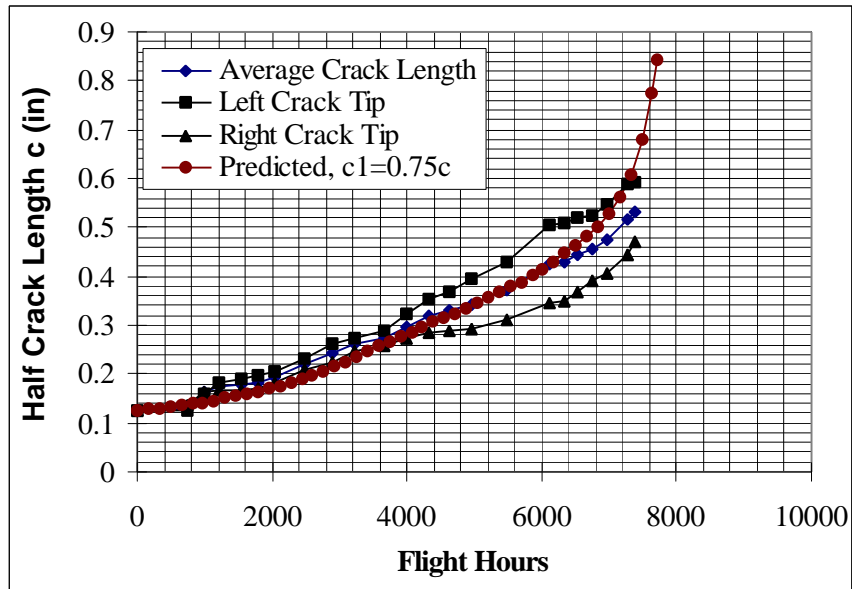


Figure 38. Comparison Between Test and Predicted Crack Growth in Machined Pocket

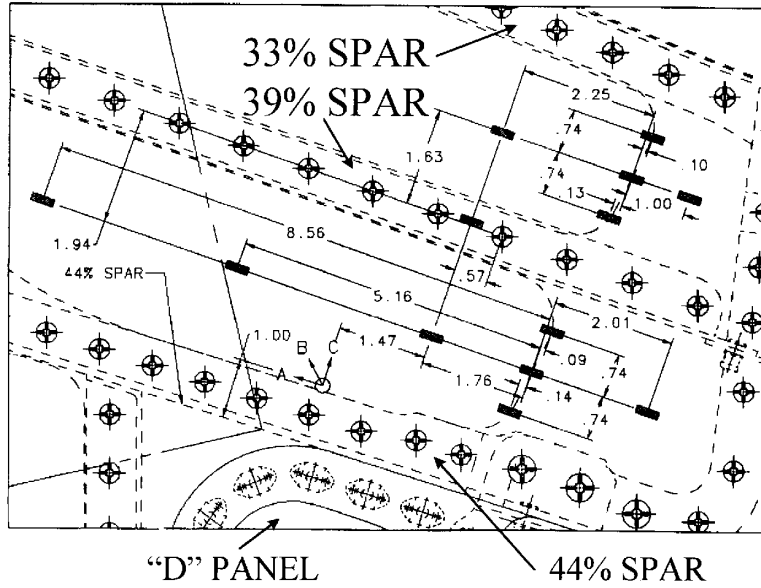


Figure 39. Strain Gage Locations in the Pocket Area of T-38 Wing Skin

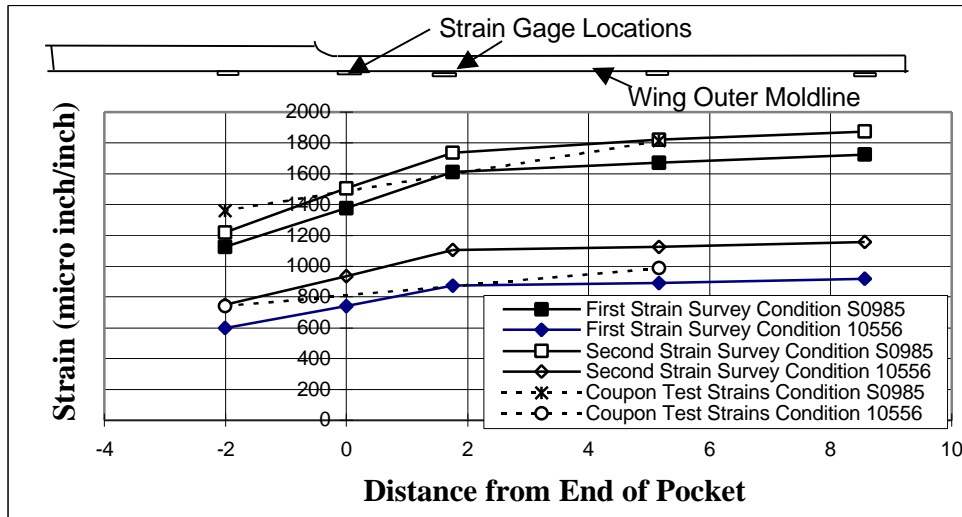


Figure 40. Wing Strain Survey

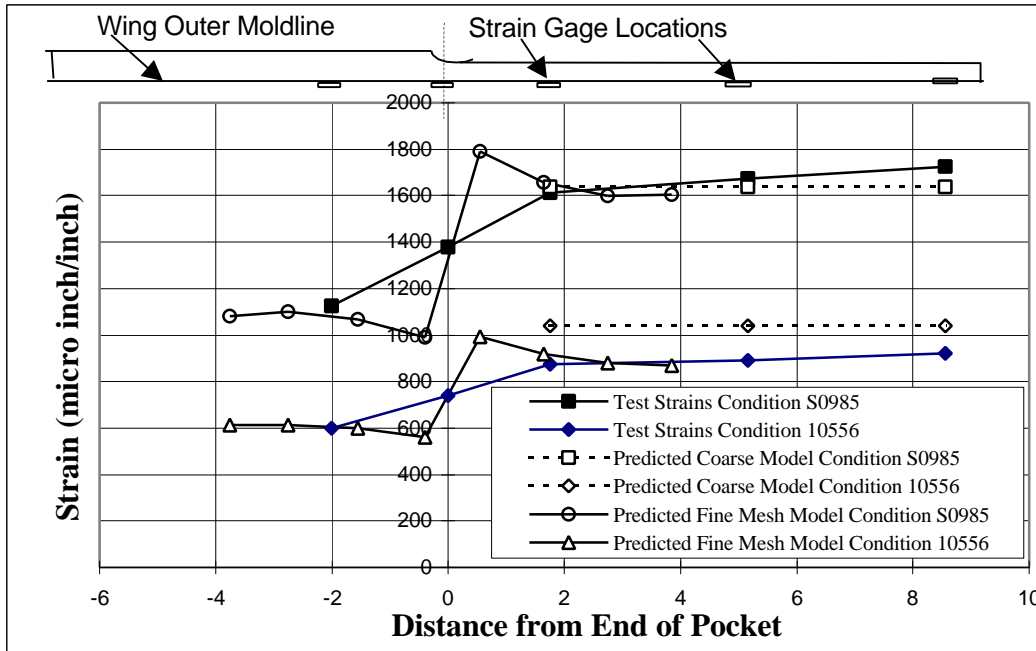


Figure 41. Comparison of Observed and Predicted Strains

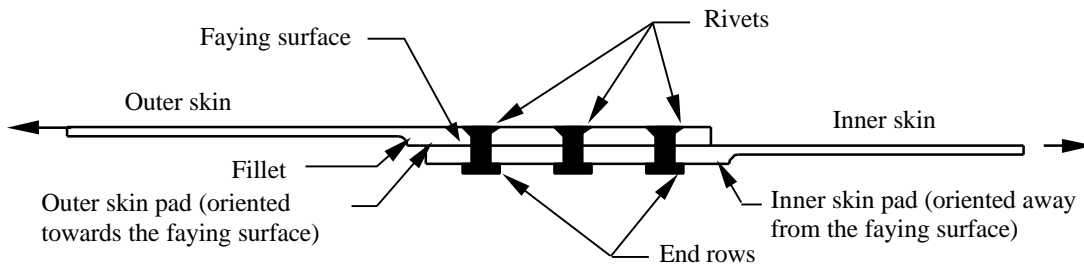


Figure 42. Padded Single Shear Lap Splice

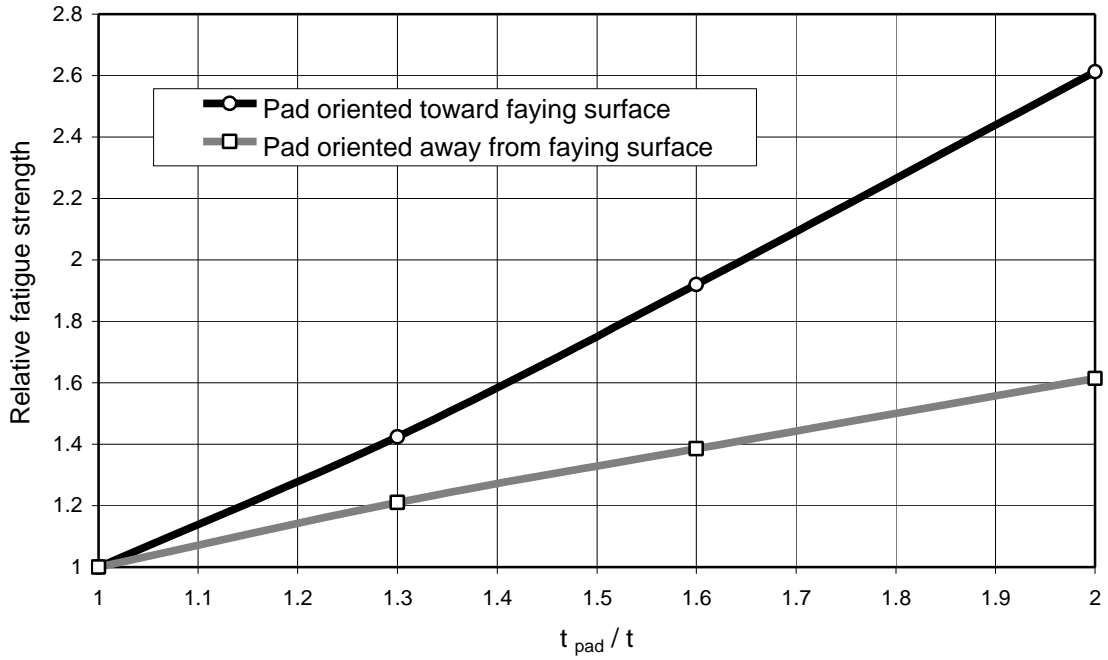


Figure 43. Effect of Pad Orientation on Joint Relative Fatigue Strength (for a Padded Lap Joint with Pads Oriented as Shown in Figure 42.)

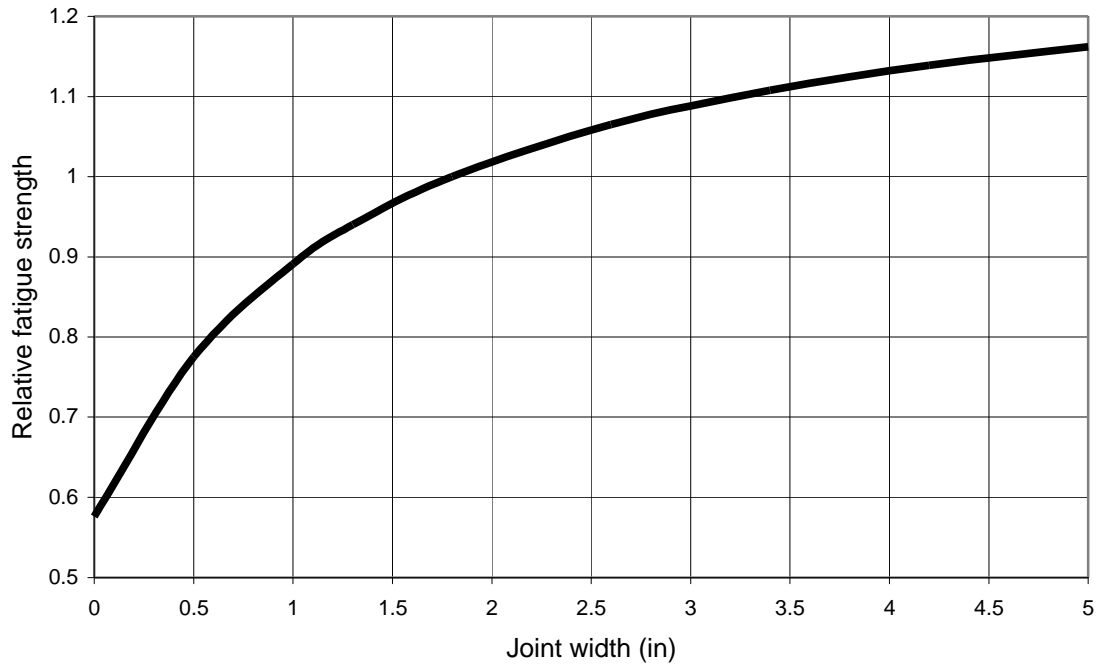
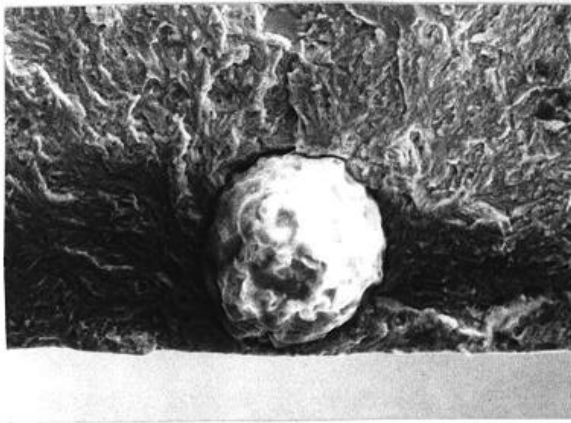
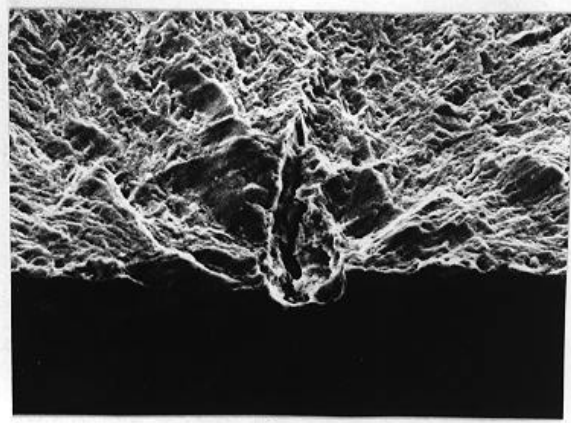


Figure 44. Effect of Overlap Width on Joint Relative Fatigue Strength for .040 in Aluminum Skins



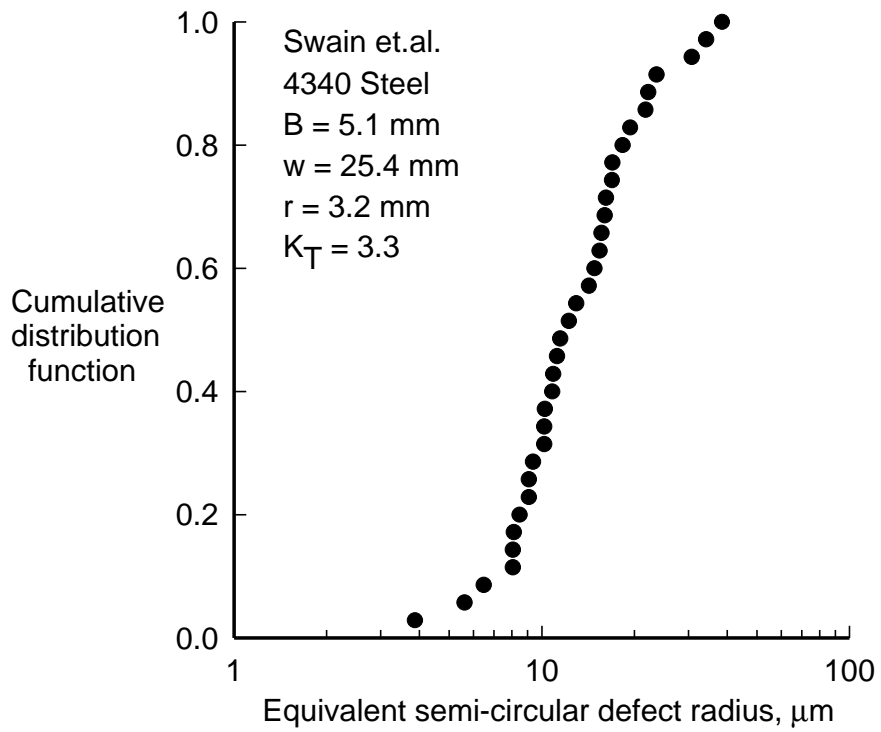
◄—————► .025 mm

(a) Spherical Inclusion Particle



◄—————► .025 mm

(b) Stringer Inclusion Particle

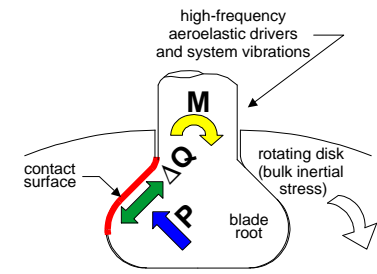


(c) Cumulative Distribution Function for Defects in 4340 Steel

Figure 45. Cumulative Distribution Function for Initiation Sites in 4340 Steel and an Example of a Spherical and Stringer Inclusion Particles at Initiation Sites

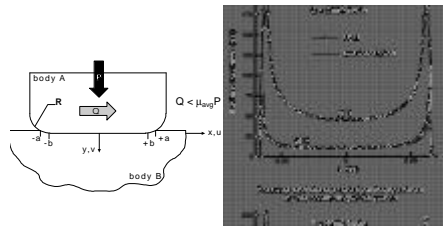
High Cycle Fatigue & Fretting

HCF drivers and near-surface fretting fatigue damage in dovetail joints pose a threat to engine structural integrity



Relevant Research Tasks

- model contact conditions
- tribology of fretting in engine alloys
- fretting fatigue experiments
- design-based metrics for engine lifing

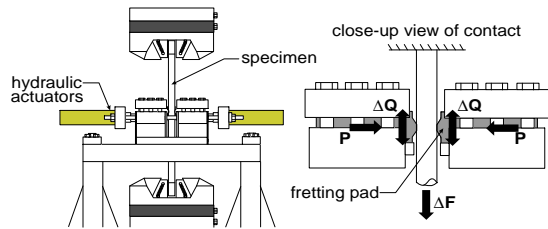


Contact Modeling

- nominally-flat contacts yield sharp near-surface stress gradients
- quasi-analytical method, FEM used to model near-surface conditions
- additional model resolves effects of LCF/HCF loads on fretting fatigue

Figure 45 (d).

Fretting Fatigue Testing



- test with Ti-6Al-4V, nominally flat fretting pads
- characterize interfacial damage
- quantify evolution of friction
- observe fretting fatigue failures

- applied load histories linked to near-surface stress field
- near-surface stresses used with multiaxial fatigue life parameter & smooth-bar strain-life data for Ti-6Al-4V
- correlation between predicted and observed failures

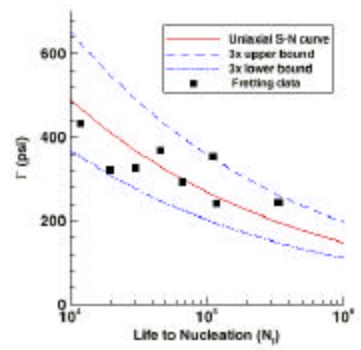


Figure 45 (e).

Fretting Fatigue in Aerospace Structures

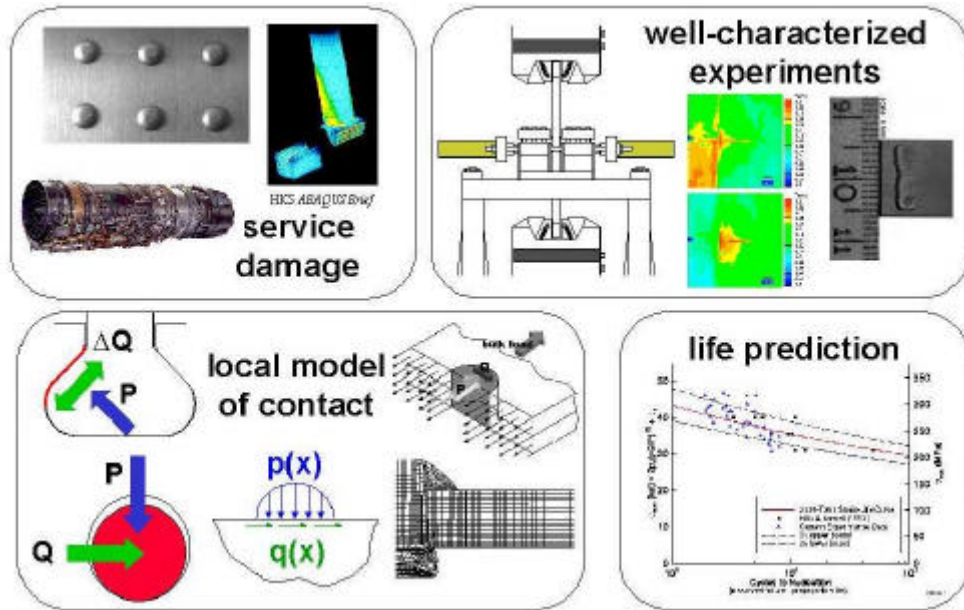


Figure 45 (f).

Predicting Fretting Fatigue in Lap Joints

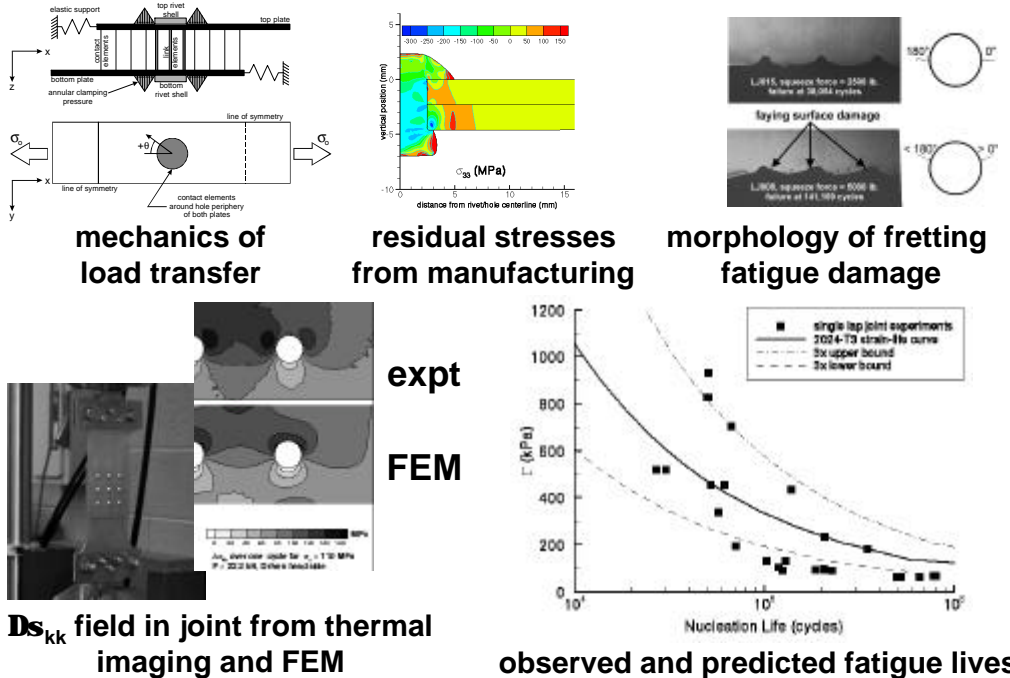


Figure 45 (g).

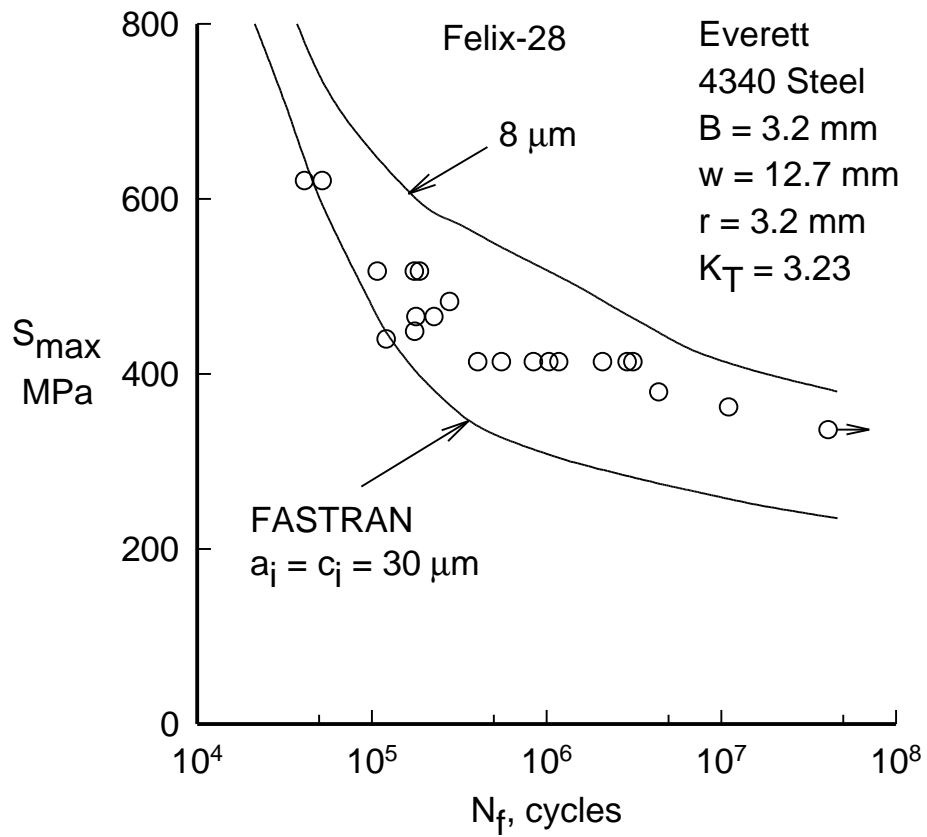


Figure 46. Measured and Predicted Failure Lives for 4340 Steel Notched Specimens Under the Helicopter Spectrum Felix-28

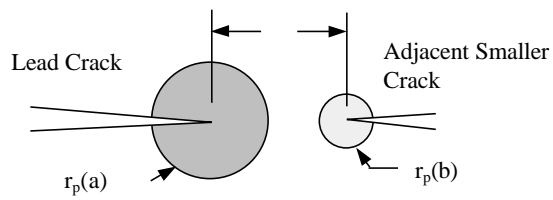


Figure 47.

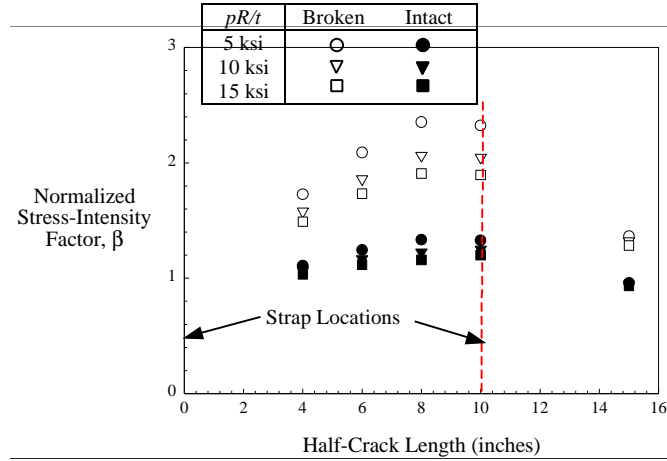


Figure 48.

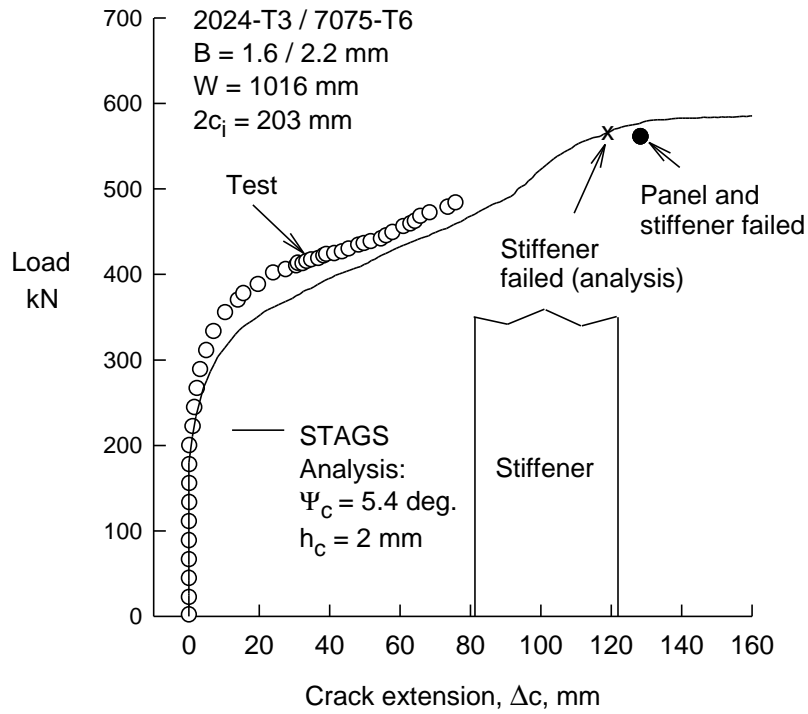


Figure 49. Measured and Predicted Load-Against-Crack Extension for a Stiffened Panel With a Single Crack

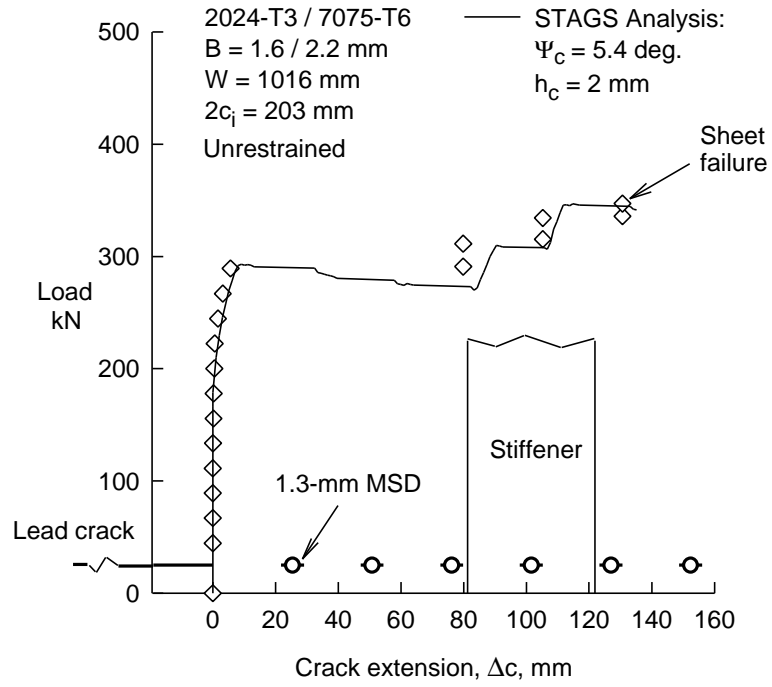


Figure 50. Measured and Predicted Load-Against-Crack Extension for a Stiffened Panel With 1.3-mm Multiple-Site Damage (MSD) Cracking

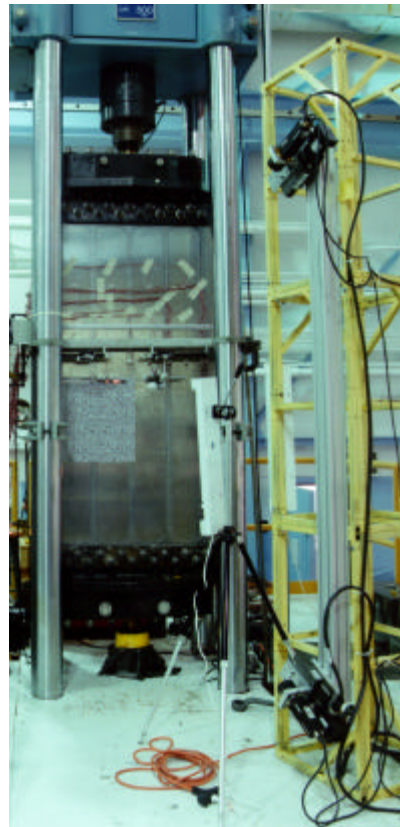


Figure 51.

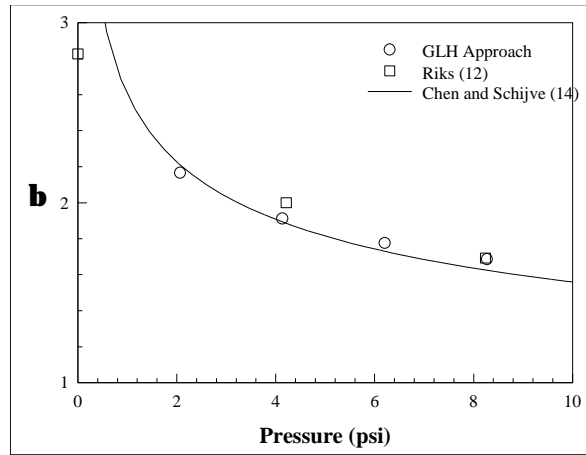


Figure 52.

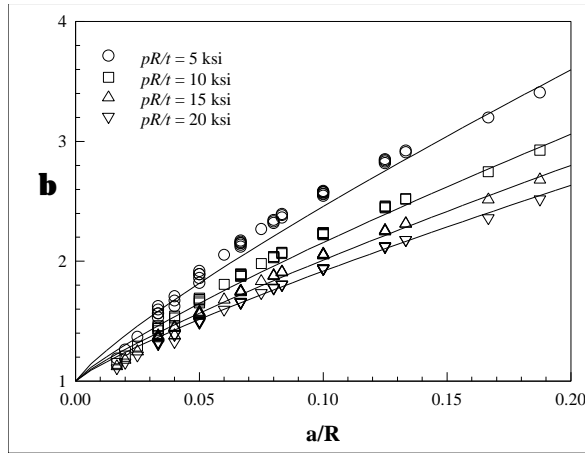


Figure 53.

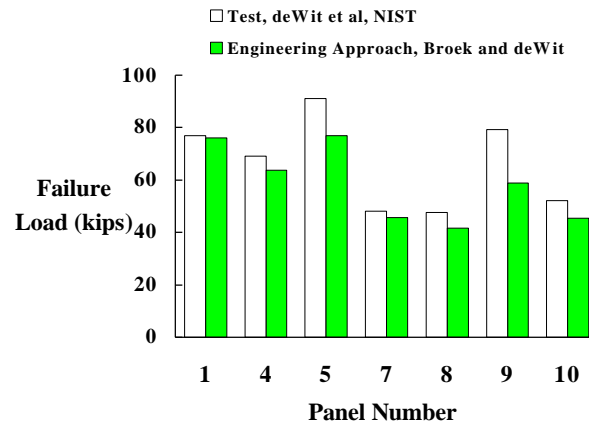


Figure 54.

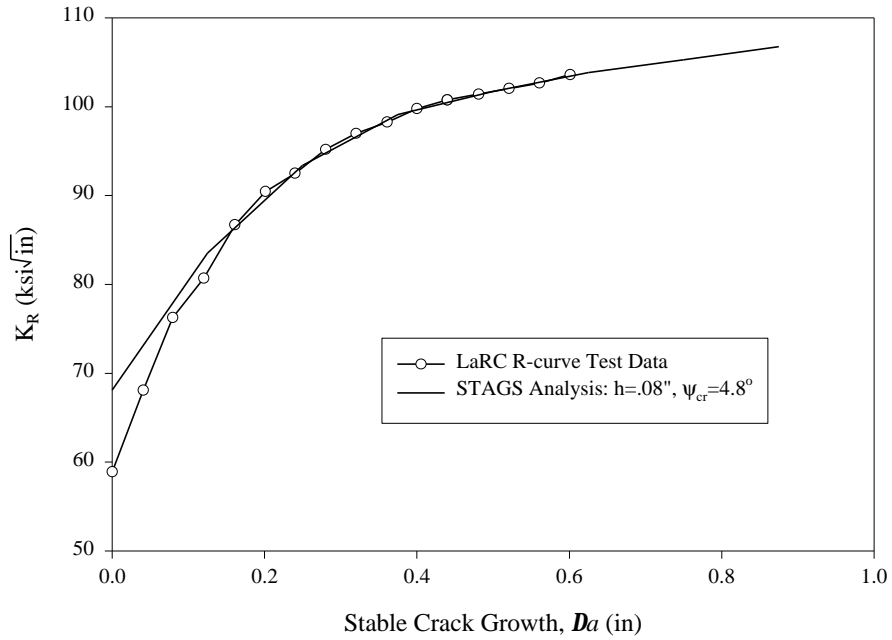
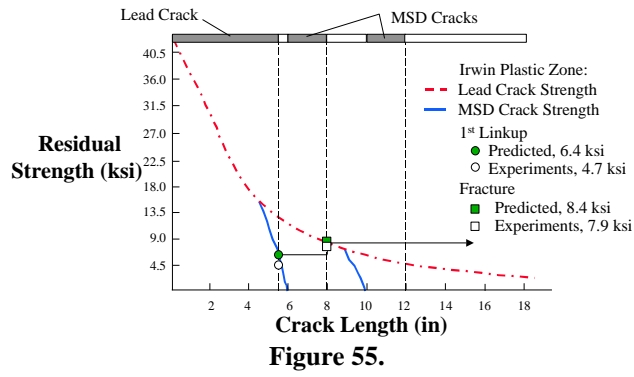


Figure 56. Comparison of Stable Tearing Results (K_R) from Test and STAGS Analysis

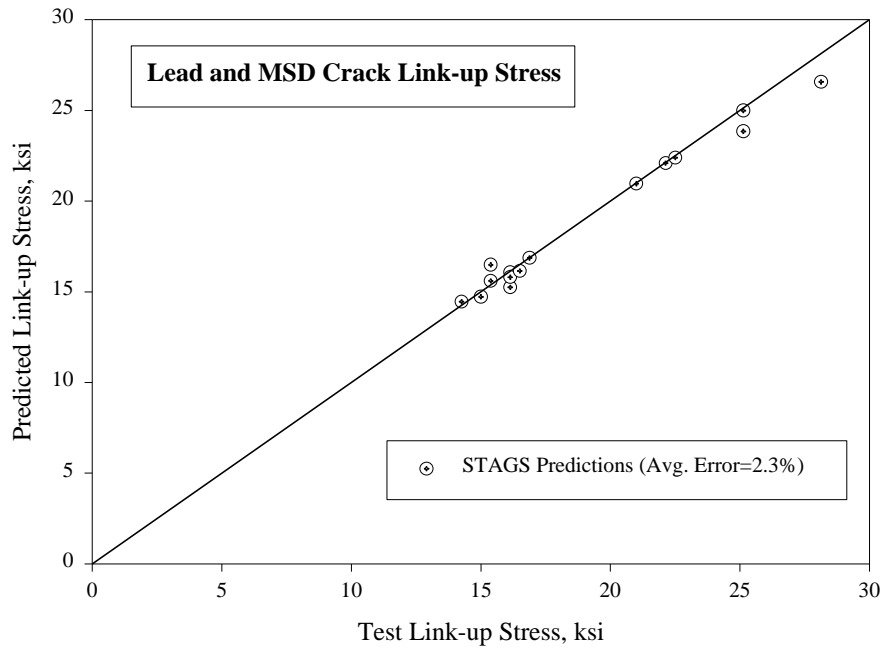


Figure 57. Test Versus STAGS-Calculated Link-Up of Lead and MSD Cracks

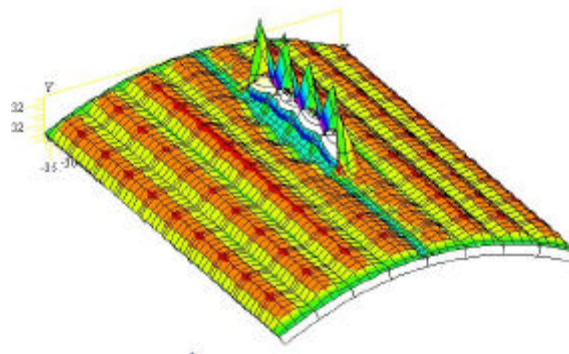


Figure 58.

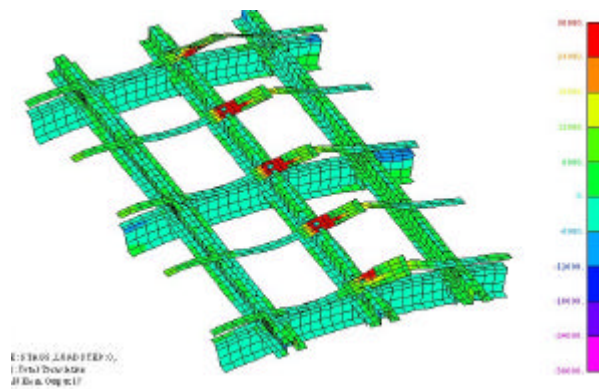


Figure 59.

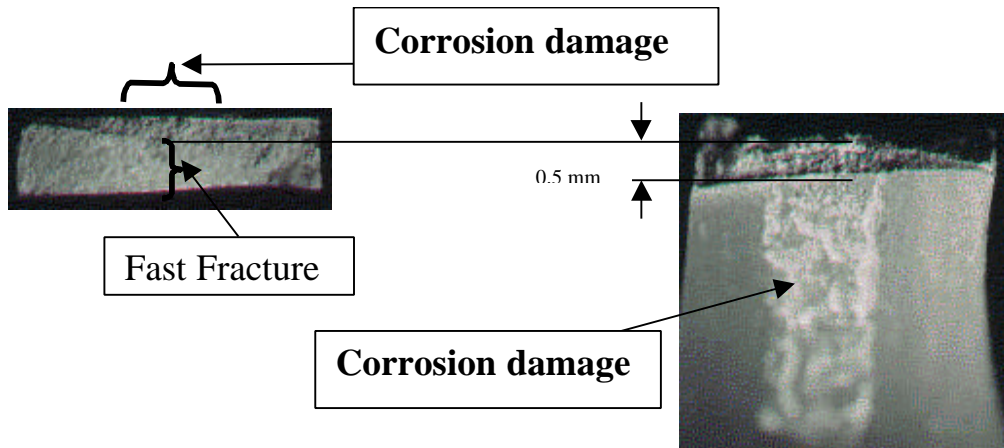


Figure 60. Photograph of Fracture Surface Showing Crack Propagated Deeper (0.5 mm) From the Corroded Region When Compared to Uncorroded Region of Specimen #2. (Range of Pit Depth (60-100 μm))

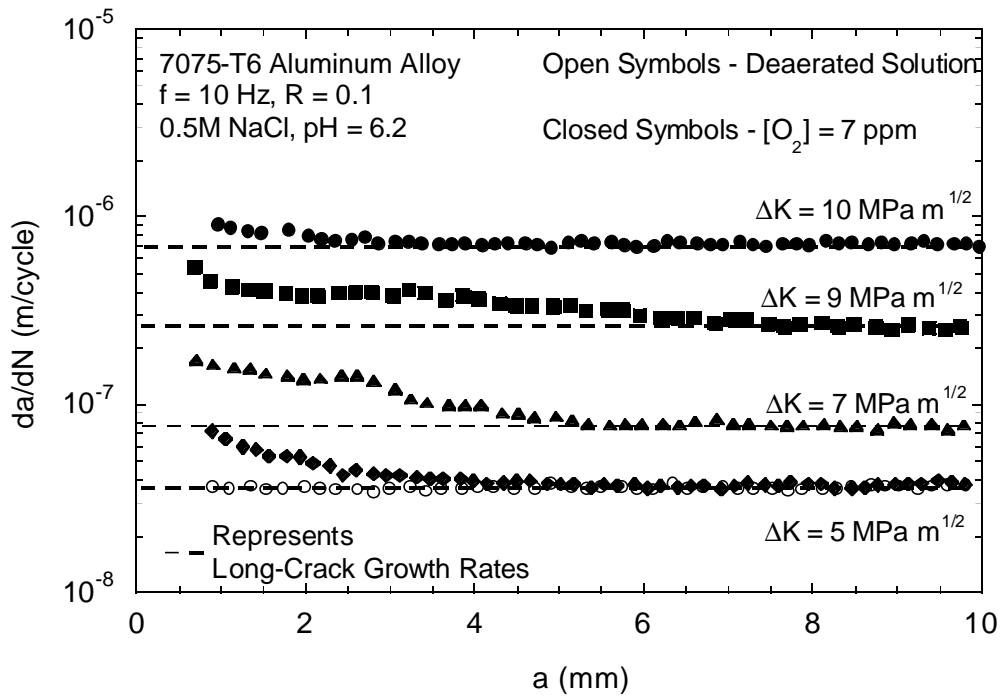


Figure 61. Corrosion Fatigue Crack Growth Response Showing the Presence of a Chemically Short Crack-Growth Regime in the 7075-T6 Aluminum Alloy

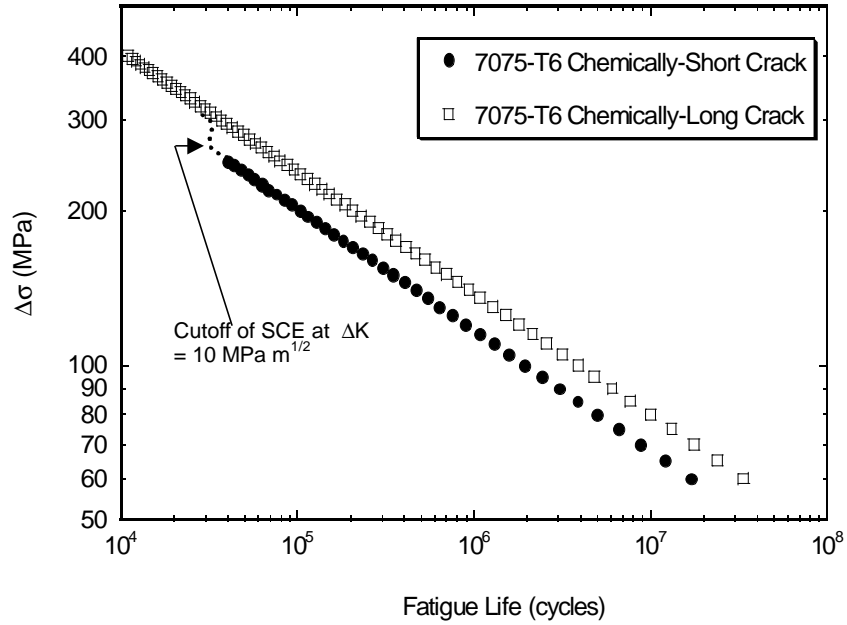


Figure 62. Estimated Reduction in the Fatigue Life From a Crack Length of 0.03 to 1 mm for a 7075-T6 Aluminum Alloy When Considering the Chemically Short-Crack Effect

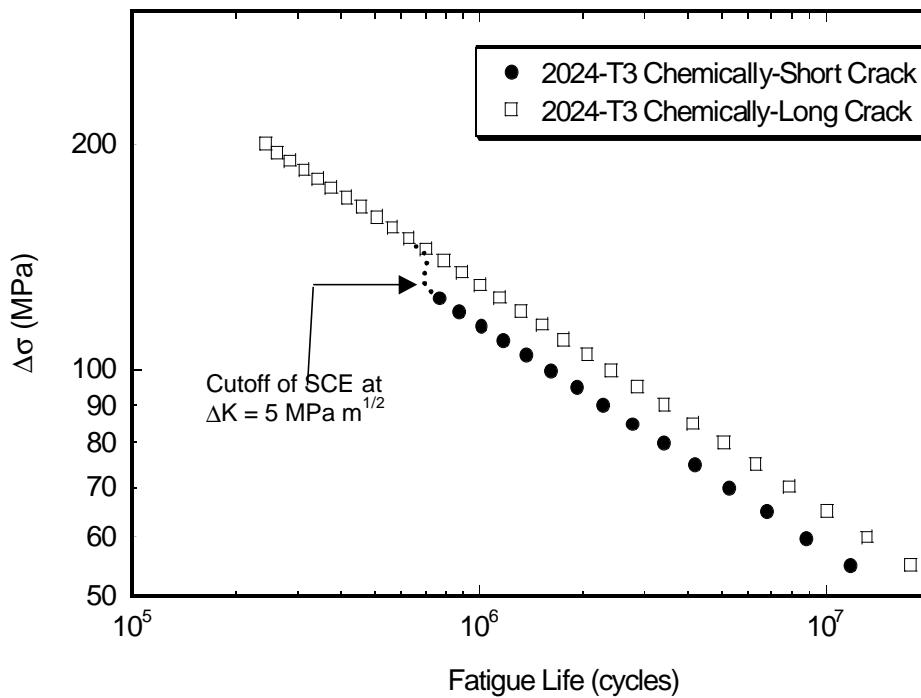


Figure 63. Estimated Reduction in the Fatigue Life From a Crack Length of 0.03 to 1 mm for a 2024-T3 Aluminum Alloy When Considering the Chemically Short-Crack Effect

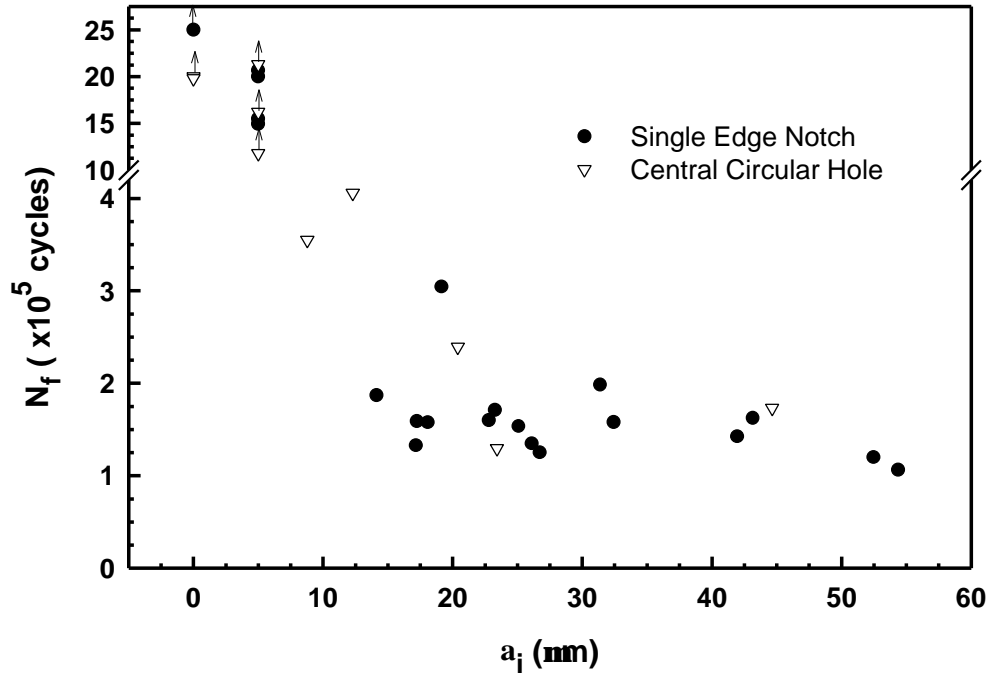


Figure 64. Fatigue Lives of Pre-Corroded, Notched Specimens (at $k_t \Delta \sigma = 288$ MPa) of 2024-T3 Aluminum Alloy as a Function of Pit Depth

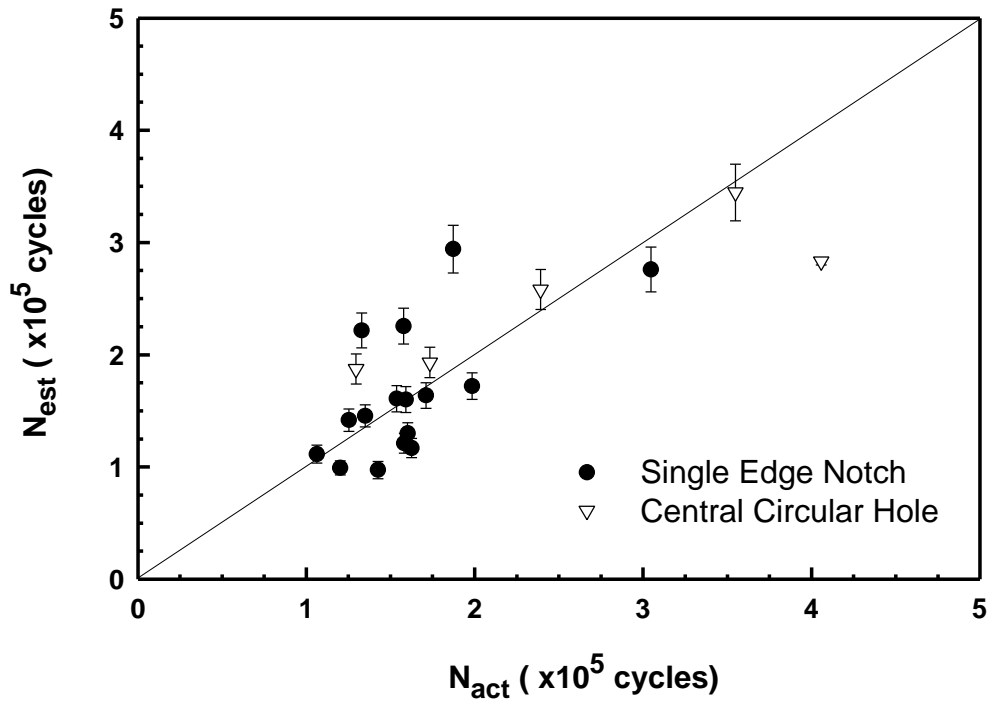


Figure 65. A Comparison Between Estimated and Actual Fatigue Lives for Pre-Corroded 2024-T3 Aluminum Alloy

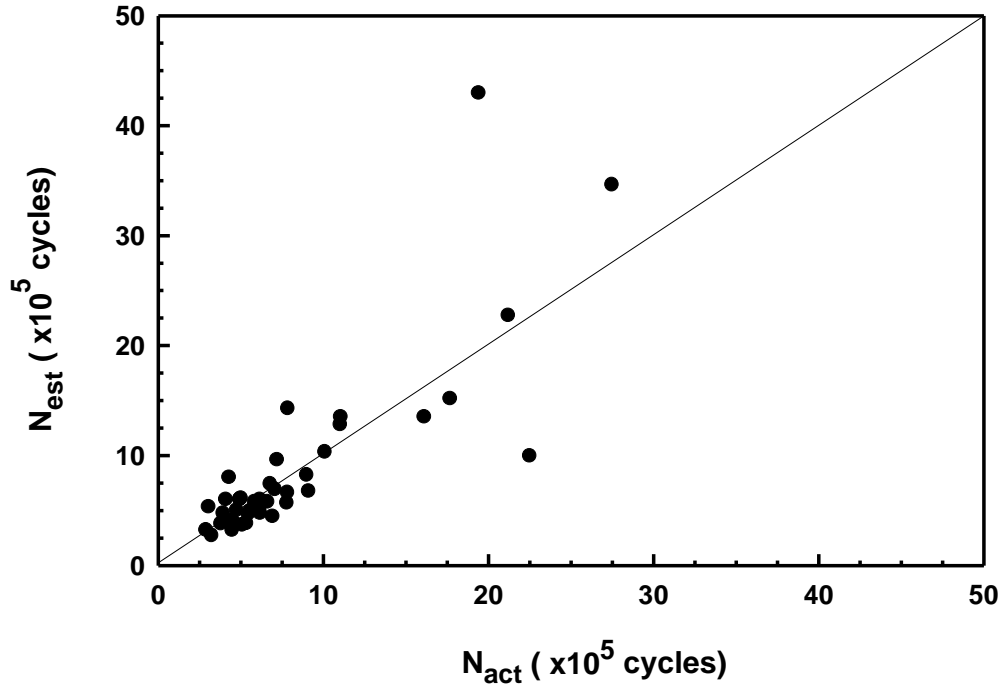


Figure 66. A Comparison Between Estimated and Actual Fatigue Lives for Pre-Corroded 2024-T4 Aluminum Alloy (Harmsworth)

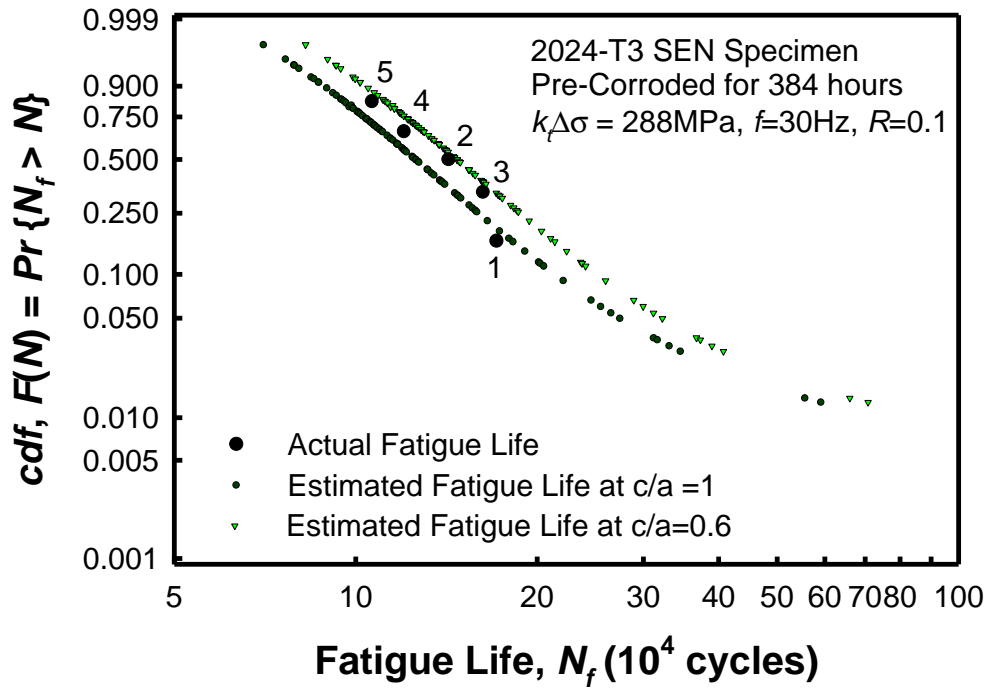


Figure 67. A Comparison Between the Distributions in Estimated and Actual Fatigue Lives of 2024-T3 Aluminum Alloy Specimens Pre-Corroded for 384 Hours (16 Days)

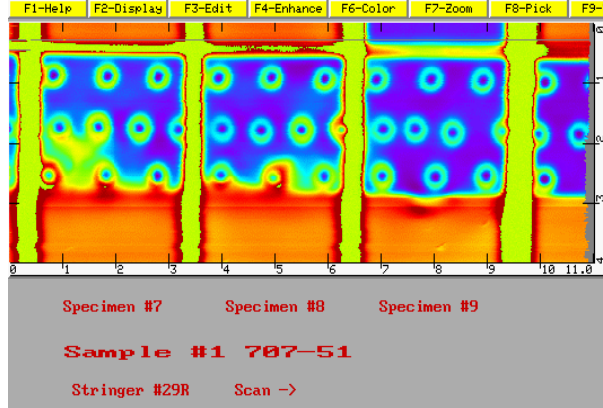


Figure 68. NDI Scan of KC-135 Lap Joint

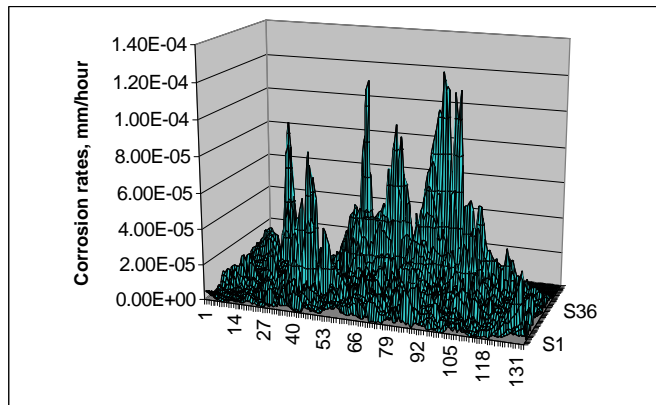
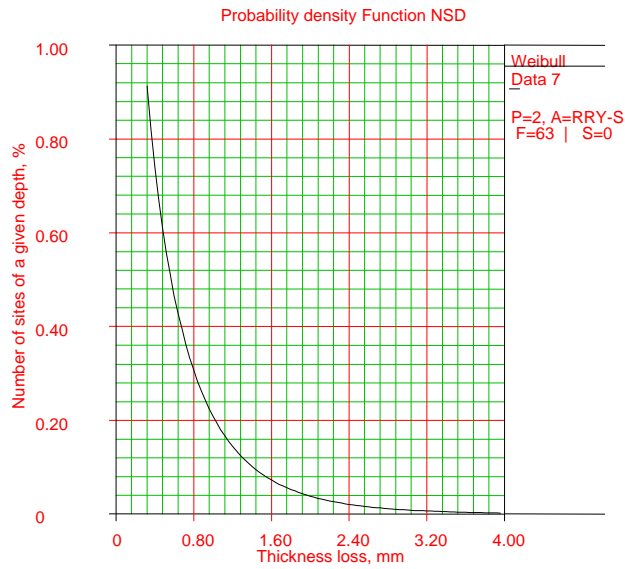
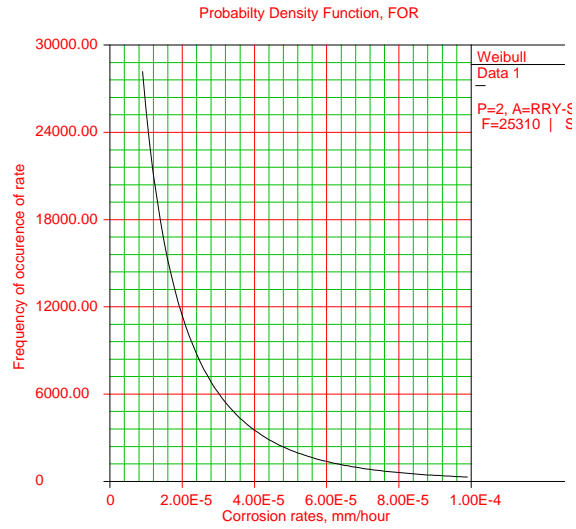


Figure 69. Corrosion Rates Distribution of KC-135 Lap Joint Exposed to 2M CI Solution for 45 Hours



$\beta=0.81, \eta=0.40, \rho=0.98$

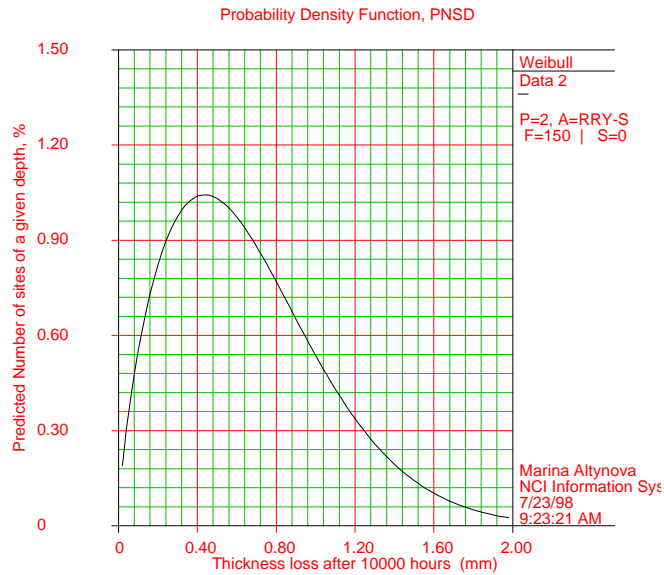
Figure 70. Weibull PDF NSD of KC-135 Lap Joint



$\beta=0.70, \eta=1.07E-5, \rho=0.96$

Figure 71. Weibull PDF for (p) of the Corrosion Rates for KC-135 Lap Joint Exposed to 2M CI-Solution for 45 Hours

$$PNSD(h_f) = \int_{p=0}^{p=\frac{h_f}{\Delta t}} NSD(h_f - p * \Delta t) * FOR(p) dp$$



$\beta=1.68, \eta=0.75, \rho=0.84$

Figure 72. Calculated Probability Density Function PNSD of Final Corrosion Damage of the KC-135 Lap Joint After 10,000 Hours in 2.0 M CI-Solution

Time Δt (hours)	% of damage sites deeper than $h_{cr} = 1.00$ mm	% of damage sites deeper than $h_{cr} = 1.50$ mm
5,000	12.0	3.7
10,000	17.9	8.5
15,000	21.5	10.1
20,000	24.6	12.1

Figure 73. Predicted Number of Damage Sites Deeper Than Critical Depth h_{cr} After Different Periods of Time Δt Since NDI. Corrosion Conditions are 2 M CI- and 98% Relative Humidity at Room Temperature

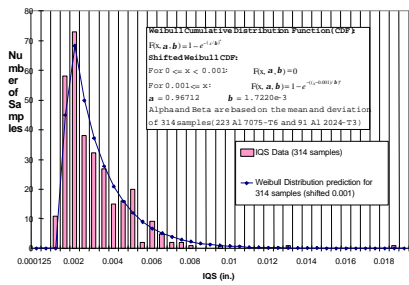


Figure 74 Spectrum of Initial Flaw Sizes Extracted from Test Data.

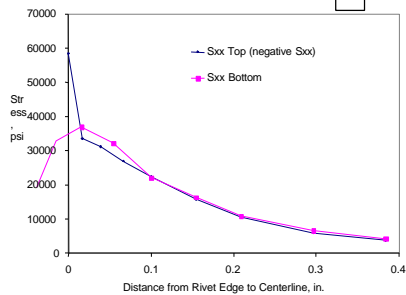


Figure 78. Corrosion Pilling Increases Sustained Stress

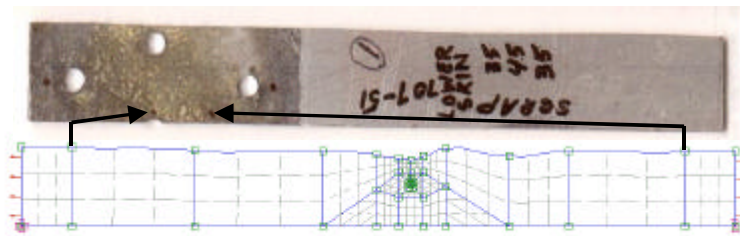


Figure 75. FEA model of Corroded Surface Topography

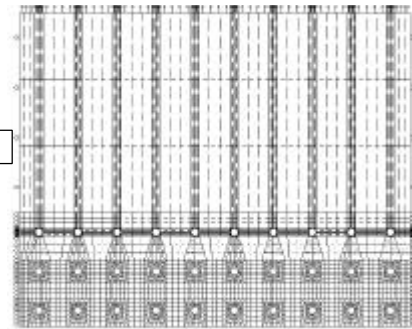
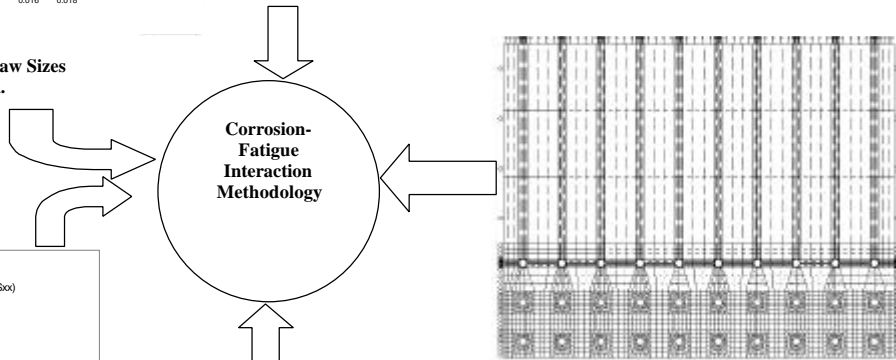


Figure 76. FEA Model of Multi-site Damage Scenario

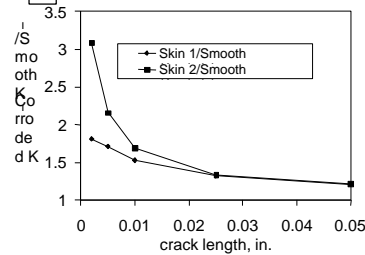


Figure 77. Stress Intensity Amplifications Caused by Corrosion

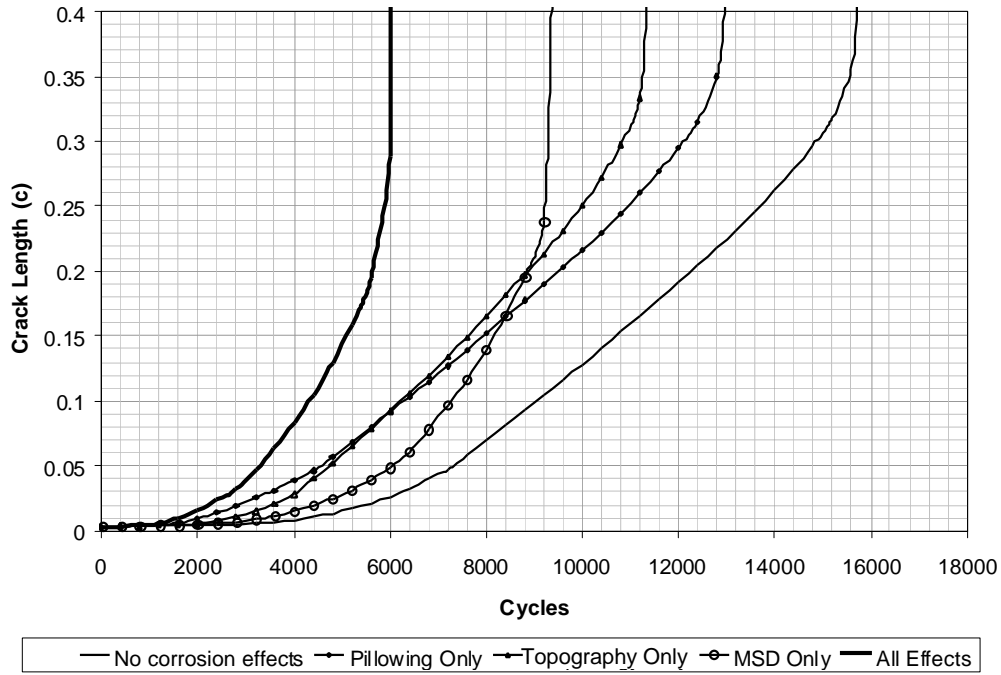


Figure 79. Corrosion Effects on Crack Growth Life

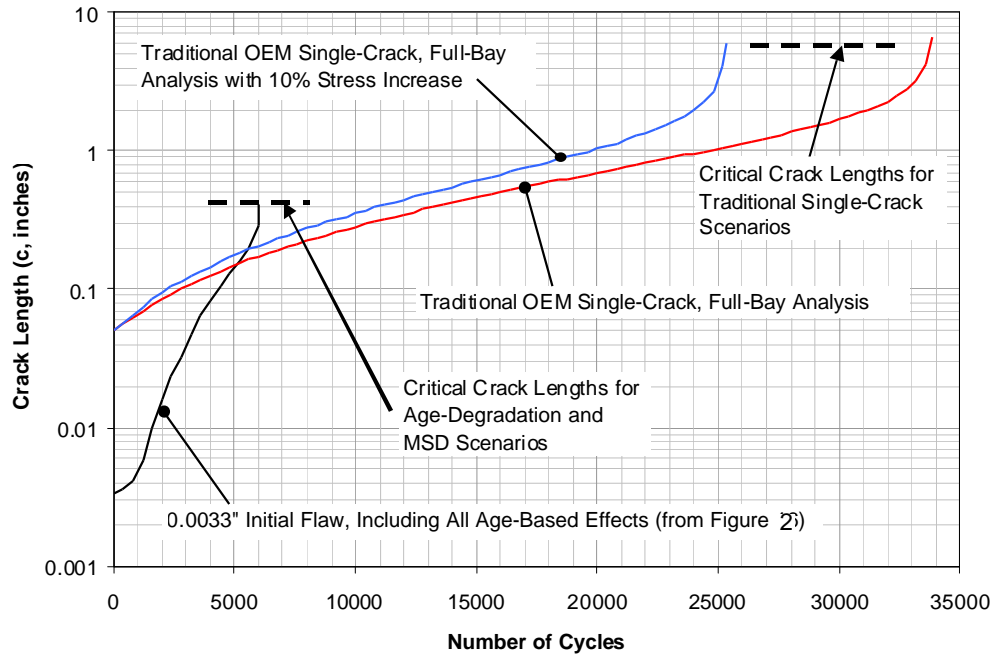


Figure 80. Comparison of Proposed Corrosion-Fatigue Interacton Approach with Traditional Crack Growth Life Analyses

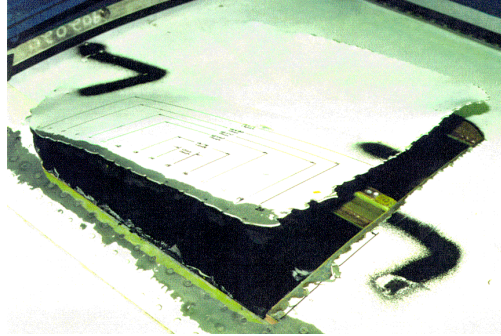
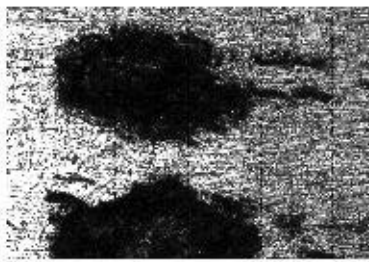


Figure 81.



Stage I
Formation of debris
[analyzed after 44100 cycles]



Stage II
Removal of material
[after 96200 cycles]



Stage III
Nucleation of cracks
[after 12840 cycles]

Figure 82. Digitized Confocal Images Showing the Stages in the Nucleation and the Development of Fretting Damages on the Faying Surface of 7075-T6 Aluminum Alloy Specimen, $\sigma_{max} = 172$ MPa (25 ksi), $\sigma_n = 13.8$ MPa (2 ksi), $R = 0.1$, $f = 10$ Hz, Lab Air

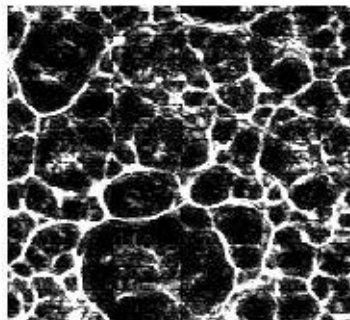


Figure 83. Digitized Image Showing Fretting Nucleated Multiple Pits on the Faying Surface of 2024-T3 Aluminum Alloy Specimen (Analyzed After Fracture, 80100 Cycles)

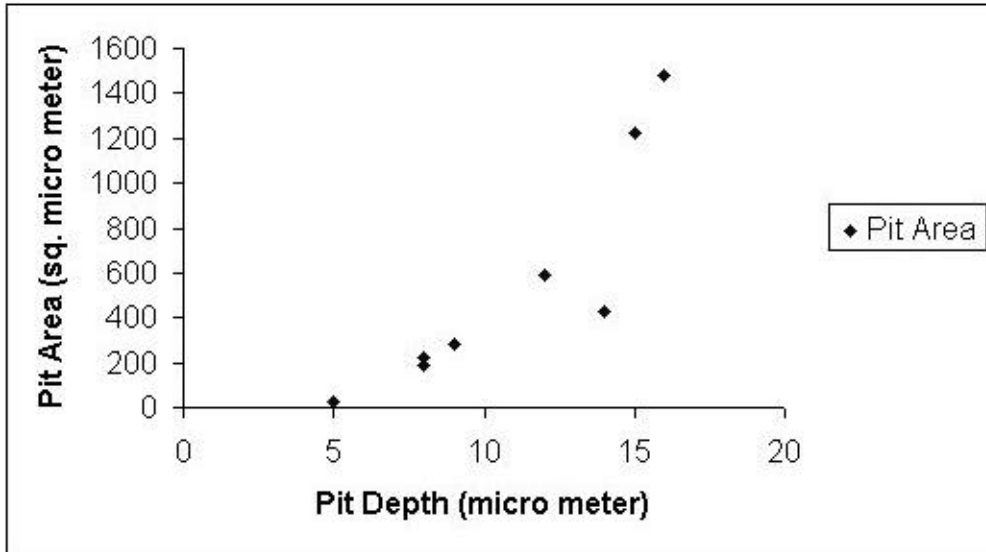


Figure 84. Correlation Between Pit Depth and Pit Area, Material: 2024-T3 Aluminum Alloy, Normal Stress = 13.8 MPa (2 ksi), Max. Fatigue Stress = 207 MPa (30 ksi), Environment: Lab Air

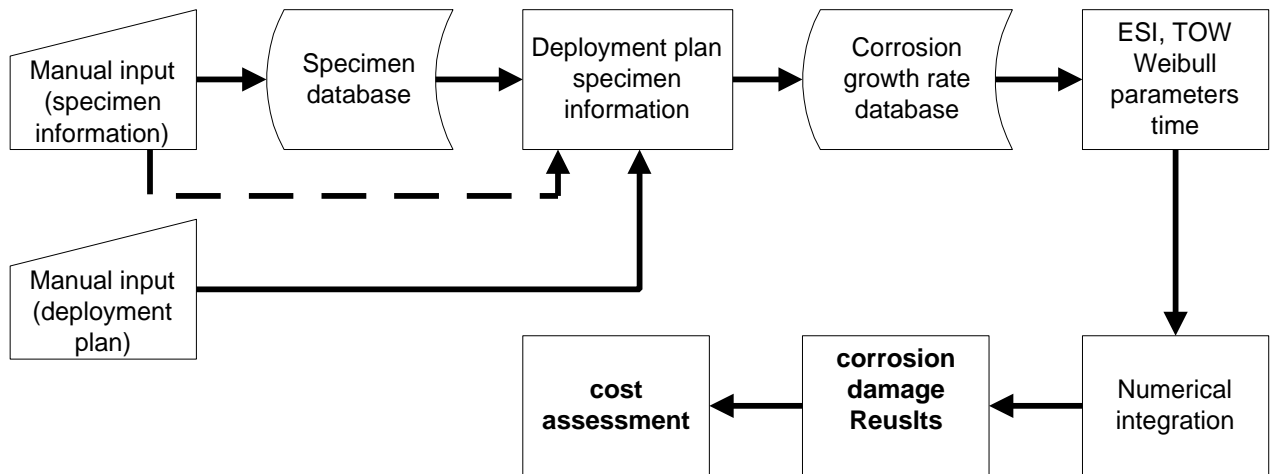


Figure 85. Flowchart of Computer Program for Lap Joint Corrosion Prediction

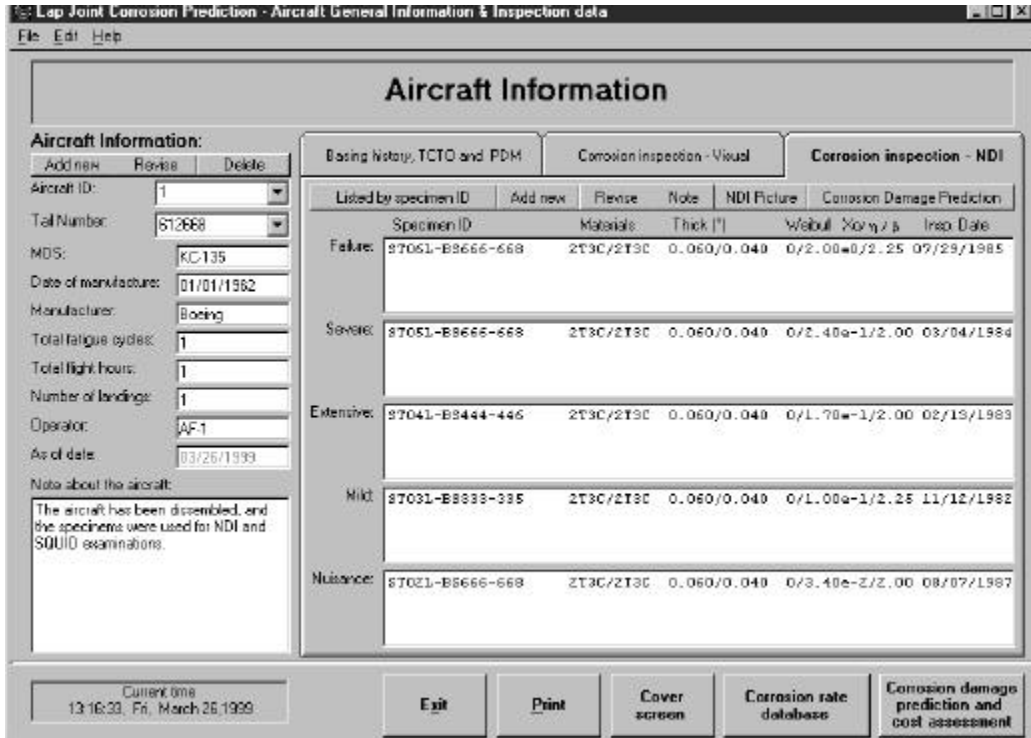


Figure 86. Specimen Database Screen

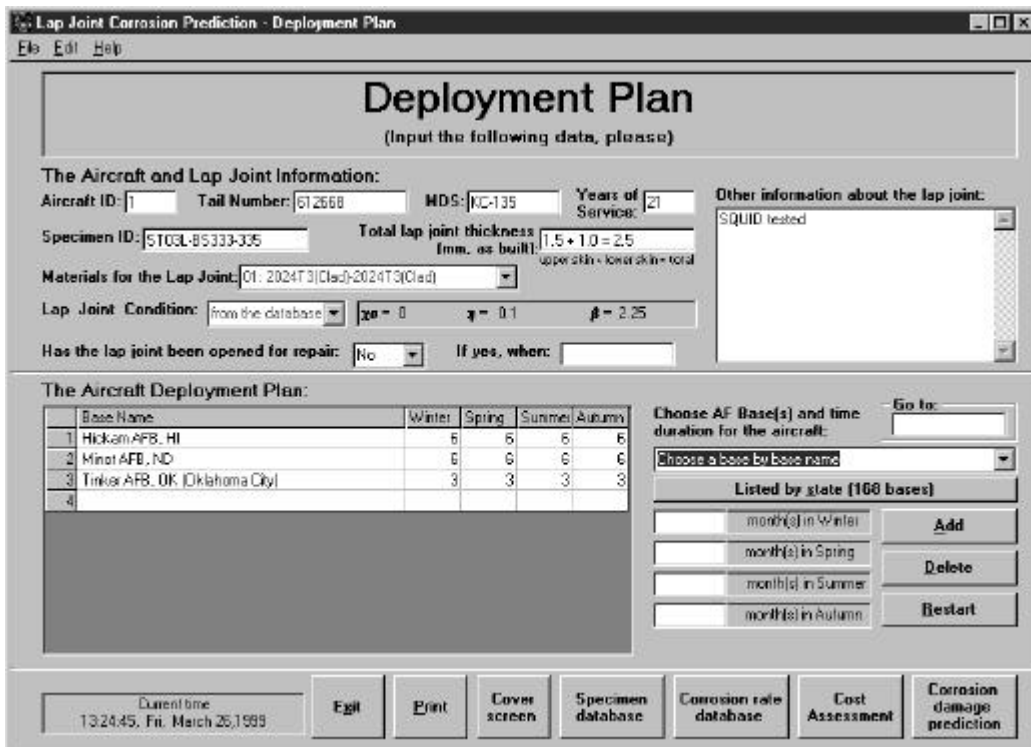


Figure 87. Deployment Plan and Aircraft/Specimen Information Screen

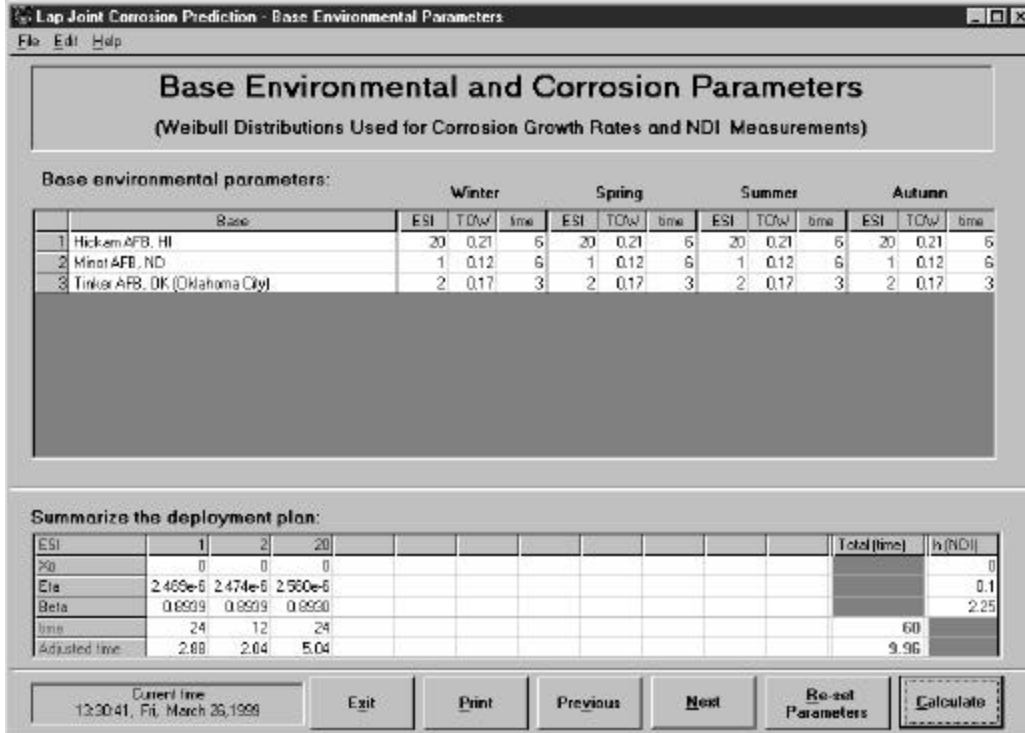


Figure 88. Corrosion Parameters Screen (ESI, TOW and Weibull Parameters From Database)

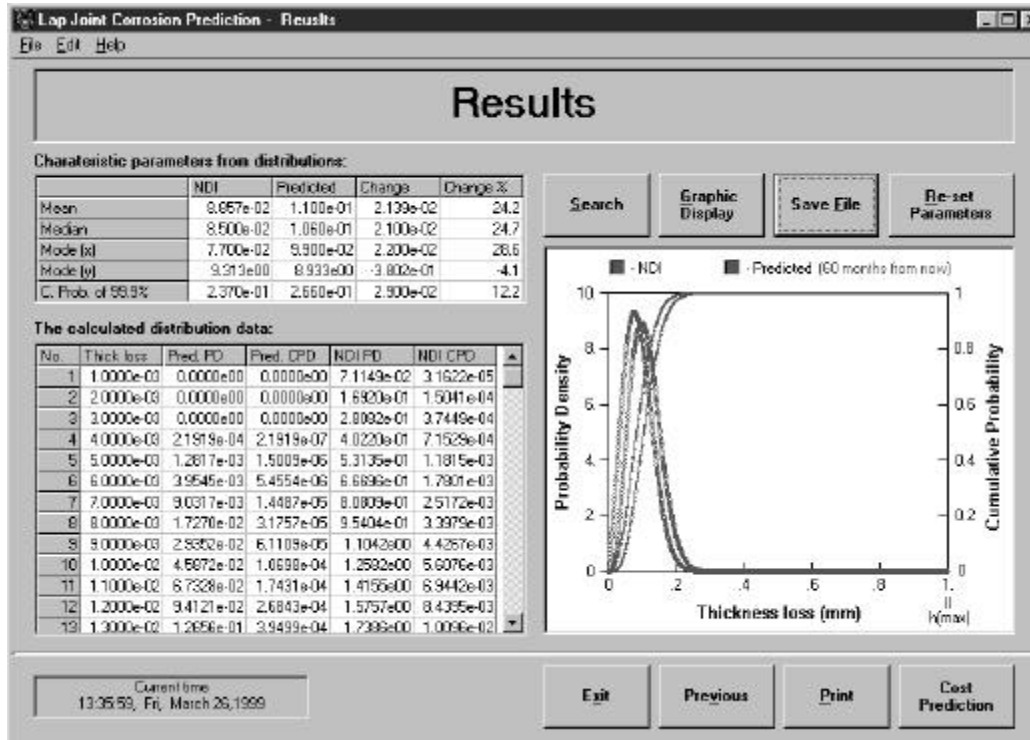


Figure 89. Results of Calculated Distributions

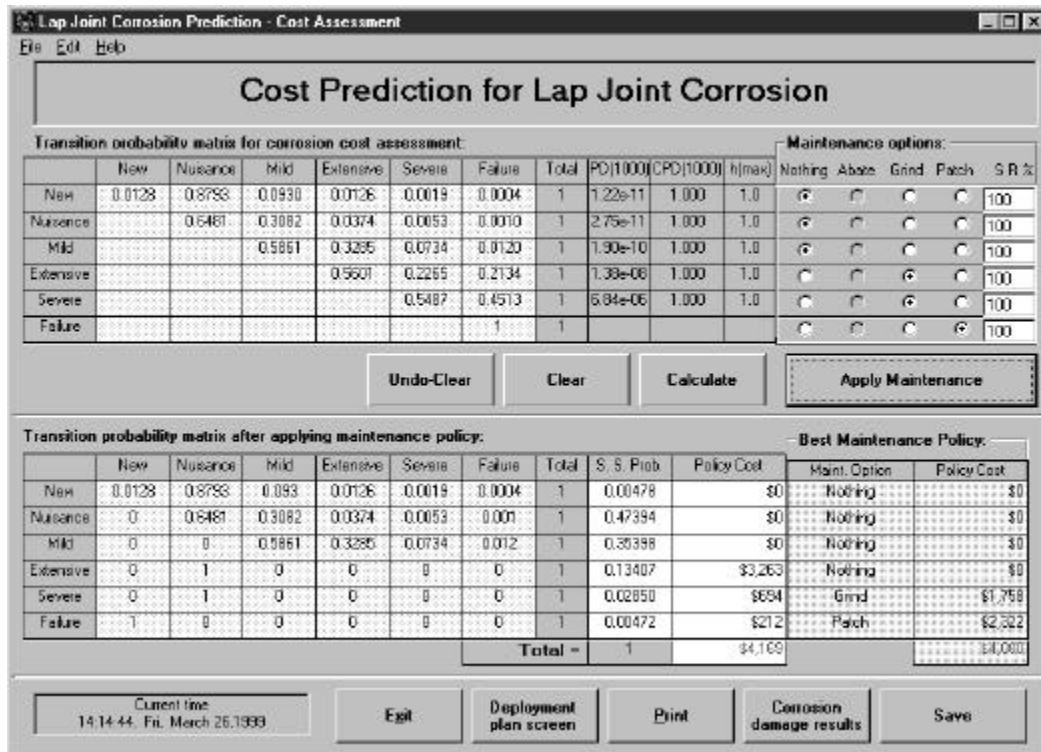


Figure 90.

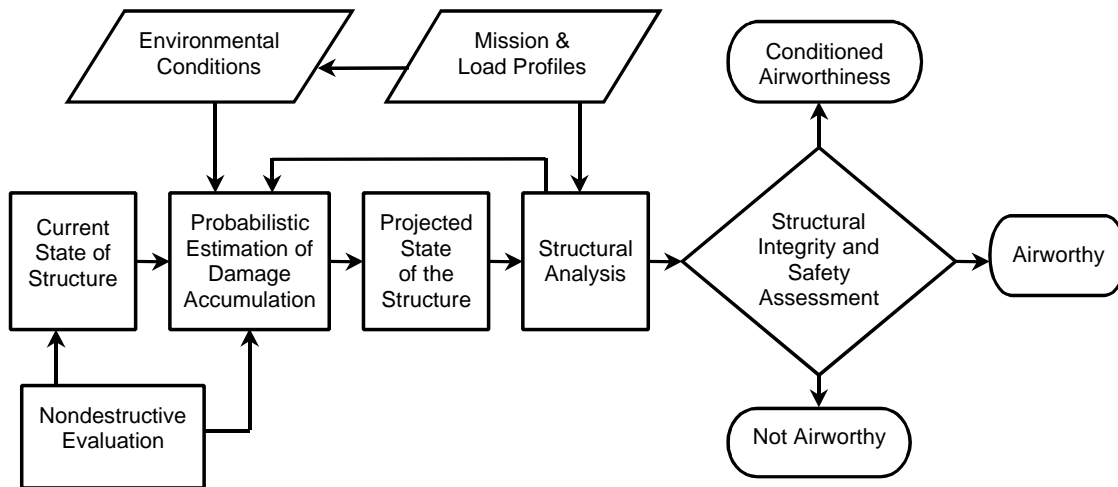


Figure 91. Airworthiness, Structural Integrity and Durability Assessments

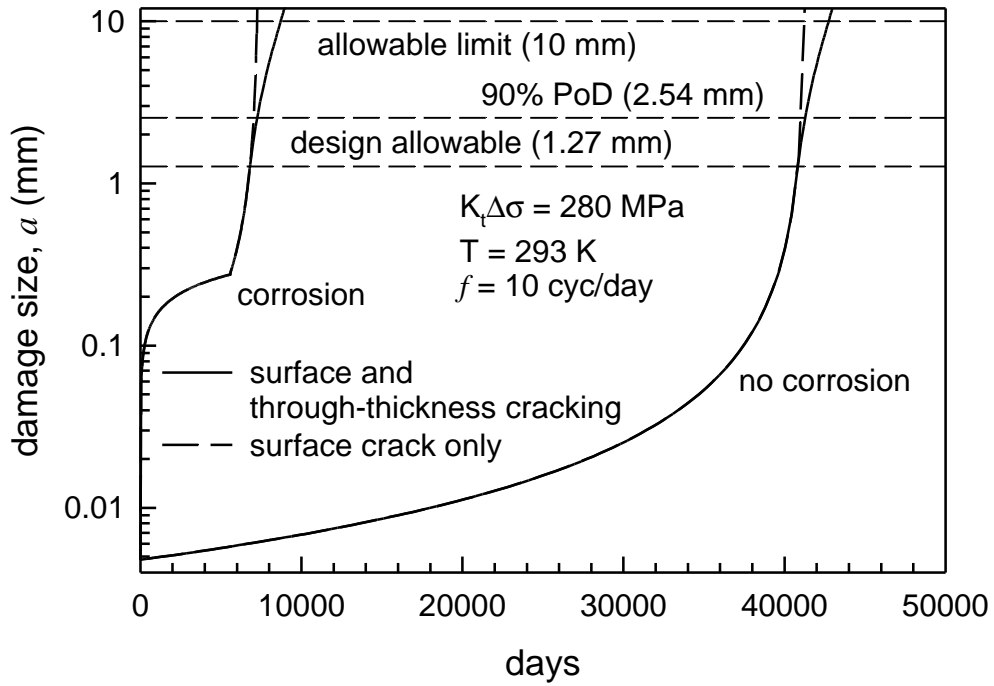


Figure 92. Average Damage Size Modeled by Pitting Corrosion with Corrosion Fatigue Crack Growth, and Environmentally Assisted Fatigue Crack Growth Only

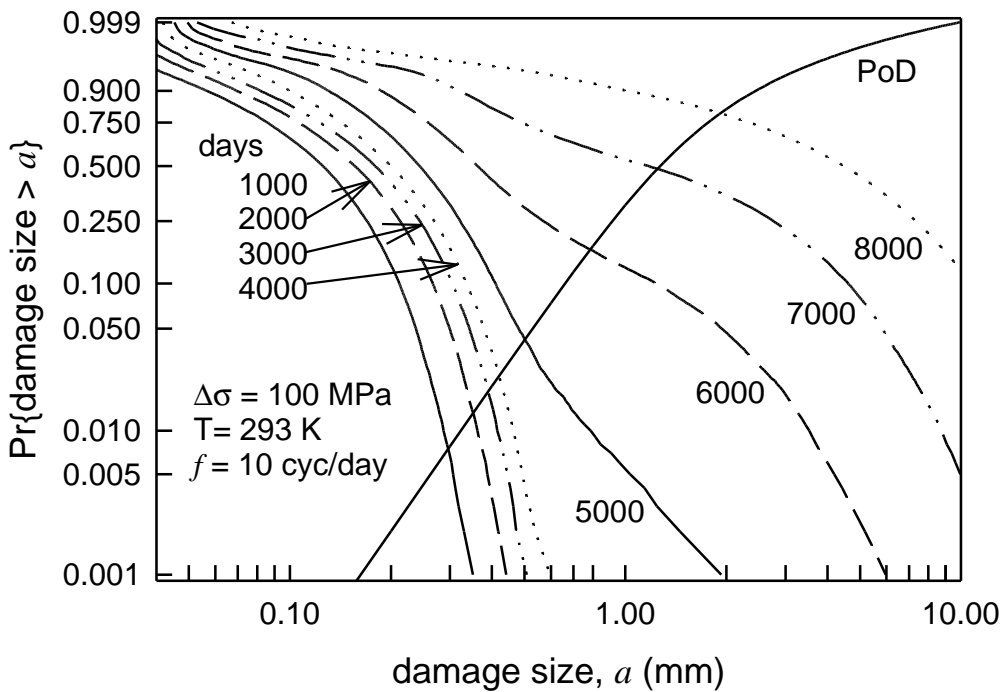


Figure 93. PoO of Damage Size Versus Time and a Typical PoD

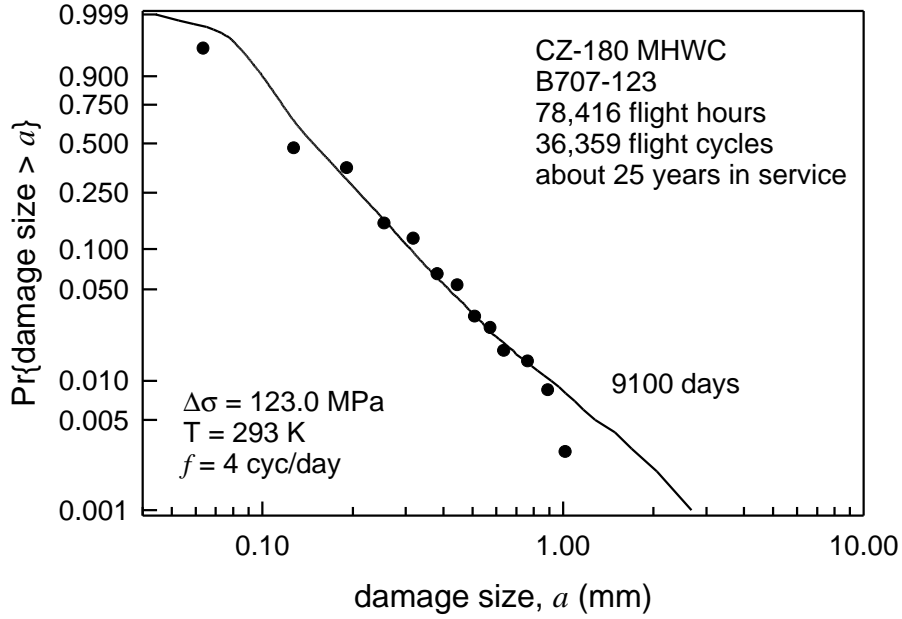


Figure 94. Comparison Between Predicted and Observed Fastener Hole Damage in Lower Wing Panels of a 100 Series B707 Aircraft

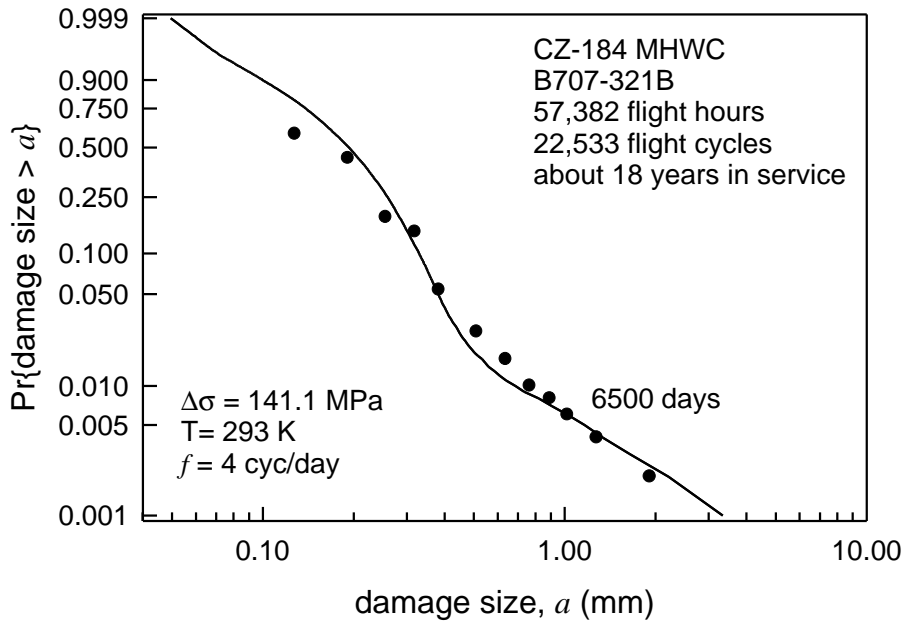


Figure 95. Comparison Between Predicted and Observed Fastener Hole Damage in Lower Wing Panels of a 300 Series B707 Aircraft

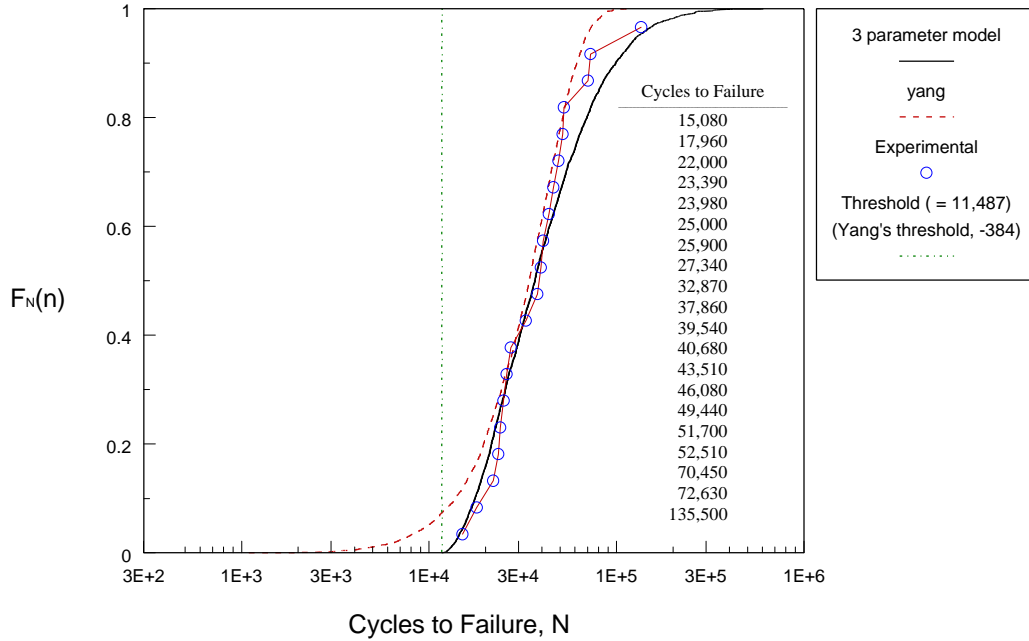


Figure 96. Distribution Function for Fatigue Life for [90/45/-45/0]s Thornel 300-Rigidite 5208 Gr/Ep Subjected to an Applied Loading of $S_{max} = 60.57$ [ksi] with a Stress Ratio = 1/36

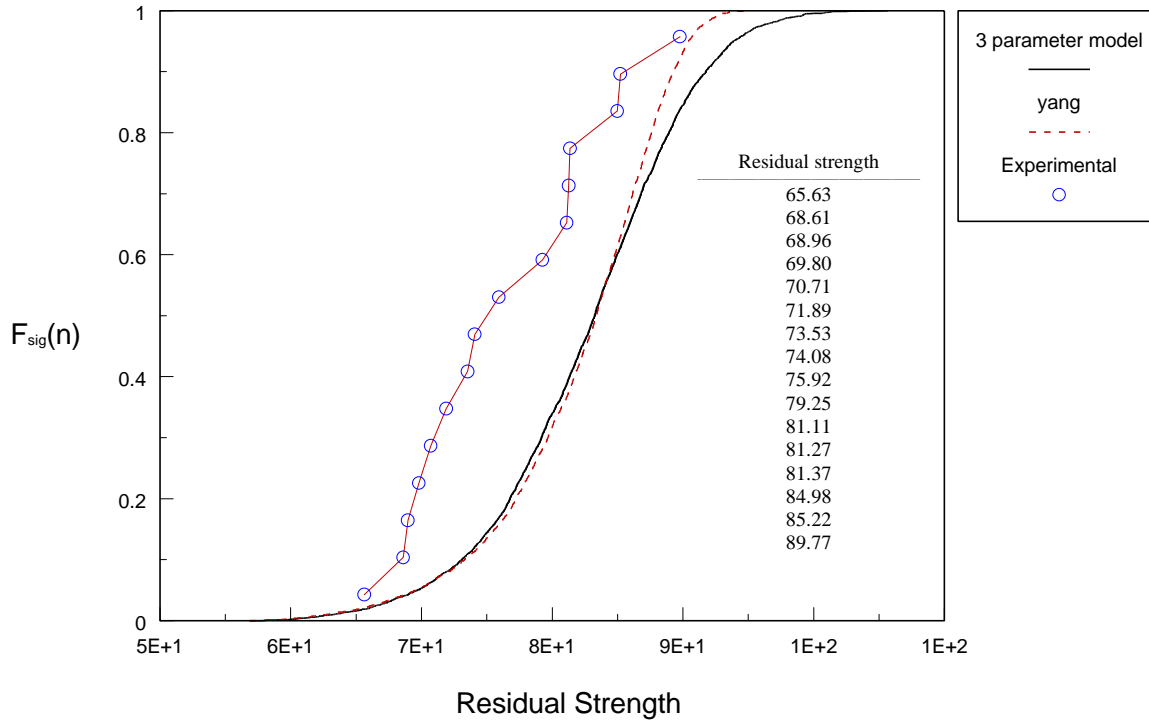


Figure 97. Distribution Function of Residual Strength for [90/45/-45/0]s Thornel 300- Rigidite 5208 Gr/Ep Subjected to $S_{max} = 56.53$ [ksi], Stress Ratio = 1/36 and $n = 56,000$ Cycles

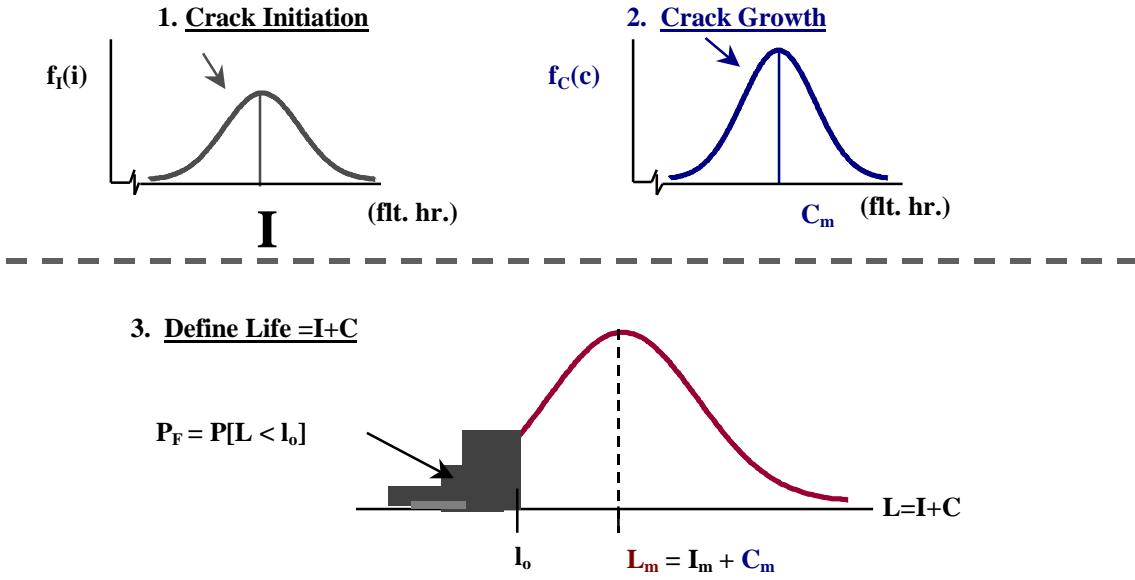


Figure 98.

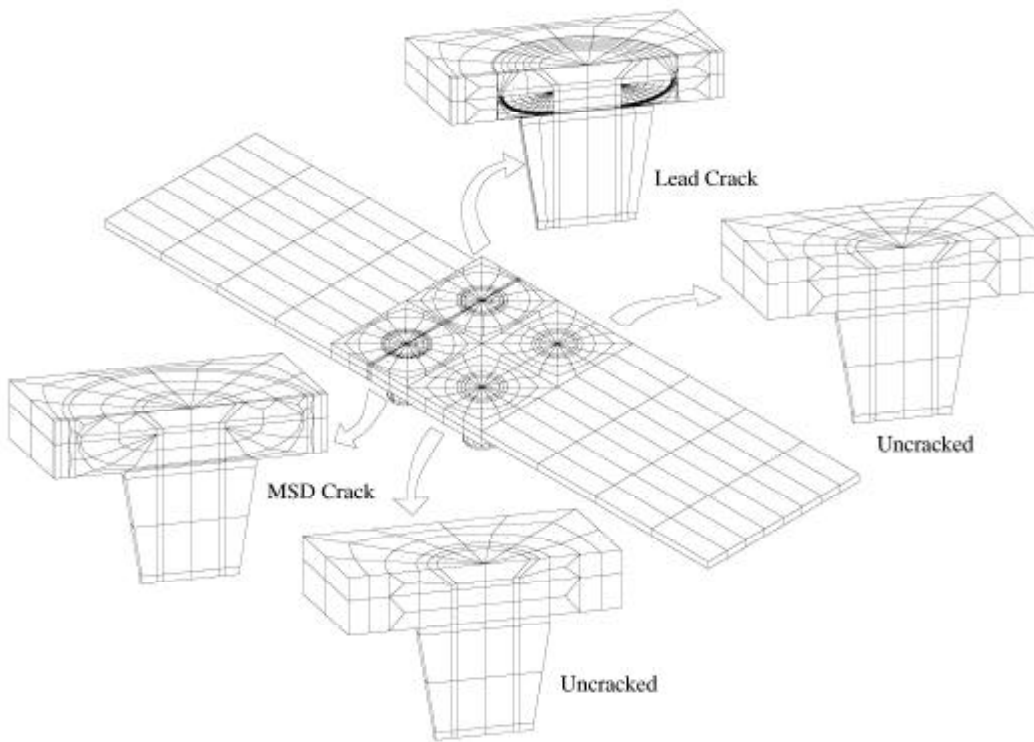


Figure 99. DIAL Finite Element Model for Two-Row Single Shear Cracked Joint with Countersunk Fasteners

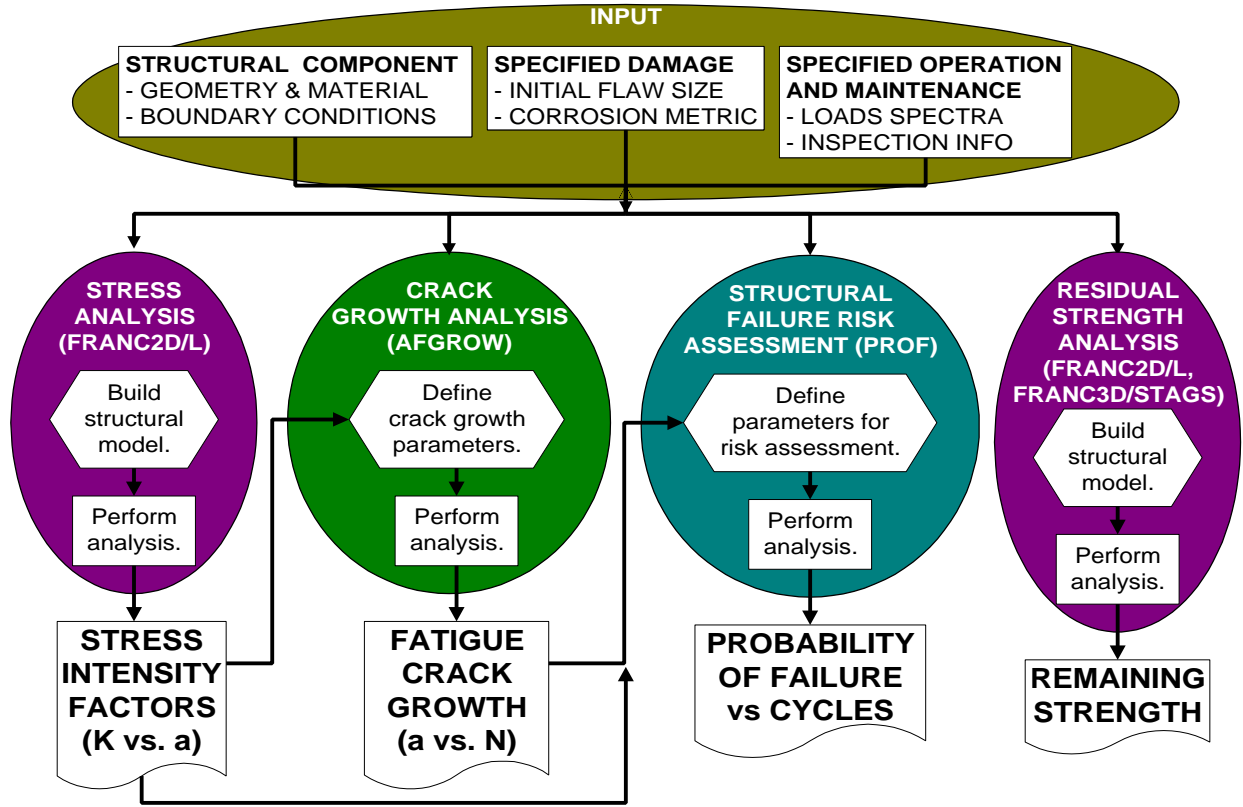


Figure 100. Analysis Tools for DaDTA of Riveted Lap Joints

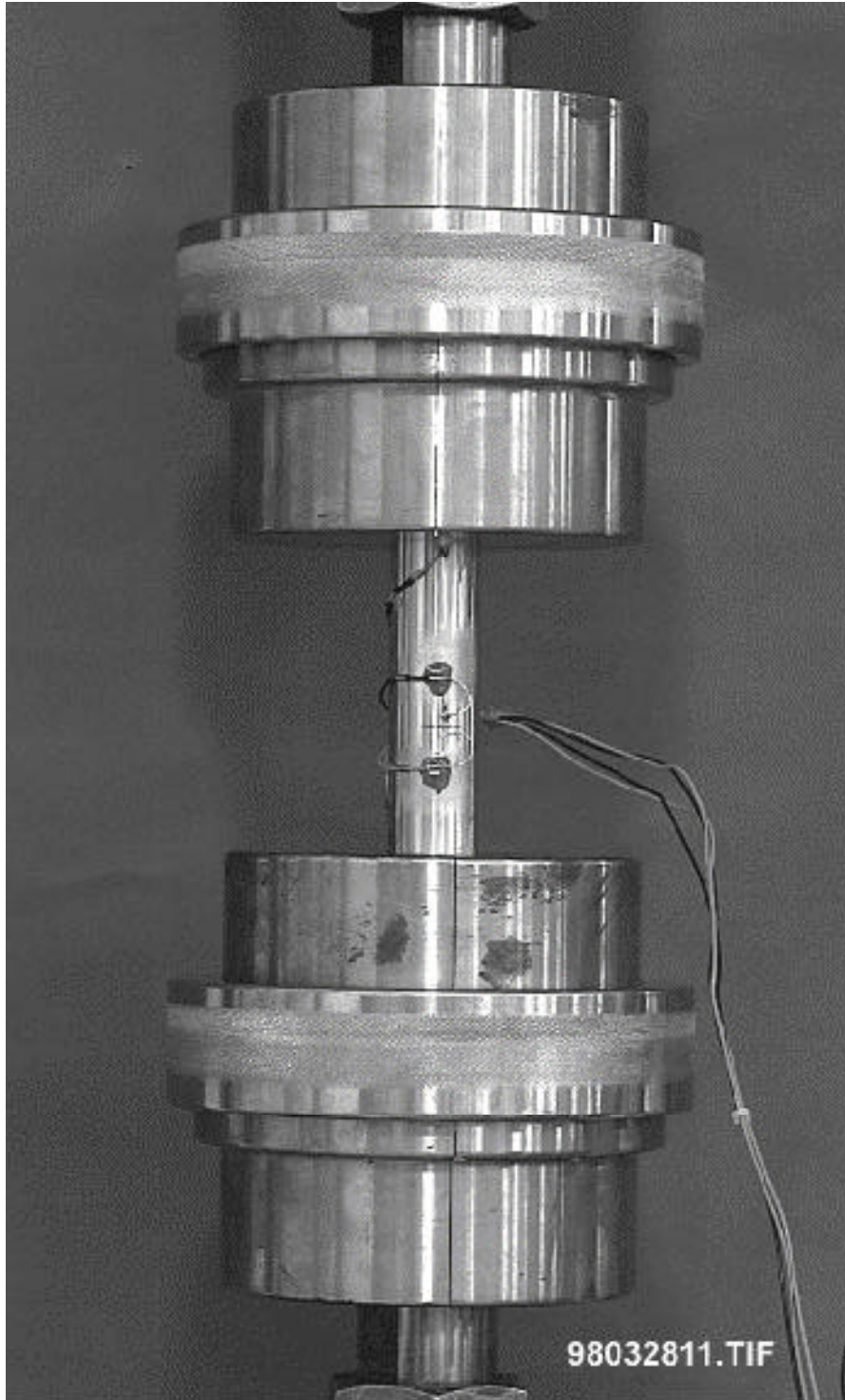


Figure 101. Typical Test Setup for Crack Growth in High Strength Bolts

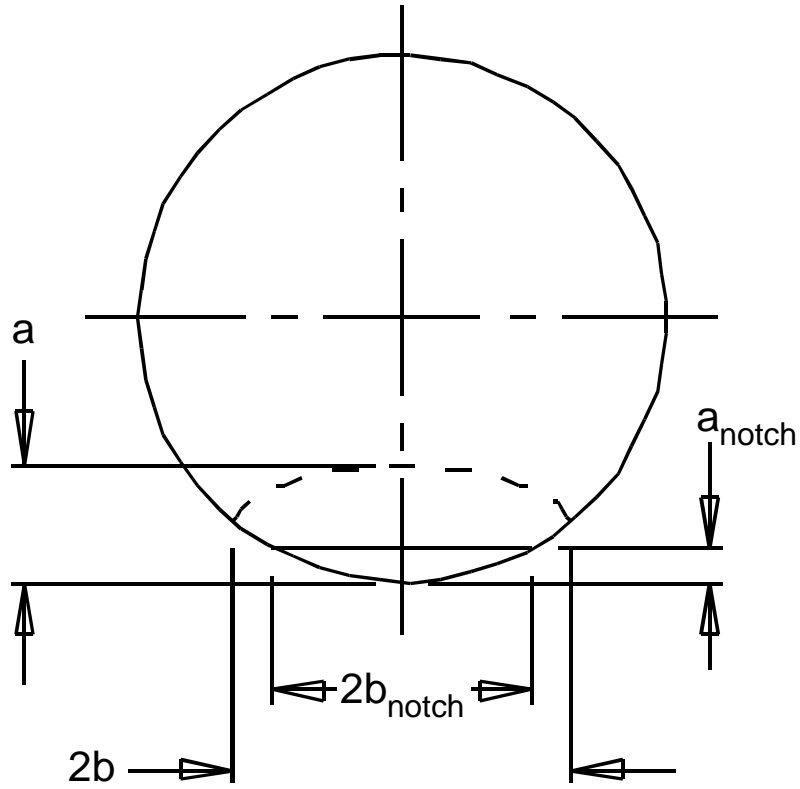


Figure 102. Fatigue Crack Notch, a_{notch} , and Typical Cracking Pattern, a

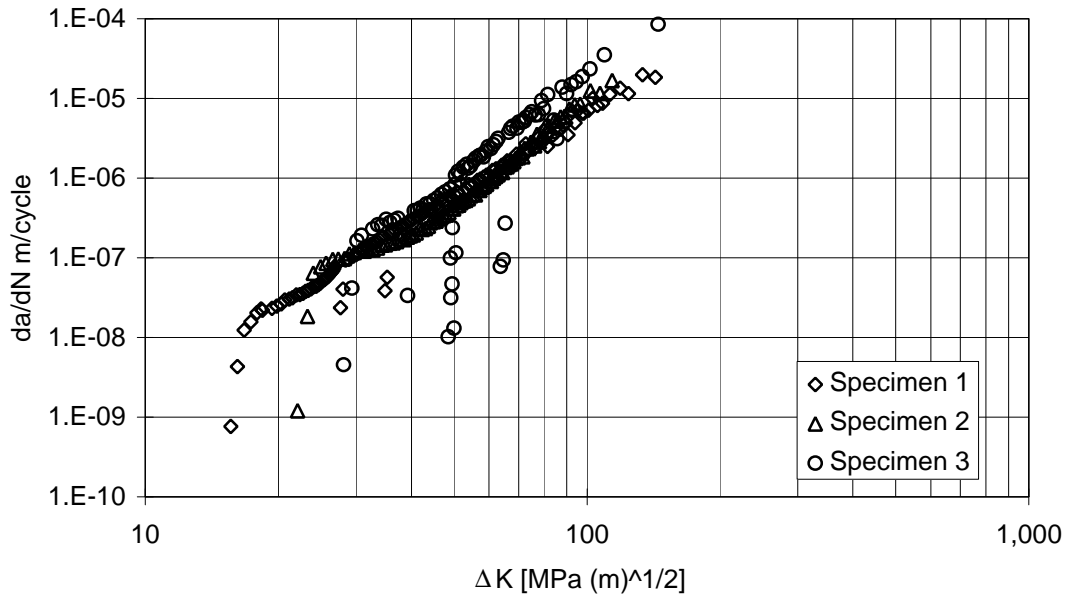


Figure 103. Typical Fatigue Crack Growth Data

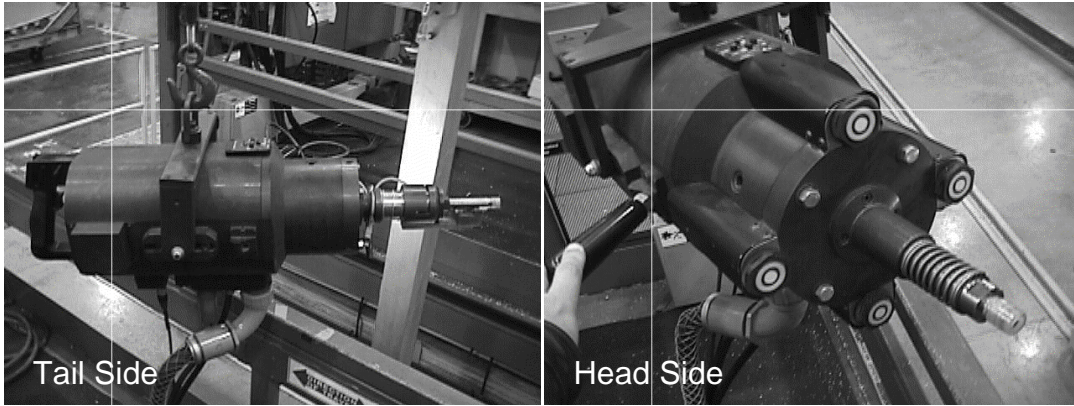


Figure 104. Hand Held Low Voltage Electromagnetic Riveting Apparatus

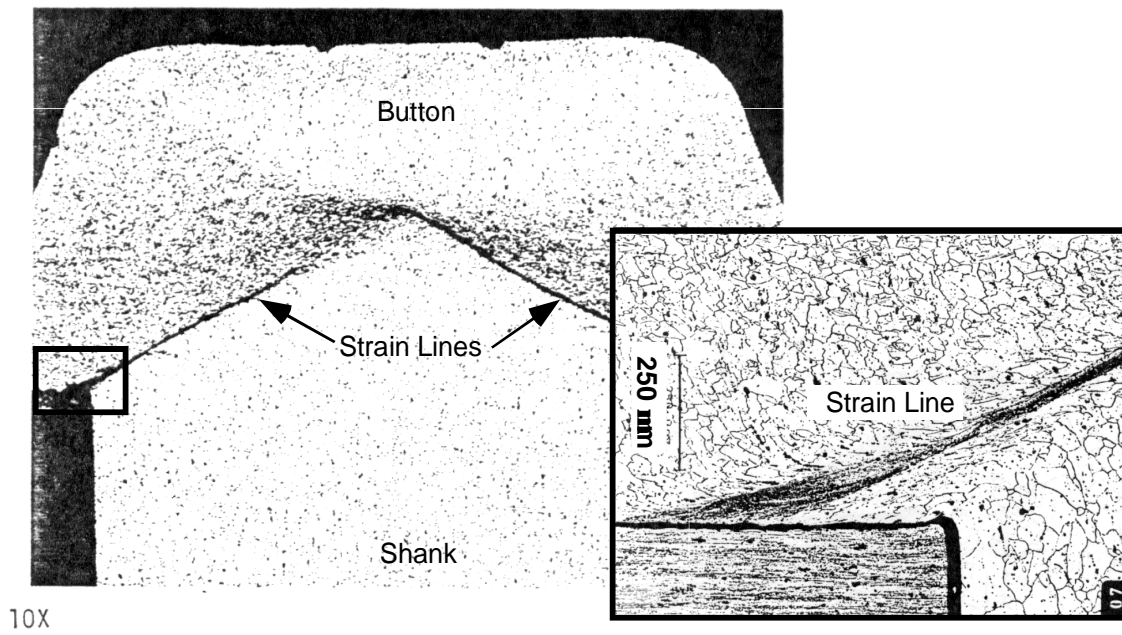


Figure 105. Resultant Intergranular Corrosion Along Strain Lines in EMR Installed Rivet After 500 Hours in 5% Salt Solution

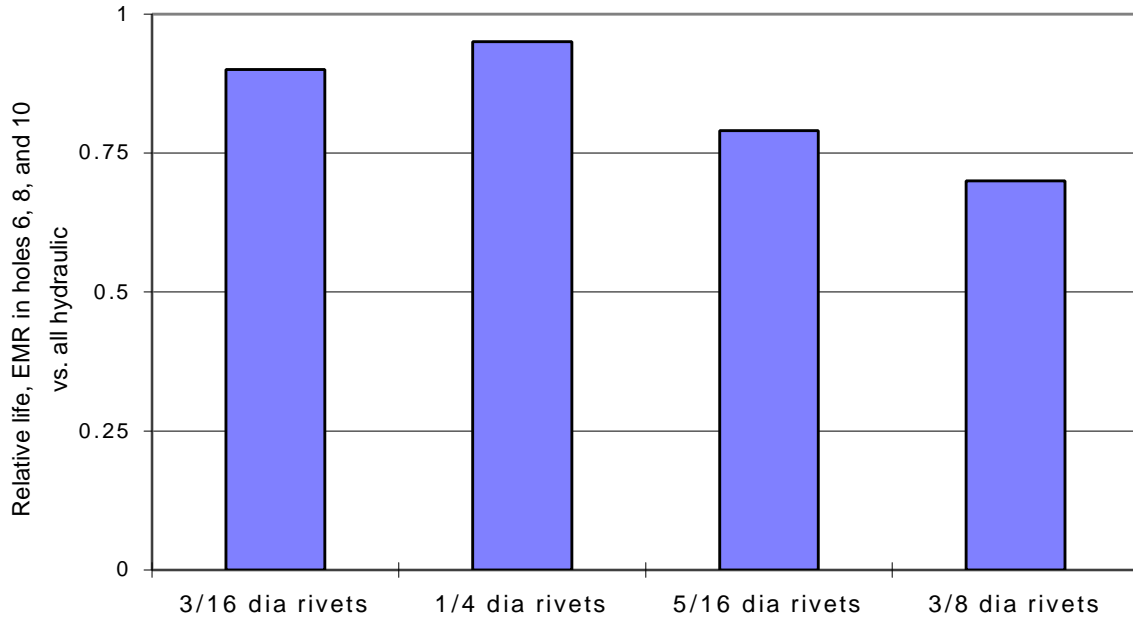


Figure 106. Fatigue Life Comparison of Simulated Temporary Fastener Replacement EMR with Baseline Hydraulic Specimens

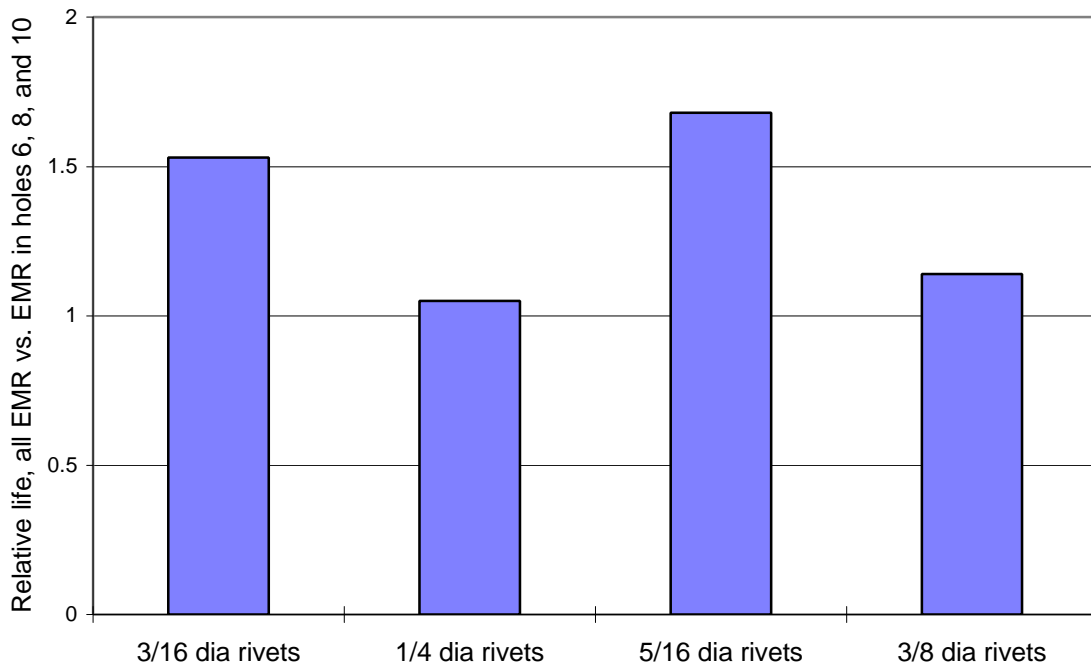


Figure 107. Fatigue Life Comparison of Simulated Temporary Fastener Replacement with All EMR Rivets

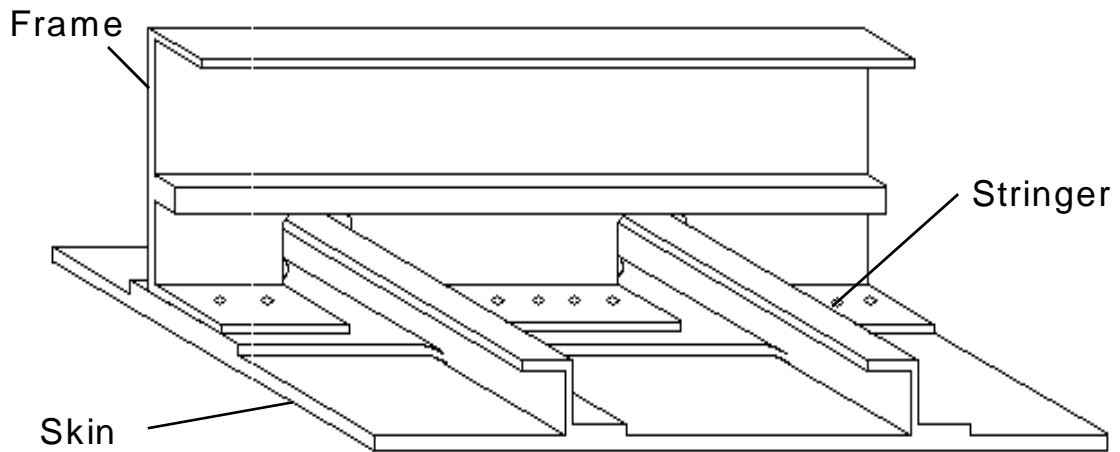


Figure 108. Panel Structural Configuration

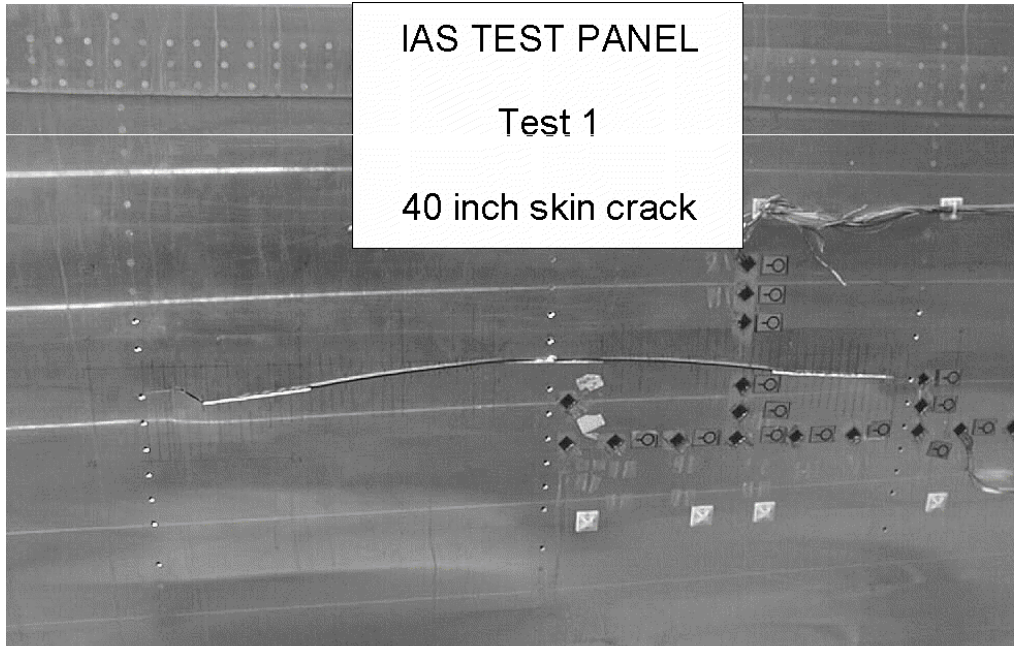


Figure 109. Test 1 – 40 Inch Skin Crack

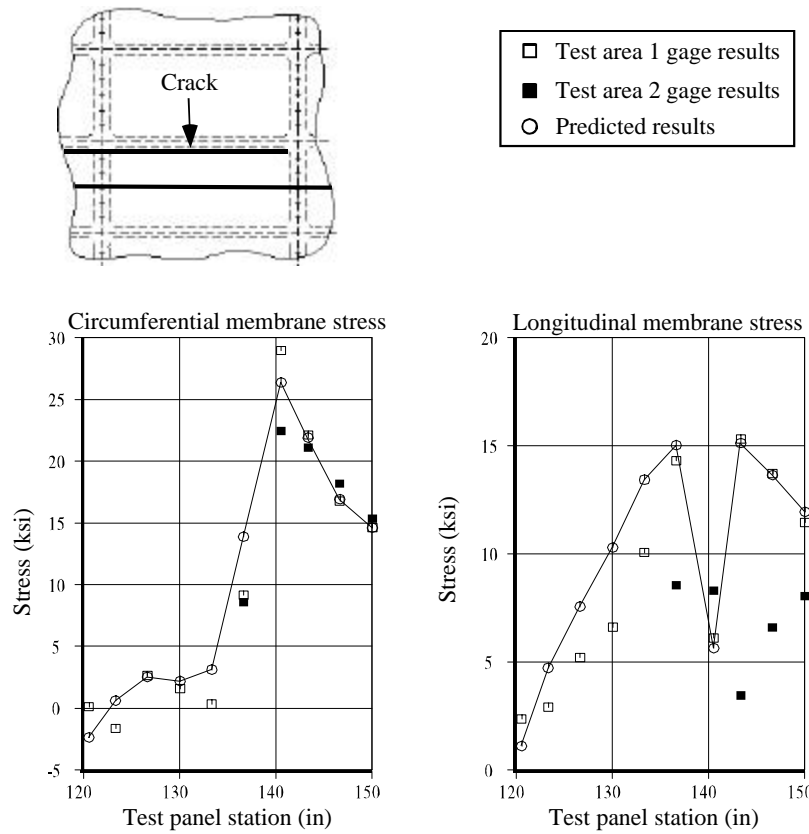


Figure 110. Comparison of Predicted and Test Stress Results for Integral Skin Stringer Panel

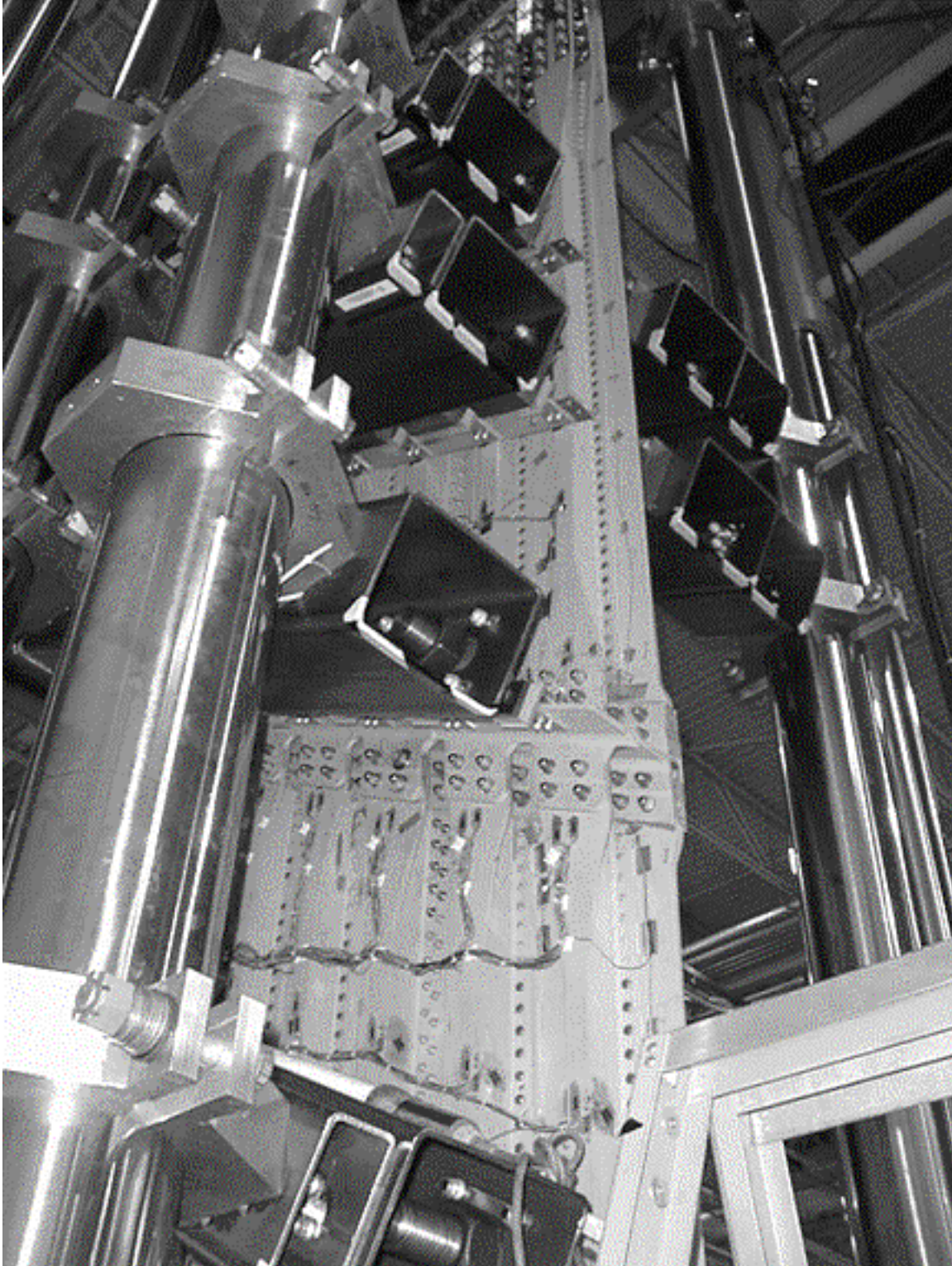


Figure 111. 767-400ER High Load Transfer Panel Installed in the Test Fixture



Figure 112.



Figure 113.

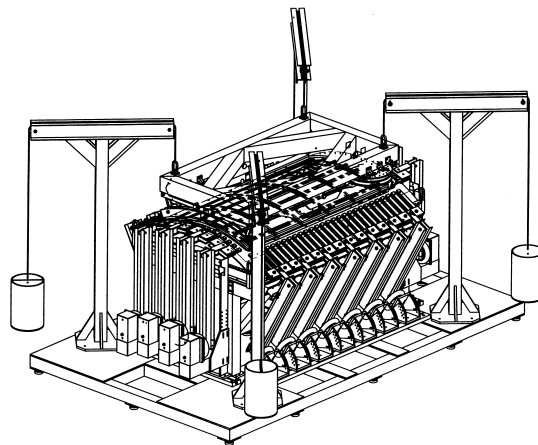


Figure 114.



Figure 115.

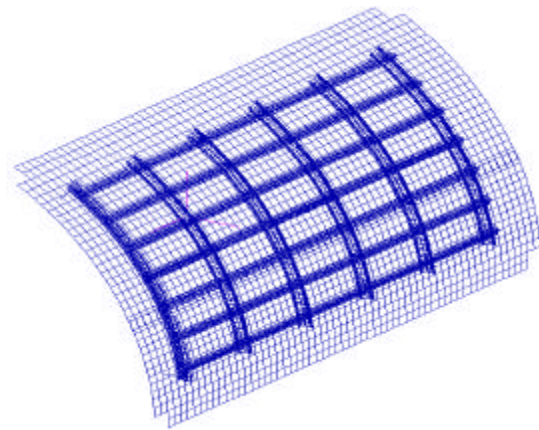
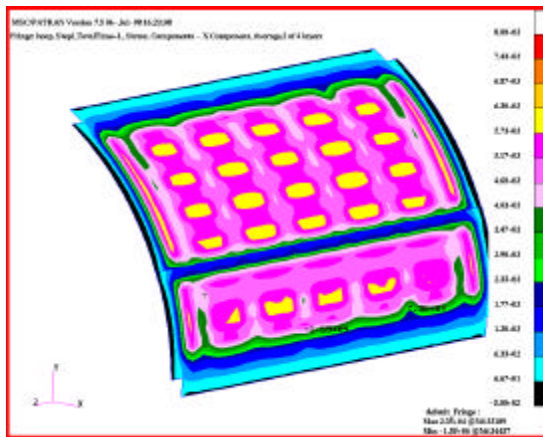


Figure 116.

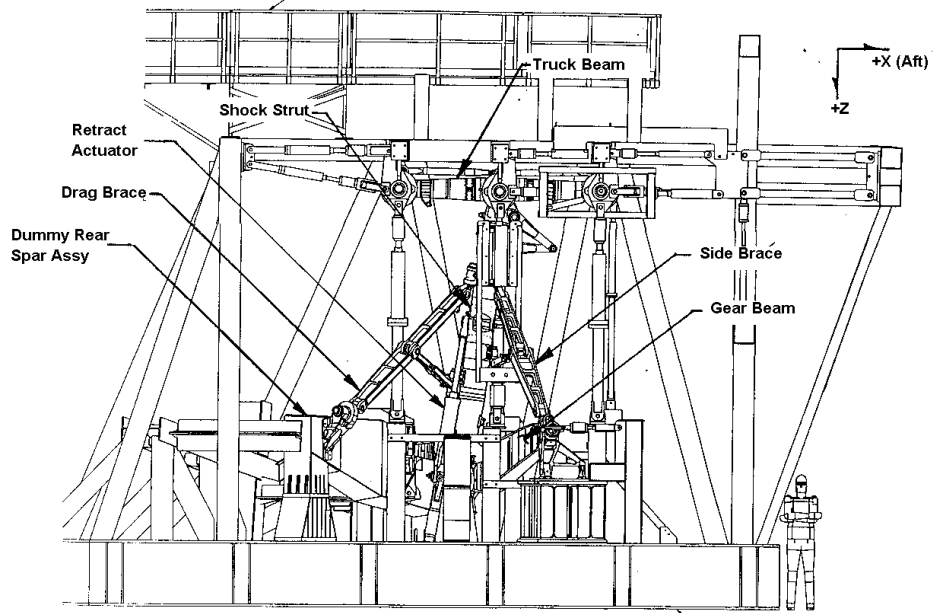


Figure 117. 777 Main Landing Gear Test Fixture with Main Landing Gear Installed

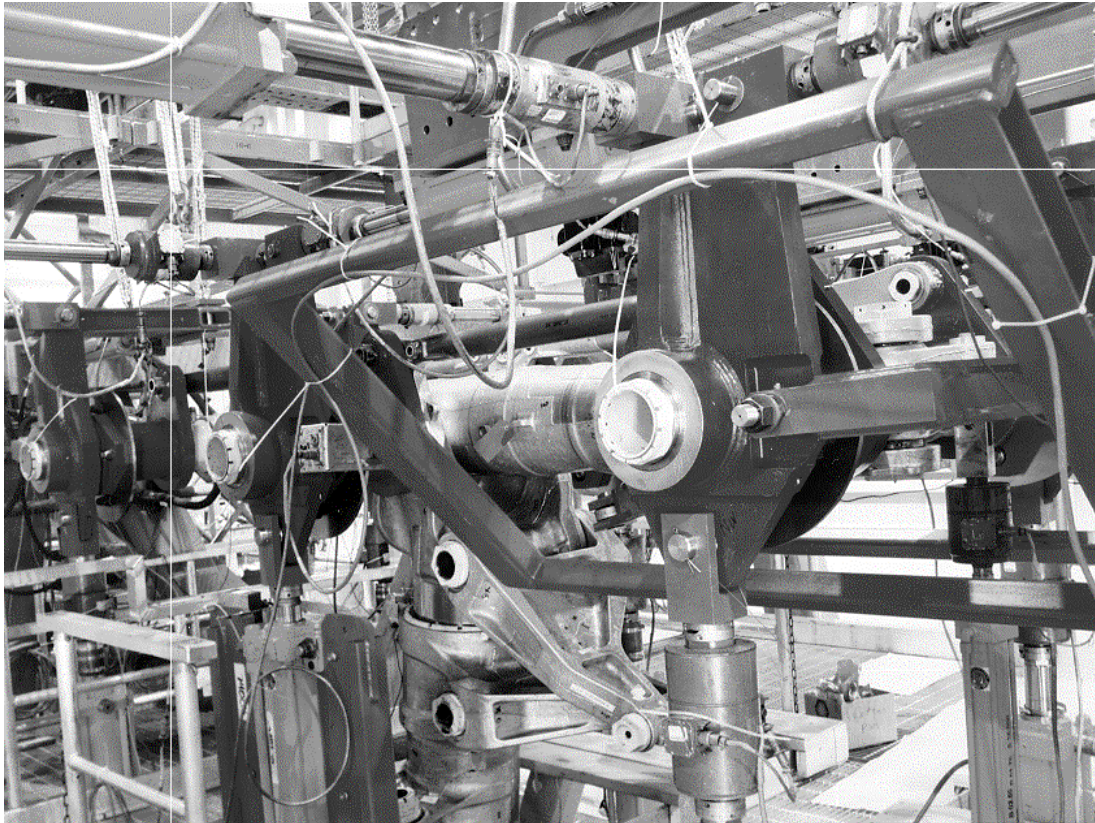


Figure 118. 777 Landing Gear Wheel Block Test Fixture



Figure 119.

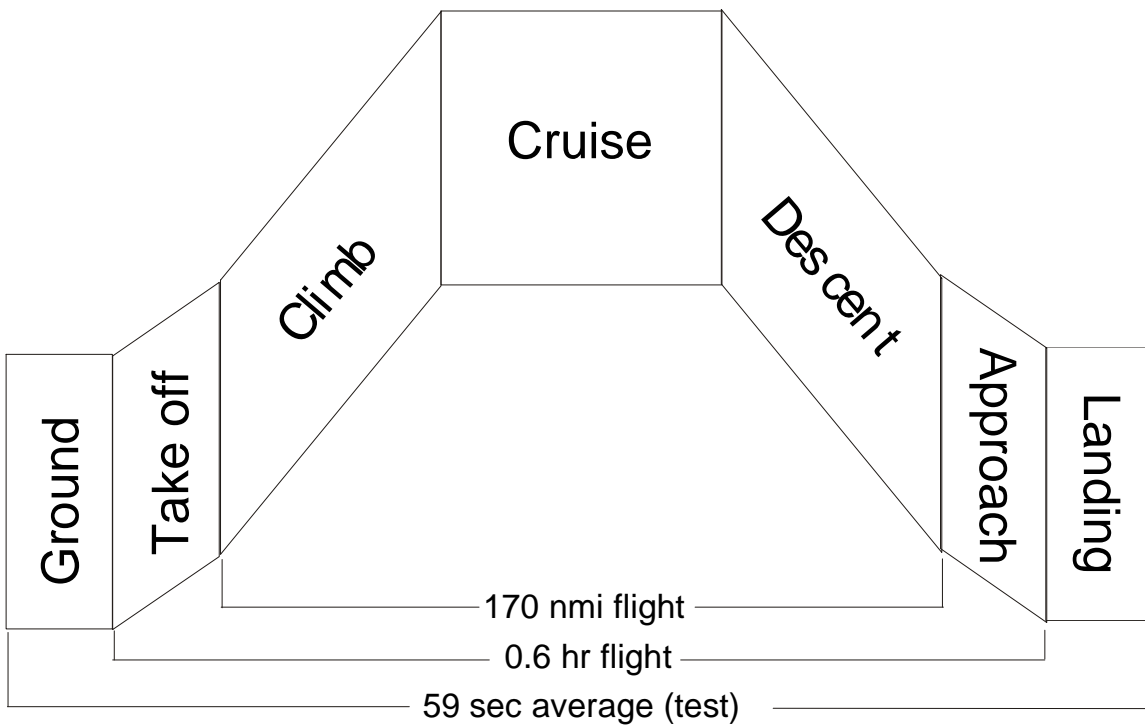


Figure 120. Base Flight Profile



Figure 121. 737-800 Full Scale Fuselage Fatigue Test Setup

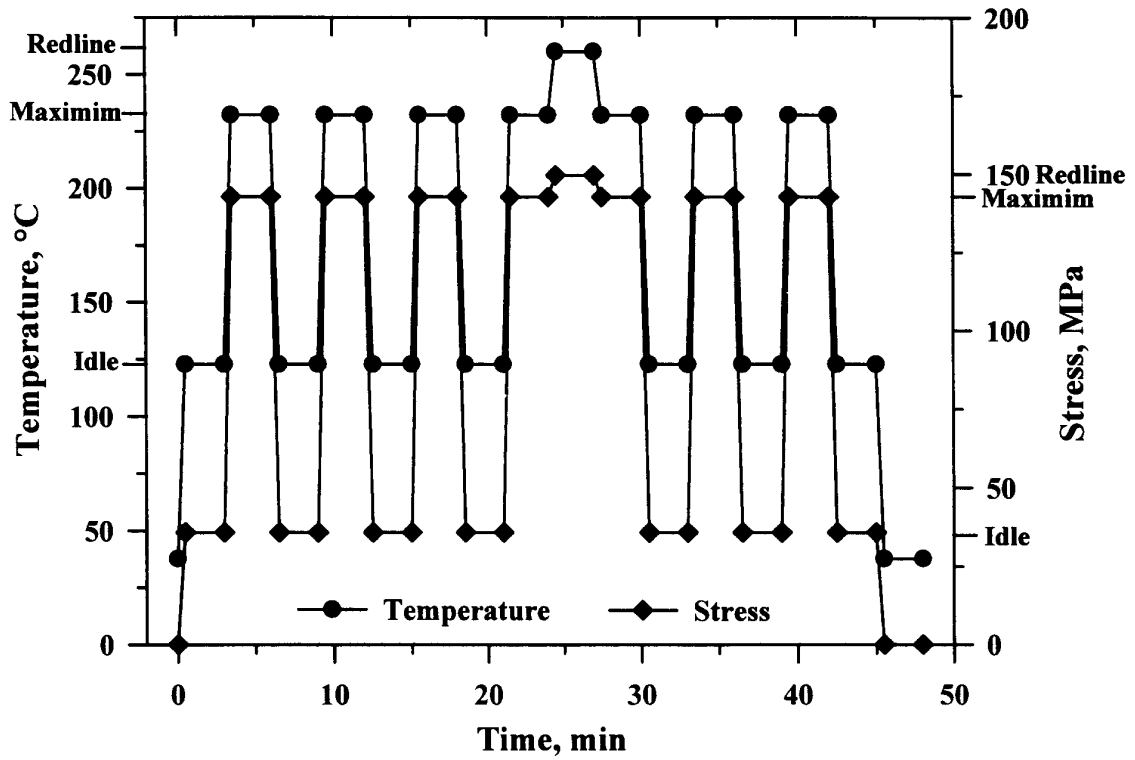
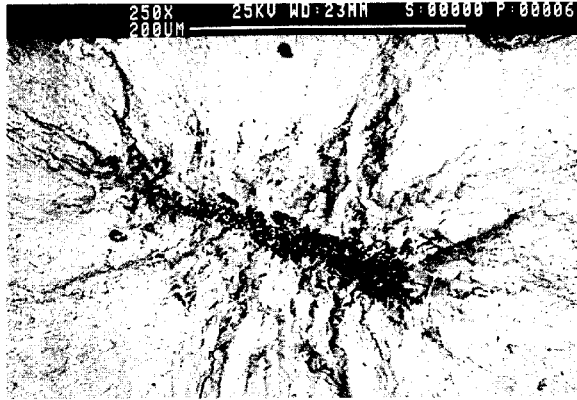


Figure 122. Thermomechanical Fatigue Mission Cycle Used for the T650-35/PMR-15 SMC Inner Vane Endwall Application Showing Idle, Maximum, and Redline Conditions for Temperature and Stress



Oxide Inclusions



Large Grains



Pores

Figure 123. Defects Limiting the Fatigue Life of a PM Disk Superalloy Identified

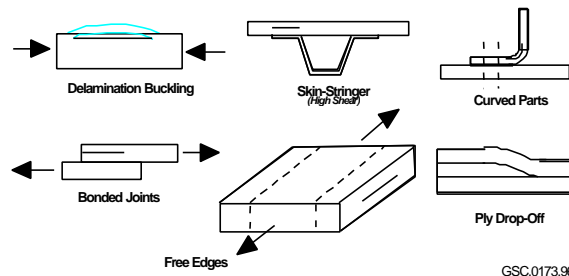


Figure 124.

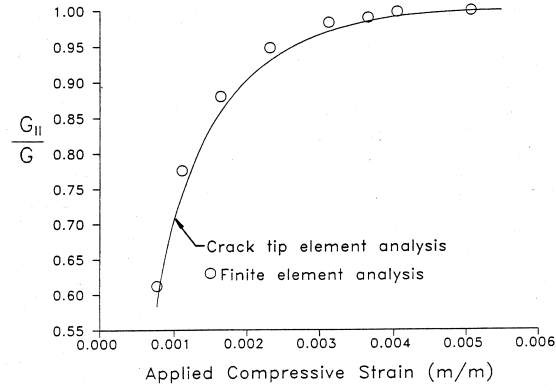


Figure 125.

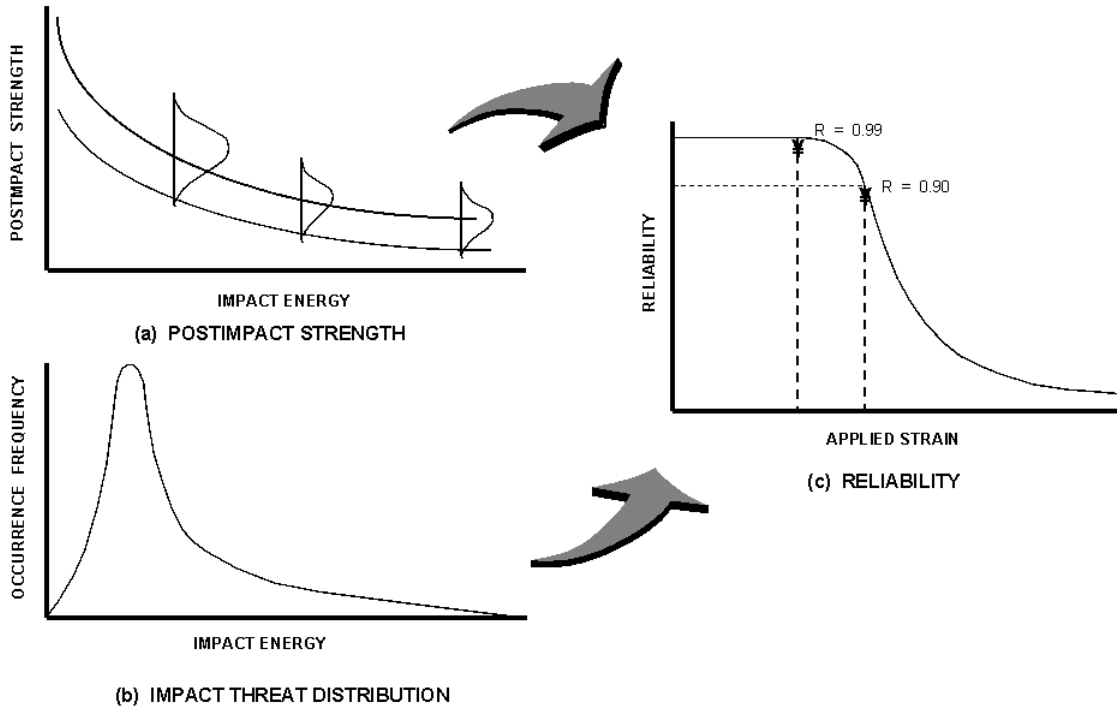


Figure 126. Schematic of the Integrated Reliability Analysis Methods

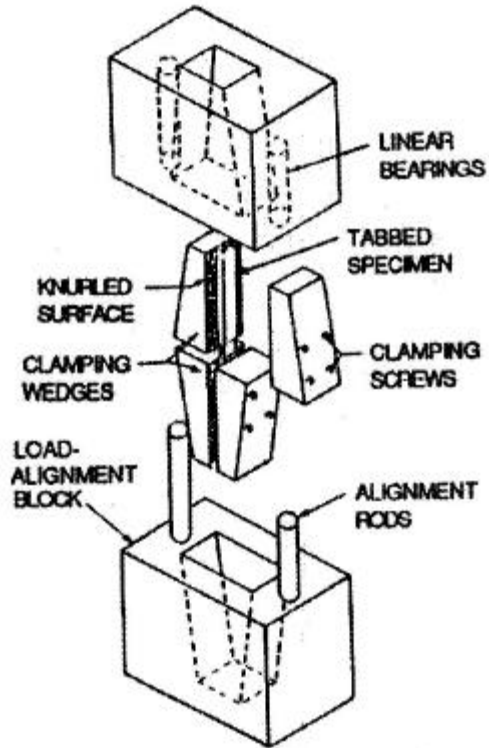


Figure 127. IITRI Compression Test Fixture

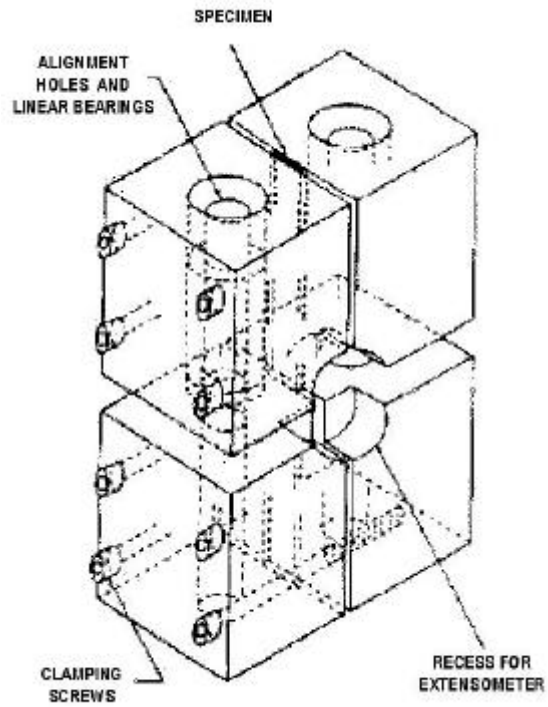


Figure 128. CLC Compression Test Fixture

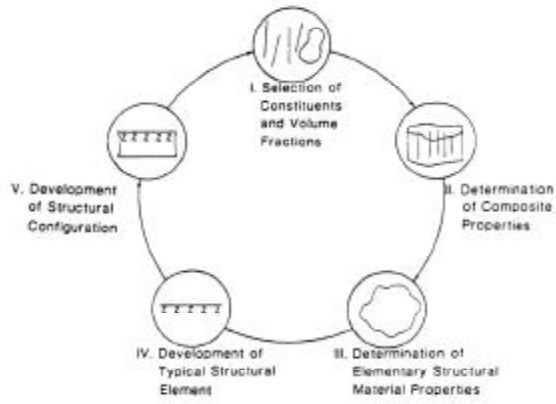


Figure 129.

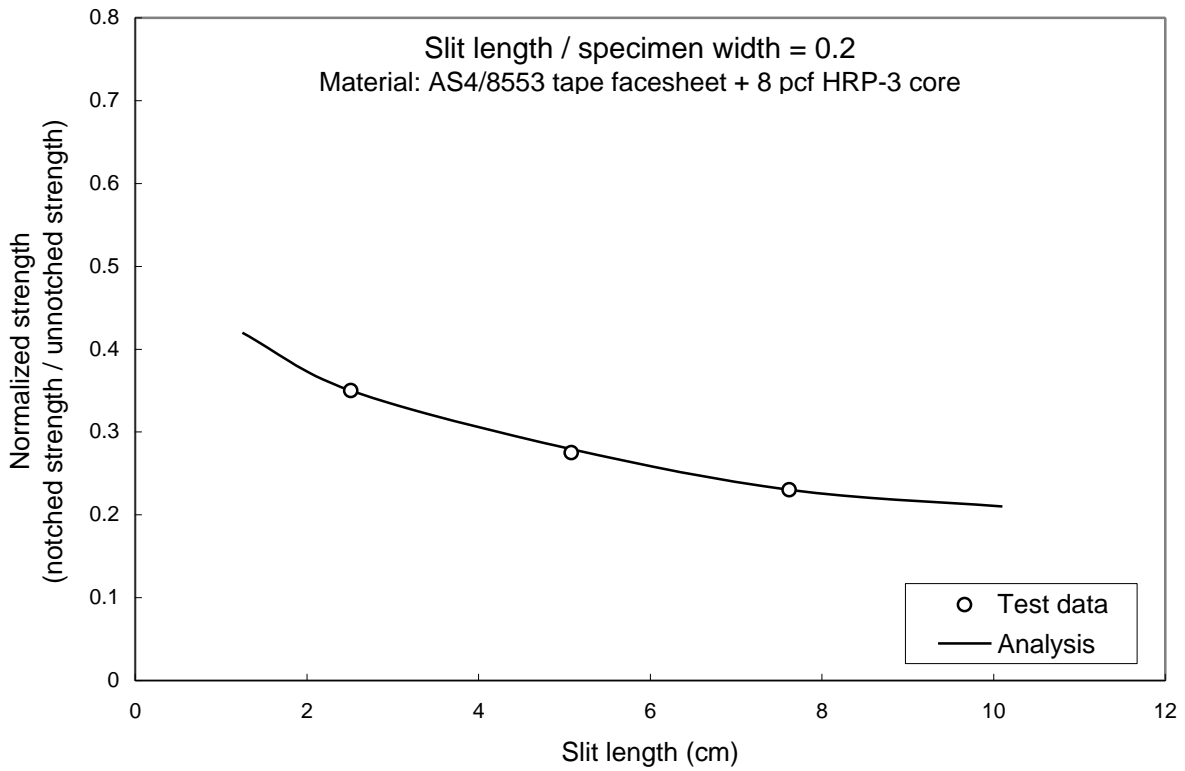


Figure 130. Comparison Between Analysis Method and Test Data

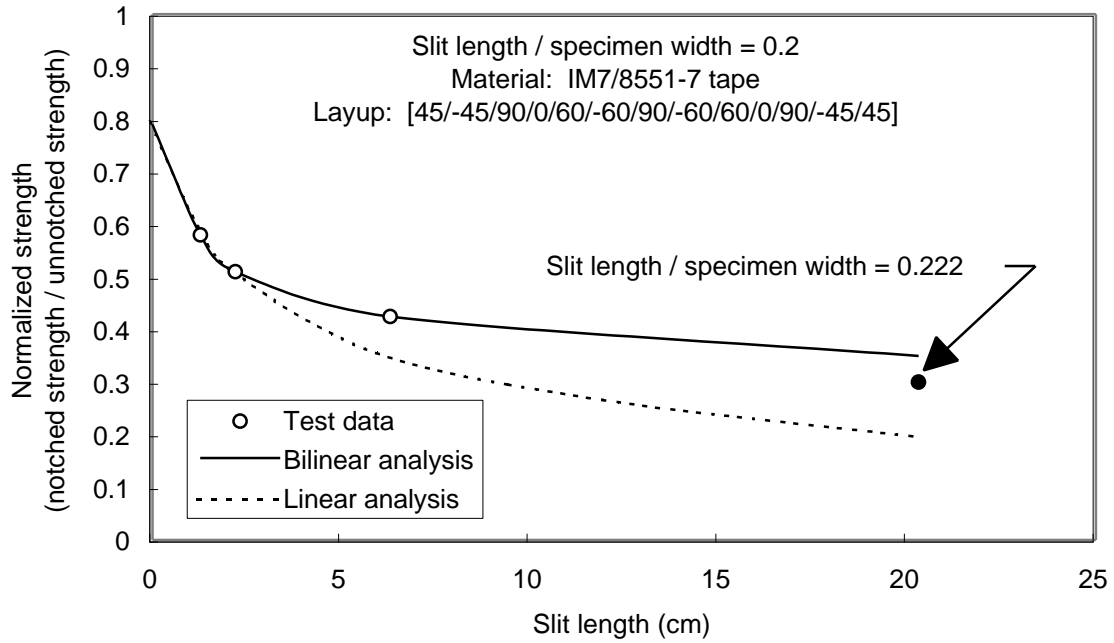


Figure 131. A Comparison Between Test Data and Linear and Bilinear Strain-Softening Law

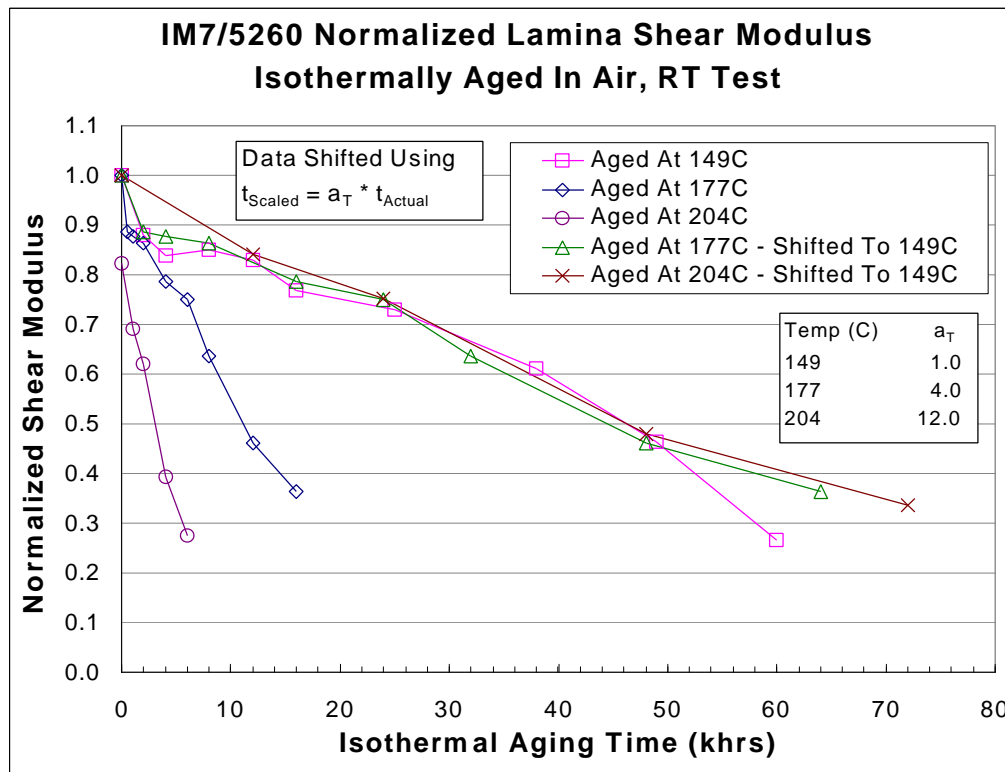


Figure 132. Normalized IM7/5260 Lamina Shear Modulus From $[\pm 45]_{2s}$ Tensile Test After Isothermal Aging in Air at 149° to 204° C

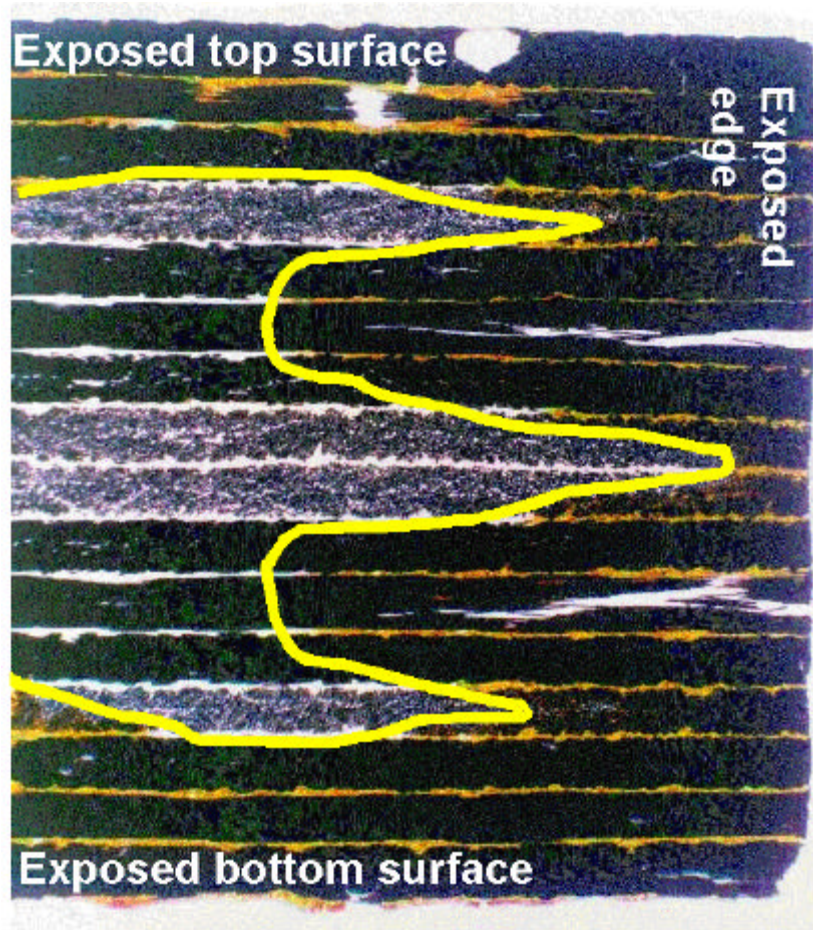


Figure 133. Thin Microsection of IM7/5260 Laminate Aged in Air at 204° C for 4,000 hr (Line Borders Damage Region)

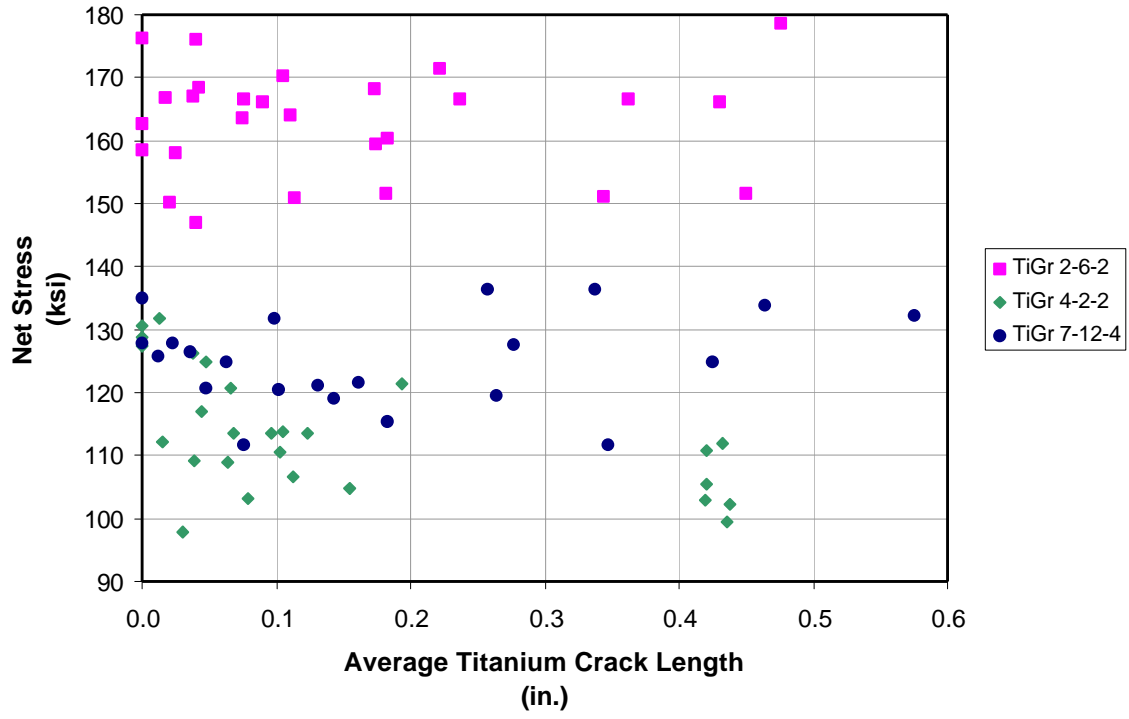
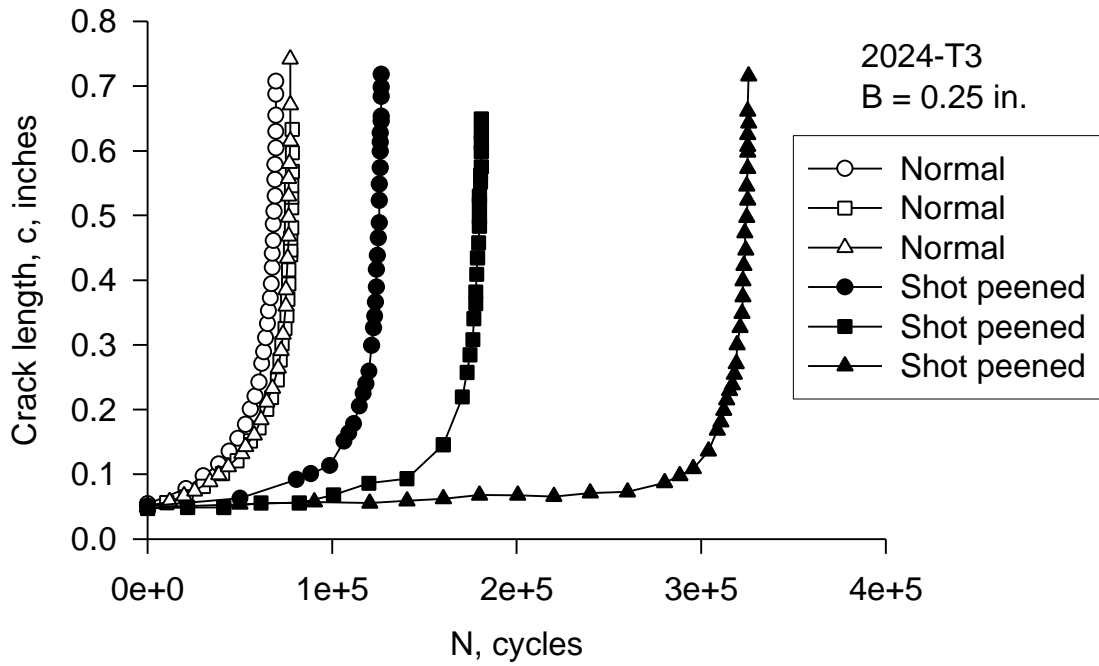


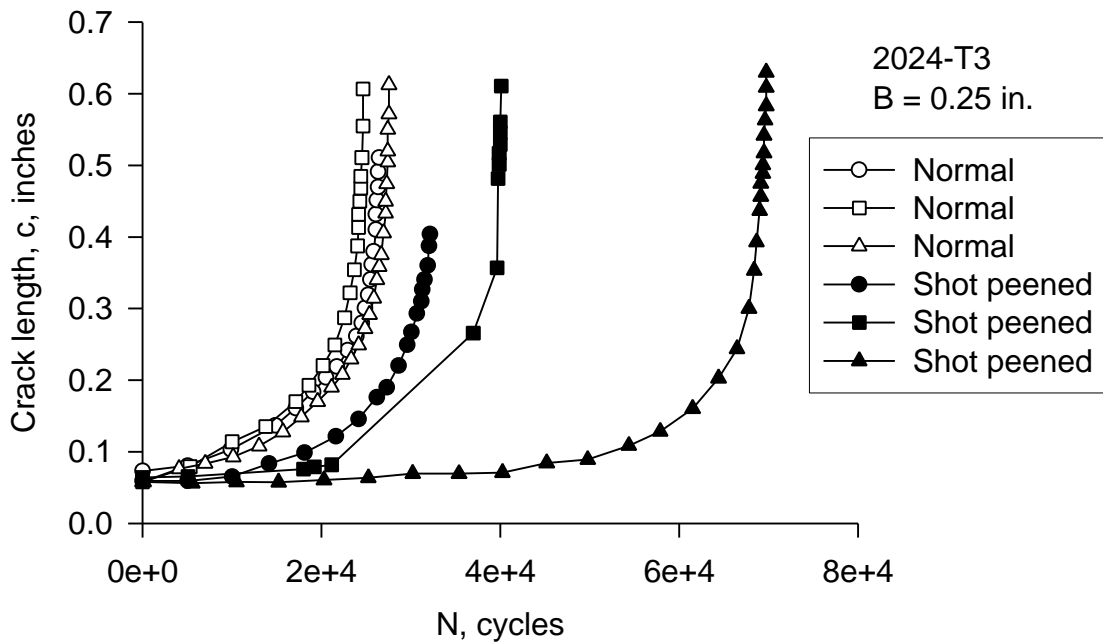
Figure 134. Residual Strength of TiGr OHT Specimens After Fatigue Precracking



Figure 135.



(a) Nominal stress = 15 ksi



(b) Nominal stress = 20 ksi

Figure 136. Comparison of Fatigue Crack Growth in Normal and Shot-Peened Fatigue Specimens

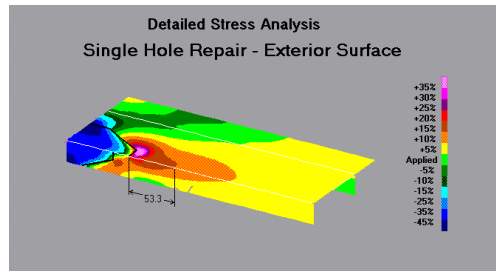


Figure 137.



Figure 138.



Figure 139.

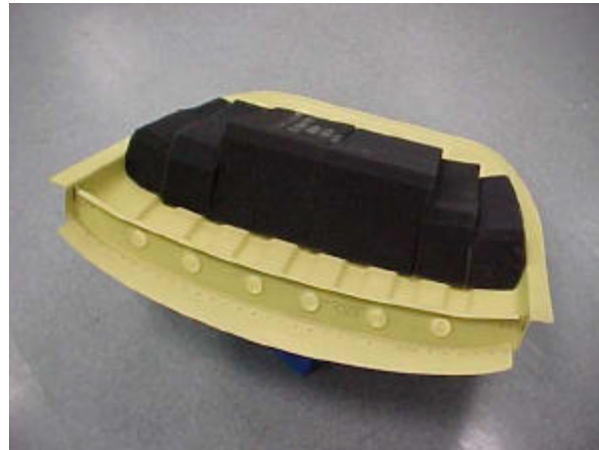


Figure 140.



Figure 141.

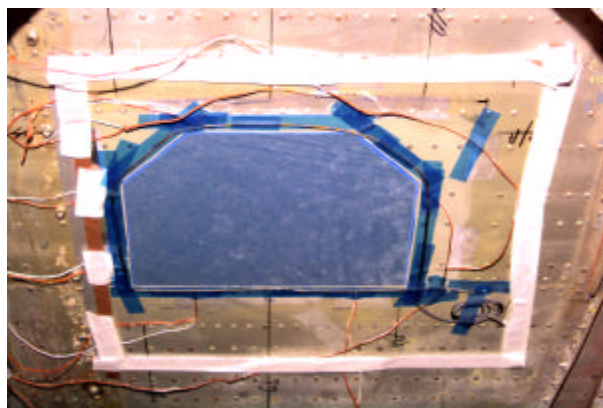


Figure 142.



Figure 143.



Figure 144.

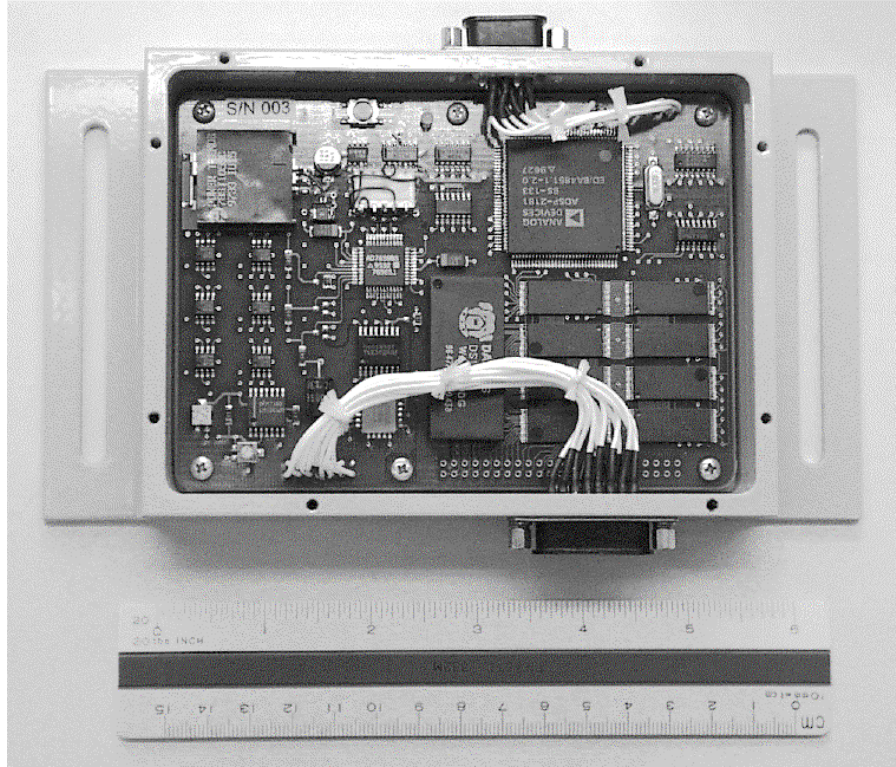


Figure 145. Damage Dosimeter

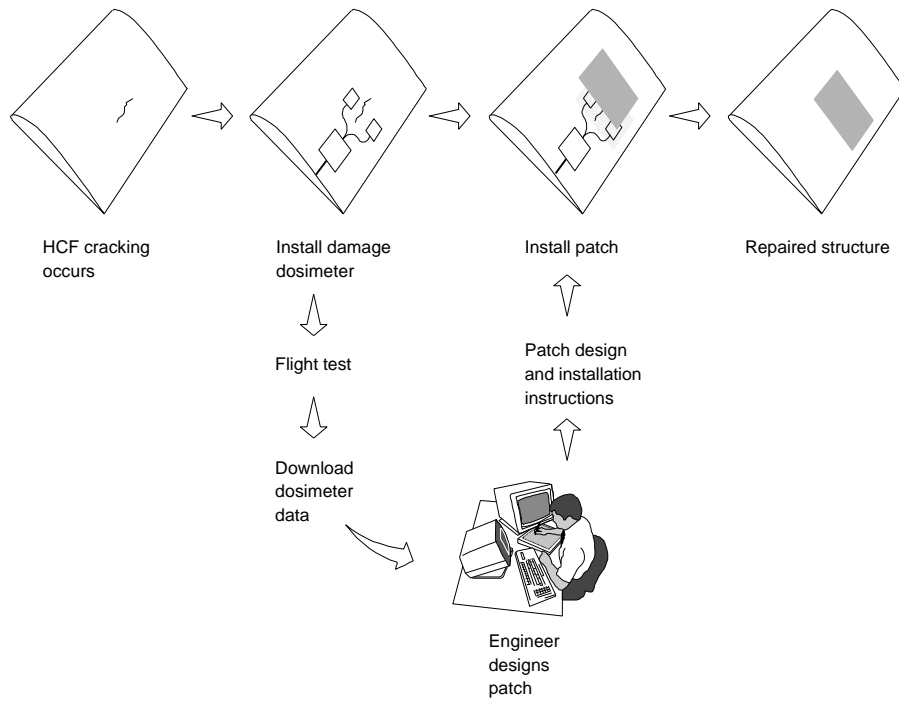


Figure 146. Durability Patch Design Process

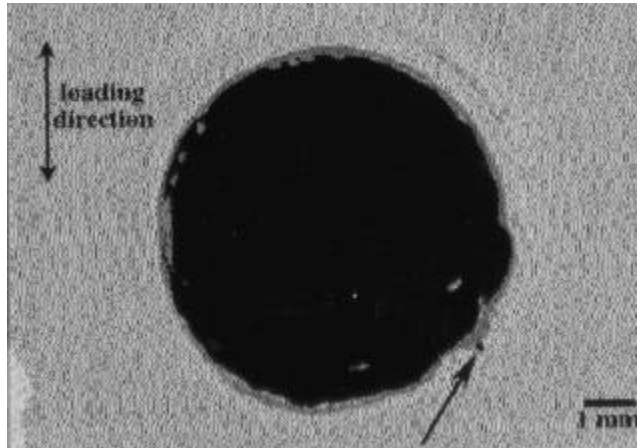


Figure 147. Early Indication of Subsurface Crack in Scanning Acoustic Micrograph

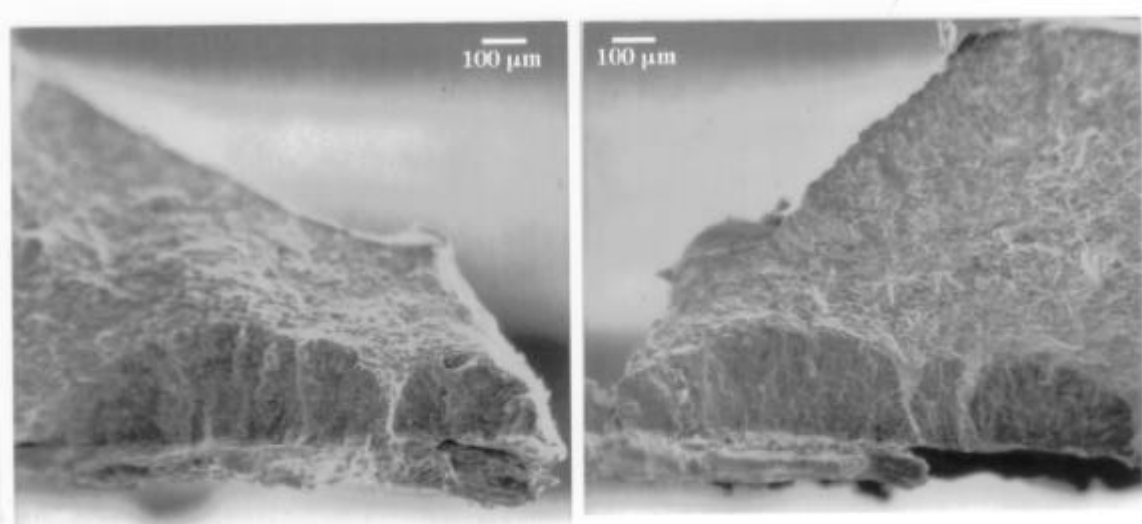


Figure 148. Fracture Surface of Specimen Shown in Figure 140. Multiple Initiation Sites of Crack on Each Side of the Rivet Hole are Viewed

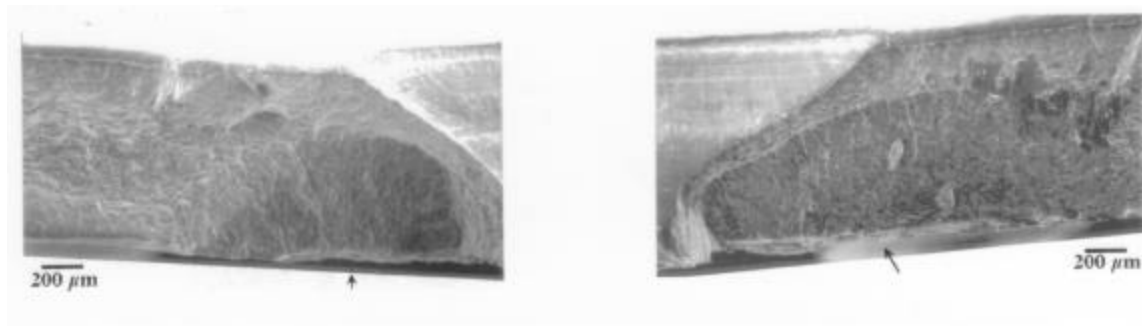


Figure 149. Fatigue Fracture Surface of Specimen Fatigued at Maximum Nominal Stress of 103 MPa and Showing Initiation of Crack Some Distance From the Fracture Surface

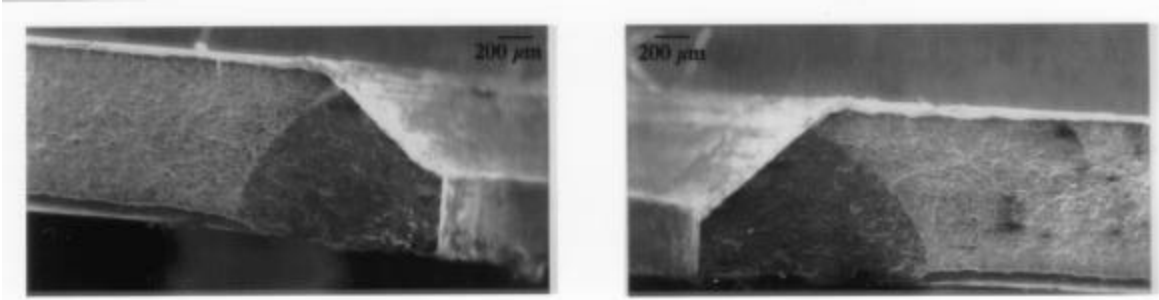


Figure 150. Fatigue Fracture Surface of Specimen Fatigued at Maximum Nominal Stress of 154 MPa and Showing Initiation of Crack at the Corner Where the Knife Edge Meets the Fayed Surface



Figure 151. Pulsed-Eddy Current (PEC) Device

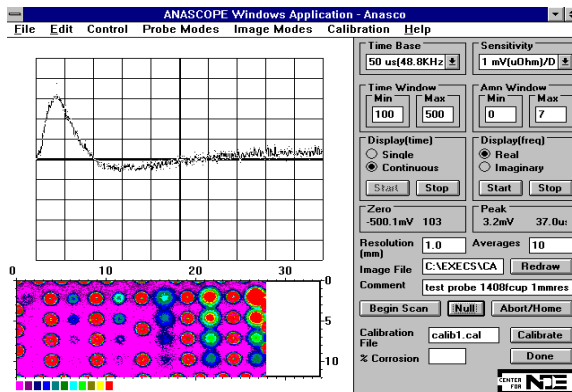


Figure 152. PEC Output Display

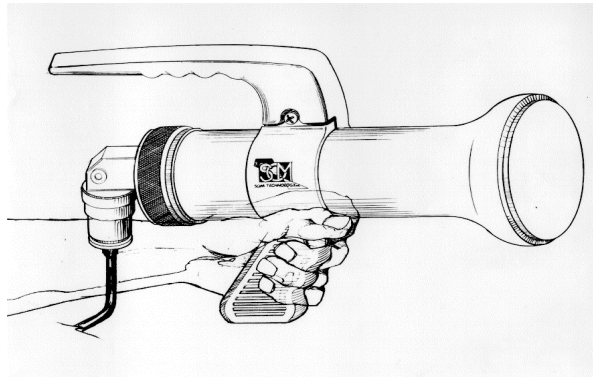


Figure 153. Hand-Held Scanning Head

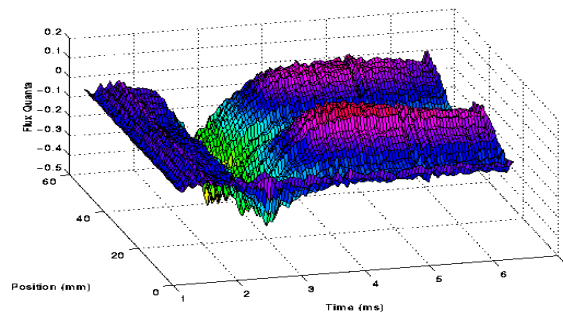


Figure 154. 25 mm Crack Under 10 mm Al

NASA Rotating Probe

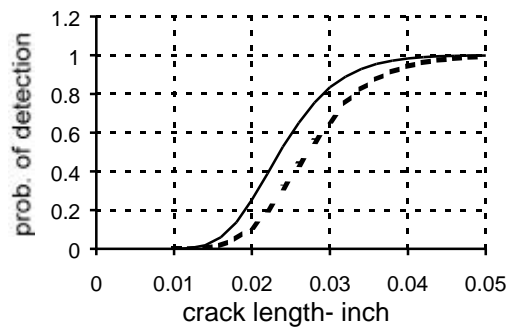


Figure 155.



Figure 156.

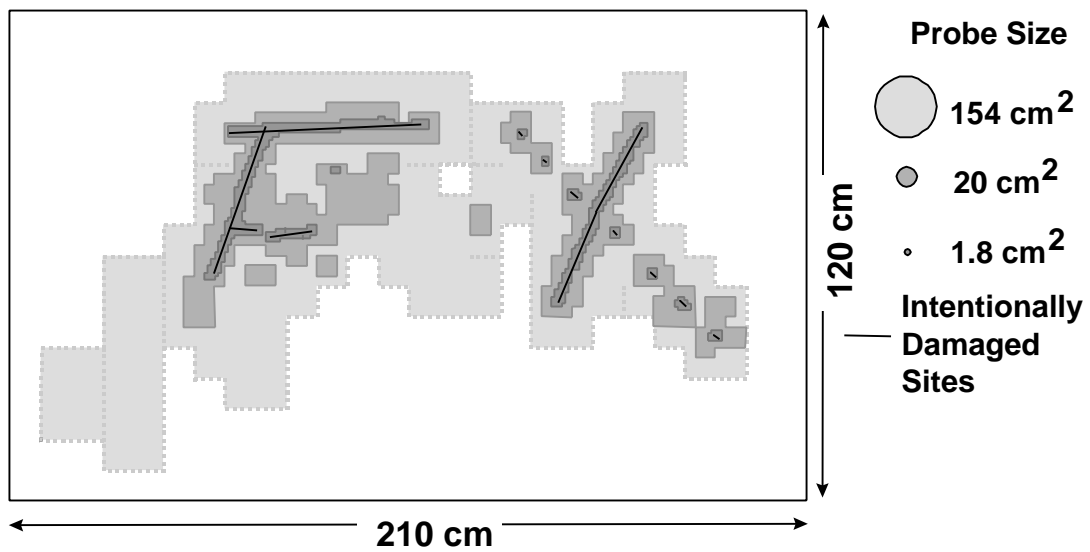


Figure 157. Scanning Test of a 25,200 cm² Painted Al7075-T6 Coupon with Three Prototype Probes of Different Sizes: 154, 20, and 1.8 cm². Shaded Areas Represent Damaged Sites, and Were Detected When Either Part or All of the Intentionally Damaged Site Was Underneath the Probe. Darker Areas Were Detected with Smaller Probes. A Couple of Non-Intentionally Damaged Sites Were Also Detected.

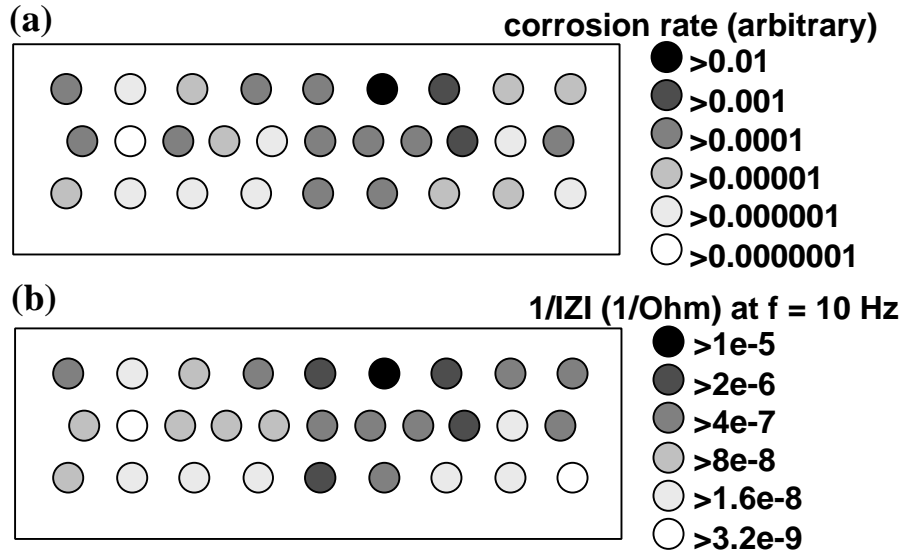


Figure 158. Maps Reflecting the Degree of Hidden Corrosion in Part of a Side Fuselage From an Aged Boeing 727 Aircraft. (a) Values Estimated From the Corrosion Rates Measured at Each Rivet. (b) Values Estimated From the Inverse of the Impedance Magnitude at 10 Hz Measured at Each Rivet. Each Circle Represents a Rivet. Black Represents the Most Corroded Areas, Whereas White Represents the Non-Corroded Areas.

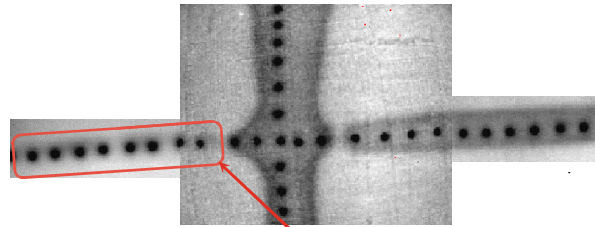


Figure 159. Example of Disbonded (Left) and Bonded Doubler Regions on a B747 Aircraft

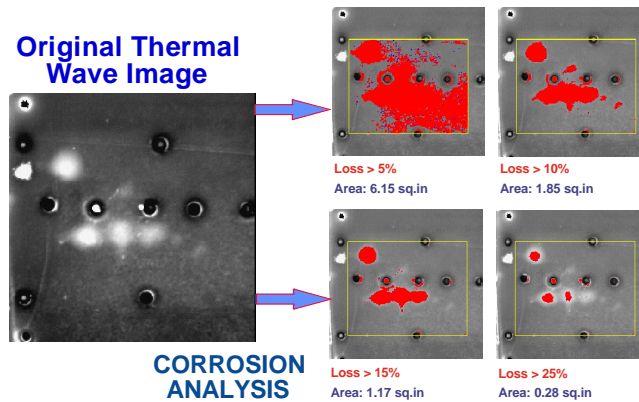


Figure 160. Example of Corrosion Analysis of a Two-Layer Corrosion Test Specimen

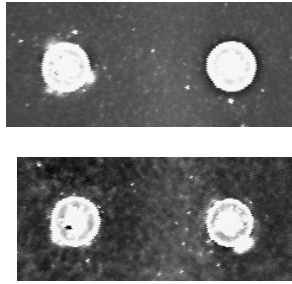
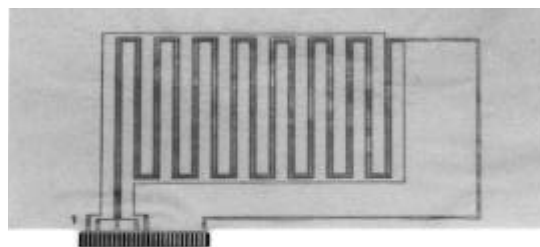


Figure 161. Intergranular Corrosion Creeping Out From Under the Countersunk Fastener Heads (Bright Areas) on 3 of the 4 KC-135 Wing Fasteners Displayed



Figure 162. ETC Portable Scanner Applied to AlliedSignal Engine Component



MWM Sensor

Figure 163.

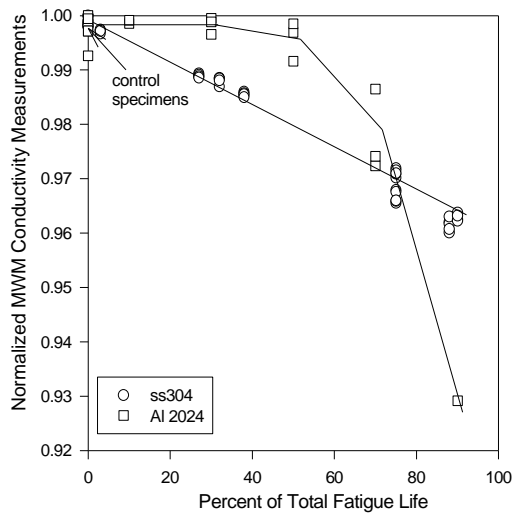


Figure 164.

Transport Inspector PoDs

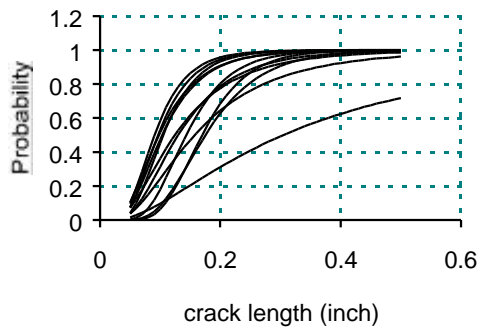


Figure 165.

Commuter PoDs

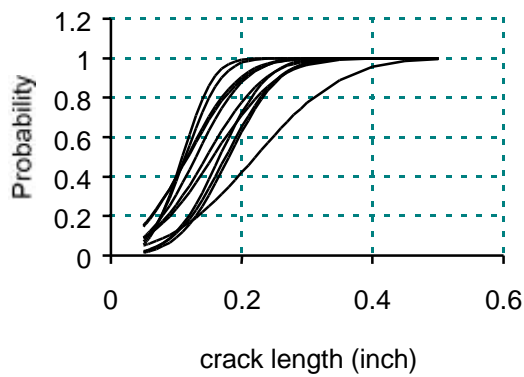


Figure 166.

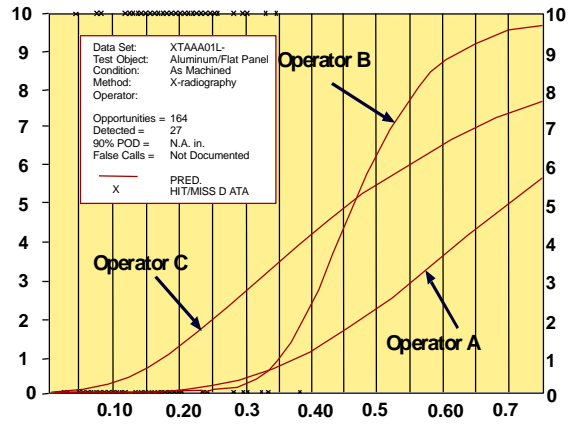
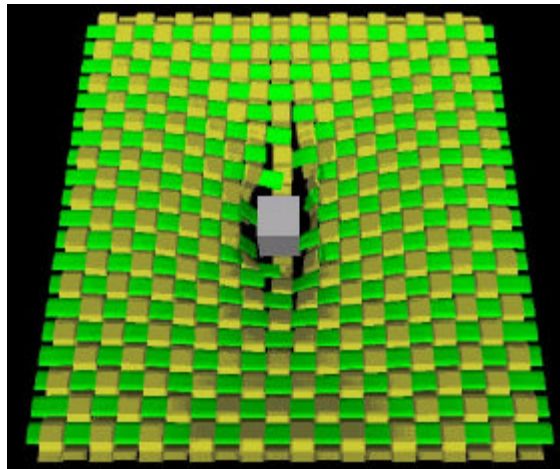


Figure 167. Example of PoD Curves From the NDE Capabilities Data



DYNA 3D Model of Fragment Impact

Figure 168.



Figure 169.

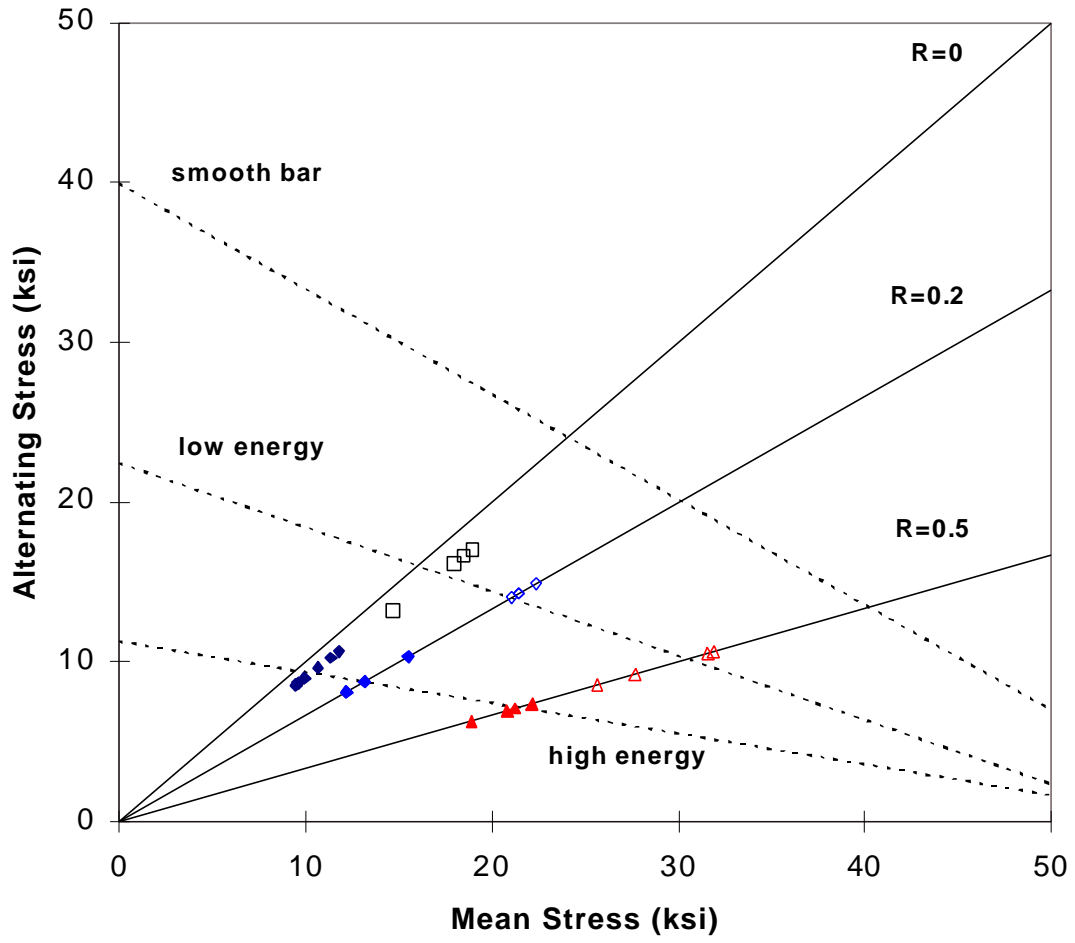


Figure 170. Goodman Diagram for γ -TiAl Specimens Tested at 650° C

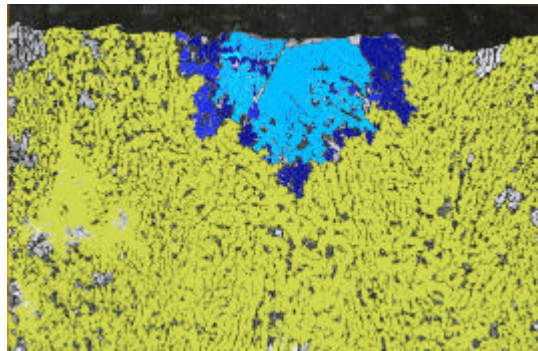
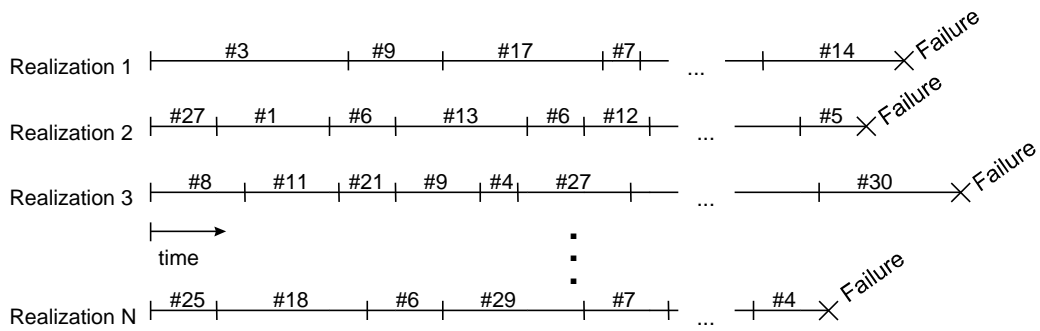


Figure 171.



Figure 172.



#1 Troop Assault SLS	#11 Troop Assault 35°C	#21 Troop Assault 35°C HA
#2 Resupply SLS	#12 Resupply 35°C	#22 Resupply 35°C HA
#3 Aeromed. Evac. SLS	#13 Aeromed. Evac. 35°C	#23 Aeromed. Evac. 35°C HA
#4 Replacing Units SLS	#14 Replacing Units 35°C	#24 Replacing Units 35°C HA
#5 Trans. of Recon. SLS	#15 Trans. of Recon. 35°C	#25 Trans. of Recon. 35°C HA
#6 Reinforce/Repos. SLS	#16 Reinforce/Repos. 35°C	#26 Reinforce/Repos. 35°C HA
#7 Troop Extract. SLS	#17 Troop Extract. 35°C	#27 Troop Extract. 35°C HA
#8 Aerial Comm. Post SLS	#18 Aerial Comm. Post 35°C	#28 Aerial Comm. Post 35°C HA
#9 Sling Load SLS	#19 Sling Load 35°C	#29 Sling Load 35°C HA
#10 Training SLS	#20 Training 35°C	#30 Training 35°C HA

Figure 173. Schematic of Random Mission Mix Loading. Note Both the Random Selection of Missions and the Variation in the Block Length.

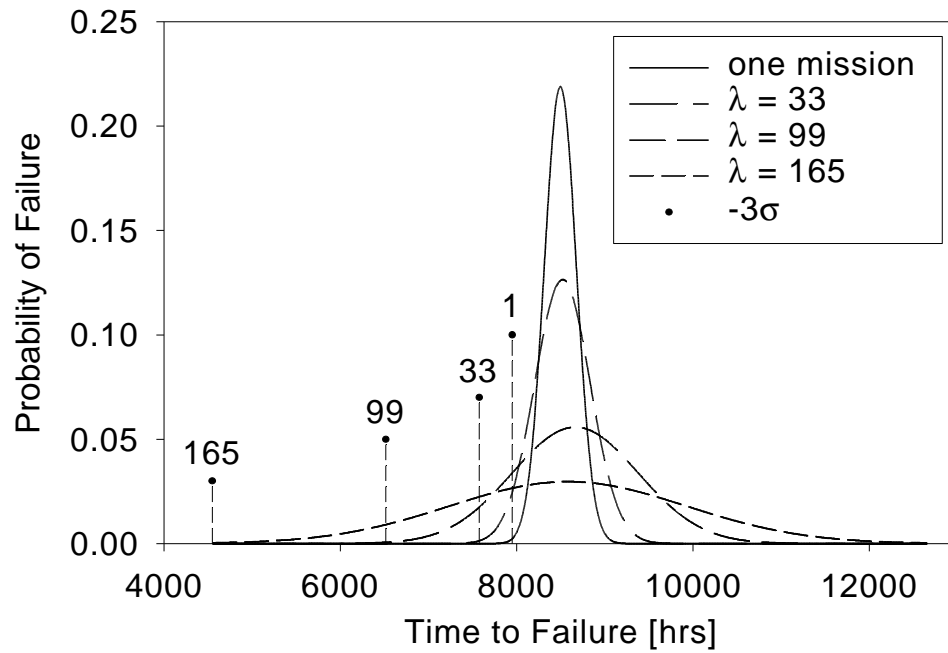


Figure 174. Failure Distributions Derived from Simulation Results. The Labeled Drop Lines Indicate Life at Mean Minus 3 Standard Deviations for Each Simulation Run. λ is the Expected Mission Repeat Count (Poisson Distribution Parameter).

REVIEW OF CANADIAN AERONAUTICAL FATIGUE WORK 1997-1999

Jerzy P. Komorowski
David L. Simpson

INSTITUTE FOR AEROSPACE RESEARCH
NATIONAL RESEARCH COUNCIL OF CANADA

SUMMARY

This paper provides a review of Canadian work associated with fatigue of aeronautical structures during the period 1997-1999. All aspects of structural technology are covered including full scale tests, loads monitoring, fracture mechanics, composite materials and engine fatigue.

Organisation Abbreviations Used in Text

AETE	Aerospace Engineering Test Establishment (DND)
AMRL	Aeronautical and Maritime Research Laboratory (Australia)
BARA	Bombardier Aerospace Regional Aircraft
BADS	Bombardier Aerospace Defence Services
CF	Canadian Forces
DGAETM (FT)	Director General Air Equipment Technical Management (Fighters and Trainers)
DND	Department of National Defence
DTA	Directorate of Technical Airworthiness
IAR	Institute for Aerospace Research
NRC	National Research Council of Canada
RAAF	Royal Australian Air Force
RCAF	Royal Canadian Air Force
RMC	Royal Military College of Canada
QETE	Quality Engineering Test Establishment
USN	United States Navy
UTIAS	University of Toronto Institute for Aerospace Studies

1 INDEX

1	INDEX.....	2
2	INTRODUCTION.....	4
3	FULL SCALE TESTING.....	5
3.1	Full-Scale Testing Review.....	5
3.2	CF18 - Hornet.....	5
3.3	CF18 International Follow-On Structural Project (IFOSTP) Centre Fuselage Test.....	6
3.4	CF18 IFOSTP Wing Test – Loads Derivation.....	7
3.5	FT 245 Wing Test Configuration.....	11
3.6	FT 245 Actuator Loads Calculations.....	13
3.7	Maritime Patrol Aircraft CP-140 Orion.....	15
3.8	The Bombardier Global Express Certification.....	16
3.9	DHC-8-400 (Dash 8) Certification.....	17
3.10	Landing Gear Programs.....	18
3.10.1	Messier-Dowty Inc.....	18
3.10.2	Menasco Aerospace.....	20
4	LOADS MONITORING AND MEASUREMENT ACTIVITIES.....	21
4.1	Operational Loads Monitoring - Body of Knowledge.....	21
4.2	CT114 - Tutor.....	21
4.3	CT133 Silverstar Operational Loads Monitoring Program.....	22
4.4	CF18 Fatigue Life Tracking Improvements.....	23
4.5	CC130 – Hercules.....	24
4.5.1	Operational Loads Monitoring/Individual Aircraft Tracking (OLM/IAT).....	24
4.5.2	CC130 Wing Finite Element Modelling.....	25
4.5.3	Centre Wing Service Life Extension Program/Fuselage Life Assessment Program.....	26
4.5.4	Centre Wing Strain Survey/Aft Fuselage Strain Survey.....	26
4.5.5	"Hot Spot" Strain Surveys.....	27
4.6	CP140 (P3) Structural Data Recording System.....	27
4.7	DHC-8 Service Load Monitoring.....	29
4.8	Total Data Integrity Initiative (TDI ²).....	29
4.9	Squadron Level Software (SLS).....	30
5	FRACTURE MECHANICS AND CRACK PROPAGATION STUDIES.....	30
5.1	A Study on the Use of Neuber’s Rule in Fatigue Crack Initiation Predictions.....	30
5.2	Fatigue Life Extension of Ageing CP140 Aircraft.....	30
5.3	Probabilistic Crack Growth Analysis Software Development.....	33
5.4	Shot Peening Certification Program for CF18 Y470.5 Bulkhead Location X19.....	33
5.5	CT114 Coupon Test Program.....	33
5.6	CT133 Coupon Test Program.....	34
5.7	Parametric Crack Growth Analysis.....	34
6	FAILURE INVESTIGATIONS.....	35
6.1	CF18 (Hornet).....	35
6.1.1	Failure Analysis of Fatigue Coupons from 7050-T7452 Forging.....	36
6.1.2	A Metallographic study of Fatigue–Critical Fastener Holes in a CF18 Structural Component [].....	37
6.1.3	CF18 Heavy Weight Outboard Engine Thrust Mount.....	38
6.1.4	CF18 Main Landing Gear Planing Link Bolts - Failure Analysis.....	38
6.1.5	CF18 Trailing Edge Flap Outboard Hinge/Lug Crack.....	38
6.1.6	CF18 Front Spar Fractographic Analysis.....	38
6.1.7	CF18 LAU 7 Missile Launcher Crack Assessment.....	39
6.1.8	Failure of PH 13-8 Mo Aircraft Components.....	39
6.2	CC130 (Hercules).....	39
6.2.1	CC130 Longeron Attachment Fitting Crack.....	40
6.2.2	CC130 Strut Web, and Bulkhead Failure.....	40
6.2.3	CC130 Fuselage Station FS 880 Extrusion Ring Segment Failure.....	40
6.2.4	Failure of RH T-Bow Beam Fitting of CC130 Aircraft.....	41
6.2.5	CC130 Rear Spar Web Fatigue Damage Assessment.....	41

6.3	CP140 (P3 Orion)	42
6.3.1	CP140 Nose Landing Gear Actuator Failure	42
6.4	CH124 (Sea King).....	42
6.4.1	CH12437 Pylon Assembly Failure.....	43
6.4.2	Failure of a CH124 Sea King T58 Engine Mount.....	43
6.5	CC142 (Dash-8) Main Wheel Failure	43
6.6	CT114 Tutor	44
6.6.1	CT114 Tutor Wing Cracks.....	44
7	AGING AIRCRAFT ISSUES.....	44
7.1	Integrating Real Time Age Degradation Into the Structural Integrity Process	44
7.2	Pillowing Corrosion Cracking in Al 2024-T3 Fuselage Lap Joints	46
7.3	MSD and Corrosion Fatigue in Lap Splice Specimens.....	48
7.3.1	Experimental Technology	48
7.3.2	Risk assessment of fuselage splice joints with multiple site damage.....	51
7.3.3	Analytical and FE modelling of riveted lap joints	52
7.3.4	Three dimensional geometrically non-linear finite element model of a lap joint specimen.....	54
7.4	Retrosession and re-ageing (RRA).....	55
7.5	Bonded Patch Repair Technology.....	55
7.5.1	Three-dimensional FE modelling of bonded repair of thick section.....	55
7.5.2	Thick Section Bonded Patch Technology	57
7.5.3	CT114 Tutor Boron Doubler Repair to Lower Wing Skin Damage	59
7.5.4	Composite Patch Repair - CC130 Lower Wing Skin.....	60
7.5.5	Thermal Analysis of Composite Patch Repair	60
8	EXPERIMENTAL AIRCRAFT	61
8.1	UTIAS Ornithopter	61
9	COMPOSITE MATERIALS AND STRUCTURES	63
9.1	CF18 Flight Control Surfaces Moisture and Water Ingress	63
9.2	Field Level Assessment of Low Viscosity Adhesives	64
9.3	Shear buckling test and analysis of fibre metal laminates (FML).....	65
10	GAS TURBINE ENGINES - FATIGUE AND DAMAGE TOLERANCE	66
10.1	Thermal Fatigue Testing of Nozzle Guide Vanes in the NRC/IAR Burner Rig	66
10.2	Damage Tolerance Assessment of Nene X Turbine Disc	66
10.3	Damage Tolerance of Modified Waspaloy Disc Material.....	67
10.4	Modelling the Crack Tip Elastic-Plastic Field in Anisotropy Crystalline Solids.....	68
11	NONDESTRUCTIVE INSPECTION	69
11.1	Development of POD From In-Service NDI Data.....	69
11.2	The Edge of Light Technique: Towards Quantitative Enhanced Visual NDI.....	69
11.3	Probability of Detection of Impact Damage in Composite Structures	70
11.4	Pulsed Eddy Current Method Development for Hidden Corrosion Detection in Aircraft Structures	71
12	ACKNOWLEDGMENTS	72
13	REFERENCES	73

2 INTRODUCTION

Canadian industry, universities and government agencies were solicited for information describing their fatigue technology related activities over the period 1997 to 1999. This review covers work performed or being performed by the following organisations:

Bombardier Aerospace

- Defence Services
- Regional Aircraft (deHavilland)
- Business Aircraft

Celeris Aerospace Inc.

Department of National Defence

- Canadian Forces
- Director for Technical Airworthiness
- Quality Engineering Test Establishment
- Air Vehicles Research Section
- Royal Military College

IMP Group Limited

- IMP Aerospace

National Research Council of Canada

- Institute for Aerospace Research

Martec Ltd

Menasco Aerospace

Messier-Dowty Inc.

SPAR

Carleton University, Department of Aerospace and Mechanical Engineering

University of Toronto Institute for Aerospace Studies (UTIAS)

Full addresses of the contributors are available through the Canadian National ICAF Delegate at:

D. L. Simpson
 Director
 Structures, Materials and Propulsion Laboratory
 Institute for Aerospace Research
 National Research Council of Canada
 Montreal Road, Building M-14
 Ottawa, ON, K1A 0R6, Canada

Phone: 613-993-0899 FAX: 613-952-7136 Email: david.simpson@nrc.ca

3 FULL SCALE TESTING

3.1 Full-Scale Testing Review

The development of the technology for full-scale aircraft structural testing has been reviewed by Hewitt [1] by examining a number of tests performed at the Institute for Aerospace Research. An increased complexity is seen in all aspects of the tests over the years. The number of load conditions is more, the required fidelity of loading is higher, the demand for data is increased and the testing equipment itself is far more complex. Hewitt discusses some of the issues brought about by this increased complexity from the test engineer's perspective.

The implications of increasing the number of load conditions and spectrum length were examined and Hewitt argues that the number of load conditions used in some recent tests is excessive. The requirements for increased fidelity of loading require that more attention be paid to the matching process used to derive actuator loads. Some non-traditional ways of optimising actuator loads to give this increased loading fidelity were presented. A combination of automatic end point load verification and a strain-monitoring scheme was suggested to reduce the excessive amount of data that often seems to be requested by certification authorities and life cycle managers.

Finally, the test equipment itself is more complex and the large number of channels and their associated interactions make tuning these systems very complex. Hewitt suggests that system simulation can be used for this task and some initial developments using MatLab and state space systems were given.

3.2 CF18 - Hornet

In the last 3 years, the CF18 fleet has seen significant changes in its fatigue management and approach to lifing.

The most important changes have been a result of the International Follow-On Structural Test Project (IFOSTP). IFOSTP is a collaborative project between the Royal Australian Air Force and the Canadian Forces to perform a full-scale test on the F/A-18 aircraft. The IFOSTP project has 3 components. The centre fuselage test, coded FT55, is funded by the CF and conducted at Bombardier Defence Services in Mirabel. The wing test, coded FT245, is a collaborative effort jointly funded by the CF and the National Research Council of Canada and is being performed at Institute for Aerospace Research of the NRC in Ottawa (NRC/IAR). Finally, the empennage test, coded FT46, is performed in Australia at the Aeronautical and Maritime Research Laboratory (AMRL) under sponsorship of the RAAF. The AMRL is also performing a free standing bulkhead test.

All tests have made significant progress over the past 2 years. The NRC/IAR wing test is now mostly assembled and the loads development is nearing the end. The test is quasi-static and the loads take into consideration the dynamic effects of buffet and turbulence. Test start is scheduled for late 1999. The centre fuselage test has achieved over 12,000 simulated flying

hours of testing. The spectrum applied to the test is representative of CF and RAAF usage. A significant number of defects were found during the major inspection at ~12,000 hours leading to important fleet management decisions.

A large number of airworthy class modifications have been generated in response to the defects found on the test. These modifications must be incorporated on the fleet for it to reach its 6,000 hour life expectancy. The modifications cover a wide array of structural defects, with severity ranging from minor to flight critical. In response to some cracking in the main wing carry-through bulkheads on the test and subsequently confirmed in service, the CF have placed some high time/high damage aircraft and those with cracks in repairable reserve pending modification.

3.3 CF18 International Follow-On Structural Project (IFOSTP) Centre Fuselage Test

The application of fatigue loading to the FT55 centre fuselage test article started in May 1995. In June 1997, the two-lifetime 12,000 hour milestone was attained after 11,375 simulated flight hours (SFH) and 700 hours of flying before the aircraft was retired from the fleet. FT55 was then subjected to a comprehensive inspection program, which included the removal of the wings and landing gear.

As the two-lifetime milestone represents a certification target for secondary structure (under the Canadian Forces Lifting Policy) as well as durability critical areas exhibiting good inspectability, the 11,375 SFH inspection program was very extensive. Comprised of approximately 300 cards, the inspection program addressed 100% of the test article visually and all known critical areas through either NDI or detailed visual means, depending on the perceived level of risk. A detailed assessment of the fracture critical structure, the three wing-carry-through bulkheads, was performed in order to identify required actions and to maximise the probability that they successfully reach their certification target at 15,600 SFH (2.7 lifetimes per Canadian Forces Lifting Policy). As a result of this assessment, six preventive modifications were developed and installed on the test article at 11,375 SFH.

In some areas, it was shown that repairs can be performed after defect discovery. These areas will be managed on a safety-by-inspection basis. Additional effort was made to improve inspectability and thus mitigate risk. This improvement in inspectability was achieved by developing special inspection techniques, which in some cases included inspection cut-outs in the secondary structure covering the critical areas to improve access. Two areas of the 453 bulkhead addressed in this manner were found to be cracked with significant consequences on the test program and the fleet. For these two locations, a special inspection program was activated, leading to the discovery of cracks in the majority of the Canadian fleet. The cracks are developing in flanges, parallel with the main load path of the bulkhead through a warping effect in a high curvature area, aggravated by discontinuities in both the mating crease longeron and the mold line skin which is spliced over these areas. In total, 25 areas of the centre fuselage specimen were either repaired or modified during the 11,375 SFH downtime. As a result, a large portion of the instrumentation, approximately 60% of the available 500 strain gauge channels was reassigned to evaluate repairs and known or potential defects.

The test resumed in January 1999. Three areas were left with defects in order to evaluate their damage tolerance characteristics and their potential for life management by inspection. One of these was the inner wing front spar at hole 172 just inboard of the leading edge flap transmission attachment lugs, exceptionally considered as a representative test area although outside of the test section. The first cracking was found in the left hand wing at ~7800 hours. The wing was replaced and the initial wing torn down. Significant cracking was found in a number of other holes in the spar near the leading edge flap transmission. At 11,375 SFH, cracking was discovered on the right hand wing at hole 172. A one-inch crack across a hole in the lower flange was detected with a boroscope. Approximately 400 SFH later, the crack was detected in the web of the spar and successfully stop drilled (and cold worked) in order to allow the test article to reach the next scheduled inspection at 12,350 SFH in March 1999. At the downtime, a more detailed non-destructive inspection of the front spar in the leading edge transition area revealed 6 additional cracked fastener holes. A decision was made by DND to replace this inner wing with a spare wing to complete the test. A program is underway to determine the type and extent of the modifications required in this area. These modifications will likely be installed, at a later date after some testing, on the CF18 IFOSTP wing test scheduled to start at the NRC at the end of 1999.

FT55 is scheduled for another major downtime at 13,325 SFH in October 1999, similar in scope to the 11,375 SFH downtime. The achievement of the 15,600 target is scheduled for mid-2001.

3.4 CF18 IFOSTP Wing Test – Loads Derivation

Early in 1997, an investigation, aimed at quantifying the impact of buffet loads at critical locations of the wing structure (wing root, wing fold and trailing edge surface actuators), was completed. A methodology was developed for predicting strain sequences, with or without dynamic activity, from a time trace of aircraft flight parameters representing actual flying. The methodology is based on the use of strain data recorded at high frequency during RAAF and United States Navy (USN) flight tests.

In support to the IFOSTP wing test, the RAAF Aircraft Research and Development Unit (ARDU) flight test agency completed a critical flight test program (ARDU Task 0166) in December 1997. This program gathered data for manoeuvre and dynamic loads generation as well as for interpretation of the full-scale test results. It is important to note that before the collected flight test data was used for loads derivation purposes, extensive efforts were put into the verification of data integrity. This covered identification of corrupted or bad segments of flight parameters, loads and strains and correction of spikes in the recorded data

As previously reported, the basis of the test spectrum for the wing test is an approximate 300 hour block of MSDRS data with representative statistics in terms of mission split and important aircraft parameters [2]. Strain sequences were developed for control points from this data block but do not include a full representation of the higher cycle buffet loads due to the MSDRS sampling frequencies. Using this data block and the resultant strain sequences as a basis, procedures were developed for inserting the higher frequency dynamic strain sequences at appropriate points in the spectrum based on aircraft parameters, primarily, angle of attack and dynamic pressure. This allowed the generation of representative full block strain sequences with

and without dynamic activity for selected locations on the wing (wing root, wing fold and trailing edge surfaces actuator).

Through analytical predictions and coupon testing, it was shown, for these sequences, that a significant portion (25% - 80%) of fatigue damage at the selected wing control point locations comes from buffet loading. These findings warranted that a method be developed to account for buffet damage in the IFOSTP wing full-scale fatigue test.

A robust process for the prediction of manoeuvre and dynamic loads at a set of wing control points to use for truncation studies was developed and thoroughly validated. The process is made up of three main blocks: (1) enhancement of the MSDRS data which is used as input to the loads calculation for the flight spectrum; (2) calculation of manoeuvre loads; and (3) calculation of dynamic loads originating from buffet and turbulence. This process is illustrated in Figure 1.

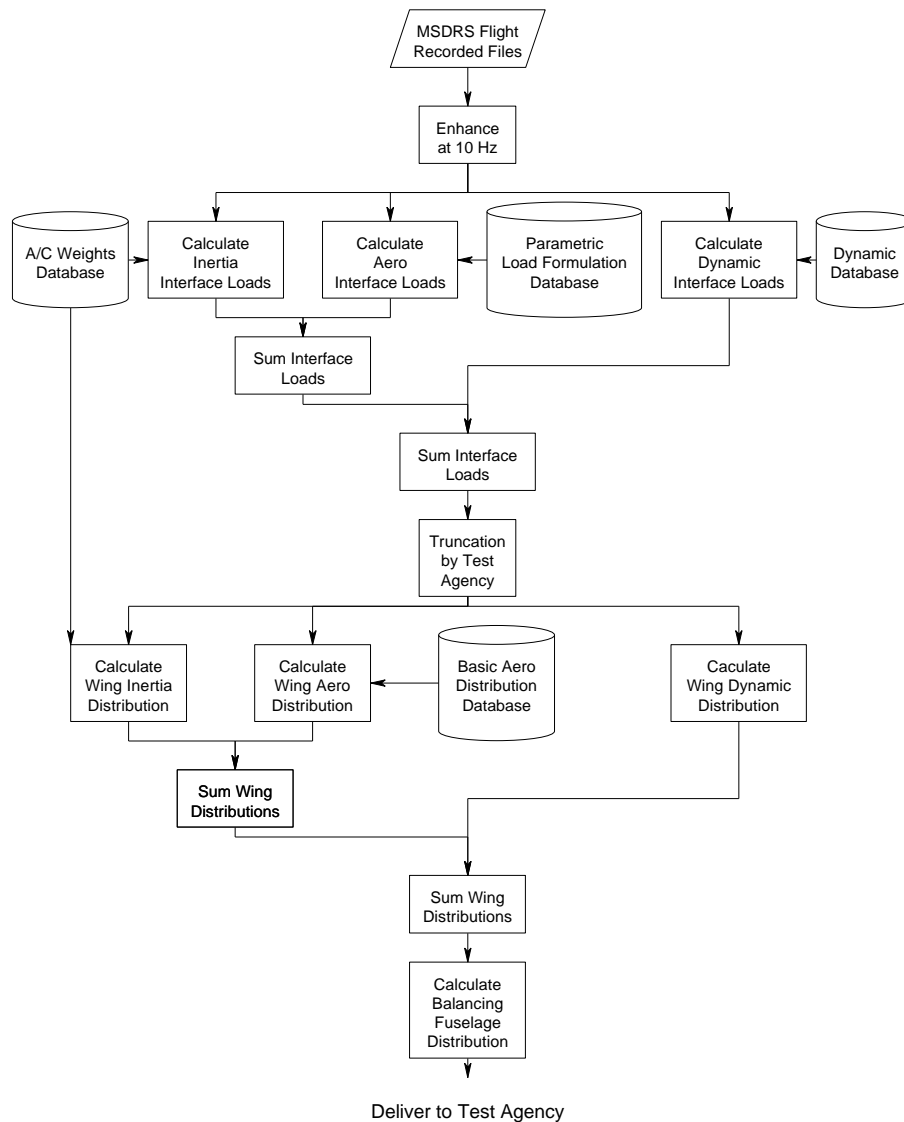


Figure 1: CF18 IFOSTP Wing Loads Calculation Process

The available parameters and sampling rate of the MSDRS data used as input for the loads calculation are inadequate for accurate prediction of loads for the IFOSTP wing test. Therefore, some of the MSDRS flight parameters were enhanced by simple splining and interpolation. Additional parameters such as rotational accelerations and dynamic pressure are calculated from the available data, and control surface deflections are approximated from a simplified set of the aircraft control laws.

Manoeuvre loads at each of the wing control points are calculated using a parametric technique. The inertial component of the manoeuvre loads is obtained by using simple kinematics equations relating aircraft translational and rotational speeds (rates) and accelerations to the aircraft mass properties breakdown. The aerodynamic component is calculated through a set of parametric equations relating the aerodynamic component of the loads to basic aircraft flight parameters. The latter parametric equations for the aerodynamic component of the manoeuvre loads were derived from extensive statistical analysis of the data collected in the RAAF ARDU flight test programs. The parametric equations derived enable accurate predictions of loads for the various configurations of wing stores being part of the basic flight spectrum.

For the prediction of dynamic loads at the wing control points, a method was developed to allow prediction of dynamic loads originating from buffet or turbulence flight regimes by using as input the time trace of the aircraft Angle Of Attack (AOA) and dynamic pressure (Q). This method was the result of an extensive investigation done into characterising the dynamic response of the wing as a function of aircraft flight parameters. It basically consists of collating the dynamic loads measured from flight test into an array of AOA / Q bins. This array then becomes the reference data from which dynamic loads can be predicted by using as input the AOA / Q time trace(s) for the manoeuvre(s) of interest.

Figure 2 illustrates the results of the validation for the dynamic load reconstruction methodology for one of the wing control points.

In December 1998, after a thorough validation exercise of comparing calculated loads to in-flight measured loads for a series of Air Combat Manoeuvres and Ground Attack missions, a major milestone of the loads derivation effort was met by the generation of a series of 24 load sequences to be used for truncation of the flight spectrum before the major effort of calculating fully balanced loads distributions. For each wing, 10 Hz manoeuvre-only load sequences at four locations and 483 Hz manoeuvre + dynamic load sequences at eight other locations were calculated for the 326 flight hours of the baseline IARPO3a Canadian spectrum. The same was also done for the baseline Australian spectrum APO2b (294 spectrum flight hours) in order to confirm the representations of the test spectrum for both countries.

The other major accomplishments in terms of developing engineering tools for external loads derivation were:

- the development of a general method for determining load distributions that can be used in a quasi-static full-scale fatigue test to simulate the dynamic effects of buffet and turbulence;
- the preparation of a database of basic CF18 aerodynamic distributions that will be used for calculation of manoeuvre loads distributions;

- the development of an optimiser routine that modifies appropriate basic aerodynamic distributions from the database to match a set of interface loads' constraints within a prescribed tolerance. This is used to predict the aerodynamic component of external loads distributions acting on the wing during manoeuvring.

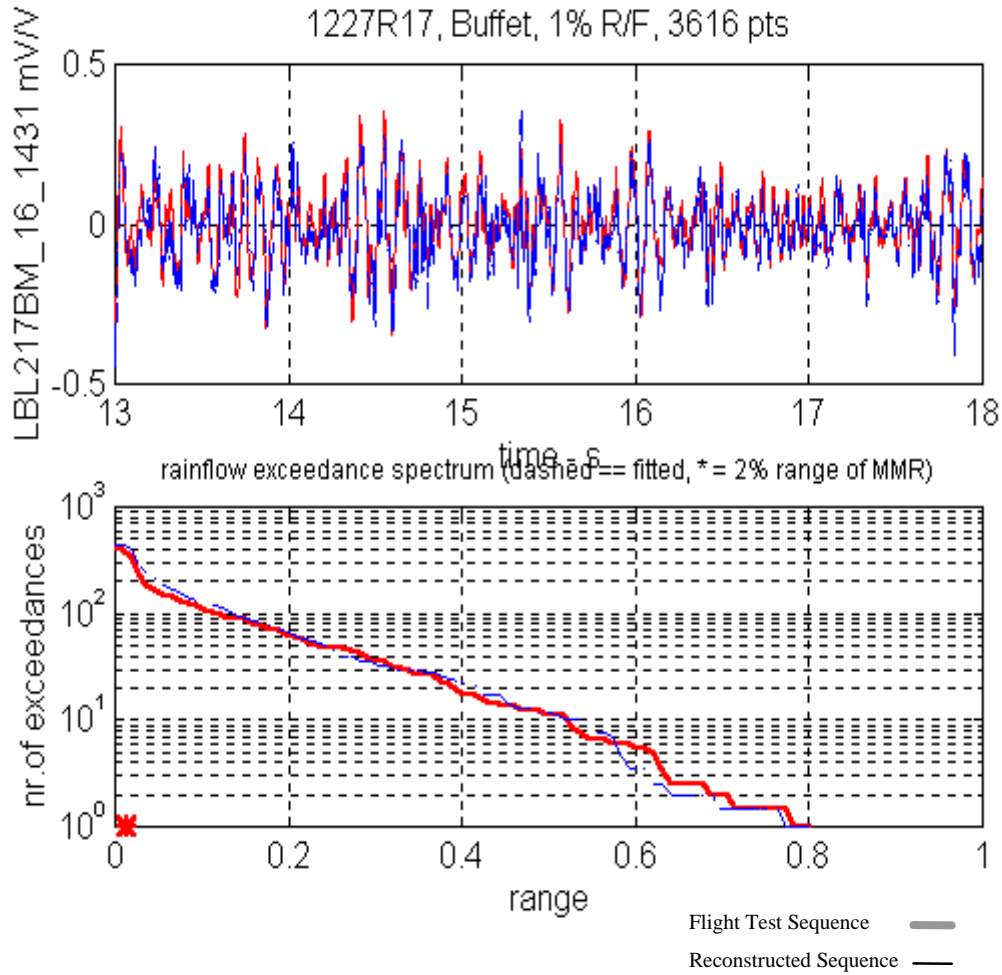


Figure 2: CF18 IFOSTP Validation of the Wing Dynamic Load Reconstruction Methodology for the Wing Tip Moment Measurand.

The method developed for determining load distributions to simulate the dynamic effects of buffet and turbulence is essentially the derivation of load distributions tailored to match measured dynamic loads. The goal of this approach is to define finely-gridded external force distributions for each time-step of the buffet (or turbulence) time-history. To assure that these distributions relate to the measured buffet (or turbulence) loads, the methodology actually uses the flight test measured loads to establish the distributions' shape and magnitude. The measured buffet (or turbulence) loads are used as constraints to the load distributions to be derived and are therefore termed "Control Point Loads". The external force distributions are derived through the use of an optimisation technique that is based on a multi-parameter regression. With fine gridding of external forces and generally only a few points in the structure where buffet (or turbulence) loads are measured, only an under-determined system of equations can be defined. This system was

expanded such that it could be solved numerically and also to ensure that the solution is sensible and acceptable for application to the full scale fatigue test.

Using Wind Tunnel Test (WTT) results as reference data, a database of basic aerodynamic distributions was developed giving a set of 76 differential pressure values over the wing platform for various points in the Mach/AOA envelope. This was done for the three main under-wing store configurations included in the baseline flight spectrum. Also, as the WTT data was limited in certain areas of the Mach/AOA envelope, interpolation /extrapolation techniques were developed for predicting a suitable distribution that the aforementioned optimiser can then use as a starting point for external loads distributions prediction at any point in the Mach/AOA envelope.

By August 1999, the development of the load distributions calculation process will be completed and fully balanced external loads distributions will be derived for the set of residual load lines after truncation, filtering and binning of the nominal interface loads sequences as discussed above. The derived external loads distributions will be, for the wing test article, manoeuvre loads distributions and loads distributions simulating the dynamic effects of buffet and turbulence and these will be supplemented with the necessary loads distributions required to ensure appropriate loading and balance of the reaction stub wing and fuselage.

3.5 FT 245 Wing Test Configuration

The general philosophy in designing the test arrangement for the FT245 Wing Test was that wherever loads are introduced into the test specimen itself, other than through loading pads, they must be via actual F/A-18 transition structure. This was to ensure that loads are introduced in a representative manner. The test article itself is a right hand inner and outer wing box. However, to ensure correct loading, the wing is mounted on a representative fuselage and has representative flaps, ailerons and pylon attachments. A left-hand inner wing is used to react the right hand wing loads.

The fuselage is restrained in the vertical direction at the nose gear landing strut and at both horizontal tail spindles. Fore and aft restraint is provided through an attachment to the arresting hook attachment. Lateral restraint is achieved through attachments to the forward fuselage and the vertical stabiliser attachment fitting. A series of 10 actuators are used to provide a representative longitudinal bending moment distribution in the fuselage, particularly in the area of the wing lug attachments, in order both to ensure representative loading in the wing attachments and to minimise premature failure of the transition fuselage.

The left-hand stub wing is loaded by 6 actuators via 3 contour boards located at the inboard and outboard pylon stations and the wing fold. A further 47 actuators are used to load the inner and outer right hand test wing and the control surfaces and stores for a total of 63 actuators. A schematic of the test arrangement is shown in Figure 3 and a photograph of the test in its present state of assembly is shown in Figure 4.

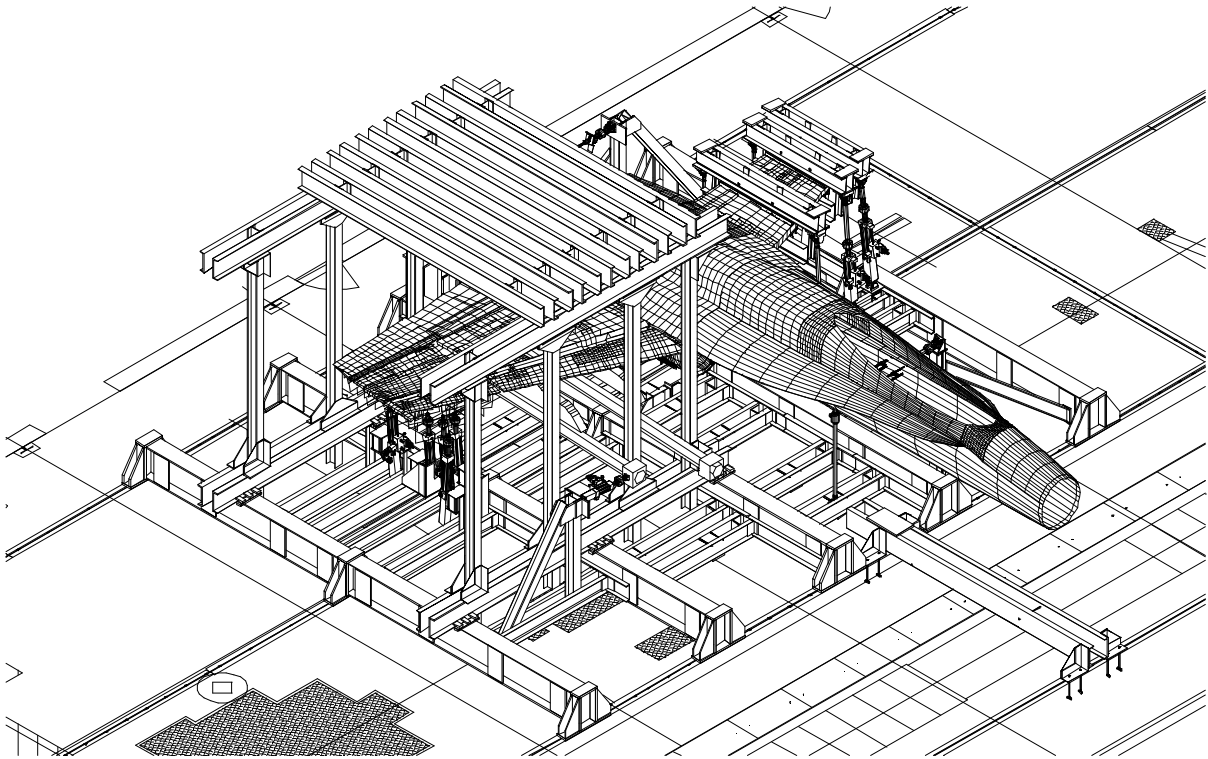


Figure 3. Schematic of F/A-18 Full Scale Wing Fatigue Test

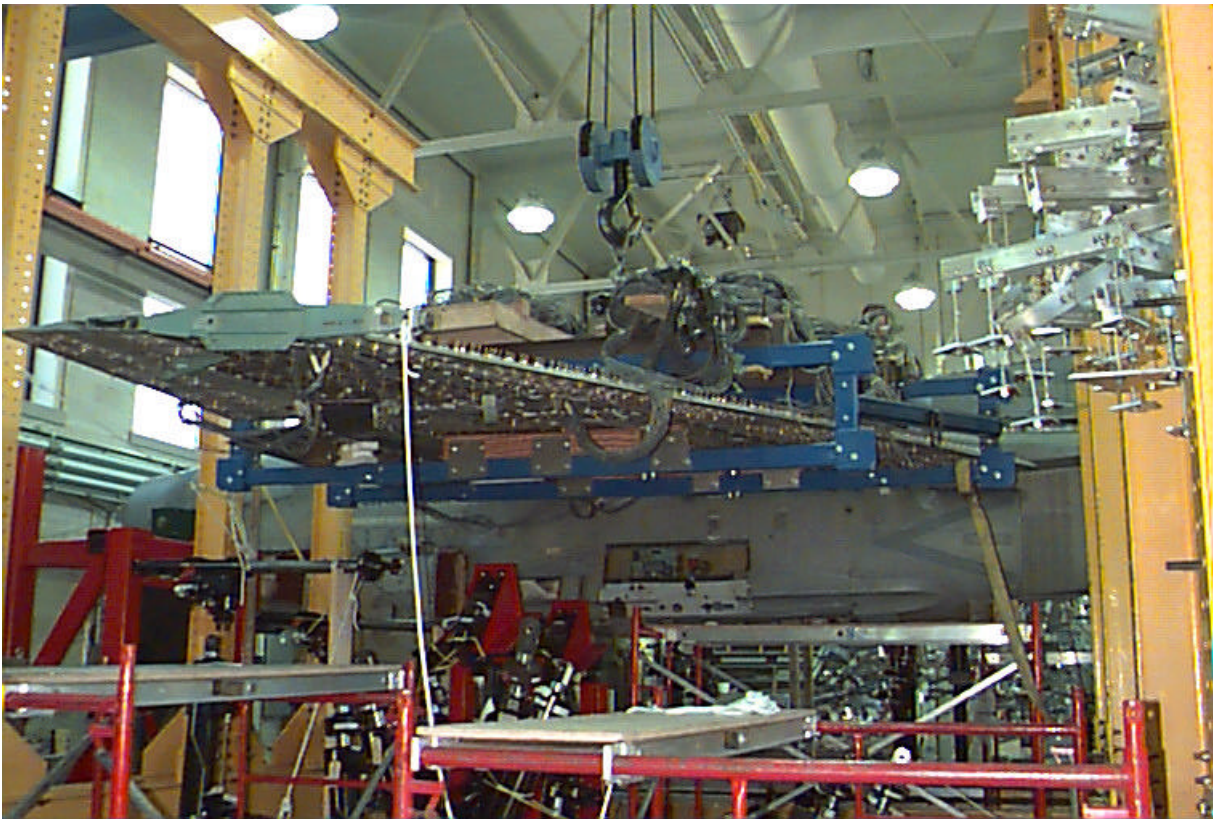


Figure 4 FT245 test wing being installed in the test rig.



Figure 5. Example of Thin Disc Loading Pads

Attachments to the wing and control surfaces are via thin aluminium disks that are bonded directly to the surface with either an acrylic or epoxy adhesive, depending upon the substrate. This design is being used to both reduce fixturing weight over that of the more typical neoprene pads and to ensure local stiffness is not introduced into the specimen. Several of these pads are shown in Figure 5 on the aileron.

Test loads will be controlled by an MTS Aero-90™ system. This consists of digital servo-controllers and a Windows-based operator interface. The system includes continual end point checking so that the operator will know if any end points are outside of a defined error limit. Data from 512 strain gauges will be recorded and monitored via a high level multiplexed system, while an additional 60 strain gauges and 6 displacements will be recorded on a high speed system integral with the controllers. The data acquisition and control systems are fully integrated and allow sophisticated on-line trend monitoring.

3.6 FT 245 Actuator Loads Calculations

Loads matching in previous wing tests has typically been accomplished by matching shear, moment and torque at a number of stations along the wing. This works well as long as there are only two actuators in the chordwise direction. Active control technology and digital flight control systems with varying control laws create a situation whereby a large number of load conditions need to be matched at a higher fidelity. The impact of this is that more actuators are required in the chordwise direction. This configuration creates a situation where torque matching can be achieved by many combinations of actuator loads which means that unrepresentative loading can arise and still meet balance criteria. Another approach is necessary.

The shear, moment and torque diagrams are usually derived from the integration of aerodynamic and inertia panel loads. It therefore makes more sense to try to match these panel loads rather than quantities derived from them that contain less information. If the panel loads are matched, the test engineer can be confident that representative loading is being applied. This technique has been used on the FT 245 wing test. Figure 6 shows an input panel load distribution for the complete right hand wing and Figure 7 shows the results of the two optimising techniques in terms of spanwise shear, bending and torque. The Optload results were obtained using traditional linear programming to optimise the shear, moment and torque on the control surfaces

and wing box separately. This had to be done because there were too many actuators in the chordwise direction for a sensible solution. The full wing results were obtained from one optimisation of the panel loads for the complete wing. The results are not significantly different.

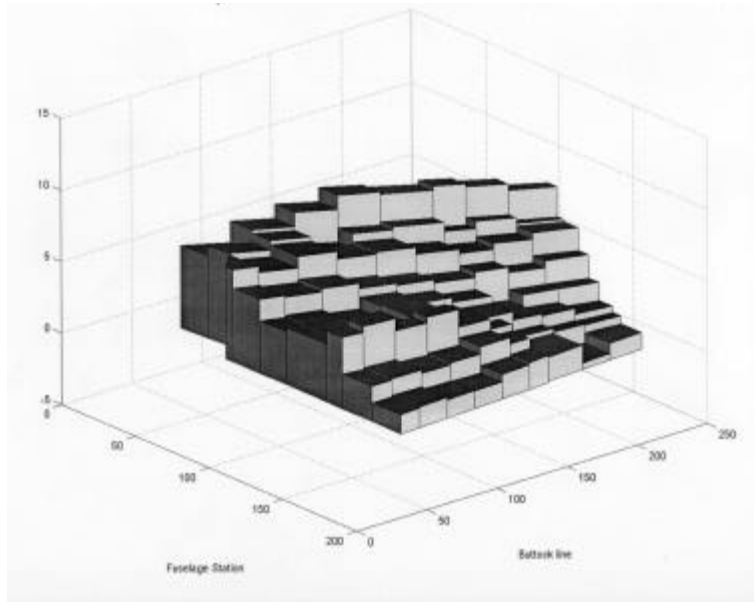


Figure 6. Input Panel Load Distribution

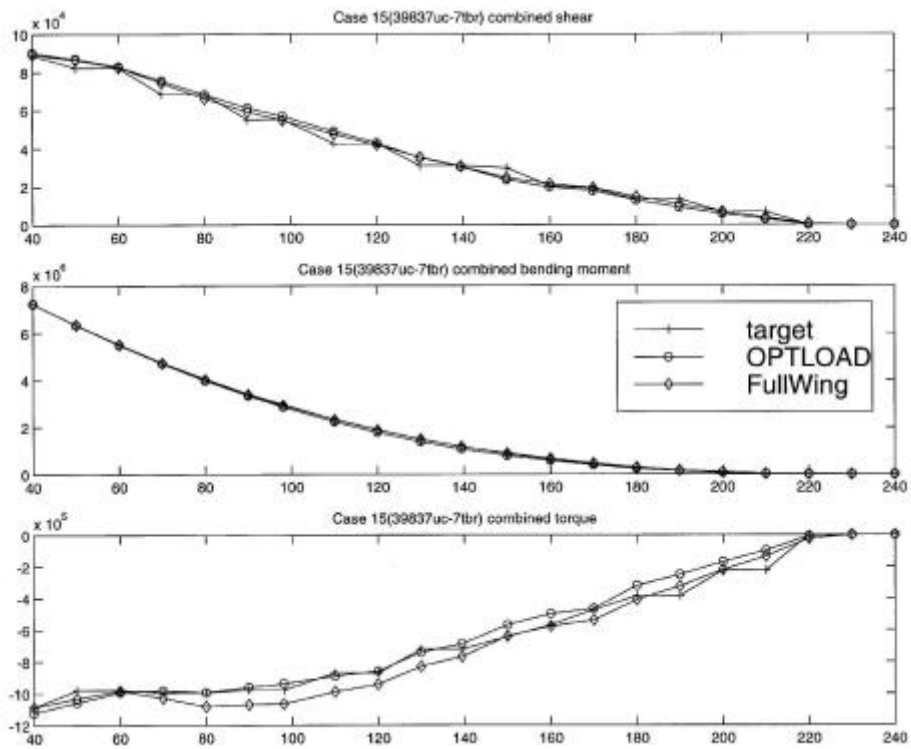


Figure 7. Comparison of Spanwise Loads Matching using Different Methods

However, if the output panel loads for the two cases, as shown in Figure 8, are compared with the input loads it is clear that the optimisation using panel loads gives much more representative loading.

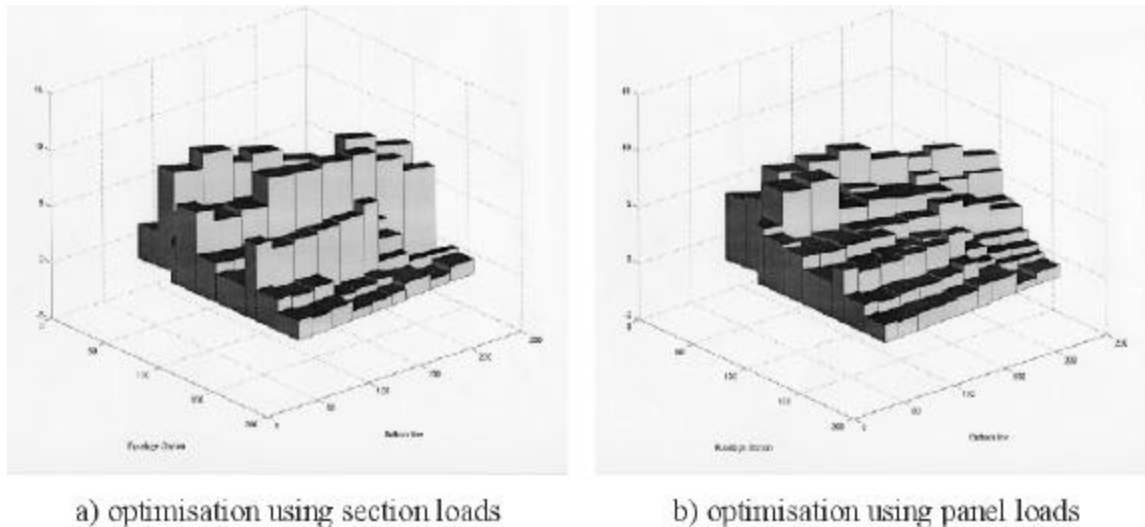


Figure 8. Comparison of Output Panel Load Distributions

It should be noted that the distribution of b) is not a final distribution but one obtained during the development of the optimisation process.

3.7 Maritime Patrol Aircraft CP-140 Orion

The Canadian Forces (CF) acquired their CP-140 fleet (Canadian designation for the P-3C) in 1981 with an intended 20-year service life. The estimated life expectancy of the aircraft has since been extended to 2010, with considerations being given to push it past 2015. In 1998, individual CP-140 aircraft have reached, and then exceeded, the 100% Fatigue Life Index (FLI) milestone. At the current utilisation rate, the fleet average will stand at 100% in early to mid-year 2000. Support engineering activities in recent years have therefore focused on the continued structural airworthiness of the aircraft past its safe life limit.

During the procurement phase of the CP-140, the CF commissioned Lockheed to assess the aircraft compliance to the MIL-A-83444 Standard and to provide the tools necessary to manage the fleet using Damage Tolerance principles. The original Lockheed maintenance program has since been amended to better suit the CF maintenance policies and to maximise the useful life of the airframe. Some of these activities include:

- a. The increase of inspection intervals through the implementation of NDI techniques and through the use of a crack growth based Individual Aircraft Tracking (IAT) program developed by Lockheed. As a result of these efforts, fatigue critical locations are now inspected on a five-year cycle corresponding to the Third Line Inspection and Repair (TLIR);

- b. Continued efforts towards the eventual transition of the parametric, paper form based IAT system to an automated Loads Monitoring system. The 18 CP-140 and 3 CP-140A in service with the CF have already been fitted with the SEI Structural Data Recorder Sets that record a number of flight and structural parameters; and
- c. Participation in the USN P-3C Service Life Assessment Program as a Foreign Military Sales customer. This effort consists of a full-scale fatigue test that will assess the safe life potential of a P-3C aircraft partially refurbished under the USN Sustained Readiness Program. The CF are contributing to the loads validation portion of the program by building a powered P-3C model that will be tested in the NRC/IAR high speed and low speed wind tunnels. In addition, the CF and the RAAF plan to fund extended testing of the SLAP test article so that sufficient data is generated to allow certification of the basic structure.

In parallel to the fatigue management effort, the CF have devoted considerable effort to evaluate the structural condition of its fleet from a corrosion perspective and assess the requirement for a major refurbishment program that would be needed to achieve a 2015+ retirement date. Several years ago, the CF conducted a Reliability Centred Maintenance Analysis study for the CP-140 that identified a number of potential structurally significant areas that were not covered by the current maintenance plans. The CF initiated a sampling inspection program in 1998 that addresses these locations. Under this program, detailed visual inspections will concentrate on the centre wing area, internal surfaces of fuselage skins, frames and cut-outs as well as the internal surfaces of the forward and aft pressure bulkheads. In addition, NDI mapping techniques will be used to assess the condition of wing, fuselage and empennage lap joints.

3.8 The Bombardier Global Express Certification

The Bombardier Global Express, Figure 9, the first aircraft in its category resulting from a new "clean sheet" design, received certification from Transport Canada in July 1998. The Transport Canada type certificate for the Global Express meets Airworthiness Manual Chapter 525, Change 6.

The United States Federal Aviation Administration (FAA) awarded type approval for the ultra long-range business jet on Nov. 13, 1998, certifying the aircraft to higher FAA standards than any other jet. It is the only aircraft in its class to meet the latest FAA standards, including FAR Parts 25, up to Amendments 25-97. The decision cleared the way for Bombardier to begin delivering the first group of Global Express aircraft to operators world-wide. The aircraft obtained type approval from the European Joint Aviation Authorities (JAA) on May 12th, 1999.

Bombardier Aerospace Regional Aircraft (BARA) - deHavilland was responsible for the design, analysis and manufacture of the rear fuselage and vertical stabiliser, as well as assembly of the complete aircraft. Although the damage tolerance evaluation was primarily analytical, a number of component fatigue tests are being carried out to supplement the analysis. For the pressure shell portion of the structure, special high altitude compliance requirements were met, which necessitated certification to two residual strength criteria; the customary one based on fracture strength plus a second based on permitted crack opening area.



Figure 9. Bombardier Global Express

3.9 DHC-8-400 (Dash 8) Certification

The new DHC-8-400 is the largest, heaviest and fastest version of the Dash 8 series. Although the structural concepts, and to a large extent many of the structural details, have not changed from earlier versions, this aircraft is being treated as a new design for certification purposes. Like previous DHC-8 versions, the entire structure is being certified as damage tolerant, with the exception of the landing gear and their immediate support structure, which is classified as safe-life. A total of 254 Primary Structural Elements (PSEs) is being evaluated by a combination of analysis and testing to define a fatigue crack inspection program for the entire primary structure. Inspection intervals for both visual inspection and NDI are being determined for all PSEs where a choice of inspection methods may be advantageous to operators. A fatigue test, Figure 9, of the complete aircraft to 2 design lifetimes is being carried out using the following 4 major components:

- 1) wing/nacelles/fuselage/vertical stabiliser
- 2) horizontal stabiliser
- 3) nacelle
- 4) inner and outer flaps.

This test program of major components is being supplemented by a further 14 fatigue tests of smaller components for which analytical damage tolerance substantiation alone is not considered to be adequate.

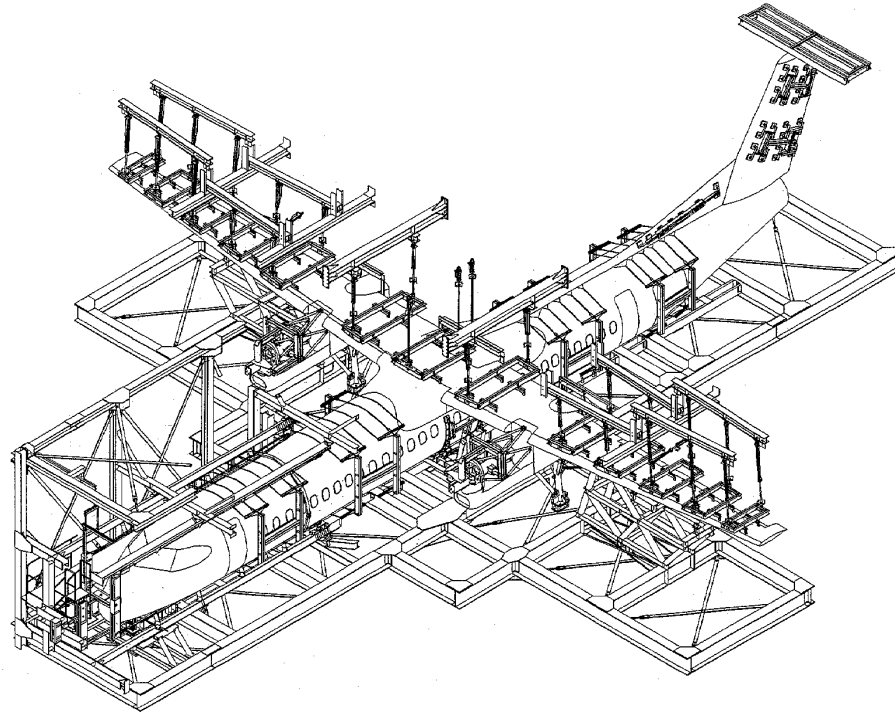


Figure 10. Dash 8-400 Test Rig

3.10 Landing Gear Programs

3.10.1 Messier-Dowty Inc.

The F/A18 E/F nose landing gear qualification program conducted at Messier-Dowty Inc (Montreal) included the following test lab activities:

- Free Extension testing of the nose landing gear, retraction actuator, steering manifold retraction and endurance
- Feature testing of the launch bar assembly and
- Drop testing of the nose landing gear.

Deliveries of the F/A18 E/F gear started in October 1998. In 1999 the program continued with re-testing of the retraction endurance for drag brace design modifications to reduce hydraulic leakage, retraction actuator design modification to reduce wear on piston head (introduced a HVOF coating for the purpose), and steer manifold design modification to improve durability.

Similar activities were conducted on the Bombardier Global Express landing gear systems and were completed in 1998. Fatigue test program and strength test programs were conducted on the

main landing gear struts (Figure 11). Cyclic testing to demonstrate retraction endurance of the Global Express main landing gear struts was recently completed.

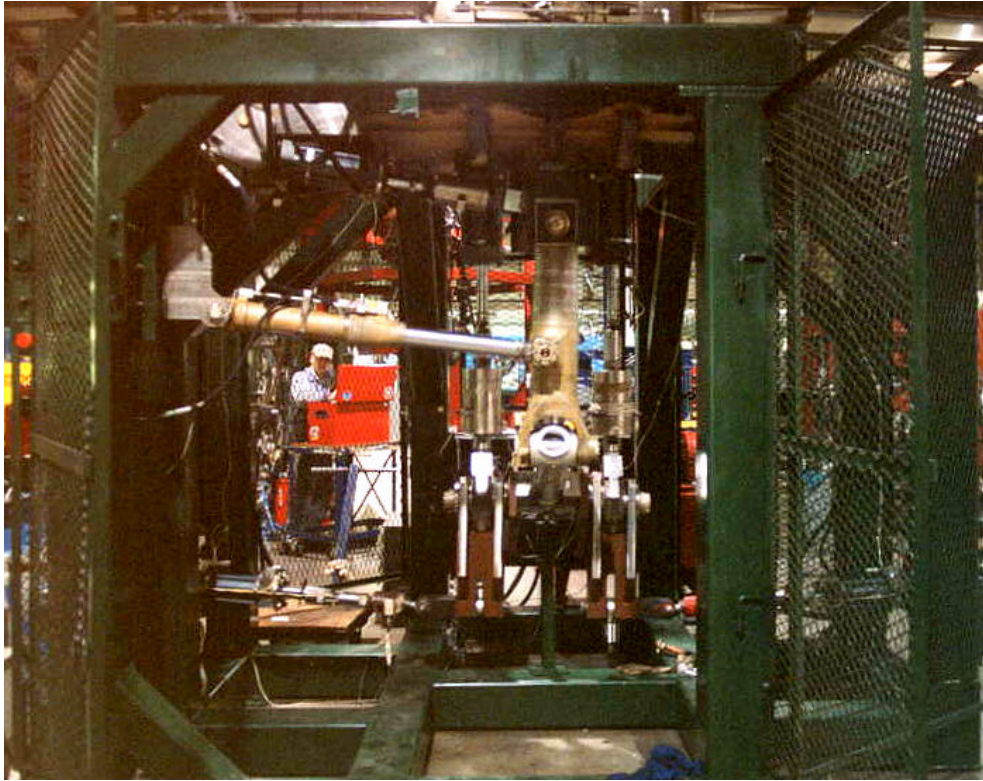


Figure 11. Global Express Main Landing Gear Fatigue Test Rig

The in-service Bombardier DHC-8 (Dash 8) nose landing gear was re-tested and strain gauge surveys of the fatigue test article were performed to evaluate reported problems. The source problems did not correlate with the results from earlier qualification testing. Single engine taxiing at airports was identified as causing limited lives on some NLG components and the new test program addressed this issue.

The V-22 main landing gear fatigue test program has continued. Recently, investigations on the drag brace were added to the program. Under the V-22 light-weight landing gear program, strength testing of a titanium matrix drag brace was successfully performed. Currently, fatigue and endurance tests on the drag brace are in progress.

Other programs at Messier-Dowty Inc. are in progress. In 1998, the rig design of the Hawk 4000 and BA 609 landing gear systems were completed. Drop testing of the Hawk 4000 MLG and BA 609 MLG and NLG assemblies have been completed. Strength and fatigue testing is planned for the latter part of 1999. The DO 328 Main Landing Gear Drop Test Program is in progress. Investigations and fatigue testing of the A340 Centre Landing Gear are continuing. A fatigue test program of a re-designed cylinder and a free extension test program are ongoing.

3.10.2 Menasco Aerospace

The Menasco Aerospace Test and Development Laboratory does structural and performance testing of landing gear and flight controls. Fatigue testing is currently in progress on the F-22 Raptor Main and Nose Landing Gears, the V-22 Osprey Tilt-rotor helicopter Nose Landing Gear, the Bombardier Dash-8 Series 400 Main and Nose Landing Gears, and the Bombardier CRJ-700 700 Main and Nose Landing Gears. Past programs have included C-17 and Fokker-100 landing gear fatigue tests.

A typical test involves four lives of fatigue loading, with up to 70,000 flights per life. The duration of such a test is measured in years, so it becomes critical to optimise test speed, and enhance reliability to keep the test running around the clock. Further, the use of closed-loop computer-controlled load systems capable of managing very large numbers of load cases is needed to support the increasingly refined, flight-by-flight fatigue spectra.

Menasco uses Kelsey K-7000 and Cyber control systems to control loads applied via servo-controlled hydraulic actuators, with load cell feedback. Testing is performed in modular structural test rigs with custom interface structures and custom dummy wheels. The dummy wheels are installed on the landing gear axles using aircraft wheel bearings; they incorporate load application points to pass fatigue loads into the test article in a way that simulates actual service loading. A typical test requires side, drag and vertical loads on each axle, applied at two different landing gear piston strokes (one representative of landing cases, one for ground handling cases.) The vertical loads are reacted by filling the shock strut with hydraulic fluid such that its air-spring characteristics are removed. Piston stroke changes are effected by opening a hydraulic line to the shock strut, and allowing fluid in or out of the gear while the vertical loading systems move the piston to the new stroke in closed-loop position control. A stroke change is accompanied by a corresponding change in the side and drag actuators, whose alignment along aircraft axes must be maintained. For this, the actuators are mounted on sliding assemblies, and move to the new piston stroke position by actuators and directional valves, or screw-jacks operating in closed-loop position control.

Menasco employs three tiers of safety systems to protect the specimen: (1) low-level mechanical systems to prevent accidental overload in the event of a control system failure including load actuators sized with minimum overload margin, relief valves on actuator ports to limit maximum load, and micro-switches to detect gear deflection outside of the expected envelope; (2) control system software limits to detect excessive following error, load cell readings out of range, and other, measurement-based limit conditions; and (3) an independent loads monitoring system to check each load endpoint against the target load.

In some fatigue tests, loading rates are maximised by using scaled load ramp times proportional to the change in load between two targets such that a longer time is used to ramp from one load to a very different load, while short ramp times are used to for smaller magnitude changes. Further, the Kelsey control systems incorporate a system which continually tries to run the test faster and faster, until a pre-set following error limit is tripped, at which time the speed is knocked down and immediately begins creeping up again. The load rate is dependent on the response and tuning of the control system, as well as the stiffness of the test article in the

direction of applied load. Load rates of 10,000 lb/s (44.5kN/s) are not uncommon with a well-tuned system. Load ramps are typically of a half-sine shape, so that the rate of change is at a maximum midway through the ramp, and zero at the endpoints. This increases control accuracy at the endpoints where it is needed. The control systems use integral as well as proportional gain settings to further improve load fidelity at endpoints. Fatigue tests run continuously and unattended other than periodic lubrication, maintenance and inspection.

4 LOADS MONITORING AND MEASUREMENT ACTIVITIES

4.1 Operational Loads Monitoring - Body of Knowledge

As part of an internal program review conducted by the Canadian Forces, Martec Limited has been contracted to prepare a technical document presenting a synopsis of the current Operational Loads Monitoring (OLM) body of knowledge. The objectives of this documents were; to provide the reader with a sound knowledge of the OLM concepts; to detail the project management activities that are necessary for the implementation of a cost effective and efficient OLM program; to discuss key issues and lessons learned that have emerged from past OLM programs; and to provide information handling strategies that are capable of offering cost-effective solutions to the challenges of managing large quantities of data. This document is intended for the structural integrity specialists and the aircraft fleet managers who lack the engineering experience or background technical knowledge of the OLM processes. It has been structured to emphasise the information generation nature of OLM as opposed to the more traditional hardware/software system engineering approach so characteristic of OLM procurement projects. OLM technical concepts are discussed and a typical OLM data processing flow and system architecture are presented. A project management framework for the efficient conduct of OLM activities has been proposed. This framework considers the OLM project as an information handling process and provides focus on the key activities that will ensure successful OLM projects. Lessons learnt from previous projects are also discussed. Technical issues to ensure reliable fatigue damage assessment and an efficient fatigue damage data processing flow have been discussed. Finally new strategies for future programs or improvement of current programs are proposed.

4.2 CT114 - Tutor

As a result of in-service failures, the CT114 Tutor jet trainer was the subject of two separate full-scale fatigue tests conducted by the National Research Council of Canada. The wing was tested in the early 1970's and the aft fuselage and empennage were tested in the mid-1980's. Early fatigue monitoring of the aircraft was based primarily on partial fleet fitting of recording accelerometers recording data at the aircraft nominal centre of gravity. Analysis of various flight load surveys conducted by the Canadian Forces demonstrated the requirement for more detailed data in order to properly manage training fleet resources and to monitor the intense Snowbird and Fighter Lead-In Trainer (FLIT) roles. As reported in previous ICAF reviews, a decision was made in 1992 to equip the CT114 Tutor aircraft fleet with an Operational Loads Monitoring (OLM) system to provide this data. The installation phase of the CT114 OLM project was completed in 1998. A total of 50 Tutor aircraft, including nine Snowbird aircraft, were instrumented with an eight-channel Moog/Esprit Elaps IIC located in the avionics compartment

in the nose of the aircraft. Four flight parameters: altitude, airspeed, N_z and Roll rate plus strain at four critical locations in the empennage and tail are recorded.

The incorporation of OLM into regular fleet operations has been performed smoothly, even though integration problems have at times, impaired system serviceability. In-service data is transferred directly to the ASIP contractor at Bombardier Aerospace, Defence Services where data management software was developed on a PC platform to perform data validation, reconciliation with supplementary mission data, data storage and analysis. The General Integrated Fatigue Tracking System (GIFTS) software also generates fatigue tracking reports on major individual components, individual aircraft, individual squadrons and the overall fleet. It also allows the investigation of the severity of specific missions or roles.

The OLM data is used primarily to determine the fatigue accumulation in the wing and the empennage and to permit the assessment of the damage rates accumulated by the Snowbird and FLIT roles. As a result of reduction of the 1996 and 1997 Snowbird OLM data, a serious discrepancy was found between the loading assumptions made for the full-scale tests and the actual usage in the Snowbird solo role. The OLM data was instrumental in identifying manoeuvres still being flown that had been prohibited after an earlier accident. These manoeuvres have a serious negative impact on the CT114 fatigue accumulation. The actions taken as a result of this data reduction effort resulted in the replacement of three tail assemblies and the prohibition of certain manoeuvres from the Snowbird repertoire.

The life-cycle management approach to the CT114 fleet is currently in transition from a safe-life concept to safety-by-inspection approach. To support this new approach, a coupon test program has been initiated in order to validate the inspection intervals of six critical locations in the wing/fuselage fitting area (see section 5.5). The results of the CT114 coupon test will be available by the end of 1999 and should provide justification to retain the Tutors in the Snowbird role for at least 10 more years without major structural repairs.

4.3 CT133 Silverstar Operational Loads Monitoring Program

The CT133 (T-33) aircraft is currently the aircraft with the longest service in the Canadian Forces inventory, having commenced operations in the RCAF in the early 1950's. The Canadian Forces intend to operate a fleet of approximately 25 CT133 Silverstars well into the next century in roles ranging from electronic warfare to CF18 training support, including target towing for Navy gunnery practice. Retirement of the CF116 Freedom Fighter (CF-5) required the venerable T-33 to take on additional roles formerly performed by higher performance aircraft. In order to assess the impact of the new roles and the carriage of even heavier external pods on the fatigue posture of the CT133 fleet, a Loads Environment Spectral Survey was undertaken in 1992. The results of that effort demonstrated the requirement for detailed monitoring and assessment of the fatigue life of the CT133.

The fleet is currently being instrumented with an OLM system through its Depot Level Inspection and Repair program at Kelowna Flightcraft, British Columbia. All 25 DLIR aircraft, corresponding to the future fleet establishment, will receive an OLM installation. A total of 19 aircraft have now been completed and are back in service.

The OLM instrumentation consists of an accelerometer and a rate sensor at the aircraft C of G to capture normal acceleration and roll rate, as well as a pressure transducer to collect airspeed and altitude information directly from the pilot static system. Two aircraft have also received four strain gauges with backups, located in the wing and the aft fuselage longeron, to complement the Loads Environment Spectrum Survey (LESS). The recorder is a Moog/Esprit ELAPS IIC located in the avionics compartment in the nose of the aircraft.

Results of the LESS conducted between 1993-96 demonstrated severe in-service usage which invalidated the safe life management approach, mostly due to the impossibility of calculating accumulated fatigue damage from past usage. A new safety-by-inspection approach is currently under development. It will tailor the inspection intervals of the most critical structural areas using an in-service usage spectrum and results of a damage tolerance coupon test program. The usage spectrum will be developed from transfer functions between flight parameters and stress at critical points of the wing and the aft fuselage, using strain data from the OLM instrumented aircraft and an upcoming flight test calibration program at AETE.

The incorporation of OLM within regular fleet operations is being performed. A number of integration problems have at times impaired system serviceability. The impact of having to generate good data returns from four dispersed squadrons has affected the program. It is currently very difficult to efficiently control the quality and consistency of both the OLM and supplementary mission data. Technical and managerial solutions are being investigated. In-service data is transferred directly to the ASIP contractor at Bombardier Aerospace, Defence Services where a data management software was developed on a PC platform to perform data validation, reconciliation with supplementary mission data, data storage and analysis. The General Integrated Fatigue Tracking System (GIFTS) software also generates usage spectrum at critical structural areas. It also allows the investigation of the severity of specific missions or roles.

4.4 CF18 Fatigue Life Tracking Improvements

Efforts to improve the accuracy of the CF18 fatigue tracking for the aircraft centre fuselage are complete. The fatigue usage of each aircraft was re-evaluated by Bombardier and the results implemented by the CF. The aircraft fatigue usage is now referenced to the Canadian Forces Baseline Operational Spectrum. This is the same spectrum that is currently being applied to Canadian IFOSTP centre fuselage and wing tests.

Work is underway to establish a proper strategy to track the fatigue usage of the aircraft aft fuselage. The dynamic loading experienced by the aircraft aft fuselage is not captured by the MSDRS aft fuselage strain gauges because of frequency. Various methodologies were considered (including PSD method) however, the apparent large variation in the aft fuselage structure reactions from one aircraft to another is making this task difficult.

The possibility of eliminating the strain gauge at the wing root location is under investigation. The maintenance cost of these gauges is relatively high. The Parametric Loads Formation method used to derive the IFOSTP loads spectrum has been adapted to replace the data from

these gauges. A decision on the use of this method for fatigue tracking purposes is currently under review.

The result of these OLM improvements is a more robust usage database that can be directly used in the CF comprehensive structural maintenance plan for the CF18. Fleet managers are able to forecast overhaul requirements based on fatigue usage. This program has become the centre of the CF18 fleet maintenance management. It has spun-off a very complex modification induction model that is catered to each aircraft. It has combined resources availability and operational requirements to manage the scheduling of a very extensive structural upgrade programme.

4.5 CC130 – Hercules

4.5.1 Operational Loads Monitoring/Individual Aircraft Tracking (OLM/IAT)

The CC130 Hercules (OLM/IAT) Data Analysis System (DAS) program is a multi-organisational activity to develop and validate a Data Analysis System for application to critical primary structures on CC130 aircraft [3, 4, 5, 6, 7, 8]. The system will be using actual flight load data collected by the Marconi Operational Loads Monitoring / Individual Aircraft Tracking Systems installed on the CC130 fleet. The objective is to rationalise operations, fleet management, maintenance and inspection schedules/priorities and consequences of decisions using individual aircraft flight data that will be approximately 1 month old. Currently the best information available is collated, analysed and reported on a yearly basis. Since the reporting turnaround of this data is 6 months, the most current information is approximately 1.5 years old.

Responsibilities and activities for the system are as follows. SPAR has overall responsibility. Martec is undertaking the finite element analyses required to develop the load transfer functions and load module for the system. QETE has selected and is in the process of validating the damage tolerance crack growth module to calculate damage progression and determine appropriate inspection/maintenance intervals. QETE, with support from RMC, is also undertaking material testing to generate a representative materials and operational service usage spectrum database for determining mission severity factors.

Martec data will be used for the evaluation of accumulated fatigue damage for the wing fatigue critical locations. The transfer functions have been generated using the Martec developed NASTRAN aeroelastic model for the CC130 aircraft [9]. This model employs key aircraft flight parameters from the flight data recorder as input, and generates the global aircraft loading. The model has been validated with the original manufacturer data and has proven to be accurate. In the model, aerodynamic loads are computerised using the doublet lattice small perturbation method. The aerodynamic panel models include the wing, fuselage and horizontal stabiliser with elevator. The structural model includes a global mass and stiffness representation of the wing while the fuselage and tailplane are modelled as beams (stick model). The local detailed model from which the transfer functions will be calculated is embedded into the wing global model. The gust loading on the wing is treated as a quasi-static load event, but the loading is modulated using dynamic magnification functions that have been derived from aeroelastic gust analyses. Both the manoeuvre loads model and gust dynamic magnification functions will be validated using flight test data. The Transfer Function methodology used for the CC130 aircraft is well

suited for this transport aircraft type loading. Figure 12 briefly describes the transfer functions development process.

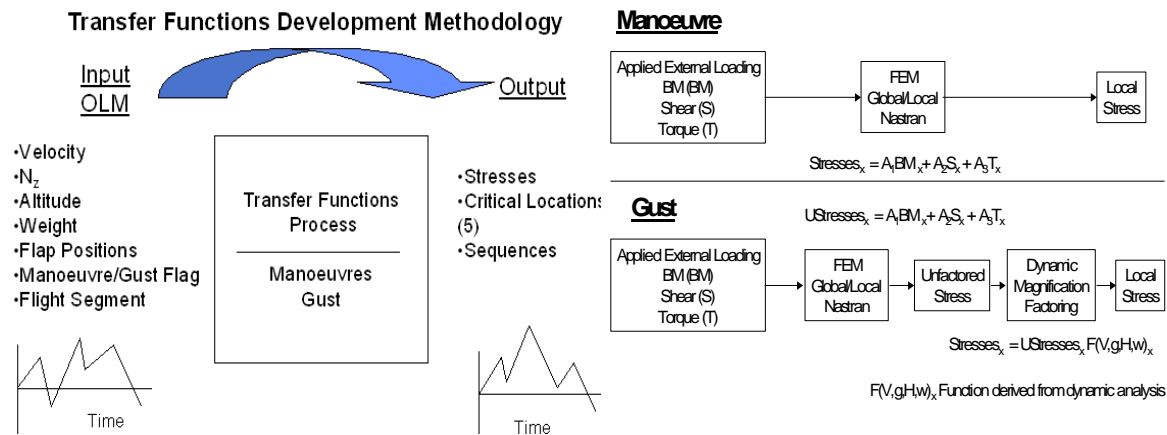


Figure 12. Transfer Functions Development Process

4.5.2 CC130 Wing Finite Element Modelling

Under contract from DND, Martec Limited has been assigned the responsibility of transfer function development. These functions will be used to convert aircraft flight parameters into local stress sequences at fatigue critical locations.

To perform this work, Martec Limited has developed a global stiffness and mass representative finite element model of the CC130 wing structure. The modeled structure is an “H” model wing corresponding to the current configuration flown by the Canadian Forces. In addition, six models of fatigue critical structural details were developed and imbedded into the global wing model for follow-on global/local analyses. Martec is using the global/local finite element analysis method for a wide range of analysis problems. This method has shown to be computationally efficient while providing good accuracy in stress prediction. For the transfer functions project, all models developed are MSC/NASTRAN finite element models and have been generated using the HyperMESH and FEMAP pre/post processors. The global model was validated against available stress and deflection data and has proven to be an accurate representation of the wing stiffness and mass. Stress predictions were within 5% to 10% accuracy while deflections were within 10% of those measured during ground testing. Figure 13 shows the CC130 wing global wing model with imbedded local models for two fatigue critical locations located at WS95 and OWS 357.

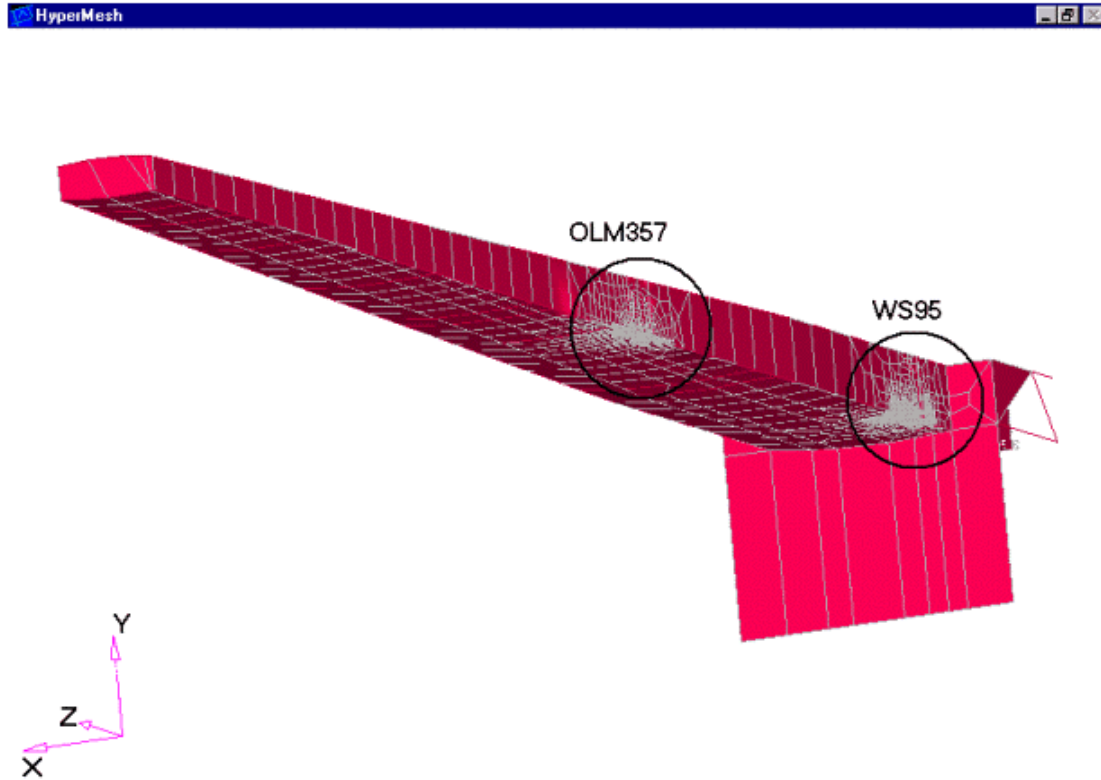


Figure 13. CC130 Global/Local FEM

4.5.3 Centre Wing Service Life Extension Program/Fuselage Life Assessment Program

Work is being conducted to assess the life expectancy of both the centre wing and the fuselage. The centre wing assessment considers three options: continued maintenance on condition, replacement, and an improvement program. The two fuselage options are continued maintenance and a fuselage improvement program. The assessments consider the past usage severity, anticipated future usage, service experience and, in the case of the centre wing, full scale test results. Additionally, to assist in assessing the current aircraft status, a number of in-depth inspections and a limited fleet-wide sampling inspection program were conducted for the centre wing and a similar program is currently underway for the fuselage.

4.5.4 Centre Wing Strain Survey/Aft Fuselage Strain Survey

In 1998, the CC130 centre and outer wings were instrumented with a series of strain gauges, accelerometers and position sensors providing a total of 65 channels of data that were recorded for 11 flight regimes. This data provides the basis for the OLM/IAT validation activities and furthers the centre wing improvement study option analyses. A similar initiative was conducted in 1997 for the aft fuselage to assess specific problems relating to longeron and ring segment attachment area cracking.

4.5.5 "Hot Spot" Strain Surveys

To aid in rapid assessment of the validity of structural integrity analyses and associated dispositions, the trial and development of a hot spot recording capability is being pursued. This entails the use of extremely compact, highly capable, and self-contained equipment that can be fitted to an aircraft to collect strain data in an independent manner.

4.6 CP140 (P3) Structural Data Recording System

The Canadian Forces (CF) have an established program for Individual Aircraft Tracking (IAT) of the CP140/CP140A, variants of the Lockheed P-3C fleet. This program uses data recorded manually on Flight Engineer Logs and represents tracking methods that are conservative and reactive. The Fatigue Life Index (FLI) and inspection intervals derived are thought to be overly conservative.

In 1993, the CF established a policy to assign airframe punishing training missions to three training aircraft, designated CP140A Arcturus, specifically configured for this role. Such severe usage results in high crack growth rates yielding short inspection intervals for these aircraft when calculated using the methods of the existing IAT program. To address this situation, the CF established an aircraft tracking system based on actual aircraft data. To this end, each of the CP140A aircraft was equipped with a Structural Data Recording System (SDRS) to record flight parameters and structural loads.

Based on the experience with the SDRS on the three CP140A, the CF decided that it was warranted to have the system installed on all CP140 aircraft. A fleet fit installation of the SDRS on all CP140 Aurora aircraft was completed in 1997. Support is provided to the CP140/CP140A SDRS program by means of an Aircraft Structural Integrity Program (ASIP) contracted to IMP Group Limited.

Currently, each of the Canadian CP140/CP140A aircraft, is equipped with a SDRS to facilitate Individual Aircraft Tracking (IAT). One of the objectives of the system is to provide usage-monitoring data that will enable the CF to quantify individual aircraft fatigue usage and crack growth rates from which optimised inspection times can be calculated. Thus inspection frequency and costs can be reduced while the safety of the aircraft is ensured.

Oore and Crocker [10] provided a brief description of the SDRS and related experience acquired with the system usage and data collection. An overview of the parameters recorded by the SDRS is presented as well as examples of data recorded in flight and their significance. Strain sensor recording rise/fall criteria are discussed in the context of minimising the volume of recorded data while capturing significant data. A rise/fall criteria sensitivity study was conducted to optimise selection of the triggering gate value, is also presented in [10]

Since the SDRS zeros strain sensor readings at the beginning of each flight, a strain offset determination method was developed to calculate absolute strain values. This method has been substantiated by calibration tests that included validation of a Finite Element (FE) model of the wing and verification of the SDRS strain measuring system. Studies performed to assess the

adequacy of the SDRS strain resolution are also presented, in terms of the resolution effect on the calculated fatigue life and crack growth (Figure 14, and Figure 15), using the Monte Carlo simulation approach. Overall it is demonstrated that SDRS data can be used to generate sufficiently accurate stress spectra for fatigue and crack growth analyses.

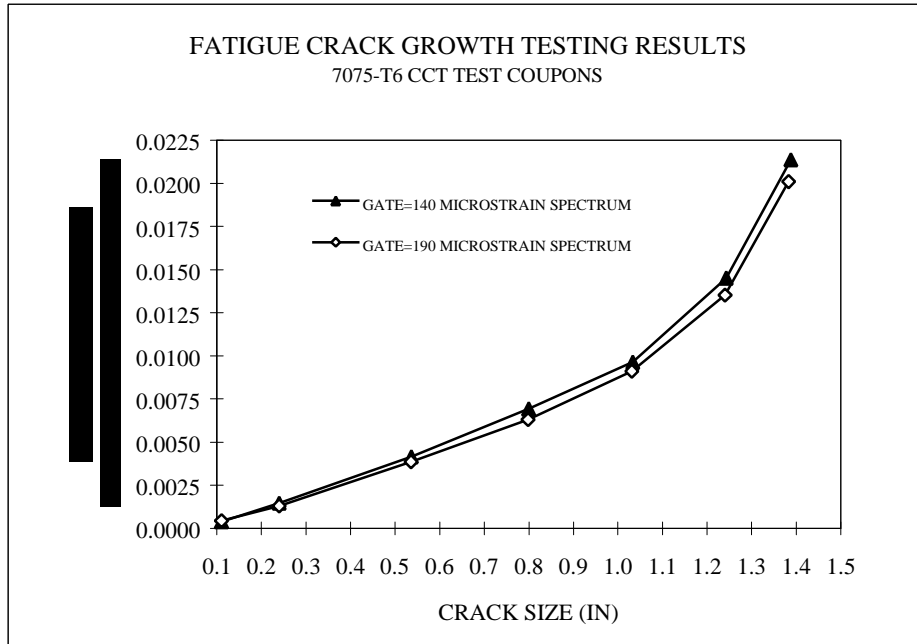


Figure 14. Rise/Fall Gate Effect on Fatigue Crack Growth

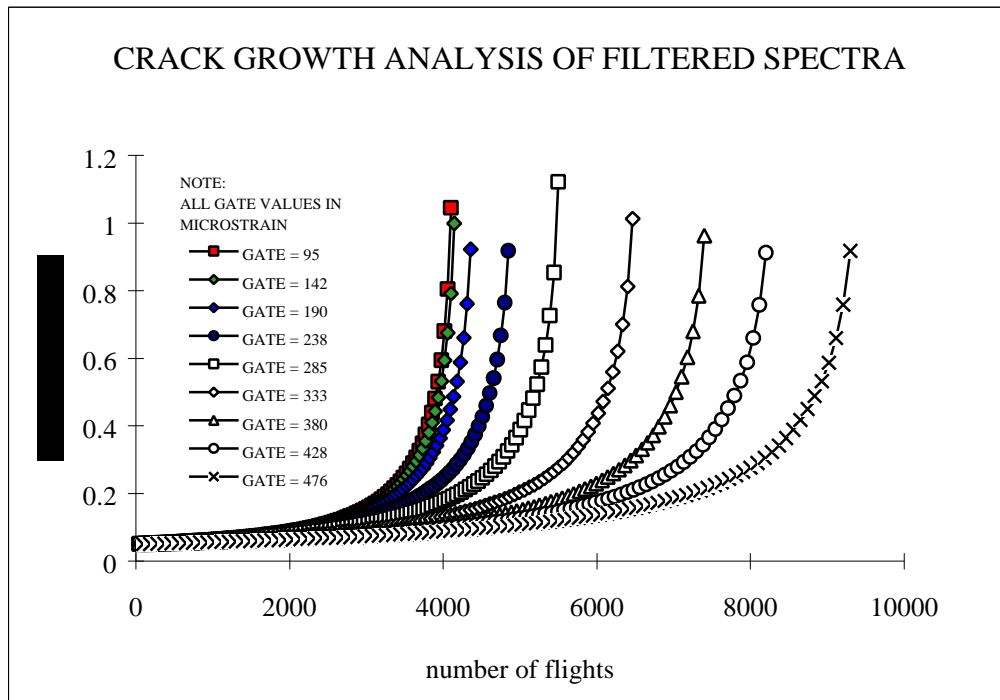


Figure 15. Fatigue Crack Growth Testing Results

4.7 DHC-8 Service Load Monitoring

Two DHC-8-200 aircraft currently operated in Australia in a coastal patrol role have been instrumented to record rain-flow counted vertical centre of gravity acceleration data. This data will be used to determine what changes are required to the fatigue crack inspection intervals specified for aircraft operated in the normal passenger carrying role.

4.8 Total Data Integrity Initiative (TDI²)

Celeris Aerospace Canada Inc., in conjunction with Smiths Industries, Grand Rapids Michigan have developed the Total Data Integrity Initiative (TDI²) for aircraft Operational Loads Monitoring. TDI² recognises that the ultimate aim of an OLM program is to provide useful and valid Life-Cycle Management Data that enable fleet operators and maintainers to make sound decisions about the use and life of their aircraft. It is postulated that this aim cannot be achieved without a rigorous and disciplined approach to both the engineering and data-management aspects of an OLM program and that both issues have to be addressed concurrently, not separately. Techniques for the practical implementation of TDI² have been developed and will be tested on an upcoming CF18 flight test program in late 1999. During the flight test program a Smith's Integrated Data Acquisition and Recording System (IDARS) will be installed in a flight test aircraft and used to monitor a variety of structural and engine parameters. The results obtained will be compared with detailed flight test data to evaluate the fidelity of the data recorded. Through this program, it is hoped to explore and/or demonstrate:

- the fidelity of data that can be obtained from “fourth-generation” recorders;
- the benefits of having voice data available to analyse unusual incidents;
- potential multi-fleet applications of TDI² concepts, thereby minimising OLM software development and user training time;
- download site data validation techniques that will result in valid data return rates in excess of 95% or better;
- the use of the Internet/Intranet for on-aircraft troubleshooting of individual recorders;
- the transfer of large quantities of data via Internet/Intranet to facilitate rapid data analysis and response; and
- the use of Web-Enabled tools, modern database technology and on-line data query/retrieval capabilities, to facilitate the rapid dissemination of data trends to different levels of users including, squadron-level personnel, maintenance engineers, life-cycle managers and fleet managers.

As part of this ongoing initiative, it is also intended to establish a “Loads Monitoring Central” on the World Wide Web. The aim of Loads Monitoring Central is to provide a central location where information about the practical aspects of establishing and running an Operational Loads Monitoring Program can be obtained and a forum where implementation and/or ongoing OLM application problems can be discussed.

References on TDI² are contained in the papers section of the Celeris Website (<http://www.celeris.ca>).

4.9 Squadron Level Software (SLS)

The Squadron Level Software (SLS) was developed by Celeris Aerospace Inc. as part of the Canadian Forces ongoing CF18 Operational Loads Monitoring program. This software takes processed MSDRS fatigue data provided by the CF18 System Engineering Support Contractor (SESC), Bombardier, and processes it to allow operational squadrons to evaluate their Fatigue Life Expended (FLE) and Fuel Usage against parameters such as mission, squadron, aircraft configuration, aircraft tail number and pilot. A user-friendly graphic user interface enables operational squadrons to rapidly evaluate the FLE and fuel consumption of individual aircraft and optimise them in accordance with current operational parameters. The system was originally developed and used as a single-user system. However, recent user feedback has identified requirements to expand SLS to a multi-user, browser enabled application for use in an Internet or Intranet environment.

A software demonstration package can be found on the SLS Web-site at <http://sls.celeris.ca>.

5 FRACTURE MECHANICS AND CRACK PROPAGATION STUDIES

5.1 A Study on the Use of Neuber's Rule in Fatigue Crack Initiation Predictions

A study on the applicability of Neuber's rule [11] in the local strain method of fatigue life prediction was undertaken by a Master's student in the Mechanical and Aerospace Department of Carleton University in collaboration with the Structures, Materials and Propulsion Laboratory of IAR. The method was examined for two geometries through a finite element analysis. In addition, the ability of the local strain method to predict the lives of the coupons subjected to spectrum loading was assessed by comparing local strain predictions for the two coupons with results from a coupon test program. The findings of the study verified the applicability of Neuber's rule in plane stress situations. A method of estimating multi-axial elastic-plastic notch stresses and strains was verified to be an effective means of accounting for notch root multi-axiality. A method of estimating total life, composed of crack initiation and crack propagation, was proposed which accounts for the notch size effect displayed in sharply notched specimens.

5.2 Fatigue Life Extension of Ageing CP140 Aircraft

The need to extend the life of ageing CP140/CP140A aircraft made the use of a refined fatigue analysis essential. Calculating local stresses and strains, and performing fatigue analysis on a cycle-by-cycle basis (strain-life approach), results in a more accurate fatigue life estimation than using nominal stresses and elastic stress concentration factors (stress-life approach). In some cases, depending on the cycle sequence, the fatigue life estimated using the strain-life approach is longer than that estimated using the stress-life approach.

The stress spectrum used in the original fatigue analysis for the CP140 Aurora aircraft was based on six mission profiles that were assumed representative of the aircraft utilisation in the fleet plus

a mix of these missions representative of the overall activity of the CF fleet. The stress spectra used are based on assumed, not monitored, missions and do not accurately represent the actual stress encountered by the aircraft. The need for a more realistic stress spectra and fatigue evaluation of the ageing CP140 aircraft prompted the initiation of the Loads/Environmental Spectra Survey (L/ESS) programs for the CP140 fleet. In 1992-1993 the CP140A Arcturus aircraft joined the Canadian Forces (CF) fleet. The CP140A was expected to have abnormally severe usage spectrum due to the large percentage of crew training missions it will be flying. A more refined fatigue and crack growth analysis was desired at that time to achieve longer inspection intervals. The decision was made to install the Structural Data Recording Set (SDRS) AN/ASH-37A aboard each CP140A aircraft to monitor the strains, and to produce a unique spectrum for each CP140A aircraft. The whole CP140 fleet has since been retrofitted with the SDRS.

IMP performed fatigue analysis to predict the fatigue life of the CP140/CP140A aircraft using “STFE” software which employs the strain-based approach and performs fatigue analysis on a cycle-by-cycle basis. The fatigue life predictions using the STFE software were made with the following information:

- Material properties obtained from strain controlled fatigue tests which include:
 - a- Strain-life data; and
 - b- Cyclic stress-strain data.
- Stress-strain history at the critical location;
- Rain-flow cycle counting technique to identify damaging events;
- Smith-Watson-Topper mean stress parameter; and
- Miner’s linear damage summation.

The software was first verified with a spectrum obtained from a full-scale fatigue test performed on the P3V-1 aircraft wing and landing gear. The software analysis results agreed well with the full-scale fatigue test results. The software was then applied to two critical points of the CP140/CP140A aircraft for the following two studies:

In the first study, the fatigue analysis of the two critical points for the CP140/CP140A was performed first using the stress-life approach. The analysis used the SDRS data derived for the CP140/CP140A fleet. The results obtained from this analysis were compared to the results obtained from the cycle-by-cycle fatigue analysis to determine if the fatigue analysis using the strain-life approach, instead of the stress-life approach, will improve the fatigue life of the CP140/CP140A fleet when applying the same fatigue spectra (SDRS data). The comparison showed a significant improvement in fatigue life prediction of the two critical points examined owing to the cycle-by-cycle fatigue analysis. Figure 16 shows the comparison for critical point 12 in terms of the fatigue damage per 100 flight hours. The CP140 Aircraft are tail numbered from 102 to 118, while the CP140A aircraft are tail numbered from 119 to 121.

In the second study, the stress-life approach fatigue analysis of the two critical points for the CP140/CP140A was performed first using the mission mix profile. Results obtained from this analysis were compared to the results obtained from the cycle-by-cycle fatigue analysis of the SDRS spectra. The comparison was done to determine if the fatigue analysis using the strain-life

approach and the SDRS data, instead of the stress-life approach and the mission mix profile data, would improve the fatigue life of the CP140/CP140A fleet. The comparison showed again an improvement in the fatigue life of the two critical points examined due to the use of SDRS data and the cycle-by-cycle analysis. Figure 17 shows the fatigue damage results obtained per 100 flight hours for critical point 12.

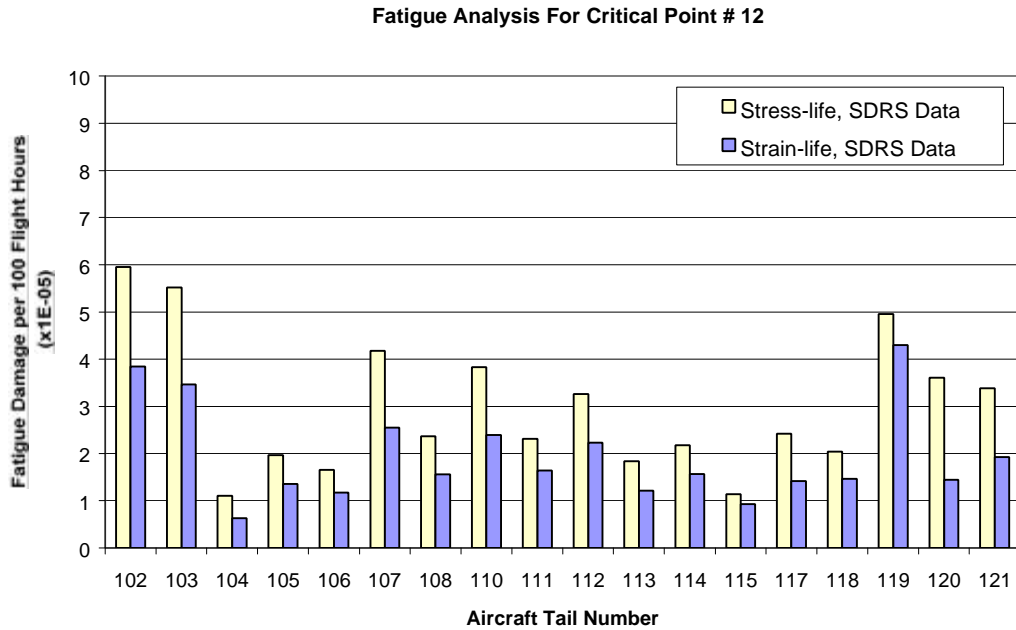


Figure 16. Fatigue Life Comparison for Critical Point # 12 Using SDRS Data

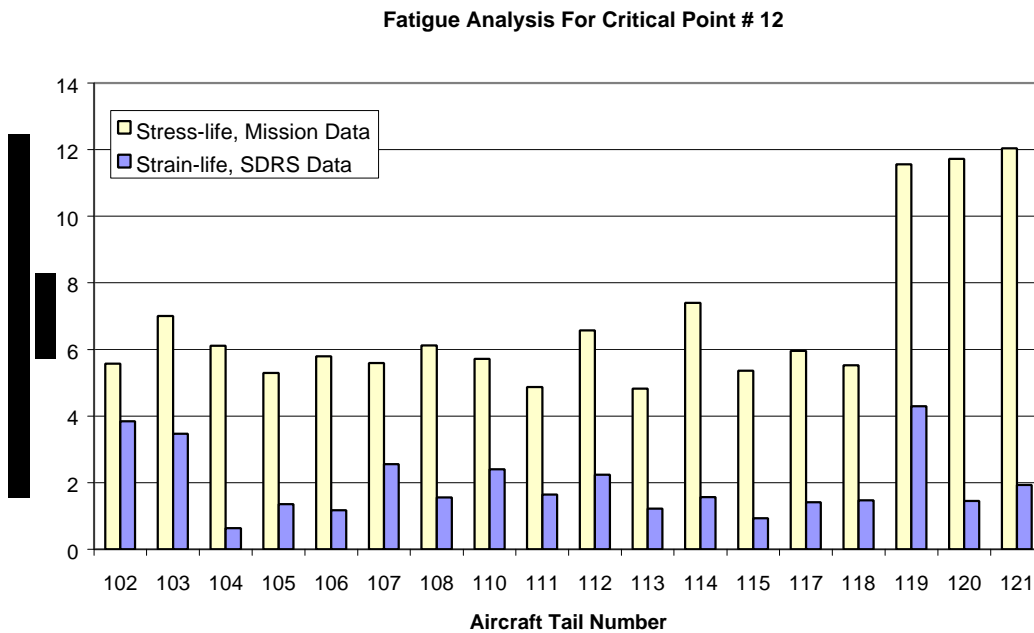


Figure 17. Fatigue Life Comparison for Critical Point # 12 Using Mission Mix and SDRS Data

5.3 Probabilistic Crack Growth Analysis Software Development

Bombardier developed a Structural Probabilistic Risk Management software (PRISM) for DND. This software, completed in 1997, is being used to perform a feasibility study for optimisation of maintenance scheduling on the Canadian Forces CC130 Hercules. Results will be officially presented to DND in May 1999.

A benchmarking exercise of PRISM with the USAF PROF software is also underway. It will compare results obtained with each respective software for the same test cases. Results are expected in June 1999.

5.4 Shot Peening Certification Program for CF18 Y470.5 Bulkhead Location X19

DGAETM(FT), DTA, QETE, RMC and École Polytechnique are participating in a program to evaluate the benefit of shot peening in a critical location of the Y470.5 bulkhead of the CF18 aircraft. During the original McDonnell Douglas ST16 full scale test, this location had developed cracks. The current test program is an attempt to quantify the benefit of shot peening at different stages of the fatigue damage accumulation, i.e. shot peening pristine material, shot peening after accumulation of 40% of the baseline crack formation life, shot peening after accumulation of 65% of the baseline crack formation life, shot peening after accumulation of 80% of the baseline crack formation life, as well as the benefit of repetitive shot peening processes (first shot peening done after the accumulation of 65% of the baseline crack formation life, second shot peening following an additional 88% of the baseline crack formation life) including the benefit of polishing the surfaces prior to shot peening.

A special coupon has been developed simulating the X19 location and a spectrum representative of the joint CF and RAAF CF18 International Follow-On Structural Test Program, IFOSTP, full scale test program is being used. At this point it has been determined that there is at least a 2.4 times increase in the baseline crack formation life after shot peening of "crack-free" surfaces irrespective of the prior history and accumulated damage. Statistical analysis of the limited current data, including those coupons which exhibited cracking below the threshold of inspectability of convention Eddy Current NDI pencil probes, has been undertaken. At this point in time with 8 to 10 data points per condition and using a 1/1000 crack formation risk level, statistical analysis indicates that the Shot Peening Life Improvement factor ranges from 4.1 for coupons shot peened at time 0% of Baseline Crack Formation Life (BCFL); 4.1 for coupons shot peened at 40% of BCFL; 3.8 for coupons shot peened at 40% of BCFL; 3.3 for coupons shot peened at 65% of BCFL; and 1.2 for coupons shot peened at 80% of BCFL. While these tests results show some optimism about shot peening repair, DND is currently assessing how this information will be utilised for fleet-wide management purposes. Further testing is underway to supplement the material database.

5.5 CT114 Coupon Test Program

The CT114 Tutor aircraft is in the process of being retired from its current trainer role. However, the Canadian Forces are considering continuing to use the aircraft in the Snowbird aerobatic demonstration team role. QETE is in the process of investigating / defining testing

requirements for main wing attachment fittings in order to develop a safety-by-inspection program [12] for an aircraft that has to date been lifed using safe life principles. The goal of this program is to determine what the inspection, repair and maintenance requirements will be to enable the Snowbird team to continue using CT114 Tutor aircraft to the year 2015.

5.6 CT133 Coupon Test Program

The CT133 Silver Star aircraft was originally designed in the 1940's prior to any design requirement for fatigue or damage tolerance. The airframe was lifed by means of full-scale test conducted by the OEM for the USAF. Canadian usage of the aircraft has been historically benign in comparison with the load spectrum used for the full scale test. The role for this aircraft has changed several times and most recently a Load Environment Stress Survey has found the usage spectrum to be much closer to the Lockheed test spectrum, particularly for those aircraft which are used at fighter bases as threat simulators and electronic warfare. Because of the raised profile of the aircraft and lack of serious problems reported in the fleet and during DLIR, it is expected that the fleet is still in reasonably good health. The CF is pursuing a safety-by-inspection approach to establish and maintain continued structural airworthiness for the CT133. Structurally critical components removed from aircraft will be tested to the current usage spectrum to establish crack growth behaviour and determine appropriate inspection intervals.

5.7 Parametric Crack Growth Analysis

As part of a preliminary repair design study to repair fatigue damage to the CC130 Hercules lower wing skin Martec conducted an extensive parametric crack growth analysis. This analysis was conducted to determine the level of loads transfer (strain reduction) needed from the composite doubler repair to achieve the required fatigue life improvement to the affected area. Fatigue crack growth analyses were conducted using a baseline representative in-service wing root strain spectrum for the CC130 aircraft lower wing skin. Crack growth analysis using an initial crack size of 0.2" were conducted for a number of load transfer conditions through the composite doubler and assumed three levels of load by-pass through the fastener at which the fatigue cracking was found to have initiated. The result indicated that for a load transfer through the composite patch ranging from 20% to 30% the expected fatigue Life Improvement factor for the repair was between 2.2 to 3.4. Life Improvement Factor (LIF) is the ratio of the time, in spectrum flying hours, for a crack to grow to critical size for the repair condition over the baseline unrepaired condition. Follow-on repair design considered a load transfer of 25% as the target design value for the repair. Figure 18 summarises the results of the analysis conducted to peg the required load transfer.

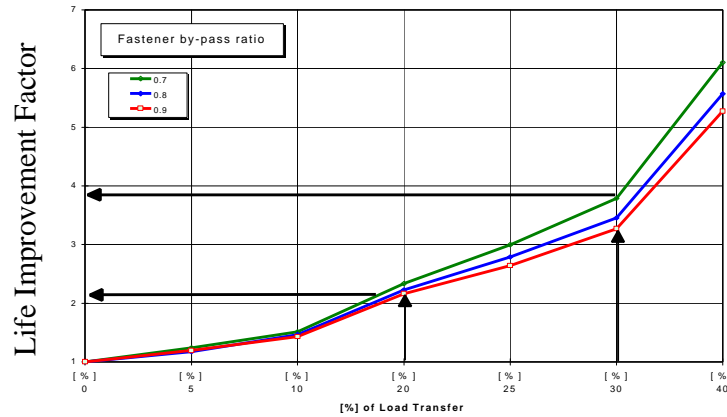


Figure 18. Parametric Crack Growth Analysis

6 FAILURE INVESTIGATIONS

This report includes descriptions of numerous failure investigations. These are organised by aircraft type and are preceded by summary table.

6.1 CF18 (Hornet)

Part	Problem	Diagnosis/Resolution
Fatigue Coupons from 7050-T7452 Hand Forging (IFOST)	Premature failure of some samples	higher than normal content of constituent particles from certain location of forged block
Front wing spar machined from 7050-T7452 die forging	Cracks at critical fastener holes –origin of cracks unknown	Grain structure parallel to the axis of the hole.
Inner Wing Front Spar (IFOSTP FT55)	Fatigue cracks originating from the four critical fastener holes near the leading edge flap transmission mount	Fatigue loading attributable to the various simulated aircraft mission profiles caused all cracks under study. No specific surface condition, manufacturing or material related factor was found which could be considered contributing or causal to the formation of the fatigue cracks.
Heavy weight outboard engine thrust mount (PH 13-8 Mo)	In-service damage (wear, pitting, galling and fretting) was found to exceed the Structural Repair Manual (SRM) rework limits	Static loading of representative mount to 130% Ultimate Load revealed that maximum bearing stress was 54% lower than calculated and that Margin of Safety exceeds 0.55
Main Landing Gear (MLG) Planing Link Bolts.	Head of the planing link lower attachment bolt on the left hand assembly had separated from the bolt shank.	Failure mode was predominately intergranular, typical of stress corrosion cracking (SCC). Rigging procedures to be changed to include corrosion inhibitor sealant, bolt inspection for corrosion and torque control.
MLG Door Attachment Hardware	Two bolts failed in tension, one by shearing of the threads – primarily overload	Rigging procedure modified

Trailing Edge Flap Outboard Hinge/Lug	Fatigue cracked hinge lugs	Consideration to be given to performing a fleet wide damage assessment on the component using a method such as the Walker model which could assist in the optimisation of inspection methods and intervals.
4 o'clock main spraybar pigtail from engine	Failed in fatigue	Extended measures already adopted to prevent fatigue failure in the other main spraybars to include the ones in the 4 o'clock position as well
LAU 7 Missile Launcher	A 140 mm crack discovered in the rail radius at the front hanger position	Part failed in fatigue followed by tensile overload – further investigation recommended

6.1.1 Failure Analysis of Fatigue Coupons from 7050-T7452 Forging

One element of the joint CF/RAAF CF18 IFOST program at the NRC/IAR is a coupon fatigue test study in support of the test spectrum development. A series of flat coupons were manufactured from a hand forging Aluminium alloy 7050 in the T-7452 temper condition. During the course of testing, it was found that some samples failed after a low number of cycles while others survived for much longer. The difference was far greater than normal scatter and, furthermore, there was no intermediate value between the groups of results. Extensive failure analysis of fracture surface using metallography and SEM examination showed that the content of constituent particles, of the type shown in Figure 19, was considerably higher in short-life coupons, which coupled with the rough machined surface in the notch, could explain the reduced fatigue life. The fact that the short life coupons exhibited multiple crack initiation sites, was consistent with higher than normal content of constituent particles in certain locations in the forged block. It became apparent towards the end of this investigation that all short-life coupons were from the same region to the forging. Under a separate investigation quality assurance and evaluation of microstructure and fatigue properties of the 7050-T7452 hand forging is being investigated [13].

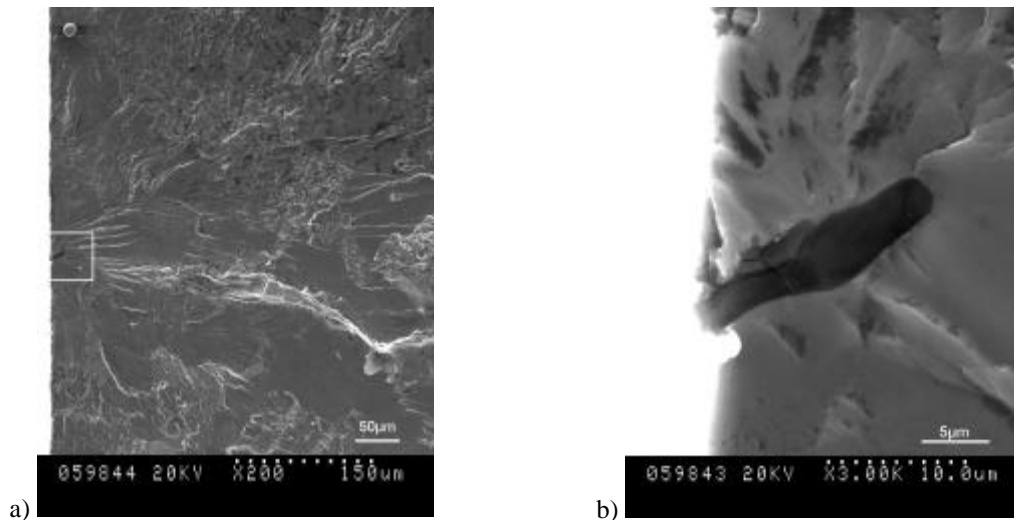


Figure 19. Crack initiation site in short life coupon: (a) SEM micrograph at low magnification; (b) high magnification view of window in (a) showing a former site of a brittle constituent particle or porosity

6.1.2 A Metallographic study of Fatigue–Critical Fastener Holes in a CF18 Structural Component [14]

The CF18 front starboard wing spar (Figure 20), is machined from aluminium alloy 7050-T7452 die forging. An inspection report from McDonnell Douglas indicated the presence of cracks at fastener holes in the equivalent component of an F18A Hornet aircraft. Under the NRC/IAR IFOSTP wing test program, a study was undertaken to assess the origin of such cracks. Eddy current inspections revealed cracks at fastener hole 172 (Figure 21). SEM examination and metallography were performed to assess the microstructure at this critical location. It was found that the grain orientation near the hole was parallel to the axis of the hole. A preferable microstructure for the grain would be to follow the outline of the part. The grain structure in the component may have contributed to the susceptibility to fatigue crack formation at Fastener Hole 172.

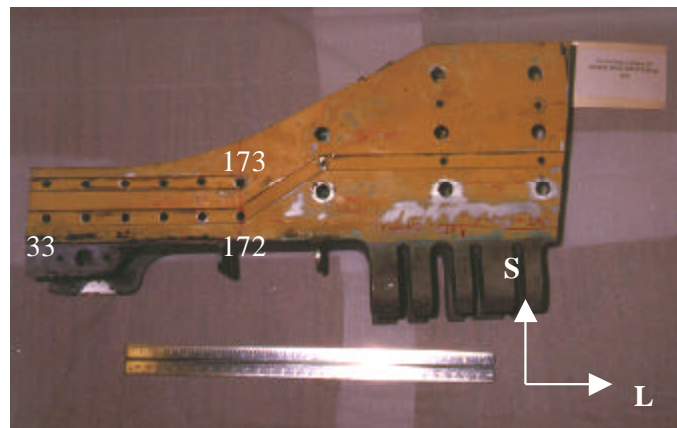


Figure 20. The as-received portion of the CF18 Inner Wing Front Spar right hand side. Fastener hole 172 is identified. L is the longitudinal and S is the short transverse direction in the forging material

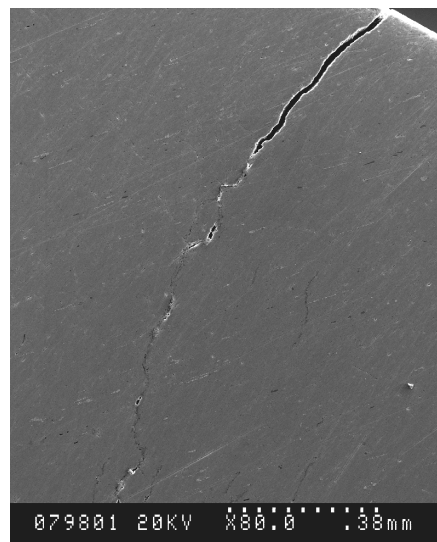


Figure 21. SEM micrograph showing one of the cracks found during Eddy Current inspection at Fastener Hole 172

6.1.3 CF18 Heavy Weight Outboard Engine Thrust Mount

In-service damage (wear, pitting, galling and fretting) to CF18 Heavy Weight Outboard Engine Thrust Mount [15] was found to exceed the Structural Repair Manual (SRM) rework limits. A static test was required to determine whether a 5.5% nominal race dimension reduction was possible; analysis of the original dimensions indicated that the Margin of Safety (M.S.)= 0. To determine what the actual load capacity of a reworked mount would be, QETE designed a test to statically test a fleet representative mount to 130% of the Ultimate Load condition (complete stall of engine at sea level) using progressive reduction in race dimension. Strain gauging on the mount indicated that at 130% of the Ultimate Load condition, the maximum bearing stress was 54% lower than analytically calculated. As well, the outboard hinge lug has an M.S = 0.55; the pin bearing outboard M.S. = 0.6 and the thrust bearing surface M.S. = 0.57. Most importantly there was no evidence of plastic deformation. The maximum stress near the thrust bearing surface, using the von Mises failure criteria, was ~ 75% below engine mount yield strength (PH 13-8 Mo).

6.1.4 CF18 Main Landing Gear Planing Link Bolts - Failure Analysis

CF18736 was undergoing normal maintenance when it was discovered that the head of the planing link lower attachment bolt on the left hand main landing gear (MLG) assembly had separated from the bolt shank [16]. The bolt was replaced and forwarded to QETE to determine the cause of failure. QETE determined that the failure mode was predominately intergranular, typical of stress corrosion cracking (SCC). The SCC had initiated at corrosion pitting that had occurred in the radius of the bolt head. Recommended correction actions include that the MLG rigging procedures be amended to detail proper application of the corrosion inhibitor sealant and that the bolts be visually inspected during the normal rigging procedures and replaced if there is corrosion in the bolt head radius. Over-torqueing may have be a contributing factor. The assembly is configured so that operating loads should not be transferred to the planing link lower attachment bolt head therefore the only stress on the bolt head should be due to torque application. The normal torque applied to this bolt is not sufficient to generate the stress required to initiate SCC in this particular material.

6.1.5 CF18 Trailing Edge Flap Outboard Hinge/Lug Crack

QETE analyzed a cracked trailing edge flap (TEF) hinge lug [17]. Shortly thereafter, another crack was found on another TEF hinge. Both of these cracks were found on regularly scheduled eddy current inspections. Examination using the SEM revealed that both cracks propagated by means of fatigue. Both the cracks were progressing into the rear portion of the hinge.

6.1.6 CF18 Front Spar Fractographic Analysis

During a teardown inspection of the CF18 International Follow-On Structural Test FT55 centre fuselage test article, several cracks in the Inner Wing Front Spar were detected [18]. QETE conducted a detailed mapping of the fatigue damage and performed a fractographic analysis of the fatigue cracks originating from the four critical fastener holes near the leading edge flap

transmission mount. A non-destructive test evaluation confirmed the presence of two cracks in hole 170 and one crack in hole 172. Failure analysis determined that fatigue loading attributable to the cyclic stresses induced by the various simulated aircraft mission profiles caused all cracks under study. No specific surface condition, manufacturing or material related factor was found which could be considered contributing or causal to the formation of the fatigue cracks.

6.1.7 CF18 LAU 7 Missile Launcher Crack Assessment

A 140 mm crack was found in a LAU7 Missile Launcher on a CF18 aircraft [19]. The crack was located in the rail radius at the front hanger position. An evaluation of the fracture surface determined that the crack initiated in a small region of fatigue (45 mm x 0.4 mm), which correlated to the wear marks left on the rail surface by the hanger. The rest of the fracture surface was consistent with tensile overload. All material tests indicated that the part material met specifications. It was concluded that this part failed in fatigue followed by tensile overload caused by extreme stresses and hanger movement. Further investigation into the loading and mechanics of this part was recommended.

6.1.8 Failure of PH 13-8 Mo Aircraft Components

Failure investigations of two aircraft components, one from a landing gear and the other from an ejector rack mechanism have been completed [20]. Both were made from PH 13-8 Mo (UNS S13800) precipitation hardening stainless steel which had been heat treated to the H1000 and H950 tempers respectively and then chromium plated. The parts were characterised metallographically and mechanically and were found to be compliant. Detailed fractographic examination revealed that the first stage of both failures was similar: sub-surface initiation of numerous cracks with a wide range of orientations and cleavage like features. Hydrogen embrittlement was identified as the most likely mechanism of failure.

6.2 CC130 (Hercules)

Part	Problem	Diagnosis/Resolution
Vertical Stabiliser Longeron Attachment Fitting	Routinely replaced due to cracking	Stress Corrosion Cracking of 7075-T6 fittings. It was recommended that progressively all 7075-T6 fittings be replaced with newer 7075-T73 construction.
Strut Web, and Bulkhead FS 858	The left hand strut, bulkhead rib and webbing fractured	The new rib did not align properly with the existing structure, the damage likely originated because structural deformation was placing abnormal loads on the components.
Ramp Support Fittings	Increased replacement frequency	Fitting failures found to have initiated by fatigue, due to operational loads, fleet wide replacement recommended, fittings uninspectable.
RH T-Bow Beam Fitting (MLG area)	Steel fitting replacing original aluminium fitting failed after several years	This is the first known failure of a modified fitting and may be an isolated incident related to this specific installation. Fleet to be monitored and if additional failures of the modified fittings are experienced corrective heat treatment(s) be applied to impart both toughness and strength to the component.

Extrusion Ring Segment FS 880	T extrusion forming the inboard cap of the FS880 side bulkhead had cracked. The crack began approx. 2" above the bottom of the extrusion and continued upwards for approx. 4.15" on the inboard face and 4.85" on the outboard face.	Fatigue crack took approximately 3400 cycles to grow from 0.015" to 0.14" in depth. No material deficiency was detected. It was recommended that an ultrasonic NDT inspection technique be developed to detect similar flaws prior to catastrophic failure.
Rear Spar Web – centre wing	A number of older aircraft were found cracked	Damage consistent with Lockheed full scale test. Slow growth observed, however concern over rapid jump of cracks to link fastener holes.
Nose Wheel Steering Collar Bolts	Following wheel shimmy two aft steering collar shear bolts broke.	Fatigue initiation and propagation followed by catastrophic overload. These features were typical of an under-torqued assembly. Increase in the torque recommended.

6.2.1 CC130 Longeron Attachment Fitting Crack

During CC130 progressive structural inspection (PSI) at SPAR, technicians have been routinely replacing cracked longeron attachment fittings on the vertical stabiliser. QETE investigated the cause of cracking [21]. Examination of the fracture surfaces revealed that the cracks had progressed by means of stress corrosion cracking (SCC). Material tests showed that the component was manufactured from 7075-T6 Aluminium, a material that is susceptible to this type of failure. The component drawing called for 7075-T73 but an earlier version called for 7075-T6. It was determined that the components under investigation were likely original equipment and therefore manufactured from 7075-T6 Aluminium. The extensive cracking had taken place without catastrophic failure, indicating that structure had some fail-safety. Pending the results of a more complete fail-safe analysis. QETE recommended that when the tail is removed on PSI, the components should be inspected and any that are found to be 7075-T6 material should be replaced.

6.2.2 CC130 Strut Web, and Bulkhead Failure

While deployed in Thule, Greenland, a C130 was undergoing a post flight inspection when a number of the components near the cargo ramp were found damaged. The left hand strut, bulkhead rib and webbing located at fuselage station (FS) 858 were fractured [22]. These components along with other supporting fittings were sent to QETE for analysis. During the investigation QETE determined that one of the supporting components, the ramp support fitting, was also cracked. All the failed components displayed features of fatigue growth followed by overload. Although the cracks on each of the components likely grew concurrently, rubbing on the rib fracture surface indicated that it fractured first but was hidden by insulation blankets. The damage was only discovered when the strut, which is visible, failed.

6.2.3 CC130 Fuselage Station FS 880 Extrusion Ring Segment Failure

During a post periodic inspection run-up of a C130 aircraft a bang was heard coming from the rear of the aircraft. Inspection of the aft area revealed that a T extrusion, which forms the

inboard cap of the FS880 side bulkhead had cracked [23]. The crack began approximately 2 inches above the bottom of the extrusion and continued upwards for approximately 4.15 inches on the inboard face and 4.85 inches on the outboard face. Flaking paint on the inboard face and the large size of the crack made it readily visible in the aircraft, except for the lowest 0.7 inches which extended under the cap used to attach the side bulkhead to the sloping longeron. Opening of the crack revealed the presence of fatigue cracking, most likely formed as a result of pressurisation cycles, prior to the overload failure. It was also determined that the fatigue crack took approximately 3400 cycles to grow from 0.015 to 0.14 inches in depth. The extrusion met specifications and no material deficiency was detected which would have initiated the failure.

6.2.4 Failure of RH T-Bow Beam Fitting of CC130 Aircraft

The bow beam fitting is a structural component of the CC130 airframe in the main landing gear area. As a result of fatigue problems a modification was made several years ago which replaced the original aluminium fittings with identically sized steel fittings. QETE investigated the failure of a steel fitting. LPI and MPI inspections confirmed the presence of cracks at the fastener hole locations [24]. The fracture surface was heavily oxidised and the fractographic features were obscured. Careful Scanning Electron Microscopic (SEM) examination of the obliterated fracture surface revealed signs of fatigue cracks which seemed to have initiated from the machined surface of the fastener hole. Heavy oxidation implied that the crack had existed for some time in an aggressive service environment. However, final fracture appeared to have been caused by overload. Metallurgical examination and hardness data indicated that the fitting was manufactured from an annealed low carbon steel, comparable to the specified steel alloy. This is the first known failure of a modified fitting and may be an isolated incident related to this specific installation.

6.2.5 CC130 Rear Spar Web Fatigue Damage Assessment

In an attempt to accurately assess the structural status of the older CC130 aircraft in the CF fleet, a major survey involving visual and non-destructive inspection (NDI) of several critical areas of the centre wing section has been conducted. The goal of the survey was to determine if the Canadian CC130 aircraft were experiencing damage at the same locations as occurred on the Lockheed full scale test and to quantify the extent of this damage. One of the locations on the centre wing, which suffered significant damage during the full scale test, was the rear spar web. When this area was examined, a number of CF aircraft were found cracked and subsequently repaired [25].

QETE conducted a detailed NDI and fractographic evaluation of the failed components to assist in relating the level of damage present in the Canadian fleet to the results of the full scale test program. QETE confirmed the presence of the flaws found by the contractor in the four panels examined as well as one additional flaw. It was determined that one NDI method (eddy current) was much more effective than the other method utilised (LPI) because of debris present in the cracks. The locations of the damage in the panels were identical to that seen in the full scale test but to a much lesser extent. However, the fractographic evidence proved that the crack growth was slow and stable to a small size then very rapidly jumped to link fastener holes. This evidence indicates that although the Canadian CC 130 aircraft have only 10 % or less of the

damage in comparison to that developed in the component during the full scale test, the wing can not be considered to have 90 % of its life remaining.

6.3 CP140 (P3 Orion)

Part	Problem	Diagnosis/Resolution
Engine Bleed Air Duct	Broke apart requiring the shutdown of the engine	Fatigue cracking observed, special inspection of the fleet revealed more cracks. More extensive inspection of ducts at regular intervals recommended.
Engine starter flange	Found broken in two after a flight, causing the starter to separate from the gearbox. (8 cases)	Improper alignment or looseness in the starter inlet duct led to abnormal vibration loads. The failure occurred by high cycle, low stress fatigue most likely vibration induced.
Nose Landing Gear Actuator component (pin and yoke)	Fatigue failure	It is recommended that the pins of the nose landing gear be inspect using MPI on a periodic schedule to find cracks before the pins fail.

6.3.1 CP140 Nose Landing Gear Actuator Failure

QETE investigated the failure of a CP140 Nose Landing Gear Actuator component [26]. Visual and microscopic inspection of the yoke revealed that there were no fatigue features evident and that the part had failed in overload. The pin was examined visually and using the Scanning Electron Microscope (SEM). The macroscopic features, such as ratchet marks, indicated that the pin failed in fatigue by unidirectional bending. Cracking most likely initiated at the outer surface of the plating as indicated by striations visible in the plating fracture surface. The crack then continued in the steel towards the drilled hole in the center of the pin. This section of the fracture was extensively corroded. Just before reaching the drilled hole, the crack changed direction abruptly. The fatigue cracking then continued at the other side of the hole and propagated towards the outer surface of the pin. The final failure zone was quite small. There were no unusual surface features such as corrosion pits or tool marks, which could have facilitated crack initiation. Since one half of the pin displayed such extensive corrosion, it was evident that the crack had been in the pin for some time. This indicates that Nondestructive Testing (NDT) using Magnetic Particle Inspection (MPI) at periodic intervals would find these defects and prevent further failures. It was concluded that the pin failed by fatigue, which took place over some time, followed by failure of the yoke in overload after the pin had failed completely. It is recommended that the pins of the nose landing gear be inspect using MPI on a periodic schedule to find cracks before the pins fail.

6.4 CH124 (Sea King)

Part	Problem	Diagnosis/Resolution
Pylon and sponson assembly components	Several components failed	Primary mode of failure was fatigue. Lack of service history prevented definite determination of the root cause.
Main Gearbox (MGB) Input Bevel Gear	Removed from service because the chip detector light would not extinguish.	Tooth lands and ends of the gear in this investigation had been carburized. The residual stresses that would have been induced by the carburization served to assist in the initiation of the chips. NDI of input bevel gears at main gear box overhaul contractor initiated.

Main Gearbox #2 Filter Bowl Bolt	Massive oil leak	Fatigue, caused by the use of a thread seal instead of a duo-seal during filter bowl installation.
Accessory Drive Gearbox	In flight #2 engine failure	Fatigue caused by cyclic loading. This situation was created by a missing shim (0.050 in.) behind the accessory bevel gear, leading to the failure in overload of the front frame accessory drive (FFAD) shaft.
T58 Engine Mount	Broken engine mount	Fatigue followed by overload. The bearing staking profile. The staking was four times deeper than specified, which would have developed extra internal stresses that were the most likely cause of fatigue initiation. Special inspection and EC NDI recommended.
Tail Wheel Support	Failures on landing	The supports were machined too thin in the critical area. This resulted in the initiation of fatigue cracks and subsequent overload fracture.
Rudder Flight Control Cables	Time expired cable inspection	Fatigue failure of cable wires in the sections of cables that travel over the guide pulleys. Cables to be replaced prior to 1100hrs. Extended service not recommended.

6.4.1 CH12437 Pylon Assembly Failure

QETE investigated the failure of several CH124 pylon and sponson assembly components [27]. The primary mode of failure in each case was found to be fatigue. Without service history information, it was not possible to determine conclusively the cause of the failures, however possible factors were identified as age and increased loading as the result of operational requirements. Failure of one component probably contributed to failure of others. The first component to fail was identified as the web (PN S6120-66105-6).

6.4.2 Failure of a CH124 Sea King T58 Engine Mount

During an after flight check of a CH124 Sea King helicopter, one engine was found to swing outboard freely due to a broken engine mount [28]. This mount had failed in fatigue on one side of the bearing followed by overload on the other side. All dimensions and material properties were as specified, except for the bearing staking profile. The staking was four times deeper than specified, which would have developed extra internal stresses that were the most likely cause of fatigue initiation. The age of the engine mount may have also been a factor in the fatigue initiation.

6.5 CC142 (Dash-8) Main Wheel Failure

QETE investigated the failure of a Dash-8 main wheel assembly [29]. The complete wheel assembly, including tire, was received along with the broken piece, which was approximately 12" in length. The fracture surface was examined visually and in the Scanning Electron Microscope (SEM). Macroscopic features of the fracture surface were indicative of fatigue. The SEM revealed two distinct initiation sites located near the centre of the failed region, on the inside of the bead wall. There was no evidence of any metallurgical flaws at the initiation sites. The remainder of the wheel was stripped of paint and a Liquid Penetrant Inspection was carried out with no further defects found. Energy Dispersive X-ray analysis and eddy current

conductivity testing showed that the material was consistent with 2024-T3 aluminium alloy. The tire exhibited a considerable amount of side wall damage in the area of the wheel failure. It is the opinion of QETE that the damage to the tire was a result, rather than a cause of the wheel failure. It is concluded that the wheel failed by fatigue with no material, manufacturing or mechanical flaws found which would have contributed to the initiation. It was considered possible that the crack had grown relatively quickly and was either not present or sufficiently large to be detected during the prior NDT inspection.

6.6 CT114 Tutor

Part	Problem	Diagnosis/Resolution
Left Hand Wing Main Lower Spar Cap	Cracks found	Fatigue. Cause under investigation.
Main Wheel Drive Key Mounting Screw	Failure	Bending fatigue. Improper maintenance resulting in loose seating of the drive key screw.

6.6.1 CT114 Tutor Wing Cracks

Tutor aircraft, CT114108, was found to have through cracks in the left hand wing main lower spar cap [30]. One crack was in the radius near the main lug, the other crack occurred nearby, extending between two adjacent fastener holes. Fractographic examination of the crack surfaces revealed striations and the cause of failure was found to be fatigue in both cases. The crack between the fastener holes was smeared indicative of significant shear loading in this area. Striation spacing in the radius crack was found to be larger at the crack formation site and the crack appeared to slow down as it got larger. The ability to resolve striation spacing for the crack between the two fastener holes was limited; however, from the information available, it appeared that crack growth was initially slow and consistent. Crack growth became more rapid as the crack neared the second fastener hole. There was no evidence of cracking on the opposite sides of the two holes.

As well, a 6.5 inch (165 mm) crack was found in aircraft CT114141 in the right hand main spar upper cap forward upper upper flange approximately 17 inches from the centre hole of the main lug. The cause of failure is currently under investigation.

7 AGING AIRCRAFT ISSUES

7.1 Integrating Real Time Age Degradation Into the Structural Integrity Process

The NRC/IAR have been collaborating with Analytical Processes and Engineering Solutions (APES) to develop the rationale, approaches, and techniques to evolve the structural integrity process to include the effects of corrosion, sustained stress corrosion cracking, and other age related degradation effects. The demands for extended use of the ageing aircraft fleets around the world are providing new challenges to the aerospace community to ensure continued safety, readiness, and reduced costs. Integrity can be built into a product with the existing processes, but can not be proclaimed into an existing aircraft system. For an existing fleet, the challenge is to maintain safety and readiness while keeping control of operating and maintenance costs.

The principal focus of this collaboration is to describe a process for incorporating the "age degradation" aspects of aircraft into the existing infrastructure of the design, manufacturing, and maintenance of aircraft systems. The tailoring of the structural integrity process enables the industry and the user communities to meet the needs, opportunities, and challenges being presented by the Ageing Aircraft Fleet. The economic and safety impact of the continued use of some aircraft necessitates an enhancement to the existing system. A viable method of utilising the proposed approach presented in reference [31] in a fashion to realise benefits throughout the full life cycle of aircraft systems.

TASK I	TASK II	TASK III	TASK IV	TASK V
DESIGN INFORMATION	DESIGN ANALYSES & DEVELOPMENT TESTS	COMPONENT & FULL SCALL TESTING + DEMONSTRATION	FORCE MANAGEMENT DATA PACKAGE	FORCE MANAGEMENT
Integrity Master Plan	Materials & Joint Allowables	Static Tests	Final Design Analyses Strength Summary	Load s/Environment Spectra Survey
Structural Design Criteria w/Corrosion & SSCC	Loads Analysis	Durability Tests	Durability Summary	Individual Airplane Tracking Data
Damage Tolerance & Durability Control Plans	Sonic, Vibration & Flutter Analysis	Damage Tolerance Tests	Corrosion Summary	Individual Airplane Maintenance Time s
Corrosion Tolerance Control Plan	Design Service Loads Spectra	Assembly Process Verif. Test w / Revisions & Updates	Force structural Maintenance Plan	Structural Maintenance Records
Selection of Mat'ls & Processes	Design Chemical/Thermal Environment Spectra	Analytical Process Verification Test	DTA, CTA, & SSCC Summary	Cost Assessment Process
Cost Trade Studies w/Corrosion & SSCC	Stress Analysis	Flight & Ground Operations Tests	Load s/Environment Spectra Survey	Repair Tracking
Design Service Life and Design Usage	Damage Tolerance Analysis	Sonic Tests	Individual Airplane Tracking Program	System Feedback Lessons Learned & Info
Critical Comp. & Selection	Durability Analysis	Flight Vibrations Tests	Operational Database Cracking Corrosion Repairs Cost	
Priority Process Definition	Corrosion Tolerance Analysis	Flutter Tests		
Methodology & Analysis	LCC Assessment	Interpretation & Evaluation of Test Results	Corrosion Protection Verification Loads/Stress Database FEA Models Files Geometry	
Review Approval Plan				

Figure 22. Proposed changes to ASIP tasks to account for corrosion

Modifications to the existing structural integrity processes are required to:

- include technical issues associated with actual use and effects of the field environment;
- consider maintenance practices and information gained from maintenance programs that were not included in the design criteria or covered in the in-service maintenance plans;
- provide the end users with the appropriate technical information and engineering tools to effectively assess and manage ageing aircraft;
- ensure that all disciplines adequately interact during the design phase to address the issues of degradation of the assembled aircraft in the field environment;
- incorporate recent advances in corrosion assessment and prediction technologies that are not included in conventional practices and procedures.

Current structural integrity processes focus on usage related degradation such as static strength, fatigue and damage tolerance but do not fully address real time related degradation phenomena such as corrosion. There are cost and safety benefits to integrating consideration of real time based degradation mechanisms with the current structural integrity processes as proposed in Figure 22.

The NRC/IAR projects briefly described in the following sections are focused on the development of technologies needed to support the integration of corrosion with structural integrity processes.

7.2 Pillowing Corrosion Cracking in Al 2024-T3 Fuselage Lap Joints

At the 1997 ICAF Symposium [32], Komorowski et al predicted the possibility of occurrence of high aspect ratio cracks caused by pillowing in corroded lap splices. This type of cracking has been confirmed in the first and second layer skins, in longitudinal and circumferential joints and in both retired and operational aircraft [33] [34]. The majority of the cracks, which will be referred to as “pillowing cracks”, had not penetrated through the thickness and were undetected using conventional non-destructive and visual inspection techniques. Table 1 lists the different aircraft where these pillowing cracks have been found.

Table 1. Recorded Incidences of Pillowing Cracks

Type of Aircraft	Hours / Cycles	Location of crack	Layer	WFU / CUT
L1011	38,040 / 31,370	33R / BS589-609	First	Dec. 93 / Sept. 93
B727-235	55,640 / 48,660	4R / BS1100	Second	Sept. 92 / May 93
B727-200	D Check	S30 / BS1090	First	In service / Aug 95
B727-100	61,890 / 54,150	S19R / BS600-640	Second	July 94 / July 96
B727-90C	72,400 / 56,700	S19-26L / BS440	First	In service / Oct 95
B727-235	56,870 / 49,530	S19R / BS700-720	First	Mar 92 / Feb 93
A300	10,400 / 6,940	S31L / FR26-31	First	In service / Oct 81
B727-295	61,854 / 55,465	S19R / BS660-680	First	Jan 90 / Feb 98
B727-295	63,349 / 55,676	S19R / BS720A-720B	First	Aug 89 / Feb 98

Thus far, six cracks from three aircraft have been examined using scanning electron microscopy, three from B727-90C, one of which was through the thickness, two from an L1011 and one from a B727-295 which was also severely exfoliated. The dimensions of the cracks along the faying

surface, a, and through the thickness, b, are given in Table 2 along with the approximate crack shape.

An investigation was initiated at the NRC/IAR to determine the fracture mode for these pillowing cracks [35]. It should be pointed out that very little corrosion damage (such as pitting) or fretting damage was present around the rivet holes. These types of cracks have been found to occur in groups and tend to form a star-shape pattern, particularly if the corrosion pillowing was significant around the hole. Also, the crack growth in the through the thickness direction is not perpendicular to the surfaces but occurs at an angle. All the fracture surfaces examined showed extensive intergranular cracking along with numerous secondary cracks as shown in Figure 23.

Table 2. Dimensions of Pillowing Cracks

Aircraft Type	Faying surface, a, mm (in.)	Through the thickness, b, mm (in.)	Ratio(a/b)	Approximate crack shape
B727-90C	7.125 (0.281)	0.991 (0.039)	7.16	
	2.692 (0.106)	0.891 (.035)	3.02	
	5.876 (0.231)	0.336 (0.013)	17.5	
L1011	10.5 (0.413)	0.432 (.017)	24.3	
	6.431 (0.253)	0.574 (.023)	11.2	
B727-295	3.074 (0.121)	0.672 (.027)	4.57	

Upon closer examination of the fracture surface, fatigue striations were found, which indicates that this crack was growing under fatigue loading. As can be seen in Figure 23, this crack had four distinct fracture regions, each having a different crack depth. These regions suggest the presence of four initiation sites, which could not be easily identified.

Sections from different corroded lap joints were cold mounted and polished to determine the type of damage that is occurring along the faying surfaces. The results suggest that in areas away from the rivet hole where the residual stress from corrosion pillowing is small, intergranular cracking occurs at the bottom of corrosion pits, as shown in part one of Figure 24. However, in the vicinity of the rivet holes, stress corrosion cracks occur which grow at a slant through the thickness, as shown in part two of Figure 24. Once again, these cracks occur at the bottom of corrosion pits. However, it is not known at this time which mode of damage occurred first, corrosion pits or stress corrosion cracking. The slanted growth characteristic is typical of stress corrosion cracking in material where grains are substantially elongated as in Al 2024-T3 sheet.

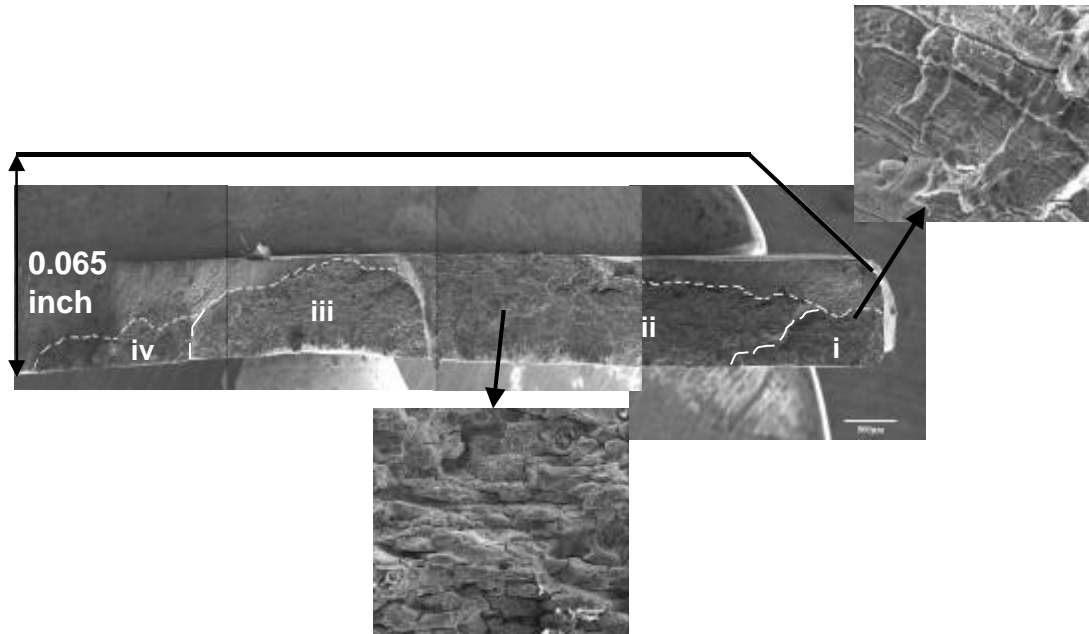


Figure 23. Scanning electron micrograph of pillowing crack found in L1011 lap joint;
(a) intergranular cracking, (b) fatigue striations

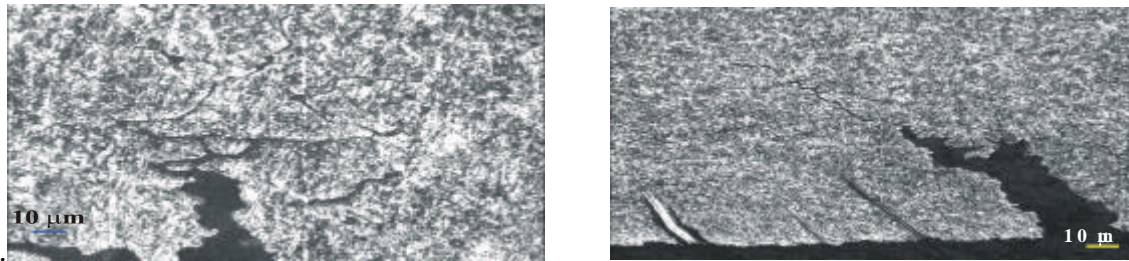


Figure 24. The first part shows optical micro graph showing intergranular cracking along faying surface away from the rivet hole, and the second one is an optical micro graph showing stress corrosion cracking along faying surface near rivet hole.

7.3 MSD and Corrosion Fatigue in Lap Splice Specimens

7.3.1 Experimental Technology

The NRC/IAR and Carleton University have developed cost-effective experimental technology for representative fatigue and corrosion/fatigue testing of longitudinal fuselage skin splices. In experimental fatigue and corrosion/fatigue studies, the specimen and test procedures must be representative of the aircraft and its operating environment. This presents several problems:

- full-scale testing or fuselage panel testing would be costly, because many specimens would be required;

- simple splice specimens of the sort usually used for preliminary design purposes do not reliably simulate aircraft conditions; in particular the MSD failure mode, the out-of-plane bending stresses, and the load transfer from cracked areas to the surrounding structure. Consequently, the initiation and crack growth characteristics are not representative;
- the accelerated corrosion process and its application in conjunction with fatigue loading must simulate many years of operation in a complex and variable environment.

The requirement for a representative yet inexpensive means of fatigue-testing splices has been met by developing the MSD test specimen concept is illustrated in Figure 25. The version in the figure is a generic lap-splice version of the specimen in 2024-T3 Alclad which is representative of some narrow-body ageing aircraft. The key feature of the concept is the use of bonded side straps to simulate the load transfer from cracked areas to surrounding structure that occurs on aircraft. This allows MSD cracks to develop and link-up in a typical manner, with typical crack growth rates, and without premature failure of the specimen. A shaped doubler at each end of the specimen is used to fine-tune the hoop stress distribution. A finite element model of the hoop stress distribution is shown in Figure 26. This illustrates how the MSD specimen models the typical hoop stress distribution across a frame-bay, including out-of-plane bending stresses. For fully representative studies, the specimen would be tailored to the aircraft of interest and might be made 20 inches (~500 mm) wide to represent a full frame-bay. For corrosion/fatigue tests, a corrosion process previously developed at the NRC has been adapted for use with the MSD test specimen and has been verified by comparing corrosion damage in corroded MSD specimens with that in naturally corroded aircraft splices [36].

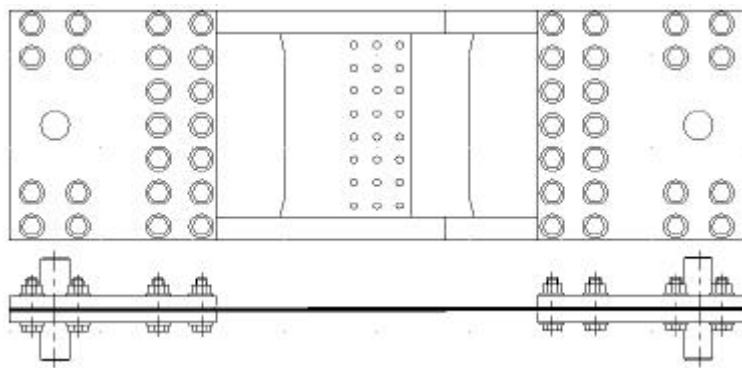


Figure 25. MSD Specimen

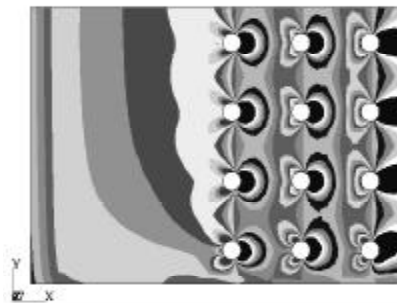


Figure 26. Half-width FE model of hoop stress distribution at faying surface of countersunk sheet in MSD specimen

A statistically designed series of fatigue-tests of corroded and non-corroded MSD specimen is currently under way. In the corroded specimens, the interior of the splice is being pre-corroded to an average thickness loss of between 5% and 6% per sheet. At this level of corrosion, which requires an exposure of several months, most of the cladding is usually consumed and there are localised regions of substantial attack into the core 2024-T3. Test results from the first ten specimens in the series show a 50% reduction in fatigue life due to corrosion. For comparative and modelling purposes it can be useful to view MSD crack growth data as aggregate crack growth curves showing the sum of all individual MSD crack lengths at any given time (cycles). The aggregate crack growth curves for all ten tests are shown in Figure 27, and clearly show the separation between the corroded and non-corroded populations. There have also been significant changes in failure mode, and several observations on corrosion/fatigue interaction have been made that may be important in corrosion/fatigue modelling [37].

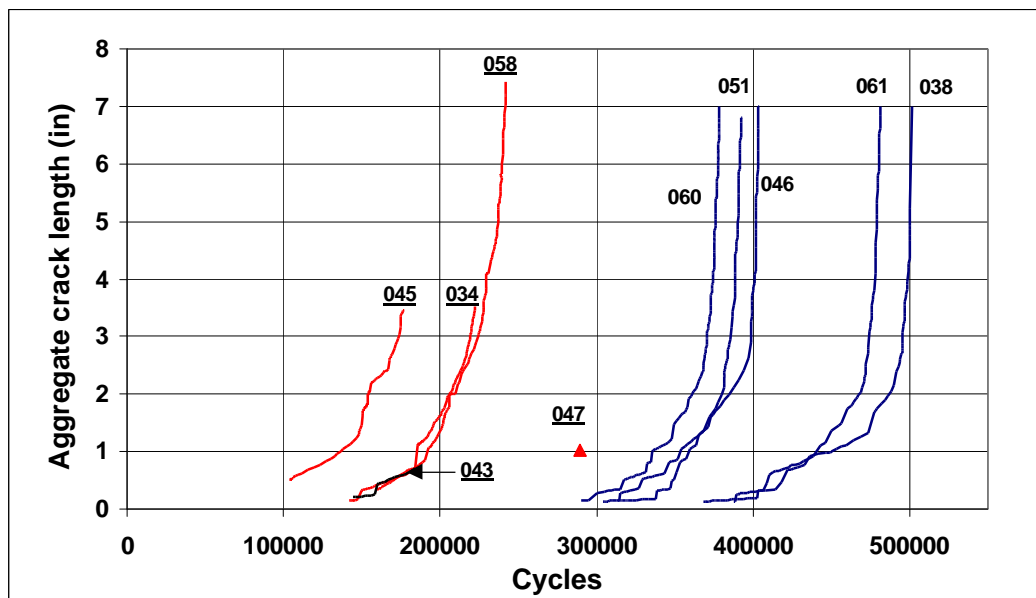


Figure 27. Aggregate crack growth curves from fatigue tests of pre-corroded (serial No. underlined) and non-corroded MSD specimens

The MSD experimental program has included applications development work and new research in several relevant technologies, including NDE of cracks and corrosion, experimental stress analysis, modelling of experimental data, and cost-effective finite element modelling of a fuselage frame-bay/splice for the purpose of tailoring MSD specimens to specific aircraft. Some of these are mentioned elsewhere in this ICAF Review. The work has included an interesting new application of acoustic emission monitoring (AEM) for the detection and monitoring (plotting of crack growth curves) of hidden cracks under rivet heads in collaboration with a Canadian company, Acoustic Emission Monitoring Services Inc [38]. This work is important in view of the current interest in modelling the detailed fatigue and corrosion/fatigue processes in fuselage skin splices.

7.3.2 Risk assessment of fuselage splice joints with multiple site damage

Multiple site fatigue damage (MSD) in a longitudinal skin splice is an important issue to be addressed in dealing with the fatigue life of ageing aircraft. It has been recognised as a major airworthiness problem and has prompted major international research efforts. The NRC/IAR program described in the preceding section generated extensive test data using corroded as well as non-corroded MSD specimens. These data provide the basis for developing analytical prediction models. The test data show that crack development in a MSD environment has characteristics that are quite different from and more stochastic than those related to a single crack situation. It is therefore necessary to use a probabilistic approach to examine and characterise the fatigue behaviour of splices. In the current research on corrosion risk assessment, stochastic models are developed using the MSD specimen test data for the fatigue crack initiation, growth, and link-up characteristics of the splice that could be used in durability and damage tolerance analysis [39].

In the present analysis, all cracks in the specimen at a given moment are treated as one aggregate crack and the splice is considered to have failed when the aggregate crack length (sum of all the crack lengths) reaches a specific value. The first step in the probabilistic analysis for each of the two failure criteria (first linkup and final failure) is to characterise the crack growth of each specimen using growth functions to fit the data of aggregate crack length versus the number of load cycles. Then a crack growth model is established by incorporating a stochastic variable in the equation. All the parameters in the equation are determined from the data calculated using the growth functions. Finally a single growth function involving a stochastic variable is developed in which the initial crack length can either be deterministic or stochastic. Using this equation, various probabilistic effects of MSD are calculated such as the percentiles and the distribution of crack size and, more importantly, the probability of failure at any given time. Figure 28 shows the predicted probability of failure with comparison to the test data from the MSD specimens.

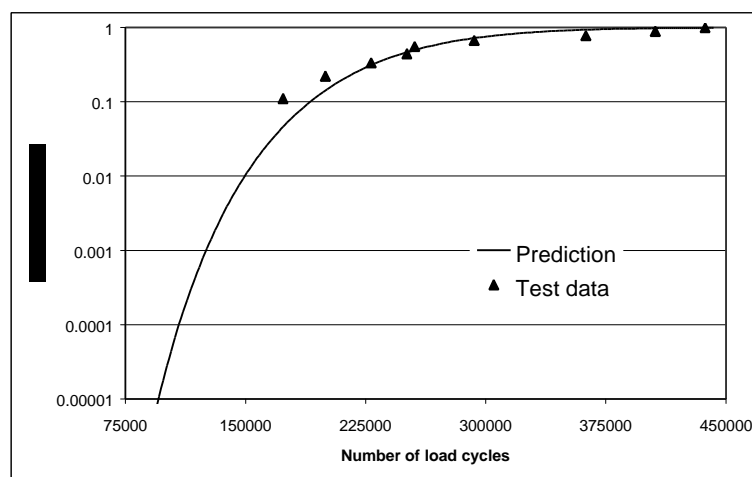


Figure 28. Probability of failure of splice joints with MSD

Sophisticated fracture mechanics analysis for each specimen at every growth stage is not used, and so the approach is less complex than risk analysis using deterministic crack growth prediction and distributed initial flaw sizes. Since all stochastic characteristics are inherently

included in the test data, the model based on the data might also be expected to provide a more reasonable assessment of failure probability. In addition, provided sufficient test data is available, this modelling approach can be used to deal, in a relatively simple manner, with the problems with fatigue and corrosion interactions in splices.

The test data needed for this method of probabilistic analysis of MSD in splices can be obtained from full scale fuselage and panel fatigue tests performed during aircraft certification, but it is preferable that a larger sample of data be obtained using less costly methods such as the MSD specimen concept used in this work.

7.3.3 Analytical and FE modelling of riveted lap joints

The objective of this research is to develop efficient modelling procedures for mechanically fastened composite joints and riveted lap joints in aircraft structure. Both analytical and numerical methods have been investigated. This is challenging work because of the complex geometry and load transfer in the joints. An important consideration about the modelling procedures is to maintain a good balance between accuracy and the computational efficiency.

In analytical modelling, a mixed form complex variational approach has been developed for composite joints containing multiple rivet holes under a unidirectional load [40] and this approach has recently been extended to deal with composite joints under general bi-axial loading conditions [41] [42], as shown in Figure 29. Based on this approach, a computer program has been developed for optimum design of bolted patch repair of composite panels with an elliptical damage hole, as shown in Figure 30.

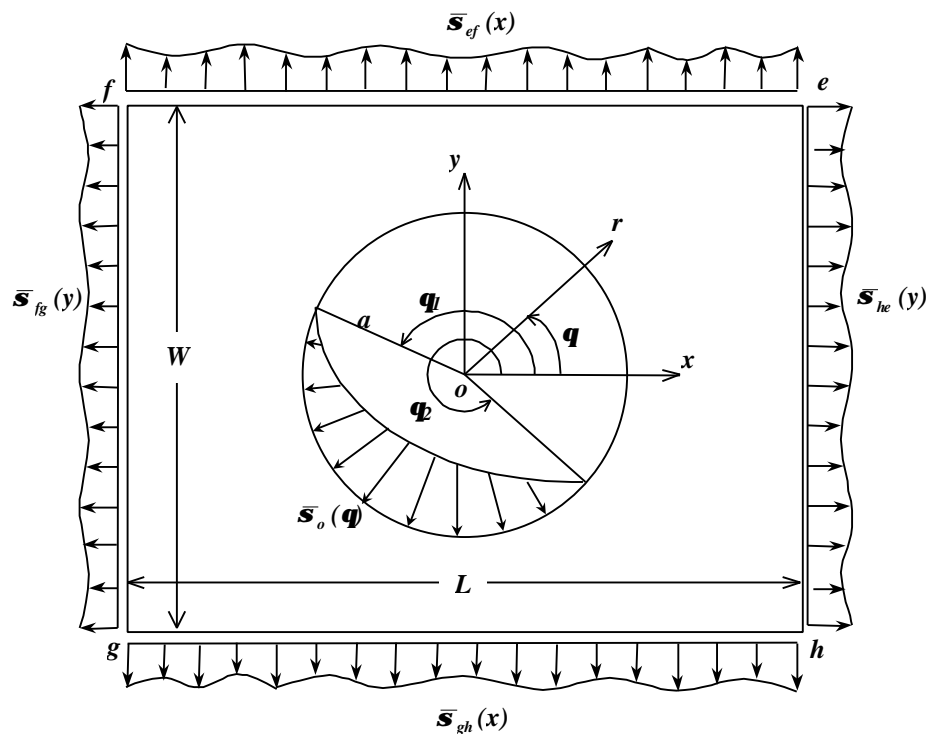


Figure 29. Geometric configuration of a bi-axially loaded joint

In finite element analysis, a two-dimensional modelling technique has been developed for riveted lap joints with relatively complicated geometry and loading conditions. A rivet idealisation was proposed in which the rivet was modelled as an elastic beam with two end disks and the rivet-hole interactions were simulated using gap elements as illustrated in Figure 31 for a four-rivet

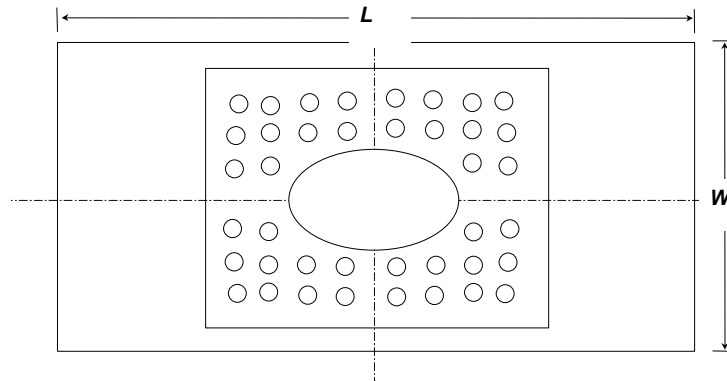


Figure 30. Bolted patch repair of composite panel with elliptical damage hole

joint. The effects of the number of gap elements were examined from the accuracy and computational efficiency points of view [43]. This modelling technique has been used to determine the stress distributions in an MSD specimen [44] [45] and the comparison of results between analysis and test is shown in Figure 32. A detailed discussion on development of the analytical and numerical modelling procedures for lap joints involving single and multiple rivet holes has been prepared [46].

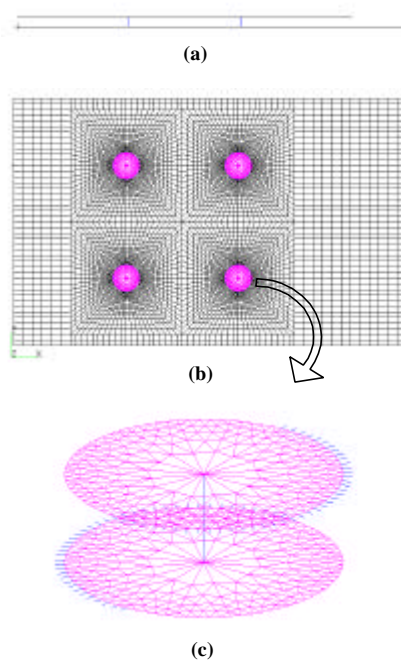


Figure 31. Finite element modelling of a four-rivet joint. (a) front view, (b) top view, and (c) rivet representation.

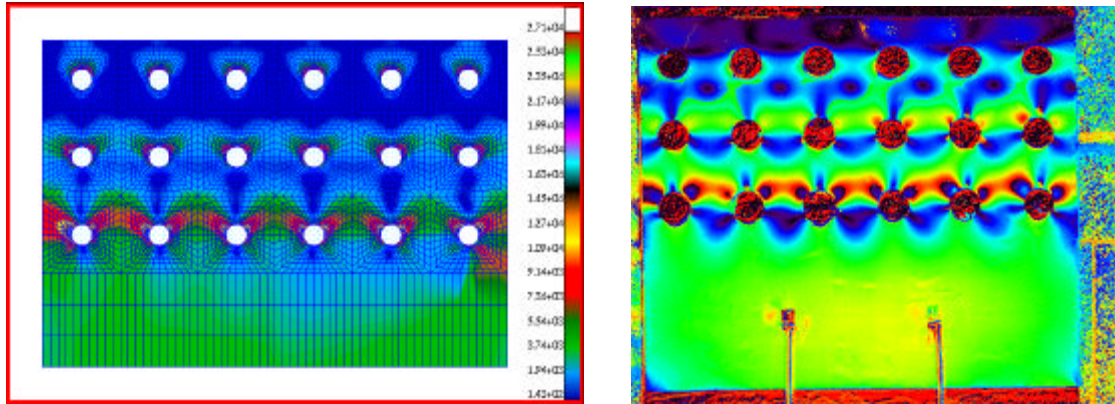


Figure 32. Maximum shear strain in lap joint --- comparison of finite element results and photoelastic measurement

7.3.4 Three dimensional geometrically non-linear finite element model of a lap joint specimen

For the purpose of full-field strain analysis a photoelastic coating is applied to the surface of the target specimen. Fringe patterns result when the strained coating is viewed in polarised light conditions. The use of multiple photoelastic images, if acquired digitally, allows for a quantitative analysis that can be compared to the results of a finite element model.

The method of automated photoelastic analysis presently used at NRC/IAR is a six-image phase stepping approach developed by Patterson and Wang [47] and modified for use with a reflection polariscope [48]. NRC/IAR has developed software that can convert one white-light and six monochromatic digital photoelastic images to pseudo-colour images representing the maximum shear strain and principal strain directions [49]. An application of the analysis is shown below.

The specimen is a simple riveted lap joint of two overlapping 0.040-in (1mm) thick aluminium sheets fastened by three rows of rivets spaced one inch apart. The photoelastic coating covers the overlapping region and an additional 2 inches (50mm) into the far field of the front sheet. Only one-half of the photoelastic coating is shown in, Figure 33. The comparisons of the maximum in-plane shear strains from a photoelastic analysis and those calculated by the finite element two dimensional model described in the previous section was not totally satisfactory. A three dimensional finite element model was generated to model one half of the simple riveted specimens as well as the photoelastic coating. The adhesive layer that bonded the photoelastic coating to the outer skin was not modelled. The FE model was generated using first order brick elements and the material properties used were $E=10,500$ ksi (72.4GPa), $\nu=0.33$ for the skins, $E=10,700$ ksi (73.8GPa), $\nu=0.33$ for the rivets and $E=360$ ksi (2.48GPa), $\nu=0.38$ for the photoelastic coating. Symmetrical boundary conditions were applied to one edge of the model. One end of the model was fixed in all directions while a displacement loading was applied at the opposite end. The results shown in (c) are from the middle of the photoelastic coating. A much better correlation between the model and photoelastic results was obtained at the expense of model complexity and computing time.

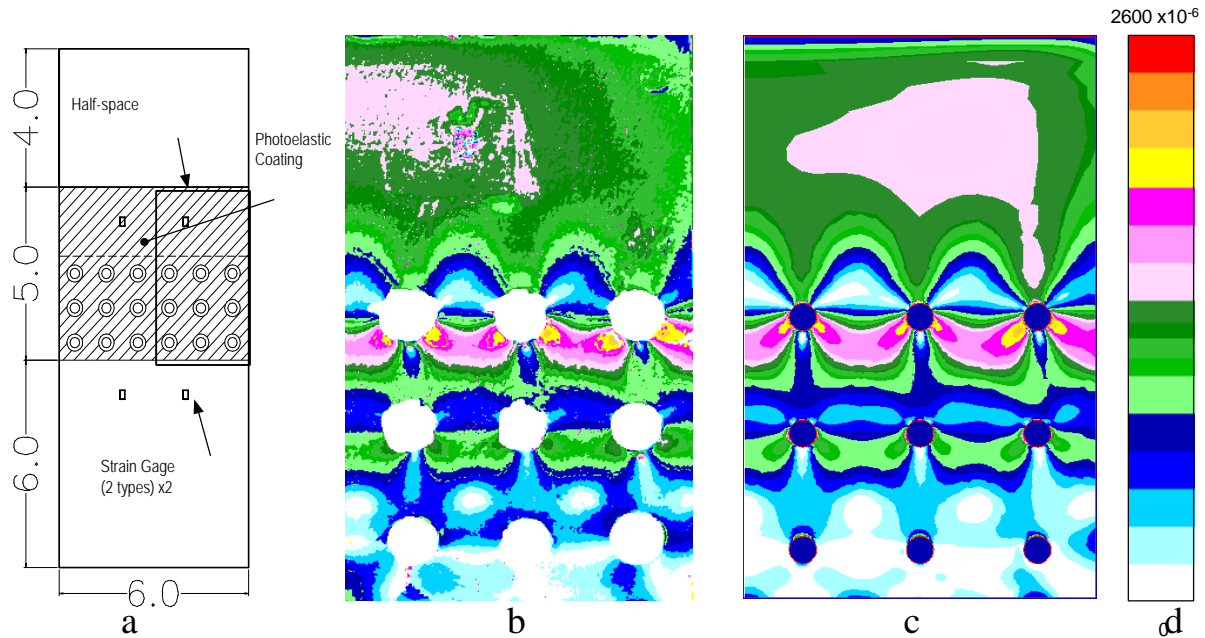


Figure 33. Comparison of photoelastic results and 3D geometrically non-linear FE model

a) Lap joint schematic; b) Photoelastic results; c) FEM results; d) Colour scale

7.4 Retrogression and re-ageing (RRA)

Retrogression and re-ageing (RRA) is a heat treatment process performed on the aluminium alloy 7075 in the T6xxx temper condition to improve its resistance to corrosion, while at the same time maintaining the high strength levels required for aircraft structural applications. For large extruded or forged parts, we have determined that the most practical process involves retrogression at 195 degrees C for 40 minutes, followed by rapid cooling and full re-ageing at 120 degrees C for 24 hours.

NRC/IAR has performed a large number of tests to confirm that this treatment does not adversely affect a variety of mechanical properties including axial fatigue ($R=0$) for which all RRA results were in the scatter band for T6 [50]. It was determined, however, that water quenching after the retrogression step gave better fatigue strengths than forced air quenching. Fatigue crack growth rates (single edge notch specimens) for RRA treatments were consistently better than for the original T6 condition.

7.5 Bonded Patch Repair Technology

7.5.1 Three-dimensional FE modelling of bonded repair of thick section

Analysis work was carried out at NRC/IAR to validate the design of the patch repair which will be used at the X-19 location of the CF18 Y470.5 bulkhead. Analysis work has been conducted with the objectives to: (i) evaluate the effects of the patch stacking sequence and the fibreglass

layer used in the adhesive, (ii) determine the patch efficiency, and (iii) gain confidence in the experimental observations.

Three-dimensional finite element modelling techniques have been proposed for bonded patch repair of thick sections at NRC/IAR [51] [52], using the commercial software packages: MSC/PATRAN and MSC/NASTRAN. In the present work, similar modelling techniques were employed to simulate and analyse the three flat bar specimens tested. Relatively fine meshes of solid elements were used for the three-dimensional analyses. The strains at the positions where the strain gauges were located on the test specimens were compared with those measured in the experiments. A good agreement was achieved between the results of testing and finite element analyses, as shown in Figure 34. The distributions of the maximum shear stress and peel stress in the adhesive and the tensile stress in the substrate were calculated and plotted along the central bondline. In addition to the stress concentrations in the adhesive, the calculated results showed an increase in the tensile stress in the substrate near the patched edge, as shown in Figure 35. This finding provided an explanation for the observed failure mode of the test specimens [53].

In addition to the finite element analysis, closed-form solutions were developed for analysis of bonded composite-to-metal joints subject to axial tensile or compressive load on the substrate [54]. Two joint configurations were considered which simulate bonded composite patch repair for fatigue life enhancement and crack patching. While the metallic substrate is of uniform thickness, the composite patch had a thickness tapered from the central portion to its edges. The model calculates axial forces/stresses in the substrate and patch, shear stress in the adhesive, and peel stresses on the substrate-adhesive and patch-adhesive interfaces. The residual stresses after curing due to thermal mismatch between the substrate and patch are also considered. Based on the stress results obtained and the strength allowables of the joint member materials, the joint failure load is predicted and the failure mode is examined. Eight typical failure modes are considered and the associated safety margins are determined.

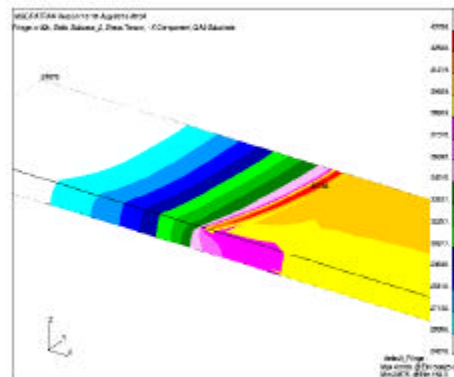


Figure 34. Comparison of strain data at different location of bonded joint

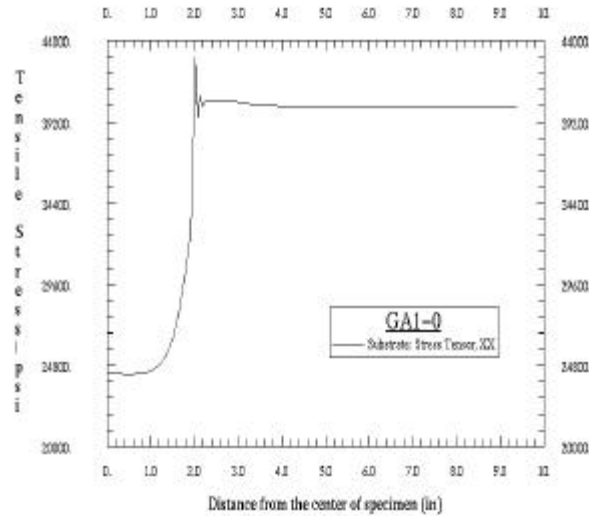


Figure 35. Stress distribution along bondline in substrate of bonded joint

7.5.2 Thick Section Bonded Patch Technology

During the original F-18 full scale fatigue test at McDonnell Douglas, fatigue cracks developed on the Y470.5 wing carry-through bulkhead at the X-19 location. To address the problem, DND tasked NRC and Martec Ltd. to investigate the feasibility of using an adhesively bonded graphite composite three-sided patch to reduce the strain in the affected area. The repair was considered as a fatigue enhancement and was required to delay the onset of a fatigue crack initiation predicted to occur at the lower inside pocket. The composite patch was required to meet a far field limit strain of 3750 microstrain in a corner with a K_t of 1.7. Figure 36 shows the composite repair installed on the FS470.5 bulkhead at the X-19 location. The initial design, testing and processing specification for the patch was carried out by NRC [55, 56]. Martec carried out further design development and numerical analysis. The repair design difficulties were enhanced by the presence of a significant stress gradient through the thickness of the bulkhead flanges and through out-of-plane deflections of the lower flange. The stress analysis conducted involved extensive FEA based methods using the global/local approach, Figure 37. The loads were derived by BADS using full scale fatigue test strain measurements performed at a large number of locations in the affected area [57, 58].

Experimental validation of the patch design was used to:

- to establish a patch stacking sequence that would provide a 30% strain reduction in the underlying aluminium structure,
- to evaluate the candidate design under static loading and fatigue loading, constant amplitude and F-18 spectrum (Figure 38),
- to measure the effect of dry operating temperatures (-29°C , RT, $+60^{\circ}\text{C}$) on the performance of the patch,
- to measure the thermal residual strains in the aluminium structure caused by the 85°C cure cycle,
- to establish a patch failure sequence and a patch failure morphology,

- to evaluate the capability of ultrasonic non-destructive inspection to find patch defects, adhesive disbonds and aluminium substrate fatigue cracks.

Ten ply graphite (Hexcel W3T282-42-F155 prepreg) plain weave fabric patches were investigated. The patches were B-staged and cocured in place with CYTEC FM 73 adhesive. For electrical isolation, a single ply of dry 120 E-glass plain weave fabric was placed between the graphite and the adhesive. Patch efficiency, including thermal effects at +24°C, was measured to be 35 percent. Static and fatigue loading to far field +3750 microstrain tension and -1000 microstrain compression resulted in no patch failures or a decrease in patch efficiency.

Two patches were installed by NRC on the F-18 full scale test currently underway at BDS. Patch performance is being monitored using strain gauges and NDI. Four patches have also been installed on the fuselage used as transition structure for the FT-245 wing test at NRC.

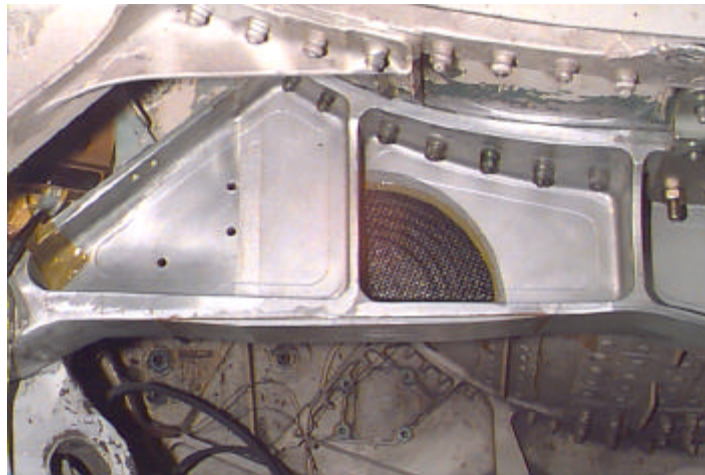


Figure 36. CF18, Y470.5 X-19 Composite Patch

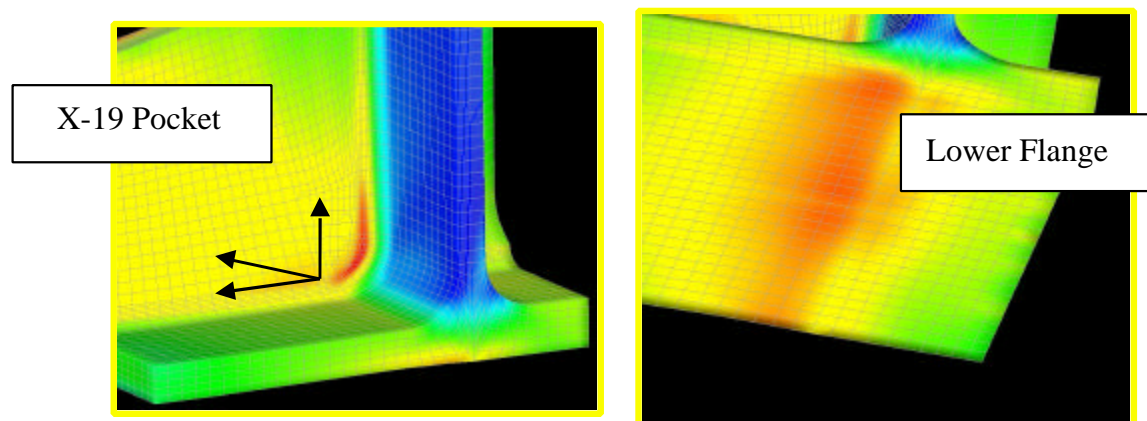


Figure 37. Numerical Analysis Results for X-19 Pocket and Lower Flange

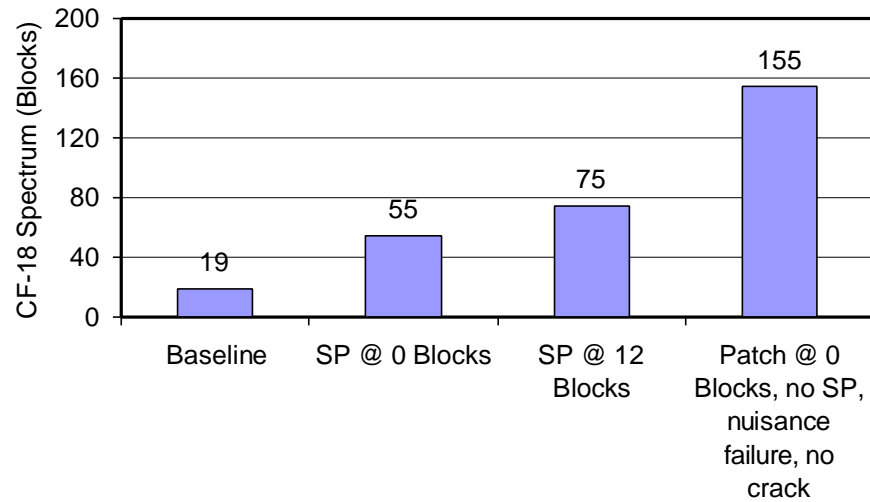


Figure 38. CF-18 Y470.5 X-19 Composite Patch Fatigue Test
Blocks to Crack Initiation (1 Block = 325 SFH), SP (shot peening)

7.5.3 CT114 Tutor Boron Doubler Repair to Lower Wing Skin Damage

Martec Limited was requested to design a composite patch repair and to propose improvements to a Phosphoric Acid Non-Tank Anodising (PANTA) surface treatment process specification provided by the repair contractor.

The lower wing skin damage combined a large wrinkle 0.050" (1.27mm) deep with a 0.008" (.2032mm) material removal at the bottom of the crease. The boron patch repair was considered as a fatigue enhancement. The aim of the repair was to reduce the stress concentration resulting from the crease to that of local stress due to the existing lower wing skin rivet holes. The final repair consisted of a six plies $[0^\circ, \pm 45^\circ]_s$ laminate bonded to the metallic surfaces using three layers of FM73 film adhesive 0.01" of thickness. A vacuum bag co-curing process at 82°C was used to cope with the wing curvature, to minimise the residual thermal strains and to avoid any post cure deformation of the 0.05" (12.7mm) thick lower wing skin. Martec also designed a non-destructive inspection (NDI) specimen with imbedded defects that emulated the repair conditions. The specimen was fabricated to qualify NDI technicians to perform the in-service recurring inspection needed to ensure the integrity of the bond. Stringent quality control procedures that included traveller single lap shear specimens and Boeing Wedge coupons were implemented during the repair installation. Figure 39 shows a drawing of the NDI specimen used to qualify the NDI technician.

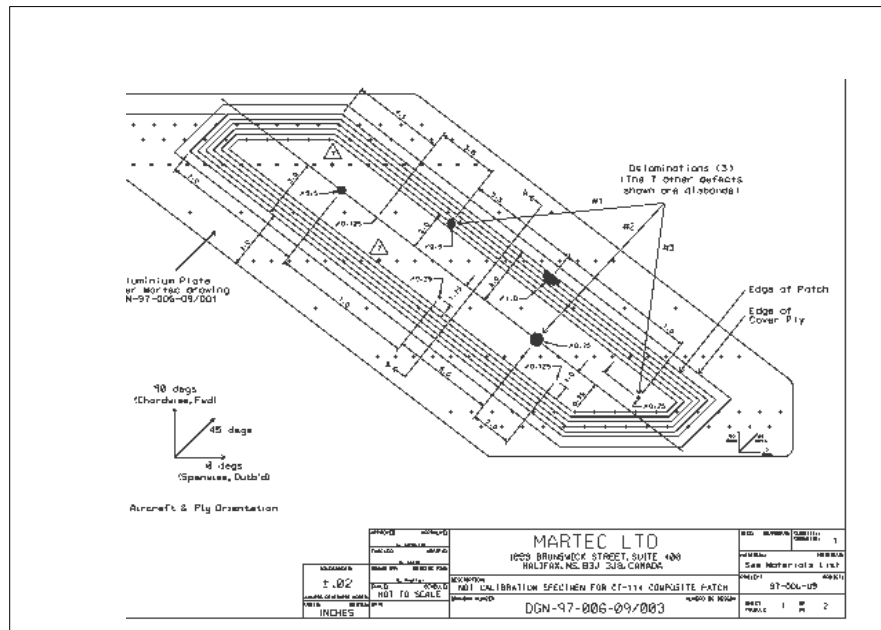


Figure 39. CT114 Repair NDI Specimen

7.5.4 Composite Patch Repair - CC130 Lower Wing Skin

Martec Limited and its sub-contractors were tasked to design, manufacture and install a composite patch to repair fatigue damage to the CC130 lower wing skin. The fatigue damage consisted of a 0.5" (12.7mm) crack originating from a fastener hole at wing station (WS) 85, stringer #23, and running aft towards the rear spar cap. Based on parametric fatigue analysis results, a 25% load transfer through the patch was required to achieve the desired fatigue life enhancement. The final design consisted of a boron/epoxy composite patch bonded to the wing structure using FM-73 film adhesive. Two different installation processes were developed for this specific installation: Phosphoric Acid Non Tank Anodising (PANTA) and Gritblast/Silane/BR127 (GSB), both of which were validated using modified Boeing wedge test coupons. From a cost and performance point of view, the composite doubler repair proved to be more efficient than the proposed classical mechanically fastened aluminium doubler.

7.5.5 Thermal Analysis of Composite Patch Repair

During the bonding process of composite doubler, residual strains in the substrate materials are locked in due to the different Coefficients of Thermal Expansion (CTE) between the composite repair material and the metallic substrate. From a fatigue stand point, these thermal residual strains can reduce the benefits of the repair by increasing the mean stress level, as thermal effects induce tension strains into the metallic substrate. The use of numerical models (FEM) enables the coupling of static design considerations with thermal residual strains in the repair design and analysis, thus providing a better appreciation of the impact of thermally induced strain into the fatigue performance of bonded repair.

As part of a research program into composite patching repair technologies, Martec Limited has conducted research to improve the current methods for the numerical evaluation of thermally induced strain in composite repairs. The objectives of this research were:

- to increase the understanding of thermal residual strains induced by the curing process for real life structures;
- improve on the current FEA technique for the evaluation of thermal residual strains;
- apply the improved methodology to a practical composite repair problem;
- and assess the impact of residual thermal strains on the effective load transfer for a typical repair.

From this research, a new methodology for the evaluation of thermal residual strains was developed and validated using experimental data obtained from laboratory measurements and strain data performed on two full scale aircraft structures (CF18 and CC130), that had composite repair to metallic aircraft structures implemented. This new technique has proven to be highly accurate in the numerical evaluation of thermally induced strains by showing agreement with experimental data to within $\pm 10\%$ accuracy. Technical information in this project is documented in reference [59].

8 EXPERIMENTAL AIRCRAFT

8.1 UTIAS Ornithopter

A full-scale piloted ornithopter shown in Figure 40 is being readied for test flight later this year. The aircraft is being developed by a group headed by J.D. DeLaurier at University of Toronto Institute for Aerospace Studies (UTIAS). The purpose of the project is to develop human piloted engine-powered ornithopter (flapping-wing aircraft). A scaled proof-of-concept model flew successfully in 1991. In 1998, the full-scale ornithopter completed several taxi runs. It accelerated to 80 km/h and the aircraft lifted-off for a full flapping cycle [60].



Figure 40. UTIAS Ornithopter during taxi trials.

A wing spar fatigue test was conducted to support the design. The spar is made of carbon fibre caps and plywood/Kevlar shear web integrally built with the leading edge made of Kevlar epoxy shell with carbon spar. The structure is filled with foam core [60]. The objective of this test was to observe the effects of cyclic loading in the composite spar over a period of 72 hours of simulated flight conditions at 1.05 Hz. The required loads to simulate these flight conditions for Spar #6 are summarised in Table 3 below. Unfortunately, not all four of the load objectives could be met and a compromise had to be reached. The actual loads are given for comparison.

Moments	Required		Actual	
	Up (288 ⁰)	Down (108 ⁰)	Up	Down
Bending ft*lb.(Nm)	2333(3167)	-1011(-1372)	2304(3128)	564.0(765.6)
Twist ft*lb.(Nm)	540.0(733.0)	123.0(167.0)	533.3(724.0)	122.5(166.3)

Table 3: Required and Actual Loads for cyclic loading test

The reason for this compromise was the inability to build a simple test rig that could apply both the positive torque and the negative bending moment in the simulated down stroke. The design team believed that modelling the twisting moment was more important than the negative bending moment. This is based on previous experience in testing of sample spars, which had proved that torsion failures were the most common and usually catastrophic.

The final design of the test rig consisted of two weights attached to the torque arm at the end of the spar by a series of cables and sheaves. The first weight of 94 lbs.(42.7kg) was to generate the moments in the down stroke, with the secondary weight of 220 lbs.(100kg) adding enough moment to reach the upstroke conditions. The pneumatic piston was used to lift the secondary weight, releasing the cable tension. The piston's down-stroke was not powered, but controlled by a vent attached to the exit port. The vent was used to adjust the fall of the secondary weight. Two switches that were wired to the control valve limited the piston's travel. Thus, the air pressure (piston speed) and the vent are used to control the frequency of the test rig. A schematic of the set-up is given below in Figure 41.

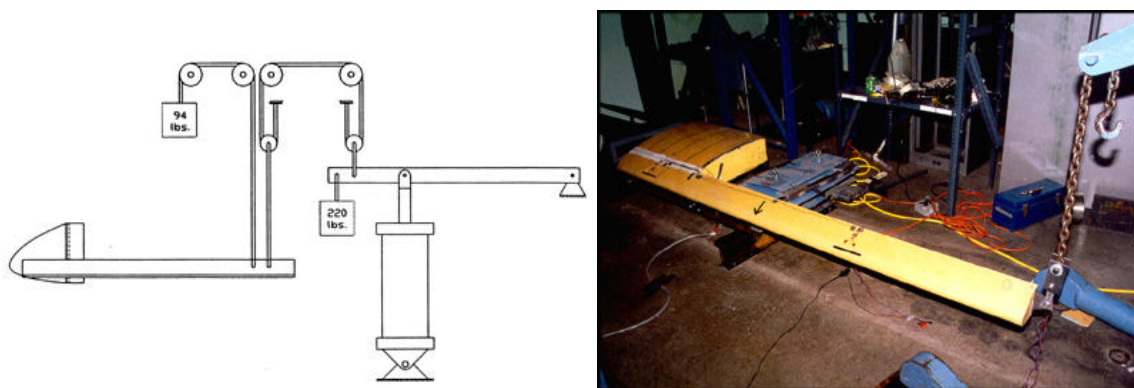


Figure 41. The Cyclic Loading Test Rig schematic and test spar photo.

The progress of fatigue test was initially very slow, as the ¼"(6mm) steel cables repeatedly broke. The causes were determined to be the improper size combination of cable and sheave,

and the heat being generated by friction. An attempted solution included the replacement of the steel cables with a larger one having a ¼"(6mm) diameter and the installation of a new sheaves with bushings. Unfortunately, this did not fully remedy the problem. Only after the installation of a hi-tech rope called TECH12, two high-grade Harken pulleys and small bungee cords did the system work flawlessly. The bungee cords were used to reduce the shock loading within the system. Springs were also added to reduce the swinging of the two weights.

The results of the torsion tests, initially taken every 6 hours, and then every 12 are given below in Figure 42. These tests were performed to monitor the possibility of any changes in the characteristics of Spar #6. The results indicated that the twisting stiffness values remained fairly constant over the test period of 72 hours. This was also supported by the fact that the minor damage, which occurred during the 3.8g proof test, did not worsen or propagate any further.

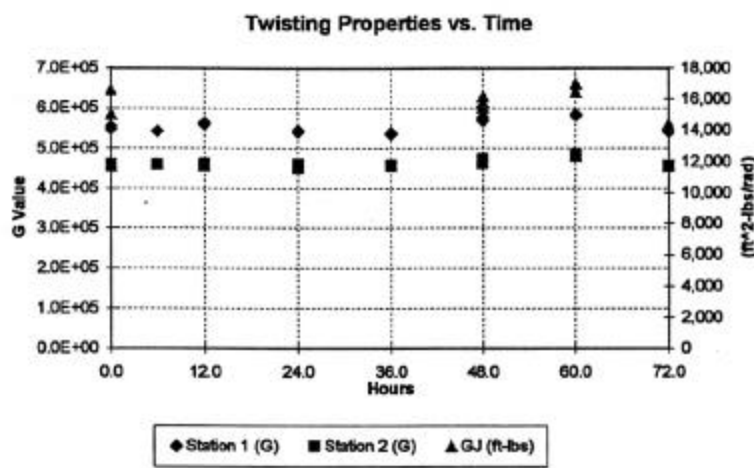


Figure 42. Effects of Cyclic Loading on the Twisting Properties of Spar #6 over 72 hours

9 COMPOSITE MATERIALS AND STRUCTURES

9.1 CF18 Flight Control Surfaces Moisture and Water Ingress

A water ingress problem has been found in CF18 flight control surfaces, with the most affected component being CF18 rudders [61]. To date, 3 US Navy F/A-18's have lost rudders during operations due to this problem. Figure 43a) shows CF18 with an in-service failure due to water ingress that occurred in 1999. Figure 43b) shows the failed rudder next to one which is intact.

This is a potential problem with all control surfaces. At the source of the problem there is evidence of an adhesive failure between the honeycomb and the adhesive (disbond). There was no adhesive found on the honeycomb with the naked eye. In the final overload failure area, there is evidence of a cohesive failure, delamination and peeling. Currently 3 techniques are being used to inspect these components: x-ray (Bombardier) - which is able to find water ingress and corrosion; Neutron Radiography (RMC) - which is able to find water ingress, moisture and corrosion; and, Ultrasonic C-Scan (QETE) - which can detect disbond, water ingress and to some extent moisture. The ultimate goal of the program is to correlate inspection results with residual

strength of the rudder to aid decision making on repair action. As well, it is the intent of the program to determine to what extent water ingress can be tolerated and at what point repair/retirement must be considered. To date there are no design limits or criteria available by which one is able to dispose the structure.

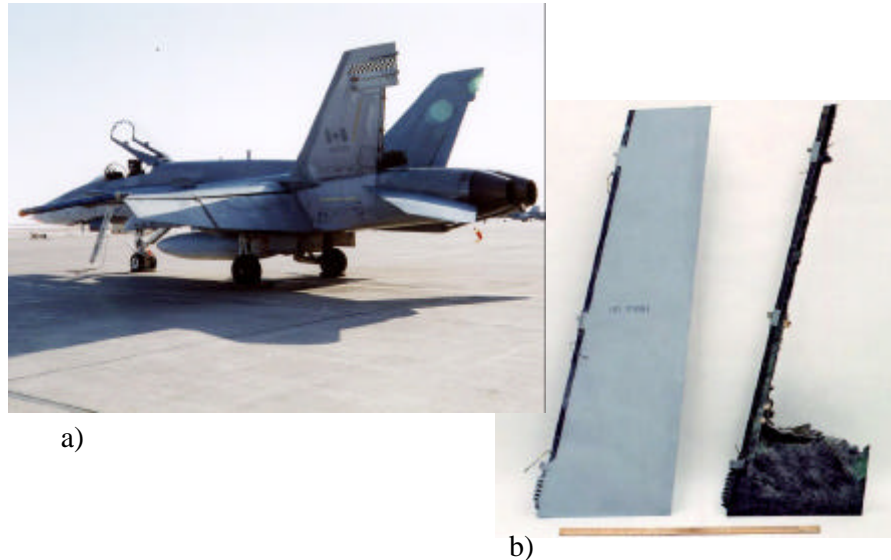


Figure 43. a) Rudder failed in-service, b) intact and failed rudder.

9.2 Field Level Assessment of Low Viscosity Adhesives

QETE has been involved in a co-ordinated effort between the CF and the USN (NADEP) to evaluate 3 two part epoxy adhesive systems. QETE developed the test plan for this task under the Composite Repair Engineering Development Program (CREDP) [62 63 64]. The intent is to determine the performance of time-expired structural repair adhesives and correlate this performance with a simple field level assessment of viscosity. The CF evaluated HYSOL EA956 and EA9396; the USN evaluated HYSOL EA9321. The viscosity measurements were correlated with strength and time at 1 month intervals once a change in viscosity was noted. Storing the adhesives at 100°F (37.8°C) and 140°F (60°C) was used to accelerate ageing. Mechanical testing was conducted at dry/room and wet/elevated temperature conditions using single lap shear and 4 point bed interlaminar shear specimens. Immersing specimens for 48 hours in boiling water simulated the wet condition. Though all adhesive kits were aged in exactly the same manner, there were variations observed between and within batches; however, this did not interfere with the program since the concern was with the symptoms of age, i.e. viscosity, not the age itself. For the EA956 adhesive it was established that ~13 minutes for the adhesive to flow 3 inches (75mm) on the vertical flow test apparatus (with spacer washer, as per ASTM D2202 Test Method for Slump of Caulking Compounds and Sealants) was the maximum allowable to ensure that the minimum single lap shear dry strength of 1600 psi (11 MPa) was maintained. For the EA9396 adhesive, as long as the adhesive could be processed, the minimum single lap shear dry strength of 3500 psi (24 MPa) was obtainable. In this case the corresponding time-to-flow was ~11 minutes. As a result of this test program, the CF18 Structural Repair Manual has set a 10

minute time limit on time-to-flow for both EA956 and EA9396 adhesives as the measure of an acceptable adhesive.

9.3 Shear buckling test and analysis of fibre metal laminates (FML)

Under a collaborative program between NRC/IAR and Bombardier Aerospace Regional Aircraft (de Havilland) on Fibre Metal Laminate (FML) Durability, a test technique for the development of FML shear buckling allowables has been proposed and verified [65 66]. For this task, a picture-frame test fixture and a total of 33 shear panel specimens made of aluminium (baseline) and of fibre metal laminates were designed and manufactured by NRC/IAR. Preliminary test work on three shear panels (Aluminium 2024-T3, ARALL3-3/2, and GLARE3-2/1) was conducted at NRC/IAR. In the preliminary test work, general test procedures were established and the buckling data was collected for the three specimens. To help determine the test procedures, finite element analyses were carried out for the three specimens. A photo-elastic study of the shear buckling test was also carried out to record the buckling shape and the maximum shear strain. The comparison between the results from test and finite element analysis indicated that the finite element model provided reasonably good predictions of the buckling loads. This helped in the establishment of test procedures. It was shown that the test rig can simulate the shear loading condition, but that the panel is not in a pure shear strain state. Figure 44 provides some results of the test and analysis work for shear buckling of a FML specimen.

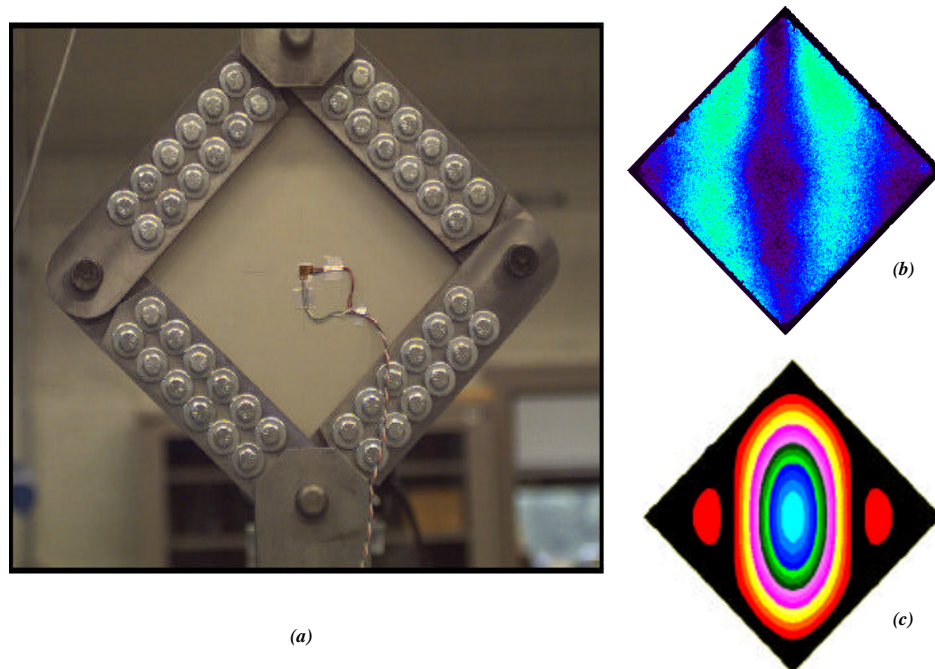


Figure 44. Shear buckling test and analysis of FML panel
 (a) test set-up, (b) photo-elastic image, and (c) finite element analysis

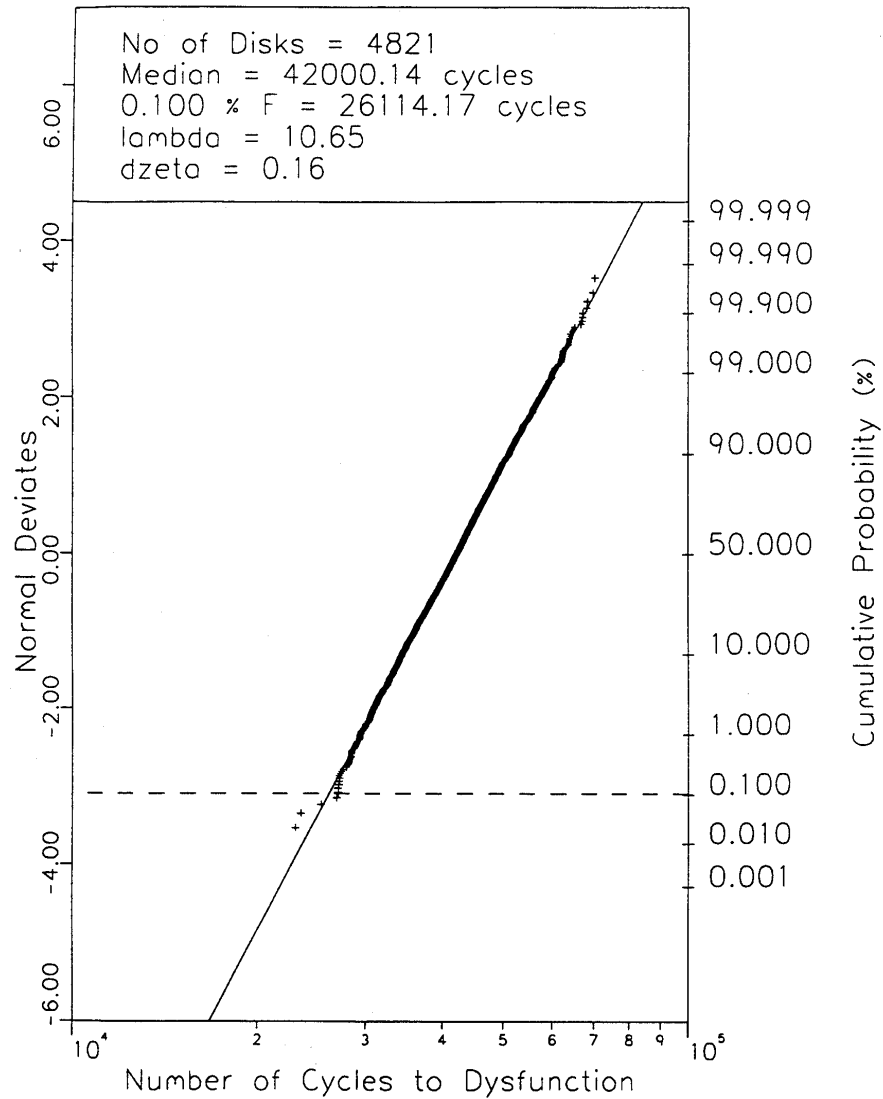
10 GAS TURBINE ENGINES - FATIGUE AND DAMAGE TOLERANCE

10.1 Thermal Fatigue Testing of Nozzle Guide Vanes in the NRC/IAR Burner Rig

In the Canadian Forces, approximately 80% of the Allison T56 first stage nozzle guide vanes (NGV1's) are scrapped during overhaul due to severe thermal fatigue damage in the airfoil. There is a strong incentive to repair these expensive components and return them to service. A number of engine overhaul/repair vendors have developed braze repair processes for these components. The effectiveness of these repairs needs to be assessed before they are implemented in the fleet. In this regard, the NRC/IAR has developed test techniques to evaluate the thermal fatigue resistance of NGV1's in a burner rig [67]. Several burner rig tests have been conducted on new NGV1's and unserviceable parts that were braze-repaired by different vendors. The results show crack initiation sites in the burner rig tested parts are consistent with those in service exposed parts. Typically, initiation occurred near the cooling holes in the airfoils; additional cracks also initiated in the leading edge of the airfoil at the airfoil-outer band junction. In the repaired parts, only some of the brazed repaired cracks re-initiated, the majority of cracks were initiated at new sites. Compared with the new parts, the repaired parts exhibited earlier thermal fatigue crack initiation and faster growth. At the end of a 1300-cycle test, the total length of the cracks in the repaired parts was approximately double that of similar cracks in the new parts. In follow-on work, NGV1's that are coated with thermal barrier coatings will be tested in the burner rig to assess the effectiveness of these coatings in increasing the thermal fatigue resistance of the components.

10.2 Damage Tolerance Assessment of Nene X Turbine Disc

Work on damage tolerance assessment of the turbine disc, the impellor and the shaft of the CF Nene X engine was initiated in 1998. The objectives of the project are to predict a safe inspection interval (SII) for each component and to apply damage tolerance based life cycle management concepts to maintain these critical components in the field. The work on the turbine disc was recently completed. The NRC/IAR deterministic and probabilistic fracture mechanics based damage tolerance algorithms were used to predict a safe inspection interval for the disc and to assess the risks associated with various inspection strategies [68] [69]. It was concluded that the turbine discs could be maintained using damage tolerance based inspection concepts at depot level, Figure 45.



Lognormal Analysis for Safe Inspection Intervals

Figure 45. Log-normal analysis of PFM generated data for Nene-X turbine discs simulating the effect of worst possible scatter in FCGR data and uncertainties associated with the LPI technique

10.3 Damage Tolerance of Modified Waspaloy Disc Material

A project on damage tolerant microstructural design for Modified Waspaloy turbine disc material has been initiated and the microstructural design philosophy developed at NRC/IAR is being adapted to design a damage tolerant microstructure for P/M Ni base turbine disc alloys. Work is focussed on designing microstructures for improving creep strength and short as well as long fatigue crack growth of the material with minimum penalty on the low cycle fatigue crack initiation life. Initial results are very promising.

10.4 Modelling the Crack Tip Elastic-Plastic Field in Anisotropy Crystalline Solids

In the fatigue lifetime assessment of structural materials for use in aero-engines, the period of crack initiation and short crack growth generally accounts for most of the total life. This is especially true for high strength nickel- base superalloys and when the applied stress level is relatively low. Therefore, the determination of short crack growth rates for these and other structural materials is of considerable engineering significance.

The propagation behaviour of long fatigue cracks can be completely described by the linear elastic fracture mechanics based stress intensity factor range ΔK . However, when the crack length becomes small, the crack growth rate may not be appropriately described by ΔK . For the reliable design and life assessment of components that may contain short cracks, it is necessary to take into account the effects of the following microstructural features: (i) anisotropy, (ii) crack tip plasticity, and (iii) grain size. Existing analytical models usually consider only features (ii) and/or (iii). The effects of anisotropy, which is an intrinsic feature of individual grains, have not been considered in past analysis due to the mathematical difficulty associated with the problem. As a result, existing models cannot be applied to some important materials used in aerospace systems, such as titanium alloys or nickel-base superalloys, both of which can exhibit strong anisotropy. Work is underway at NRC/IAR to correct this deficiency.

The work completed to date has considered a crack in either an unbounded or a bounded anisotropic material, as shown in Figure 46. The elastic-plastic analysis is based upon the use of the continuously distributed dislocation theory (CDDT) and the Stroh formalism. A closed form solution for the problem has been obtained for several crack types [70]. The crack tip opening displacement (CTOD) and the energy release rate are explicitly derived. The effects of anisotropy and grain size on crack tip elastic-plastic yields are considered. By comparing the model for an anisotropic medium with that for an isotropic medium, it is shown that the plastic zone sizes are identical in both cases and are independent of the material constants. However, the CTOD and the energy release rate parameter differ for the two cases. The model is thus well suited to describe the effects of anisotropy on short crack growth.

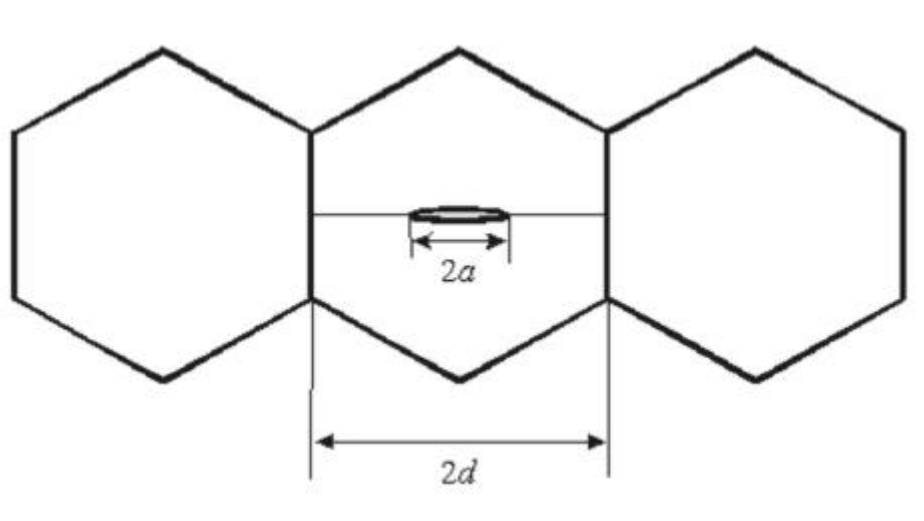


Figure 46. Schematic of a crack-tip slip band blocked by grain boundary

11 NONDESTRUCTIVE INSPECTION

11.1 Development of POD From In-Service NDI Data

The economic drive towards using aircraft beyond their initial design life has created a great interest in damage-tolerance based maintenance. The DT approach relies on routine non-destructive inspections (NDI) and requires that the NDI performance to be quantified in terms probability of detection (POD). The most common approach for determining NDI POD is to perform inspections on representative components or specimens simulating the actual parts. Although this approach is practical, it is very expensive. A more economic approach is to use the actual field inspection data as the basis for determining POD. This requires the accurate determination of the size of the detected crack, the inspection history of the area and a representative crack growth curves. Using this information, hits as well as misses can be determined and from this, the POD can be calculated. The approach is particularly attractive for airframe inspection techniques since most airframe structures cannot be easily or economically simulated for round-robin inspection programs. The POD data are needed to determine the safe inspection intervals in the damage-tolerance maintenance approach.

The NATO Research and Technology Organisation recently conducted a workshop on this topic [71] and an RTO Working Group has been formed to carry this forward. In addition, under auspices of The Technical Co-operation Program (TTCP) and with funding from the Canadian Department of National Defence, an operating assignment is underway to develop POD from in-service data. The objectives of the assignment are: (i) to develop a methodology for the calculation of POD and confidence levels using in-service inspection data and (ii) to use the available data from the field inspections or full-scale fatigue tests for POD development.

To date, in collaboration with the Crosscurrent Research & Policy Consulting LTD., the problems and uncertainties associated with the POD analysis based on field inspection data have been investigated. Also, NDI data available at NRC/IAR from an earlier Tutor full-scale fatigue test and the data available at DND on the CF18 full-scale fatigue test carried out at Bombardier Aerospace Defence Services have been analysed.

11.2 The Edge of Light Technique: Towards Quantitative Enhanced Visual NDI

The Edge of Light[®] (EOL) technique was invented at NRC/IAR and is being applied to the quantitative measurement of surface characteristics [72]. The technique enhances surface topography at a minute scale, which makes possible the detection and measurement of defects such as surface breaking cracks, surface finish, or corrosion. The technique also has forensics applications in the detection of forged or altered documents, fingerprints, and counterfeit currency. Figure 47 shows a comparison of a photograph with an EOL inspection of a section of a Boeing 727 aircraft. Corrosion between layers in the riveted specimen has pushed the layers apart between the rivets, causing a deformation known as pillowing. The EOL technique shows this clearly, and can measure the pillowing and infer the amount of hidden corrosion from this measurement as shown in Figure 48 [73].

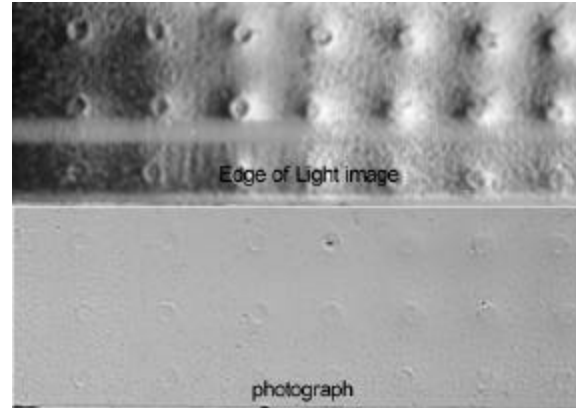


Figure 47. A comparison of an Edge of Light inspection with a photograph of a corroded lap splice joint from a Boeing 727

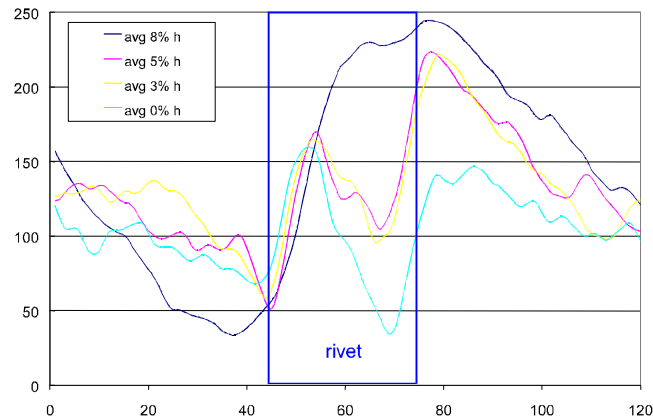


Figure 48. EOL Brightness Profiles: Horizontal Through Rivet Centres

11.3 Probability of Detection of Impact Damage in Composite Structures

The D Sight enhanced visual NDT technique was applied to the inspection of impact damage in composites at NRC/IAR. Recently, a POD study was performed to assess the sensitivity and reliability of D Sight in this application. The results showed that experienced NDI inspectors, some of whom have no training with the D Sight Aircraft Inspection System (DAIS), can achieve very high rates of detection on impact damage sites of 0.025 mm, depending on the roughness of the undamaged background (Figure 49, Figure 50). This is one to two orders of magnitude better than the typical Barely Visible Impact Damage design limits which are in use today, for which the reliability of visual inspections are not substantiated by experimental data [74].

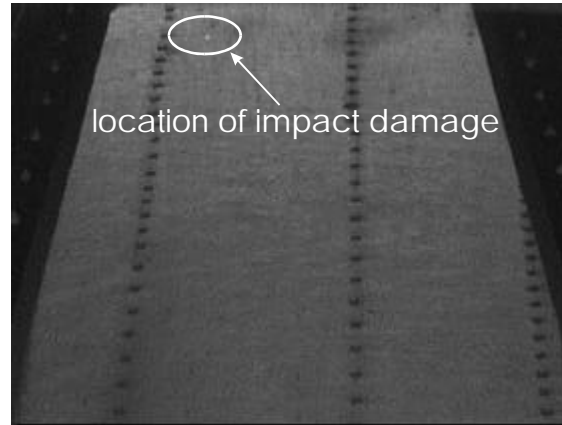


Figure 49. An example of a D Sight inspection of a CF-18 vertical stabiliser, with a 0.001" (0.025 mm) deep impact

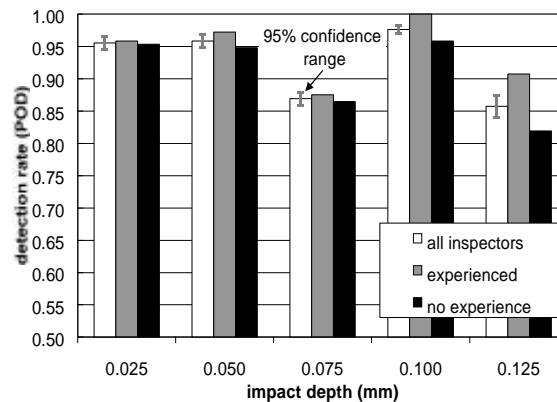


Figure 50. Detection rates for the DAIS 500 inspection of impact damage on a CF-18 vertical stabiliser

11.4 Pulsed Eddy Current Method Development for Hidden Corrosion Detection in Aircraft Structures

Early aircraft corrosion detection and characterisation requires more sensitive and quantitative NDI methods than those available with most conventional techniques. In the case of multi-layered aircraft structures, there is a requirement to accurately measure both the amounts of metal loss and pillowing from the corrosion product while determining the location and extent of damage on each affected layer. The Defence Research and Development Branch and the Royal Military College of Canada within the Department of National Defence (DND) in collaboration with IAR/NRC have initiated a pulsed eddy current (PEC) development activity that addresses these important issues and a unique pulsed eddy current system has been designed for this purpose.

The present capabilities and future potential for characterising corrosion is currently being assessed using both laboratory and actual in-service multi-layered specimens. In each case, the unique features of the time-based pulsed eddy current signals are analysed to detect corrosion in

aircraft fuselage structures and discriminate between the affected layers. Because this method permits a time-based analysis, B-scans and C-scans are also used for both analysis and graphical presentation of the results. The PEC system demonstrates sensitivity to at least 5% total metal loss, or 0.05 mm thinning in the second layer. This method, therefore, offers the ability to discriminate between first or second layer corrosion. The effects of limiting factors, such as lift-off and varying air gaps, are also being investigated. Figure 51 demonstrates good agreement between maps from X-ray and PEC process.

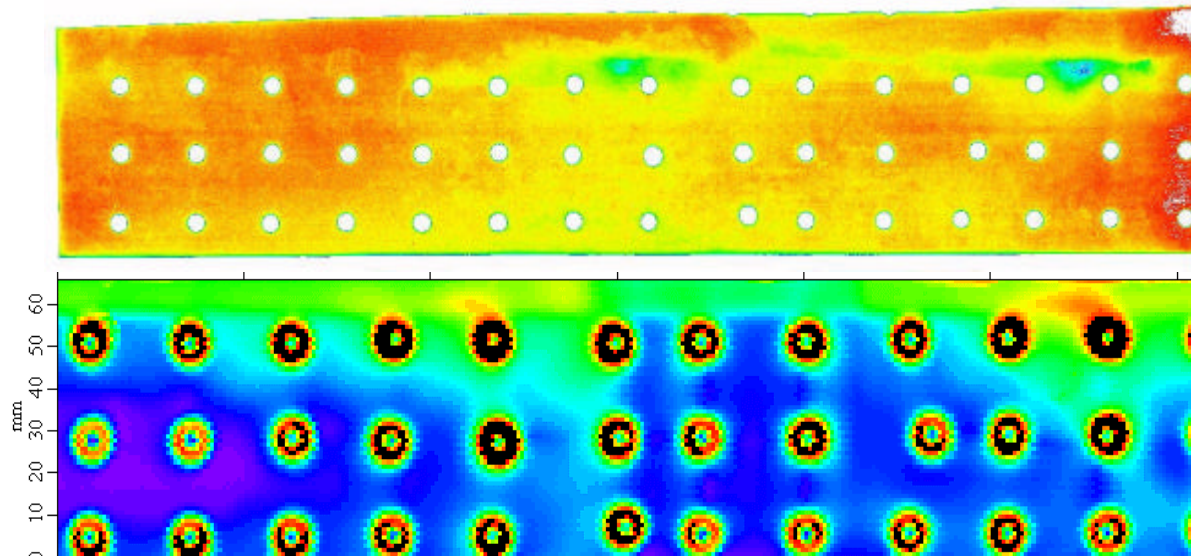


Figure 51: X-ray map (top) and PEC scan (bottom) of corroded lap joint

12 ACKNOWLEDGMENTS

The authors gratefully acknowledge the following individuals and their organizations for contributions without which this review would not be possible:

- DND: Maj. N. Landry DGAETM, Maj J.-F. Leclerc DGAETM, K. McRae CRAD, M. Yanishevsky QETE
- NRC/IAR: N. C. Bellinger, G. Eastaugh, D. Forsyth, A. Fahr, R. Hewitt, R. Holt, J-P Immagerion, A. Koul, A. Merati, C. Poon, M.D. Raizenne, S. Sparling, Y. Xiong
- Industry: P. Trau - AIAC, J. Roussel – Bombardier Aerospace, B. Leigh – Bombardier Aerospace, G. Sinzig – Bombardier Aerospace, M. Perrella – Menasco, R. Eybel - Messier-Dowty, S. Hall – Celeris Aerospace, M. Oore – IMP Aerospace, M. Zgela Martec
- University: J. DeLaurier – UTIAS, P. Straznicky – Caleton U.

We are particularly grateful to Melanie Lambert and Colleen Cameron for their assistance in the preparation of the manuscript.

13 REFERENCES

- 1 R.L. Hewitt, "Full-Scale Aircraft Structural Testing – Sandbags to Simulation", Proceedings of International Conference on Mechanical Testing of Materials and Structures, The Hong Kong University of Science and Technology, October 24-26, 1998.
- 2 R.L. Hewitt, R.J. Hiscocks, G. Bernard, "Load spectrum determination for an aircraft with digital flight control system – CF18 centre fuselage example. CASI Journal, 42(1), 5-9.
- 3 A. Douchant, "Validation of an Analysis Software Program for Fatigue Crack Growth Predictions for Use with the CC130 Hercules Data Analysis System", Quality Engineering Test Establishment, Department of National Defence, QETE Report A008096, June 1997.
- 4 A. Douchant, "Phase II(a): Establishing Inter-Laboratory Correlation, Using Aluminium 7075 T6511 Plate Material, for the CC130 Hercules Data Analysis System", Quality Engineering Test Establishment, Department of National Defence, QETE Report A008096-01, June 1997.
- 5 A. Douchant, "Phase II: Generation of a Fatigue Crack Growth Properties Database and Fatigue Crack Growth Life Predictions Using Aluminium 7075 T6511 and 7075 T73511 Extrusion for the CC130 Hercules Data Analysis System", Quality Engineering Test Establishment, Department of National Defence, QETE Report A008096-02, January 1998.
- 6 A. Douchant, "Phase III: Fatigue Crack Growth Life Predictions Using Aluminium 7075 T6511 Extrusion for the CC130 Hercules Data Analysis System", Quality Engineering Test Establishment, Department of National Defence, QETE Report A020797, July 1998.
- 7 TBD, "Phase IV: CC130 Reanalysis of Fatigue Crack Growth Life Predictions Using the OEM Material Database", Quality Engineering Test Establishment, Department of National Defence, QETE Report A020398, in progress.
- 8 TBD, "Phase V: CC130 Mission Severity Studies / Spectrum Tests for the CC130 Hercules Data Analysis System", Quality Engineering Test Establishment, Department of National Defence, QETE Report A020298, in progress.
- 9 C. DesRochers & R. Govzdic "Transfer Function Development using Neural Network Approach", CASI Conference 1996 Ottawa.
- 10 M. Oore, D. Crocker, "CP140 (P3) STRUCTURAL DATA RECORDING SYSTEM" RTO-MP-7 November 1998 (presented at AGARD Specialist Meeting held in Brussels May 1998).
- 11 S.K. Visvanatha, "A Study on the Use of Neuber's Rule in Fatigue Crack Initiation Predictions", Masters Thesis, Department of Mechanical and Aerospace Engineering, Carleton University, September, 1998.

-
- 12 M. Yanishevsky, "CT114 Safety-by-Inspection Coupon Test Program", Quality Engineering Test Establishment, Department of National Defence, QETE Report A023898, in progress.
 - 13 A.A. Merati, R.T. Holt," Failure Analysis of High Kt and Low Kt Fatigue Coupons from 7050-T7452 Forging", NRC/IAR, LTR-ST-2158, October, 1998.
 - 14 A.A. Merati, R.T. Holt, J. Twidale, "A Metallographic study of Fatigue–Critical Fastener Holes in CF18 Right Hand Front Wing Spar ", NRC/IAR, LTR-ST-2148., September, 1998
 - 15 B. Lefèbvre, B. Benoit, G. Baker and A. Douchant, "CF18 Heavy Weight Outboard Engine Thrust Mount Static Load Test ", Quality Engineering Test Establishment, Department of National Defence, QETE Report A017496, in progress.
 - 16 R. McRae, "CF18 Main Landing Gear Planing Link Bolts - Failure Analysis", Quality Engineering Test Establishment, Department of National Defence, QETE Report A023297, in progress.
 - 17 R. McRae, "CF18 T.E.F. Outboard Hinge/Lug Crack Investigation", Quality Engineering Test Establishment, Department of National Defence, QETE Report A003397, October 1997.
 - 18 B. Lefèbvre, "CF18 Front Spar Fractographic Analysis", Quality Engineering Test Establishment, Department of National Defence, QETE Report A010298, February 1999.
 - 19 L. Sorensen, "CF18 LAU 7 Missile Launcher Crack Assessment", Quality Engineering Test Establishment, Department of National Defence, QETE Report A005798, September 1998.
 - 20 M. Roth, "Failure Investigations of PH 13-8 Mo Aircraft Components", Quality Engineering Test Establishment, Department of National Defence, QETE Report H010198, December 1998.
 - 21 R. McRae, "CC130 Longeron Attachment Fitting Crack Investigation", Quality Engineering Test Establishment, Department of National Defence, QETE Report A024296, in progress.
 - 22 R. McRae, "CC130 Strut Web, and Bulkhead Failure Investigation", Quality Engineering Test Establishment, Department of National Defence, QETE Report A006697, in progress.
 - 23 K. Lemke, "CC130 FS Extrusion Ring Segment Failure Investigation", Quality Engineering Test Establishment, Department of National Defence, QETE Report A023397, March 1998.
 - 24 A.L.M Abdel-latif, "Failure Investigation of RH T-Bow Beam Fitting of CC130 Aircraft", Quality Engineering Test Establishment, Department of National Defence, QETE Report A012396, February 1997.
 - 25 K. Lemke, "CC130 Rear Spar Web Fatigue Damage Assessment", Quality Engineering Test Establishment, Department of National Defence, QETE Report A013897, July 1998.

-
- 26 J. Schwemler, "CP140 Nose Landing Gear Actuator Failure Investigation", Quality Engineering Test Establishment, Department of National Defence, QETE Report A027397, June 1998.
 - 27 K. Sander, "CH12437 Pylon Assembly Failure", Quality Engineering Test Establishment, Department of National Defence, QETE Report A015796, January 1998.
 - 28 L. Sorensen, "Failure Investigation of a CH124 Sea King T58 Engine Mount", Quality Engineering Test Establishment, Department of National Defence, QETE Report A003498, September 1998.
 - 29 J. Schwemler, "CC142 Main Wheel Failure Investigation", Quality Engineering Test Establishment, Department of National Defence, QETE Report A002698, July 1998.
 - 30 K. Sander, "CT114 Tutor Wing Cracks", Quality Engineering Test Establishment, Department of National Defence, QETE Report A022097, in progress.
 - 31 C. L. Brooks, D.L. Simpson, "Integrating Real Time Age Degradation Into the Structural Integrity Process", NATO-RTO Air Vehicle Technology Panel Workshop on Fatigue in the Presence of Corrosion, Corfu, Greece, 7-8 October, 1998, in "Fatigue in the Presence of Corrosion", RTO meeting proceedings 18, March 1999.
 - 32 J.P. Komorowski, N.C. Bellinger and R.W. Gould, "The Role of Corrosion Pillowing in NDI and in the Structural Integrity of Fuselage Joints", Proceedings of the 19th Symposium of the International Committee on Aeronautical Fatigue, Edinburgh, 16-20, June 1997.
 - 33 N.C. Bellinger, J.P. Komorowski and R.W. Gould, "Damage Tolerance Implications of Corrosion Pillowing on Fuselage Lap Joints", Journal of Aircraft, Vol. 35, No. 3, May-June, 1998, pp. 487-491.
 - 34 J.P. Komorowski, N.C. Bellinger and R.W. Gould, "Local Stress Effects of Corrosion in Lap Splices", NATO-RTO Air Vehicle Technology Panel Workshop on Fatigue in the Presence of Corrosion, Corfu, Greece, 7-8 October, 1998, in "Fatigue in the Presence of Corrosion", RTO meeting proceedings 18, March 1999.
 - 35 N.C. Bellinger, J.P. Komorowski and R.W. Gould, "Corrosion Pillowing Cracks in Fuselage Joints", Proceedings of the Second Joint NASA/FAA/DoD Conference on Aging Aircraft, Williamsburg, Virginia, 31 August-3 September, 1998.
 - 36 G.F.Eastaugh, A.A.Merati, and D.L.Simpson, P.V.Straznicky, J.P.Scott, R.B.Wakeman, and D.V.Krizan, "An Experimental Study of Corrosion/Fatigue Interaction in the Development of Multiple Site Damage in Longitudinal Fuselage Skin Splices", NATO-RTO Air Vehicle Technology Panel Workshop on Fatigue in the Presence of Corrosion, Corfu, Greece, 7-8 October, 1998, in "Fatigue in the Presence of Corrosion", RTO meeting proceedings 18, March 1999.

-
- 37 G.F.Eastaugh, A.A.Merati, and D.L.Simpson, P.V.Straznicky and D.V.Krizan, "The Effects of Corrosion on the Durability and Damage Tolerance Characteristics of Longitudinal Fuselage Skin Splices", 1998 USAF Aircraft Structural Integrity Program Conference, San Antonio, 1-3 December 1998.
- 38 S.L. McBride, J.P. Scott, G.F. Eastaugh, "Use of Acoustic Emission Monitoring to Detect, Locate and Measure Multiple Site Damage (MSD) Fatigue Crack Growth Underneath Rivet Heads", Second Joint NASA/FAA/DOD conference on Aging Aircraft, Williamsburg, 31 August - 3 September 1998.
- 39 Y. Xiong and G. Shi, "Stochastic crack growth model for failure prediction of fuselage splice joints with multi-site damage", LTR-ST-2152, NRC/IAR, 1999.
- 40 Y. Xiong, "An analytical method for failure prediction of multi-fastener composite joints", International Journal of Solids and Structures, Vol. 33, pp. 4395-4409, 1996.
- 41 Y. Xiong and C. Poon, "Stresses around a Bi-Axially Loaded Fastener Hole in a Laminate of Finite Geometry", Journal of Thermoplastic Composite materials, Vol. 11, 1998.
- 42 Y. Xiong, "A Stress Analysis Method for Bi-Axially Loaded Fastener Hole in Finite Composite Laminate", ASME Journal of Applied Mechanics, Vol. 65, No. 3, pp. 787-789, 1998.
- 43 O.K. Bedair and Y. Xiong, "Finite Element Modelling of Riveted Composite Joints using MSC/PATRAN and MSC/NASTRAN", LM-ST-831, NRC/IAR, December 1998.
- 44 O.K. Bedair, Y. Xiong, G. Eastaugh and C. P. Martinez-Cerbu, "A Finite Element Modelling Approach for Riveted Joints in Aircraft Structures", presented at the 11th Canadian Symposium on Aerospace Structures and Materials, the 45th CASI Annual Conference, Calgary, May 1998.
- 45 O.K. Bedair, G. Eastaugh and Y. Xiong, "Finite Element Models of Fuselage Frame-Bay with Longitudinal Splice in Challenger Aircraft", to be published as a Laboratory Report, NRC/IAR 1999.
- 46 Y. Xiong and O.K. Bedair, "Analytical and Finite Element Modelling of Riveted Lap Joints in Aircraft Structure", *AIAA Journal*, Vol. 37, No. 1, pp. 93-99, 1999.
- 47 E.A. Patterson, and Z.F. Wang, (1991) "Towards full field automated photoelastic analysis of complex components", *Strain*, Vol.27 (May), pp. 49-56.
- 48 S.A. Sparling, J. Gagnon, and J.P. Komorowski, "Photoelastic analysis by 6-image phase stepping with RGB input ", LTR-ST-2154, NRC/IAR (1999).
- 49 D.V. Krizan, and S.A. Sparling, "A photoelastic study of a multiple site damage (MSD) specimen and a simple riveted lap joint (SRLJ)", LTR-ST-2197, NRC/IAR (1999).

-
- 50 R.T Holt, M.D. Raizenne, W. Wallace, D.L. DuQuesnay, "RRA Heat Treatment of Large Al 7075-T6 Components", Proceedings of NATO/RTA AVT Panel meeting on "New Metallic Materials for the Structure of Ageing Aircraft", Corfu, Greece, 19-23 April 1999.
- 51 Y. Xiong, "Three Dimensional Analysis of X-19 Specimen", IAR LM-ST-810, Institute for Aerospace Research, National Research Council, October 1997.
- 52 Y. Xiong and M.D. Raizenne, "A Global-Local Three Dimensional Finite Element Modelling Approach for Bonded Patch Repair of Thick Sections", CASI J., Vol. 43, No. 4, December 1997.
- 53 G. Shi, Y. Xiong and M.D. Raizenne, Finite Element Modelling and Analysis of Flat Bar Specimens for Composite Repair, LTR-ST-2172, NRC/IAR, October 1998.
- 54 Y. Xiong, "An Analytical Model for Stress Analysis and Failure Prediction of Bonded Joints with Tapered Edges", Transactions of the Canadian Society for Mechanical Engineering, Vol. 22, No. 2, 1998.
- 55 D. Raizenne, N. Roohi, M. Sova, M. Brothers "Experimental Verification of Graphite Composite Three-Sided Patches for CF-18 IFOSTP FT55 Y470.5 Bulkhead X-19 Location Progress Report 1", NRC LTR-ST-2127, February 1998
- 56 D. Raizenne, N. Roohi, G. Shi, "Experimental Verification of Graphite Composite Three-Sided Patches for CF-18 IFOSTP FT55 Y470.5 Bulkhead X-19 Location Progress Report 2", NRC LTR-ST-2179, March 1999.
- 57 J. Eiblmeier, "Design and Analysis of a Composite Reinforcement for the CF-18 FSY470.5 Bulkhead", CASI Conference 1998 Calgary.
- 58 J.F. Leclerc, "X-19 Structural Reinforcement Detailed Design and Analysis", TRM Meeting 1998 Australia.
- 59 J.F. Roberge, J. Eiblmeier, M. B. Zgela, "Thermal Analysis of Composite Repair to Metallic Aircraft Structure" Martec TR-98-17, October 1998
- 60 J.D. Delaurier, "The development and testing of a Full-Scale Piloted Ornithopter", CASI Journal, Vol. 45, No.2, June 1999, pp. 72-82
- 61 M. Montambeault, "CF18 Rudders Evaluation", Quality Engineering Test Establishment, Department of National Defence, QETE Report A017496, in progress.
- 62 A. Savard, "Development of a Field Level Material Test Method for Two Part Low Viscosity Adhesives EA9396", Quality Engineering Test Establishment, Department of National Defence, QETE Report A018895, November 1998.

-
- 63 A. Savard, "Development of a Field Level Material Test Method for Two Part Low Viscosity Adhesives EA956", Quality Engineering Test Establishment, Department of National Defence, QETE Report A018795, March 1998.
- 64 O. Nespoli and A. Savard, "Test Plan for the Qualification of a Field Level Material Test Method for Rapid Assessment of Two-Part Low Viscosity Adhesives, Quality Engineering Test Establishment, Department of National Defence, QETE Report A018695, June 1996.
- 65 G. Shi and Y. Xiong, Finite Element Analysis for Shear Buckling of Fiber Metal Laminates, LM-ST-830, NRC/IAR, Ottawa, November 1998.
- 66 G. Shi, Y. Xiong, S. Sparling, and G. Elliott, "Shear Buckling Test and Analysis of Fiber Metal Laminates", LTR-ST-2167, NRC/IAR, Ottawa, January 1999.
- 67 P. Au, J-P. Immarigeon, A.K. Koul, "Test methods for evaluating the mechanical properties and durability of gas turbine materials, repairs and coatings", Keynote address, International Conference on Mechanical Testing of Materials & Structures, The Hong Kong University of Science & Technology, Hong Kong, Oct 24-26, 1998.
- 68 A.K. Koul, W. Beres, S. Cheng, R. He and X-J Wu, "Predictions of the Slls for the Nene X Turbine Disc", IAR-NRC Report, LTR-ST-2142, July 1998.
- 69 S.M. Cheng, W. Beres, A.K. Koul, R. He and X-J Wu, "Fracture Mechanics Analysis of the Nene X Engine Turbine Disc", Submitted to Eng. Frac. Mechanics J, 1999.
- 70 W. Deng, A.K. Koul, and J.-P. Immarigeon, "Modeling the crack tip elastic-plastic field in anisotropic crystalline solids", NRC/IAR Internal Report, 1998 (to be submitted to International Journal of Fracture).
- 71 Airframe Inspection Reliability under Field/Depot Conditions, NATO RTO MP-10, AC/323(AVT)TP/2, November 1998
- 72 D.S. Forsyth, J.P. Komorowski, A. Marincak, R.W. Gould, "The Edge Of Light Enhanced Optical NDI Technique", CASI J. vol. 43 No. 4, December 1997, pp. 231-235.
- 73 D.S. Forsyth, J.P. Komorowski, R.W. Gould, A. Marincak, "Automation of Enhanced Visual NDT Techniques", Canadian Society for NDT, 1st Pan American Conference for Nondestructive Testing, Toronto, ON. September 1998. Also published in: NDT.net - January 1999, Vol.4 No.1
- 74 D.S. Forsyth, R.W. Gould, and J.P. Komorowski, "Double Pass Retroreflection Versus Visual Inspection Of Impact Damage In Composites", NATO/RTO Workshop on Airframe Inspection Reliability Under Field/Depot Conditions, Brussels, May 13-14 1998.

REVIEW OF AERONAUTICAL FATIGUE INVESTIGATIONS IN ISRAEL

APRIL 1997-MARCH 1999

**A. Berkovits
Faculty of Aerospace Engineering
Technion-Israel Institute of Technology
Haifa 32000, Israel**

SUMMARY

The review summarizes fatigue and fracture mechanics work in Israel. It includes contributions from Israel Aircraft Industries, Ltd. (IAI), Israel Air Force (IAF), Tel Aviv and Ben Gurion Universities and Technion-Israel Institute of Technology.

Prepared for presentation at the 26th ICAF Conference

Seattle, 12 and 13 July, 1999

TABLE OF CONTENTS

11.1 INTRODUCTION

11.2 STRESS INTENSITY FACTORS

- 11.2.1 3D P-Version Finite Element Stress Intensity Analysis of Repaired Structure (A. Brot, IAI)
- 11.2.2 Stress Distribution and Stress-Intensity Factor for a Preloaded End-Pad (A. Brot, IAI)
- 11.2.3 Notch at a Bonded Joint (L. Banks-Sills, Tel Aviv University)
- 11.2.4 Interface Fracture at Butt Joints (L. Banks-Sills, Tel Aviv University)
- 11.2.5 Generalized Thermal Stress Intensity Factors in 2-D Domains
(Z. Yosibash, Ben Gurion University)
- 11.2.6 Edge Singularities in Elastic Anisotropic Three-Dimensional
Domain (Z. Yosibash, Ben Gurion University)
- 11.2.7 Stress Intensity Factors for Multiple Cracks in Pressurized Thick Cylinders
(M. Perl, Ben Gurion University)

11.3 FAILURE PREDICTION AND RELIABILITY

- 11.3.1. Probabilistic Failure Analysis by Simulation (A. Brot, IAI)

11.4 AIRCRAFT PROJECTS

- 11.4.1 Galaxy Executive Jet (A. Brot, IAI)
 - 11.4.1.1 Cabin Window Fatigue and Damage-Tolerance Test
 - 11.4.1.2 Full-Scale Fatigue Test
 - 11.4.1.3 Empennage Fatigue and Damage-Tolerance Test
 - 11.4.1.4 Main Landing-Gear Fatigue Test
 - 11.4.1.5 Nose Landing-Gear Landing-Impact, Fatigue Load-Spectrum
- 11.4.2 F-5 Structural Upgrades (A. Brot, IAI)

11.5 COMPOSITES

- 11.5.1 Composite Repair of Aging Aircraft - Brite-Euram Research Program (A. Brot, IAI)
- 11.5.2 Composite Repair of a Metallic Spar (A. Brot, IAI)
- 11.5.3 CH53 Helicopter Battle Damage Repair (A. Brot, IAI)
- 11.5.4 Development Program for Designing Primary Structures from GLARE
Material (A. Brot, IAI)

11.6 JOINTS AND MATERIALS

- 11.6.1 Fatigue Damage Healing by a Laser Surface Treatment (E. Altus, Technion)
- 11.6.2 Effect of Prestrain on Fracture Toughness (L. Banks-Sills, Tel Aviv University)

11.7 SMART STRUCTURES AND HEALTH MONITORING

- 11.7.1 Health Monitoring of Airborne Structures Using Optical Fiber Sensors (A. Brot, IAI)
- 11.7.2 Corrosion Detection (A. Brot, IAI)
- 11.7.3 Vibratory Methods of Health Monitoring in Smart Structures (A. Berkovits, Technion)

11.8 REFERENCES

FIGURES 1-21

11.1 INTRODUCTION

The Israel National Review summarizes R&D work pursued by fatigue and fracture mechanics organizations in Israel in the two years since the last Review [1]. Material for the Review was gathered from:

Israel Aircraft Industries, Ltd. (I.A.I.)
 Israel Air Force (IAF)
 Technion-Israel Institute of Technology
 Tel Aviv University
 Ben Gurion University

The source of the material is acknowledged in brackets after the title of each subsection. (Work submitted by IAI also includes the contributions of S. Afnaim, E. Blass, A. Brot (editor), D. Chester, S. Girshovich, Z. Granot, I. Kressel, V. Krylov, A. Nathan, U. Sol and M. Zeidman.)

11.2 STRESS INTENSITY FACTORS

11.2.1 3D P-Version Finite Element Stress Intensity Analysis of Repaired Structure (A. Brot, IAI)

A paper was presented at the Second NASA/FAA/DoD Conference on Aging Aircraft in Williamsburg, Virginia [2] regarding a fast, simple and relatively accurate method for calculating the effect of a composite material repair bonded to metallic parent structure. P-version, three dimensional, parametric, finite-element analysis was used to calculate load transfer to the composite material repair as well as stress intensity factors for cracks in the parent metallic structure. Cracks at cutouts under composite patches were also analyzed. The parametric nature of the model permitted changing of geometry or crack size with ease.

Aspects of the work which were presented in the paper include:

- Solutions for both a center crack and for a crack at a cutout under a composite patch.
- Finite element analyses (energy method and displacement extrapolation method) to calculate K_I for a crack under the composite patch.
- Parametric modeling in order to isolate the dominant factors of composite patch design.
- Simple modeling of complex problems, a consequence of p-version finite element procedures.
- Calculation of residual stresses due to difference in thermal expansion coefficient between the patch and aluminum.
- Typical application: Composite patch over cutout on fighter aircraft front spar.

Figure 1 shows the result of a parametric study, and presents the normalized stress intensity plotted vs. normalized crack size for various ratios of plate stiffness to patch stiffness. As expected, the stress intensity in the cracked parent material decreases as the relative stiffness of the patch increases.

Another interesting observation is the nearly constant stress intensity factor, K , as a function of crack size, a . This is consistent with results reported using the Rose model developed in [3] and [4].

11.2.2 Stress Distribution and Stress-Intensity Factor for a Preloaded End-Pad (A. Brot, IAI)

A longitudinal crack was found in a fuselage fitting of a fighter aircraft, in the bore of a fastener hole. In this structure two segments of longeron are fastened together by back-to-back end-pad fittings, by a single preloaded bolt. The crack was aligned along the bore of the end-pad hole, as is shown in Fig. 2. Since the fitting could not be repaired, it was decided to replace the entire longeron. In order to allow the aircraft to continue to fly until the replacement longeron could be obtained, a fracture mechanics analysis of the fitting was performed to determine the critical crack size and to establish aircraft limitations corresponding to flight safety.

A fail-safe analysis of the aircraft was first performed. It was assumed that one longeron was totally failed and forces were obtained for the remaining longerons. On this basis, it was determined that the aircraft could fly safely, with the vertical load-factor limited to three, even with a totally failed longeron.

The stress field in the end-pad fitting was analyzed. A finite-element model of the fitting was built which accounts for the influence of the mating part of the longeron on the fitting considered, as well as the influence of the preloaded bolt. Calculations were performed using Stress Check[®], which utilizes high precision, p-version finite-elements and is designed especially to solve problems of fracture mechanics. The distribution of the circumferential stresses around the hole of the fitting is shown in Fig. 2.

The analysis of the cracked fitting was performed using the finite-element model of the fitting. Stress-intensity factors for the radial crack in the circular plate under bending were determined, as a function of the crack length and the load factor. The critical crack length for the given load factor, as well as maximum allowable load-factor for a given crack length, were obtained. On this basis, it was confirmed that the aircraft could operate safely, under controlled limitations, until the replacement longeron could be obtained.

11.2.3 Notch at a Bonded Joint (L. Banks-Sills, Tel Aviv University)

The stress intensity factors of the bimaterial notch are important in many applications in which bonded parts are employed. In recent work two methods were developed for determining the stress intensity factors for elements in which two linear elastic, homogeneous wedges are edge-bonded to one another (Fig. 3). The analyses include (1) an influence function method, which yields an analytic solution for infinite geometries [5], and (2) use of conservative integrals, together with numerical methods for finite geometries [6].

For the geometry in Fig. 3 the stresses at the intersection between the interface and free surface are generally singular, the singularity depending upon material properties and the notch angles θ_1 and θ_2 . Thus, the stresses in this neighborhood behave as

$$\sigma_{ij} \sim \frac{K_1}{\left(\frac{r}{L}\right)^{\omega_1}} f_{ij}^{(1)}(\theta) + \frac{K_2}{\left(\frac{r}{L}\right)^{\omega_2}} f_{ij}^{(2)}(\theta) \quad (1)$$

where L is a characteristic length, and the functions for each stress component $f_{ij}^{(k)}(\theta)$ are known universal functions of geometry and material constants. There are two stress intensity factors, K_1 and K_2 , each the amplitude of the singularity of strength ω_i , which may be real or complex. By the influence function method [5], the complex stress intensity factor $K = K_1 + i K_2$ is determined analytically from

$$K = \int_0^{\infty} K^*(r_0) dr_0 \quad (2)$$

where $K^*(r_0)$ is the influence function and $r = r_0$ is a point along the interface. A dislocation is placed along the interface at $r = r_0$ in order to determine $K^*(r_0)$. Solutions were obtained for a bonded strip subjected to remote tension perpendicular to the bond line, a temperature decrease and pure shear.

Both conservative line and area integrals were developed in [6] to determine the stress intensity factor K_1 for a bonded strip. These expressions were generalized [7] to obtain the complex stress intensity factor K for arbitrary notch geometry when the eigenvalue is real. Assuming there are no body forces, the conservative integral was developed from Bett's reciprocal principle as

$$K = \int_{\Gamma} (\tilde{T}_i' u_i - T_i \tilde{u}_i') ds \quad (3)$$

where ds is the differential arc length, and Γ is an arbitrary path beginning on the lower notch flank and ending on the upper one. The tractions $T_i = \sigma_{ij} n_j$ and the displacement field u_i are determined numerically. The primed traction and displacement field are complex. The real part is the eigensolution for K_1 and the imaginary part is the corresponding eigensolution for K_2 .

The integral in (3) may be converted into an area integral given by

$$K = \int_A (\sigma_{ij} \tilde{u}_i' - \tilde{\sigma}_{ij}' u_i) q_{1,j} dA \quad (4)$$

where σ_{ij} and u_i are the stress and displacement field in the region A obtained from a numerical analysis of the problem, and $\tilde{\sigma}_{ij}'$ and \tilde{u}_i' are the eigensolution. The region A is chosen to be a ring, which begins at the lower flank of the notch and ends at the upper flank. The function q_1 is taken to be zero on the outer curve of A and unity on the inner curve and must be continuously differentiable within A .

In [6] the integrals in (3) and (4) were employed to calculate K_1 for a bonded strip of finite height subjected to remote stress normal to the bond line. All results obtained by the area integral were shown to be path-independent, and agreed to within 3 percent of the analytic solution obtained by the influence function method.

11.2.4 Interface Fracture at Butt Joints (L. Banks-Sills, Tel Aviv University)

Cracks often develop at or just below an interface between two materials at a butt bond. A methodology was developed for measuring the interface fracture toughness of a crack along an interface [8]. The bimaterial Brazilian disk specimen in Fig. 4 was employed to measure the critical interface energy release rate G_{ic} . The specimen was analyzed by means of the finite element method and a conservative integral in order to determine stress intensity factors $K_1^{(f)}$ and $K_2^{(f)}$ as a function of loading angle θ , and non-dimensional crack length a/R . Curve fitting was employed to obtain calibration functions for these parameters.

Residual stresses develop in the specimens during curing, and lead to stress intensity factors $K_1^{(r)}$ and $K_2^{(r)}$. A weight function derived for interface cracks [9] was employed in [7] and [10] to obtain the stress intensity factors resulting from residual curing stresses.

The total stress intensity factors are given by

$$K_j^{(T)} = K_j^{(f)} + K_j^{(r)} \quad (5)$$

where $j=1,2$. The interface energy release rate is related to the stress intensity factors by the expression

$$G_i = \frac{1}{H} (K_1^2 + K_2^2) \quad (6)$$

where H is a material parameter.

Results of tests carried out [7] to determine G_{ic} of a glass/epoxy pair are shown in Fig. 5. The abscissa Ψ is the phase angle or mode mixity, given by

$$\Psi = \tan^{-1} \left[\frac{\text{Im}(KL^{i\varepsilon})}{\text{Re}(KL^{i\varepsilon})} \right] \quad (7)$$

where the complex stress intensity factor $K = K_1 + iK_2$, and L is a length parameter chosen here as $600 \mu\text{m}$. The parameter ε is related to material properties. If $\varepsilon = 0$, which occurs for homogeneous bodies, $\Psi = \tan^{-1}(K_2 / K_1)$. It may be observed that the critical energy release rate G_{ic} increases with increasing $|K_2|$.

11.2.5 Generalized Thermal Stress Intensity Factors in 2-D Domains (Z. Yosibash, Ben Gurion University)

Computation of thermal generalized stress intensity factors (TGSIFs) in linear thermo-elastic two-dimensional problems with singular points subjected to steady state temperature distribution was addressed in [11]. The stress tensor in the vicinity of singular points exhibits singular behavior characterized by the strength of the singularity and the associated TGSIFs. The p-version finite element program Stress Check[®] was used first to compute the temperature field, which usually exhibits singular behavior of the fluxes in the vicinity of the singular point, and then to impose this thermal loading in the elastic analysis, exciting the TGSIFs. A post-processing technique based on the complementary weak form in conjunction with Richardson extrapolation was applied to extract the TGSIFs. Significantly, the proposed method is suitable not only for singularities associated with crack tips, but also for multi-material interfaces and non-homogeneous materials. Numerical results of crack-tip singularities (mode I, mode II and mixed modes) and singular points associated with a two-material inclusion and a 90° dissimilar materials wedge, were presented in [11]. For example the body in Fig. 6 was heated uniformly by $\Delta\tau = 100 \text{ deg}$. Fig. 7 shows the x- and y-components of the homogeneous first eigen-stress vector, for two isotropic, homogeneous rectangular blocks with different material properties, bonded together ($L/h_1 = 10, L/h_2 = 5$).

11.2.6 Edge Singularities in Elastic Anisotropic Three-Dimensional Domain (Z. Yosibash, Ben Gurion University)

Computation of eigen-pairs characterizing the linear elastostatic solution in three-dimensional anisotropic domains in the vicinity of edge singularities was investigated. Such singularities may be caused by re-entrant corners, abrupt changes in boundary conditions or in material properties. Edge singularities in three-dimensional domains are of great interest with regard to failure initiation. The eigen-pairs characterize the straining modes, and their amplitudes quantify the energy residing in particular straining modes. For this reason, eigen-pairs and their amplitudes are directly or indirectly involved in failure theories.

The problem of determining edge eigen-pairs numerically was dealt with on the basis of the modified Steklov formulation, using the p-version finite element method. The method is very accurate, efficient and robust, and provides complex eigen-pairs if they exist. Details on the method are presented in [12] and many case studies including multi-material inclusion problems, cracks in dissimilar materials, and multi-material interfaces at free and clamped edges are presented in [13].

Examples of special interest are laminated composite patches used for the repair of aging aircraft containing fatigue cracks. These patches are usually bonded to metallic structures and typically terminate at an angle γ as illustrated in Fig. 8. Edge singularities along the patch edge at the intersection of faces A and B were investigated, assuming a zero-thickness adhesive layer between a graphite-epoxy composite patch and metal structure of 7075-T aluminum alloy.

Plots of eigen-values as a function of the fiber orientation angle (β), and the termination angle (γ) are presented in Fig. 9. (The third eigen-value is unity.) These plots enable visualization of the optimal combination of angles β and γ , which produces the highest first two eigen-values.

11.2.7 Stress Intensity Factors for Multiple Cracks in Pressurized Thick Cylinders (M. Perl, Ben Gurion University)

In two previous papers, the interaction effects for two separate cases of large arrays of semi-elliptical, internal, surface cracks in a thick-walled, cylindrical pressure vessel were studied. Arrays of radial cracks and longitudinal-coplanar crack arrays were considered separately. Circumferential crack density and longitudinal crack spacing were found to have opposing effects on the prevailing stress intensity factors (SIFs). In a later paper [14] combined arrays of both radial and longitudinal cracks were considered, and their interaction effects were studied. The mode I SIF distribution for numerous configurations of combined semi-circular and semi-elliptical crack arrays were evaluated. The 3-D analysis was performed by the finite element method and the submodeling technique, employing singular elements along the crack front. The effects of crack density in the circumferential direction, and of relative spacing in the longitudinal direction, on the SIFs were studied for combined arrays of up to 32 circumferentially equispaced radial cracks longitudinally spaced, for a range of crack depth to wall thickness ratios from 0.05 to 0.4 and for ratios of crack depth to semi-crack length from 0.2 to 1.5. Results indicated that the SIFs are considerably affected by the interaction among the cracks, and depend upon the circumferential density and longitudinal spacing, the crack depth and ellipticity, as well as the three-dimensional nature of the problem.

The effect of crack length unevenness on the mode I SIFs for large uniform arrays of radial cracks of unequal depth, in fully or partially autofrettaged thick-walled cylinders, was investigated in [15]. The analysis was based on the previously proposed two-crack-length level model. Values for K_{IA} - the SIF due to the compressive residual stress field - for arrays of from 4 to 1024 cracks, a wide range of crack lengths, and levels of autofrettage from 30 to 100 percent were evaluated by the finite element method for a cylinder of outer to inner radius ratio of 2. The results showed that the unevenness in the SIFs depends on all three parameters. However, the interaction range between adjacent cracks is determined only by the relative length of the cracks and the density of the array.

Erosion geometry effects on the mode I SIF for a crack emanating from the deepest point of erosion in an autofrettaged, pressurized, thick-walled cylinder were investigated [16,17]. The problem was solved by the FEM and knowledge of the asymptotic behavior of short cracks. Autofrettage was simulated by thermal loading, based on the von Mises yield criterion, and SIFs were determined by the nodal displacement method. SIFs were evaluated for crack length to wall thickness ratios of 0.01 to 0.45, the crack emanating from the tip of erosions of different geometries. In Part I of this paper [16], two configurations were considered: semi-circular erosions of depths of 5 percent of the cylinder wall thickness and thumbnail erosions of depth to wall thickness ratios of 0.05 to 0.4. While deep cracks were almost unaffected by erosion, the effective SIF for relatively short cracks was found to be significantly enhanced by the presence and geometry of the erosion, which might reduce the fatigue life of the cylinder. However, since erosion depth and ellipticity are believed to have equally important impact on the SIFs, Part II of the paper [17] delved further into these two parameters using the following configurations: semi-circular erosions of relative depths of up to 10 percent of the cylinder wall thickness; and semi-elliptical erosions with depth to width ratios of 0.3 to 2.0. Deep cracks were found to be practically unaffected by the erosion, similar to the results presented in [16]. The effective SIF for relatively short cracks was found to be dramatically enhanced by the stress concentration factor, which represents the depth of erosion as well as its tip radius. As a result of the increased effective SIF, a decrease in the vessel fatigue life of up to an order of magnitude may occur.

11.3 FAILURE PREDICTION AND RELIABILITY

11.3.1. Probabilistic Failure Analysis by Simulation (A. Brot, IAI)

The 1997 Israel National Review [1] described the activities performed by IAI on the development of probabilistic inspection strategies using a computer simulation program called INSIM. Work has continued on this topic and papers were presented at the 1997 ICAF Symposium [18], the 38th Israel Annual Conference on Aerospace Sciences [19] and the 1998 USAF Structural Integrity Program Conference [20].

An IAI paper [18], presented at the 1997 ICAF Symposium, contained a critical review of damage-tolerance methodology as performed by a probabilistic simulation of the fatigue process. This simulation was performed, using the INSIM computer program. This study included an evaluation of:

- The trade-off process built into the damage-tolerance regulations for determining inspection intervals.
- How damage-tolerance deals with the effects of increased load-transfer and shot-peening.
- The ability of the existing damage-tolerance regulations to deal successfully with the aging aircraft problem.
- The benefits and dangers of the "inspection threshold".
- The ability of the present damage-tolerance methodology to deal with multi-site damage.

In [18] it was concluded that the existing damage-tolerance methodology is not capable of achieving a consistent level of safety for the great variety of conditions which it must address. Recommendations for the future evolution of the damage-tolerance regulations were included.

Reference [19] dealt with multi-site damage configurations. The effects of hole pitch to hole diameter ratio, number of fastener rows, NDI method and inspection interval on the expected probability of failure were presented. The results showed that reasonable probabilities of failure can be achieved at low values of pitch/diameter (with no inspections) or at high values of pitch/diameter (with frequent inspections). Five MSD design configurations that minimize the probability of failure were recommended.

In [20], a comparison was made between four fatigue life regulations used by the FAA, US Air Force, US Navy and the UK military organisation. Significant differences were found in the criteria that each regulation imposes in order to control the fatigue life of an airframe structure. Table 1 contains a comparison of the four sets of fatigue life regulations. The INSIM computer simulation program was used to simulate in a probabilistic manner, service life variation, service load severity, time to crack initiation, crack growth life and crack detection capability.

Three types of structures were selected for evaluation: a lower wing skin detail, a typical splice with a high level of load-transfer, and a typical multi-site damage splice structure. All three structures were sized separately to meet the USAF, FAA, USN and UK military regulations. The INSIM computer simulation was then applied to each structure, assuming an aging aircraft scenario. The probability of failure was calculated for each design under each regulation. The numerical results were then compared from the standpoint of safety, weight and maintenance complexity. Figure 10 compares the expected probability of failure of a multi-site damage structure designed to each of the four sets of regulations.

It was concluded that, in certain instances, the FAA damage-tolerance regulations impose inspections that appear to be unnecessary. In low load-transfer applications, the damage-tolerance policy of the FAA and USAF may add unnecessary weight. For high load-transfer configurations, the FAA and USAF regulations do not insure adequate safety under severe aging aircraft conditions. The US Navy Specifications and UK DEF Standards provide a more balanced approach by accounting for crack initiation as well as crack growth. None of the regulations deal adequately with multi-site damage configurations.

11.4 AIRCRAFT PROJECTS

11.4.1 Galaxy Executive Jet (A. Brot, IAI)

The Galaxy, wide-body executive jet, seen in Fig. 11 during test flight, flew for the first time in December 1997 and received its type certificates from the CAA of Israel and the FAA in December 1998. The Galaxy has a transatlantic range and a maximum cruise speed of Mach 0.85. It can transport up to 18 passengers in a corporate configuration and up to nine passengers in an executive configuration. The Galaxy is powered by two PW306A jet engines. The Galaxy primary structure is metallic except for the ailerons, elevators and rudder that are made from composite materials.

The Galaxy airframe structure has been substantiated to the FAR-25 damage-tolerance requirements. In addition, fatigue and damage-tolerance component tests were performed in order to support the damage-tolerance analyses. Several of these tests were described in the 1997 National Review. This review describes activities performed after the 1997 review was prepared. Reference [21], which will be presented at the 1999 ICAF Symposium, contains a summary of the damage-tolerance substantiation of the Galaxy Executive Jet.

11.4.1.1 Cabin Window Fatigue and Damage-Tolerance Test

The 1997 ICAF National Review described a cabin window fatigue and damage-tolerance component test that had then been started. A section of fuselage, containing the structure surrounding the cabin window, was pressure tested for two lifetimes. Upon completion of the two lifetimes, initial flaws were introduced into the structure at three critical locations and the pressure loading was continued for approximately one additional lifetime, in order to evaluate the crack growth characteristics of the design. The test concluded with a residual strength check that demonstrated the damage-tolerance of the structure under a condition of extensive cracking. Figure 12 shows the window structure, under the residual strength condition, with a large crack extending from an initial flaw introduced in the window frame. The test demonstrated that the crack will be arrested by the neighboring fuselage frame and will not result in failure of the fuselage.

11.4.1.2 Full-Scale Fatigue Test

The Galaxy has been designed to a service life objective of 36,000 hours and 20,000 flight cycles. In order to substantiate this service life objective, the aircraft is being tested in a full-scale fatigue test for a duration of two lifetimes. The test-article for the full-scale fatigue test consists of all the structural members of the fuselage and both wings. The empennage is being fatigue tested separately. The test aircraft was mounted to the test fixture at the nose landing gear attachment and at the engine mount fittings. Figure 13 is a photograph of the Galaxy aircraft mounted in its loading fixture.

The fatigue spectrum loading consists of randomly selected flight-by-flight sequences, reflecting the anticipated usage of the aircraft. A flight consists of the various flight and ground events that the aircraft will experience. Approximately 20 events per flight have been included in the 2000-flight spectrum block.

The test article was divided into 29 loading zones, each of which is independently loaded during each event of the spectrum, using 42 servo-hydraulic actuators. In addition, the passenger cabin and baggage compartment are pressurized with compressed air during the airborne events of the spectrum. The zone loading for each event was determined using a "constrained least-square error method" which minimized deviations in loading of the important structural parameters. Approximately 500 strain-gages were bonded to the test article.

Testing began in December 1998 with a strain survey and is being followed by two lifetimes of spectrum loading. Strains are monitored periodically. NDI is performed at specific intervals. If cracks are detected, crack-gages will be bonded to the crack-tip in order to monitor crack growth rates. Upon completion of two lifetimes, further test objectives will be defined. Testing reached 5000 flights by the end of March 1999.

11.4.1.3 Empennage Fatigue and Damage-Tolerance Test

The entire empennage assembly has been mounted to an aft-fuselage structure for fatigue testing, as is shown in Figure 14. The test includes the elevator and rudder, manufactured from composite materials. The loading spectrum includes vertical and lateral loading resulting from gusts and maneuvers as well as measured buffeting loads arising from thrust reverser deployment. The horizontal and vertical tails were divided into 10 loading zones, each of which is independently loaded during each event of the spectrum, using servo-hydraulic actuators. Approximately 150 strain-gages were bonded to the structure for periodic strain monitoring.

The empennage test started in December 1998. The empennage is being tested for two lifetimes, followed by one additional lifetime of damage-tolerance testing. The composite material elevator and rudder will be tested for damage-tolerance under manufacturing and service inflicted damage as well as under barely-visible impact damage. Testing reached 5000 flights by the end of March 1999.

11.4.1.4 Main Landing-Gear Fatigue Test

The main landing gear spectrum loads are being applied in the vertical, drag and side directions in the Galaxy landing-gear test shown in Fig. 15. A truncated fatigue-load spectrum of the ground-loads is used for this test, after

combining and simplifying some of the ground-operations. Six operational stages were taken within each flight-cycle: taxi, turning, braking, pivoting, rotation and landing-impact. The test spectrum was truncated to include approximately 20 events per flight. Groups of 1,000 of these flights were assembled into each block of flight cycles for the fatigue test load spectrum.

Using this fatigue loading-spectrum, the Galaxy landing-gear has begun testing to five lifetimes. By the end of March 1999, the main-gear had completed 5000 flights.

11.4.1.5 Nose Landing-Gear Landing-Impact, Fatigue Load-Spectrum

Landing conditions determined for the Galaxy by the method of Chester in [22] (based on data in [23] and [24] for the F-104G and AIRBUS 300B aircraft) gave forces that were found to be excessive. In order to reduce the magnitude of this part of the fatigue load-spectrum, a study of nose-gear landing-impacts on the first 20 flights of the Galaxy flight test aircraft was undertaken. It was found that the horizontal position of the center of gravity had a much more significant effect on the vertical loads than did variations in the aircraft mass. This was due to the relative stiffnesses of the nose and main tires and shock-absorbers. The equivalent mass at the nose-gear was in fact greater than the value previously obtained from the analytic method in [22], and was about 3.1 times the "static-mass" on average. (Other aircraft generally present a lower value of equivalent-mass ratio.) However, the sinking-speeds at the nose of Galaxy averaged only 0.41 m/sec. (1.34 ft./sec.) in practice. This resulted in the spectrum of vertical impact loads on landing being smaller than the values determined at first. The detailed results of this study are given in [25], a poster paper at the 1999 ICAF Symposium.

11.4.2. F-5 Structural Upgrades (A. Brot, IAI)

The IAI structural departments continue to support the various F-5 upgrade programs being performed at IAI. Although most of the modernization programs emphasize an avionics upgrade, a significant effort is expended to ensure that the aging structure can sustain the changing load configuration and extended life expectation.

11.5 COMPOSITES

11.5.1 Composite Repair of Aging Aircraft - Brite-Euram Research Program (A. Brot, IAI)

IAI functions as the technical director of a European Brite-Euram research program regarding composite material repair of metallic structure for aging commercial aircraft. Hellenic Aerospace Industry Ltd. (HAI) in Greece provides overall management of the program. The other partners are Alenia in Italy, Cytec in the UK, Générale de Micro Informatique (GMI) in France and Industrial Aeronautica de Portugal (OGMA) in Portugal. Two universities in Greece, Democritus University of Thrace (DUT) and the National Technical University of Athens (NTUA) are also participating in the program.

The objective of the program is to produce a methodology for standardized composite material bonded repairs of metallic structure for aging commercial aircraft. Bonded composite repairs have a number of advantages over metallic fastened repair, including uniform and efficient load paths, elimination of fastener hole stress concentrations, good fatigue characteristics and corrosion resistance. Bonded composite repairs have been used in many military applications over the past 20 years; for example: the F-111 wing pivots, C-141 wing skins, C-130 wing stiffeners, the B1 dorsal longeron, and the repair of Mirage and Kfir lower wing skins. Today this type of repair is entering the commercial arena. Examples include the boron epoxy doubler repair of the L-1011 door corner.

The tasks of the European Consortium research program include:

- Candidate Structural Detail Survey
- Composite/Adhesive Material Allowables
- Analytical Methodology (including load, stress, fatigue and crack growth)
- Repair Procedure
- Repair Equipment

- Non-Destructive Inspection of Repair
- Substantiation and Validation Testing
- Development of Standards and Manual

A major effort in the program is devoted to analytical methodology for calculating fatigue and crack growth of the metallic structure under the composite material patch.

The final deliverable will include a manual for standardized composite material bonded repairs of characteristic metallic structural components. The manual will serve as a technological basis for expanding the infrastructure with respect to bonded composite repairs, including patch design, analytical methodology, material data base, curing process, surface preparation, and NDI.

A summary of this activity is contained in [26], which will be presented at the 1999 ICAF Symposium.

11.5.2 Composite Repair of a Metallic Spar (A. Brot, IAI)

IAI considered potential candidate structure for development and implementation of composite repair technology. Structure that would pose technological challenges was a prime candidate with which to demonstrate approaches and methodology. A military aircraft forward spar web was chosen because of the following complexities and challenges:

- Large stresses and high stress concentration factors around the cutout.
- Protruding lip around the cutout.
- Requirement to leave an opening in the patch for wiring or tubing.
- Relatively large thickness of metallic parent material.
- Criticality of location based on past history of cracking.
- Hot/wet environment.

The objectives of the work were:

- To develop methodology for applying bonded composite material repairs to metallic structure.
- To develop methods of analyzing the load transfer, stress and stress intensities of the repaired structure.
- To examine the effectiveness of various patch configurations in reducing the stress concentrations and stress intensity factor in the original structure.

Finite element models were created in order to calculate the stress in the parent metallic material, the load transferred to the composite patch and the shear load in the adhesive layer. The calculated reduction in stress intensity factors due to the composite patch as is shown in Fig. 16. The stress distribution on the reinforced web, based on the finite element model that was developed for this application, is shown in Fig. 17.

Testing is being performed to verify the graphite-epoxy co-cured composite repair designed for this application. EDM notches were inserted, precracking was performed and spectrum loading is now being applied to both the repaired and unrepaired test specimens. Reference [27] describes this analytical and test program in more detail.

An interesting observation to date is the trade-off regarding patch stiffness near the cutout. On the one hand, a stiffer patch reduces the high stress concentration loads in the aluminum parent material at the cutout. On the other hand, a very stiff patch at the cut-out may draw excessive load, and cause failure in the patch or adhesive.

11.5.3 CH53 Helicopter Battle Damage Repair (A. Brot, IAI)

Israel Aircraft Industries (IAI) is presently involved with the Israeli Air force in developing a composite material battle damage repair for the CH53 helicopter blade. Various types of blade damage have been defined including damage to the skin and/or the honeycomb core. Also, different types of repairs were stipulated, including a "fast-fix" for a ferry flight (return to base) and a more serious repair which would allow full envelope operation for 100 flight hours.

A number of repair concepts were investigated, all keeping within the stringent battle damage time constraints. Two of the more promising methods included:

- Rapid wet lay up of fiberglass fabric and fast cure epoxy resin patches.
- Precured composite patches with fast cure epoxy resin.

Material process development was supported by comprehensive analytical calculations of the composite material of the blade and the repair, in order to ensure that the damage would not extend and become critical, and to verify the restoration of original strength when necessary. The program includes diverse testing to verify the quality and functionality of the various repairs:

- Extensive “suction” testing to ensure sufficient adhesion of the patches at room temperature as well as in both hot and cold environments.
- A dynamic test of a turning blade, testing various types of repairs, is shown in Fig. 18.
- Static verification testing of the composite material repair.

11.5.4 Development Program for Designing Primary Structures from GLARE Material (A. Brot, IAI)

Interest in the well-known high resistance of fiber-metal laminates to crack growth and fatigue has led IAI to commence a program for fatigue testing a stiffened panel of GLARE 3-3/2 material of 1.4 mm thickness. The component is rectangular, flat and double-skinned with omega-shaped spacers that are riveted to both sheets, as shown in Fig. 19. The test-rig is designed to apply cyclic pressure on one side of the panel, the edges of which are supported by extruded angles. This represents the kind of support afforded a bulkhead of similar design, at its fuselage attachment. For purposes of direct comparison, the panel will be cyclically loaded simultaneously and in parallel with a similar panel of monolithic aluminum-alloy material of the same overall size and type of construction.

11.6 JOINTS AND MATERIAL

11.6.1 Fatigue Damage Healing by a Laser Surface Treatment (E. Altus, Technion)

A laser surface treatment, which enhances fatigue resistance of 6Al-4V titanium alloy, has been studied using a 0.8kw CW CO₂ laser. The laser treatment proved useful both for improving the near surface microstructure of undamaged specimens, thereby increasing the original fatigue life, and for healing in-service structures subjected to cyclic loading. The combination of both effects was studied [28].

Laser surface treatment was applied at different stages of fatigue life, to three-point bending specimens loaded cyclically. A significant improvement in fatigue life, with a distinct optimal treatment point at about 2/3 of the original lifetime, was obtained under certain treatment conditions. In addition, changes in surface microstructure such as grain size and shape distribution, and in alloy phase ratios, were identified. Surface treatment with a laser caused a relative reduction in the α -phase and grain size. Other changes of grain boundary geometry due to the treatment were also studied.

Conclusions were: a) Improving fatigue resistance by laser surface treatment is observed only under very specific treatment conditions. b) There are two different mechanisms involved: micro-structural change and healing. c) It is expected that the healing mechanism can be applied successfully many times, to increase the fatigue life many fold.

11.6.2 Effect of Prestrain on Fracture Toughness (L. Banks-Sills, Tel Aviv University)

In a study [29] of the effect of plastic prestrain on the fracture toughness K_{IC} , experiments were carried out on three-point bend specimens of 7075-T7371 aluminum-alloy. Several specimen groups were prepared by subjecting long strips of the material to different uniform tensile overloads. Long dog-bone specimens were fabricated with nominal overall length 630 mm and a gage length of 390 mm. Each of these specimens was subjected to one of five

different tensile overloads perpendicular to the material rolling direction, producing a plastic permanent set or prestrain. The overload caused a constant plastic prestrain of 0.96, 2.0, 3.2, 3.96 and 5.1 percent within the material.

It was found that as the prestrain level was increased, the fracture toughness was reduced by a factor of up to approximately 20 percent (see Fig. 20). A micro-mechanistic model [30] was employed to determine K_{IC} values from the current yield stress. The trend shown by the model was similar to that determined by the tests.

11.7 SMART STRUCTURES AND HEALTH MONITORING

11.7.1 Health Monitoring of Airborne Structures Using Optical Fiber Sensors (A. Brot, IAI)

Structures, especially those made of layered composite material, are susceptible to in-service damage that sometimes is difficult and expensive to track. The time, equipment and manpower required for periodical nondestructive tests, in addition to the grounding time of the fleet, add considerably to the operating costs of commercial and military aircraft. In between these periodic tests, it is assumed that a certain amount of damage occurs without being detected. To avoid catastrophic failure due to this damage, the structure has to be designed with relatively high margins of safety, which usually results in added weight. This hard-to-detect damage reduces considerably the reliability of composite structures, and is probably one of the main reasons that composite materials are not often used in critical aircraft parts.

Next generation aircraft are expected to be economic and safe to operate, yet, the structure has to withstand an increase in performance and loads. These requirements call for a new concept in structure inspection methods. Instead of increase of the designed margin of safety, decrease of the time interval between inspections, or avoidance of composite materials in critical structural parts, an in-flight health monitoring system is suggested, based on an array of strain sensors.

The well known electrical strain gage is not suitable for the purpose of in-flight strain mapping. The heavy and complex wiring and the sensitivity of the readings to electromagnetic fields make the electric strain gage impractical when a large number of measuring points is required.

At Israel Aircraft Industries, investigation and development of the use of strain sensors made of optical fibers for use in structure made of composite materials are continuing. Many such sensors can be positioned along one optical fiber, which may be embedded in and protected by the composite layered structure. The sensors, made of optical fibers, are indifferent to electromagnetic field, lightweight, corrosion resistant and do not produce heat or electric sparks.

A process of embedding optical fiber strain sensors into composite materials laminates, as well as the technology of interfacing these optical fibers with the optical measuring equipment, was developed and tested. Optical fibers with Bragg sensors, embedded in composite test coupons, were successfully used to measure strains in a laboratory setting. This technology development was accompanied by development of an analytical method to predict the influence of the embedded fiber and its coating on the thermomechanical properties of laminated composite materials. A full-size demonstrator was designed and is expected to be tested under realistic flight loads during the coming year.

11.7.2 Corrosion Detection (A. Brot, IAI)

The economic necessity of keeping military and commercial aging aircraft in service has resulted in the emerging importance of developing methods for the early detection of corrosion. A program was started to evaluate conventional and newer methods for detecting corrosion. Specimens were manufactured having various severity levels of pitting and exfoliation corrosion. These specimens are being tested by conventional and developmental methods, in order to assess each method in its ability to detect corrosion, estimate its severity and determine its extent. The relative cost advantage of each method will be estimated. A report will be issued when the study is completed.

11.7.3 Vibratory Methods of Health Monitoring in Smart Structures (A. Berkovits, Technion)

Vibration methods for the identification of global health-monitoring of structures resurface from time to time. The detection and characterization of local damage requires the use of relatively high frequencies, on the order of 15-50 kHz. In an on-going research project at the Technion [31] changes in resonant frequency, damping coefficient, and vibrational energy due to local damage, such as fatigue cracks and impact damage, are being studied in composite plates. Both optical sensors and conventional vibration sensors are being used.

Detection of simulated fatigue cracks on the order of 1 or 2 mm in length, and delaminations over small areas in graphite-epoxy stiffened plates, using piezoelectric sensors and FTP modal analysis, has been highly successful for modes up to the fourth natural frequency. Experimental results were well predicted by a modified Bolotin analysis [32,33]. The present algorithm is very efficient, and achieves computed results within 8 percent of the time required for previous Bolotin analyses. Also it gives valid results over a significantly larger portion of the plate. Representative calculated mode shapes are shown in Fig. 21.

The approach is now being extended with the use of optical, laser-illuminated fibers embedded in the composite material plates.

11.8 REFERENCES

1. Berkovits, A., "Review of Aeronautical Fatigue Investigations in Israel", April 1995-March 1997, Minutes 25th ICAF Conf., ICAF Doc. No. 2164, Edinburgh 1997.
2. Nathan, A. "Composite Repair of Aging Metallic Structure – P-Version 3D Finite-Element Approach", *Proceedings of the 2nd Joint NASA/FAA/DoD Conference on Aging Aircraft*, Williamsburg, VA, USA, September 1998, pp. 153-162.
3. Rose, L. R. F., "An Application of the Inclusion Analogy for Bonded Reinforcements", *Int. J. Solids and Structures*, **17**, 1981, pp. 827-838.
4. Rose L. R. F., "Theoretical Analysis of Crack Patching", in *Bonded Repair of Aircraft Structures*, eds. A.A. Baker, R. Jones, Martinus Nijhoff Publishers, 1988, pp. 77-106.
5. Banks-Sills, L., Yang, Y.Y. and Munz, D., "An Influence Function for Stress Intensity Factors of Bimaterial Notched Bodies", *International J. of Fracture*, **85**, 1997, pp. 333-350.
6. Banks-Sills, L., "A Conservative Integral for Determining Stress Intensity Factors of a Bimaterial Strip", *International J. of Fracture*, **86**, 1997, pp. 385-398.
7. Banks-Sills, L., "The Bimaterial Notch Problem", in *IUTAM Symposium on Non-Linear Singularities in Deformation and Flow*, eds. D. Durban and J.R.A. Pearson, Kluwer Academic Publishers, 1999, pp. 55-61.
8. Banks-Sills, L., Travitzky, N., Ashkenazi, D. and Eliasi, R., "A Methodology for Measuring Interface Fracture Properties of Composite Materials", to appear in *International J. of Fracture*.
9. Banks-Sills, L., "Weight Functions for Interface Cracks", *International J. of Fracture*, **60**, 1993, pp. 89-95.
10. Banks-Sills, L., Ashkenazi, D. and Eliasi, R., "Determination of the Effect of Residual Curing Stresses on an Interface Crack by Means of the Weight Function Method", *Computational Mechanics*, **19**, 1997, pp. 507-510.
11. Yosibash, Z., "Thermal Generalized Stress Intensity Factors in 2-D Domains", *Computer Meth. Appl. Mech. Engrg.*, **157**, 1998, pp. 365-385.

12. Yosibash, Z., "Numerical Analysis of Edge Singularities in Three-Dimensional Elasticity", *Int. J. Numer. Meth. Engrg.*, 1997, pp. 4611-4632.
13. Yosibash, Z., "Computing Edge Singularities in Elastic Anisotropic Three-Dimensional Domains", *Int. J. Fracture*, **86**(3), 1997, pp. 221-245.
14. Perl, M., Levy, C. and Wang, J., "Interaction Effects of Combined Arrays of Radial and Longitudinal Semi-Elliptical Surface Cracks in Pressurized Thick-Walled Cylinder", *ASME J. of Pressure Vessel Tech.*, **119**, 1997, pp. 167-174.
15. Perl, M. and Alperowitz, D., "The Effect of Crack Length Unevenness on Stress Intensity Factors Due to Autofrettage in Thick-Walled Cylinders", *ASME J. of Pressure Vessel Tech.*, **119**, 1997, pp. 274-278.
16. Levy, C., Perl, M. and Fang, H., "Cracks Emanating from an Erosion in a Pressurized Autofrettaged Thick-Walled Cylinder. Part I: Semi-Circular and Arc Erosions", *ASME J. of Pressure Vessel Tech.*, **120**, 1998, pp. 349-353.
17. Perl, M., Levy, C. and Fang, H., "Cracks Emanating from an Erosion in a Pressurized Autofrettaged Thick-Walled Cylinder. Part II: Erosion Depth and Ellipticity Effects", *ASME J. Pressure Vessel Techn.*, **120**, 1998, pp. 354-358.
18. Brot, A., "A Critical Review of Damage-Tolerance Methodology by Means of Probabilistic Simulation of the Fatigue Process", in "*Fatigue in New and Aging Aircraft*" (R. Cook and P. Poole, eds.) Proc. 19th ICAF Symp., Edinburgh, Scotland, June 1997, EMAS Publ., UK, Vol. 1, pp. 403-420, 1997.
19. Brot, A., "Designing Aircraft Structures to Avoid Multi-Site Damage Failures", *Proceedings of the 38th Israel Annual Conference on Aerospace Sciences*, Israel, February 1998, pp. 171-179.
20. Brot, A., "Military and Federal Fatigue Life Regulations – Do They Insure Safety?", *Proceedings of the 1998 USAF Aircraft Structural Integrity Program Conference*, San Antonio, TX, USA, December 1998 (in print).
21. Brot, A. et al, "Damage-Tolerance Substantiation of the Galaxy Executive Jet", to be presented at the 20th ICAF Symposium, July 1999.
22. Chester, D.H., "The Equivalent Masses at Nose Landing-Gears During Landing-Impacts and When Taxiing Over Runway Perturbations" *Israel Journal of Technology*, **23**, 1986/7, pp. 7-12.
23. Buxbaum, O. and Gassner, E., "Cumulative Frequency Distribution of Aircraft Landing Gear Loads" RAE Library Translation 1462, June 1970.
24. Buxbaum, O., "Landing Gear Loads of Civil Transport Airplanes", *Proceedings of the 11th ICAF Symposium*, ICAF Doc. No. 1216, May 1981, pp. 0/1-0/36.
25. Chester, D. H. and Brot, A., "Development of a Fatigue Spectrum for Nose-Gear Landing Impact on the Galaxy Executive Jet", to be presented at the 20th ICAF Symposium, July 1999.
26. Nathan, A., "Bonded Composite Repairs for Aging Commercial Aircraft – a Multi-National Research Effort", to be presented at the 20th ICAF Symposium, July 1999.
27. Peled, D. et al, "Composite Patch Repair on Aluminum Primary Structures", Presented at the *39th Israel Annual Conference on Aerospace Sciences*, Israel, February 1999.
28. Altus, E. and Konstantino, E., "Fatigue Damage Healing by a Laser Surface Treatment", *J. Eng. Fracture & Fatigue* (in print).

29. Banks-Sills, L. and Dunye, I., "A Note on the Effect of Plastic Strain on Fracture Toughness", *Engineering Fracture Mechanics*, **57**, 1997, pp. 67-73.
30. Ritchie, R.O., Knott, J.F. and Rice, J.R., "On the Relationship between Critical Tensile Stress and Fracture Toughness in Mild Steel", *J. Mech. Phys. Solids*, **21**, 1973, pp. 395-410.
31. Pevzner, P., Weller, T. and Berkovits, A., "Further Modification of Bolotin Method in Vibration Analysis of Rectangular Plates", submitted to AIAA Journal, 1999.
32. King, W.W. and Lin, C.-C., "Applications of Bolotin's Method to Vibration of Plates", *AIAA J.*, **12**(3), 1974, pp. 399-401.
33. Pevzner, P., Berkovits, A. and Weller, T., "Vibration Analysis of Clamped Rectangular Composite Plates Including a Crack in the Interior Region", TAE 817, Faculty of Aerospace Eng., Technion-Israel Institute of Technology, Haifa, Jan. 1998.

Table 1 Comparison of Fatigue Life Regulations

Regulation	Principal Options	Crack Initiation Life	Crack Growth Life	Inspections	Miscellaneous
Commercial Aircraft FAA / JAA [FAR-25 / JAR-25]	None	Not Applicable	Time to grow from a_i to a_c	<u>Threshold</u> : Related to crack growth <u>Interval</u> : 50% of the time from a_d to a_c	<i>All critical structure must be inspected periodically</i>
USAF [MIL-A-87221]	Slow Crack Growth – Inspected Structure	Not Applicable	Time to grow from a_i to a_c	<u>Threshold</u> : Related to crack growth <u>Interval</u> : 50% of the time from a_d to a_c	
	Slow Crack Growth – Uninspected Structure	Not Applicable	Time to grow from a_i to a_c . Must exceed 2 LT	None Required	
USN [MIL-A-8866C (AS)]	None	To exceed 4 LT	Time to grow from $a_i = 0.01''$ to a_c . Must exceed 1 LT	None Specified	Critical Crack Size must exceed 0.25''
UK Military [DEF-STAN-00-970]	Safe-Life	To exceed 3 LT and To exceed 1.5 LT with all loads “amplified” by 1.2	Not Applicable	None Required	Intended Option for most structures
	Inspection Dependent	For determining threshold inspection only	Time to grow from a_i to a_c	<u>Threshold</u> : Related to crack initiation life <u>Interval</u> : To result in a 99.9% overall P.O.D.	

Abbreviations: a_i = initial crack (usually 0.05 in); a_c = critical crack size under required residual loads; a_d = detectable crack size; LT = Design Lifetime; P.O.D. = Probability of Detection

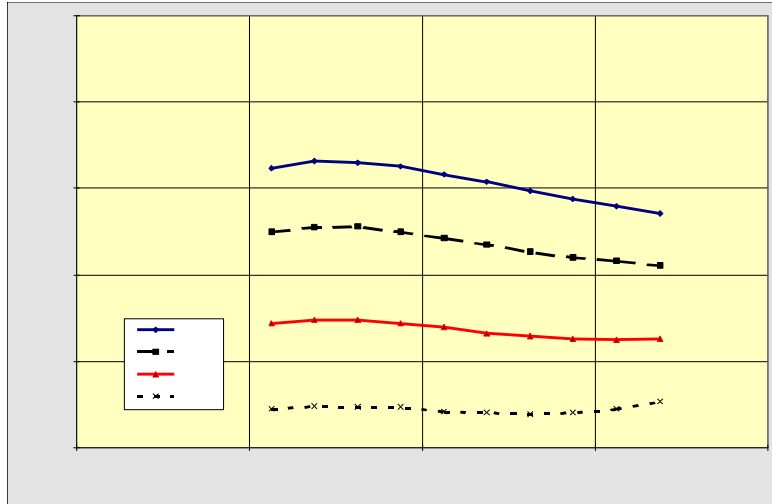


Figure 1. Parametric Study – Stress Intensity as a Function of Plate/Patch Stiffness

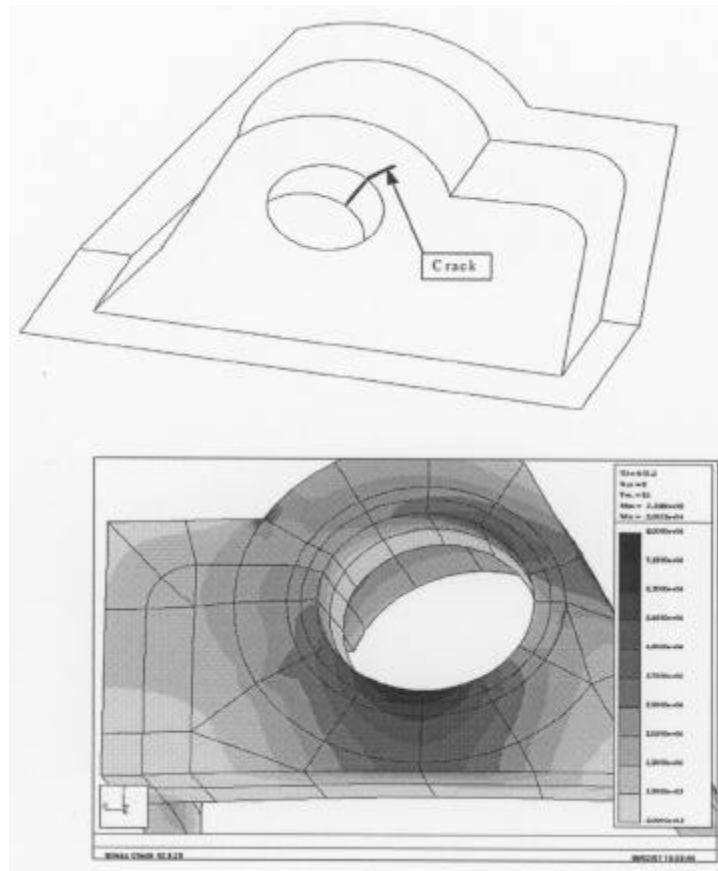


Figure 2. Cracked End-Pad Fitting and P-Version Finite-Element Model (shown from the direction of the mating face)

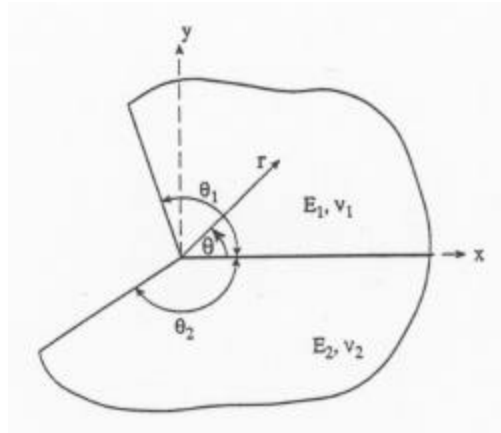


Figure 3. Bimaterial notch geometry

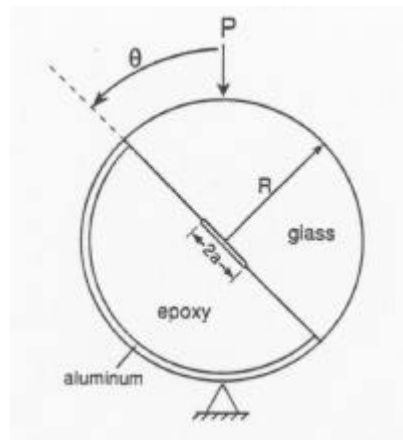


Figure 4. Bimaterial Brazilian disk specimen

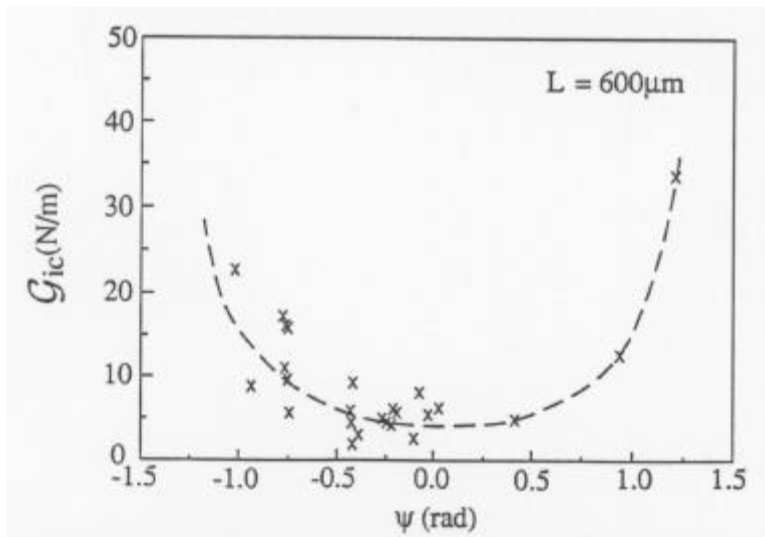


Figure 5. Critical interface energy release rate for glass and epoxy

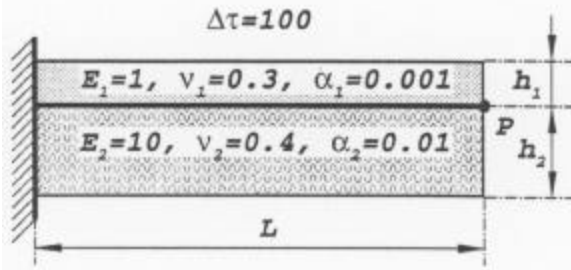


Figure 6. Configuration of dissimilar bonded blocks

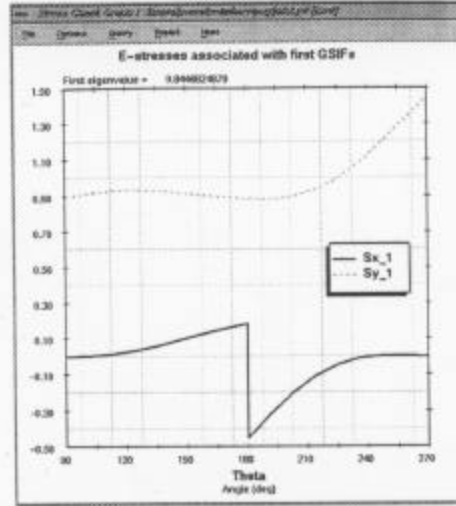


Figure 7. $(F_{11})_1(\theta)$ and $(F_{22})_1(\theta)$ eigenvalues for dissimilar bonded blocks

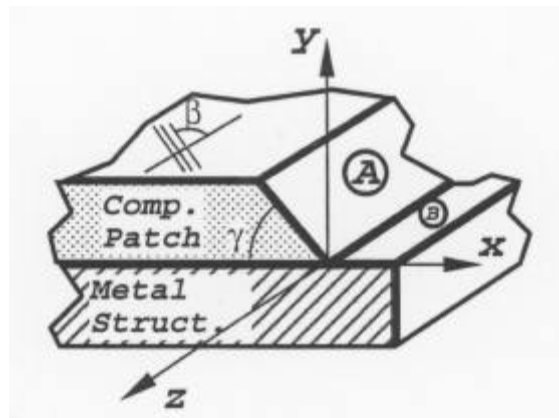


Figure 8. Composite patch attached to metal structure

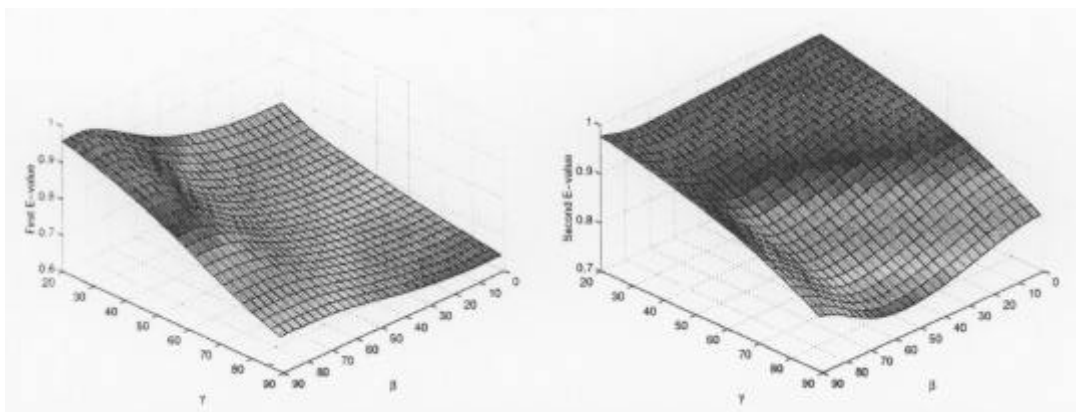


Figure 9. First two eigenvalues as a function of the fiber orientation angle (β), and terminating angle γ for a composite patch attached to a metal structure

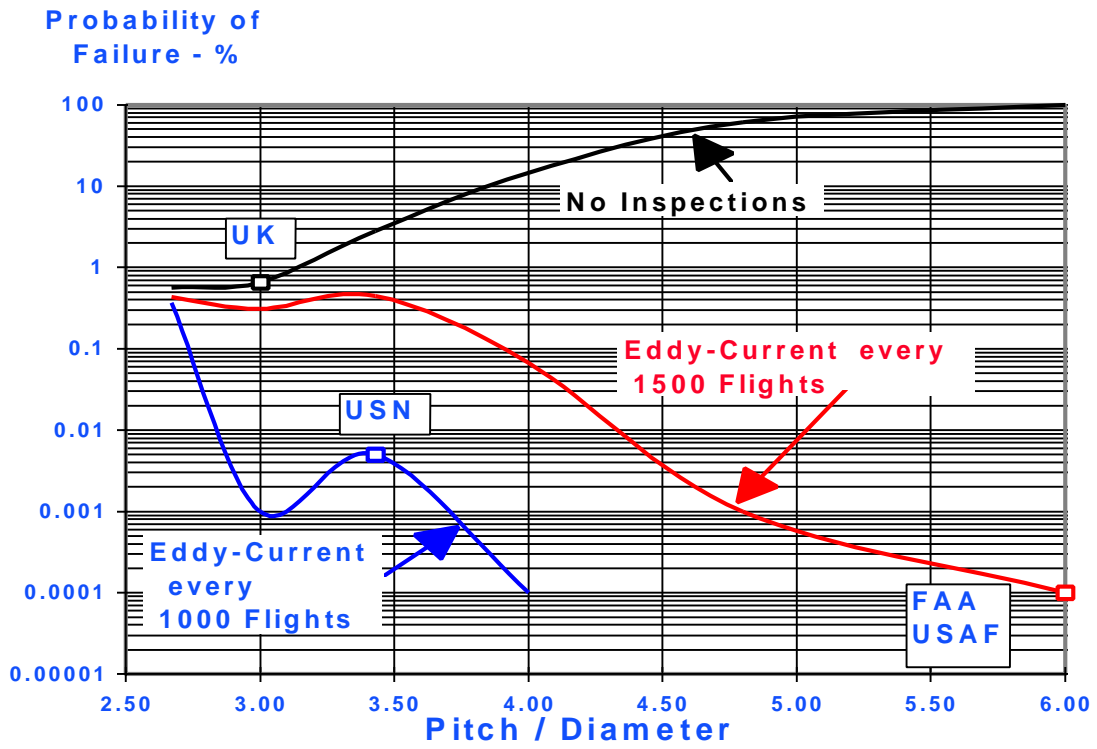


Figure 10. Probability of Failure of Multi-Site Damage Splice



Figure 11. Galaxy Executive Jet during Test Flight

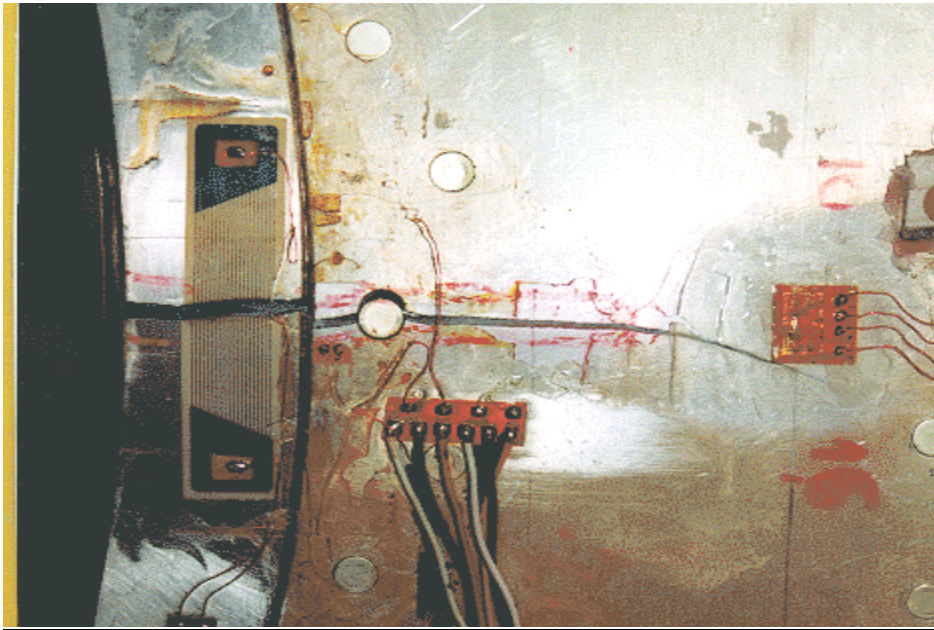


Figure 12. Galaxy Cabin Window Structure Residual Strength Test With a Crack Extending from Initial Flaw Introduced in Window Frame



Figure 13: Galaxy Full-Scale Fatigue Test Aircraft in Loading Fixture

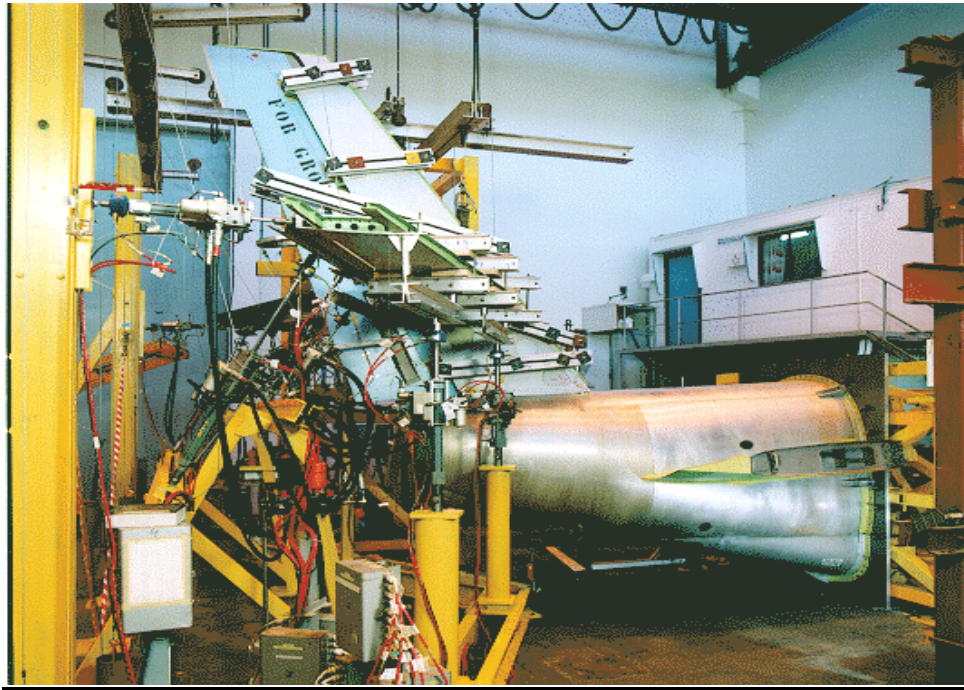


Figure 14. Galaxy Empennage Mounted in Fixture for Fatigue and Damage-Tolerance Test

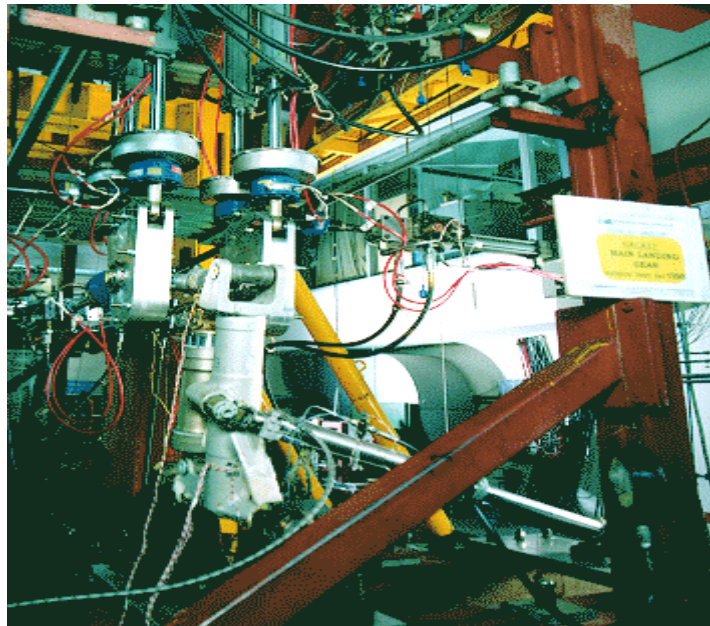


Figure 15. Galaxy Main Landing Gear Fatigue Test (landing gear mounted upside down in loading fixture)

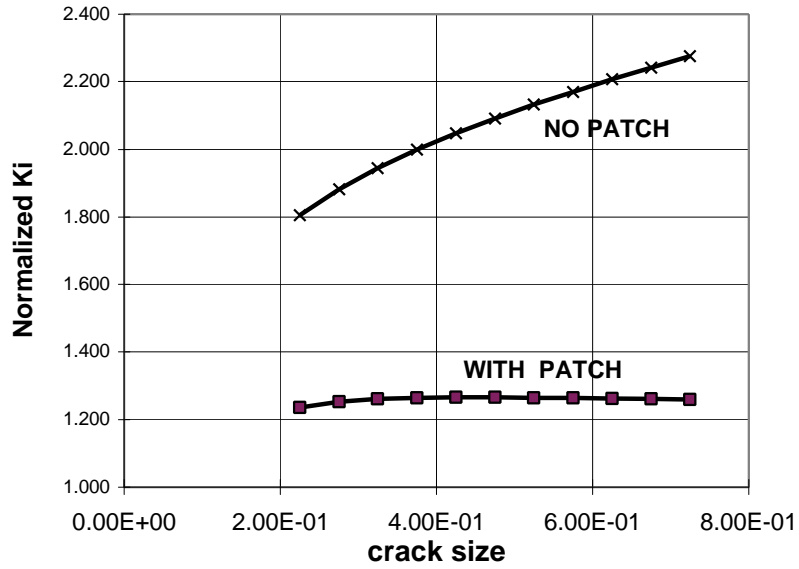


Figure 16. Normalized Stress Intensity for Normalized Crack Size (With and Without a Patch at a Spar Cut-Out)

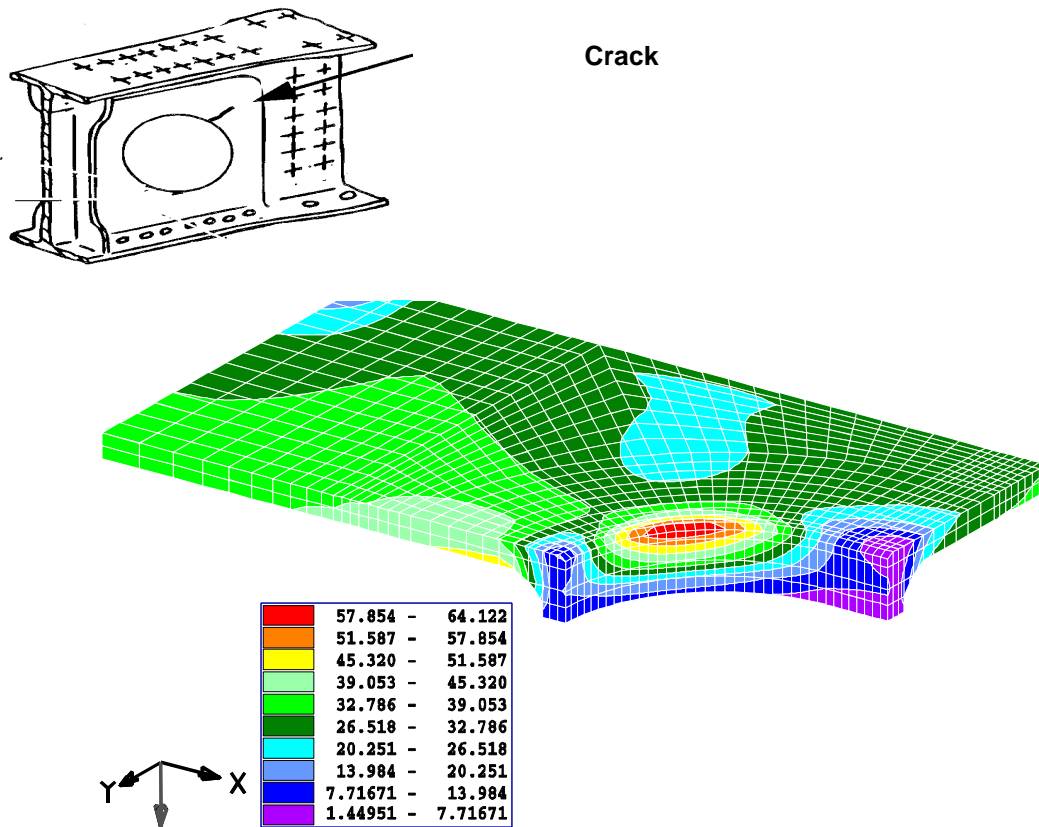


Figure 17. Stress Distribution around Reinforced Spar Web



Figure 18. Dynamic Testing of Helicopter Blade

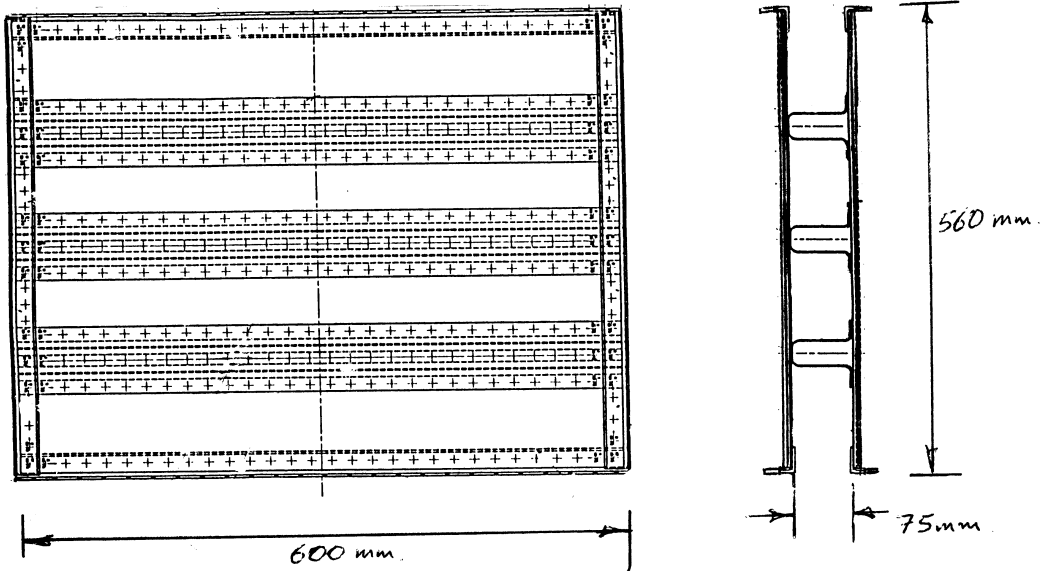


Figure 19. Fatigue Test Panel Fabricated from GLARE

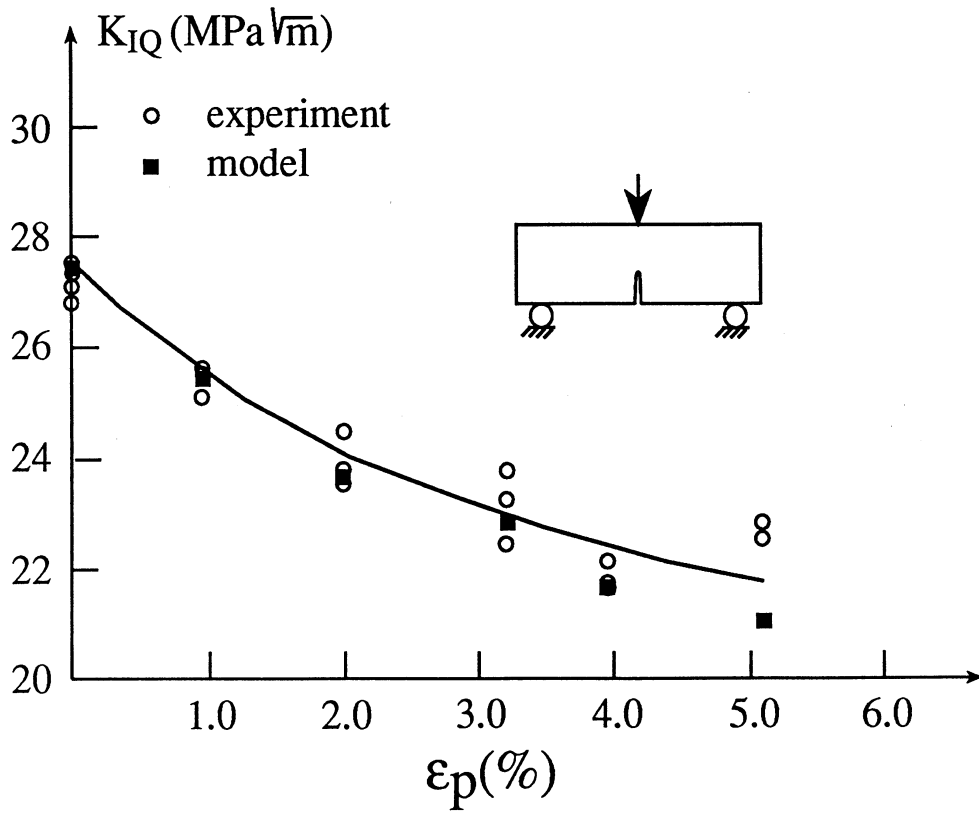


Figure 20. Fracture Toughness Dependence on Prestrain

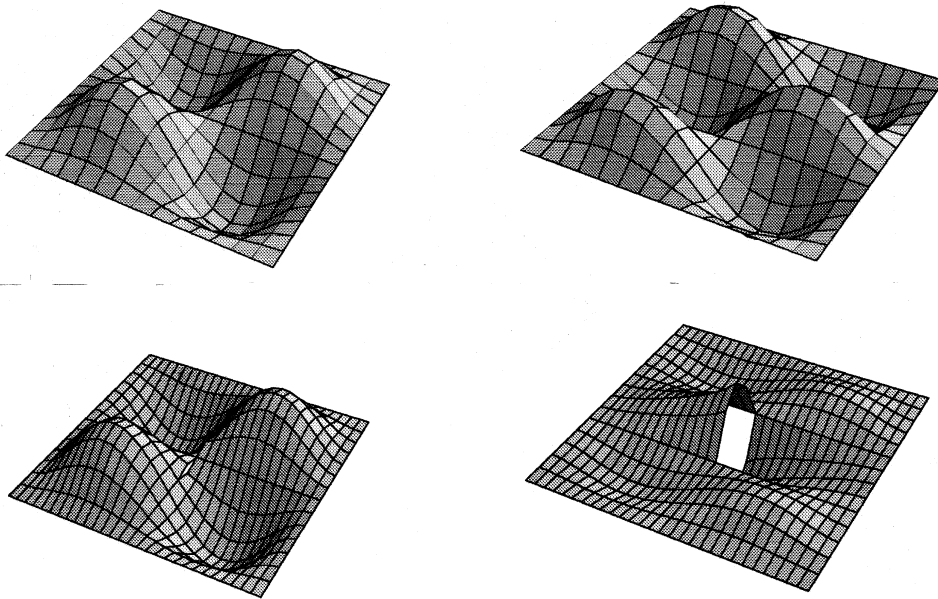


Figure 21. Deflected Shapes of Undamaged and Cracked Composite Plates

**REVIEW OF AERONAUTICAL FATIGUE INVESTIGATIONS IN JAPAN
DURING THE PERIOD JUNE 1997 TO JUNE 1999**

Edited by

Akira Kobayashi
Science University of Tokyo

and

Toshiyuki Shimokawa
National Aerospace Laboratory

For Presentation at the 26th Conference of
the International Committee on Aeronautical Fatigue

Bellevue, Washington, USA, July 12-13, 1999

CONTENTS

	Page
12.1 INTRODUCTION	12/3
12.2 METALS	12/3
12.2.1 Fatigue Strength of Stainless Steel in Post Yield Region	12/3
12.3 COMPOSITES	12/4
12.3.1 Microscopic Fatigue Damage Evolution in Quasi-Isotropic CFRP Laminates	12/4
12.3.2 Effects of Loading Frequency and Environment on Fatigue Delamination-Crack Growth of CFRP	12/4
12.3.3 Strength Degradation of High Temperature Polymeric Composite Materials for the Next-Generation SST Structures by Isothermal Aging	12/5
12.4 JOINTS	12/6
12.4.1 Evaluation of Plugged Hole Effect on Fatigue Life	12/6
12.5 COMPONENT TESTING	12/7
12.5.1 Fatigue Tests of Fuselage Structure Model by Pneumatic Cycles	12/7
12.5.2 Cast Front Pressure-Bulkhead – Damage Tolerance Test	12/7
12.5.3 Flaw Tolerance Verification Tests for MH2000 Helicopter	12/8
12.5.4 Static Tests of Composite Leading Edges of Vertical & Horizontal Stabilizers for Dash8 Q400	12/9
12.5.5 DADT Tests of Metallic Control Surface for Dash8 Q400	12/9
12.6 FULL-SCALE TESTING	12/10
12.6.1 Full-Scale Strength Tests for Japanese New Military Aircraft	12/10
12.7 AGING AIRCRAFT PROBLEM	12/11
12.7.1 Residual Strength of Aged Small Aircraft	12/11
12.8 AIRCRAFT ENGINE MANAGEMENT	12/11
12.8.1 Proactive Approach for Engine Reliability Improvement	12/11
12.9 AIRCRAFT ACCIDENTS	12/12
12.9.1 Aircraft Accident Investigation in Japan	12/12
12.10 ICAF DOCUMENTS DISTRIBUTED BY JAPAN DURING 1997-1999	12/14
ACKNOWLEDGMENT	12/15
FIGURES AND TABLES	12/16
	(Last page 12/39)

12.1 INTRODUCTION

A. Kobayashi, National Delegate

The present national review reports aeronautical fatigue activities in Japan during 1997 to 1999. The very review is due to contributions by Aeronautical Fatigue Research Committee members of Japan Society for Aeronautical and Space Sciences, especially to the key members affiliated with the following:

National Aerospace Laboratory (NAL)
 Third Research Center, Technical Research and Development Institute (TRDI), Japan Defense Agency (JDA)
 Aircraft Accident Investigation Commission
 Mitsubishi Heavy Industries, Ltd. (MHI)
 Kawasaki Heavy Industries, Ltd. (KHI)
 Fuji Heavy Industries, Ltd. (FHI)
 All Nippon Airways (ANA)
 Japan Aircraft Development Corporation (JADC)
 University of Tokyo
 Kobe University
 Science University of Tokyo

The above-mentioned members are greatly appreciated for their concentrated endeavor to achieve such a fruitful review. Mr. Tadao Kamiyama, former National Delegate of Japan, is acknowledged for his everlasting encouragement during the course of compilation of the present review.

12.2 METALS

12.2.1 Fatigue Strength of Stainless Steel in Post Yield Region

N. Yoshikawa and S. Machida, Fuji Heavy Industries, Ltd. (FHI)

FHI has been developing a new rotor system for a medium-sized helicopter. One design requirement for helicopter rotor blades is an anti-erosion or anti-abrasion characteristic. To satisfy this requirement, a metal abrasion strip is bonded on the leading edge of composite rotor blades. Figure 1 shows the typical construction of a composite rotor blade.

Titanium, electro-formed nickel, and stainless steel are widely used as a material of an abrasion strip. Since stainless steel is less expensive for material itself and processing than titanium and electro-formed nickel, stainless steel was selected for a new rotor system.

The stainless steel abrasion strip is loaded very high-strain cycles due to high flexibility of Glass Fiber Reinforced Plastics (GFRP) which is used for a blade spar. In this particular case, i.e., during a high-speed cruise-flight, the endurance loading cycle was estimated as the maximum strain to be 4,200 μ m and the minimum strain to be 2,200 μ m. This strain cycle exceeds the yield strain of ASTM 5517 stainless steel (AISI 301, 1/4 hard) that is selected in this study. Moreover, the *S-N* data under these high-strain loading were not published.

Fatigue tests were conducted to obtain the *S-N* data. The specimen configuration is illustrated in Figure 2, of which shape is based on ASTM E 466. The testing machine used was a MTS Model 810. The loading frequency was 10Hz, which was the maximum speed achieved by this machine, though the actual loading frequency of the rotor blade is about 20Hz. The strain ratio *R* (min. strain/max. strain)=0.5 was used for all fatigue tests.

The yielding of this material was clearly observed during the initial loading. At first, a fatigue test was carried out at 135% of the estimated maximum strain and the specimen did not fail. Then, the maximum stain level was increased to 165%; however, no failure occurred. Finally the fatigue strain level was enhanced to 180% and three specimens were fatigue tested. Total five specimens were fatigue tested and four specimens ran out. The test results are plotted in Figure 3. From these test results, the fatigue strength for infinite life, i.e. the fatigue limit, of this stainless steel was estimated to be very close to 1800 μ m-strain amplitude. Since the estimated actual strain amplitude is about

1000 μ m as described above, this stainless steel is confirmed to have enough fatigue strength and to be usable as the material of an abrasion strip.

12.3 COMPOSITES

12.3.1 Microscopic Fatigue Damage Evolution in Quasi-Isotropic CFRP Laminates

N. Takeda, University of Tokyo, S. Ogihara and A. Kobayashi, Science University of Tokyo

Microscopic damage initiation and growth behavior in quasi-isotropic CFRP laminates under tensile fatigue loading were investigated. Transverse cracks and delaminations were quantitatively evaluated as a function of the number of stress cycles at various loading levels. Damage observation was conducted by using an optical microscope and a soft X-ray radiography.

Experiment

The material used was T800H/3900-2 CFRP with interlaminar-toughened layers supplied by Toray Inc. The T800H/3900-2 prepreg system has tough and fine Polyamide particles on its surfaces, which results in formation of the interlaminar-toughened layers at every ply interface in the laminates. The fiber volume fraction was about 55%. The laminate configurations were quasi-isotropic [$\pm 45/0/90$]s, [$0/\pm 45/90$]s, and [$45/0/90/-45$]s in order to discuss the effect of stacking sequences on microscopic fatigue damage.

Tensile fatigue tests were conducted at the stress ratio, $R=0$, with a frequency of 5Hz under load control conditions of sinusoidal waves. The maximum stress levels, S , were selected as 60%, 40% and 25% of the static tensile strength of each laminate. During fatigue tests, the testing machine was periodically stopped, and the onset and growth of transverse cracks and delamination were observed. Transverse crack evolution on the edge was observed as a function of the number of stress cycles. Delamination onset and growth in the width direction were detected by the X-ray observation. The number of transverse cracks per unit observed-length and the area of delamination per unit observed-area were defined as the transverse crack density and delamination ratio, respectively.

Experimental Results

Figure 4 shows fatigue damage progress in a [$\pm 45/90$]s laminate on the basis of the edge observation by an optical microscope. The first microscopic damage observed in all specimens was transverse cracks in 90° ply. In [$\pm 45/0/90$]s and [$0/\pm 45/90$]s laminates, delamination at $q/90$ and $90/90$ interface was also observed. Microscopic damage in each ply and interface initiated at free edge and grew in the width direction as the number of stress cycles increased. Figures 5 and 6 indicate transverse crack density in 90° and $\pm 45^\circ$ plies as a function of the number of stress cycles, respectively. Transverse crack density measured by X-ray observation means the number of transverse cracks, which went through in the width direction, per observed-length. Figure 7 shows a delamination ratio as a function of the number of stress cycles. Transverse cracks and delaminations initiate at earlier stage at higher stress levels in all the laminates. It will be possible to model their microscopic damage progress on the basis of the precise damage observation.

12.3.2 Effects of Loading Frequency and Environment on Fatigue Delamination-Crack Growth of CFRP

Y. Nakai, Kobe University

The delamination-crack growth behavior under isothermal and thermo-mechanical fatigue was investigated for unidirectional CF/epoxy laminates (Toray P3060-15). The thickness of the laminates was 8 mm. An initial notch was introduced into a specimen by inserting a small piece of Teflon film between prepregs. Fatigue tests were conducted under constant ΔK conditions either in air or in water. DCB and ENF specimens were employed for Mode I and Mode II crack-growth tests, respectively.

Mode I Fatigue Crack Growth

During constant ΔK tests, the loading frequency was changed to examine the effect of loading frequency on crack growth in air. Figure 8 shows the cycle-based crack-growth rate, da/dN , in air. Independent of the loading

frequencies, the cycle-based crack growth rate is almost constant, and it can be concluded that Mode I fatigue crack growth is dependent on the number of load cycles (cycle-dependent) in air.

The time-based fatigue crack growth rate is defined crack growth per unit time and denoted by da/dt . Figure 9 presents da/dt in water under two different loading frequencies. Since the time-based crack growth rate is independent of the loading frequencies, the Mode I fatigue crack growth is dependent on the total test time (time-dependent) in water.

Figure 10 indicates the crack growth behavior under variable test temperature. In the test, isothermal fatigue tests were conducted, but the test temperature was changed between 24°C and 80°C at every crack-extension of 5 mm. The crack growth rate drastically decreased when the test temperature decreased from a temperature higher than 50°C to that lower than 50°C. The crack growth behavior was not affected by other type of temperature change.

Thermo-mechanical fatigue tests were conducted either in air or in water. The highest test temperature was 70°C and the lowest was 35°C. The fatigue crack growth rates, da/dN , under thermo-mechanical fatigue tests for the stress ratio $R=0.5$ are shown in Figure 11(a). The crack growth rates obtained by an out-of-phase fatigue test were higher than those obtained by an in-phase fatigue test. Under isothermal fatigue at 35°C or 70°C, crack growth rates were too high to be measured, *i.e.*, specimens fractured just after the start of a fatigue test at $\Delta K=0.52 \text{ MPa}\cdot\text{m}^{1/2}$. It means that the crack growth rates in both types of thermo-mechanical fatigue tests were lower than those obtained by isothermal fatigue tests in air.

The delamination-crack growth rates for $R = 0.1$ are shown in Figure 11(b). For this stress ratio, the growth rates were not constant with crack extension. It indicates that the crack tip shielding by fiber bridging is larger for lower stress ratio. The growth rates in both types of thermo-mechanical fatigue tests are lower than the lowest growth rate in isothermal tests. The growth rates under in-phase thermo-mechanical fatigue are lower than those obtained by out-of-phase thermo-mechanical fatigue tests. These behaviors are the same as those for $R=0.5$.

Figure 12 indicates the crack growth rates in water. The crack growth rates obtained by isothermal fatigue tests in water were higher as the temperature became lower. The rates obtained by thermo-mechanical fatigue tests were almost equal to those obtained by isothermal fatigue tests, of which test temperature was equal to that at the maximum load in the thermo-mechanical fatigue test.

Mode II Fatigue Crack Growth

Figure 13 presents the time-based crack growth rate, da/dt , as a function of crack length from the initial notch. Since the crack growth rate is independent of the loading frequencies, the Mode II fatigue crack growth is time-dependent either in air or in water.

As shown in Figure 14, the growth rate at 25°C is higher than that at 70°C. Contrary to Mode I fatigue crack growth, no effect of the test temperature change was observed in Mode II fatigue crack growth.

12.3.3 Strength Degradation of High Temperature Polymeric Composite Materials for the Next-Generation SST Structures by Isothermal Aging*

T. Shimokawa, National Aerospace Laboratory (NAL)

NAL and three major Japanese aircraft industries, *i.e.*, FHI, KHI, and MHI, are conducting a joint research program of structural material evaluation for a SST of the next-generation. As a part of this program, this study investigated the strength degradation of high temperature polymer composites by isothermal aging. Namely, the tensile and compressive strengths of notched specimens, and the short beam shear (SBS) strength were investigated for three kinds of carbon/high-temperature polymer composites at room and isothermal-aging temperatures, before and after isothermal aging up to 15,000 hours. The three kinds of carbon/high temperature polymer-composite laminates tested were made of two kinds of carbon/bismaleimide prepreg systems, G40-800/5260 and MR50K/MR2000N, and a carbon/amorphous thermoplastic polyimide prepreg system, T800H/PI-SP, which are current candidate composites for the SST structures.

The two kinds of panels with quasi-isotropic stacking sequences, 24 plies $(45/0/-45/90)_{3S}$ for tensile notched specimens, and 32 plies $(45/0/-45/90)_{4S}$ for compressive notched specimens, were circular-hole notched before thermal aging. The panels for SBS specimens were a unidirectional laminate, 20 plies (0_{20}) . The panels were isothermally aged for 5,000, 10,000, and 15,000 hours at 120°C or 180°C in air circulating ovens. Specimens were machined from virgin and isothermally aged panels. Figure 15 shows the geometry of panels for isothermal aging and specimens tested. Prior to static tests, specimens were dried in a vacuum oven. The notched tensile and notched compressive strengths were represented by nominal strength calculated using the nominal thickness based on the nominal prepreg thickness and the net width. The SBS strength was represented by net strength calculated using the measured thickness.

Figure 16 presents the relationship between notched tensile strength and thermal aging time for two batches of G40-800/5260 laminates. In the case of isothermal aging at 180°C, fairly large strength degradation was observed.

Figure 17 shows the relationships between notched compressive strength and isothermal aging time for the three kinds of high temperature polymer composites. In the case of the G40-800/5260 bismaleimide composite and thermal aging at 120°C, the strength at room temperature does not reduce with thermal aging time, but that at 120°C slightly reduces. In the case of 180°C aging, the strength remarkably decreases with thermal aging time, and after 5,000 hours, this drop is almost proportional to thermal aging time. In the case of the MR50K/MR2000N bismaleimide composite and thermal aging at 180°C, the strength significantly decreases with isothermal aging time. The strength degradation is especially great from 5,000 to 10,000 hours, and dulls after 10,000 hours. In the case of the T800H/PI-SP polyimide composite, the strength degradation by isothermal aging at 120°C and 180°C, up to 15,000 hours, was not found.

The SBS strength was represented by the maximum stress that could commonly be determined for all test cases, though this definition was questionable as a SBS strength. Figure 18 depicts the obtained results of SBS strength versus isothermal aging time for three kinds of high temperature composites. The test number is five for each case. The SBS strengths of the G40-800/5260 composite at room temperature and 180°C, after thermal aging at 180°C, reduced with fluctuations. The SBS strength of the MR50K/MR2000N composite at 180°C indicated a fairly large drop with thermal aging time. The scatter of the SBS strength was high after the thermal aging at 180°C. In the case of the T800H/PI-SP composite, there was no reduction of the SBS strength after thermal aging at 120°C and 180°C.

* T. Shimokawa, Y. Hamaguchi, Y. Kakuta, H. Katoh, T. Sanda, H. Mizuno, and Y. Toi, "Effect of Isothermal Aging on Ultimate Strength of High Temperature Composite Materials for SST Structures", Journal of Composite Materials, Vol. 33, 1999 (to be published).

12.4 JOINTS

12.4.1 Evaluation of Plugged Hole Effect on Fatigue Life

T. Kitagawa, Kawasaki Heavy Industries, Ltd. (KHI)

The fatigue life of a plate with a plugged hole is known to be longer than that of a plate with an open hole. The author quantitatively evaluated the plugged-hole effect by conducting fatigue tests.

Figure 19 shows the specimen configurations. The detail of specimens is as follows:

Material: 7075-T6, $t=0.063$ inch

Number: 7 specimens

Group A: having 6 open holes

Group B: having 6 plugged holes with AD-rivets (MS20470AD4-6)

Fatigue loading is:

P_H (high load) = 780 lbs ($f_t = 20.0$ ksi)

R (Stress ratio) = 0.03

Figure 20 indicates the fatigue test results. The hole filling effect with AD-rivets can be clearly recognized. The averaged life of the specimens with plugged holes is approximately 20 times greater than that of the specimens with open holes.

12.5 COMPONENT TESTING

12.5.1 Fatigue Tests of Fuselage Structure Model by Pneumatic Cycles

H. Terada, T. Okada, and P. Dybskiy, National Aerospace Laboratory (NAL)

If uni-axial fatigue test results for simple fastener joints accurately predict the fatigue life of a fuselage structure under complex operational load conditions, remarkable saving time and money can be expected.

In order to obtain the correlation between the test results of simple fastener joints and the fatigue life of a fuselage structure mentioned above, fatigue tests are being conducted using an approximately 1/3 scale model of the B-737 fuselage structure. Three specimens were manufactured to evaluate the effects of fatigue loads by simple pressurization, pressurization and bending, and the combination of pressurization, bending, and torsion on the fatigue damage process of the structure separately. The specimen geometry and testing conditions are listed in Tables 1 and 2, respectively.

Approximately 70% of the internal volume of the specimen was reduced by Styrofoam cores inserted. The cylindrical structure was made of four curved panels fastened by triple row counter-sunk rivets. The external appearance of fatigue testing is shown in Figure 21. The specimen is fixed to the right end truss. The counter-balancing weight is used at the left free end to cancel the weight of the specimen. Doublers were used at the both end-bays to avoid the failure at these areas. In the case of applying bending and torsional loads to the specimen, a pair of hydraulic actuators are used at the free end. Strains were measured to monitor the strain history and evaluate the effect of the stiffeners. These results were compared with those of FEM analysis. Fatigue crack propagation was monitored through a 30-power CCD-microscope remotely controllable in x, y, and z directions.

A fatigue test by simple pressurization was ended last year and the second fatigue test, i.e., by the synchronized combination of pressurizing and bending, is under way.

The results of the fatigue test by simple pressurization are as follows:

1. Fatigue crack initiation was observed at the edge of several rivets of the top row fasteners after 90,000 cycles. Variety of growth rates was obtained at each crack.
2. After approximately 100,000 cycles, three cracks became dominant and their growth was faster than other cracks. One of these dominant cracks linked-up after 117,800 cycles and unstable fast-fracture took place at 118,931 cycles. The failure mode was flapping at that bay as shown in Figure 22.

12.5.2 Cast Front Pressure-Bulkhead – Damage Tolerance Test

M. Hirahara, Japan Aircraft Development Corporation (JADC), and S. Taura, Mitsubishi Heavy Industries, Ltd. (MHI)

Introduction

It is generally believed that substantial reduction in the production cost is achieved by incorporating monolithic cast parts; however, cast parts have been used only for secondary structures which were not flight-critical. This study was carried out to apply casting to the primary structure of a commercial airplane of the 80- to 100-seater class by the joint team including the Boeing Commercial Airplane Group (BCAG), the Hitchcock Industries Inc. (HII), and JADC. A front pressure-bulkhead was selected as a candidate of primary cast structures. MHI conducted damage tolerance tests of the cast front pressure-bulkhead under the contract with JADC. Summary of the test is described below.

Objectives of Damage Tolerance Tests

Since any monolithic part generally provides no crack stopper, if a crack initiates, it will grow rapidly without any

structural interference within a flight and finally lead to a catastrophic failure. Therefore, this study aimed at the following objectives:

1. To confirm the accuracy of a DT analysis tool to predict crack propagation before a crack grows up to the critical length.
2. To determine a crack growth profile after a crack reached the critical length, which the DT tool cannot well predict.

Cast Bulkhead Design

In order to make an apple-to-apple comparison against a front pressure-bulkhead of a conventional build-up type, the design constraints were defined as identical to those of the B 737 airplane. The maximum differential pressure was determined to be 9.6 psi and the service life to be 75,000 cycles. The configuration of a cast bulkhead was developed mainly by BCAG and HII in consideration of the casting process and required functions. It has double curved shells which are interconnected by internal rays and a circumferential ring at the outer edge, with several types of intercostals to which adjacent skins and stringers etc. are attached. On the forward face of the front shell, inspection opening is provided. Figure 23 indicates the cast bulkhead.

Analysis and Test

Before DT test, FEM analysis and subsequent DT analysis (NASA FLAGRO modified) were conducted. DT analysis results showed that some cracks in high-stress area would propagate rapidly under cyclic pressure loading. DT test was conducted for a test article with several artificial cracks in high-stress locations, including the locations in which DT analysis predicted rapid crack growth. DT test was continued under cyclic loading (1-9.6 psi) up to one design life. Figure 24 presents the test setup. Three artificial cracks, rapid growth of which was predicted by DT analysis, grew as evaluated. Also, the crack growth rate was gradually decreased once the crack reaches the critical length, then finally almost stopped. This is because the stress concentration around a crack tip was relaxed due to load redistribution. This was confirmed by the strain survey after the test. See Figure 25 for an example. The crack growth predicted by the analysis tool well matched to the test data when FEM was well tuned as illustrated in Figure 26.

Conclusions

1. A good correlation was observed between the analysis results and the test data, regarding crack growth before reaching the critical length.
2. After exceeding the critical length, crack growth was stopped due to the relaxation in stress concentration. It means that a large monolithic structure can be “Damage Tolerant” with an appropriate design that provides a redundant load path.

12.5.3 Flaw Tolerance Verification Tests for MH2000 Helicopter

Z. Yamaguchi, Mitsubishi Heavy Industries, Ltd. (MHI)

MHI has been developing “Mitsubishi MH2000” aiming at the first-class multi-purpose helicopter through the 21st century, which is the first helicopter of purely Japanese make for both engine and airframe.

Figure 27 indicates the MH2000 in flight. The Civil Aviation Bureau of Japan granted the certification of this helicopter in June 1997 as a basic type.

MHI conducted many static and fatigue tests during the development and certification process. One of them was a verification test of the flaw tolerance of main/tail rotor composite parts, such as main rotor blades, a pitch horn/rod, and tail rotor blades. Figure 28 presents the composite components of the main and tail rotor systems. Figure 29 shows the detail of the main rotor blade.

Figure 30 presents the test set-up for the inboard portion of a main rotor blade. The test specimen was impact-damaged on selected critical locations. Then it was fatigue tested under repeated operational loads, including an axial tensile load, which was equivalent to a centrifugal load, and G-A-G-cycle load. Finally it was followed by the limit-load static test. The test results showed no damage propagation and no failure.

The final certification of fatigue strength and life was given by the analysis based on the test data of each component combined with the *S-N* curves obtained by other fatigue tests.

12.5.4 Static Tests of Composite Leading Edges of Vertical & Horizontal Stabilizers for Dash8 Q400

Z. Yamaguchi, Mitsubishi Heavy Industries, Ltd. (MHI)

Bombardier Dash8 Q400 is a short-range regional turboprop airplane of a new generation. MHI is participating in the design and manufacturing of the fuselage and empennage, and conducted the static tests of the composite leading edges of vertical & horizontal stabilizers as certification tests. The purpose of these tests was to demonstrate the structural integrity of the leading edges of vertical & horizontal stabilizers under the ultimate load after environmentally conditioned.

The leading edges are made of Aramid Fiber/Nomex Honeycomb Composites. The test set-up for the leading edge of the vertical stabilizer (as a typical example) is shown in Figure 31. The specimen size is about 114 inch long, 14 inch deep, and 12 inch wide. The loading pads (total 24 pieces) and the strain gauges (total 18 pieces) were bonded to the outer surface of the specimen. Test loads were applied with two independent hydraulic actuators through the tension and compression pads and the whiffletrees. The windward and leeward sides of the vertical stabilizer were loaded respectively. The specimen was supported rigidly to the test fixture that simulated the front spar of the vertical stabilizer. The dummy spar was fabricated with commercial steel to simulate the contour of the contact surface. The bolts used were the same size to the actual ones. The test specimen and monitor coupons were conditioned in a humidity chamber controlled at 76.6°C and 95% R.H. until the moisture content of 7-plyes ARAMID monitor coupons reached 5.05 weight %. The ultimate load was applied to the test specimen in the following steps, 0-20-40-60-80-100-120-130-140-145-150-100-80-40-0 % of the limit load. The load, deflection, and strain were recorded at each step. The specimen supported the ultimate load for more than 3 seconds. The structural integrity of the vertical stabilizer leading-edge was demonstrated under the ultimate load (150% of the limit load). No damage was detected by visual inspection and tapping after the test. The leading edges of the horizontal stabilizer were also tested in the same manner. The test results showed that the composite leading-edges have the ultimate load capability.

12.5.5 DADT Tests of Metallic Control Surface for Dash8 Q400

Z. Yamaguchi, Mitsubishi Heavy Industries, Ltd. (MHI)

MHI conducted DADT (Durability And Damage Tolerance) tests for an elevator to verify the DADT analysis, which is used for designing the metallic control surface for Dash8 Q400. The elevator design was changed from a manual control system (Dash8 S300) to a powered control system. The load condition of Q400 is much severer than that of S300. The specimen size is about 180 inches long, 4 inches deep, and 20 inches wide.

The testing load-spectrum simulated the air and inertia loads of this aircraft. A unit block of the load spectrum is equivalent to 2,000 flight loading and repeated 40 times for one lifetime, namely, 80,000 flights. For the durability and damage tolerance qualification using a single test specimen, the required number of flights to be loaded is 268,800 flights, i.e., 3.36 lifetimes, for the intact structure. The test set-up for the elevator is shown in Figure 32. The elevator was bolted to the test fixture. Reaction forces were measured with dummy actuator rods. The test loads were applied by two hydraulic servo actuators, which were capable of loading up to one ton via whiffletrees and 28 loading pads. 12 displacement meters and 76 strain gauges including 8 for dynamical monitors were installed to the specimen. To acquire the actual stress/displacement of the elevator and to monitor the test set-up, the strain survey was conducted at every half design-life.

This specimen satisfied the DADT requirement and the DADT analysis method provided a conservative prediction in fatigue crack propagation.

12.6 FULL-SCALE TESTING

12.6.1 Full-Scale Strength Tests for Japanese New Military Aircraft

M. Yasue and M. Ito, Third Research Center, Technical Research and Development Institute (TRDI), Japan Defense Agency (JDA)

Development of the Japanese New Small Observation Helicopter (XOH-1)

Since 1992 TRDI has developed the XOH-1 in Figure 33 for the Japan Ground Self Defense Force. The XOH-1 is the Japanese fully indigenous rotorcraft. The main missions of the XOH-1 are observation, reconnaissance, command, and control in the divisions of aviation units and anti-tank helicopter units. The XOH-1 is a four-bladed single rotor helicopter with tandem seats and twin engines. The normal gross weight is approximately 3.5 tons. The technical features in terms of the structure for the XOH-1 are the composite hingeless-rotor-hub system and the ducted tail-rotor. The full-scale strength tests, tie-down tests, and flight tests have been performed in the development. TRDI will have completed the development by the end of 1999.

Full-Scale Static Strength Tests of the XOH-1

In 1996 TRDI started the full-scale static strength tests of the XOH-1 using a test article as shown in Figure 34. More than hundred test cases which simulate flight loads, landing loads, ground loads, control system loads, crash loads, and etc. have been conducted to certify that the XOH-1 has enough static strength for the design loads. In 1998 the static strength tests have been completed successfully with minor modifications already applied and qualified during the test period.

Fatigue Tests of Main Landing Gears of the XOH-1

Employing the test article for the full-scale static strength test, TRDI conducted fatigue tests of the main landing gears of the XOH-1. The landing and ground load-spectra for two lifetimes, which are 44,000 landings, were applied to the main landing gears on a flight-by-flight basis. The counter loads were also applied to the airframe. The fatigue tests have been completed successfully without any problem.

Fatigue Tests of Rotors of the XOH-1

Since 1996 bench fatigue tests have been conducted for the specimens of rotor components, a main rotor hub, main rotor blades, and a tail rotor hub. For each component, six specimens were prepared for the ground-air-ground loads and other six for the high-cycle in-flight loads. Figure 35 shows loading systems. The specimens of a main rotor hub were subjected to the loads simulating the centrifugal force, lift force, torque force of rotation, flapping moment, lead lag moment, and pitch link angle. As to the specimens of main rotor blades, the centrifugal force, flapping moment, lead lag moment, and pitch link angle were simulated. The specimens of a tail rotor hub were applied to the centrifugal force, thrust force, torque force of rotation, and hub moment. The tests are being conducted successfully and will be completed by the end of 1999.

Development of the Japanese Next Generation Support Fighter (XF-2)

TRDI has developed the XF-2 in Figure 36 based on the USAF F-16 under the Japan-US joint-development program since 1988. The main modifications from the F-16 in terms of the airframe structure are the enlargement of the wing, the stretch of the fuselage, and the application of composite materials to the wings and fuselage. The development of the airframe was specified in the XF-2 ASIP Master Plan based on the MIL-STD-1530A. The full-scale strength tests and flight tests have been performed in the development. TRDI will have completed the development by the end of 1999.

Full-Scale Static Strength Tests of the XF-2

In 1995 TRDI started the full-scale static strength tests of the XF-2. More than hundred test cases which simulate flight loads, landing loads, ground loads, external store loads, control system loads, and etc. have been conducted to certify that the XF-2 has enough static strength for the design loads. Figure 37 shows a view in the test case of symmetrical pull up. As of March 1999, most of the test cases have been completed with some modifications, which are already applied and qualified.

Full-Scale Fatigue Strength Tests of the XF-2

Since 1995 the full-scale fatigue strength tests of the XF-2 have been conducted using three test articles, a full-scale single seat airframe, a two-seat forward fuselage component, and a horizontal tail component. Figure 38 shows test loading systems. The fatigue tests are composed of a durability test for two lifetimes and a damage tolerance test for two lifetimes after the durability test. The test spectra, developed in accordance with MIL-A-008866B with some modifications due to the mission of the XF-2, were applied to each test article on a flight-by-flight basis. A schematic of loading pattern for the test article of a single-seat airframe is shown in Figure 39. Inspection programs developed in accordance with MIL-A-83444 were conducted at the specified intervals. In March 1999 the whole fatigue strength tests were completed successfully with the data for in-service inspections and maintenance.

12.7 AGING AIRCRAFT PROBLEM

12.7.1 Residual Strength of Aged Small Aircraft**

In order to confirm the integrity of the primary structures, residual strength was investigated for three aged FA-200-180 small aircraft. Figure 40 shows the test set-up. FA-200-180 belongs to the acrobatic category and these three airplanes had been used in training for about 25 years at Civil Aviation College. Flight cycles of these airplanes were between 6,161 and 7,202 and the amount of flight hours were between 10,782 and 12,539. Static tests were carried out under pull-up-maneuvers loading cases when the positive limit-load factor, 6.0, was achieved, because the primary structures of the FA-200-180 were designed under these loading cases. Strains and displacements on the fuselage and wing together with the applied load were monitored at each load step.

There were no plastic strains at the limit load and these airplanes supported the ultimate load without failure for 3 seconds. The ratios of the failure load to the limit load were 198%, 200% and 199% and the scatter of the residual strength was very small. These limit load ratios agreed with that measured at the development stage. The degradation in the static strength of the primary structures caused by aging was not confirmed.

** Summarized by T. Okada, National Aerospace Laboratory (NAL), from “T. Ueda and T. Sotozaki, ‘Residual Strength of Aged Small Aircraft,’ Proceedings of 36th Aircraft Symposium, Japan Society for Aeronautical and Space Sciences and Japan Aeronautical Engineers’ Association, 1998, pp. 557-560 (in Japanese).”

12.8 AIRCRAFT ENGINE MANAGEMENT

12.8.1 Proactive Approach for Engine Reliability Improvement

S. Sugiura, All Nippon Airways (ANA)

Since current reliability management is reactive approach, an engineering action will be taken after engine failure. Therefore, the fleet-leader operator will always suffer from new problems. ANA is the fleet cycle-leader in many cases and will experience aging problems which impact on not only aircraft operation but also aircraft production and spare parts planning. Recently, the author developed a new reliability management program that is more proactive in identifying new problems before actual service problems will occur. This program was proposed to the PW4084/4090 Working Together Team (WTT) which consists of Boeing, PWA, United Airlines, Korea Airlines, and ANA in July 1997 and has been adopted by the WTT as a SUGI Method for a reliability management tool. The procedure of this program is introduced in brief as follows:

Step-1 Design/System Description

Explain the design feature and function of the engine hardware/systems

Step-2 Potential Failure Mode Analysis

Failure mode analysis for all the components and parts (FMEA and FTA). Evaluate problem initiation (leading indication of the problem) and discuss how the problem propagates utilizing a step by step failure analysis to

identify a possible failure consequence. If the failure consequence is significant (if affect Safety, IFSD, Unplanned Engine Removal, Planned Engine Removal, RTO, Dispatch Critical, and High Cost Parts Rejection: they are defined as significant problems), proceed to the next step.

Step-3 Significant Problem Analysis

If the design has been proven to prevent the problem (by enough experience and derivative design substantiated by the test results), no more analysis is required. Discuss the problem characteristics: Is the problem age-related or random? What is the problem propagation rate? How to detect the problem before each failure sequence? Figure 41 indicates a flow chart to analyze significant problems.

Step-4 Early Problem Identification Strategy

Determine the tool to detect the problem initiation (leading indicator). Dependent on the problem characteristic, determine what kind of tool is the most effective to identify the problem initiation.

Select the tool as follows:

1. PACER Engine (Engine Endurance Test)
2. Rig Test using the high cycle parts provided from an operator or PACER Engine
3. Threshold Sampling for the fleet leader operator
4. Opportunity Sampling Data (Trend Data analysis)

What is the requirement to detect the problem initiation?

1. NDT (Visual, FPI, USI, etc.)
2. Destructive Test
3. Laboratory Evaluation
4. Trend Data Monitoring
5. Bench Test (for Component)

Step-5 Problem Management Program

To avoid an arbitrary failure event, determine the most effective and economical Management Program based on the result of discussion on Step-3 and Step-4. If the problem is not manageable (problem occurs at random and propagates to fail very quickly), a redesign should be mandatory.

Step-6 Review the result of Test/Sampling/Data analysis

Identify an actual problem and the age of the problem initiation by the Test/Sampling/Data analysis.

Step-7 Amend the Maintenance Requirement and Redesign if Necessary

Introduce the Problem Management Program that is discussed in Step-5 based on the age of the problem initiation and review the design for improvement.

Step-8 Review and Refine the Program

Review the problems not predictable and refine the program.

12.9 AIRCRAFT ACCIDENTS

12.9.1 Aircraft Accident Investigation in Japan

T. Yabuki, Aircraft Accident Investigation Commission

Statistics Obtained by Accident Investigation

As of December 31, 1998, the number of civil aircraft registered in Japan were 2,785 including 1,238 airplanes (of which 396 were multi-turbine engine airplanes), 951 helicopters, 596 gliders including motorglider. The number of accidents that the Aircraft Accident Investigation Commission investigated for past 5 years is shown in Table 3. In 1997 and 1998, the accident investigation reports were issued for 73 accidents, of which 79.5% of causal factors were related to pilots, 8.2% to mechanical failure, and 12.3% to weather or others.

Accidents Due to Fatigue Failure

Table 4 shows the detail classification of accidents due to mechanical failure. The number in parenthesis indicates the accidents caused by fatigue failure. There were four cases related to fatigue failure. One case occurred in a twin turbine-engine airplane that came to rest on the runway after landing because the nose landing gear could not be locked. The retractable drag-leg assembly, one of parts for the nose-landing-gear retraction-mechanism, was found broken by fatigue. This airplane was operated as a pilot-trainer. Other two cases were similar causal accidents. Two helicopters having a single turbine-engine were crashed to the ground due to sudden engine-stop in flight when they were landing using the autorotation landing mode. These accidents occurred by the fatigue failure of an engine accessory (FCU) drive gear. Another case was an accident of a transport category airplane that came to rest on the ground due to the take-off rejection by the engine failure, which was caused by a fatigue failure of a high-pressure turbine-blade.

Example 1: Failure of Nose-Landing-Gear Retraction-Mechanism in Flight

Aircraft Identification: Piper PA-42-720

Part Identification: Nose Landing Gear Retract Mechanism Idler Link: P/N75178-02, fatigue failure occurred at the bolt hole connected to the retraction-actuator piston-rod-end

Time in Service: 5,137+47/18,219 Landing Gear Operating Cycles

Summary

This airplane was powered by twin turbine engines with the maximum weight of 10,530 lbs., and was utilized for a pilot-trainer at an airline. The accident involving this airplane occurred in May 1998. During touch-and-go training and the landing gears retracted, an abnormal noise was produced and a landing-gear warning-light illuminated. Though the efforts to extend all landing gears including emergency procedures were attempted, forced landing was made with only main landing gear extended. The nose gear was collapsed, and the lower skins and structure of nose section were damaged. According to the detailed examination, fatigue failure was found at the fracture surface of Idler Link shown in Figure 42 and the origin of fatigue failure was the forward outboard face of the Idler-link bolt hole. This failure was caused by repeated bending force of low cycles applied to the idler link by the retraction actuator.

Example 2: Gear Failure Due to Excessive Wear Caused by Engine Vibration

Aircraft Identification: Bell 214B

Engine Identification: Lycoming T5508D

Part Identification: Accessory Gearbox, Bevel Gear Assembly/Spar Gear (P/N2-080-016-04)

Time in Service of Accessory Gearbox: 3,935+03

Time in Service of Bevel Gear Assembly/Spar Gear: 1,769+14

Summary

This helicopter was powered by a single turbo-shaft engine with the maximum weight of 13,800 lbs. and was utilized for cargo transportation. The engine is composed of seven-stage axial and one-stage centrifugal compressors, and one-stage gas-generator turbine and two-stage power turbines, which generates 2,050 SHP output. The accident involving this helicopter occurred in September 1997. The helicopter engaged in a slinging work of construction materials. During hovering over the tower construction site for high-voltage electric-power-lines in a mountain, emergency landing was made on the construction site and the helicopter lied over due to a sudden engine stop. The disassembling investigation of the engine accessory gearbox in Figure 43 found that the spar gear with an internal spline connected to the accessory drive bevel-gear was broken into four pieces as shown in Figure 44. Therefore, the accessories were not driven and fuel was not supplied to the engine, resulting in a sudden stop of the engine. According to the detailed examination, fatigue failure was found on the teeth root of the spar-gear internal-spline. This failure occurred due to the abnormal wear of the gear caused by engine vibration.

Example 3: Bevel Gear Fracture Due to Improper Machine Work

Aircraft Identification: Aerospatiale AS350B

Engine Identification: Turbomeca Arriel 1B

Part Identification: Accessory Gearbox, Accessory Drive Intermediate Gear, Assembly/Bevel Gear

(Horizontal Gear: P/N0.292.10.276.0-S355B/41 teeth)

Time in Service of Accessory Gearbox: 1,759+56/TSO 51+16

Summary

This helicopter was powered by a single turbo-shaft engine, and was utilized for multi-purpose business use. The engine in Figure 45 is composed of one-stage axial and one-stage centrifugal compressors, a two-stage gas generator turbine, and a one-stage power turbine, which generates 641 SHP output. The accident involving this helicopter occurred in January 1997. During a flight for aerial photographic work, the engine suddenly stopped. Autorotation landing was attempted to a rice field, then the tail cone of the helicopter hit to the ground and the main rotor blades cut the tail boom. The disassembling investigation of the engine gearbox found that the horizontal bevel gear (41 teeth), driven by the accessory drive power-shaft gear, was separated into two pieces (hub and web) as shown in Figure 46. According to the maintenance records, the engine was overhauled outside Japan and the gearbox housing was repaired by an improper machine work. Since a measurement check for the machine work was not properly conducted, the misalignment of gear teeth occurred. The detailed examination revealed that a fatigue crack initiated at a tooth root and propagated during a small number of cycles.

Example 4: Sudden Engine Stop Due to HPT Blades Fracture by Intergranular Oxidation During Take off

Aircraft Identification: Douglas DC-10-30

Engine Identification: General Electric CF-6-50C

Part Identification: High Pressure Module/ 1st Turbine Blade

Total Time in Service of Engine: 61,891+00 / 19,023 Flight Cycles

Total Time in Service of Parts: 30,913+00 / 6,182 Flight Cycles

Summary

This large transport airplane was of a wide-body type having three turbo-fan engines and operated by a commercial air carrier for international scheduled flights. The engine is composed of four-stage axial LPC, 14-stage HPC, two-stage LPT, and four-stage HPT as shown in Figure 47. Take-off thrust was 51,800 lbs. The accident involving this airplane occurred in June 1996. Just after lift-off, the right engine failed and take-off was aborted. Then the aircraft overran the runway and was engulfed in fire. The disassembling investigation of the No.3 engine revealed that all of the HPT stage I blade airfoils (80) were broken at the root or at the mid-chord of the airfoils and severely blackened shown in Figures 48 and 49. The minute metal adhered to the first NGV of HPT module and all of the trailing edge of NGV burned off. According to the detailed examination, fatigue failure triggered by inter-granular oxidation was observed on the airfoil fracture surface of the first HPT blade shown in Figure 50.

12.10 ICAF DOCUMENTS DISTRIBUTED BY JAPAN DURING 1997-1999

- No. 2165 "Microscopic fatigue failure process in interleaved and toughness-improved GFRP cross-ply laminates," N. Takeda, S. Ogihara, A. Kobayashi, and D. -Y. Song
- No. 2167 "Local fatigue damage accumulation around notch attending crack initiation," Y. Iino
- No. 2168 "Fracture characteristics of Ti-6Al-4V and Ti-5Al-2.5Fe with refined microstructure using hydrogen," M. Niinomi, B. Gong, T. Kobayashi, Y. Ohyabu, and O. Toriyama
- No. 2178 "A new method of dynamic measurements of the plastic deformation occurring at a fatigue crack tip," M. Shimojo, T. Nagatomo, Y. Higo, and S. Nunomura
- No. 2179 "A fatigue-crack-growth-based analysis of two-step corrosion fatigue tests," S. Ishihara, A. J. McEvily and K. Shiozawa
- No. 2180 "Fatigue behavior in notched component of alpha+beta and beta titanium alloys under combined axial-torsional loading," T. Hoshide, T. Hirota, and T. Inoue
- No. 2181 "On the transition of fatigue crack growth from stage I to stage II in a corrosive environment," R. Hamano
- No. 2183 "Failure analysis and prevention in SCC and corrosion fatigue cases," K. Komai

- No. 2186 “Effect of adhesive layer thickness on fatigue strength of adhesively bonded butt, scarf and butterfly type butt joints,” M. Imanaka and T. Iwata
- No. 2187 “Crack initiation and small fatigue crack growth behavior of squeeze-cast Al-Si aluminum alloys,” K. Shiozawa, Y. Tohda, and S-M. Sun
- No. 2192 “A method for determining stress ratio of fatigue loading from the width and height of striation,” K. Furukawa, Y. Murakami, and S. Nishida
- No. 2193 “Mechanism of the two stage plastic deformation following an overload in fatigue crack growth,” M. Shimojo, M. Chujo, Y. Higo, and S. Nunomura
- No. 2194 “The entering behavior of environmental gases into the plastic zone around fatigue crack tips in titanium,” M. Shimojo, R. Iguchi, T. H. Myeong, and Y. Higo
- No. 2195 “Evaluation of stress corrosion resistance and corrosion fatigue fracture behavior of ultra-high-strength P/M Al-Zn-Mg alloy,” K. Minoshima, M. Okada and K. Komai
- No. 2207 “Effects of toughened interlaminar layers on fatigue damage progress in quasi-isotropic CFRP laminates,” N.Takeda, S. Kobayashi, S. Ogihara, and A. Kobayashi

ACKNOWLEDGMENT

Mr. Hisaya Katoh, a research engineer of National Aerospace Laboratory (NAL), is acknowledged for his assistance in compiling this review.

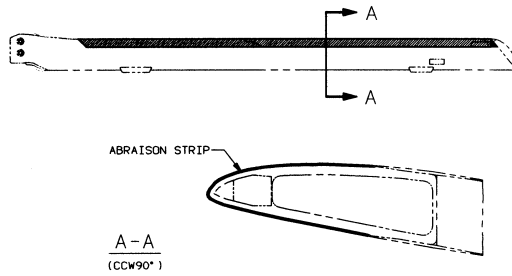


Figure 1 Typical construction of a composite rotor blade bonded with an abrasion strip.

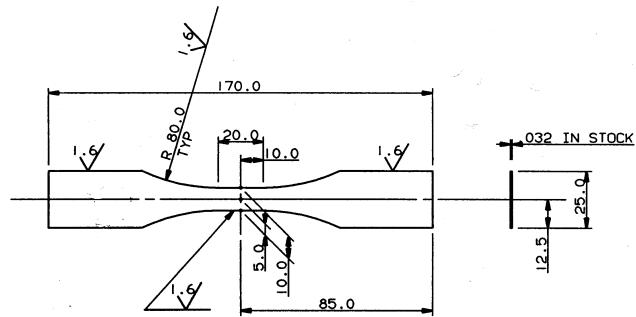


Figure 2 Specimen configuration; dimensions in mm.

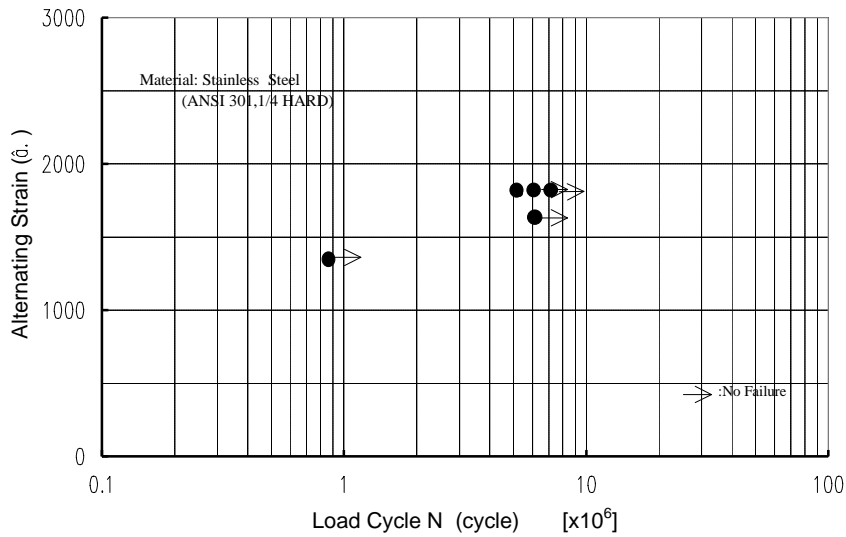
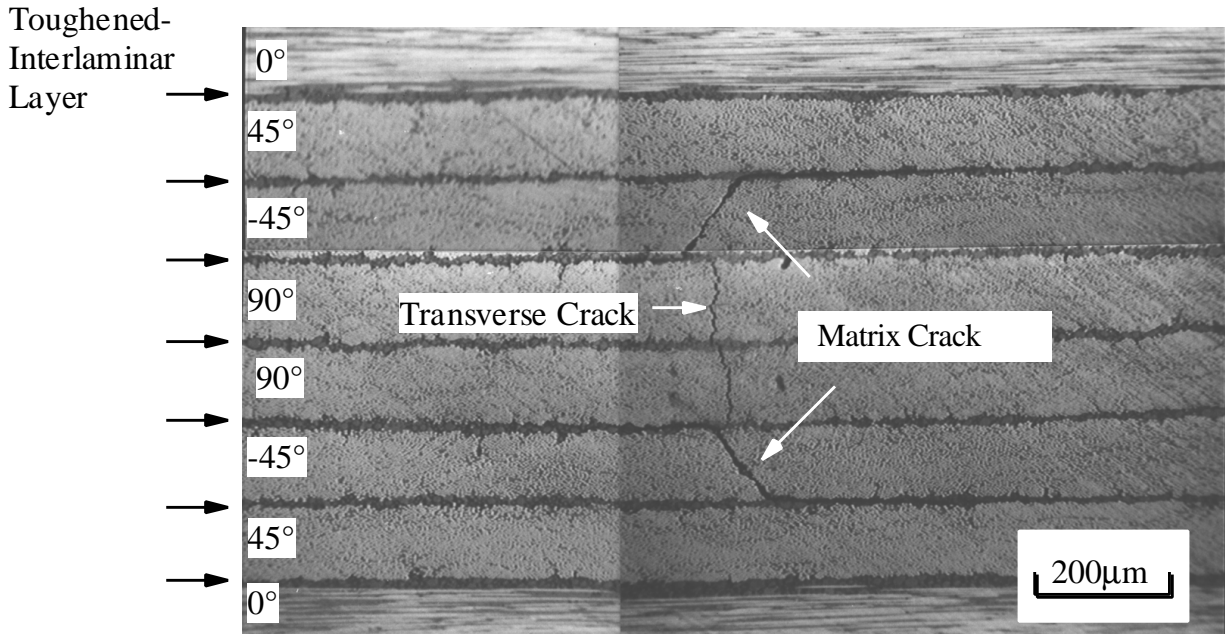
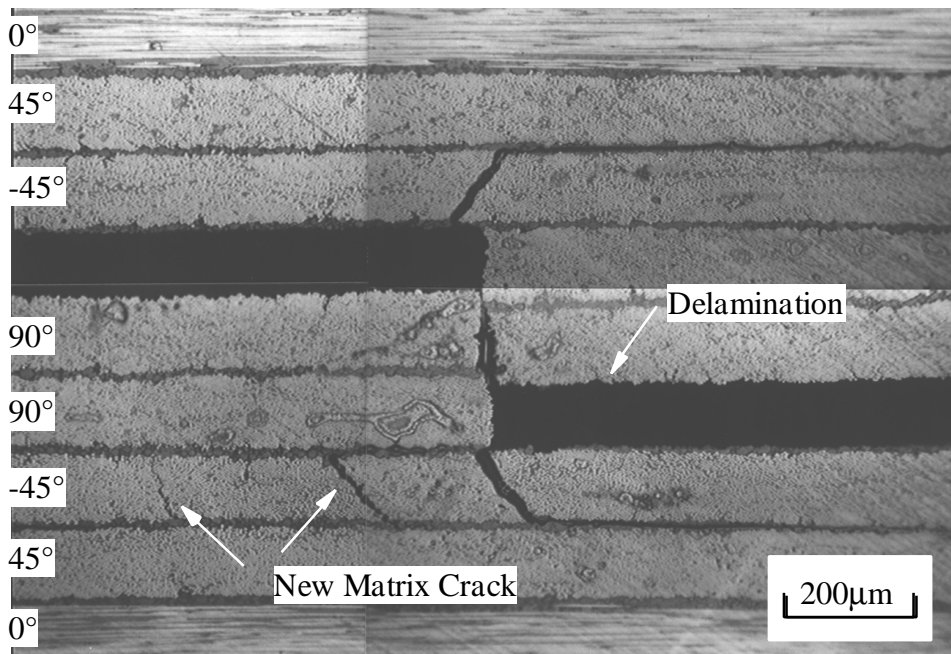


Figure 3 Fatigue test results.

(a) $n=1,000$ (b) $n=10,000$ Figure 4 Damage progress in $[0/\pm 45/90]_s$ laminates at the maximum stress level $S=0.6$.

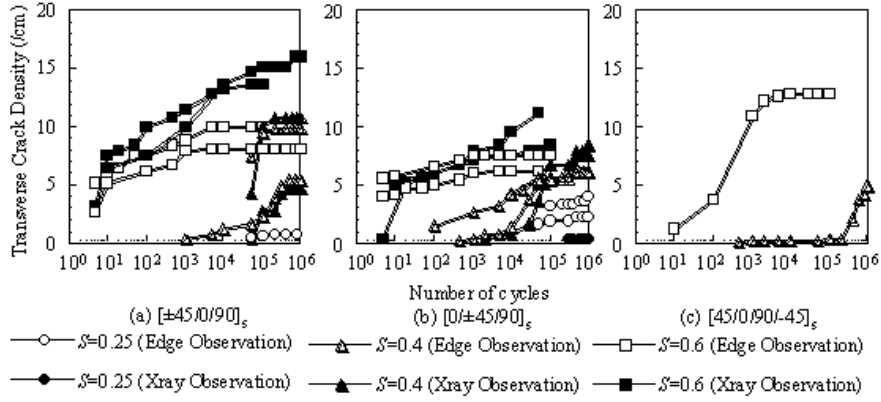


Figure 5 Transverse crack density in 90° plies as a function of number of stress cycles.

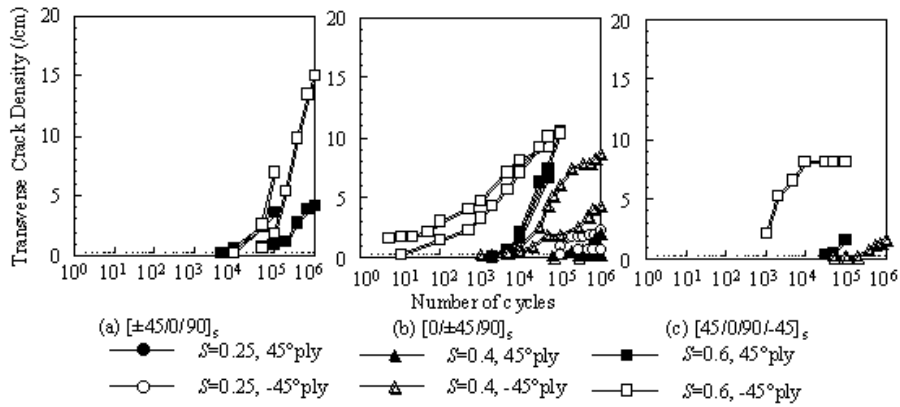


Figure 6 Transverse crack density in ±45° plies as a function of number of stress cycles.

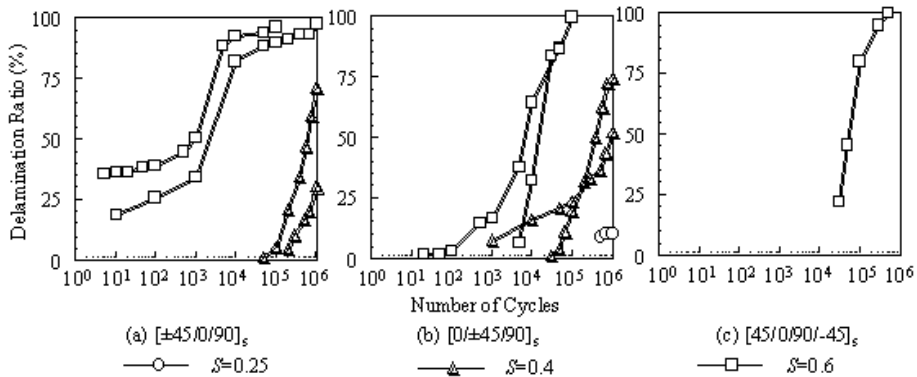


Figure 7 Delamination ratio as a function of number of stress cycles.

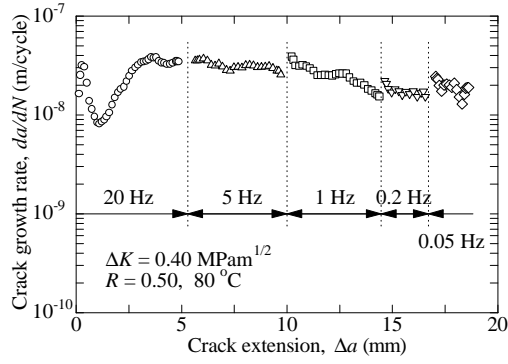


Figure 8 Effect of loading frequency on fatigue crack growth in air under isothermal fatigue.

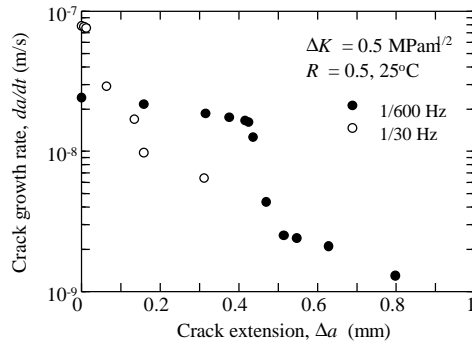


Figure 9 Effect of loading frequency on fatigue crack growth in water under isothermal fatigue.

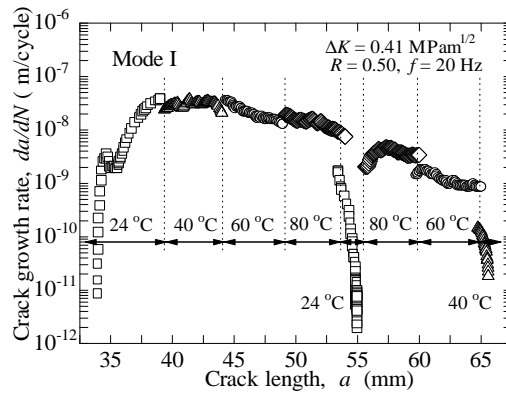
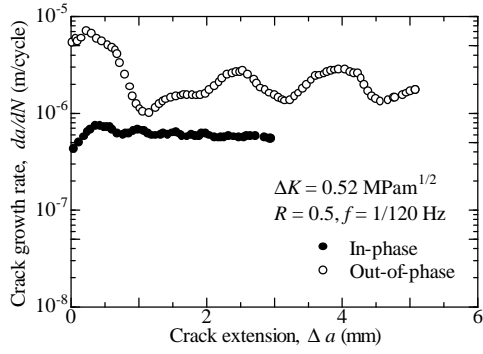
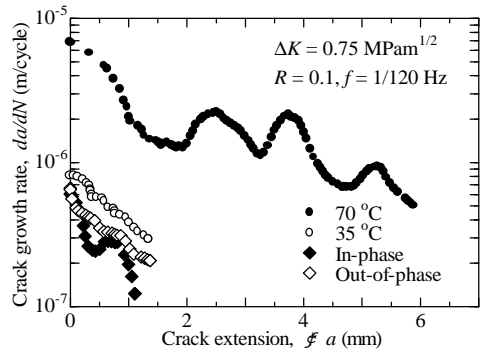


Figure 10 Effect of temperature change on fatigue crack growth under isothermal fatigue test.



(a) $R=0.5$



(b) $R=0.1$

Figure 11 Fatigue crack growth behavior under thermo-mechanical fatigue in air.

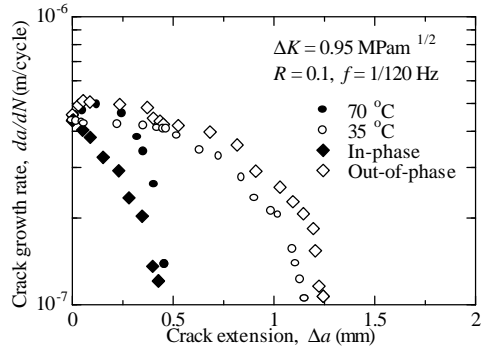
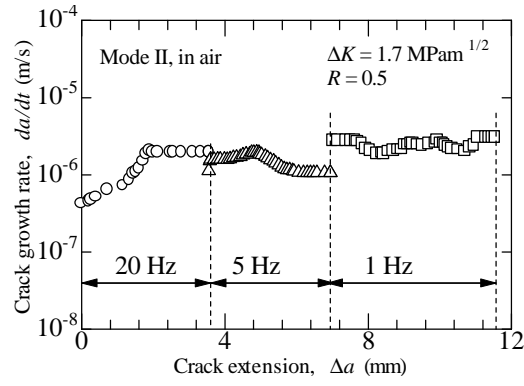
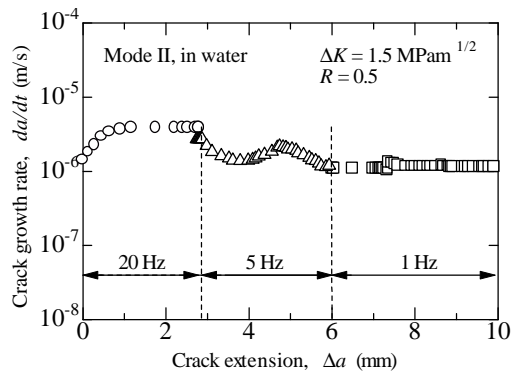


Figure 12 Fatigue crack growth behavior under thermo-mechanical fatigue in water.



(a) In air



(b) In water

Figure 13 Effect of loading frequency on Mode II fatigue crack growth.

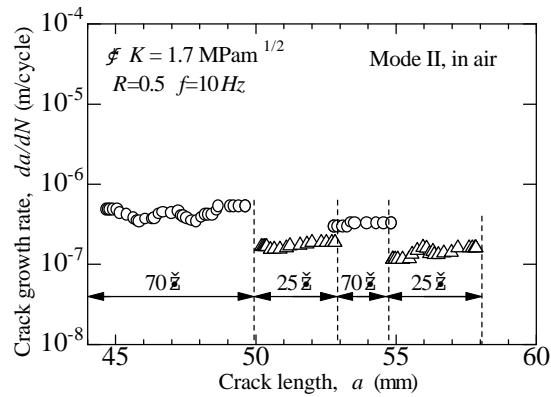


Figure 14 Effect of temperature changes on fatigue crack growth.

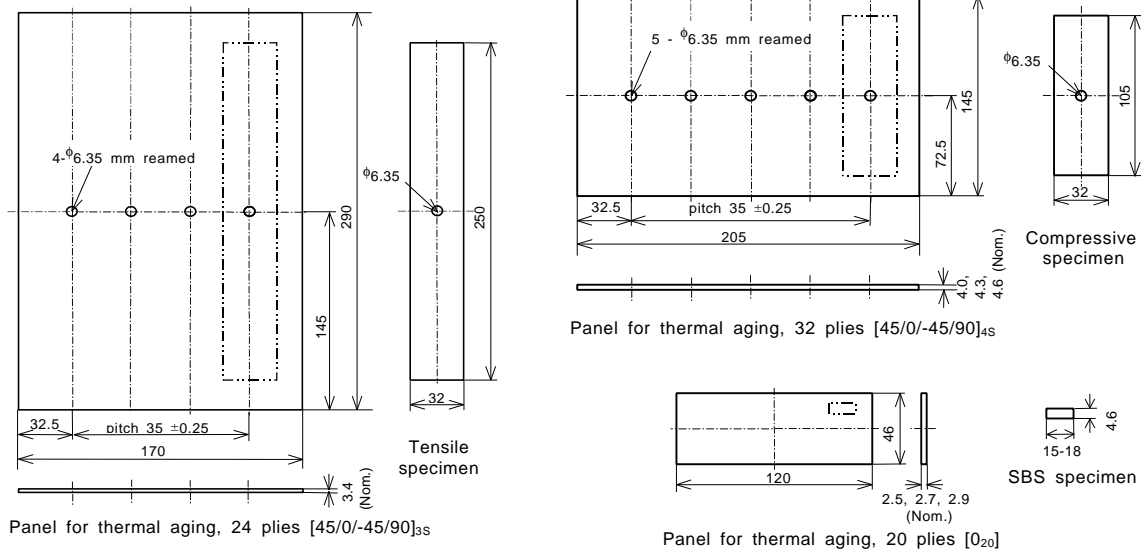


Figure 15 Geometry of panels for isothermal aging and specimens tested; dimensions in mm.

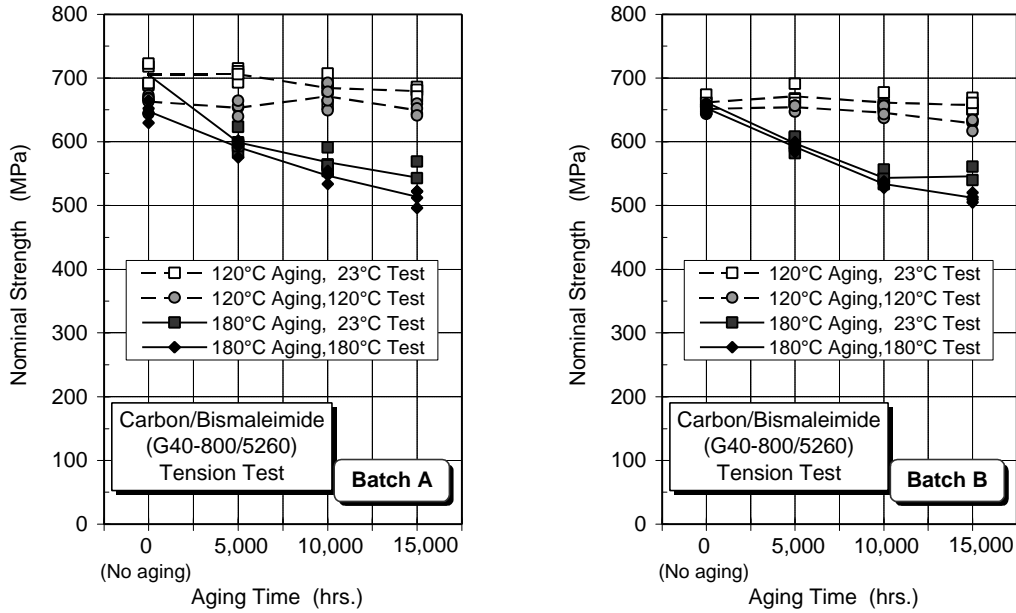


Figure 16 Open-hole tensile strength of G40-800/5260 carbon/bismaleimide composite versus isothermal aging time for two batches A and B.

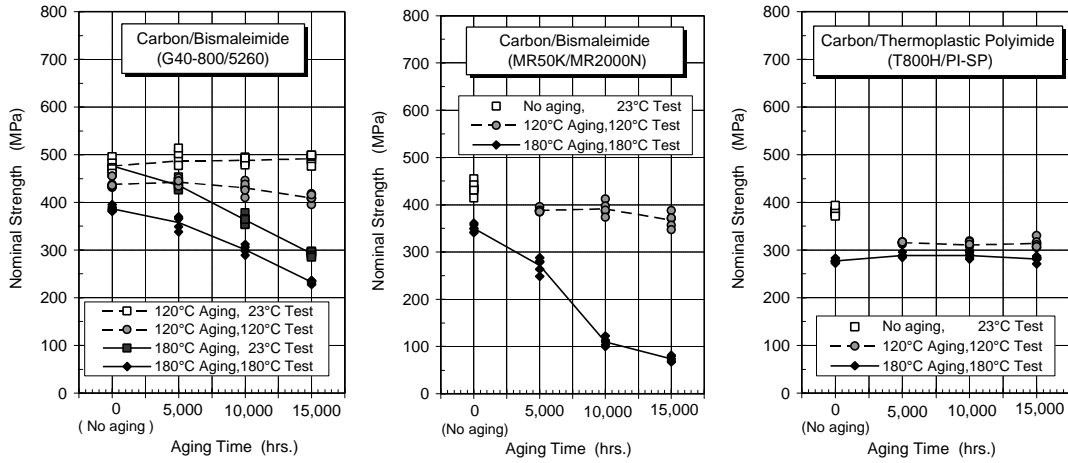


Figure 17 Open-hole compressive strength versus isothermal aging time for three kinds of carbon/high-temperature polymeric composites.

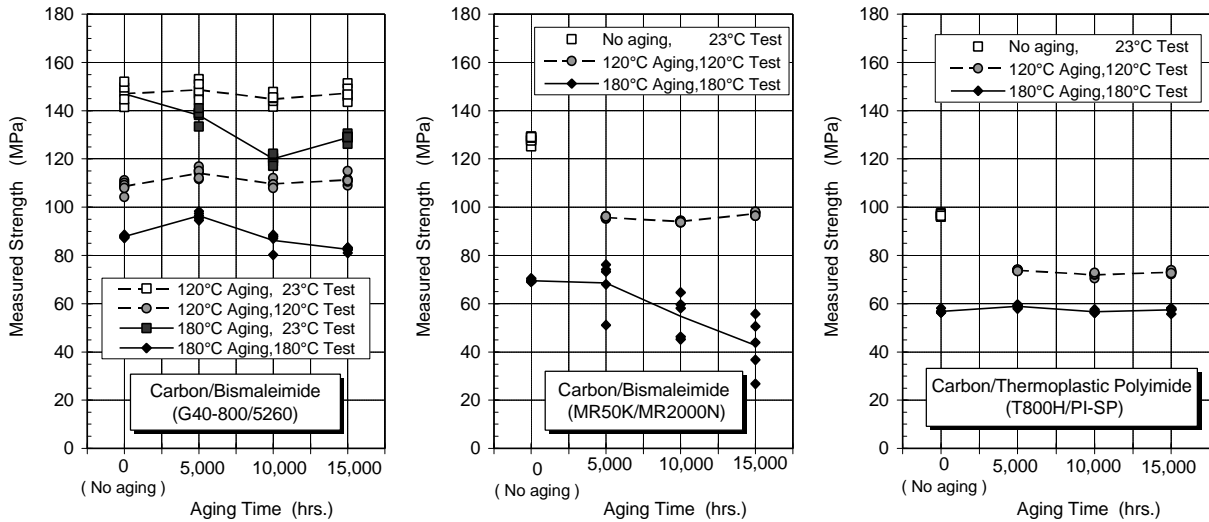


Figure 18 Short beam shear (SBS) strength versus isothermal aging time for three kinds of carbon/high-temperature polymeric composites.

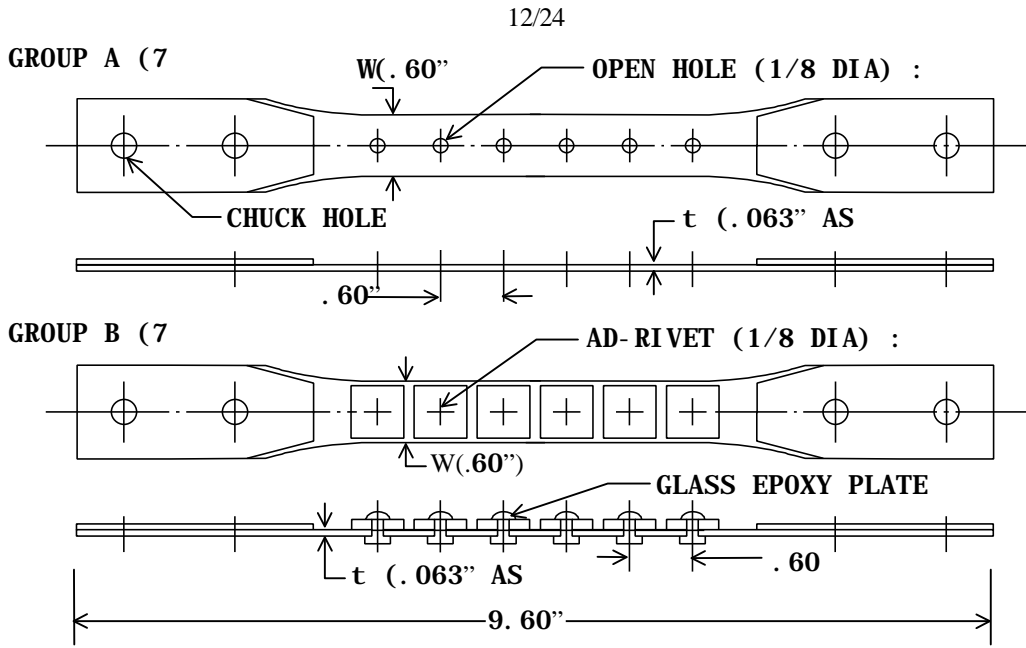


Figure 19 Geometry of specimens; dimensions in inch.

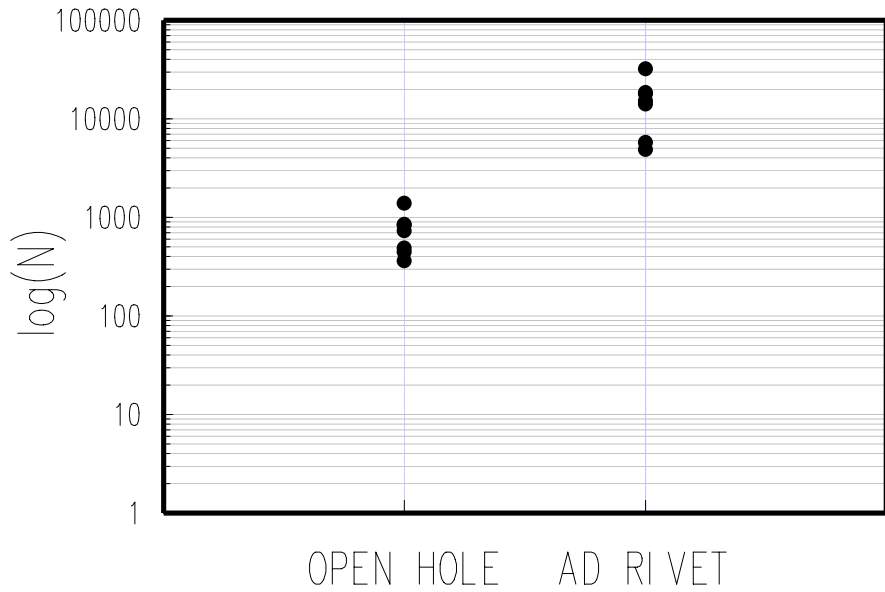


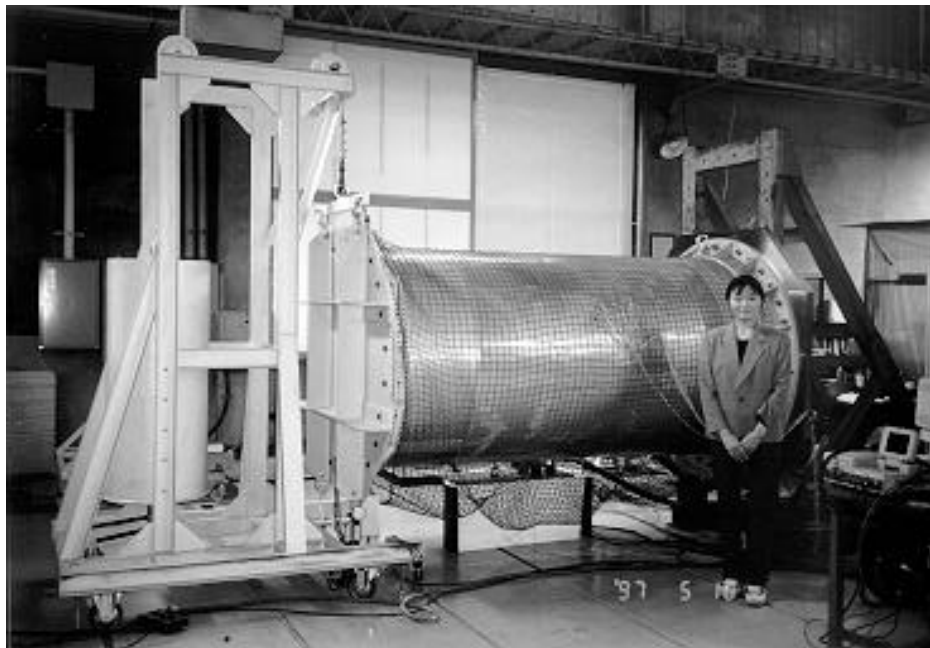
Figure 20 Fatigue test results.

Table 1 Specimen geometry.

Skin thickness	0.81 mm
Radius	625 mm
Length	2500 mm
Number of Frames	5
Number of Stringers	18

Table 2 Testing conditions.

Loading rate	1 cycle/min
Max. pressure	1.26 atm. (100 MPa at skin)
Min. pressure	0.10 atm.
Load ratio	0.08

**Figure 21 Aspect of fatigue testing.**

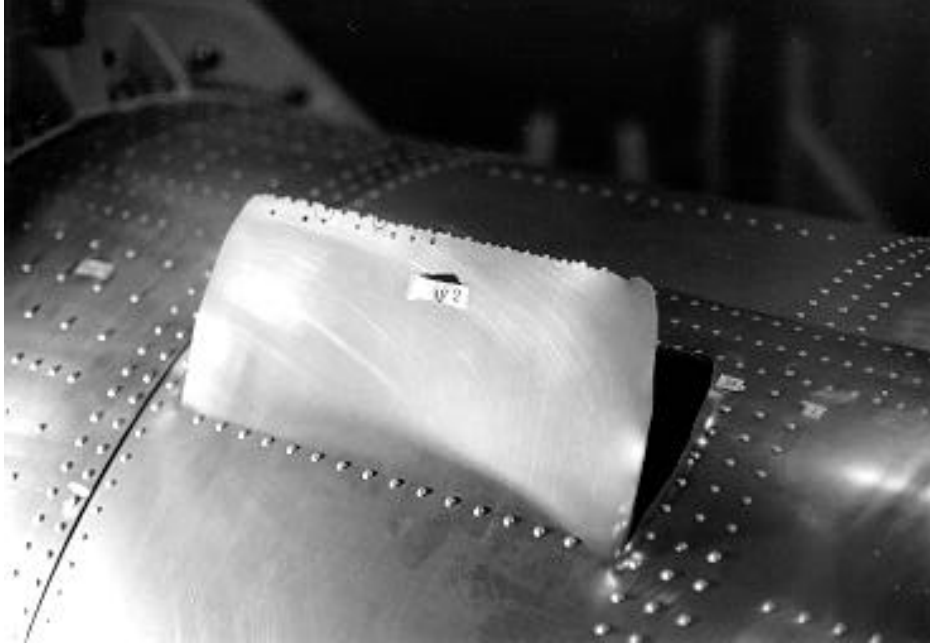


Figure 22 An example of flapping failure.

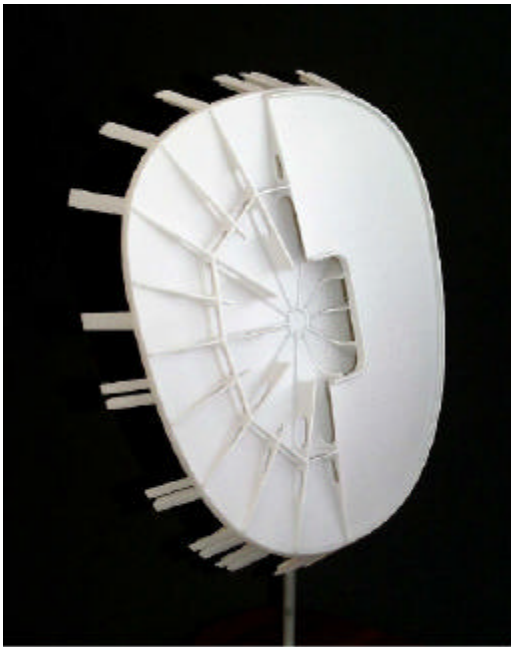


Figure 23 Cast front bulkhead (model).



Figure 24 DT test setup.

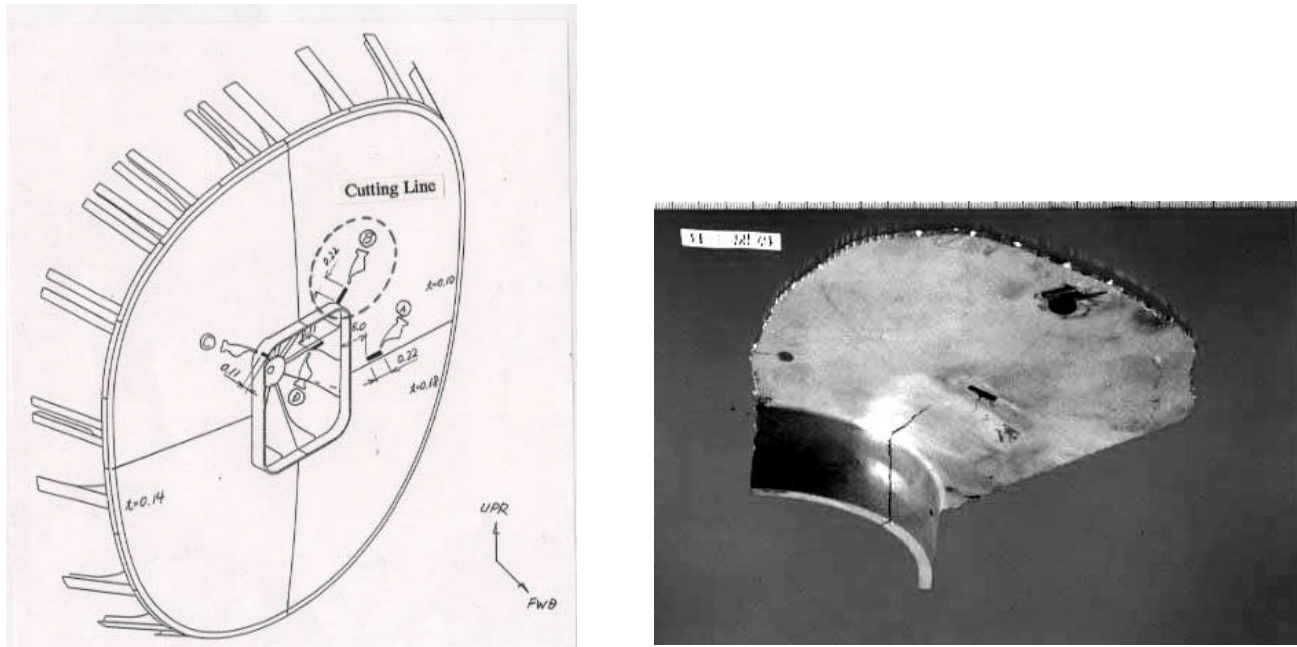


Figure 25 Crack in the door flange.

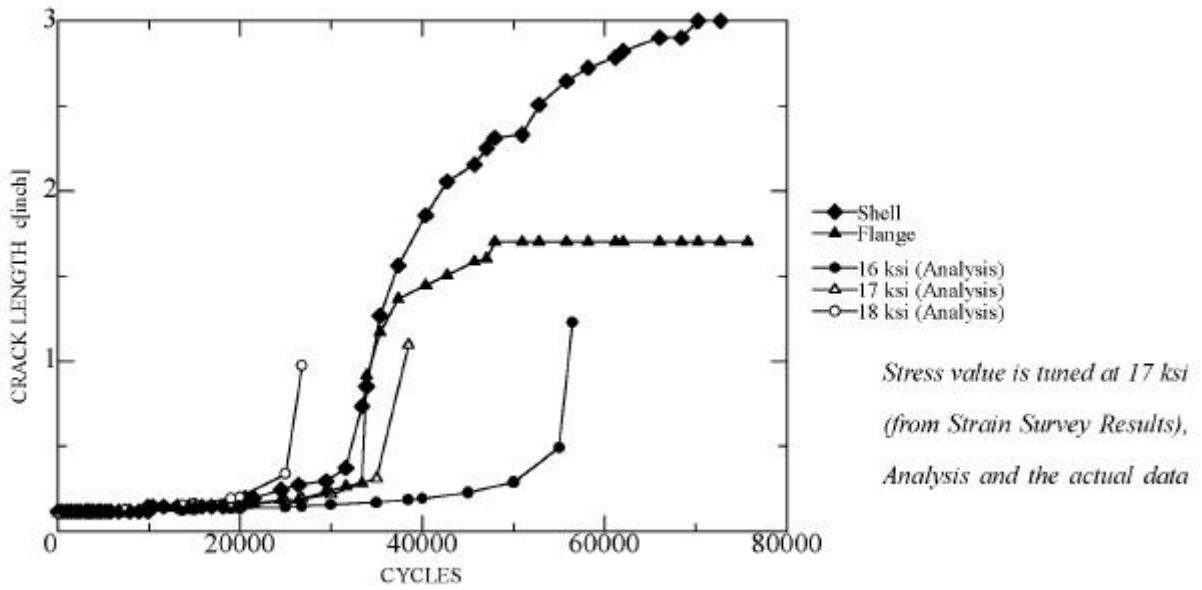


Figure 26 Analysis results versus actual data.



Figure 27 MH2000 flying around Yokohama Minato-Mirai 21.

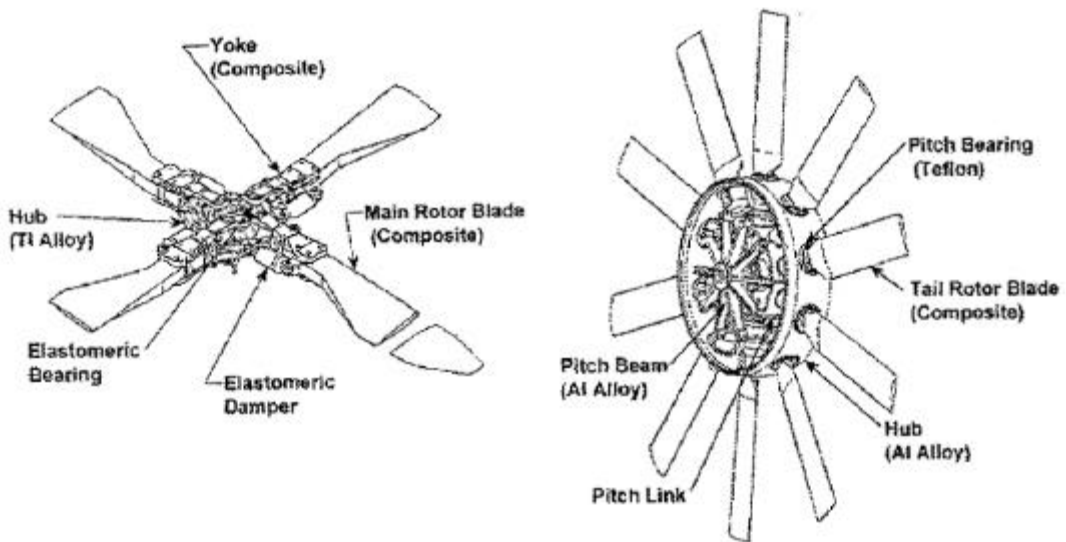


Figure 28 Main and tail rotor systems of MH2000.

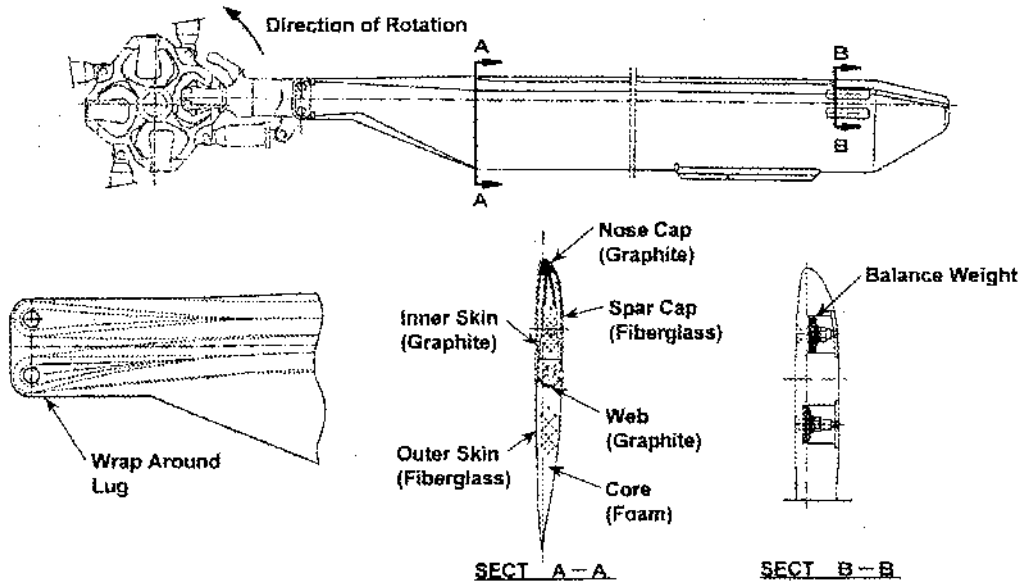


Figure 29 Main rotor blade.

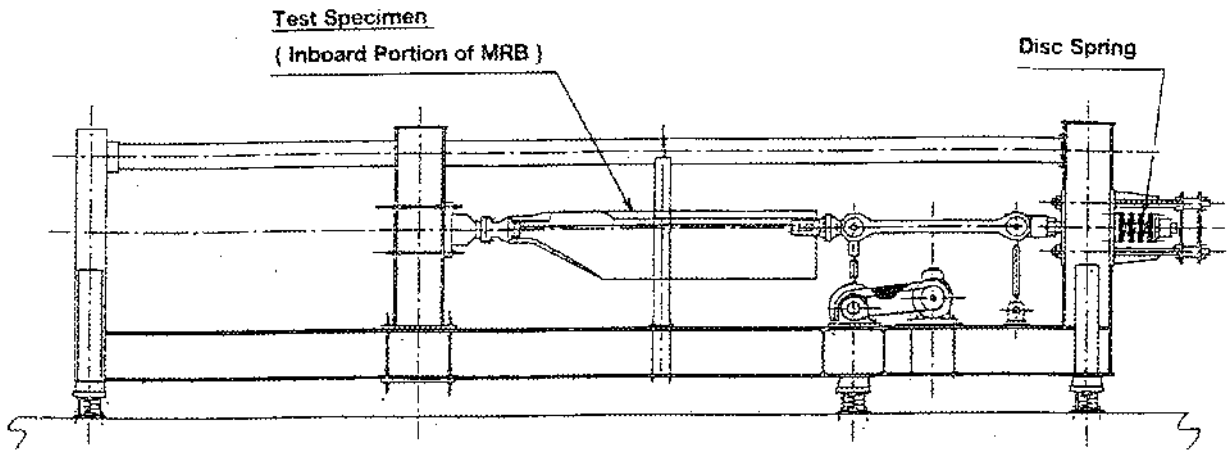


Figure 30 Test set-up for a main rotor blade.



Figure 31 Test set-up for a vertical stabilizer leading-edge.



Figure 32 Test set-up for an elevator.



Figure 33 Japanese new small observation helicopter (XOH-1).



Figure 34 Full-scale static strength test.

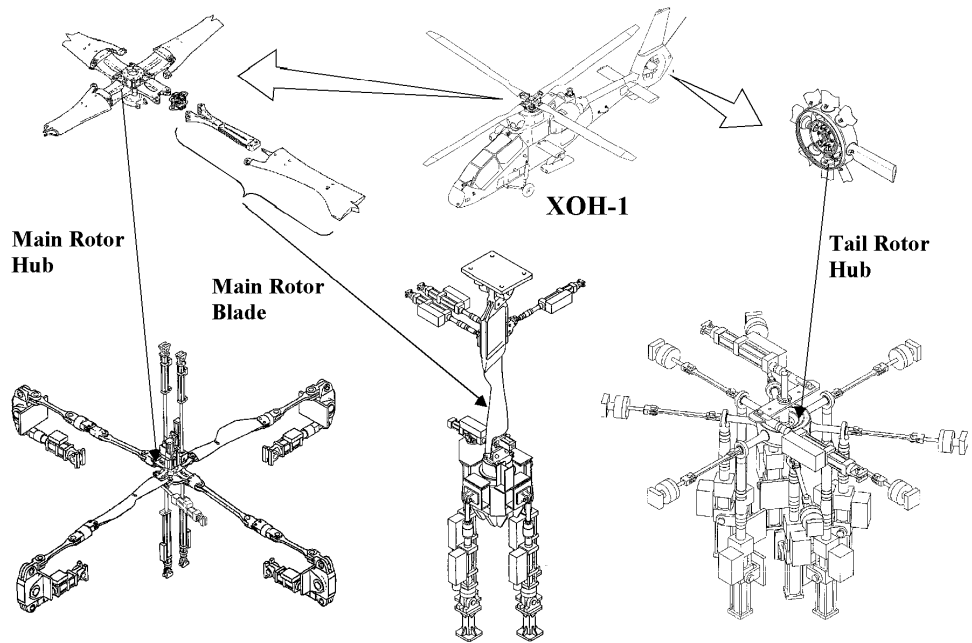


Figure 35 Loading systems of fatigue tests for rotor components.



Figure 36 Japanese support fighter (XF-2) of the next generation.

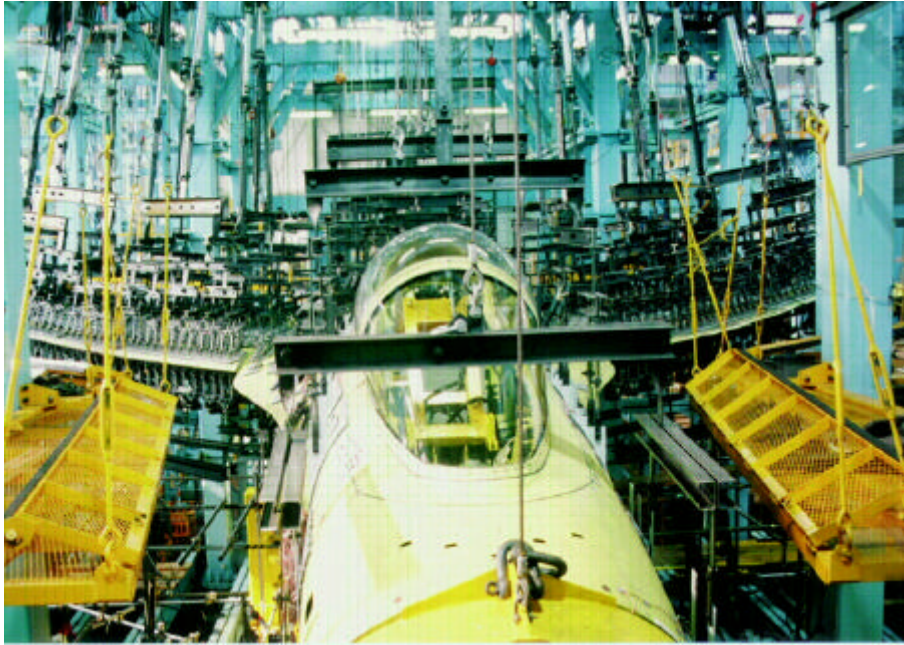


Figure 37 Test view at the 100% design limit load of symmetrical pull up.

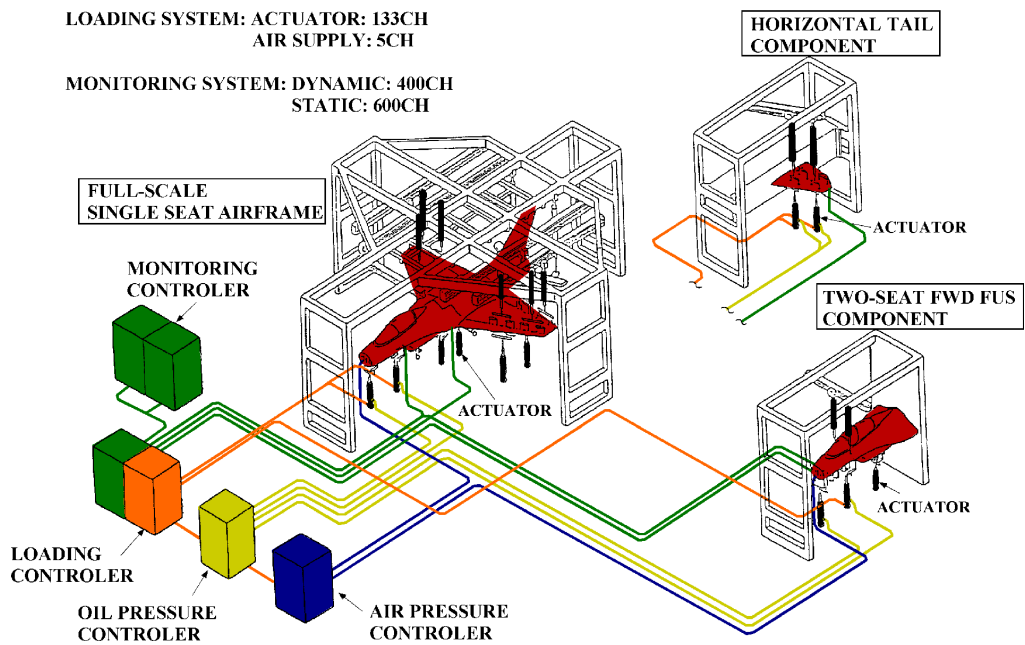


Figure 38 Testing system of full-scale fatigue strength tests.

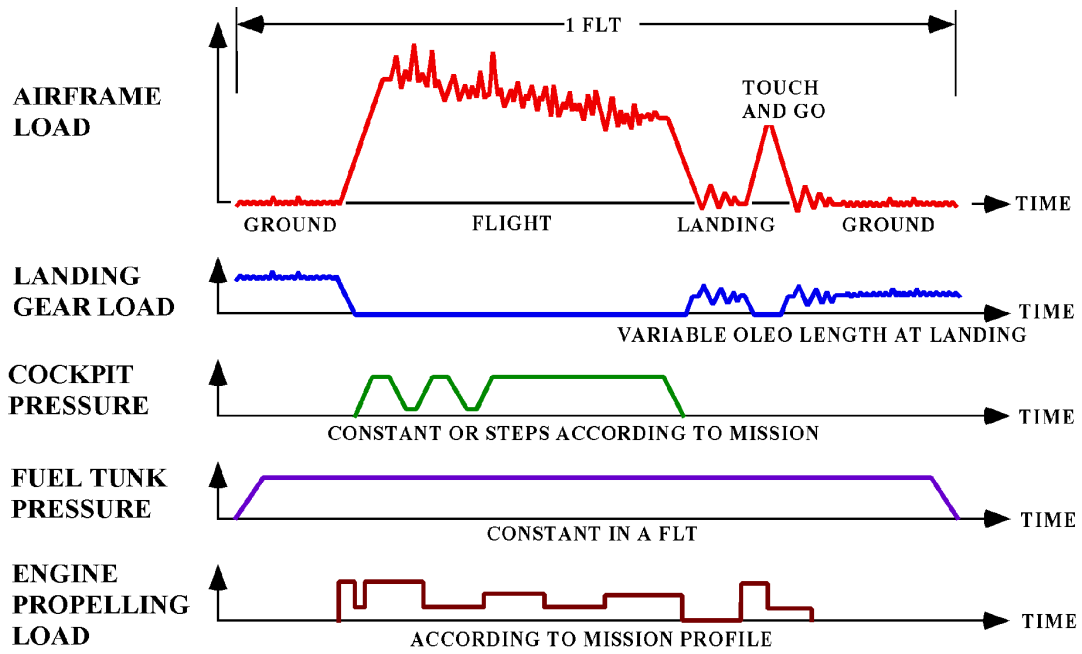


Figure 39 Schematic loading pattern for the single-seat-airframe fatigue test.



Figure 40 Static test set-up.

Table 3 Number of accidents investigated in Japan for past five years.

Year	1994	1995	1996	1997	1998	Total
Airplane	7	11	19	14	18	69
Helicopter	13	6	8	8	6	41
Glider/Motor Glider	2	1	4	3	6	16
Other (ULP etc.)	8	10	5	5	6	34
Total Accidents	30	28	36	30	36	160

Table 4 Number of accidents caused by mechanical failure during 1997 through 1998.

Kind of Aircraft	Cause				Total
	Airframe		Power Plant		
	1997	1998	1997	1998	
Airplane	0	1 (1)	1 (1)	1	3 (2)
Helicopter	0	0	1 (1)	1 (1)	2 (2)
Glider/Motor Glider	0	0	0	0	0
Others (ULP etc.)	0	2	0	0	2
Total	0	3 (1)	2 (2)	2 (1)	7 (4)

Note: The number in parenthesis indicates the accidents by fatigue failure.

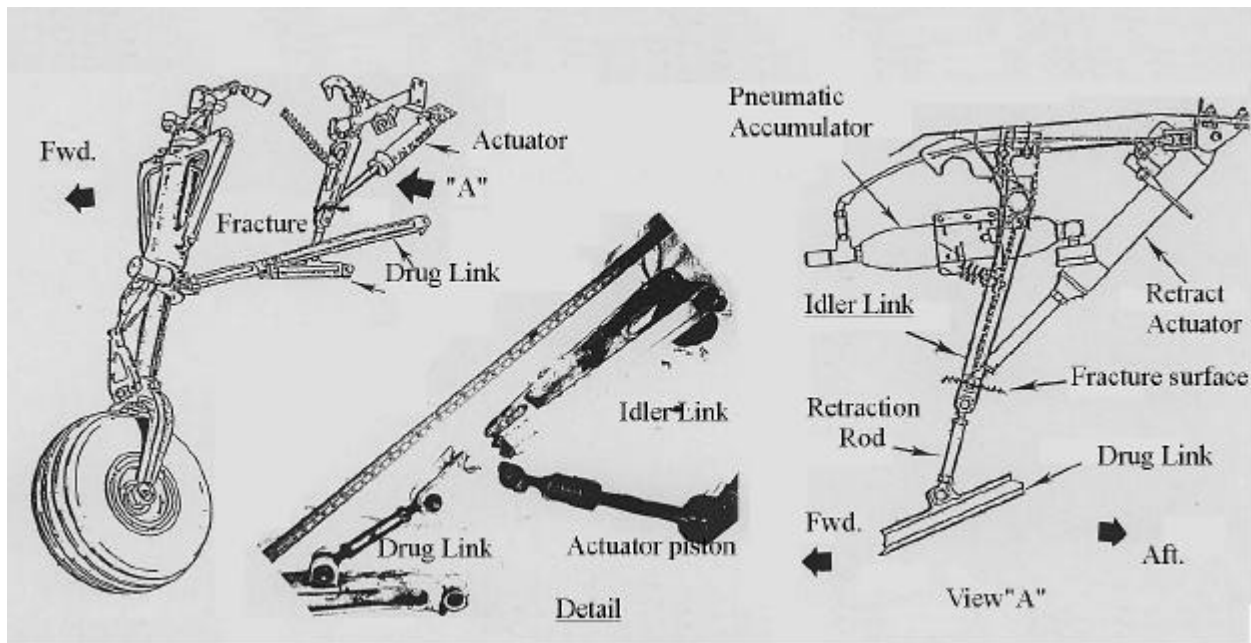


Figure 41 Retraction mechanism of the nose landing gear.

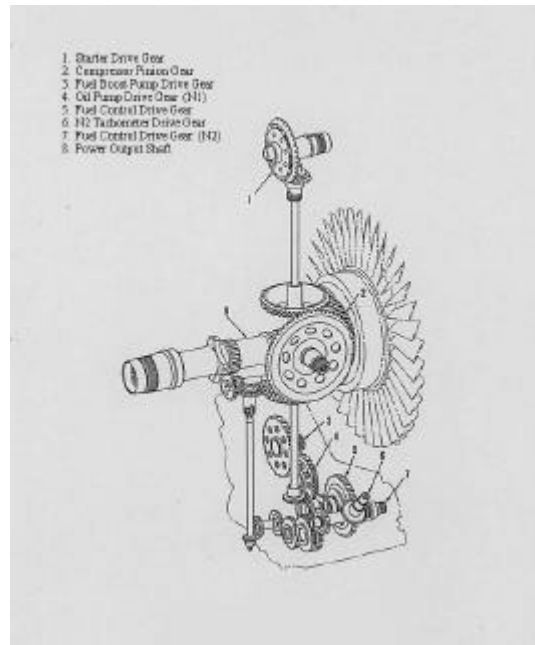


Figure 42 Engine accessory drive gear train.

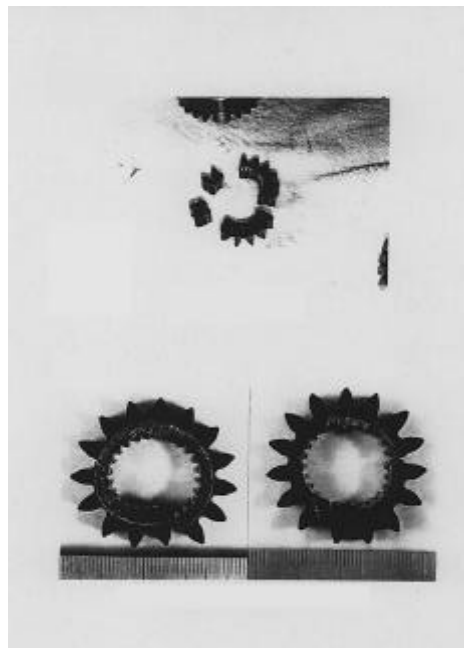


Figure 43 Spar gear broken into four pieces.

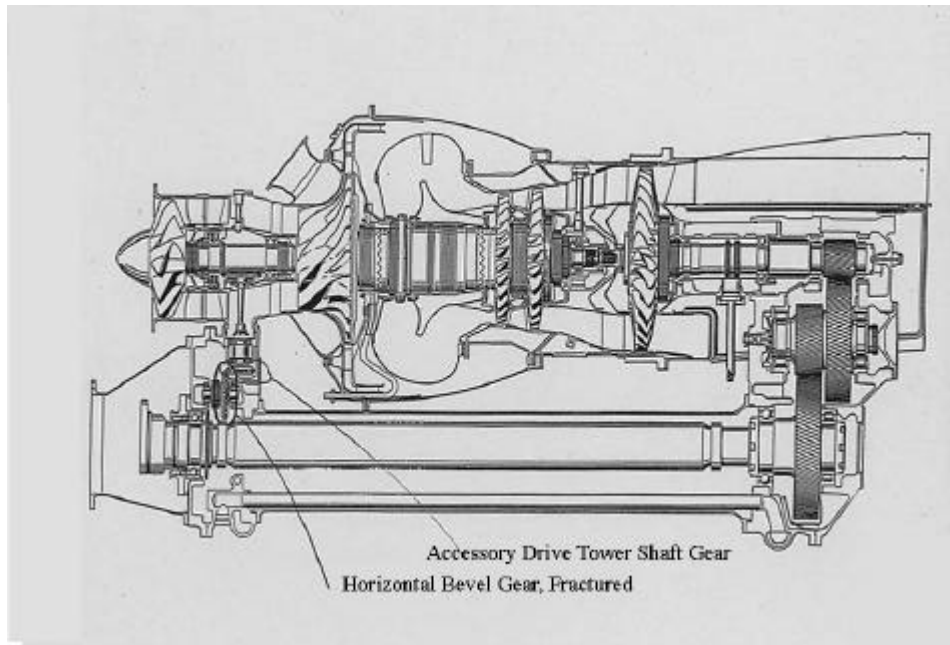


Figure 44 Engine cut view.

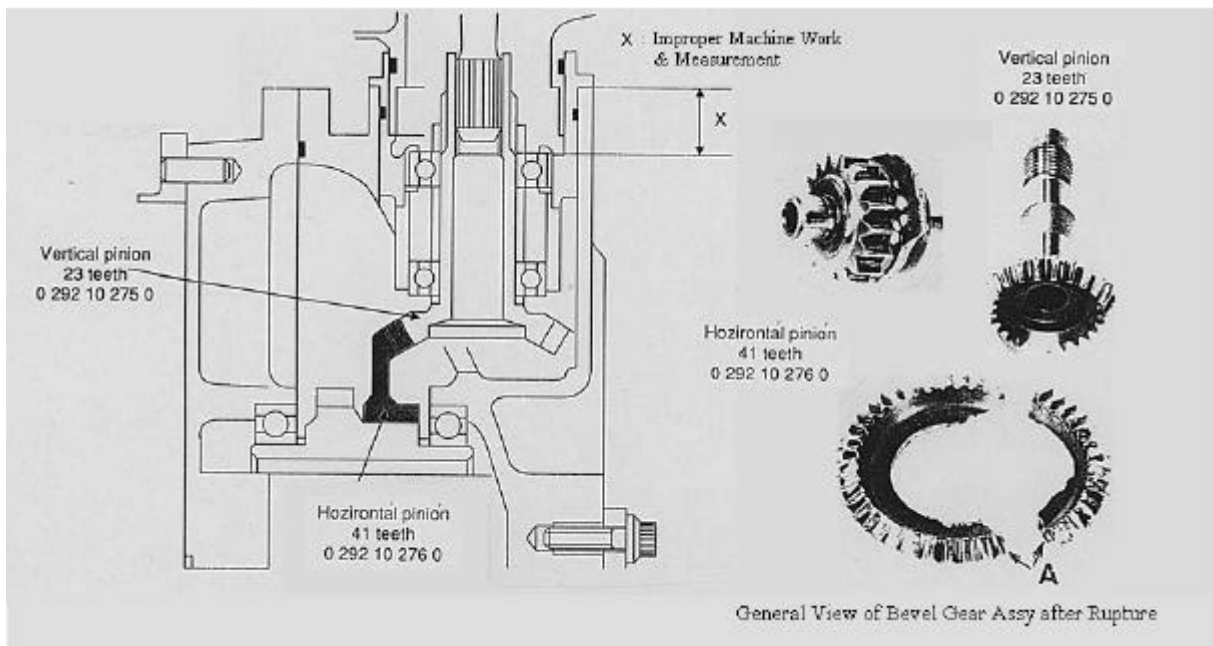


Figure 45 Accessory drive gear inlet module.

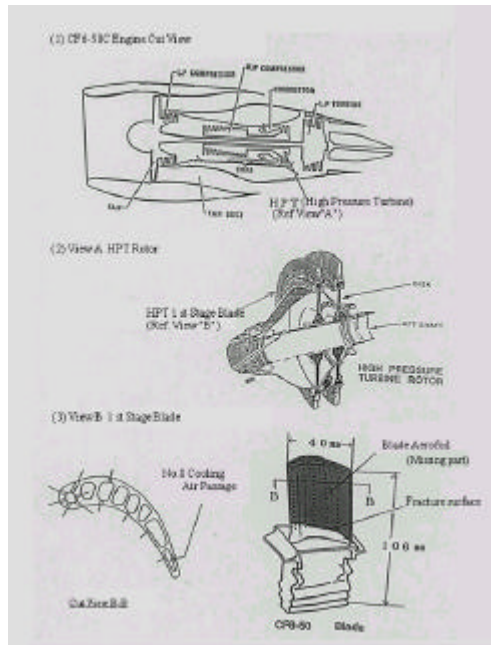


Figure 46 Cut view of an engine and a HPT blade.

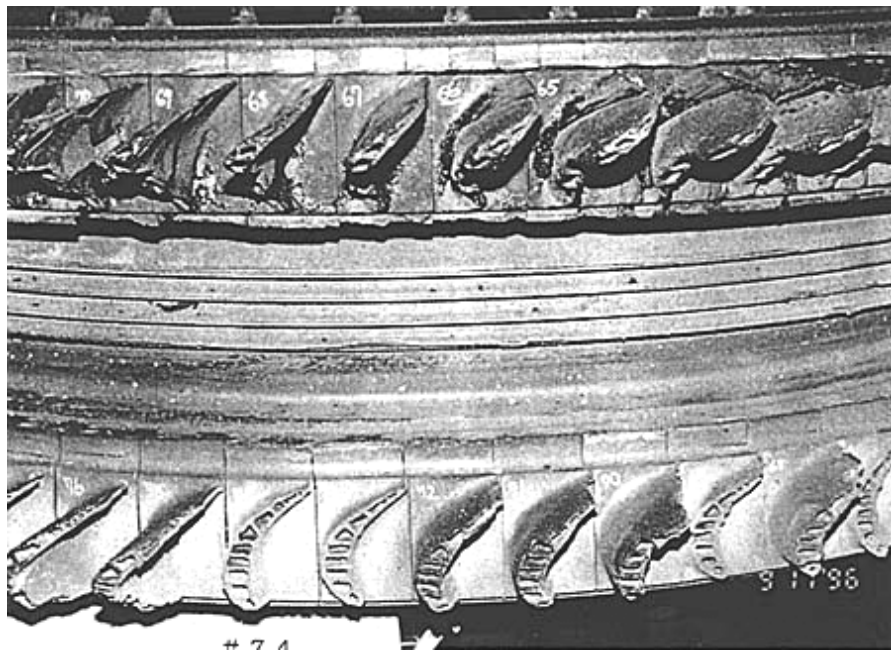


Figure 47 A part of No.3 engine without HPT blades.

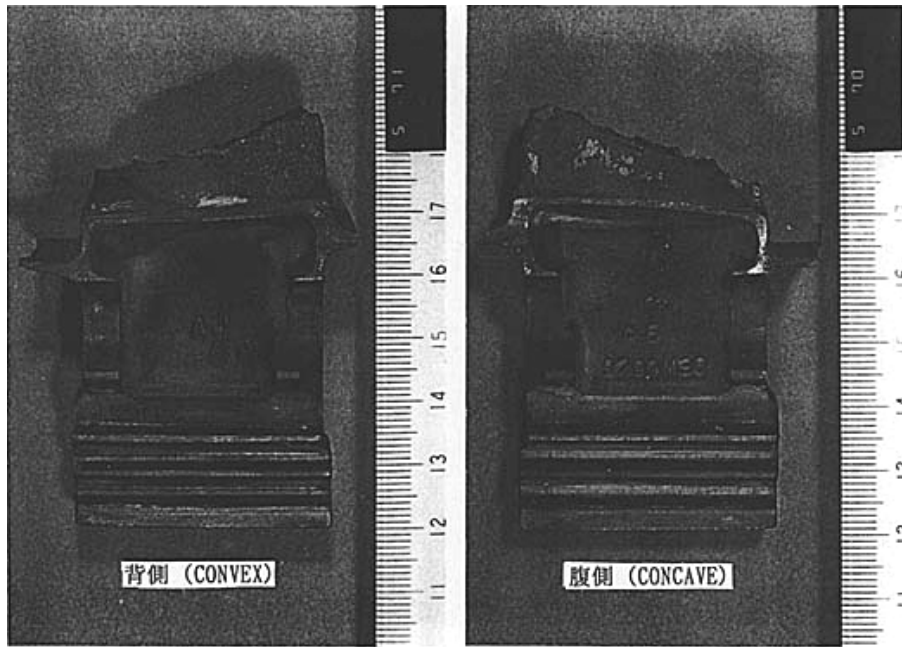


Figure 48 Fracture of first stage no.74 blade.

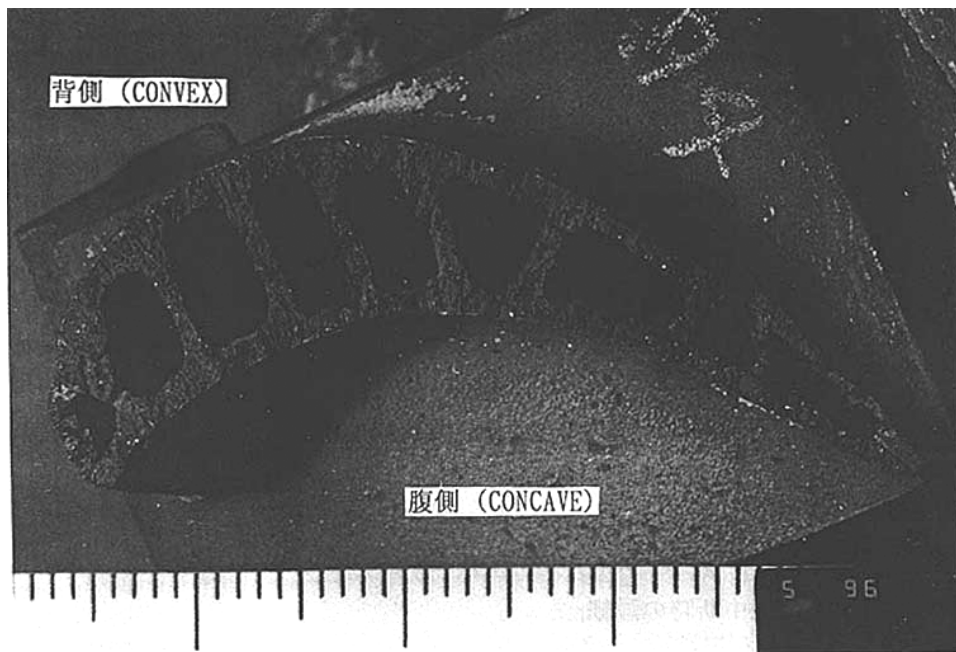


Figure 49 Fracture surface of the first stage No.74 blade.

26TH ICAF CONFERENCE AGENDA

SUNDAY, 11 JULY 1999

1500 - 1700 **REGISTRATION** - Hyatt Regency Bellevue, Wintergarden Atrium



MONDAY, 12 JULY 1999

0730 - 1700 **REGISTRATION** - Meydenbauer Center

0730-0900 **CONTINENTAL BREAKFAST**

0900 - 0910 Welcome, Administrative Remarks and Introduction of the ICAF General Secretary
J. Rudd, USAF Research Laboratory

0910 - 0920 Conference Opening and ICAF General Secretary's Review
O. Buxbaum, Fraunhofer-Institut Fur

0920 - 0930 Introduction of the Keynote Speaker
J. Rudd, USAF Research Laboratory

0930 - 1000 Keynote Speaker
Mr. Terry Neighbor, SES, Director, Plans and Programs
Directorate, USAF Research Laboratory

SESSION A

Chairman: C. Martin, Aeronautical and Maritime Research Laboratory (Australia)

1000 - 1030 The Netherlands
H. Ottens, National Aerospace Laboratory NLR

1030 - 1100 **BREAK**

SESSION B

Chairman: J. Rouchon, Centre d'Essais Aeronautique de Toulouse (France)

1100 - 1145 United Kingdom
P. Poole, Defence Research Agency DRA

1145 - 1230 Sweden
A. Blom, The Aeronautical Research Institute of Sweden (FFA)

1230 - 1345 **GROUP LUNCHEON**

SESSION C

Chairman: A. Blom, The Aeronautical Research Institute of Sweden (FFA) (Sweden)

1345 - 1430 Canada
D. Simpson, National Research Council of Canada

1430 - 1500 Israel
A. Berkovits, Technion-Israel Institute of Technology

1500 - 1530 Switzerland
M. Guillaume, TTA, SF Emmen

1530 - 1615 **BREAK**

SESSION D

Chairman: H. Ottens, National Aerospace Laboratory NLR (The Netherlands)

1615 - 1700 France
J. Rouchon, Centre d'Essais Aeronautique de Toulouse

1700 **ADJOURN**

TUESDAY, 13 JULY 1999

- 0700 - 1730** **REGISTRATION** - Meydenbauer Center
- 0700-0800** **CONTINENTAL BREAKFAST**
- SESSION E**
Chairman: P. Poole, Defence Research Agency DRA (United Kingdom)
- 0800 - 0845** Australia
C. Martin, Aeronautical and Maritime Research Laboratory (AMRL)
- 0845 - 0915** Italy
A. Slavetti, Universita di Pisa
- 0915 - 1000** Germany
C. Dalle Donne, Deutsche Forschungsanstalt fur Luft-Raumfahrt e. V. (DLR)
- 1000 - 1030** **BREAK**
- SESSION F**
Chairman: A. Berkovits, Technion-Israel Institute of Technology (Israel)
- 1030 - 1100** Japan
A. Kobayashi, Science University of Tokyo
- 1100 - 1145** United States
J. Rudd, USAF Research Laboratory
- 1145 - 1200** Announcements Related to Tours and Conference Reception
J. Rudd, USAF Research Laboratory
- 1200 - 1300** **GROUP LUNCHEON**
- 1215** Bus departs for Boeing Plant Tour (Box Lunch)
- 1300** Bus departs for Boeing Plant Tour
- 1300** Bus departs for Fatigue Technology Plant Tour
- 1300** Bus departs for B.F. Goodrich Plant Tour
- 1300** Bus departs for Boeing Lab Tour
(Busses will return to Hotels at completion of tours)
- 1800** **BUSSES DEPART HOTEL FOR CONFERENCE RECEPTION -
Boeing Museum of Flight**
- 2100** Busses return to hotels

20TH ICAF SYMPOSIUM AGENDA



WEDNESDAY, 14 JULY 1999

- 0730 - 1700** **REGISTRATION** - Meydenbauer Center
- 0730 - 0900** **CONTINENTAL BREAKFAST**
- 0900 - 0910** Welcome and Administrative Remarks
J. Rudd, USAF Research Laboratory
- 0910 - 1010** Introduction of the Plantema Memorial Lecturer
J. Lincoln, USAF Aeronautical Systems Center
Plantema Memorial Lecture: “Advances in Fatigue and Fracture Mechanics Analyses for Aircraft Structures”
J. Newman, NASA, Langley Research Center
Presentation of the Plantema Medal
O. Buxbaum,
- 1010 - 1040** **BREAK**
- 1040 - 1045** Introduction of Symposium Keynote Speaker
U. Goranson, Boeing Commercial Airplane Group
- 1045-1115** Symposium Keynote Speaker
Mr. David O. Swain, Boeing Vice President, Engineering
- SESSION 1 - VISIONARY APPROACHES**
Chairman: D. Simpson, National Research Council of Canada (Canada)
- 1115 - 1145** Effect of Inspection Uncertainty on Aircraft Structural Integrity
J. Lincoln, USAF Aeronautical Systems Center
- 1145 - 1215** Corrosion and the Management of Structural Integrity
G. Clark, Aeronautical and Maritime Research Laboratory (Australia)
- 1215 - 1330** **GROUP LUNCHEON**
- SESSION 2 - FATIGUE I**
Chairman: A. Salvetti, Universita di Pisa (Italy)
- 1330 - 1400** A Practical Engineering Approach to Predicting Fatigue Crack Growth in Riveted Lap Joints
C. Harris, J. Newman Jr. and R. Piascik, National Aeronautics and Space Administration (USA)
- 1400 - 1430** Fatigue and Damage Tolerance Design of Large Airbus Wing Structures
E. Hunt, M. Jones and A. Williams, British Aerospace Airbus, Ltd. (UK)
- 1430 - 1500** Stress Intensity Factors and Crack Interaction of Part Elliptical Through Cracks in Adjacent Holes
J.J.M. De Rijck, J. Schijve and A. Vlot, Delft University of Technology and *S. Fawaz*, Air Force Research Lab (Netherlands)
- 1500 - 1530** **BREAK**
- SESSION 3 - FATIGUE II**
Chairman: D. Dalle Donne, Deutsche Forschungsanstalt fur Luft-Raumfahrt e.V. (DLR) (Germany)
- 1530 - 1600** Fatigue Crack Growth and Residual Strength Analysis of Twist Spectrum Loaded Integrally Stiffened Panels Simulating a Lower Wing Skin Two Bay Crack Scenario
M. Kulak, R. Bucci, H. Skyut and G. Bray, Alcoa Technical Center and *J. Newman Jr.*, NASA Langley Research Center (USA)
- 1600 - 1630** Fatigue and Damage Tolerance Aspects of High Speed Machined Airframe Parts
H. Ansell, SAAB AB (Sweden)
- 1630 - 1715** Poster Presentations
- 1745** Busses Depart Hotels for Symposium Reception

THURSDAY, 15 JULY 1999

- 0730 - 1700** **REGISTRATION** - Meydenbauer Center
- 0730 - 0800** **CONTINENTAL BREAKFAST**
- SESSION 4 - WIDESPREAD FATIGUE DAMAGE**
Chairman: M. Guillaume, TTA, SF Emmen (Switzerland)
- 0800 - 0830** C-141: A Probabilistic Approach to Predict the Onset of Widespread Fatigue Cracking in Fuselage Structure
R. Alford, US Air Force and R. Bell and S. Shah, Lockheed Martin Aero Systems (USA)
- 0830 - 0900** An Experimental and Theoretical Analysis of Multi-site Damaged Butt-joints
G. Cavallini and R. Galatolo, University of Pisa and D. Guiliano, Cattaneo Aermacchi S.P.A. (Italy)
- 0900 - 0930** Methodologies for the Assessment of Widespread Fatigue Damage in Aircraft Wing Structures
R. Collins and S. Kimmins, British Aerospace Airbus (UK)
- 0930 - 1000** Experimental and Analytical Assessments of Widespread Fatigue Damage in Aircraft Fuselage Structure
J. Bakuckas Jr, E. Akpan, C. Bigelow and P. Tan, Federal Aviation Administration (USA)
- 1000 - 1030** **BREAK**
- SESSION 5 - CORROSION/FATIGUE**
Chairman: C. Martin, Aeronautical and Maritime Research Laboratory (AMRL) (Australia)
- 1030 - 1100** Stress Corrosion Propagation: Damage Tolerance Approach
D. Gilletta de Saint-Joseph, Dassault-Aviation (France)
- 1100 - 1130** Review of Pitting Corrosion Fatigue Models
D. Hoepfner and V. Chandrasekaran, University of Utah and A.M. Taylor, FASIDE International, Inc. (USA)
- 1130 - 1200** Corrosion Modeling of KC-135 Lap Joints
R. Kinzie and D. Peeler, US Air Force and G Cooke, NCI Information Systems Inc. (USA)
- 1200 - 1315** **GROUP LUNCHEON**
- SESSION 6 - COMPOSITE REPAIR**
Chairman: A. Blom, The Aeronautical Research Institute of Sweden (Sweden)
- 1315 - 1345** Issues in the Certification of Bonded Composite Patch Repairs for Cracked Metallic Aircraft Structures
A. Baker, Aeronautical & Maritime Research Laboratory (Australia)
- 1345 - 1415** Bonded Composite Repairs for Aging Commercial Aircraft - A Multi-National Research Effort
A. Nathan, Israel Aircraft Industries (Israel)
- 1415 - 1445** **BREAK**
- SESSION 7 - METALLIC REPAIR**
Chairman: A. Kobayashi, Science University of Tokyo (Japan)
- 1445 - 1515** Fiber Metal Laminate Patches for Bonded Repair of Aircraft Fuselages
A. Vlot, C. Guijt and J. Greer, Delft University of Technology and S. Verhoeven and H Woerden, USAF Academy (Netherlands)
- 1515 - 1545** Evaluation of a Modified Stress Intensity Factor for Cold Expanded Holes
L. Reid, J. Restis and T. Swift, Fatigue Technology Inc. (USA)
- 1700** Busses Depart Hotels for Symposium Banquet

FRIDAY, 16 JULY 1999

- 0730 - 1700** **REGISTRATION** - Meydenbauer Center
- 0730 - 0800** **CONTINENTAL BREAKFAST**
- SESSION 8 - PROBABILISTIC METHODS**
Chairman: H. Ottens, National Aerospace Lab (NLR) (The Netherlands)
- 0800 - 0830** A Probabilistic Failure Analysis of Fuselage Splice Joints with Multiple Site Fatigue Damage
Y. Xiong, G. Shi and G. Sastaugh, Institute for Aerospace Research (Canada)
- 0830 - 0900** Fatigue Variability and Life Prediction: A Probabilistic Approach
B. Hillberry, Purdue University (USA)
- 0900 - 0930** A Novel Probabilistic Fatigue Crack Growth Model Based on the Crack Closure Model
G. Wang and A. Blom, The Aeronautical Research Institute of Sweden (Sweden)
- 0930 - 1000** Probabilities of Occurrence and Detection, and Airworthiness Assessment
R. Wei and G. Harlow, Lehigh University (USA)
- 1000 - 1030** **BREAK**
- SESSION 9 - DAMAGE TOLERANCE**
Chairman: A. Berkovits, Technion-Israel Inst of Technology (Israel)
- 1030 - 1100** Fractographic Investigation of Pressure Cabin MSD
R. Wanhill, W. Van Der Hoeven, H. Ten Hoeve and H. Ottens, National Aerospace Laboratory NLR (Netherlands)
- 1100 - 1130** Improved Design Criteria for a Large Airbus Aircraft to Meet Future Damage Tolerance Requirements
R. Boetsch and R. Hein, Airbus Industrie and A. Davy, Aerospatiale (France)
- 1130 - 1200** Damage Tolerance Substantiation of the Galaxy Executive Jet
A. Brot, S. Afnaim and Z. Granot, Israel Aircraft Industries Ltd. (Israel)
- 1200 - 1315** **GROUP LUNCHEON**
- SESSION 10 - OVERVIEWS**
Chairman: P. Poole, Defence Research Agency DRA (United Kingdom)
- 1315 - 1345** Damage Tolerance in Helicopter Airframes - Is Crack Growth Practical?
M. Overd, GKN Westland Helicopters (UK)
- 1345 - 1415** Current Status of Research and Development Activities for the Fuselage of a Large Airbus Aircraft
M. Schmidt and N. Ohrloff, Daimler-Benz Aerospace Airbus and T. Fleischer, IMA Materials and Research Applied Engineering (Germany)
- 1415 - 1445** Risk and Economic Implications of DADTA for Foreign Military Operations of Non USAF Fleets
K. Schrader, O. Burnside, J. Cardinal and W. Sparks, Southwest Research Institute (USA)
- 1445 - 1515** **BREAK**
- SESSION 11 - EXPERIMENTAL TECHNIQUES**
Chairman: J. Rouchon, Centre d Essais Aeronautique de Toulouse (France)
- 1515 - 1545** Full Scale Fatigue Test of the Pilatus PC9/A Trainer Aircraft
I. Anderson and R. Parker, Aeronautical & Maritime Research Laboratory (Australia)
- 1545 - 1615** Extended Full-Scale Testing of the 777 Fuselage
G. Das, J. Lusk and M. Starha, Boeing Commercial Airplane Group (USA)
- 1615 - 1645** Supplemental Structural Inspection Program and Results for ANA B747SR and B767 Airplane
K. Yoshioka and N. Wakita, All Nippon Airways (Japan)
- 1645 - 1715** Results of the DORNIER 328 Operational Load Recording Campaign
R. Brunbauer, B. Hebing, R. Teske and H. Hugh, Fairchild-Dornier (Germany)
- 1715 - 1730** Closing Remarks
J. Rudd, USAF Research Laboratory

ICAF GENERAL SECRETARY

Prof. Dr. O. Buxbaum

Fraunhofer-Institut for Betriebsfestigkeit (LBF)
Bartningstrasse 47
D-64289 Darmstadt, Germany

ICAF NATIONAL DELEGATES

Colin A. Martin

Aeronautical & Maritime Research
Laboratory (AMRL)
506 Lorimer Street
Fishermens Bend
Victoria 3207 Australia

D. L. Simpson

Structures & Materials Laboratory
Nat'l Research Council of Canada
Montreal Road
Ottawa, Ontario K1A 0R6 Canada

J. Rouchon

Structures & Airframe
Materials Department
Centre d'Essais Aeronautique
de Toulouse (CEAT)
23 Avenue Henri Guillaumet
F-31056 Toulouse Cedex, France

Dr. Claudio Dalle Donne

German Aerospace Center (DLR)
Linder Höhe
D-51147 Cologne, Germany

Prof. A. Berkovits

Faculty of Aerospace Engineering
Technion-Israel Inst of Technology
Technion City, Haifa 3200
Israel

Prof. A. Salvetti

Dipartimento de
Ingegneria Aerospaziale
Universita di Pisa
Via Diotisalvi 2
I-56100 Pisa, Italy

Prof. Dr. A. Kobayashi

Dept of Mechanical Engineering
Faculty of Science & Technology
Science University of Tokyo
Noda, Chiba 278 Japan

Harold Ottens

Nat'l Aerospace Lab (NLR)
P O Box 153
NL-8300 AD Emmeloord
The Netherlands

Prof. Dr. A. F. Blom

The Aeronautical Research
Institute of Sweden (FFA)
P O Box 11021
S-16111 Bromma, Sweden

Dr. Michel Guillaume

F/A-18 Full Scale Fatigue Test Manager
TTA, SF Emmen
PO Box 301
CH-6032 Emmen, Switzerland

Dr. P. Poole

Structural Materials Centre
Def Research Agency (DRA)
Farnborough, Hants GU146TD
United Kingdom

J. L. Rudd

AFRL/VAA Bldg 45
2130 Eighth Street, Ste 1
Wright-Patterson Air Force Base
Ohio 45433-7542 USA

ICAF '99 FINAL ATTENDANCE LIST

MR JOHN ACH
 CHIEF STRUCTURAL INTEGRITY BRANCH
 USAF AFRL/VASE
 RESEARCH LAB
 RM 504
 2790 D ST
 WRIGHT-PATTERSON AFB OH 45433-7402
 937-255-6104 X 244 **FAX:** 937-656-4999
e-Mail: *john.ach@va.afrl.af.mil*

DR VINOD AGARWALA
 SR STAFF SCIENTIST
 NAVAL AIR WARFARE CTR
 M/S 3 BLDG 2188
 PATUXENT RIVER MD 20670-1908
 301-342-8002 **FAX:** 301-342-0316
e-Mail: *agarwalavs@navair.navy.mil*

MR ALEXANDER AIZIC
 ENGINEERING SPECIALIST
 BOMBARDIER INC
 ENGINEERING DEPT
 PO BOX 6087 STATION A
 MONTREAL QUEBEC
 CANADA H3C 3G9
 514-855-2312 **FAX:** 514-855-2115
e-Mail: *alex.aizic@eng.canadair.ca*

MR ROBERT ALLEN
 STRUCTURAL TEST LAB MANAGER
 LOCKHEED MARTIN AERO SYSTEMS CO
 DEPT 73-55
 M/S 0484
 86 S COBB DR
 MARIETTA GA 30063-0484
 770-494-5991 **FAX:** 770-494-2028
e-Mail: *doug.allen@lmco.com*

MR ANASTASSIOS ANINOS
 GENERAL SECRETARY
 HELLENIC AERO ENGINEERS SOCIETY
 14 EGINIS ST
 GLYFADA ATHENS 166 74
 GREECE
 ++30-1-8945230 **FAX:** ++30-1-9362992
e-Mail: *enin@tee.gr*

DR HANS ANSELL
 APPOINTED PROFESSIONAL SPECIALIST
 SAAB AB
 SE 581 88 LINKOPING
 SWEDEN
 +46 13 181698 **FAX:** +46-13-183363
e-Mail: *hans.ansell@saab.se*

SNQ LDR STEVE ARMITAGE
 AIRCRAFT STRUCTURAL INTEGRITY
 ROYAL AIR FORCE
 LOGISTICS SUPPORT SERVICES
 RAF WYTON ROOM BOOG LSS (AMDS)
 HUNTINGDON PE17 2EA CAMBS
 UNITED KINGDOM
 44-1480-52451 X923 **FAX:** 44-1480-446820
e-Mail:

MS ANASTASIA ARSENIEN
 LEAD ENGINEER
 BOEING
 DAMAGE TOLERANCE
 M/S 04-JJ
 16526 DENSMERE AVE
 SHORELINE WA 98133
 425-342-7154 **FAX:** 425-266-9259
e-Mail: *anastasia.arsenien@pss.boeing.com*

MR MAGNUS AXELSSON
 ENGINEER STRUCTURES
 CONAIR AVIATION LTD
 PO BOX 220
 ABBOTSFORD BC
 CANADA V 2S 4N9
 604-855-1171 **FAX:** 604-852-5199
e-Mail: *maxelsson@conair.ca*

MR ROBERT BADER
 CONSULTANT
 1613 KINGSWAY DR
 XENIA OH 45385-9589
 937-255-6639 **FAX:** 937-255-3740
e-Mail: *robert.bader@va.wpafb.af.mil*

MR ASAD BAIG
 CC 130 ASIP PM
 SPAR AEROSPACE LTD
 ENGINEERING DEPT
 EDMONTON INTERNATIONAL AIRPORT
 EDMONTON ALBERTA
 CANADA T5S 272
 780-890-6503 **FAX:** 780-890-6543
e-Mail: *baiga@spar.ca*

DR ALAN BAKER
 DEFENCE SCIENCE & TECHNOLOGY ORG
 AIRFRAMES & ENGINES DIV
 506 LORIMER STREET
 HELBOURNE VICTORIA 3199
 AUSTRALIA
 61-3-9626-7495 **FAX:** 61-3-9626-7087
e-Mail: *alan.baker@dsto.defence.gov.au*

ICAF '99 FINAL ATTENDANCE LIST

DR JOHN BAKUCKAS JR
 STRCTRL TEST FACILITY MANAGER
 FEDERAL AVIATION ADMIN
 WILLIAM J HUGHES TECH CTR
 M/S AAR-431
 ATLANTIC CITY INT'L AIRPORT NJ 08405
 609-485-4784 **FAX:** 609-485-4004
e-Mail: *john.bakuckas@tc.faa.gov*

MR WILLIAM BECKER
 AERO SALES MANAGER
 MTS SYSTEMS CORPORATION
 26500 W AGOURA ROAD #202
 CALABASAS CA 91302
 818-878-9512 **FAX:** 818-878-9515
e-Mail: *bill.becker@mts.com*

DR JAMES BALDWIN
 ASS'T PROFESSOR
 UNIVERSITY OF OKLAHOMA
 AERO & MECHANICAL ENGINEERING
 RM 212
 865 ASP AVE
 NORMAN OK 73019
 405-325-1090 **FAX:** 405-325-1088
e-Mail: *baldwin@ou.edu*

MS LAUREL BECKMAN
 AEROSPACE ENGINEER
 NAVAIRSYSCOM
 AIR-4.3.3.4
 BLVD 2187 STE 2340A UNIT 5
 48110 SHAW ROAD
 PATUXENT RIVER MD 20670-1906
 301-342-9350 **FAX:** 301-342-9406
e-Mail: *beckmanlt@navair.navy.mil*

MR JAMES BALDWIN
 SR SPECIALIST ENGINEER
 BOEING
 737-700C CONVERTIBLE
 M/S K01-11
 PO BOX 7730
 WICHITA KS 67277-7730
 316-526-8982 **FAX:**
e-Mail: *james.baldwin@wichita.boeing.com*

MR ROBERT BELL
 SENIOR SPECIALIST ENGINEER
 LOCKHEED MARTIN
 AERO SYSTEMS
 M/S 0160
 86 S COBB DR
 MARIETTA GA 30063-0160
 770-494-2166 **FAX:** 770-494-9610
e-Mail: *bob.bell@lmco.com*

DR DALE BALL
 SPECIALIST SENIOR
 LOCKHEED MARTIN TAS
 FATIGUE & FRACTURE ANALYSIS STRUCTURES
 M/S S862
 PO BOX 748
 FT WORTH TX 76101
 817-777-3760 **FAX:** 817-777-2115
e-Mail: *dale.l.ball@lmco.com*

MR JOHN BENNETT
 PRINCIPAL STRESS ENGINEER
 BRITISH AEROSPACE REGIONAL AIRCRAFT
 SERVICE SUPPORT-STRUCTURES
 CHESTER RD WOODFORD
 CHESHIRE SK7 1QR
 ENGLAND
 0161-439-5050 X4321 **FAX:** 0161-955-3227
e-Mail:

MR STEVEN BASIC
 PRINCIPAL ENGINEER
 BOEING CO
 STRUCTURES TECHNOLOGY
 M/S K02-17
 PO BOX 7730
 WICHITA KS 67277-7730
 316-526-1292 **FAX:** 316-526-4232
e-Mail: *steven.basic@wichita.boeing.com*

PROF AVRAHAM BERKOVITS
 BRUM BERKOVITS
 TECHNION-ISRAEL INSTITUTE OF TECHNOLOGY
 FACULTY OF AEROSPACE ENGINEERING
 TECHNION CITY
 HAIFA 32000
 ISRAEL
 972-4829-3808 **FAX:** 972-4823-1848
e-Mail: *aerbrum@aerodyne.technion.ac.il*

MR BERNHARD BAUDISCH
 DAIMLER CHRYSLER AEROSPACE
 FATIGUE DEPT
 PO BOX 80 11 60
 MUNICH BAYERN 81663
 GERMANY
 49-89-607-24736 **FAX:** 49-89-607-32158
e-Mail: *bernhard.baudisch@m.dasa.de*

MS CASSIE BERRY FOHN
 ENGINEER
 SCHWARTZ ENGINEERING CO
 11503 JONES-MALTSBERGER 200
 SAN ANTONIO TX 78247
 210-490-7496 **FAX:** 210-490-2540
e-Mail: *cfohn@schwartzeng.com*

ICAF '99 FINAL ATTENDANCE LIST

DR CATHERINE BIGELOW
SECT HEAD AIRFRAME STRCTRS
FEDERAL AVIATION ADMIN
WILLIAM J HUGHES TECH CTR
M/S AAR-341
ATLANTIC CITY INTL AIRPT NJ 08405-0001
609-485-6662 **FAX:** 609-485-4004
e-Mail: *cathy.bigelow@tc.faa.gov*

MR PER BJORKLUND
SR STRUCTURES ENGINEER
CONAIR AVIATION LTD
PO BOX 220
ABBOTSFORD BC
CANADA V2J 4N9
604-855-1171 **FAX:** 604-852-5199
e-Mail: *pbjorklund@conair.ca*

MR EMANUEL BLASS
TEST ENGINEER & QA
ISRAEL AIRCRAFT INDUSTRIES LTD
GROUND TEST LABS
DEPT 4454
BEN GURION INTL AIRPORT 70100
ISRAEL
972-3-9357769 **FAX:** 972-3-9353082
e-Mail: *ebllass@engdiv.iai.co.il*

DR ANDERS BLOM
TECHNICAL DIRECTOR
FFA (AERONAUTICAL RESEARCH INST. OF
SWEDEN)
STRUCTURES & MATERIALS
PO BOX 11021
S-161 11 BROMMA
SWEDEN
46-8-555-49260 **FAX:** 46-8-258-919
e-Mail: *abm@ffa.se*

MR REGIS BOETSCH
DEPUTY DEPARTMENT MANAGER
AIRBUS INDUSTRIE
ENGINEERING DIRECTORATE
1 ROND POINT MAURICE BELLONTE
31707 BLAGNAC CEDEX
FRANCE
33 5 62 11 01 21 **FAX:** 33 5 61 93 48 19
e-Mail: *regis.boetsch@airbus.fr*

MR ARTHUR BRAUN
DIVISION MANAGER
MTS SYSTEMS CORP
AEROSPACE STRUCTURES & MATERIALS DIV
14000 TECH DR
M/S 231
EDEN PRAIRIE MN 55347
612-937-4045 **FAX:** 612-937-4515
e-Mail: *art.braun@mts.com*

MR JOSEPH BRAUN
PRESIDENT
SYSTEMS & ELECTRONICS INC
190 GORDON ST
ELK GROVE VILLAGE IL 60007-1120
847-228-0985 **FAX:** 847-228-1164
e-Mail: *jbraun@sysei.com*

MR CHARLES BRIKMANIS
SPECIALIST DADT GROUP JAPAN F-2
LOCKHEED MARTIN
TACTICAL AIRCRAFT SYSTEMS
PO BOX 748
MS 9323
FT WORTH TX 76008
817-762-2730 **FAX:** 817-762-2634
e-Mail: *chaz.k.brikmanis@lmco.com*

MR WOLFGANG BROECKER
DIPL ING
IABG
EINSTEINSTR 20
85521 OTTOBRUNN
GERMANY
49-89-6088-3454 **FAX:** 49-89-6088-2673
e-Mail: *broecker@iabg.de*

MR JOHN BROOKS
USAF AFRL/VASE
BLDG 65 RM 504
2790 D ST
WRIGHT-PATTERSON AFB OH 45433-7402
937-255-6104 X 233 **FAX:** 937-656-4999
e-Mail: *john.brooks@va.af.mil*

MR ABRAHAM BROTH
HEAD OF FATIGUE DEPT
ISRAEL AIRCRAFT INDUSTRIES LTD
FATIGUE DEPT
BEN-GURION AIRPORT
4441
ISRAEL
972-3-935-3398 **FAX:** 972-3-935-5055
e-Mail: *abrot@engdiv.iai.co.il*

MR ALBERT BRUETSCH
AEROSPACE ENGINEER
USAF SM-ALC/LAFME
M/S LAFME
5020 DUDLEY BLVD
MCCLELLAN AFB CA 95652-1391
916-643-5300 **FAX:** 916-643-1405
e-Mail: *bruetschal@fusun1.mcclellan.af.mil*

ICAF '99 FINAL ATTENDANCE LIST

MR ROBERT BRUNBAUER
FAIRCHILD-DORNIER
DORNIER LUFTFAHRT GMBH
PO BOX 11 03
D-82230 WESSLING
GERMANY
+49-8153-30-26-08 **FAX:** +49-8153-30-48-86
e-Mail:

DR ROBERT BUCCI
SR TECH CONSULTANT
ALCOA INC
100 TECHNICAL DR
ALCOA CTR PA 15069-0001
724-337-2671 **FAX:** 724-337-5436
e-Mail: *robert.vucci@alcoa.com*

MR JAMES BURD
FAA DER DAMAGE TOLERANCE
GULFSTREAM AEROSPACE CORP
STRUCTURES
M/S G07
PO BOX 2206
SAVANNAH GA 31402-2206
912-965-3591 **FAX:** 912-965-5266
e-Mail: *james_burd@macmail.git.gulfaero.com*

DR OTTO BUXBAUM
PROFESSOR
FRAUNHOFER-INST FOR BETRIEBSFESTIGKEIT
LBF
BARTNINGSTRABE 47
D-64289 DARMSTADT
GERMANY
+49-6151-7051 **FAX:** +49-6151-705214
e-Mail:

MR STEPHEN CAMPBELL
SCIENTIST
DEFENCE OPERATIONAL TECHNOLOGY SUPPORT
ESTABLISHMENT (DOTSE)
MATERIALS & STRUCTURES GROUP
PRIVATE BAG 32901
AUCKLAND
NEW ZEALAND
64-9-4455848 **FAX:** 64-9-4455520
e-Mail: *s.campbell@dotse.mil.nz*

MR JAMES CANDELA
AEROSPACE ENGINEER
NAVAIR
STRUCTURES DIV UNIT 5
BLDG 2187 STE 2340
48110 SHAW RD
PATUXENT RIVER MD 20670-1906
301-342-0295 **FAX:**
e-Mail:

MR DOUGLAS CANNINGTON
SPECIALIST ENGINEER
LOCKHEED MARTIN
73-71
ZONE 0595
86 SOUTH COBB DRIVE
MARIETTA GA 30063
770-494-2234 **FAX:** 770-494-6995
e-Mail: *d.j.cannington@lmco.com*

MR JOSEPH CARDINAL
PRINCIPAL ENGINEER
SOUTHWEST RESEARCH INST
STRUCTURAL ENGINEERING
6220 CULEBRA RD
SAN ANTONIO TX 78238-0510
210-522-3323 **FAX:** 210-522-3042
e-Mail: *jcardinal@swri.org*

MR DOUGLAS CARMODY
TECHNICAL LEAD STRUCTURAL SCIENCES
NORTHROP GRUMMAN
VEHICLE ENGINEERING
2000 NASA BLVD
M/S H11-223
MELBOURNE FL 32902
407-726-7821 **FAX:** 407-951-6048
e-Mail: *carmodo@mail.northgrum.com*

DR GIULIANO CATTANEO
ENGINEER
AERMACCHI SPA
PRJ/STR
VIA PAOLO FORESIO 1
VENEGONO SUPERIORE (VARESE) 21090
ITALY
39-0331-813688 **FAX:** 39-0331-813691
e-Mail: *giuliano.cattaneo@aermacchi.it*

MR STEPHEN CAULFIELD
STRESS ENGINEER
SHORT BROTHERS PLC
STRESS DEPT
AIRPORT RD PO BOX 241
BELFAST BT3 9D7
N IRELAND
01237-463457 **FAX:** 01232-462093
e-Mail: *caulfields@shorts.co.uk*

PROF GIORGIO CAVALLINI
UNIVERSITY OF PISA
DEPT OF AEROSPACE ENGINEERING
VIA DIOTISALVI, 2
PISA
ITALY 56126
39 50 550200 **FAX:** 39 50 553654
e-Mail: *g.cavalline@ing.unipi.it*

ICAF '99 FINAL ATTENDANCE LIST

MR HEH-CHYUN CHEN
 SR ENGINEER
 BOEING COMM AIRPLANE GRP
 STRUCTURES
 M/S 04-JJ
 PO BOX 3707
 SEATTLE WA 98124-2207
 425-294-6792 **FAX:** 425-266-9259
e-Mail: *heh-chyun.c.chen@boeing.com*

DR QI CHEN
 BOEING CO
 DAMAGE TECHNOLOGY
 15943 S E 46TH WAY
 BELLEVUE WA 98006
FAX:
e-Mail:

MR DAVID CHESTER
 ISRAEL AIRCRAFT INDUSTRIES LTD
 ENGINEERING DIV
 DEPT 4441
 BEN-GURION AIRPORT 70100
 ISRAEL
 972-3-935-3294 **FAX:** 972-3-935-5055
e-Mail: *abrot@engdiv.iai.co.il*

DR MARIO CHIARELLI
 UNIVERSITY OF PISA
 DEPT OF AEROSPACE ENGINEERING
 VIA DIOTISALVI 2
 PISA
 ITALY 56126
 39-050-550200 **FAX:** 39-050-553654
e-Mail: *chiarelli@ing.unipi.it*

MR JOHN CHRISTIANSEN
 APPLICATIONS ENGINEER
 MTS SYSTEMS CORP
 M/S 231
 14000 TECHNOLOGY DR
 EDEN PRAIRIE MN 55344-2290
 612-937-4865 **FAX:** 612-937-4515
e-Mail:

MR STAMATIOS CHRYSSEAFITIS
 VICE PRESIDENT
 HELLENIC AERO ENGINEERS SOCIETY
 5 PRASSAKAKI STR
 THESSALONIKI 546 22
 GREECE
 ++301-9407522 **FAX:** ++301-9362848
e-Mail:

MR DON CLARK
 ENGINEERING SR SPECIALIST
 LOCKHEED MARTIN AERO SYSTEMS CO
 SURVEILLANCE & COMMAND PROGS 70-E1
 86 S COBB DR
 M/S 0595
 MARIETTA GA 30063
 770-494-8318 **FAX:** 770-494-5414
e-Mail: *don.p.clark@lmco.com*

MR GRAHAM CLARK
 HEAD FATIGUE & FRACTURES DETECT & ASSES
 DSTO AMRL AUSTRALIA
 DEPT OF DEFENCE
 506 LORIMER STREET
 FISHERMENS BEND VIC 3207
 AUSTRALIA
 61 3 9626 7497 **FAX:** 61 3 962 7089
e-Mail: *graham.clark@dsto.defence.gov.au*

MR PAUL CLARK
 RESEARCH ASSISTANT
 UNIVERSITY OF UTAH
 MECHANICAL ENGINEERING
 MEB RM 2202
 40 SOUTH CENTRAL CAMPUS DR
 SALT LAKE CITY UT 84112-9208
 801-581-4130 **FAX:** 801-585-9826
e-Mail: *clark@eng.utah.edu*

FLTLT PAUL CONNOR
 AS12A
 ROYAL AUSTRALIAN AIR FORCE
 AIRCRAFT STRUCTURAL INTEGRITY
 DIRECTORATE GENERAL TECH AIRWORTHINESS
 RAAF BASE WILLIAMS LAVERTON VIC 3027
 AUSTRALIA
 011-61-3-92563502 **FAX:** 011-61-3-92563488
e-Mail: *paconnor@raaf.defence.gov.au*

MR ROBIN COOK
 TECHNICAL LEADER
 DEFENCE EVALUATION AND RESEARCH AGENCY
 STRUCTURAL METATERIALS CENTRE
 ROOM 2008, A7 BUILDING
 GARNBOROUGH HANTS GU14 0LX
 UNITED KINGDOM
 44-1252-395387 **FAX:** 44-1252-397298
e-Mail: *rcook@dera.gov.uk*

MR GARTH COOKE
 SR SYSTEMS ENGINEER
 NCI INFORMATION SYSTEMS INC
 3150 PRESIDENTIAL DRIVE
 FAIRBORN OH 45324
 937-427-0252 **FAX:** 937-427-3790
e-Mail: *gcooke@nciinc.com*

ICAF '99 FINAL ATTENDANCE LIST

MR DALE COPE
 KC-135 STRUCTURES ENGINEER
 THE BOEING CO
 MILITARY PROGRAMS
 PO BOX 7730
 M/S K86-71
 WICHITA KS 67277-7730
 316-526-9873 **FAX:** 316-523-3130
e-Mail: *dale.a.cope@boeing.com*

DR EDUARDO DE LOS RIOS
 SENIOR RESEARCH FELLOW
 UNIVERSITY OF SHEFFIELD
 MECHANICAL ENGINEER
 MAPPIN ST
 SHEFFIELD S13JD
 UNITED KINGDOM
 44-114-2227723 **FAX:** 44-114-2227890
e-Mail: *e.rios@sheffield.ac.uk*

MR BRITT COVINGTON
 AERO ENGINEER
 USAF HQ AFSC/SEFE
 STE 250C
 9700 G AVE SE
 KIRTLAND AFB NM 87117-5670
 505-846-0990 **FAX:** 505-846-6826
e-Mail: *covingt@kafb.saia.af.mil*

MR JOHANNES DE RIJCK
 MSC
 DELFT UNIVERSITY OF TECH NIMR
 AEROSPACE ENGINEERING
 KLUYVER WEG 1
 2629 HS DELFT
 THE NETHERLANDS
 31-15-278-6279 **FAX:** 31-15-278-1151
e-Mail: *rijck@tudelft.nl*

DR JASON DAI
 SR ENGINEER
 STRUCTURAL INTEGRITY ENGINEERING
 9509 VASSAR AVE
 CHATSWORTH CA 91311
 818-718-2195 **FAX:** 818-718-2212
e-Mail: *jdai@sieinc.com*

MR MARK DERRISO
 ELECTRONICS ENGINEER
 USAF AFRL/VAST
 2790 D ST
 WRIGHT-PATTERSON AFB OH 45433
 937-255-5059 X282 **FAX:** 937-255-6210
e-Mail: *mark.derriso@va.af.mil*

DR CLAUDIO DALLE DONNE
 GERMAN AEROSPACE CTR (DLR)
 INST OF MATERIALS RESEARCH
 LINDER HOHE
 D-51147 COLOGNE
 GERMANY
 +49-2203-601-4608 **FAX:** +49-2203-696480
e-Mail: *claudio.dalle-donne@dlr.de*

MR GARY DESANTIS
 SR ENGINEER
 SIE ENGINEERING
 9509 VASSAR AVE
 CHATSWORTH CA 91311
 818-718-2195 X 125 **FAX:** 818-718-2212
e-Mail: *gdesantis@sieinc.com*

MR GIRIN DAS
 ENGINEER
 BOEING COMMERCIAL AIRPLANE GROUP
 STRUCTURAL DAMAGE TECHNOLOGY
 PO BOX 3707
 M/S 67-FF
 SEATTLE WA 98124-2207
 425-237-6548 **FAX:** 425-234-1499
e-Mail: *gkd0311@servere.ca.boeing.com*

DR PAVLO DYBSKIY
 NATIONAL AEROSPACE LAB
 STRUCTURES DIVISION
 7-44-1 JINDAIJI-HIGAHIMACHI CHOFU-SHI
 TOKYO 182-8522
 JAPAN
 81-0-422-40-3384 **FAX:** 81-0-422-40-3376
e-Mail: *dybskiy@nal.go.jp*

MR MAXWELL DAVIS
 SR RESEARCH SCIENTIST
 ROYAL AUSTRALIAN AIR FORCE
 AIRCRAFT STRUCTURAL INTEGRITY SECTION
 NDTSL SEWING
 RAAF AMBERLEY 4306
 AUSTRALIA
 61-7-5461-3086 **FAX:** 61-7-5461-3260
e-Mail: *mjdavis@raaf.defence.gov.au*

MR ROBERT EASTIN
 NRS-FRACTURE MECHANICS
 FEDERAL AVIATION ADMINISTRATION
 AIR-100 DEPT
 3960 FARAMOUNT BLVD
 LAKEWOOD CA 90712-4137
 562-627-5205 **FAX:** 562-627-5209
e-Mail: *robert.eastin@faa.gov*

ICAF '99 FINAL ATTENDANCE LIST

MR MICHAEL EDWARDS
AEROSPACE ENGINEER
NAVAL AIR SYSTEMS CMD
STRUCTURES DIV
BLDG 2187 UNIT 5
PATUXENT RIVER MD 20670
301-342-9341 **FAX:** 301-342-9404
e-Mail: edwardsml@navair.navy.mil

DR PETER EDWARDS
MANAGING DIRECTOR
PP DATA LTD
RECTORY COTTAGE, RECTORY ROAD WOOD
NORTON
DEREHAM NORFOLK NR20 5BA
UNITED KINGDOM
44-01362-683509 **FAX:** 44-01362-683572
e-Mail: edwards@ppdata.demon.co.uk

MR WILLIAM ELLIOTT
SUPERVISORY AEROSPACE ENGINEER
US AIR FORCE
420 SECOND ST
STE 100
ROBINS AFB GA 31098-1640
912-926-9835 **FAX:** 912-926-1743
e-Mail: welliott@ti.robins.af.mil

MR TIMOTHY FALLON
AEROSPACE ENGINEER
NAVAL AIR SYSTEMS CMD
STRUCTURES DEPT
48110 SHAW RD
BLDG 2187 STE 2320A
PATUXENT RIVER MD 20670-1906
301-342-9325 **FAX:** 301-342-9406
e-Mail: fallontr@navair.navy.mil

MR MICHAEL FALUGI
AERO ENGINEER
USAF AFRL
RESEARCH LAB
STE 1
2130 EIGHTH ST
WRIGHT-PATTERSON AFB OH 45433-7542
937-255-3157 **FAX:** 937-656-7723
e-Mail:

DR THOMAS FARRIS
PROFESSOR AND HEAD
PURDUE UNIVERSITY
SCHOOL OF AERONAUTICS & ASTRONAUTICS
1282 GRISSOM HALL
WEST LAFAYETTE IN 47907-1282
765-494-5117 **FAX:** 765-494-0307
e-Mail: farrist@ecn.purdue.edu

MAJ SCOTT FAWAZ
DEPUTY BRANCH CHIEF
US AIR FORCE
STRUCTURAL INTEGRITY BRANCH
BLDG 65 RM 504
2790 D ST
WRIGH-PATTERSON AFB OH 45433
937-255-6104 EXT 239 **FAX:** 937-656-4999
e-Mail: scott.fawaz@va.wpafb.af.mil

DR DAVID FORD
FR-TEK P/L
196 MONBULK RD
VICTORIA
AUSTRALIA 3791
613-9752-0121 **FAX:**
e-Mail:

MR ROYCE FORMAN
SR SCIENTIST FRACTURE MECHANICS
NASA JOHNSON SPACE CTR
2101 NASA RD ONE
M/S EM2
HOUSTON TX 77058
281-483-8926 **FAX:** 281-244-1301
e-Mail: royce.g.forman@jsc.nasa.gov

MR RONALD FRANCIS
STRCTS ENGINEERING MANAGER
NAVAL AIR SYSTS CMD
NADEP JAX 4.3.3
STE 5
6255 LAKE GRAY BLVD
JACKSONVILLE FL 32244
904-779-3544 **FAX:** 904-779-3520
e-Mail: francisrl@navair.navy.mil

LT COL ROBERT FREDELL
CHIEF, INTERNATIONAL PROG
USAF EOARD
PSC 802 BOX 14
FPO AE 09499
44 207 514 4505 **FAX:** 44 207 514 4960
e-Mail: rfredell@eoard.af.mil

MR CARL FRENCH
ENGINEER
BOEING
OKLAHOMA CITY SUPPORT
2600 LIBERTY PARKWAY
MIDWEST CITY OK 73110
405-739-1410 **FAX:** 405-739-1416
e-Mail: carl.a.french@boeing.com

ICAF '99 FINAL ATTENDANCE LIST

MR MINAS FYTOS
 MANAGER INSPECTION LABS
 OLYMPIC AIRWAYS
 TECHNICAL OPS DEPT
 ATHENS AIRPORT-WEST TD/IC
 ATHENS 166 04
 GREECE
 301-936-2084 **FAX:** 301-936-2879
e-Mail:

MR WALDIR GOMES GONCALVES
 SR STRUCTURES ENGINEER
 EMBRAER-EMPRESA BRASILEIRA DE
 AERONAUTICA SA
 STRUCTURAL ENGINEERING
 AV BRIG FARIA LIMA 2170 180-GEE
 SOA JOSE DOS CAMPOS 12227-901
 SAO PAULO
 55-12-345-2734 **FAX:** 55-12-345-1384
e-Mail: *waldir.goncalves@embrair.com.br*

MR TODD GALLAGHER
 AEROSPACE ENGINEER
 NAPRA DET NAPLES
 ENGINEERING
 PSC 817
 BOX 28
 FPO AE 09622
 39-081-568-5497 **FAX:** 39-081-568-5536
e-Mail: *tgallagh@naples.navy.mil*

MR M DAN GOODYEAR
 AERO TECHNICAL MANAGER
 ALCOA
 STE 222 BLDG 200
 1201 ROBERTS BLVD
 KENNESAW GA 30144
 724-337-2037 **FAX:** 724-339-4075
e-Mail: *dan.goodyear@alcoa.com*

DR FRANK GALLERNEAU
 ONERA
 DMSE
 29 AVENUE DE LE DIVISION
 LEDEX 92322 CHATILLON
 FRANCE
 33 1 4673 4695 **FAX:** 33 1 46 73 41 58
e-Mail: *gallerneau@onera.fr*

DR ULF GORANSON
 CHIEF ENGINEER
 BOEING COMMERCIAL AIRPLANE GROUP
 STRUCTURES LABS & TECH STANDARDS
 PO BOX 3707
 MC 45-10
 SEATTLE WA 98124-2207
 206-655-9922 **FAX:** 206-544-1047
e-Mail: *ulf.g.goranson@boeing.com*

DR JOCELYN GAUDIN
 INGENNEUI
 AEROSPATIALE CCR
 LOUIS-BLERIOT CORP RES CTR
 12 RUE PASTEUR BP 76
 SURESNES 92152
 FRANCE
 33 1 4697 3767 **FAX:** 33 1 4697 3730
e-Mail:

MS RUTH GRAHAM
 UNIVERSITY OF HULL
 SCHOOL OF ENGINEERING
 COTTINGHAM RD
 HULL YORKSHIRE HUG 7RX
 UNITED KINGDOM
 +44 1482 466350 **FAX:** +44 1482 466664
e-Mail: *r.h.graham@edm.hull.ac.uk*

MR ALLEN GEORGESON
 BOEING CO
 MS 67-FF
 PO BOX 3707
 SEATTLE WA 98124
FAX:
e-Mail: *allen.m.georgeson@boeing.com*

MR PAUL GREEN
 TECHNOLOGIST
 BAE MA&A
 STRUCTURAL ENGINEERING
 WARTON AERODROME W427C
 PRESTON LANCASHIRE PR4 1AX
 UNITED KINGDOM
 +44-1772-856203 **FAX:** +44-1772-855689
e-Mail: *paul-d.green@bae.co.uk*

MR DANIEL GILLETTA DE SAINT-JOSEPH
 ENGINEER
 DASSAULT-AVIATION
 STRESS OFFICE
 BP 24
 MERIGNAC CEDEX 33701
 FRANCE
 33 5 56 13 96 64 **FAX:** 33 5 56 13 97 27
e-Mail:

MAJ JAMES GREER JR
 DIRECTOR CASTLE
 US AIR FORCE ACADEMY
 HQ USAFA/DFEM
 STE 6H2
 2354 FAIRCHILD DR
 USAF ACADEMY CO 80840-6240
 719-333-3618 **FAX:** 719-333-2944
e-Mail: *jim.greer@usafa.af.mil*

ICAF '99 FINAL ATTENDANCE LIST

MR PASI GREUS
 MSC ENG
 FINNISH AIR FORCE
 PO BOX 210
 FIN-33101 TAMPERE
 FINLAND
 358-3-181-64111 **FAX:** 358-3-181-64044
e-Mail: *pasi.greus@Intv.fi*

MR MICHAEL GRUBER
 STRUCTURES ENGINEER
 BOEING CO
 STRUCTURAL DAMAGE TECH
 10-16 BLDG M/S 67-FF
 PO BOX 3707
 SEATTLE WA 98056
 425-237-6759 **FAX:** 425-234-1499
e-Mail: *michael.l.gruber@boeing.com*

MR CORNELIS GUIJT
 RESEARCH ENGINEER
 USAF HQ DFEM
 STE 6H2
 2354 FAIRCHILD DR
 US AIR FORCE ACADEMY CO 80840-6240
 719-333-3043 **FAX:** 719-333-2944
e-Mail: *guytcb.dfem@usafa.af.mil*

DR MICHEL GUILLAUME
 SWISS NAT'L DELEGATE
 SWISS AIRCRAFT & SYSTEMS
 ENGINEERING & PROJECTS
 SF EMMEN
 CH 6032
 SWITZERLAND
 41-41-268-4173 **FAX:** 41-41-268-39-47
e-Mail: *michel.guillaume@sf.admin.ch*

MR DANIEL HAENNI
 DIPL MASCH-ING ETH TM LEADER
 PILATUS AIRCRAFT LTD
 CORP UTILITY STRUCTURAL ANALYSIS
 GRUOBSTRASSE 3
 ENNETMOOS CH-6372
 SWITZERLAND
 41-41-619-64-64 **FAX:** 41-41-619-64-52
e-Mail: *dhaenni@pilatus-aircraft.com*

MR RICK HALLIWILL
 LOCKHEED MARTIN AERO SYSTEMS CO
 2585 KINGSWOOD DR
 MARIETTA GA 30066
 770-494-7645 **FAX:** 770-494-5400
e-Mail: *rick.l.halliwill@lmco.com*

DR D GARY HARLOW
 PROFESSOR
 LEHIGH UNIVERSITY
 MECHANICAL ENGINEERING & MECHANICS
 PACKARD LAB
 19 MEMORIAL DR W
 BETHLEHEM PA 18015-3085
 610-758-4127 **FAX:** 610-758-6224
e-Mail: *dgh0@lehigh.edu*

MR DAVID HARPER
 CHIEF ENGINEER
 USAF HQ AFSC/SEF
 9700 AVE G SE
 KIRTLAND AFB NM 87117
 505-846-0996 **FAX:** 505-846-6826
e-Mail: *david.harper@kafb.saia.af.mil*

MR PAAVO HEIKKINEN
 DC-10 PROJECT ENGINEER
 FINNAIR
 ENGINEERING
 M/C EB/2G
 01053 FINNAIR
 FINLAND
 358-9-818-6419 **FAX:** 358-9-818-6797
e-Mail: *paavo.heikkinen@finnair.fi*

MR JAMES HELBLING
 MANAGER/TEAM LEADER
 NORTHROP GRUMMAN CORP
 F-5/T-38 ENGINEERING
 M/S 9780/9
 1 HORNET WAY
 EL SEGUNDO CA 90245-2804
 310-332-6004 **FAX:** 310-331-6648
e-Mail: *james_helbling@mail.northgrum.com*

MR SHANE HILL
 SR ENGINEER
 AMRL
 C/O LOCKHEED MARTIN TAS
 M/Z 6465
 PO BOX 748
 FT WORTH TX 76101
 817-777-2612 **FAX:** 817-763-1014
e-Mail: *shane.hill@dsto.defence.gov.au*

DR BEN HILLBERRY
 PURDUE UNIVERSITY
 SCHOOL OF MECH ENGR
 1288 MECHANICAL ENGINEERING BLDG
 WEST LAFAYETTE IN 47907-1288
 765-494-5721 **FAX:** 765-494-0539
e-Mail: *hillberr@ecn.purdue.edu*

ICAF '99 FINAL ATTENDANCE LIST

DR DAVID HOEPPNER
 PROFESSOR
 UNIVERSITY OF UTAH
 DEPT OF MECHANICAL ENGINEERING
 50 S CENTRAL CAMPUS DR
 RM 2202
 SALT LAKE CITY UT 84112-9208
 801-581-3851 **FAX:** 801-585-5889
e-Mail: *hoeppner@mech.utah.edu*

DR LARS JARFALL
 VARGARDSVAGEN 14
 LINKOPING S-58941
 SWEDEN
 46-13-160709 **FAX:** 46-13-160709
e-Mail:

MR GEOFF HUME
 STRUCTURES ENGINEER
 BRITISH AEROSPACE MA&A
 STRUCTURAL ENGINEERING
 BROUGH
 EAST YORKSHIRE HU15 1EQ
 ENGLAND
 01482-663119 **FAX:**
e-Mail: *geoff.hume@bae.co.uk*

MAJOR BERND JESGULKE
 AEROSPACE ENGINEER
 NATO/HQ NAEWF
 FCLE
 B-7010 SHAPE
 BELGIUM
 32-65-444647 **FAX:** 32-65-347216
e-Mail: *jesgulke@naewfc.nato.int*

DR EDWARD HUNT
 PROFESSIONAL ENGINEER
 BRITISH AEROSPACE AIRBUS LTD
 NEW FILTON HOUSE
 DEPT B56
 BRISTOL BS99 7AR
 UNITED KINGDOM
 +44-117-9365796 **FAX:** +44-117-9365903
e-Mail: *edward.hunt@bae.co.uk*

MR KEVIN JONES
 ENGINEER
 GULFSTREAM AEROSPACE
 FATIGUE & DAMAGE TOLERANCE
 ML/S G07
 PO BOX 2206
 SAVANNAH GA 30003-2206
 912-965-7629 **FAX:** 912-965-5266
e-Mail: *kevin.jones@gulfaero.com*

MR JOHN INGRAM
 STAFF ENGINEER
 LOCKHEED MARTIN
 ADV STRUCTURES & MAT'LS
 M/S 0648
 86 S COBB DR
 MARIETTA GA 30063-0648
 770-494-8172 **FAX:** 770-494-8345
e-Mail: *ed.ingram@lmco.com*

MR YOSHIKI KAKUTA
 SR RESEARCHER
 NATIONAL AEROSPACE LAB
 STRUCTURES DIVISION
 6-13-1 OHSAWA MITAKE
 TOKYO 181-0015
 JAPAN
 81-422-40-3565 **FAX:** 81-422-40-3549
e-Mail: *kakuta@nal.go.jp*

DR PHILIP IRVING
 PROFESSOR
 CRANFIELD UNIVERSITY
 DAMAGE TOLERANCE
 CRANFIELD
 BEDS MK43 OAL
 UNITED KINGDOM
 44-1234-754129 **FAX:** 44-1234-752376
e-Mail: *p.e.iring@cranfield.ac.uk*

MS BRIDGETTE KAPLAN
 SR ENGINEER
 BOEING CO
 STRUCTURES TECHNOLOGY
 M/S K01-11
 PO BOX 7730
 WICHITA KS 67277-7730
 316-523-2961 **FAX:** 316-526-4232
e-Mail: *bridgette.kaplan@wichita.boeing.com*

DR MAKOTO ITO
 JAPAN DEFENSE AGENCY
 1-6-1-943 SAKAE
 TACHIKAWA TOKOYO
 JAPAN
 425-28-3071 **FAX:** 425-28-3071
e-Mail: *makotoy@jda-trdi.go.jp*

MR HISAYA KATOH
 RESEARCH ENGINEER
 NATIONAL AEROSPACE LABORATORY
 STRUCTURES DIVISION
 6-13-1 OSAWA
 MITAKA-SHI TOKYO 181-0015
 JAPAN
 81-422-40-3566 **FAX:** 81-422-40-3549
e-Mail: *katoh@nal.go.jp*

ICAF '99 FINAL ATTENDANCE LIST

MR KENRO KAWABATA
 MANAGER ACFT PROJ ENGINEERING DEPT
 KAWASAKI HEAVY INDUSTRIES LTD
 AIROSPACE DIV
 1KAWASAKI-CHO
 KAKAMIGAHAR CITY GIFU 504-8710
 JAPAN
 0583 82-5947 **FAX:** 0583 82-0924
e-Mail: kawabata-kenro@khu.co.jp

MR RICHARD KINZIE
 MATERIALS ENGR
 USAF AFRL/MLS-OLR
 420 2ND ST
 ROBBINS AFB GA 31098
 912-926-3284 **FAX:** 912-926-6619
e-Mail: richard.kinzie@robins.af.mil

MR DENNIS KEENE
 DEPARTMENT OF DEFENSE
 US AIR FORCE
 420 SECOND ST
 STE 100
 ROBINS AFB GA 31098
 912-926-4489 **FAX:** 912-926-1743
e-Mail: dennis.keene@robins.af.mil

MR JAMES KLEIN
 CHIEF FLIGHT SYSTEMS ENGINEER
 USAF
 FLIGHT TRAINING SYSTEM PROGRAM OFFICE
 BLDG 56
 2100 MONAHAN WAY
 WRIGHT-PATTERSON AFB OH 45433
 937-255-9306 X243 **FAX:** 937-255-8516
e-Mail: james.klein@yt.wpafb.af.mil

MR MIKA KEINONEN
 STRESS ENGINEER
 PATRIA FINAVITEC OY
 ENGINEERING DEPARTMENT
 LENTOKONETEHTAANTIE 3
 HALLI 35600
 FINLAND
 358-0-3-5809392 **FAX:** 358-0-3-5809600
e-Mail: mika.keinonen@patria.fi

DR AKIRA KOBAYASHI
 JAPANESE NAT'L DELEGATE, PROFESSOR
 SCIENCE UNIVERSITY OF TOKYO
 MECHANICAL ENGINEERING DEPT
 YAMASAKI 2641
 NODA CHIBA 278
 JAPAN
 81-471-24-1501 **FAX:** 81-471-23-8096
e-Mail: ogihara@rs.noda.sut.ac.jp

MR THEODOR KERMANIDIS
 PROFESSOR
 UNIVERSITY OF PATRAS
 MECHANICAL ENGINEERING & AERONAUTICS
 26500 PATRAS
 GREECE
 00 30 61 991027 **FAX:** 00 30 61 997190
e-Mail: kermanid@mech.upatrs.gr

DR ALBERT KOBAYASHI
 PROFESSOR EMERITUS
 UNIVERSITY OF WASHINGTON
 MECHANICAL ENGINEERING
 P.O. BOX 352600
 SEATTLE WA 98195-2600
 206-543-5488 **FAX:** 206-685-8047
e-Mail: ask@u.washington.edu

DR JINSEONG KIM
 RESEARCH SCIENTIST
 LYNNTech INC
 7610 EASTMARK DR
 STE 202
 COLLEGE STATION TX 77840
 409-693-0017 **FAX:** 409-764-7479
e-Mail: lunntech@tca.net

MR JERZY KOMOROWSKI
 ACTING STRUCTURES GROUP LEADER
 NATIONAL RESEARCH COUNCIL CANADA
 INSTITUTE FOR AEROSPACE RESEARCH
 MONTREAL RD M14
 OTTOWA ONTARIO
 CANADA KIA 0R6
 613-993-3999 **FAX:** 613-952-7136
e-Mail: jerzy.komorowski@nrc.ca

DR STEPHEN KIMMINS
 PROFESSIONAL ENGINEER
 BRITISH AEROSPACE AIRBUS
 STRUCTURES TECHNOLOGY
 NEW FILTON HOUSE
 B599 7AR FILTON BRISTOL
 UNITED KINGDOM
 44-117-936-5847 **FAX:** 44-117-936-5903
e-Mail: steve.kimmins@bae.co.uk

MR MAKOTO KOSAI
 SR SPECIALIST ENGINEER
 BOEING
 STRUCTURAL DAMAGE TECHNOLOGY
 MC 67-FF
 PO BOX 3707
 SEATTLE WA 98124-2207
 425-237-4881 **FAX:** 425-234-1499
e-Mail: makoto.kosai@boeing.com

ICAF '99 FINAL ATTENDANCE LIST

MR KEIJO KOSKI
RESEARCH SCIENTIST
VTT MANUFACTURING TECHNOLOGY
MARITIME & MECHANICAL ENGINEERING
PO BOX 1705
FIN-02044 VTT ESPOO
FINLAND
358-9-456-6549 **FAX:** 358-9-455-0619
e-Mail: *keijo.koski@vtt.fi*

MR PAUL KRISTENSEN
MANAGING DIRECTOR
STRUCTURAL MONITORING SYSTEMS LTD
LVL 18 152 ST GEORGE'S TERRACE
PERTH WA 6000
AUSTRALIA
61-8-9288-4596 **FAX:** 61-8-9386-5122
e-Mail: *capt.pk@p085.aone.net.au*

MR MICHAEL KULAK
ALCOA TECHNICAL CENTER
100 TECHNICAL DR
ALCOA CENTER PA 15069
724-337-5874 **FAX:** 724-337-5436
e-Mail: *michael.kulak@alcoa.com*

MR RIKU LAHTINEN
M SC (TECH)
FINNISH AIR FORCE HEADQUARTERS
PO BOX 30
TIKKAKSOKI FIN-41161
FINLAND
358-14-181-0111 **FAX:** 358-14-181-4350
e-Mail:

PROF AGOSTINO LANCIOTTI
PROFESSOR
UNIVERSITY OF PISA
AEROSPACE ENGINEERING
VIA DIOTISALVI 2
PISA
ITALY 56126
39-050-550200 **FAX:** 39-050-553654
e-Mail: *a.lanciotti@ing.unipi.it*

MR MICHAEL LANGENBUCHER
DIPL-ING
DAIMLER CHRYSLER AEROSPACE
FATIGUE DEPT
PO BOX 801160
MUNICH 81663
GERMANY
0049-0-89-607-20781 **FAX:** 0049-0-83-607-32158
e-Mail: *michael.langenbucher@m.dasa.de*

MR MARC LANGON
STRUCTURAL TESTING ENGINEER
DGA / CEAT
STRUCTURES & AIRPLANE MAT'LS
23 AVENUE H GUILLANMER
31056 TOULOUSE CEDEX
FRANCE
33 5 61 58 74 19 **FAX:** 33 5 61 58 74 78
e-Mail: *ceat.structures@wanadoo.fr*

PROF LUIGI LAZZERI
PROFESSOR
UNIV OF PISA
DEPT OF AEROSPACE ENGINEERING
VIA DIOTISALVI 2
PISA
ITALY 56126
39-050-550200 **FAX:** 39-050-553654
e-Mail: *aero.lazzeri@ing.unipi.it*

MR BOB LEE
SR STRUCTURAL LIFE ANALYST
RAYTHEON SYSTEMS CO
FLIGHT SCIENCES DEPARTMENT
PO BOX 154580
M/S 1134
WACO TX 76715-4580
254-867-7409 **FAX:** 254-867-2115
e-Mail: *leek@readwo.com*

DR JOHN LINCOLN
TECH ADVISOR
USAF ASC/EN
BLDG 560
2530 LOOP RD W
WRIGHT-PATTERSON AFB OH 45433-7101
937-255-5312 **FAX:** 937-656-4546
e-Mail: *lincoliw@asc-en.wpafb.af.mil*

MR CHARLES LIPSCOMB
AERO ENGINEER
NAVAL AVIATION DEPOT
P3-FST CODE 4.3.3 BLDG 2
NAVAL AIR STATION
JACKSONVILLE FL 32212
904-542-5407 X216 **FAX:** 904-512-2417
e-Mail:

MR KO-WEI LIU
PRIN ENG
THE BOEING CO
M/S CO52/0660
2401 E WARDLOW ROAD
LONG BEACH CA 90807-4418
310-982-5422 **FAX:** 310-982-5164
e-Mail: *ko-wei.liu@boeing.com*

ICAF '99 FINAL ATTENDANCE LIST

MR STEVEN LOVATO
PROJECT ENGINEER
FEDERAL EXPRESS
AIRCRAFT STRUCTURES ENGINEERING
3131 DEMOCRAT
M/S 5413
MEMPHIS TN 38118
901-224-4829 **FAX:** 901-224-4819
e-Mail: *smlovato@fedex.com*

MR RA'ED MA'AYTA
SENIOR STRESS ENGINEER
ROYAL AIR FORCE
REPAIR DESIGN AUTHORITY
RAFRDA-RAF ST ATHAN
BARRY VALE OF GLAMORGAN WALES CF61 4WA
UNITED KINGDOM
01446-798578 **FAX:** 01446-798985
e-Mail:

MR SHIGERU MACHIDA
SUPERVISOR
FUJI HEAVY INDUSTRIES LTD
AEROSPACE DIVISION
1-1-11 YONAN
TOCHIGI 320-8564 UTSUNOMIYA
JAPAN
81-28-659-5710 **FAX:** 81-28-659-5895
e-Mail: *machidas@pow2.ae.subaru-fhi.co.jp*

MR WILLIAM MADLEY
GENERAL MANAGER
AEROSTRUCTURES
PO BOX 4331
MELBOURNE 3001
AUSTRALIA
61-3-9626-7991 **FAX:** 61-3-9681-9813
e-Mail: *bill.madley@dsto.defence.gov.au*

SQNLDR DAVID MAHONEY
ROYAL AUSTRALIAN AIR FORCE
OFFICE OF THE AIR ATTACHE
1601 MASSACHUSTES AVE NW
WASHINGTON DC 20036
202-797-3044 **FAX:** 202-483-5184
e-Mail:

MR HARRY MAHOOD
CEO
MASDAA INC
OFFICE OF THE CEO
14 WENONAH DR
MISSISSAUGA ONTARIO
CANADA L5G 3W1
905-274-5338 **FAX:** 905-274-5390
e-Mail: *mahoodh@msn.com*

MR COLIN MARTIN
RESEARCH LEADER
DEFENCE SCIENCE & TECHNOLOGY ORG
506 LORIMER STREET FISHERMENS BEND
MELBOURNE VICTORIA 3207
AUSTRALIA
9-626-7481 **FAX:** 9-626-7089
e-Mail: *colin.martin@dsto.defence.gov.au*

MS SUZANNE MASTERSON
BOEING COMMERCIAL AIRPLANES GRP
M/S 67-FF
PO BOX 3707
SEATTLE WA 98124-2207
206-237-1053 **FAX:** 206-234-1499
e-Mail: *sam8795@es5012.ca.boeing.com*

MR CHRISTOPHER MAZUR
STRUCTURES ENGINEER
BOEING CO
STRUCTURAL DAMAGE TECH
M/S 67-FF 10-16 BLDG
PO BOX 3707
SEATTLE WA 98124-2207
425-237-9575 **FAX:** 425-234-1499
e-Mail: *christopher.j.mazur@boeing.com*

MR JAMES MAZZA
MTLS ENGINEER
USAF AFRL/MLSA
STE 1
2179 TWELFTH ST
WRIGHT-PATTERSON AFB OH 45433
937-255-7778 **FAX:** 937-656-4419
e-Mail: *james.mazza@afrl.af.mil*

MR STEPHEN MCCLURE
AEROSPACE ENGINEER
NAWCAD
AIR 4.3.3.2
638 RADFORD CIRCLE
WOODSTOCK GA 30188
770-494-1802 **FAX:** 770-494-7883
e-Mail: *mccluresp@naviar.navy.mil*

MR NIAL MCCUSKER
STRUCTURES ENGINEER
BRITISH AEROSPACE MA&A
STRUCTURAL ENGINEERING
BROUGH
EAST YORKSHIRE HU15 1EQ
ENGLAND
01482-664298 **FAX:**
e-Mail: *niall.mccusker@bae.co.uk*

ICAF '99 FINAL ATTENDANCE LIST

DR PETER MCKEIGHAN
 MANAGER
 SOUTHWEST RESEARCH INSTITUTE
 MATERIALS ENGINEERING DEPT
 6220 CULEBRA ROAD
 SAN ANTONIO TX 78238
 210-522-2016 **FAX:** 210-522-5122
e-Mail: *pmckeighan@swri.org*

MR ALLEN MOORE
 INDUSTRIAL ENGINEER
 USAF AFRL/MLMA
 WRIGHT-PATTERSON AFB OH 45433
 937-255-3701 **FAX:** 937-255-1268
e-Mail:

MRS ALISON MEW
 SR ENGINEER
 DERA
 LAND/AIR STRUCTURES
 RM 2008, GRIFFITH BLDG (A7) IVELY RD
 FARNBOROUGH, HANTS GU14 OLX
 ENGLAND
 +44-1252-395455 **FAX:** +44-1252-394006
e-Mail: *abmew@dera.gov.uk*

MR TERRY MOORE
 TEST SPECIALIST II
 BOEING
 PHANTOM WORKS
 M/S 4E-94
 PO BOX 3707
 SEATTLE WA 98124-2207
 206-662-2086 **FAX:** 206-662-2126
e-Mail: *terry.r.moore@boeing.com*

MR ERIC MEYER
 ASSOC TECHNICAL FELLOW
 BOEING
 DEPT 350
 M/S S1063511
 PO BOX 516
 ST LOUIS MO 63166
 314-232-4097 **FAX:** 314-232-6885
e-Mail: *eric.s.meyer@boeing.com*

MR JOHN MORGAN
 AERO ENGINEER
 USAF OC-ALC/LABEF
 B-1B SYSTEM SPT ENGINEERING
 STE 2AB85A
 3001 STAFF DR
 TINKER AFB OK 73145-3006
 405-736-7264 **FAX:** 405-736-5598
e-Mail: *morgan.john@b1b.tinker.af.mil*

MR HANS-JORG MEYER
 DIPL-ING
 DAIMLER CHRYSLER AEROSPACE AIRBUS
 EDC DEPT
 HUNEFELDSTR. 1-5
 D - 28183 BREMEN
 GERMANY
 421-5382912 **FAX:** 421-5384998
e-Mail: *hans-joerg.meyer@airbus.dasa.de*

MR JOHN MORRISH
 AERONAUTICAL ENGINEERING 1
 ROYAL NEW ZEALAND AIR FORCE
 DIRECTORATE OF AERONAUTICAL ENGINEERING
 HDQUARTERS NEW ZEALAND DEFENCE FORCE
 WELLINGTON
 NEW ZEALAND
 0064-4-4986531 **FAX:** 0064-4-4986818
e-Mail: *ael@hq.af.mil.nz*

DR JENNIFER MILLER
 AEROSPACE ENGINEER
 NAVAIR
 STRUCTURES
 UNIT 5
 48110 SHAW RD
 PATUXENT RIVER MD 20670-1906
 301-342-8099 **FAX:** 301-342-9406
e-Mail: *millerj2@navair.navy.mil*

MR KOICHI MURAYAMA
 ENGINEER
 MITSUBISHI HEAVY IND LTD
 NAGOYA AERO SYS
 10 OYE-CHO MINATO-KU
 NAGOYA 455-8515
 JAPAN
 052 611 2194 **FAX:** 052 611 9365
e-Mail: *kouichi_murayama@mx.nasw.mhi.co.jp*

MR JUERGEN MOEWS
 PILATUS AIRCRAFT LTD
 STRUCTURAL ENGINEERING
 AMRL 506 LORIMER ST
 PO BOX 4331 MELBOURNE VIC 3001
 AUSTRALIA
 61-3-9626-7191 **FAX:** 61-3-9626-7072
e-Mail: *juergen.moews@dsto.defence.gov.au*

LT MICHAEL MYERS
 LD ENGINEER ACFT REPAIR
 USAF AFRL/VASE
 RM 504
 2790 D ST
 WRIGHT-PATTERSON AFB OH 45433
 937-255-6104 X243 **FAX:** 937-656-4999
e-Mail: *michael.myers@va.af.mil*

ICAF '99 FINAL ATTENDANCE LIST

DR RAJIV NAIK
 MATERIALS SPECIALIST
 PRATT & WHITNEY
 MATERIALS BEHAVIOR & EVALUATION
 PO BOX 109600
 M/S 707-22
 WEST PALM BEACH FL 33410-9608
 561-796-5213 **FAX:** 561-796-7454
e-Mail: *nikra@pwfl.com*

PROF GRIGORY NESTERENKO
 DAMAGE TOLERANCE/INTEG STIFF & RIV STRCT
 CENTRAL AEROHYDRODYNAMIC INST
 1 ZHUKOVSKY STR
 ZHUKOVSKY MOSCOW REG 140160
 RUSSIA
 7-095-556-40-02 **FAX:** 7-095-556-43-37
e-Mail: *slc@tsagi.rssi.ru*

MR BRIAN NASRALLA
 AIRCRAFT STRUCTURAL REPAIR ENGINEER
 BOEING FLIGHT SAFETY
 STRUCTURES TRAINING
 M/S 20-72
 PO BOX 34787
 SEATTLE WA 98124-1787
 206-662-8081 **FAX:** 206-662-8239
e-Mail: *brian.g.nasralla@boeing.com*

DR JAMES NEWMAN
 SR SCIENTIST
 NASA LANGLEY RESEARCH CTR
 MECHANICS OF MAT'LS BRANCH
 2 W RIED ST
 M/S 188E
 HAMPTON VA 23681
 804-864-3487 **FAX:** 80-864-8911
e-Mail: *j.c.newman.jr@larc.nasa.gov*

MR ARNOLD NATHAN
 MANAGER R&D OF AIRCRAFT STURCTURES
 ISRAEL AIRCRAFT INDUSTRIES
 DEPT 4441
 BEN GURION INTERNATIONAL AIRPORT
 70100
 ISRAEL
 972-3-935-3868 **FAX:** 972-3-935-5055
e-Mail: *anathan@engdiv.iai.co.il*

MR TRUNG NGUYEN
 AERO ENGINEER
 NAVAL AIR SYSTEMS CMD
 STRUCTURES AIR 4.3.3.2
 BLDG 2187
 M/S 5
 PATUXENT RIVER MD 20670
 301-342-9329 **FAX:** 301-342-9404
e-Mail: *nguyentt@navair.navy.mil*

MR GEORGE NEAT
 CHIEF
 US DOT/VOLPE CTR
 OFFICE OF SAFETY & SECURITY
 KENDALL SQUARE
 M/S DTS-74
 CAMBRIDGE MA 02142
 617-494-2679 **FAX:** 617-494-3096
e-Mail: *neat@volpe.dot.gov*

MR MATTHEW NORDSTRUM
 ENGINEER
 BOEING CO
 STRUCTURAL DAMAGE TECH
 MS 67-FF
 PO BOX 3707
 SEATTLE WA 98124-2207
 425-237-6570 **FAX:** 425-234-1499
e-Mail: *matthew.c.nordstrum@boeing.com*

MR TERRY NEIGHBOR
 DIRECTOR
 USAF AFRL/XP
 RESEARCH LAB
 STE 1 BLDG 15
 1864 4TH ST
 WRIGHT-PATTERSON AFB OH 45433-7131
 (937) 255-5248 **FAX:** (937) 656-4824
e-Mail: *terry.neighbor@afrl.af.mil*

MR MICHAEL O'GRADY
 SUPV STRUCTURAL MAT'LS LAB
 BOEING
 STRUCTURES
 BLDG 45-12
 DC COMPLEX 9-90.1
 SEATTLE WA
 206-655-8866 **FAX:**
e-Mail: *michael.o'grady@pss.boeing.com*

MR ROGER NESJE
 PRINC ENGINEER
 ROYAL NORWEGIAN AF
 MATERIAL COMMAND
 PO BOX 7
 KJELLER N2027
 NORWAY
 4763808312 **FAX:** 4763808300
e-Mail: *roger.nesje@lfk.mil.nw*

MR STEN OBERG
 STRUCTURES SPECIALIST
 THE SWEDISH CIVIL AVIATION ADMINISTRATION
 AVIATION SAFETY DEPT
 AIRWORTHINESS SECTION
 NORRKOEPING S-601 79
 SWEDEN
 46-11-19-20-67 **FAX:** 46-11-19-25-75
e-Mail: *sten.oberg@fltsafety.lfv.se*

ICAF '99 FINAL ATTENDANCE LIST

MR KIRK ODIAN
 SR ENGINEER
 SIE ENGINEERING
 9509 VASSAR AVE
 CHATSWORTH CA 91311
 818-718-2195 **FAX:** 818-718-2212
e-Mail: *kodian@sieinc.com*

MR MARK OFSTHUN
 SR SPECIALIST ENGINEER
 BOEING CO
 STRUCTUREAL DAMAGE TECH
 MS 67-FF
 PO BOX 3707
 SEATTLE WA 98124-2207
 206-237-0198 **FAX:** 206-234-1499
e-Mail:

DR SHINJI OGIHARA
 SCIENCE UNIV OF TOKYO
 MECHANICAL ENGINEERING
 2641 YAMASAKI
 NODA, CHIBA 278
 JAPAN
 81-471-24-1501 X 3957 **FAX:** 81-471-23-8096
e-Mail: *ogihara@rs.noda.sut.ac.jp*

MR TAKAO OKADA
 NATIONAL AEROSPACE LAB
 STRUCTURES DIVISION
 7-44-1 JINDAJI HIGASHIMACHI
 CHOFU 182-8522
 JAPAN
 81-422-40-3398 **FAX:** 81-422-40-3376
e-Mail: *tokada@nal.go.jp*

MR JAVIER ORTIZ-APENTE
 DESIGN ENGINEER
 BOEING CO
 POST PROD ENGINEERING
 M/S 2M-14
 SEATTLE WA
 206-544-7756 **FAX:** 206-544-9297
e-Mail: *javier.r.ortiz-aponte@boeing.com*

MR HAROLD OTTENS
 NAT'L AEROSPACE LAB (NLR)
 PO BOX 153
 NL-8300 AD EMMELOORD
 THE NETHERLANDS
 31-527-248289 **FAX:** 31-527-24-8210
e-Mail: *ottens@nlr.nl*

MR MICHAEL OVERD
 HEAD OF STRUCTURES & MAT'LS
 GKN WESTLAND HELICOPTERS
 BOX 267 LYSANDER ROAD
 YEOVIL, SOMERSET BA20 2YB
 ENGLAND
 +44-01935-702452 **FAX:** +44-01935-704015
e-Mail: *overdm@gkn-whl.co.uk*

MR BJORN PALMBERG
 SENIOR RESEARCH ENGINEER
 FFA (AERONAUTICAL RESEARCH INSTITUTE OF
 SWEDEN)
 STRUCTURES AND MATERIALS
 PO BOX 110 21
 SE-161 11 BROMMA
 SWEDEN
 46-8-555-492-42 **FAX:** 46-8-258919
e-Mail: *pgb@ffa.se*

MR RAY PARKER
 AERONAUTICAL & MARITIME RESEARCH LAB
 PO BOX 4331
 MELBOURNE VICTORIA 3001
 AUSTRALIA
FAX: 61 3 9626 7264
e-Mail: *ray.parker@dsto.defence.gov.au*

DR ARUN PASRICHA
 ENGINEERING SPECIALIST
 NORTHROP GRUMMAN CORP
 STRUCTURAL CERTIFICATION AIR COMBAT
 ONE HORNET WAY
 9L14/64
 EL SEGUNDO CA 90245-9160
 310-332-2122 **FAX:** 310-332-9160
e-Mail: *pasriar@mail.northgrum.com*

DR DEB PEELER
 MATERIALS SCIENTIST
 USAF AFRL/MLS
 RM 122
 2179 12TH ST
 WRIGHT-PATTERSON AFB OH 45433
 937-255-4251 **FAX:** 937-656-7129
e-Mail: *dpeeler@wl.wpafb.af.mil*

MR DONALD PETTIT
 DEPARTMENT MANAGER
 LOCKHEED MARTIN AERO SYSTEMS
 STRUCTURAL TEST LAB
 M/S 0484
 86 S COBB DR
 MARIETTA GA 30063-0484
 770-494-5313 **FAX:** 770-494-2028
e-Mail: *don.e.pettit@lmco.com*

ICAF '99 FINAL ATTENDANCE LIST

DR ROBERT PIASCIK
 SR SCIENTIST
 NASA LANGLEY RESEARCH CTR
 M/S 188E
 TWO W REID ST
 HAMPTON VA 26381-0001
 757-864-3483 **FAX:** 757-864-8911
e-Mail: *r.s.piascik@larc.nasa.gov*

MR DAVID REES
 CHIEF ENGINEER
 AEROSTRUCTURES AUSTRALIA
 LEVEL 14, 222 KINGSWAY
 SOUTH MELBOURNE VIC 3205
 AUSTRALIA
 61-3-9686-8081 **FAX:** 61-3-9696-8195
e-Mail: *david.rees@aerostructures.com.au*

MR YVES PILON
 DADT SECTION LEAD
 SINO SWEARINGEN AIRCRAFT CO
 DURABILITY & DAMAGE TOLERANCW
 1770 SKY PLACE BLVD
 SAN ANTONIO TX 78216
 210-258-3941 **FAX:** 210-258-3953
e-Mail: *ypilon@sj30jet.com*

MR LEN REID
 VICE PRESIDENT ENGINEERING
 FATIGUE TECHNOLOGY INC
 100 ANDOVER PARK WEST
 SEATTLE WA 98188
 206-246-2010 **FAX:** 206-244-9886
e-Mail: *engineering@fatiguetechnology.com*

MR JOUNI PIRTOLA
 ENGINEERING MANAGER
 PATRIA FINAVITEC OY
 ENGINEERING DEPARTMENT
 LENTOKONETEHTAANTIE 3
 HALLI 35600
 FINLAND
 358-0-3-5800260 **FAX:** 358-0-3-5809600
e-Mail: *jouni.pirtola@patria.fi*

MR JUDE RESTIS
 ENGINEERING MANAGER
 FATIGUE TECHNOLOGY INC
 100 ANDOVER PARK WEST
 SEATTLE WA 98188
 206-246-2010 **FAX:** 206-244-9886
e-Mail: *jrestis@fatiguetechnology.com*

DR PETER POOLE
 STRUCTURAL MATERIALS CENTRE
 DEF RESEARCH AGENCY (DRA)
 FARNBOROUGH
 HANTS GU146TD
 UNITED KINGDOM
 01252 395004 **FAX:** 01252 397298
e-Mail:

MR W MICHAEL REYER
 AEROSPACE ENGINEER
 FEDERAL AVIATION ADMINISTRATION
 SMALL AIRPLANE DIRECTORATE, ACE-111
 601 E 12TH STREET
 KANSAS CITY MO 64112
 816-426-6941 **FAX:** 816-426-2169
e-Mail: *michael.rayer@faa.gov*

MR JONATHAN POPE
 NAVAIR
 STRUCTURES DIVISION
 BLDG 2187 UNIT 5
 48110 SHAW RD
 CALIFORNIA MD 20619
 301-342-9328 **FAX:** 301-342-9404
e-Mail: *popejm@navair.navy.mil*

MAJ ERICA ROBERTSON
 DEPUTY CHIEF STRUCTURES DIV
 USAF AFRL/VAS
 BLDG 45 ROOM 113
 2130 8TH ST
 WRIGHT-PATTERSON AFB OH 45433-7542
 937-255-3031 **FAX:** 937-255-3740
e-Mail: *erica.robertson@va.wpafb.af.mil*

DR MOHAN RATWANI
 GENERAL MANAGER
 R-TEC
 4 LATIGO LN
 ROLLING HILLS ESTATE CA 90274-7697
 310-378-9236 **FAX:** 310-378-7697
e-Mail: *mohanr@aol.com*

MR CHRISTOPHER ROOT
 E-2C/C-2A
 NAVAL AIR SYSTEMS COMMAND
 NAVAL AVIATION DEPOT NORTH ISLAND
 P.O. BOX 357058
 SAN DIEGO CA 92135
 619-545-3941 **FAX:** 619-545-7314
e-Mail: *rootcb@navair.navy.mil*

ICAF '99 FINAL ATTENDANCE LIST

MR JEAN ROUCHON
 FRENCH NATIONAL DELEGATE
 CEAT
 STRUCTURES & AIRFRAME MATERIALS DEPT
 23 AVENUE HENRI GUILLAUMET-F
 31056 TOULOUSE CEDEX
 FRANCE
 33-561-58-7390 **FAX:** 33-561-58-7478
e-Mail: *jean.rouchon@wanadoo.fr*

MR JEAN ROUSSEL
 MANAGER TECH ENGINEERING
 BOMBARDIER AEROSPACE
 TECHNICAL ENGINEERING
 10000 CARGO A-4 ST
 MIRABEL QUEBEC
 CANADA J7N 1H3
 450-476-4056 **FAX:** 450-476-4451
e-Mail: *jean.rousseau@defence.bombardier.com*

MR JAMES RUDD
 CHIEF STRUCT INTEGRITY BRANCH
 USAF AFRL/VAA
 BLDG 45 STE 1
 2130 EIGHTH ST
 WRIGHT-PATTERSON AFB OH 45433
 937-255-3031 **FAX:** 937-255-3740
e-Mail:

MR PATRICK SAFARIAN
 FEDERAL AVIATION ADMIN FAA
 SEATTLE AIRCRAFT CERT OFFICE
 ANM-1205
 1601 LIND AVE SW
 RENTON WA 98012
 425-227-2775 **FAX:** 425-227-1181
e-Mail: *patrick.saferian@faa.gov*

MR ALAN SAFERSTEIN
 AEROSPACE ENGINEER
 NAVAL AVIATION DEPOT
 STRUCTURAL MOD & PROD SUPPORT
 COMMANDING OFFICER
 JACKSONVILLE FL 32212
 904-542-5407 X215 **FAX:** 904-542-2417
e-Mail: *safersteinam@navair.navy.mil*

DR CHARLEY SAFF
 BOEING FELLOW
 BOEING COMPANY
 STRUCTURAL TECHNOLOGY
 PO BOX 516
 M/S S1021322
 ST LOUIS MO 63166
 314-233-8623 **FAX:** 314-777-1171
e-Mail: *charles.r.saff@boeing.com*

PROF ATTILIO SALVETTI
 PROFESSOR
 UNIVERSITA PISA
 AEROSPACE ENGINEERING
 VIA DIOTISALVI 2
 PISA
 ITALY 56126
FAX: 39-050-553654
e-Mail:

MR CYRILLE SAVES ST GERMES
 RESEARCH ENGINEER
 AEROSPATIALE AIRBUS
 METALLIC RESEARCH
 316 ROUTE DE BAYONNE
 31060 TOULOUSE CEDEX
 FRANCE
 33 5 61 18 53 04 **FAX:** 33 5 61 93 69 55
e-Mail:
cyril.saves-saint-germes@avions.aerospatiale.fr

MR GREG SCARICH
 PRINCIPAL ENGINEER
 NORTHROP GRUMMAN
 STRUCTURES AIR COMBAT SYSTS
 ONE HORNET WAY
 M/S 90245-2804
 EL SEGUNDO CA 90245-2804
 310-332-4228 **FAX:** 310-332-9160
e-Mail: *scarigr@mail.northgrum.com*

MR HANS-JUERGEN SCHMIDT
 DIPL-ING
 DAIMLER CHRYSLER AREO AIRBUS
 FATIGUE & FRACTURE MECHANICS
 PO BOX 950109
 HAMBURG D 21111
 GERMANY
 49 40 7437 2252 **FAX:** 49 40 7437 4193
e-Mail: *hans.schmidt@airbus.dasa.de*

SQD LDR NICHOLAS SCHONER
 OC RAFROA
 ROYAL AIR FORCE
 REPAIR DESIGN AUTHORITY
 RAF ST ATHAN
 BARRY VALE OF GLAMORGAN WALES CF62 4LB
 UNITED KINGDOM
 01446-798126 **FAX:** 01446-798985
e-Mail:

MR WARREN SCOTT
 AIRCRAFT CATALOGER
 DEPARTMENT OF DEFENSE
 DEFENSE LOGISTICS INFORMATION SERVICE
 STE 7
 74 WASHINGTON AVE N
 BATTLECREEK MI 49017-3084
 616-961-5509 **FAX:** 616-961-5660
e-Mail: *wscott@dliis.dla.mil*

ICAF '99 FINAL ATTENDANCE LIST

MR SURENDRA SHAH
SR SPECIALIST ENGINEER
LOCKHEED MARTIN AERO SYSTEMS CO
DEPT 73-25
86 S COBB DR
MS 0160
MARIETTA GA 30063-0160
770-494-2391 **FAX:** 770-494-9610
e-Mail: *surendra.r.shah@lmco.com*

MR DAVID SIMPSON
DIRECTOR
NAT'L RESEARCH COUNCIL OF CANADA
STRUCTURES & MATERIALS LAB
MONTREAL RD
OTTAWA ONTARIO
CANADA KIA 0R6
613-993-0899 **FAX:** 613-952-7136
e-Mail: *david.simpson@nrc.ca*

MR PETER SHARP
RESEARCH SCIENTIST
DSTO
AERONAUTICAL & MARITIME RESEARCH LAB
PO BOX 4331
MELBOURNE 3001
AUSTRALIA
61-3-9626-7395 **FAX:** 61-3-9626-7089
e-Mail: *khan.sharp@dsto.defence.gov.au*

MR GERALD SINZIG
SR PRINCIPAL ENGINEER
BOMBARDIER AEROSPACE
ENGINEERING STRESS DEPT
123 GARRAT BLVD M/S N45-34
TORONTO ONTARIO
CANADA M3K 1Y5
416-375-3813 **FAX:** 416-375-7699
e-Mail: *gsinzig@dehavilland.ca*

DR TOSHIYUKI SHIMOKAWA
HEAD OF FATIGUE STRENGTH LABORATORY
NATIONAL AEROSPACE LABORATORY
STRUCTURES DIVISION
6-13-1 OHSAWA
MITAKA TOKYO 181-0015
JAPAN
+81-422-47-5911 **FAX:** +81-422-31-6198
e-Mail: *shimoka@nal.go.jp*

MR JOHNNY SMITH
GROUP ENGINEER
RAYTHEON AIRCRAFT CO
TECHNICAL ENGINEERING
PO BOX 85
M/S 931-B6
WICHITA KS 67201
316-676-7719 **FAX:** 316-676-8381
e-Mail: *johnny_smith@raytheon.com*

MR ROBERT SHOOTER
STRUCTURES ENGINEER
BRITISH AEROSPACE MA&A
STRUCTURAL ENGINEERING
BROUGH
EAST YORKSHIRE HU15 1EQ
ENGLAND
01482-664129 **FAX:**
e-Mail: *rob.shooter@bae.co.uk*

MR BOB SOMERVILLE
BOEING CO
MS 45-12
PO BOX 3707
SEATTLE WA 98124
206-655-1602 **FAX:** 206-544-1047
e-Mail: *robert.w.somerville@boeing*

MR DANIEL SHRAGE
STRUCTURAL ENGINEER
USAF AFRL
BLDG 65
2790 D ST
WRIGHT-PATTERSON AFB OH 45433
937-255-6104 **FAX:**
e-Mail: *daniel.shrage@va.afrl.af.mil*

MR THOMAS SOVAR
SPECIALIST ENGINEER
THE BOEING CO
M/S 67-FF
PO BOX 3707
SEATTLE WA 98124-2207
425-237-6487 **FAX:** 425-234-1499
e-Mail: *thomas.e.sovar@boeing.com*

MR CLYDE SIMMERMAN JR
AEROSPACE ENGINEER
NAVAL AIR SYSTEMS CMD
AIR 4.3.3.2
UNIT 5 STE 2340
48110 SHAW RD
PATUXENT RIVER MD 20670-1906
301-342-9339 **FAX:** 301-342-9404
e-Mail: *simmernance@navair.navy.mil*

MR HANS STAHL
HEAD OF STRUCTURE REPAIR ENGINEERING
DAIMLER CHRYSLER AEROSPACE AIRBUS
STRUCTURE REPAIR ENGINEERING
PO BOX 950109
HAMBURG 21111
GERMANY
49-40-74373482 **FAX:** 49-74374193
e-Mail: *hans.stahl@airbus.dasa.de*

ICAF '99 FINAL ATTENDANCE LIST

MR BRIAN STEPHENS
AEROSPACE ENGINEER
NAVAL AVIATION DEPOT
CODE 4.3.3 - H3ISST
PSC BOX 8021
CHERRY POINT NC 28533-0021
252-464-5644 **FAX:** 252-464-6431
e-Mail: *stephensbe@navair.navy.mil*

MR THOMAS SWIFT
ENGINEERING CONSULTANT
FATIGUE TECHNOLOGY INC
118 OXEN HOLME RD
LA9 7HQ KENDAL CUMGRIA
UNITED KINGDOM
44-1539-727509 **FAX:** 44-1539-735967
e-Mail: *tomswiftk@aol.com*

SQN LDR MARK STUBBS
HEAD OF AIRFRAME SECTION
ROYAL AIR FORCE
AIRCRAFT ENGINEERING AIRFRAMES
RAF WYTON SLAF BLOCK L
HUNTINGDON PE17 2PY CAMBS
UNITED KINGDOM
44-0-1480-52451 X6396 **FAX:** 44-0-1480-446565
e-Mail: *slaf@logistics.org.uk*

DR MATTHEW SZOLWINSKI
ASSISTANT PROFESSOR
RENSELAER POLYTECHNIC
MECHANICAL/AERO ENGINEER
110 8TH ST
M/S 2046 JEC
TROY NY 12180-3590
518-276-2024 **FAX:** 518-276-6025
e-Mail: *szolwin@rpi.edu*

MR DAVID SWAIN
VICE PRESIDENT ENGINEERING
BOEING

FAX:
e-Mail:

MS AMY TAYLOR
RESEARCH ENGINEER
UNIVERSITY OF UTAH
MECHANICAL ENGINEERING
50 S CENTRAL CAMPUS DR
RM 2202
SALT LAKE CITY UT 84112
801-581-4025 **FAX:** 801-585-9826
e-Mail: *ahtaylor@mech.utah.edu*

MR GEOFFREY SWANTON
PROFESSIONAL OFFICER
DSTO AMRL
3217 RIVER PARK DR #2912
FT WORTH TX 76116
817-763-8982 **FAX:** 817-763-1014
e-Mail: *gswanton@flash.net*

MR YVES THERIAULT
SECTION CHIEF
BOMBARDIER AEROSPACE
AIRFRAME STRESS
1800 MARCEL-LAUAIN BLVD
ST LAURENT QUEBEC
CANADA H4R 1K2
514-855-5001 X51605 **FAX:** 514-855-2111
e-Mail: *yves.theriault@eng.canadair.ca*

DR DAVID SWARTZ
TECHNICAL SPECIALST
FEDERAL AVIATION ADMIN
2500 EAST VALLEY RD C-2
RENTON WA 98055
425-227-2172 **FAX:** 425-227-1159
e-Mail: *dave.swartz@faa.gov*

DR MARK THOMSEN
ENGINEER
BOEING COMMERCIAL AIRPLANE GROUP
STRUCTURAL MATERIALS LABORATORY
PO BOX 3707
M/S 45-12
SEATTLE WA 98124-2207
206-655-1601 **FAX:** 206-544-1047
e-Mail: *mark.l.thomsen@boeing.com*

MR STEVEN SWIFT
PRINCIPAL ENGINEER, FATIGUE EVALUATION
CIVIL AVIATION SAFETY AUTHORITY
AIRWORTHINESS
GPO BOX 2005
CANBERRA ACT 2601
AUSTRALIA
61-2-6217-1833 **FAX:** 61-2-6217-1914
e-Mail: *swift_sj@casa.gov.au*

MR STEPHAN TIPTON
B-1 LEAD ENGINEER
USAF OC-ALC/LABEF
STE 2AB79A
3001 STAFF DR
TINKER AFB OH 73145-3006
405-736-7446 **FAX:** 405-736-5598
e-Mail: *tipton.steve@b1b.tinker.af.mil*

ICAF '99 FINAL ATTENDANCE LIST

MR HIN TSANG
 SR STRUCTURES ENGINEER
 TRANSPORT CANADA
 AIRCRAFT CERT BRANCH
 330 SPARKS ST AAROD/S
 OTTAWA ONTARIO
 CANADA KIA ON8
 613-952-4397 **FAX:** 613-996-9178
e-Mail: *tsangh@tc.gc.ca*

DR CHANDRASEKARAN VENKATESAN
 RESEARCH ASST PROFESSOR
 UNIVERSITY OF UTAH
 MECHANICAL ENGINEERING
 50 S CENTRAL CAMPUS DR
 RM 2202
 SALT LAKE CITY UT 84112
 801-581-4025 **FAX:** 801-585-9826
e-Mail: *chandru@mech.utah.edu*

MR TRIANTAFILLOS TSITINIDIS
 PRESIDENT
 HELLENIC AERO ENGINEERS SOCIETY
 38 M ALEXANDROU N SMIRNI
 ATHENS 17122
 GREECE
 ++30-1-9325309 **FAX:** ++30-262-59992
e-Mail: *aero@tee.gr*

MS MARTA VICARIO
 AGUSTA UN'AZIENDA FINMECCANICA
 FATIGUE OFFICE
 VIA G AGUSTA 520
 21017 CASCINA COSTA DI SAMARATE (VA)
 ITALY
 39-0331-229752 **FAX:** 39-0331-229341
e-Mail: *fatica@agusta.it*

MR MICHAEL TYSON
 ENGINEERING PROGRAM MANAGER
 LOCKHEED MARTIN
 SURVEILLANCE & COMMAND
 86 S COBB DR
 MZ 0595
 MARIETTA GA 30063-0595
 770-494-5280 **FAX:** 770-494-5414
e-Mail: *m.j.tyson@lmco.com*

MR DENNIS VICKERY
 BOEING CO
 STRUCTURAL MATERIALS TEST LAB
 MS 45-12
 SEATTLE WA
FAX:
e-Mail:

MR ANDREAS UEBERSAX
 DIPL. ING. ETH
 SWISS AIRCRAFT AND SYSTEMS ENTERPRISE
 CORP.
 FATIGUE ENGINEERING
 PO BOX 301
 EMMEN CH-6032
 SWITZERLAND
 41-41-268-21-13 **FAX:** 41-41-268-39-91
e-Mail: *andreas.uebersax@sf.admin.ch*

MR MARCELO FRAY VILLAR
 STRUCTURAL ENGINEER
 EMBRAER
 STRUCTURAL ENGINEERING
 AV BRIG AFARIA LIMA 2170
 SAQ JOSE DOS CAMPOS 1227-901
 SAO PAULO
FAX:
e-Mail: *fray@embraer.com.br*

MR PIM VAN DEN DIJSSEL
 MKTG & SALES MANAGER
 FOKKER CONTROL SYSTEMS
 PO BOX 7600
 SCHIPHOL 1117 ZJ
 THE NETHERLANDS
 31 20 6053248 **FAX:** 31 20 605 2524
e-Mail: *pim@fokkercontrol.com*

DR A VLOT
 DELFT UNIVERSITY OF TECHNOLOGY
 AEROSPACE ENGINEERING
 KLUGVISIVEG 1
 DELFT 262G MS
 THE NETHERLANDS
 31 15 278 7158 **FAX:** 31-1527-87-151
e-Mail: *a.vlot@lr.tudelft.nl*

MR SCOTT VANDERSALL
 C-130 STRUCTURAL ENGINEER
 US AIR FORCE
 265 OCMULGEE CT
 ROBINS AFB GA 31098-1647
 912-926-7198 **FAX:** 912-328-1257
e-Mail: *scott.vandersall@robins.af.mil*

MR NOBORU WAKITA
 MANAGER
 ALL NIPPON AIRWAYS
 STRUCT ENGINEERING IN AFRM MAINT CTR
 3-5-4 HANEDA AIRPORT
 144-0041TOKOYO
 JAPAN
 81-3-5756-5052 **FAX:** 81-3-5756-5037
e-Mail: *n.wakita@ana.co.jp*

ICAF '99 FINAL ATTENDANCE LIST

MR KEN WALKER
CONSULTANT
PO BOX 855
FILMORE CA 93016
805-524-5069 **FAX:** 805-524-5069
e-Mail: *ekwenger@csiway.com*

MR KEVIN WALKER
F-111 DADTA SUPPORT TASK MANAGER
DSTO
AIRFRAMES & ENGINES DIV AMRL
506 LORIMER ST
FISHERMENS BEND VIC 3207
AUSTRALIA
61-3-9626-7961 **FAX:** 61-3-9626-7089
e-Mail:

MR SIMON WALKER
STRUCTURES ENGINEER
BRITISH AEROSPACE MA&A
STRUCTURAL ENGINEERING
BROUGH
EAST YORKSHIRE HU15 1EQ
ENGLAND
01482-664142 **FAX:**
e-Mail: *simon.k.walker@bae.co.uk*

DR GENG-SHENG WANG
THE AERO RESEARCH INST OF SWEDEN
STRUCTURES DEPARTMENT
BOX 11021
161 11 BROMMA
SWEDEN
46-8-555-49-144 **FAX:** 46-8-258919
e-Mail: *wgs@ffa.se*

MR JIAN-JUEI WANG
PRINCIPAL ENGINEER/SCIENTIST
THE BOEING COMPANY
DURABILITY AND DAMAGE TOLERANCE
2401 E. WARDLOW RD
M/S C078-0209
LONG BEACH CA 90807-5309
562-982-2786 **FAX:** 562-982-7367
e-Mail: *jian-juei.wang@boeing.com*

DR ROY WATANABE
BOEING CO
M/S 67-FF
PO BOX 3707
SEATTLE WA 98124
425-237-4720 **FAX:** 425-234-1499
e-Mail: *roy.t.watanabe@boeing.com*

DR ROBERT WEI
PROFESSOR
LEHIGH UNIVERSITY
DEPT OF MECHANICAL ENG & MECHANICS
327 SINCLAIR LABORATORY
7 ASA DRIVE
BETHLEHEM PA 18015
610-758-3587 **FAX:** 610-758-6555
e-Mail: *rpw0@lehigh.edu*

MR IAN WHITTAKER
TECH FELLOW
THE BOEING CO
M/S 67-FF
PO BOX 3707
SEATTLE WA 98124
206-237-9909 **FAX:** 206-234-1499
e-Mail: *ian.c.whittaker@boeing.com*

MR HENRICUS WOERDEN
MSC
DELFT UNIVERSITY OF TECHNOLOGY
AEROSPACE ENGINEERING
KLUYVERWEG 1
DELFT 262G HS
NETHERLANDS
3115-279-6279 **FAX:** 3115-278-1151
e-Mail: *arwo@dutlbcz.lr.tudelft.nl*

DR YUEXI XIONG
RESEARCH OFFICER
NATIONAL RESEARCH COUNCIL CANADA
INSTITUTE FOR AEROSPACE RESEARCH
M-14 MONTREAL RD
OTTAWA ONTARIO
CANADA K1A 0R6
613-991-6926 **FAX:** 613-952-7136
e-Mail: *yuexi.xiong@nrc.ca*

MR TSUYOSHI YABUKI
DEPUTY CHIEF ACFT ACCIDENT INVESTIGATOR
JAPAN AIRCRAFT ACCIDENT INVESTIGATION COM
MINISTRY OF TRANSPORT
2 CHOME 1 BAN 3 KASUMIGASEKI
CHIYODA-KU TOKYO 100-8989
JAPAN
81-3-3581-7609 **FAX:** 81-3-3580-7973
e-Mail: *tsuyoshi-yabuki@so.motnet.go.jp*

MR YOUNG-IN YOON
DOCTORAL STUDENT
UNIVERSITY OF UTAH
MECHANICAL ENGINEERING
50 S CENTRAL CAMPUS DR
RM 2202
SALT LAKE CITY UT 84108
801-581-3030 **FAX:** 801-585-9826
e-Mail: *yyoon@mech.utah.edu*

ICAF '99 FINAL ATTENDANCE LIST

MR JAMES YOST
CHIEF ENGINEER
YOST ENGINEERING
4105 PLANTATION DR
FT WORTH TX 76116
817-244-3502 **FAX:**
e-Mail:



“Structural Integrity for the Next Millennium”

International Committee on Aeronautical Fatigue

12 - 16 July 1999

**Meydenbauer Center
Bellevue, Washington - USA**



National Delegates

Front Row (L-R): Dr. P. Poole, United Kingdom; J. Rouchon, France; D.L. Simpson, Canada; Prof. Dr. O. Buxbaum, Germany (General Secretary); J.L. Rudd, USA; and Prof. A. Salvetti, Italy

Back Row: Prof. Dr. A. Kobayashi, Japan; Colin A. Martin, Australia; Prof. A. Berkovitz, Israel; Silvain Michel, Switzerland; Claudio Dalle Donne, Germany; Harold Ottens, The Netherlands; and Prof. Dr. A.F. Blom, Sweden



◀ *Seattle Skyline*

*Meydenbauer Center
Meeting Site* ▶





Meeting Registration
UTC Staff



ICAF General Secretary
Otto Buxbaum



Meeting Chairman
Jim Rudd



*Conference
Keynote Speaker*
Terry Neighbor



Delegates and Guests
Spirit of Washington Dinner Train Event

Exhibit Hall ▶



*Tour of Fatigue
Technology Inc. Facilities*



▲
*Conference Reception
at the
Boeing Museum of Flight*



▲
*Symposium Keynote Speaker
David Swain*

Plantema Lecturer
Jim Newman ▶



◀ *Symposium Paper Presentation*



Symposium Reception - Puget Sound Cruise

Poster Session





Guests Organize the Days Activities



Attendees Return from Lunch to Auditorium



▲ *Guests Arrive for Symposium Banquet at Kiana Lodge* ▼





ICAF SPONSORS

- USAF Research Laboratory
- Boeing Commercial Airplane Group
- Fatigue Technology Incorporated
- NASA - Langley Research Center
- Northrop Grumman Corporation
- MTS Systems Corporation



New ICAF General Secretary David Simpson (l) Presents Gift to Retiring Otto Buxbaum



Long Time ICAF Supporters and Members of the Organizing Committee (l-r) Len Reid, Ulf Goranson, Govind Chinani, Art Braun and Bob Bader